

The Handbook of Environmental Chemistry 115

Series Editors: Damià Barceló · Andrey G. Kostianoy

Shunitz Tanaka
Masaaki Kurasaki
Masaaki Morikawa
Yuichi Kamiya *Editors*

Design of Materials and Technologies for Environmental Remediation



Springer

The Handbook of Environmental Chemistry

Volume 115

Founding Editor: Otto Hutzinger

Series Editors: Damià Barceló • Andrey G. Kostianoy

Editorial Board Members:

**Jacob de Boer, Philippe Garrigues, Ji-Dong Gu,
Kevin C. Jones, Abdelazim M. Negm, Alice Newton,
Duc Long Nghiem, Sergi Garcia-Segura, Paola Verlicchi**

In over four decades, *The Handbook of Environmental Chemistry* has established itself as the premier reference source, providing sound and solid knowledge about environmental topics from a chemical perspective. Written by leading experts with practical experience in the field, the series continues to be essential reading for environmental scientists as well as for environmental managers and decision-makers in industry, government, agencies and public-interest groups.

Two distinguished Series Editors, internationally renowned volume editors as well as a prestigious Editorial Board safeguard publication of volumes according to high scientific standards.

Presenting a wide spectrum of viewpoints and approaches in topical volumes, the scope of the series covers topics such as

- local and global changes of natural environment and climate
- anthropogenic impact on the environment
- water, air and soil pollution
- remediation and waste characterization
- environmental contaminants
- biogeochemistry and geoecology
- chemical reactions and processes
- chemical and biological transformations as well as physical transport of chemicals in the environment
- environmental modeling

A particular focus of the series lies on methodological advances in environmental analytical chemistry.

The Handbook of Environmental Chemistry is available both in print and online via <https://link.springer.com/bookseries/698>. Articles are published online as soon as they have been reviewed and approved for publication.

Meeting the needs of the scientific community, publication of volumes in subseries has been discontinued to achieve a broader scope for the series as a whole.

Design of Materials and Technologies for Environmental Remediation

Volume Editors: Shunitz Tanaka · Masaaki Kurasaki ·
Masaaki Morikawa · Yuichi Kamiya

With contributions by

S. Afrin · Y. Akemoto · M. Akter · R. Akter · Y. Amano ·
I.-A. Araki · A. K. M. Atique Ullah · P. Begum · Y. Dai ·
B. Fugetsu · S. Fujita · M. K. F. B. Hossain · M. S. Islam ·
H. Itabashi · Y. Kamiya · R. Kishi · S. Kobayashi ·
P. A. Krisbiantoro · Y. Kuboki · H. Kuramitz · M. Kurasaki ·
Y. Lin · E. Lopez-Echartea · M. Machida · Y. Mihara ·
C. Miyashita · M. Morikawa · M. Mori · M. Mudasir ·
N. Nuryono · R. S. Putra · M. M. Rahman · M. Ramakrishnan ·
R. Roto · T. Saito · N. Sakairi · S. C. W. Sakti · T. Sasaki ·
M. Shammi · T. Shunitz · E. Siswoyo · L. Sun ·
M. S. Syawal · M. Tajuddin Sikder · S. Tanaka · N. Wada ·
K. Yamazaki · K. Yrjälä · Yustiawati · H. Zheng

Editors

Shunitz Tanaka
Hokkaido University
Sapporo, Japan

Masaaki Kurasaki
Hokkaido University
Sapporo, Japan

Masaaki Morikawa
Hokkaido University
Sapporo, Japan

Yuichi Kamiya
Hokkaido University
Sapporo, Japan

ISSN 1867-979X

ISSN 1616-864X (electronic)

The Handbook of Environmental Chemistry

ISBN 978-981-19-5235-7

ISBN 978-981-19-5236-4 (eBook)

<https://doi.org/10.1007/978-981-19-5236-4>

© The Editor(s) (if applicable) and The Author(s), under exclusive license to Springer Nature Singapore Pte Ltd. 2023

This work is subject to copyright. All rights are solely and exclusively licensed by the Publisher, whether the whole or part of the material is concerned, specifically the rights of translation, reprinting, reuse of illustrations, recitation, broadcasting, reproduction on microfilms or in any other physical way, and transmission or information storage and retrieval, electronic adaptation, computer software, or by similar or dissimilar methodology now known or hereafter developed.

The use of general descriptive names, registered names, trademarks, service marks, etc. in this publication does not imply, even in the absence of a specific statement, that such names are exempt from the relevant protective laws and regulations and therefore free for general use.

The publisher, the authors, and the editors are safe to assume that the advice and information in this book are believed to be true and accurate at the date of publication. Neither the publisher nor the authors or the editors give a warranty, expressed or implied, with respect to the material contained herein or for any errors or omissions that may have been made. The publisher remains neutral with regard to jurisdictional claims in published maps and institutional affiliations.

This Springer imprint is published by the registered company Springer Nature Singapore Pte Ltd.

The registered company address is: 152 Beach Road, #21-01/04 Gateway East, Singapore 189721, Singapore

Series Editors

Prof. Dr. Damià Barceló

Department of Environmental Chemistry,
Barcelona, Spain
and
Catalan Institute for Water Research (ICRA)
Scientific and Technological Park of the
University of Girona
Girona, Spain
dbcqam@cid.csic.es

Prof. Dr. Andrey G. Kostianoy

Shirshov Institute of Oceanology
Russian Academy of Sciences
Moscow, Russia
and
S.Yu. Witte Moscow University
Moscow, Russia
kostianoy@gmail.com

Editorial Board Members

Prof. Dr. Jacob de Boer

VU University Amsterdam, Amsterdam, The Netherlands

Prof. Dr. Philippe Garrigues

Université de Bordeaux, Talence Cedex, France

Prof. Dr. Ji-Dong Gu

Guangdong Technion-Israel Institute of Technology, Shantou, Guangdong, China

Prof. Dr. Kevin C. Jones

Lancaster University, Lancaster, UK

Prof. Dr. Abdelazim M. Negm

Zagazig University, Zagazig, Egypt

Prof. Dr. Alice Newton

University of Algarve, Faro, Portugal

Prof. Dr. Duc Long Nghiem

University of Technology Sydney, Broadway, NSW, Australia

Prof. Dr. Sergi Garcia-Segura

Arizona State University, Tempe, AZ, USA

Paola Verlicchi

University of Ferrara, Ferrara, Italy

Series Preface

With remarkable vision, Prof. Otto Hutzinger initiated *The Handbook of Environmental Chemistry* in 1980 and became the founding Editor-in-Chief. At that time, environmental chemistry was an emerging field, aiming at a complete description of the Earth's environment, encompassing the physical, chemical, biological, and geological transformations of chemical substances occurring on a local as well as a global scale. Environmental chemistry was intended to provide an account of the impact of man's activities on the natural environment by describing observed changes.

While a considerable amount of knowledge has been accumulated over the last four decades, as reflected in the more than 150 volumes of *The Handbook of Environmental Chemistry*, there are still many scientific and policy challenges ahead due to the complexity and interdisciplinary nature of the field. The series will therefore continue to provide compilations of current knowledge. Contributions are written by leading experts with practical experience in their fields. *The Handbook of Environmental Chemistry* grows with the increases in our scientific understanding, and provides a valuable source not only for scientists but also for environmental managers and decision-makers. Today, the series covers a broad range of environmental topics from a chemical perspective, including methodological advances in environmental analytical chemistry.

In recent years, there has been a growing tendency to include subject matter of societal relevance in the broad view of environmental chemistry. Topics include life cycle analysis, environmental management, sustainable development, and socio-economic, legal and even political problems, among others. While these topics are of great importance for the development and acceptance of *The Handbook of Environmental Chemistry*, the publisher and Editors-in-Chief have decided to keep the handbook essentially a source of information on "hard sciences" with a particular emphasis on chemistry, but also covering biology, geology, hydrology and engineering as applied to environmental sciences.

The volumes of the series are written at an advanced level, addressing the needs of both researchers and graduate students, as well as of people outside the field of

“pure” chemistry, including those in industry, business, government, research establishments, and public interest groups. It would be very satisfying to see these volumes used as a basis for graduate courses in environmental chemistry. With its high standards of scientific quality and clarity, *The Handbook of Environmental Chemistry* provides a solid basis from which scientists can share their knowledge on the different aspects of environmental problems, presenting a wide spectrum of viewpoints and approaches.

The Handbook of Environmental Chemistry is available both in print and online via <https://link.springer.com/bookseries/698>. Articles are published online as soon as they have been approved for publication. Authors, Volume Editors and Editors-in-Chief are rewarded by the broad acceptance of *The Handbook of Environmental Chemistry* by the scientific community, from whom suggestions for new topics to the Editors-in-Chief are always very welcome.

Damià Barceló
Andrey G. Kostianoy
Series Editors

Preface

Environmental remediation technology is a method for removing pollutants from a polluted environment and restoring them to their original safe state. Unfortunately, pollution has persisted in many places of the world, and many new pollution problems are now occurring. As a result, the advancement of environmental remediation technology is highly expected. Some of these technologies necessitate the use of special materials to remove pollutants when conducted. For example, the adsorption method to separate pollutants necessitates the use of an adsorbent that must have excellent properties in terms of adsorptive capacity, selectivity, durability, and safety in order to be used in actual environments. As a result, research on environmental remediation technologies is being conducted to develop the materials used in these technologies. Pollutants are diverse, and pollution levels vary from one polluted site to the next. Consequently, the materials used there must serve multiple functions and be designed in accordance with the pollution situation. From this perspective, I asked researchers to present their previous and ongoing research on the development of materials applicable to environmental remediation.

The book, entitled “Design of Materials and Technologies for Environmental Remediation,” is divided into 19 chapters about environmental remediation. This book is also part of the Handbook of Environmental Chemistry series. The first half of the book includes a chapter on the concept of environmental remediation, a chapter on case studies of environmental pollution problems, and two chapters on the biological effects of heavy metals and persistent organic pollutants on human health and ecosystems. Section 7 in page 29 shows the contents of this book. This book’s general conclusion chapter has been omitted because each chapter has its own conclusion or prospective. The topics introduced in this book do not cover all the environmental remediation technologies currently being researched or all the materials used there. The majority of the topics are provided by the researchers close to me or the other editors of this book. Hence, some may argue that the contents of this book are quite biased. It is possible that the current mainstream environmental remediation technologies are missing or that recent successes in this field or studies that have had a major impact are not described in this book.

However, despite focusing on the topics related to the editors, I think we could provide interesting and promising materials and technologies for environmental remediation in this book to some extent. Another distinguishing feature of this book is that it was written by a large number of Asian researchers. This book's publication includes contributions from researchers in Japan, Indonesia, China, and Bangladesh. These countries face many environmental pollution problems now, and I hope that this book will play a role in the future and that the authors who wrote this book will act as leaders in solving these problems. Since many Asian researchers, including me, are the authors of this book, there may be some infelicitous expressions in English from the perspective of native speakers, so we would like to ask for forgiveness.

Springer Nature's publisher approved the publication project for this book in November of 2019. It took almost three years to complete this book. This period has coincided with the pandemic spread of the coronavirus all over the world. Many universities must hold online classes in response to corona, and since most of the authors of this book are also university faculty members, they must spend a significant amount of time preparing the online classes and protecting their laboratory members from the infections, which makes them extremely busy. Thus, it was expected that writing activities would be pushed back. Hence, I requested the publisher to extend the deadline for the submission of the manuscript by six months. I would like to thank all the authors who wrote during the busy schedule of the severe corona infection. I apologize for the delay in publishing this book to the authors who finished their manuscripts well ahead of schedule.

Sapporo, Japan

Shunitz Tanaka

Acknowledgements

Finally, I would like to thank Mr. Koizumi Shinichi of Springer Nature Japan, who gave me the opportunity to publish the book, Ms. Ramya Venkitachalam, a project coordinator of Springer Nature, who waited patiently for our manuscript with much support for us, and other staff members of Springer Nature. Thanks also to the editors, Dr. Kurasaki Masaaki, Dr. Morikawa Masaaki, and Dr. Kamiya Yuichi for their cooperation with me from the planning to the completion of this book. I would also like to thank my current workplaces, ES General Laboratory Co. and Hokkaido Environmental Science and Technology Center. I do not think this book would have been completed without the understanding and support of these workplaces. Naturally, I am grateful to the many students who studied hard to obtain the valuable data and many researchers who supported our studies and surveys, as well as all the authors of this book. I would like to thank Enago (www.enago.jp) for the English language review. Finally, I would like to thank my wife and my family for silently but fondly watching over my work.

Contents

Part I Background

- Environmental Pollution and Remediation** 3
Shunitz Tanaka
- Some Pollution Problems to Consider the Design for Remediation** 33
Rudy Syah Putra, Yustiawati, M. Suhaemi Syawal, Yingjie Dai,
Yongbo Lin, Md. Mostafizur Rahman, Mashura Shammi,
and Tanaka Shunitz

Part II Effects and Evaluation

- Effects of Metals on Human Health and Ecosystem** 81
Md. Mostafizur Rahman, Mst. Kaniz Fatima Binte Hossain, Sadia Afrin,
Takeshi Saito, and Masaaki Kurasaki
- Effects of Persistent Organic Pollutants (POPs) in the Ecosystem
and Human Health: Focusing on Chlorinated Chemicals** 121
Ikeda-Atsuko Araki, Chihiro Miyashita, Sumitaka Kobayashi,
Keiko Yamazaki, and Reiko Kishi

Part III Introduction of Novel Functions and Materials into Remediation Technologies

- Electrokinetic Remediation** 147
Yasuhiro Akemoto, Rudy Syah Putra, and Shunitz Tanaka
- Phytoremediation: Background, Principle, and Application, Plant
Species Used for Phytoremediation** 199
Md. Shariful Islam, Rubaiya Akter, Md. Mostafizur Rahman,
and Masaaki Kurasaki

Electrochemical Decomposition and Adsorption for Removal of Organic Pollutants from Water	225
Hideki Kuramitz	
Bioremediation: From Key Enzymes to Practical Technologies	263
Masaaki Morikawa	
Part IV Design of Environmental Materials	
Environmentally Friendly Adsorbents	293
Eko Siswoyo, Yingjie Dai, Masanobu Mori, Nobuhiko Wada, and Hideyuki Itabashi	
Preparation and Modification of Activated Carbon Surface and Functions for Environments	335
Motoi Machida and Yoshimasa Amano	
Pyrolysis to Produce Hydrochar and Biochar Carbon Material for Carbon Removal and Sustainable Environmental Technology	367
Kim Yrjälä, Muthusamy Ramakrishnan, Huabao Zheng, and Eglantina Lopez-Echartea	
Graphene Oxide for Elimination of Dyes	393
Ling Sun and Bunshi Fugetsu	
Heterogeneous Catalysts for Environmental Purification	423
Yuichi Kamiya	
Coal Fly/Bottom Ash, Hydroxylapatite, and Hydrotalcite	461
Mudasir Mudasir, Roto Roto, Yoshinori Kuboki, and Parvin Begum	
Bio-Inspired Materials for Environmental Remediation	507
Sayaka Fujita and Nobuo Sakairi	
Zero-Valent Iron and Some Other Nanometal Particles for Environmental Remediation	539
Mahmuda Akter, Md. Tajuddin Sikder, and A. K. M. Atique Ullah	
Part V Easily Collectable Adsorbents	
Magnetic Separation of Pollutants for Environmental Remediation . . .	571
Takahiro Sasaki, Satya Candra Wibawa Sakti, Nuryono Nuryono, and Philip Anggo Krisbiantoro	
Easily Collectable Floating-Up Adsorbents to Remove Pollutants	617
Yoshihiro Mihara and Shunitz Tanaka	
Remediation by Floating Plants	651
Masaaki Morikawa	

Part I

Background

Environmental Pollution and Remediation



Shunitz Tanaka

Contents

1	Introduction	4
2	Environmental Pollution Problems in Japan	6
2.1	Occurrence of “Ko-gai”: Public Pollution Problems	6
2.2	Low-Concentration Pollution Problem	8
2.3	Contamination with Radionuclides by Nuclear Power Plant Accident	11
3	Environmental Remediation	13
3.1	Concepts of Environmental Remediation	13
3.2	Classification of Remediation Technologies	14
4	Combination of Remediation Methods	24
5	Selection and Evaluation of Environmental Remediation Technology	25
6	Design of Environmental Materials for Remediation	26
7	Contents of This Book	29
8	Conclusion	30
	References	31

Abstract In this Chapter, as the background and introduction of this whole book, the following matters are mainly described. Firstly, it is stated that many environmental pollution problems occur still now in the world by various causes such as industrial activities, our daily and natural activities, and accidents and disasters. In order to solve these environmental pollution problems, the necessity of the development of environmental remediation technology is described. Next, some pollution problems, which Japan experienced previously and is currently facing, are intro-

S. Tanaka (✉)

Hokkaido University, Hokkaido Environmental Science and Technology Center, ES General Laboratory Co., Sapporo, Hokkaido, Japan

e-mail: syny-tanaka@ab.auone-net.jp

Shunitz Tanaka, Masaaki Kurasaki, Masaaki Morikawa, and Yuichi Kamiya (eds.),

3

Design of Materials and Technologies for Environmental Remediation,

Hdb Env Chem (2023) 115: 3–32, DOI 10.1007/698_2021_819,

© The Author(s), under exclusive license to Springer Nature Singapore Pte Ltd 2022,

Published online: 1 January 2022

duced, for example, Minamata disease, low-concentration pollution problems such as dioxins and endocrine disruptors, and contamination with radionuclides from the explosion of the nuclear power plants caused by the big tsunami. After that, the concept and classification of the environmental remediation technology are described. It is shown that remediation consists of three concepts: containment, separation, and decomposition, and that remediation technologies are also classified into two categories, In-situ and Ex-situ. Several representative techniques for containment, separation, and decomposition are introduced briefly. The combination of some remediation technologies and the evaluation are also described, when these remediation techniques will be applied to the actual contaminated site. It is discussed why further development of remediation technology is necessary and why the design of materials for remediation technology is necessary. Finally, a brief introduction for the structure of this book and chapters is given.

Keywords Concepts for remediation, Containment, Environmental remediation, In-situ and Ex-situ, Low-concentration pollution, Minamata disease, Separation and decomposition

1 Introduction

On the earth, humankind has enlightened and developed its civilization over a long time. According to United Nations; World Population Prospects 2019, 7.7 billion people live on the earth in 2019 [1]. Population Division of UN prospects that the world population will be 9.7 billion in 2050. In order to maintain their lives, we must secure enough amounts of water, foods, and energy for them. For more wealthy life, we have promoted industries to manufacture various kinds of products massively, and circulated them over the world. In order to maintain such our lifestyles and industrial activities, we have always developed the resources of coal and oil as energy and minerals as raw materials from every place on the earth. We have also synthesized new materials that had not existed on the earth. As a result, our lives have become convenient and prosperous. On the other hand, the environments surrounding us have been flooded with every kind of things, and often polluted with harmful substances including natural and synthesized compounds. There are various kinds of pollutants, including heavy metals, harmful organic substances, organic chlorine compounds, asbestos, radioactive substances, and so on. The more sophisticate the current industry becomes, the more diverse of the materials are required there. Consequently, the sorts of pollutant are now diversifying.

Pollution arises from various causes. Pollution often occurs as the results of industrial activities in mines and factories. It also occurs from our daily lives and

Table 1 Some recent pollution problems by accident and disasters

Events	Date	Location and country	Pollutants	Amounts of pollutant
Nuclear power plant accident	April 26th, 1986	Chernobyl, Ukraine	Radionuclides	1.2×10^{19} Bq
Oil spill from a tanker, Nakhodka	Jan. 2nd, 1997	The Japan Sea, near Shimane	Heavy oil	6,240 kL
Chemical plant explosion	Nov. 13th, 2005	The Songhua river, North-east in China	Benzene, aniline, nitrobenzene	100 tons
Nuclear power plant accident	March 11th, 2011	Fukushima, Japan	Radionuclides	0.9×10^{18} Bq
Oil-drilling station accident	April 20th, 2010	The Gulf of Mexico	Crude oil	78×10^3 kL
Oil spill from a cargo boat, Wakashio	July 25th, 2020	Mauritius, the Indian Ocean	Heavy oil	1,000 ton

natural processes such as volcanic activities. Accidents and disasters sometimes cause severe pollution problems. For example, an explosion of a chemical factory gave rise to the pollution of the Songhua River of China [2]. After the mega earthquake occurred on March 11 of 2011 in Tohoku area of Japan, the big tsunami attacked Fukushima Daiichi Nuclear Plants to lose the electricity for cooling the nuclear reactors, consequently the reactors exploded to pollute the wide areas of Fukushima and surrounding prefectures with plenty of radionuclides [3]. Some pollution problems happened recently by accidents and disasters are summarized in Table 1. And some examples of pollution problems are described in chapter “Pollution Sites Where Need Remediation”.

How should we balance economic development with environmental preservation for a sustainable society? This is an unavoidable challenge for our and our future generations to cope with. According to the Sustainable Society Foundation, a sustainable society is defined as the following society: “that meets the needs of the present generation, and that does not compromise the ability of future generations to meet their own needs, in which each human being has the opportunity to develop itself in freedom, within a well-balanced society and in harmony with its surroundings” [4]. At the UN Summit held on Sep. 25 in 2015, the SDGs (Sustainable Development Goals) to achieve a better and more sustainable future for all were adopted. The SDGs consist of 17 challenges including those related to poverty, inequality, climate change, environmental degradation, peace, and justice [5]. The SDGs should be achieved by 2030 in the world, and then every countries and individuals are required to act as aiming these goals. The following six goals seem to be particularly related to environmental remediation and the goals which remediation technologies can contribute to fully (Table 2).

Table 2 SDGs related to environmental remediation

Goal 3	Good health and well-being: ensure healthy lives and promote well-being for all at all ages
Goal 6	Clean water and sanitation: ensure access to water and sanitation for all
Goal 9	Industry, innovation, and infrastructure: build resilient infrastructure, promote sustainable industrialization and foster innovation
Goal 13	Climate action: take urgent action to combat climate change and its impacts
Goal 14	Life below water: conserve and sustainably use the oceans, seas, and marine resources
Goal 15	Life on land: sustainably manage forests, combat desertification, halt and reverse land degradation, halt biodiversity loss

2 Environmental Pollution Problems in Japan

2.1 Occurrence of “Ko-gai”: Public Pollution Problems

In Japan, many environmental pollution problems occurred in the 1950–1970s during the economic recovery and growth in Japan after the World War II. Minamata disease, Itai-itai disease, Yokkaichi air pollution, etc., are well known in the world as the representative pollution problems in Japan. These pollution problems were called “Ko-gai” in Japanese, which means “public pollution problems.” Japan’s economic growth-first policy during this period gave priority to the economic development over the consideration for the environment and consequently it led to many pollution problems. Those problems were not just the pollution which private companies caused but the pollution which Japan’s policy during those days caused. Therefore, those pollution problems are considered as the public problems, “Ko-gai.” In the 1970s, some countermeasures were conducted, and in 1973, a law, “Basic Law on Pollution Control,” which was the first environmental law in Japan, was enacted. Some environmental standards were enforced in this law, and thereafter various countermeasures to keep these standards have been carried out on the basis of this law in Japan. As a result, “Ko-gai”-type environmental pollution problems in Japan gradually decreased. In most cases of “Ko-gai”-type pollution, pollutants were released from the specific industrial process and facility, and then if any countermeasure was taken against the source of pollutants, most of pollution problems could be solved. Figure 1 shows the change in the non-achievement rate for some environmental standards after the enforcement of the environmental law [6]. The non-achievement rate has decreased rapidly after the enforcement and now the rates are below 1% in many items.

Minamata disease was one of the typical “Ko-gai” problems. The pollution problem occurred in Minamata city of Kumamoto prefecture in Kyushu island of Japan. Since the first finding of a patient of Minamata disease in 1956, many patients were found out from mainly fishermen and their family who had been fishing in Minamata Bay. The patients of Minamata disease had a disorder in motor and

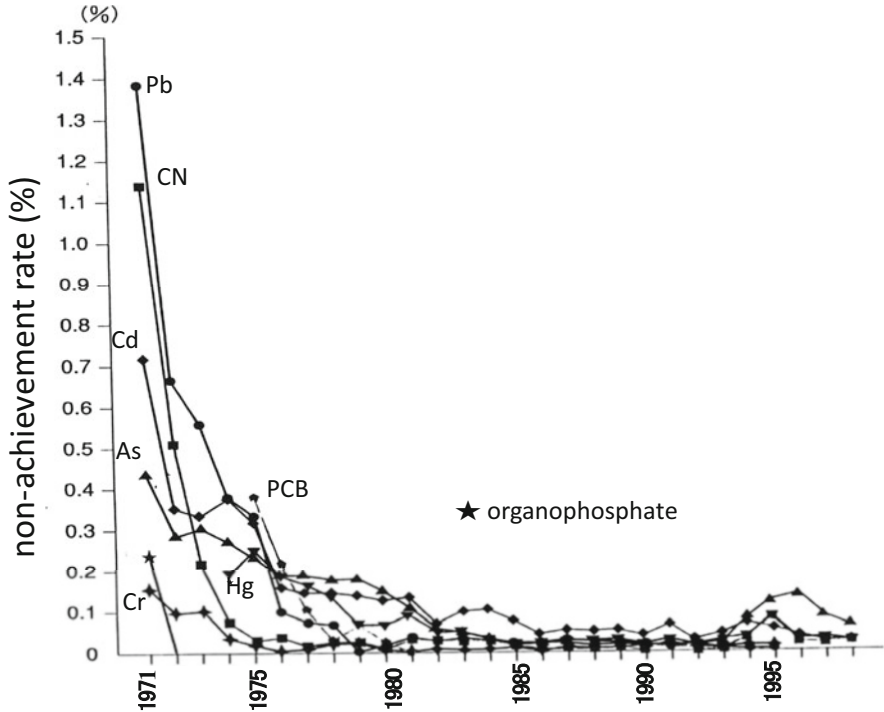


Fig. 1 Change in non-achievement rate for some environmental standards (from The Annual Report of the Environment of Japan (1995) [6])

language, and sometimes a problem in brain. It took very long time to clarify the cause of Minamata disease. In 1959, methylmercury discharged from a factory of a chemical company was suggested to be a cause by a research group of Kumamoto University. At those days, the factory had produced acetaldehyde from acetylene by using mercury salt as a catalyst. The inorganic mercury might be converted to methylmercury by the reactions during the production process. However, some authorities such as the academic society, the industrial society, and university in Japan declared other opinions about the cause of Minamata disease. Their opinions confused the clarification of the cause and made it prolong to determine the cause. Later Dr. Nishimura et al. showed the reaction mechanism for methylmercury formation during acetaldehyde production in their book as shown in Fig. 2 [7]. Methylmercury can pass through the placenta and be accumulated in a body of fetus and then many children having the disorder in motor and brain were born. In 1967, Japanese government admitted Minamata disease as a “Koh-gai,” a public disease with methylmercury. After many conflicts between fishermen and the company concerning the countermeasures and compensation, finally in 1968, the company stopped the production of acetaldehyde. In 1965, the second Minamata disease was found in Niigata Prefecture in Japan [8].

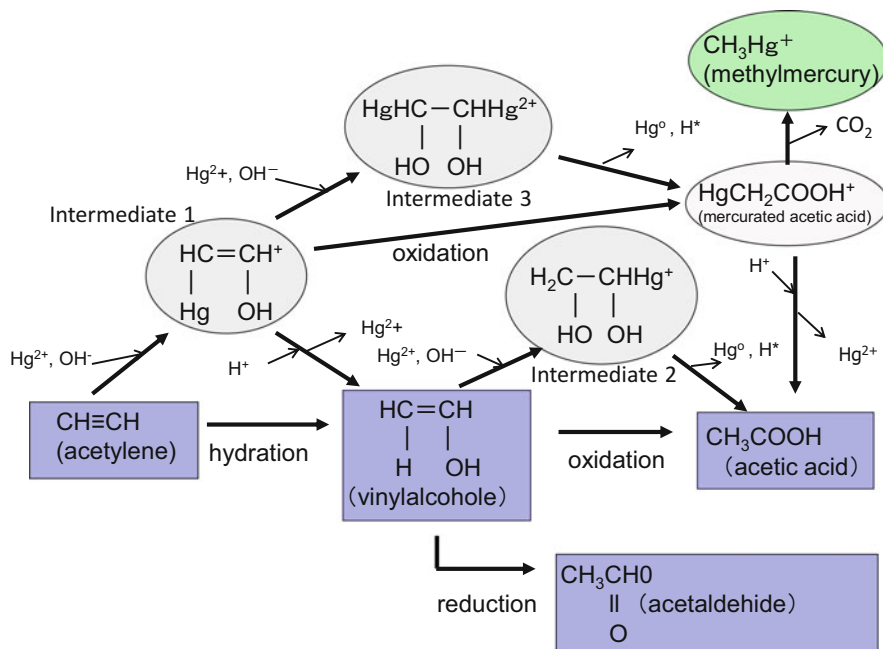


Fig. 2 Reaction mechanism for methylmercury formation during acetaldehyde production [7]

The “Ko-gai” type of the pollution problems like Minamata disease has not been completely solved in Japan. Even now, there are many designated patients of Minamata disease, and also many not-designated patients are still waiting to be recognized as a patient of Minamata disease by the struggle in court and administration. Environmental pollutions with mercury seem to be spreading all over the world, and the third and fourth Minamata diseases may occur or have occurred somewhere in the world. For this reason, the Minamata Convention on Mercury (Minamata Treaty) [9] was adopted at UN meeting held at Minamata city in 2013 with the aim of reducing and controlling the use of mercury worldwide.

In Japan, in order to cope with global environmental problems such as global warming and ozone layer depletion, a new law, the Basic Environmental Law, was established in 1993 instead the old law. In this law, preventive and diverse methods were introduced to in addition to ordinal regulatory methods and the countermeasures based on environmental education and international cooperation are recommended.

2.2 Low-Concentration Pollution Problem

In the 1990s, Japan was facing pollution problems with dioxins and environmental hormones (endocrine disrupting chemicals). These pollutions have different

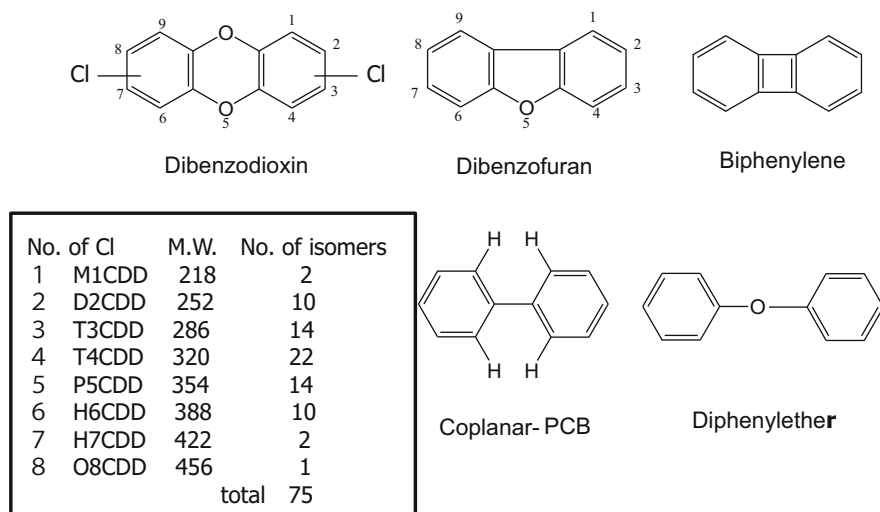


Fig. 3 Structures of dioxin and dioxin analogs

characteristics from previous pollution problems, “Koh-gai,” in the point that the pollutants affect human health and ecosystems at very low concentration. In addition, pollutants are released from unspecific and multiple sources but not from a specific factory like “Koh-gai”-type. Especially dioxins are generated even when garbage routinely discharged from our ordinary households is combusted. Dioxin generally represents polychlorinated dibenzo-dioxin and some analogs such as dibenzofuran and biphenylene are also included in Dioxins (Dioxin group). Each analog has many isomers and congeners. Figure 3 shows the structures of dioxin and dioxin analogs. Among them, 2, 3, 7, 8-dibenzo-*p*-dioxine is known to have the strongest toxicity. Dioxins are unintentionally generated chemicals at the incineration plants in city and also in hospitals, schools, companies, etc. If pollution with dioxins comes from the combustion of our household garbage, the perpetrators of dioxin pollution are ourselves who generate the garbage, and the victims are also us. In “Ko-gai” pollution problems, the perpetrators and victims could be clearly distinguished, but not in the case of dioxins pollution problems.

In Japan, a special law for dioxins (Law concerning Special Measures against Dioxins) was established in 1999 [10], although scientific information was not enough. The criteria for the concentration of dioxins in the emitted gases and water from an incinerator were established. The owner of an incinerator is obligated by this law to report the concentration of dioxins in and around the incinerator. Consequently, most of small incinerators disappeared from hospital, school, and home. People stopped burning garbage in their garden. Local governments replaced an old incinerator with a new one which could burn garbage at the higher temperature not to generate a large amount of dioxins. As a result, the amount of dioxins discharged from the incinerator has been reduced largely to be negligible now in Japan as shown in Fig. 4 [11].

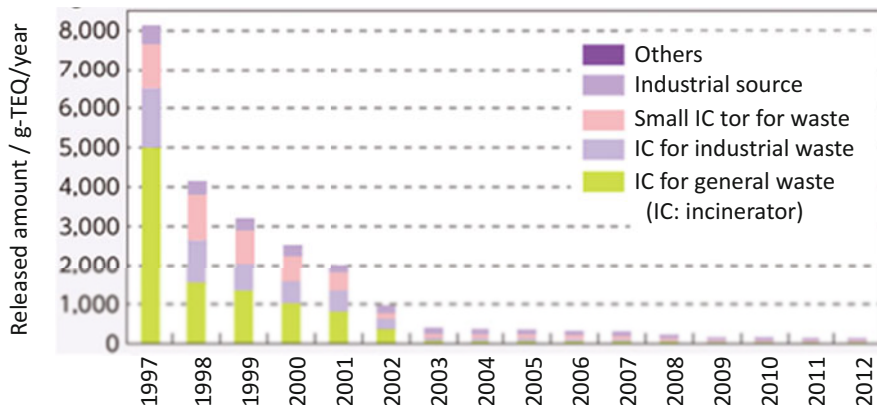


Fig. 4 Released amount of dioxins from various sources (from The Annual Report of the Environment of Japan (2014) [11])

In Japan, the pollution problem by endocrine disrupting chemicals was a notable environmental topic in the 1990s. These chemicals were called “environmental hormones” in Japan because those chemicals acted like hormones and affected human health and ecosystems, especially on reproduction and the next generation, even though at very low concentration. Many researchers joined in the studies on the detection of many kinds of chemicals in environments and the effects on human health and ecosystems. It was like a fever as involving many mass media. Two books of “Silence Spring” by Rachel Carson and “Our stolen future” by Theo Colborn must enhance not a little the concern and fears of people for the chemicals. The Japanese Ministry of the Environment has launched a program, “Strategic Programs on Environmental Endocrine Disruptors (SPEED98)” in 1998 to urgently investigate the effects of endocrine disrupting chemicals on human health and ecosystems [12]. The program concluded that few chemicals showed the endocrine disrupting effects on the human health, a few chemicals showed some effects on ecosystem and there might be still now many things which we did not know. The program was carried on to a new program, EXTEND 2010 program [13]. However, the concerns of people and the interest of the media in the endocrine disrupting chemicals declined rapidly.

Polychlorinated biphenyl (PCB) is an artificially synthesized compound. This compound is very stable chemically and biologically and has high insulated and fire-resistant properties. Therefore, PCB has been used in various purposes, insulated oil for condenser and capacitor, paint, heat-transfer fluid, transfer paper, and so on, and it was called “a dreamy chemical.” However, the toxicity of PCB to human health and ecosystem was found out and then the production and use were banned. The more stable and persistent the compound is, the longer the compound can stay in environments. Since PCB is almost insoluble in water, the concentration of PCB in water is usually very low. However, the hydrophobic and persistent properties of PCB facilitate the bio-concentration. Even though the concentration of PCB in water is very low, PCB is accumulated gradually in the living body to be a significant

concentration to give some damages. Therefore, PCB pollution problem has a common feature with the low-concentration pollution problem such as dioxins and environmental hormones. PCB has many isomers and congeners with different numbers of chlorine at the different positions. Among these congeners, the PCB isomers having no chlorine at the position of 2, 2', 6, and 6' are called "coplanar PCB: Co-PCB" because these have the co-planarity of two benzene rings. The structure of Co-PCBs is similar to that of dioxin and then they have the strong toxicity like dioxins. Therefore, Co-PCBs are regarded as one of dioxins. In Japan, the treatment of PCB oil and the products containing PCB such as condenser and capacitor has been conducted by Japan Environmental Storage and Safety Corporation (JESCO), whose treatment facilities exist at five areas in Japan and all of PCB including high and low concentration will be decomposed by 2027 [14].

The measure for the low-concentration pollution has some difficulties as follows:

1. It is difficult to detect the pollutants and then to know the pollution situation exactly.
2. It is difficult to evaluate the impacts of the pollution because it may take a long time to appear the impacts by the pollution, sometimes the impacts may appear in the next generation.
3. It is difficult to find out the effective countermeasures against the pollutants, because the concentration is too low to apply the conventional treatment methods to them. Pre-collection and accumulation of the pollutants are necessary before the treatment. In order to cope with low-concentration pollution, the novel technologies for high sensitive detection and selective accumulation of pollutants are required.

As described previously, if a pollutant is persistent and stays in the environment for a long time, the pollutant may be accumulated to the level that can affect human health by bio-concentration even at low concentration. In particular, the effects of long-term exposure on children have not yet been clarified. Currently a project for investigation of the effects of the long-term exposure on children is in progress [15]. A part of the results of the project will be described in detail in chapter "Effects of Persistent Organic Pollutants (POPs) in the Ecosystem and HUMAN health: Focusing on Chlorinated Chemicals".

2.3 Contamination with Radionuclides by Nuclear Power Plant Accident

On March 11 of 2011, an earthquake of the magnitude 9.0 attacked the northeastern Japan followed by a big tsunami. The tsunami over 20 m rushed toward the shore of the wide areas and citizens more than 15,000 died and about 2,500 have been still missing by the earthquake and tsunami [16]. The tsunami also attacked Fukushima Daiichi Nuclear Power Plants and destroyed the electric systems to cool the reactors.

Consequently, four nuclear reactors exploded to release a large amount of radionuclides into environments. The amount of released radionuclides, 0.9×10^{18} Bq, was as large as one-tenth of the amount released in the nuclear plant accident at Chernobyl [17]. The radionuclides firstly released into the atmosphere were carried by the wind to fall down into soil, farmland, and forests throughout Fukushima prefecture and the neighboring prefectures.

Two months after the accident, the Ministry of Education, Culture, Sports, Science and Technology of Japan, some universities and institutes cooperatively conducted an emergency survey of soil pollution with radionuclides within a radius of 100 km from the nuclear power plants. According to the results of the survey, it was found that the wide areas in Fukushima were polluted with radionuclides, especially with ^{134}Cs , ^{137}Cs , and others, The pollution was spreading distinctively in the northwest direction from the site of the nuclear power plants as shown in Fig. 5 [3]. The radioactive Cs has been remaining in the surface soil within several cm because Cs ions bound strongly to clay minerals in soil. The Ministry of the Environment recommended a series of the processes shown in Fig. 6 as a decontamination method for the surface soil. The upper 5 cm of the contaminated surface soil is stripped off and put into the large bags (flexible containers). These bags are stored in a temporary storage site for 3 years and then moved sequentially to an intermediate storage facility for 30 years. Lastly the contaminated soil is moved to the final disposal facility [18]. However, the amount of contaminated soil is too huge

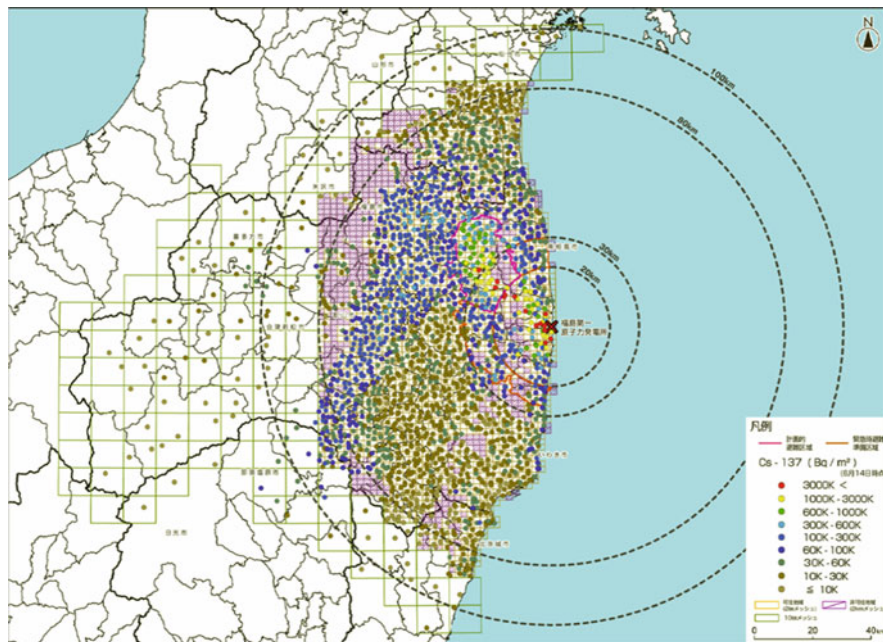
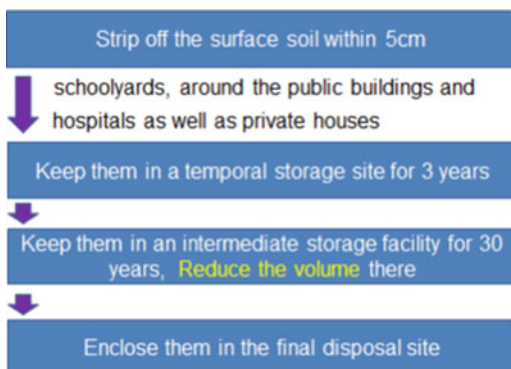


Fig. 5 Distribution of ^{137}Cs in soil around of the NPP [3]

Fig. 6 Flow of decontamination for polluted soils proposed by the Ministry of Environment, Japan



to treat and store them and the construction of the intermediate storage facilities has not so progressed. Moreover, Japanese government has not yet decided the locations for the final disposal facility. It is doubtful whether the decontamination would proceed as planned or not. Even now, 9 years after the accident, there are many residents who cannot return to their homes because the areas around their houses have been designated as the evacuation areas.

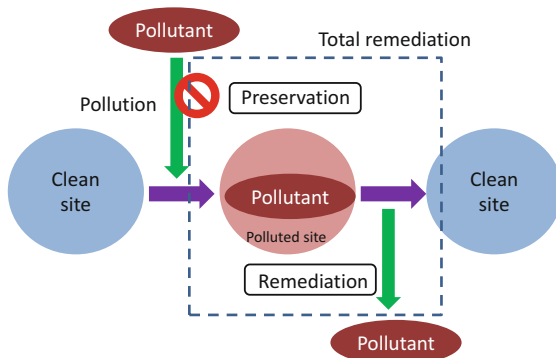
If radionuclides could be removed from contaminated soil by any methods, the volume of the contaminated soil could be reduced to scale down the number and size of the storage facilities. Many researchers have intended to develop various kinds of treatment methods using phytoremediation, adsorption, hydrothermal method, electrochemical method, etc. So far, the practical methods which can be applied to actual contaminated soil have not yet been found out because most of the reported methods have disadvantages in terms of processing time and cost. A Korean researcher, Kim studied on the removal of radionuclides from contaminated soil by a combined method of soil washing and electro-kinetic method [19]. We also investigated EK method to remove Cs ion from soil and some results of these studies are described in chapter “Electrokinetic Remediation”.

3 Environmental Remediation

3.1 Concepts of Environmental Remediation

What we should do firstly to keep the earth’s environments clean is to not release pollutants to environments. In all processes of manufacturing, we have to introduce pollutant-free processes by developing new technologies. These technologies are called conservation/preservation, zero-emission technology, and sometimes green chemistry for the technology in the field of chemistry. On the other hand, there are already many contaminated environments around us. For these environments, it is necessary to restore the previous clean and safe situation by removing the pollutant.

Fig. 7 True remediation technology contains the preservation technology



That process is the environmental remediation and the technology used for that purpose is the remediation technology. The remediation technologies are also called restoration, decontamination, cleaning, and so on. The definitions of these terms are not always clear.

The technologies for preservation and remediation should be complementary to each other. Even though a contaminated site could be restored completely by the remediation technology, as far as the source which releases a pollutant still exists, the site will be again contaminated with the pollutant. Therefore, the true remediation technology should contain the preservation technology which can suppress the release of the pollutant from the source and the injection to the site as shown in Fig. 7. If the ultimate preservation technologies, which can suppress the release of pollutants completely, could be established in all processes, the remediation technologies may be not necessary. So far, unfortunately such preservation technologies have not been established in most fields. The complementary roles of two kinds of the technology are shown in Fig. 8. In the figure, at first, before starting remediation, a certain amount of pollution exists. The amount of the pollution consists of not only already existing pollutants but also newly injected pollutants. The pollution is treated by the remediation technology and the amount is reduced as a function of time. At the same time, the pollution is treated by preservation technologies and the amount of the pollutant is also reduced as a function of time. Finally the remaining pollution is disappeared by the complementary actions of the remediation and preservation.

3.2 *Classification of Remediation Technologies*

The diverse environments of aqueous sphere, atmosphere, and soil can be the targets of remediation. Various kinds of substances such as metals, harmful organic matters, radionuclides, and so on are also the target substances of remediation. The situation of pollution differs from site and site, and the concentration and toxicity of pollutants

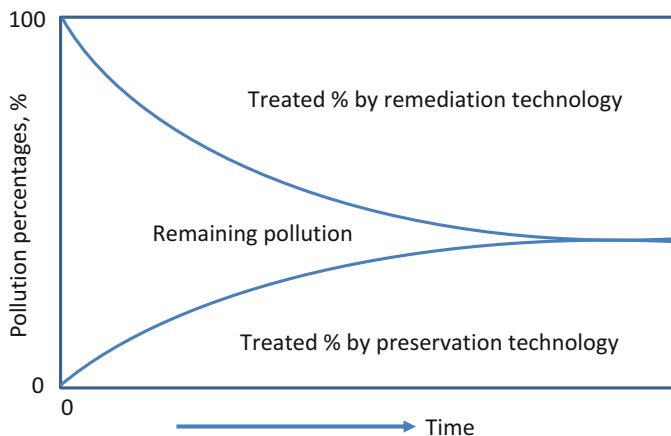


Fig. 8 Complementary relationship between remediation and preservation technologies

and the environments surrounding the polluted site are also different. The removal efficiency of pollutants required depends on the status of the site. Some site requires the complete removal of pollutant but other site not so because the reduction of pollutants by natural attenuation can be expected there after the remediation. For such diverse requirements, we have to prepare many kinds of remediation technologies.

Remediation technologies are classified into three groups depending on these concepts, containment, separation, and decomposition. In addition to these, accumulation technologies are required for the treatment of low-concentration pollutants but these technologies are included in separation. Table 3 shows the classification of some representative remediation technologies [20–22].

In containment, pollutants are converted to stable and immobile substances or enveloped into the stable material to prevent pollutants from spreading more in environments. In separation, pollutants are removed from contaminated site by various kinds of chemical, physical, and biological methods. In decomposition, harmful pollutants are converted to harmless compounds and destroyed completely to form carbon dioxide and water by various chemical and biological processes. A remediation technology may be used independently or some technologies may be combined, for example, a pollutant is firstly contained for a certain period (containment technology), then it is separated from the matrix (separation technology) and finally it is decomposed (decomposition technology).

The remediation methods are also classified into In-situ and Ex-situ methods. In-situ means on-site, that is, remediation is carried out on and in the vicinity of the contaminated site and Ex-situ means off-site, that is, contaminated matters are transported to the treatment facility and treated there as shown in Fig. 9. In a case of Ex-situ remediation for contaminated soil, the action of digging out contaminated soil in order to transport it gives a heavy load to the land, and during digging and transportation of contaminated soil, the pollutant in the soil may spill to

Table 3 Classification of representative remediation technologies [20–22]

Concept	Technology	Main principle	Materials used	In-situ or Ex-situ	Targets materials	Remarks
Containment	Slurry wall	Surrounding with low permeable clay mineral	Clay mineral and cement	In-situ	Heavy metal ions, harmful organics, oil	Low-cost, easy construction
	Deep geological disposal	Storing in deep stable stratum	Glass and canister	In-situ	High-level radioactive waste	Need a long management, no-exposure for current generation
Separation	Vitrification	Enveloping with stable glass material	SiO ₂ , Al ₂ O ₃ , graphite	In-situ and Ex-situ	Heavy metals, radionuclides, harmful organics	Need high current and voltage, 1,000 kWh/ton for In-situ
	Precipitation	Precipitation reaction	Hydroxide, sulfide and xanthate	Ex-situ and In-situ	Heavy metal ions	The secondary pollution by added reagent should be addressed
	Solidification and Stabilization	Encapsulating into solid material	Cement, pozzolanic, thermoplastic	Ex-situ and In-situ	Heavy metals and harmful organics	Some factors may interfere this process
	Solvent extraction	Distribution to organic phase	Organic solvent	Ex-situ	PCB, dioxins, pesticides, and oil	Liquefied gas and critical solution temp. solvents also have been used
	Electro-kinetic remediation	Electrophoresis, electroosmotic flow	EDTA and surfactants and so on are used as an additive	In-situ	Heavy metal ions, harmful organics	Applicable to low permeable clayey soil
	Electrochemical accumulation	Oxidative film formation on electrode	Carbon fiber electrode	Ex-situ	Phenols and aniline	Some organics are accumulated on the electrode as a polymer film
	Soil washing	Mechanically and chemically scrubbing, particle size separation	Acid, base and surfactants	Ex-situ	Oil, organics and heavy metals	Need to treat washing water used
	Soil flashing	Chelating and solubilization	Water, surfactants	In-situ	Hydrophilic and hydrophobic organics	Flushing liquids should be recovered and recycled

Adsorption	Adsorbing ability, ion-exchange, chelating	Many kinds of adsorbent, activated carbon, ion-exchange resin, chelating resin	Ex-situ and In-situ	Organics, heavy metals and radionuclides	Need to recover adsorbent after adsorption
Vapor extraction	Volatilization, vapor flow	Hot air, steam	In-situ	Volatile organics and fuels	Injection of hot air or steam facilitates volatilization
Phytoremediation	Uptake by plants	Hyperaccumulator plants	In-situ	Metals, organics	Need to manage and treat the plant used
Bioremediation	Biodegradation	Microorganisms, bacteria, fungi, actinomycetes	Ex-situ and In-situ	Fuel oil, waste oil, pesticides	Need to control moisture, oxygen, pH, and nutrients in process
Catalytic and photocatalytic reaction	Catalytic and photocatalytic reaction	Heterogeneous, homogeneous catalyst and TiO ₂	Ex-situ	Organics, NOx and SOx	Sunlight or UV light is necessary for photo-catalytic reaction
Zero valent iron	Reduction, and oxidation by hydroxyl radical (Fenton reaction)	Micro- and nano-Fe(0) particles	In-situ and Ex-situ	Chlorinated organics, nitroaromatic organics and others	ZVI is often used in the permeable reactive barriers (PRBs)
Supercritical water oxidation	Oxidative degradation and dehalogenation near the critical point	Oxygen, hydrogen peroxide	Ex-situ	Halogenated organics, PCBs and pesticides	Need high temp. and pressure and corrosion-resist equipment
Chemical oxidation	Oxidation reaction	Ozone, hydrogen peroxide, hypochlorite, chlorine	Ex-situ	Amines, chlorinated organics, cyanide, mercaptans, and others	Combining with UV photolysis improves the efficiency of degradation
Electro-degradation	Electrolysis	SnO ₂ electrode	Ex-situ	Organics	Some organics can be decomposed at the electrode
Thermal degradation	Incineration, pyrolysis	Auxiliary fuel	Ex-situ	Various kinds of organics	More toxic compounds sometimes may be formed under the inadequate incineration condition
Decomposition					

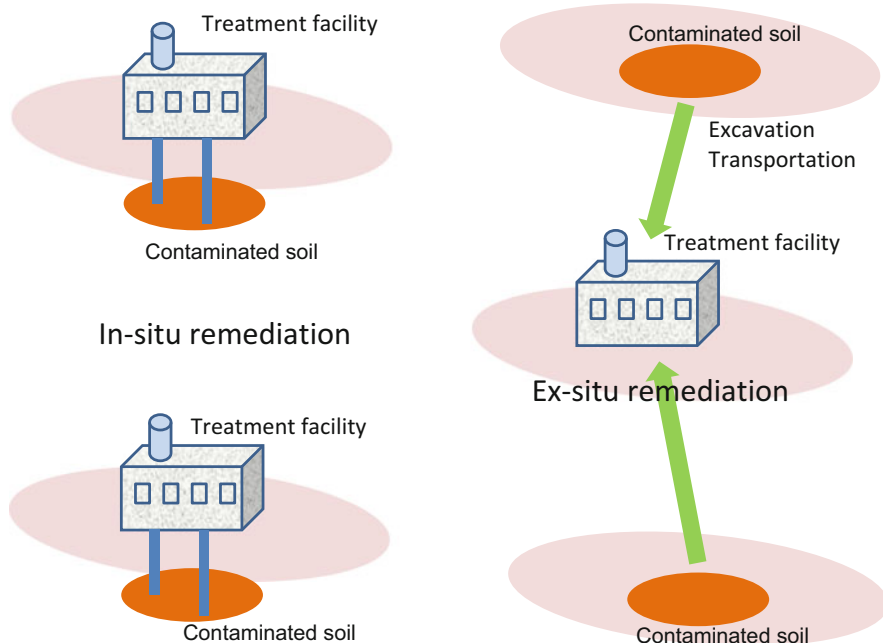


Fig. 9 In-situ and Ex-situ remediation technologies

environments and cause the secondary pollution. Therefore, recently In-situ remediation methods which do not need digging and transportation are preferred more than Ex-situ remediation.

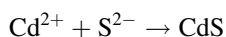
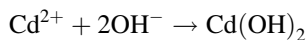
3.2.1 Containment

In containment, to prevent pollutants from spreading in environments, pollutants are confined in a limited area by various chemical and physical methods or converted into immobile forms. The concept of the containment is based on the following relation on the risk of chemicals.

$$\text{Risk} = \text{Severity of Effect} \times \text{Possibility of Exposure}$$

The risk of a pollutant is represented as the product of the severity of the effect from pollutant and the possibility of the exposure of us with the pollutant. Even though a pollutant has a very high toxicity, if the possibility that we are exposed with the pollutant would be almost zero, then the total risk by the pollutant might be almost zero. Containment is a process to minimize the possibility of the exposure with pollutants. Many methods are applied and developed to minimize the exposure with pollutants. One of these methods is to make pollutant itself immobile. Some precipitation reactions are used for the purpose, for example, heavy metal ions such

as Cd(II) react with hydroxide and sulfide to form precipitation of $\text{Cd}(\text{OH})_2$ and CdS , respectively. These precipitations are water-insoluble and can stay as a solid in soil for a long time.



Hexavalent Cr(VI) is very toxic and carcinogenic. It is so water-soluble that can move easily in environments. While trivalent Cr(III) is one of essential elements and forms the precipitate with hydroxide in neutral pH. Therefore, the reduction of Cr(VI) to Cr(III) contributes to prevent Cr(VI) from spreading in environments. Some natural organic matters such as fulvic and humic acids can be used as a reductant for Cr(VI) [23]. Another method to minimize the spreading of pollutants is to envelop the pollutants with stable materials such as concrete, glass, and clay minerals. For example, heavy metal ions and radionuclides are solidified with concrete and glass. Vitrification is a method to envelop the pollutants into glass. In this method, pollutants such as heavy metal ions and radionuclides are heated with SiO_2 and Al_2O_3 as the raw materials for glass at the higher temperature than $1,100^\circ\text{C}$. The vitrification can be applied to the actual contaminated site as an In-situ method. Two electrodes are embedded near the contaminated soil and a large amount of the electricity of 4,000 V/400 A is applied between the electrodes, and the soil between the electrodes is heated at $1100\text{-}1500^\circ\text{C}$. Usually natural soil consists of mainly SiO_2 and Al_2O_3 and then soil is vitrified to confine the pollutants in the glass [20].

Clay mineral has a very low permeability for water. If a wall made with slurry prepared by mixing clay mineral, concrete, and water is constructed like surrounding a contaminated site as shown in Fig. 10, the wall can shut pollutants off from

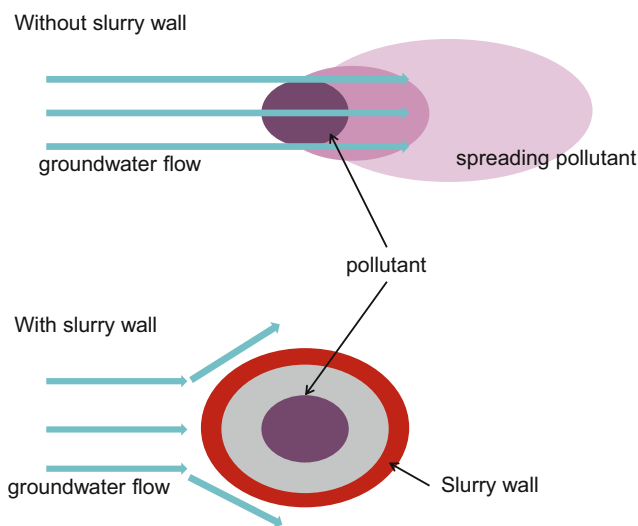


Fig. 10 Slurry wall method

spreading. The wall is called “slurry wall” and from the reason of relatively low cost, the slurry wall is applied to many contaminated sites, especially to the site just after the disclosure of the pollution. The migrating rate of water in the slurry is known to be about 10^{-3} – 10^{-6} cm/s and then if 1 m length of the slurry wall with the lowest permeability is constructed around the contaminated site, the pollutants would be stored inside the slurry wall at least for 3 years. During this containing period, we can plan the next treatment of the pollutant and operate actually the process to remove or decompose the pollutants enclosed with the slurry wall. The containment technology is expected most for the deep geological disposal of high-level radionuclides. The effect of radiation from radionuclides on human health is very severe. In order to reduce the risk of high-level radionuclides, it is necessary to minimize the possibility of the exposure with them to almost zero. Therefore, high-level radionuclides are vitrified and then put into a canister made from stainless steel. The canister enveloped with a buffer material such as clay mineral is transported to the deep soil by passing through the vertical shaft and stored in the tunnel built in 500–1,000 m depth as shown in Fig. 11. Under this condition, the possibility that ordinal people could expose with the radionuclides in the tunnel would be almost zero. This method is expected to be a final disposal technology for high-level radioactive waste generated from nuclear atomic plants. In Finland, a deep geological disposal using the facilities of an abandoned mine, which is called “Onkalo,” is now in the practical application stage [24]. In Japan, “Horonobe Underground Research Center,” one of the research center of Japan of Atomic Energy Agency (JAEA) has conducted the studies on the deep geological disposal for high-level

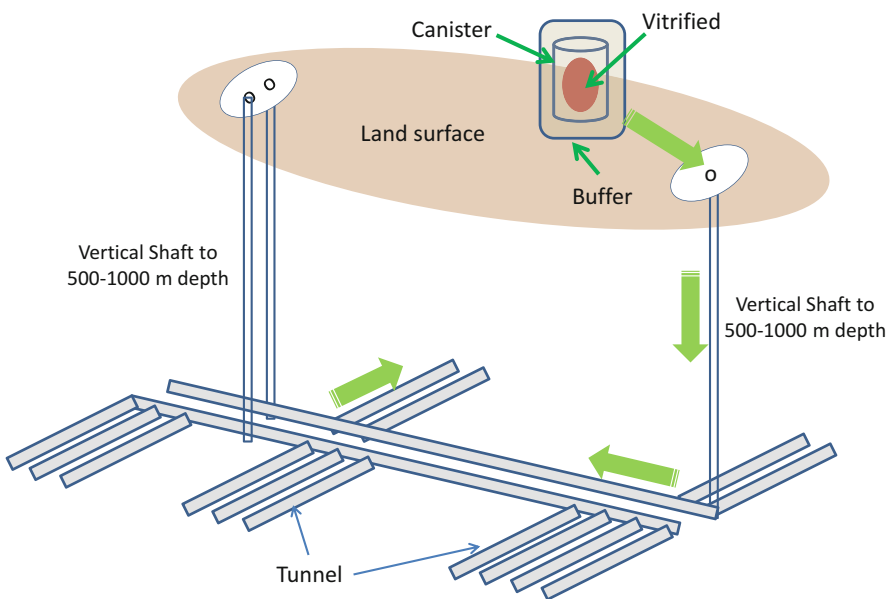


Fig. 11 Deep geological disposal of high-level radionuclides

radioactive waste by using the pits of an abandoned mine at Horonobe in Hokkaido [25]. The purpose of this center is to investigate the behaviors of high-level radionuclides in actual deep geological environments, to find out the factors which can give some effects on the behaviors and finally to verify the reliability of this method for a long period. However, this center will be used only for the research but not for the actual disposal. The national government promised the local residents that after the research completion or after the promised period, the facility will be backfilled and never used for the actual disposal. The area around Horonobe, the northern Hokkaido, is one of the leading agricultural and dairy farming areas in Hokkaido, and if the facility of Horonobe would be used as an actual disposal site, a plenty of high-level radioactive waste will be transported in this area from all over Japan, consequently rumor damages for agricultural products may be concerned.

The deep geological disposal is expected as a practically applicable method for the containment of high-level radioactive waste, but has some problems. Ordinary, the migration of radionuclides in soil is extremely limited (2 cm/year) due to the ion-exchanging capacity of soil. Therefore, even if radionuclides enclosed in the vitrified material would leak from there, soil would prevent the radionuclides from spreading into environments. However, it is known that soil organic matters such as humic substances would act as a carrier to increase the migration distance of the radionuclides in soil [26]. The behavior of radioactive materials in soil probably varies depending on various conditions. In addition, the lifetime of radionuclides often lasts for thousands or tens of thousands of years and more, and then the deep underground disposal facilities must be maintained for a long period corresponding to their lifetime. Therefore, even if the storage facility exists now in deep underground, the possibility that it may appear on the surface of the land in far-off future is not zero because the crustal movements can cause for a long period. The risk of the current generation may be zero, but the risk of later generations is not necessarily zero.

Containment methods can be viewed as the chroral transfer of the risk in a certain sense. That is, a current existing risk is contained for a certain period and transferred to the future. The negative legacy accompanied with the benefits that the current generation has received should not be handed to the later generation without any treatment by the current generation.

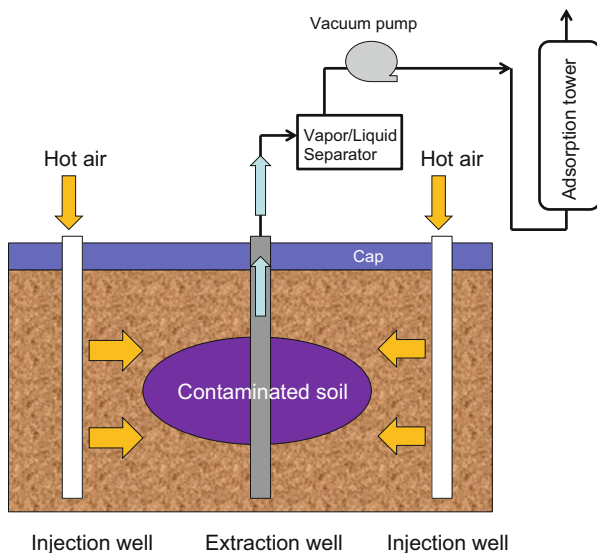
3.2.2 Separation

Some containment methods, especially slurry wall method, are relatively low-cost and easy to build up in the contaminated sites. However, contaminants have not been disappeared from that location and continue to stay there although the spreading can be suppressed. There are some threats that someday the materials and wall for the containment may be collapsed to release pollutants into environments. Therefore, it is necessary to plan the next measures during containing pollutants in the wall and to conduct the measures. Separation is a method for separating and removing pollutants from contaminated matters and sites. Various methods have been devised depending

on the type of pollutants and the situation of the contaminated site. For the separation of pollutants suspended in an aqueous solution, physical separation methods such as filtration and centrifugation can be applied to, and for heavy metal ions dissolving in the aqueous solution, various chemical and physical methods can be applied to. For example, heavy metal ions are precipitated with hydroxide or sulfide and then the precipitants are filtrated or centrifuged. Many other chemical methods such as acid elution, organic solvent extraction, ion-exchange resin, chelating resin, and adsorption are used as the fundamental separation techniques, and some of them are described in the later chapters.

Some separation techniques are used for In-situ remediation. In-situ vapor extraction method is applied to the remediation of contaminated soil with volatile organic compounds such as jet fuel, gasoline, and so on. As shown in Fig. 12, the pipes or thin wells are inserted or dug in the vicinity of the contaminated soil and volatile pollutants are sucked with a pump through the pipes or wells [21]. After passing through a gas-liquid separation, volatile pollutants are introduced to the adsorption tower filled with adsorbent like activated carbon. Finally pollutants are removed by the adsorption and clean air is exhausted to the atmosphere. By injecting hot air to the vicinity of the contaminated soil, the rapid treatment can be achieved by the acceleration of the volatilization of pollutant [22]. Soil flushing is also an In-situ separation method for contaminated soil, in which washing water is sprayed on the surface of contaminated soil and contaminants in soil are washed away as washing water soaks into the soil. The soil flushing and extraction methods using aqueous solution cannot be applied to clayey soil because the low water permeability of the clayey soil prevents water from soaking into soil. Electro-kinetic remediation is only one method which can move water in clayey soil by the electroosmotic flow. In EK as shown in Fig. 13, if a pollutant has positive or negative charges, pollutants in soil

Fig. 12 In-situ vapor extraction [21]



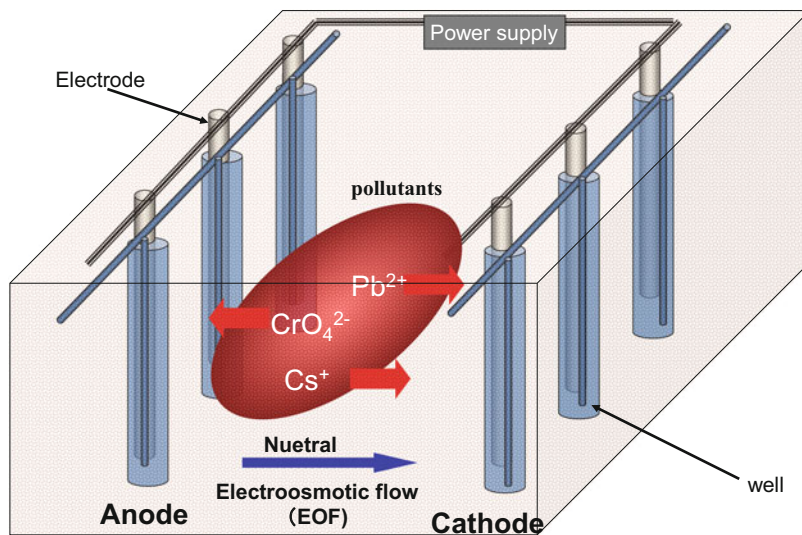


Fig. 13 Image of electro-kinetic remediation

are removed by electrophoretic migration. Even though a pollutant does not have any charges, the pollutant can be moved by the electroosmotic flow generated by applying the electricity between the electrodes inserted near the contaminated soil [27]. The details of the EK method are described in the later chapter “Electrokinetic Remediation”.

Phytoremediation is another separation method using some plants. Plants, which have the ability of the uptake of pollutants in leaves, stems, and roots, hyperaccumulator plants, can be used for removal of pollutants in contaminated soil. Phytoremediation is expected as a low-cost and easy method for treatment. Ideally, all we have to do is just to sow the plant seeds on the contaminated soil and to harvest the grown plants which have taken pollutants into some parts of the plant [28]. However, there are some limitations and disadvantages in phytoremediation. For example, the depth of soil to be able to be treated is limited by the length of the plant root. It usually takes a long time to treat and this method cannot be operated in winter season in the northern area. After harvesting, the management of the plant and some treatments are required to extract pollutants from the plant or store the plant somewhere. The details of phytoremediation are described in the later chapter “Phytoremediation”.

3.2.3 Decomposition

In the decomposition, a harmful substance is transformed to harmless one by various chemical reactions and/or microorganism process. Sometimes harmful organic substances can be completely decomposed into carbon dioxide and water but in most

cases they are just transformed to less harmful compounds. In dechlorination, chlorines are liberated from the organic chlorinated compound to form a less or no-chlorinated compound. From the early years, combustion (incineration) has been used widely as the simplest decomposition method for harmful organic compounds. However, the combustion sometimes may transform a harmful compound to more harmful one like dioxins. Dioxins, which have very strong toxicity, are often generated as the by-products of the incineration of garbage and so on. The amounts of released dioxins depend on the condition of the incineration, the lower the temperature of combustion is, the larger amount of dioxins is formed. Recently, some innovated methods to decompose organic substances, using photo-catalyst [29], supercritical water [30], electrochemical method [31], ultra-sonic waves [32], and so on have been developed.

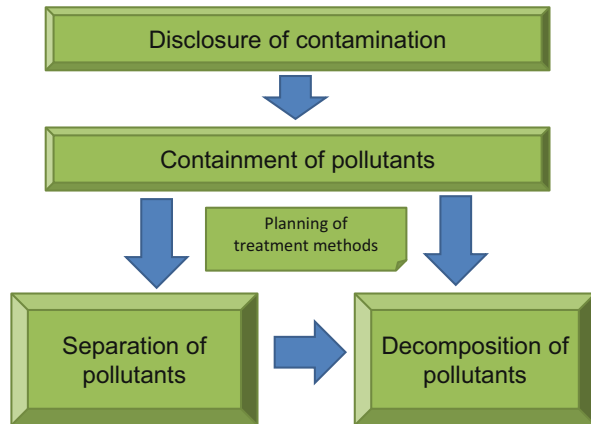
Zero valent iron (ZVI) has a high reactivity. ZVI reacts with oxygen and water to form reactive oxygen species. The reactive species dechlorinate reductively chlorinated hydrocarbon such as tetrachloroethylene and trichloroethylene to form less toxic compounds. The In-situ remediation of groundwater contaminated with TCE has been carried out by a permeable reactive barrier (PRB) containing ZVI. Nano particles of ZVI enable to remediate the groundwater and soil by the direct injection of nano-ZVI. ZVI has also a high ability to adsorb some heavy metal ions. Particularly, arsenic ions selectively adsorb on the hydroxide shell of iron around the core of ZVI [33, 34]. The details of ZVI are described in chapter “Zero Valent Iron and Some Other Nanometal Particles for Environmental Remediation”.

Metal ions can be converted from highly harmful species to less harmful. As described previously, hexavalent chromium is a toxic and carcinogenic metal ion, but trivalent chromium is one of the essential metals. Therefore, the reduction of hexavalent chromium to trivalent chromium can be considered as one of the decomposition methods. In addition, when groundwater contaminated with high nitrate ions is continued to be used as drinking water, it will cause methemoglobinemia in human, especially in children. If nitrate ions can be converted into harmless nitrogen using a catalyst, the method using a catalyst can also be a decomposition method. The treatment of nitrate ion using the catalyst is described in detail in chapter “Heterogeneous Catalysts for Environmental Purification”. Some chemical reactions are also used for the decomposition of pollutants, for example, ozone reaction [35], Fenton reaction [36], and zero valent iron (ZVI). The most promising method for decomposition is bioremediation method, whose detail is described in chapter “Bioremediation: From Key Enzymes to Practical Technologies”.

4 Combination of Remediation Methods

The remediation methods based on each concept are often used as combining several methods, rather than the individual use. For example, when contamination is discovered somewhere, a containment process such as slurry wall is first employed to prevent the pollutant from further spreading. During the containment period, the

Fig. 14 Combination of remediation technologies



method to treat the pollutant is sought and planned, and then the pollutant is separated from there and/or decomposed to harmless compounds. The flow of these processes is shown in Fig. 14.

In the restoration of paintings and works of art, the reversible restoration is always required. That is, it is desirable that the repaired parts can be removed to retake the state before the restoration. That is because the restoration sometimes undermines the value of the original work of art. The environmental remediation should be also reversible if possible, especially in the remediation based on containment. Since the better remediation methods may be developed in the future, the performed process should be reversible as making the process removed if necessary.

5 Selection and Evaluation of Environmental Remediation Technology

The status of pollution varies from site to site. What should we consider when we choose a remediation technology from many technologies? The first thing to do is to get the accurate information about the pollution situation. What is a causative substance of the pollution, how high is the concentration of the substance at the contaminated site? And how does the possibility of spreading the substance to the environments exist? When the pollution occurs in soil, the rate of spreading the pollution may be very slow, but when the pollution happens in water or air, the pollutant will diffuse rapidly. Depending on the situation of the pollution, we should select a remediation technology which is best matted to the pollution. The toxicity of the pollutant is also an important factor in the selection of remediation technology. When the pollutant is very toxic like radionuclides, sufficient attention must be paid to all of the activities during the remediation process. In addition, the final residual concentration of the pollutants after the remediation needs to be considerably low so that it can ensure the safety. The geological or social geographical information of the

contaminated site is also very important to choose the adequate remediation technology. The geological information around the contaminated site will give insights on the direction of pollutant diffusion, and the social geographical information is necessary to obtain the cooperation and agreement with the local people who live around the contaminated site during, before, and after the remediation process. Furthermore, the time required for remediation, the extent of remediation, and the cost of remediation are also important.

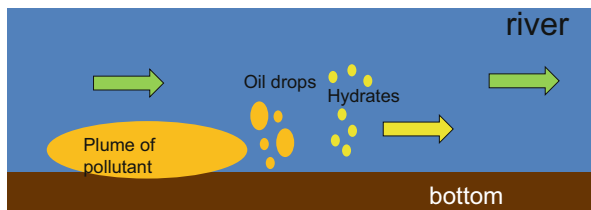
In order to evaluate various methods for soil remediation comprehensively, an assessment by scoring to the following criteria; (1) overall cost, (2) ability to clean to an acceptable level, (3) time to complete clean up, (4) reliability and maintenance, (5) data needs, (6) safety, and (7) community acceptability, has been proposed.

6 Design of Environmental Materials for Remediation

Many environmental remediation technologies have been currently developed and some of them are now available for actual contaminated sites. However, there are some specific cases of the pollution that cannot be treated only by the conventional remediation technologies. Therefore, it is necessary to design the novel methods and materials useful for the specific remediation. Many researchers have made much effort to develop newly designed methods and materials to be able to deal with the specific cases and some studies by them are introduced in this book. I had some experiences where I felt the necessity to design newly the methods and materials for the remediation. Some pollution problems that I have experienced are introduced in chapter “Pollution Sites Where Need Remediation” and our developments of the designed materials are described in some chapters, especially in chapters “Magnetic Separation of Pollutants for Environmental Remediation” and “Easily Collectable Floating-up Adsorbents to Remove Pollutants”. Here I would like to introduce one of my experiences that led us to our development of the new designed environmental materials. In November of 2005, an explosion accident occurred at a petrochemical plant in Jilin City of China, where is located in the Songhua River basin, and about 100 tons of benzene, aniline, and nitrobenzene in the plant flowed into the Songhua River. Among these pollutants, nitrobenzene has a specific gravity of about 1.20 heavier than that of water and is slightly soluble in water. Therefore, nitrobenzene was supposed to have flowed down along with the river water at the bottom of the river while dissolving in water to some extent as shown in Fig. 15. I and my colleagues conducted a survey of pollution of the Songhua River at this time with a researcher of Northeast Forestry University of China, as the detail of this pollution is described in chapter “Pollution Sites Where Need Remediation”. However, eventually I could not do anything in the remediation and the recovery of the pollutants in the Songhua River.

How to collect the oily pollutants which are flowing down with the river water at the bottom of the river? According to the UNEP report, the local government of China injected a large amount of activated carbon and plant materials as adsorbent in

Fig. 15 Expected situation at the Songhua River: the plume of pollutant moves with the river water at the bottom and oily drops and hydrates of the pollutant also move along the river water



the vicinity of the gate for the water intake as the source of drinking water to recover pollutants. Unfortunately the effects of the adsorbents and the recovery amounts of pollutants by the adsorbents were not described in that report [2]. Activated carbon is not so expensive but plenty of activated carbon needs to recover the pollutants released into the river. Therefore, the adsorbent used under such situation should be low-cost and also environmental friendly materials. The enhancement in the function of activated carbon by modification is described in chapter “Preparation and Modification of Activated Carbon Surface and Functions for Environments” and the environmental friendly and low-cost adsorbents using paper sludge, some plants, and natural products are described in chapters “Environmentally Friendly Adsorbents” and “Coal Fly/Bottom Ash, Hydroxylapatite and Hydrotalcite”. The recovery of pollutant flowing down at the bottom of river is one of the special challenges that conventional treatment methods and materials cannot be applied to. It is essential to develop newly designed materials that can cope with such pollution situations. This specific situation gave authors a motivation to develop the adsorbents which can be collected easily after adsorption of pollutants on them. One of such adsorbents was a modified magnetite with hydrophobic compounds and it aimed to collect the adsorbent by a magnet after adsorbing oily materials like nitrobenzene in water. The magnetic separation of oily drops with modified magnetite was firstly developed by the researchers of Kawasaki Heavy Industries Ltd. [37]. Their study was also motivated by an accident of the oil spill from the Russian tanker, “Nakhodka,” near the coast of Shimane prefecture in the Japan Sea in 1997. In this accident, a large amount of fuel oil spilled from the ship and polluted a wide area of the coastline. The modified magnetite with hydrophobic compound can surround around oily drops of fuel oil and the oil droplets surrounded with the modified magnetite can be collected by a magnet. Our challenges were to clarify whether this technology could be applied to the collection of organic solvents such as nitrobenzene and chlorobenzene, furthermore, to expand this method for the collection of heavy metal ions and organic matters by introducing some adsorbing abilities into the modified magnetite. The image of easily collectable adsorbents by a magnet is shown in Fig. 16.

Another challenge is to develop the adsorbent that can float up on the surface of water after adsorbing pollutants. In the case of the Songhua river accident, a heavier pollutant than water such as nitrobenzene would flow down at the bottom of the river as described previously. In order to collect such pollutants with adsorbent, the adsorbent should once sink down at the bottom of the water to make contact with pollutants and stay there to adsorb the pollutants. Finally if the adsorbent could float

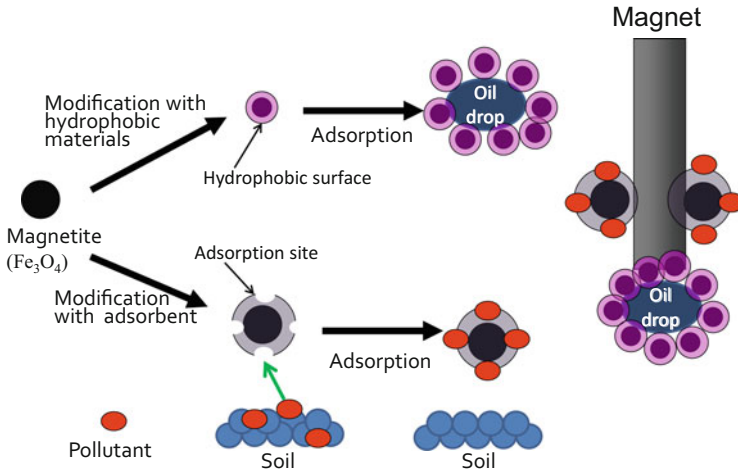


Fig. 16 Modified magnetite and magnetic separation

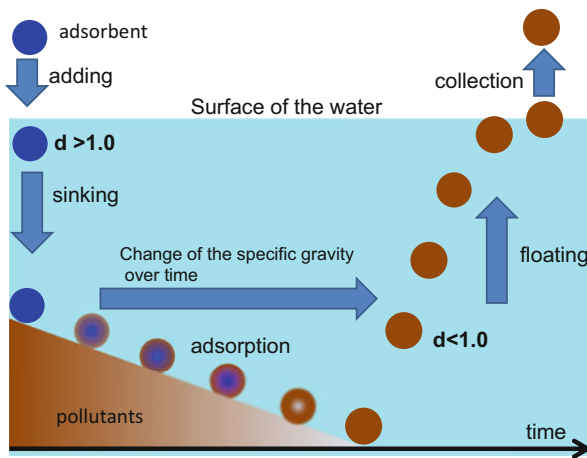


Fig. 17 Floating adsorbent and easy collection

up to the surface of the water, the adsorbent can then be collected relatively easily from the water surface as shown in Fig. 17. In order to develop such an adsorbent, we attempted to introduce a weight and a float to the adsorbent. When a heavier weight than the buoyancy due to a float is initially attached to the adsorbent, the adsorbent will sink down at the bottom of the water. However, if the weight gradually dissolves in water, this adsorbent would float up to the surface of the water after a certain time. In the process of the development of this type of adsorbents, we found out the very interested adsorbent which repeated the floating up to the surface and sinking down to the bottom a dozen and so times. This behavior is suitable for the collection of

pollutant diffused in bulk solution. Lastly if the adsorbent could float up the water surface, we can collect the pollutant with the adsorbent easily. The details on this adsorbent are described in chapter “Easily Collectable Floating-up Adsorbents to Remove Pollutants”.

7 Contents of This Book

This book consists of five parts. Part I including two chapters is a background for environmental remediation and the introduction of some pollution problems. The necessity of environmental remediation and the classification of the technologies for remediation are dealt in chapter “Environmental pollution and remediation”. In this chapter, the necessity of the design of the environmental materials and methods for remediation is also described. Some case studies of recent pollution problems which authors have been concerned in are introduced in chapter “Pollution Sites Where Need Remediation”. In Part II including two chapters, the effects of pollutants on human health and ecosystem and the evaluation are described. The cases of heavy metals are described in chapter “Effects of Metals on Human Health and Ecosystem” and the cases of harmful organic substances in chapter “Effects of Persistent Organic Pollutants (POPs) in the Ecosystem and HUMAN health: Focusing on Chlorinated Chemicals”. Part III including four chapters shows some representative remediation technologies such as electro-kinetic remediation (chapter “Electrokinetic Remediation”), phytoremediation (chapter “Phytoremediation”), electrolysis for accumulation and decomposition of pollutants (chapter “Electrochemical Accumulation and Decomposition”) and bioremediation (chapter “Bioremediation: From Key Enzymes to Practical Technologies”) as relating to the design of the new functions and materials which can be applicable to these technologies. In Part IV including eight chapters, the developments of some designed environmental materials are introduced. The preparation and characterization of the developed materials are described and also the application or the possibility of the application is shown in each chapter. The developments of environmental friendly adsorbents are dealt in chapter “Environmentally friendly adsorbents”, and the studies on modified activated carbon (chapter “Preparation and Modification of Activated Carbon Surface and Functions for Environments”), hydro-char and bio-char (chapter “Hydrochar and biochar”), graphene (chapter “Graphene Oxide for Elimination of Dyes”), heterogeneous catalyst (chapter “Heterogeneous Catalysts for Environmental Purification”), adsorbents based on natural products (chapter “Coal fly/bottom ash, hydroxylapatite and hydrocalcite”), solidified DNA and cyclo-dextrin (chapter “Bio-Inspired Materials for Environmental Remediation”), zero valent iron (chapter “Zero Valent Iron and Some Other Nanometal Particles for Environmental Remediation”) are introduced. Finally in Part V including three chapters, easily collectable adsorbents and floating plants are described. The floating adsorbent can be collected easily from the surface of water. The adsorbents with magnetism can be collected easily by a magnet. The floating plants like algae, which can intake some pollutants, can be also collected

easily from the water surface. The results of our studies on magnetic separation using the modified magnetite are shown in chapter “Magnetic Separation of Pollutants for Environmental Remediation”. The floating adsorbents and plants are introduced in chapters “Easily Collectable Floating-up Adsorbents to Remove Pollutants” and “Remediation by Floating Plants”, respectively.

8 Conclusion

An ideal world is one that does not need any remediation technologies. For that purpose, it is necessary that zero-emission technology has been established in every process and no pollutants are emitted into the environment. However, in reality, it will take a long time to develop the complete zero-emission technology. Even if such a technology would be developed, it will take plenty of time and cost to deploy it to every process. In the meantime, pollutants will continue to be discharged into the environment. Moreover, there are many environments around us that have already been polluted. Even if a zero-emission system is completed and deployed, a system failure may occur due to accidents or disasters, resulting in pollution. Therefore, the remediation technology is an essential technology at all time. The inexpensive and efficient remediation methods can replace an expensive preservation technology. However, the establishment of the complete remediation techniques does not mean that the release of pollutants into the environment is permitted if efficient remediation techniques are available. Until the complete zero-emission system will be established, we have to supplement it with remediation technology. As described previously, the remediation and preservation techniques are complementary. Therefore, it seems to be indispensable to develop the remediation technology and to design the useful materials for the remediation as well as the preservation technology.

Acknowledgments I would like to appreciate Springer Ltd. for giving me the opportunity to write the environmental remediation, especially the design of the methods and materials for the remediation. I thank Mr. Koizumi of Springer Nature Japan because his invitation mails and visit to me led to the publishing of this book. I also thank Ms. Ramya, a regional manager of Springer, because she supported us in many issues related to the publication of this book, such as the contract and editing and so on. I would like to say many thanks to ES general laboratory Co., because the company supported me and then I could focus on the writing of this book in the office of the company. Of course, I have to thank to every authors, they prepared their manuscripts under the special condition of the severe infection of COVID-19. I also want to say much thanks to my students and colleagues of the Research Institute of Environmental Earth Science, Hokkaido University. Lastly, I thank my wife and my family, they always watch over me kindly.

References

1. United Nations, Department of Economic and Social Affairs, Population Division. <https://population.un.org/wpp2019/>
2. United Nation Environment Program (UNEP) (2005) The Songhua River Spill China, field mission report
3. The Ministry of Education, Culture, Sports, Science and Technology and the Ministry of Agriculture, Forestry and Fisheries (2012) Urgent research on the distribution of radioactive materials released from the accident of the Fukushima Daiichi Nuclear Power Station of Tokyo Electric Power Company. http://radioactivity.mext.go.jp/ja/distribution_map_around_FukushimaNPP/#distribution_map
4. Home Page(HP) of Sustainable Society Foundation. <http://www.ssfindex.com/ssi/ssi-2016/>
5. HP of United Nations. Sustainable development goals. <https://www.un.org/sustainabledevelopment/sustainable-development-goals/>
6. The Ministry of Environment, Japan (1995) The annual report of the environment of Japan. <http://www.env.go.jp/policy/hakusyo/img/207/fb1.5.2.1.gif>
7. Nishimura H, Okamoto T (2001) Science of Minamata Disease (Minamata-byo no Kagaku). Nippon Hyoron Sya (in Japanese)
8. HP of Niigata Prefecture. An outline of Niigata Minamata disease. <https://www.pref.niigata.lg.jp/sec/seikatueisei/1195661749709.html>
9. Minamata convention on mercury. http://www.mercuryconvention.org/Portals/11/documents/conventionText/Minamata%20Convention%20on%20Mercury_e.pdf
10. Law concerning special measures against Dioxins (1999) <https://www.env.go.jp/en/chemi/dioxins/law.pdf>
11. The Ministry of Environment, Japan (2014) The annual report of the environment of Japan. http://www.env.go.jp/policy/hakusyo/h26/html/hj14020503.html#n2_5_3_3
12. Environment Agency's basic policy on environmental endocrine disruptors, strategic programs on environmental endocrine disruptors SPEED '98. http://www.env.go.jp/en/chemi/ed/bda_speed98.pdf
13. The Ministry of Environment, Japan (2010) EXTEND 2010. http://www.env.go.jp/chemi/end/extend2010/extend2010_full.pdf
14. Japan Environmental Storage and Safety Corporation (JESCO). http://www.jesconet.co.jp/business/contents/pcb_committee/guideline.html
15. The Ministry of Environment, Japan, Japan Environment and Children's Study for the Future Crew of the Earth. <http://www.env.go.jp/chemi/ceh/en/index.html>
16. Cabinet Office Japan, Disaster Management in Japan. www.bousai.go.jp/kohou/kouhoubousai/h23/63/special_01.html
17. The Tokyo Electric Power Co. (2012) Estimation of the amount of radioactive material released into the atmosphere in the Fukushima Daiichi Nuclear Power Station accident. <https://www3.nhk.or.jp/news/genpatsu-fukushima/20160311/>
18. The Ministry of Environment, Japan. Environmental remediation. josen.env.go.jp/soil/storage_procedure.html
19. Kim GN, Yang BI, Choi WK, Lee KW (2009) Development of vertical electrokinetic-flushing decontamination technology to remove ^{60}Co and ^{137}Cs from a Korean nuclear facility site. *Sep Purif Tech* 68:222–226
20. Freeman HM, Harris FF (eds) (1995) Hazardous waste remediation. Chapter 20: In-situ vitrification treatment. Technomic Publishing, pp 195–202
21. Sharma HD, Reddy KR (eds) (2004) Geoenvironmental engineering: site remediation, waste management, and emerging waste management technologies. Wiley
22. Wilson DJ, Clarke AN (eds) (1994) Hazardous waste site soil remediation. Marcel Dekker
23. Nakayasu K, Fukushima M, Sasaki K, Nakamura H, Tanaka S (1999) Comparative studies of reduction behavior of chromium (VI) by humic substances and their precursors. *Environ Toxicol Chem* 18:1085–1090

24. Posiva. Final disposal. http://www.posiva.fi/en/final_disposal/#X7DlXOVxfIU
25. Japan Atomic Energy Agency (JAEA), Horonobe Underground Research Center. <https://www.jaea.go.jp/04/horonobe/>
26. McCarthy JF, Zachara JM (1989) Subsurface transport of contaminants. *Environ Sci Technol* 23(5):496–502
27. Acar YB, Alshawabkeh AN (1993) Principles of electrokinetic remediation. *Environ Sci Technol* 27:2638
28. Kruger EL, Anderson TA, Coats JR (1997) Phytoremediation of soil and water contaminants. American Chemical Society
29. The Pollution-related Health Damage Compensation and Prevention Association. Practical use of photo-catalytic materials as coating agents on walls of buildings and other structures for removal of airborne nitrogen oxides. www.erca.go.jp/yobou/taiki/research/h16_03.html
30. Sako T, Sugeta T, Otake K, Sato M, Tsugumi M, Hiaki T, Hongo M (1997) Decomposition of dioxins in fly ash with supercritical water oxidation. *J Chem Eng Jpn* 30(4):744–747
31. Tanaka S, Nakata Y, Kimura T, Yustiawati MK, Kuramitz H (2002) Electrochemical decomposition of bisphenol A using Pt/Ti and SnO₂/Ti anodes. *J Appl Electrochem* 32:197–201
32. Nakamura Y, Nagamori M, Karouji K (2002) Simultaneous and multi component decomposition of volatile organic compounds. *Ultrason Technol* 14(3):2–8 (in Japanese)
33. Fua F, Dionysiou DD, Liu H (2014) The use of zero-valent iron for groundwater remediation and wastewater treatment: a review. *J Hazard Mater* 267:194–205
34. Su C, Puls A (2001) Arsenate and arsenite removal by zerovalent iron: kinetics, redox transformation, and implications for in situ groundwater remediation. *Environ Sci Technol* 35:1487–1492
35. Benitez FJ, Beltran-Heredia J, Acero JL, Rubio FJ (1999) Chemical decomposition of 2,4,6-trichlorophenol by ozone, Fenton's reagent, and UV radiation. *Ind Eng Chem Res* 38(4):1341–1349
36. Qiu M, Shou J, Lu Y (2014) Degradation of organic compounds by fluidized bed Fenton process. *J Chem Pharm Res* 6(7):2033–2038
37. Sugiyama K, Fukunaga K, Kuramochi Y, Iwata A, Nishijima S, Takeda S, Nakahira A. Oil spill recovery method using magnetic material by magnetic separation. Japanese Patent 2000-176306 (in Japanese)

Some Pollution Problems to Consider the Design for Remediation



Rudy Syah Putra, Yustiawati, M. Suhaemi Syawal, Yingjie Dai, Yongbo Lin, Md. Mostafizur Rahman, Mashura Shammi, and Tanaka Shunitz

Contents

1	Introduction	34
2	Pollution Problems in Indonesia	35
2.1	Current Environmental Issues in Indonesia	35
2.2	Pollution with Mercury by Illegal Gold Mining in Indonesia	45
3	Nitrobenzene Pollution in Songhua River in China	51
3.1	Background	51
3.2	Responses	53
3.3	Data Analysis	55

R. S. Putra

Department of Chemistry, Faculty of Mathematics and Natural Sciences, Universitas Islam Indonesia, Yogyakarta, Indonesia

Environmental Remediation Research Group, Department of Chemistry, Faculty of Mathematics and Natural Sciences, Universitas Islam Indonesia, Yogyakarta, Indonesia
e-mail: rudy.syahputra@uii.ac.id

Yustiawati and M. S. Syawal

Research Center for Limnology and Water Resources, The National Research and Innovation Agency (BRIN), Cibinong, West Java, Indonesia
e-mail: yusti@limnologi.lipi.go.id; syawal@limnologi.lipi.go.id

Y. Dai

College of Resources and Environment, Northeast Agricultural University, Harbin, China
e-mail: yingjiedai@neau.edu.cn

Y. Lin

School of Life Sciences, Guangzhou University, Guangzhou, China
e-mail: linyongbo@gzhu.edu.cn

M. M. Rahman and M. Shammi

Department of Environmental Sciences, Jahangirnagar University, Dhaka, Bangladesh
e-mail: rahmanmm@juniv.edu

T. Shunitz (✉)

Hokkaido University, Sapporo, Hokkaido, Japan
e-mail: syny-tanaka@ab.auone-net.jp

Shunitz Tanaka, Masaaki Kurasaki, Masaaki Morikawa, and Yuichi Kamiya (eds.), 33

Design of Materials and Technologies for Environmental Remediation,

Hdb Env Chem (2023) 115: 33–78, DOI 10.1007/698_2022_896,

© The Author(s), under exclusive license to Springer Nature Singapore Pte Ltd 2022,

Published online: 24 August 2022

3.4	Conclusions	61
4	Salt Damages in Bangladesh	61
4.1	Introduction	61
4.2	Process of Salinity	62
4.3	Seasonal Variation in Salinity	63
4.4	Groundwater Extraction and Salinity	65
4.5	Shrimp Cultivation	65
4.6	Impacts of Salinity on Agriculture	66
4.7	Impact of Salinity on Public Health and Well-Being	67
4.8	Impacts of Salinity on the Mangrove Ecosystem	68
4.9	Concluding Remarks	68
5	Soil Contamination of Railroad Station with Lead	69
5.1	Introduction	69
5.2	Contents of Lead and Tin in the Contaminated Soils	70
5.3	Chemical Species of Lead in Soil by Sequential Extraction	71
5.4	Isotope Analysis of Lead in Soil Samples	71
5.5	Conclusion	73
6	Conclusion	73
	References	74

Abstract In this chapter, four different types of pollution problems in four countries are introduced. These are pollution with mercury by small-scale gold mining activities in Indonesia, pollution with nitrobenzene in the Songhua River in China, salt damages in Bangladesh, and soil contamination with lead in railroad stations in Japan. Some authors actually participated in the survey and investigation of these pollution problems. Although any remediation technologies have not been applied to these pollution sites, these pollution problems were important for us to consider the design of the materials used for the remediation and the remediation technologies.

Keywords Pollution with mercury, Pollution with nitrobenzene, Salt damages, Small-scale gold mining, Soil contamination with lead

1 Introduction

There are many polluted environments around us. A large variety of pollutants affect a wide range of polluted sites, from the hydrosphere such as oceans, rivers, and lakes to the atmosphere and soil. There are many kinds of pollutants such as heavy metals, organic pollutants, oils, radioactive substances, salts, and asbestos. Some organic pollutants are artificially synthesized, and others are naturally produced and unintentionally produced during human activity. Many pollutants show the toxicity at the relative high concentration but some affect the living body even at the trace amounts. If pollution is left untreated, it will spread more and more and its impact on people and ecosystems will increase. Therefore, it is necessary to remove pollutants from the contaminated areas and restore the original safe and clean environment.

Many pollution sites where need the remediation exist all over the world and it is impossible to describe all of them.

In this chapter, we mainly focus on four pollution problems that we have been involved in, especially in Asian four countries. The researchers who have surveyed the pollution together joined in writing of this chapter. One is mercury pollution of rivers due to small-scale gold mining activities in Indonesia. In 2001 and 2002, we conducted the surveys of the gold mining in the rivers of Java and Central Kalimantan and measured the mercury concentration in river water and sediments. The second is the spill accident of some chemical substances into the Songhua River in the northeastern region of China in 2005. In March of 2006, 6 months later the accident, we visited the Songhua River and measured nitrobenzene in river water, surface ice, and fish samples.

The third is the problem of salt damage in Bangladesh. The rise in the sea level due to global warming, the frequent occurrence of high tides and strong monsoon due to the recent abnormal weather, and human activities like shrimp cultivation cause the salt damage to groundwater and soil in the coastal area in Bangladesh. We surveyed these areas and confirmed the high conductivity in well water. The salt damage is common problems for many countries having the low coastal area.

The fourth is soil pollution with lead of railway stations in Japan. We conducted a joint research with JR Hokkaido and considered the causes of the lead pollution.

For these pollution problems, we had not performed the remediation actually. However, these were very important for us to consider the remediation technology and the materials applicable to the remediation.

2 Pollution Problems in Indonesia

2.1 *Current Environmental Issues in Indonesia*

2.1.1 Citarum River

In 2013, the Citarum River in West Java and the Kahayan River in Central Kalimantan were named among the world's 10 most polluted places with Chernobyl in Ukraine according to a report of Green Cross Switzerland and Blacksmith Institute [1]. The Citarum River which provides 80% surface water for the city of Jakarta and irrigates farms that supply 5% of Indonesia's rice is the most polluted river due to household garbage and untreated industrial wastewater. A photograph in Fig. 1 shows the rubbish dumped in the Citarum River.

More than 2,000 companies in the area, primarily textile factories built near the river, discharged enormous amounts of wastewater directly into the river [3–5]. About nine million people live in close contact with the river, where levels of fecal coliform are more than 5,000 times mandatory limits [6]. In addition, heavy metal concentration such as lead (Pb) is more than 1,000 times the U.S. standard of drinking water, while other heavy metals concentration such as aluminum, iron, and



Fig. 1 The water in the Citarum river is full of trash, detergents, household waste, and hazardous waste [2]

manganese is significantly higher than the standard limit [4]. The toxic waste kills the rivers and fosters diseases such as dermatitis. Table 1 shows the average value of water quality in the Citarum River basin at a different location from 2001 to 2009.

Environmental degradation also leads to regular flooding in cities such as Bandung because of deforestation and drains blocked with garbage [5]. However, fishing is still widely practiced along the river, and the catchment has been contaminated by heavy metals and microplastics, which are consumed in areas adjacent to the river. In recent years, the volume of farmed fish in the Saguling reservoir has reduced by 5,000 metric tons per year because of deterioration of water quality leading to lower dissolved oxygen levels in the Citarum River basin [7]. Additionally, the number of fish species in the river has decreased by 60% since 2008 [6].

In 2018, the Indonesian government established the Citarum Harum – a seven-year revitalization program with the goal of Citarum’s water drinkable in 2025. The program has been supported by the Asian Development Bank (ADB) since 2013, which includes combating soil erosion and agricultural runoff by reforesting surrounding mountains, extracting the toxic sediment, prohibiting discharging wastewater from factories, and setting up environmental education projects [2]. Table 2 shows the innovation of the ADB program to increase the sanitation and wastewater management based on a formulated scenario for treating domestic and industrial water.

Table 1 Average values (2001–2009) of water quality in the Citarum River basin [7]

Component	Unit	Wangisagara	Majalaya	Sapan	Cijeruk	Dayeuh kolot	Burujui	Nanjung
BOD	mg/L	2.9	7.7	27.8	26.0	24.2	24.7	27.3
COD	mg/L	10.1	19.7	78.8	64.4	60.2	59.7	70.1
PO ₄ -P	mg/L-P	0.2	0.3	0.6	0.5	0.6	0.7	0.8
NH ₃ +NO _{3,2}	mg/L-N	0.8	1.8	4.2	4.1	4.6	5.4	5.6
Fecal coliform	U/100 mL	5.8 × 10 ⁵	5.3 × 10 ⁵	1.5 × 10 ⁶	1.4 × 10 ⁷	3.5 × 10 ⁶	1.3 × 10 ⁶	1.3 × 10 ⁶

Table 2 Benefits of improved sanitation and wastewater management [7]

Benefit	Monetized	Quantified
Health	Averted fecal-oral disease from improved on-site sanitation and wastewater management	Reduced cases of food poisoning from consumption of fish infected by algal blooms or heavy metal
	Averted health impacts of less exposure during flooding events	
Water	Reduced water treatment costs to households and industries	Increased business investment due to availability of cheap and clean water
	Improved fish yields from farming in downstream lakes	Reduced frequency and costs of flood events due to preventing further land subsidence from excessive groundwater extraction
Environment	Reduced frequency of river and reservoir dredging due to sludge extraction before wastewater release	Improved quality of life for riverside communities
	Rise in land prices due to improved esthetics of riverside and lakeside real estate	Conservation: preserved biodiversity Tourism opportunities due to improved esthetics of riverside and lakeside locations

2.1.2 Kahayan River

The Kahayan River is used by local people for many purposes, including drinking water supply, washing, bathing, transportation, and fishing. Recently, gold mining activities have been distributed over the Kahayan and Rungan Rivers watersheds. Commonly, these activities are conducted in the upstream villages. In 2004, about 1,000 units of gold mining equipment were being used in the Kahayan watershed and 200 units in the Rungan watershed [8]. Significantly, gold mining contributes 19.4–29.1% of the annual revenue of the Palangka Raya region, although it is a significant source of water pollution [9]. The primary pollution of the river is associated with the artisanal small-scale gold mining (ASGM) that uses mercury (Hg) in the gold extraction process [10]. The mercury forms an amalgam with gold concentrate and then is burned off in a rudimentary smelting process. The remaining mercury concentration in aquatic systems is readily converted to organic methyl mercury by a process that is thought to be mediated by SO_4^{2-} reducing bacteria, and surficial sediments are regarded as the primary sites of microbial methyl mercury production [11]. Bioaccumulation through the food chain increases the human risk of chronic methyl mercury exposure, mainly in those populations with high intakes of fish or fish products [12]. Total mercury concentrations in fish (*Mystus nemurus*) obtained from both rivers ranged from 0.02 to 0.48 ng/mg wet wt., which is close to the USEPA guideline value for human consumption.

Additionally, the highest total mercury concentration in a water sample came from a tributary of the Kahayan River, which was higher than Indonesia's drinking water standard for total mercury (1,000 ng/l) [10]. Recently, the gaseous elemental mercury (GEM) was measured to clarify the human health risk of inhalation in three

artisanal small-scale gold mining (ASGM) areas of Palu (Central Sulawesi, 342,000 residents), Muara Aman (Bengkulu in Sumatra, about 1,000 residents), and Palangka Raya (Central Kalimantan, 236,000 residents). The results showed that the health of residents of Palu—not only in the ASGM area but also in the city—may be at risk due to GEM inhalation. In Muara Aman, the health of people who engage in gold refining and gold shop employees may be at risk, whereas the health of residents of Palangka Raya appears not to be at risk [13].

The United Nation's Minamata Convention on Mercury was signed by the Indonesian government on 10 October 2013 and then followed with the ratification on 22 September 2017, which requires a reduction in the use of mercury and mercury compounds at mining sites [14]. Therefore, Indonesia has acted a vital step to limit anthropogenic mercury releases into the environment. However, ASGM activities are closely related to poverty and thus are likely pessimistic about continuing [13].

Currently, the Ministry of Environment and Forestry (KLHK) of Indonesia has reported that in 2021, around 59% of 564 rivers in Indonesia will be heavily polluted. The sources of pollution are industrial waste, such as oil, gas, mining, domestic or household waste, and livestock waste. Previously in 2015, around 79.5% of rivers across the country were reported in severe pollution conditions. Therefore, there is an improvement in water quality in Indonesia today [15].

2.1.3 Crude Oil Sludge

Currently, Indonesia's oil production reached nearly 740,000 barrels of oil per day (BOPD) which is predicted to produce approximately 51,000 m³ of crude oil sludge annually [16, 17]. Pertamina Ltd. at Unit Tanjung business operation, South Kalimantan, Indonesia, has produced 300 m³ per year crude oil sludge from 5,000 BOPD of oil production. This large quantity does not include a stockpile of crude oil sludge by other oil and gas companies operating in Indonesia. Santa Fe Ltd. in Papua and Vico Ltd. in Kalimantan store about 20,000 and 15,000 m³ of crude oil sludge. Pertamina Ltd. stockpiles as much as 15,000 m³ of crude oil sludge in Cilacap and Balikpapan, 500 m³ in Plaju, and 16,000 m³ in Indramayu of oil processing facility [18]. To date, the number of crude oil sludge production will vary due to stringent standards regulated by the Indonesian government. Oil and gas exploration and production (E and P) are necessary and responsible for various environmental pollutions worldwide. Table 3 shows common waste associated with E and P activities. Physically, crude oil sludge forms as sticky mud and has a viscosity of 450 cP. The hydrocarbon compounds in crude oil sludge are dominated by a long carbon chain (i.e., from C11 to C44). The organic phase in crude oil sludge contained heavy petroleum residue. At the same time, oil-contaminated soil is contaminated soil or sand with petroleum oil or its derivative compounds.

Table 4 shows general characteristics of crude oil sludge collected from Balongan oil refinery unit, Cirebon, Indonesia, and oil-contaminated soil collected from Bula oil field, Seram, Indonesia.

Table 3 Common waste associated with E and P activities [16]

Waste	Components	E and P activities					
		S	D	C	P	M	A
Oil spill/leaks	Hydrocarbon, chemicals	√	√	√	√	√	
Contaminated soil	Hydrocarbon, chemicals, heavy metals	√	√	√	√	√	√
Domestic waste	Organic, solids, oil and grease, nutrients	√	√	√	√	√	√
Lubricant waste	Hydrocarbon, heavy metals	√	√			√	
Ballast water	Hydrocarbon, heavy metals				√		
Boiler blowdown	Biocides, heavy metals, scale		√			√	
Drilling fluid, mud, and cutting	Biocides, metals, surfactants, viscosifiers		√		√		
Produced water	Hydrocarbon, heavy metals, organic, ammonia, H ₂ S, BTEX		√		√		
Produced sand	Hydrocarbon, heavy metals				√		
Oil sludge/bottom waste	Hydrocarbon, chemicals, heavy metals				√		√

S seismic survey, D exploratory drilling, C construction, P production, M maintenance, A abandonment

Table 4 Characteristics of oil sludge and oil-contaminated soil [16]

Parameter	Oil sludge	Oil-contaminated soil	National standard ^a
Density, g/L	878.8	1,024.5	–
Viscosity, cP	450		–
TPH, %	30–33	20–22	–
Water, %	2.61	4.50	–
Solid, %	35.63	73.8	–
Volatile hydrocarbon, %	7.65	14.4	–
Non-volatile hydrocarbon	54.61	9.5	–
Organic-C (dry wt.), %	28.49	–	–
Heavy metals (mg/L)			
As	0.0002	0.57	5
Ba	0.429	1.37	100
B	0.011	–	500
Cd	<0.001	0.03	1
Cr	<0.001	<0.005	5
Cu	<0.001	0.01	10
Pb	<0.001	<0.004	5
Hg	0.0013	0.12	0.2
Se	0.0008	–	1
Ag	<0.001	–	5
Zn	0.124	0.06	50

^a Ministry of Environment of Indonesia No.128/2003

Table 5 TPH content after 24 h soil washing and 30 days bioremediation [16]

Treatment	Time (days)	TPH content (%)		
		Control (exp.1)	Biosurfactant (exp.2)	Tween80 (exp.3)
Soil washing	Initial	32.00	32.00	32.00
	1	29.40 (8.13)	20.20 (36.90)	24.00 (25.00)
Bioremediation	2	29.40 (8.13)	20.20 (36.90)	24.00 (25.00)
	4	27.04 (15.50)	15.84 (50.50)	19.70 (38.44)
	7	26.40 (17.50)	12.10 (62.19)	16.45 (48.59)
	15	24.20 (24.38)	9.60 (67.50)	12.58 (60.69)
	21	21.77 (31.97)	4.05 (87.34)	9.84 (69.25)
	30	17.31 (45.91)	2.96 (90.75)	6.66 (79.19)

Value in bracket is the removal percentage of TPH

Standard practice on the treatment of crude oil sludge is physical/chemical extraction and then centrifugations to recover oil while the remaining residue is treated by mean bioremediation or co-processing method, which utilizes the incineration to burn waste at high temperature (1,500°C) in cement kiln. According to the environmental regulation, total petroleum hydrocarbon (TPH) in crude oil sludge must be reduced until 15% (w/w) before the bioremediation can be applied to treat crude oil sludge. The surfactants, either synthetic or bio-products, are added to the soil washing process to reduce TPH content in crude oil sludge. Additionally, these surfactants also enhanced the bioremediation process itself [16, 19]. Table 5 shows TPH content in crude oil sludge after 24 h soil washing and 30 days bioremediation process.

Crude oil sludge is treated by soil washing to reduce oil content before bioremediation continues. Experiment 1 (exp.1) is washed with tap water, while exp.2 and exp.3 are washed with biosurfactant from *Azotobacter sp.* and Tween80 at 10-fold CMC value. Significantly, TPH decreased by 37% when oil sludge was washed with a biosurfactant (exp.2). After oil content is recovered and removed from an experimental reactor, bioremediation is continued for 30 d. The highest removal of TPH is 91% from crude oil sludge by biosurfactant compared with Tween80 (79%). Therefore, the significant growth of petrophilic bacteria in bioremediation is enhanced by surfactants [20, 21]. The applied field of bioremediation on petroleum-contaminated soil showed that the addition of specific degrader microbe and biosurfactants could remove 46 g total petroleum hydrocarbon per kg soil from 4.883 m³ for 16 months treatment [22]. Chevron Pacific Indonesia (CPI) is the biggest oil producer in Indonesia, which contributes up to 40% of national oil production. Currently, this company operates nine treatment facilities with 42.000 m³ of contaminated soil per treatment cycle and has successfully treated more than half a million cubic meters of contaminated soil from the Sumatra operation area from 2003 to 2011 [16]. Figure 2 shows the enhancement mechanism of microbial degradation with biosurfactants produced by petrophilic bacteria.

An assuring technique that can enhance the biodegradation efficiency of hydrophobic compounds is the employment of biosurfactants. The present of biosurfactant

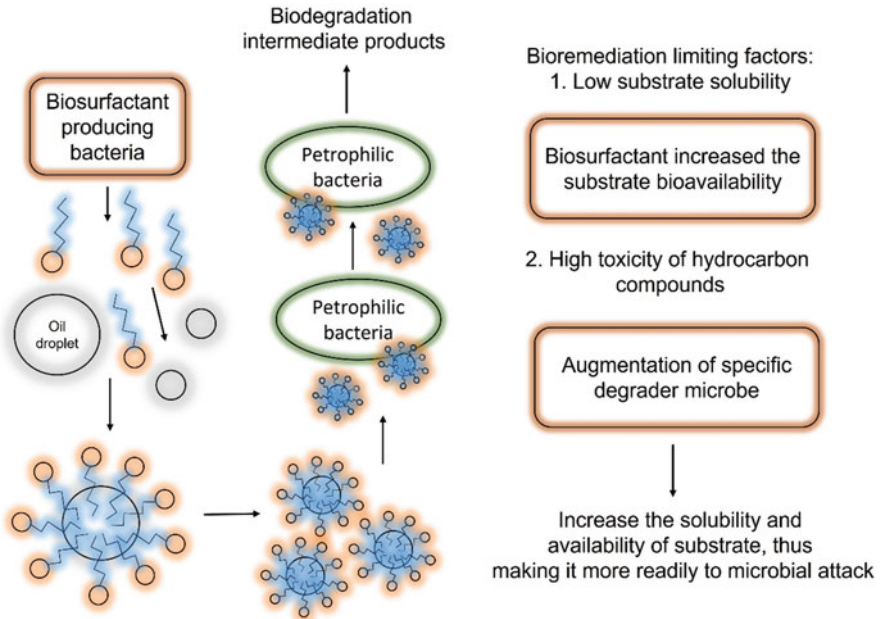


Fig. 2 Mechanisms of biosurfactant in degradation of hydrophobic compounds [18]

can improve a low solubility compounds biodegradation by two mechanisms are as follow: (1) enhancement of the solubility employing emulsification of the hydrophobic compounds, making it more available for microorganism attack and (2) facilitated transport and mobilization of hydrophobic compounds, allowing it to connect more with microbial cells [18]. By decreasing the interfacial and surface tension with biosurfactant addition, the surface area of the hydrophobic compound will increase, which leads to enhanced bioavailability and mobility. Furthermore, the emulsification mechanisms are promoted by the high molecular mass of biosurfactants, whereas the mobilization mechanisms are promoted by common molecular types of biosurfactants [23, 24].

2.1.4 Tailing Soil

PT. Freeport Indonesia (PTFI) is a copper and gold mining company operating in the Mimika Regency, of the Papua Province, since 1972. Currently, the company processes 220,000–240,000 tons of ore per day. The ore processing is conducted at the mill (MP-74) using a well-known flotation process, which produces concentrate and tailings. Tailings are finely ground natural rock residue from the processing of mineralized ore amounting to approximately 97% of the processed ore, and only 3% represent the concentrate containing copper, gold, and silver. Tailings produced by company operations are deposited in a designated area of 230 km² in the lowlands

Table 6 Characteristics of deposited tailing in conservation area [25]

Characteristics	Type 1	Type 2	Type 3	Type 4
Particle size	Medium-course	Medium-fine	Mix medium-fine/very fine	Very fine
Drainage	Very good	Moderate	Bad-water logged/inundated	Very bad
Moisture	Moderate	High	Very high	Very high
Nutrient	Very low	Low	Low-moderate	Low
Land use	Forest/agroforestry	Agriculture with ameliorative	Wetland/aquaculture	Mangrove

of Mimika Regency of the Papua Province of Indonesia. Tailing’s soil is classified as *Entisolic* and is characterized by low to very low content of Nitrogen (N), Phosphorous (P), Potassium (K), and organic carbon and high Calcium (Ca), Magnesium (Mg), Copper (Cu), Iron (Fe), Manganese (Mn), Zinc (Zn), Sulfur (S), and pH level ranging from medium to high (pH 6–8). The high pH level of tailings soil reduces the mobility of nutrients and metals in soil solution and the availability of these elements to plants [25].

To minimize the lateral impacts, the company builds and maintains two levees along 54 km in the east and 52 km in the west sides of the deposition area. The area between the two levees is the Modified Ajkwa Deposition Area (Mod-ADA), which was used about 230 km² for the deposition area of tailing in the lowlands. The area has no longer actively received tailings that use as reclamation areas. In this area, the deposited inactive tailing soil is divided into four zones based on tailing particle size, geomorphology, hydrogeology, and appropriate vegetation types. Additionally, the number of soil organisms (bacteria, fungi, and actinomycetes) in the tailing areas are medium to high population, which can play their roles in the decomposition of soil organic matter [26]. Those areas are converted into the natural forest by re-vegetation and productive agricultural land. Table 6 shows the characteristic of deposited tailing in the reclamation area.

Based on tailing characteristics there are three programs that have been considered to reclaim the tailing soil after the final mine closure: (1) allows the natural succession to occur in the tailing area, (2) convert the tailing area into agriculture (includes estate crops plantation, forest plantation, or agroforestry), and (3) convert the area where natural succession process has occurred after several years into agriculture, forest plantation, or agroforestry. Additionally, the company started these reclamation programs before the final mine closure as the strategic plans to determine an appropriate plant that can grow in the tailing area. Field reclamation has been conducted since 1992 by covering 6,430,000 m² of the area with agriculture, forestry, and agroforestry plants. Until 2011, around 160 plant species have been successfully grown in the area [25]. In addition, a part of a plant has been confirmed by laboratory testing that the metal concentration in the plant is lower than the limits of environmental standards of the Indonesian government, as shown in Table 7.

Table 7 Heavy metal concentration in the plant that had been grown in the tailing [25]

Plant type	Plant name	Treatment	Heavy metal conc. (mg/kg wet weight)			
			As	Cu	Pb	Zn
Fruit	Banana	Tailing	<0.20	1.70	<0.20	3.52
	(<i>Musa L.</i>)	Non-tailing	<0.20	1.10	<0.20	1.72
	Melon	Tailing	<0.20	0.45	<0.20	1.32
	(<i>Cucumis melo L.</i>)	Non-tailing	<0.20	0.46	<0.20	1.15
	Watermelon	Tailing	<0.20	0.40	<0.20	1.11
	(<i>Citrullus lanatus</i>)	Non-tailing	<0.20	0.57	<0.20	1.21
	Pineapple	Tailing	<0.20	1.81	<0.20	1.48
	(<i>Ananas comosus</i>)	Non-tailing	<0.20	0.54	<0.20	1.16
Vegetable	Chili pepper	Tailing	<0.20	1.33	<0.20	2.49
	(<i>Capsicum annum</i>)	Non-tailing	<0.20	1.88	<0.20	2.36
	Eggplants	Tailing	<0.20	0.96	<0.20	1.43
	(<i>Solanum melongena L.</i>)	Non-tailing	<0.20	1.01	<0.20	1.75
	Spinach	Tailing	<0.20	2.83	<0.20	2.65
	(<i>Spinacia oleracea</i>)	Non-tailing	<0.20	2.59	<0.20	2.66
	Tomatoes	Tailing	<0.20	0.54	<0.20	1.75
	(<i>Solanum lycopersicum</i>)	Non-tailing	<0.20	0.56	<0.20	2.13
	Long bean	Tailing	<0.20	0.92	<0.20	1.32
(<i>Vigna unguiculata</i>)	Non-tailing	<0.20	0.99	<0.20	6.06	
Food plant	Sweet potatoes	Tailing	<0.20	1.60	<0.20	2.22
	(<i>Ipomoea batatas</i>)	Non-tailing	<0.20	1.06	<0.20	3.20
	Sago palm	Tailing	<0.20	0.38	<0.20	0.42
	(<i>Metroxylon sagu</i>)	Non-tailing	<0.20	0.41	<0.20	0.98
Forest plant	<i>Adina nerifolia</i>	Tailing	<0.20	2.67	<0.20	4.55
		Non-tailing	<0.20	2.55	<0.20	4.72
	<i>Fiqus armitii</i> Miq.	Tailing	<0.20	1.69	<0.20	7.63
		Non-tailing	<0.20	2.51	<0.20	8.03
	<i>Nauclea orientalis</i>	Tailing	<0.20	3.17	<0.20	5.50
		Non-tailing	<0.20	1.62	<0.20	5.36
The standard limit of National Food and Drug Administration of Indonesia No. 03725/B/SK/B/VII/SK			1.00	5.00	2.00	40.00

Highland reclamation program in overburden stockpile areas at Grasberg open-pit mine area has been recently reclaimed by transplants using a tissue culture technique to provide mass micropropagation [27]. The area is located at 4,100–4,300 m above sea level, where only subalpine and alpine plant species can grow in this area. As the Grasberg mine transitioned from open pit to underground operations in 2016, more mining areas would be reclaimed. The total area reclaimed as of December 2011 was 200 ha, and up to 637 ha will be reclaimed until 2020. A single ha mine requires 2,500 clumps of transplants, so thus 1.6 million clumps of transplants are required up to 2020. The primary means of plant establishment is transplanting native grasses,



Fig. 3 Reclamation area of overburden stockpile at Cartenz [28]

shrubs, and ferns harvested from the surrounding, relatively undisturbed areas and from previously planted areas that serve as a plant source. A photograph in Fig. 3 shows the reclamation in the overburdened stockpile at the Cartenz area. The grasses and shrubs are divided and replanted in the pots at the Grasberg nursery, acclimated to the conditions, then transplanted onto the overburdened stockpiles [27].

2.2 Pollution with Mercury by Illegal Gold Mining in Indonesia

Artisanal small-scale gold mining activities have been conducted in many countries, such as Brazil, Mongol, Indonesia, etc. The gold mining areas in Indonesia are mostly distributed in Sumatra, Java, Kalimantan, Sulawesi, and Papua islands. Small-scale gold mining usually uses elemental mercury for gold extraction which is called as amalgamation process; this activity threatens the environment because the mercury used in the process has not been completely recovered and partially discharged into environments and it will be released to the river, surrounded area, and atmosphere where the activities are carried out near. Consequently, mercury pollution cannot be avoided, this small-scale gold mining activities are considered as illegal gold mining [29]. After long process for drafting, President of Republic Indonesia has launched Presidential Decree No.21 year 2019 that determined national action to reduce and remove mercury in small-scale gold mining. The reduction target of mercury utilization in sector of small scale of gold mining is

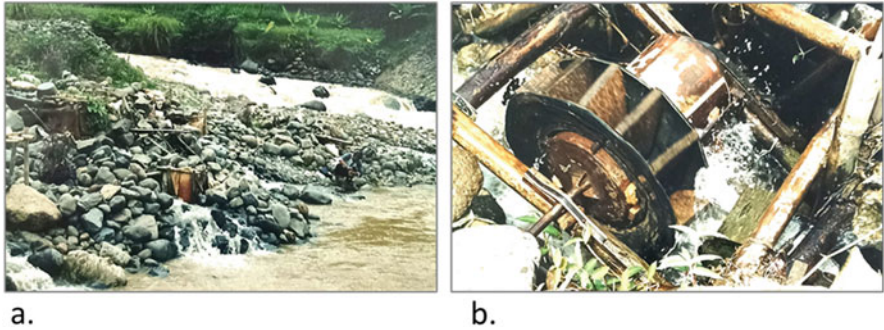


Fig. 4 Gold mining activities using mercury in Cikaniki River of West Java; (a) The Cikaniki River where gold mining activities have been performed, (b) A drum with an impeller for extracting gold with mercury

100% (zero mercury) by 2025. Therefore, mercury concentration in river water should be monitored to avoid environmental damage in the future.

2.2.1 Past and Current Situations of Illegal Gold Mining

In 2001 and 2002, Yustiawati et al. surveyed the mercury pollution caused by small-scale gold mining activities in some rivers of Indonesia, the Cikaniki and Cidikit Rivers in West Java, and the Kahayan River in Central Kalimantan. Different methods and equipment have been used in the rivers in West Java and Central Kalimantan. In the Cikaniki and Cidikit Rivers, the small drum with an impeller has been used as shown in Fig. 4. Soil containing small amounts of gold ore, cement, water, and elemental mercury are put into the drum. The drum is set in a small stream in the middle or edge of the river as shown in Fig. 4. The drum continues to be rotated by hydraulic power to mix well soil with mercury; in this process gold will be extracted and bounded with mercury. After rotating for several days, mercury contained gold was separated from soil. A small ball of amalgam Hg with gold can be obtained by squeezing out the excess mercury from the amalgam by using a piece of cloth. The last, the amalgam was heated with a burner to evaporate mercury from the amalgam to get pure gold. The outline of the mining process is shown in Fig. 5. Amalgamation process is the primary method to extract gold from gold ore or alluvial gold because about 90% of gold will be trapped in amalgam by this method. From several steps of gold mining processes, especially the separation process of Hg amalgam from soil and the evaporation process, mercury could be discharged into the environments, then mercury contamination occurs. On the other hand, in the Kahayan River, the gold sands have been collected from the bottom of the river by a special device built up on a raft as shown in Fig. 6. The river sands are pumped up with huge amount of water and flowed down on a slider, whose surface was covered with a carpet having long fibers. The lighter ordinal sands can flow down out of the slider but the heavier gold sands can be trapped between the long fibers. After the

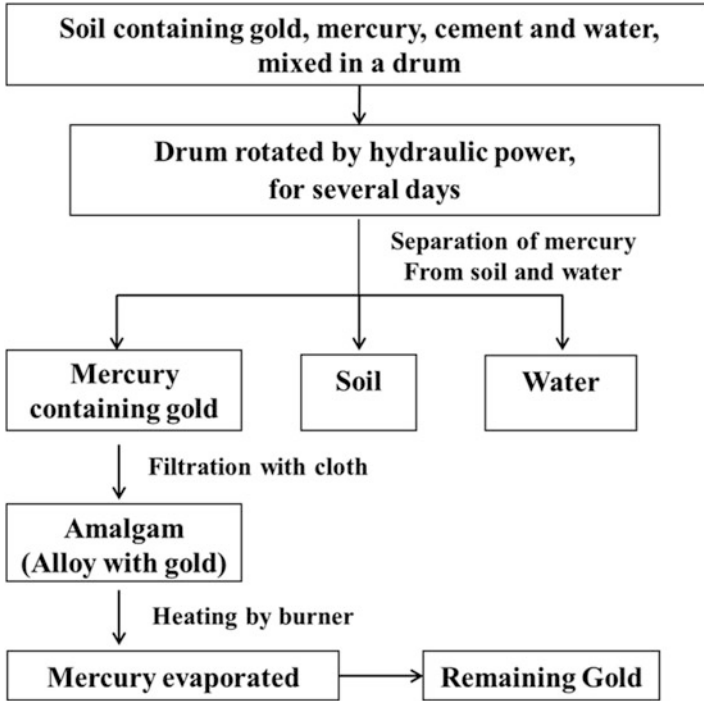


Fig. 5 Mining processes for extraction of gold from soil in the Cikaniki River



Fig. 6 Gold mining activities at the Kahayan River in Central Kalimantan, some devices set up in the river

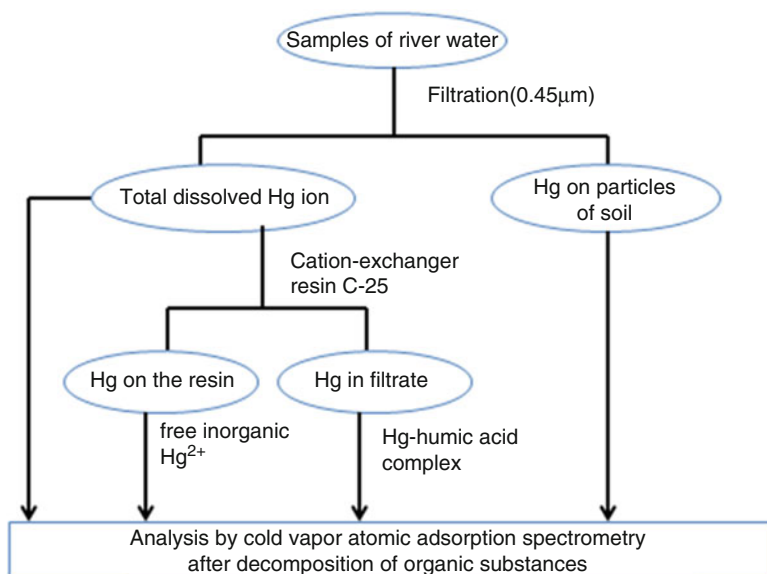


Fig. 7 Procedure for speciation analysis of mercury

Table 8 Mercury concentration of river water samples

No.	Sampling location	Total Hg ($\mu\text{g/L}$)		Hg bound with HA ($\mu\text{g/L}$)	
		2001	2002	2001	2002
1.	R. Cikaniki 1	4.86	1.13	0.09	0.15
2.	R. Cikaniki 2	2.74	0.71	0.23	0.09
3.	R. Cikaniki 3	3.63	0.37	0.11	0.07
4.	R. Cidikit 1	0.24	0.34	0.07	0.02
5.	R. Cidikit 2	0.82	0.39	0.06	0.01
6.	R. Cidikit 3	0.44	0.49	0.08	0.02
7.	R. Kahayan	–	0.08	–	nd

nd not detected

process run for several days, the carpet was dried, and gold dusts in the fibers are recovered. In this activity, elemental mercury was not used in the river but used in worker's house to extract gold from the collected gold sands. In this study, the concentrations of mercury in the water samples of three rivers in West Java and Central Kalimantan were measured [30].

The river waters were collected in October 2001 and September 2002 at three sampling sites ranging from upstream to downstream chosen at each river. By filtration of the water using $0.45 \mu\text{m}$ membrane filter, mercury in the river water was separated into dissolved Hg and adsorbing Hg on suspended particles (particulate mercury). Moreover, the dissolved mercury was separated into cationic and anionic species by adding C-25 cation-exchanger resin into the filtered solution.

After digestion of organic matters in the solution by KMnO_4 in acidic solution, mercury in the solution was measured by a Mercury Analyzer (Hiranuma HG-300). The procedure of the speciation analysis for mercury is shown in Fig. 7. Since most of anionic species of mercury were thought to exist as a complex with humic substances, the conditional stability constant and the complexing capacity of humic acid with Hg were calculated by using a Scatchard plot [31].

Mercury was detected in all the water samples of the Cikaniki and Cidikit rivers in 2001 and 2002. The concentrations of the total Hg and HA-bound mercury species in the Cikaniki and Cidikit rivers are shown in Table 8. The total concentration of mercury in the Cikaniki River in 2001 was higher than the maximum tolerable concentration (0.002 mg/L) of Indonesian Government regulations for river water. However, the concentration in 2002 had drastically decreased because of the reduction in the number of gold mining operations due to the regulation of the gold mining activities on the river by the government. Most of mercury existed as the adsorbing species on suspended particles, which were suggested to be clay minerals from the SEM images and the elemental analysis data by X-Ray spectroscopy. These results indicated that the separation between mercury and soil in the gold mining process had not achieved completely and the mixture of fine mercury drops and soil was discharged into the river. Anionic species of HA-bound mercury were also found in the sample waters but in relatively low concentration. Mercury was detected in water samples of the Cidikit River; however, the concentration was less than the maximum tolerable concentration. The concentration of mercury in the river water of the Kahayan River was much lower than those of the Cikaniki and Cidikit rivers, because the gold mining process at the Kahayan River was different from that of the Cikaniki and Cidikit rivers, where mercury was not used in the river directly. From the experiment in Laboratory, the conditional stability constant and the complexing capacity of a humic acid, which was prepared from soil sampled at Jangraga, with mercury were estimated by Scatchard plot and the values were 6.5 as the log K' and 0.38 μM , respectively [30].

From 2013 to 2017, Tomiyasu et al. also surveyed the mercury pollution around the Cikaniki River which was caused by small-scale gold mining activities. The average of annual concentration of total filtered Hg was in the range of 1.2–12.5 $\mu\text{g/L}$ [32]. They reported that the concentration of mercury in 2013 in the river water near the mining site was 9 times higher than the environmental standard in Indonesia [33]. They found that the forest soil was also polluted with mercury, whose concentration was approximately 20 times higher than the maximum permitted level of mercury in the soils of Indonesia. They suggested that the mercury released by mining activity was dispersed through the atmosphere and deposited on the surface. From the vertical total Hg profile and the distribution of organic matters in soil, they suggested that mercury deposited from atmosphere was retained at the soil surface and suppressed to move toward a deeper layer. In order to estimate the atmospheric mercury levels, they used the native epiphytic fern *Asplenium nidus* (*A. nidus*) as a biomonitor. They collected the *A. nidus* fronds in natural forests and village areas where the gold mining activities are conducted and measured the total mercury concentration in the fronds after the acid-digestion. The mercury concentrations in

A. nidus were higher at the mining village ($5.4 \times 10^3 \pm 1.6 \times 10^3 \text{ ng g}^{-1}$) than at the remote site ($70 \pm 30 \text{ ng g}^{-1}$). They concluded that the atmospheric pollution with mercury was found in areas at least 1 km away from the mining villages [34]. Some researchers reported the impact of mercury contamination to the environment of the Cikaniki River. Aquatic biotas are at higher risk affected by mercury pollution. The Caddisflies (Trichoptera) are one of the aquatic insects that live in freshwater; meanwhile, in river and stream they are mostly found in the larvae stage [35]. The Caddisflies (Trichoptera) have the important role in aquatic food chain. They degrade organic material in river sediment, and also are as the food sources for fish [36]. While the Trichoptera are contaminated by mercury, then they are consumed by fish, it leads to the accumulation of mercury in fish. Furthermore, it will threaten human health because if the Hg contaminated fishes are consumed by human, the accumulated mercury will move to the human. Yoga et al [37] observed the effect of mercury on the aquatic insects, Trichoptera, the results indicated that tracheal gill of Trichoptera had become darkening until 91%, those insects were found in some segments of the Cikaniki River. Moreover, the increase in the concentration of particulate Hg and the total suspended solid (TSS) in the Cikaniki River conducted the reduction in secondary production of *Chematophyche* spp. [38]. Susintowati and Hadisusanto studied the mercury accumulation in benthic organisms (the aquatic organism that live in bottom sediment river), then they found that mercury is higher accumulated in non-sessile benthos than in sessile benthos [39].

Castilhos et al. investigated the pollution with mercury in fish which were collected mainly from the rivers in the artisanal gold mining areas of North Sulawesi and Central Kalimantan of Indonesia. They reported that more than 45% of fish samples in a river collected of North Sulawesi had the mercury concentration in the muscles above the WHO guideline for human consumption ($0.5 \mu\text{g/g}$). On the other hand, the mean mercury concentrations in fish samples from Galangan area in Central Kalimantan were two to four times lower than the WHO guideline, i.e. $0.5 \mu\text{g/g}$ [40].

2.2.2 Remediation of Mercury Contaminated Water and Soil

Mercury contamination in soil and water as impact of illegal gold mining activities threatens environment and human health. When the wastes were disposed to the river, then river water are used for irrigation of paddy field, mercury will be accumulated in aquatic biota and plants; furthermore, mercury will enter into food chains, it may cause serious health problems. Therefore, it is necessary to remediate the soil and water that have been contaminated by mercury. There are many remediation methods that could be applied to the contaminated soil and water. Phytoremediation is one of remediation methods that are often used to remove or reduce heavy metals in contaminated soil and water. Hidayati et al. studied to identify the plants that have potency to uptake and accumulate mercury from water and soil. Phytoextraction was conducted to some indigenous plants. Some

indigenous plants where growing in Pongkor gold mining area indicated to have high tolerance to mercury and survived in mercury contaminated condition. These plants have potential to be used for phytoremediation to clean up the river water from mercury contamination. These indigenous plants were *Lindernia crustacea* (L.) F.M., *Digitaria radicata* (Presl) Miq., *Zingiber* sp., *Commelina nudiflora*, *Colocasia* sp., *Paspalum conjugatum*. The highest accumulated Hg was found in *Lindernia crustacea*, which was about 89.13 ppm [29].

Another remediation method is to use microorganism to remove environmental contaminant. Irawati et al. reported that *Brevundimonas* sp. HgP1 and *Brevundimonas* sp. HgP2 were highly mercury resistant bacteria that were isolated from a gold mine in Pongkor village with MIC of 575 ppm. *Brevundimonas* sp. HgP1 has the ability to accumulate Hg^{2+} up to 1.09 and 2.7 mg/g dry weight of cells and removed 64.38 and 57.10% Hg^{2+} from the medium containing 50 and 100 ppm $HgCl_2$, respectively [41]. The ability of *Brevundimonas* sp. HgP1 and HgP2 to grow in the presence of highly $HgCl_2$ was suitable to be applied in waste water treatment. These microorganisms play an important role to decompose organic matter and also to reduce the toxic effect of mercury in waste water treatment.

2.2.3 Conclusion

Regarding the environmental pollution in Indonesia, the issue of illegal small-scale gold mining was mainly described in this section. Anyone can easily conduct this mining process because it can be carried out without any special equipment or technology. The elemental mercury used in technology is also relatively inexpensive to obtain, so it has not been rigorously recovered. Therefore, a significant amount of mercury is released into the river during the separation process from the soil and into atmosphere during the evaporation process of mercury. As a result of investigation, it has been found that not only the water and soil of the river near the mining site but also the plants and soil of the remote forest are contaminated through the atmosphere. Mercury mining activities should be terminated as soon as possible, and some remediation technologies should be done for soils contaminated with high concentration of mercury.

3 Nitrobenzene Pollution in Songhua River in China

3.1 Background

On November 13, 2005, an explosion occurred at a petrochemical plant of Jilin Petrochemical Company of Petro China near the Songhua River in Jilin City, Jilin Province of China (see Fig. 8). The explosion and its subsequent pollution leakage caused serious impact. Five persons were confirmed dead, nearly 70 people were wounded, and more than 10,000 residents were evacuated [42]. The explosion



Fig. 8 Explosion in Jilin petrochemical plant

had resulted in a spill of approximately 100 tons of chemicals, including benzene, aniline, and nitrobenzene (NB), into the Songhua River. After the accident, the explosion caused a pollution plume of 80 km long on the surface of the Songhua River, which was mainly composed of benzene and NB [43, 44]. China's State Environmental Protection Administration (SEPA) said publicly on that day that the Songhua River had suffered "major water pollution" after the 13th November 2005 explosion at the chemical plant. The highest concentrations of benzene and NB in the Songhua River exceeded the standard by 108 times (the standard limit of benzene is 0.01 mg/L in water) and 29.1 times (the standard limits of NB is 0.017 mg/L in water), respectively, after the accident [45].

The Songhua River is a major river in northeast China and the main water source of many cities and villages it passes by, including Harbin, the capital of Heilongjiang Province with a population of four million (in 2005). It also was the source of drinking water in Harbin in 2005, so this pollution incident paralyzed the water supply system in Harbin. The Municipal Government of Harbin had to temporarily shut down its water supply, leaving around four million people temporarily without access to tap water but bottled water provided by the government (www.unep.org). Pollutants flowed down the Songhua River and passed through many cities. Pollutant trajectory and arrival time are shown in Fig. 9. The Songhua River (1927 km), which flows through Jilin and Heilongjiang provinces, merges with the Heilongjiang River (called the Amur River in Russia) and forms a national border with Russia, and eventually flows into the Sea of Okhotsk [46]. The incident caused



Fig. 9 Pollutant trajectory and arrival time

a serious water crisis domestically and internationally in the region along the river and became one of the top 10 international pollution events in 2005 [47].

Pollutants entering the Songhua River may affect the organisms in the water, crops on the river bank, ice and groundwater. We mainly evaluated the safety of ice layer, sediment, aquatic products, groundwater, coastal agricultural and animal husbandry products, and urban water supply by sorting out the investigation data. In order to investigate the pollution hazards caused by the explosion and comprehensively evaluate the safety situation of the Songhua River after decades of time, this paper studies whether the pollution event will bring harm to human-beings by analyzing the specific data.

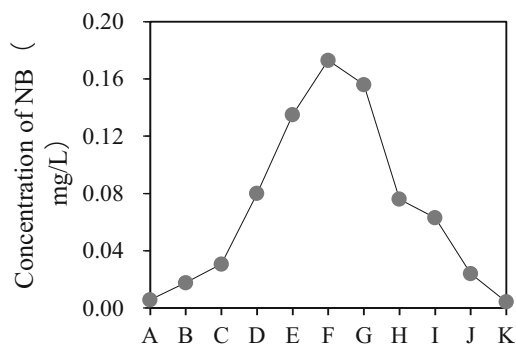
3.2 Responses

After the explosion accident, China government have taken a series of remedial measures. We mainly studied from two aspects: first, the emergency response to pollution accidents shortly after the explosion accident performed by Jilin and

Heilongjiang provincial governments in China (two polluted provinces along the Songhua River), and second, the pollution control measures from 2006 to 2010 followed by the government of China after the pollution.

3.2.1 Emergency Measures After the Explosion Accident

After the accident occurred, Jilin and Heilongjiang provincial governments in China took the following measures according to the requirements of their plan: first, the Jilin Petrochemical company quickly closed the discharge outlet of the pollutant to cut off the pollution source [48]. Second, on November 14, 2005, Fengman Hydro-power Station located upstream of the explosion source increased the discharge in a short time and rapidly reduced the concentration of NB and other pollutants in the water [48]. Third, Harbin adopted underground deep well for a temporary water supply, and about 1,200 t activated carbon was put into the drinking water at the purification plant of Harbin using the Songhua River water as the water source to adsorb pollutants [48]. Then, the 80 km long pollution plume arrived in Jiamusi city of Heilongjiang Province, located downstream the explosion source on December 8, 2005. The concentration of NB in Jiamusi section of the Songhua River began to rise and reached the peak value between 8:00 a.m. and 14:00 p.m. on December 10, 2005, which was more than 10 times of the standard concentration as shown in Fig. 10. Jiamusi City has the same emergency treatment mode as Harbin. On



A:4:00, December 8, 05 **B:**10:00, December 8, 05 **C:**16:00, December 8, 05

D:6:00, December 9, 05 **E:**14:00, December 9, 05 **F:**8:00, December 10, 05

G:14:00, December 10, 05 **H:**6:00, December 11, 05 **I:**14:00, December 11, 05

J:6:00, December 12, 05 **K:**16:00, December 12, 05

Fig. 10 Real-time monitoring results of NB content in Jiamusi section [50]. **A:** 4:00, December 8, 05, **B:** 10:00, December 8, 05, **C:** 16:00, December 8, 05, **D:** 6:00, December 9, 05, **E:** 14:00, December 9, 05, **F:** 8:00, December 10, 05, **G:** 14:00, December 10, 05, **H:** 6:00, December 11, 05, **I:** 14:00, December 11, 05, **J:** 6:00, December 12, 05, **K:** 16:00, December 12, 05

December 12, 2005, the pollution plume left Jiamusi city [49]. Then it continued to flow along the downstream, passed through Tongjiang city and Fuyuan county of China, and finally flowed into Heilongjiang River.

3.2.2 Five Years Prevention and Control Plan (2006–2010)

In 2006, the Chinese government approved and implemented the Plan for the Prevention and Control of Water Pollution in the Songhua River Basin (2006–2010) (hereinafter referred to as the Plan), arranging 116 pollution control projects with a total investment of US \$1.9 billion (RMB 13.4 billion; Conversion rate: 1 USD = 7 RMB), 70 municipal sewage treatment plants were built, and 2.95 million tons of sewage treatment capacity were added per day [51]. In order to understand the follow-up situation of the Songhua River pollution and avoid more serious consequences, the Ministry of Science and Technology of China commissioned scientific research institutions to carry out a comprehensive safety assessment on the Songhua River. Due to the low latitude and long ice age of the Songhua River, in order to avoid the secondary pollution caused by pollutants in ice and sediment, the environmental protection departments paid close attention to this and strengthened the monitoring of some key river sections. At the same time, in order to ensure the food safety related to the Songhua River, the evaluation project team collected hundreds of fish samples in Songhua River, and hundreds of milk, eggs, and meat samples from agricultural irrigation areas and animal husbandry bases that might be affected within 10 km along the Songhua River and detected and analyzed the residual NB in them. In order to ensure the safety of water use, the project team investigated and evaluated the drinking water sources along the Songhua River and closely monitored the groundwater. Comprehensive evaluation of the safety situation of the Songhua River was carried out [52].

On the other hand, Jilin and Heilongjiang provincial governments resolutely eliminated a number of enterprises that used the backward technology with large water consumption and heavy pollution. In 2008, Heilongjiang province carried out a comprehensive investigation on potential environmental safety hazards in many key industries, key enterprises, sewage reservoirs, tailings ponds, and other environmental risk sources as well as drinking water sources. 4,461 enterprises were inspected [51], 173 enterprises were shut down for treatment, 352 enterprises were treated within a time limit, 215 enterprises were rectified within a time limit, and 134 enterprises were subject to administrative punishment [53].

3.3 Data Analysis

In order to evaluate the effectiveness of the above measures and understand the subsequent situation of the Songhua River pollution, the safety situation of the Songhua River was evaluated from three aspects: the concentration change of NB

in Songhua River, the inter-annual variation of other chemical index concentration in the Songhua River, and the safety evaluation of agricultural, livestock, and fish products.

3.3.1 Determination of NB Concentration

The date when the explosion occurred in Jilin was 13 November 2005, and the date when the pollution plume arrived at Harbin city was 24 November 2005 (Harbin is around 600 km downstream of the explosion site). The ice and water samples were collected from the city of Harbin and Jilin on the Songhua River, in March, May, and October of 2006 and March of 2009 at each sampling site (see Fig. 11) [42].

The analytical data of ice and water samples collected from the Songhua River are given in Tables 9 and 10. Table 9 shows that the NB concentrations in water samples were 0.025 $\mu\text{g/L}$ to 0.19 $\mu\text{g/L}$. The concentration of NB was much lower than that of NB (0.58 mg/L) in the pollution plume that arrived at Harbin city on 24 November 2005. From data of March to October in 2006, the concentration of NB in the upper reaches of Harbin decreased significantly. The NB concentration in Harbin basin is slightly lower than that in Jilin City basin, which proves that the area near the explosion source is the most polluted area. The concentration of NB in ice was also very low in spite of the ice formed during the winter season of the accident. In the



Fig. 11 Map for the sampling sites near the Songhua River. A, Downstream; B, upper stream; C, branch in Harbin; D, downstream; E, upper stream; F, Fengman hydroelectric power station in Jilin [42]

Table 9 Concentration of nitrobenzene in the water samples collected from the Songhua River

Collection date	Sites		Concentration of nitrobenzene/ $\mu\text{g/L}$
March-06	Harbin	A (downstream)	0.19
	Harbin	B (upper stream)	0.03
May-06	Harbin	A (downstream)	0.03
	Harbin	B (upper stream)	0.03
October-06	Harbin	A (downstream)	0.04
	Harbin	B (upper stream)	0.04
	Harbin	C (branch)	0.02
	Jilin	D (downstream)	Not detected ^a
	Jilin	E (upper stream)	0.05
	Jilin	F (Fengman hydroelectric power station)	0.11

^a The detection limit of the nitrobenzene in water is 0.01 $\mu\text{g/L}$

Table 10 Concentration of nitrobenzene in the ice samples collected from the Songhua River in Harbin

Collection date	Sites	Concentration of nitrobenzene/ $\mu\text{g/L}$
March-06	B (near surface)	0.65
	B (surface)	0.04
	B (0.2 m below the surface)	0.03
	B (1 m below the surface)	0.05
	A (surface)	0.02
March-09	A (0.2 m below the surface)	0.08
	B (0.2 m below the surface)	0.04
	C (0.2 m below the surface)	0.10

Table 11 Fish samples collected in Songhua River at Harbin city

Fish samples	Collecting date	Species	Size/cm	Nitrobenzene quantity/ ng/g
A	March-06	Yellow catfish	25	30.2
B	March-06	Yellow catfish	14	19.7
C	October-06	Carp	30	13.6
D	October-06	Longnose gudgeon	12	15.8
E	October-06	White fish	10	9.86
F	October-07	Crucian carp	15	2.73
G	October-07	Yellow catfish	13	3.31
H	October-07	Perch	14	1.14

data, the content of NB in ice is very low, and the accident happened during the freezing period of the Songhua River, which indicates that NB and other pollutants in water are excluded from ice when water is frozen to form ice. NB was detected in most of the water and ice samples taken in the Songhua River. However, the concentration of NB in any water and ice samples was sufficiently low [42].

At the same time, the results as shown in Table 11, the monitoring of fish shows that the content of NB in the fish was decreasing gradually [54]. The content of NB in the same species of fish decreased significantly from March to October in 2006, while the content of NB in other species of fish still showed a downward trend, with the biggest difference of 30 times [54].

According to the above data, we can find that most of the pollutants such as NB have been taken away by the river water, and the NB content in the fish in the river has also been greatly reduced, and all of them have dropped below the standard value. Combined with the data of NB content in the water, it can be concluded that the pollution of the Songhua River water has changed to the level of non-toxic to human-beings.

3.3.2 Detection of each Index in the Songhua River

Thanks to the large amount of the capital investment in the five-year plan (2006–2010), the research groups obtained rich practical data through experiments. Through the comparison of previous experimental data, the comprehensive treatment of water projects has achieved certain results.

According to the situation of exceeding the standard of each index section in the Songhua River Basin, from 2001 to 2015, the main pollutants were permanganate

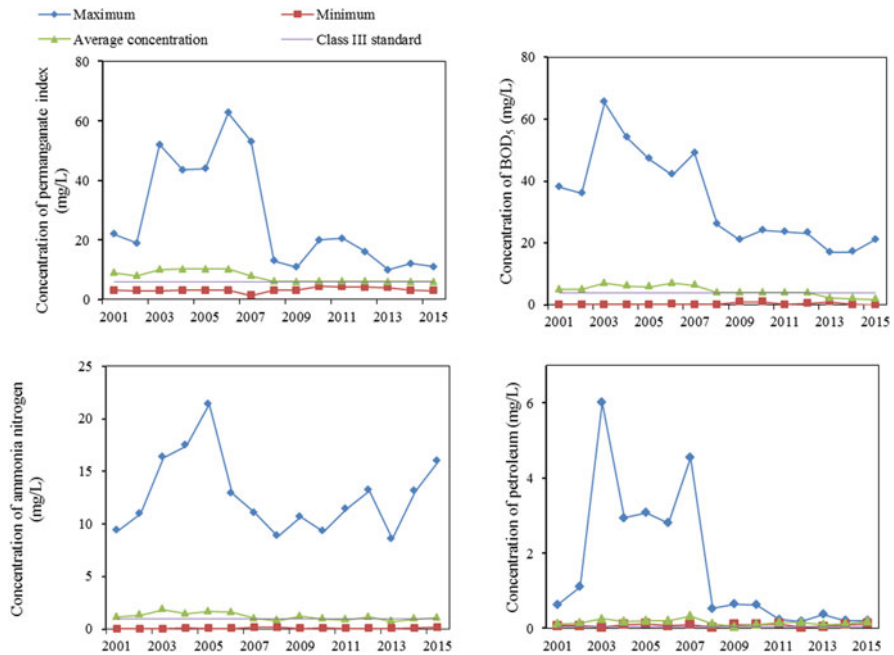


Fig. 12 The concentration change trend of main over-standard indexes was analyzed [49]

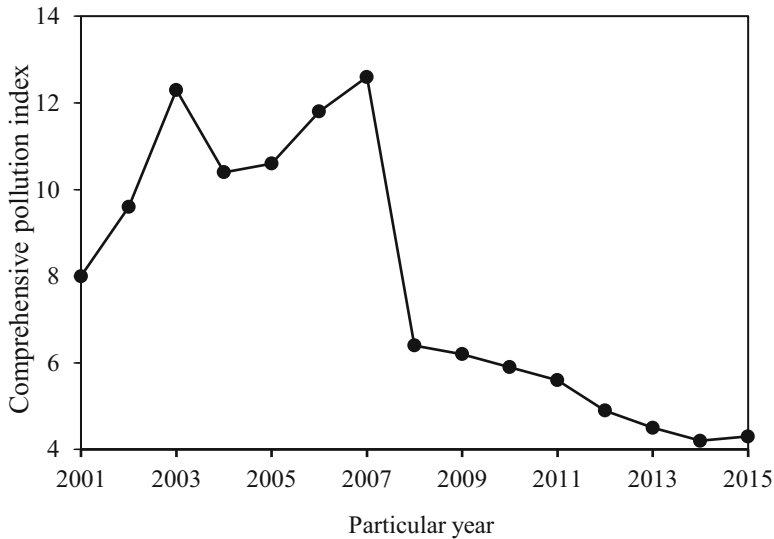


Fig. 13 Inter-annual variation of comprehensive pollution index of river basin water quality [49]

index, petroleum, BOD₅ (five-day biochemical oxygen demand), and ammonia nitrogen, and then the four indicators above were selected to analyze the concentration change trend, as shown in Fig. 12 [49].

From the inter-annual trend chart, we can see that after the explosion in 2005, BOD₅ rapidly rose to an unprecedented peak, and the other three indicators also reached their peaks in the following 2006–2007. Subsequently, China took some emergency measures to solve the pollution problem. What makes us pleased is that the implementation of emergency measures has achieved remarkable results. The potassium permanganate index and ammonia nitrogen concentration decreased rapidly by about 80% from 2007 to 2008. For petroleum, the BOD₅ also showed a very rapid decline and entered a relatively long-term stable state of low concentration around 2008 (except that the BOD₅ showed an upward trend after 2013) [49].

The water quality of the Songhua River Basin is generally improved. As shown in Fig. 13, from 2001 to 2007, the overall pollution level increased and maintained at a high level. After 2007, it showed a downward trend, and tended to be stable from 2013 to 2015, and the pollution was significantly reduced [49]. In general, the pollution degree of each index has been reduced, the overall water quality of comparable section in the Songhua River Basin deteriorated first and then improved. Thanks to the effective pollution control measures taken by the central government of China, the comprehensive pollution index in the Songhua River has dropped to a very low level since 2008.

3.3.3 Safety Assessment

As the Ministry of Science and Technology of China entrusts scientific research institutions to protect the specific data of comprehensive safety assessment of the Songhua River, we can only collect the macro experimental results from news reports or press conferences. The conclusion is as follows.

Whether NB Frozen into Ice and Sediment Causes Secondary Pollution

According to the research results, the amount of NB frozen into ice was less. In addition, the sediment of the Songhua River is mainly sandy, and the amount of NB sunk into the sediment was probably limited. In addition, due to the large amount of water when the river opens in spring, the melting of ice body and the release of sediment in this spring would not lead to the water quality of the Songhua River exceeding the standard. The concentration of NB in some stagnant areas and buffer zones may have increased [52].

Food Safety of Aquatic Products

The assessment project team collected hundreds of fish samples in the Songhua River, detected and analyzed the samples of different river sections, different habits, and different species of fish samples, as well as fish in fish ponds within 2 km along the Songhua River and carried out experiments on the enrichment and release of NB in fish. The results showed that the content of NB in fish in the Songhua River dropped to the safe level after 25–30 days. The content of NB in the fish in the Songhua River and the fish cultured in fish ponds along the coast met the safe content index and then the fish could be eaten [52].

On the Drinking Safety of Groundwater on Both Sides of the River

The assessment project team investigated and evaluated the drinking water sources and decentralized drinking water sources along the Songhua River and closely monitored the groundwater. The results showed that among the 48 monitoring wells along the Songhua River, no trace of NB was detected except for some monitoring wells which were lower than the drinking water source standards in China. Therefore, the safety of groundwater drinking is guaranteed [52].

Food Safety of Agricultural and Livestock Products on Both Sides of the Songhua River

The assessment project team investigated the agricultural irrigation areas and livestock breeding bases that may be affected within 10 km along the Songhua River, detected and analyzed the NB residues in hundreds of milk, eggs, and meat samples, and carried out the simulation test of the impact of NB wastewater on typical agricultural products. The results showed that NB was not detected in milk, eggs, and meat samples along the Songhua River, and the agricultural and livestock products along the river could be safely consumed [52].

The Impact on Crop Growth

The results of simulation test on soybean, corn, rice, wheat, and vegetable showed that when the river water met the national surface water standard, no adverse effects

on seed germination and seedling growth were found. Therefore, the use of the Songhua River water for irrigation would not affect the growth of crops [52].

Safe Water Supply in Cities

The evaluation project group has carried out a variety of tests on the removal of pollutants, the results showed that the removal effect of NB by powdered activated carbon was very good, and more technical basis for this method was obtained. This technical achievement can be used for safe water supply in cities in the future when a small amount of pollutants such as NB in water sources exceed the standard [52].

3.4 Conclusions

After the accident, NB as the main pollutant has seriously affected the environment and human life in the polluted areas. The Chinese government has taken timely some measures to reduce the impact of pollution on residents and curb the possibility of pollution diffusion. The water pollution control of the Songhua River Basin has achieved remarkable results under the long-term adherence of the Chinese government and steady progress has been made in the emission reduction of the total pollutants. Due to this serious accident, China has paid more and more attention to environmental protection, invested a lot of manpower and material resources in the prevention and control work, and paid close attention to the water quality and pollution control of the Songhua River.

According to the above data and literature research, we can know that the possibility of the secondary pollution in the Songhua River is extremely low. In the continuous investment and pollution control, the safety of fish in the river, agricultural and livestock products along the coast, domestic water and drinking water have been guaranteed. At present, the water quality and soil on both sides of the Songhua River have been greatly restored. However, environmental problems still need us to take seriously, never relax, and avoid the occurrence of such hazardous events again.

4 Salt Damages in Bangladesh

4.1 Introduction

Coastal areas are the shifting geomorphological boundaries between land and ocean. Increasing anthropogenic influences in the coastal areas and water resources has resulted in the reduction of freshwater flows, the dwindle of the groundwater resources, the alternation in the mixtures of freshwater and brackish water in the estuaries, and the increase in more marine influences within the region [55]. Saltwater intrusion is a problematic concern occurring in coastal water resources all over the

world. Groundwater resources such as aquifers and surface water resources such as rivers, canals, and lakes are severely affected by the salinity intrusion [56, 57]. The Mekong River Delta in Vietnam, the Ganges–Brahmaputra–Meghna (GBM) Delta in Bangladesh, and other river deltas in India are prone to be contaminated by saline water. Drinking water resources are vulnerable to saltwater intrusion. Subsequently, in these regions, 25 million-plus people are at the risk of the salinity contamination in the drinking water. Furthermore, climate change is likely to overstress the saltwater contamination, which negatively impacts on the human health in these regions [58]. The saltwater intrusion also arises by fluctuating the salinity from sea levels rise, seasonal cyclones, tidal surges, and the upstream withdrawal of freshwater from the ground [59]. In addition, the coastal zones are also threatened by the collective influences of different heavy metals such as arsenic, iron, and manganese contamination [57, 60]. Besides, the seasonal fluctuation of boron, nitrate, and fluoride concentration in the groundwater also poses significant health risks for adults and children [61]. Consequently, coronary diseases, such as high blood pressure and hypertension, are a common public health problem in the coastal zones [58]. Moreover, periodic droughts and low rainfall caused by climate change intensify the water resources' salinity problem and threaten the water quality, affecting the water and food security. As a result, the coastal zones of Bangladesh are one of the severely poverty-ridden areas.

4.2 Process of Salinity

The edge between fresh groundwater and saline groundwater is denoted as the freshwater–saltwater interface. The dynamic process of fresh surface water from the rivers and the groundwater released to the estuaries prevents the inland movement of saline groundwater and the surface water. The saltwater intrusion may occur naturally in the coastal zones, depending on the hydraulic connection of freshwater aquifers and saline water. The difference in the water density of sea and fresh water typically results in a higher hydraulic head or water pressure in the saline seawater than the freshwater. Here, the higher hydraulic head difference will cause the saline water from the sea entering inland. This is the natural mechanism of the seawater intrusion in the coastal zones.

Geographically, the presence of a large coastal belt in Bangladesh is prone to be exposed to saltwater intrusion. But it is a matter of concern that the seawater intrusion occurs mainly by the anthropogenic activities influencing more than the natural system. In the following sections, we describe the results of our survey on the extent of the salinity problem in coastal Bangladesh. We also have discussed the nature and prevalence of the salinity intrusion in different seasons, notably monsoon and dry seasons, and the underlying anthropogenic causes of the salinity intrusion in the coastal districts.

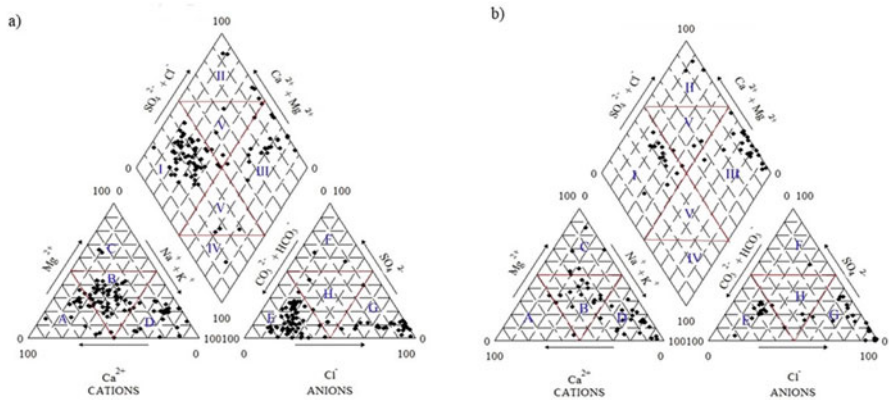


Fig. 14 In the monsoon season, Ca–Mg–HCO₃ dominates in river water due to the heavy monsoon discharge from the upstream that pushes off the Na–Cl type seawater toward the south (a). Major river water in the dry season contains Na–Cl type seawater compared to the Ca–Mg–HCO₃ type (b). During the dry season, limited river water discharge from the upstream causes a salinity front pushing toward the north [62]

4.3 Seasonal Variation in Salinity

The coastal rivers in Bangladesh demonstrate a pronounced seasonal contrast in terms of hydrogeochemistry. The contents of anions and cations in the surface waters vary in the monsoon season and dry season, resulting in the different salinity levels. The distinction in such salinity lies in water discharge from the Ganges–Brahmaputra–Meghna (GBM) and the internal rainfall drainage [62]. The surface water in monsoon is characterized by Ca–Mg–HCO₃ type water compared to the dry season by Na–Cl type water (Fig. 14a, b).

When rainfall sets in the pre-monsoon season, the salinity in the coastal districts varies from 0.01 ppt to 17 ppt (parts per thousand) in the surface waters. When rainfall descends in the post-monsoon season, the salinity reaches up to 38.2 ppt (Fig. 15a, b). Due to India’s Farakka Barrage water diversion since 1975, different threshold criteria were changed substantially, including the monthly dry season average (December–May) and annual minimum flows [62]. As an inactive delta of the Himalayan rivers, Bangladesh’s southwestern zone is severely affected by an extreme salinity level. This part is also the hub for all kinds of natural disasters, including storm surges, tidal floods, and cyclones that help the seawater intrude inland [63].

Moreover, this part of Bangladesh is highly vulnerable to the impacts of climate change as well. Global warming is also slightly related to this seawater intrusion. As the sea level is rising due to global warming, the associated impacts of inundation are responsible for increasing coastal region’s salinity. A recent study showed that the 5 ppt saline front could penetrate about 40 km inland for the sea level rise (SLR) of

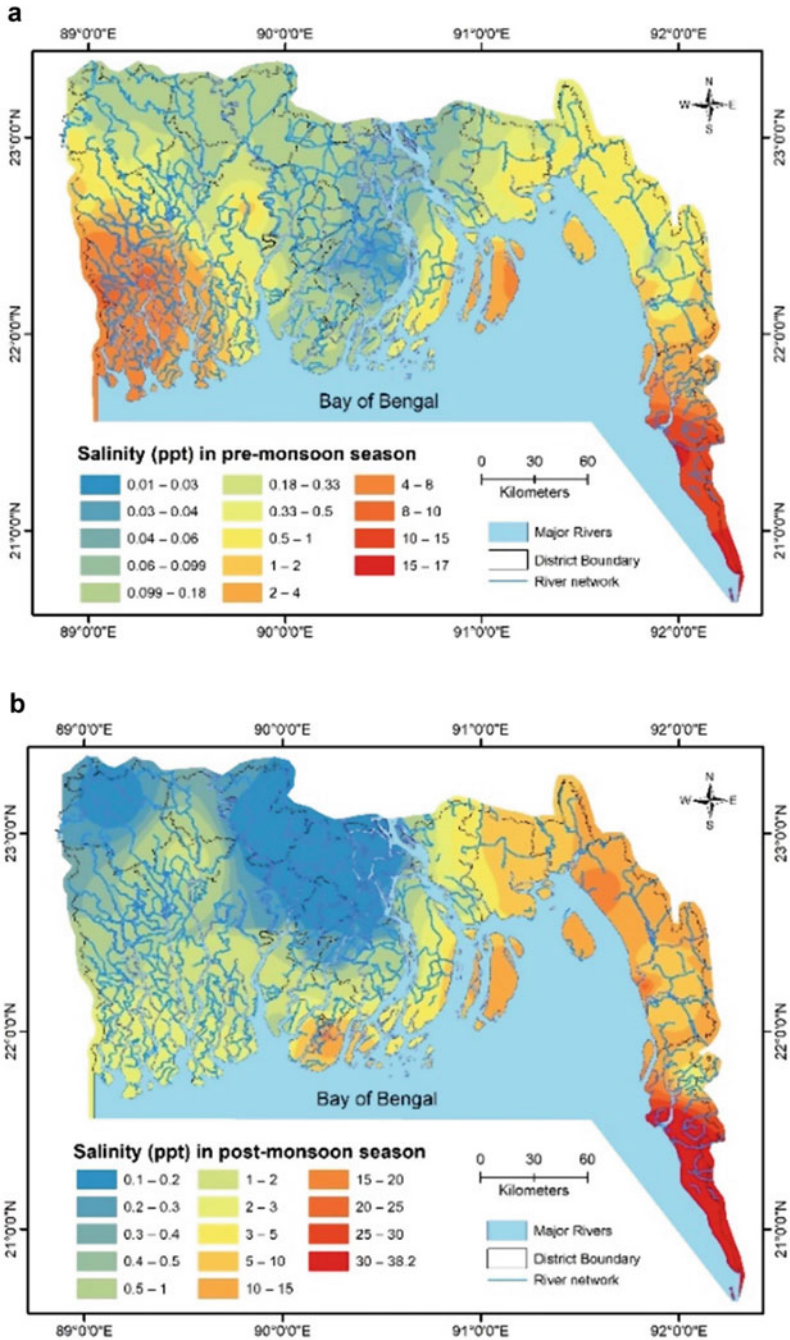


Fig. 15 Spatial distribution of salinity in parts per thousand (ppt) in pre-monsoon season (a) and post-monsoon season (b) in the coastal rivers and estuaries of Bangladesh [64]

88 cm, which reached likely to only the freshwater pocket of the Tentulia River in Meghna estuary [63].

4.4 Groundwater Extraction and Salinity

Groundwater extraction is another significant reason behind the seawater intrusion in the coastal areas of Bangladesh. We are relentlessly pumping groundwater near the coastal zones for irrigation and drinking purposes, causing the groundwater resources to be threatened by saline intrusion [65]. Most of the shallow tube well water samples had higher Soluble Sodium Percentage (SSP) values compared to the surface waters. On the other hand, Sodium Adsorption Ratio (SAR), an essential indicator of irrigation water quality, indicated the surface water and groundwater with low sodium hazard [66]. The hydrochemical analysis disclosed that the groundwater in this area was neutral to slightly alkaline, and leading cations were Na^+ , Mg^{2+} , and Ca^{2+} along with chief anions Cl^- and HCO_3^- . Most of groundwater had total dissolved solid (TDS) $>1,000$ mg/L, and more than 40% of the groundwater had EC $>2,250$ $\mu\text{S}/\text{cm}$, which indicates the saline water intrusion in south-central coastal districts of Bangladesh [65]. The pronounced differences in the electrical conductivity of groundwater are shown in Table 12. From the coastal belt toward inland the seasonal difference in groundwater salinity becomes significant. Some of the coastal districts show significant increase in salinity in the monsoon seasons compared to the dry season.

4.5 Shrimp Cultivation

In addition to natural salinity intrusion and groundwater extraction, poor water management and upstream intervention are other significant reasons for saline water intrusion in the coastal districts. Shrimp cultivation is related to more significant environmental consequences, such as sedimentation, soil salinization, pollution, and biodiversity loss [63, 68–70]. This shrimp cultivation is intensifying the

Table 12 Reported references with groundwater electrical conductivity from coastal districts

Coastal districts	Groundwater electrical conductivity	References
Batiaghata Upazila, Khulna	1,000 $\mu\text{S}/\text{cm}$ to for shallow tube well in the monsoon season	[66]
Gopalganj district	Dry season: 274 to 9,190 $\mu\text{S}/\text{cm}$; monsoon season: 600 to 9,380 $\mu\text{S}/\text{cm}$	[65]
Barguna and Patuakhali district	Pre-monsoon season: 719 to 37,300 $\mu\text{S}/\text{cm}$; Post-monsoon range from and 741 to 34,100 $\mu\text{S}/\text{cm}$	[61]
Along with the coastal belts	Dry season: 27 to 50,500 $\mu\text{S}/\text{cm}$ (mean: 5990.77 $\mu\text{S}/\text{cm}$); monsoon season: 24 to 44,600 $\mu\text{S}/\text{cm}$ (mean: 5459.12 $\mu\text{S}/\text{cm}$)	[67]

salinity problem over time. Salinity in the shrimp-cultivated area is 500% higher compared to the non-shrimp-cultivated areas [68]. Subsequently, a considerable number of land-use change occurred by constructing the drainage channels for shrimp and crab cultivation (aquaculture) and the remaining agriculture practices. In the Bagerhat district, agricultural land decreased around 303 km² (7.97 km²/year), while aquaculture increased dramatically at 486 km² (12.78 km²/year) from 1980 to 2018 [63, 71]. It is perceivable that shrimp farming is a significant economic adaptation to the rapidly salinizing delta that may produce economic growth [72]. Yet, it has not been a useful adaptation for the delta's poor and marginalized areas in its present form.

4.6 Impacts of Salinity on Agriculture

In the previous section, we have mentioned the changes in agricultural land-use patterns. The land-use change has increased salinity over the years, harmed the coastal people's agricultural production, endangered food security, livestock farming, livelihoods, health, and well-being. The salt accumulated in the agricultural soils from the increase in salinity affected groundwater for irrigation [73]. Located in the Khulna district, Batiaghata Upazila has the highest salinity in the groundwater and surface waters (EC <700 mS/cm). Even during the rainy season, both surface and groundwater sources for irrigation are saline with the extreme risk of salinity. Moreover, during monsoon season, rainwater flushes saline soil from the adjacent farmlands and accumulates salts in the ponds [66]. In the same area, soil samples collected from 2004 to 2011 indicated that soil salinity was lowest in September due to the rainfall-flushing of soil, while the highest soil salinity was observed in March–May during the pre-monsoon season, which was naturally dry as shown in Fig. 16.

Soils affected with salinity impair crop production as the number of cations and anions is higher than the optimum amount. On the southwest coast of Bangladesh, salinity changes occur due to the hydrological alteration, which affects the ecosystem [74]. In Bangladesh's southwestern zone, Aman rice variety is the prime cultivated rice variety but the Boro, Aus, and other types of rice variety are not profitable to be grown in the soil enriched with salts. So, farmers have to raise less-profitable rabi crops like vegetables. On average yearly, 0.2 million metric tons of rice production is reduced in this coastal region because of seawater intrusion [63]. Subsequently, shrimp cultivation is a unique adaptation technique to sustain livelihood in the South-west coast [72] and cultivate saline tolerant variety, pond-sand filter, rainwater harvesting, leveling land, applying potassium sulfate fertilizer, and avoid fallowing land in the dry season [75].

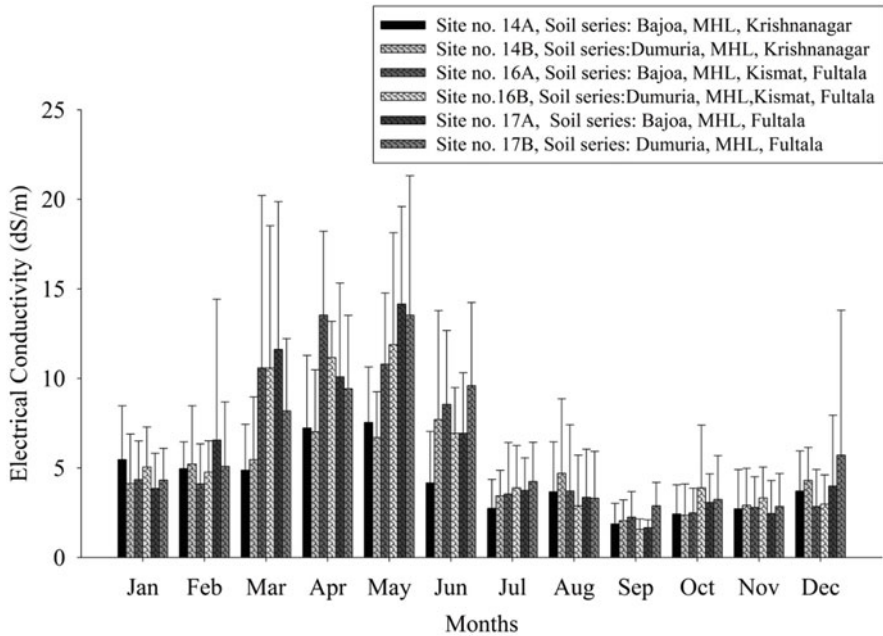


Fig. 16 Salinity of six different soil series from Batiaghata Upazila, Khulna district from 2004 to 2011 collected from Soil Research Development Institutes (SRDI) where MHL means medium high land [66]

4.7 Impact of Salinity on Public Health and Well-Being

Increasing salt intake has substantial negative impacts on human health and well-being. Groundwater provides the single primary drinking water resource in the coastal zones other than rainwater [76]. Because of saltwater intrusion, poor people face acute salinity problems in drinking water, which brings detrimental consequences on the coastal communities’ public health and sanitation [64]. Usually, younger women and younger girls are responsible for collecting drinking water from long distances on foot every day [76]. It is also challenging for pregnant women to collect water irrespective of their physical condition. Saline water is also a crucial factor for hypertension or high blood pressure in the coastal areas. It also contributes to an increased risk of (pre)eclampsia among pregnant women and infant mortality [64]. People exposed to the moderate potable salinity (TDS $\geq 2,000$ mg/L) had 42% ($p < 0.05$) higher chance of being hypertensive than those who consumed freshwater, which may lead to heart diseases [77].

The social, educational, mental, and physical well-being of women and girls is also compromised as they are engaged in collecting water for household chores such as cooking, bathing, washing clothes [63]. The most regrettable reality is that water-borne diseases such as diarrhea and cholera are prevalent in these areas, as potable

water remains inaccessible in the dry season. The high salinity also gives severe damages to the building infrastructures, including the buildings of the primary and secondary schools and colleges, roads, and communication facilities. Consequently, due to damage of school buildings the school dropout rate among young boys and girls in these areas is higher. Subsequently, the harassment to young women and girls sometimes happens by these men and adolescent boys, creating social mayhems [63, 72]. Moreover, salinization and waterlogging also may create a sequence of poverty, unemployment, and consequently uneducated population.

4.8 Impacts of Salinity on the Mangrove Ecosystem

The Sundarbans, the world's largest mangrove forest covering Khulna, Satkhira, and Bagerhat districts, lies in Bangladesh's extreme southwestern zone. As the salinity in this region increases, it is likely to alter this unique forest's regular habitat pattern. Anthropogenic activities such as shrimp cultivation, over-extraction of groundwater for drinking and irrigation, and transboundary and upstream water diversion projects are the major contributor to the alarming salinization process in Bangladesh's regions mentioned above and they negatively affect the mangrove ecosystem [77].

The drastic change in the salinity profile and hydrochemistry has a critical effect on the Sundarban mangrove forest and its biodiversity, known as a world heritage site. Banerjee et al. [78] showed that the variability in salinity has a significant impact on the growth of *Heritiera fomes* (locally known as *Sundari*), which can serve as an indicator species of salinity variation. The species die when the Sundarbans' rivers and canals are inundated by the saltwater excess more than the average and remain waterlogged for a long period [78, 79]. Any damage in the Sundarbans eventually leads to the losses in heritage, biodiversity, and livelihoods. As the Sundarbans are the reservoir of several saline ecosystems, any significant damage may result in the tremendous loss of the ecosystems.

4.9 Concluding Remarks

Considering the seriousness and impacts of the salinity on the present environmental, climatic, and socio-economic conditions existing in Bangladesh's coastal regions, we need to address more the salinity intrusion and its associated problems such as soil salinization, drinking water crisis, public health problem, and social issues with a great importance.

5 Soil Contamination of Railroad Station with Lead

5.1 Introduction

The railway in Japan started in 1872 by operation between Shinbashi in Tokyo and Yokohama (29 km) [80]. Since then, railways have spread throughout the country as developing in industries in Japan. The railway business in Japan was firstly operated by both of a national and many private companies, and then they were unified in a State-owned enterprise, Japan National Railways (JNR: Koku-tetsu). However, after long operation by JNR, in order to eliminate the deficit and streamline its operation, JNR was privatized in 1987 to be divided into seven private companies. JR Hokkaido is one of the seven private companies and operates the railway business in Hokkaido exclusively.

The railway in Hokkaido was established relatively early time in 1880 between Temiya and Sapporo to transport coal from coal minings in Horonai area to Otaru port [80]. In 1983 during the JNR era, there were 37 lines and more than 4,027 working kilometers in Hokkaido. After privatization, the deficit lines were abolished gradually, and, in 2021, JR Hokkaido has the working kilometer of 2,488 km of the 14 lines [81]. Since the coal industry was once flourishing in Hokkaido, railways needed to transport coal from the mining sites to the port in order to provide huge amounts of coal mined in Hokkaido to the main land by ship. However, along with the decline of the coal industry, the transportation of coal by railroads also decreased rapidly. Asahikawa Station and Iwamizawa Station had played an important role as a hub station for coal and personnel transportation. Since a steam engine was used as a locomotive in those days, these stations needed vast ground for supplying fuel and water to the locomotives and replacing the locomotives and freight cars. However, due to the changes in economic structures and the modernization of railway facilities such as the spread of diesel and electric engines, it is no longer necessary to have as vast ground as before. In the processes of the redevelopment of the grounds, soil survey was conducted in these stations and soil contamination with lead was disclosed.

Various causes for the lead pollution in these stations have been surmised, for example, anti-knock agents added to gasoline, lead solutions in lead storage battery, and paint containing lead. White metal, one of alloy of lead and tin, has been used as a bearing material. It was possible that the fine particles of the alloy were scattered due to the abrasion of the white metal in the bearing unit. However, the exact cause has not yet been identified at present. Understanding the exact situation of the pollution and chemical species of pollutants in soil is important to identify the cause and decide the adequate remediation methods.

Ohkawa et al. measured the lead and tin contents in the soils of Asahikawa and Iwamizawa stations and analyzed the distribution of the chemical species of lead in soil by sequential extraction method [82]. It is known that the lead isotope abundance gives the important information to identify the cause of the pollution

[4, 5]. They tried to obtain the basic knowledge on the cause of pollution and soil remediation by the lead isotope composition of each fractionated lead species.

Soil samples were collected from one contaminated site in Asahikawa station (A-1) and two sites of Iwamizawa station (I-1 and I-2). A soil obtained from our university campus was used as an unpolluted soil. In addition to the soil samples, two kinds of white metal, a crown shaft and a lead storage battery used in JR Hokkaido previously were provided by the company as the samples to compare the lead isotopic abundance with each other. Automobile emission particles (NIES No. 8) were used as a standard sample for checking the accuracy of the measurement of isotopic abundance [83].

5.2 Contents of Lead and Tin in the Contaminated Soils

Table 13 shows the amounts of lead and tin in contaminated soils of the stations and an unpolluted soil. In the soils of both stations, the lead contents were higher than the environmental standard for soil in Japan, 150 ppm, especially A-1 contained five times more than the environmental standard of lead. The lead concentration in unpolluted soil was sufficiently low compared to the environmental standard value. Few amounts of tin in the unpolluted soil N and the polluted soil A-1 were detected. On the other hand, relatively high amounts of tin were detected in the soil samples of I-1 and I-2. Some kinds of white metal with the different ratio of tin to lead (Sn/Pb) have been used as the bearing material of the wheel axles of railway vehicles. The ratios of the Sn/Pb in I-1 and I-2 were relatively close to those of white metals as shown in the table. The contamination of the soil in Iwamizawa station may be caused by scattering of fine alloy particles due to abrasion of the white metal during wheel rotation into soil.

Table 13 Contents of lead and tin and the ratio in contaminated soils

Sample	Pb content (ppm)	Sn content(ppm)	The ratio of Sn/Pb
A-1	832 (780)	Less than 5	< 0.006
I-1	360 (140–160)	21	0.058
I-2	289 (230–290)	72	0.249
N	33.7	Less than 5	< 0.147
White metal no. 6			1.098
White metal no. 7			0.164
White metal no. 8			0.093
White metal no. 9			0.071
White metal no. 10			0.012

The environmental standard of lead for soil in Japan, 150 ppm

The values of the parentheses are those reported by JR Hokkaido

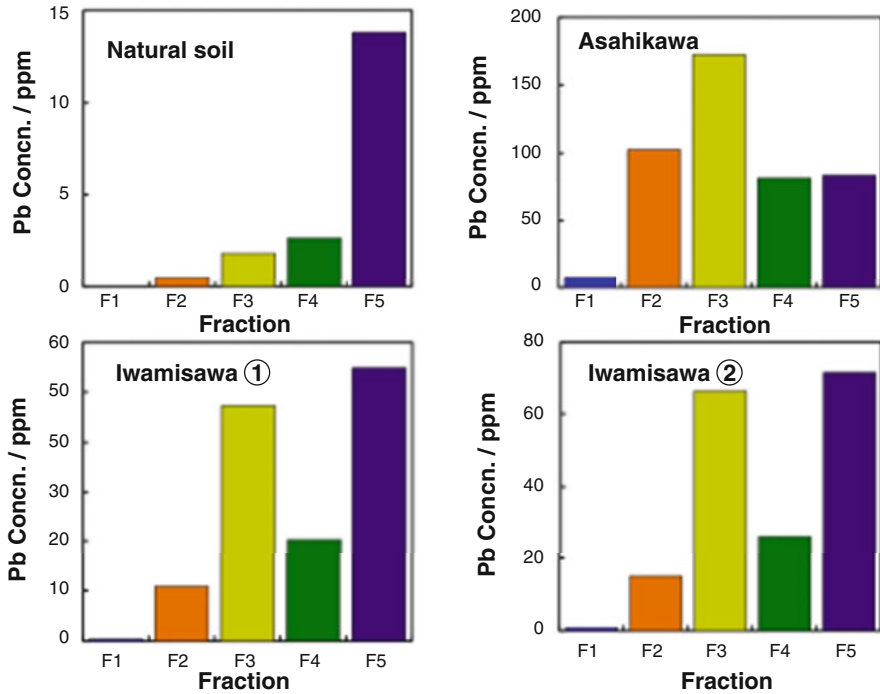


Fig. 17 Sequential fractional extraction of lead from soil samples

5.3 Chemical Species of Lead in Soil by Sequential Extraction

The results of sequential fractional extraction of lead in the soil samples are shown in Fig. 17a–d. Most of the lead in the natural soil (N) was fractionated into the F5, the residue, and few amounts of lead were fractionated into the F1–4. However, the amounts of lead distributed in the F3 (iron-manganese oxide bound state) were relatively large in the contaminated soils. A-1 soil contained some amount of lead in F2, whereas I-1 and I-2 soils contained more in F4 than in F2. The lead fractionated in F1 (ion exchangeable species) was very small in all soil samples including the natural soil.

5.4 Isotope Analysis of Lead in Soil Samples

Lead has four stable isotopes, ^{204}Pb , ^{206}Pb , ^{207}Pb , and ^{208}Pb . Three isotopes except ^{204}Pb are the final products of the radioactive decay of U and Th. Therefore, it is well known that the isotopic composition of lead differs depending on the mineral deposit [84]. The sources of the lead in samples can be presumed from the differences in the

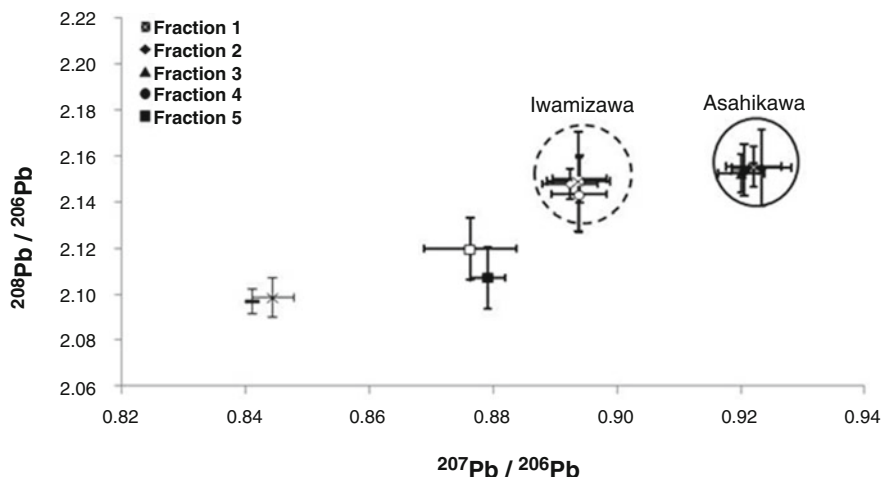


Fig. 18 Comparison of lead isotope ratio in the Asahikawa and Iwamizawa soils. Closed circle is Asahikawa soil data and Open circle is Iwamizawa soil data, ×: Japanese parent rock, —: Japanese soil [88]. Error bar is 2σ

isotopic composition [85, 86]. Therefore, the lead isotope abundance gives the important information to identify the cause of the pollution.

Ohkawa et al. attempted to clarify the cause of pollution of the station soils by measuring the lead isotope composition of lead species fractionated by the sequential fractionation extraction method. The measurement of the isotope ratio of lead was conducted by ICP-MS. A solid-phase extraction column with chelate resin (NOBIAS CHELATE PA-1, Hitachi High-Technology, Japan) was used to concentrate lead ion and remove impurities in the lead solution. 10 ppb of thallium ion was added to the solution as the internal standard. The detail condition for the measurement is described in their previous paper [87].

The plots of the isotope ratio, $^{208}\text{Pb}/^{206}\text{Pb}$ vs. $^{207}\text{Pb}/^{206}\text{Pb}$, of lead in the fractions of Asahikawa soil and Iwamizawa soils by sequential fractional extraction are shown in Fig. 18. For comparison, the reported ratios of lead in natural soil and the host rock in Hokkaido [88] are plotted in the same figure.

The lead isotope ratios of the fraction of F1–F4 obtained by sequential fractional extraction were similar to each other but significantly different from that of F5. In general, lead in F5 is said to be the lead that has existed in the land originally and lead in the other fractions has been artificially derived later. However, the lead isotope ratios of F5 in these soils were different from that of the host rock in Hokkaido. Therefore, the lead in F5 might be also added to there from the different source a long time ago. The lead isotope ratio of the deeper soil (1–3 m) corresponded to the values of the host rocks and soils in Hokkaido reported by Murozumi et al. [88] within the error range. From this result, it is considered that the lead in the deeper soil is that which originally existed in the land. The lead isotope ratio of white metal (WM) was relatively close to those of F1–F4 of Iwamizawa soil.

From these evidences, it is presumed that the cause of lead pollution in the Iwamizawa station might be due to the alloy of lead and tin, white metal used in the bearing unit.

5.5 Conclusion

In order to estimate the cause of the lead pollution in railroad stations, the sequential fraction extraction and lead isotope ratio measurement were applied to the soil samples. The distribution pattern of the chemical species (F1–F5) of lead in the polluted soils was different from that of the unpolluted natural soil. Tin was detected in the soil of Iwamizawa station but not in the soil of Asahikawa station. The lead isotope ratios of F1 to 4 of each contaminated soil were similar to each other but different from that of F5. The lead isotope ratio in the deep soil was different from that of the surface layer soil. These results mean that the lead pollution had been introduced into the surface layer soil artificially. The lead isotope ratio of white metal (WM) used as the bearing material was relatively close to those of F1–F4 of Iwamizawa soil. From these evidences, it is presumed that the cause of lead pollution in the Iwamizawa station might be due to the alloy of lead and tin, white metal used in the bearing unit. However, tin was not detected in the soil of Asahikawa station and the lead isotope ratio of the soil was different from that of white metal. Consequently, it was not possible to identify the cause of the lead pollution of Asahikawa station. The additional information is necessary to identify the cause exactly.

6 Conclusion

In order to find the adequate remediation technology suitable to a polluted site, we have to know the pollution situation exactly, the sort of the pollutant, the concentration and the toxicity as well as the chemical species. In this chapter, four cases of the investigation of pollution problems which occurred in different countries, Indonesia, China, Bangladesh, and Japan, were described. In a certain site among these contaminated areas, the contamination has already been almost completely eliminated, and in other sites the contaminated soil has already been treated or transported to the disposal site. On the other sites, the human activities and natural phenomena which can cause pollution have been still continuing, and then pollution has been progressing. The remediation seems to be not easy for all four pollution cases shown here. How to recover the pollutants that move with river water, and how to remediate the wide-spreading pollution such as salt damage caused by the rise in sea level? It is not easy to obtain the answer. However, these pollution problems were very important to consider the design for the remediation techniques and the materials used there.

References

1. Djuwita MR, Hartono DM, Mursidik SS, Budhi Soesilo TE (2021) Pollution load allocation on water pollution control in the Citarum River. *J Eng Technol Sci* 53(1):210112. <https://doi.org/10.5614/j.eng.technol.sci.2021.53.1.12>
2. Ramirez-Lovering D (2021) Cleaning up Indonesia's Citarum River, one of the world's most polluted waterways. Retrieved 26 Jan 2022 from <https://lens.monash.edu/@design-architecture/2021/08/26/1383691/cleaning-up-citarum-river-one-of-the-worlds-most-polluted-waterways>
3. Sumartias S (2020) The community responses over the Citarum river West Java. *Eur J Mol Clin Med* 7(1):3724–3732
4. Carrubba A (2020) Rotten river: life on one of the world's most polluted waterways – photo essay. Retrieved 26 January 2022 from <https://www.theguardian.com/global-development/2020/nov/02/rotten-river-life-on-one-of-the-worlds-most-polluted-waterways-photo-essay>
5. Asian Development Bank (ADB) (2014) Cleaning up Indonesia's Citarum basin. Retrieved 6 Feb 2022 from <https://www.adb.org/features/cleaning-indonesias-citarum-basin>
6. Asian Development Bank and the World Bank (2013) Downstream impacts of water pollution in the upper Citarum River, West Java, Indonesia, Water, and Sanitation Program: Technical Paper
7. B1 Report (2012) Water quality in Citarum River report: planning interventions to improve water quality in upper Citarum River. ADB TA 7189-INO Package B. Sponsored by Asian Development Bank (ADB), pp 1–58
8. Yamada T, Inoue T, Dohong S, Darung U (2005) Mercury contamination in river water and sediment in Central Kalimantan, Indonesia. Annual report for April 2004 – March 2005 on environmental conservation and land use Management of Wetland Ecosystems in Southeast Asia, Core University Program between Hokkaido University, Japan, and Research Center for Biology, LIPI, Indonesia. Sponsored by Japan Society for Promotion of Science, pp 115–120
9. Meguri M, Ujihira M, Tachibana H, Nyoman S (2006) Study on the present situation of placer gold mining and improvement of gold processing method in Central Kalimantan. Annual Report for April 2005 – March 2006 on environmental conservation and land use Management of Wetland Ecosystems in Southeast Asia, Core University Program between Hokkaido University, Japan, and research Center for Biology, LIPI, Indonesia. Sponsored by Japan Society for Promotion of Science, pp 149–153
10. Elvince R, Inoue T, Tsushima K, Takayanagi R, Ardianor U, Darung S, Gumiri S, Dohong O, Nagafuchi TK, Yamada T (2008) Assessment of mercury contamination in the Kahayan River, Central Kalimantan, Indonesia. *J Water Environ Technol* 6(2):103–112. <https://doi.org/10.2965/jwet.2008.103>
11. Ullrich S, Ilyushchenko MA, Uskov GA, Tanton TW (2007) Mercury distribution and transport in a contaminated river system in Kazakhstan and associated impacts on aquatic biota. *J Appl Geochem* 22:2706–2734. <https://doi.org/10.1016/j.apgeochem.2007.07.005>
12. Jewett SC, Duffy LK (2007) Mercury in fishes of Alaska, with emphasis on subsistence species. *Sci Total Environ* 387(1–3):3–27. <https://doi.org/10.1016/j.scitotenv.2007.07.034>
13. Nakazawa K, Nagafuchi O, Kawakami T, Inoue T, Elvince R, Kanefuji K, Nur I, Napitupulu M, Basir-Cyio M, Kinoshita H, Shinozuka K (2021) Human health risk assessment of atmospheric mercury inhalation around three artisanal small scale gold mining areas in Indonesia. *Environ Sci Atmos*. <https://doi.org/10.1039/d0ea00019a>
14. Minamata Convention on Mercury Home (2021) Retrieved 25 Jan 2022 from <https://www.mercuryconvention.org>
15. Environment Ministry. 59 Percent of Indonesian Rivers Severely Polluted. Retrieved 25 January 2022 from <https://en.tempo.co/read/1488257/environment-ministry-59-percent-of-indonesian-rivers-severely-polluted>

16. Helmy Q, Kardena E (2015) Petroleum oil and gas industry waste treatment: common practice in Indonesia. *J Pet Environ Biotechnol* 6(5):241. <https://doi.org/10.4172/2157-7463.1000241>
17. Ministry of Energy and Mineral Resources Republic of Indonesia (2020) Handbook of energy and economic statistics of Indonesia, ISSN 2528-3464
18. Effendi AJ, Kardena E, Helmy Q (2019) Biosurfactant-enhanced petroleum oil bioremediation. In: Kumar V et al (eds) *Microbial action on hydrocarbons*, Springer Nature Singapore Pte Ltd, pp 143–179. https://doi.org/10.1007/978-981-13-1840-5_7
19. Helmy Q, Kardena E, Nurachman Z, Wisjnuaprpto. (2010) Application of biosurfactant produced by *Azotobacter vinelandii* AV01 for enhanced oil recovery and biodegradation of oil sludge. *IJCEE-IJENS* 10(1):7–14
20. Helmy Q, Suryatmana P, Kardena E, Funamizu NW (2008) Biosurfactants production from *Azotobacter sp.* and its application in biodegradation of petroleum hydrocarbon. *J Appl Indust Biotechnol Trop Region* 1:1–4
21. Helmy Q, Kardena EW (2009) Performance of petrofilic consortia and effect of surfactant tween 80 addition in the oil sludge removal process. *J Appl Sci Environ Sanit* 4:207–218
22. Helmy Q, Laksmono R, Kardena E (2015) Bioremediation of aged petroleum oil contaminated soil: from laboratory scale to full scale application. *Procedia Chem* 14:326–333. <https://doi.org/10.1016/j.proche.2015.03.045>
23. Bustamante M, Durán N, Díez MC (2012) Biosurfactants are useful tools for the bioremediation of contaminated soil: a review. *J Soil Sci Plant Nutr* 12(4):667–687. <https://doi.org/10.1351/PAC-CON-09-02-10>
24. Cameotra SS, Makkar RS (2010) Biosurfactant enhanced bioremediation of hydrophobic pollutants. *Pure Appl Chem* 82(1):97–116. <https://doi.org/10.4067/S0718-95162012005000024>
25. Puradyatmika P, Prewitt JM (2012) Tailings reclamation trials at P.T. Freeport Indonesia in Mimika, Papua, Indonesia. In: Fourie AB, Tibbett M (eds) *Proceedings of the seventh international conference on mine closure*. Australian Centre for Geomechanics, Perth, pp 173–186. https://doi.org/10.36487/ACG_rep/1208_17_Puradyatmika
26. Fifi Djuuna IA, Masora M, Puradyatmika P (2011) Soil microorganisms numbers in the tailing deposition ModADA areas of Freeport Indonesia, Timika, Papua. *Biodiversitas* 12(4):198–203. <https://doi.org/10.13057/biodiv/d120403>
27. Ermayanti TM, Mukhsia A (2012) Applications of tissue culture for the production of native plant species to accelerate the alpine reclamation program at P.T. Freeport Indonesia. In: Fourie AB, Tibbett M (eds) *Proceedings of the seventh international conference on mine closure*. Australian Centre for Geomechanics, Perth, pp 1–10. https://doi.org/10.36487/ACG_rep/1208_44_Ermayanti
28. PTFI (2022) Overburden and mine acid water. Retrieved 30 Jan 2022 from <https://ptfi.co.id/en/overburden-and-acid-mine-water>
29. Hidayati N, Juhaeti T, Syari F (2009) Mercury and cyanide contamination in gold mine environment and possible solution of cleaning up by phytoextraction. *HAYATI J Biosci* 16(3):88–94
30. Yustiawati, Syawal MS, Terashima M, Tanaka S (2006) Speciation analysis of mercury in river water in West Java, Indonesia. *TROPIC* 15:425–428
31. Taga M, Tanaka S, Fukushima M (1989) Measurement of copper complexing ability of humic acids by using diethylamino ethyl SephadexA-25 column. *Anal Sci* 5:597–600
32. Tomiyasu T., Hamada YK, Kodamatani H, Hidayati N, Rahajoe JS. (2019) Transport of mercury species by river from artisanal and small scale gold mining in West Java, Indonesia
33. Tomiyasu T, Kono Y, Kodamatani H, Hidayati N, Rahajoe JS (2013) The distribution of mercury around the small-scale gold mining area along the Cikaniki river, Bogor, Indonesia. *Environ Res* 125:12–19
34. Kono Y, Rahajoe JS, Hidayati N, Kodamatani H, Tomiyasu T (2012) Using native epiphytic ferns to estimate the atmospheric mercury levels in a small-scale gold mining area of West Java, Indonesia. *Chemosphere* 89:241–248

35. Derka T, Zamora-Muñoz C, Tierno de Figueroa JM (2019) Aquatic insects. Biodiversity of Pantepui. Academic Press, pp 167–192. <https://doi.org/10.1016/b978-0-12-815591-2.00008-2>
36. Bouchard Jr RW (2004) Guide to aquatic macroinvertebrate of the upper Midwest. Water Resources Center, University of Minnesota, St. Paul. 208 p
37. Yoga GP, Lumbanbatu D, Riani E, Wardianto Y (2014) Pengaruh Pencemaran Merkuri di Sungai Cikaniki terhadap Biota Trichoptera (Insekta). LIMNOTEK 21(1):11–20. (in Indonesian)
38. Yoga GP, Lumbanbatu DT, Riani E, Wardiatno Y (2014) Secondary production of the net-spinning caddisfly, *Cheumatopsyche* spp.(Trichoptera: Hydropsychidae) in mercury contaminated river. J Trop Biol Conserv 11:1–12
39. Susintowati, Hadisusanto S (2015) Mercury accumulation of macrobenthos based on feeding and NICHESAT lampoon ceased Traditional gold mining, Banyuwangi District, east Java. KnE Life Sciences vol 2, pp 451–457 (ISSN2413-0877). The 3rd international conference on biological sciences 2013. (The 3rd ICBS-2013)
40. Castilhos ZC, Rodrigues-Filho S, Rodrigues APC, Villas-Bôas RC, Siegel S, Veiga MM, Beinhoff C (2006) Mercury contamination in fish from gold mining areas in Indonesia and human health risk assessment. Sci Total Environ 368:320–325
41. Irawati W, Patricia, Soraya Y, Baskoro A (2012) A study on mercury-resistant bacteria isolated from a gold mine in Pongkor Village, Bogor, Indonesia. HAYATI J Biosci 19(4):197–200. EISSN: 2086-4094
42. Dai Y, Terui N, Lin Y, Tanaka S, Jin K, Hirama Y, Teduka M, Zhang M, Shen X, Fugrstu B (2010) Determination of nitrobenzene in water and ice samples collected from the Songhua River after an explosion of a petrochemical plant and investigation on enclosing behavior of nitrobenzene into ice. Anal Sci 26:519–523
43. Li D, Yang M, Li Z, Qi R, He J, Liu H (2008) Change of bacterial communities in sediments along Songhua River in northeastern China after a nitrobenzene pollution event. FEMS Microbiol Ecol 65:494–503
44. Li Z, Yang M, Li D, Qi R, Liu H, Sun J, Qu J (2008) Nitrobenzene biodegradation ability of microbial communities in water and sediments along the Songhua River after a nitrobenzene pollution event. Environ Sci 20:778–786
45. Wang S (2006) Treatment of Songhua River water by catalytic ozonation process using nanosize TiO₂. Harbin Institute of Technology. Dissertation for the Master Degree, Harbin
46. Zhang L, Zhang Y, Yang Y, Tao R (2007) The response of contamination accident of Songhua River and relevant consideration. Saf Environ Eng 14:13–15
47. Jiang J, Chen Y, Wang B (2019) Pollution source identification for river chemical spills by modular-Bayesian approach: a retrospective study on the ‘Landmark’ spill incident in China. Hydrology 6:74
48. Zhang H, Xu X, Zhang X (2009) Treatment technology of organic waste water in sudden accident – a case study of nitrobenzene pollution in the Songhua River. J Water Resources Water Eng 20:67–71
49. Lin L, Shi Y, Luo H, Zhang Y, Yu Y, Chen Y (2016) Study on the characteristics of water pollution change of Songhua River basin in 2001-2015. Environ Monit China 6:58–62
50. Zhu L, Xu H, Wang M, Sun D, Teng R, Gao Y (2006) Monitoring and post impact assessment of nitrobenzene in Jiamusi section of Songhua River, Heilongjiang. Med Pharm 29:7–7
51. Li P (2009) Comprehensively promote the prevention and control of water pollution in the Songhua River basin. Environ Prot 13:39–40
52. Information Office of the State Council (2006) Ecological environmental impact assessment of Songhua River water pollution achieved phased results
53. Anniversary of water pollution in Songhua River: a number of problematic enterprises were shut down, Heilongjiang daily on 24 Nov 2006. <http://news.sina.com.cn/c/2006-11-24/085910585361s.shtml>

54. Eriko T, Dai Y, Lin Y, Bushi F, Shunitz T, Kazuo J, Yujin H (2009) Determination of nitrobenzene in fish samples of Matsuhana River after chemical plant explosion. *Bunseki Kagaku* 58:807–813
55. Loitzenbauer E, Mendes CAB (2012) Salinity dynamics as a tool for water resources management in coastal zones: an application in the Tramandaí River basin, southern Brazil. *Ocean Coast Manag* 55:52–62
56. Werner AD, Bakker M, Post VEA, Vandenbohede A, Lu C, Ataie-Ashtiani B, Simmons CT, Barry DA (2013) Seawater intrusion processes, investigation and management: recent advances and future challenges. *Adv Water Resour* 51:3–26
57. Abedin M, Habiba U, Shaw R (2014) Community perception and adaptation to safe drinking water scarcity: salinity, arsenic, and drought risks in coastal Bangladesh. *Int J Disaster Risk Sci* 5:110–124
58. Hoque MA, Scheelbeek PF, Vineis P, Khan AE, Ahmed KM, Butler AP (2016) Drinking water vulnerability to climate change and alternatives for adaptation in coastal south and South East Asia. *Clim Change* 136:247–263
59. Khan A, Ireson A, Kovats S, Mojumder S, Khusru A, Rahman A, Vineis P (2011) Drinking water salinity and maternal health in coastal Bangladesh: implications of climate change. *Environ Health Perspect* 119:1328–1332
60. Rahman MM, Islam MA, Bodrud-Doza M, Muhib MI, Zahid A, Shammi M, Tareq SM, Kurasaki M (2018) Spatio-temporal assessment of groundwater quality and human health risk: a case study in Gopalganj, Bangladesh. *Expo Health* 10(3):167–188
61. Islam MA, Zahid A, Rahman MM, Rahman MS, Islam MJ, Akter Y, Shammi M, Bodrud-Doza M, Roy B (2017) Investigation of groundwater quality and its suitability for drinking and agricultural use in the south-central part of the coastal region in Bangladesh. *Expos Health* 9(1): 27–41
62. Shammi M, Rahman MM, Islam MA, Bodrud-Doza M, Zahid A, Akter Y, Quaiyum S, Kurasaki M (2017) Spatio-temporal assessment and trend analysis of surface water salinity in the coastal region of Bangladesh. *Environ Sci Pollut Res* 24(16):14273–14290
63. Abedin MA, Habiba U, Shaw R (2012) Impacts of salinity, arsenic, and drought in South-Western Bangladesh. *Environ Dis Risk Manag* 9:165–193
64. Shammi M, Rahman M, Bondad SE, Bodrud-Doza M (2019) Impacts of salinity intrusion in community health: a review of experiences on drinking water sodium from coastal areas of Bangladesh. *Healthcare* 7(1):50
65. Islam MA, Rahman MM, Bodrud-Doza M, Muhib MI, Shammi M, Zahid A, Akter Y, Kurasaki M (2018) A study of groundwater irrigation water quality in south-central Bangladesh: a geo-statistical model approach using GIS and multivariate statistics. *Acta Geochimica* 37(2): 193–214
66. Shammi M, Karmakar B, Rahman M, Islam MS, Rahaman R, Uddin K (2016) Assessment of salinity Hazard of irrigation water quality in monsoon season of Batiaghata Upazila, Khulna District, Bangladesh and adaptation strategies. *Pollution* 2(2):183–197
67. Islam ARMT, Siddiqua MT, Zahid A, Tasnim SS, Rahman MM (2020) Drinking appraisal of coastal groundwater in Bangladesh: an approach of multi-hazards towards water security and health safety. *Chemosphere*:26933
68. Islam MA, Sattar MA, Alam MS (1999) Scientific report on impact of shrimp farming on soil and water quality of some selected areas in the Greater Khulna District. Dhaka, Bangladesh: Research and Development Collective (RDC)
69. Ahmed N, Cheung WW, Thompson S, Glaser M (2017) Solutions to blue carbon emissions: shrimp cultivation, mangrove deforestation and climate change in coastal Bangladesh. *Mar Policy* 82:68–75
70. Akber M, Islam M, Ahmed M, Rahman MM, Rahman MR (2017) Changes of shrimp farming in southwest coastal Bangladesh. *Aquacult Int* 25:1883–1899. <https://doi.org/10.1007/s10499-017-0159-5>

71. Hasan MH, Hossain MJ, Chowdhury MA, Billah M (2020) Salinity intrusion in southwest coastal Bangladesh: an insight from land use change. In: Haque A, Chowdhury A (eds) *Water, flood management and water security under a changing climate*. Springer, Cham. https://doi.org/10.1007/978-3-030-47786-8_8
72. Johnson FA, Hutton CW, Hornby D, Lázár AN, Mukhopadhyay A (2016) Is shrimp farming a successful adaptation to salinity intrusion? A geospatial associative analysis of poverty in the populous Ganges–Brahmaputra–Meghna Delta of Bangladesh. *Sustain Sci* 11(3):423–439
73. Clarke D, Williams S, Jahiruddin M, Parks K, Salehin M (2015) Projections of on-farm salinity in coastal Bangladesh. *Environ Sci Process Impacts* 17(6):1127–1136
74. Gain A, Giupponi C (2014) Impact of the Farakka Dam on thresholds of the hydrologic flow regime in the lower Ganges River basin (Bangladesh). *Water* 6(8):2501–2518
75. Shammi M, Das A, Salma U, Sakib AZ, Rahman MM (2020) Effectiveness of adaptation measures for reducing the effect of salinity intrusion in agriculture practice: a case study from Kalapara Upazila, Bangladesh. *Bangladesh J Environ Res* 11:38–54
76. Ahmed AU, Neelormi S, Adri N, Alam MS, Nuruzzaman K (2007) Climate change, gender and special vulnerable groups in Bangladesh. Draft final report. BASTOB and Center for Global Change (CGC), Dhaka, p 84
77. Scheelbeek PF, Chowdhury MA, Haines A, Alam DS, Hoque MA, Butler AP, Khan AE, Mojumder SK, Blangiardo MA, Elliott P (2017) Drinking water salinity and raised blood pressure: evidence from a cohort study in coastal Bangladesh. *Environ Health Perspect* 125: 057007
78. Banerjee K, Gatti RC, Mitra A (2017) Climate change-induced salinity variation impacts on a stenocious mangrove species in the Indian Sundarbans. *Ambio* 46(4):492–499
79. Dasgupta S, Sobhan I, Wheeler D (2017) The impact of climate change and aquatic salinization on mangrove species in the Bangladesh Sundarbans. *Ambio* 46(6):680–694
80. Oikawa Y (2014) History of Japanese railroad, the volume of the closing days of the Tokugawa Shogunate and the Meiji Era (written in Japanese). Iwanami Shinsho
81. JR Hokkaido HP, https://www.jrhokkaido.co.jp/corporate/company/com_02.html
82. Tessier A, Campbell PGC, Bisson M (1979) Sequential extraction procedure for the speciation of particulate trace metals. *Anal Chem* 51:844
83. Araya M, Funasaka K, Katahira K, Matsui S (2006) Determination of lead source in urban road runoff due to automobile traffic. *J Jpn Soc Water Environ* 29(11):693
84. Mukai H, Yoshinaga J (1995) Isotope ratio analysis of environmental and biological samples by ICP-MS. *J Environ Chem* 5:789–798
85. Hirao Y, Mabuchi H, Fukuda E, Tanaka H, Imamura T, Todoroki H, Kimura K, Matsumoto E (1986) Lead isotope ratios in Tokyo Bay sediments and their implications in the lead consumption of Japanese industries. *Geochem J* 20:1–15
86. Mukai H, Furuta N, Fujii T, Ambe Y, Sakamoto K, Hashimoto Y (1993) Characterization of sources of lead in the urban air of Asia using ratios of stable lead isotopes. *Environ Sci Technol* 27:1347–1356
87. Ohkawa Y, Rudy S, Fujiwara N, Jin K, Tanaka S (2012) Presumption of the source of lead contaminated soil by isotope analysis of Lead and ICP-MS with sequential extraction. *Bunseki Kagaku* 61:95–101
88. Murozumi M, Nakamura S, Yoshida K (1982) Impacts of aerosol lead to natural ecosystems. *Nippon Kagaku Kaishi* 9:1479–1484

Part II

Effects and Evaluation

Effects of Metals on Human Health and Ecosystem



Md. Mostafizur Rahman, Mst. Kaniz Fatima Binte Hossain, Sadia Afrin, Takeshi Saito, and Masaaki Kurasaki

Contents

1	Introduction	82
2	Properties of Metals	86
3	Sources of Metal Pollution	86
4	Metal Toxicity	87
4.1	Modes of Action	88
4.2	The Factors Affecting Metal Toxicity	88
5	Metals and Their Effect on Human and Environment	91
5.1	Pb and Its Effects	91
5.2	Hg and Its Effects	93
5.3	Cd and Its Effects	96
5.4	Cu and Its Effects	98
5.5	As and Its Effects	101
5.6	Cr and Its Effects	103
5.7	Mn and Its Effect	105
5.8	Al and Its Effects	107
5.9	Ag and Its Effect	108
6	Combined Effects of Heavy Metals	110
7	Concluding Remarks	113
	References	114

M. M. Rahman (✉) and S. Afrin
Department of Environmental Sciences, Jahangirnagar University, Dhaka, Bangladesh
e-mail: rahmanmm@juniv.edu

M. K. F. B. Hossain and T. Saito
Faculty of Health Sciences, Hokkaido University, Sapporo, Japan
e-mail: taksaito@med.hokudai.ac.jp

M. Kurasaki
Faculty of Environmental Earth Science, Hokkaido University, Sapporo, Japan
e-mail: kura@ees.hokudai.ac.jp

Shunitz Tanaka, Masaaki Kurasaki, Masaaki Morikawa, and Yuichi Kamiya (eds.),
Design of Materials and Technologies for Environmental Remediation,
Hdb Env Chem (2023) 115: 81–120, DOI 10.1007/698_2021_825,
© The Author(s), under exclusive license to Springer Nature Singapore Pte Ltd 2022,
Published online: 1 January 2022

Abstract Heavy metals are one of the main constituents of the earth and have played an important role in living organisms. However, ingestion of large amounts of even essential heavy metals can cause serious damage and continue to cause many sufferings as pollutants in the environment. This chapter outlines the toxicity common to the general properties of heavy metals, and then details the effects of individual heavy metals on living organisms, mainly human health. And finally, it also describes the effect of reducing the antioxidant heavy metals that coexist with the adverse health effects of these heavy metals.

Keyword Co-exposure, General properties, Heavy metals, Lethal dose, Reactive oxygen species, Toxicity

1 Introduction

Heavy metals are important biologically as trace nutrients, however, the toxic effects of the heavy metals in human physiology are very concerning. Thus, for comprehensive understanding of metals' mechanism of actions, there is a need to know about involving functions and actions, such as their concentrations, speciation, and toxicokinetics which make them detrimental [1]. There is an urgent need to address properly their environmental sources, leaching criteria, chemical alterations, and their modes of action that contaminating the surrounding environment and ecosystem, where life persists. Several researches depicted that these metals are released into the environment by two pathways: one is natural and the other is anthropogenic means, especially mining and industrial activities, and automobile exhausts [2]. Metals accumulate into the groundwaters, by passing along water pathways and ultimately assembling in the aquifer, or they are washed away by run-off into surface waters, as a result water and soil pollution occur. The toxicity and poisoning level of metals are being triggered by their exchange mechanism. When metals are ingested, they form several cellular stresses including formation of reactive oxygen species (ROS), altering their structures, and inhibit the biomolecular reactions and functions in biological systems. This chapter focuses on certain heavy metals and their effects on human and ecosystem [3]. Metals are crucial components of the environment. Their presence in the environment is quite unique because it is troublesome to dispel them from the environment entirely once they enter in the environment. Metal comprises such toxic substances which are visible in several environmental and occupational conditions. The effect of these toxic metals on human health currently is of great interest due to the omnipresence of metal exposure [4]. For decades, various metals are being evicted from the Earth and utilized in industries and production worldwide. So, the problems raising in the environment from these toxic metal usages have such serious aspects. Metals are natural material (except for Plutonium and Uranium) also categorized as globally-distributed pollutants. Metals are being depressive now-a-days creating environmental disruptions

such as they accumulated in the human body. Even if their exposure level is minor, they could be potentially toxic [5]. For example, Iron (Fe) and Copper (Cu) are vital for life and play a vital role in enzyme system functioning. Other metals are xenobiotics in nature, they do not have any crucial benefits for human and other living organisms, e.g., lead (Pb) and mercury (Hg) at trace level exposure can be toxic. Though these metals are of great importance, they can be detrimental at high exposure. The very basic tenet of toxicology follows as: “the dose makes the poison” [6]. U.S. Agency for Toxic Substances and Disease Registry (ATSDR, 2017) lists all the metals with their potential hazards, disposal, and toxicity level. According to the list, the order of three most hazardous metals is Pb, Hg, arsenic (As), respectively. Cadmium (Cd) is the sixth most hazardous metal according to ATSDR [7]. The metal exposure has several routes such as inhaling tiny particulate matter, ingesting them through foods, metals can be vaporized and inhaled [8]. The amount of metals that was accumulated in the digestive tract could be different based on the metal’s chemical form and individual’s nutritional condition. After metal accumulated in the tract, it spreads throughout the organs and tissues. Metals usually accumulated in some storage areas such as liver, kidneys, and bones for decades, as through kidneys and digestive tract, excretion primarily occurs. Metal toxicity mainly affects the brain and kidneys, though some corresponding metals such as As are able to cause cancer [9]. An individual with acute dose of metal toxicity has some symptoms which involves hypertension (exposure to lead), headache, renal toxicity (exposure to Cd), and weaknesses in body. Also these toxicities might occur even the individual has no symptoms. The diagnosis of this kind of toxicity level can be so difficult otherwise the technical body must have that expertise and knowledge to able to do correct diagnosis [10]. Due to metal toxicity, the genetic factors may become vulnerable and that study needs much intensive inquisition. A diagram of sources of heavy metal and human exposure has been presented in Fig. 1. It is also concerning that metals exposures now at low condition can cause several chronic diseases and hinder necessary functioning [11].

Dose-response relationship is an important part of the principles of pharmacokinetics and pharmacodynamics. In this relationship, the required dose and frequency with the therapeutic index for a drug are determined for a population. The therapeutic index is the ratio of the minimum toxic concentration to the median effective concentration. This index helps to measure drug’s efficacy and safety. Increasing the drug dose with a minimal therapeutic index enhances the toxicity probability or drug ineffectiveness. Thus, this relationship differs by population and it is influenced by patient-related factors such as age, pregnancy, and organ function [12]. Dose-response curve has been shown in Fig. 2.

In fish, metals can transport through various pathways [12]:

- Through gills as diffusion occurs in membranes into bloodstream
- Skin contact as diffusion occurs in the bloodstream
- By drinking water
- Ingesting sediments
- Transportation in food chain

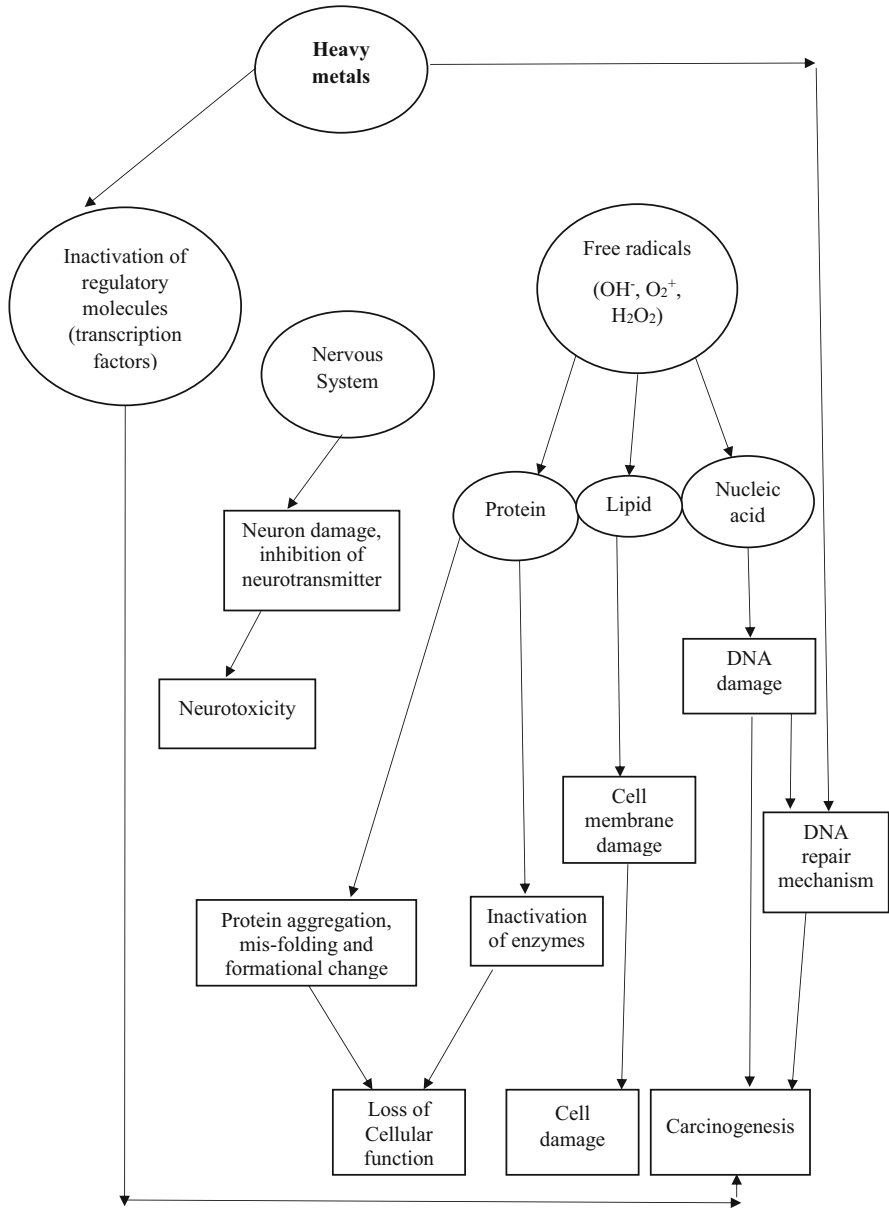


Fig. 1 Sources of heavy metals and human exposure (Modified after [2])

In humans, metals are transported through several pathways such as through lungs when humans inhale lead dust and particulate matters, through skin, by drinking metal-polluted water, through food chain, by eating contaminated food

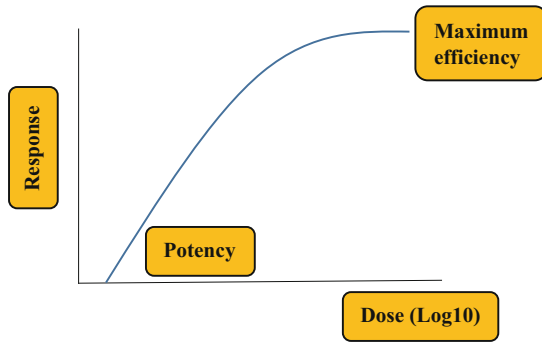


Fig. 2 Dose-Response curve

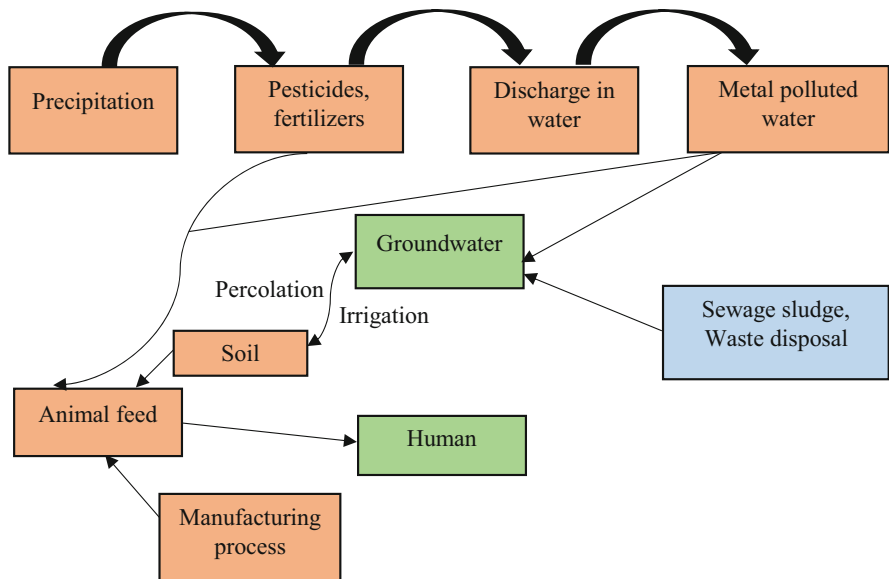


Fig. 3 Human exposure to metals through food chain (Modified after [13])

(such as for Pb, acidic juices and foods will liquefy lead from the food and juice containers). Children playing with toys that may contain Pb paint [12]. Human exposure to metals through food chain has been illustrated in Fig. 3.

The categories of metals are bit different in case of concentration. It can be essential and non-essential. Metals in low concentrations are crucial for good health and in high concentrations these are lethal [12]. Some essential metals are: chromium (Cr), Cu, zinc (Zn), nickel (Ni), manganese (Mn), and selenium (Se). Non-essential metals are: aluminum (Al), Pb, As, Hg, Cd, gold (Au), silver (Ag), and tin (Sn).

Many factors are responsible for metal toxicity in body such as metal solubility, metal's ability to bind with the biological sites, extent of metabolized metal complex

formation, and much more [14]. Thus, this metal toxicity can cause severe impacts on human health as well as on the environment.

2 Properties of Metals

Metals have some notable properties which make them crucial and also make them globally-distributed pollutant [12]. Some mentionable properties are:

- Metals have luster, malleability, and ductility.
- They are the elements of rocks and mineral ores in low concentration.
- Anthropogenic activities trigger erosion, as a result metals are released in the environment.
- They remain solid at room and normal temperature.
- They form cations (positively charged ions).
- They are good conductors of electricity and heat.
- They dissolve in water and are easily concentrated in aquatic organisms.
- They trigger point and non-point source pollution.

3 Sources of Metal Pollution

Metals (toxic) can be accumulated in the environment through discharging industrial effluents, organic wastes, refuse burning, power generation, and transportation. Wind can also be a major metal pollution source because metals can be steered many places even miles away through this force, if metals are in particulate (gaseous) form [5]. Metal pollutants are then finally carried out from the air into the ground and the surface of waterways. In this way, air is also an important source for the metal pollution in the environment. Metals which are released from industrial effluents are severe pollution causing source of hydrosphere. Also the movement of drainage water from contaminated catchment areas is responsible for such pollution [15].

Mining is one of the major sources of metal pollution. Because of the mining activities, the mine tailing is being disposed in the waterbodies, which forms acid rock drainage (ARD). And then from both abandoned and operating mines, the mine tailing and ARD are released into the groundwater and surface water [12]. Some toxic metals used in industrial production [5] are shown in Table 1.

Other mentionable sources are agricultural activities which involve use of fertilizers; soil amendments from bio-solids; coal combustion such as As, Cd, Se, and Zn; urban run-off such as Cu, Pb, and Zn; industrial waste; solid waste disposal such as batteries, tires, and appliances [16]. Regulatory limits of heavy metals are given in Table 3.

Table 1 Toxic metals used in industrial production

Metal	Manufacturing purposes
As	Fertilizer, metal hardening, paints, textile
Cd	Fertilizer, electronics, paints
Cr	Metal plating, tanning, rubber
Cu	Plating, rayon, electrical
Pb	Paints, battery
Ni	Electro-plating, iron steel
Zn	Galvanizing, iron plating, steel
Hg	Chlor-alkali, scientific apparatus, chemicals

Table 2 The favorable organs of some toxic metals

Metal	Favorable organs
As	Skin and pulmonary nervous system
Cd	Skeletal, pulmonary, and renal system
Cr	Pulmonary system
Mn	Nervous system
Pb	Nervous system, renal system, hematopoietic system
Ni	Pulmonary system and skin
Sn	Nervous and pulmonary system
Hg	Renal system and nervous system

4 Metal Toxicity

Metals have impacts on human, animals, and aquatic organisms. There is an adverse biological effect of metals on organism's survival, activity, growth, metabolism, and reproduction. Mainly, the chemical activity of metal ions with the enzymatic and membrane system often causes metal ions toxicity to mammal species. Toxic metals usually target those organs which have the possibility to persist highest metal concentration such as brain and bone marrow, etc. This possibility depends on the exposure route and chemical characters of metal compounds such as lipid solubility and molecular size. Human exposure to toxic metals can also be carcinogenic such as chromium and nickel are associated with cancer causing agent [17]. The favorable organs of some toxic metals are shown in Table 2. Metals can cause both acute and chronic poisoning in human and animals [12].

Toxicity can be measured in two ways: LC_{50} and EC_{50} . LC_{50} is the lethal concentration 50 which causes death in 50% of the organisms of exposed population. EC_{50} is the effective concentration 50 which causes nonlethal negative effect in 50% of the exposed organisms. If there is lower amount of LC_{50} or EC_{50} , then the metal has more toxicity [12]. Regulatory limits of some heavy metals according to EPA Environmental Protection Agency, OSHA Occupational Safety and Health Administration, FDA Food and Drug Administration have been presented in (Table 3).

Table 3 Regulatory limits of some heavy metals (*EPA* Environmental Protection Agency, *OSHA* Occupational Safety and Health Administration, *FDA* Food and Drug Administration, *ppm* parts per million, *mg* milligram)

Metals	EPA regulatory limit in drinking water (ppm)	FDA limit in food or bottled water (ppm)	OSHA limit in air (workplaces) (mg/m ³)
Arsenic	0.01	–	10
Cadmium	0.005	0.005	5
Chromium	0.1	1	1
Selenium	0.05	–	0.2
Manganese	0.05	–	5
Mercury	0.002	1	0.1
Sliver	0.0001	–	0.01
Zinc	5	–	5
Lead	0.15	–	0.15
Aluminum	0.2	–	5
Barium	2.0	–	0.5

4.1 Modes of Action

Metals cause structural damage to organs especially to the tissues such as Hg injures brain. Metals inactivate the enzyme and the enzyme co-factors [18]. Metals interact in three ways as follows;

- Additivity where two metals have twice the effect of either metal ($1 + 1 = 2$);
- Synergism where two metals have more effect than twice the effect of either metal ($1 + 1 = 3$), such as Cd and Cu, Cd and Cr, Cu and Ag, and Zn and Ag;
- Antagonism where two metals have less than twice the effect of either metal ($1 + 1 = 1.5$), such as Zn and Cd, Zn and Pb, Hg and Se, and Hg and Cd [18].

Heavy metal toxicity mechanism in human has been illustrated in Fig. 4.

4.2 The Factors Affecting Metal Toxicity

Some factors [6, 12, 19] that affect metal toxicity in human and animals are given below:

- *Metal concentration*: In high concentration metals can cause acute effects. And in low concentration they may cause chronic effects.
- *Time of exposure and mood of exposure*: Furthermore, the continuous exposure is more hazardous than discontinuous exposure.
- *Bioavailability or speciation*: Metal concentration is not an indicator of its biological effect. Metals need to be present in the dissolved form to interact with the surface or tissues for better detection of its biological system. Metal

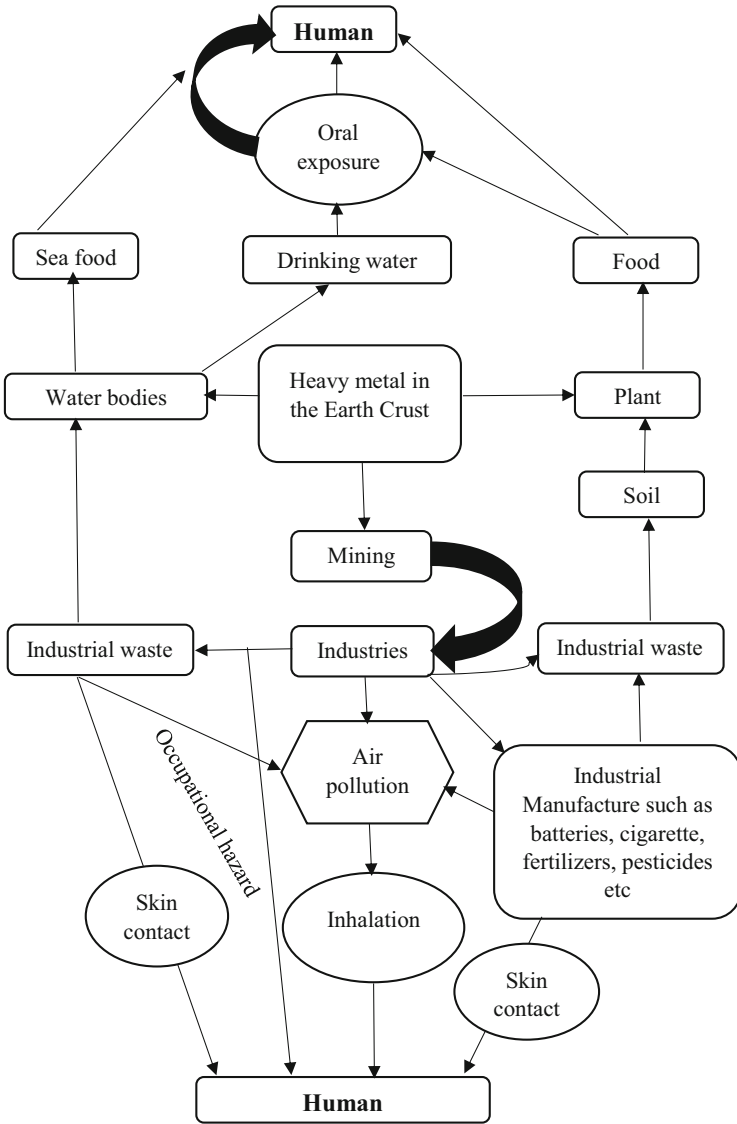


Fig. 4 Heavy metal toxicity mechanism in human (O figures → exposure routes)

bioavailability is affected by speciation. Speciation refers to different chemical forms where metal exists as its neutral element, ions, and organic forms. For example: organic and inorganic mercury, Cr^{+6} and Cr^{+3} .

- *pH*: At low pH metals are more toxic. Concentration of hydrogen ion has an impact on the metal speciation such as aluminum. In sediment, metals are being

released due to lower pH levels. On the other hand, metals are being bound in the sediment due to higher pH levels.

- *Buffering capacity*: Buffering capacity of waterbodies relies on the carbonate and bicarbonate ions concentration and affects the aquatic ecosystem susceptibility to ARD. In the buffered waterbody, metals are less lethal.
- *Salinity*: Comparing with saltwater, metals are more toxic in the freshwater because they are more bioavailable in freshwater. Chemical speciation of metal is affected by salinity, for example: Cd in the form of Cd^{+2} is more bioavailable than its elemental form and dominant in freshwater. On the other hand, Cd creates chloride complexes, which makes them less toxic and bioavailable.
- *Water temperature*: If water temperature increases, then metal toxicity also increases. $Q_{10} = 2$ (in coldblooded animals metabolism rate is doubled with every 10°C water temperature increase). With increasing water temperature, respiratory rate, membrane permeability, and absorption rates also increase.
- *Hardness*: In soft water, metals are mostly toxic. Whereas the toxicity depends on calcium (Ca) ion concentration (Ca^{+2}), it gives protective effect. Water quality criteria for metals are based on water hardness in US, Canada, and Europe.
- *Species and individual differences*: Aquatic animals are more delicate than aquatic plants. Daphnia is planktonic freshwater crustacean where shrimp is impressible marine crustaceans. In each species, there are sensitivity differences.
- *Age and body size*: Young animals are more sensorial than adults. Young animals don't have developed detoxification enzymatic system. They have high metabolic rate, as a result more toxic metals are taken faster by them.
- *Persistence*: The time required for 50% of the metals dose to be reduced from organisms is termed as half-life. Metals such as Hg, Cd, and Pb have longer half-lives in mammal species and ultimately can create prolonged effects.
- *Detoxification*: Metal exposure can lead to metallothionein (low molecular weight protein), it has the ability to bind with some metals such as Cd, Cu, and Zn and thus lessen their toxicity. The system can be submerged if concentration of metal is too high and also if there is a continuous metal exposure.

One of the notable phenomena of metal toxicity is bio-concentration or bioaccumulation. Bioaccumulation is the phenomenon which is responsible for the increase of metal concentration in the organisms comparing with their concentrations in sediments or water. All the metals sustain bioaccumulation. Animals which live in sediment are more susceptible to metal exposure at high level [20].

Bio-magnification is another phenomenon which is responsible for metal toxicity. The term “bio-magnification” refers to the increase of metal concentration gradually in the higher trophic levels of food chain. Usually, predators sustain more metal concentration than the preys. Animals on higher trophic level have the highest metal concentration, mainly pertaining to mercury and cadmium, manganese, and selenium also [20].

Biotransformation refers to the metal alteration by the organism. Thus, the metal toxicity can be both increased and decreased. For examples, converting organic Hg

with inorganic Hg can increase Hg toxicity whereas the conversion of inorganic As to organic As can decrease the As toxicity [21].

5 Metals and Their Effect on Human and Environment

There are some concerning metals that can cause residential and occupational hazards. Out of 35 metals, 23 metals are considered as heavy metals, such as As, Cd, cesium (Cs), Cr, cobalt (Co), Cu, Fe, Pb, bismuth (Bi), antimony (Sb), Au, Mn, Ni, platinum (Pt), Ag, Hg, Sn, Zn, uranium (U), vanadium (V), and tellurium (Te) [22]. They can be naturally occurring. Though some of them are required in trace amount for health, higher concentration of these can be dangerous for health. Metal can affect the human body and environment in several ways [23]. Heavy metals can damage energy levels, hinder the human body function, even damage organs such as liver, kidneys, brain, and blood, and cause Parkinson's disease, Alzheimer's disease. It can induce either acute or chronic health effects. Long-term exposure of such metals can even cause cancer [24]. Some heavy metals above the tolerable concentration can be found in the environment. For proper defensive measure to avoid excessive exposure, the knowledge of heavy metals is required [25]. Some important metals such as Pb, Hg, Cd, Cu, As, Cr, Mn, Al, and Ag with their effects on human health and the environment are discussed here in the below.

5.1 *Pb and Its Effects*

For decades, intensive focus has been provided on Pb in environmental health research. Pb is mined and used in industries and production for millennium, thus modern industrialization introduced mass production of household products, paint, candies, toys, ceramics, cans and other products in the twentieth century. For the past 60 years, Pb has been used as antiknock vehicle fuel additives, which is major source of environmental disruption worldwide [26]. The annual production rate of Pb is raising from 5.4 million tons currently. Around 60% Pb has been used in battery manufacturing, rest of them are used in solder, cable, gasoline additive and plastic production etc. Such productions are posing a considerable risk to individuals as well as the prevailing communities. Because of the risks, several developing countries have taken necessary actions which have limited the actual exposure of Pb over the last 25 years [27]. Several sources are responsible for Pb pollution in the environment such as gasoline and pigments, factory chimneys, ore smelting, pesticides and fertilizers, metal plating, battery wastes, soil wastes, automobile exhaust and so on. Pb accumulation pathway in human are diverse such as inhaling Pb dust, drinking Pb contaminated water, eating contaminated food (acidic juices and foods will liquefy Pb from the food and juice containers. Children playing with toys that

may contain Pb paint [13, 28]. Pb is easy to find and mine, has multipurpose. Pb undergoes corrosion and stain, delivers brightness to paint dye, gives support to be attached on the woods. Pb^{+2} is the most bioavailable form of Pb and successfully binds with sediments [27]

Several factors are responsible for the Pb exposure effects, such as water having low pH (acid rain water) can release more Pb from Pb solder plumbing in respect of high pH water [29]. In soil environment, Pb tends to persist in root vegetables like onions and vegetables such as spinach [30]. If people do not have enough Ca, Zn, or Fe in their diets, then there is a high possibility to absorb more Pb in their diets [28].

For the toxicity level measurement, humans have focused on the method development such as GFAAS (Graphite Furnace Atomic Absorption Spectroscopy), a technique used for surveillance and research, which can be used for the precise Pb measurement in blood (mg/dL). According to general dose, children and adults Pb exposure can create a great health problem such as coma, renal failure, effects on metabolism, intelligence (low exposure) and even death (at high dose) [31]. Children are particularly vulnerable to neurotoxic effects of Pb. According to epidemiologic studies, Pb exposure at low level in children (<5 years) was found in the range of 5–25 mg/dL which may hinder their intellectual development [28]. Because of that Centers for Disease Control (CDC) has lowered the allowable concentration of Pb in children blood ranging from 25 to 10 mg/dL. And it is also recommended that children from 6 months to 5 years old must do universal blood Pb screening [32].

Impacts of Pb on Human Health Even at markedly low level exposure, Pb is very viral for humans. Pb can cause both chronic and acute health effects depending on the dose and exposure condition. Pb mainly targets the nervous system, hematopoietic system and renal system, thus causing anemia, neurological, cardiovascular, renal, gastrointestinal, hematological, and reproductive effects. Through blood examination, Pb exposure to human can be measured. Pb tends to persist in the bones in re-mobilized form hence can cause Pb exposure late in the individual life [2]. Primary sources of Pb exposure are industrial dust and fumes inhalation and contaminated food consumption. Inhalation is one of the most prominent exposure pathway for human triggering point source pollution such as Pb contaminated sites and generated waste from production contains Pb which is then burnt. Another major source of Pb pollution is drinking contaminated water [28]. Home dusts can contain Pb paint which can be inhaled by both adults and children and ingested by children through eating behavior. Pb can have several deleterious effects on human health such as by accumulating in teeth and bones, Pb can persist there and can act as transporter of Pb in the bloodstream because half-life of Pb is around 20 years [4]. Pb mainly targets the bone marrow and brain as reservoir. So, Pb toxicity is much more severe if the diet is calcium deficient. There is no safe level for children. By measuring Pb concentration in blood, Pb exposure can be evaluated. Around 250 parts per billion (ppb) was taken into account as safe level till 1970. And then according to the revised recommendation, the safe level of Pb was checked from 50 to 100 ppb [12]. Pb has some neurological impacts also such as hyperactivity, imperfect attention span, and low IQ in children. Pb interferes with Ca transportation

in the neuron membranes. The linkage between Pb exposure and cancer is yet to be evaluated though more studies are needed to address the probable linkage between Pb exposure and several cancers [33].

Impacts of Pb on Aquatic Organisms Pb can be found in water up to 500 ppb injures algae. Pb obstructs the necessary enzymes to perform photosynthesis, lessen the absorption capacity of water, inhibits growth (greater than 50 ppb injures fishes) [12].

Impact of Pb on Animals Pb creates poisons for animals, which is termed as avian plumbism for birds. This disease is caused by high concentration of exposure in animals. Pb enters into animal's body through several processes [2]. Pb is toxic for several organs such as kidneys, heart, bones, hematopoietic system, nervous system, and reproductive system. Pb also affects the red blood cell formation by inhibiting aminolevulinic acid dehydrogenase (ALAD). Pb affects the enzymes of sulfhydryl group and erythrocyte thiol contents. It is viral for domestic animals such as cattle, dogs, and small animals. In animals, Pb poisoning can be acute and chronic which can readily cause death [19].

Physiological and Biochemical Impacts of Pb Pb also interferes in the enzymatic process for hemoglobin synthesis. Pb causes birth defects, kidney dysfunction, anemia (usually found in children having Pb concentration > 400 parts per billion in bloods). Around 1,200 toys were tested by using X-ray fluorescence analyzer. It was found that Pb levels were at 12–23 ppt in weight [10].

5.2 Hg and Its Effects

Hg is a naturally occurring metal which is an odorless liquid, colorless as vapor and has silver-white shiny feature. It is very viral and also bioaccumulative. It has severe impacts on the environment, particularly in the water environment. Primary sources of Hg pollutions are some man-made activities such as wastewater discharge, incineration, mining, agriculture, and so on [34]. Hg can be toxic for biological system even if they prevail in trace amount. Hg is used in several activities worldwide such as: in chlor-alkali 13%, batteries 9%, dental amalgam 9%, electronic equipment (5%), vinyl chloride monomers 21%, lamps (4%), measuring devices 9%, gold mining 22%, and others 8%. Hg toxicity is based on the form in which it accumulates in body such as elemental form, organic or inorganic form (alkyl-Hg compounds: methyl-Hg, dimethyl-Hg, and ethyl-methyl Hg). Hg remains in nature in these forms: elemental, organic, and inorganic Hg, having their own different toxicity levels. These three forms can be found in water environment such ocean, river, lakes where it is taken up by the microorganisms and converted to methyl-Hg within them, thus causing bio-magnification and aquatic environment disturbances. Human methyl-Hg exposure mostly occurs due to consuming these contaminated aquatic lives [15]. In case of methyl-Hg (potential neurotoxin), ingestion of

contaminated food is one of the major reasons of Hg toxicity exposure, mainly for fishes. About 80% of inhaled elementary Hg vapor is accumulated in the lungs tissue where they enter in the blood-brain barrier causing neurological and renal effects [35]. Neurological effects are considered as hindering human brain development. Though elemental Hg ingestion does not cause high level of toxicity but deaths have been recorded. Elemental Hg vapor inhalation has caused some severe symptoms such as insomnia, memory loss, thyroid, headache, shivering, also damages kidney [19]. Also, organic and inorganic Hg toxicity can be triggered by using fairness creams, soaps, and medicines. Hg passes easily through the placental barrier and blood-brain barrier causing severe exposure during pregnancy. According to International Agency for Research on Cancer, methyl-Hg is regarded as a potential carcinogen [7].

Hg Speciation Speciation of Hg can be in various forms such as elemental Hg or metallic Hg (Hg^0), inorganic Hg (Hg^{+2}), organic Hg (methyl-Hg). As bacteria (methylate Hg^{+2}) at water-sediment interface, methylation is forwarded by low pH and high dissolved organic carbon. Methyl-Hg (CH_3Hg^+) is the most persistent, lethal, and lipophilic form [12].

Impacts of Methyl-Hg on Fish Fishes are relatively impassible to toxic effects of methyl-Hg and can endure up to 10 times as much methylmercury as humans. Methylmercury storage in muscle tissue can detoxify methyl-Hg. If the levels of methyl-Hg are high, then unfavorable conditions may arise such as decreasing rates of egg hatching, impairing growth, and development [15].

Impacts of Methyl-Hg on Human Health Hg exposure may cause Alzheimer's disease [36]. This disease is considered as one of the top four death causing diseases, particularly responsible for mortality in the USA. This disease has affected over five million people, which will increase to 16 million affected by 2050 [37]. Methyl-Hg exposure may cause autism spectrum disorder which is a neurological disorder [17]. Several impacts can be seen due to methyl-Hg exposure such as memory loss, weak muscles, hand paralysis, disability in eye-hand coordination, vision and speech loss, impairment in consciousness. Children are at higher risk of methyl-Hg exposure, birth defects, cause cancer, prolonged exposure can damage kidneys even death [2]. Methylmercury toxicity mechanism in human body and affected organs (critical) has been illustrated in Fig. 5.

Impact of Hg on Animals Hg has detrimental effects on neurological and reproductive systems of wildlife. This effect has been for a while as contaminating source of freshwater bodies [12]. Hg enters into the animal's body, persists in the tissue for prolonged period, affecting their physiology. Fish from the water body, the birds (eagles and loons) which eats these fishes all are interconnected in this process [5]. A recent study by New York State scientists and other researchers in the Adirondack region reiterated this problem by showing that common loons (below) with high Hg levels exposure produced fewer off-springs (chicks) [18].

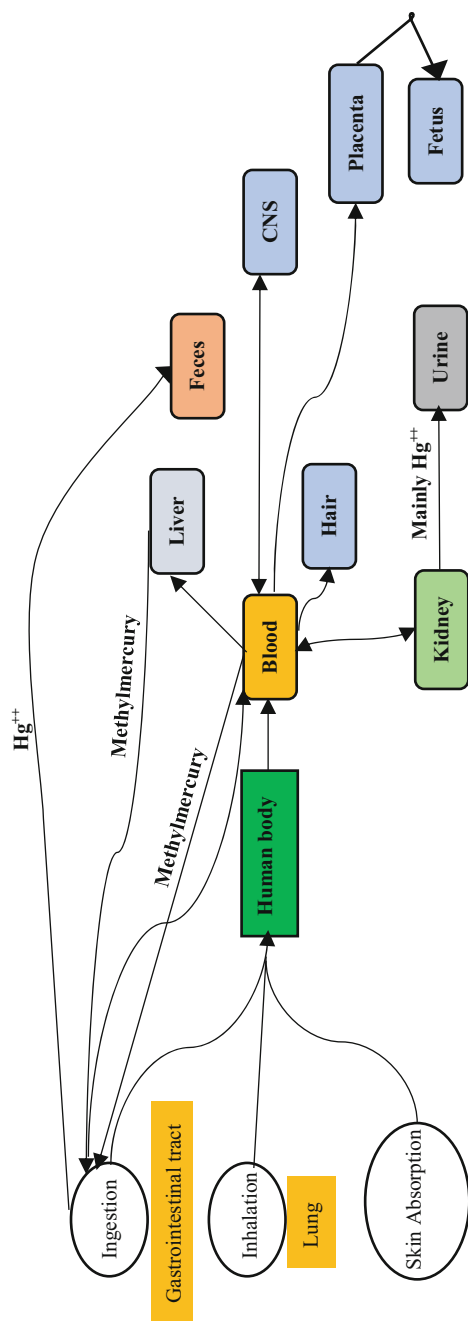


Fig. 5 Methylmercury toxicity mechanism in human body and affected organs (critical)

Minamata Bay Incident In 1907, Chisso factory near Minamata Bay started to produce acetaldehyde and vinyl chloride. And then in 1932, mercuric oxide (HgO) catalyst started to be used in production. Because of this continuous discharge, around 150 tons of Hg was discharged from the period of 1932 to 1968. Hg was present in that the bay in the form of bacteria methylated Hg^{+2} . Minamata Bay had many fishes, so people and seabirds ate those fishes from the bay. Methyl mercury concentration is millions of times stronger in top food chain than water. As a result, such disease called “Minamata disease” was occurred. In 1956, a complete linkage between the Minamata disease and methyl mercury was identified [38].

5.3 Cd and Its Effects

Cd is not such crucial element for human biological functions. Cd exposure has some effects on human health and ecosystem [39]. Mammal species can be exposed to Cd through inhalation (tobacco smoking) and ingestion pathway. Cd mainly targets renal and pulmonary system. Major health impacts from Cd exposure were recorded through dietary exposure. These exposures can cause kidney, lung, and bone damage [40]. Around 90% of Cd exposures through dietary intakes recorded for non-smokers. Cd can be viral for animals, organisms, and plants. Cd deposited in toxic form in the environment causes bioaccumulation in the kidneys and liver of both vertebrates and invertebrates. Cd can enter into the environment from various man-made sources. Wastewater is one of the notable sources of Cd contamination in the environment [41]. Industrial air emissions and worldwide use of fertilizers in soil for agricultural activity are also some emerging sources of Cd. Iron and steel production (20% Cd exposure), fossil fuel (33% Cd exposure), waste incineration (2% Cd exposure), cement, and other (1.2% Cd exposure) such human activities are responsible for human Cd exposure [42]. Plants such as rice and tobacco which are grown in contaminated soils can take up Cd and Pb through inhalation and human dietary exposures. Furthermore, Cd contaminated soil can cause human exposure when it is disturbed, and the Cd dust inhaled by humans [43].

Cd Toxicity Cd hinders Zn metabolism, disturbing Zn containing enzymes. Thus, gastrointestinal absorption occurs and ultimately replaces Zn in metallothionein. It also binds with Ca which may cause osteoporosis, Cd deposition in bones may cause hypercalciuria. It decreases Cu concentration in liver and decreases ceruloplasmin concentration in plasma. It also binds with Fe, decreases the concentration of hemoglobin and hematocrit, thus causing [44]. Cd exposure toxicity has been illustrated in Fig. 6.

Effects of Cd on Human Health Cd can cause acute and chronic health effects such as anemia, deformation in skeletons, loss of bones, kidney dysfunction, obstructs necessary enzymes to perform absorption in tubules of kidney. It can be a potential carcinogen on higher dose [46]. Diets such as rich in red meat, sea fishes can often contain high Cd intakes, cause kidney and liver damage, elevated

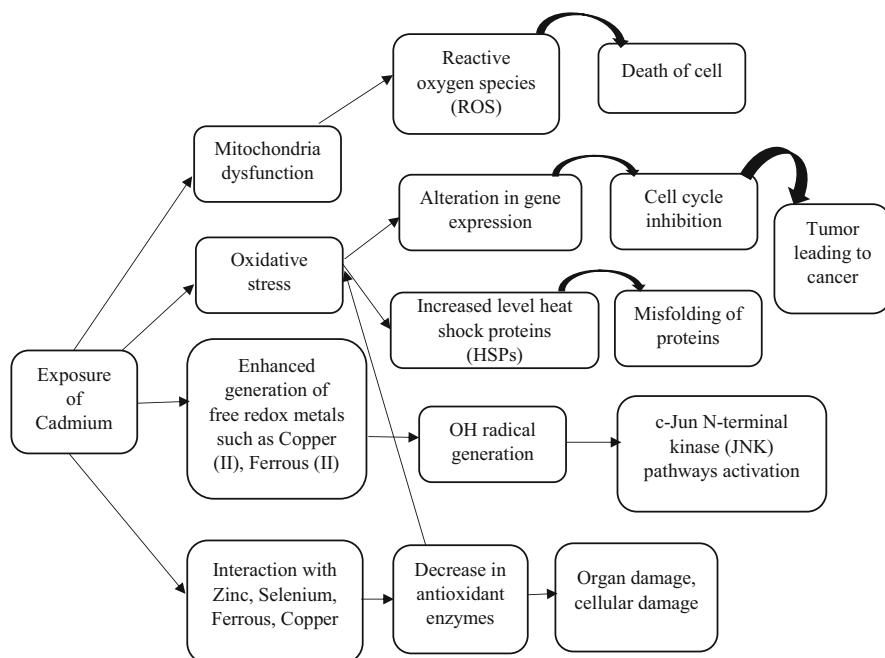


Fig. 6 Cd exposure toxicity mechanism in human body (Modified after [45])

frequency of stone (kidney) formation. Smokers are marked as the higher risk bearer than people with less iron levels. The secondary health effects of Cd are skeletal damage which is caused by the damage in kidney through Cd exposure [47].

Effects of Cd on Aquatic Organisms Cd can also affect aquatic organism's health: Such as Cd impairs the growth of aquatic plants, deformities in skeleton of fishes (in bones Cd replaces Ca), reduces the survival rate of shell fish, as well as causes kidney tubules dysfunction in fishes [46].

Effects of Cd on Animals In animals, prolonged inhalation or ingestion exposure of Cd causes detrimental effects on the liver, lung, kidney, bone, nervous system, immune system, and blood. Cd can affect the bone tissues on young animals [43].

Cd and Itai-Itai Disease Kamioka Mine situated 40 km away of Fuchu Town had discharged untreated effluent containing Cd to the rice paddies from 1920. Rice plants absorb Cd spontaneously. So, people of the area consumed those contaminated rice for around 30 years and were disclosed to 600–1,000 mg of Cd everyday which exceeds twice the toxicity level. In 1950, people from Fuchu Town, Japan (near Toyama City in Jinzu River Basin) confronted several pains in joint, muscle, and bones, also they faced severe dysfunctions in kidney. Even caused death of some people living there [48].

5.4 *Cu and Its Effects*

Cu is categorized by the USEPA as Group D carcinogen though it has not been listed in new cancer classification category. Cu is an essential natural metal, needed in trace amount (5–20 ppm) as nutrient [5]. Cu presents in soil at an average concentration of 50 ppm. It is found in plants and animals. It acts as an essential nutrient for human and for animal where it is needed in small quantity. It is an important component of human body because it reacts with iron and creates red blood cells in body. It is a component of enzymes which helps to form hemoglobin and hemocyanin and also supports carbohydrate metabolism. It is responsible for functioning of more than 30 enzymes. It helps to grow healthy hair in humans. Moreover, at concentration of more than 20 ppm, Cu^{+2} is viral [49]. The chief sources of Cu releasing in the environment are mining, sanitary fittings, containers, smelting, birth control pills, and Cu refining, industrial production such as wires, pipes, and fossil fuel combustion. Water line pipes are usually made of Cu and bath settings also are made from bronze and brass alloys which comprise Cu [12]. The chief source of Cu in drinking water is Cu leaching from water pipes and bath settings because of acidic water. Even Cu in water leaves some blue-green spots in bath settings. The other primary sources are as pesticides in agricultural field, used to remove algae from waterbody. Some metabolic studies recorded that oral ingestion of Cu ranges from 24 to 60%. The absorption capacity of Cu depends on some factors such as dietary condition, Fe and Zn presence in food. No studies have been conducted to measure the skin and inhalation exposure of Cu. Though few studies depicted that skin absorption of Cu was very low, the Recommended Allowance (RA) of Cu for adults is 0.9 mg/day. The highest safe level of Cu intake for a lasting period of time (chronic exposure) is 10 mg/day. Metals, beans, cocoa, shell fish are rich in Cu [50].

Toxicity of Cu Cu is able to bind with sediments and organic matter in soil. Cu is highly viral for aquatic organisms. Adrenaline, aldosterone, and cortisol are released due to stress. Adrenal gland is also affected by stress, retaining Cu and reduces Zn. Aldosterone mechanism follows by Na and Cu which secretion increase the reduction of Zn and Mg. Zn is important for toxic heavy metal removal (Cu). Mood swing and mind can become troubled when brain starts to be saturated by Cu. Cu saturation may limit the presence of important neurotransmitters in brain which helps to keep brain Cu functioning static [51]. Cu binds with necessary protein-enzymes such as ceruloplasmin and metallothionein to enter into the cell and mitochondria use these proteins in the Krebs cycle to form ATP. Liver mainly receives adrenal glands signal to form these proteins. Any dysfunction in adrenal glands and liver may relate to unbound and release Cu thus Cu will start to accumulate in blood [12]. Cu may also accumulate in lysosomes, mitochondria causing necrosis and cellular degeneration. Higher Cu level in blood may cause erythrocyte membrane weakness causing fragility thus hemolysis (hemolytic crisis). Cu may cause hemoglobin oxidation forming methemoglobin (cannot carry oxygen). Fish species such as shell fish and fin fish are around ten to hundred times more susceptible to Cu than mammal species [12]. Algae are more sensitive to Cu mammal species (around

1,000 times). When dissolved organic carbon is present in the waterbody then Cu is less viral. The Cu level in blood, hair, liver biopsy are some reliable indicators of copper toxicity. Hemoglobin level, serum copper, and serum ceruloplasmin can be helpful for the diagnosis, as Cu accumulates deep in the liver and brain [5].

Impact of Cu on Human Health and Animals Cu plays an important role in human body function. For example, in bones and connective tissue, Cu is necessary to bind with Ca to form connective tissue and repair them all. Such imbalances may cause osteoporosis, skin, nails and hair damage also. Cu plays an important role in cell's energy production. Cu is required in the electron transport system which is termed as energy cycles final stage and produces cellular energy. Any imbalances here may cause depression, fatigue, and low energy Cu [51]. For immune system, Cu must be in balance with Zn. Any imbalance may cause infections such as yeast and fungal infections. Cu can affect thyroid gland, glandular system, adrenal system. Cu imbalance may cause premenstrual syndrome, cysts, miscarriages, sexual malfunction, even hyperthyroidism, Wilson disease, Menkes disease, and Grave's disease [52]. These all can occur because of stress and Hg exposure as well. It may affect reproductive system, for example Cu is related to estrogen metabolism which is necessary for pregnancy and women's fertility and man's potency. It can affect the nervous system also. Cu increases the production of the neurotransmitters such as epinephrine, dopamine, and norepinephrine. Cu imbalance may affect psychological and neurological conditions such as loss of memory in young people, schizophrenia, anxiety, and depression. Cu deficiency may cause anemia, hindering white blood cells formation, osteoporosis in infants and children, and defects in tissue, skeletal problems. There is relatively low copper toxicity in humans because of Cu detoxification process by metallothioneins in kidney and liver [53]. The drinking water standards for Cu are developed depending on the taste, not on the toxicity risk. Acute or short-term effects of Cu are: more Cu ingestion may cause temporary gastrointestinal distress with nausea, abdominal pain, and vomiting. High Cu dose can damage liver, even can cause death. High level Cu exposure may cause red blood cells decimation, ultimately causing anemia [49]. Chronic or long-term effects of Cu are: kidney and liver damage (high dose), mammal species have versatile mechanism to store Cu in the body that they are usually protected from over plus dietary copper levels. Wilson's disease is a genetic inherited disorder in which Cu stores in liver. Liver toxicity has some severe symptoms such as jaundice, swelling, headache usually does not appear at young age [2]. It can be a potential carcinogenic, causing cancer. Studies have showed that Cu has high cancer risks, especially in workplaces, as workers are exposed to chemicals having carcinogenic capacity. Though in animal, Cu cancer risk has not been found. Cu has some reproductive and developmental effects also. Though the developmental effects have not been recorded in human but in animals some effects have been occurred such as animal growth and developmental processes can be hampered at high Cu dose, hinder bone formation, lessen the body mass and litter capacity [51] Copper toxicity mechanism in human body and their outcome have been illustrated in Fig. 7.

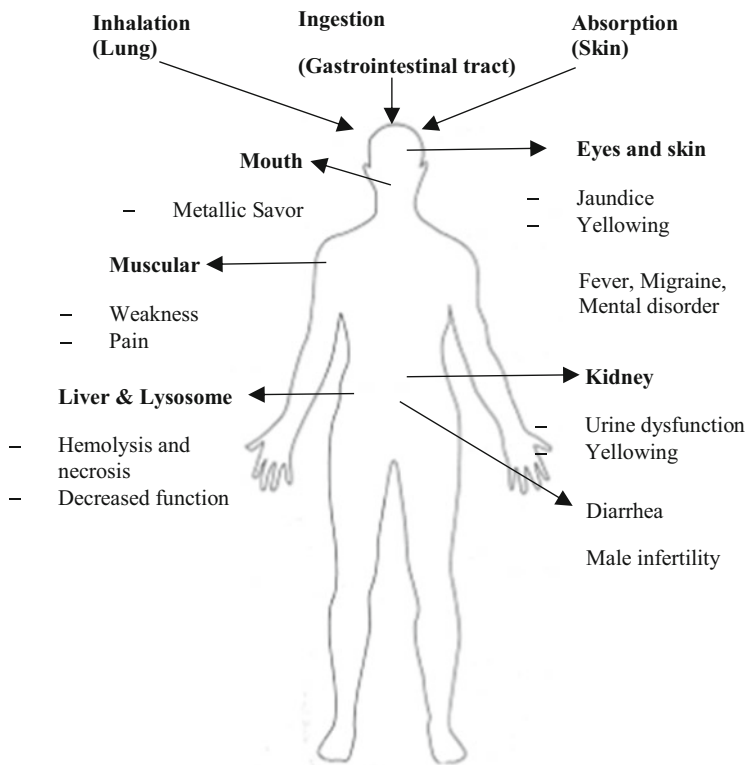


Fig. 7 Copper toxicity mechanism in human body and their outcome

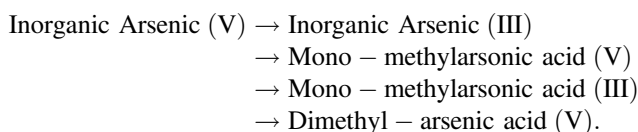
Impact of Cu on Fish Fish species such as shellfish have some considerable individual effects of Cu such as it lowers the metabolism rate of clams especially in estuaries. It also affects shell fish population by lowering the egg and sperm production in sea, exposing to Cu concentration around 10–20 ppb [12]. In fin fish, Cu inhibits osmoregulation by intervening the sodium uptake process in the gills. Cu also has some neurotoxic effects such as it meddles with olfaction, as a result disrupted olfaction process obstructs migration, salmon habitation, and predator avoidance. Cu has effects on their food intake and growth, damages kidney, lessens the survival rate of juvenile fish. Cu has some sub-fatal effects on rainbow trout also. Stress in rainbow trout occurs at relatively low Cu exposure (1.4 ppb), causes hyperactivity in population, increases cortisol level in bloodstream, in liver it forms metallothionein [54].

Cu Effects on Ecosystem Cu limits the algal growth, responsible for death of beneficial insects such as mayflies, causes emergence of insects which can undergo water pollution. These variations will have an impact on fish species appearances. Cu has continuing effect throughout the ecosystem [5].

5.5 *As and Its Effects*

As can be present in three allotropic forms: grey, yellow, and black. The stable form is silver-gray and brittle-crystalline solid. As rusts easily in air and at high temperatures, thus, it forms As trioxide. Non-metallic form of As is not that much reactive. As and its compounds are widely used in special type of glass manufacturing, also in wood preservation [2]. As gas AsH_3 is an important dopant gas in micro-chip industry, although it is extremely viral which requires strict guidelines. China is the chief exporting country of As worldwide. World resources of As in Cu and Pb ores are around 10 million tons. In the nineteenth and twentieth century, As and its compounds were used in medicine. As is found in small concentration naturally on Earth's crust. It is found in minerals and soil and thus enter into the air, land, and water through run-off and dust. As originates from various sources such as microorganisms that release volatile methyl-arsines to around of 20,000 tons per annually and from volcanoes that release about 3,000 tons of As annually. Anthropogenic activities are more responsible for such As pollution. By burning fossil fuel, man-made activities release around 80,000 tons of As annually. As is known as potential poison though it is needed in trace amount for human (maybe) and animals. The required intake of As is around 0.01 mg/day which is as much as low. As is a hard component that can't be turned to water-soluble form or volatile form easily. As is an unstable metal, so for that high concentration does not actually stay at a site for a longer period. Despite this characteristic, it might have some negative impacts too because it disperses easily. Because of human encroachment activities, such as melting and mining, the As forms, which were immobilized, have started to mobilize now. As a result, they can be found in many places where it is not supposed to be found. Many As forms may be found in combination with minerals and sulfur such as Arseno-pyrite (AsFeS) and orpiment. From As's oxide form, the worldwide production of As is around 50,000 tons annually, excessively used in industries [55].

As Toxicity As toxicity may arise from bio-transformation activity, where detrimental inorganic As compounds are methylated by microorganisms such as bacteria, algae, fungi, and even by human forming mono-methylarsonic acid (MMA) and dimethyl-arsenic acid (DMA). In this process, inorganic As is enzymatically transformed to end metabolite (methylated arsenicals), which is responsible for chronic As exposure [18].



In bio-methylation process, the end products are mono-methylarsonic acid and dimethyl-arsenic acid. These compounds are excreted through urine, which indicates chronic As exposure. Under specific conditions, mono-methylarsonic acid (MMA)

in the form of MMA (III) generally is not excreted and stays as intermediate product in the human cell. It is highly toxic compared with other forms, which can ultimately cause As related carcinogenesis [56].

Effects of As on Human Health As has some toxic effects though inorganic form of As is found naturally. Humans can be exposed to excessive As concentration through eating contaminated food, inhalation of polluted air, and drinking contaminated water. Through skin absorption or skin contact with water and soil, humans and animals can be exposed to As [50]. Soluble form of inorganic As may have immediate toxic effects. So, ingesting large quantity can cause severe gastrointestinal problems such as vomiting, dysfunction in blood, impairment in nervous system, and even death. If not that deadly, these large doses may diminish blood cell formation, disruption in red blood cells formation in the blood circulation, liver enlargement, skin colorization, limbs sensation impairment and can cause brain damage. The interrelationship between As exposure and health effects is of great concern [33]. From the studies it is depicted that As causes high blood pressure, heart attacks, and other circulatory disease. Though in case of diabetes and reproductive effects, As sensitive is not recorded yet, it causes long-term neurological effects and causes cancer at sites other than lung, bladder, kidney, and skin. Also, it causes skin changes such as hyperkeratosis and colorization. These effects have been visible in several studies [50]. Dose–response relationships and As risks have been demonstrated in various studies. Drinking-water having As concentrations of 50 $\mu\text{g/L}$ can cause As related skin damage. Inhaling As through occupational exposure can cause lung cancer. It has also been recorded that the risk of As related health effects increased at cumulative exposure levels $\geq 0.75 \text{ (mg/m}^3\text{)} \times \text{year}$ (e.g., 10 years of exposure to a work area air concentration of 50 $\mu\text{g/m}^3$ As) [12].

In food, As can find in lower amounts, but in fish and sea food As concentrations can be high because in water fishes absorb As through discharge. Fishes that absorb high amount of inorganic As can be dangerous for human health. At workplace, people can be exposed to higher levels of As due to occupational exposure. Also, in houses (furniture), farmlands (pesticide use), people can be exposed to As. Inorganic As exposure may cause several health problems such as stomach irritation, less formation of red and white blood cells, lung irritation, skin type change. Also several studies have concluded that exposing to high amount of inorganic As may develop the chance of several cancer formation such as lymphatic cancer, lung cancer, skin cancer, and liver cancer. Also a very alarming exposure to inorganic As may cause skin irritations, increased infections, heart failure, miscarriages, infertility in women, brain damage, and more. Ultimately, inorganic As can cause DNA damage. A toxic dose of As oxide is considered as 100 mg. Organic form of As does not harm DNA or cause any cancer. But exposure to significant concentration of organic As can have impact on human health such as stomach aches and nervous system damage [57].

Effects of As on Plants and Animals Human interferences prolongs As cyclic process in the environment. As a result, huge amounts of As are being discharged in the environment, animals, and aquatic organisms. Pb, Zn, and Cu producing

industries may produce As [5]. In agricultural processes As can be released in the environment, once it is entered in the environment, it can't be removed, so the amount increases over time by both anthropogenic and natural activities. Thus, causing prolonged health effects to plants and animals everywhere. Plant absorbs As readily, in these foods, high concentration of As might be present. Inorganic As is very toxic. So, toxic inorganic As concentration is found in surface water which readily changes the genetic mechanisms of aquatic animals, especially of fish populations. This kind of toxicity is being generated by As accumulation in bodies of organisms that eat those fishes from freshwater. Generally, bird eats these fishes that have high concentration of As presence causing As poisoning to aquatic organisms, fish populations start to die and decompose [58].

5.6 Cr and Its Effects

Cr is a hard metal with silver-gray color. It does not rust in air, when it is heated, it forms chromic oxide (green). Cr is impermeable to oxygen. According to International Agency for Research on Cancer (IARC), Cr and its trivalent compounds have been listed within Group 3 (it is not classified as carcinogenicity characteristics to human). OSHA does not consider Cr as a carcinogen [2]. Cr is an essential metal that is found in coal, petroleum, steel, catalysts, fertilizers, pigment oxidants, and metal plating tanneries. Cr is used in industrial production such as electroplating, coating of silver mirror, metallurgy, paint and pigment production, dyeing catalyst, leather tanning, mold making for bricks, paper and pulp production. Cr in the form of Cr (IV) oxide- (CrO_2) is used to produce magnetic tape. As a result, the industrial activity plays a concerning role in Cr releasing in the environment causing harmful effects to human, plants, animals, and ultimately to ecosystem. Anthropogenic activities such as sewage disposal, fertilizer usage trigger the chromium release in the environment. As well as agricultural practices are responsible for the Cr contamination. In recent year, Cr in hexavalent form Cr^{+6} is severely responsible for environmental Cr contamination [12]. Cr is mined in the form of Cr which is FeCr_2O_4 ore. Cr ores are mined worldwide. Around 14 million tons of chromite ore are being extracted. Worldwide reserves of Cr ore are 1 billion tons [3].

- *Cr ions on Human Health:* Through breathing, drinking, eating or skin absorption, human can be exposed to Cr and its compounds. In air and water, Cr is found in lesser amount. In drinking water, its concentration is low also. But contaminated water might contain Cr (IV) or Cr (VI). The main route of Cr exposure to human body is through food that contains Cr (III). This form of Cr is readily found in fruits, vegetables, yeasts, meats etc. The way of food packaging, preparation, and storage may change the Cr quantity in food. Food storing in cans and tanks may increase the concentration of Cr in the food. Cr (III) acts as nutrient for humans and its deficiency can cause heart diseases, diabetes, metabolic activity disruptions. But human exposure to high amount of Cr (III) may

affect human health such as causing skin rashes. Unlike Cr (III), Cr (IV) is very toxic to human health. Especially at workplace, people working in textile and steel factories may expose to this compound. Also tobacco users have the highest chance of Cr (IV) exposure. This compound can cause severe health impacts such as from leather items, allergy and skin reaction may happen (skin rashes). Inhalation of Cr (VI) may cause nose bleeding and irritations. Some severe health problems of Cr (VI) are: skin rashes, liver damage, kidney damage, genetic mechanism alteration, immune system damage, ulcer, stomachaches, respiratory diseases, cancer (lung), and even death. The human health problems to Cr exposure depend on the Cr's oxidation form. Cr in its metal form has low toxicity. Cr in hexavalent form is very toxic. Some adverse health effects of the Cr (VI) form are: ulcer formations, nasal septum's mucous membrane perforation, bronchitis, edema, allergic reactions, skin irritations, dermatitis, and respiratory diseases (breathing shortness, nasal itchiness) [12, 59]. According to National Toxicology Program (NTP), Cr and its trivalent compounds can be considered as carcinogen. NTP provided evidence of Cr carcinogenicity in animals. Some forms of Cr that can show carcinogenicity are: Cr (VI): Calcium chromate, chromium trioxide, strontium chromate, and zinc chromate. Hexavalent form (Cr^{+6}) of Cr is the most viral, though some other forms of Cr such as Cr (III) compounds are less toxic and cause little or no health problems. On the other hand, Cr (VI) tends to be corrosive, thus cause swelling and redness of skin (allergic reactions) to the body. Furthermore, inhalation of Cr^{+6} may cause anemia, nose lining irritation, and nose ulcers. It may cause stomach ulcers (mostly in chromate worker), sperm damage in male reproductive system. Therefore high Cr^{+6} dose can cause severe respiratory, hepatic, gastrointestinal, and neurological effects and even death. High chromium exposure can cause inhibition of erythrocyte glutathione reductase, which readily lessens the ability to convert methemoglobin to hemoglobin. In both in vivo and in vitro experiments, it has been seen that in several ways chromate compounds can cause DNA damage and chromosomal aberrations and DNA transcription. Human can be exposed to higher dose of Cr (VI) through drinking water. Also, some potential evidences show that Cr can induce carcinogenicity to human, in animals chromium can cause stomach tumors [60].

5.6.1 Effects of Cr in Plants and Animals

Cr and its compounds differ in characteristics and cause effects on plants and animals. Through anthropogenic process and natural processes, Cr in the form Cr (III) and Cr (VI) enters in the soil, water, and air and ultimately in the entire environment. Steel, textile, and leather production industries are main responsible body for this high concentration Cr (III) exposure to living things. Thus, Cr level in the water has been increased by discharging industrial effluents in the water body [16]. Man-made activities such as coal combustion are also responsible for the high concentration dispersal of Cr in the air. Waste disposal will eventually increase its

amount in the soil. In the air, Cr is end to persist and then goes to soil or water. Cr readily attaches with the soil particles as a result Cr does not flow through the groundwater. Sediment would absorb Cr in water and produce unstable form. Finally, only smaller amount of Cr can be dissolved in water. Cr (III) is a crucial element for organisms which can disrupt sugar metabolism causing heart diseases, when the daily uptake is too low [61]. Cr (VI) is dangerous to organisms. Cr (IV) can change the genetic mechanisms and can cause different type of cancer. Crops have some system which regulates the Cr concentration in a significant way that it remain at low level and did not cause any impairment. If there are higher concentrations of Cr in soil, that will eventually increase the Cr concentration in crops too. Cr uptake of crops is influenced by soil acidification process. Plant usually takes up only Cr (III). This is an important chromium form, but negative effects can occur when concentration will be much higher [5]. In fish, Cr does not accumulate in their body. Metal products disposal may trigger the high Cr concentration in surface water. That can damage fish gills present at the point of disposal. In animals, Cr can cause severe health hazards such as birth defects, infertility, weakness, ulcer, tumor, respiratory diseases, and disability to fight disease [3].

5.7 Mn and Its Effect

Mn is a very important element for iron and steel production. In present days, steel making comprises 85–90% of total demand and other most of the demand. Mn is the basic component of cheap stainless steel formation and widely used in aluminum alloys. Mn in the form of Mn dioxide is used as a catalyst. Mn is widely used to de-colorize glasses and create violet color glasses. Potassium permanganate is one of the strong oxidants and is used as disinfectant widely. Manganese oxide (MnO) and manganese carbonate (MnCO₃) are used in fertilizers and ceramics and MnCO₃ is used especially for making other Mn compounds [1].

Mn is a crucial element for all and found readily in soils, where it remains as oxides and hydroxides, and it moves through its different oxidation states. Mn's principal form is pyrolusite (MnO₂) and also present in the form of rhodochrosite (MnCO₃). In around 25 million tons of mining activities, five million tons of the metal are being recovered, and reserves exceeds around 3 billion tons metal. Some organisms, such as diatoms, mollusks, and sponges, store manganese. Fish can store up to 5 ppm Mn and mammals can store up to 3 ppm in their tissue, though they have already around 1 ppm [2].

Effect of Mn on Human Health and Animals Mn is one of the three toxic essential trace metals, which is not only necessary for survival but also can be toxic when high Mn concentration will prevail in human body. When people do not make up to the recommended daily allowance (RDA) or exceed the limit, in both conditions it starts to decrease the health condition. Human can be exposed to manganese through several routes such as eating food, for example eating spinach

or tea or the food which contains highest concentrations of grains and rice, soya beans, oyster, eggs, nuts, olive oil, and green beans. After Mn absorption in the body, it will transport to the blood and then liver, kidney, pancreas, and finally to the endocrine glands. Mn has severe impact on brain and respiratory tract. The symptoms of high dose manganese exposure are: forgetfulness, dullness, nerve damage, and hallucinations which can cause Parkinson's, bronchitis, schizophrenia, paralysis, sleepiness, emotional disturbance, insomnia, headache, and lung embolism. Especially impotence in men can occur if men are exposed to Mn for prolonged period. Other alarming health effects of Mn are: glucose intolerance, blood clotting, fatness, skeleton disorder, birth defects, hair color changes, depressed cholesterol level, neurological effects. Long or chronic health effects of Mn can be triggered by dust and fume inhalation. From these kinds of diseases, nervous system becomes weak and may cause physical disability. Severe pneumonia and other respiratory infections have been recorded among workers who are exposed to Mn dust or fume and experimental suspicious tumorigenic agents [62].

So, Mn is a crucial metal for body but in recent days it has been listed as global toxic metal. Mn was introduced as gasoline additive in the form of methylcyclopentadienyl Mn tri-carbonyl (MMT). MMT is considered as occupational manganese hazard and connected with Parkinson's disease with several syndromes such as tremor, gait disorder, cognitive disorder, and postural instability. High dose of manganese exposure can cause neurotoxicity. Mn can cause neurological disease termed as "Mn" by forming Mn rigidity, tremor, mass formation, mood disorder, and memory dysfunction. The symptoms of Mn are quite similar to the symptoms of Parkinson disease. Therefore, the main differences between Mn and Parkinson disease are the symptoms and disease progression and also Mn is not susceptible to levodopa (L -DOPA) administration [2].

Effect of Mn on the Ecosystem Mn and its compounds are found in the soil and water as small particles. Also they can be in the air as dust particles. They tend to settle on the land within few days. Mn and its compounds are released in the environment through industrial activities and fossil fuel burning. From the human exposure, manganese can penetrate into the surface, groundwater, and sewage water. Mn accumulates in the soil easily because it is used as pesticides [63].

Effect of Mn on Animals For animals Mn is an important element for animals of around 36 enzymes, used for carbohydrate, fat, and protein metabolism. Even at low level exposure, Mn can interfere with bone formation, reproduction and growth of animals [64]. Ultimately it could be viral for animal even at low level. Mn compounds can cause brain, lung, and liver damage, vascular disturbances, low blood pressure, inhibit the development of animal fetuses. Then Mn skin absorption may cause tremors [8]. From several studies on test animals, it has been depicted that acute Mn poisoning can develop tumor in animals [5].

Effect of Mn on Plants In plants, after the uptake from the soil, Mn ions are transported to the leaves. Even at low level Mn absorption, it can cause disorder in plant mechanisms. Mn plays an important role in division of water into hydrogen

and oxygen for plant uptake. Mn may trigger both toxicity and deficiency problems in plants. Mn deficiency is common in low pH soil. Both deficient and high toxic level of Mn in soils may cause cell wall swelling, leaf withering, and creating brown spots on leaf. The interconnection between deficient and toxic concentration can be measured by detecting optimal Mn concentration for plants [11].

5.8 Al and Its Effects

Al has only one naturally occurring isotope which is Al-27 and that is not radioactive. Al is a poor metal, mainly found in the form of ore bauxite and is versatile for its light weight, strength, and counteraction capacity to oxidation. Meanwhile, Al is oxidized but remains in unstable form than most other metals. Al is used in industrial productions of various products which is very significant for the worldwide economy. Metal recovery from scrap through recycling has become a vital element of the Al industry. Metal industrial production is around 20 million tons per year and also the same quantity is recycled. The Al ore reserves are around 6 billion tons worldwide. Al is used as building material, electrical transmission wire, in packaging, transportation material because of its durability, strength, and lightweight. Al is also utilized as structural components which is emergent for aerospace industry. Al is the second most usable metal after iron. The pure aluminum usually forms alloys with other metals such as Cu, Mn, Zn, and silicon. Al is highly conductive and cheap comparing with Cu. Al was first used for household electrical lining in 1960 [2]. Al is also used in telescope mirrors and modern mirror as thin reflective coating [64]. But Al tends to be sensitive towards thermal expansion as well as can't sustain pressure, because of these characteristics galvanic erosion occurs. The most recent Al technology development is the Al foam production through adding to molten metal usually a metal hybrid, from which hydrogen gas is released. So, for this phenomena, the molten Al need to be thickened by consolidating silicon carbide or Al oxide fibers before this is performed. Thus this Al foam is widely used in space shuttle and traffic tunnels [5].

Effect of Al on the Environment Al is abundant in the earth's surface, present in the percentage of around 7.5% to 8.1% of earth crust. Al can't be found readily in its free form. Al in the form of Al hydroxide provides benefits to the soil properties. Al being a reactive metal is extracted from its ore, Al oxide (Al_2O_3). Comparing with other metals, Al is quite hard to refine because Al is oxidized very easily and that oxidized compound is very stable. And because of these characteristics, Al is used in several applications. It can cause acidifying problems. Al oxide (crystal form) helps to form gemstone which is called as "Corundum." Al oxide with other metals creates some versatile compounds such as with cobalt it makes blue sapphires and with chromium it makes red rubies, with iron traces it makes topaz which is a yellow Al silicate. They all can be easily produced artificially [65].

Effect of Al on Human Health Due to the abundance, human can expose to Al at an alarming rate. At high concentration exposure, Al can cause health disorders. Al's water-soluble form (ions) such as Al chlorine may cause detrimental health effects. In humans, Al exposure may occur through skin absorption and ingestion such as eating contaminated food. Some chronic or long-term effects of Al are: central nervous system damage, memory loss, acute trembling, dementia, and much more. Al is considered as occupational hazard causing metal, as it can create water-soluble form. Workers who are exposed to Al and are being used in production procedure may undergo lung disorders. Also, pulmonary diseases and kidney damage may occur by inhaling Al oxide powder and Al dust. Inhalation of silica and iron oxide air can cause severe diseases such as "Shaver's disease". Especially, in kidney dialysis process, Al can also penetrate in kidney patient's body [66].

Effects of Al on Animals and Plants Al can store in plants and can create health hazards for animals which take these plants as food. In acidic lake, Al concentration is high. In high acidic condition, fish and amphibian population cannot sustain because of the reaction of Al ions with fish protein of gill and embryos of frog. It has been observed that high Al concentration has impacts on fishes, birds, and other animals which take these insects and fishes and also on the animals that take in Al through air inhalation. Animals that take in Al through air may incur lung disorder, loss in weights, and activity downfall [2]. Another notable adverse effect of Al in environment is the Al ions that make reaction with phosphates, thus there are lesser amounts of phosphate available for water organisms to intake. Also, in groundwater of acidified soil, Al concentration can be found at a higher level. Thus indicating, Al can injure the tree roots that are connected to groundwater [27].

5.9 Ag and Its Effect

Ag is a rare metal in the Earth crust as the 67th naturally abundant metal. Pure Ag is very ductile, malleable, and lustrous form of Ag. With nanotechnology development, Ag nanoparticles (Ag-NanoParticles) are being used widely in various sectors [67]. Ag is not chemically active but it can react with nitric acid and sulfuric acid. It is stable in water. It has greater cost and highest electrical conductivity. In crude oil and steam well, Ag concentration can be high. Ag can be found as monovalent in its every form, the predominant forms are its oxide, fluoride, and sulfide. It can react with hydrogen sulfide in the air and creates tarnish (Ag sulfide). Ag is a precious metal, especially Ag nitrate is widely used in electronic manufacturing, appliances, mirror and jewelry making, and photography. Ag bromide and Ag iodide both are used from the very beginning of photography era, also applicable for black and white image. It is used as a catalyst in several oxidation reactions. Ag and its compounds are also used in dentistry and battery manufacturing [8].

Anthropogenic activities can increase the concentration of Ag in the environment such as mining of metal, photo-processing, hazardous waste disposal, smelting, and

lots more. Several studies have demonstrated that the few forms of Ag are much more toxic than other metals, because both soluble and insoluble forms of Ag can cause toxicities which also include the occurrence of occupational exposure [5].

Effect of Ag in the Environment In mineral rich soil, Ag can be found in high concentration around 44 ppm. Ag can be absorbed by plants in the range of 0.03–0.5 ppm. Ag metals are natural crystals and its deposits are found worldwide. The major Ag ores “Stephanite” and “Acanthite” can be found in Bolivia, Mexico, and Honduras. Refining of several metals can form some by-product in the form of Ag compounds. Around 17,000 tons of Ag are mined annually [68].

Effect of Ag on Human Health Ag and its compounds are being used worldwide which allows the Ag exposure to human health through various routes such as inhalation, ingestion, and skin absorption. According to ATSDR (2008), human can be exposed to Ag dust or fume through occupational exposure. Skin contact occurred through using different kind of burn creams and jewelry. Through needles and dental amalgams, Ag can also enter into human body. Soluble Ag compounds are more easily absorbed than insoluble Ag [69], causing potential health hazard. Chronic exposure to Ag mainly affects some key organs of human body such as kidney, eye, liver, lung and brain, and causes damage to them. Similarly, prolonged exposure to Ag nitrate can lower blood pressure and lower respiratory rate. Ag in its salt form, AgNO_3 , can be lethal in the concentrations of more than 2 g. Soluble Ag compounds have the ability to accumulate the muscle and brains in smaller quantity [70]. Soluble Ag compounds are absorbed by tissue slowly (prolonged period), creating blacking pigmentation on skin, which termed as “Argyria.” Such permanent pigmentation developed due to argyria (on skin) and argyrosis (on eyes). This is mainly the result of inhalation and Ag solid material attack on the skin and eyes. It can be severe corneal harm, when it comes to eye contact. Through skin absorption, it can cause skin irritation. This disease can also be occurred by using medicine containing Ag and colloidal Ag. Localized agrarian caused direct skin absorption of Ag, where it enters in the body in very slight amount through sweat glands. This deposition causes small round patches (light brown or black color) on the skin. It mainly affects the hands, mucous membranes, and eyes [71]. In eyes, Ag fine particles may enter through air and form localized agrarian over time. Generalized agrarian causes skin, eye, and nail pigmentation through Ag compound (AgNO_3) ingestion, inhalation, and skin surface contact. Once it enters into the body, it passes through the bloodstream and accumulates in the several tissues. Sun-exposed areas are more vulnerable to these types of exposure. Long-term Ag exposure can cause allergy and dermatitis. Inhalation of Ag vapor can cause throat or lungs irritation, headache, breathing difficulties and respiratory problems, unconsciousness, confusion, drowsiness, weakness, and even death [71]. Excess concentration of Ag may be very detrimental. Comparing with other route, ingestion of Ag is much hazardous for health because it can accumulate in the lung for prolonged period. Thus, it can cause anemia, pneumonia, narcosis, nausea, vomiting, stomachache, and diarrhea. Long-term overexposure can cause permanent nervous system and brain damage. Continuous exposure of methyl ethyl ketone through inhalation can form hexane

(neurotoxin) [67]. According to ATSDR, Ag in any of its form is not considered as carcinogen and viral to nervous, immune, and reproductive system.

6 Combined Effects of Heavy Metals

Living organisms in nature are exposed to not only one xenobiotic substance, but also a combination of toxic substances through multiple routes of exposure. Combinations of exposure depend on the environmental factors and occupational variability. Though abundant information on the effect and toxicity of single metal are widely available, studies on effects of multiple metals are relatively very few.

Tabacova et al. [72] examined placental As and Cd in relation to lipid peroxides and glutathione levels in 49 maternal-infant pairs from a copper smelter area and reported that combined exposure of metals resulted in lower glutathione antioxidant protection and higher concentrations of lipid peroxides [72]. Dimitrova et al. [73] studied the combined effect of Zn and Pb on the hepatic superoxide dismutase-catalase system in carp (*Cyprinus carpio*), and it was found that superoxide dismutase and the catalase activity were increased at a 24-h exposure and decreased at a 5-day exposure.

Combined effect of Cu and Cd on *Chlorella vulgaris* growth and photosynthesis-related gene transcription was explored by Qian et al. [74]; and it was found that the combination of these two metals decreased cell growth and chlorophyll content, and increased ROS content synergistically. The transcript abundance of *psbA* and *rbcL* were reduced, though not in a synergistic interaction; however, the transcript abundance of *psaB* was increased synergistically by metal combination [74].

Combined treatment of Pb and Cd is reported to be additive type of toxicity in Sprague–Dawley rats, when administrated orally [75]. Yuan et al. [75] informed that combined treatment of Pb and Cd in acute toxicity studies significantly altered physiological and biological properties of blood, resulted in microcytic hypochromic anemia and damages of different intensities to the liver and kidney, where target organs of the metals were testicles, liver, and kidneys. The minimum dose to observe adverse effect was suggested as less than 29.96 (29.25 + 0.71; $\text{Pb}(\text{NO}_3)_2 + \text{CdCl}_2$) mg/(kg bw day) oral administration for 90 consecutive days. Similar additive toxicity of Pb and Cd was reported by Hambach et al. [76], depicting Pb increased the effect of Cd on early renal biomarkers (e.g., retinol binding protein, N-acetyl- β -d-glucosaminidase, intestinal alkaline phosphatase) in metallurgic refinery workers.

According to Hernández-García et al. [77] the major cell death process was apoptosis when isolated red blood cells of common buzzard were exposed to a mixture of Pb and Cd (1:10). It was reported by Wu et al. [78] that Pb and Cd significantly inhibit cellulase activity on earthworm (*Eisenia fetida*) in a combined exposure. The combined toxic effects of Pb and Cd were complex, and probably influenced by the competitive adsorption and bioavailability of both metals [78].

The effect of Hg and Cd on the packing and elasticity of biomimetic lipid monolayers was investigated by Le et al. [79] using various lipid combinations. It was shown that the metal-mixture (HgCl₂:CdCl₂; 1:1) showed alterations in the lateral lipid packing as depicted by area expansion and enhanced film rigidity.

Antagonistic effect was reported by Smith et al. [80], while investigating the influence of Cd on Pb accumulation in pregnant and non-pregnant mice by exposing them to Cd and Pb contaminated soil. The existing Cd depicted a major influence on the Pb and Fe accumulation in the kidneys and liver, respectively. Cd reduced Pb accumulation in all mice irrespective of status [80]. Vellinger et al. [81] investigated the interactive effect of As and Cd in a freshwater amphipod (*Gammarus pulex*) and reported similar antagonistic interaction between metals on mortality. Metal concentrations in tissues were lower in binary mixtures than in single metal exposures at similar concentration [82]. In another research Vellinger et al. [82] observed that mobilization of the detoxification systems (such as reduction in glutathione content, γ -glutamyl-cysteine ligase activity, and metallothionein concentration) were increased in *G. pulex* in response to the binary exposure. They suggested that this response indicates the changes in energy reserve utilization, as well as a possible energy reallocation from locomotion to detoxification [81].

Jadhav et al. [83] examined the sub-chronic exposure of metal-mixture (As, Cd, Pb, Hg, Cr, Mn, Fe, and Ni) via drinking water in male rat. It was observed that contaminants can alter systemic physiology of rats by altering the functional and structural integrity of kidneys, liver, and brain [83]. The mixture decreased body weight and water consumption and increased weights of brain, liver, and kidneys. Moreover, necrotic changes were observed in those organs. The same research group [84] in a similar study reported that the sub-chronic exposure of metal-mixture (As, Cd, Pb, Hg, Cr, Ni, Mn, and Fe) via drinking water can induce immune toxicity in male rats, and found that the hematopoietic and immune systems of male rats were toxicologically sensitive to joint mixtures. It was also suggested that it leads to anemia and suppression of humoral and cell-mediated immune responses [84].

Low doses of Pb, Cd, and As in a mixture increase delta-aminolevulinic acid (ALA), Fe, and Cu in male Sprague Dawley rats [85]. It was also observed to increase a significant amount of Cu in kidney [85]. Exposure with a mixture of Pb, As, and Cd to BALB/C 3T3 cells resulted in miRNA and mRNA expressions which could be responsible for the cellular death, growth disruption, and inhibited proliferation [86].

Tully et al. [87] investigated the effects of As, Cd, Cr, and Pb on gene expression regulated by a battery of 13 different promoters in recombinant HepG2 cells. They informed that Cd, Cr, and Pb exhibited significant dose-dependent induction of the stress-responsive promoter human metallothionein-IIA (hMTIIA).

Combined effect of Cu, Cd, and Pb on *Cucumis sativus* growth and bioaccumulation was evaluated by An et al. [88]. Binary combinations of Cu + Cd, Cu + Pb, and Cd + Pb resulted in all three types of interactions: additive, synergistic, and antagonistic responses on growth [88]. Ternary combination of Cu + Cd + Pb produced an antagonistic response for the growth. The bioaccumulation of one metal was influenced by the presence of other metals in metal mixtures [88]. Similarly

synergistic, antagonistic, or additive effects of the toxicity were reported in different metal mixtures by Lin et al. [89], when the combined toxicity of eight common heavy metals (Pb, Cd, Hg, Cu, Zn, Mn, Cr, Ni) mixtures were studied in HL7702 cells.

The bioaccumulation of heavy metals and growth response of rice plants after exposure to combined contamination by Cu, Cd, and Pb was conducted [90] in a pot experiment. Yizong et al. [90] showed that Pb promoted both root and shoot absorption of Cu and Cd, and Cu affected Cd and Pb absorption in the root, but Pb concentrations in both root and shoot were not affected by Cd application.

The features of morphological changes in the urinary bladder of mature rats were investigated under combined influence of heavy metals (Zn, Cu, Fe, Mn, Pb, and Cr) by Romaniuk et al. [91]. This metal combination caused intense morphological alterations in all structures of the urinary bladder of rats, which may initiate the dysfunctions of bladder; and these alterations rely on the period of heavy metals intake [91].

Antonio et al. [92] reported that in pregnant rat the mixed exposure of Cd and Pb has additive influence on decreasing Na^+/K^+ -ATPase function, where Cd activity was effected by Pb to cause inhibition of the Na^+/K^+ -ATPase pump. This inhibition results in intracellular K^+ depletion, intracellular Na^+ accumulation, and intracellular free Ca^{+2} increase, causing intense cognitive dysfunction [92]. Another research group [93] reported binary exposure of Pb and As in brain and informed that in the presence of As, action of Pb drastically enhanced and affects the hippocampus. Moreover, the ternary mixture of Pb, As, and Cd triggers intracellular Ca^{+2} release, ROS generation, encourages the extracellular signal-regulated pathway (ERK), c-Jun N-terminal kinases (JNK), and mitogen-activated protein kinase3 (MAPK3) pathway, causing neuronal oxidative stress [94].

The complex interaction of metals (As, Cd, Hg, and Pb) can change the essential neuronal cell integrity by down-regulation of neuronal nitric oxide synthase (n-NOS), metallothionein-3 (MT-III), catalase, superoxide dismutase (SOD), brain-derived neurotrophic factor (BDNF), glutathione peroxidases (GPx), glutathione (GSH), and glutathione S-transferase (GS) and results in oxidative stress [14]. The oxidative stress by various cellular signaling pathways results in programmed neuronal cell death and cognitive dysfunction [94].

Vinodhini and Narayanan [95] evaluated the impact of toxic heavy metals (Cd + Pb + Cr + Ni) on the hematological parameters in common carp (*Cyprinus carpio L.*). They reported decreased hemoglobin and PCV as well as elevated RBC count and blood glucose [95]. Chandanshive et al. [96] studied the effect of heavy metal model mixture on blood hematological parameters in the laboratory acclimatized fish *Labeo rohita*, where a significant reduction of erythrocyte count and hematocrit level was reported.

Combined effects of Cd, As, and Pb in a comparative study using conceptual models and the antioxidant responses in the brackish water flea were examined by Yoo et al. [97]. Yoo et al. [97] reported that the combinations of As+Pb and Cd + Pb showed synergistic effects, whereas Cd + As+Pb and Cd + As combinations showed additive, but antagonistic effects were not observed in any combinations.

Interestingly, in several combined treatment experiments one metal exhibited protective effect against another metal toxicity. For instance, Firat and Kargin [98] investigated the combined effects of heavy metals on serum biochemistry of Nile Tilapia (*Oreochromis niloticus*) and found that concentrations of Cd and Zn metals in the serum were lower in combined metals-exposed fish than in fish exposed to individual metals, thereby exhibiting protective effect.

Examining the combined effect of Cd and Zn in PC12 cells, Rahman et al. [99] reported that Zn effectively inhibited Cd-induced apoptotic cell death via suppressing mitochondrial apoptosis pathway and reserving Cd-induced production of reactive oxygen species (ROS). Zn limited Cd-induced apoptosis by decreasing cytochrome *c* release from the mitochondria, and down-regulating the pro-apoptotic protein caspase 9 and Bax, as well as up-regulating anti-apoptotic Bcl-x [99]. Similarly, evaluating the effect of Zn in the presence of Hg in PC12 cells, Hossain et al. [100] reported Zn triggers glutathione and Nrf2-mediated protection against inorganic Hg-induced cytotoxicity and intrinsic apoptosis. Combined exposure of Hg and Zn exhibited improvement in cell viability, cell membrane, DNA damage, ROS amount, and apoptotic cells, along with a significant increase of pro-survival mTOR, akt, ERK1, Nrf2, HO1, Bcl-2 and Bcl-xL, and decrease in apoptotic p53, Bax, cytochrome *c* and cleaved caspase 3 [100].

Alike Zn, Selenium (Se) also expressed ameliorative actions against As-induced cytotoxicity via modulating autophagy/apoptosis [101]. Rahman et al. [101] explained that Se modulates As-induced intrinsic apoptosis pathway via enhancing mTOR/Akt autophagy signaling pathway by retaining antioxidant molecules and hindering the cellular accumulation of As in the cells. Similar Se-amelioration was reported by Hossain et al. [102, 103] against Cd and Hg influenced toxicity in PC12 cells. Co-presence of Se with Cd protects against Cd-induced cytotoxicity in PC12 cells through inhibition of Cd-induced oxidative stress and suppression of mitochondrial apoptosis [102]. Co-exposure also displayed increased antioxidant glutathione and glutathione peroxidase 1 (GPx1) levels, and decreased DNA fragmentation and cell membrane damage [102]. Hossain et al. [103] also reported that Se attenuates inorganic Hg-induced cytotoxicity and intrinsic apoptosis in PC12 cells modulating antioxidant properties and ROS generation.

These studies in biological system indicate that the interaction among different metals is very complex. These complex interactions depend on environmental factors, exposure time, and exposed animals. Intensive understanding on the associated mechanism of action and exploration of the substantial impact on biological system is needed.

7 Concluding Remarks

There are still many unknown parts about the biological effects of heavy metals. It has been reported that even heavy metals that are recognized as harmful to health, such as Cd and As, have a negative effect on living organisms if they are not

completely present. The general understanding is that excessive intake or excess exposure of heavy metals is harmful, even in the case of absolutely essential heavy metals for physical and biological activities such as Cu and Zn. Heavy metal exposure to human, animals, and plants involves several different routes such as by water and food consumption, skin absorption, inhalation of metal dust and fume in the air and especially at workplace through occupation exposure. Usually many heavy metals are considered as toxic even at low level. The chief heavy metal toxicity mechanism is influenced by the free radical formation which can cause biological molecule (lipid, protein, nucleic acid) damage, oxidative stresses, DNA damage. Ultimately these metals act as potential carcinogens and neurotoxins. Some metals can be chronic where other metals can be acute even after prolonged exposure, ultimately causing organ damage and diseases in the body such as liver, brain, kidney and lungs damage and connected diseases. Recently, there have been many reports that the toxicity of these heavy metals can be alleviated by simultaneous or pre-administration of essential heavy metals such as Se, Zn, or Cu. These heavy metals also induce oxidative stress and show toxicity when administered in large amounts. However, these metals can help in relieving oxidative stress under permissible and proper dose. Many studies have various discussions about the mechanism, but it seems that more detailed research is needed in the future.

References

1. Bradl H (2002) Heavy metals in the environment: origin, interaction and remediation, vol 6. Academic, London
2. Engwa GA, Ferdinand PU, Nwalo FN, Unachukwu MN (2019) Mechanism and health effects of heavy metal toxicity in humans. Poisoning in the modern world – new tricks for an old dog? IntechOpen, pp 1–23
3. Duffus JH (2002) Heavy metals – a meaningless term? Pure Appl Chem 74(5):793–807
4. Flora SJS, Flora GJS, Saxena G (2006) Environmental occurrence, health effects and management of lead poisoning. In: Cascas SB, Sordo J (eds) Lead: chemistry, analytical aspects, environmental impacts and health effects. Elsevier, pp 158–228
5. Mahurpawar M (2015) Effects of heavy metals on human health. Int J Res Granthaalayah:1–7
6. McCally M (2003) Life support: the environment and human health. J Sociol Soc Welfare 30(4):19
7. Agency for Toxic Substances and Disease Registry (2017) Investigating Environmental Hazards to Advance Community Health. U.S. Department of Health & Human Services
8. Nagajyoti PC, Lee KD, Sreekanth TVM (2010) Heavy metals, occurrence and toxicity for plants: a review. Environ Chem Lett 8(3):199–216
9. Nriagu JO (1996) History of global metal pollution. Science 272:223–224
10. Singh DJ, Kamalhdad AS (2011) Effects of heavy metals on soil, plants, human health and aquatic life. Int J Res Chem Environ 1(2):15–21
11. Tchounwou PB, Yedjou CG, Patlolla AK, Sutton DJ (2012) Heavy metal toxicity and the environment. Experientia Suppl 101:133–164
12. Solomon F (2008) Impacts of metals on aquatic ecosystems and human health. University of Washington Water Center
13. Muhib MI, Chowdhury MAZ, Easha NJ (2016) Investigation of heavy metal contents in cow milk samples from area of Dhaka, Bangladesh. Food Contam 3:16

14. Duruibe JO, Ogwuegbu MOC, Egwurugwu JN (2007) Heavy metal pollution and human biotoxic effects. *Int J Phys Sci* 2(5):112–118
15. Trasande L, Landrigan PJ, Schechter C (2005) Public health and economic consequences of methyl mercury toxicity to the developing brain. *Environ Health Perspect* 113(5):590–596
16. Esmaeilzadeh M, Jaafari J, Mohammadi AA, Panahandeh M, Javid A, Javan S (2019) Investigation of the extent of contamination of heavy metals in agricultural soil using statistical analyses and contamination indices. *Hum Ecol Risk Assess Int J* 25(5):1125–1136
17. Bjørklund G, Skalný AV, Rahman MM, Dadar M, Yassa HA, Aaseth J, Chirumbolo S, Skalnaya MG, Tinkov AA (2018) Toxic metal(loid)-based pollutants and their possible role in autism spectrum disorder. *Environ Res* 166:234–250
18. Jaishankar M, Tseten T, Anbalagan N, Mathew BB, Beeregowda KN (2014) Toxicity, mechanism and health effects of some heavy metals. *Interdiscip Toxicol* 7(2):60–72
19. Morais S, Costa FG, Pereira ML (2012) Heavy metals and human health, in environmental health – emerging issues and practice. *InTech Open*, pp 227–246
20. McGreer JC, Brix KV, Skeaff JM, DeForest DK, Brigham SI (2003) Inverse relationship between bioconcentration factor and exposure concentration for metals: implications for hazard assessment of metals in the aquatic environment. *Environ Toxicol Chem* 22(5):1017–1037
21. Juwarkar AA, Yadav SK (2010) Bioaccumulation and biotransformation of heavy metals. *Biotechnology*:266–284
22. Mosby CV, Glanze WD, Anderson KN (1996) Mosby medical encyclopedia. The Signet, St. Louis. Revised Edition
23. Florea A-M, Busselberg D (2006) Occurrence, use and potential toxic effects of metals and metal compounds. *Biometals* 19:419–427
24. Järup L (2003) Hazards of heavy metal contamination. *Br Med Bull* 68(1):167–182
25. Ferner DJ (2001) Toxicity, heavy metals. *eMed* 2(5):1
26. Yongsheng W, Qihui L, Qian T (2011) Effect of lead on growth, accumulation and quality component of tea plant. *Procedia Eng* 18:214–219
27. Hirner AV, Emons H (2004) Organic metal and metalloid species in the environment: analysis, distribution, processes and toxicological evaluation. Springer, Berlin, pp 205–219
28. Mahaffey KR (1990) Environmental lead toxicity: nutrition as a component of intervention. *Environ Health Perspect* 89:75–78
29. Moore CP, Cock JH (1985) Cassava forage silage as a feed source for zebu calves in the tropics. *Trop Agric (Trinidad)* 62(2):142–144
30. Ward JD, Spears JW, Gengelbach GP (1995) Differences in copper status and copper metabolism among Angus, Simmental, and Charolais cattle. *J Anim Sci* 73(2):571–577
31. Agency for Toxic Substances and Disease Registry (2018) Protecting People from Harmful Environmental Exposures. U.S. Department of Health & Human Services
32. Centers for Disease Control and Prevention (2019) Annual review: towards a decade of action
33. Akbor MA, Rahman MM, Bodrud-Doza M, Haque MM, Abu Bakar Siddique M, Ahsan MA, Bondad SEC, Uddin MK (2020) Metal pollution in water and sediment of the Buriganga River, Bangladesh: an ecological risk perspective. *Desalin Water Treat* 193:284–301
34. Chen CW, Chen CF, Dong CD (2012) Distribution and accumulation of mercury in sediments of Kaohsiung River mouth, Taiwan. *APCBEE Procedia* 1:153–158
35. Alina M, Azrina A, Mohd-Yunus AS, Mohd-Zakiuddin S, Mohd-Izuan EE, Radyaqsa M (2012) Heavy metals (mercury, arsenic, cadmium, plumbum) in selected marine fish and shellfish along the straits of Malacca. *Int Food Res* 19(1):135–140
36. Bjørklund G, Hofer T, Nurchi VM, Aaseth J (2019) Iron and other metals in the pathogenesis of Parkinson’s disease: toxic effects and possible detoxification. *J Inorg Biochem* 199:110717
37. Crous-Bou M, Minguillón C, Gramunt N (2017) Alzheimer’s disease prevention: from risk factors to early intervention. *Alz Res Therapy* 9:71

38. Semionov A (2018) Minamata disease – review. *World J Neurosci* 8:178–184
39. Han JX, Shang Q, Du Y (2009) Effect of environmental cadmium pollution on human health. *Health* 1(3):159–166
40. Henson MC, Chedrese PJ (2004) Endocrine disruption by cadmium, a common environmental toxicant with paradoxical effects on reproduction. *Exp Biol Med* 229(5):383–392
41. Regoli L (2005) The relative contributions of different environmental sources to human exposure and the EU cadmium risk assessment meeting of UNECE task force on heavy metals. Presentation for the UNECE Long-Range-Trans-boundary Air Pollutants – Task Force on Heavy Metals
42. Järup L, Akesson A (2009) Current status of Cd as an environmental health problem. *Toxicol Appl Pharmacol* 238:201–208
43. Flora SJS, Mittal M, Mehta A (2008) Heavy metal induced oxidative stress & its possible reversal by chelation therapy. *Indian J Med Res* 128:501–523
44. Lalor GC (2008) Review of cadmium transfers from soil to humans and its health effects in the Jamaican environment. *Sci Total Environ* 400:162–172
45. Jain J, Gauba P (2017) Heavy metal toxicity-implications on metabolism and health. *Int J Pharm Bio Sci* 8(4):452–460. <https://doi.org/10.22376/ijpbs.2017.8.4.b452-460>
46. Satarug S, Garrett SH, Sens MA, Sens DA (2011) Cadmium, environmental exposure, and health outcomes. *Cien Saude Colet* 16(5):2587–2602
47. Bernard A (2008) Cadmium & its adverse effects on human health. *Indian J Med Res* 128(4):557–564
48. Nishijo M, Nakagawa H, Suwazono Y, Nogawa K, Kido T (2017) Causes of death in patients with Itai-itai disease suffering from severe chronic cadmium poisoning: a nested case-control analysis of a follow-up study in Japan. *BMJ Open* 7(7):e015694
49. Agency for Toxic Substances and Disease Registry (2017) Public Health Statement Copper. ATSDR Publication CAS#7440-50-8
50. Ali H, Khan E, Ilahi I (2019) Environmental chemistry and ecotoxicology of hazardous heavy metals: environmental persistence, toxicity, and bioaccumulation. *J Chem*:1–14. 6730305
51. Taylor AA, Tsuji JS, Garry MR (2020) Critical review of exposure and effects: implications for setting regulatory health criteria for ingested copper. *Environ Manag* 65:131–159
52. Hefnawy A, Elkhaiaf H (2015) The importance of copper and the effects of its deficiency and toxicity in animal health. *Int J Livest Res* 5(12):1–20
53. Nkwunonwo UC, Odika PO, Onyia NT (2020) A review of the health implications of heavy metals in food chain in Nigeria. *Sci World J*:1–11. 6594109
54. Woody DCA (2012) Effects of copper on fish and aquatic resources. *The Nature Preservancy*
55. Mazumder G (2008) Chronic arsenic toxicity & human health. *Indian J Med Res* 128(4):436–447
56. Singh N, Kumar D, Sahu A (2007) Arsenic in the environment: effects on human health and possible prevention. *J Environ Biol* 28(2 Suppl):359–365
57. Chowdhury UK, Biswas BK, Chowdhury TR, Samanta G, Mandal BK, Basu GC (2000) Groundwater arsenic contamination in Bangladesh and West Bengal, India. *Environ Health Perspect* 108(5):393–397
58. Saha JC, Dikshit AK, Bandyopadhyay M, Saha KC (1999) A review of arsenic poisoning and its effects on human health. *Crit Rev Environ Sci Technol* 29(3):281–313
59. Shrivastava R, Upreti RK, Seth PK, Chaturvedi UC (2002) Effects of chromium on the immune system. *FEMS Immunol Med Microbiol* 34(1):1–7
60. Agency for Toxic Substances and Disease Registry (ATSDR) (2011) Case studies in environmental medicine (CSEM): chromium toxicity
61. Dayan AD, Paine AJ (2001) Mechanisms of chromium toxicity, carcinogenicity and allergenicity: review of the literature from 1985 to 2000. *Hum Exp Toxicol* 20(9):439–451
62. Milatovic D, Gupta RC, Yin Z, Zaja- Milatovic S, Aschner M (2017) Manganese. In: *Reproductive and developmental toxicology*, pp 567–581

63. Röllin H (2011) Manganese: environmental pollution and health effects. In: Encyclopedia of environmental health, chapter: manganese: environmental pollution and health effects. Elsevier, Nriagu, pp 617–629
64. Wright DA, Welbourn P (2002) Environmental toxicology (Cambridge environmental chemistry series 11). Cambridge University Press, Cambridge
65. Krewski D, Yokel RA, Nieboer E, Borchelt D, Cohen J, Harry J, Kacew S, Lindsay J, Mahfouz AM, Rondeau V (2007) Human health risk assessment for aluminium, aluminium oxide, and aluminium hydroxide. *J Toxicol Environ Health B* 10(1):1–269
66. Vardar F, Ünal M (2007) Aluminum toxicity and resistance in higher plants. *Adv Mol Biol* 1: 1–12
67. Akter M, Sikder MT, Rahman MM (2018) A systematic review on silver nanoparticles-induced cytotoxicity: physicochemical properties and perspectives. *J Adv Res* 9:1–16
68. Miyayama T, Arai Y, Hirano S (2012) Environmental exposure to silver and its health effects. *Nihon Eiseigaku Zasshi* 67(3):383–389
69. Rosenman KD, Seixas N, Jacobs I (1987) Potential nephrotoxic effects of exposure to silver. *Br J Ind Med* 44:267–272
70. Fung MC, Bowen DL (1996) Silver products for medical indications: risk-benefit assessment. *J Toxicol Clin Toxicol* 34(1):119–126
71. Drake PL, Hazelwood KJ (2005) Exposure-related health effects of silver and silver compounds: a review. *Ann Occup Hyg* 49(7):575–585
72. Tabacova S, Baird DD, Balabaeva L, Lolova D, Petrov I (1994) Placental arsenic and cadmium in relation to lipid peroxides and glutathione levels in maternal-infant pairs from a copper smelter area. *Placenta* 15:873–881
73. Dimitrova MS, Tishinova V, Velcheva V (1994) Combined effect of zinc and lead on the hepatic superoxide dismutase-catalase system in carp (*Cyprinus carpio*). *Comp Biochem Physiol* 108C:43–46
74. Qian H, Li J, Sun L, Chen W, Sheng GD, Liu W, Fu Z (2009) Combined effect of copper and cadmium on *Chlorella vulgaris* growth and photosynthesis-related gene transcription. *Aquat Toxicol* 94:56–61
75. Yuan G, Dai S, Yin Z, Lu H, Jia R, Xu J, Song X, Li L, Shu Y, Zhao X (2014) Toxicological assessment of combined lead and cadmium: acute and sub-chronic toxicity study in rats. *Food Chem Toxicol* 65:260–268
76. Hambach R, Lison D, D'Haese PC, Weyler J, De Graef E, De Schryver A, Lamberts LV, Van Sprundel M (2013) Co-exposure to lead increases the renal response to low levels of cadmium in metallurgy workers. *Toxicol Lett* 222:233–238
77. Hernández-García A, Romero D, Gómez-Ramírez P, María-Mojica P, Martínez-López E, García-Fernández A (2014) In vitro evaluation of cell death induced by cadmium, lead and their binary mixtures on erythrocytes of common buzzard (*Buteo buteo*). *Toxicol In Vitro* 28: 300–306
78. Wu B, Liu Z, Xu Y, Li D, Li M (2012) Combined toxicity of cadmium and lead on the earthworm *Eisenia fetida* (Annelida, Oligochaeta). *Ecotoxicol Environ Saf* 81:122–126
79. Le MT, Hassanin M, Mahadeo M, Gailer J, Prenner EJ (2013) Hg- and Cd-induced modulation of lipid packing and monolayer fluidity in biomimetic erythrocyte model systems. *Chem Phys Lipids* 170:46–54
80. Smith E, Gancarz D, Rofe A, Kempson IM, Weber J, Juhasz AL (2012) Antagonistic effects of cadmium on lead accumulation in pregnant and non-pregnant mice. *J Hazard Mater* 199:453–456
81. Vellinger C, Parant M, Rousselle P, Usseglio-Polatera P (2012) Antagonistic toxicity of arsenate and cadmium in a freshwater amphipod (*Gammarus pulex*). *Ecotoxicology* 21:1817–1827
82. Vellinger C, Gismondi E, Felten V, Rousselle P, Mehennaoui K, Parant M, Usseglio-Polatera P (2013) Single and combined effects of cadmium and arsenate in *Gammarus pulex*

- (Crustacea, Amphipoda): understanding the links between physiological and behavioural responses. *Aquat Toxicol* 140:106–116
83. Jadhav S, Sarkar S, Patil R, Tripathi H (2007) Effects of subchronic exposure via drinking water to a mixture of eight water contaminating metals: a biochemical and histopathological study in male rats. *Arch Environ Contam Toxicol* 53:667–677
 84. Jadhav S, Sarkar S, Ram G, Tripathi H (2007) Immunosuppressive effect of subchronic exposure to a mixture of eight heavy metals, found as groundwater contaminants in different areas of India, through drinking water in male rats. *Arch Environ Contam Toxicol* 53:450–458
 85. Whittaker MH, Wang G, Chen XQ, Lipsky M, Smith D, Gwiazda R, Fowler BA (2011) Exposure to Pb, Cd, and As mixtures potentiates the production of oxidative stress precursors: 30-day, 90-day, and 180-day drinking water studies in rats. *Toxicol Appl Pharmacol* 254:154–166
 86. Martínez-Pacheco M, Hidalgo-Miranda A, Romero-Córdoba S, Valverde M, Rojas E (2014) mRNA and miRNA expression patterns associated to pathways linked to metal mixture health effects. *Gene* 533:508–514
 87. Tully DB, Collins BJ, Overstreet JD, Smith CS, Dinse GE, Mumtaz MM, Chapin RE (2000) Effects of arsenic, cadmium, chromium, and lead on gene expression regulated by a battery of 13 different promoters in recombinant HepG2 cells. *Toxicol Appl Pharmacol* 168:79–90
 88. An YJ, Kim YM, Kwon TI, Jeong SW (2004) Combined effect of copper, cadmium, and lead upon *Cucumis sativus* growth and bioaccumulation. *Sci Total Environ* 326:85–93
 89. Lin X, Gu Y, Zhou Q, Mao G, Zou B, Zhao J (2016) Combined toxicity of heavy metal mixtures in liver cells. *J Appl Toxicol* 36:1163–1172
 90. Yizong H, Ying H, Yunxia L (2009) Heavy metal accumulation in iron plaque and growth of rice plants upon exposure to single and combined contamination by copper, cadmium and lead. *Acta Ecol Sin* 29:320–326
 91. Romaniuk A, Sikora V, Lyndin M, Smiyarov V, Sikora V, Lyndina Y, Piddubnyi A, Gyryavenko N, Korobchanska A (2017) The features of morphological changes in the urinary bladder under combined effect of heavy metal salts. *Interv Med Appl Sci* 9(2):105–111
 92. Antonio MT, Corredor L, Leret ML (2003) Study of the activity of several brain enzymes like markers of the neurotoxicity induced by perinatal exposure to lead and/or cadmium. *Toxicol Lett* 143:331–340
 93. Mejía JJ, Díaz-Barriga F, Calderón J, Ríos C, Jiménez-Capdeville ME (1997) Effects of lead–arsenic combined exposure on central monoaminergic systems. *Neurotoxicol Teratol* 19:489–497
 94. Rai A, Maurya SK, Khare P, Srivastava A, Bandyopadhyay S (2010) Characterization of developmental neurotoxicity of As, Cd, and Pb mixture: synergistic action of metal mixture in glial and neuronal functions. *Toxicol Sci* 118:586–601
 95. Vinodhini R, Narayanan M (2009) The impact of toxic heavy metals on the hematological parameters in common carp (*Cyprinus carpio* L.). *Iran J Environ Health Sci Eng* 6:23–28
 96. Chandanshive S, Sarwade P, Humbe A, Mohekar A (2012) Effect of heavy metal model mixture on haematological parameters of *Labeo rohita* from Gharni Dam Nalegaon. *Latur Int Multidisc Res J* 2:10–12
 97. Yoo JW, Cho H, Lee KW, Won EJ, Lee YM (2021) Combined effects of heavy metals (Cd, As, and Pb): comparative study using conceptual models and the antioxidant responses in the brackish water flea. *Comp Biochem Physiol C* 239:108863
 98. Firat Ö, Kargin F (2010) Individual and combined effects of heavy metals on serum biochemistry of Nile tilapia *Oreochromis niloticus*. *Arch Environ Contam Toxicol* 58:151–157
 99. Rahman MM, Ukiana J, Lopez RU, Sikder MT, Saito T, Kurasaki M (2017) Cytotoxic effects of cadmium and zinc co-exposure in PC12 cells and the underlying mechanism. *Chem Biol Interact* 269:41–49

100. Hossain KFB, Hosokawa T, Saito T, Kurasaaki M (2021) Zinc-pretreatment triggers glutathione and Nrf2-mediated protection against inorganic mercury-induced cytotoxicity and intrinsic apoptosis in PC12 cells. *Ecotoxicol Environ Saf* 207:111320
101. Rahman MM, Lopez-Uson AR, Sikder MT, Tan G, Hosokawa T, Saito T, Kurasaki M (2018) Ameliorative effects of selenium on arsenic-induced cytotoxicity in PC12 cells via modulating autophagy/apoptosis. *Chemosphere* 196:453–466
102. Hossain KFB, Rahman MM, Sikder MT, Saito T, Hosokawa T, Kurasaki M (2018) Inhibitory effects of selenium on cadmium-induced cytotoxicity in PC12 cells via regulating oxidative stress and apoptosis. *Food Chem Toxicol* 114:180–189
103. Hossain KFB, Rahman MM, Sikder MT, Hosokawa T, Saito T, Kurasaaki M (2021) Selenium modulates inorganic mercury induced cytotoxicity and intrinsic apoptosis in PC12 cells. *Ecotoxicol Environ Saf* 207:111262

Effects of Persistent Organic Pollutants (POPs) in the Ecosystem and Human Health: Focusing on Chlorinated Chemicals



Ikeda-Atsuko Araki, Chihiro Miyashita, Sumitaka Kobayashi,
Keiko Yamazaki, and Reiko Kishi

Contents

1	Background: Persistent Organic Substances in the Environment	123
2	Chlorinated Chemicals in Humans	127
2.1	Exposure Levels in Humans	127
2.2	Health Effects	132
2.3	Findings from a Birth Cohort: Hokkaido Study	132
3	Conclusions and Recommendations for Future Research	140
	References	141

Abstract Persistent organic pollutants (POPs) are manmade chemical substances and their by-products remain in the environment for long periods of time. Based on the increasing threat of POPs to human health and the environment, the Stockholm Convention was adopted and enforced. The initial POPs listed were chlorinated chemicals such as polychlorinated biphenyls (PCBs), dioxins, chlorinated pesticides and insecticides such as 1,1,1-trichloro-2,2-bis(*p*-chlorophenyl)ethane (DDT). Even

I-A. Araki (✉)

Hokkaido University Center for Environmental and Health Sciences, Hokkaido, Japan

WHO Collaborating Centre for Environmental Health and Prevention of Chemical Hazards,
Hokkaido, Japan

Hokkaido University Faculty of Health Sciences, Hokkaido, Japan

e-mail: AAraki@cehs.hokudai.ac.jp

C. Miyashita, S. Kobayashi, K. Yamazaki, and R. Kishi

Hokkaido University Center for Environmental and Health Sciences, Hokkaido, Japan

WHO Collaborating Centre for Environmental Health and Prevention of Chemical Hazards,
Hokkaido, Japan

e-mail: miyasita@med.hokudai.ac.jp; sukobayashi@cehs.hokudai.ac.jp;

kyamazaki@cehs.hokudai.ac.jp; rkishi@cehs.hokudai.ac.jp

Shunitz Tanaka, Masaaki Kurasaki, Masaaki Morikawa, and Yuichi Kamiya (eds.),

121

Design of Materials and Technologies for Environmental Remediation,

Hdb Env Chem (2023) 115: 121–144, DOI 10.1007/698_2021_823,

© The Author(s), under exclusive license to Springer Nature Singapore Pte Ltd 2022,

Published online: 1 January 2022

after their ban and elimination from the market, POPs are still widely distributed throughout the environment around the globe, including in human body. High-dose exposure to dioxins and DDT may cause cancer. However, the effects of relatively low doses in the general population are still under consideration. Foetuses and neonates may be particularly sensitive to exposure to these chemicals, and the life-long health effects of prenatal exposure to chemicals need to be investigated. The Hokkaido Study on Environment and Children's Health (The Hokkaido Study) is an on-going birth cohort established in 2001. The Hokkaido Study comprises two cohorts: the Sapporo cohort with 514 pregnant women recruited in the second to third trimester from one gynaecology hospital in Sapporo during 2002–2005 and the Hokkaido cohort with 20,926 pregnant women recruited in the first trimester in cooperation with 37 gynaecology hospitals and clinics all over Hokkaido Prefecture during 2003–2012. In the Sapporo cohort, detectable levels of dioxins, PCBs, and chlorinated pesticides were found in maternal blood during pregnancy. Increasing levels of these chemicals in the maternal blood were associated with decreased birth size, delayed neurodevelopment at an early age, and up- or down-regulation of thyroid and reproductive hormones at birth. Increased levels of dioxins were also associated with reduced levels of IgE at birth, but increased risk of otitis media incidence up to 18 months and wheezing up to 7 years of age. Specific genetic polymorphisms modify the maternal blood dioxin levels so that there is a possibility of genetically vulnerable populations to dioxins. Exposure to PCBs modifies DNA methylation at birth, which may partly explain the adverse effect mechanisms on health outcomes. Long-term follow-up is necessary to determine the life-long effects of such exposure in early life.

Keywords Dioxins, Exposure levels, Health effects, Organochlorine pesticides, Persistent organic pollutants, Polychlorinated biphenyls

Abbreviations

AHR	Aromatic hydrocarbon receptor
BSID-II	Bayley Scales of Infant Development Second Edition
CI	Confidence interval
<i>cis</i> -HCE	Heptachlor epoxide
CYP1	Cytochrome 450 family 1
DDE	Dichlorodiphenyldichloroethylene
DDT	Dichlorodiphenyltrichloroethane
DHEA	Dehydroepiandrosterone
DLC	Dioxin-like compound
e-waste	Electronic waste
FSH	Follicle stimulating hormone
HCB	Hexachlorobenzene
HCH	Hexachlorocyclohexane

HRGC/HRMS	High-resolution gas chromatography/high-resolution mass spectrometry
IARC	International Agency for Research on Cancer
IGF2	Insulin-like growth factor 2
ISAAC	International Study of Asthma and Allergies in Childhood
LINE1	Long interspersed element 1
MDI	Mental development index
NHANES	National Health and Nutrition Examination Survey
NHATS	National Human Adipose Tissue Survey
OCPs	Organochlorine pesticides
OH-PCBs	Hydroxylated PCBs
OR	Odds ratio
p,p'-DDE	1,1-Dichloro-2,2-bis(4-chlorophenyl)ethane
p,p'-DDT	1,1,1-Trichloro-2,2-bis(<i>p</i> -chlorophenyl)-ethane
PCB	Polychlorinated biphenyl
PCDD	Polychlorinated dibenzo- <i>p</i> -dioxins
PCDF	Polychlorinated dibenzofuran
PFOA	Perfluorooctanoic acid
PFOS	Perfluorooctane sulfonic acid
PFOSF	Perfluorooctane sulfonyl fluoride
POPs	Persistent organic pollutants
SNPs	Single nucleotide polymorphisms
TCDD	Tetrachlorodibenzo- <i>p</i> -dioxin
TEF	Toxic equivalency factor
TEQ	Toxic equivalent
WHO	World Health Organization
β-BHC	Beta-hexachlorocyclohexane

1 Background: Persistent Organic Substances in the Environment

Persistent organic pollutants (POPs) are manmade chemical substances and their by-products remain in the environment for exceptionally long periods [1]. Owing to their long half-lives, they are widely distributed throughout the global environment in soil, water, air, wild animals, and human bodies. Because of the high solubility of the POPs in fatty tissue, they bio-accumulate in especially high concentrations (up to 70,000 times than background concentrations) in the living organs of animals at higher levels of the food chain. Initially, 12 POPs were listed under the Stockholm Convention to protect human health and the environment and were categorised into three categories: pesticides (aldrin, chlordane, 1,1,1-trichloro-2,2-bis(*p*-chlorophenyl)ethane (DDT), dieldrin, endrin, heptachlor, hexachlorobenzene (HCB), mirex, and toxaphene), industrial chemicals (HCB, polychlorinated

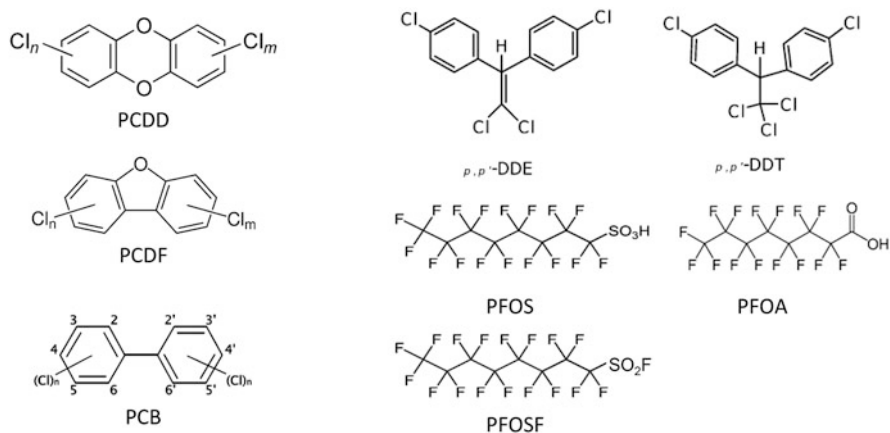


Fig. 1 Chemical structures of Persistent Organic Pollutants (POPs) discussed in this chapter

biphenyls (PCBs)), and by-products (HCB, polychlorinated dibenzo-*p*-dioxin (PCDD), and polychlorinated dibenzofuran (PCDF). Subsequently, 16 classes of chemicals were added to the Stockholm Convention, including perfluorooctanesulfonic acid (PFOS) with its salts, perfluorooctane sulfonyl fluoride (PFOSF), perfluorooctanoic acid (PFOA) with its salts, and PFOA-related compounds (Stockholm Convention, <http://www.pops.int/TheConvention/ThePOPs/tabid/673/Default.aspx>). Their chemical structures are shown in Fig. 1.

PCBs have 209 congeners, and PCB-153 is one of the most detected non-dioxin-like PCBs used for comparison of exposure levels among different populations [2]. Dioxin-like (DL) PCBs have 12 congeners, and the potential toxicity of DL-PCBs is considered to be higher than that of PCBs. DL compounds (DLCs) or the more generally used term “dioxins” include seven PCDDs, 10 PCDFs, and 12 DL-PCBs. Most dioxins are by-products of manufacturing processes such as smelting, chlorine bleaching of paper pulp, and the production of certain herbicides and pesticides. A major cause of the release of dioxins into the environment is the incomplete burning of solid and hospital waste by uncontrolled waste incinerators. Dioxins can also result naturally from volcanic eruptions, forest fires, and other natural processes. In Japan, the Ministry of Environment monitors the dioxin levels in the environment [3]. As shown in Fig. 2, technologies were developed for controlled waste incineration with low dioxin emissions, so that the secular trend of dioxin levels in the environment decreased since the 1990s and remained stable at relatively low levels, although detectable.

Organochlorine pesticides (OCPs), including DDT, aldrin, and endrin are classic pesticides that are classified as POPs. They have been banned for agricultural or domestic uses in accordance with the Stockholm Convention, except DDT usage to control malaria in a few developing countries. Figure 3 shows the *p,p'*-DDT and 1,1-dichloro-2,2-bis(*p*-chlorophenyl) ethylene (*p,p'*-DDE) levels in wildlife in

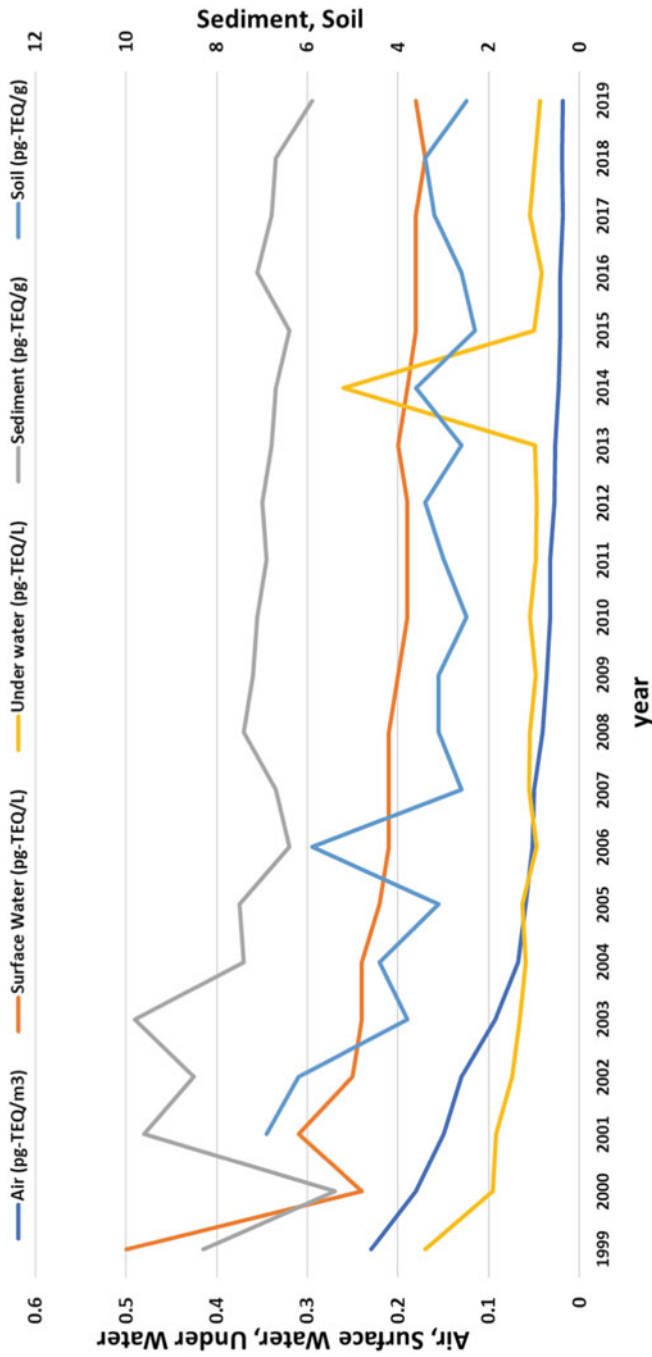


Fig. 2 Dioxin concentration in environmental samples in Japan (data from Ministry of Environment, Japan [3])

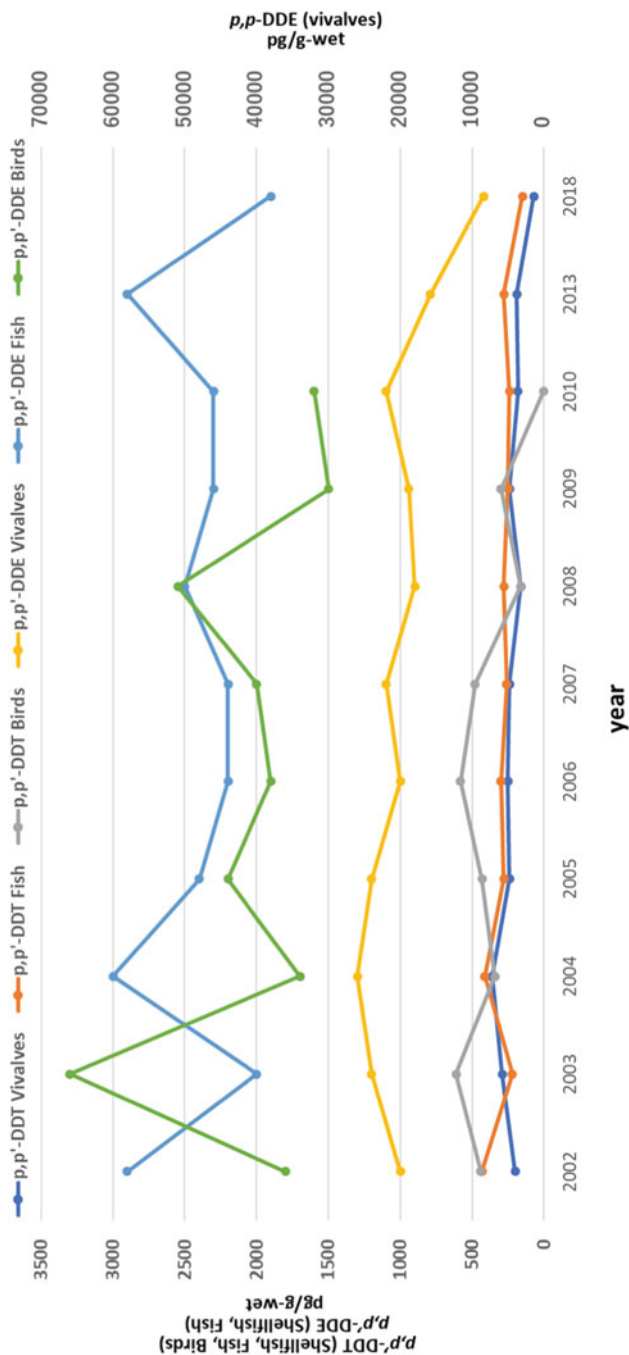


Fig. 3 DDT and DDE concentrations in wildlife in Japan (monitoring data from Ministry of Environment, Japan [3])

Japan [3]. Since the early 1970s, DDT has not been used in Japan; however, owing to its long half-life and persistent properties, it can still be detected, although the levels remain low.

Among the newly added chemicals to the Stockholm Convention, PFOS and PFOA should be especially considered. PFOS and PFOA are synthetic chemicals with unique surfactant properties that are resistant to oil, water, grease, or soil. They have been intentionally used in industrial applications such as electric and electronic parts, firefighting foam, photo imaging, hydraulic fluids, leather, paper, and consumer products such as textiles for more than 60 years [4]. In contrast to chlorinated compounds such as PCBs and dioxins, PFOS and PFOA do not accumulate in lipids, but bind to blood proteins. The presence of detectable concentrations in animals at higher trophic levels (polar bear, caribou, walrus) has generated concern regarding the biomagnification potential of PFOS and PFOA in food webs [5].

2 Chlorinated Chemicals in Humans

2.1 Exposure Levels in Humans

The potential toxic effects of DLCs are related to the binding affinity of aryl hydrocarbon receptors (AHR). Based on the estimated AHR affinity, the World Health Organization (WHO) assigned a toxic equivalency factor (TEF) for each of the 29 DLCs. The TEF is used to identify the toxic effects of the 29 DLCs based on their relationship with the most toxic compound, 2,3,7,8-tetrachlorodibenzo-*p*-dioxin (TCDD), by assigning it a basic coefficient value of 1 TEF, and then assigning each of the other 28 DLCs a coefficient value ranging downward from 1 (TCDD and 1,2,3,7,8-pentachlorodibenzo-*p*-dioxin PeCDD) to 0.00003 (mono-ortho PCBs) (Table 1). The toxic equivalent quantity (TEQ) is then calculated by multiplying the concentrations of the individual congeners of DLC with its TEF [6].

Dioxin levels among different populations are shown in Table 2. Historically, there have been a few incidents of dioxin pollution. Yusho was a disease caused by a widespread consumption of dioxin-contaminated rice-bran oil in the Kyusyu area in Japan. PCDFs were the main culprits and the DLC levels in the blood were found to be as high as 214.5 pg/g-TEQ factor lipid [2, 7]. A similar rice-bran oil contamination occurred in Taiwan as well, called Yucheng in 1978–79. High levels (6,550 pg/g-TEQ lipid) of PCDD/PCDFs in the blood were observed in Yucheng patients [2]. High TCDD contamination was also found in a Vietnamese hotspot where the United States veterans used the herbicide Agent Orange during the Vietnam War in the 1960s. The level was as high as 1,832 pg/g lipid in breast milk collected in 1970. The levels of total dioxins and PCDD/PCDF in pooled Vietnamese blood from 1991 to 1992 were 1,145 pg/g lipid, which is approximately 50 TEQ [8]. Even after 40 years, total PCDDs/PCDFs levels of 25 pg/g lipid were detected among males who live close to the former US air base [9]. On 10 July 1976, a chemical manufacturing plant accident occurred in Seveso, Italy, causing severe exposure to

Table 1 Toxic equivalency factor (TEF) for each of the dioxin-like compound (DLC)

Congener	WHO 2005 TEF
17 congeners of PCDDs/PCDFs	
PCDDs (polychlorinated dibenzo-p-dioxins)	
2,3,7,8-TCDD	1.0
1,2,3,7,8-PeCDD	1.0
1,2,3,4,7,8-HxCDD	0.1
1,2,3,6,7,8-HxCDD	0.1
1,2,3,7,8,9-HxCDD	0.1
1,2,3,4,6,7,8-HpCDD	0.0
OCDD	0.0
PCDFs (polychlorinated dibenzofurans)	
2,3,7,8-TCDF	0.1
1,2,3,7,8-PeCDF	0.0
2,3,4,7,8-PeCDF	0.3
1,2,3,4,7,8-HxCDF	0.1
1,2,3,6,7,8-HxCDF	0.1
2,3,4,6,7,8-HxCDF	0.1
1,2,3,7,8,9-HxCDF	0.1
1,2,3,4,6,7,8-HpCDF	0.010
1,2,3,4,7,8,9-HpCDF	0.010
OCDF	0.0001
12 congeners of dioxin-like PCBs	
Non-ortho-PCBs	
344'5'-TCB (PCB 81)	0.0001
33'44'-TCB (PCB 77)	0.0001
33'44'5'-PenCB (PCB 126)	0.1
33'44'55'-HxCB (PCB 169)	0.03000
Mono-ortho-PCBs	
2'344'5'-PeCB (PCB 123)	0.00003
23'44'5'-PeCB (PCB 118)	0.00003
2,344'5'-PeCB (PCB 114)	0.00003
233'44'-PeCB (PCB 105)	0.00003
23'44'55'-HxCB (PCB 167)	0.00003
233'44'5'-HxCB (PCB 156)	0.00003
233'44'5'-HxCB (PCB 157)	0.00003
233'44'55'-HpCB (PCB 189)	0.00003

TCDD. After 17 years, the TCDD levels in plasma remained as high as the median 2,3,7,8-TCDD and total dioxin levels of 73.3 and 95.0 pg/g -TEQ lipid, respectively, for those who lived near the most contaminated site [10].

Among the general population, two review papers, Marquès and Domingo [11] and Arisawa [12] summarised the blood PCDD/PCDF levels in the general population on several continents. In the populations living in the surroundings of a hazardous waste incineration plant in Constanti, Tarragona County, Spain, the

Table 2 Exposure levels of dioxin among different populations

Country	Years	Chemicals and levels	Remarks	Reference
<i>High exposure cases</i>				
Kyusyu, Japan		DLCs: 215.4 pg/g-TEQ lipid in blood	Yusho rice-bran oil contamination	[2]
Taiwan	1978–1979	PCDD/PCDFs 6,550 pg/g-TEQ lipid in blood	Yucheng rice-bran oil contamination	[2]
Vietnam	1970	Total PCDDs/PCDFs 1832 pg/g lipid in breast milk	Agent Orange during Vietnam war	[8]
	1991–1992	Total PCDDs/PCDFs 1,145 pg/g lipid (50 pg/TEQ lipid)	Central region ($n = 183$)	[8]
	2010	Total PCDDs/PCDFs: 25 pg/g lipid in blood	Phu cat (hotspot) ($n = 97$)	[9]
Seveso, Italy	1993	2,3,7,8-TCDD: 73.3 pg/g-TEQ fat Total dioxin 95.0 pg/g-TEQ fat	Population affected chemical manufacturing plant accident at very high contaminated site	[10]
<i>General populations</i>				
Constanti, Spain	1998	Mean levels of PCDD/PCDF 27 pg/g-TEQ fat	Nonoccupationally exposed subjects living in the vicinity of a new hazardous waste incinerator (HWI) ($n = 22$)	[11]
	2018	Mean levels of PCDD/PCDF 6.79 pg/g-TEQ fat	Nonoccupationally exposed subjects lived for at least the last 10 years in locations of Tarragona County near the HWI ($n = 40$)	[11]
Germany	1991	PCDD/PCDF: 42.7 pg/g-TEQ lipid in blood	The subjects were suspected to have been exposed to assumed PCDD/F sources in connection with fire accidents or exposure to contaminated materials like dust, soil, or degradation products of combustion processes ($n = 95$)	[13]
	1996	PCDD/PCDF: 20.74 pg/g TEQ lipid in blood		
Belgium	1998	17 PCDD/PCDF: 22.9 pg/g-TEQ fat in blood	About 700 anonymous blood donors	[14]
	2000	PCDD/PCDF: 23.1 pg/g-TEQ fat in blood	General population of donors ($n = 232$)	[14]
Japan	2002	PCDD/PCDF: 26.7 pg/g-TEQ lipid in blood	Living widely in 75 different residential areas of 25 prefectures of all over Japan ($n = 259$)	[15]

(continued)

Table 2 (continued)

Country	Years	Chemicals and levels	Remarks	Reference
	2006	PCDD/PCDF: 21.0 pg/g-TEQ lipid in blood	Living widely in 75 different residential areas of 25 prefectures of all over Japan Ff ($n = 291$)	[15]
	2011	PCDD/PCDF: 14.0 pg/g-TEQ lipid	Survey on the exposure to dioxins and other chemical compounds in humans (SEDOCCH) surveys ($n = 86$)	[16]
	2016	PCDD/PCDF: 9.0 pg/g-TEQ lipid	SEDOCCH surveys ($n = 80$)	[16]
Taiwan	2001– 2006	17 PCDD/PCDFs: 11.5 pg/g-TEQ fat in serum	Five urban areas (Taipei, Hsinchu, Taichung, Tainan, and Kaohsiung) and one rural area ($n = 251$)	[17]
The USA	1980– 1981	PCDD/PCDFs: 55 pg/g-TEQ lipid in blood	National Health and aging trends stud NHATS ($n = 57$)	[18]
	1990– 2000	PCDD/PCDFs: 15.4 pg/g-TEQ lipid in blood	The National Health and Nutrition Examination Survey (NHANES) ($n = 1,271$)	[19]
	2001– 2002	PCDD/PCDFs: 18.05 pg/g-TEQ lipid in blood	NHANES ($n = 1,244$)	[19]
	2003– 2004	PCDD/PCDFs: 13.90 pg/g-TEQ lipid in blood	NHANES ($n = 1,290$)	[19]
Tswana South Africa	2005	PCDD/PCDF: 4.0 pg/g-TEQ lipid in blood	Rural (Ganyesa) and urban (Potchefstroom) regions in the north west province, pooled blood ($n = 693$)	[21]
Agbogbloshie, Ghana	2011	PCDD/PCDF: 12.1 pg/g-TEQ lipid in blood	e-waste dumpsite exposed ($n = 21$)	[22]
	2011	PCDD/PCDF: 4.52 pg/g-TEQ lipid in blood	Non-exposed ($n = 21$)	[22]

mean levels of PCDD/PCDF reduced gradually from 27 pg/g-TEQ fat in 1998 to 6.79 pg/g-TEQ fat in 2018 [11]. In Germany, Wittsiepe et al. reported a significant decrease of PCDD/PCDF in blood from 42.67 pg/g-TEQ lipid in 1991 to 20.74 pg/g-TEQ lipid in 1996 in the general population [13]. In Belgium, Debacker et al. measured total PCDD/PCDF levels in blood donated to Red Cross and reported approximately similar levels of 22.9 pg/g-TEQ fat in 1998 and 23.1 pg/g-TEQ fat in 2000 [14]. Among the general population in Japan, a significant decrease of PCDD/PCDF in blood was also observed, from 26.7 pg/g-TEQ lipid in 2002 to 21.0 pg/g-TEQ lipid in 2006 [15]. Another cross-sectional study of The Ministry of the

Environment of Japan from 2011 to 2016 also observed a decreasing trend from the median 14.0 pg/g-TEQ lipid in 2011 to 9.0 pg/g-TEQ lipid in 2016 [16]. In the general population of urban and rural areas in Taiwan, blood samples were collected from 251 participants in 2001–2006, with median concentration of 11.5 pg/g WHO-TEQ fat for 17 PCDD/PCDFs [17]. In the USA, concentrations of PCDD/PCDFs in blood are available from the National Human Adipose Tissue Survey (NHATS) and National Health and Nutrition Examination Survey (NHANES). In NHATS 1980–1981, the median level was 55 pg/g WHO-TEQ lipid [18], whereas the levels decreased in 1990–2000, 2001–2002, and 2003–2004, to 15.4 pg/g TEQ lipid, 18.05 pg/g TEQ lipid, and 13.90 pg/g TEQ lipid, respectively [19]. In Africa, Ssebugere recently summarised the human and environmental exposure levels [20]. In a South African population health study in 2005, the median PCDD/PCDF level from pooled blood samples was 4.0 pg/g-TEQ lipid [21]. In Africa, approximately 90% households in rural areas burn biomass such as wood, coal, household waste, and agricultural residues, which could lead to a potential exposure to dioxins [21]. Another study was conducted in an electric and electronic equipment waste recycling site in the northern part of Ghana in 2011 [22]. Compared to unexposed individuals, the median PCDD/PCDF levels in the exposed individuals at the Electronic waste (e-waste) dumpsite were significantly higher, 4.52 pg/g-TEQ lipid vs 12.1 pg/g-TEQ lipid, respectively. Overall, Consonni examined the levels of PCDD/PCDFs and dioxin-like PCBs across 26 countries through 187 studies with 29,687 participants from the general population from 1989 to 2010 and concluded that European countries showed higher levels of dioxins than Asian, North American, and Oceanian countries. A clear decrease in PCDDs and PCDF levels has been documented over two decades [23].

Although studies examining the levels of DDT and its metabolite DDE in the blood of the general population were limited, the WHO and UNEP examined DDT and DDE in pooled samples of human breast milk [6]. The early stage of life is the most sensitive to chemical exposure. The third, fourth, and fifth surveys were conducted in 2000–2003, 2005–2007, and 2008–2010, respectively, and the number of pooled breast milk samples from donors were 102, 16, and 28, respectively, from a total of 47 countries. The levels of the total DDT metabolites, *o,p'*-DDT, *p,p'*-DDT, *o,p'*-DDE, *p,p'*-DDE, *o,p'*-DDD, and *p,p'*-DDD, were higher among Asian populations, notably the highest in Tajikistan (8,502 ng/g lipid), followed by that in India and Hong Kong. The majority of countries showing relatively high levels of DDT are located in tropical areas and are associated with malaria problems [6]. However, the examined DDT levels in breast milk in all such countries were under or near the calculated safe levels of the provisional total daily intake (10 µg/kg/day) defined by WHO [6]. Thus, the results do not limit breastfeeding because of its considerable benefits to the infant.

2.2 *Health Effects*

Several industrial cohorts of workers with phenoxy herbicide and chlorophenol exposure have been reported. Other studies have reported a high-dose exposure from the Seveso disasters, to US military personnel in Vietnam, Yusho, and to Yucheng patients, who were exposed to 10–1,000 times higher dioxins than the general population [24, 25]. Based on sufficient evidence from these human high-dose studies and animal experiments, dioxins have been found to be carcinogenic and the International Agency for Research on Cancer (IARC) classified TCDD as a Group 1 carcinogen to humans [26]. In addition, the mechanism of action for TCDD-induced cancer in humans applies to other dioxins and DLCs; thus, dioxin-like PCBs with a PCB TEF of 77, 81, 105, 114, 118, 123, 126, 156, 167, 169, and 189 were also classified in Group 1 in 2016 [26]. Simultaneously, it should be noted that the strong evidence of carcinogenesis is based on studies with participants with two to three times higher order of exposure than the general population [24]. Besides cancer, short-term but high-level exposure to dioxins may cause dermatological effects such as acneiform eruptions, chloracne, and pigmentation [24]. According to the results of epidemiological and animal studies, the reproductive, developmental, and neurodevelopmental toxicities, immunotoxicity, alteration of male-to-female ratio, and effects on thyroid hormones, liver, and tooth development are under consideration [26].

The health effects of DDT at accidentally high doses may include excitability, tremors, and seizures [27]. The IARC classified DDT in Group 2A, which includes substances probably carcinogenic to humans. The effects of exposure to DDT, DDE, and DDD in children are not well known. Animal studies suggest that exposure to DDT and DDE can mimic the action of hormones and may affect the reproductive and nervous systems [27]. Recent studies indicate that perinatal exposure to low doses of organochlorine pesticide may alter sex steroid hormones, birth weight, and neurodevelopment [2].

Foetuses and neonates may be particularly sensitive to exposure to dioxins, PCBs, and chlorinated pesticides. Especially, the life-long health effects of prenatal exposure to chemicals require investigation [28].

2.3 *Findings from a Birth Cohort: Hokkaido Study*

2.3.1 *Overview of the Hokkaido Study*

The Hokkaido Study on Environment and Children's Health (Hokkaido Study) is an on-going birth cohort study established in 2001 and one of the oldest birth cohort studies in Asia. The Hokkaido Study comprises two cohorts: the Sapporo cohort where 514 pregnant women were recruited at mid-term from one gynaecology hospital in Sapporo during 2001–2004 (Fig. 4) and the Hokkaido cohort that

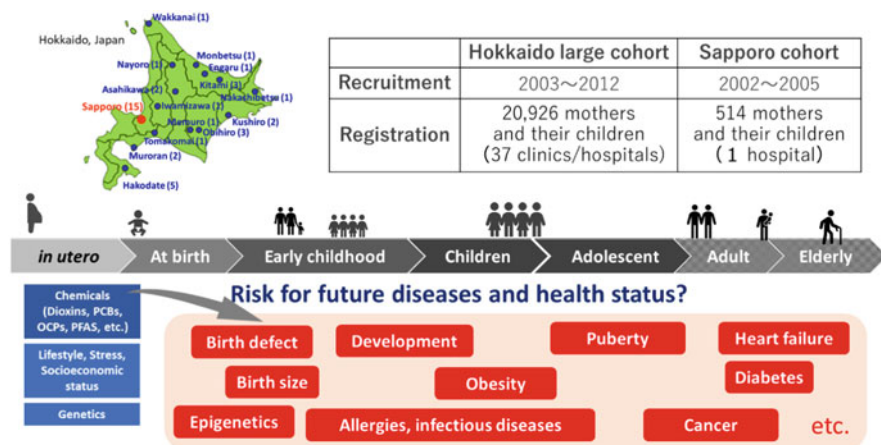


Fig. 4 Profile of The Hokkaido Study on Environment and Children's Health. Upper left: Locations of the participating obstetrician and gynaecology clinics and hospitals. Upper right: Recruitment information for the two cohorts. Lower tier: Cohort study flow

recruited 20,926 pregnant women in their first trimester in cooperation with 37 gynaecology hospitals and clinics all over Hokkaido Prefecture during 2002–2012. The primary aims of the study in both cohorts included (1) examining the adverse effects of relatively low perinatal environmental chemical exposure on birth outcomes, including birth defects and growth retardation; (2) following the development of allergies, infectious diseases, and neurobehavioral developmental disorders and performing a longitudinal observation of child development; (3) identifying high-risk groups with genetic susceptibilities to environmental chemical exposures; and (4) identifying the additive effects of lifestyle including tobacco smoking and folic acid intake encountered in the daily environment [29–32].

In the Sapporo cohort, maternal blood samples and cord blood during second to third trimester were collected for environmental chemical and biomarker measurements. The levels of 29 congeners of dioxins and dioxin-like PCBs (DL-PCBs) (seven PCDDs, 10 PCDFs, four non-ortho, and eight mono-ortho PCBs), 58 congeners of other PCBs, and five congeners of hydroxylated PCBs (OH-PCBs) were measured using high-resolution gas chromatography/high-resolution mass spectrometry (HRGC/HRMS) at the Fukuoka Institute of Health and Environmental Sciences. The TEQ levels were calculated by multiplying the levels of individual congeners with the TEF values defined by the WHO in 2005 [33]. The levels of 29 OCPs [5 chlordanes (*cis*-chlordane, *trans*-chlordane, *cis*-nonachlor, *trans*-nonachlor, and oxychlordane), six DDTs (*o,p'*-DDT, *p,p'*-DDT, *o,p'*-DDE, *p,p'*-DDE, *o,p'*-DDD, and *p,p'*-DDD), three drins (aldrin, dieldrin, and endrin), three heptachlors (heptachlors, *cis*-heptachlor epoxide (HCE), and *trans*-HCE), HCB, four hexachlorocyclohexane (HCH) isomers (α -HCH, β -HCH, γ -HCH, and δ -HCH), Mirex, and six toxaphenes (Parlar-26, Parlar-41, Parlar-40, Parlar-44, Parlar-50, and Parlar-62)] were analysed with gas chromatography/negative-ion

chemical-ionisation mass spectrometry (GC/NCIMS) and gas chromatography/high-resolution mass spectrometry (GC/HRMS) at IDEA Consultants, Inc. For health-related outcomes, information on gestational age at birth, infant sex, and birth size was obtained from medical records. Data on asthma and allergies were collected from the parents using the International Study of Asthma and Allergies in Childhood (ISAAC) criteria [34], along with the history of doctor-diagnosed infectious disease information through follow-up questionnaires at 18 months, and 3.5 and 7 years. Child neurodevelopment was examined face-to face according to the Bayley Scales of Infant Development second edition (BSID-II) at 6–7 and 18 months of age. Maternal and child thyroid hormone data were obtained from a mass screening test at the Sapporo City Institute of Public Health. Steroid and reproductive hormone levels were measured using cord blood samples with LC/MS and immunoassay. Single nucleotide polymorphisms (SNPs) were performed using allelic discrimination assays with fluorogenic probes and 5' nuclease (TaqMan) (Applied Biosystems, Foster, CA, USA) for maternal genotyping. For epigenetics, offspring patterns of insulin-like growth factor 2 (IGF2), H19, and long interspersed element 1 (LINE1) DNA methylation in cord blood were also examined by pyrosequencing.

2.3.2 Exposure Levels in Pregnant Women

The exposure levels of dioxins, PCBs, and chlorinated pesticides in the Sapporo cohort are shown in Table 3. Dioxins and PCBs in maternal blood levels were comparable or relatively lower than those in European countries and the USA [35]. Factors associated with higher levels of dioxins and PCBs in the Sapporo cohort were higher maternal age, nulliparas, non-smoking, higher educational levels, higher household income, higher frequency of fish intake, beef intake, alcohol consumption during pregnancy, and non-breastfeeding [36, 37]. Dioxins and PCBs are highly lipophilic and have a half-life ranging from a few years to decades; thus, it is common to find positive correlations between age and blood levels. Fish intake is a major source of exposure to dioxins and PCBs in Japan [2, 36]. Interestingly, maternal smoking significantly reduced the dioxin levels. This can be explained by the activation of AhR by tobacco smoke, which induces an eventual reduction in dioxins and PCBs [36].

Simultaneously, dioxins are metabolised by cytochrome 450 family 1 (CYP1) and AhR. Examining the genetic polymorphisms in dioxin-metabolising genes, as shown in Fig. 5, we found that maternal dioxin levels varied between genotype holders [38]. Specifically, the concentrations of 2,3',4,4',5-PeCB, 2,3,3',4,4'-PeCB, 2,3',4,4',5,5'-HexCB were significantly higher among mothers with a dominant AA+GA genotype compared to GG in AhR ($G > A$, Arg554Lys), and the concentration of 2,3,4,7,8-PeCDF was higher among mothers with a recessive TC + TT genotype compared to CC in CYP1A1 ($T > C$, *MesI*) [38]. The results suggest that certain genotype modify the internal dioxin levels in blood, so that pregnant women are genetically susceptible to dioxin, which may further affect the next generation.

Table 3 Exposure levels of POPs in pregnant woman's blood of Sapporo cohort

	Sample size (<i>n</i>)	25% tile	Median	75% tile	Maximum
Dioxins (pg/g lipid)					
Total PCDDs	364	365.5	460.9	609.0	1602.4
Total PCDFs	364	14.4	18.0	22.6	52.9
Non-ortho PCBs	364	53.4	76.0	99.5	281.7
Mono-ortho PCBs	364	7747.1	11471.7	15641.8	49632.0
Total dioxins	364	8149.7	11968.1	16432.2	50477.5
Dioxins (pg/g-TEQ lipid)					
Total PCDDs	364	5.1	6.9	9.2	29.3
Total PCDFs	364	1.8	2.4	3.1	7.8
Non-ortho PCBs	364	2.8	4.2	5.9	23.2
Mono-ortho PCBs	364	0.2	0.3	0.5	1.5
Total dioxins	364	10.1	13.9	18.4	43.4
Total 70 PCBs (ng/g lipid)	426	107.4	148.1	232.8	41460.4
Chlorinated pesticides (pg/g-wet)					
Oxychlorane	379	39.7	56.0	90.7	250.9
Cis-nonachlor	379	10.0	14.4	23.8	38.1
Trans-Nonachlor	379	71.5	107.6	176.5	513.5
p,p'-DDD	379	1.5	2.3	4.5	9.0
o,p'-DDE	379	1.3	1.8	3.4	6.2
p,p'-DDE	379	651.0	1011.5	1931.5	4575.7
o,p'-DDT	379	3.5	4.9	9.1	17.2
p,p'-DDT	379	23.2	34.0	59.2	121.5
Dieldrin	379	16.4	22.6	36.1	71.5
Cis-heptachlor epoxide	379	26.4	37.3	63.4	200.5
Hexachlorobenzene	379	101.7	130.1	180.3	245.5
β-Hexachlorocyclohexane	379	154.5	244.8	494.6	1667.1
Mirex	379	6.0	8.3	14.4	35.0
Parlar-26	379	4.4	6.7	12.4	20.8
Parlar-50	379	6.5	9.7	18.1	29.3

Among the 29 OCPs tested in maternal blood, 21 were detected [39]. Notably, even after 20 to 30 years of being banned, most of them were still detected, including Mirex, Parlar-26, and Parlar-50, which have never been used in Japan. Maternal age and pre-pregnancy body mass index were positively associated with concentrations, whereas past conceptions reduced the levels of certain compounds [39].

2.3.3 Associations Between Health Outcomes

As seen in Table 3, maternal blood levels of dioxins and PCBs during pregnancy in the Sapporo cohort were relatively low. However, these levels were associated with health outcomes, as shown in Table 4. These results suggest that prenatal exposure to

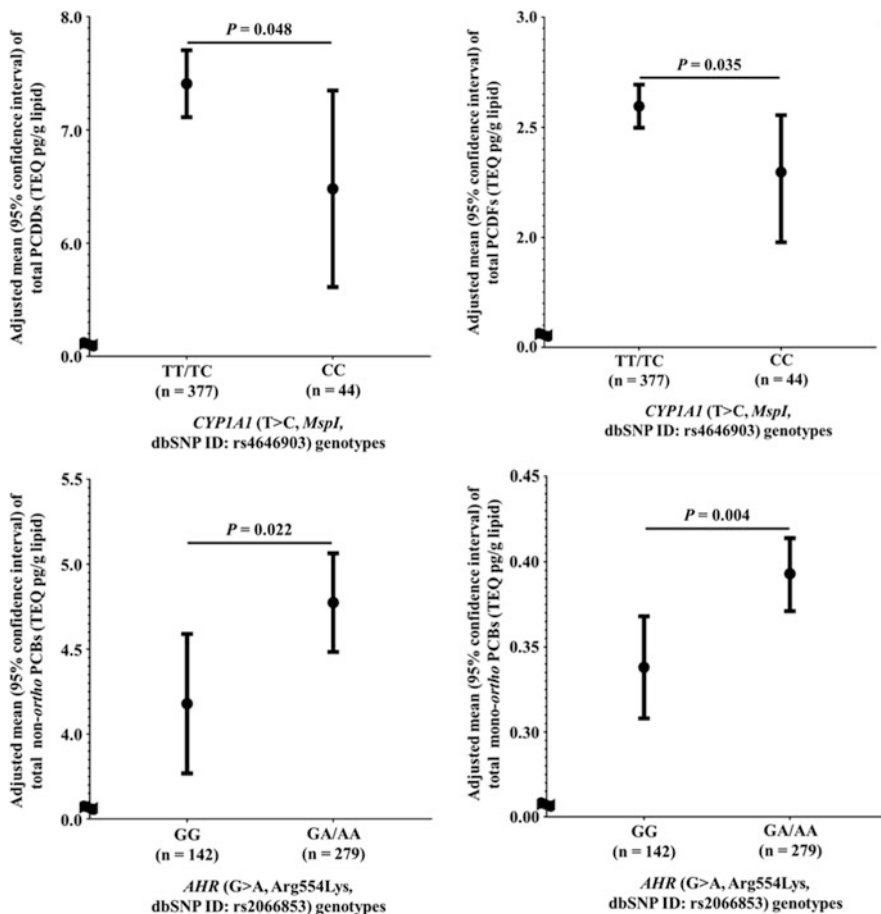


Fig. 5 Variation in maternal dioxin levels and genotypes of genetic polymorphisms. The generalised linear models were adapted and adjusted for maternal age, height, weight before pregnancy, caffeine intake during pregnancy, alcohol consumption during pregnancy, parity, smoking status during pregnancy, educational level, annual household income, inshore fish intake during pregnancy, deep-sea fish intake during pregnancy, and blood sampling period. Upper tier: CYP1A1 (T > C, MspI, dbSNP ID: rs4646903) genotypes: (a) total PCDD levels, (b) total PCDF levels. Lower tier: AHR (G > A, Arg554Lys, dbSNP ID: rs2066853) genotypes: (c) total non-ortho PCB levels, (d) total mono-ortho PCB levels

dioxin reduces the birth weight, especially in boys [40]. Total PCDD TEQ, PCDF TEQ, PCDD/PCDF TEQ, and total TEQ reduced the birth weight, along with each congener, for example, a 10-fold increase in 2,3,4,7,8-PeCDF reduced the birth weight by 24.6 g (95% confidence interval (CI): -387, -61.5) [40]. However, no association was found with PCBs [41]. Concentrations of PCBs are positively associated with free thyroxine, especially in boys [42]. Dioxins are also positively and inversely associated with a variety of steroid and reproductive hormones at birth,

Table 4 Dioxins and PCBs exposure and health outcomes

Exposures	Outcomes	Findings	Reference
Birth size			
PCDD/ PCDFs	Birth weight	Significant inverse association between dioxin levels and birth weight, remarkably among boys. Individual congener assessment found 2,3,4,7,8-PeCDF had a significant negative influence (per log ₁₀ unit: $\beta = -24.5$ g, 95% CI -387.4 to -61.5)	[40]
PCBs	Birth weight	No association	[41]
Hormones at birth			
PCB	Thyroid hormones	Log ₁₀ Σ dioxin (TEQ) was associated with increased FT ₄ ($\beta = 0.224$ ng/dL, 95% CI 0.016 to 0.433) overall, and the association was more significant among boys ($\beta = 0.299$ ng/dL, 95% CI 0.011 to 0.587)	[42]
Dioxins	Reproductive hormones	Among males, dioxins were related to decreased testosterone/estradiol ratios, sex hormone-binding globulin, and inhibin B whereas increased adrenal androgen/glucocorticoid ratios and follicle stimulating hormone and dehydroepiandrosterone (DHEA) levels. In females, increase in mono-ortho PCBs was related to increased cortisol, cortisone, and DHEA levels and adrenal androgen/glucocorticoid ratios	[43]
Neurodevelopment			
PCDD/ PCDFs	BSID-II at 6 months	Several dioxin isomers showed adverse effects on mental motor development in 6-month-old male infants	[44]
PCDD/ PCDFs, PCBs	BSID-II at 18 months	No association was observed between any of the dioxin isomers and neurodevelopment in males. In contrast, the levels of six dioxin isomers were significantly positively associated with mental development, and this unexpected finding might be attributable to residual confounding factors	[45]
Dioxins	K-ABC at 3.5 years	K-ABC (intelligence) scores were not associated with prenatal exposure to dioxins	[46]
Immune functions			
Total DL-PCBs	IgE at birth	Total dioxin-like compounds were associated with decreased cord IgE in males ($\beta = -1.01$; 95% CI: -1.79 , -0.23)	[47]
Dioxins	Otitis media	Among all infants: Polychlorinated dibenzofuran was associated with increased risk among male infants (OR 2.5, 95% CI 1.1–5.9) Among boys: 2,3,4,7,8-pentachlorodibenzofuran was associated with increased risk of otitis media (OR 5.3, 95% CI 1.5–19)	[37]

(continued)

Table 4 (continued)

Exposures	Outcomes	Findings	Reference
Dioxins	Wheeze eczema otitis media at 3.5 and 7 years	Total DLCs were associated with increased risk of wheeze in children up to aged 7 years (OR: 7.81; 95% CI: 1.4–43)	[47]
Genetic susceptibility			
Dioxin (total TEQ)	GSTM1 (non-null/null)	Per 10-fold increase of certain dioxin congeners TEQ reduced –214 to –346 g reduction of infant birth weight among mother with <i>GSTM1</i> null type	[48]
Epigenetics			
PCBs	DNA methylations at IGF-2, H19, and LINE1	Ten-fold increase of deca CBs increase 0.017 (95% confidence interval [CI]: 0.003–0.031) H19 methylation levels (%) among all infants. We observed a dose-dependent association of the decaCB levels in maternal blood with the H19 methylation levels among female infants (<i>P</i> value for trend = 0.040) Ten-fold increase of heptaCBs increase 0.005 (95% CI: 0.000–0.010) LINE-1 methylation levels (%) likewise a dose-dependent association of heptaCB levels was observed with LINE-1 methylation levels among female infants (<i>P</i> value for trend = 0.015)	[49]

increasing the specific ratios of testosterone/estradiol and adrenal androgen/glucocorticoid [43]. Higher levels of dioxin remarkably delayed neurodevelopment at 6 months, with total PCDD, total PCDD/PCDFs, and PCDD isomer 1,2,3,4,6,7,8-HpCDD affecting mental developmental index and the four maternal PCDD isomers, 1,2,3,7,8,9-HxCDD, 1,2,3,4,6,7,8-HpCDD, 2,3,7,8-TCDF, 1,2,3,7,8-PeCDF, and 1,2,3,6,7,8-HxCDF significantly associated with lower psychomotor developmental index [44]. However, these associations were not found at 18 months and 3.5 years of age. Moreover, higher levels of dioxin showed even positive associations with development [45, 46]. This unexpected finding might be attributed to residual confounding factors or benefits of fish intake, which increases the dioxin exposure levels as well. Among the tests for immune functions, dioxin levels were inversely associated with IgE in cord blood among male infants [47]. An increase in dioxin levels increased the history of otitis media incidence up to 18 months of age with an odds ratio (OR) of 2.5 [95% confidence interval (CI): 1.1, 5.9] after a 10-fold increase in PCDF, and an OR of 5.3 (95% CI: 1.5, 19) among all infants and 2,3,4,7,8-PeCDF among boys [37]. A 10-fold increase in total DLCs was associated with an increased risk of wheezing in children up to 7 years of age (OR = 7.81; 95% CI: 1.4, 43) [47]. The effects of dioxin exposure in utero were more pronounced in boys.

We also examined the genetic susceptibility to dioxins. Among mothers with specific gene polymorphisms, the *GSTM1* null type, per 10-fold increase in certain dioxin congeners TEQ reduced the infant birth weight by 214 to 346 g [48]. Finally,

Table 5 Associations between organochlorine pesticides and health outcomes

Outcomes	Findings	Reference
Hormone levels at birth		
Thyroid hormones	For maternal free T4, inverse associations were found with levels of <i>o,p'</i> -DDE, <i>o,p'</i> -DDT, and dieldrin, and the weighted quantile sum analysis showed that <i>o,p'</i> -DDT (48.6%), <i>cis</i> -HCE (22.8%), dieldrin (15.4%) were the primary contributors to the significant mixture exposure effect of OCPs on maternal FT4. For infants free T4, positive association with <i>cis</i> -nonachlor and mirex was found. The most contributory compounds in the multiple exposure effect were <i>trans</i> -nonachlor (27.1%) and <i>cis</i> -nonachlor (13.8%)	[50]
Reproductive hormones	Among boys in categorical quartile models, testosterone and DHEA were inversely and positively associated with OCPs, respectively. Estradiol-testosterone and adrenal androgen-glucocorticoid ratios tended to increase with increasing OCP concentrations in the higher quartile, while the testosterone-androstenedione ratio tended to decrease. Sex hormone-binding globulin and prolactin showed an inverse association with OCPs. Among girls, the linear regression model showed that only <i>p,p'</i> -DDT was inversely associated with the level of DHEA and the adrenal androgen-glucocorticoid ratio, but was positively associated with cortisone levels	[51]
Neurodevelopment		
BSID-II at 6 and 18 months	Children born to mothers with <i>cis</i> -HCE in the highest quartile had mental developmental index scores -9.8 (95% confidence interval: $-16.4, -3.1$) lower than children born to mothers with concentrations of <i>cis</i> -heptachlor epoxide in the fourth quartile (P for trend <0.01)	[53]

we examined the epigenetic mechanisms of DNA methylation. Associations between the DNA methylation of IGF-2, H19, and LINE1 genes in infants and PCB levels in maternal blood were examined [49]. These results suggest that exposure to PCBs in utero may increase H19 and LINE1 methylation levels in cord blood, particularly in girls.

The findings of organochlorine pesticide use and health outcomes are shown in Table 5. Organochlorine pesticide levels were inversely associated with maternal free T4 but positively associated with infantile free T4. Examining the mixed exposure, *o,p'*-DDT (48.6%), *cis*-heptachlor epoxide (22.8%), and dieldrin (15.4%) were primary contributors in mothers, whereas *trans*-nonachlor (27.1%) and *cis*-nonachlor (13.8%) in infants [50]. Similar to dioxins, OCPs also alter child steroids and reproductive hormones at birth [51]. Linear regression models after sex stratification showed that chlordanes, *cis*-HCE HCB Mirex, and toxaphenes in maternal blood were inversely associated with testosterone, cortisol, cortisone, sex hormone-binding globulin, prolactin, androstenedione-dehydroepiandrosterone (DHEA), and testosterone-androstenediones ratios in boys. Furthermore, these

OCPs were positively correlated with DHEA, follicle stimulating hormone (FSH), and adrenal androgen-glucocorticoid and FSH-inhibin B ratios in boys. In girls, the linear regression model showed that only *p,p*-DDT was inversely associated with the DHEA levels and the adrenal androgen-glucocorticoid ratio, but positively associated with cortisone levels. Studies in the USA and Russia reported a delay in the onset of puberty with higher prenatal exposure to OCPs; therefore, further follow-up of the children is warranted [52]. Regarding child development, children born to mothers with *cis*-HCE in the highest quartile had significant lower Mental Development Index (MDI) scores -9.8 (95% CI: $-16.4, -3.1$) than those born to mothers with concentrations in the fourth quartile (P for trend <0.01) at 18 months of age [53]. However, caution should be exercised, as this is the only compound with statistical significance among the 15 compounds.

3 Conclusions and Recommendations for Future Research

The use of POPs has already been banned under the Stockholm Convention. There is clear evidence that the concentrations of PCBs, dioxins, and OCPs have been decreasing. However, these chemicals are still detected in the environment, wild animals, and the human body because of their long half-lives. Beyond the health of an individual, it is crucial to protect the land, air, and water globally. Development of technology to accelerate the degradation of these chemicals and remediation of the environment is urgent.

The Hokkaido Study suggest that an exposure to even relatively low levels of these chemicals in utero may alter child hormone levels at birth and induce lower birth size, delay in neurodevelopment, alterations in immune functions, and increase in infectious diseases and allergies. Longer follow-up is required to examine the residual effects at a later age. In addition, the levels of these chemicals in blood are generally highly correlated. Thus, the examination of mixed chemicals using sophisticated statistical methods is required.

The United Nations has a set of 17 sustainable development goals to achieve a healthier and more sustainable future for all [54]. Chemical and waste management are related to achieving each of these goals, especially #3 (good health and well-being), #14 (life below water), and #15 (life on land). The accumulation of scientific knowledge and reinforcement of actions on scientific evidence are important for future generations.

Acknowledgement This research was supported by Grants-in Aid for Scientific Research from the Japan Ministry of Health, Labour, and Welfare; the Japan Society for the Promotion of Science; the Ministry of Education, Culture, Sports, Science, and Technology; and Environment Research and Technology Development Fund.

References

1. Stockholm Convention. <http://www.pops.int/TheConvention/ThePOPs/tabid/673/Default.aspx>
2. Miyashita C (2020) Environmental pollution and recent data on Asian children's health in relation to pre-and early post-natal exposure to persistent organic pollutants, including PCGs, PCDD/PCDFs, and organochlorine pesticides. In: Kishi R, Grandjean P (eds) Health impacts of developmental exposure to environmental chemicals. Springer, Singapore, pp 279–300
3. Ministry of the Environment Japan. <https://www.env.go.jp/chemi/kurohon/>. 7 Mar 2021
4. Houman G, Yamazaki K (2020) Effects of developmental exposure to perfluoroalkyl substances on health outcomes in pregnant women and offspring. In: Kishi R, Grandjean P (eds) Health impacts of developmental exposure to environmental chemicals. Springer, Singapore, pp 279–300
5. WHO/UNEP (2012) State of the science of endocrine disrupting chemicals-an assessment of the state of the science of endocrine disruptors prepared by a group of experts for the United nations Environment Programme (UNEP) and World Health Organization (WHO)
6. van den Berg M, Kypke K, Kotz A et al (2017) WHO/UNEP global surveys of PCDDs, PCDFs, PCBs and DDTs in human milk and benefit-risk evaluation of breastfeeding. *Arch Toxicol* 91(1):83–96
7. Lü YC, Wong PN (1984) PCB poisoning in Japan and Taiwan. Dermatological, medical, and laboratory findings of patients in Taiwan and their treatments. *Prog Clin Biol Res* 137:81–115
8. Schecter A, Dai LC, Thuy LTB et al (1995) Agent Orange and the Vietnamese: the persistence of elevated dioxin levels in human tissues. *Am J Public Health* 85:516–522
9. Manh HD, Kido T, Okamoto R et al (2014) Serum dioxin levels in Vietnamese men more than 40 years after herbicide spraying. *Environ Sci Technol* 48(6):3496–3503
10. Consonni D, Sindaco R, Agnello L et al (2012) Plasma levels of dioxins, furans, non-ortho-PCBs, and TEQs in the Seveso population 17 years after the accident. *Med Lav* 103(4):259–267
11. Marques M, Domingo JL (2019) Concentrations of PCDD/Fs in human blood: a review of data from the current decade. *Int J Environ Res Public Health* 16:5366
12. Arisawa K (2018) Recent decreasing trends of exposure to PCDDs/PCDFs/dioxin-like PCBs in general populations, and associations with diabetes, metabolic syndrome, and gout/hyperuricemia. *J Med Investig* 65:151–161
13. Wittsiepe J, Schrey P, Ewers U et al (2000) Decrease of PCDD/F levels in human blood – trend analysis for the German population, 1991–1996. *Environ Res* 83(1):46–53
14. Debacker N, Sasse A, van Wouwe N et al (2007) PCDD/F levels in plasma of a Belgian population before and after the 1999 Belgian PCB/DIOXIN incident. *Chemosphere* 67(9):S217–S223
15. Uemura H, Arisawa K, Hiyoshi M et al (2008) PCDDs/PCDFs and dioxin-like PCBs: recent body burden levels and their determinants among general inhabitants in Japan. *Chemosphere* 73(1):30–37
16. Muzembo BA, Iwai-Shimada M, Isobe T et al (2019) Dioxins levels in human blood after implementation of measures against dioxin exposure in Japan. *Environ Health Prev Med* 24(1):6
17. Hsu JF, Lee CC, Su HJ et al (2009) Evaluation of background persistent organic pollutant levels in human from Taiwan: polychlorinated dibenzo-p-dioxins, dibenzofurans, and biphenyls. *Environ Int* 35(1):33–42
18. Ferriby LL, Knutsen JS, Harris M et al (2007) Evaluation of PCDD/F and dioxin-like PCB serum concentration data from the 2001–2002 National Health and Nutrition Examination Survey of the United States population. *J Expo Sci Environ Epidemiol* 17(4):358–371
19. LaKind JS, Hays SM, Aylward LL et al (2009) Perspective on serum dioxin levels in the United States: an evaluation of the NHANES data. *J Expo Sci Environ Epidemiol* 19(4):435–441
20. Ssebugere P, Sillanpaa M, Matovu H et al (2019) Human and environmental exposure to PCDD/Fs and dioxin-like PCBs in Africa: a review. *Chemosphere* 223:483–493

21. Pieters R, Focant JF (2014) Dioxin, furan and PCB serum levels in a South African Tswana population: comparing the polluting effects of using different cooking and heating fuels. *Environ Int* 66:71–78
22. Wittsiepe J, Fobil JN, Till H et al (2015) Levels of polychlorinated dibenzo-p-dioxins, dibenzofurans (PCDD/Fs) and biphenyls (PCBs) in blood of informal e-waste recycling workers from Agbogbloshie, Ghana, and controls. *Environ Int* 79:65–73
23. Consonni D, Sindaco R, Bertazzi PA (2012) Blood levels of dioxins, furans, dioxin-like PCBs, and TEQs in general populations: a review, 1989–2010. *Environ Int* 44:151–162
24. Kogevinas M (2001) Human health effects of dioxins: cancer, reproductive and endocrine system effects. *Hum Reprod* 7(3):331–339
25. Mitoma C, Uchi H, Tsukimori K et al (2015) Yusho and its latest findings – a review in studies conducted by the Yusho group. *Environ Int* 82:41–48
26. World Health Organization (2019) Preventing disease through healthy environments: exposure to dioxins and dioxin-like substances: a major public health concern. Geneva, Switzerland. Contract No.: WHO/CED/PHE/EPE/19.4.4
27. Agency for Toxic Substances and Disease registry. Toxic substances portal - DDT, DDE, DDD. <https://www.cdc.gov/TSP/substances/ToxSubstance.aspx?toxid=20>. 7 Mar 2021
28. Kishi R, Grandjean P (eds) (2020) Health impacts of developmental exposure to environmental chemicals. Springer, Singapore
29. Kishi R, Araki A, Minatoya M et al (2017) The Hokkaido birth cohort study on environment and Children's health: cohort profile-updated 2017. *Environ Health Prev Med* 22(1):46
30. Kishi R, Kobayashi S, Ikeno T et al (2013) Ten years of progress in the Hokkaido birth cohort study on environment and children's health: cohort profile-updated 2013. *Environ Health Prev Med* 18(6):429–450
31. Kishi R, Sasaki S, Yoshioka E et al (2011) Cohort profile: the Hokkaido study on environment and children's health in Japan. *Int J Epidemiol* 40(3):611–618
32. Kishi R, Ikeda-Araki A, Miyashita C, Itoh S, Kobayashi S, Bamai YA, Yamazaki K, Tamura N, Minatoya M, Ketema RM, Poudel K, Miura R, Masuda H, Itoh M, Yamaguchi T, Fukunaga H, Ito K, Goudarzi H (2021) Hokkaido birth cohort study on environment and children's health: cohort profile 2021. *Environ Health Prev Med* 26(1):1–20
33. Van den Berg M, Birnbaum LS, Denison M et al (2006) The 2005 World Health Organization re-evaluation of human and mammalian toxic equivalency factors for dioxins and dioxin-like compounds. *Toxicol Sci* 93(2):223–241
34. Beasley R (1998) Worldwide variation in prevalence of symptoms of asthma, allergic rhinoconjunctivitis, and atopic eczema: ISAAC. *Lancet* 351(9111):1225–1232
35. Kishi R, Araki A, Minatoya M et al (2018) Birth cohorts in Asia: the importance, advantages, and disadvantages of different-sized cohorts. *Sci Total Environ* 615:1143–1154
36. Miyashita C, Sasaki S, Saijo Y et al (2015) Demographic, behavioral, dietary, and socio-economic characteristics related to persistent organic pollutants and mercury levels in pregnant women in Japan. *Chemosphere* 133:13–21
37. Miyashita C, Sasaki S, Saijo Y et al (2011) Effects of prenatal exposure to dioxin-like compounds on allergies and infections during infancy. *Environ Res* 111(4):551–558
38. Kobayashi S, Sata F, Sasaki S et al (2013) Genetic association of aromatic hydrocarbon receptor (AHR) and cytochrome P450, family 1, subfamily A, polypeptide 1 (CYP1A1) polymorphisms with dioxin blood concentrations among pregnant Japanese women. *Toxicol Lett* 219(3):269–278
39. Kanazawa A, Miyasita C, Okada E et al (2012) Blood persistent organochlorine pesticides in pregnant women in relation to physical and environmental variables in the Hokkaido study on environment and children's health. *Sci Total Environ* 426:73–82
40. Konishi K, Sasaki S, Kato S et al (2009) Prenatal exposure to PCDDs/PCDFs and dioxin-like PCBs in relation to birth weight. *Environ Res* 109(7):906–913

41. Miyashita C, Sasaki S, Ikeno T et al (2015) Effects of in utero exposure to polychlorinated biphenyls, methylmercury, and polyunsaturated fatty acids on birth size. *Sci Total Environ* 533: 256–265
42. Baba T, Ito S, Yuasa M et al (2018) Association of prenatal exposure to PCDD/Fs and PCBs with maternal and infant thyroid hormones: the Hokkaido study on environment and children's health. *Sci Total Environ* 615:1239–1246
43. Miyashita C, Araki A, Mitsui T et al (2018) Sex-related differences in the associations between maternal dioxin-like compounds and reproductive and steroid hormones in cord blood: the Hokkaido study. *Environ Int* 117:175–185
44. Nakajima S, Saijo Y, Kato S et al (2006) Effects of prenatal exposure to polychlorinated biphenyls and dioxins on mental and motor development in Japanese children at 6 months of age. *Environ Health Perspect* 114(5):773–778
45. Nakajima S, Saijo Y, Miyashita C et al (2017) Sex-specific differences in effect of prenatal exposure to dioxin-like compounds on neurodevelopment in Japanese children: Sapporo cohort study. *Environ Res* 159:222–231
46. Ikeno T, Miyashita C, Nakajima S et al (2018) Effects of low-level prenatal exposure to dioxins on cognitive development in Japanese children at 42 months. *Sci Total Environ* 618:1423–1430
47. Miyashita C, Bamai YA, Araki A et al (2018) Prenatal exposure to dioxin-like compounds is associated with decreased cord blood IgE and increased risk of wheezing in children aged up to 7 years: the Hokkaido study. *Sci Total Environ* 610–611:191–199
48. Kobayashi S, Sata F, Miyashita C et al (2017) Dioxin-metabolizing genes in relation to effects of prenatal dioxin levels and reduced birth size: the Hokkaido study. *Reprod Toxicol* 67:111–116
49. Kobayashi S, Sata F, Miyashita C et al (2017) Gender-specific association of exposure to non-dioxin-like polychlorinated biphenyls during pregnancy with methylation levels of H19 and long interspersed nuclear element-1 in cord blood in the Hokkaido study. *Toxicology* 390:135–145
50. Yamazaki K, Itoh S, Araki A et al (2020) Associations between prenatal exposure to organochlorine pesticides and thyroid hormone levels in mothers and infants: the Hokkaido study on environment and children's health. *Environ Res* 189:109840
51. Araki A, Miyashita C, Mitsui T et al (2018) Prenatal organochlorine pesticide exposure and the disruption of steroids and reproductive hormones in cord blood: the Hokkaido study. *Environ Int* 110:1–13
52. Araki A, Jensen TK (2020) Endocrine-distributing chemicals and reproductive function. In: Kishi R, Grandjean P (eds) *Health impacts of developmental exposure to environmental chemicals*. Springer, Singapore, pp 101–129
53. Yamazaki K, Araki A, Nakajima S et al (2018) Association between prenatal exposure to organochlorine pesticides and the mental and psychomotor development of infants at ages 6 and 18 months: the Hokkaido study on environment and children's health. *Neurotoxicology* 69:201–208
54. Kishi R, Araki A (2002) Further direction of research and policy making of environment and children's health. In: Kishi R, Grandjean P (eds) *Health impacts of developmental exposure to environmental chemicals*. Springer, Singapore, pp 545–557

Part III
Introduction of Novel Functions
and Materials into Remediation
Technologies

Electrokinetic Remediation



Yasuhiro Akemoto, Rudy Syah Putra, and Shunitz Tanaka

Contents

1	Introduction	148
2	Principles	149
3	Design of Experimental Conditions	152
3.1	Equipment Scale and Material	152
3.2	Electrical Conditions	152
3.3	Energy Resource	154
3.4	Soil Properties	155
3.5	Impacts on the Environment	155
3.6	Cost Efficiency	156
4	Advanced EK Remediation	157
4.1	Solubilization	158
4.2	Humic Substances	159
4.3	Accumulation	162
4.4	Decomposition and Transformation	167
5	Electro-Assisted Phytoremediation	169
5.1	Influence of Electrode Configuration	170

Y. Akemoto (✉)

Hokkaido Research Organization, Industrial Technology and Environment Research
Department, Research Institute of Energy, Environment and Geology, Sapporo, Hokkaido,
Japan

e-mail: akemoto-yasuhiro@hro.or.jp

R. S. Putra

Department of Chemistry, Faculty of Mathematics and Natural Sciences, Universitas Islam
Indonesia, Yogyakarta, Indonesia

Environmental Remediation Research Group, Faculty of Mathematics and Natural Sciences,
Universitas Islam Indonesia, Yogyakarta, Indonesia

e-mail: rudy.syahputra@uui.ac.id

S. Tanaka

Faculty of Environmental Earth Science, Hokkaido University, Sapporo, Hokkaido, Japan

Hokkaido Center of Environmental Science and Technology, Sapporo, Hokkaido, Japan

ES General Laboratory Co., Sapporo, Hokkaido, Japan

e-mail: shunitz@ees.hokudai.ac.jp

Shunitz Tanaka, Masaaki Kurasaki, Masaaki Morikawa, and Yuichi Kamiya (eds.),

Design of Materials and Technologies for Environmental Remediation,

Hdb Env Chem (2023) 115: 147–198, DOI 10.1007/698_2022_843,

© The Author(s), under exclusive license to Springer Nature Singapore Pte Ltd 2022,

Published online: 16 April 2022

5.2	Application of EAPR Systems on Contaminated Water	174
5.3	Combination with Other Technologies for the Remediation of Contaminated Water	177
6	Disaster Pollution	180
6.1	Saline Soil	180
6.2	Radioactive Species	180
6.3	Cesium Pollution	181
6.4	Interaction with Soil Components	182
6.5	Application for Contaminated Radioactive Waste	184
7	Conclusion	185
	References	186

Abstract Electrokinetic (EK) remediation is an in situ soil treatment technology that applies electric fields such as electromigration and electroosmotic flow (EOF). This technology is advantageous for environmental remediation applications in two ways. First, electromigration and EOF are limited between electrodes, such that the treatment area is easy to control. Second, EOF occurs independent of soil properties, may be applied to low-permeability soils, and is capable of moving soluble substances. Insoluble forms, such as substances that strongly interact with soil components and precipitated forms such as oxides or hydroxides, are difficult to remove. Various strategies have been investigated to achieve remediation. Inorganic or organic acids, chelating reagents, and surfactants have been found to enhance the removal efficiency of pollutants from soil. In addition, various technologies, such as membrane separation, decomposition, phytoremediation, and adsorption, have been combined to improve the removal efficiency.

This chapter introduces the principles of EK remediation, the necessary experimental conditions, and the design of applications for effective environmental remediation.

Keywords Accumulation, Clay mineral, Electrokinetic remediation, Electromigration, Electroosmotic flow (EOF), Humic substances, In situ soil remediation, Phytoremediation, Solubilization

1 Introduction

Electrokinetic (EK) remediation is a soil remediation technology that uses an electric field. The principles and applications of EK remediation were published in *Environmental Science and Technology* (American Chemical Society Publications) in 1993 [1, 2]; around this year, several fundamental papers relating to EK remediation were published [3–6]. Since then, the number of publications on EK remediation has increased. The first International Symposium on Electrokinetic Remediation (EREM) was held in Albi (France) in 1997 and has since been held annually around the world [7].

EK remediation covers a wide range of target pollutants including organic substances such as organochlorine compounds, polyaromatic hydrocarbons (PAHs), oils, and pesticides, to inorganic substances such as heavy metals, radionuclides, salts, and anionic species. Organic pollutants are transformed into low-risk substances by chemical oxidation or reduction reactions, heating, and biodegradation. To apply these techniques as in situ soil remediation, various reagents and microorganisms can be introduced into the soil via the EK process. Unlike organic pollutants, inorganic pollutants cannot be decomposed and need to be removed from contaminated areas. Inorganic pollutants often exist in poorly soluble forms, such as oxides and fractions interacting with soil components. As such, studies have investigated the use of complex reagents or acids to create low-pH conditions to solubilize heavy metals [8–10].

In general, pollutants are removed from the soil and transferred into the electrolyte where the electrodes are inserted. An alternative method is the accumulation of pollutants in a specific area to reduce the volume of waste that requires treatment following the EK process. This EK process is applicable to soil, sludge, sediment, ash, and concrete [11–13].

This chapter introduces the principles of EK remediation, the necessary experimental conditions, and several applications. Finally, the potential of EK process as a decontamination method for radioactive waste generated by the Fukushima Daiichi Nuclear Power Plant accident in Japan is considered.

2 Principles

EK remediation can remove pollutants from soil via electromigration and electroosmotic flow (EOF). Figure 1 presents a conceptual diagram of EK remediation. Electromigration is the movement of electrically charged substances towards the polar opposite of its electric charge: a cationic substance moves toward the cathode

Fig. 1 Conceptual diagram of electrokinetic remediation

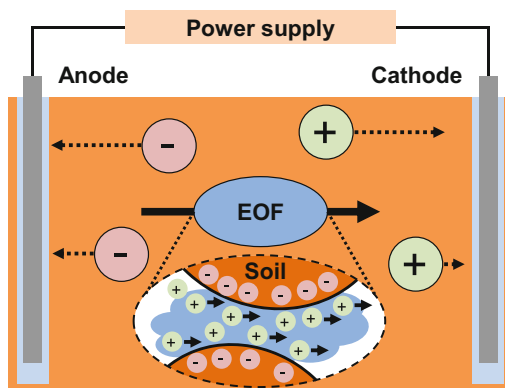


Table 1 The ionic mobility of major ions at 25°C

Cation	Mobility/ $10^{-8} \text{ m}^2 \text{ V}^{-1} \text{ s}^{-1}$	Anion	Mobility/ $10^{-8} \text{ m}^2 \text{ V}^{-1} \text{ s}^{-1}$
H ⁺	36.98	OH ⁻	20.9
Cs ⁺	8.16	Fe(CN) ₆ ⁴⁻	11.7
NH ⁺	7.78	CrO ₄ ²⁻	8.98
K ⁺	7.76	SO ₄ ²⁻	8.45
Pb ²⁺	7.50	CN ⁻	8.24
Fe ³⁺	7.29	Cl ⁻	8.06
Cr ³⁺	7.08	C ₂ O ₄ ²⁻	7.84
Al ³⁺	6.44	NO ₂ ⁻	7.58
Ca ²⁺	6.28	NO ₃ ⁻	7.54
Sr ²⁺	6.28	C ₆ H ₅ O ₇ ³⁻	7.41
Cu ²⁺	5.98	CO ₃ ²⁻	7.32
Cd ²⁺	5.70	ClO ₄ ⁻	7.11
Hg ²⁺	5.66	SCN ⁻	7.02
Fe ²⁺	5.65	F ⁻	5.85
Mn ²⁺	5.65	CH ₃ COO ⁻	4.32
Mg ²⁺	5.60	HC ₂ O ₄ ⁻	4.25
Zn ²⁺	5.58	H ₂ AsO ₄ ⁻	3.59
Na ⁺	5.29	H ₂ PO ₄ ⁻	3.49

The values are the molar ionic conductivity divided by the Faraday constant [15].

side and an anionic substance moves toward the anode side. The electromigrative velocity ($u_{e,m}$) is given by Eq. 1 [14]:

$$u_{e,m} = v_i z_i n \tau F \nabla E \quad (1)$$

For ionic species i , v_i is the ionic mobility ($\text{m}^2 \text{V}^{-1} \text{s}^{-1}$), z the ionic valence, n the soil porosity, τ the tortuosity of the soil, F the Faraday constant (C mol^{-1}), and ∇E the potential gradient (V m^{-1}). Notably, n and τ are dimensionless and depend on the soil properties; typically, the range of n is 0.1–0.7 and that of τ is 0.01–0.84 [1]. The ionic mobility (v_i) is a specific value for each substance, and the electromigrative velocity ($u_{e,m}$) increases with the potential gradient. Table 1 details the ionic mobility (v_i) of the major ions.

EOF is the water transportation in soil that occurs with the application of an electric potential. This phenomenon has already been observed and has been used as a dewatering technique for soil [16]. The velocity of the EOF ($u_{e,o}$) is expressed by the Helmholtz–Smoluchowski equation (Eq. 2):

$$u_{e,o} = \frac{\varepsilon \zeta}{\mu} \nabla E \quad (2)$$

where ε is the permittivity of water ($\text{C V}^{-1} \text{m}^{-1}$), ζ the zeta potential of the soil particle (V), and μ the viscosity of water (Pa s). The velocity of the EOF is

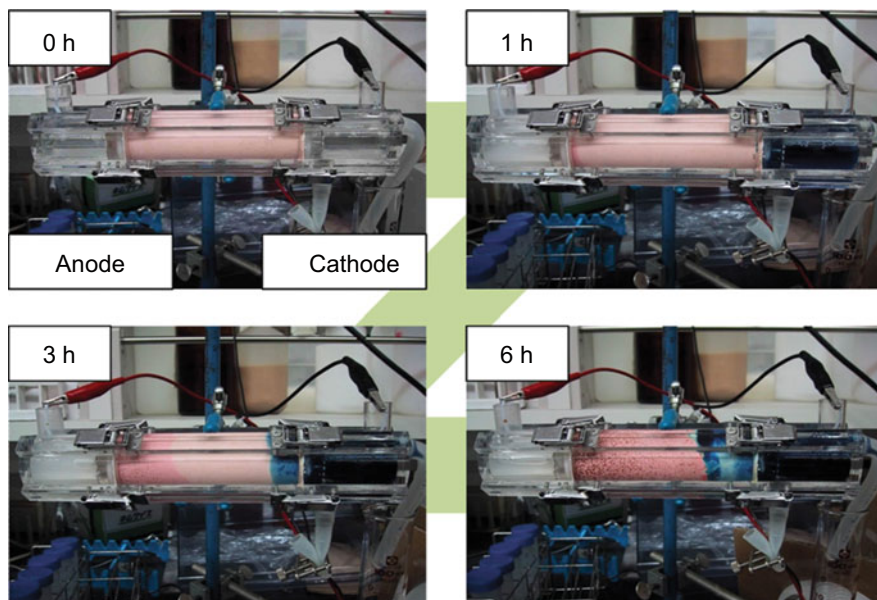
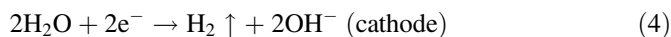
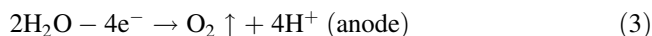


Fig. 2 Illustration of soil pH change during the electrokinetic process. Note: left and right sides are the anode and cathode; red and blue zones indicate acid and basic regions, respectively

approximately 10 cm day^{-1} under a potential gradient of 100 V m^{-1} at 20°C [5]. The velocity of the EOF and electromigration increases with the potential gradient, on the other hand, soil acidification and alkalization occur near the electrode by electrolysis. Typically, soil particles have a negative charge and the EOF direction is toward the cathode side. The zeta potential of the soil particles is neutralized or positively charged under acidic conditions. When soil particles have a positive charge, the EOF direction is from the cathode to the anode side, which means that the velocity and direction of the EOF are dependent on the soil environment.

Electrolysis significantly affects the soil pH (Eqs. 3 and 4).



Hydrogen ions (H^+) are generated at the anode and introduced into the soil by electromigration, which creates an acidic region near the anode. Likewise, hydroxide ions (OH^-) also form a basic region near the cathode. As H^+ and OH^- have a higher ionic mobility than other ionic species (Table 1), the soil pH slope forms quickly under low buffering ability. The authors attempted to visually demonstrate the pH change in the soil using a methyl yellow and thymolphthalein, as shown in Fig. 2. In the figure, the left side is the anode and the right side is the cathode; the initial soil is light pink, and over time red and blue zones appear in the vicinity of each electrode. The red and blue zones are indicative of acidic and basic regions, respectively.

Figure 2 shows that H^+ and OH^- generated by electrolysis are introduced into the soil, and the acidic and basic interface is formed slightly closer to the cathode side because the ionic mobility of H^+ is higher than that of OH^- . This acidification promotes the solubilization of heavy metals in the soil, enhancing their removal efficiency by EK remediation. Conversely, low pH conditions make it difficult to reuse the soil for agricultural use, for which soil neutralization is often required after remediation. The EOF velocity is also dependent on the zeta potential of the soil particles (Eq. 2); however, in most cases the zeta potential is neutralized in the acidic region, and the EOF velocity decreases. As such, the effective use of EOF for pollutant removal requires that the soil pH is maintained around neutral.

3 Design of Experimental Conditions

Certain aspects of the experiment should be carefully designed to investigate EK remediation. This section introduces the experimental conditions used in several previous studies.

3.1 *Equipment Scale and Material*

Many researchers have designed rectangular or cylindrical equipment. In many cases, polyvinyl chloride (PVC) or acrylic resin, characterized by high electrical resistance and ease of processing and molding, has been used as the main construction material; the equipment for EK remediation consists of one migration chamber and two electrode chambers (Fig. 3). The electrode chamber has an opening for the addition of the electrolyte and the insertion of instruments that measure pH and electrical conductivity (EC). The pH control system is combined with EK equipment to create a constant soil pH environment during the experiment. The interface of the soil and electrolyte is separated using filter paper or nylon cloth to prevent the elution of soil from the migration chamber to the electrode chamber. In a lab-scale experiment, 100 g to a few kilograms of soil is used to evaluate the effectiveness of the EK process, while a scale of approximately 40–4,000 m³ is used for field-scale experiments [2, 17].

3.2 *Electrical Conditions*

The electrode materials of EK remediation require acidic and basic resistance. As platinum or iridium oxide-coated titanium is inert under acidic conditions, these materials have been used in lab-scale experiments as electrodes. Mesh-like electrodes made of these materials have been used to prevent interference with the EOF.

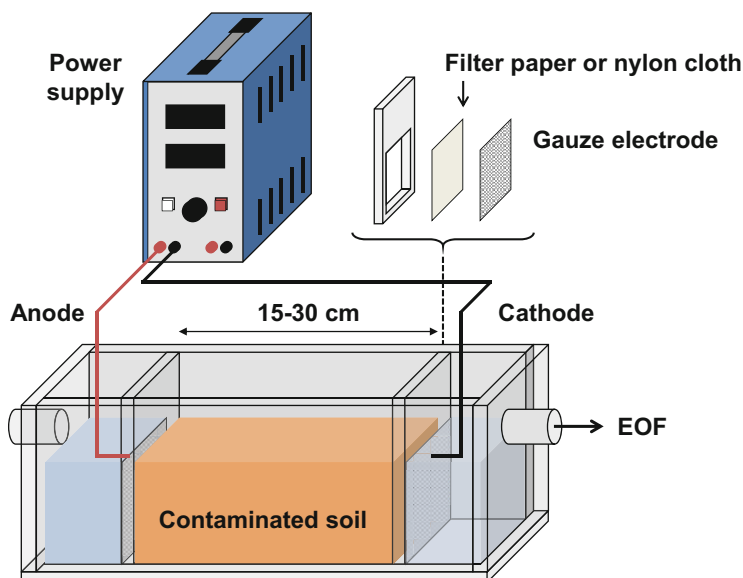


Fig. 3 Schematic of the equipment used in electrokinetic remediation

The size and number of electrodes are dependent on the extent of the treatment area; typically, field-scale experiments require a large size or many electrodes. As these inert materials are expensive, stainless-steel or graphite carbon is used as the electrodes in field-scale experiments. The injection of iron (Fe) ions because of the corrosion of the iron electrode from electrolysis may be used to decompose organic pollutants by a chemical reaction (described in Sect. 4.4.2).

The range of the potential gradient is commonly $0.1\text{--}5\text{ V cm}^{-1}$; this gradient is closely related to the distance between the anode and cathode in field-scale experiments. The duration of the treatment increases with the distance between the anode and cathode; therefore, this distance should be set appropriately [18]. In field-scale experiments, the distance between the anode and cathode is set between 1 and 2 m [19, 20]. For example, an electric potential of 100 V is required for a 1 V cm^{-1} potential gradient at an electrode distance of 1 m. A potential gradient of $0.1\text{--}5\text{ V cm}^{-1}$ has often been used as it considers the transmission capacity, safety, and environmental impact depending on the country. On the other hand, Athmer and Ho stated that a potential gradient of 1 V cm^{-1} is not practical as the soil temperature exceeds 100°C after a week [21]. A higher potential gradient can reduce the remediation period owing to the higher electromigration and EOF velocity (Eqs. 1 and 2). Therefore, the potential gradient and operating time should be balanced. The estimated electric resistance of humans is $\sim 5\text{ M}\Omega$; however, when the skin surface is wet, the resistance decreases. For safety reasons, people should stay away from the treatment area during processing. Additionally, the enclosures should be made of wood or nonconductive materials, as a metal fence may be subject to corrosion.

Various arrays of electrodes have been reported to accumulate pollutants in specific areas and achieve effective soil acidification. The positioning of the anode at the bottom of the soil and the cathode on the ground surface enables the accumulation of cationic pollutants near the ground surface. A triangular or hexagonal arrangement of the anode can effectively acidify the soil. This acidification prompts the accumulation of heavy metals around the cathode in the center, where the alkalization area is minimized [18, 22, 23]. Various studies have investigated different electrolytes for enhanced pollutant removal efficiency, the details of which are introduced in Sect. 4.

3.3 *Energy Resource*

Renewable energy has been evaluated as a potential energy resource for EK remediation. Solar panels can only generate electricity during the day light hours. Typically, EK remediation operates over weeks or months, in which the intermittency of the applied voltage does not significantly affect the removal efficiency. Yuan et al. found no significant difference between the removal efficiency of cadmium (Cd) using a conventional power supply and solar energy. They also found that running costs using solar energy were reduced by approximately 60% compared to conventional power supply [24]. When the electric potential is continuously supplied, the soil pH changes rapidly, and polarization occurs in the soil. This polarization lowers the electromigration velocity and extends the remediation period. On the other hand, the application of pulsed electric fields using solar panels can minimize this soil polarization and contribute to reducing the operating time and running cost [25]. Although the diffusion of pollutants without a potential gradient after sunset is a concern, most studies have found it to be negligible [26]. Solar energy has been applied to remove fluorine (F) from contaminated soil and manganese (Mn) and nitrogen in ammonium form (NH_3) from residuals following hydro-metallurgy [27, 28]. Wind power has also been examined as a potential energy resource for the removal of herbicides from soil. In terms of the potential gradient, there seems to be no significant difference between conventional power supply and wind power energy [29]. However, in these renewable energy sources, the effects of weather conditions are not negligible. Microbial fuel cells (MFCs) are independent of weather conditions and may be applied without large facilities, such as solar panels and wind power generation. MFCs use electrons produced when microorganisms oxidize organic matter; several studies have used MFC as a power supply for the EK process to remove pesticides or heavy metals from soil [30, 31]. The current density obtained by the MFC is relatively lower than that used in the conventional EK process; thus, a longer remediation period is required. Moreover, as microbial activity decreases at low temperatures, the application of MFCs in cold regions is limited. However, MFCs have the advantage of not requiring an external power supply and frequent maintenance.

Renewable energy has a relatively low environmental impact compared to fossil-fuel-derived energy. As such, renewable energy demonstrates good potential as a power supply for EK remediation, although it would be necessary to become more widespread.

3.4 Soil Properties

Soil is a complex material comprising metal oxides, organic matter, and microorganisms. Its use at the beginning of the experiment is not always a good approach as there is a possibility of unexpected reactions occurring in the soil. In lab-scale experiments, clay minerals have often been used as model soil to evaluate EK remediation. Specifically, kaolinite or pyrophyllite has been used in various studies because these minerals have a low adsorption capacity, low buffering capacity for pH, and low swelling, which make these soils suitable for observing the migration behavior of pollutants, complex formation reactions, and the decomposition process. However, the interactions between substances such as cesium (Cs) vary depending on the type of clay mineral. As such, the removal behavior of Cs is significantly affected by the type of clay (described in Sect. 6). Once the migration and reaction are evident in the model soil, several horticultural or actual soils containing pollutants can be evaluated.

3.5 Impacts on the Environment

Sections 3.1, 3.2, 3.3, and 3.4 introduce the concept of the experimental conditions for EK remediation. In addition to the removal efficiency, the impact of the EK process on the environment must also be considered as sustainable remediation technology.

The first is the effect of the EK process on soil components. Section 2 discusses that acidic and basic regions are generated by the EK process without any buffer solution. Soil particles consist of silicate, aluminum, and iron oxides; these elements (particularly aluminum) are eluted in an acidic environment [32]. As a high concentration of Al is toxic to plants [33], the elution of these elements needs to be continuously monitored.

The second is the loss of nutrients as a result of the EK process. As electromigration and EOF do not possess selectivity for each substance in the soil, all ionic or dissolved substances will move alongside the pollutants; this phenomenon introduces the potential to remove nutrients. One study also reported the injection of nitrogen compounds as nutrients introduced into the soil by the EK process [34]. The EK process is also effective for creating suitable soil conditions for agricultural use after remediation.

The third is the effect of the EK process on soil microorganisms. These microbes play important roles in the decomposition of plant remains, nitrogen fixation, and material circulation. Ethylenediaminetetraacetic acid (EDTA) has been used to enhance the removal efficiency of heavy metals; however, it reduces microbial cell numbers and diversity [35]. The increased toxicity of pentachlorophenol (PCP) due to soil acidification during the EK process also reduces the microbial cell numbers [36]. Thus, several previous studies have reported that the addition of substances to enhance pollutant removal efficiency or accumulation of pollutant has a significant impact on microbial activity. Alternatively, negatively charged microorganisms have been injected into the soil using electromigration and EOF to decompose PAHs [37]. These studies indicate that the electric field does not directly have an adverse effect on microbial activity [38]. Since environmental remediation is not only removal of pollutant, the environmental impacts of EK remediation should be determined and built upon to develop a sustainable means of soil remediation.

3.6 Cost Efficiency

Detailed studies on the cost of EK remediation are scarce. Athmer reported on cost efficiency and indicated that the cost of EK remediation was estimated at \$200 m⁻³. The area and depth of the contaminated site, treatment time, and site preparation (such as building removal) were major factors influencing cost, whereas the cost of electricity was a minor factor in the suite of cost variables associated with EK remediation [39]. With a narrow or shallow contaminated area, the cost of excavating a well to insert electrodes may be reduced. In general, buildings should be removed to prevent the straying voltage. However, if the target field is flat land, such as agricultural land, building removal is not required. Compared with these factors, energy consumption is considered predictable; on average, the ratio of electricity to total cost is 15% [39]. In the first field application, the total energy consumption was 65 kWh m⁻³ after 43 days of operation, but it was estimated to be 85 kWh m⁻³ to reach the Dutch reference level [2]. Jeon et al. showed that the energy consumption was 67.5 kWh m⁻³ after 35 days of operation [25], while Kim et al. reported a consumption of 170 kWh m⁻³ over 37 weeks [40]. The highest contributing factor to the total cost is installation, which includes labor, equipment, and materials. These cost estimations are also dependent on soil properties, remediation period, removal efficiency, and target pollutants. When the cost of EK remediation is lower than \$90 t⁻¹, it is estimated to be less than that of an excavation process [39], and as the excavation process only transports pollutants to another location, it is not necessarily considered a fundamental remediation. Many field applications are thus required to obtain detailed cost estimates to establish EK remediation as an in situ remediation process.

4 Advanced EK Remediation

Clay and clayey soils have very low water permeability, and as such, conventional pollutant removal technologies cannot achieve sufficient removal efficiency for these soils. In particular, the use of acid and surfactant solutions as additives for soil washing and flushing is ineffective, as they cannot infiltrate in clayey soil. Despite the occurrence of useful reagents that can dissolve and decompose pollutants, it is difficult to carry out these reactions in soil without transporting these reagents to the desired locations. The EK process is the only method that can transport these reagents and water-soluble pollutants in clayey soils via electromigration and EOF.

Therefore, the EK process enables the introduction of various chemical reactions into the soil to remove and decompose pollutants. Complex formations between metal ions and ligands such as EDTA, solubilization of hydrophobic compounds with surfactants and cyclodextrin, and redox reactions may occur in soil during the EK process. The Fenton reaction to decompose harmful organic substances and dechlorination using zero-valent iron (Fe) may also be demonstrated in soil by the EK process. The introduction of these reactions into the EK process enables expansion of the targets in applications. Figure 4 illustrates the introduction of several chemical reactions into the soil. Based on this idea, this section also introduces the usefulness of some reactions in soil for EK remediation.

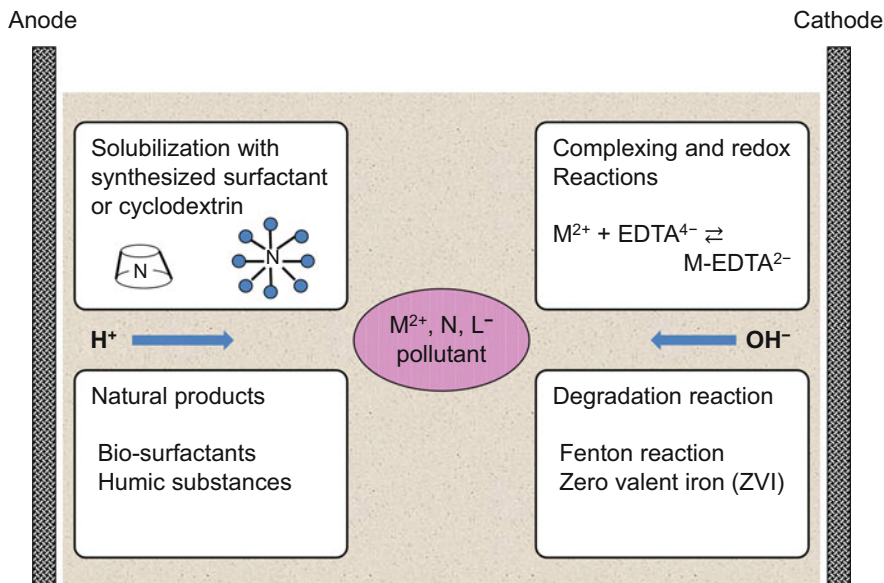


Fig. 4 Introduction of chemical reactions into the soil

4.1 Solubilization

In the environment, heavy metals exist in insoluble forms such as oxides, sulfides, bound to Fe-Mn oxides, and hydroxides [41–44]. To solubilize these heavy metals, several types of acids have been injected into the soil directly or added into the electrolyte, and the cation exchange membrane is located between the soil and cathode to prevent the penetration of OH^- into the soil [45–48]. For example, the removal efficiency of zinc (Zn) and nickel (Ni) from contaminated soil was shown to improve 20-fold using nitric acid, which was added to the cathode electrolyte to maintain a constant pH [49]. However, for inorganic acids such as nitric and hydrochloric acids, the nitrate ions may cause secondary contamination, and the chloride ions may produce toxic chlorine gas due to the electrode reaction at the anode.

EDTA has been used to form complexes with many types of heavy metals and solubilize these metals [8, 50–52]. EDTA forms negative complex ions with divalent metal ions, as shown in Eq. 5.



This complex moves toward the anode side by electromigration [8]; as this is the opposite of the EOF direction, the net velocity of the complex is reduced by that of the EOF. Therefore, this is not always the best condition for the EK process. EDTA is advantageous in that it can dissolve insoluble heavy metals; however, its low biodegradability may cause secondary contamination. To this end, several alternative chelating reagents have been investigated. Niinae et al. reported that the removal efficiency of lead (Pb) from soil using EDTA and [S,S]-ethylenediamine disuccinic acid ([S,S]-EDDS) did not significantly differ for each chelating reagent [9]. Similar to the Pb-EDTA complex, the Pb-EDDS complex, which has a negative charge, moves toward the anode side. Several organic acids, such as acetic, citric, oxalic, and lactic acids, have also been used as enhancement reagents because of their low environmental impact [53–55]. Citric acid is most commonly used in the EK process as it forms a complex with heavy metals and prevents precipitation as a hydroxide. As this complex maintains heavy metals in soluble form over a wide pH range, it contributes to a higher removal efficiency. Several surfactants, such as sodium dodecyl sulfate (SDS) and Tween 80, have been used to increase the removal efficiency of insoluble organic pollutants, such as organochlorine compounds and PAHs [56–60]. Although these surfactants have an excellent ability to solubilize these insoluble organic pollutants, there is potential for these surfactants to be adsorbed on clay minerals [61]. Similar to nitrate ions, surfactants may remain in the environment and cause secondary contamination. Cyclodextrin is a by-product that forms during the decomposition of starch by microorganisms; it is highly biodegradable and has a low affinity for soil. It has high potential for use as an enhancement reagent during the EK process. Maturi and Reddy attempted the simultaneous removal of Ni and phenanthrene from contaminated soil using

cyclodextrin. Phenanthrene was solubilized by cyclodextrin and moved toward the cathode side by EOF [62]. Biosurfactants are biosynthesized substances and metabolites of yeast and bacteria; they are amphipathic and have low toxicity and environmental impact. Gonzini et al. reported the EK remediation of contaminated soil with gasoil using rhamnolipid as an enhancement reagent produced from *Pseudomonas aeruginosa*. Rhamnolipid is a biosurfactant, and gasoil is solubilized with rhamnolipids. Gonzini et al. found that 86.7% of the solubilized gasoil was removed and transported to the cathode side by EOF after 15 days [63]. In addition, biosurfactants are also effective in removing heavy metals [64] and show high potential as enhancement reagents in EK remediation because of their low environmental impact.

4.2 Humic Substances

Humic substances are natural products of the decomposition of plant remains through microbial activity. These substances are amorphous and heterogeneous mixtures of different types of compounds produced by microorganisms. However, humic substances are widely distributed in the environment and play an important role in material circulation. Humic substances have both hydrophilic groups, such as hydroxyl and carboxyl groups, where the hydrophobic parts are aromatic rings and alkyl chains in their structure. As such, these humic substances can enhance solubilization of pollutants due to functions as surfactant, oxidation or reduction reactions, and complex formation.

4.2.1 Removal of Cu-Oxine with Humic Acid

Some studies have reported removal methods in which the EK process uses solubilization reactions of hydrophobic and oily compounds with surfactants in soil (Sect. 4.1). However, the use of synthesized surfactants may at times lead to secondary pollution; if natural surfactants are used, this risk may be reduced. Humic acid (HA) is one of the main organic constituents in soil, and it is characterized by a surface-active property as its structure consists of hydrophobic and hydrophilic parts. HA acts as a surfactant to solubilize the hydrophobic compounds in water. We attempted to introduce HA in the EK process to remove the scarcely water-soluble Cu-oxine complex from soil, which is a type of herbicide. First, we investigated the movement of HA in kaolin, a clay mineral used as a model clayey soil, under an electric field. In a migrating chamber, a kaolin zone with a high HA concentration was established in the center of the chamber and sandwiched with pure kaolin, as shown in Fig. 5. A potential gradient of 2.2 V cm^{-1} was applied between the cathode and anode in the electrode chamber. As HA has a negative charge in neutral and alkaline pH regions, it was expected to migrate to the anode side by electromigration; however, we observed the movement of HA to the cathode,

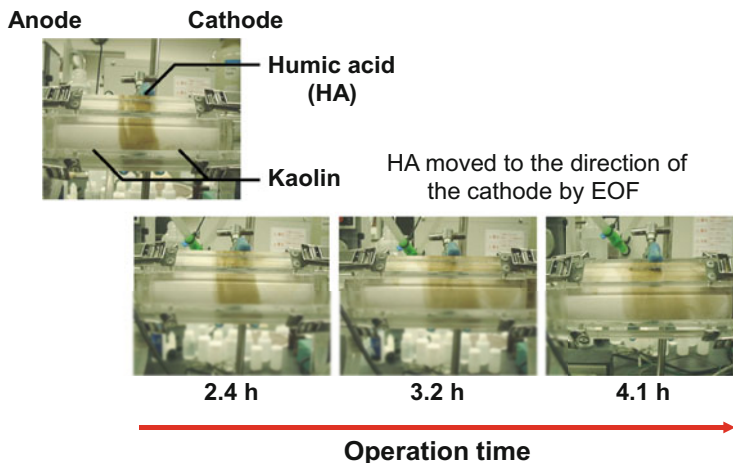


Fig. 5 Movement of humic acid (HA) in kaolin. HA: 58 mg g^{-1} , water content: 31%, potential gradient: 2.2 V cm^{-1}

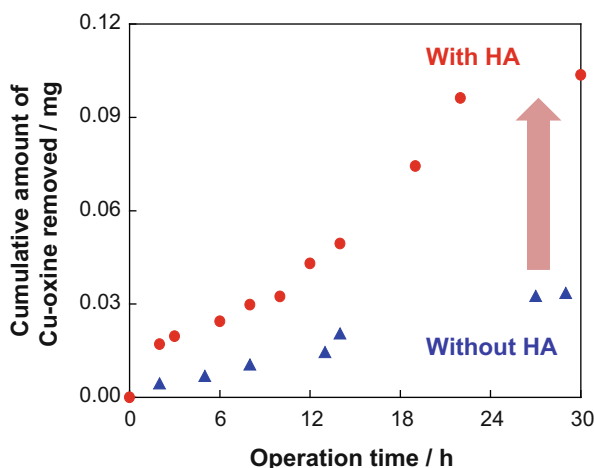


Fig. 6 Removal of Cu-oxine from soil with HA. Cu-oxine: 230 mg g^{-1} , HA: 58 mg g^{-1} , water content: 31%, pH 7, applied potential: 2.2 V cm^{-1}

as shown in Fig. 5. This may be due to the higher velocity of the EOF to the cathode side than the electromigration of HA to the anode side in kaolin. Based on these results, a kaolin layer containing a large amount of HA was established on the more anodic side than the site in which kaolin was contaminated with Cu-oxine. Then, HA was transported to the polluted site by the EOF, and Cu-oxine was solubilized with HA and moved to the cathode side accompanied by HA. Figure 6 shows that the presence of HA enhanced the removal efficiency of Cu-oxine three-fold compared to

the removal efficiency in the absence of HA. It was clarified that the introduction of natural surfactants such as HA into the EK process facilitates the establishment of an environmentally friendly removal method using solubilization reactions in the soil [65].

4.2.2 Reduction and Removal of Cr(VI)

Chromium (Cr) is one of the most frequently reported heavy metals in contaminated soils. Cr(VI) is toxic to the human body, whereas Cr(III) has relatively low toxicity [66]. Typically, Cr(VI) is reduced to Cr(III) via several reactions for environmental protection. As soil organic matter (SOM), such as HA, is known to reduce Cr(VI) to Cr(III), we attempted to reduce and remove Cr(VI) from soil using EK remediation with HA and its precursors (tannic and gallic acids). The model contaminated soil with Cr(VI) was prepared using kaolin and potassium dichromate, and Cr behavior was observed under a potential gradient of 2 V cm^{-1} . When the model soil did not include HA, Cr existed as $\text{Cr}_2\text{O}_7^{2-}$ and moved to the anode via electromigration. When the model soil included HA or its precursors, the Cr concentration near the anode decreased, and a high Cr concentration was detected in the cathode and EOF reservoir. These results show that Cr(VI) was reduced to Cr(III) by HA and its precursors; Cr was then removed as the cationic species by electromigration and EOF [67].

The reduced Cr(III) is considered to have been present as a Cr(III)-SOM complex, which is stable and rarely re-oxidized or decomposed [68, 69]. We recovered Cr(VI) in the anode electrolyte from the soil using EK remediation and passed this electrolyte through a column filled with immobilized tannin resin, which was then recirculated to the anode for reuse as an electrolyte (Fig. 7). After 14 h under a potential gradient of 2 V cm^{-1} , approximately 83% of Cr(VI) was removed from the soil and accumulated in the immobilized tannin column [70].

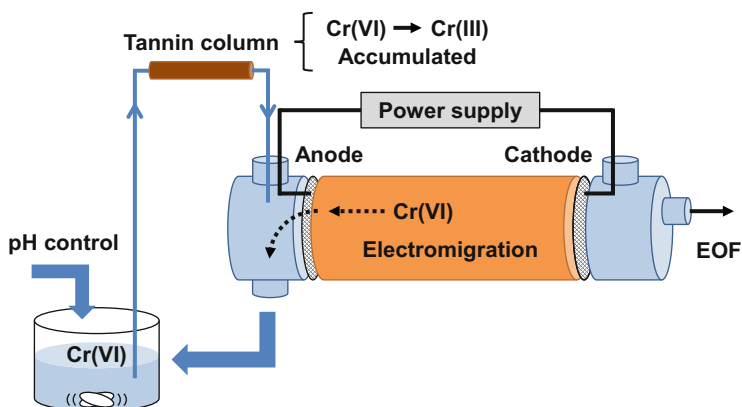


Fig. 7 Conceptual EK process with an immobilized tannin column

4.2.3 Complex Formation

HA has the ability to complex with several heavy metals owing to its functional groups [71–74]; we investigated the application of this ability to remove Pb from contaminated soil using the EK process. The contaminated soil was prepared using $\text{Pb}(\text{NO}_3)_2$, and the Pb removal efficiency after 72 h of operation was 48.0% without HA compared to 72.6% with HA. Although HA has a negative charge, it moves to the cathode side by the EOF (Fig. 5). HA interacts with Pb and consequently weakens the interaction between Pb and clay minerals, resulting in greater Pb removal when HA is used [75]. As the HA behavior is dominated by the EOF, it is preferable to locate HA in the anode chamber for its continuous supply. However, when HA was added as an anode electrolyte, it remained in the anode chamber even after 72 h of operation. The generation of EOF was limited to the surface of solid media such as clay minerals, and EOF was not generated in the liquid media. Therefore, HA should be added to the soil for enhancement of the removal efficiency [76].

Humic substances are known to interact with various other compounds because of their ability to activate and form complexes [77–79]. As these substances have a low environmental impact and interact with various compounds regardless of their inorganic or organic nature, they are expected to contribute to the development and improvement of EK remediation.

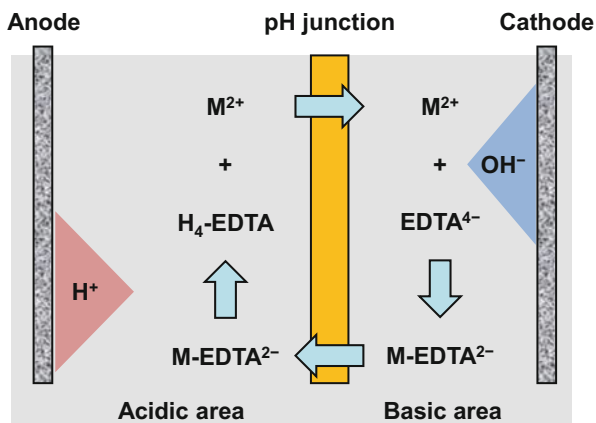
4.3 Accumulation

EK remediation is also used to accumulate pollutants at specific sites in soils or liquids. This accumulation simplifies the management of contaminated waste and reduces the amount of waste that requires treatment following EK remediation. Various methods, such as chemical reactions and membrane separation, have been investigated.

4.3.1 pH Junction

In EK remediation, the electrolysis of water occurs at both electrodes, where the anode and cathode are acidified and alkalinized by the formed H^+ and OH^- , respectively. The generated H^+ and OH^- invade the soil, and the acidification and alkalization occur continuously. In using the EK process to remediate actual contaminated sites, the solution of each chamber should be neutralized to protect water and soil from acidification or alkalization. However, soil acidification may improve the removal efficiency of metal ions in soil by accelerating ion exchange with protons. Without neutralizing treatment in both electrode chambers, the acidification and alkalization of soil gradually spread from the anode and cathode, respectively

Fig. 8 Accumulation of metal ions in the pH junction [81]



(Fig. 2). Finally, the acid and base fronts in the soil meet within a narrow region, where the soil pH changes sharply; this region is known as the pH junction.

Metal ions are released from soil by ion exchange with protons and are then transported to the cathode side by electromigration and enter the pH junction; these metal ions accumulate at this junction: metal hydroxide precipitates because of the rapid increase in pH at this site. With the introduction of ligands such as EDTA from the cathode chamber, the metal-EDTA complex on the cathode side of the pH junction becomes negatively charged as there is an alkali region where the complex may be stable. Then, the metal-EDTA complex is transported to the anode side of the pH junction. Once the metal-EDTA complex enters the anode side, the metal complex dissociates to form a free metal cation and EDTA as there is an acidic region. Metal cations move to the cathode side (to the pH junction) by electromigration and form the EDTA complex, which is then transported back to the anode side. Eventually, the metal ion can only exist at the pH junction, resulting in the accumulation of metal ions in the pH junction, as shown in Fig. 8. To experimentally confirm this hypothesis, Cu-contaminated kaolin was placed in half of the anode side of the migration chamber, and kaolin containing EDTA was placed in the remaining half of the cathode side. After completion of the EK process, we confirmed that Cu ions accumulated around the pH junction, as shown in Fig. 9. Thus, we demonstrated the potential of a pH junction to remove and accumulate heavy metal ions within a specific area via EK process [80].

4.3.2 Electrodialysis

The separation mechanism used for electrodialysis is also applied to soil remediation, which is known as electro-dialytic soil remediation (EDR) [46]. EDR is implemented in combination with an ion exchange membrane; the anion exchange membrane (AEM) is located near the anode side, and the cation exchange membrane (CEM) is located near the cathode side. Although H^+ produced by electrolysis

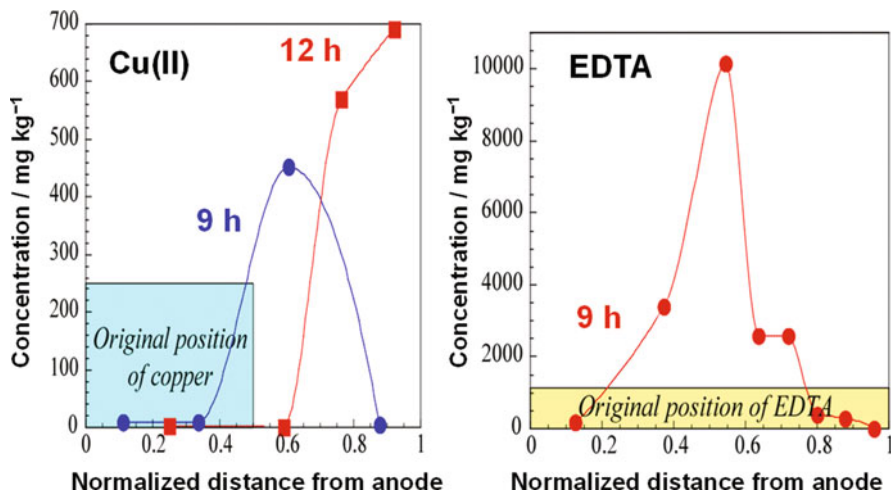


Fig. 9 Distribution of Cu and EDTA in the migration chamber after EK treatment with pH junction. Applied current: 50 mA [80]

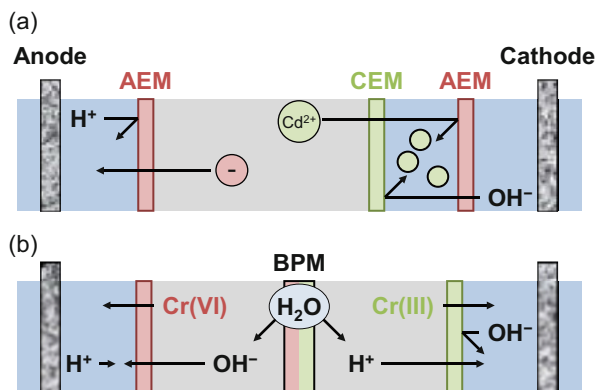


Fig. 10 (a, b) Conceptual electrodynamic soil remediation (EDR). *AEM* anion exchange membrane, *CEM* cation exchange membrane, *BPM* bipolar membrane

typically penetrates the soil, it cannot pass through the AEM; similarly, the penetration of OH^- is prevented by the CEM. Therefore, soil acidification and alkalization are minimized in the EDR (Fig. 10), and the electric current may be used by focusing on pollutants because of the inhibited mobilization of H^+ and OH^- [82, 83]. Jakobsen et al. reported the accumulation of Cd in solution between AEM and CEM by EDR. Cd in soil moved toward the cathode side via electromigration and EOF and passed through the CEM on the soil side. As it could not pass through the AEM on the cathode side, it accumulated in the solution between the AEM and CEM (Fig. 10a) [84]. The bipolar membrane (BPM) consists of anion and cation

exchange layers, which can dissociate water into H^+ and OH^- in the intermediate layer by the electric field. Liu et al. reported that BPM effectively removed Cu and Ni from contaminated sludge, and Cr was simultaneously separated by electric charge and removed (Fig. 10b) [85, 86].

4.3.3 Entrapment Zone

Groundwater contaminated by organic or inorganic pollutants, originating from either soil leaching or anthropogenic activities, is a major environmental issue. Groundwater remediation is the highest priority for many countries that use groundwater for drinking purposes. While the pump-and-treat method is a traditional technique for contaminated groundwater, the excavation and disposal of contaminated soil that alters the groundwater is no longer considered an adequate solution [87]. The demand for soil and groundwater treatment techniques is increasing and the development of new low-cost, efficient, and environment-friendly remediation processes has become an important study in the last two decades.

The concept of using a treatment zone in combination with EK remediation for pollutant removal from soil and groundwater was widely discussed at the fifth EREM 2005 symposium [88]. EK remediation is an emerging technology that can be used to remove contaminants in situ from heterogeneous fine-grained soils. Pump-and-treat technology and permeable reactive barrier (PRB) are uneconomical and impractical for application to fine-grained soils because of the low hydraulic conductivity of these soils [18, 89, 90]. During in situ EK remediation, the contaminant flux migrates from the anode towards the cathode owing to the combined effects of electromigration and electroosmosis, which are the main mechanisms at play during heavy metal removal [91]. Employing the entrapment zone (EZ) for EK remediation as a more effective removal technique involves the use of a PRB placed across the flow path of a contaminated plume. As the plume flows through the EZ under the EK, contaminants are entrapped, immobilized, and precipitated, without requiring soil excavation or groundwater pumping.

Enhanced EK remediation using EZ reactive material has shown promising results for heavy metal removal (e.g., Cr, Cu, As, Pb, and Ni) from soil, as it prevents heavy metal leaching from groundwater [92–97]. The EZ can be either installed vertically (one-dimensional, 1D) or horizontally (two-dimensional, 2D); it follows the electrode configuration between the anode and cathode to reach the contaminated plume at depth during the EK movement (Fig. 11).

Some reactive materials have been applied to remove heavy metals from the soil, such as zero-valent iron (ZVI) [92], granular carbon [93], atomizing slag [98], red mud [94], combined nanomagnetic Fe_3O_4 , and chelating agents [96]. Low-cost or free waste recycling and reutilization materials have also been evaluated as potential EZs, such as dewatering drinking water sludge [95], tannery waste [99], and recyclable food scrap ash [97]. These EZ materials are considered promising for the cleanup of heavy metals in groundwater because of their practicality, reasonable

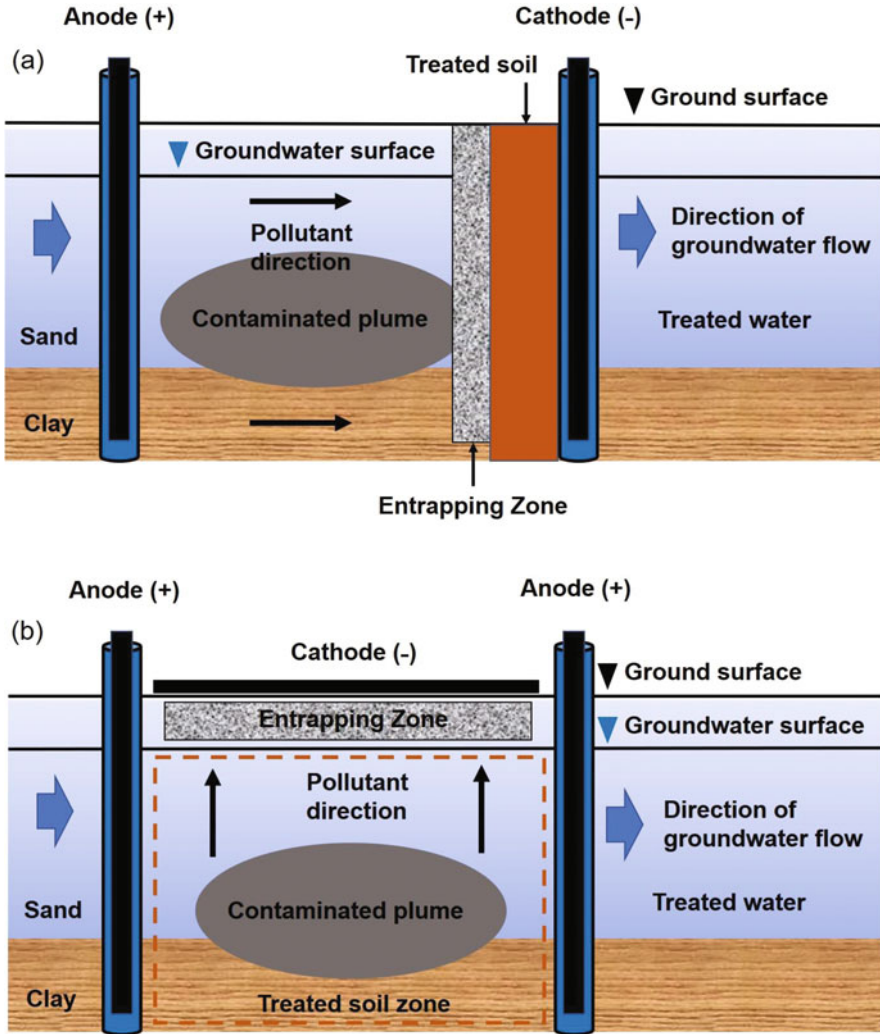


Fig. 11 Schematic of the entrapment zone (EZ) electrokinetic remediation system. The EZ may be installed (a) vertically or (b) horizontally, as per the electrode configuration in the EK remediation

cost, and effectiveness. Czurda and Haus highlighted the three major features of this technology. First, a low direct current through the installed electrode in a contaminated plume causes the flow of water and soluble contaminants to move into or through the EZ. Second, reactive materials in the EZ decompose the soluble contaminants or adsorb contaminants for immobilization or subsequent removal and disposal. Third, a water management system, in which water accumulates at the cathode by EOF, is recycled back to the anode for acid–base neutralization [100].

4.4 Decomposition and Transformation

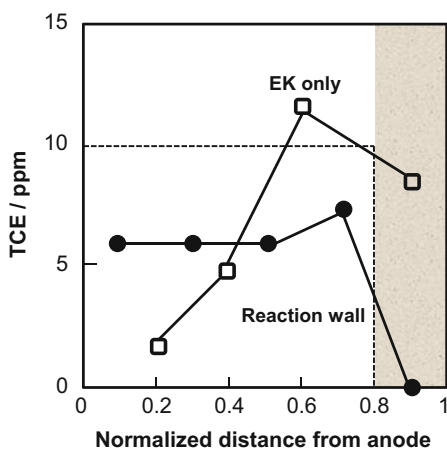
As mentioned in Sect. 4.1, organic pollutants are often poorly soluble, and several solubilization methods have been used to remove them. In contrast, several organic pollutants may be decomposed and transformed into substances with a low environmental impact using a chemical reaction. To enhance these reactions, several reagents such as oxidants, catalysts, and metals have been introduced into the soil via the EK process.

4.4.1 ZVI Reaction Zone

Many studies on remediation methods that decompose and adsorb pollutants in groundwater and soil have reported using ZVI, which has strong reductive and adsorption abilities [101]. PRB containing ZVI has been used as an in situ remediation method for actual polluted soils [102]. Pollutants such as organochlorine compounds in soil are introduced into the PRB using a groundwater stream and detoxified via dechlorination using ZVI. However, the PRB cannot be used in clayey soils because of its low-permeability to groundwater.

During the EK process, the EOF transports organochlorine compounds in clayey soils to the reaction zone of ZVI. We attempted to remove and treat trichloroethylene (TCE) in kaolin using the ZVI reaction zone built up in the EK process. Kaolin containing 10 ppm TCE was used as the model polluted soil, and kaolin containing 1,000 ppm ZVI was used as the reaction zone. TCE contaminated kaolin was set in the anodic two-thirds of the migrating chamber and the ZVI-kaolin was set in the remaining part of the chamber. A direct current (DC) voltage of 20 V (potential gradient of 2 V cm^{-1}) was applied between the two electrodes in each electrode chamber for 48 h. Figure 12 shows the distribution of TCE in kaolin after 48 h of EK operation with and without the ZVI reaction zone. TCE was transported to the

Fig. 12 Removal of TCE from contaminated soil by electrokinetic (EK) remediation with an iron reaction wall. Potential gradient: 2 V cm^{-1} , operation time: 48 h [103]



cathode side by the EOF, and the TCE concentration in the ZVI reaction zone was almost zero. A sufficient amount of TCE was detected in the kaolin at the same position in the absence of a ZVI zone; this may be because TCE was dechlorinated by ZVI in the reaction zone and converted into other compounds [103].

The combination of a ZVI reaction zone and the EK process enabled the in situ remediation of polluted soil with organochlorine compounds, despite the low-permeability of the clayey soil [104]. The EK process can control the water flow between electrodes and introduce pollutants into the reaction zone, as opposed to using a groundwater stream.

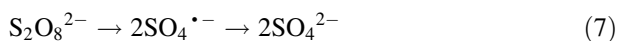
The combination of ZVI with the EK process was applied to reduce Cr(VI) to Cr(III). Citric acid and Fe(II) are known to reduce Cr(VI), and Fe(III) is a catalyst that enhances the reduction by citric acid. In ZVI, Fe(II) eluted from ZVI by citric acid, and the end product, Fe(III) from ZVI, contributed to the removal of Cr(VI) from the contaminated soil [105]. The reduction of nitrate ions to ammonium by ZVI has also been reported, and the effective induction of nitrate ions into the ZVI zone via the EK process has been investigated [106, 107]. The reaction wall from iron effectively dechlorinated TCE in laboratory- and field-scale experiments; this process is known as the Lasagna system [108, 109]. These results indicate that the iron reaction wall effectively transformed and removed the organic and inorganic pollutants from soil during the EK process.

4.4.2 Decomposition

The Fenton reaction is an effective means of achieving the decomposition of organic pollutants; this reaction uses OH radicals generated from the reaction of H₂O₂ with iron [110].



Yang and Long created a PRB consisting of scrap iron powder and demonstrated the decomposition of phenol via the penetration of H₂O₂ using the EK process [111]. Park et al. reported that H₂O₂ penetrated the soil through the EK process and reacted with iron in the soil to decompose phenanthrene at the site [112]. Fe ions generated through the corrosion of the iron electrode were used in the Fenton reaction to decompose diesel oil or petroleum in soil [113, 114]. H₂O₂ is a promising reagent with a low environmental impact as it is converted to water after the oxidation reaction. Persulfates have also been used to decompose organochlorine pollutants as they generate nontoxic by-products. At high temperatures, persulfates decompose to reactive SO₄ radicals and then to SO₄²⁻.



Chowdhury et al. indicated that persulfates, which move toward the anode side as an anion, are effective in the decomposition and removal of tetrachloroethene (PCE) in low-permeability soils [115].

5 Electro-Assisted Phytoremediation

Phytoremediation is an environment-friendly technology and a safe and cheap method for removing contaminants. This process introduces plants into a contaminated environment and allows them to take up contaminants and store them in the plant tissues, such as roots and leaves [116]. Phytoremediation has been used to clean up heavy metals, pesticides, xenobiotics, organic compounds, toxic aromatic pollutants, and acids mine drainage [117]. However, such technology does not guarantee consistent effectiveness and it may not be suitable for all types of contaminated sites. The restoration of a contaminated site by phytoremediation requires a long treatment time in which the cleanup depth is determined by the length of the plant roots. If the concentration of the toxic compound is very high, plants alone cannot efficiently remediate the soil [118, 119]. Phytoremediation may be applied to a low to moderate contaminant concentration, where the bioavailability of contaminants in the soil is below the phytotoxicity of the threshold limit, which enables plants to germinate and grow [120].

Electro-assisted phytoremediation (EAPR) technology was first introduced by Hodko et al. [121] and Bedmer et al. [122] to overcome the limitations of phytoremediation. Following this, studies have recently proposed improvements in the plant uptake of heavy metals from soil [120, 123–127]. In an EAPR system, a low intensity DC electric field is applied to the contaminated plume, which is located deeper than the root zone while being in the vicinity of growing plants. The electric field enhances the bioavailability of metal ions toward plant roots through the EK phenomenon (i.e., electromigration, electrophoresis, and electroosmosis). This enables subsequent extraction, generating stressful conditions for the plants [91, 128]. Hyperaccumulator plants that translocate greater amounts of heavy metals from the roots to the aerial parts of plants, such as shoots and leaves, are considered the best candidates for EAPR technology [129]. This method also enables the use of plants with relatively shorter roots, encouraging the use of a variety of plant species during the phytoremediation process [130]. In addition, the EK process is also used to deliver water and nutrients required for plant growth; for example, there may be higher levels of nutrients available to the roots growing under the EAPR system [121]. The sequential application of an electrical field in soil remediation is possible for both technologies. Phytoremediation may be applied at the site after EK remediation to remove the residual concentration of contaminants, which results in cleaner soil. The use of phytoremediation following EK remediation may contribute to the recovery of soil properties that have been altered or damaged by EK remediation, improving soil structure through the influence of the root system. However, EAPR technology is more effective and efficient as a remedial strategy than the

sequential use of these technologies. A number of variables have a significant effect on the EAPR technique for contaminated soil remediation: the application of alternating current (AC) or DC, voltage or current level, mode of voltage application (continuous or periodical), evolution of soil pH, electrolyte solution (e.g., low concentration of weak organic acid or electrolyte salt), and the possible addition of facilitating agents to enhance the mobility and bioavailability of contaminants [91, 119]. Table 2 summarizes the laboratory conditions used in prominent studies on aquatic EAPR systems, which are introduced in the following sections.

5.1 Influence of Electrode Configuration

The electrode configuration in the EAPR system can also be installed horizontally or vertically, allowing the solution to exchange between the electrode and the subsurface environment. This is essential for the proper functioning of EK remediation. To date, most bench-scale and large-scale EAPR systems conducted in contaminated soil have horizontal 1D configurations [128, 139, 140]. The effect of the vertical 1D electrode configuration on the efficiency of the EAPR system was investigated in a DC electric field to favor the transport of Pb toward the root zone [141]. The vertical application of the electric field extended the phytoremediation process beyond the root zone. The combination of the effect of the vertical electric field and addition of a chelating agent prevent the leaching of Pb into groundwater [142].

Limited numerical sensitivity analyses have been conducted on 2D or axisymmetric electrode configurations on EAPR systems [121, 143, 144]. In this configuration, the cathode is placed at the center, while anodes are placed around the perimeter of the cathode to generate 2D nonlinear electric fields. These configurations were also used to increase the acidic environment generated by the anode and decrease the basic environment generated by the cathode [18]. In the 1D electrode configuration, the electric current density (i.e., current per unit area) was independent of the electrode location. However, in 2D configurations, the electric current density and strength of the electric field increased linearly with the distance from anode to the cathode [18]. Hodko et al. proposed 1D and 2D electrode configurations in the EAPR system to increase the depth phytoremediation in Pb-contaminated soil (Fig. 13). This prevents the leaching of mobilized metals into groundwater [121]. In one of the proposed electrode configurations, the cathode was placed in the middle and surrounded by anodes in the soil perimeter to be treated. However, there is no detailed information regarding metal transport and redistribution in the soil following treatment.

Putra et al. first investigated the effectiveness of the 2D electrode configuration in the EAPR system for the removal of Pb from commercial topsoil spiked with 100 mg kg^{-1} of $\text{Pb}(\text{NO}_3)_2$ [130]. Kentucky bluegrass (*Poa pratensis*) was cultivated in a rectangular EAPR cell ($290 \text{ (L)} \times 240 \text{ (W)} \times 60 \text{ (H)} \text{ mm}$); graphite anodes were installed vertically in the four corners of the cell. The combined mesh net-wire and rod of the stainless-steel cathode were placed on the soil surface. The effectiveness

Table 2 Summary of electro-assisted phytoremediation (EAPR) in aquatic laboratory studies

Plant (scientific name)	Contaminant	Application	Voltage/intensity	Reference
Lettuce (<i>Lactuca sativa</i>)	Spiked water with 5 mg L ⁻¹ of cadmium (CdCl ₂)	Hydroponic culture, a nutrient solution contaminated with Cd. Continuous AC and oxygen supply to the solution; batch reactor; 60 days period	AC: 1 V cm ⁻¹ , 10 Hz or 50 Hz	[131]
Duckweed (<i>Lemna minor</i>)	Spiked water with 150 µg L ⁻¹ of arsenate (Na ₂ HAsO ₄ ·7H ₂ O)	Hydroponic culture, spiked surface water contaminated with As Continuous DC with stainless steel as anode and cathode; semi-continuous system; 6 days period	DC: Set up with different voltages of 0.7 V, 5 V, and 1.4 V	[132]
Water lettuce (<i>Pistia stratiotes</i>)	Spiked water with 100 mg L ⁻¹ Pb solution and Cu (CuSO ₄ ·5H ₂ O)	Hydroponic culture, a nutrient solution contaminated with Pb and Cu Continuous DC with the Ti anode and designed stainless steel of cathode-pot net-wire; batch reactor; 7 days period	DC: Constant 2 V	[133]
Water hyacinth (<i>Eichornia crassipes</i>)	Spiked water with 100 mg L ⁻¹ Pb solution and Cu (CuSO ₄ ·5H ₂ O)	Hydroponic culture, a nutrient solution contaminated with Pb and Cu Continuous DC with the Ti anode and designed stainless steel of cathode-pot net-wire; batch reactor; 7 days period	DC: Constant 2 V	[134]
Water hyacinth (<i>Eichornia crassipes</i>)	Wastewater from the chemical laboratory	Plant growth in wastewater Continuous DC with the Ti anode and designed stainless steel of cathode-pot net-wire. First 2 h with a batch system and then continued for 2 h with a flow system	DC: Constant 5 V	[135]
Water hyacinth (<i>Eichornia crassipes</i>)	Leachate	Plant growth in leachate Continuous DC with the Ti anode and designed stainless steel of cathode-pot net-wire; batch reactor; 11 days period	DC: Constant 2 V	[136]

(continued)

Table 2 (continued)

Plant (scientific name)	Contaminant	Application	Voltage/intensity	Reference
Vetiver grass (<i>Vetiveria zizanioides</i>)	Spiked water with 30 mg L ⁻¹ Cu (CuSO ₄ ·5H ₂ O) and 12 mg L ⁻¹ Fe (FeSO ₄ ·7H ₂ O)	Hydroponic culture, a nutrient solution with Pb and Cu concentration Continuous DC with the Ti anode and designed stainless steel of cathode-pot net-wire; batch reactor. Aeration supply to the solution; 7 days period	DC: Constant 2 V	[137]
Rough horsetail (<i>Equisetum hyemale</i>)	Batik (textile) wastewater	Plant growth in wastewater Continuous DC with the Ti anode and designed stainless steel of cathode-pot net-wire. Combined electrocoagulation and EAPR system with the semi-continuous flow. Electrocoagulation is 1 h and then continued with 7 days of EAPR	DC: 20 V of electrocoagulation and 5 V of EAPR	[138]

of the 2D electrode configuration was evaluated in a rapid assessment (48 h) using an agar medium. The results show that the concentration of Pb²⁺ increases from the bottom of the tray at the anode toward the cathode through the V-shape in the agar medium and accumulates in the middle of the cathode area (Fig. 14). A similar behavior was observed when the electrode configuration was used on Pb-contaminated soil over 15 days of the EAPR process. However, the migration of Pb²⁺ in the contaminated soil was significantly slower than that in the agar medium because of the strong bonding with organic matter and clay minerals in the soil. These results indicate that the 2D electrode configuration can be used in EAPR systems. In the soil experiment, *P. pratensis* grew better in experiments with the electric current than with no current, based on the observed biomass production. Furthermore, the electric field improved the upward movement of Pb ions entering the rhizosphere, after which the metal was extracted from the soil by plant roots.

Recently Putra et al. evaluated the effectiveness of a 2D electrode configuration to remove Pb and Cu from spiked contaminated water with 100 mg L⁻¹ of Pb(NO₃)₂ and CuSO₄ [133, 134]. Floating aquatic plants such as water hyacinth (*Eichornia crassipes*), and water lettuce (*Pistia stratiotes*) were cultivated in 15 L of rectangular EAPR cells (400 (L) × 250 (W) × 350 (H) mm), with half-strength Hoagland solution. In this study, a designed stainless-steel mesh of an electrode-pot as the cathode was installed on the surface below the water table to increase the ion concentration around the plant roots, and the anode was a titanium (Ti) rod that

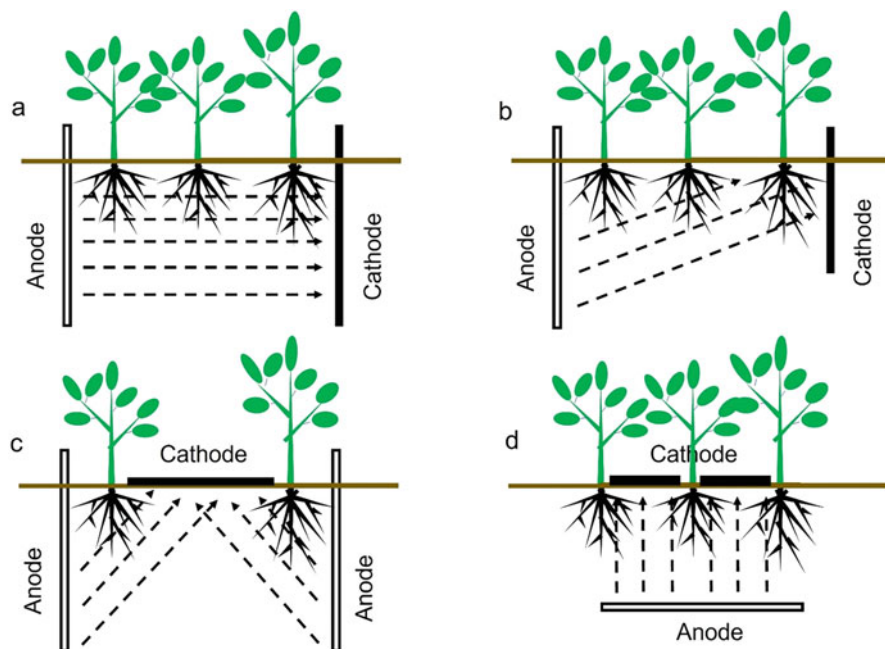


Fig. 13 Possible electrode configurations on the EAPR system to prevent leaching of contaminants to groundwater and to extend the depth of the phytoremediation beyond the roots. Direct-current of electric field was induced by horizontal (a), reversed polarity (b), axi-symmetrical/radial (c) and vertical (d) electrodes configuration [119]

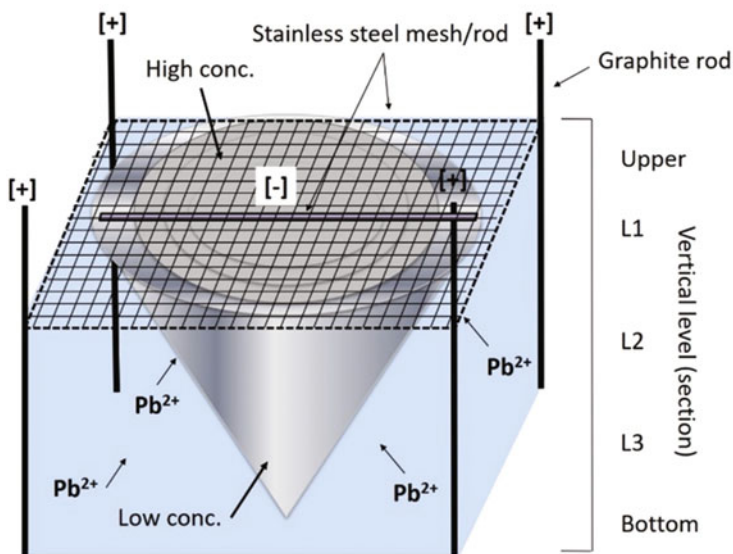


Fig. 14 A V-shape of concentrated lead in agar medium after 48 h of electrical processing at a constant current of 50 mA. Agar medium was prepared by dissolving 100 g agar in a 3.8 L solution of $150 \text{ mg L}^{-1} \text{ Pb(NO}_3)_2$ and $2.5 \text{ mmol L}^{-1} \text{ KNO}_3$ as a background electrolyte ($n = 3$)

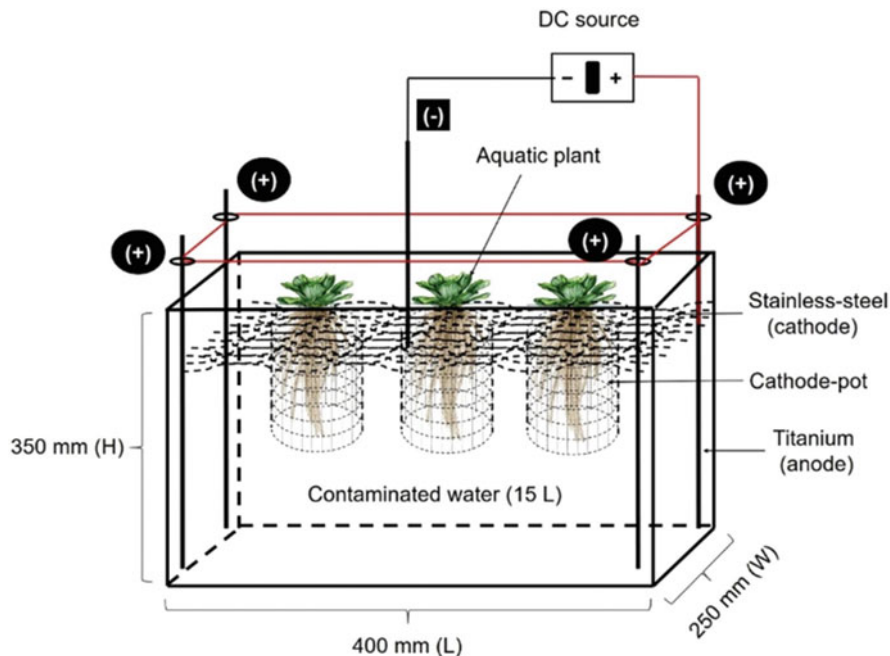


Fig. 15 Schematic of the designed electrode-pot as the cathode used to evaluate the effectiveness of a 2D configuration within an aqueous EAPR system

was installed vertically in the four corners of the reactor (Fig. 15). Periodically, the solution was sampled from the EAPR cell at three levels (bottom, middle, and upper) to evaluate the effectiveness of Pb and Cu ion migration over a 7 days period. The results showed that the Pb^{2+} and Cu^{2+} concentrations significantly decreased from the bottom point in the first 2 days. At this point, Pb^{2+} concentrations decreased to as low as 60–93%, whereas Cu was as low as 80–99% of the initial concentration, depending on the plant species used in the experiment. These results indicate that the 2D electrode configuration with the installed electrode-pot as the cathode effectively transported metal ions toward the surface near the plant roots. Additionally, *E. crassipes* and *P. stratiotes* grew better with an electric current. This was reflected by the higher total chlorophyll and chlorophyll a/b ratio, compared to plants in the phytoremediation with no current.

5.2 Application of EAPR Systems on Contaminated Water

Phytoremediation has been investigated for its ability to remove heavy metals from groundwater in contaminated mine sites [145]. The viability of arbuscular mycorrhizal fungi (AMF) with phytoremediation to promote the biodegradation of organic

pollutants in groundwater was discussed by Fester [146]. A phytoremediation study in Taiwan showed that herbaceous plants could store higher quantities of heavy metals than woody plants. However, woody plants such as camphor trees (*Cinnamomum camphora*) may be used for the long period of phytoextraction of Cd from soil and groundwater, as these trees accumulate high quantities of Cd in their leaves and branches [147]. As such, it was difficult to evaluate the remediation of contaminants in a stream of groundwater at the laboratory scale. However, most EAPR studies at this scale have been conducted in hydroponic cultures.

The application of the EAPR system to remove Cd from hydroponic contaminated water was reported by Bi et al. [131]. This study determined whether 1 V cm^{-1} of AC electric field with two different frequencies (10 and 50 Hz) could improve Cd adsorption in the roots of lettuce (*Lactuca sativa*), and the possible translocation of Cd^{2+} to the shoots of the plant. A 5 mg L^{-1} Cd concentration (i.e., CdCl_2) was used in the hydroponic solution. The results showed that the AC electric field had a positive effect on biomass production in a non-contaminated medium compared to the control plants. However, the biomass of plants grown in Cd-contaminated medium with an AC electric field was higher than that of plants grown without electrical treatment. Metal ion uptake was also accelerated by the presence of an electric field in the medium, which favored the translocation of Cd^{2+} to the aerial parts of the plant. In addition, chlorophyll content was higher in plants grown in the Cd-contaminated medium when treated with an electrical field compared with the control. These results showed that these plants can cope with Cd toxicity in the growth medium. Overall, the efficiency of phytoremediation was $>90\%$ and 44% under the influence of the 50 Hz and 10 Hz AC electrical field, respectively. This study also detected selective metal uptake by plants. The high adsorption of certain metal ions induced a competition effect in plants, which may limit the capacity of the plant to adsorb other metal ions [119]. In this study, Cu was a competing metal ion and was present at a low concentration (0.025 mg L^{-1}). In general, these results confirm the viability of the EAPR system for the treatment of heavy metals in contaminated groundwater.

The viability of the EAPR system to remediate As-contaminated water was evaluated by Kubiak et al. [132]. For over a decade, As was recognized as one of the most hazardous contaminants on Earth. In Bangladesh and West Bengal, elevated As concentrations are often associated with high Fe and Mn levels. Although human exposure to As may occur from a variety of sources, drinking water poses the greatest threat [148, 149]. In this study, *Lemna minor* was grown in spiked surface water without any precleaning with an As concentration of $150 \mu\text{g L}^{-1}$. The surface water contained various other elements including Mn (2.9 mg L^{-1}), Cu (0.05 mg L^{-1}), Fe (1.39 mg L^{-1}), barium (Ba) (0.13 mg L^{-1}), and phosphorus (P) (0.25 mg L^{-1}). The 1D electrode configuration of the stainless-steel electrodes in the reactor was positioned horizontally. The cathode plate was positioned at the bottom of the reactor, and the 1 cm anode mesh was positioned below the water table such that the plant roots were next to the anode. Two experiments were conducted

over 6 h: (1) an experiment with a consecutive increase in the applied voltage (i.e., 0.7, 2.1, and 5 V), and (2) an experiment with constant voltage (1.4 V). No enhanced adsorption of As in plants was observed when the electric field was applied during the phytoremediation. However, a high decrease in As concentration in the aqueous medium test was observed when an electric current was applied. The preliminary results showed that the applied DC voltage removed 90% of the As ions from the spiked surface water. This study proposed several explanations for the competition between P and As in plant adsorption. In addition, the spiked As concentration in the water may have been too low for the insignificant uptake of As by plants to be observed. There may also be plant species that are more suitable for As phytoremediation.

An evaluation of the EAPR system for the removal of heavy metals (i.e., Pb, Cu, Cd, and Fe) and uptake by *E. crassipes* from leachate was demonstrated in a laboratory-scale experiment by Putra and Hastika [136]. A similar dimension of the EAPR batch reactor was used in this study, as shown in Fig. 15. An EAPR system was implemented over 11 days at a constant DC voltage of 2 V. The results showed that the concentrations of Fe, Cu, Cd, and Pb in the leachate decreased significantly from 78%, 22%, 32%, and 30% of the initial concentrations, respectively. The presence of the DC electric field in the aqueous medium accelerated the metal ion uptake by the plant and the high translocation of metal ions to the aerial plant biomass. The total chlorophyll content and chlorophyll a/b ratio showed that the application of the DC electrical field in hydroponic phytoremediation may assist *E. crassipes* in coping with stress conditions. High concentrations of heavy metals from leachate were accumulated in the plant.

Putra et al. reported a continuous model of the EAPR system for wastewater treatment in a chemical laboratory [135]. This study aimed to decrease the biochemical oxygen demand (BOD), chemical oxygen demand (COD), and heavy metal concentrations (i.e., Pb and Cu) from wastewater. A configuration of four EAPR cells was connected by a single circulation wastewater treatment, hereafter referred to as the colony system (Fig. 16). The viability of *E. crassipes* in the colony system was evaluated using EAPR treatment for a large volume of effluent (i.e., 40 L). The results from these studies were used to predict the viability of these technologies for the remediation of industrial effluents under actual conditions. Each EAPR cell was constructed according to previously reported methods, as shown in Fig. 15. The EAPR process was carried out in the batch system for the first 2 h and then continued with the flow system for a further 2 h at a constant DC voltage of 5 V. The results showed that the BOD and COD did not change within the first 2 h in the batch and flow processes, indicating that the colony system of the EAPR cell was ineffective in decreasing the organic components in the wastewater. However, the Pb and Cu concentrations decreased by as much as 46% and 47%, respectively, from the initial concentrations. The results indicated that the colony system of the EAPR cell may only be used to decrease heavy metal concentrations in wastewater.

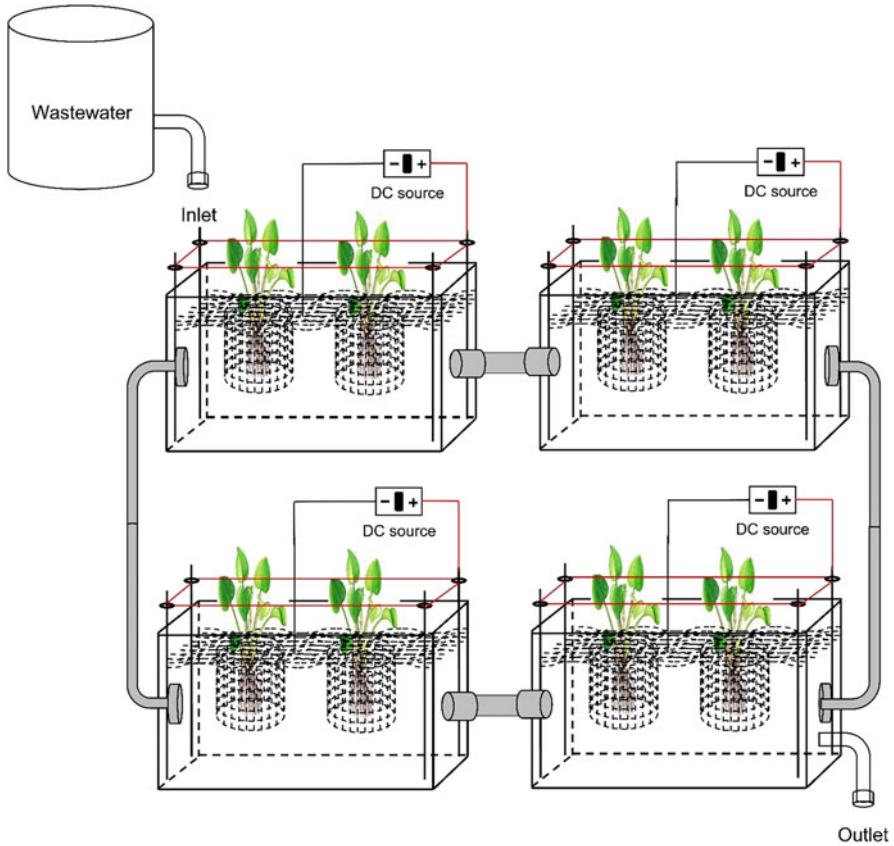


Fig. 16 Flow circulation of wastewater treatment in the EAPR system. The effluent is circulated in the colony unit of EAPRs cell prior to discharging into an open body of water

5.3 Combination with Other Technologies for the Remediation of Contaminated Water

A semi-continuous process of the combined electrocoagulation and EAPR system for the treatment of textile effluent successfully decreased the COD and heavy metal (i.e., Pb and Cr) concentrations [138]. The colony system of the EAPR cells was used to evaluate the viability of rough horsetail (*Equisetum hyemale*) as an accumulator plant during the process. Many studies have shown that electrocoagulation is an efficient method for removing COD from wastewater in petroleum refineries [150], mineral processing [151], electroplating [152], textiles [153], and batik [154]. This method boasts efficiencies between 83% and 99% and generates fewer sludge products than other alternative methods [155]. In this study, electrocoagulation was conducted for 1 h under a constant DC voltage of 20 V, whereas each EAPR

cell in the colony system proceeded for 7 days at a constant DC voltage of 5 V. First, the effluent was flown into 10 L of an electrocoagulation reactor (350 (L) \times 200 (W) \times 200 (H) mm). This was constructed using Al as the anode and stainless-steel sheets as the cathode. Each cathode consisted of three sheets (300 (L) \times 200 (W) mm; 3 mm thick). Electrocoagulation was performed to decrease the COD concentration in wastewater. The clarified solution from the electrocoagulation process continued to flow into the 17 L EAPR cells of the colony system to remove any remaining heavy metals prior to discharge into an open body of water. The results showed that after 1 h of electrocoagulation, the COD concentration decreased by as much as 70%, and heavy metal concentrations decreased by as much as 25% and 7% for Cr and Pb, respectively. At the end of the EAPR system, the COD concentration continued to decrease to 80.9%, and the Cr and Pb concentrations decreased by as much as 35% and 25%, respectively.

An electrical system in a designed cathode-pot electrode induced more rapid adsorption of metal ions in the EAPR system, which progressively increased phytotoxicity such that the plants died earlier than during a normal phytoremediation process [134, 135]. Therefore, the EAPR system is supplemented by pumping air into the wastewater to increase healthy plant growth such that the plant can live longer in a stressful environment (Fig. 17). The effectiveness of the aerated-EAPR system in the removal of Cu and Fe from contaminated water was first reported by

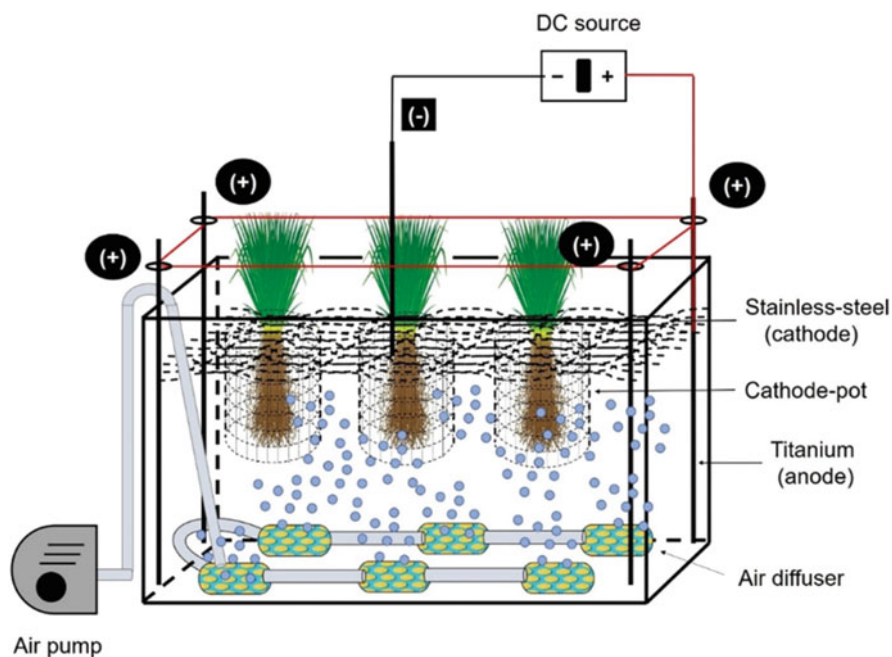


Fig. 17 Aerated-EAPR system on water remediation. The aeration could extend the plant growth and overcome earlier phytotoxicity on the plant

Putra et al. [137], who used the hydroponic growth of vetiver grass (*Vetiveria zizanioides*). This plant may be hydroponically cultivated in a wastewater medium to remove Cu up to 15 mg kg^{-1} of plant biomass. The plant was found to survive even when the soil was contaminated with Cu up to $50\text{--}100 \text{ mg kg}^{-1}$ soil [156]. Furthermore, plants were able to accumulate up to 17 and 3 times the mg Pb kg^{-1} dry weight in the roots and shoots, respectively, when exposed to a Pb concentration of $1,200 \text{ mg L}^{-1}$. This demonstrates that the plants had wider adaptability and could grow in various extreme locations for heavy metal remediation [157].

A similar dimension to the previously reported EAPR batch reactor was applied in an aerated-EAPR study, as shown in Fig. 15. An aerated-EAPR system with vetiver grass was applied over a 7-d period by a constant DC voltage of 2 V and an airflow rate of 10 L min^{-1} . The plant was grown in 15 L of spiked water containing 30 mg L^{-1} of Cu and 12 mg L^{-1} of Fe. The effectiveness of aerated-EAPR, aerated-phytoremediation, and phytoremediation was compared by observing the phytomorphological changes in plants, chlorophyll levels (i.e., total chlorophyll and chlorophyll a/b ratio), and decreasing heavy metal concentrations in the contaminated water. Chlorophyll content and the chlorophyll a/b ratio are indicators of photosynthetic activity and are also often used as indicators of stress in plants. These parameters have been used to direct and assess the exposure of plants to environmental contaminants [158, 159]. The results of the study showed that the Cu and Fe concentrations decreased in contaminated water by as much as 87% and 99% for aerated-EAPR, which was higher than that of aerated-phytoremediation (82% and 99%) and phytoremediation (15% and 56%), respectively. The profile of heavy metal uptake by plants indicated that the electro-assisted and aeration systems could enhance phytoremediation with different results. For example, the concentration of heavy metals in the roots according to the method used was as follows: phytoremediation > aerated-phytoremediation > aerated-EAPR. In contrast, the heavy metal concentration had a higher translocation from roots to shoots of plants in the aerated-EAPR system. High chlorophyll content in plants under the aerated-EAPR system indicated that aeration and electro-assistance did not disrupt the circulation of nutrients in plant tissues.

EAPR is an innovative, green, and sustainable technology that combines the merits of phytoremediation and EK remediation. Using a 2D electrode configuration of the electrode-pot as the cathode in floating aquatic plants and hydroponic experiments, this technology improved metal uptake and favored the translocation of metals from roots to shoots. The colony system of EAPR cells in a continuous flow process may therefore be used in the future to treat industrial effluents. Electrocoagulation and the EAPR system may be applied to decrease organic and heavy metal contamination in textile effluents (i.e., batik wastewater).

The application of aerated-EAPR systems for wastewater treatment sought to increase the bioavailability of contaminants to avoid earlier plant toxicity, with the aim of facilitating the healthy growth of plants in a longer remediation period. Generally, our findings show that the decrease in contaminant concentrations from aqueous media using the EAPR system was more rapid than phytoremediation in the soil.

6 Disaster Pollution

Suitable remediation technologies should be adopted based on the characteristics of the contaminated environment. For example, pollution from natural disasters can generate a vast contaminated area and involves various substances where treatment occurs over a protracted period. This section describes the potential of EK remediation for the Great East Japan Earthquake of 2011.

6.1 Saline Soil

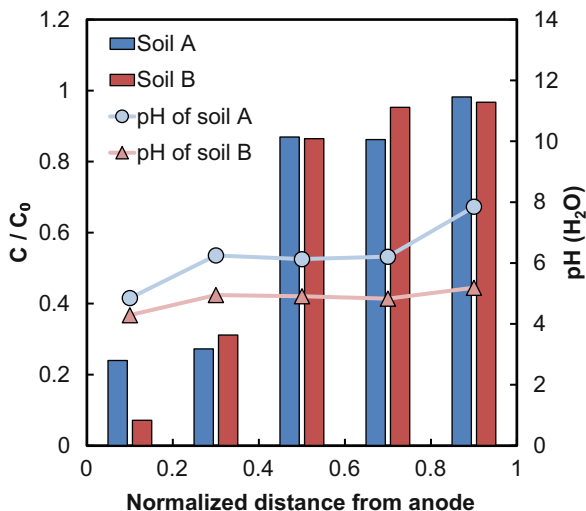
Plant growth becomes difficult in soils containing high concentrations of salt, and salt damage has often been observed in irrigated agriculture in drylands and reclaimed land and is also observed in greenhouses where water supply by rain is limited. A tsunami caused by an earthquake transports a large amount of salt via seawater to the land; consequently, the concentration of salt in the soil rapidly increases. For the Great East Japan Earthquake, approximately 23,600 ha of agricultural fields were salt damaged; the electrical conductivity (EC) exceeded 700 mS m^{-1} in the soils of the Iwate Prefecture, Japan [160]. Sodium ions, the main cations in seawater, change the aggregate structure of soil particles, creating finer soil particles, which lowers soil porosity and reduces permeability [161, 162]. Generally, the water infiltration method, in which pure water is introduced to soil and elutes salt from soil, is applied for the desalination of saline soil. However, this method loses its effectiveness in low-permeability soils such as clayey soil; it requires a large amount of water and remediation occurs over an exceptionally long period. Therefore, we investigated the potential of the EK remediation for desalinating saline soil. The model saline soil was prepared using NaCl and two types of agricultural soil (andosol; the organic content of soil A was 4.8% and soil B was 11.3%) in Aomori Prefecture, Japan. Figure 18 shows that Na^+ moves toward the cathode side, with no significant difference in Na^+ distribution in each soil [163]. In this experiment, although distilled water was used as the electrolyte, the soil pH did not change significantly owing to its pH buffering capacity. Lee et al. reported that over 90% of nitrate ions were removed from contaminated soil in a greenhouse (initial concentration of $27,985 \text{ mg kg}^{-1}$) by the EK process after 54 days of operation [164].

These results indicate that the EK process is an effective method for remediating saline soils.

6.2 Radioactive Species

The Korea Atomic Energy Research Institute (KAERI) has been developing various remediation technologies for contaminated areas and waste for some time, owing to

Fig. 18 Distribution of Na^+ and soil pH after the EK process. Soil A and B had 4.8% and 11.3% organic content. Potential gradient: 1 V cm^{-1} , operation time: 24 h



the presence of radioactive species around the research reactor (TRIGA; Training, Research, Isotope, General, Atomic) in Seoul, Republic of South Korea [165, 166]. At these sites, uranium (U) exists as a hydroxide or is adsorbed onto soil components. Kim et al. applied EK remediation to soils contaminated with U and were able to reduce the concentration to below the clearance level (1 Bq g^{-1}) after 34 days by using nitric acid to maintain a low pH in the cathode electrolyte. The number of days required for remediation increased with the initial concentration of radioactive species; with an initial concentration of 100 Bq g^{-1} , the clearance level could be achieved in 49 days [167].

In Berkshire, United Kingdom, there is a site contaminated with plutonium (Pu) at the Atomic Weapons Establishment Aldermaston site. Pu is also considered to exist in a poorly soluble form of oxide or hydroxide in soil. Agnew et al. reported that Pu formed a complex with citric acid, and Pu was removed as an anionic complex using EK remediation. They also attempted pilot-scale experiments with 2.4 m^3 of soil, finding that the removal efficiency varied depending on the distance from the electrode; for approximately 0.4 m^3 of soil the Pu concentration was below 1.7 Bq g^{-1} after 60 days of operation [168].

These results indicate that EK remediation may be an excellent tool for the treatment of soils contaminated by radioactive species.

6.3 Cesium Pollution

In March 2011, the Fukushima Daiichi Nuclear Power Plant accident occurred, and a large amount of radionuclides was released into the environment. The volume of contaminated soil was estimated to be approximately 21.4 Mm^3 [169]; therefore,

there is an urgent need for an effective remediation technology. In particular, ^{137}Cs has a half-life of ~ 30 y, which represents a long-term impact on human activity and ecosystems. This section introduces some research on EK remediation for the removal of Cs, including stable isotope ^{133}Cs .

Al-Shahrani and Roberts investigated the behavior of ^{133}Cs in kaolin using EK remediation. The removal efficiency of ^{133}Cs from contaminated soil ($450 \text{ mg Cs}^+ \text{ kg}^{-1}$) was 38% and 79% after 48 h and 10 days, respectively. However, the removal efficiency of ^{133}Cs from actual soil around the Sellafield nuclear facility (United Kingdom) showed a decrease [170]. Oguri et al. reported that approximately half of the ^{133}Cs was removed from a model contaminated andosol ($4,000 \text{ mg Cs}^+ \text{ kg}^{-1}$) after 36 h of EK operation (potential gradient: 1.3 V cm^{-1}) [171]. A soil chamber with a 20° slope was designed to apply the EK process for a mountain field. Horticultural soil containing ^{133}Cs (50 mg kg^{-1}) was prepared and filled into the equipment, and the EK process was applied with acetic acid (0.01 mol L^{-1}) as the electrolyte. The removal efficiency of ^{133}Cs was 87% after 21 days of operation; however, with soil particles that were less than $40 \mu\text{m}$, its removal efficiency decreased, and only 60% of ^{133}Cs was removed [172]. Igawa et al. reported that the removal efficiency of ^{133}Cs from model soil (18 mg kg^{-1}) prepared using black soil in Tochigi Prefecture, Japan, was only 0.25% after 49 h of operation [173]. Kim et al. prepared a model contaminated soil using the soil around a research reactor ($514 \text{ mg Cs}^+ \text{ kg}^{-1}$), where several organic acids (EDTA, citric, oxalic, and acetic acid) were evaluated as electrolytes. After 15 days of operation, acetic acid was the most effective in removing ^{133}Cs from soil, with a removal efficiency of 84.2% [174]. Jung et al. applied the EK process to model contaminated soil at the Hanford site ($668 \text{ mg Cs}^+ \text{ kg}^{-1}$) in the United States, which also suffers from radioactive contamination, and obtained a 47% removal efficiency of ^{133}Cs after 68 days of operation [175]. These removal efficiencies vary in each study, and this variance may be due to the soil type.

6.4 Interaction with Soil Components

Andosols are widely distributed in Japan and contains volcanic ash and humic substances. Section 4.2 explains that humic substances have various functional groups and interact with many cationic species. However, the interaction between Cs^+ and humic substances is relatively weak because Cs^+ is monovalent ion and large ionic diameter [176]. On the other hand, Fukushima Prefecture is rich in clay minerals such as biotite and vermiculite derived from Abukuma granite. These clay minerals are known to have a strong interaction with Cs^+ ; for example, the desorption efficiency of Cs^+ from biotite decreases with aging time [177]. These effects maintain Cs^+ on the ground surface and inhibit its deeper dispersion into the soil [178, 179]. Takahashi et al. reported that humic substances interfered with the

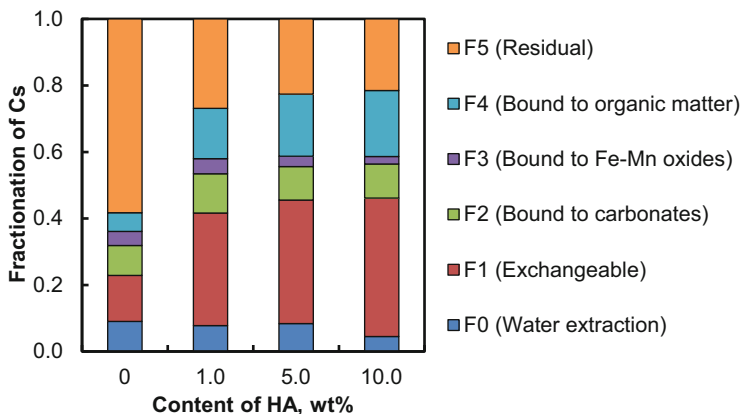


Fig. 19 Fractionation of Cs in the presence of differing humic acid (HA) content in horticultural vermiculite

interaction between Cs^+ and clay minerals and induced the high mobility of radioactive Cs^+ [180]. As Cs^+ is strongly affected by these soil components, we evaluated these effects using model soil and HA.

The model soil was prepared using vermiculite for horticultural use and HA. It was thoroughly mixed following the addition of ^{133}Cs . The fractionation of Cs in various HA model soil contents was evaluated using a modified sequential extraction analysis [181]. Figure 19 shows that approximately 60% of Cs^+ in horticultural vermiculite without HA is present as F5 (residual); this is the species that strongly adsorb and fix Cs^+ . The ratio of F0 (water extraction) and F1 (exchangeable) was approximately 20%. The fractionation of Cs as F5 decreased with increasing HA content. When horticultural vermiculite containing 10 wt% of HA was used, almost half of the Cs was present as F0 and F1, which was characterized by a weak interaction. The fractionation of F0 and F1 increased with HA content as Cs^+ interacted with functional groups such as the carboxyl group of HA, which is easily desorbed by ion exchange [182]. As HA was also transported by the EK process (see Sect. 4.2), it was anticipated that Cs^+ would be removed by HA. This estimate cannot be quantitatively discussed in terms of organic matter content; however, based on the findings of several previous studies, weakly bound Cs^+ may have been removed.

The strong interaction between Cs^+ and clay minerals makes it difficult to decontaminate Cs-polluted soils. We compared the removal efficiency of Cs^+ from pyrophyllite and horticultural vermiculite using EK process. Although pyrophyllite and vermiculite are 2:1 type clay minerals, their basal spacing and electric charge are different. The adsorption capacity of pyrophyllite and horticultural vermiculite for Cs^+ were 1.2 and 18.8 mg g^{-1} , respectively. We prepared soils with differing vermiculite content, in which the concentration of Cs^+ was adjusted to 0.1 mg g^{-1} . After the application of the EK process for 3 days, the removal efficiency of Cs^+

from pyrophyllite was 21%. This efficiency decreased with an increase in vermiculite content, and most Cs was not removed from the 100% vermiculite. These results indicate that the strength of the interaction with Cs^+ significantly differed for each 2:1 type clay mineral [183]. The basal spacing of pyrophyllite was 0.93 nm, and this value was comparable to the total thickness of one octahedral sheet and two tetrahedral sheets, indicating that there was no space to receive Cs^+ in the interlayer of pyrophyllite. In addition, pyrophyllite is ideally uncharged, whereas vermiculite has a negative charge due to its isomorphous substitution on the tetrahedral sheet. As such, pyrophyllite cannot fix Cs^+ into its structure. In contrast, biotite and vermiculite have a sufficiently large basal spacing to uptake Cs^+ in its interlayer, and the adsorbed Cs^+ is not easily desorbed [184]. These properties of clay minerals also significantly affect the removal behavior of Cs^+ by the EK process, and some new approaches should be considered to design effective remediation.

6.5 Application for Contaminated Radioactive Waste

The EK process has been applied to various contaminated soils and waste materials. Kim et al. indicated that the concentration of ^{137}Cs in ash from the incineration facility in Fukushima Prefecture decreased from 30–40 Bq g^{-1} to below 2.0 Bq g^{-1} after 10 days of operation [185]. Additionally, over 90% of Cs and cobalt (Co) from the radioactive contaminated concrete particles below 0.5 cm ($\sim 2 \text{ Bq g}^{-1}$) was removed over 25 days of the EK process [186]. These results indicate that the EK process is effective in remediating radioactive wastes.

The groundwater around the Fukushima Daiichi Nuclear Power Plant was also contaminated after the accident. We designed a lab-scale EK process to prevent contaminated groundwater from dispersing into the environment (Fig. 20a). The model flow channel was prepared using pyrophyllite and glass beads, and uncontaminated pyrophyllite was filled between the flow channel and the electrode chamber. CsCl solution (10 mg L^{-1}) was supplied to the “inlet,” and then eluted from the “outlet.” When no potential gradient was applied, Cs^+ was detected along the flow channel and was present in the “outlet” solution (6.9 mg L^{-1}) (Fig. 20b). However, at a potential gradient of 1 V cm^{-1} , Cs^+ accumulated in the soil near the cathode side by electromigration and EOF (Fig. 20c). The concentration of Cs^+ in the “outlet” solution decreased by more than 85%, indicating that the EK process has the potential to control the distribution of Cs^+ in groundwater [187]. In 2017, a frozen soil wall was constructed around the Fukushima Daiichi Nuclear Power Plant, which prevented groundwater penetration. Unfortunately, tritium and trace amounts of ^{137}Cs ($3\text{--}4 \text{ Bq kg}^{-1}$) have been observed [188], highlighting the need to continuously monitor the behavior of radionuclides.

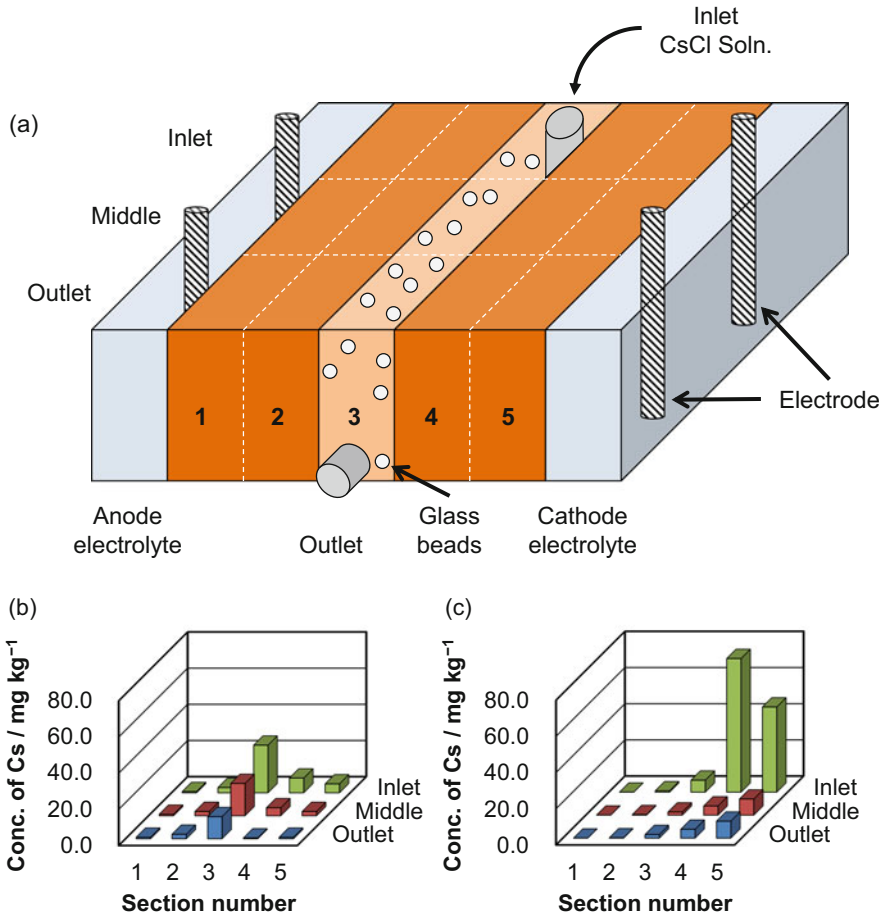


Fig. 20 (a) Schematic of the EK process for the model groundwater scenario; (b) distribution of Cs in soil without the potential gradient; and (c) with the potential gradient (1 V cm^{-1})

7 Conclusion

EK remediation has various advantages and shows potential as an environmental remediation technology; the treatment range can be controlled between the electrodes, and it may be applied to low-permeability soils. Substances with low environmental impact have been developed and combined with EK remediation to increase the effectiveness of its use in treating soils. Chapters “Magnetic Separation of Pollutants for Environmental Remediation” and “Easily Collectable Floating-up Adsorbents to Remove Pollutants” describe the development of adsorbents such that they may be easily collected after adsorbing pollutants; these adsorbents may be applied as remediation technology for aquatic environments [189–191]. A process in

which novel adsorbents recover pollutants removed from the soil by EK remediation may also be designed. Moreover, the EK process has been investigated for the ferritization of heavy metals to make them insoluble, prolong the longevity of the PRB, and dewater solids such as sludge and sediment [192–194]. As of 2020, there are few effective technologies for the in situ remediation of contaminated soils with heavy metals. Although the EK process presents some challenges, its advantages can be utilized in various fields.

Acknowledgments This research was supported by Assoc. Prof. Masahiko Kan (Hokkaido University of Education Sapporo) and the late Assoc. Prof. Masami Fukushima (Faculty of Engineering, Hokkaido University). Some parts of this chapter are the doctoral and master's research of Dr. Akira Sawada, Mr. Tomoyuki Kimura, Mr. Ken-Ichi Takase, Mr. Yasuhisa Ohkawa, Mr. Chihiro Kitagawa, and Mr. Ryosuke Miyamura (Graduate School of Environmental Science, Hokkaido University). We would like to thank Editage (www.editage.com) for English language editing.

R.S.P. would like to thank the Ministry of Research, Technology and Higher Education of Republic of Indonesia for their financial support through the 2014–2020 research program in part of this study. Also greatly appreciate all students involved in the Environmental Remediation Research group. Furthermore, additional financial support from Directorate of Research and Community Services of Universitas Islam Indonesia is gratefully acknowledged.

Y.A. and S.T. are grateful to Ms. Toko Iwamura and Ms. Seira Takahashi (Graduate School of Environmental Science, Hokkaido University) for their dedicated support in preparing this chapter.

References

1. Acar YB, Alshawabkeh AN (1993) Principles of electrokinetic remediation. *Environ Sci Technol* 27:2638–2647. <https://doi.org/10.1021/es00049a002>
2. Lageman R, Electroreclamation. (1993) Applications in the Netherlands. *Environ Sci Technol* 27:2648–2650. <https://doi.org/10.1021/es00049a003>
3. Acar YB, Alshawabkeh AN, Gale RJ (1993) Fundamentals of extracting species from soils by electrokinetics. *Waste Manag* 13:141–151. [https://doi.org/10.1016/0956-053X\(93\)90006-I](https://doi.org/10.1016/0956-053X(93)90006-I)
4. Probst RF, Hicks RE (1993) Removal of contaminants from soils by electric fields. *Science* 260:498–503. <https://doi.org/10.1126/science.260.5107.498>
5. Shapiro AP, Probst RF (1993) Removal of contaminants from saturated clay by electroosmosis. *Environ Sci Technol* 27:283–291. <https://doi.org/10.1021/es00039a007>
6. Acar YB, Gale RJ, Alshawabkeh AN, Marks RE, Puppala S, Bricka M, Parker R (1995) Electrokinetic remediation: basics and technology status. *J Hazard Mater* 40:117–137. [https://doi.org/10.1016/0304-3894\(94\)00066-P](https://doi.org/10.1016/0304-3894(94)00066-P)
7. The 18th international symposium on electrokinetic remediation (2020). <https://erem2020.sciencesconf.org/?forward-action=index&forward-controller=index&lang=en>. Accessed 24 Nov 2020
8. Yeung AT, Hsu C, Menon RM (1996) EDTA-enhanced electrokinetic extraction of lead. *J Geotech Eng* 122:666–673. [https://doi.org/10.1061/\(ASCE\)0733-9410\(1996\)122:8\(666\)](https://doi.org/10.1061/(ASCE)0733-9410(1996)122:8(666))
9. Niinae M, Nishigaki K, Aoki K (2008) Removal of lead from contaminated soils with chelating agents. *Mater Trans* 49:2377–2382. <https://doi.org/10.2320/matertrans.M-MRA2008825>
10. Ryu S-R, Jeon E-K, Baek K (2017) A combination of reducing and chelating agents for electrolyte conditioning in electrokinetic remediation of As-contaminated soil. *J Taiwan Inst Chem Eng* 70:252–259. <https://doi.org/10.1016/j.jtice.2016.10.058>

11. Reddy KR, Donahue M, Saichek RE, Sasaoka R (1999) Preliminary assessment of electrokinetic remediation of soil and sludge contaminated with mixed waste. *J Air Waste Manage Assoc* 49:823–830. <https://doi.org/10.1080/10473289.1999.10463849>
12. Ueda T, Kameda T, Nanasawa A (2011) A new electrochemical rehabilitation method for reinforced concrete employing the DFRCC anode system. *Sep Purif Technol* 79:204–207. <https://doi.org/10.1016/j.seppur.2011.02.027>
13. Ueda T, Wakitani K, Nanasawa A (2012) Influence of electrolyte temperature on efficiency of electrochemical chloride removal from concrete. *Electrochim Acta* 86:23–27. <https://doi.org/10.1016/j.electacta.2012.05.026>
14. Reddy KR, Cameselle C (2009) Overview of electrochemical remediation technologies. In: Reddy KR, Cameselle C (eds) *Electrochemical remediation technologies for polluted soils, sediments and groundwater*. Wiley, Hoboken, pp 3–28
15. The Chemical Society of Japan (2021) *Handbook of chemistry* (in Japanese), 6th edn. Maruzen Publishing, Tokyo
16. Casagrande IL (1949) Electro-osmosis in soils. *Géotechnique* 1:159–177. <https://doi.org/10.1680/geot.1949.1.3.159>
17. Lageman R, Clarke RL, Pool W (2005) Electro-reclamation, a versatile soil remediation solution. *Eng Geol* 77:191–201. <https://doi.org/10.1016/j.enggeo.2004.07.010>
18. Alshawabkeh AN, Yeung AT, Bricka MR (1999) Practical aspects of in-situ electrokinetic extraction. *J Environ Eng* 125:27–35. [https://doi.org/10.1061/\(ASCE\)0733-9372\(1999\)125:1\(27\)](https://doi.org/10.1061/(ASCE)0733-9372(1999)125:1(27))
19. Acar YB, Alshawabkeh AN (1996) Electrokinetic remediation. I: pilot-scale tests with lead-spiked kaolinite. *J Geotech Eng* 122:173–185. [https://doi.org/10.1061/\(ASCE\)0733-9410\(1996\)122:3\(173\)](https://doi.org/10.1061/(ASCE)0733-9410(1996)122:3(173))
20. Kim W-S, Jeon E-K, Jung J-M, Jung H-B, Ko S-H, Seo C-I, Baek K (2014) Field application of electrokinetic remediation for multi-metal contaminated paddy soil using two-dimensional electrode configuration. *Environ Sci Pollut Res* 21:4482–4491. <https://doi.org/10.1007/s11356-013-2424-0>
21. Athmer CJ, Ho SV (2009) Field studies: organic-contaminated soil remediation with Lasagna technology. In: Reddy KR, Cameselle C (eds) *Electrochemical remediation technologies for polluted soils, sediments and groundwater*. Wiley, Hoboken, pp 625–646
22. Niinae M, Aoki Y, Aoki K (2005) Numerical modeling for electrokinetic soil processing-acidification of soil. *Resour Process* 52:136–144 (in Japanese). <https://doi.org/10.4144/rpsj.52.136>
23. Niinae M, Aoki Y, Aoki K (2006) Effect of electrode configuration on cleanup efficiency of heavy metals by electrokinetic soil remediation. *Resour. Process.* 53:49–57 (in Japanese). <https://doi.org/10.4144/rpsj.53.49>
24. Yuan S, Zheng Z, Chen J, Lu X (2009) Use of solar cell in electrokinetic remediation of cadmium-contaminated soil. *J Hazard Mater* 162:1583–1587. <https://doi.org/10.1016/j.jhazmat.2008.06.038>
25. Jeon E-K, Ryu S-R, Baek K (2015) Application of solar-cells in the electrokinetic remediation of As-contaminated soil. *Electrochim Acta* 181:160–166. <https://doi.org/10.1016/j.electacta.2015.03.065>
26. Millán M, Bucio-Rodríguez PY, Lobato J, Fernández-Marchante CM, Roa-Morales G, Barrera-Díaz C, Rodrigo MA (2020) Strategies for powering electrokinetic soil remediation: a way to optimize performance of the environmental technology. *J Environ Manag* 267. <https://doi.org/10.1016/j.jenvman.2020.110665>
27. Zhou M, Zhu S, Liu Y, Wang X (2013) Removal of fluorine from contaminated soil by electrokinetic treatment driven by solar energy. *Environ Sci Pollut Res* 20:5806–5812. <https://doi.org/10.1007/s11356-013-1595-z>
28. Wu S, Liu R, Liu Z, Du J, Tao C (2019) Electrokinetic remediation of electrolytic manganese residue using solar-cell and leachate-recirculation. *J Chem Eng Jpn* 52:710–717. <https://doi.org/10.1252/jcej.19we010>

29. Souza FL, Llanos J, Sáez C, Lanza MRV, Rodrigo MA, Cañizares P (2016) Performance of wind-powered soil electroremediation process for the removal of 2,4-D from soil. *J Environ Manag* 171:128–132. <https://doi.org/10.1016/j.jenvman.2016.01.032>
30. Cao X, Song H, Yu C, Li X (2015) Simultaneous degradation of toxic refractory organic pesticide and bioelectricity generation using a soil microbial fuel cell. *Bioresour Technol* 189: 87–93. <https://doi.org/10.1016/j.biortech.2015.03.148>
31. Habibul N, Hu Y, Sheng GP (2016) Microbial fuel cell driving electrokinetic remediation of toxic metal contaminated soils. *J Hazard Mater* 318:9–14. <https://doi.org/10.1016/j.jhazmat.2016.06.041>
32. Wada S-I, Umegaki Y (2001) Major ion and electrical potential distribution in soil under electrokinetic remediation. *Environ Sci Technol* 35:2151–2155. <https://doi.org/10.1021/es001335j>
33. Panda SK, Baluška F, Matsumoto H (2009) Aluminum stress signaling in plants. *Plant Signal Behav* 4:592–597. <https://doi.org/10.4161/psb.4.7.8903>
34. Elektorowicz M, Boeva V (1996) Electrokinetic supply of nutrients in soil bioremediation. *Environ Technol* 17:1339–1349. <https://doi.org/10.1080/09593331708616503>
35. Kim S-H, Han H-Y, Lee Y-J, Kim CW, Yang J-W (2010) Effect of electrokinetic remediation on indigenous microbial activity and community within diesel contaminated soil. *Sci Total Environ* 408:3162–3168. <https://doi.org/10.1016/j.scitotenv.2010.03.038>
36. Lear G, Harbottle MJ, Sills G, Knowles CJ, Semple KT, Thompson IP (2007) Impact of electrokinetic remediation on microbial communities within PCP contaminated soil. *Environ Pollut* 146:139–146. <https://doi.org/10.1016/j.envpol.2006.06.037>
37. Wick LY, Mattle PA, Wattiau P, Harms H (2004) Electrokinetic transport of PAH-degrading bacteria in model aquifers and soil. *Environ Sci Technol* 38:4596–4602. <https://doi.org/10.1021/es0354420>
38. Lear G, Harbottle MJ, van der Gast CJ, Jackman SA, Knowles CJ, Sills G, Thompson IP (2004) The effect of electrokinetics on soil microbial communities. *Soil Biol Biochem* 36: 1751–1760. <https://doi.org/10.1016/j.soilbio.2004.04.032>
39. Athmer CJ (2009) Cost estimates for electrokinetic remediation. In: Reddy KR, Cameselle C (eds) *Electrochemical remediation technologies for polluted soils, sediments and groundwater*. Wiley, Hoboken, pp 583–587
40. Kim D-H, Yoo J-C, Hwang B-R, Yang J-S, Baek K (2014) Environmental assessment on electrokinetic remediation of multimetal-contaminated site: a case study. *Environ Sci Pollut Res* 21:6751–6758. <https://doi.org/10.1007/s11356-014-2597-1>
41. Martin R, Sanchez DM, Gutierrez AM (1998) Sequential extraction of U, Th, Ce, La and some heavy metals in sediments from Ortigas river, Spain. *Talanta* 46:1115–1121. [https://doi.org/10.1016/S0039-9140\(97\)00374-3](https://doi.org/10.1016/S0039-9140(97)00374-3)
42. Li F, Fan Z, Xiao P, Oh K, Ma X, Hou W (2009) Contamination, chemical speciation and vertical distribution of heavy metals in soils of an old and large industrial zone in Northeast China. *Environ Geol* 57:1815–1823. <https://doi.org/10.1007/s00254-008-1469-8>
43. Giannis A, Pentari D, Wang JY, Gidarakos E (2010) Application of sequential extraction analysis to electrokinetic remediation of cadmium, nickel and zinc from contaminated soils. *J Hazard Mater* 184:547–554. <https://doi.org/10.1016/j.jhazmat.2010.08.070>
44. Ohkawa Y, Rudy SP, Fujiwara N, Jin K, Tanaka S (2012) Presumption of the source of lead contaminated soil by isotope analysis with sequential extraction. *Bunseki Kagaku* 61:95–101 (in Japanese). <https://doi.org/10.2116/bunsekikagaku.61.95>
45. Puppala SK, Alshawabkeh AN, Acar YB, Gale RJ, Bricka M (1997) Enhanced electrokinetic remediation of high sorption capacity soil. *J Hazard Mater* 55:203–220. [https://doi.org/10.1016/S0304-3894\(97\)00011-3](https://doi.org/10.1016/S0304-3894(97)00011-3)
46. Hansen HK, Ottosen LM, Kliem BK, Villumsen A (1997) Electrodialytic remediation of soils polluted with Cu, Cr, Hg, Pb and Zn. *J Chem Technol Biotechnol* 70:67–73. [https://doi.org/10.1002/\(SICI\)1097-4660\(199709\)70:1<67::AID-JCTB662>3.0.CO;2-V](https://doi.org/10.1002/(SICI)1097-4660(199709)70:1<67::AID-JCTB662>3.0.CO;2-V)

47. Giannis A, Gidarakos E (2005) Washing enhanced electrokinetic remediation for removal cadmium from real contaminated soil. *J Hazard Mater* 123:165–175. <https://doi.org/10.1016/j.jhazmat.2005.03.050>
48. Suzuki M, Shoji T, Yoshimura N (2007) Research on heavy metal recovery using the electrokinetic phenomenon. *Electr Eng Jpn* 158:1–7. <https://doi.org/10.1002/ej.20312>
49. Kim D-H, Ryu B-G, Park S-W, Seo C-I, Baek K (2009) Electrokinetic remediation of Zn and Ni-contaminated soil. *J Hazard Mater* 165:501–505. <https://doi.org/10.1016/j.jhazmat.2008.10.025>
50. Niinae M, Aoki K (2006) Effect of pH on enhanced electrokinetic remediation of cadmium contaminated soils by EDTA. *Resour Process* 53:185–190 (in Japanese). <https://doi.org/10.4144/rpsj.53.185>
51. Alcántara MT, Gómez J, Pazos M, Sanromán MA (2012) Electrokinetic remediation of lead and phenanthrene polluted soils. *Geoderma* 173–174:128–133. <https://doi.org/10.1016/j.geoderma.2011.12.009>
52. Gu Y, Yeung AT, Li H (2018) Enhanced electrokinetic remediation of cadmium-contaminated natural clay using organophosphonates in comparison with EDTA. *Chin J Chem Eng* 26: 1152–1159. <https://doi.org/10.1016/j.cjche.2017.10.012>
53. Zhou D-M, Deng C-F, Cang L, Alshwabkeh AN (2005) Electrokinetic remediation of a Cu–Zn contaminated red soil by controlling the voltage and conditioning catholyte pH. *Chemosphere* 61:519–527. <https://doi.org/10.1016/j.chemosphere.2005.02.055>
54. Yuan L, Xu X, Li H, Wang N, Guo N, Yu H (2016) Development of novel assisting agents for the electrokinetic remediation of heavy metal-contaminated kaolin. *Electrochim Acta* 218: 140–148. <https://doi.org/10.1016/j.electacta.2016.09.121>
55. Fu R, Wen D, Xia X, Zhang W, Gu Y (2017) Electrokinetic remediation of chromium (Cr)-contaminated soil with citric acid (CA) and polyaspartic acid (PASP) as electrolytes. *Chem Eng J* 316:601–608. <https://doi.org/10.1016/j.cej.2017.01.092>
56. Karagunduz A, Gezer A, Karasuloglu G (2007) Surfactant enhanced electrokinetic remediation of DDT from soils. *Sci Total Environ* 385:1–11. <https://doi.org/10.1016/j.scitotenv.2007.07.010>
57. Alcántara MT, Gómez J, Pazos M, Sanromán MA (2010) Electrokinetic remediation of PAH mixtures from kaolin. *J Hazard Mater* 179:1156–1160. <https://doi.org/10.1016/j.jhazmat.2010.03.010>
58. Fan G, Cang L, Fang G, Zhou D (2014) Surfactant and oxidant enhanced electrokinetic remediation of a PCBs polluted soil. *Sep Purif Technol* 123:106–113. <https://doi.org/10.1016/j.seppur.2013.12.035>
59. Suanon F, Tang L, Sheng H, Fu Y, Xiang L, Herzberger A, Jiang X, Mama D, Wang F (2020) TW80 and GLDA-enhanced oxidation under electrokinetic remediation for aged contaminated-soil: does it worth? *Chem Eng J* 385:123934. <https://doi.org/10.1016/j.cej.2019.123934>
60. Fardin AB, Jamshidi-Zanjani A, Darban AK (2021) Application of enhanced electrokinetic remediation by coupling surfactants for kerosene-contaminated soils: effect of ionic and nonionic surfactants. *J Environ Manag* 277:111422. <https://doi.org/10.1016/j.jenvman.2020.111422>
61. Ko S-O, Schlautman MA, Carraway ER (2000) Cyclodextrin-enhanced electrokinetic removal of phenanthrene from a model clay soil. *Environ Sci Technol* 34:1535–1541. <https://doi.org/10.1021/es990223t>
62. Maturi K, Reddy KR (2006) Simultaneous removal of organic compounds and heavy metals from soils by electrokinetic remediation with a modified cyclodextrin. *Chemosphere* 63:1022–1031. <https://doi.org/10.1016/j.chemosphere.2005.08.037>
63. Gonzini O, Plaza A, Di Palma L, Lobo MC (2010) Electrokinetic remediation of gasoil contaminated soil enhanced by rhamnolipid. *J Appl Electrochem* 40:1239–1248. <https://doi.org/10.1007/s10800-010-0095-9>

64. Tang J, He J, Tang H, Wang H, Sima W, Liang C, Qiu Z (2020) Heavy metal removal effectiveness, flow direction and speciation variations in the sludge during the biosurfactant-enhanced electrokinetic remediation. *Sep Purif Technol* 246:116918. <https://doi.org/10.1016/j.seppur.2020.116918>
65. Sawada A, Tanaka S, Fukushima M, Tatsumi K (2003) Electrokinetic remediation of clayey soils containing copper(II)-oxinate using humic acid as a surfactant. *J Hazard Mater* 96:145–154. [https://doi.org/10.1016/S0304-3894\(02\)00168-1](https://doi.org/10.1016/S0304-3894(02)00168-1)
66. Arakawa H, Watanabe N, Tamura R, Rao CP (1998) Reduction of potassium chromate by tannins. *Bull Chem Soc Jpn* 71:1993–1998. <https://doi.org/10.1246/bcsj.71.1993>
67. Tanaka S, Sawada A (1999) Effect of humic substances and their precursors on removal of hexavalent chromium in soil by electroremediation. *J Environ Chem* 9:391–398 (in Japanese). <https://doi.org/10.5985/jec.9.391>
68. Tanaka S, Nakayasu K, Fukushima M (1997) Suppression effect of humic substances on oxidation of chromium (III) to chromium (VI). *Toxicol Environ Chem* 58:17–23. <https://doi.org/10.1080/02772249709358394>
69. Fukushima M, Nakayasu K, Tanaka S, Nakamura H (1997) Speciation analysis of chromium after reduction of chromium (VI) by humic acid. *Toxicol Environ Chem* 62:207–215. <https://doi.org/10.1080/02772249709358508>
70. Sawada A, Mori K, Tanaka S, Fukushima M, Tatsumi K (2004) Removal of Cr(VI) from contaminated soil by electrokinetic remediation. *Waste Manag* 24:483–490. [https://doi.org/10.1016/S0956-053X\(03\)00133-8](https://doi.org/10.1016/S0956-053X(03)00133-8)
71. Taga M, Tanaka S, Fukushima M (1989) Measurement of copper complexing ability of humic acids by using diethylaminoethyl Sephadex A-25 column. *Anal Sci* 5:597–600. <https://doi.org/10.2116/analsci.5.597>
72. Fukushima M, Nakayasu K, Tanaka S, Nakamura H (1995) Chromium(III) binding abilities of humic acids. *Anal Chim Acta* 317:195–206. [https://doi.org/10.1016/0003-2670\(95\)00410-6](https://doi.org/10.1016/0003-2670(95)00410-6)
73. Yamamoto M, Nishida A, Otsuka K, Komai T, Fukushima M (2010) Evaluation of the binding of iron(II) to humic substances derived from a compost sample by a colorimetric method using ferrozine. *Bioresour Technol* 101:4456–4460. <https://doi.org/10.1016/j.biortech.2010.01.050>
74. Tan L, Zhao C, Tan X, Wang X, Feng J, Fang M, Ai Y, Hayat T, Sun L, Wang X (2019) Effect of co-existing Co²⁺ ions on the aggregation of humic acid in aquatic environment: aggregation kinetics, dynamic properties and fluorescence spectroscopic study. *Sci Total Environ* 674:544–553. <https://doi.org/10.1016/j.scitotenv.2019.04.119>
75. Iwamura T, Akemoto Y, Tanaka S (2020) Enhancement effect of humic acid on removal of lead from soil by electrokinetic process. *Anal Sci* 36:627–630. <https://doi.org/10.2116/analsci.19SBN04>
76. Iwamura T (2016) Enhancement effect of humic acid for the remediation of lead contaminated soil by electrokinetic process, Master thesis, Hokkaido University (in Japanese)
77. Tanaka S, Oba K, Fukushima M, Nakayasu K, Hasebe K (1997) Water solubility enhancement of pyrene in the presence of humic substances. *Anal Chim Acta* 337:351–357. [https://doi.org/10.1016/S0003-2670\(96\)00422-9](https://doi.org/10.1016/S0003-2670(96)00422-9)
78. Kodama R, Sazawa K, Miyamoto T, Zhu Q, Igarashi M, Oda K, Kuramitz H, Fukushima M (2018) Potential risk of coupling products between tetrahalobisphenol A and humic acid prepared via oxidation with a biomimetic catalyst. *Chemosphere* 204:63–70. <https://doi.org/10.1016/j.chemosphere.2018.03.141>
79. Yamamoto M, Iwai H, Matsuo M, Liu D, Fukushima M (2020) Mechanism of the elution of iron from a slag-compost fertilizer for restoring seaweed beds in coastal areas-characteristic changes of steelmaking slag and humic acids derived from the fertilizer during the elution process. *Anal Sci* 36:545–551. <https://doi.org/10.2116/ANALSCI.19SBP04>
80. Kimura T, Takase K, Tanaka S (2007) Concentration of copper and a copper-EDTA complex at the pH junction formed in soil by an electrokinetic remediation process. *J Hazard Mater* 143:668–672. <https://doi.org/10.1016/j.jhazmat.2007.01.011>

81. Tanaka S (2019) Development of separation technologies for environmental remediation. *Anal Sci* 35:241–248. <https://doi.org/10.2116/analsci.18R002>
82. Ottosen LM, Hansen HK, Laursen S, Villumsen A (1997) Electrodialytic remediation of soil polluted with copper from wood preservation industry. *Environ Sci Technol* 31:1711–1715. <https://doi.org/10.1021/es9605883>
83. Ottosen LM, Hansen HK, Hansen CB (2000) Water splitting at ion-exchange membranes and potential differences in soil during electrodialytic soil remediation. *J Appl Electrochem* 30: 1199–1207. <https://doi.org/10.1023/A:1026557830268>
84. Jakobsen MR, Fritt-Rasmussen J, Nielsen S, Ottosen LM (2004) Electrodialytic removal of cadmium from wastewater sludge. *J Hazard Mater* 106:127–132. <https://doi.org/10.1016/j.jhazmat.2003.10.005>
85. Liu Y, Chen J, Cai Z, Chen R, Sun Q, Sun M (2017) Removal of copper and nickel from municipal sludge using an improved electrokinetic process. *Chem Eng J* 307:1008–1016. <https://doi.org/10.1016/j.cej.2016.08.133>
86. Liu Y, Ke X, Wu X, Ke C, Chen R, Chen X, Zheng X, Jin Y, Van der Bruggen B (2020) Simultaneous removal of trivalent chromium and hexavalent chromium from soil using a modified bipolar membrane electrodialysis system. *Environ Sci Technol* 54:13304–13313. <https://doi.org/10.1021/acs.est.0c04105>
87. Maitra S (2019) Permeable reactive barrier: a technology for groundwater remediation—a mini review. *Res J Life Sci Bioinform Pharm Chem Sci* 5:203–217. <https://doi.org/10.26479/2019.0501.21>
88. De Battisti A, Ferro S (2007) Electrokinetic remediation: methods of remediation of soils and ground waters (EREM 2005). *Electrochim Acta* 52:3345–3348. <https://doi.org/10.1016/j.electacta.2006.09.033>
89. Yeh C, Lin C, Wu C (2010) A permeable reactive barrier for the bioremediation of BTEX-contaminated groundwater: microbial community distribution and removal efficiencies. *J Hazard Mater* 178:74–80. <https://doi.org/10.1016/j.jhazmat.2010.01.045>
90. Mumford KA, Rayner JL, Snape I, Stark SC, Stevens GW, Gore DB (2013) Design, installation and preliminary testing of a permeable reactive barrier for diesel fuel remediation at Casey Station, Antarctica. *Cold Reg Sci Technol* 96:96–107. <https://doi.org/10.1016/j.coldregions.2013.06.002>
91. Yeung AT (2011) Milestone developments, myths, and future directions of electrokinetic remediation. *Sep Purif Technol* 79:124–132. <https://doi.org/10.1016/j.seppur.2011.01.022>
92. Cang L, Zhou D-M, Wu D-Y, Alshawabkeh AN (2009) Coupling electrokinetics with permeable reactive barriers of zero-valent iron for treating a chromium contaminated soil. *Sep Sci Technol* 44:2188–2202. <https://doi.org/10.1080/01496390902976699>
93. Saeedi M, Jamshidi A, Shariatmadri N, Falamaki A (2009) An investigation on the efficiency of electro kinetic coupled with carbon active barrier to remediate nickel contaminated clay. *Int J Environ Res* 3:629–636
94. Cappai G, De Gioannis G, Muntoni A, Spiga D, Zijlstra JJP (2012) Combined use of a transformed red mud reactive barrier and electrokinetics for remediation of Cr/As contaminated soil. *Chemosphere* 86:400–408. <https://doi.org/10.1016/j.chemosphere.2011.10.053>
95. Putra RS, Tanaka S (2011) Aluminum drinking water treatment residuals (AL-WTRs) as an entrapping zone for lead in soil by electrokinetic remediation. *Sep Purif Technol* 79:208–215. <https://doi.org/10.1016/j.seppur.2011.02.015>
96. Nasiri A, Jamshidi-Zanjani A, Khodadadi Darban A (2020) Application of enhanced electrokinetic approach to remediate Cr-contaminated soil: effect of chelating agents and permeable reactive barrier. *Environ Pollut* 266:115197. <https://doi.org/10.1016/j.envpol.2020.115197>
97. Kim D, Han J (2020) Remediation of multiply contaminated ground via permeable reactive barrier and electrokinetic using recyclable food scrap ash (FSA). *Appl Sci* 10:1194. <https://doi.org/10.3390/app10041194>

98. Chung HI, Lee MH (2007) A new method for remedial treatment of contaminated clayey soils by electrokinetics coupled with permeable reactive barriers. *Electrochim Acta* 52:3427–3431. <https://doi.org/10.1016/j.electacta.2006.08.074>
99. Nieto Castillo A, García-Delgado RA, Cala Rivero V (2012) Electrokinetic treatment of soils contaminated by tannery waste. *Electrochim Acta* 86:110–114. <https://doi.org/10.1016/j.electacta.2012.04.132>
100. Czurda K, Haus R (2002) Reactive barriers with fly ash zeolites for in situ groundwater remediation. *Appl Clay Sci* 21:13–20. [https://doi.org/10.1016/S0169-1317\(01\)00088-6](https://doi.org/10.1016/S0169-1317(01)00088-6)
101. Zhao X, Liu W, Cai Z, Han B, Qian T, Zhao D (2016) An overview of preparation and applications of stabilized zero-valent iron nanoparticles for soil and groundwater remediation. *Water Res* 100:245–266. <https://doi.org/10.1016/j.watres.2016.05.019>
102. Sharma HD, Reddy KR (2004) *Geoenvironmental engineering: site remediation, waste containment, and emerging waste management technologies*. Wiley
103. Kimura T, Tanaka S (2006) Removal of organochlorine compounds contaminated soil by electrokinetic remediation combined with iron wall. *J Japan Soc Water Environ* 29:101–105 (in Japanese). <https://doi.org/10.2965/jswe.29.101>
104. Czinnerová M, Vološčuková O, Marková K, Ševců A, Černík M, Nosek J (2020) Combining nanoscale zero-valent iron with electrokinetic treatment for remediation of chlorinated ethenes and promoting biodegradation: a long-term field study. *Water Res* 175:115692. <https://doi.org/10.1016/j.watres.2020.115692>
105. Zheng Y, Yan Y, Yu L, Li H, Jiao B, Shiau Y, Li D (2020) Synergism of citric acid and zero-valent iron on Cr(VI) removal from real contaminated soil by electrokinetic remediation. *Environ Sci Pollut Res* 27:5572–5583. <https://doi.org/10.1007/s11356-019-06820-5>
106. Suzuki T, Moribe M, Oyama Y, Niinae M (2012) Mechanism of nitrate reduction by zero-valent iron: equilibrium and kinetics studies. *Chem Eng J* 183:271–277. <https://doi.org/10.1016/j.cej.2011.12.074>
107. Suzuki T, Oyama Y, Moribe M, Niinae M (2012) An electrokinetic/Fe⁰ permeable reactive barrier system for the treatment of nitrate-contaminated subsurface soils. *Water Res* 46:772–778. <https://doi.org/10.1016/j.watres.2011.11.048>
108. Ho SV, Athmer C, Sheridan PW, Hughes BM, Orth R, McKenzie D, Brodsky PH, Shapiro A, Thornton R, Salvo J, Schultz D, Landis R, Griffith R, Shoemaker S (1999) The Lasagna technology for in situ soil remediation. 1. Small field test. *Environ Sci Technol* 33:1086–1091. <https://doi.org/10.1021/es980332s>
109. Ho SV, Athmer C, Sheridan PW, Hughes BM, Orth R, McKenzie D, Brodsky PH, Shapiro AM, Sivavec TM, Salvo J, Schultz D, Landis R, Griffith R, Shoemaker S (1999) The Lasagna technology for in situ soil remediation. 2. Large field test. *Environ Sci Technol* 33:1092–1099. <https://doi.org/10.1021/es980414g>
110. Fukushima M, Tatsumi K (2001) Degradation pathways of pentachlorophenol by photo-Fenton systems in the presence of iron(III), humic acid, and hydrogen peroxide. *Environ Sci Technol* 35:1771–1778. <https://doi.org/10.1021/es001088j>
111. Yang GCC, Long Y-W (1999) Removal and degradation of phenol in a saturated flow by in-situ electrokinetic remediation and Fenton-like process. *J Hazard Mater* 69:259–271. [https://doi.org/10.1016/S0304-3894\(99\)00059-X](https://doi.org/10.1016/S0304-3894(99)00059-X)
112. Park J-Y, Kim S-J, Lee Y-J, Baek K, Yang J-W (2005) EK-Fenton process for removal of phenanthrene in a two-dimensional soil system. *Eng Geol* 77:217–224. <https://doi.org/10.1016/j.enggeo.2004.07.012>
113. Tsai T-T, Sah J, Kao C-M (2010) Application of iron electrode corrosion enhanced electrokinetic-Fenton oxidation to remediation diesel contaminated soils: a laboratory feasibility study. *J Hydrol* 380:4–13. <https://doi.org/10.1016/j.jhydrol.2009.09.010>
114. Paixão IC, López-Vizcaíno R, Solano AMS, Martínez-Huitle CA, Navarro V, Rodrigo MA, dos Santos EV (2020) Electrokinetic-Fenton for the remediation low hydraulic conductivity soil contaminated with petroleum. *Chemosphere* 248:126029. <https://doi.org/10.1016/j.chemosphere.2020.126029>

115. Chowdhury AIA, Gerhard JI, Reynolds D, O'Carroll DM (2017) Low permeability zone remediation via oxidant delivered by electrokinetics and activated by electrical resistance heating: proof of concept. *Environ Sci Technol* 51:13295–13303. <https://doi.org/10.1021/acs.est.7b02231>
116. Cluis C (2004) Junk-greedy greens: phytoremediation as a new option for soil decontamination. *BioTeach J* 2:61–67
117. Gratão PL, Prasad MNV, Cardoso PF, Lea PJ, Azevedo RA (2005) Phytoremediation: green technology for the clean up of toxic metals in the environment, Brazilian. *J Plant Physiol* 17: 53–64. <https://doi.org/10.1590/S1677-04202005000100005>
118. Ghosh M, Singh SP (2005) A review on phytoremediation of heavy metals and utilization of it's by products. *Asian. J Energy Environ* 6:214–231
119. Cameselle C, Chirakkara RA, Reddy KR (2013) Electrokinetic-enhanced phytoremediation of soils: status and opportunities. *Chemosphere* 93:626–636. <https://doi.org/10.1016/j.chemosphere.2013.06.029>
120. Cameselle C, Gouveia S, Urréjola S (2019) Benefits of phytoremediation amended with DC electric field. Application to soils contaminated with heavy metals. *Chemosphere* 229:481–488. <https://doi.org/10.1016/j.chemosphere.2019.04.222>
121. Hodko D, Van Hyfte J, Denvir A, Magnuson JW (2000) Methods for enhancing phytoextraction of contaminants from porous media using electrokinetic phenomena, US Patent No. 6,145,224
122. Bedmar MCL, Perez-Sanz A, Martinez-Inigo MJ, Benito AP (2009) Influence of coupled electrokinetic phytoremediation on soil remediation. In: Reddy KR, Cameselle C (eds) *Electrochemical remediation technologies for polluted soils, sediments and groundwater*. Wiley, Hoboken, pp 417–437
123. Fengxiang XM (2015) Coupled electro-kinetic remediation and phytoremediation of metal (loid) contaminated soils. *J Bioremed Biodegr* 06:2–4. <https://doi.org/10.4172/2155-6199.1000e163>
124. Chirakkara RA, Reddy KR, Cameselle C (2015) Electrokinetic amendment in phytoremediation of mixed contaminated soil. *Electrochim Acta* 181:179–191. <https://doi.org/10.1016/j.electacta.2015.01.025>
125. Luo J, Yang D, Qi S, Wu J, Gu XS (2018) Using solar cell to phytoremediate field-scale metal polluted soil assisted by electric field. *Ecotoxicol Environ Saf* 165:404–410. <https://doi.org/10.1016/j.ecoenv.2018.09.031>
126. Chang J-H, Dong C-D, Shen S-Y (2019) The lead contaminated land treated by the circulation-enhanced electrokinetics and phytoremediation in field scale. *J Hazard Mater* 368:894–898. <https://doi.org/10.1016/j.jhazmat.2018.08.085>
127. Luo J, Xing X, Qi S, Wu J, Gu XWS (2019) Comparing the risk of metal leaching in phytoremediation using *Noccaea caerulea* with or without electric field. *Chemosphere* 216:661–668. <https://doi.org/10.1016/j.chemosphere.2018.10.167>
128. O'Connor CS, Lepp NW, Edwards R, Sunderland G (2003) The combined use of electrokinetic remediation and phytoremediation to decontaminate metal-polluted soils: a laboratory-scale feasibility study. *Environ Monit Assess* 84:141–158. <https://doi.org/10.1023/A:1022851501118>
129. Baker AJM, Brooks RR (1989) Terrestrial higher plants which hyperaccumulate metallic elements - a review of their distribution, ecology and phytochemistry. *Biorecovery* 1:81–126
130. Putra RS, Ohkawa Y, Tanaka S (2013) Application of EAPR system on the removal of lead from sandy soil and uptake by Kentucky bluegrass (*Poa pratensis* L.). *Sep Purif Technol* 102: 34–42. <https://doi.org/10.1016/j.seppur.2012.09.025>
131. Bi R, Schlaak M, Siefert E, Lord R, Connolly H (2010) Alternating current electrical field effects on lettuce (*Lactuca sativa*) growing in hydroponic culture with and without cadmium contamination. *J Appl Electrochem* 40:1217–1223. <https://doi.org/10.1007/s10800-010-0094-x>

132. Kubiak JJ, Khankhane PJ, Kleingeld PJ, Lima AT (2012) An attempt to electrically enhance phytoremediation of arsenic contaminated water. *Chemosphere* 87:259–264. <https://doi.org/10.1016/j.chemosphere.2011.12.048>
133. Putra RS, Cahyana F, Novarita D (2015) Removal of lead and copper from contaminated water using EAPR system and uptake by water lettuce (*Pistia Stratiotes* L.). *Procedia Chem* 14:381–386. <https://doi.org/10.1016/j.proche.2015.03.052>
134. Putra RS, Novarita D, Cahyana F (2016) Remediation of lead (Pb) and copper (Cu) using water hyacinth [*Eichornia crassipes* (Mart.) Solms] with electro-assisted phytoremediation (EAPR). *AIP Conf Proc* 1744:020052. <https://doi.org/10.1063/1.4953526>
135. Putra RS, Trahadinata GA, Latif A, Solehudin M (2017) Wastewater treatment of chemical laboratory using electro assisted-phytoremediation (EAPR), in. *AIP Conf Proc* 1823:020077. <https://doi.org/10.1063/1.4978150>
136. Putra RS, Hastika FY (2018) Removal of heavy metals from leachate using electro-assisted phytoremediation (EAPR) and up-take by water hyacinth (*Eichornia crassipes*). *Indones J Chem* 18:306. <https://doi.org/10.22146/ijc.29713>
137. Putra RS, Viani V, Setianingrum I, Dwi Sintadani E, Uuliyah D, M. (2019) Faiq Faridani, enhancement of EAPR system using aeration process on the removal of heavy metal (Cu and Fe) in the wastewater and up-take by vetiver grass (*Vetiveira zizaniodes* L). *Mater Sci Forum* 948:3–8. <https://doi.org/10.4028/www.scientific.net/MSF.948.3>
138. Putra RS, Annisa AD, Budiarijo S (2020) Batik wastewater treatment using simultaneous process of electrocoagulation and electro-assisted phytoremediation (EAPR). *Indones J Chem* 20:1221–1229. <https://doi.org/10.22146/ijc.47898>
139. Aboughalma H, Bi R, Schlaak M (2008) Electrokinetic enhancement on phytoremediation in Zn, Pb, Cu and Cd contaminated soil using potato plants. *J Environ Sci Heal Part A* 43:926–933. <https://doi.org/10.1080/10934520801974459>
140. Lim J-M, Salido AL, Butcher DJ (2004) Phytoremediation of lead using Indian mustard (*Brassica juncea*) with EDTA and electrodis. *Microchem J* 76:3–9. <https://doi.org/10.1016/j.microc.2003.10.002>
141. Wang JY, Huang XJ, Kao JCM, Stabnikova O (2006) Removal of heavy metals from kaolin using an upward electrokinetic soil remedial (UESR) technology. *J Hazard Mater* 136:532–541. <https://doi.org/10.1016/j.jhazmat.2006.01.029>
142. Zhou D-M, Chen H-F, Cang L, Wang Y-J (2007) Ryegrass uptake of soil Cu/Zn induced by EDTA/EDDS together with a vertical direct-current electrical field. *Chemosphere* 67:1671–1676. <https://doi.org/10.1016/j.chemosphere.2006.11.042>
143. Renauld PO, Probststein RF (1987) Electro-osmotic control of hazardous waste. *Physicochem Hydrodyn* 9:345–460
144. Jin M, Sharma MM (1991) A model for electrochemical and electrokinetic coupling in inhomogeneous porous media. *J Colloid Interface Sci* 142:61–73. [https://doi.org/10.1016/0021-9797\(91\)90033-5](https://doi.org/10.1016/0021-9797(91)90033-5)
145. Adams A, Raman A, Hodgkins D (2012) How do the plants used in phytoremediation in constructed wetlands, a sustainable remediation strategy, perform in heavy-metal-contaminated mine sites? *Water Environ J* 27:373–386. <https://doi.org/10.1111/j.1747-6593.2012.00357.x>
146. Fester T (2013) Arbuscular mycorrhizal fungi in a wetland constructed for benzene-, methyl tert -butyl ether- and ammonia-contaminated groundwater bioremediation. *Microb Biotechnol* 6:80–84. <https://doi.org/10.1111/j.1751-7915.2012.00357.x>
147. Yeh TY (2021) Current status of soil and groundwater remediation technologies in Taiwan. *Int J Phytoremediation* 23:212–218. <https://doi.org/10.1080/15226514.2020.1803202>
148. Zabłudowska E, Kowalska J, Jedynak Ł, Wojas S, Skłodowska A, Antosiewicz DM (2009) Search for a plant for phytoremediation – what can we learn from field and hydroponic studies? *Chemosphere* 77:301–307. <https://doi.org/10.1016/j.chemosphere.2009.07.064>
149. Vithanage M, Dabrowska BB, Mukherjee AB, Sandhi A, Bhattacharya P (2012) Arsenic uptake by plants and possible phytoremediation applications: a brief overview. *Environ Chem Lett* 10:217–224. <https://doi.org/10.1007/s10311-011-0349-8>

150. Safari S, Azadi Aghdam M, Kariminia H-R (2016) Electrocoagulation for COD and diesel removal from oily wastewater. *Int J Environ Sci Technol* 13:231–242. <https://doi.org/10.1007/s13762-015-0863-5>
151. Jing G, Ren S, Gao Y, Sun W, Gao Z (2020) Electrocoagulation: a promising method to treat and reuse mineral processing wastewater with high COD. *Water* 12:595. <https://doi.org/10.3390/w12020595>
152. Kong X, Zhou Y, Xu T, Hu B, Lei X, Chen H, Yu G (2020) A novel technique of COD removal from electroplating wastewater by Fenton—alternating current electrocoagulation. *Environ Sci Pollut Res* 27:15198–15210. <https://doi.org/10.1007/s11356-020-07804-6>
153. Ghanbari F, Moradi M, Eslami A, Emamjomeh MM (2014) Electrocoagulation/floatation of textile wastewater with simultaneous application of aluminum and iron as anode. *Environ Process* 1:447–457. <https://doi.org/10.1007/s40710-014-0029-3>
154. Utomo B, Masykuri M, Musyawaroh AP, Wanguyun AG (2019) The performance of batik wastewater treatment by electro coagulation process under variations of electrodes. *Ecol Environ Conserv* 25:32–36
155. Barrera-Díaz C, Linares-Hernández I, Roa-Morales G, Bilyeu B, Balderas-Hernández P (2009) Removal of biorefractory compounds in industrial wastewater by chemical and electrochemical pretreatments. *Ind Eng Chem Res* 48:1253–1258. <https://doi.org/10.1021/ie800560n>
156. Suelee AL, Hasan SNMS, Kusin FM, Yusuff FM, Ibrahim ZZ (2017) Phytoremediation potential of vetiver grass (*Vetiveria zizanioides*) for treatment of metal-contaminated water. *Water Air Soil Pollut* 228:158. <https://doi.org/10.1007/s11270-017-3349-x>
157. Andra SS, Datta R, Sarkar D, Makris KC, Mullens CP, Sahi SV, Bach SBH (2010) Synthesis of phytochelatin in vetiver grass upon lead exposure in the presence of phosphorus. *Plant Soil* 326:171–185. <https://doi.org/10.1007/s11104-009-9992-2>
158. Marwood CA, Solomon KR, Greenberg BM (2001) Chlorophyll fluorescence as a bioindicator of effects on growth in aquatic macrophytes from mixtures of polycyclic aromatic hydrocarbons. *Environ Toxicol Chem* 20:890–898. <https://doi.org/10.1002/etc.5620200425>
159. Chantachon S, Kruatrachue M, Pokethitiyook P, Upatham S, Tantanararit S, Soonthornsarathool V (2004) Phytoextraction and accumulation of lead from contaminated soil by vetiver grass: laboratory and simulated field study. *Water Air Soil Pollut* 154:37–55. <https://doi.org/10.1023/B:WATE.0000022926.05464.74>
160. Satoh T (2015) Actual soil conditions of tsunami-hit farmland: 1. Influence of soil physical conditions on eluviation of salt in terms of soil EC in non-cropped paddy fields in Iwate prefecture (progress review: tsunami affected farmland). *Jpn J Soil Sci Plant Nutr* 86:396–398 (in Japanese). https://doi.org/10.20710/dojo.86.5_396
161. Nishimura T, Toride N (1999) Fundamentals and applications of soil colloid science (12) -Hydraulic properties and soil erosion. *J Agric Eng Soc Jpn* 67:277–284 (in Japanese). https://doi.org/10.11408/jjsidre1965.67.3_277
162. Ishiguro M (2015) Fundamental information about measures of desalinization: 1. Fundamentals of solute transport for desalinization (progress review: tsunami affected farmland). *Jpn J Soil Sci Plant Nutr*. 86:381–386 (in Japanese). https://doi.org/10.20710/dojo.86.5_381
163. Akemoto Y, Ohkawa Y, Putra RS, Kan M, Tanaka S (2012) Removal of sodium ion from sea-water contaminated soil by using electrokinetic process. In: International symposium on electrokinetic remediation, Sapporo, pp 99–100
164. Lee Y-J, Choi J-H, Lee H-G, Ha T-H, Bae J-H (2011) Pilot-scale study on in situ electrokinetic removal of nitrate from greenhouse soil. *Sep Purif Technol* 79:254–263. <https://doi.org/10.1016/j.seppur.2011.02.011>
165. Kim G-N, Oh W-Z, Won H-J, Choi W-K (2003) Removal of cesium and cobalt from soil around TRIGA reactor using electrokinetic method. *J Ind Eng Chem* 9:306–313
166. Kim G-N, Choi W-K, Jung C-H, Moon J-K (2007) Development of a washing system for soil contaminated with radionuclides around TRIGA reactors. *J Ind Eng Chem* 13:406–413

167. Kim G-N, Shon D-B, Park H-M, Lee K-W, Chung U-S (2011) Development of pilot-scale electrokinetic remediation technology for uranium removal. *Sep Purif Technol* 80:67–72. <https://doi.org/10.1016/j.seppur.2011.04.009>
168. Agnew K, Cundy AB, Hopkinson L, Croudace IW, Warwick PE, Purdie P (2011) Electrokinetic remediation of plutonium-contaminated nuclear site wastes: results from a pilot-scale on-site trial. *J Hazard Mater* 186:1405–1414. <https://doi.org/10.1016/j.jhazmat.2010.12.016>
169. Hashimoto S, Ugawa S, Nanko K, Shichi K (2012) The total amounts of radioactively contaminated materials in forests in Fukushima, Japan. *Sci Rep* 2:416. <https://doi.org/10.1038/srep00416>
170. Al-Shahrani SS, Roberts EPL (2005) Electrokinetic removal of caesium from kaolin. *J Hazard Mater* B122:91–101. <https://doi.org/10.1016/j.jhazmat.2005.03.018>
171. Oguri Y, Miyake K, Fukuda H, Kaneko J, Hasagawa J, Ogawa M, Shiho M (2004) Application of PIXE analysis to the study of electrokinetic removal of cesium from soil. *Int J PIXE* 14: 49–56. <https://doi.org/10.1142/S0129083504000094>
172. Miura T, Kabir M, Suzuki M, Shunsuke N, Mori S (2016) Effect of organic acids on cesium removal from contaminated soil by the electrokinetic remediation. *J Inst Electrostat Jpn* 40: 14–19 (in Japanese)
173. Igawa M, Ishiyama K, Nanzai B (2018) Removal of cesium ions from soil by electrokinetic remediation. *Bull Soc Sea Water Sci Jpn* 72:88–95 (in Japanese). https://doi.org/10.11457/swsj.72.2_88
174. Kim G-N, Jung Y-H, Lee J-J, Moon J-K, Jung C-H (2008) An analysis of a flushing effect on the electrokinetic-flushing removal of cobalt and cesium from a soil around decommissioning site. *Sep Purif Technol* 63:116–121. <https://doi.org/10.1016/j.seppur.2008.04.006>
175. Jung HB, Yang J-S, Um W (2015) Bench-scale electrokinetic remediation for cesium-contaminated sediment at the Hanford site, USA. *J Radioanal Nucl Chem* 304:615–625. <https://doi.org/10.1007/s10967-014-3852-0>
176. Helal AA, Arida HA, Rizk HE, Khalifa SM (2007) Interaction of cesium with humic materials: a comparative study of radioactivity and ISE measurements. *Radiochemistry* 49:523–529. <https://doi.org/10.1134/S1066362207050141>
177. Mukai H, Tamura K, Kikuchi R, Takahashi Y, Yaita T, Kogure T (2018) Cesium desorption behavior of weathered biotite in Fukushima considering the actual radioactive contamination level of soils. *J Environ Radioact* 190–191:81–88. <https://doi.org/10.1016/j.jenvrad.2018.05.006>
178. Tanaka K, Takahashi Y, Sakaguchi A, Umeo M, Hayakawa S, Tanida H, Saito T, Kanai Y (2012) Vertical profiles of iodine-131 and cesium-137 in soils in Fukushima prefecture related to the Fukushima Daiichi Nuclear Power Station accident. *Geochem J* 46:73–76. <https://doi.org/10.2343/geochemj.1.0137>
179. Malins A, Kurikami H, Nakama S, Saito T, Okumura M, Machida M, Kitamura A (2016) Evaluation of ambient dose equivalent rates influenced by vertical and horizontal distribution of radioactive cesium in soil in Fukushima prefecture. *J Environ Radioact* 151:38–49. <https://doi.org/10.1016/j.jenvrad.2015.09.014>
180. Takahashi Y, Fan Q, Suga H, Tanaka K, Sakaguchi A, Takeichi Y, Ono K, Mase K, Kato K, Kanivets VV (2017) Comparison of solid-water partitions of radiocesium in river waters in Fukushima and Chernobyl areas. *Sci Rep* 7:12407. <https://doi.org/10.1038/s41598-017-12391-7>
181. Tessier A, Campbell PGC, Bisson M (1979) Sequential extraction procedure for the speciation of particulate trace metals. *Anal Chem* 51:844–851. <https://doi.org/10.1021/ac50043a017>
182. Kitagawa C (2015) Effect of soil organic matter on the interaction of clay minerals with cesium ion. Master thesis, Hokkaido University (in Japanese)
183. Akemoto Y, Kan M, Tanaka S (2019) Static adsorption of cesium ions on kaolin/vermiculite and dynamic adsorption/desorption using the electrokinetic process. *J Chem Eng Jpn* 52:662–669. <https://doi.org/10.1252/jcej.18we312>

184. Akemoto Y, Sakti SCW, Kan M, Tanaka S (2021) Interpretation of the interaction between cesium ion and some clay minerals based on their structural features. *Environ Sci Pollut Res* 28:14121–14130. <https://doi.org/10.1007/s11356-020-11476-7>
185. Kim G-N, Kim S, Park H-M, Kim W-S, Park U-R, Moon J-K (2013) Cs-137 and Cs-134 removal from radioactive ash using washing–electrokinetic equipment. *Ann Nucl Energy* 57: 311–317. <https://doi.org/10.1016/j.anucene.2013.02.016>
186. Kim G-N, Choi W-K, Lee K-W (2010) Decontamination of radioactive concrete using electrokinetic technology. *J Appl Electrochem* 40:1209–1216. <https://doi.org/10.1007/s10800-010-0088-8>
187. Miyamura R (2015) Study on removal of cesium ions in soil water using interfacial electrokinetic technique. Master thesis, Hokkaido University (in Japanese)
188. Shozugawa K, Hori M, Johnson TE, Takahata N, Sano Y, Kavasi N, Sahoo SK, Matsuo M (2020) Landside tritium leakage over through years from Fukushima Dai-ichi nuclear plant and relationship between countermeasures and contaminated water. *Sci Rep* 10:19925. <https://doi.org/10.1038/s41598-020-76964-9>
189. Sasaki T, Tanaka S (2011) Adsorption behavior of some aromatic compounds on hydrophobic magnetite for magnetic separation. *J Hazard Mater* 196:327–334. <https://doi.org/10.1016/j.jhazmat.2011.09.033>
190. Narita Y, Sakti SCW, Akemoto Y, Tanaka S (2019) Ultra-rapid removal of cationic organic dyes by novel single- and double-stranded DNA immobilized on quaternary ammonium magnetic chitosan. *J Environ Chem Eng* 7:103308. <https://doi.org/10.1016/j.jece.2019.103308>
191. Mihara Y, Zhang S, Syahputra R, Akemoto Y, Itoh S, Tanaka S (2020) Functionalization of shirasu-balloons surface for removal of cadmium ions from contaminated soil. *Anal Sci* 36: 553–560. <https://doi.org/10.2116/analsci.19SBP06>
192. Kimura T, Takase K, Terui N, Tanaka S (2007) Ferritization treatment of copper in soil by electrokinetic remediation. *J Hazard Mater* 143:662–667. <https://doi.org/10.1016/j.jhazmat.2007.01.010>
193. Ghaemina M, Mokhtarani N (2018) Remediation of nitrate-contaminated groundwater by PRB-electrokinetic integrated process. *J Environ Manag* 222:234–241. <https://doi.org/10.1016/j.jenvman.2018.05.078>
194. Martin L, Alizadeh V, Meegoda J (2019) Electro-osmosis treatment techniques and their effect on dewatering of soils, sediments, and sludge: a review. *Soils Found* 59:407–418. <https://doi.org/10.1016/j.sandf.2018.12.015>

Phytoremediation: Background, Principle, and Application, Plant Species Used for Phytoremediation



Md. Shariful Islam, Rubaiya Akter, Md. Mostafizur Rahman,
and Masaaki Kurasaki

Contents

1	Introduction	200
2	Principles of Phytoremediation	203
3	Factors Considering for Effective Phytoremediation Technique	207
3.1	Enrichment Factor (EF)	207
3.2	Translocation Factor (TF)	208
3.3	Bio-Concentration Factors (BCF)	208
3.4	Phytodesalination Capacity (PDC)	210
4	Applications	210
4.1	Phytoremediation of Organic Pollutants	210
4.2	Phytoremediation of Heavy Metals/Inorganic Pollutants	211
4.3	Improved Quality of Wastewater Through Phytoremediation	212
4.4	Use of Halophytes to Remediate Saline Soils	212
5	Plants Species Suitable for Phytoremediation	213
6	Advantages of Phytoremediation	213
7	Post-Harvest Management of Plants for Phytoremediation	216
8	Limitations of Phytoremediation	216
9	Conclusion	217
	References	218

M. S. Islam (✉)

Department of Agricultural Chemistry, Patuakhali Science and Technology University, Dumki,
Patuakhali, Bangladesh

e-mail: sharifacm@pstu.ac.bd

R. Akter and M. M. Rahman (✉)

Department of Environmental Sciences, Jahangirnagar University, Dhaka, Bangladesh

e-mail: rahmanmm@juniv.edu

M. Kurasaki

Faculty of Environmental Earth Sciences, Hokkaido University, Sapporo, Japan

e-mail: kura@ees.hokudai.ac.jp

Shunitz Tanaka, Masaaki Kurasaki, Masaaki Morikawa, and Yuichi Kamiya (eds.),

Design of Materials and Technologies for Environmental Remediation,

Hdb Env Chem (2023) 115: 199–224, DOI 10.1007/698_2021_831,

© The Author(s), under exclusive license to Springer Nature Singapore Pte Ltd 2022,

Published online: 8 January 2022

Abstract Environmental contamination is increasing day by day due to different natural and anthropogenic activities that lead to the soil, water, and food chain contamination. This becomes a major challenge to decontaminate the natural environment. Thus, ultimately the environmental pollutants are being taking tolls from the living being of this planet. There are a lot of potential approaches to remove pollutants from the environmental matrices including the phytoremediation. The phytoremediation is a low-risk and environmentally friendly clean-up method where plants are used to decontaminate the environment. In this chapter, efforts were given to accumulate and synthesize the published research data on phytoremediation technologies with their principles, mechanisms, and application to remove the contaminants from the soil and water environment. Phytoremediation techniques including phytoextraction, phytofiltration, rhizofiltration, phytostabilization, phytodesalination, phytodegradation, phytovolatilization, and phytomining are briefly discussed. Based on the recent literature, organic, inorganic, desalination, and wastewater treatment through phytoremediation techniques were presented with the achieved outcome. Fundamental considering factors such as enrichment factor, bioaccumulation factor, bio-concentration factor, phytodesalination capacity were also presented here. A comprehensive spectrum of potentially applicable phytoremediators was listed in this chapter which might open up the opportunity to advance further research in this particular remediation technique. Moreover, this chapter also gives an overview of the advantages and limitations of the phytoremediation techniques. In addition, post-harvest safe management of phytoremediator plants was also discussed. This chapter might be a good source of scientific evidence on phytoremediation that will be useful for the further advancement of research in this particular field.

Keywords Environmental remediation, Metals, Organic pollutants, Phytoextraction, Salinity

1 Introduction

“Phytoremediation” comes from two words: *phyto* and *remedium*. *Phyto* comes from greek prefix meaning “plant” and *remedium* comes from Latin root meaning “to correct” or “to remove an evil.” Phytoremediation simply refers to remediate or to remove contaminants from soil or water using plant species. It can also be termed as the use of plants with or without associating microbes to reduce the toxicity or the concentration of contaminants from the environments [1].

Phytoremediation is defined as “the efficient use of plants to remove, detoxify or immobilize environmental contaminants in a growth matrix (soil, water or sediments) through the natural biological, chemical or physical activities and processes of the plants” [2].

Environmental contamination

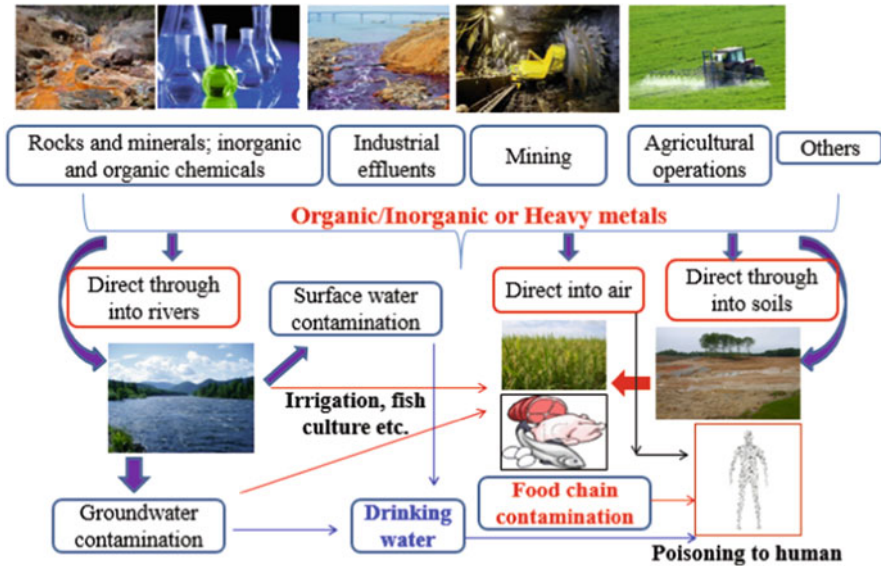


Fig. 1 Environmental contamination in soil, water, and food chain

Environmental contamination is increasing with time due to different natural and anthropogenic activities that leads to the soil, water, and food chain contamination and ultimately poisoning to the living being of this planet (Fig. 1). Different remediation technologies have been assigned to remove the contaminants from the environment like physico-chemical approaches like precipitation, membrane filtration (reverse osmosis), adsorption, ion exchange, permeable reactive barrier, etc., [3] and biological approaches like bioremediation and phytoremediation. But these physico-chemical approaches need high technological knowledge, expensive and create secondary pollutions. Microbes are used in bioremediation techniques which are difficult to harvest from contaminated sites and only can be used for removal of biodegradable pollutants.

On the other hand, phytoremediation has received much attention since 2000. It is used for the removal of organic, inorganic, radionuclides, single or multiple contaminants removal from the in-situ and ex-situ environment. It has low operational and maintenance cost. Phytoremediation has high public acceptance for esthetic and ecological restoration. It has comparatively high enhancement perception compared to other traditional physical and chemical remediation technologies. Different environmental remediation technologies are shown in Fig. 2. About 50,000 publications related to phytoremediation have been published in the last 20 years [4].

Phytoremediation is driven by solar and it is also a low-cost clean-up green technology [5]. Phytoremediation technology can reduce the cost 5% less than the alternative technology [6]. In phytoremediation technology it cost \$60,000–\$

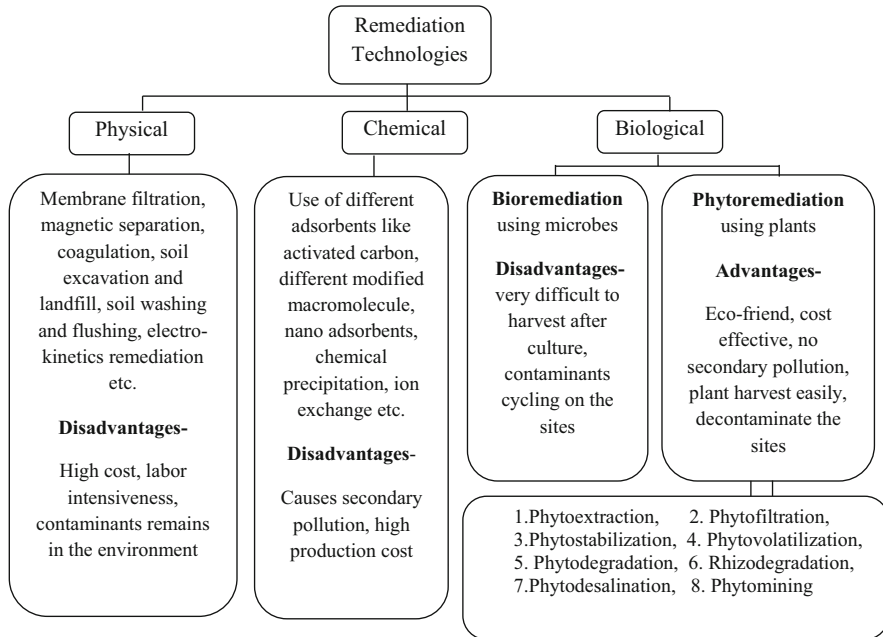


Fig. 2 Flowchart of different environmental remediation technologies

100,000, whereas other conventional methods cost \$400,000 [6]. Plants generally uptake the pollutants without affecting the soil and water environment and it ensures the quality and utility of the medium. Green plants have some special characteristics. They can uptake pollutants and neutralize toxicity by various mechanisms.

Phytoremediation is suitable for large-scale sites. In large field site other conventional methods are not suitable whereas phytoremediation is cost effective and practical [7]. From economic purpose, it can be said that the application of phytoremediation is divided into three types. They are: (1) Phytostabilization as risk contaminant; (2) Phytomining as Ni, Tl, and Au, etc., metal extraction [8]; (3) Phytoextraction as durable land management. Through phytoextraction process soil quality gradually improves. It helps soil in subsequent crop cultivation with higher market value [9]. Even, willow, jatropha, and poplar can be used as they are fast-growing and high biomass productive plants for both phytoremediation and energy production [10]. It is an alternative solution to chemicals and bulldozers and it has become popular as “Green Clean” terminology [11]. It is a sustainable technology with a good future perspective in the field of environmental pollution remediation. Phytoremediation is environment friendly and it does not disturb the natural environment.

2 Principles of Phytoremediation

The principle of phytoremediation technique is that plant roots either break the contaminant down in the soil or absorb the contaminant up, then store the contaminant in the stems and leaves of the plants. The root system provides an enormous surface area that absorbs and accumulates the water and nutrients essential for growth, as well as other non-essential contaminants. Plant roots also cause changes at the soil–root interface as they release inorganic and organic compounds (root exudates) in the rhizosphere. These root exudates affect the number and activity of the microorganisms, the aggregation and stability of the soil particles around the root, and the availability of the contaminants. Phytoremediation can be applied in the field of agricultural field for removal of contaminant and land preparation for cultivation, industrial and mining sites, commercial waste disposal sites to remove the contaminants from these sites [12]. It can be effectively carried out for remediation of heavy metals, petroleum hydrocarbons, chlorinated solvents, pesticides, radionuclides, explosives, and excess nutrients [13]. The classification of phytoremediation is given below:

- *Phytoextraction:*

Phytoextraction is also familiar as phytoabsorption, phytoaccumulation or phytosequestration. It can be defined as the use of pollutant-accumulating plants by absorbing or storing in their harvestable parts, i.e. shoots, leaves to remove metals or organic pollutants from soil or water. In phytoextraction, pollutants are translocated and accumulated in these plants part [14–16] (Fig. 3).

Metals are often translocated to shoots by phytoextraction process. It is an effective biochemical process [17, 18].

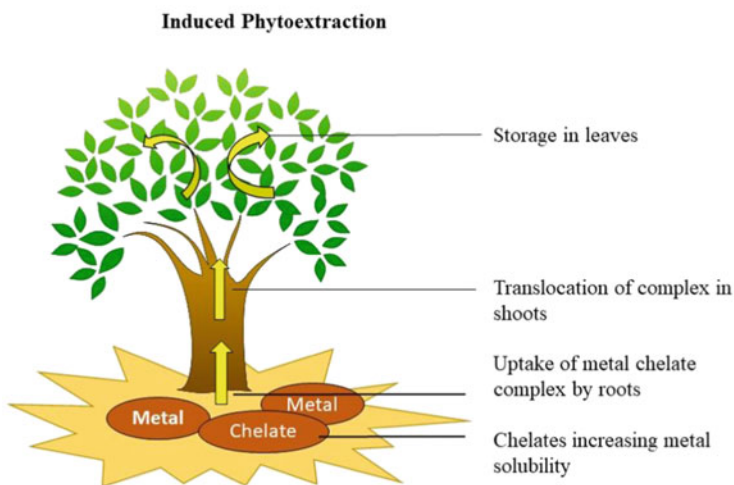


Fig. 3 The process of induced phytoextraction in the process of chelates

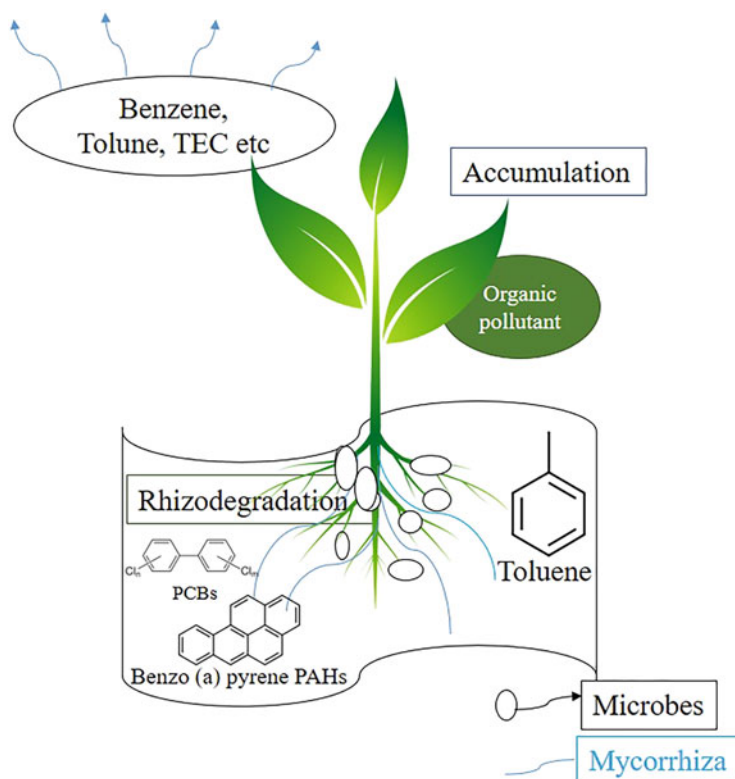


Fig. 4 Plant–microbes symbiotic relation for phytoremediation of organic pollutants

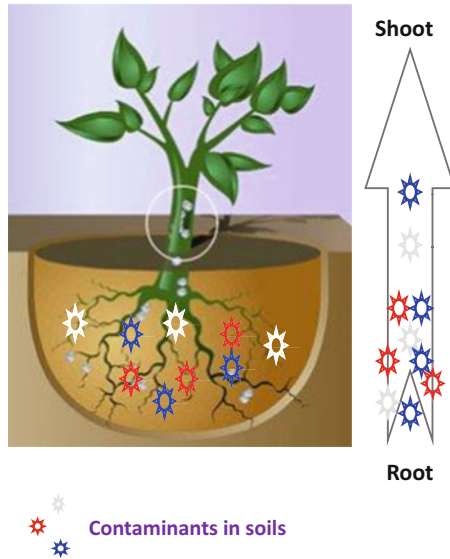
- *Phytodegradation:*

Phytodegradation is defined as the use of plants to degrade organic pollutants by plants with the help of enzymes such as oxygenase and dehalogenase. It does not depend on microorganisms in the rhizosphere [9]. In this process plants accumulate organic xenobiotics from the contaminated environments. Through this metabolic process plants detoxify the environment. For this reason, green plants are also termed as “Green Liver” for the biosphere. But it has some limitation too. It cannot remove the metals as they are nonbiodegradable. It can remove the organic pollutants only. Nowadays, genetically modified plants such as transgenic poplars are used for phytoremediation. Scientists have also shown their interest to study about synthetic insecticides and herbicides in this purpose.

- *Rhizofiltration:*

Rhizofiltration is termed as the breakdown of organic pollutants mainly metals from water and soil by plants root and microorganisms in the rhizosphere [19]. Rhizosphere refers to 1 mm around the root and is under the influence of the plant [20]. Plant–microbes symbiotic relation for phytoremediation of organic pollutants is shown in Fig. 4.

Fig. 5 Phytoremediation of soil environment



Through this process plants can accumulate about 10–100 times higher in the rhizosphere by the secretion of exudates containing carbohydrates, amino acids, flavonoids. Rhizofiltration stimulates carbon and nitrogen source to the soil. Thus, it creates a nutrient rich soil where microbial activities are stimulated. In addition, plants also release certain enzymes capable of degrading organic contaminants in soils [21].

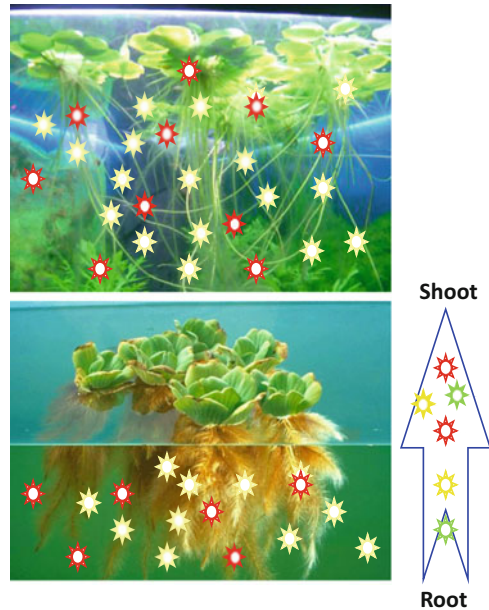
- *Phytostabilization:*

Phytostabilization is also known as phytoimmobilization. It is defined as the use of plants to stabilize the contaminant in the soil or to reduce the bioavailable pollutants from the environment [22]. Phytostabilization helps in reducing the mobility of pollutants. Thus, it prevents pollutant to enter into the food chain or migration in groundwater [23]. In rhizosphere, plants can immobilize heavy metals in soils through sorption by roots, precipitation, complexation, or metal valence reduction [24]. The toxicity varies upon the metal valences. Plants help in converting hazardous metals to relatively less toxic condition by excreting redox enzymes. It also helps in decreasing possible metal stress and damage such as Cr (VI) to Cr (III); Cr (III) is less toxic and less mobile [25]. Phytostabilization also helps in limiting the heavy metals in biota and in minimizing leaching into underground water. Phytostabilization has some limitation too. It is not a permanent solution as heavy metals remain in soil. It can limit the movement only. However, it is a management strategy to stabilize the potential toxic contaminants [9] (Fig. 5).

- *Phytovolatilization:*

Phytovolatilization refers to the use of plants to uptake pollutants by converting them to volatilize pollutant and subsequent release into the atmosphere. It is used for mainly organic pollutants. It is also used for heavy metals like Hg and

Fig. 6 Phytofiltration of water environment



Se. But, the limitation of the study is that the pollutants are removed partially from soil to the atmosphere. It can be redeposited again in the atmosphere. Phytovolatilization is termed as the most controversial of phytoremediation technologies [26].

- *Phytofiltration:*

Phytofiltration refers to the use of plants to remove pollutants from water environment such as surface water and waste water [19]. Phytofiltration may work like rhizofiltration (use of plant roots) or blastofiltration (use of seedlings) or caulofiltration (use of excised plant shoots; Latin caulis = shoot). In this process, the contaminants are absorbed or adsorbed. Thus, the contaminants are limited their movement to underground waters. The process is shown in Fig. 6.

- *Phytodesalination:*

The most emerging technique of phytoremediation is phytodesalination [27]. Phytodesalination is defined as the use of halophytic plants to remove salts and ions from salt-affected soils. By desalinating soil, it helps in supporting the normal growth of plants [28]. Studies shows that halophytic plants are comparatively better adapted with saline environment naturally compared to glycophytic plants [29]. According to the studies, two halophytes, *Suaeda maritima* could remove 504 kg and *Sesuvium portulacastrum* could remove 474 kg of sodium chloride from 1 ha of saline soil in a period of 4 months. Therefore, *S. maritima* and *S. portulacastrum* could be successfully used for not only to accumulate NaCl from highly saline soils but also for crop production after a few repeated cultivation and harvest [30]. Another study has reported accumulation of about 1 t ha^{-1} of Na^+ ions in the above-ground biomass of the

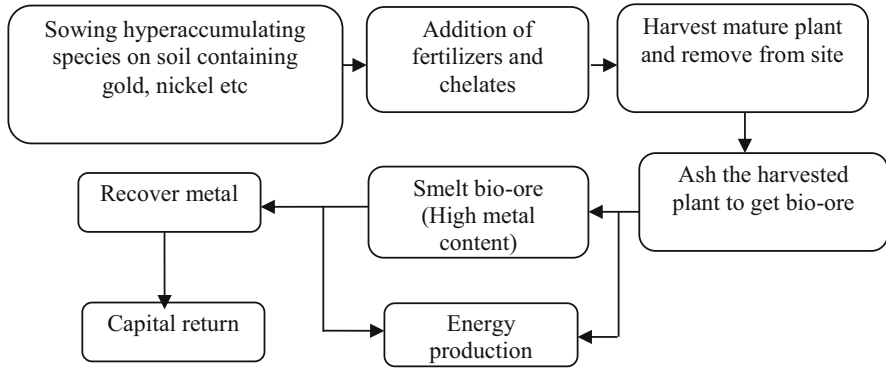


Fig. 7 Integrated process of metal recovery or phytomining (modified from Sheoran et al. [8])

obligate halophyte *S. portulacastrum* cultivated on a salinized soil. The resultant decrease in salinity and sodicity of the phytodesalinized soil significantly reduced the negative effects on the growth of the test culture of the glycophytic crop, *Hordeum vulgare* [26].

- **Phytomining:**

Phytomining has opened a new corner named “bio-ore.” Bio-ore is used to recover or extract heavy metals from the remaining ash. Energy is also got from phytomining. An advantage of phytomining is that the energy comes from the combustion of biomass can be sold [31]. The commercial use of phytomining often depends on the efficiency of phytoextraction and current market value of the processed metals. However, it has been commercially used for Ni. It is found that it is less expensive than the conventional extraction methods. Using *Alyssum murale* and *Alyssum corsicum*, one can grow biomass containing $400 \text{ kg Ni ha}^{-1}$ with production costs of $\$250\text{--}500 \text{ ha}^{-1}$. The process of phytomining is shown in Fig. 7.

Here different phytoremediation techniques available are shown Fig. 8 and summarized in Table 1.

3 Factors Considering for Effective Phytoremediation Technique

3.1 Enrichment Factor (EF)

The EF is calculated to derive the degree of contamination and heavy metal accumulation in environment and in plants growing on contaminated site with respect to substrate (soil, water, etc.) and plants growing on uncontaminated soil [33]. It can be calculated by

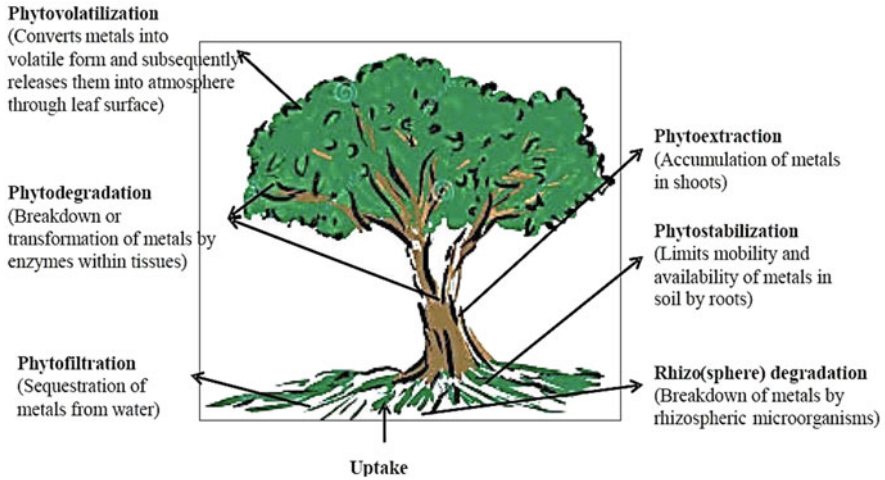


Fig. 8 Different phytoremediation techniques

$$EF = \frac{\text{Conc. of metal in substrate or plant parts at contaminated site}}{\text{Conc. of metal in substrate or plant parts at uncontaminated site}}$$

3.2 Translocation Factor (TF)

The TF or mobilization ratio is calculated to determine the relative translocation of metals from the substrate (soil, water) to the various plant components (root, stem, and leaf) [34, 35]. It can be calculated by.

$$TF = \frac{\text{Concentration of metal in plant tissue (root, stem, or leaf)}}{\text{Concentration of metal in corresponding water or root}}$$

3.3 Bio-Concentration Factors (BCF)

The BCF provides an index of the ability of the plant to accumulate the metal with respect to the metal concentration in the substrate [36]. The result of BCF can be calculated ($L\ kg^{-1}$) as follows.

Table 1 Different mechanisms of phytoremediation techniques and target contaminants (modified from Ghosh and Singh [32])

Techniques	Definition	Mechanism	Contaminants
Phytoextraction	Use plants to absorb, translocate, and store toxic contaminants from a soil matrix into their root and shoot tissue	Hyper accumulation from soil	Inorganic
Phytofiltration or Rhizofiltration	Use of roots to uptake and store contaminants from an aqueous growth matrix	Hyperaccumulation from water	Inorganic or organic
Phytostabilization	Plant-mediated immobilization or binding of contaminants into the soil matrix, thereby reducing their bioavailability	Complexation	Inorganic
Phytovolatilization	Use of a plant's ability to uptake contaminants from the growth matrix and subsequently transform and volatilize contaminants into the atmosphere	Volatilization by leaves	Inorganic or organic
Phytodegradation	Use of plants to uptake, store, and degrade contaminants within its tissue	Degradation by enzymatic reactions within plant	Organic
Phytomining	Phytoaccumulation of mining elements as bio-ore	Hyperaccumulation of mining elements as bio-ore	Inorganic
Rhizodegradation	Use of rhizospheric associations between plants and symbiotic soil microbes to degrade contaminants	Degradation in the rhizosphere by microorganisms	Organic
Phytodesalination	Accumulation of salts in shoot parts and desalination of saline soil and water	Hyper accumulation of salt from soil and water	Inorganic

Table 2 Definition of BCF

BCF values	Class
<1	Excluder
>1	Accumulator
≥1,000	Hyperaccumulator

$$\text{BCF} = \frac{\text{Concentration of metal in the plant parts (root, stem, or leaf) (mg kg}^{-1}\text{)}}{\text{Concentration of metal in the substrate water (mg L}^{-1}\text{)}}$$

Depending on the BCF values, plants can be classified as follows [37] (Table 2).

The following concentration criteria for different metals and metalloids in dried foliage with plants growing in their natural habitats: 100 mg kg⁻¹ for Cd, Se and Tl; 300 mg kg⁻¹ for Co, Cu and Cr; 1,000 mg kg⁻¹ for Ni, Pb and As; 3,000 mg kg⁻¹ for Zn; 10,000 mg kg⁻¹ for Mn. Generally, hyperaccumulators achieve 100-fold

higher shoot metal concentration (without yield reduction) compared to crop plants or common nonaccumulator plants.

3.4 *Phytodesalination Capacity (PDC)*

PDC from hydroponic experiment can be estimated by measuring pot surface area, total biomass per pot, Na ion concentration in plants, and plant productivity (plant dry weight per hectare), by using the following formula as described by Islam et al. [38].

$$\text{PDC} = \text{Productivity} \times \text{Na ion concentration}$$

Results of PDC are expressed as kg per hectare wetland or pond or any confined water body or soil.

4 Applications

4.1 *Phytoremediation of Organic Pollutants*

Phytoremediation of organic pollutants has some limitations too. Plants cannot degrade these volatile compounds fully within plant system and often organic pollutants are found in heterogeneous streams mixed with other chemicals and distributed in a highly non-uniform manner. Naturally, microorganisms can rapidly degrade the lower concentration of organic pollutants in the environment. Zayed et al. [37] reported that plant can uptake pentachlorophenol at concentration above 10 mg kg^{-1} due to soil microorganism degraded them at lower concentration. Organic xenobiotics with a $\log K_{ow}$ (octanol/water partition coefficient) <1 are considered to be very water-soluble, and plant roots do not generally accumulate them at a rate surpassing passive influx into the transpiration stream [39]. Contaminants with a $\log K_{ow} > 3.5$ show high sorption to the roots, but slow or no translocation to the stems and leaves. However, plants readily take up organic xenobiotics with a $\log K_{ow}$ between 0.5 and 3.5, as well as weak electrolytes (weak acids and bases or amphoteres as herbicides). These compounds seem to enter the xylem faster than the soil, and rhizosphere micro flora can degrade them, even if the soil is enriched with degrading bacteria [40]. Once taken up, plants metabolize these contaminants, although some of them, or their metabolites, such as trichloroethene, which is transformed into trichloro acetic acid, can be toxic. Alternatively, plants preferentially release volatile pollutants, such as benzene, toluene, ethylbenzene and xylene compounds and trichloroethene and their metabolites, into the environment by evaporation via the leaves, which calls into question the merits of phytoremediation [41]. Some enhanced engineered phytoremediation

technologies were used by some researchers to mitigate these toxic evaporated organic pollutants. Ma et al. [42] examined that the endophytic bacteria equipped with the appropriate degradation pathway increased *in planta* degradation of toluene. After surface-sterilized lupine seeds were successfully inoculated with the recombinant strain, the engineered endophytic bacteria strongly degraded toluene, resulting in a marked decrease in its phytotoxicity, and a 50–70% reduction of its evapotranspiration through the leaves. Thus, it is difficult to remediate organic pollutants using plant itself only, without cooperation of microorganisms.

4.2 Phytoremediation of Heavy Metals/Inorganic Pollutants

Phytoremediation technology is widely used as the removal of metals or inorganic pollutants. Worldwide metal pollution has been recognized as serious environmental pollution. Industrialization has also created disturbance in natural biogeochemical cycle. Various extraction process and different industrial activity have released Cd, As, Pb, Hg, Cr, Ni, Cu, Zn, and so on, into the environment [43]. Heavy metals are non-degradable, and accumulate in food chain. Further, most of them are toxic and carcinogenic for human. Nowadays, heavy metal recovery or treatment is of great concern because of their recalcitrant and persistent characteristics [44]. Phytoremediation technology is a successful technology for heavy metal remediation. Here, plant acts like hyperaccumulator. One of the hyperaccumulators is *Thlaspi caerulescens* accumulated up to 26,000 mg kg⁻¹ Zn, without showing injury; and up to 22% of soil exchangeable Cd from contaminated site [45]. Another one is *Brassica juncea*, commonly called as Indian mustard, has been found to be a good ability to transport lead from the roots to the shoots. Some calculations indicate that *Brassica juncea* is capable of removing 1,550 kg of lead per acre [46]. On a worldwide basis, plant species having more than 1,000 mg kg⁻¹ metal removing ability are known more than 320 plant species for Ni, 30 plant species for Co, 34 plant species for Cu, 20 plant species for Se, 14 plant species for Pb, and one plant species for Cd. The species involved in hyper accumulation have been tabulated [47]. Metal removing ability exceeding 10,000 mg kg⁻¹ has been recorded 11 plant species for Zn and ten plant species for Mn [47]. *Pteris vittata* has been shown to accumulate as much as 14,500 mg As kg⁻¹ fronds from soil without showing toxicity symptoms [48]. *Micranthemum umbrosum* can absorb 1,220 mg As kg⁻¹ and 800 mg Cd kg⁻¹ from a contaminated water environment [47, 49]. Nowadays, scientists are trying to find more suitable plants or develop genetically engineered plants for effective phytoremediation of inorganic pollutants from the environment.

Plant uptake inorganic pollutants like heavy metals from solution through their roots and in submerged condition, whole plant body acted as an active site for absorption [3]. After entry into roots, heavy metal ions or sodium ion (in case of phytodesalination) can either be stored in the roots or translocated to the shoots primarily through xylem vessels [6, 50] where they are mostly deposited in vacuoles [38]. Heavy metal sequestration in the vacuole is one of the ways to remove excess

metal ions from the cytosol, and may reduce their interactions with cellular metabolic processes [8, 51]. The entire mechanism of phytoextraction/phytofiltration of heavy metals has five basic aspects: mobilization of the heavy metals in soil and water, uptake of the metal ions by plant roots, translocation of the accumulated metals from roots to aerial tissues, sequestration of the metal ions in plant tissues, and metal tolerance. Mechanisms governing heavy metal tolerance in plant cells are cell wall binding, active transport of ions into the vacuole, chelation through the induction of metal-binding peptides, and the formation of metal complexes [52, 53]. The most important peptides/proteins involved in metal accumulation and tolerance are phytochelatins (PCs) and metallothioneins (MTs). Plant PCs and MTs are rich in cysteine sulfhydryl groups, which bind and sequester heavy metals in very stable complexes [49, 54]. PCs are small glutathione (GSH)-derived, enzymatically synthesized peptides, which bind metals and are principal part of the metal detoxification system in plants [55–58].

4.3 Improved Quality of Wastewater Through Phytoremediation

Wastewater contains large amount of different pollutants that have serious environmental and health hazard implications on humans, animals, plants, and microorganisms in the environment and this usually leads to great environmental challenges [59]. The reuse of treated wastewater in aquaculture/agriculture practices is encouraged to minimize demand on freshwater resources. Many researchers have applied various macrophytes such as water hyacinth (*Eichhornia crassipes*), water lettuce (*Pistia stratiotes L.*), water spinach (*Ipomoea aquatica*), duckweed (*Lemna spp.*), vetiver grass (*Chrysopogon zizanioides*), common reed (*Phragmites australis*), etc. and microalgae including *Chlorella vulgaris* for phytoremediation of different types of waste water to achieve better quality water for agricultural and domestic purposes. The most important factor in the implementation of phytoremediation of contaminated water is the selection of appropriate plant that has a high uptake of nutrients and great capacity of pollutants removal and grows well in polluted water [60].

4.4 Use of Halophytes to Remediate Saline Soils

It was postulated that 6% (more than 800 million ha) of the world lands are affected by salinity, which is mainly due to natural causes (salt accumulation over long periods of time in arid and semi-arid regions) or to secondary salinity that affected in 2008 already 2% (32 million ha) of the dryland-farmed areas and 20% (45 million ha) of the irrigated lands in the world [61]. Soil phytodesalination is based on the capacity of some halophytes to accumulate enormous sodium quantities in their

shoots [38]. Preconditions for an applicable candidate for soil desalination are at least a high salt resistance, a high biomass production, a considerable shoot sodium content, and a high degree of economic utilization (such as fodder, fuel, fiber, essential oil, and oil seeds). Shoot-succulent halophytes meet these requirements since they are able to accumulate enormous Na^+ quantities within their above-ground organs. Such as, *S. portulacastrum* is a promising halophyte for phytodesalination programs. *S. portulacastrum* is a cold-sensitive species. The duration of phytodesalination process depends on soil salinity and sodicity. Zhao and Abdelhafez [62, 63] demonstrated that some halophytes (such as *Suaeda salsa*, *Suaeda fruticosa*, *Arthrocnemum indicum*, *Halocnemum strobilaceum*) can remove enormous sodium quantities from soil and accumulate them in their shoots. Ravindran et al. [64] evaluated also in six halophytes (*Suaeda maritima* Dum., *Sesuvium portulacastrum* L., *Clerodendrum inerme* Gaertn., *Ipomoea pes-caprae* Sweet., *Heliotropium curassavicum* L., and *Excoecaria agallocha* L. (a tree) the ability to reduce salinity in the upper 40 cm of soil. A similar evaluation based on soil and halophyte analyses was performed in the three perennial species: *Tecticornia indica* (or *Arthrocnemum indicum*), *Suaeda fruticosa*, and *Sesuvium portulacastrum*. Islam et al. [38] conducted a hydroponic experiment growing *Ipomoea aquatica*, *Alternanthera philoxeroides*, and *Ludwigia adscendens* at 0–7 dS m^{-1} salinity level and found that *I. aquatic* has high phytodesalination capacity (130 kg Na^+ ha^{-1}). They also revealed that spongy mesophyll cells along with sub-stomatal cells in leaf and xylem vessels along with vacuolar sequestration might be responsible for Na accumulation in the stem of these halophytes. Phytodesalination is an emerging technique used to cope with salinity/sodicity problems in arid and semi-arid regions. However, its application requires an optimization, including the choice of the convenient halophyte and the season of its culture. However, plant desalination cannot be adapted to extremely high sodium soil. Plants used for phytodesalination purposes can have several post-harvests uses (fodder, biofuel production, oil extraction, essential oil extraction, medicinal use) and can thus have two simultaneous beneficial utilizations.

5 Plants Species Suitable for Phytoremediation

Suitable plant species for phytoremediation are listed in Table 3.

6 Advantages of Phytoremediation

Phytoremediation has been identified as an emerging, low-cost, and eco-sustainable solution for heavy metal pollution prevention and control. It is the most suitable alternative technology to conventional physico-chemical remediation technologies, which are highly expensive and technically more suited to small areas, create

Table 3 Good candidates for phytoremediation

Plant	Contaminated areas	Pollutants	Reference
<i>Pteris vittata</i>	Soil	Arsenic	[64, 65]
<i>Epilobium dodonaei</i> Vill	Mining waste	Arsenic	[66]
<i>Wurmstorfia fluitans</i>	Water	Arsenic	[67]
<i>Puccinellia frigida</i>	Soil	Boron	[68]
<i>Ricinus communis</i>	Soil	Cadmium	[64, 65]
<i>Iris sibirica</i>	Wetland	Cadmium	[48]
<i>Ipomoea aquatica</i> , <i>Alternanthera philoxeroides</i> , <i>Ludwigia adscendens</i>	Water	Sodium	[38]
<i>Micranthemum umbrosum</i>	Water	Arsenic, Cadmium	[49]
<i>Sesuvium portulacastrum</i>	Soil	Sodium	[69]
<i>Helianthus annuus</i>	Soil	Chromium	[70]
<i>Rose plant</i>	Soil	Chromium	[71]
<i>Phalaris arundinacea</i>	Water	Chromium	[72]
<i>Pennisetum annuus</i>	Soil	Cobalt	[73]
<i>Brachiaria decumbens</i>	Soil	Copper	[74]
<i>Vossia cuspidata</i>	Water	Copper	[75, 76]
<i>Pistia stratiotes</i>	Wetland	Copper	[75, 76]
<i>Pisum sativum</i>	Soil	Lead	[77]
<i>Hordeum vulgare</i>	Soil	Lead	[78]
<i>Noccaea caerulea</i>	Hydroponic condition	Lead	[79]
<i>Brassica napus</i>	Soil	Zinc	[80]
<i>Epilobium dodonaei</i> Vill	Mining waste	Zinc	[66]
<i>Pistia stratiotes</i>	Wetland	Zinc	[75, 76]
<i>Cyperus alternifolius</i>	Wetland	Zinc	[64, 65]
<i>Noccaea caerulea</i>	Hydroponics	Zinc	[79]
<i>Phytolacca americana</i>	Hydroponics medium	Manganese	[81]
<i>Jatropha curcas</i>	Soil	Mercury	[82]
<i>Brassica juncea</i>	Soil	Mercury	[83]
<i>Phragmites australis</i>	Sediments	Mercury	[84]
<i>Limnocharis flava</i>	Water	Mercury	[82]
<i>Salix matsudana</i>	Hydroponics medium	Mercury	[85]
<i>Brassica juncea</i>	Soil	Nickel	[86]
<i>Typha domingensis</i>	Sediments	Nickel	[65]
<i>Tagetes erecta</i>	Water	Nickel	[87]
<i>Stanleya pinnata</i>	Soil	Selenium	[88]
<i>Brassica sp. (wild type)</i>	Soil	Selenium	[88]
<i>Lactuca sativa</i>	Water	Selenium	[89]
<i>Allium schoenoprasum</i> L. (Chive)	Soil	Ni, Co, Cd	[90]

(continued)

Table 3 (continued)

Plant	Contaminated areas	Pollutants	Reference
<i>Brassica juncea</i> L. (Indian mustard)	Soil and water	Cd, Cu, Zn, Pb	[91–95]
<i>Brassica napus</i> L. (canola)	Soil	Cd, Cu, Zn, Pb	[93, 96, 97]
<i>Cajanus Cajan</i> (L.) Milsp. (pigeon pea)	Soil	As, Cd	[98]
<i>Cicer aeritimum</i> L. (chickpea)	Soil	Cd, Pb, Cr, Cu	[99–101]
<i>Cucumis sativus</i> L. (cucumber)	Water	Pb	[92]
<i>Eichhornia crassipes</i> L. (water hyacinth)	Water	As, Cr, Zn, Cs, Co	[102–104]
<i>Jatropha curcas</i> L. (purging nut, physic nut)	Soil	Fe, Al, Cu, Mn, Cr, As	[20, 105, 106]
<i>Lantana camara</i> L. (lantana)	Soil	Zn, Hg, Pb	[107]
<i>Lens culinaris</i> Medic. (lentil)	Soil	Pb	[108]
<i>Lepidium sativum</i> L. (cress)	Soil	As, Cd, Fe, Pb, Hg	[109, 110]
<i>Lactuca sativa</i> L. (lettuce)	Soil	Cu, Fe, Mn, Zn, Ni, Cd	[109–111]
<i>Medicago sativa</i> L. (alfalfa)	Soil	Pb, Co, As, Cd	[112]
<i>Oryza sativa</i> L. (rice)	Soil	Cu, Cd	[113]
<i>Pistia stratiotes</i> L. (water lettuce)	Water	Cr, Cd, As	[114–116]
<i>Pisum sativum</i> L. (pea)	Soil	Pb, Cu, Zn, Fe, Cd, Ni	[98, 117–120]
<i>Raparus sativus</i> L. (radish)	Soil	As, Cr, As, Cd, Fe, Pb, Cu	[109, 121]
<i>Spinacia oleracea</i> L. (spinach)	Soil	Cd, Cu, Fe, Ni, Pb, Zn,	[122–126]
<i>Solanum nigrum</i> L. (black)	Soil	Cr, Cd	[127–129]
<i>Sorghum bicolor</i> L. (sorghum)	Soil	Cd, Cu, Zn, Fe	[130]
<i>Zea mays</i> L. (corn)	Soil	Cd, Pb, Zn, Cu	[126, 131]
<i>Salix Populus</i>	Soil, water	Heavy metals	[132]
<i>Brassica napus</i> , <i>B. juncea</i> , <i>B. nigra</i>	Soil, water, groundwater	Ni	[133]
<i>Cannabis sativa</i>	Soil	Radionuclides, heavy metals, Se	[134]
<i>Helianthus</i>	Soil	Radionuclides, Cd	[135]
<i>Typha</i> sp.	Soil	Pb, Cd	[136]
<i>Brassica juncea</i>	Mine wastewater	Mn, Cu, Se	[131]
<i>Glyceria fluitans</i>		Heavy metals	[137]
<i>Lemna minor</i>	Mine tailings-wetland	Heavy metals	[138]

secondary pollution and deteriorate soil fertility, and thus adversely affect agroecosystem [139]. It is an eco-friendly, non-intrusive, and esthetically pleasing remediation technology that removes metal pollutants from the contaminated sites [140, 141]. Phytoremediation technology is applicable to a broad range of contaminants, including metals and radionuclides, as well as organic compounds like

chlorinated solvents, polychloribiphenyls, polycyclic aromatic hydrocarbons, pesticides/insecticides, explosives, and surfactants.

7 Post-Harvest Management of Plants for Phytoremediation

Some possible ways to handle the plant used for phytoremediation, such as

1. Carbonization and incineration,
2. Hydrolysis and fermentation,
3. Briquetting,
4. Production of biogas, and
5. Bio-recovery or disposed as hazardous waste.

Figure 9 shows the possible way of post-harvest treatment of phytoremediator plants:

8 Limitations of Phytoremediation

Phytoremediation is highly promising technique for remediation of soil and water. But it has some limitation too. The limitation of phytoremediation is given below:

- Phytoremediation takes long time for clean-up.
- The efficiency of phytoremediation for most of the metal is usually inhibited by their low biomass and slow growth rate.
- It is difficult to mobilize more tightly bound fraction of metal ion from soil. Example: limitation of bioavailable contaminant in soil.
- Phytoremediation is applicable for low to moderate level metal contamination as in highly polluted areas plant growth does not sustain.
- If it is not possible to take proper care and mismanagement, food chain may fall in risk of contamination.

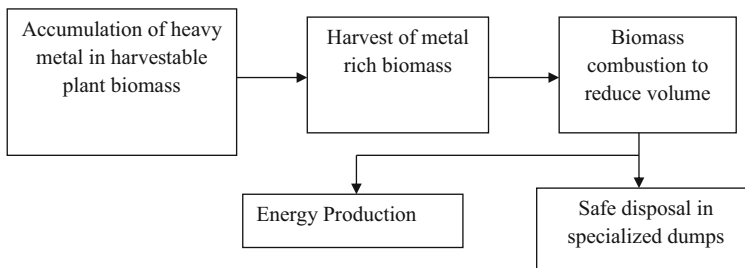


Fig. 9 Post-harvest treatment of phytoremediator plants

9 Conclusion

Phytoremediation is an alternative green remediation technology of conventional energy based costly cleaning methods that can be applied in contaminated sites without disturbing the natural environment and very less or no secondary pollution. In some cases, especially soil and water environment become improved after phytoremediation. From the above review, it is concluded that several naturally grown plants have already been identified as hyperaccumulators for the reclamation of specific toxic soil and water environment due to their high biomass, high bio-concentration factors, and translocation factors from soil to root and root to harvestable shoot with their mechanisms. There are some plants that are used for phytoremediation of water environment, their whole-body act as active sites for absorption of contaminants. Every technology has some advantages and disadvantages. Phytoremediation technology is not exception of that. Though there are some disadvantages like time consuming and post-harvest management but have more advantages than traditional methods like esthetic, conserve natural environment, act as CO₂ sinkers, O₂ producers, increases soil fertility and productivity, very less or no secondary pollution, etc. Integrated approaches along with traditional and phytoremediation can be enhancing the decontamination of the contaminated sites within short time. Researchers should focus more to develop some transgenic varieties for phytoremediation of contaminated sites.

Recommendations

Phytoremediation is a solar-driven natural technology that can be applied “in-situ” and “ex-situ” to remediate contaminated soil and water sites. Phytoremediation also possesses environmental and socioeconomic merits over other physical and chemical clean-up methods. However, some recommendation is given below for future works.

1. As phytoremediation is an interdisciplinary approach, researchers and scientists from different background are encouraged to apply their knowledge in this field.
2. Hyperaccumulation of various types of contaminant in existing plant kingdom should be explored to find more effective contaminant accumulators.
3. For phytoremediation in the field, extensive and reliable risk assessment studies should be conducted before applying any transgenic plants.
4. Unbiased and honest cost benefit analysis studies should be conducted in the field for the green technology named phytoremediation.
5. To understand the interaction among contaminant, soil, microbes, and plants, more studies should be conducted.
6. To improve understanding about the fate of metal ions in plant tissues, metal hyperaccumulation and tolerance of contaminant in plants, advancement in spectroscopic and chromatographic techniques should be exploited.
7. International forum like IUPAC should be developed for arranging meetings, seminars to discuss and promote phytoremediation technology. It can be helpful for searching solutions and challenges faced by the technology.

References

1. Greipsson S (2011) Phytoremediation. *Nat Educ Knowl* 3(10):7
2. United States Protection Agency (USEPA) (2000) Introduction to phytoremediation. EPA 600/R-99/107. U.S. Environmental Protection Agency, Office of Research and Development, Cincinnati
3. Rahman MA, Hasegawa H (2011) Review on aquatic arsenic: phytoremediation using floating macrophytes. *Chemosphere* 83:633–646
4. Google Scholar (2020) <https://scholar.google.com/>
5. Van Aken O, Zhang B, Carrie C, Uggalla V, Paynter E, Giraud E, Whelan J (2009) Defining the mitochondrial stress response in *Arabidopsis thaliana*. *Mol Plant* 2(6):1310–1324. <https://doi.org/10.1093/mp/ssp053>
6. Prasad MNV (2004) Phytoremediation of metals in the environment for sustainable development. *Proc Indian Natl Sci Acad Part B* 70:71–98
7. Garbisu C, Alkorta I (2003) Review basic concepts on heavy metal soil bioremediation. *Eur J Miner Process Environ Prot* 3(1):58–66
8. Sheoran V, Sheoran A, Poonia P (2011) Role of hyperaccumulators in phytoextraction of metals from contaminated mining sites: a review. *Crit Rev Environ Sci Technol* 41:168–214
9. Vangronsveld J, Herzig R, Weyens N, Boulet J, Adriaensen K, Ruttens A, Thewys T, Vassilev A, Meers E, Nehnevajova E, Van der Lelie D, Mench M (2009) Phytoremediation of contaminated soils and groundwater: lessons from the field. *Environ Sci Pollut Res* 16:765–794
10. Abhilash MR, Srikantaswamy S, Shiva Kumar D, Jagadish K, Shruthi L (2016) Phytoremediation of heavy metal industrial contaminated soil by *Spinacia oleracea* L. and *Zea mays* L. *Int J Appl Science* 4(1):192–199
11. Pilon-Smits E (2005) Phytoremediation. *Annu Rev Plant Biol* 56:15–39
12. Adams N, Carroll D, Madalinski K, Rock S (2000) Introduction to phytoremediation. United States Environmental Protection Agency, Office of Research and Development, Washington
13. McCutcheon SC, Schnoor JL (2002) Phytoremediation: transformation and control of contaminant. Hoboken, NJ, Wiley
14. Sekara A, Poniedzialek M, Ciura J, Jedrszczyk E (2005) Cadmium and lead accumulation and distribution in the organs of nine crops: implications for phytoremediation. *Pol J Environ Stud* 14:509–516
15. Yoon J, Cao X, Zhou Q, Ma LQ (2006) Accumulation of Pb, Cu, and Zn in native plants growing on a contaminated Florida site. *Sci Total Environ* 368:456–464
16. Rafati M, Khorasani N, Moattar F, Shirvany A, Moraghebi F, Hosseinzadeh S (2011) Phytoremediation potential of *Populus alba* and *Morus alba* for cadmium, chromium and nickel absorption from polluted soil. *Int J Environ Res* 5:961–970
17. Zacchini M, Pietrini F, Mugnozza GS, Iori V, Pietrosanti L, Massacci A (2009) Metal tolerance, accumulation and translocation in poplar and willow clones treated with cadmium in hydroponics. *Water Air Soil Pollut* 197:23–34
18. Tangahu BV, Abdullah SRS, Basri H, Idris M, Anuar N, Mukhlisin M (2011) A review on heavy metals (As, Pb, and Hg) uptake by plants through phytoremediation. *Int J Chem Eng* 2011:939161
19. Kuiper I, Lagendijk EL, Bloemberg GV, Lugtenberg BJJ (2004) Rhizoremediation: a beneficial plant-microbe interaction. *Mol Plant-Microbe Interact* 17:6–15
20. Yadav SK, Juwarkar AS, Kumar P, Thawale PR, Singh SK, Chakrabarti T (2009) Bioaccumulation and phyto-translocation of arsenic, chromium, and zinc by *Jatropha curcas* L.: impact of diary sludge and biofertilizer. *Bioresour Technol* 100:4616–4622
21. Singh S (2012) Phytoremediation: a sustainable alternative for environmental challenges. *Int J Green Herb Chem* 1:133–139
22. Erakhrumen AA (2007) Phytoremediation: an environmentally sound technology for pollution prevention, control and remediation in developing countries. *Educ Res Rev* 2:151–156

23. Wuana RA, Okieimen FE (2011) Heavy metals in contaminated soils: a review of sources, chemistry, risks and best available strategies for remediation. *ISRN Ecol* 2011:1–20
24. Wu G, Kang H, Zhang X, Shao H, Chu L, Ruan C (2010) A critical review on the bio-removal of hazardous heavy metals from contaminated soils: issues, progress, eco-environmental concerns and opportunities. *J Hazard Mater* 174:1–8
25. Padmavathiamma PK, Li LY (2007) Phytoremediation technology: hyperaccumulation metals in plants. *Water Air Soil Pollut* 184:105–126
26. Wang H-L, Tian C-Y, Jiang L, Wang L (2014) Remediation of heavy metals contaminated saline soils: a halophyte choice? *Environ Sci Technol* 48:21–22
27. Saxena G, Chandra R, Bharagava RN (2016) Environmental pollution, toxicity profile and treatment approaches for tannery wastewater and its chemical pollutants. *Rev Environ Contam Toxicol* 240:31–69
28. Sakai Y, Ma Y, Xu C, Wu H, Zhu W, Yang J (2012) Phytodesalination of a salt affected soil with four halophytes in China. *J Arid Land Stud* 22:17–20
29. Manousaki E, Kalogerakis N (2011) Halophytes present new opportunities in phytoremediation of heavy metals and saline soils. *Ind Eng Chem Res* 50:656–660
30. Ravindran KC, Venkatesan K, Balakrishnan V, Chellappan KP, Balasubramanian T (2007) Restoration of saline land by halophytes for Indian soils. *Soil Biol Biochem* 39:2661–2664
31. Anderson TA, Guthrie EA, Walton BT (1993) Bioremediation in the rhizosphere. *Environ Sci Technol* 27:2630–2636
32. Ghosh M, Singh SP (2005) A review on phytoremediation of heavy metals and utilization of its byproducts. *Appl Ecol Environ Res* 3:1–18. https://doi.org/10.15666/aecer/0301_001018
33. Kisku GC, Barman SC, Bhargava SK (2000) Contamination of soil and plants with potentially toxic elements irrigated with mixed industrial effluent and its impact on the environment. *Water Air Soil Pollut* 120:121–137
34. Barman SC, Sahu RK, Bhargava SK, Chatterjee C (2000) Distribution of heavy metals in wheat, mustard and weed grains irrigated with industrial effluents. *Bull Environ Contam Toxicol* 64(4):489–496
35. Gupta S, Nayek S, Saha RN, Satpati S (2008) Assessment of heavy metal accumulation in macrophyte, agricultural soil and crop plants adjacent to discharge zone of sponge iron factory. *Environ Earth Sci* 55(4):731–739
36. Snyder KVW (2006) Removal of arsenic from drinking water by water hyacinths (*Eichhornia crassipes*). *Water Cond Purif Int Mag* 1:41–58
37. Zayed A, Gowthaman S, Terry N (1998) Phytoaccumulation of trace elements by wetland plants: duckweed. *J Environ Qual* 27(3):715–721
38. Islam MS, Hosen MML, Uddin MN (2019) Phytodesalination of saline water by using *Ipomoea aquatica*, *Alternanthera philoxeroides* and *Ludwigia adscendens*. *Int J Environ Sci Technol* 16(2):965–972
39. Abou-Shanab RAI (2011) Bioremediation: new approaches and trends. In: Khan MS et al (eds) *Bio management of metal-contaminated soils, environmental pollution*. Springer, New York, pp 65–94
40. Cunningham SD, Ow DW (1996) Promises and prospects of phytoremediation. *Plant Physiol* 110(3):715–719
41. Tang GY, Wei LQ, Liu ZJ, Bi YP, Shan L (2012) Ectopic expression of peanut acyl carrier protein in tobacco alters fatty acid composition in the leaf and resistance to cold stress. *Biol Plant* 56:493–501
42. Ma Y, Prasad MNV, Rajkumar M, Freitas H (2011) Plant growth promoting rhizobacteria and endophytes accelerate phytoremediation of metalliferous soils. *Biotechnol Adv* 29:248–258
43. Ali H, Khan E, Sajad MA (2013) Phytoremediation of heavy metals-concepts and applications. *Chemosphere* 91:869–881
44. Fu C, Zhang JX, Liu XX, Yang WW, Yu HB, Liu J (2015) AtFes1A is essential for highly efficient molecular chaperone function in *Arabidopsis*. *J Plant Biol* 58:366–373

45. George GT, Gabriel JJ (2017) Phytoremediation of heavy metals from municipal wastewater by *Salvinia molesta* Mitchell. *Haya Saudi J Life Sci Sch* 2(3):108–115. <https://doi.org/10.21276/haya>
46. Haque N, Peralta-Videa JR, Jones GL, Gill TE, Gardea-Torresdey JL (2008) Screening the phytoremediation potential of desert broom *Baccharis sarothroides* gray growing on mine tailings in Arizona, USA. *Environ Pollut* 153:362–368
47. Reeves RD (2003) Tropical hyperaccumulators of metals and their potential for phytoextraction. *Plant Soil* 249:57–65
48. Ma N, Wang W, Gao J, Chend J (2017) Removal of cadmium in subsurface vertical flow constructed wetlands planted with *Iris sibirica* in the low-temperature season. *Ecol Eng* 109:48–56
49. Islam MS, Saito T, Kurasaki M (2015) Phytofiltration of arsenic and cadmium using *Micranthemum umbrosum*: Phytotoxicity, uptake kinetics and mechanism. *Ecotoxicol Environ Saf* 112:193–200
50. Jabeen R, Ahmad A, Iqbal M (2009) Phytoremediation of heavy metals: physiological and molecular mechanisms. *Bot Rev* 75:339–364
51. Assuncao AGL, Schat H, Aarts MGM (2003) *Thlaspi caerulescens*, an attractive model species to study heavy metal hyperaccumulation in plants. *New Phytol* 159:351–360
52. Mejare M, Bulow L (2001) Metal-binding proteins and peptides in bioremediation and phytoremediation of heavy metals. *Trends Biotechnol* 19:67–73
53. Memon AR, Schroder P (2009) Implications of metal accumulation mechanisms to phytoremediation. *Environ Sci Pollut Res* 16:162–175
54. Karenlampi S, Schat H, Vangronsveld J, Verkleij J, van der Lelie D, Mergeay M, Tervahauta A (2000) Genetic engineering in the improvement of plants for phytoremediation of metal polluted soils. *Environ Pollut* 107:225–231
55. Clemens S (2001) Developing tools for phytoremediation: towards a molecular understanding of plant metal tolerance and accumulation. *Int J Occup Med Environ Health* 14:235–239
56. Cobbett C, Goldsbrough P (2002) Phytochelatins and metallothioneins: roles in heavy metal detoxification and homeostasis. *Annu Rev Plant Biol* 53:159–182
57. Yurekli F, Kucukbay Z (2003) Synthesis of phytochelatins in *Helianthus annuus* is enhanced by cadmium nitrate. *Acta Bot Croat* 62:21–25
58. Fulekar M, Singh A, Bhaduri AM (2009) Genetic engineering strategies for enhancing phytoremediation of heavy metals. *Afr J Biotechnol* 8:529–535
59. Hanks NA, Caruso JA, Zhang P (2015) Assessing *Pistia stratiotes* for phytoremediation of silver nanoparticles and Ag(I) contaminated waters. *J Environ Manag* 164:41–45. <https://doi.org/10.1016/j.jenvman.2015.08.026>
60. Gonçalves AL, Pires JC, Simões M (2017) A review on the use of microalgal consortia for wastewater treatment. *Algal Res* 24:403–415
61. Sutton DL, Ornes WH (1975) Phosphorus removal from static sewage effluent using duckweed. *J Environ Qual* 4(3):367–370. <https://doi.org/10.2134/jeq1975.00472425000400030018x>
62. Zhao FJ, Jiang RF, Dunham SJ, McGrath SP (2006) Cadmium uptake, translocation and tolerance in the hyperaccumulator *Arabidopsis halleri*. *New Phytol* 172:646–654
63. Abdelhafez AA, Li J (2014) Geochemical and statistical evaluation of heavy metal status in the region around Jinxi River, China. *Soil Sediment Contam* 23:850–868
64. Yang J, Yang J, Huang J (2017) Role of co-planting and chitosan in phytoextraction of As and heavy metals by *Pteris vittata* and castor bean – a field case. *Ecol Eng* 109:35–40
65. Yang J, Zheng G, Yang J, Wan X, Song B, Cai W, Guo J (2017) Phytoaccumulation of heavy metals (Pb, Zn, and Cd) by 10 wetland plant species under different hydrological regimes. *Ecol Eng* 107:56–64
66. Randelovic D, Gajic G, Mutic J, Pavlovic P, Mihailovic N, Jovanovic S (2016) Ecological potential of *Epilobium dodonaei* Vill. for restoration of metalliferous mine wastes. *Ecol Eng* 95:800–810

67. Sandhi A, Landberg T, Greger M (2017) Phytofiltration of arsenic by aquatic moss (*Warnstorfia fluitans*). *Environ Pollut* 237:1098–1105
68. Rámila CDP, Contreras SA, Domenico CD, Montenegro MAM, Vega A, Handford M, Bonilla CA, Pizarro GE (2016) Boron stress response and accumulation potential of the extremely tolerant species *Puccinellia frigid*. *J Hazard Mater* 317:476–484
69. Rabhi M, Ferchichi S, Jouini J, Hamrouni MH, Koyro HW, Ranieri A, Abdely C, Smaoui A (2010) Phytodesalination of a salt-affected soil with the halophyte *Sesuvium portulacastrum* L. to arrange in advance the requirements for the successful growth of a glycophytic crop. *Bioresour Technol* 101:6822–6828
70. Farid M, Ali S, Rizwan M, Ali Q, Abbas F, Bukhari SAH, Saeed R, Wu L (2017) Citric acid assisted phytoextraction of chromium by sunflower; morpho-physiological and biochemical alterations in plants. *Ecotoxicol Environ Saf* 145:90–102
71. Ramana S, Biswas AK, Ajay, Singh AS, Ahirwar NK, Rao AS (2013) Potential of rose for phytostabilization of chromium contaminated. *Indian J Plant Physiol* 18:381–383
72. Vymazal J (2016) Concentration is not enough to evaluate accumulation of heavy metals and nutrients in plants. *Sci Total Environ* 544:495–498
73. Lotfy SM, Mostafa AZ (2014) Phytoremediation of contaminated soil with cobalt and chromium. *J Geochem Explor* 144(Part B):367–373
74. Andrezza R, Bortolon L, Pieniz S, Camargo FAO, Bortolon ESO (2013) Copper phytoextraction and phytostabilization by *Brachiaria decumbens* stapf. In vineyard soils and a copper mining waste. *Open J Soil Sci* 3:273–281
75. Galal TM, Eid EM, Dakhil MA, Hassan LM (2018) Bioaccumulation and rhizofiltration potential of *Pistia stratiotes* L. for mitigating water pollution in the Egyptian wetlands. *Int J Phytoremediation* 20(5):440–447
76. Galal TM, Gharib FA, Ghazi SM, Mansour KH (2017) Phytostabilization of heavy metals by the emergent macrophyte *Vossia cuspidata* (Roxb.) Griff.: a phytoremediation approach. *Int J Phytoremediation* 19:992–999
77. Tariq SR, Ashraf A (2016) Comparative evaluation of phytoremediation of metal contaminated soil of firing range of four different plant species. *Arab J Chem* 9:806–814
78. Katoh M, Risky E, Sato T (2017) Immobilization of lead migrating from contaminated soil in rhizosphere soil of barley (*Hordeum vulgare* L.) and hairy vetch (*Vicia villosa*) using hydroxyapatite. *Int J Environ Res Public Health* 14:1273. <https://doi.org/10.3390/ijerph14101273>
79. Dinh N, Ent AVD, Mulligan DR, Nguyen AV (2018) Zinc and lead accumulation characteristics and in vivo distribution of Zn²⁺ in the hyperaccumulator *Noccaea caerulescens* elucidated with fluorescent probes and laser confocal microscopy. *Environ Exp Bot* 147:1–12
80. Dhiman SS, Selvaraj C, Li J, Singh R, Zhao X, Kim D, Kim JY, Kang YC, Lee JK (2016) Phytoremediation of metal-contaminated soils by the hyperaccumulator canola (*Brassica napus* L.) and the use of its biomass for ethanol production. *Fuel* 183:107–114
81. Min Y, Boqing T, Miezhana T, Aoyama I (2007) Accumulation and uptake of manganese in a hyperaccumulator *Phytolacca americana*. *Miner Eng* 20:188–190
82. Marrugo-Negrete J, Durango-Hernández J, Pinedo-Hernández J, Olivero-Verbel J, Díez S (2015) Phytoremediation of mercury-contaminated soils by *Jatropha curcas*. *Chemosphere* 127:58–63
83. Shiyab S, Chen J, Han FX, Monts DL, Matta FB, Gu M, Su Y (2009) Phytotoxicity of mercury in Indian mustard (*Brassica juncea* L.). *Ecotoxicol Environ Saf* 72:619–625
84. Bonanno G, Vymazal J (2017) Compartmentalization of potentially hazardous elements in macrophytes: insights into capacity and efficiency of accumulation. *J Geochem Explor* 181: 22–30
85. Tang C, Song J, Hu X, Hu X, Zhao Y, Bing Li B, Ou D, Peng L (2017) Exogenous spermidine enhanced Pb tolerance in *Salix matsudana* by promoting Pb accumulation in roots and spermidine, nitric oxide, and antioxidant system levels in leaves. *Ecol Eng* 107:41–48

86. Kathal R, Malhotra P, Kumar L, Uniyal PL (2016b) Phytoextraction of Pb and Ni from the polluted soil by *Brassica juncea* L. J Environ Anal Toxicol 6(5):100394. <https://doi.org/10.4172/2161-0525.1000394>
87. Pal S, Singh HB, Rakshit A (2013) Potential of different crop species for nickel and cadmium phytoremediation in peri-urban areas of Varanasi district (India) with more than twenty years of wastewater irrigation history. Ital J Agron 8:e8. <https://doi.org/10.4081/ija.2013.e8>
88. Bañuelos GS, Arroyo I, Pickering IJ, Yang SI, Freeman JL (2015) Selenium biofortification of broccoli and carrots grown in soil amended with Se-enriched hyperaccumulator *Stanleya pinnata*. Food Chem 166:603–608
89. Hawrylak-Nowaka B (2013) Comparative effects of selenite and selenate on growth and selenium accumulation in lettuce plants under hydroponic condition. Plant Growth Regul 70:149–157
90. Golan-Goldhirsh A (2006) Plant tolerance to heavy metals, a risk for food toxicity or a means for food fortification with essential metals: the *Allium schoenoprasum* model. In: Twardowska I, Allen HE, Haggblom MM (eds) Soil and water pollution monitoring, protection and remediation. Springer, Amsterdam, pp 479–486
91. Belimov AA, Hontzeas N, Safranova VI, Demchinskaya SV, Piluzza G, Bullitta S, Glick BR (2005) Cadmium-tolerant plant growth-promoting bacteria associated with the roots of Indian mustard (*Brassica juncea* L. Czern.). Soil Biol Biochem 37:241–250
92. Takeda R, Sato Y, Yoshimura R, Komemushi S, Sawabe A (2006) Accumulation of heavy metals by cucumber and *Brassica juncea* under different cultivation conditions. Proc Annu Int Conf Soils Sediments Water Energy (Ma) 11:293–299
93. Turan M, Esringu A (2007) Phytoremediation based on canola (*Brassica napus* L.) and Indian mustard (*Brassica juncea* L.) planted on spiked soil by aliquot amount of Cd, Cu, Pb, and Zn. Plant Soil Environ 53(1):7–15
94. Singh A, Fulekar MH (2012) Phytoremediation of heavy metals by *Brassica juncea* in aquatic and terrestrial environment. In: Anjum NA, Ahmad I, Pereira ME, Duarte AC, Umar S, Khan NA (eds) The plant family Brassicaceae: contribution towards phytoremediation. Springer, Amsterdam, pp 153–169
95. Sharma H (2016) Phytoremediation of lead using *Brassica juncea* and *Vetiveria zizanioides*. Int J Life Sci Res 4(1):91–96
96. Sheng XF, Xia JJ (2006) Improvement of rape (*Brassica napus*) plant growth and cadmium uptake by cadmium-resistant bacteria. Chemosphere 64:1036–1042
97. Dell'Amico E, Cavalva L, Andreoni V (2008) Improvement of *Brassica napus* growth under cadmium stress by cadmium-resistant rhizobacteria. Soil Biol Biochem 40:74–84
98. Garg N, Singla P, Bhandari P (2014) Metal uptake, oxidative metabolism, and mycorrhization in pigeon pea and pea under arsenic and cadmium stress. Turk J Agric For 39:234–250
99. Wani PA, Khan MS, Zaidi A (2007) Impact of heavy metal toxicity on plant growth, symbiosis, seed yield and nitrogen and metal uptake in chickpea. Aust J Exp Agric 47:712–720
100. Kambhampati MS, Vu VT (2013) EDTA enhanced phytoremediation of copper contaminated soils using chickpea (*Cicer arietinum* L.). Bull Environ Contam Toxicol 91:310–313
101. Dasgupta S, Satvat PS, Mahinrakar AB (2011) Ability of *Cicer arietinum* (L.) for bioremoval of lead and chromium from soil. IJTES 2(3):338–341
102. Alvarado S, Guedez M, Lue-Meru MP, Nelson G, Alvaro A, Jesus AC, Gyula Z (2008) Arsenic removal from water by bioremediation with the aquatic plants water hyacinth (*Eichhornia crassipes*) and lesser duckweed (*Lemna minor*). Bioresour Technol 99:8436–8340
103. Mishra VK, Tripathi BD (2009) Accumulation of chromium and zinc from aqueous solutions using water hyacinth (*Eichornia crassipes*). J Hazard Mater 164:1059–1063
104. Saleh HM (2012) Water hyacinth for phytoremediation of radioactive waste simulate contaminated with cesium and cobalt radionuclides. Nucl Eng Des 242:425–432

105. Jamil S, Abhilash PC, Singh N, Sharma PN (2009) *Jatropha curcas*: a potential crop for coal fly ash. *J Hazard Mater* 172:269–277
106. Marrugo-Negrete J, Durango-Hernandez J, Pinedo-Hernandez J, Olivero-Verbel J, Diez S (2015) Phytoremediation of mercury-contaminated soils by *Jatropha curcas*. *Chemosphere* 127:58–63
107. Alaribe FO, Agamuthu P (2015) Assessment of phytoremediation potentials of *Lantana camara* in Pb impacted soil with organic wasted additives. *Ecol Eng* 83:513–520
108. Wani PA, Khan MS (2012) Bioremediation of lead by a plant growth promoting *rhizobium* species RL9. *Bacteriol J* 2(4):66–78
109. Gunduz S, Uygur FN, Kahramanoglu I (2012) Heavy metal phytoremediation potentials of *Lepidium sativum* L., *Lactuca sativa* L., *Spinacia oleracea* L. and *Raphanus sativus* L. *herald*. *J Agric Food Sci Res* 1(1):1–5
110. Smolinska B, Szczodrowska A (2016) Antioxidative response of *Lepidium sativum* L. during assisted phytoremediation of Hg contaminated soil. *New Biotechnol* 38(Part B):74–83
111. Achakzai AKK, Bazai ZA, Kayani SA (2011) Accumulation of heavy metals by lettuce (*Lactuca sativa* L.) irrigated with different levels of wastewater of Quetta City. *Pak J Bot* 43(6):2953–2960
112. Ghnaya T, Mnassri M, Ghabriche R, Wali M, Poschenriender C, Lutts S, Abdelly C (2015) Nodulation by *Sinorhizobium meliloti* originated from a mining soil alleviates Cd toxicity and increases Cd-phytoextraction in *Medicago sativa* L. *Front Plant Sci* 6:1–10
113. Li P, Wang X, Zhang T, Zhou D, He Y (2008) Effect of several amendments on rice growth and uptake of copper and cadmium from a contaminated soil. *J Environ Sci* 20:449–455
114. Akter S, Afrin R, Mia MY, Hossen MZ (2014) Phytoremediation of chromium (Cr) from tannery effluent by using water lettuce (*Pistia stratiotes*). *ASA Univ Rev* 8(2):149–156
115. Das S, Goswami S, Talukdar AD (2014) A study on cadmium phytoremediation potential of water lettuce, *Pistia stratiotes* L. *Bull Environ Contam Toxicol* 92:169–174
116. Farnese FS, Oliveira JA, Lima FS, Leao GA, Gusman GS, Silva LC (2014) Evaluation of the potential of *Pistia stratiotes* L. (water lettuce) for bioindication and phytoremediation of aquatic environments contaminated with arsenic. *Braz J Biol* 74(3):103–112
117. Malecka A, Piechalak A, Morkunas I (2008) Accumulation of lead in root cells of *Pisum sativum*. *Acta Physiol Plant* 30:629–637
118. Wani PA, Khan MS, Zaidi A (2008) Effects of heavy metal toxicity on growth, symbiosis, seed yield and metal uptake in pea grown in metal amended soil. *Bull Environ Contam Toxicol* 81:152–158
119. Hegedusova A, Jakabova S, Vargova A, Hegeus O, Pernyeszi TJ (2009) Use of phytoremediation techniques for elimination of lead from polluted soils. *Nova Biotechnol Chim* 9(2):125–132
120. Sharma S, Sharma P, Mehrotra P (2010) Bioaccumulation of heavy metals in *Pisum sativum* L. growing in fly ash amended soil. *Am J Sci* 6(6):43–50
121. Hatano K, Kanazawa K, Tomura K, Yamatsu T, Tsunoda K, Kubota K (2016) Molasse melanoidin promotes copper uptake for radish sprouts: the potential for an accelerator of phytoextraction. *Environ Sci Pollut Res* 23:17656–17663
122. Patel M, Subramanian RB (2006) Effect of a chelating agent on lead uptake by *Spinacia oleracea*. *Pollut Res* 25(1):77–79
123. Salaskar D, Shrivastava M, Kale SP (2011) Bioremediation potential of spinach (*Spinacia oleracea* L.) for decontamination of cadmium in soil. *Curr Sci* 101(10):1359–1363
124. Pathak C, Chopra AK, Zivastava S (2013) Accumulation of heavy metals in *Spinacia oleracea* irrigated with paper mill effluent and sewage. *Environ Monit Assess* 185:7343–7352
125. Jahanbakhshi S, Rezaei MR, Sayyari-Zahan MH (2014) Optimization of phytoremediation in Cd-contaminated soil by using Taguchi method in *Spinacia oleracea*. In: Zhang W (ed) Proceedings of the international academy of ecology and environmental sciences, vol vol 4. International Academy of Ecology and Environmental Sciences, Hong Kong, pp 185–193

126. Abhilash MR, Srikantaswamy S, Kumar D, Shiva Jagadish K, Shruthi L (2016) Phytoremediation of heavy metal industrial contaminated soil by *Spinacia oleracea* L. and *Zea mays* L. *Int J Appl Sci* 4(1):192–199
127. Wei S, Zhou Q, Koval PV (2006) Flowering stage characteristic of cadmium hyperaccumulator *Solanum nigrum* L. and their significance to phytoremediation. *Sci Total Environ* 369:441–446
128. Wei S, Li Y, Zhou Q, Srivastava M, Chiu S, Zhan J, Wu Z, Sun T (2010) Effect of fertilizer amendments on phytoremediation of Cd-contaminated soil by newly discovered hyperaccumulator *Solanum nigrum* L. *J Hazard Mater* 176:269–273
129. Ji P, Sun T, Song Y, Ackland ML, Liu Y (2011) Strategies for enhancing the phytoremediation of cadmium-contaminated agricultural soils by *Solanum nigrum* L. *Environ Pollut* 159:762–768
130. Pinto AP, Mota AM, de Varennes A, Pinto FC (2004) Influence of organic matter on uptake of cadmium, zinc, copper and iron by sorghum plant. *Sci Total Environ* 326:239–247
131. Mojiri A (2011) The potential of corn (*Zea mays*) for phytoremediation of soil contaminated with cadmium and lead. *J Biol Environ Sci* 5(13):17–22
132. Greger M, Landberg T (1999) Use of willow in phytoextraction. *Int J Phytoremediation* 1: 115–123
133. Pendias KA, Pendias H (2001) Trace elements in soils and plants. 3rd edn. CRC Press, Boca Raton, 331 p
134. Banuelos GS, Lin ZQ, Arroyo I, Terry N (2005) Selenium volatilisation in vegetated agricultural drainage sediment from the San Luis Drain, Central California. *Chemosphere* 60:1203–1213
135. Ostwald A (2000) Physiologische Grundlagen der Akkumulation von Schwermetallionen beim Faserhanf (*Cannabis sativa* L.) und das Nutzungspotential bei der Phytoremediation. PhD thesis, Universität Wuppertal
136. Elkhatib EA, Thabet AG, May AM (2001) Phytoremediation of cadmium contaminated soils: role of organic complexing agents in cadmium phytoextraction. *Land Contam Reclam* 9:301–306
137. Massacci A, Pietrini F, Iannelli MA (2001) Remediation of wetlands by *Phragmites australis*: the biological basis. *Minerva Biotechnol* 13:135–140
138. McCabe OM, Otte ML (2000) The wetland grass *Glyceria fluitans* for revegetation of mine tailings. *Wetlands* 20:548–559
139. Maszenan AM, Liu Y, Ng WJ (2011) Bioremediation of wastewaters with recalcitrant organic compounds and metals by aerobic granules. *Biotechnol Adv* 29(1):111–123
140. Lee JH (2013) An overview of phytoremediation as a potentially promising technology for environmental pollution control. *Biotechnol Bioprocess Eng* 18:431–439
141. Chirakkara RA, Cameselle C, Reddy KR (2016) Assessing the applicability of phytoremediation of soils with mixed organic and heavy metal contaminants. *Rev Environ Sci Biotechnol* 15:299–326. <https://doi.org/10.1007/s11157-016-9391-0>

Electrochemical Decomposition and Adsorption for Removal of Organic Pollutants from Water



Hideki Kuramitz

Contents

1	Removal of Organic Pollutants from Water Using Electrochemical Techniques	226
2	Electrochemical Polymerization-Based Organic Pollutant Removal	230
2.1	Electrochemical Oxidation Behavior of Bisphenol A and Its Derivatives	231
2.2	Electrochemical Adsorption Using Carbon Fibers for Removal of Bisphenol A and Its Derivatives	232
2.3	Electrochemical Adsorption Using Carbon Fibers for Removal of Other Organic Compounds	238
2.4	Electrochemical Adsorption Using Different Electrode Materials	248
3	Conclusions	259
	References	260

Abstract Water treatment based on electrochemical methods is a powerful means of degrading both biologically and chemically resistant organic compounds. Most organic pollutants can be removed or converted to chemicals of low toxicity using one or more electrochemical processes, including electrochemical oxidation/reduction, electrocoagulation, electroflotation, electrodialysis, and advanced electrochemical oxidation methods. Among the various electrochemical treatments used for organic pollutants, electrochemical adsorption offers a unique water treatment approach in that it utilizes the electrochemical oxidation reactions of target pollutants to obtain clean water via electrochemical polymerization or the formation of highly hydrophobic oxides. In the electrochemical adsorption method, the electrode exhibits dual functions both as a catalyst to promote the electrochemical reaction of the target pollutant and as an adsorbent to accumulate the products of the electrochemical reaction. In this chapter, the electrochemical oxidation of bisphenol

H. Kuramitz (✉)

Department of Environmental Biology and Chemistry, Graduate School of Science and Engineering, University of Toyama, Toyama, Japan
e-mail: kuramitz@sci.u-toyama.ac.jp

Shunitz Tanaka, Masaaki Kurasaki, Masaaki Morikawa, and Yuichi Kamiya (eds.), 225
Design of Materials and Technologies for Environmental Remediation,
Hdb Env Chem (2023) 115: 225–262, DOI 10.1007/698_2022_895,
© The Author(s), under exclusive license to Springer Nature Singapore Pte Ltd 2022,
Published online: 15 June 2022

A and its derivatives and their treatment with carbon fibers are introduced. In addition, the applications of electrochemical adsorption to other organic pollutants, such as aniline, estrogens, *p*-nonylphenol, phenol, and chlorinated phenol, are presented. Moreover, recent progress in electrochemical adsorption using various electrode materials such as carbon nanotube-covered polyester yarn, PbO₂, granular carbon, stainless steel, carbon aerogel, and polyaniline is reviewed.

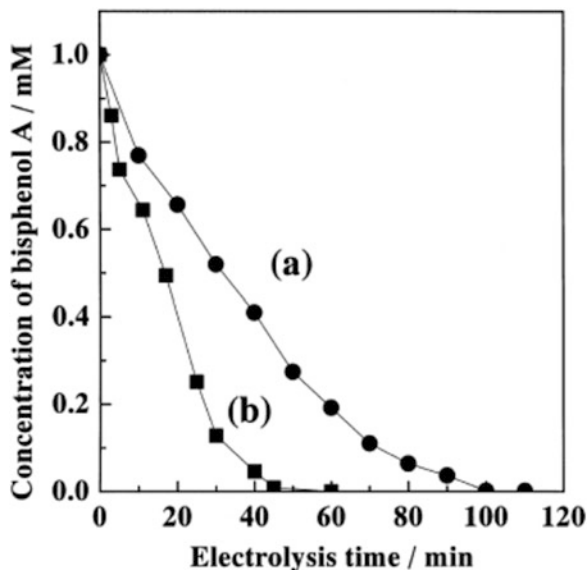
Keywords Adsorption, Decomposition, Electrocoagulation, Flotation, Photoelectrochemical

1 Removal of Organic Pollutants from Water Using Electrochemical Techniques

Electrochemical methods offer distinct advantages for the removal of organic pollutants compared with biological, physical, and chemical procedures. Biological methods are frequently inhibited by the coexistence of toxic substances and depend on conditions, such as nutrients, temperature, and pH. Conversely, electrochemical reactions are not influenced by conditions, such as toxicity, component of nutrients, or water temperature. Meanwhile, physical processes such as adsorption by activated carbon and separation by membranes may lead to limited mass transfer due to the low concentration of pollutants. Since these processes only accumulate and remove pollutants, they require further processes to recover or decompose the collected pollutants. Electrochemical methods do not require the use of harmful reactive chemicals, compared to chemical and hybrid methods. Water treatment based on electrochemical methods proceeds as long as the electrical current or potential is supplied to the electrode. Therefore, the removal of organic pollutants from water has been demonstrated using various electrochemical methods, such as electrochemical and photoelectrochemical decomposition, electrocoagulation, and flotation, which are detailed in recent review articles [1–4].

The electrochemical treatment techniques of organic compounds aim at the oxidative decomposition of organic pollutants, which have been established as advanced oxidation technologies (AOTs) because of their effectiveness, versatility, energy efficacy, ease of automation, and chemical stability. Platinum and dimensionally stable anodes (DSAs) have been used for the oxidative decomposition of various organic compounds. DSAs are also called mixed metal oxide electrodes, which are prepared by the thermal deposition of a thin layer of a metal oxide (e.g., SnO₂, PbO₂, RuO₂, and IrO₂) on a base metal [5]. In particular, the removal of various phenolic compounds has been extensively studied since the purification of wastewater containing phenolic compounds is a longstanding problem owing to the low biodegradation rate and high toxicity of phenol derivatives [6–9]. The target organic compounds are decomposed directly by electrochemical oxidation owing to the reactivity of radical species generated by the electrochemical oxidation of water

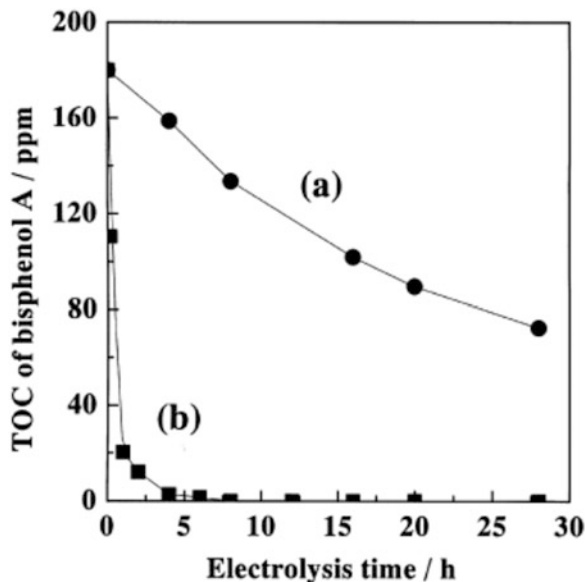
Fig. 1 Relationship between bisphenol A (BPA) concentration and electrochemical decomposition time for (a) Pt/Ti anode and (b) SnO₂/Ti anode. The electrochemical treatment was performed galvanostatically at 0.3 A in 0.1 M Na₂SO₄ [14]



or supporting electrolytes on the anode surface. Even chemically stable organic compounds that are resistant to anodic oxidation are indirectly decomposed by strong oxidants, such as hydroxyl radicals.

For example, 2,2'-bis(4'-hydroxyphenyl) propane (bisphenol A) is commonly used as a target for electrochemical decomposition-based organic pollutant removal. Because it serves as an endocrine-disrupting chemical (having estrogenic activity) [10], it is used as a raw material in the production of polycarbonate and epoxy resins. The electrochemical degradation of bisphenol A has been studied using Pt, Pt/Ti, PbO₂/Ti, SnO₂/Ti, Sb-SnO₂/Ti, and boron-doped diamond anodes [11–16]. In our previous study, the electrochemical decomposition of bisphenol A using Pt/Ti and SnO₂/Ti anodes was conducted [14]. Figure 1 shows the concentration of bisphenol A during electrochemical decomposition. The complete degradation of 1.0 mM bisphenol A was achieved using the SnO₂/Ti anode in 1 h. The SnO₂/Ti electrode was more effective for the electrochemical decomposition of bisphenol A than the Pt/Ti electrode. Figure 2 shows the changes in the total organic carbon (TOC) value of a bisphenol A solution during electrochemical decomposition using Pt/Ti and SnO₂/Ti anodes. The removal of TOC reveals the mineralization of bisphenol A during electrolysis. In both cases, the TOC value decreased with the increased electrolysis time, indicating that bisphenol A was decomposed to CO₂ and H₂O. Although approximately 50% of the TOC in the bisphenol A solution was removed in 20 h when the Pt/Ti electrode was used, the complete removal of TOC was achieved within only 6 h using the SnO₂/Ti anode. Therefore, while the conversion of bisphenol A to intermediates was fast for both anodes, the decomposition efficiency for the mineralization rate of intermediates was higher for the SnO₂/Ti anode than that for the Pt/Ti anode. Aromatic intermediates in the bisphenol A

Fig. 2 TOC removal rate using (a) Pt/Ti anode and (b) SnO₂/Ti anode. The electrochemical treatment was performed galvanostatically at 0.3 A in 0.1 M Na₂SO₄ involving 1.0 mM bisphenol A [14]



solution were identified by GC-MS after electrochemical decomposition for 2 h. In the case of the Pt/Ti electrode, *p*-benzoquinone, hydroquinone, and 2,6-bis (1,1-dimethylethyl)-4-methylphenol were observed. However, these intermediates were barely detectable in the solution treated using the SnO₂/Ti anode, suggesting that aromatic intermediates rapidly oxidized to organic acids during electrolysis using the SnO₂/Ti anode. Aliphatic acids as intermediaries are formed by further oxidation of aromatic derivatives. Changes in the concentration of some aliphatic acids during the electrochemical decomposition of bisphenol A are shown in Fig. 3. In the case of electrochemical decomposition using the Pt/Ti anode, maleic acid, citric acid, and tartaric acid were determined. Citric acid and tartaric acid are stable toward further treatment using the Pt/Ti anode, and they did not disappear even when the period of electrochemical decomposition was extended to 35 h (Fig. 3a). On the contrary, only tartaric acid was detected in the bisphenol A solution during electrolysis using the SnO₂/Ti electrode (Fig. 3b). The concentration of tartaric acid produced by the electrochemical decomposition of bisphenol A peaked at 3 h and then rapidly decreased, whereas the formation rate of tartaric acid was slow in the case of the Pt/Ti electrode, and its decomposition was not observed within the time scale of the experiment. These results indicate that bisphenol A rapidly oxidized to organic acids and further oxidized to CO₂ and H₂O, which was faster for the SnO₂/Ti anode compared to the Pt/Ti anode. Therefore, the SnO₂/Ti anode was verified to be an efficient catalytic electrode for the mineralization of bisphenol A. The electrochemical decomposition mechanism of bisphenol A is illustrated in Fig. 4. The electrochemical decomposition of bisphenol A proceeds via two pathways: In the first path, bisphenol A is decomposed to organic acids via the generation of aromatic intermediates by direct oxidization at the electrode surface. In the second path,

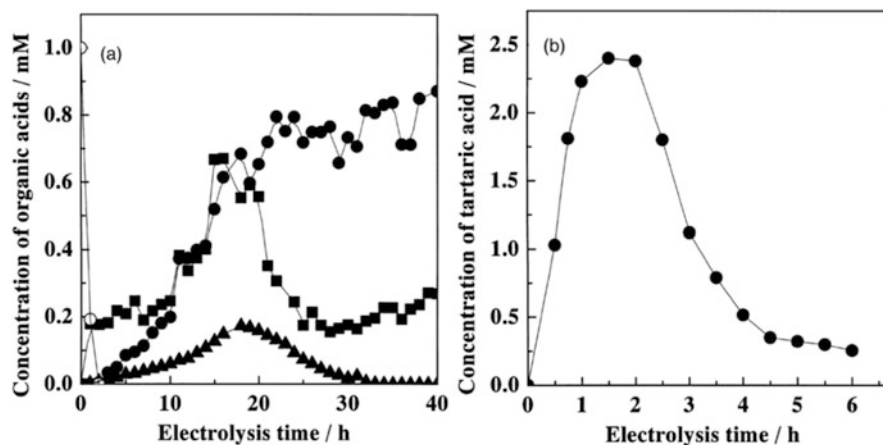


Fig. 3 Generation and destruction of aliphatic acids during the electrochemical decomposition of bisphenol A by (a) Pt/Ti anode and (b) SnO₂/Ti anode. The electrochemical treatment was performed galvanostatically at 0.3 A in 0.1 M Na₂SO₄ involving 1.0 mM bisphenol A. The concentrations of bisphenol A (*open circle*), tartaric acid (*filled circle*), citric acid (*filled square*), and maleic acid (*filled triangle*) were determined by HPLC [14]

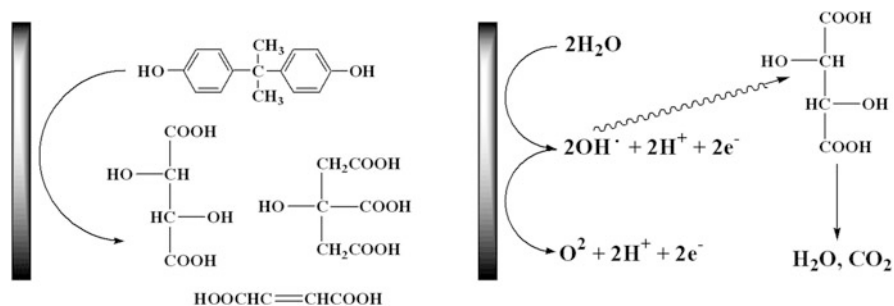
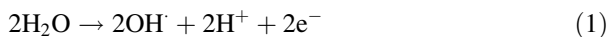


Fig. 4 Schematic diagram for the mineralization of bisphenol A by electrochemical decomposition using SnO₂/Ti anode. The generation (left) and decomposition (right) of intermediates are shown during electrolysis. The mineralization rates of the intermediates depend on the electrode material

bisphenol A and its intermediates are indirectly oxidized to CO₂ and H₂O by hydroxyl radicals. The evolution of oxygen on the anode surface upon the oxidation of water can be described by:



To mineralize bisphenol A, the mineralization efficiency of aliphatic acids as intermediates is a key factor, which is strongly related to the performance of hydroxyl radical production. The overpotential of the SnO₂/Ti anode for oxygen

evolution is high, which means the efficiency of oxygen production shown in Eq. (2) is low. Therefore, the enhanced bisphenol A mineralization capability achieved using the SnO₂/Ti anode is due to the production of hydroxyl radicals.

Further, electrochemical adsorption methods, which involve the adsorption of target organic pollutants onto the electrode and the removal of pollutants from water, have been reported. Electrochemical adsorption utilizes electrochemical reactions, especially electrochemical polymerization, to transform organic compounds into a form that can be easily adsorbed on the electrode surface. This method aims to adsorb and remove low-concentration contaminants by the electrochemical transformation of contaminants, contrary to the conventional strategies pursuing the functionalization of adsorbents in the adsorption treatment of organic contaminants. In this chapter, recent literature on this method is reviewed as follows.

2 Electrochemical Polymerization-Based Organic Pollutant Removal

Electrochemical adsorption methods require electrodes that display dual functions: to promote the electrochemical reaction with the target contaminant and to adsorb the products of the electrochemical reaction. The electrochemical oxidation of phenol and its derivatives causes the inactivation of graphite or noble metal electrodes. This is due to the deposition of the electrochemically polymerized film, which is formed when the phenoxy radical attacks unreacted substrates [17–19]. This means that phenolic compounds can accumulate and form a polymer film on the electrode surface, providing their removal from water. Therefore, we first confirm whether this method can be applied to the removal of bisphenol A. In this section, the treatment of bisphenol A and its derivatives by electrochemical polymerization is described. The electrochemical reactions of bisphenol A and its derivatives on glassy carbon electrodes are introduced, and the results obtained from their electrochemical adsorption treatment using carbon fibers are explained. Furthermore, the applications of electrochemical adsorption using carbon fibers for the removal of other organic compounds such as aniline, estrogens, *p*-nonylphenol, phenol, and chlorinated phenol are presented. Furthermore, the electrochemical adsorption techniques using different electrode materials such as carbon nanotube-covered polyester yarns, PbO₂, granular carbon, stainless steel, carbon aerogel, and polyaniline are reviewed.

Fig. 5 Linear sweep voltammograms for the oxidation of 0.1 mM bisphenol A in 0.1 M Na_2SO_4 solution at various pH values. The measurements were performed using a glassy carbon electrode at a scan rate of 0.01 V/s [21]

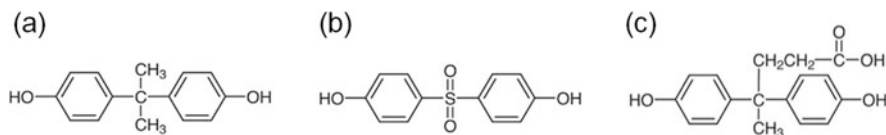
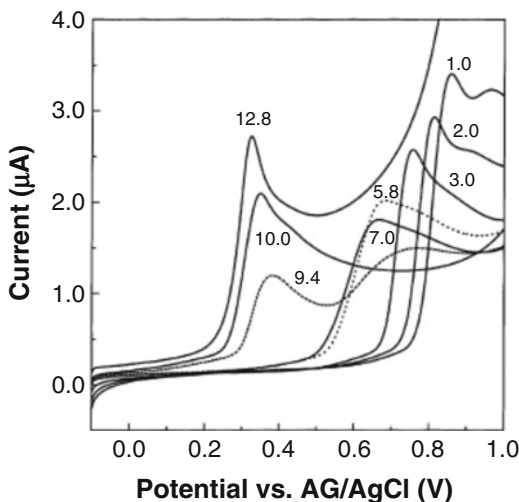


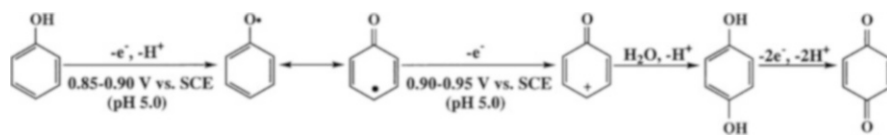
Fig. 6 Chemical structure of (a) bisphenol A, (b) bisphenol S, and (c) diphenolic acid

2.1 Electrochemical Oxidation Behavior of Bisphenol A and Its Derivatives

The linear sweep voltammograms are shown in Fig. 5 for the oxidation of bisphenol A at various pH values using a glassy carbon electrode. The oxidation potential of bisphenol A shifted to lower potentials with the increased pH. At pH 9.4, two oxidation peaks were observed. Since the pK_a of bisphenol A is 9.8 [20], these two peaks correspond to the oxidation of neutral bisphenol A and its phenolate ion. These linear sweep voltammograms indicate that the phenolate ion is more easily oxidized than neutral bisphenol A.

The chemical structures of bisphenol A, bisphenol S, and diphenolic acid are shown in Fig. 6. These compounds exhibit similar electrochemical behavior. The progressive cyclic voltammograms showed irreversible electrochemical oxidation (Fig. 7). In the first cycle, a well-defined peak current corresponding to the oxidation of these compounds was observed. The oxidation potentials of bisphenol A, bisphenol S, and diphenolic acid were 0.65, 0.97, and 0.7 V, respectively. The oxidation peak currents for these compounds disappeared completely in subsequent potential scanning, indicating that the formation of the electropolymerized film on the electrode surface blocks further monomer access to the electrode after the

oxidation by the first sweep of the potential. The electrochemical oxidation behavior of bisphenol A has been detailed in our previous chapter [21, 22]. The direct oxidation of phenolic compounds via one- and two-electron transfer generates the phenoxy radical and quinone, respectively. This electrode reaction can be expressed as follows [23]:



The electrochemical polymerization of bisphenol A, bisphenol S, and diphenolic acid on the carbon electrode surface might result from the dimerization of the phenoxy radical and/or free-radical multistep-growth polymerization with the monomer or the oxidized monomer initiated by phenoxy radicals. The increment of hydrophobicity due to dimerization may also be related to the enhanced adsorption on the electrode surface.

2.2 Electrochemical Adsorption Using Carbon Fibers for Removal of Bisphenol A and Its Derivatives

The progressive cyclic voltammograms shown in Fig. 7 indicate that the electropolymerization of bisphenol A, bisphenol S, and diphenolic acid produces a nonconducting thin film on the anode surface, which causes the passivation of the electrode surface and prevents the growth of the film. To achieve water treatment based on electrochemical adsorption, electrodes with a large surface area are desired. Therefore, we selected carbon fibers as a suitable electrode material. The SEM image

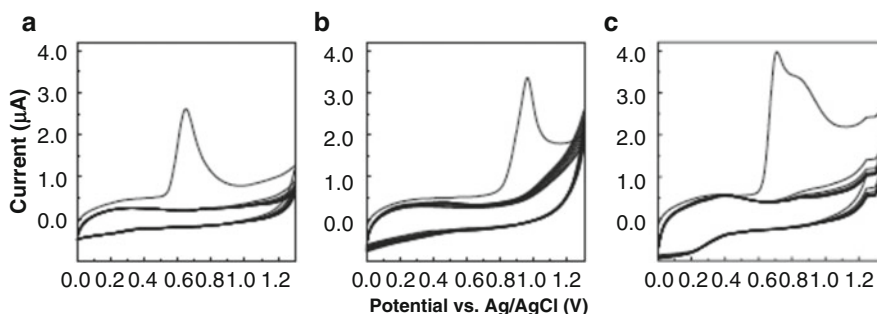


Fig. 7 Progressive cyclic voltammograms of 1.0 mM (a) bisphenol A, (b) bisphenol S, and (c) diphenolic acid in 0.1 M Na_2SO_4 solution (pH 5.8). The measurements were performed using a glassy carbon electrode at scan rate 0.015 V/s. The scanning of the potential were repeated for 10 times between 0 and 1.3 V [22]

Fig. 8 SEM image of the carbon fiber electrode

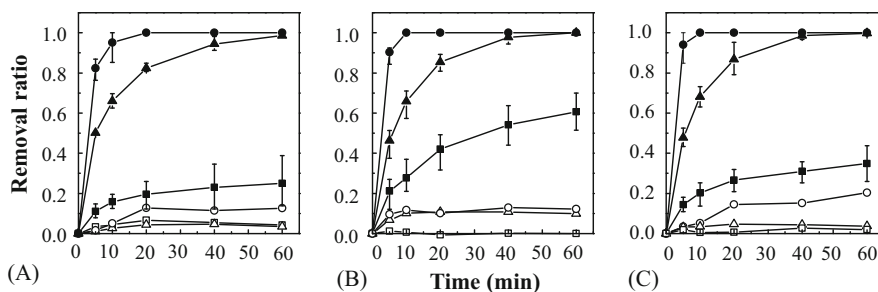
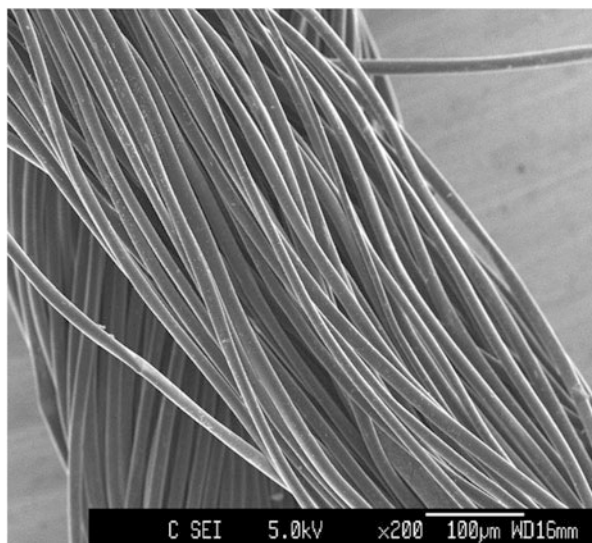


Fig. 9 Relationships between the removal ratio and the treatment time of (a) bisphenol A, (b) bisphenol S, and (c) diphenolic acid at 0.75, 1.0, and 0.8 V, respectively, in 0.1 M Na_2SO_4 containing 1.0×10^{-6} M (filled circle), 1.0×10^{-5} M (filled triangle), 1.0×10^{-4} M (filled square) bisphenol A, bisphenol S, and diphenolic acid (pH 5.8) and without applied potential in 1.0×10^{-6} M bisphenol A (open circle), 1.0×10^{-5} M bisphenol S (open triangle), and 1.0×10^{-4} M (open square) diphenolic acid [22]

of carbon fibers is shown in Fig. 8. This is a bundle of fibrous carbon with a diameter of about $10 \mu\text{m}$. In the removal experiments, carbon fibers with a surface area of ca. 650 cm^2 were used as a working electrode. A coiled platinum wire as a counter electrode was inserted in a Vycor glass tube isolated from the treated water. The removal of bisphenol A, bisphenol S, and diphenolic acid from aqueous solution by electrochemical adsorption was performed in the batch cell by stirring under a constant potential of 0.75, 1.0, and 0.8 V (vs. the Ag/AgCl electrode), respectively.

Figure 9 shows the removal efficiency during treatment for several concentrations of bisphenol A, bisphenol S, and diphenolic acid solutions using carbon fibers with or without applying a potential. While the removal of these compounds was

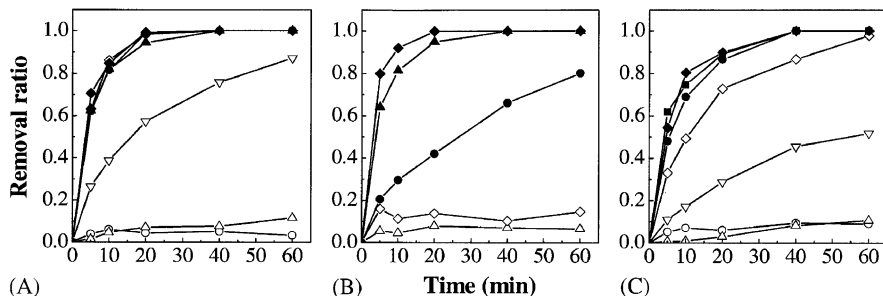


Fig. 10 Relationships between the removal efficiency and the treatment time of (a) bisphenol A, (b) bisphenol S, and (c) diphenolic acid at 0.3 (*open circle*), 0.5 (*open triangle*), 0.6 (*inverted open triangle*), 0.7 (*open diamond*), 0.8 (*filled square*), 0.9 (*filled circle*), 1.0 (*filled triangle*), and 1.2 V (*filled diamond*). The treatments were performed in 0.1 M Na₂SO₄ (pH 5.8) containing 4.0×10^{-6} M bisphenol A, bisphenol S, and diphenolic acid [22]

negligible when no potential was applied, high removal efficiency was obtained with the application of potential. At an initial concentration of 1.0×10^{-6} M for all target substances, complete removal by electrochemical oxidation was achieved in 10 min. The higher the initial concentration required longer treatment time, and the removal rate was limited to an initial concentration of 1.0×10^{-4} M. This is because the insulating film formed on the carbon fiber surface prevents further electrochemical oxidation of the monomer on the carbon fiber electrode. The surface coverage of the electropolymerized film formed by bisphenol A, bisphenol S, and diphenolic acid on the carbon fiber was estimated to be ca. $1.9(\pm 0.95) \times 10^{-9}$, $4.6(\pm 0.18) \times 10^{-9}$, and $2.7(\pm 0.72) \times 10^{-9}$ mol/cm², respectively. As shown in Fig. 10, the removal efficiency of this method strongly depends on the applied potential. Satisfactory removal curves for bisphenol A, bisphenol S, and diphenolic acid were obtained by applying a potential over 0.7, 1.0, and 0.8 V, respectively, which corresponds to the peak potentials for the oxidation of these compounds. Therefore, high removal efficiency for these compounds is not due to their hydrophobic adsorption on the carbon fiber surface. The electropolymerized bisphenol A film formed on the CF surface was characterized by FT-IR and UV/vis. Polymeric bisphenol A was characterized after extraction from carbon fibers by chloroform. These results confirmed that the electropolymerized bisphenol A film was mainly composed of aliphatic hydrocarbons including carbonyl groups.

The influence of humic acid on the removal of bisphenol A using the electrochemical adsorption was investigated. Humic acid is an abundant natural product in the environment. The content of humic acid in common surface water is 1–5 ppm, and it may exceed 40 ppm in specific places, such as peat land [24]. Humic acid is a macromolecule comprising hydrophobic and hydrophilic portions and contains carboxyl, carbonyl, alcohol, and phenolic hydroxyl groups that can form complexes with heavy metal ions and hydrophobic organic compounds. The removal of bisphenol A (4.0×10^{-6} M) from aqueous solution containing 2, 5, and 10 ppm humic acid was studied by applying a potential of 0.75 V. The results showed that

the presence of humic acid hardly influences the removal of bisphenol A. In chemical degradation methods, including photochemical and electrochemical techniques, as well as adsorption methods using activated carbon, the presence of humic acid acts competitively to remove the target substance. This method allows selective removal of bisphenol A, i.e., an electropolymerizable organic compound, from wastewater even in the presence of humic acid, unlike the treatment methods based on decomposition and adsorption.

The application of electrochemical decomposition to a flow system with a packed column-type electrode is usually difficult because of bubble generation during the electrochemical reaction. For example, electrochemical oxidative decomposition methods require the application of a high potential, which is concurrent with water electrolysis. The generation of oxygen bubbles on the anode not only diminishes the active area on the electrode surface but also prevent the flow of solution in the system. Conversely, the electrochemical adsorption method does not involve the electrolysis of water because the process is conducted at a low potential and current density. Therefore, this method is suitable to be applied to a continuous treatment process using a simple flow system with a packed-type column electrode. To achieve the continuous treatment of bisphenol A in aqueous solution, the flow system with a column-type carbon fiber electrode cell, as shown in Fig. 11, was demonstrated. In this system, the carbon fiber equivalent to $1,300 \text{ cm}^2$ surface area packed in a Vycor

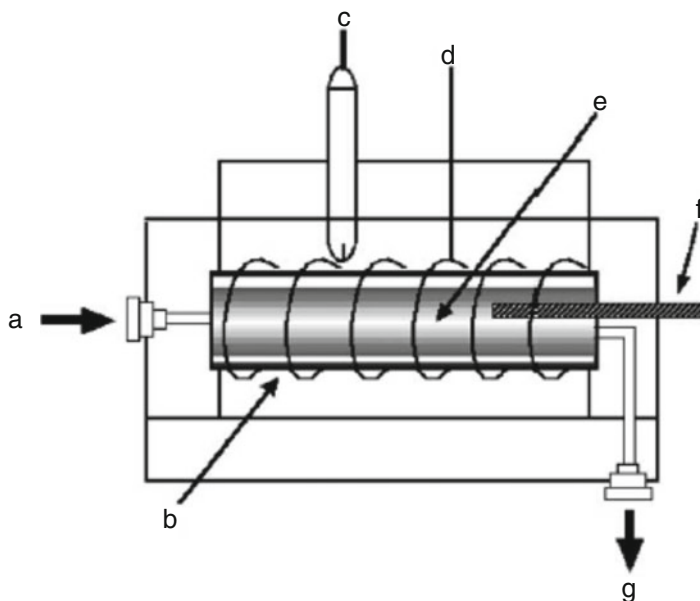


Fig. 11 Schematic of the flow-type cell for electrochemical adsorption: (a) water inlet, (b) Vycor glass tube (working electrode component), (c) reference electrode (Ag/AgCl), (d) counter electrode (a spiral platinum wire), (e) working electrode (a bundle of carbon fibers), (f) electrical connection (a platinum rod), and (g) water outlet [22]

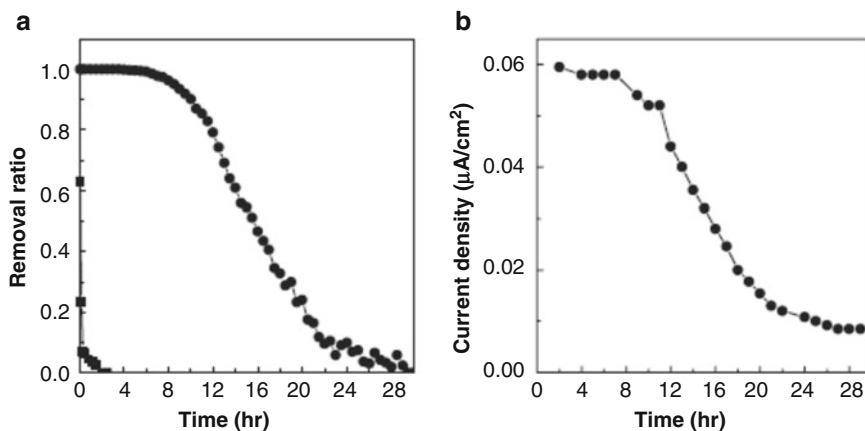


Fig. 12 (a) Continuous treatment of 5.0×10^{-6} M bisphenol A in Na_2SO_4 (pH 5.8) at a flow rate of 2 mL/min with an applied potential of 0.75 V (filled circle) and without an applied potential (filled square). (b) Changes in the current density during the treatment of 5.0×10^{-6} M bisphenol A [22]

glass tube (50×7 mm² i.d., 1 mm thickness) was used as a column-type working electrode. The effective volume of the working electrode component was ca. 0.6 cm³. The counter electrode compartment was filled with 0.1 M Na_2SO_4 (pH 5.8), and a spiral platinum wire as a counter electrode and Ag/AgCl reference electrode separately from the working electrode compartment at the outside of a Vycor glass tube. The flow rate of the sample solution was controlled by a peristaltic pump. The treated sample solutions passing through the flow cell were continuously analyzed by HPLC. The results obtained for the continuous treatment of 5.0×10^{-6} M bisphenol A solution are shown in Fig. 12a. The removal ratio for bisphenol A decreased to zero within 2 h by flowing 240 mL of bisphenol A solution without applying a potential. At an applied potential of 0.75 V, the removal ratio for bisphenol A was maintained at 100% up to 8 h by treating 960 mL of bisphenol A solution. The removal efficiency for bisphenol A decreased gradually and approached zero after ca. 24 h. The current density monitored during the treatment decreased with the reduction of the removal efficiency for bisphenol A (Fig. 12b). These results suggest that the removal of bisphenol A based on electrochemical adsorption is followed by the passivation of the carbon fiber electrode, as shown by the progressive cyclic voltammograms in Fig. 7. The effect of flow rate on the removal efficiency was investigated using several concentrations of bisphenol A solutions between 1×10^{-5} and 1×10^{-7} M (Fig. 13). For high concentrations of bisphenol A, a slight decrease was observed in the removal efficiency with the increased flow rate, but for the low concentrations of bisphenol A, the removal efficiency did not decrease regardless of the change in the flow rate from 0.5 to 8.0 mL/min. The effect of the supporting electrolyte concentration on the removal of bisphenol A was investigated at several flow rates (Fig. 14). Although the removal

Fig. 13 Effect of flow rate on the continuous treatment of bisphenol A. The removal of bisphenol A at several concentrations was performed in 0.1 M Na_2SO_4 (pH 5.8) at 0.75 V [22]

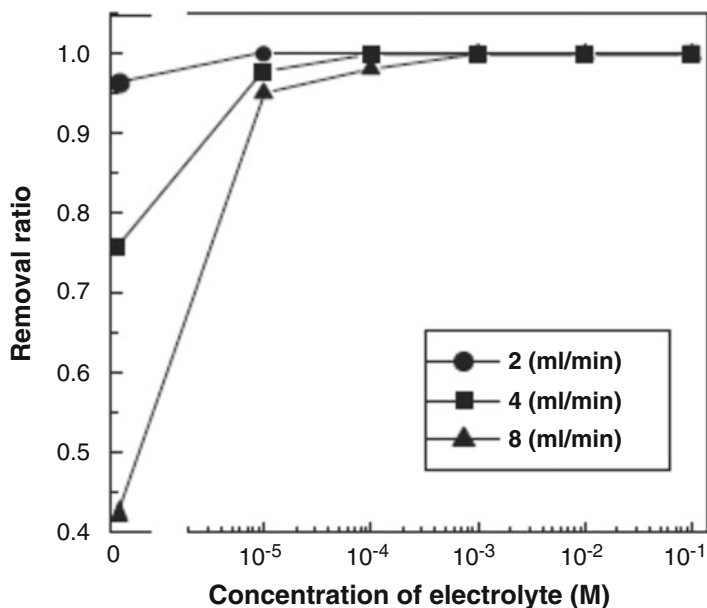
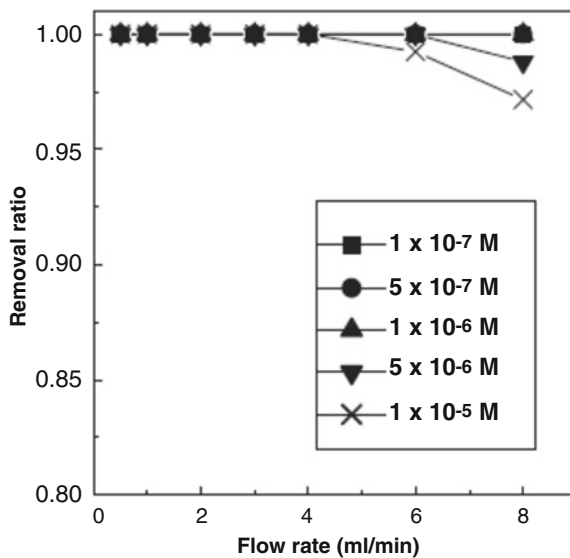


Fig. 14 Effect of supporting electrolyte concentration on the continuous treatment of bisphenol A at several flow rates. The removal of 1.0×10^{-6} M bisphenol A in various concentrations of Na_2SO_4 was performed at 0.75 V [22]

efficiency for bisphenol A (1.0×10^{-6} M) decreased with the decrease in the supporting electrolyte concentration, over 90% removal ratio was achieved at all flow rates, even in the case of an electrolyte concentration at 10^{-5} M. Therefore, this

method can be applied to bisphenol A removal directly from environmental water at a low electrolyte concentration without using a supporting electrolyte.

2.3 *Electrochemical Adsorption Using Carbon Fibers for Removal of Other Organic Compounds*

As mentioned above, the treatment method based on electrochemical adsorption was initiated for the removal of bisphenol A as a target organic pollutant. This method can be applied to other organic pollutants that polymerize or produce highly hydrophobic reaction products by electrochemical reaction at a low potential, and selective removal is possible by adjusting the value of the applied potential and the adsorption of reaction products on the electrode material. Our previous attempts to treat other organic compounds such as aniline [25], estrogens, *p*-nonylphenol [26], phenol, and chlorinated phenols [26] by electrochemical adsorption using carbon fiber electrodes are summarized below.

2.3.1 Removal of Aniline

Aniline and its derivatives are widely distributed in aqueous environment and have also been detected in drinking water because they are used as intermediates in the manufacture of a variety of organic compounds, such as colorants, pesticides, pharmaceutical agents, and synthetic resins. Aniline causes teratogenicity in aquatic organisms [27]. In humans, aniline is carcinogenic and genotoxic. Therefore, its effect on human health over a long period is alarming, even at low concentrations.

The electrochemical behavior of aniline was investigated by progressive cyclic voltammetry in several conditions. As shown in Fig. 15a, the first scanning of the potential cycle in 0.1 M aniline solution showed a well-defined peak current corresponding to the electrochemical oxidation of aniline at approximately 1.0 V. This peak decreased drastically in subsequent cycles, indicating that after aniline is initially oxidized, the electrochemical product adhering to the electrode prevents further access of the aniline monomer to the electrode surface. The redox peaks (A/A', B/B', and C/C') generated from the second scanning of the potential cycle increased with the number of cycles. This electrochemical behavior of aniline is typical of the synthesis of polyaniline on an electrode surface. There are three forms of polyaniline: leucoemeraldine, emeraldine, and pernigraniline. Redox peaks A and C indicate the transformation of leucoemeraldine to emeraldine and emeraldine to pernigraniline, respectively [28–30]. Peak B corresponds to the redox of *p*-aminodiphenylamine, which is highly hydrophobic and can act as an active center for further growth of polymeric chains on the electrode surface [28]. Figure 15b shows the result obtained from a low concentration of aniline (5.0×10^{-5} M). Other conditions are the same as those shown in Fig. 15a. The peak current corresponding

Fig. 15 Progressive cyclic voltammograms of (a) 1×10^{-1} M aniline in 1.0 M H_2SO_4 , (b) 5×10^{-5} M aniline in 1.0 M H_2SO_4 , (c) 5×10^{-5} M aniline in 0.1 M phosphate buffer (pH 6.0). The measurements were performed using a glassy carbon electrode at a scan rate of 0.05 V/s. The scanning was repeated 10 times [25]

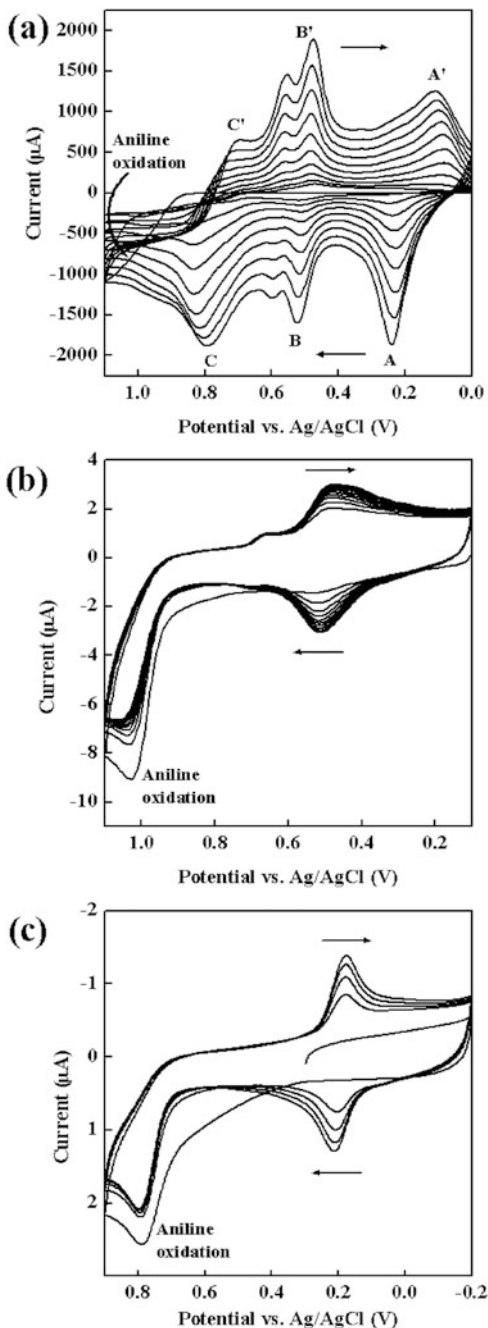
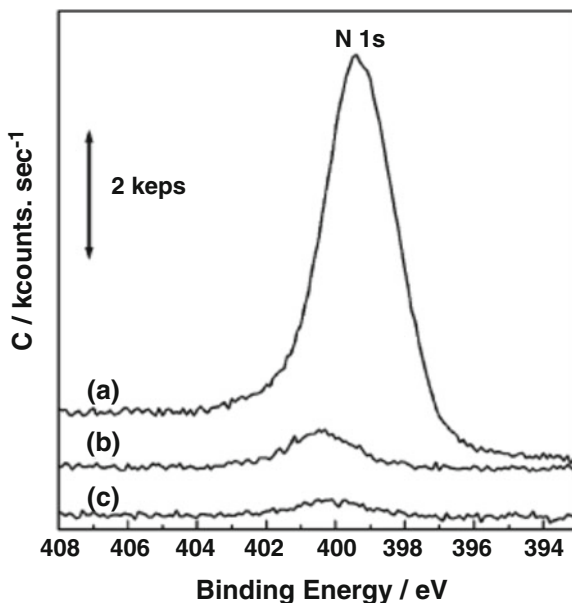


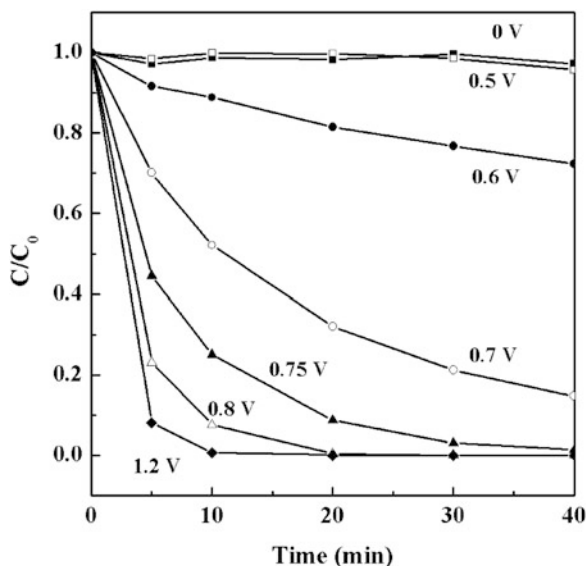
Fig. 16 XPS spectra of carbon fibers in (a) 5×10^{-5} M aniline at 0.8 V for 10 min, (b) at the same concentration of aniline for 10 min without an applied potential, (c) bare carbon fibers [25]



to the oxidation of aniline was observed at approximately 1.0 V and decreased during continuous potential scanning. A reversible redox peak aroused at 0.5 V and increased after the first cycle of potential scanning. The potential of this peak pair is similar with that of the peak B/B' in Fig. 15a. In phosphate buffer solution at pH 6.0, 5.0×10^{-5} M aniline showed a similar electrochemical response, as shown in Fig. 15c, indicating that aniline can be polymerized electrochemically at a low concentration in a neutral medium. To verify the polymerization on the carbon fiber electrode, the same measurement was performed using a string of fibrous carbon. The voltammetric response confirmed the presence of a polymerized film on the carbon fiber electrode surface. In the XPS spectra of this carbon fiber, a large amount of nitrogen was observed, as shown in Fig. 16. In the case of using the carbon fiber after soaking in aniline solution without applying a potential, little amount of nitrogen was found in the carbon fiber itself and after the carbon fiber was immersed in aniline solution without applying a potential. These results indicate that electrochemical polymeric aniline can be immobilized firmly on the carbon fiber surface.

The removal of aniline from aqueous solution based on electrochemical adsorption was studied using 5.0×10^{-5} M aniline solution (Fig. 17) and a bundle of carbon fiber as an anode. The concentration of aniline did not change unless a potential greater than 0.5 V was applied. A drastic decrement of aniline concentration was observed by applying a potential over 0.8 V, which corresponds to the oxidation potential of aniline. Therefore, the changes in the concentration of aniline are due to the electropolymerization, as shown in Fig. 15, rather than the hydrophobic adsorption of aniline monomer onto the carbon fiber surface. The maximum

Fig. 17 Relationship between the removal efficiency and the treatment time of aniline at varied potentials. C/C_0 : concentration/initial concentration. The treatments were performed in 0.1 M phosphate buffer solution (pH 6.0) containing 5.0×10^{-5} M aniline [25]



surface coverage of electropolymerized aniline on the carbon fiber was estimated to be 1.5×10^{-8} mol/cm², indicating that 1 g of carbon fiber can remove 1.9 mg of aniline. Unfortunately, aniline oxidation in neutral solution leads to the formation of a thin film with low conductivity, preventing further electrochemical polymerization of aniline. This limits the removal capacity of this method. However, this polymeric aniline film can be removed by sonication in an organic solvent (DMSO) or applying a high potential to generate oxygen or hydrogen.

It is well-known that *p*-benzoquinone is formed by aniline oxidation, especially under acidic solution conditions. The generation of *p*-benzoquinone by applying different potentials to the carbon fiber for 40 min in neutral medium including 5.0×10^{-5} M aniline is shown in Fig. 18. Approximately 5% of aniline was transformed into *p*-benzoquinone by applying a potential of 1.2 V for 40 min (Fig. 18). The generation of *p*-benzoquinone decreased with the decreased potential, and it became zero at a potential lower than 0.8 V. This indicates that the generation of *p*-benzoquinone can be suppressed by applying an appropriate potential. The expected reaction pathways in electrochemical adsorption caused by aniline oxidation are shown in Fig. 19. The initial stage in aniline polymerization is the oxidation of aniline monomer to form dimeric species (i.e., aminodiphenylamine, hydrazobenzene, and benzidine). While this treatment is in progress, 4-(phenylimino)-2,5-cyclohexadien-1-one (PC) and azobenzene are detected by GC-MS. PC and azobenzene are generated from aminodiphenylamine (ADPA) and hydrazobenzene, respectively. The oxidized forms of these dimers can generate polyaniline in the presence of aniline [31], because the oxidation potential of these dimers and oligomers of aniline are lower than that of aniline monomer [32]. The dimers and oligomers oxidize and conjugate with aniline monomer and form

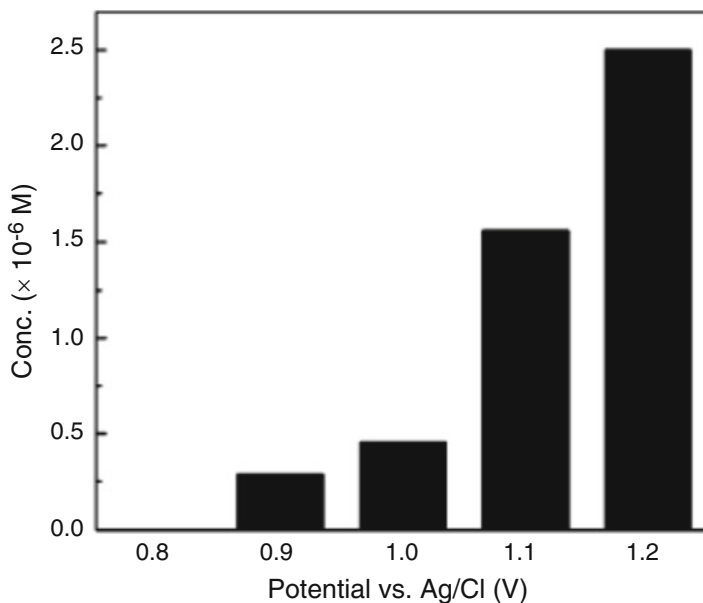


Fig. 18 Generation of *p*-benzoquinone upon electrochemical adsorption at several potentials for 40 min. The initial concentration of aniline was 5.0×10^{-5} M in 0.1 M phosphate buffer (pH 6.0). *p*-benzoquinone was identified as a byproduct by HPLC analysis [25]

polyaniline. This polymerization behavior is known as “autocatalytic behavior” [28, 30].

The continuous treatment of aniline was demonstrated using the same flow system, as shown in Fig. 11. The treatments were performed at a 5-mL/min flow rate with or without the application of a potential of 0.8 V in 0.1 M phosphate buffer solution (pH 6.0) including aniline. In the case of an applied potential of 0.8 V, 90% of aniline can be removed from 300 mL of 1.0×10^{-5} M aniline in 1 h.

2.3.2 Removal of Estrogens

Estrogen-like chemicals exist in domestic wastewater at ng/L concentrations, and the threatening effects of endocrine-disrupting chemicals on the reproductive functions of wildlife have been reported. However, estrogen-like chemicals, such as 17- β -estradiol, estrone, and synthetic estrogens, are not efficiently removed in a conventional sewage treatment plant, which aims to reduce biological oxygen demand (BOD), remove suspended solids, and disinfect. In this section, the removal of estrogens from aqueous solution by electrochemical adsorption using carbon fiber anode is introduced. This method utilizes the aromatic hydroxyl groups of estrogens for the accumulation of products on the carbon fiber surface through electrochemical oxidation reactions. The target substances to be treated were 17 β -estradiol and

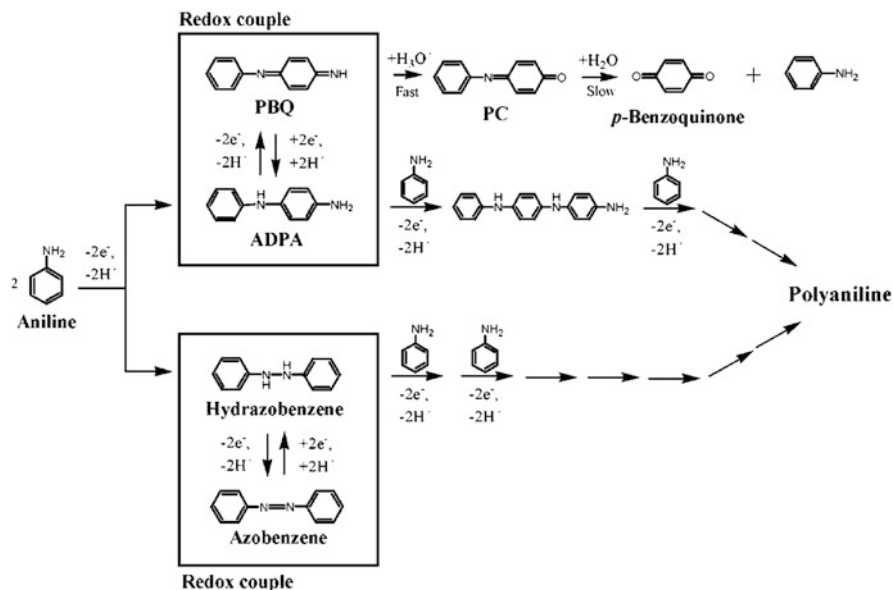


Fig. 19 Reaction pathway for the electrochemical polymerization and side reaction of low concentrations of aniline in neutral pH. PBQ: (*N*-phenyl-1,4-benzoquinonediimine), ADPA: (aminodiphenylamine), PC: (4-(phenylimino)-2,5-cyclohexadien-1-one) [25]

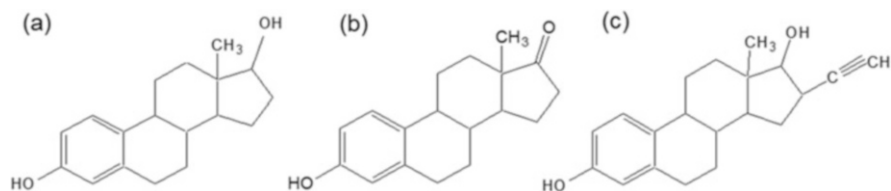


Fig. 20 Chemical structures of 17 β -estradiol, estrone, and ethynyl estradiol

estrone, which are natural estrogens possessed by humans, and ethynyl estradiol, which is a synthetic estrogen. Estrone is also produced in a reversible reaction with estradiol, although the ratio of its presence is higher than that of estradiol. Ethynyl estradiol is used widely as a birth control pill in combination with progestin and as a treatment for menstrual irregularities. Since 1999, the Pharmaceutical Affairs Law has approved pills in Japan, some of which contain a daily dose of 30–40 μ g ethynyl estradiol. The chemical structures of the target substances are shown in Fig. 20.

The progressive cyclic voltammograms of 1×10^{-4} M 17 β -estradiol, estrone, and ethynyl estradiol in 0.1 M phosphate buffer (pH 7.0) are shown in Fig. 21. All estrogens measured in this work showed an irreversible oxidation reaction derived from the hydroxyl group at 0.5 mV. As in the case of bisphenol A and its derivatives shown in Fig. 7, a decrease in the oxidation peak due to the accumulation of the target compound as a nonconductor on the electrode was observed after the repeated

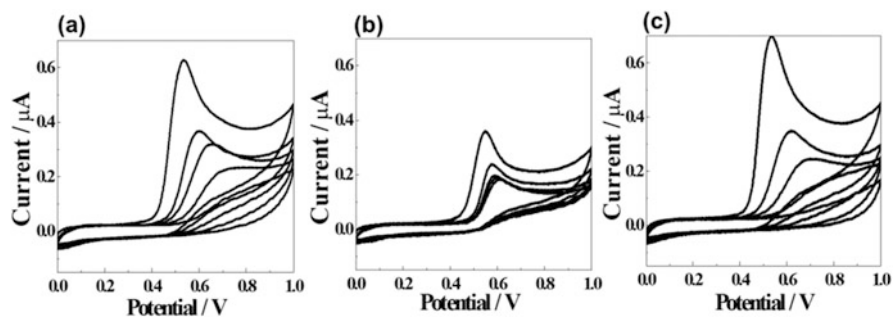


Fig. 21 Progressive cyclic voltammograms of 1×10^{-4} M (a) 17 β -estradiol, (b) estrone, and (c) ethynyl estradiol in 0.1 M phosphate buffer (pH 7.0). The measurements were performed using a glassy carbon electrode at a scan rate of 0.01 V/s. The scanning was repeated five times between 0 and 1.0 V

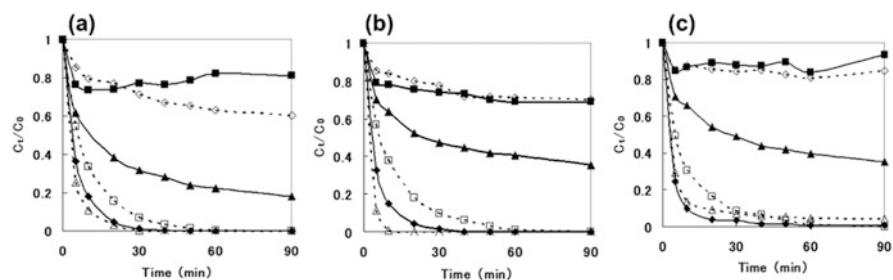


Fig. 22 Relationship between the removal efficiency and the treatment time of (a) 17 β -estradiol, (b) estrone, and (c) ethynyl estradiol at 0.4 V (open diamond), 0.5 V (filled triangle), 0.6 V (open square), 0.8 V (filled diamond), and 1.2 V (open triangle) and without a potential (filled square). The treatments were performed in 0.1 M phosphate buffer (pH 6.0) containing 1×10^{-5} M 17 β -estradiol, estrone, and ethynyl estradiol

sweeping of the potential. Slopes of -58.2 , -56.0 , and -55.6 mV/pH-unit were obtained from the linear sweep voltammograms of 1×10^{-4} M 17 β -estradiol, estrone, and ethynyl estradiol at solution pH between 2.0 and 12.0, respectively. Therefore, all the electrochemical oxidation reactions were two-electron reaction, and the continued adsorption of hydrophobic electrochemical oxidation products on the electrode surface prevented further monomer access to the electrolyte surface from bulk solution. The same behavior as that of the glassy carbon electrode was observed for all target substances when a single carbon fiber was used as the working electrode. Therefore, these estrogens can be applied for organic pollutant removal by electrochemical adsorption.

Figure 22 shows the concentration changes in 17 β -estradiol, estrone, and ethynyl estradiol solutions with an initial concentration of 1×10^{-5} M during the treatment using carbon fiber by applying different potentials. As shown in this batch-type experiment, when no potential was applied, the estrogens were hardly adsorbed on the carbon fiber surface, whereas when a potential of 0.5 V or higher was applied, the

concentration decreased significantly over time. By applying a potential of 0.6 V for 60 min, the concentration of estrogens was less than 1×10^{-7} M, which is the detection limit of the HPLC system used in this investigation. As the potential increased, the removal rate of the estrogens increased, and the concentration values decreased to below 1×10^{-7} M in 30 min. However, HPLC-UV and LC-MS results showed that byproducts were present in the solution when a potential over 1.0 were applied. The regeneration of used carbon fiber was attempted by applying a potential of -1.60 V to generate H₂, and the processing efficiency was recovered to $\sim 90\%$ in 60 min.

2.3.3 Removal of *p*-Nonylphenol

Similar to bisphenol A, *p*-nonylphenol has also attracted attention due to its potential risks as an endocrine disruptor and xenoestrogen. Alkylphenols, including *p*-nonylphenols, are used as precursors for commercially important nonionic surfactants, alkylphenol ethoxylates, and nonylphenol ethoxylates, which are used in the manufacture of antioxidants, lubricant additives, detergents, emulsifiers, solubilizers, paints, insecticides, personal care products, and plastics. *p*-Nonylphenol and its metabolites are considered biorefractory [33, 34] and toxic to aquatic organisms [35, 36].

The hydrophobic property of the alkyl chain in *p*-nonylphenol is suitable for the application of the electrochemical adsorption method. The electrochemical response of *p*-nonylphenol is typical of an irreversible electrode reaction, similar to other phenolic compounds. The oxidation peak potential of *p*-nonylphenol on the first cycle was observed as 0.3 V in 0.1 M Na₂SO₄ (pH 13.0). This value is almost the same as the oxidation potential of bisphenol A. The progressive cyclic voltammograms indicate the resulting insulating polymer film on the glassy carbon electrode surface. To evaluate the electropolymerized film formed by the oxidation of *p*-nonylphenol on the electrode surface, the changes in the electrode response of the ferrocyanide ion as a redox marker were measured. This technique can detect slight changes in electrode activity reduced by the formation of the adherent film. When the electropolymerized film was produced and adhered to the electrode surface, the peak current of the ferrocyanide ion decreased, as shown in Fig. 23. Figure 24 shows the dependence on the applied potential for the electropolymerization of *p*-nonylphenol evaluated from the electrochemical response of the ferrocyanide ion. After applying various potentials for 30 min in phosphate buffer solution (pH 9.0) involving 1.0×10^{-5} M *p*-nonylphenol, the oxidation response of potassium ferrocyanide was measured by linear sweep voltammetry. The current response of the ferrocyanide ion decreased with the increase in the applied potential and reached a constant value. The decrease in the peak current of the ferrocyanide ion was suppressed by applying at a high potential over 0.8 V due to the evolution of oxygen on the electrode surface by the electrochemical oxidation of water. The optimal potential for the electrochemical adsorption of *p*-nonylphenol was 0.6–0.8 V. The decrease in the peak current of the

Fig. 23 Cyclic voltammograms of 2.5 mM potassium ferrocyanide as a redox marker for the evaluation of the electropolymerized film of *p*-nonylphenol. The measurements were performed using a glassy carbon electrode in 0.1 M phosphate buffer (pH 7.0) at a scan rate of 0.05 V/s, after the application of a potential of 0.7 V for 5 min in 0.1 M phosphate buffer (pH 9.0) including (a) 0 M, (b) 5.0×10^{-6} M, (c) 1.0×10^{-5} M, and (d) 2.0×10^{-4} M *p*-nonylphenol [26]

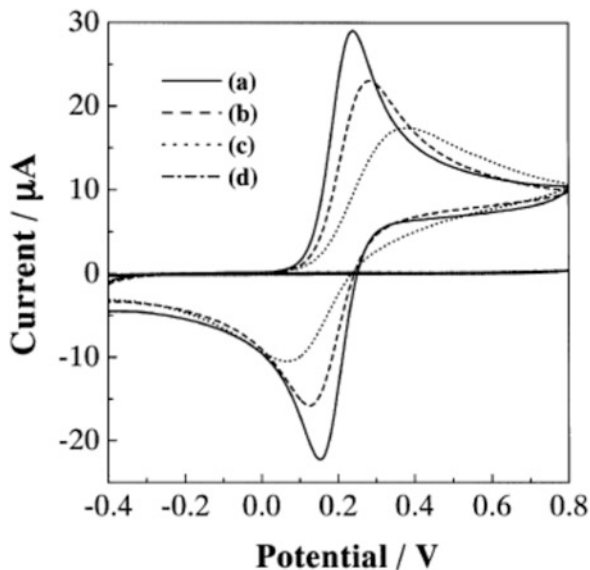
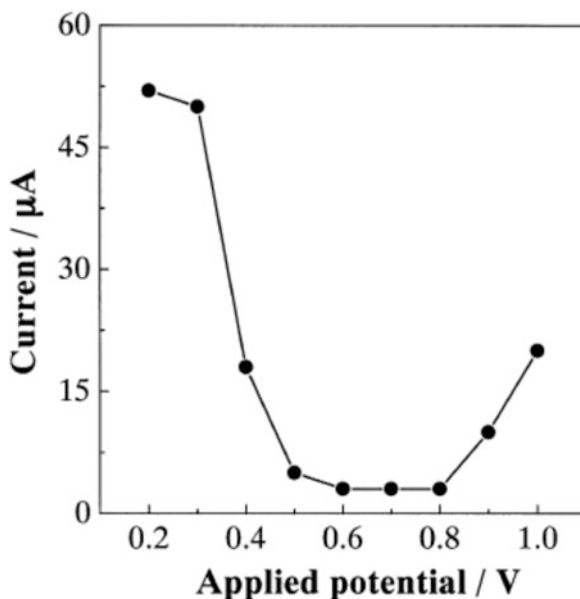


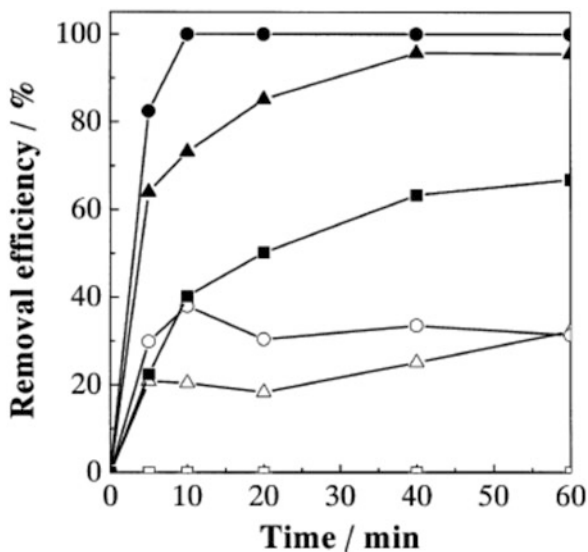
Fig. 24 Relationship between the applied potential in 0.1 M phosphate buffer (pH 9.0) including 1.0×10^{-5} M *p*-nonylphenol and the peak current of 10 mM potassium ferrocyanide obtained by linear sweep voltammetry using a glassy carbon electrode at a scan rate of 0.05 V/s [26]



ferrocyanide ion was also observed in the case of 10^{-7} M *p*-nonylphenol. Hence, even at this concentration level, the electrochemical oxidation of *p*-nonylphenol leads to the formation of an adherent film on the electrode.

The electrochemical removal of *p*-nonylphenol from an aqueous solution was attempted using carbon fibers. Figure 25 shows the removal efficiency for *p*-

Fig. 25 Relationship between the removal efficiency and the treatment time of *p*-nonylphenol with the application of a potential at 0.7 V in 5.0×10^{-6} M (filled circle), 1.0×10^{-5} M (filled triangle) and 1.0×10^{-4} M (filled square) *p*-nonylphenol in 0.1 M Na_2SO_4 (pH 5.8) and without applying a potential in 5.0×10^{-6} M (open circle), 1.0×10^{-5} M (open triangle) and 1.0×10^{-4} M (open square) *p*-nonylphenol [26]

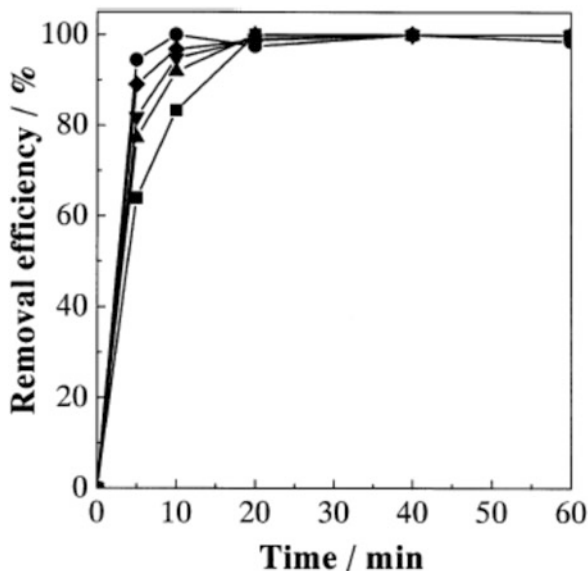


nonylphenol with or without applying a potential of 0.7 V. Without the application of potential, *p*-nonylphenol could hardly be removed, whereas a high removal efficiency was obtained with an applied potential of 0.7 V, and 100% removal was achieved within 10 min at 5.0×10^{-6} M initial concentration. The high removal efficiency is due to the electrochemical adsorption upon polymerization on the carbon fiber surface rather than hydrophobic adsorption on the carbon fiber. The maximum surface coverage of electropolymerized *p*-nonylphenol on the carbon fiber was estimated to be 5×10^{-9} mol/cm². The aromatic intermediates during electropolymerization were not observed by the HPLC system used in this study. Moreover, it was confirmed that the carbon fiber can be reused repeatedly owing to electrode regeneration. Furthermore, the applicability of the removal method at low electrolyte concentrations is highly desired. The removal ratio of *p*-nonylphenol decreased to about one-sixth when the electrolyte concentration was reduced to 1/1,000. However, since natural water contains a certain concentration of ions, this method could be applied to the removal of *p*-nonylphenol from natural water.

2.3.4 Removal of Phenol and Chlorinated Phenols

Removal of phenol and chlorinated phenols were also demonstrated using the same experimental setup described elsewhere [26]. The removal based on the electrochemical adsorption was attempted for phenol, *o*-chlorophenol, *p*-chlorophenol, 2,4-dichlorophenol, and 2,4,5-trichlorophenol. Phenol and chlorinated phenols can be found in soils and surface waters. Chlorinated phenols are mainly used to produce insecticides, antifungal agents, or pharmaceutical products. Most of them are carcinogenic, and their presence can be harmful for life. Figure 26 shows the relationship

Fig. 26 Relationship between the removal efficiency of 5.0×10^{-6} M phenol (filled square), *o*-chlorophenol (filled circle), *p*-chlorophenol (filled triangle), 2,4-dichlorophenol (inverted filled triangle), and 2,4,5-trichlorophenol (filled diamond) in 0.1 M Na_2SO_4 (pH 5.8) and the treatment time with the application of a potential [26]



between the removal efficiency of phenolic compounds (5×10^{-6} M) and the treatment time. Potentials of 0.95, 0.85, and 0.9 V were applied for the electropolymerization of phenol, *o*-chlorophenol, and other chlorophenols, respectively. The complete removal was achieved in only 20 min with all the phenolic compounds. Although trace amounts of hydroquinone/benzoquinone, catechol, and isomerized chlorophenols were observed in HPLC-UV analysis during the electropolymerization, their concentrations reached zero within 60 min [37]. Moreover, the removal of phenolic compounds was scarcely achieved unless a potential was applied. The analysis of chlorine ions was conducted by ion exclusion chromatography using a conductivity detector. However, chlorine ions could not be detected in the treated sample including 2,4-dichlorophenol for 15 and 30 min. It appears that chlorine is immobilized on the CF surface within the electropolymerized film.

2.4 Electrochemical Adsorption Using Different Electrode Materials

Water treatment based on electrochemical polymerization has been reported using several electrode materials, such as carbon nanotube-covered polyester yarns, PbO_2 , carbon, stainless steel, carbon aerogel, and polyaniline. The target compound of treatment is phenol, bisphenol, and estrogens.

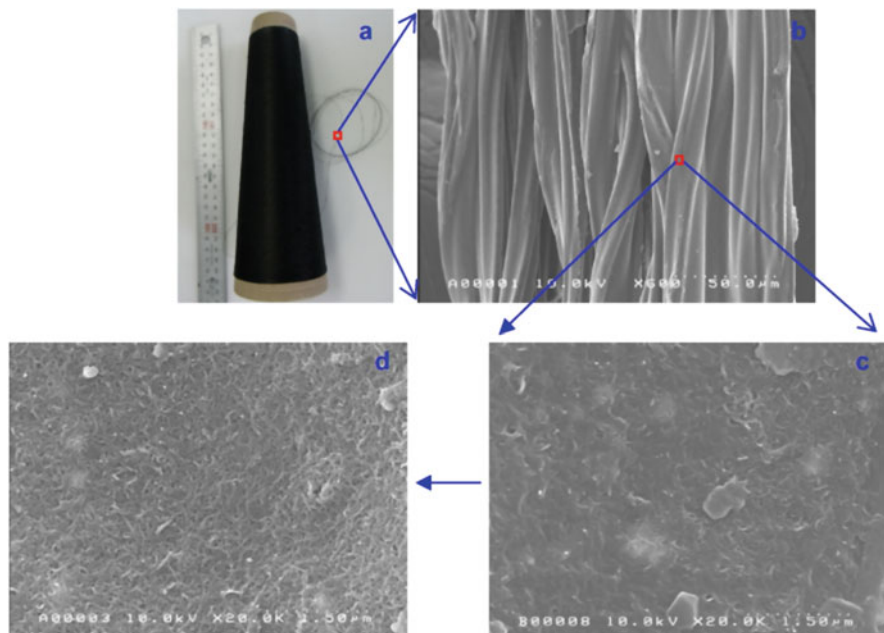


Fig. 27 (a) Photograph of the carbon nanotube-covered polyester yarns. (b) SEM image of the carbon nanotube-covered polyester yarns (c) at high-magnification before removing the binder and (d) after removing the binder [38]

2.4.1 Carbon Nanotube-Covered Polyester Yarn Electrode

The carbon nanotube-covered polyester yarn electrode was applied for bisphenol A removal by polymerization and degradation [38]. The electrode was prepared using dispersed multi-walled carbon nanotubes dyestuff, which did not contain binders and stably covered the polyester yarn surface owing to the carbon nanotube network. The carbon nanotube-covered polyester yarns (Fig. 27a) with an electric resistivity of $1,700 \Omega/\text{cm}$ were produced by a dye-print approach with the dyestuff including single dispersing multi-walled carbon nanotubes and a small amount of anionic polyurethane binder. The SEM image shows that the carbon nanotubes were coated on the polyester yarn surfaces and wrapped in the polymer (Fig. 27b, c). To produce a desired electrode, which exposes carbon nanotubes to the solution, the procedure must remove the binder and allow carbon nanotubes to remain on the surface of the polyester yarns. A washing procedure with an organic solution meets these two requirements, and ethanol as the washing liquid provides superior conductivity of the carbon nanotube-covered polyester yarns. The electric conductivity of the carbon nanotube-covered polyester yarns was improved to $87\text{--}120 \Omega/\text{cm}$, and the specific surface area was increased to $11.3 \text{ m}^2/\text{g}$.

Figure 28 shows progressive cyclic voltammograms of bisphenol A on carbon nanotube-covered polyester yarn electrode. The cyclic voltammograms exhibited

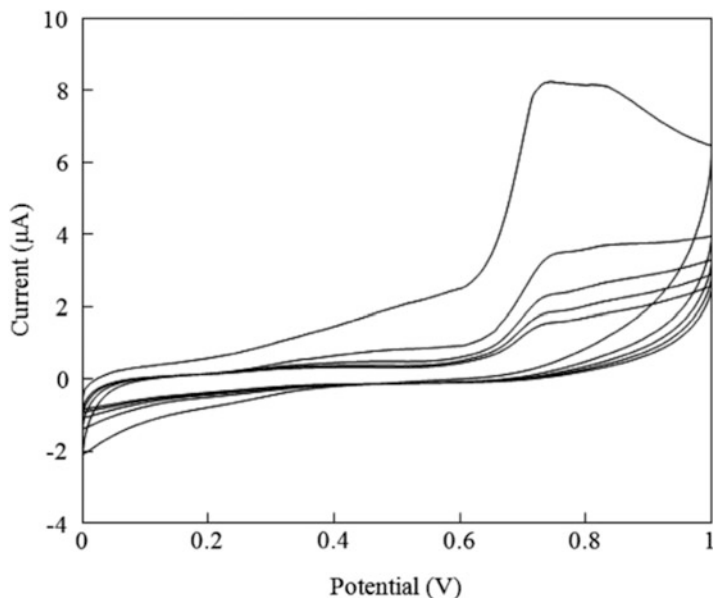


Fig. 28 Progressive cyclic voltammograms for 0.1 mM bisphenol A in 0.1 M Na_2SO_4 (pH 6.3) using the carbon nanotube-covered polyester yarn electrode. The scan rate is 50 mV/s [38]

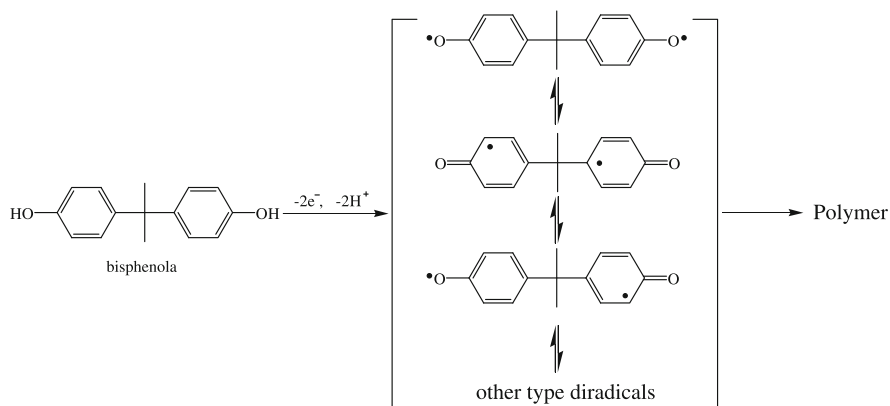


Fig. 29 Schematic diagram of the electrochemical polymerization of bisphenol A [38]

irreversible behavior, and the anodic peak height showed a gradual decrease as the scan number increased since no electrochemical active layer was formed on the electrode surface. As described in previous reports, the phenolic compounds can be electrochemically oxidized to produce phenoxyl radicals and then form dimers, which can then be further oxidized to form new radicals that couple with other radicals to produce polymers [39]. BPA is a special phenolic compound, which can be oxidized to generate some types of diradicals (Fig. 29). These diradicals continuously and randomly couple and easily form polymers.

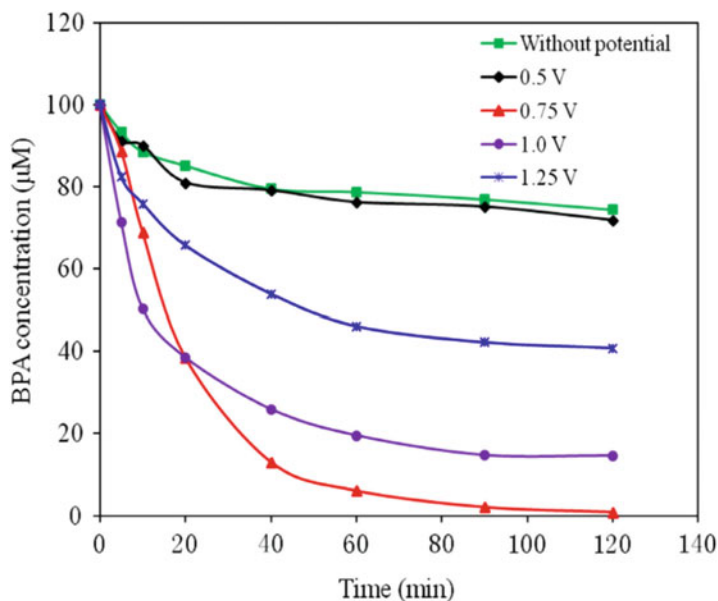


Fig. 30 Relationship between residual bisphenol A (in solution) and the treatment time at a series of applied potentials in 0.1 mM bisphenol A solution containing 0.1 M Na_2SO_4 (pH 6.3) using the carbon nanotube-covered polyester yarn electrode [38]

A series of applied potentials were investigated to evaluate the optimal potential for the efficient removal of bisphenol A (Fig. 30). The carbon nanotube-covered polyester yarns showed adsorptive capacity even without an applied potential. At a low anodic potential (0.5 V), no effect was observed on the removal of bisphenol A compared to that with no applied potential. The best removal efficiency was observed when the anodic potential was increased to 0.75 V. At higher values of the applied potential such as 1.0 or 1.25 V, the removal efficiencies decreased, which may have contributed to the occurrence of water degradation. Figure 31 shows the amount of organic carbon except bisphenol A in the residual electrolyte. These results reveal that the degradation as well as polymerization of bisphenol A occurred on the carbon nanotube-covered polyester yarn electrode. The electrochemical oxidative degradation of organic pollutants was performed on metal or metal oxide electrodes. In this work, the polymerization and degradation of bisphenol A play important roles by providing good removal efficiency at an applied potential of 0.75 V. The adsorption capacity of this electrode was 2.3×10^{-5} mol/g without an applied potential. The electrochemical removal efficiency was 8.1×10^{-5} mol/g under an applied potential of 0.75 V. The removal efficiency for the carbon nanotube-covered polyester yarn electrode was higher than that of a commercially available carbon fiber electrode. The close-packed adsorption between the curved surface of carbon nanotubes and the butterfly-shaped bisphenol A [40] may have contributed much to the high efficiency. Notably, a subsequent study found that this

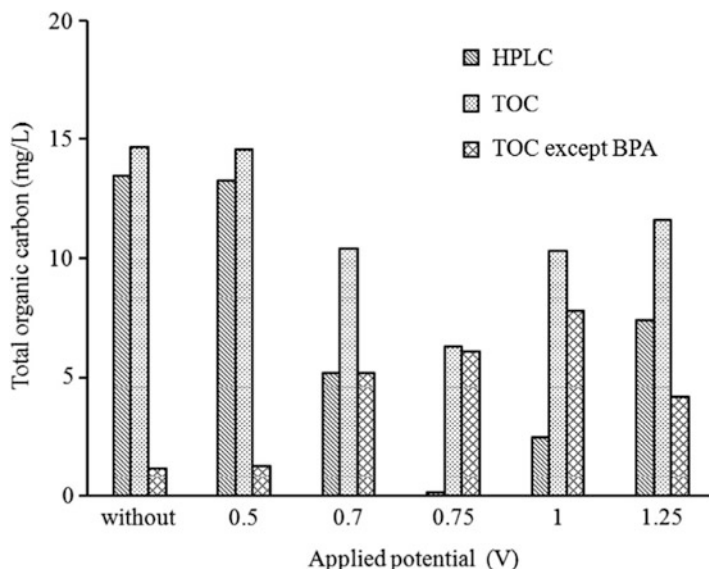


Fig. 31 Amount of organic carbon except bisphenol A in residual electrolyte calculated from the residual bisphenol A based on HPLC analysis and total carbon by TOC measurement in bisphenol A solution (initial concentration: 0.1 mM) containing 0.1 M Na₂SO₄ (pH 6.3) after 2-h electrochemical treatment at various applied potentials [38]

electrode can be reutilized after the bisphenol A polymer layer was stripped by applying a potential of 2 V in 0.1 M Na₂SO₄.

2.4.2 PbO₂ Electrode

The electrochemical removal of phenol from aqueous solution based on anodic polymerization using a PbO₂ electrode has been proposed by Tahar and Savall [39]. The polymer was formed in an alkaline solution by a process involving less than two electrons per molecule of phenol, precipitated by decreasing the solution pH, and finally filtered and disposed. The electrochemical polymerization of phenol ($C_0 = 0.105$ M) in alkaline solution (pH 13) at 86°C has been studied by galvanostatic electrolysis using a range of anode materials characterized by different O₂ overpotentials, such as IrO₂, Pt, and β-PbO₂. TOC and HPLC results have been used to follow phenol oxidation and perform the SEM of the polymer deposited on the electrode surface. The fractions of phenol converted in polymers were 25, 32, and 39% for Ti/IrO₂, Pt, and Ta/β-PbO₂, respectively, a series of materials in which the O₂-overvoltage increases. Results of bulk electrolysis conducted on Ta/β-PbO₂ at high anodic current density (200 mA/cm²) have shown that 39% of the starting phenol can be removed as polymers dispersed in the reactor under the best operating conditions. Polymeric films formed in the alkaline solution did not

fully deactivate the anodes. The use of a high anodic current density (in the potential region of water decomposition) avoids anode fouling but simultaneously favors the oxidation of the polymeric film and oxygen evolution, leading to current yield around 20%.

2.4.3 Carbon Electrode

Zareie et al. [41] reported the removal of phenol from wastewater in the form of non-passivating polymer suspended in the reactor can be achieved using a carbon electrode and high anodic current density in the presence of NaCl. The most orderly polymer formed at an initial phenol concentration of 912 mg/L, current density of 32.9 mA/cm², and NaCl concentration of 120 g/L at 25°C (Fig. 32). Higher operational parameters yielded disorderly formed polymer aggregates with decreased surface density, as shown in STM images. Along with the polymer, only toxic mono-, di-, and trichlorophenols were formed as intermediate compounds during electrochemical conversion, which were polymerized and/or oxidized to final products. FT-IR analysis and the enlarged STM image implied the repeating phenol units in the polymer structure. The renewal of the oxidizing agent formed at the electrode by agitation likely caused most of the phenol oxidation to occur in the bulk solution without electrode fouling. This process requires the use of large amounts of salt but offers the removal of phenol from wastewater in the form of a solid polymer.

Tahar and Savall reported the electrochemical polymerization of phenol on a vitreous carbon electrode in alkaline and acidic aqueous solution at different temperatures in the range of 25–85°C by cyclic voltammetry and chronoamperometry

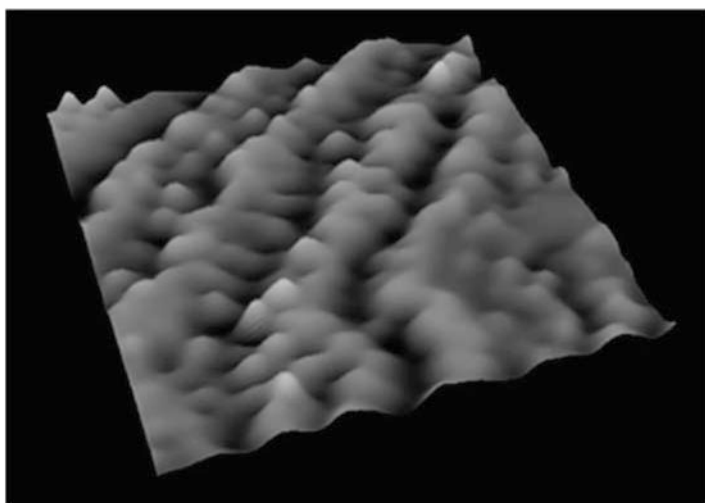


Fig. 32 STM image (20 nm × 20 nm) of the polymer (current density: 32.9 mA/cm²; NaCl concentration: 120 g/L; temperature: 25°C; initial phenol concentration: 912 mg/L [41])

[42, 43]. The electrochemical oxidation of phenol in the alkaline solution led to the complete deactivation of the electrode, irrespective of the temperature used, as a result of the deposition of the adhesive and the insulating polymeric film. The electrochemical activity of the electrode was progressively restored by repeated potential scans in the range of water stability only when conducted at high temperatures. The electrode reactivation was explained by the increase in the polymeric film permeability for both electrons (electron tunneling) and phenol molecules (diffusion). Chronoamperometric measurements conducted in the potential region of water stability have shown that electrode passivation was reduced or prevented at high temperatures. For chronoamperometry performed at the onset of oxygen evolution, the electrode remained active even at low temperatures because the discharge of water involved the production of hydroxyl radicals that destructively oxidized the polymeric film. The effect of temperature on electrode reactivation was determined by current measurement at an electrolysis time of 300 s; an increase of the temperature from 25 to 85°C amplified the current from 0.212 to 5.373 mA. In the acidic aqueous solution, the repeated potential scans in the region of water stability did not reactivate the electrode, irrespective of the temperature used. Chronoamperometric curves recorded at different potentials in the region of water decomposition showed that the electrochemical activity of the electrode was partially restored even when performed at low temperature (25°C).

Sakakibara et al. reported the continuous treatments of trace endocrine-disrupting chemicals, such as estrone, 17 β -estradiol, ethinyl estradiol, bisphenol A, *p*-nonylphenol, 4-t-octyl phenol, and pentachlorophenol using a multi-packed granular glassy carbon electrode reactor [44–46]. Figure 33 shows the interior of the reactor and its configurations in continuous treatments of estrogens. The reactor consists of two compartments filled up with glassy carbon (or Pt/Ti) granular anodes

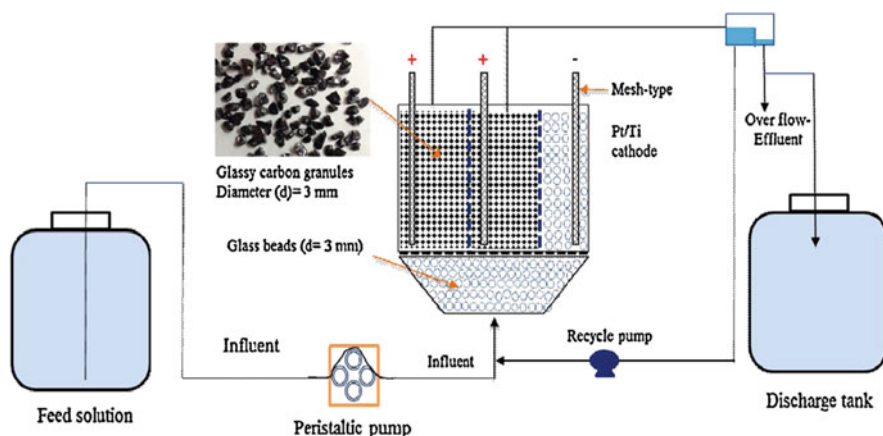


Fig. 33 Electrolytic reactor equipped with a multi-packed granular glassy carbon electrode for continuous treatments of estrogens through the polymerization and regeneration of electrolytic cells [46]

and a Pt/Ti mesh cathode. The total liquid volume and surface area of anodes were about 500 mL and 2,000 cm², respectively. A portion of the liquid inside the anode compartments was recycled to ensure completely mixed conditions. The cathode and anode chambers were separated by a porous Teflon sheet and glass beads. Experimental results showed that the target chemicals were effectively removed through electropolymerization on the granular glassy carbon (and Pt/Ti) by the reactor over 150 days. The removal efficiencies were nearly the same in the presence and absence of humic substances. The morphology of the passivated electrode was analyzed using SEM and compared with that of the unused electrode. As shown in Fig. 34b, the accumulation of a thick polymer layer (approx. 1 μm) over 95 days for 1 μg/L ethinyl estradiol was obtained, while the new electrode displayed a smooth surface (Fig. 34a). This proposed system can achieve the removal of trace estrogens and the regeneration of electrolytic cells simultaneously for long-term wastewater treatment. Figure 35 shows the result of the continuous treatment of ethinyl estradiol over the

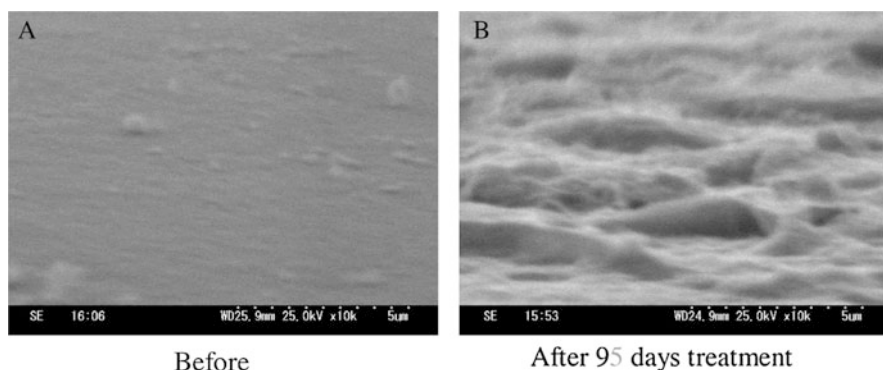


Fig. 34 SEM analysis of glassy carbon surfaces after continuous treatments of 1 μg/L ethinyl estradiol [46]

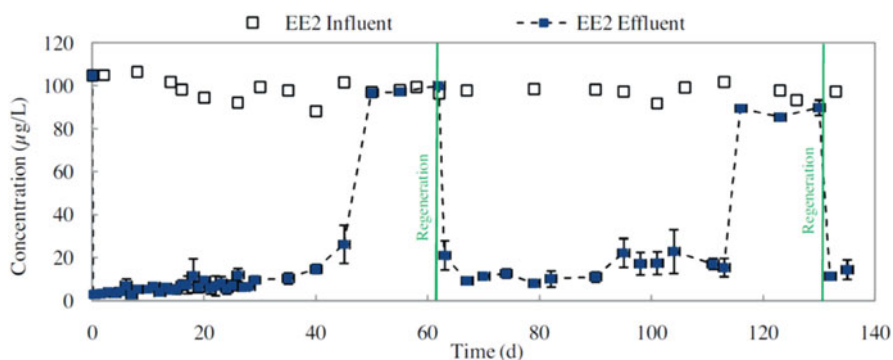


Fig. 35 Continuous treatment of ethinyl estradiol and electrode regeneration [46]

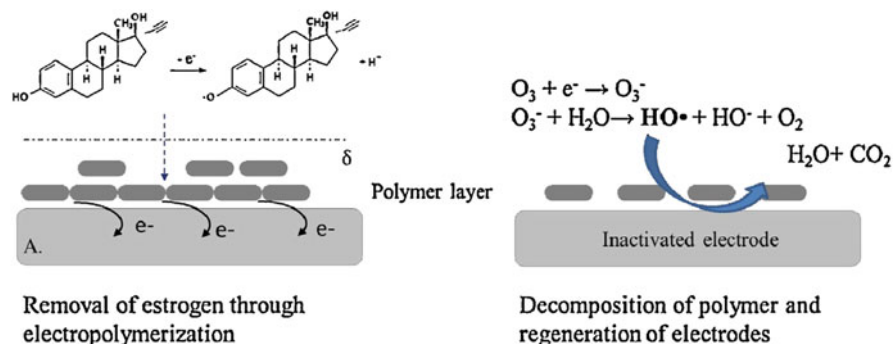


Fig. 36 Proposed mechanism of the electrochemical polymerization of ethinyl estradiol and electrode regeneration [46]

course of 135 days. Experimental results indicate an effective removal and recovery of the electrode after regenerations. The removal of ethinyl estradiol was observed through three stages. The first stage shows a stable removal of ethinyl estradiol. The second stage shows an increase of effluent concentration approaching the influent, and the third stage shows a steady state of passivation. The applied potential from 0.8 to 1.0 V indicated that the first stage denotes the removal of ethinyl estradiol through the polymerization process. The passivation of the electrode in stage 2 could be explained by the formation of the polymeric layer on the surface of the electrodes. The polymer formed during continuous treatment was quickly decomposed, and electrodes were regenerated completely by $\cdot\text{OH}$ radicals produced through the reduction of ozone. Figure 36 illustrates a proposed mechanism of the electrochemical polymerization of ethinyl estradiol occurring on the anode surface and the regeneration of the passivated electrodes. Ethinyl estradiol in the bulk solution approaches the electrode surface through a diffusion mechanism. On the anode, one electron is transferred, and ethinyl estradiol is deprotonated to form a phenoxy radical. Further chemical reactions are denoted to dimer and/or semiconducting polymer formation. The regeneration of the passivated electrode was conducted based on the oxidative capacity of $\cdot\text{OH}$ radicals, which can decompose almost all organic chemicals. The decomposition of the polymer was conducted in the presence of 1.8 and 3.0 mg/L dissolved ozone combined with polarization for 120 and 30 min, respectively. During the regeneration process, the passivated electrodes function as cathodes, which allow the reduction of the dissolved ozone into $\cdot\text{OH}$ radicals. After regenerations, ethinyl estradiol was removed effectively, and the electrolytic reactor has worked properly for a period of 50 days before the second regeneration. This result indicates the feasibility of the simultaneous removal and regeneration of the electrode for continuous treatment of estrogen. Calculated overall energy consumptions were less than 10 Wh/m^3 , demonstrating extremely low energy dependency of the method.

2.4.4 Stainless Steel Electrode

Zhang et al. reported the electrochemical polymerization treatment of phenol in wastewater and the reclamation of phenol using stainless steel anodes [47]. The electrochemical polymerization reaction was analyzed by cyclic voltammetry, and the polyphenol product was analyzed by SEM and FT-IR. The effects of phenol concentration and bath voltage were investigated using the solution with an original COD value of approximately 500 mg/L. After the electrochemical polymerization treatment, the concentration of phenol was 0.087 mM with a removal efficiency of 95.6%, and COD was 68 mg/L with a removal efficiency of 86.5%.

2.4.5 Carbon Aerogel Electrode

Carbon aerogels are highly porous, amorphous, nanostructured, sponge-like materials prepared by a sol-gel process. The treatments based on electrochemical polymerization using carbon aerogels as an anode have been reported for phenol, 2-chlorophenol, and bisphenol A [48, 49]. Grinberg et al. reported that the electropolymerized films formed from phenol and derivatives strongly adhere to carbon aerogel and are homogeneously distributed in the pores using cyclic potential from 0 to 0.8 V [48]. Hou et al. reported the removal of bisphenol A using a carbon aerogel electrode with a large specific surface area (445 m²/g) and mesoporosity [49]. For treating 0.1 mM bisphenol A in neutral pH solution (PBS, pH 7), the removal capacity using potential cycling in the range of 0–0.8 V can be enhanced to 0.029 mmol/g. This value was much higher than that of adsorption without applying a potential (0.010 mmol/g), suggesting that the enhanced removal of bisphenol A from water can be successfully achieved using carbon aerogel electrodes by electrooxidation via phenoxy radicals, associated with the deposition of the electrochemically polymerized poly(bisphenol A) film on the electrode surface. Additionally, the generation of other toxic intermediates was restricted by applying relatively low voltages below the potential of oxygen evaluation. Therefore, this study can provide a possible route to treating bisphenol A solutions at low concentrations by electrochemical polymerization with highly porous carbon electrode materials.

2.4.6 Polyaniline Electrode

The removal of phenols from the aqueous solutions using polyaniline electrodes has been achieved by Zhai et al. [50]. The polyaniline coated on a glassy carbon electrode was prepared in a solution containing 0.2 M aniline and 1.0 M HCl at 0.75 V. Phenol and 3-nitrophenol in an aqueous solution including 0.1 M NaCl at pH 4.0 can be polymerized on the polyaniline electrode to form polyaniline/polyphenol and polyaniline/poly(3-nitrophenol) composites, respectively. NaCl helps in avoiding the second pollutant discharge; and considering the fact that polyaniline

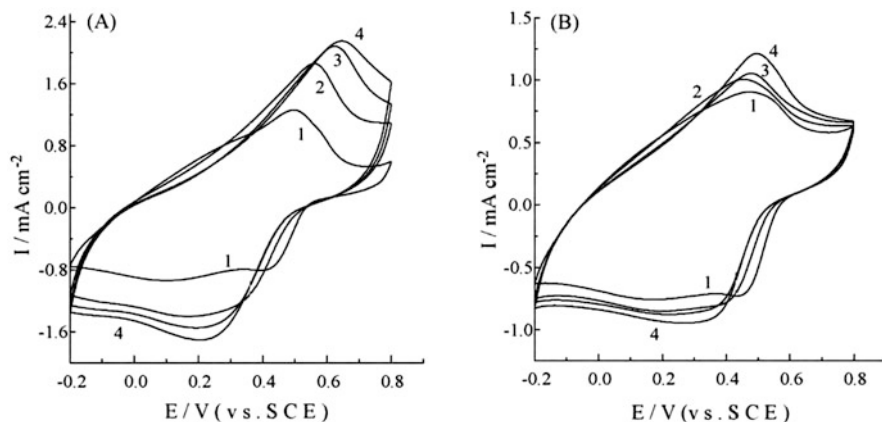


Fig. 37 (a) Cyclic voltammograms of polyaniline electrode in 0.1 M NaCl at pH 4.0 (Curve 1) and polyaniline/polyphenol and (b) polyaniline/poly(3-nitrophenol) in 0.1 M NaCl at pH 4.0 (Curves 2–4) synthesized by potential cycling (shown in Fig. 37) using 20, 40, and 60 cycles, respectively, at a scan rate of 60 mV/s [50]

lost its redox activity at $\text{pH} > 4.0$, the pH value of the NaCl solution was controlled at pH 4.0 in this work. Polyaniline plays a vital role in lowering the passivation of the electrode, which enabled the consecutive electrochemical polymerization of phenol and 3-nitrophenol. The growth of the polyaniline/polyphenol and polyaniline/poly(3-nitrophenol) films in the electrolytic process was proved by the increased area of the cyclic voltammograms as the electrolysis proceeded. Curve 1 in Fig. 37 shows the cyclic voltammogram of the polyaniline electrode. Curves 2–4 in Fig. 37a show the cyclic voltammograms of polyaniline/polyphenol in 0.1 M NaCl solution at pH 4.0, which were obtained from 20, 40, and 60 cycles using potential cycling in 5 mM phenol, respectively. The area of Curve 2 is larger than that of Curve 1, indicating that phenol was polymerized on the polyaniline electrode, and the quantity of electricity of Curve 2 became larger than that of Curve 1. Figure 37a shows that the oxidation peak potential shifts toward the positive potentials as the potential cycle for the synthesis of polyphenol increases, which is mainly attributed to the IR drop of the polyaniline/polyphenol film due to the low conductivity of polyphenol. The increase in the area of cyclic voltammograms and the shift in the oxidation peak potential toward the positive potential direction indicate the growth of the polymer film. Figure 37b shows similar results obtained from polyaniline/poly(3-nitrophenol). These results demonstrate that phenol and 3-nitrophenol in the aqueous solution can be removed by electrochemical polymerization on the polyaniline electrode.

The SEM images show that the polyaniline film consisted of interwoven nanofibers with an average diameter of 55 nm with lengths varying from 240 to 310 nm. The phenolic polymers were formed on the polyaniline nanofibers and the neighboring polyaniline nanofibers, indicating that the presence of polyaniline nanofibers is advantageous to the formation of the phenolic polymers on polyaniline

since the catalytic activity of polyaniline is mainly attributed to the free radicals in polyaniline. The nanostructures of polyaniline provide a large specific surface area, which increases the impact possibility between the free radicals in polyaniline and reactants and phenolic compounds. As a result, the nanostructures of polyaniline play a key role in enhancing the electrochemical catalytic polymerization rates of phenolic monomers. The IR spectra of polyaniline/polyphenol and polyaniline/poly(3-nitrophenol) composites differed from that of polyaniline, which is also supported by the phenolic polymers polymerized on the polyaniline electrode.

3 Conclusions

Electrochemical adsorption is an efficient water treatment method for the removal of organic pollutants from water. In this method, target organic compounds can undergo an electrochemical reaction, and the obtained compounds can be accumulated on the electrode surface. Unlike conventional adsorption approaches pursuing the functionalization of the adsorbent, this method aims to remove target organic contaminants by changing their adsorption properties through electrochemical oxidation reactions, including electrochemical polymerization. Therefore, the electrode functions as both an electrochemical catalyst and an adsorbent. Electrochemical adsorption methods have been applied to the removal of bisphenol A and its derivatives, aniline, estrogens, and other phenol derivatives using carbon fiber electrodes possessing a large surface area and excellent electrical conductivity. In this method, a target organic pollutant is accumulated on the carbon fiber anode surface at a low potential using a low current density. Therefore, this method offers a low-cost and environmentally friendly approach to removing organic pollutants from water because it does not require the generation of hydroxyl radicals, unlike electrochemical decomposition methods using DSAs for the mineralization of organic pollutants. In addition, continuous treatments have been achieved for several organic pollutants using the flow system with a column-type carbon fiber electrode. Progress has been made in electrochemical adsorption for the removal of phenolic compounds including phenol, bisphenol A, and estrogen using various electrode materials, such as carbon nanotube-covered polyester yarns, PbO_2 , granular carbon, stainless steel, carbon aerogel, and polyaniline. Methods for the regeneration of electrodes, which act as adsorbents, have also been demonstrated by washing and electrolysis. Moreover, a system for long-term wastewater treatment that can simultaneously remove organic pollutants and regenerate electrodes has been reported. By tailoring the function of the electrode used as an adsorbent and catalyst in electrochemical adsorption, it is expected that the electrochemical method can be applied to the treatment of other organic pollutants in the future.

References

1. Feng Y, Yang L, Liua J, Logan BE (2016) Electrochemical technologies for wastewater treatment and resource reclamation. *Environ Sci Water Res Technol* 2:800–831. <https://doi.org/10.1039/C5EW00289C>
2. Titchou FE, Zazou H, Afanga H, Gaayda JE, Akbour RA, Nidheesh PV, Hamdani M (2021) An overview on the elimination of organic contaminants from aqueous systems using electrochemical advanced oxidation processes. *J Water Process Eng* 41:102040. <https://doi.org/10.1016/j.jwpe.2021.102040>
3. Cong VH, Sakakibara Y, Komori M, Kishimoto N, Watanabe T, Mishima I, Ihara I, Tanaka T, Yoshida Y, Ozaki H (2016) Recent developments in electrochemical technology for water and wastewater treatments. *J Water Environ Technol* 14(2):25–36. <https://doi.org/10.2965/jwet.15-029>
4. Torres NH, Santos GOS, Ferreira LFR, Américo-Pinheiro JHP, Eguiluz KIB, Salazar-Banda GR (2021) Environmental aspects of hormones estriol, 17 β -estradiol and 17 α -ethinylestradiol: electrochemical processes as next-generation technologies for their removal in water matrices. *Chemosphere* 267:128888. <https://doi.org/10.1016/j.chemosphere.2020.128888>
5. Krstić V, Pešovski B (2019) Reviews the research on some dimensionally stable anodes (DSA) based on titanium. *Hydrometallurgy* 185:71–75. <https://doi.org/10.1016/j.hydromet.2019.01.018>
6. Comninellis C, Pulgarin C (1993) Electrochemical oxidation of phenol for wastewater treatment using SnO₂ anodes. *J Appl Electrochem* 23:108–112. <https://doi.org/10.1007/BF00246946>
7. Comninellis C, Nerini A (1995) Anodic oxidation of phenol in the presence of NaCl for wastewater treatment. *J Appl Electrochem* 25:23–28. <https://doi.org/10.1007/BF00251260>
8. Rodgers JD, Jedral W, Bunce NJ (1999) Electrochemical oxidation of chlorinated phenols. *Environ Sci Technol* 33:1453–1457. <https://doi.org/10.1021/es9808189>
9. Polcaro AM, Palmas S, Renoldi F, Mascia M (2000) Three-dimensional electrodes for the electrochemical combustion of organic pollutants. *Electrochim Acta* 46:389–394. [https://doi.org/10.1016/S0013-4686\(00\)00596-X](https://doi.org/10.1016/S0013-4686(00)00596-X)
10. Krishnan AV, Stathis P, Permuth SF, Tokes L, Feldman D (1993) Bisphenol-A: an estrogenic substance is released from polycarbonate flasks during autoclaving. *Endocrinology* 132:2279–2286. <https://doi.org/10.1210/en.132.6.2279>
11. Cui YH, Li XY, Chen GH (2009) Electrochemical degradation of bisphenol A on different anodes. *Water Res* 43(7):1968–1976. <https://doi.org/10.1016/j.watres.2009.01.026>
12. Korshin GV, Kim J, Gan LL (2006) Comparative study of reactions of endocrine disruptors bisphenol A and diethylstilbestrol in electrochemical treatment and chlorination. *Water Res* 40(5):1070–1078. <https://doi.org/10.1016/j.watres.2009.01.026>
13. Boscolo Boscoletto A, Gottardi F, Milan L, Pannocchia P, Tartari V, Tavan M (1994) Electrochemical treatment of bisphenol-A containing wastewaters. *J Appl Electrochem* 24:1052–1058. <https://doi.org/10.1007/BF00241198>
14. Tanaka S, Nakata Y, Kimura T, Yustiawati, Kawasaki M, Kuramitz H (2002) Electrochemical decomposition of bisphenol A using Pt/Ti and SnO₂/Ti anodes. *J Appl Electrochem* 32:197–201. <https://doi.org/10.1023/A:1014762511528>
15. Murugananthan M, Yoshihara S, Rakuma T, Shirakashi T (2008) Mineralization of bisphenol A (BPA) by anodic oxidation with boron-doped diamond (BDD) electrode. *J Hazard Mater* 154(1–3):213–220. <https://doi.org/10.1016/j.jhazmat.2007.10.011>
16. Zaviska F, Drogui P, Blais JF, Mercier G (2012) Electrochemical treatment of bisphenol-A using response surface methodology. *J Appl Electrochem* 42:95–109. <https://doi.org/10.1007/s10800-011-0376-y>
17. Comninellis C, Vercesi GP (1991) Characterization of DSA[®]-type oxygen evolving electrodes: choice of a coating. *J Appl Electrochem* 21:335–345. <https://doi.org/10.1007/BF01020219>
18. Gattrell M, Kirk DW (1993) A study of the oxidation of phenol at platinum and preoxidized platinum surfaces. *J Electrochem Soc* 140:1534–1540. <https://doi.org/10.1149/1.2221598>

19. Ioto PI, Kalcheva SV (1998) Mechanistic approach to the oxidation of phenol at a platinum/gold electrode in an acid medium. *J Electroanal Chem* 442(1–2):19–26. [https://doi.org/10.1016/S0022-0728\(97\)00455-5](https://doi.org/10.1016/S0022-0728(97)00455-5)
20. Del Olmo M, Zafra A, Gonzalez-casado A, Vilchez JL (1998) The use of β -cyclodextrin inclusion complexes for the analysis of bisphenol A residues in water by spectrofluorimetry. *Int J Environ Anal Chem* 69(1):99–110. <https://doi.org/10.1080/03067319808032577>
21. Kuramitz H, Nakata Y, Kawasaki M, Tanaka S (2001) Electrochemical oxidation of bisphenol A. Application to the removal of bisphenol A using a carbon fiber electrode. *Chemosphere* 45(1):37–43. [https://doi.org/10.1016/S0045-6535\(01\)00032-7](https://doi.org/10.1016/S0045-6535(01)00032-7)
22. Kuramitz H, Matsushita M, Tanaka S (2004) Electrochemical removal of bisphenol A based on the anodic polymerization using a column type carbon fiber electrode. *Water Res* 38(9):2331–2338. <https://doi.org/10.1016/j.watres.2004.02.023>
23. Papouchado L, Sandford RW, Petrie G, Adams RN (1975) Anodic oxidation pathways of phenolic compounds. 2. Stepwise electron transfer and coupled hydroxylations. *J Electroanal Chem* 65:275–284. [https://doi.org/10.1016/0368-1874\(75\)85123-9](https://doi.org/10.1016/0368-1874(75)85123-9)
24. Nanayama Y, Sazawa K, Yustiawati Y, Syawal MS, Fukushima M, Kuramitz H (2021) Effect of humic acids on the toxicity of pollutants to *Chlamydomonas reinhardtii*: investigation by a microscale algal growth inhibition test. *Environ Sci Pollut Res* 28:211–219. <https://doi.org/10.1007/s11356-020-10425-8>
25. Matsushita M, Kuramitz H, Tanaka S (2005) Electrochemical oxidation for low concentration of aniline in neutral pH medium: application to the removal of aniline based on the electrochemical polymerization on a carbon fiber. *Environ Sci Technol* 39(10):3805–3810. <https://doi.org/10.1021/es040379f>
26. Kuramitz H, Saitoh J, Hattori T, Tanaka S (2002) Electrochemical removal of *p*-nonylphenol from dilute solutions using a carbon fiber anode. *Water Res* 36(13):3323–3329. [https://doi.org/10.1016/S0043-1354\(02\)00040-4](https://doi.org/10.1016/S0043-1354(02)00040-4)
27. Zok S, Goerge G, Kalsch W, Nagel R (1991) Bioconcentration, metabolism and toxicity of substituted anilines in zebrafish (*Brachydanio rerio*). *Sci Total Environ* 109(110):411–421. [https://doi.org/10.1016/0048-9697\(91\)90196-L](https://doi.org/10.1016/0048-9697(91)90196-L)
28. Duić L, Mandić Z, Kovač S (1995) Polymer-dimer distribution in the electrochemical synthesis of polyaniline. *Electrochim Acta* 40(11):1681–1688. [https://doi.org/10.1016/0013-4686\(95\)00086-T](https://doi.org/10.1016/0013-4686(95)00086-T)
29. Yang H, Bard AJ (1992) The application of fast scan cyclic voltammetry. Mechanistic study of the initial stage of electropolymerization of aniline in aqueous solutions. *J Electroanal Chem* 339(1–2):423–449. [https://doi.org/10.1016/0022-0728\(92\)80466-H](https://doi.org/10.1016/0022-0728(92)80466-H)
30. Stilwell DE, Park SM (1988) Electrochemistry of conductive polymers II. Electrochemical studies on growth properties of polyaniline. *J Electrochem Soc* 135:2254–2262. <https://doi.org/10.1149/1.2096248>
31. Shim YB, Won MS, Park SM (1990) Electrochemistry of conductive polymers VIII: in situ spectroelectrochemical studies of polyaniline growth mechanisms. *J Electrochem Soc* 137:538–544. <https://doi.org/10.1149/1.2086494>
32. Gospodinova N, Terlemezyan L (1998) Conducting polymers prepared by oxidative polymerization: polyaniline. *Prog Polym Sci* 23:1443–1484. [https://doi.org/10.1016/S0079-6700\(98\)00008-2](https://doi.org/10.1016/S0079-6700(98)00008-2)
33. Ahel M, Conrad T, Giger W (1987) Persistent organic chemicals in sewage effluents. 3. Determinations of nonylphenoxy carboxylic acids by high-resolution gas chromatography/mass spectrometry and high-performance liquid chromatography. *Environ Sci Technol* 21:697–703. <https://doi.org/10.1021/es00161a011>
34. Giger W, Brunner PH, Schaffner C (1984) 4-Nonylphenol in sewage sludge: accumulation of toxic metabolites from nonionic surfactants. *Science* 225:623–625. <https://doi.org/10.1126/science.6740328>

35. Argese E, Marcomini A, Miana P, Bettiol C, Perin G (1994) Submitochondrial particle response to linear alkylbenzenesulfonates, nonylphenol polyethoxylates and their biodegradation derivatives. *Environ Toxicol Chem* 13:737–742. <https://doi.org/10.1002/etc.5620130507>
36. McLeese DW, Zitko V, Sergeant DB, Burridge L, Metcalfe CD (1981) Lethality and accumulation of alkylphenols in aquatic fauna. *Chemosphere* 10:723–730. [https://doi.org/10.1016/0045-6535\(81\)90003-5](https://doi.org/10.1016/0045-6535(81)90003-5)
37. Boudenne J-L, Cerclier O (1999) Performance of carbon blacks-lurry electrode for 4-chlorophenol oxidation. *Water Res* 33:494–504. [https://doi.org/10.1016/S0043-1354\(98\)00242-5](https://doi.org/10.1016/S0043-1354(98)00242-5)
38. He J, Hongwen Y, Fugetsu B, Tanaka S, Sun L (2013) Electrochemical removal of bisphenol A using a CNT-covered polyester yarn electrode. *Sep Purif Technol* 110:81–85. <https://doi.org/10.1016/j.seppur.2013.03.011>
39. Tahar NB, Savall A (2009) Electrochemical removal of phenol in alkaline solution. Contribution of the anodic polymerization on different electrode materials. *Electrochim Acta* 54:4809–4816. <https://doi.org/10.1016/j.electacta.2009.03.086>
40. Pan B, Lin D, Mashayekhi H, Xing B (2008) Adsorption and hysteresis of bisphenol A and 17 α -ethinyl estradiol on carbon nanomaterials. *Environ Sci Technol* 42:5480–5485. <https://doi.org/10.1021/es8001184>
41. Zareie MH, Körbahti BK, Tanyolaç A (2001) Non-passivating polymeric structures in electrochemical conversion of phenol in the presence of NaCl. *J Hazard Mater* 87(1–3):199–212. [https://doi.org/10.1016/S0304-3894\(01\)00278-3](https://doi.org/10.1016/S0304-3894(01)00278-3)
42. Tahar NB, Savall A (2009) Electropolymerization of phenol on a vitreous carbon electrode in alkaline aqueous solution at different temperatures. *Electrochim Acta* 55(2):465–469. <https://doi.org/10.1016/j.electacta.2009.08.040>
43. Tahar NB, Savall A (2011) Electropolymerization of phenol on a vitreous carbon electrode in acidic aqueous solution at different temperatures. *J Appl Electrochem* 41:983–989. <https://doi.org/10.1007/s10800-011-0327-7>
44. Sakakibara Y, Kounoike T, Kashimura H (2010) Enhanced treatment of estrogen and endocrine disrupting chemicals (EDCs) by a granular bed electrochemical reactor. *Water Sci Technol* 62: 2218–2224. <https://doi.org/10.2166/wst.2010.400>
45. Cong VH, Iwaya S, Sakakibara Y (2014) Removal of estrogens by electrochemical oxidation process. *J Environ Sci* 26(6):1355–1360. [https://doi.org/10.1016/S1001-0742\(13\)60611-7](https://doi.org/10.1016/S1001-0742(13)60611-7)
46. Cong VH, Sakakibara Y (2015) Continuous treatments of estrogens through polymerization and regeneration of electrolytic cells. *J Hazard Mater* 285:304–310. <https://doi.org/10.1016/j.jhazmat.2014.12.010>
47. Zhang W, Bao L, Zhang X, He J, Wei G (2012) Electropolymerization treatment of phenol wastewater and the reclamation of phenol. *Water Environ Res* 84(11):2028–2036. <https://doi.org/10.2175/106143012x13415215906771>
48. Grinberg A, Korin E, Bettelheim A (2005) Removal of phenol and derivatives from aqueous solutions by electropolymerization in aerogel carbon electrodes. *Electrochem Solid State Lett* 8(4):E42–E44. <https://doi.org/10.1149/1.1870712>
49. Hou CH, Huang SC, Chou PH, Den W (2015) Removal of bisphenol A from aqueous solutions by electrochemical polymerization on a carbon aerogel electrode. *J Taiwan Inst Chem Eng* 51: 103–108. <https://doi.org/10.1016/j.jtice.2015.01.009>
50. Zhang Y, Li Q, Cui H, Zhai J (2010) Removal of phenols from the aqueous solutions based on their electrochemical polymerization on the polyaniline electrode. *Electrochim Acta* 55(24): 7219–7224. <https://doi.org/10.1016/j.electacta.2010.07.002>

Bioremediation: From Key Enzymes to Practical Technologies



Masaaki Morikawa

Contents

1	Microbial Degradation of Stable Hydrocarbon Pollutants	264
1.1	Alkane Monooxygenase/Hydroxylase	266
1.2	Rieske Dioxygenase	267
2	Efficacy of Biofilm Formation by Naphthalene Degrading Bacteria for Bioremediation	268
2.1	Naphthalene Degradation by T102 Biofilms and Planktonic Cells	270
2.2	Comparison of Expression Levels of nahA in T102 Biofilms and Planktonic Cells ..	271
2.3	Fitness of T102 Biofilms and Planktonic Cells in Petroleum Contaminated Soils ..	273
2.4	Naphthalene Degradation Activity of Soils Containing T102 Biofilms and Planktonic Cells	276
2.5	Summary	277
3	Biosurfactants	277
3.1	Isolation of BS-Producing Bacteria	278
3.2	Production and Purification of BS	279
3.3	Types and Structures of BS	280
3.4	Structure-Activity Relationships of BS	283
3.5	Synthetic Mechanisms of Arthrofactin and Encoding Gene Cluster	284
4	Conclusion	287
	References	287

Abstract The most well-known bioremediation technology is the decomposition and purification of recalcitrant petroleum-based hydrocarbon contaminants by specific microorganisms. Here, first of all, we will learn how they have evolved ingenious enzyme systems. In order to overcome the rate-limiting step of the initial decomposition reaction, the oxygen attracted to the iron-coordinated active center attacks the stable carbon-carbon covalent bond and hydroxylates it brilliantly. Following this step a series of energy consuming reaction continues in the first half. However, since product compounds can be finally used as respiratory

M. Morikawa (✉)

Faculty of Environmental Earth Science, Hokkaido University, Sapporo, Hokkaido, Japan
e-mail: morikawa@ees.hokudai.ac.jp

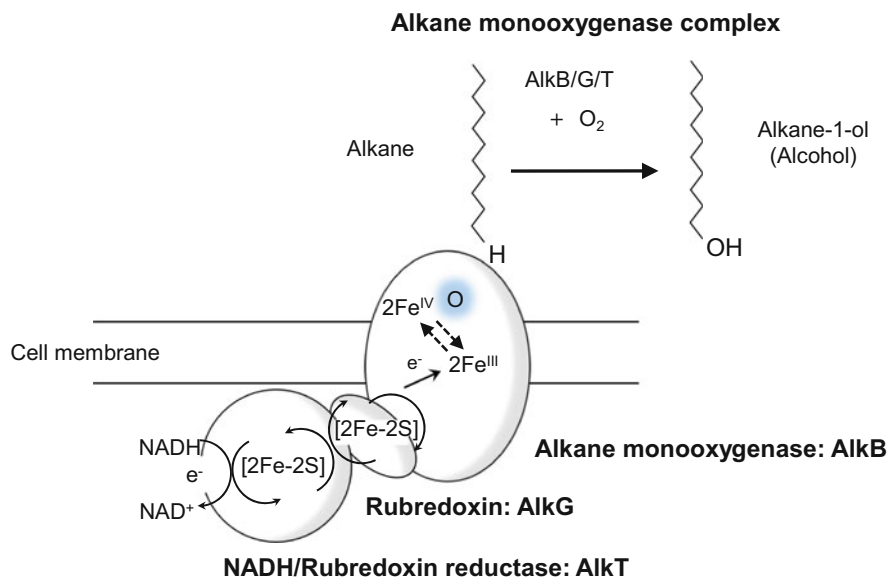


Fig. 1 Alkane monooxygenase complex is composed of three proteins, NADH/Rubredoxin reductase (AlkT), Rubredoxin (AlkG), and Alkane monooxygenase (AlkB). AlkB is embedded into cell membrane. Electron from NADH is transmitted to dinuclear Fe in AlkB through 2Fe-2S cluster in AlkT and AlkG. Dioxygen molecule binds to 2Fe in AlkB followed by single oxygen molecule attacking the terminal carbon of alkane

substrates, cells can acquire energy in the end. Secondly, it will be demonstrated that formation of a microbial biofilm is a potential bioaugmentation technology that is advantageous in survival competition with robust indigenous microorganisms at a contaminated site. Finally, we will see how microorganisms have elegantly developed projectiles for effective dispersion and emulsification of water-immiscible hydrocarbon compounds.

Keywords Bioaugmentation, Biofilms, Biosurfactants, Degradation, Hydrocarbon, Oxygenases

1 Microbial Degradation of Stable Hydrocarbon Pollutants

The most significant aspect in microbial metabolisms is their marvelously wide acceptability of substrate electron donors and acceptors in order to obtain chemical energy from the environments. This feature makes microorganisms nature based attractive players for environmental remediation technology in terms of degradation of harmful recalcitrant compounds, including stable hydrocarbons. Microbial

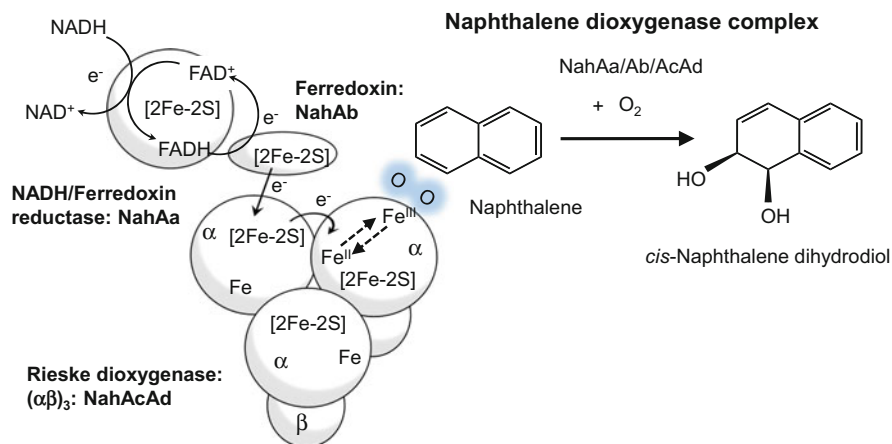


Fig. 2 Reaction mechanisms of three-component naphthalene dioxygenase (NahAa/Ab/AcAc) FAD(H): Flavin adenine dinucleotide <https://doi.org/10.1038/nchembio.71>

degradation of hydrocarbons has been reported in the temperature range from -5 to 70°C [1–3]. Transformation of highly reduced and inert hydrocarbon compounds is with no doubt a challenging and difficult biochemical reaction for a single enzyme. However, several multi-component enzyme systems enable microorganisms to utilize hydrocarbons as carbon and energy (electron) sources. Initial biological attack to hydrocarbons is generally the oxygenation/hydroxylation that requires molecular dioxygen as a co-substrate. Dioxygen, an excellent terminal electron acceptor, also contributes to the ring cleavage reaction of homo- and hetero-cyclic aromatic hydrocarbons. Although the dioxygen molecule is omnipresent and highly soluble in water, activation and splitting this triplet ground-state molecule to wed with inert hydrocarbons need special devices. In the world of enzymes, biocatalysts, non-heme iron, heme iron, or flavin nucleotide are designated as a fantastic hidden dagger for this purpose [4]. Donation of electron to these catalytic centers is supported by a series of partner proteins in the multi-component enzyme system, including NADH (Nicotinamide Adenine Dinucleotide) dehydrogenase to yield two electrons and an electron carrier protein ferredoxin or rubredoxin connecting to dioxygenase or monooxygenase components (Figs. 1 and 2).

A group of metalloenzyme families, carrying an iron coordinating active site whichever heme or non-heme type, play crucial roles for the binding and activation of dioxygen or monooxygen in various oxidative transformation of environmental pollutants. These include hydroxylation of hydrocarbons and also cleavage of aromatic ring structure. Dioxygen or monooxygen molecule binds to the iron active sites of monooxygenase or dioxygenase component, AlkB or NahAcAd and generates competent iron-peroxo and iron-oxo intermediates to generate a substrate-based radical. These reactive intermediate species allow the enzyme to insert oxygen molecule to the substrate compounds. The product alcohol compounds are further oxidized, for example, to aldehydes and fatty acids by dehydrogenase enzymes and

finally degraded completely to CO_2 and H_2O through metabolic pathways. The catechol (diol) ring structure is split by catechol dioxygenase before transformation to aldehydes or fatty acids.

Environmental pollution by halogenated hydrocarbons among polychlorinated aromatic compounds such as polychlorinated biphenyls, PCB, and dibenzodioxins is of highly concerned. These exert dermal toxicity, immunotoxicity, reproductive deficits, teratogenicity, endocrine toxicity, and carcinogenicity/tumor promotion [5]. However, a wide range of bacteria such as *Arthrobacter*, *Bacillus*, *Corynebacterium*, *Luteibacter*, *Microbacterium*, *Pseudomonas*, *Rhodococcus*, and *Williamsia* sp. have been reported thankfully to be capable of utilizing toxic PCBs as carbon and electron sources [6]. Initial oxidation by these bacteria is generally the reaction by biphenyl dioxygenase which functions as a three-component enzyme system similar to naphthalene dioxygenase enzyme as described below (Fig. 2).

On the other hand, another group of halogenated hydrocarbons are degraded by not oxidation but reduction reaction, the so-called halo-respiration which is one of the unique anaerobic respirations of bacteria. This means that the target compounds are not used as electron donors for microorganisms but as electron acceptors. These reactions proceed under anoxic conditions in the presence of organic electron donor compounds including methanol. *Dehalococcoides ethenogens* is the most popular dehalogenating bacteria that consistently dominates at the contaminated sites by tetrachloroethylene, PCE. *D. ethenogens* converts PCE to trichloroethylene, dichloroethylene, and finally to ethene (ethylene) that is further degraded to CO_2 and H_2O by aerobic respiration by other symbiotic microorganisms. This reductive dehalogenase also adopts [Fe-S] cluster, [4Fe-4S] at the catalytic site for transferring electron. It has been also indicated that a cobalamin (B_{12}) molecule exists at proximate position of [4Fe-4S] cluster and the coordinated Co atom of the cobalamin directly binds to halogen atom suggesting its contribution to dehalogenation reaction [7]. Here, we are surprised again wonderful tactic of enzyme evolution to complete its difficult mission to detoxify non-natural and recalcitrant pollutants. It may also worth to note that bacteria, prokaryotic microorganisms, never transform pollutants kindly for saving biosphere environments including human health but they need to do so for their living.

1.1 Alkane Monooxygenase/Hydroxylase

Alkane monooxygenase/hydroxylase is a three-component system comprising a soluble mononuclear iron and FAD containing NADH/rubredoxin reductase (AlkT), a [2Fe-2S] soluble rubredoxin (AlkG), and an integral-membrane diiron oxygenase (AlkB) (Fig. 1). This type of multi-component enzyme system is widely distributed in bacteria [8]. AlkB adopts the oxygen rebound mechanism in order to hydroxylate alkanes but preferably from C5 to C16 alkanes. This mechanism involves homolytic cleavage of the C–H bond by an electrophilic oxo-iron intermediate to generate a substrate-based radical. Diiron ligand site of AlkB is composed of

eight histidine motifs. These histidine residues are also potential ligands for the diiron atoms contained within alkane monooxygenase. This protein family has hydrophobic six alpha helices that would be capable of spanning the membrane bilayer. Unfortunately, active site structure of AlkB has not been solved yet, however, spectroscopic and genetic evidence suggests a nitrogen-rich coordination environment located near the inner surface of the cytoplasmic membrane with as many as eight histidines coordinating two irons and a carboxylate residue bridging these two metals. A particular amino acid residue located in the middle of trans-membrane helix-2 of AlkB has been shown to be important to determine the alkyl length of the substrate. When this amino acid has a bulky side chain like tryptophan, the long-chain alkyl groups (C13<) are not acceptable in the substrate binding cleft.

1.2 *Rieske Dioxygenase*

Rieske dioxygenase catalyzes the primary cis-dihydroxylation of arene (monocyclic and polycyclic aromatic hydrocarbon) substrates, which is the initial step of many bacterial degradation pathways. Rieske protein was first reported by John Rieske et al. [9], which has a characteristic [2Fe-2S] cluster with 2-His-2-Cys bidentate ligand. Besides a mononuclear iron active site, Rieske dioxygenases carry a dinuclear [2Fe-2S] cluster in which one iron (Fe1) is coordinated by two histidines while the other iron (Fe2) is coordinated by two cysteines. Fe2 remains in a ferric state regardless of the reduction state of the cluster, while Fe1 is converted from a ferric state to a ferrous state when reduced during the reaction. The reaction of the three-component type Rieske dioxygenase requires two electrons from an NAD(P)H and consecutively transferred to the terminal dioxygenase component through a ferredoxin (monomer) and a reductase (monomer). In a single large subunit, the Rieske-type cluster and the mononuclear iron center are too far apart to allow for electron transfer at a distance ~ 43 Å. However, the quaternary structure (trimer of hetero-dimer or homo-trimer type with three-fold symmetry) allows for electron transfer from a Rieske-type cluster to a mononuclear iron center from a neighboring subunit, which is only 5 Å apart (Fig. 2, [10]). A key role in this electron transfer has been ascribed to an absolutely conserved aspartic acid residue Asp205 in NahAc that bridges between the two metal sites. Structural studies also implicate a side-on binding of a dioxygen to form catalytically active iron(III)-peroxide intermediate which is subsequently converted to a high-valent iron(IV)-oxo or iron(V)-oxo-hydroxo intermediate. After cis-dihydroxylation of the substrate, catalytic mononuclear iron will return to iron(II) resting-state configuration [11, 12].

2 Efficacy of Biofilm Formation by Naphthalene Degrading Bacteria for Bioremediation

Among the strategies to clean up pollutants it is widely recognized that biological treatments, the so-called bioremediation technologies, have the advantage over chemical and physical treatments in terms of their compatibility with natural system thus minimizing environmental impacts [13]. Active on-site bioremediation includes technologies that activate indigenous microbial populations, biostimulation, or introduce specific competent foreign bacteria to the contaminated site, bioaugmentation. Although bioaugmentation is expected to be a quicker and more effective technology than biostimulation, low fitness and poor colonization of the introduced bacteria to the contaminated sites often make efficacy of bioaugmentation poor [14, 15]. The activity and viability of the introduced bacteria often decreases at the contaminated sites when compared with those observed under laboratory conditions, probably due to diverse environmental stresses [16, 17]. These include predation by protozoa, competition with other bacteria, unfavorable pH and temperature conditions, and poor availability of nutrients and oxygen. Catabolite repression by other organic compounds also decreases the expression level of the degradation genes. However, bioaugmentation can become more effective if both microbial ecology and population sizes are taken into account [15, 18, 19]. One of the options for effective clean-up methods of contaminated sites is the use of carrier materials so as to maintain sufficient activity of inoculants during prolonged periods. There are several reports demonstrating that immobilized or encapsulated cells effectively degrade pollutants at the contaminated sites [20, 21]. However, the cellular and molecular mechanisms underlying these technologies are largely unknown.

Biofilms are a multicellular structure of microorganisms formed on surfaces that exhibit sociality under control of quorum sensing signaling molecules [22]. Biofilms are often encased in sticky extracellular polymeric substances such as exopolysaccharides. Forming biofilms is considered a natural strategy of microorganisms to construct and maintain a favorable niche in stressful environments [17, 23]. We propose that application of biofilms to bioproduction and bioaugmentation processes is a natural and rational choice [24]. Indeed, there are several reports that demonstrate the efficacy of biofilm formation by useful bacteria and their use in bioremediation and biotransformation technologies [25–28]. We have demonstrated benefits of biofilm formation by hydrocarbon-degrading bacterium for stable bioremediation. Shimada et al. compared degradation activities and its persistence in contaminated soils inoculated with biofilms or planktonic cells of naphthalene degrading bacterium *Pseudomonas stutzeri* T102 [29]. When compared with artificially immobilized and encapsulated cells, the advantage of biofilms is that the high density and tolerance of the constituent cell is naturally achieved. Moreover, biofilms can be introduced to contaminated sites free of supports that might cause additional environmental pollution. The secondary purpose of the study was to examine the potential of model biofilms toward developing bioaugmentation technology.

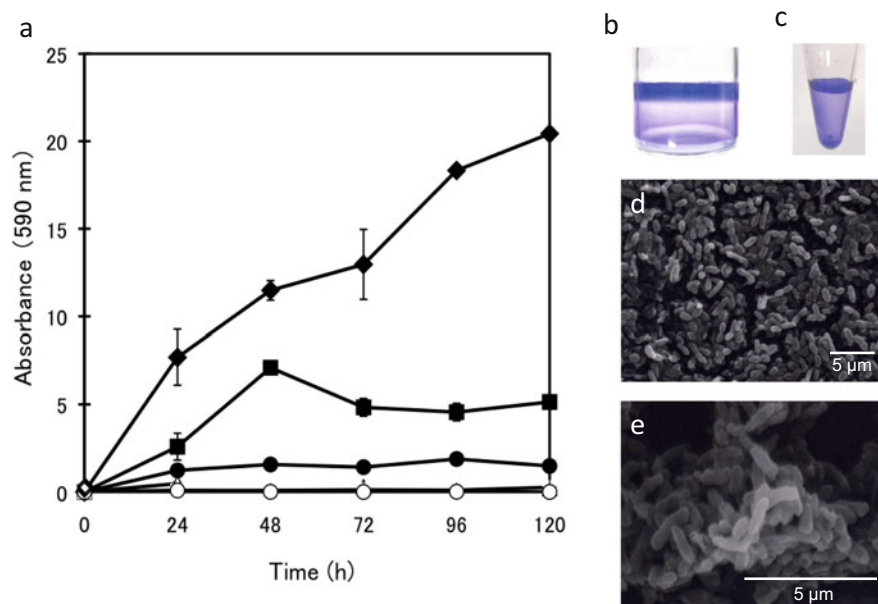


Fig. 3 (a) Biofilm formation by hydrocarbon degrading bacteria. Biofilms were formed at the indicated temperatures in 1.5 mL polypropylene tubes containing 0.5 mL Y medium. Data points are the averages of triplicate assays and error bars represent standard deviations. Symbols are as follows: closed diamond, *P. stutzeri* T102 (30°C); closed square, *Gordonia* sp. C3 (30°C); closed circle, *Oleomonas sagaranensis* HD1 (30°C); open triangle, *Rhodococcus* sp. TMP2 (20°C); open diamond, *Rhodococcus* sp. T12 (20°C); cross, *Shewanella* sp. SIB1 (20°C); open circle, *Arthrobacter* sp. CAB1 (30°C). The latter four strains did not produce biofilms in the culture systems. (b) Crystal violet staining of *P. stutzeri* T102 biofilms in a 20 mL glass bottle; (c) in a 1.5 mL polypropylene test tube. (d, e) Scanning electron micrographs. All biofilms were formed at 30°C for 48 h. (For interpretation of the references to color in this figure legend, the reader is referred to the web version of this article)

Pseudomonas stutzeri are ubiquitous and useful environmental bacteria with their high degradation abilities for harmful chemical compounds including biocides, halogenated alcohols, and hydrocarbons [30]. Among the tested laboratory strains, *P. stutzeri* T102, which was isolated from sludge of an oil reservoir tank in Okinawa [31], formed the biofilms on the surface of various materials including polypropylene, polystyrene, polyethylene terephthalate, acrylic, and glass bottles. *P. stutzeri* T102 is capable of degrading PAHs, such as naphthalene and dibenzothiophene. When using a batch culture system for biofilm formation, the amount of T102 biofilms continued increasing even after 120 h (Fig. 3a). Thus, we chose T102 as a model bacterial strain for further experiments. Gross et al. (2007) tested 69 bacterial strains for biofilm forming capacity and showed that many of the best biofilm formers belonged to *Pseudomonas* [32]. Our experimental result is consistent with their result. Since T102 is a facultative aerobic strain, it formed ring-shape biofilms near the air-liquid interface on the inner surface of glass bottles

(Fig. 3b). However, they formed rather uniform biofilms in small plastic tubes, such as 1.5 mL polypropylene tubes and 96 well polystyrene plates probably due to the small depth of the liquid phase, better aeration condition, reduced hydrophobicity and zeta potential of the tube materials (Fig. 3c). It may be worse to note that a major outer membrane protein, OmpA exhibited opposite effects on the biofilm formation in glass bottles and plastic tubes where surface hydrophobicity is different [33]. This suggests that each environmental bacterium has different surface condition for its optimal biofilm formation. Scanning electron microscopy demonstrated that the macroscopically uniform biofilms of T102 are also not flat but highly structured (Fig. 3d, e).

2.1 Naphthalene Degradation by T102 Biofilms and Planktonic Cells

There are reports that biofilm-associated cells are more dormant and inactive than planktonic cells [34–36]. This feature of biofilms partly explains their high resistance to environmental stresses [37]. It was thus a concern that T102 biofilms might exhibit less naphthalene degradation activity than planktonic cells. In order to examine this possibility, the activities of T102 biofilm and planktonic cells were compared in a pure liquid-culture system (Fig. 4). Biofilms of T102 were formed in glass bottles. After cultivation at 30°C for 24 h without shaking, free planktonic cells were carefully removed from the bottles and the biofilm formed inside walls

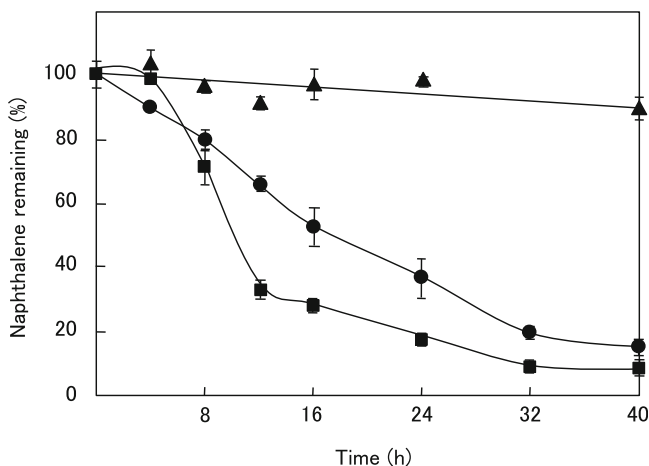


Fig. 4 Comparison of naphthalene degradation activity of T102 biofilm and planktonic cell cultures. Data points are the average of triplicate assays; error bars represent standard deviations. Initial CFUs for biofilm and planktonic cell cultures were 21,470,000 and 23,360,000, respectively. Symbols are as follows: no cells, triangle (*filled triangle*); T102 biofilm cell culture, square (*filled square*); T102 planktonic cell culture, circle (*filled circle*)

(ca 2×10^7 CFUs) was rinsed once with sterile water. The biofilms were soaked in a mineral medium containing 20 ppm naphthalene and the bottles were tightly sealed with butyl rubber stoppers and incubated at 30°C without shaking. Planktonic cells were separately grown in a shaking flask. Mid-exponential phase cells were harvested by centrifugation and washed and suspended with a small amount of medium. BM-medium containing the planktonic cells at the same CFU value (ca 2×10^7 CFUs) as the biofilm samples was prepared in glass bottles with 20 ppm naphthalene added. The bottles were sealed and kept at 30°C as described previously. All the samples were prepared in triplicate for each sampling time and a negative control included that contained no cells. Sample bottles were taken every 4 h until 16 h and then every 8 h until 48 h. Remaining amounts of naphthalene in the samples were analyzed by gas chromatography.

Experimental results revealed that T102 biofilms did not degrade naphthalene during the first 4 h but after that time they degraded naphthalene faster than planktonic cells (Fig. 4). This interesting observation was reproducible in several independent experiments. T102 biofilms degraded 14 ppm or 70% of initial naphthalene (20 ppm) in 12 h and exhibited a maximum degradation rate of 1.7 ppm h^{-1} between 4 and 12 h. On the other hand, T102 planktonic cells started to degrade naphthalene immediately after incubation. The degradation rate was almost constant, about 0.5 ppm h^{-1} for 16 h, and it took 28 h for the degradation of 14 ppm of naphthalene. About 1.6 ppm (8%) of the initial naphthalene was absorbed to the butyl rubber septum of the bottle cap and remained un-degradable. This means that naphthalene was almost completely eliminated from the culture of T102 biofilms after 32 h. We hypothesized that initial delay for degradation by biofilms may be the time that it takes the naphthalene to penetrate through the extracellular matrix of the biofilm so that the genes responsible for degradation of naphthalene might be induced.

2.2 Comparison of Expression Levels of *nahA* in T102 Biofilms and Planktonic Cells

It is known that a set of genes *nahAa*, *nahAb*, *nahAc*, and *nahAd* form an operon and encode a ferredoxin, ferredoxin oxidoreductase, and naphthalene dioxygenase large and small subunits, respectively (Fig. 2; [4, 38]). All these genes are essential for the aerobic degradation of naphthalene and related compounds. Thus, we analyzed the expression level of *nahAc*, which encodes the large subunit of naphthalene dioxygenase, in T102 biofilms and planktonic cells (Fig. 5). Total RNA was extracted from T102 cells and cDNA was synthesized from DNase-treated RNA as previously described [39]. RT-PCR amplification was performed using a primer set targeting *nahAc* in T102. The PCR products were separated on 1.5% agarose gels and stained by ethidium bromide. Contrary to our hypothesis, *nahAc* in T102 biofilms expressed *nahAc* at constant levels from the start of incubation through to

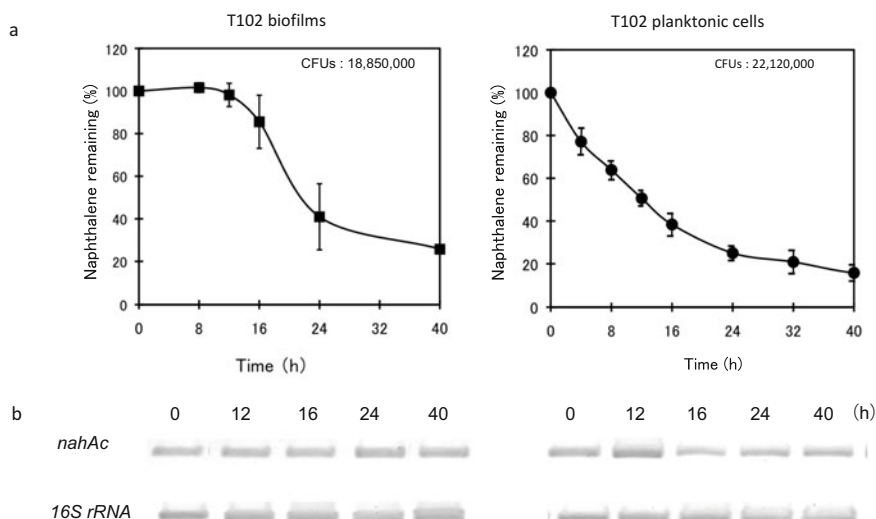


Fig. 5 (a) Naphthalene degradation activity of T102 biofilm (left) and planktonic (right) cell cultures, respectively. Initial CFUs were 18,850,000 (biofilm culture) and 22,120,000 (planktonic cell culture). Data points are the average of triplicate assays; error bars represent standard deviations. (b) RT-PCR analyses of *nahAc* and 16S rRNA gene expression in the T102 biofilms (left) and planktonic cells (right), respectively

40 h (Fig. 5b). Constant gene expression was also confirmed for *nahAa*, *nahAb*, and *nahAd* (results not shown). These results suggest that the initial lag and subsequent high naphthalene degradation periods exhibited by T102 biofilms are not due to changing gene expression levels of *nahAabcd*. The *nahAabcd* operon in *Pseudomonas putida* has been reported to be inducible under regulation of *nahR* [40]. In this experiment expression of *nahA* genes was observed at 0 h, before naphthalene was added to the medium. This suggests that *nahR* does not exist or does not function to regulate naphthalene degradation in *P. stutzeri* T102, which has been isolated from the bottom sludge of a petroleum reservoir tank where naphthalene is always abundant.

When we carefully observed the culture, we noticed that a part of T102 detached, dispersed and grew planktonically in the culture bottle containing T102 biofilms (Fig. 6a). Thus, we carefully separated these detached cells from biofilms, and examined the expression level of *nahAc*. It was found that the expression level of *nahAc* in the detached cells was clearly and significantly higher than that in biofilms from 12 to 20 h (Fig. 6b). This result allowed us to conclude that degradation of naphthalene was largely due to the activity of detached cells rather than biofilms. The naphthalene degradation activities of T102 biofilms, detached, and planktonic cells, were determined as 0.02, 1.1, and 0.3 $\mu\text{g CFUs}^{-1} \text{h}^{-1}$, respectively. The degradation activity of the biofilms was much lower than planktonic cells probably due to depletion of oxygen in biofilms where cells were densely packed and due to

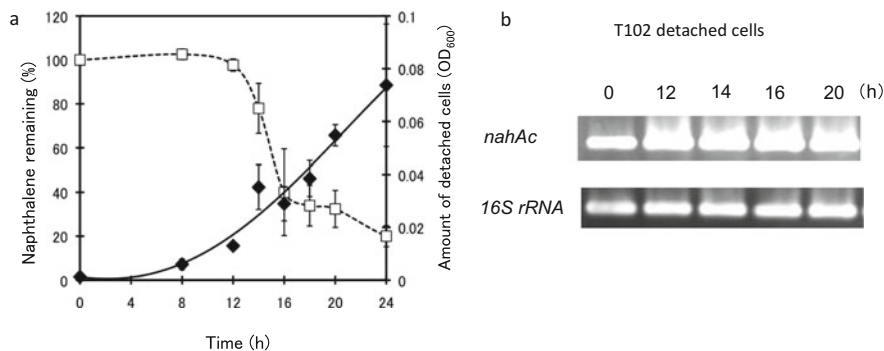


Fig. 6 (a) Naphthalene degradation activity (open square) and the amount of detached cells (closed diamonds) in a T102 biofilm flask. Data points are the average of triplicate assays and error bars represent standard deviations. (b) RT-PCR analyses of *nahAc* and 16S rRNA gene expression in the detached cells. Only the cells sample at 0 h was taken from biofilms

poor naphthalene penetration through the matrix that encases biofilm-associated cells.

2.3 Fitness of T102 Biofilms and Planktonic Cells in Petroleum Contaminated Soils

The observation that T102 biofilms were capable of producing highly active detached cells prompted us to test their performance in soils contaminated with natural petroleum. Petroleum contaminated soils were taken from Ishikari petroleum field (Hokkaido, Japan) and used for following experiments without sterilization. For biofilm samples, T102 biofilms were formed in advance at 30°C for 24 h in a screw cap polypropylene tubes containing 0.4 mL medium. The liquid culture containing planktonic cells was removed from the tubes leaving biofilms inside wall. Contaminated soils, 0.5 g, and the same amount of filtered cell free spent medium from planktonic cell cultures were added to each tube. Then, two different conditions were set for biofilm samples, one was the “intact biofilm samples” with no treatment, the other was “dispersed biofilm samples” which were vortexed for 2 s to detach and disperse the biofilm pieces into the soils. For planktonic cell samples, 0.5 g of the soils in 2 mL tubes were supplemented with mid-log phase planktonic cell cultures containing similar colony forming units, CFUs, to above biofilm samples. A soil sample with no inoculation of T102 cells was also prepared as a negative control. The soil samples inoculated with “intact biofilms,” “dispersed biofilms,” “planktonic cells,” or no inoculation were incubated at 30°C using the naphthalene vapor exposure method [41]. Naphthalene vapor was continuously supplied by placing a small quantity of naphthalene crystals in a sample tube that was loosely capped and placed on wet paper to avoid desiccation. The Petri dishes

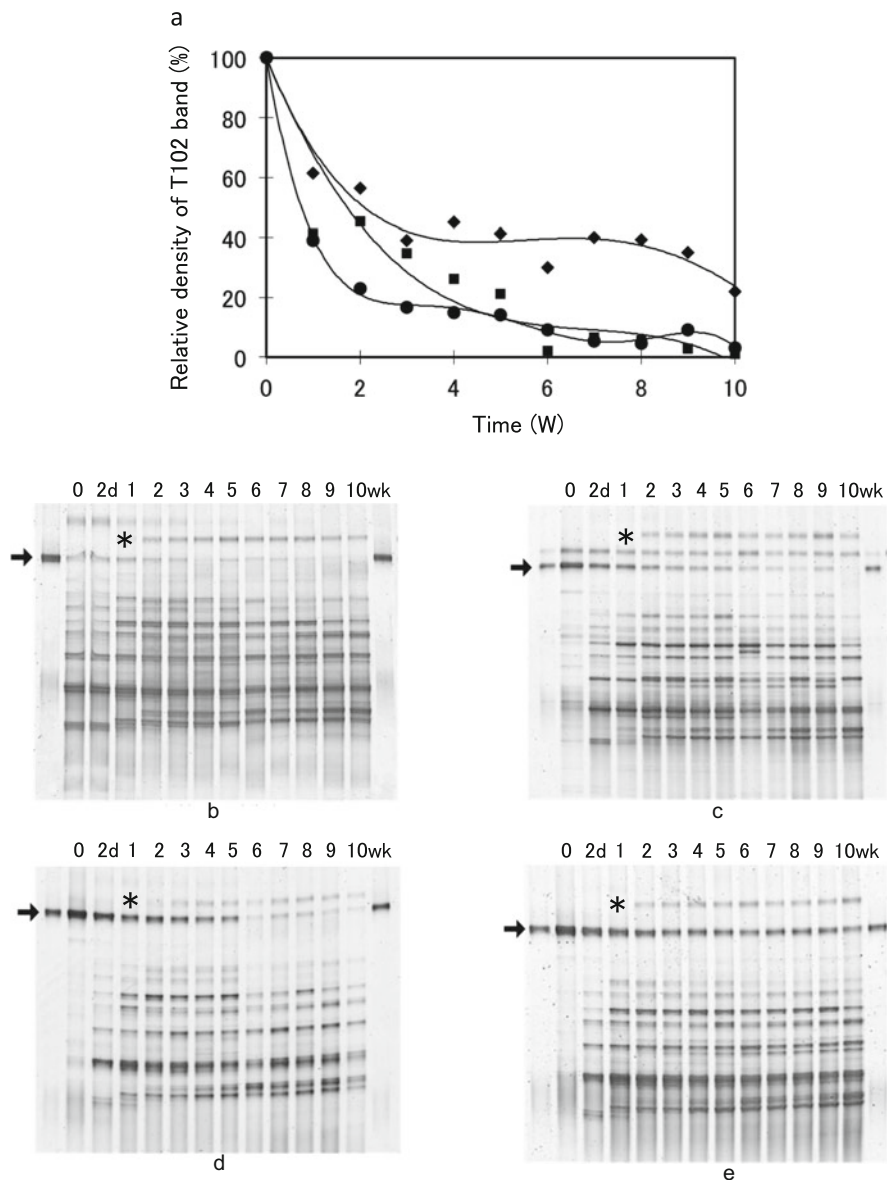


Fig. 7 (a) Comparison of the fitness of T102 cells inoculated differently in contaminated soils. Relative density of 16S rRNA-PCR products band of T102 in each DGGE gel is plotted in the graph. Symbols are as follows: T102 dispersed biofilms (triangle, *filled triangle*); T102 intact biofilms (square, *filled square*); T102 planktonic cells (circle, *filled circle*) DGGE gel data for the bacterial community analyses from 0 to 10 weeks. (b) native community without T102 inoculation; (c) Inoculation of T102 planktonic cells; (d) Inoculation of T102 intact biofilm; (e) Inoculation of T102 dispersed biofilm. The arrows indicate position of the 16S rRNA-PCR band of T102. Asterisks * indicate the position of indigenous naphthalene degrader

containing sample tubes and naphthalene crystals were sealed with parafilm, which is permeable to oxygen.

To estimate the fitness of *P. stutzeri* T102 in the soils, we used the community DNA fingerprinting method denaturant gradient gel electrophoresis (DGGE) to assess variation in bacterial community composition among samples (Fig. 7). Although this method is semi-quantitative due to different efficiency of DNA extraction and PCR depending on the bacterial strains, it is useful to analyze population changes of single strains over the time. Moreover, distribution of the DNA bands in DGGE gels provides a rough overview of the bacterial community dynamics upon introduction of T102 biofilm and planktonic cells to the soils. Total DNA was prepared from the culture and PCR amplified 16S rRNA gene fragments were separated on an 8% polyacrylamide gel with a denaturing gradient of urea and formamide ranging from 20 to 50%. The density of DNA bands corresponding to *P. stutzeri* T102 16S rRNA genes was estimated using imaging software (Fig. 7a).

We observed that the “dispersed biofilm” sample maintained a rather dense T102 DNA bands for 10 weeks and kept over 40% of its original density level for 8 weeks (Fig. 7e). The density of T102 DNA bands of “planktonic cells” and “intact biofilms” samples decreased more rapidly than that of “dispersed biofilms,” and they almost disappeared (ca 2% remained) after 10 weeks (Fig. 7c, d). The decrease in the amount of T102 DNA bands was more significant within the first 3 weeks than later for all experimental conditions. The amount of T102 DNA in the “intact biofilms” sample continuously decreased over the period. This may be because the nutrients and oxygen were more rapidly depleted around the sessile “intact biofilms” than “planktonic cells” and “dispersed biofilms.” The duration for which each sample kept over 20% of the initial density of T102 DNA was 10, 5, and 2 weeks for “dispersed biofilms,” “intact biofilms,” and “planktonic cells” inoculates, respectively (Fig. 7a). These results indicate that “dispersed biofilms” are more tolerant and stable than “intact biofilms” and “planktonic cells” in the petroleum contaminated soils. A band of increasing intensity, indicated by an asterisk, in all samples may be an indigenous naphthalene degrader since it also appeared in the sample without T102 inoculation (Fig. 7a).

The above experimental results are consistent with previous knowledge that biofilm-associated cells are generally more tolerant to environmental stresses than their planktonic counterparts. The environmental robustness of biofilm-associated cells could be attributed to both specific gene expression and physicochemical toughness provided to the densely packed cells by extracellular matrices [42–44]. Next, we examined the naphthalene degradation activities of contaminated soils containing either T102 biofilm or planktonic cells.

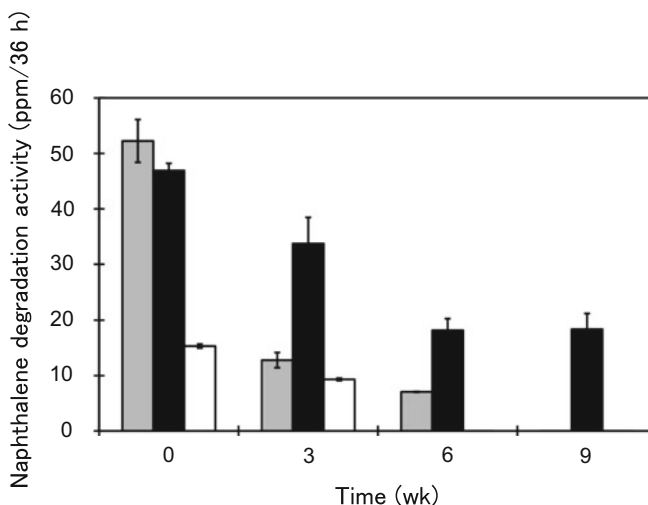


Fig. 8 Naphthalene degradation activity of soils with T102 planktonic cells (shaded bar), dispersed T102 biofilms (closed bar), and no T102 cells (open bar). Data points are the average of triplicate assays and error bars represent standard deviations

2.4 Naphthalene Degradation Activity of Soils Containing T102 Biofilms and Planktonic Cells

As shown above, the liquid-culture system inoculated with T102 biofilms exhibited naphthalene degradation activity comparable to or even higher than with T102 planktonic cells (Fig. 4). PCR-DGGE analysis suggested that populations of T102 remained higher in soils inoculated with “dispersed biofilms” rather than the “planktonic cells” during incubation for 10 weeks in contaminated soils. Thus, we expected that the soil sample containing “dispersed biofilms” should exhibit higher degradation activities than “planktonic cells” over the period. But it was difficult to measure naphthalene degradation directly in the contaminated soil samples because the soils contained large amounts of various hydrocarbons and the signal/noise ratio in GC analysis was quite low. We decided to measure naphthalene degradation activity of each soil sample in BM-medium containing an additional 100 ppm naphthalene (Fig. 8). The entire soil sample, 0.5 g, in the 1.5 mL polypropylene tube was transferred into a 50 mL screw capped glass bottle containing 20 mL of BM-medium and 100 ppm naphthalene in methanol solution. Bottles were tightly closed and incubated at 30°C for 36 h. Extraction of remaining naphthalene and GC/FID analysis were performed as previously described. It was demonstrated that “dispersed biofilms” and “planktonic cells” initially degraded 48 and 52 ppm naphthalene in 36 h, respectively. Their degradation activities gradually decreased as the incubation time increased. When their activities were compared after 9 weeks of incubation, “dispersed biofilms” still degraded 19 ppm naphthalene while

“planktonic cells” and no inoculation samples degraded only <0.1 ppm. Petroleum contaminated soils that were taken from Ishikari oil field contained various hydrocarbon compounds such as straight-, branched- and cyclo-alkanes, and PAHs including naphthalene. Thus, it was not surprising that the soils contained significant amounts of naphthalene degrading bacteria. The degradation of naphthalene with no inoculation could be attributed to these indigenous bacteria. Densitometry of the T102 bands of “dispersed biofilms” and “planktonic cells” in DGGE gel revealed that 35 and 9% of the initial band intensities remained after 9 weeks, respectively. These results suggest that the specific naphthalene degradation activity of “dispersed biofilms” including detached cells was much higher than “planktonic cells” in the petroleum contaminated soils after 9 weeks.

2.5 Summary

Biofilms confer microbial cells with high resistance to environmental stresses and facilitate their survival in complex microenvironments that help generate diverse cellular heterogeneity and activities. Naphthalene degradation rate of *P. stutzeri* T102 biofilms was initially low but later became higher than that of T102 planktonic cells. The rapid degradation activity of biofilm cultures could be attributed to producing detached cells. It was shown that “*biofilms act as aircraft carriers that launch super-active fighter cells*” which may contribute to the continued degradation of harmful environmental contaminants. T102 cells were also shown to be more durable and active in the petroleum contaminated soils when they are introduced as “dispersed biofilms” rather than as “planktonic cell” suspensions. These experimental results suggest that inoculation of contaminated sites with pollutant degrading biofilms may enhance bioaugmentation as a durable and effective bioremediation technology.

3 Biosurfactants

Biosurfactants (*biological surfactants*), namely BS, are a group of surfactants produced by living organisms. Surfactants are generally considered as chemical products such as detergents and emulsifiers that are abundantly used in various industries. Surfactants are also useful compounds for environmental remediation by accelerating microbial degradation. People may think of them as harmful substances that are far from living organisms, but this is not the case. For example, phospholipids, a major component of cell membranes in all living organisms, are biomolecules with amphiphilicity can also function as surfactants. Furthermore, glycolipids such as cerebroside and ganglioside, which are abundant in the brain, are not exception. In other words, biological complex lipids mostly can function as BS in the broad sense. Thus, surfactants are molecular species that are closely related to living organisms.

A group of microorganisms are known to produce and secrete complex lipids with strong surfactant activity outside the cells, which are generally called biosurfactants, BS [45]. The physiological significance of BS to the producing bacteria is still unclear, but it is natural that for microorganisms growing in hydrophobic environments such as oil fields, the ability to emulsify hydrocarbon compounds for efficient uptake as carbon and energy sources is advantageous for survival. In fact, microorganisms with BS production activity are widely distributed in oil fields, including *Bacillus*, *Pseudomonas*, and *Rhodococcus* [46, 47]. It is a rational idea to activate the domestic or introduce foreign BS-producing bacteria to the site of oil contaminated soils and oceans [48–53]. In the case of *Serratia*, a plant pathogen, BS are secreted to improve the affinity with the wax-covered leaf surface useful for invasion [54]. On the other hand, some BS have antimicrobial activity, which may also be of great benefit not only to the producing bacteria but also to the host plants [55]. In addition, BS have been shown to be important in the formation of three-dimensional structures of microorganisms (so-called biofilms) formed by microorganisms attached to solid surfaces and interfaces, and it can be said that BS are one of the tools that microorganisms have devised to secure their ecological niche while resisting various environmental stresses [56, 57]. The development and effective use of such special natural products is expected to contribute to the realization of a sustainable society with low environmental impact [58].

3.1 Isolation of BS-Producing Bacteria

Isolation of BS-producing bacteria can be performed by using the accumulation of an emulsified layer or the decrease in surface tension of the culture solution as an index. Emulsified layer is observed when culturing bacteria with water-insoluble hydrophobic substance such as a hydrocarbon compound as a carbon source. There is also a simpler method which is called as a plate test. It is convenient to use a blood agar medium on the market, and hemolytic spots due to BS activity are formed around the colonies of the producing bacteria [59]. The authors accidentally found that an agar plate medium prepared by spreading a small amount of crude oil to form thin membrane on the top, prepared for the purpose of isolating hydrocarbon-degrading bacteria, was very useful for selecting biosurfactant-producing bacteria. That is, first, a sample containing microorganisms is spread on this medium to form colonies, and second the surface of the plate medium is observed under the reflected light of a fluorescent lamp and a circular zone in which the oil film is excluded can be observed around the colonies of the biosurfactant-producing bacteria (Fig. 9, [60]). At first, we thought that I had discovered a novel crude oil-degrading bacterium which is capable of evaporating liquid hydrocarbons by directly cutting C–C bond to yield hydrocarbon gasses such as methane or ethane, but later it was revealed that this oil exclusion circle was due to BS activity. Since the size of this oil film exclusion zone is directly proportional to the BS molecular activity and the amount

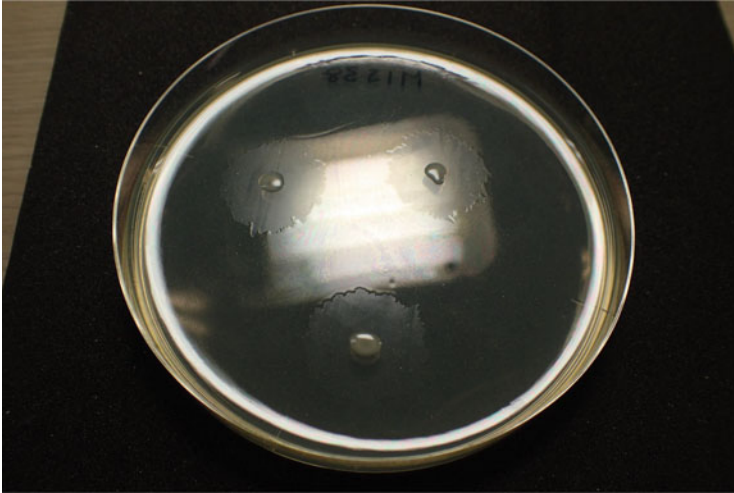


Fig. 9 Easy BS halo assay for detecting BS production. There are three colonies of BS producing bacteria surrounded by oil displacement zone, BS halo. BS halo can be visualized by different reflection of the light. The size of BS halo directly correlates with the amount and activity of BS [59]

of BS production. Finally, excellent BS-producing bacteria can be obtained by picking up colonies that form a large zone.

3.2 Production and Purification of BS

When the BS-producing bacteria are grown in liquid-culture using a hydrophobic substrate such as a hydrocarbon compound or vegetable oil, significant amount of emulsified layer is formed by the function of produced BS that cells and hydrocarbon compounds cannot be easily removed by centrifugation. However, in the case of sufficiently highly BS-producing yeasts, whose cell size is much bigger than bacteria, the hydrophobic substrate is almost completely consumed. A bottom white cell layer and biosurfactant containing brown layer are formed under the aqueous culture solution after simply left stand for 1 day. On the other hand, *Bacillus* and some *Pseudomonas* bacteria show relatively good biosurfactant productivity even without hydrophobic substrates. That is, the BS can be recovered by acid precipitation or calcium precipitation by adding hydrochloric acid or calcium chloride to the supernatant obtained by precipitating and removing the bacterial cells from culture solution by centrifugation. In addition, since BS form giant micelles in an aqueous solution, they can be concentrated using an ultrafiltration membrane having an excluded molecular weight of about 10 kDa, which is used for protein concentration [59]. In addition, since BS are involved in biofilm formation by microorganisms, good productivity is often seen in solid cultures using soybean meal or okara, and in

this case, hexane or ethyl acetate can directly solubilize and extract BS instead of from an aqueous solution [61]. This method enables us to concentrate BS compound easily by evaporation of the organic solvent.

3.3 Types and Structures of BS

Biosurfactant molecules are also composed of hydrophobic and hydrophilic part similarly to chemical surfactants. Since the hydrophobic part of BS is commonly fatty acid esters, their classification can be mainly divided into (1) glycolipid type, (2) lipopeptide type, (3) fatty acid type, and (4) polymeric type based on the structure of the hydrophilic part, but the first two types are most used in industry.

3.3.1 Glycolipid-Type BS

Although there are various types of glycolipid BS depending on the sugar, only the structures of popular rhamnolipids and sophorolipids are shown here.

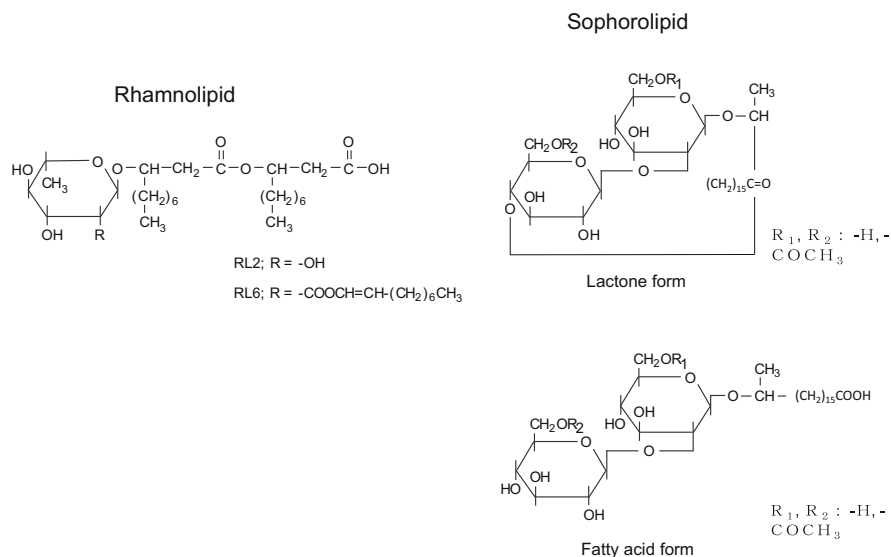


Fig. 10 Structure of two major glycolipid type BS, Rhamnolipid and Sophorolipid

Rhamnolipid

Rhamnolipid is a glycolipid-type biosurfactant produced mainly by bacteria of the genus *Pseudomonas*, and was first reported as an antibacterial substance against tuberculosis-causing *Mycobacterium tuberculosis* [62]. Since then, six types of homologous compounds with different monosaccharides, disaccharides, or fatty acid chain lengths (RL1–RL6) have been identified. Figure 10 shows the structures of typical RL2 and RL6. Hisatsuka, K. et al. reported in 1971, when “petroleum (utilizing) fermentation” was in its heyday, that hydrocarbon-degrading *Pseudomonas aeruginosa* produced rhamnolipids, which was involved in its sound growth [63].

Sophorolipid

In 1961, Gorin, P.A. et al. found sophorolipids in the fermented products of the yeast *Torulopsis magnoliae* and *Torulopsis bombicola* (later *Candida bombicola*, now *Starmerella bombicola*) [64]. As mentioned earlier, it has been found that the productivity of the biosurfactant sometimes is greatly increased by feeding vegetable oil as a carbon source along with glucose. This is probably due to the bacterium that produces lipase, and the fatty acids, which are degradation products of vegetable oil, are rapidly utilized for BS synthesis. This compound is characterized by the ether linkage of hydroxy fatty acids to the sugar (sophorose) backbone and the intramolecular condensation of the carboxyl terminus of the fatty acid with the hydroxyl group of the sugar to form a lactone (Fig. 10). The acid and lactone forms are produced in mixture in the culture medium, and the lactone can be converted to the more water-soluble acid form by ring-opening under alkaline conditions if necessary.

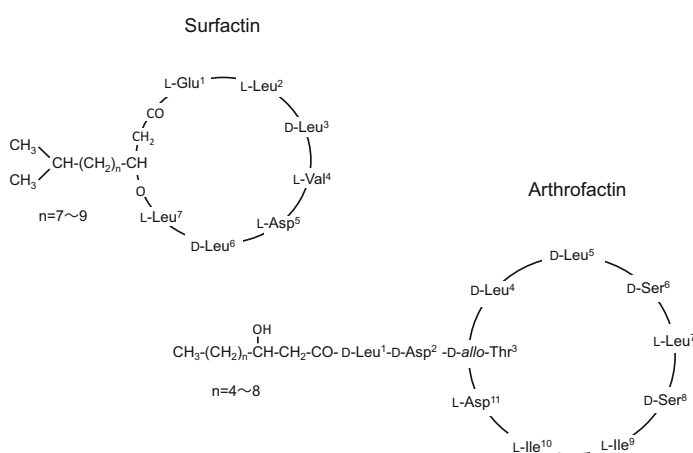


Fig. 11 Structure of two major lipopeptide type BS, Surfactin and Arthrofactin

3.3.2 Lipopeptide-Type Biosurfactant

The best known lipopeptide-type biosurfactant is surfactin, which was reported as a thrombolytic agent produced by *Bacillus subtilis* [65]. Its structure is also unique: a peptide, consisting of seven amino acid residues including two D-form amino acid residues, forms a lactone via amide and ester bonds with fatty acids (Fig. 11). Since then, a series of cyclic lipopeptides with different structures have been reported from bacteria of the genus *Bacillus*, including lichenysin, fengycin, plipastatin, iturin, and bacillomycins [66]. *Serratia* spp. and *Pseudomonas* spp. have also been reported to produce cyclic lipopeptides serawettin, arthrofactin, and syringomycin. Arthrofactin is a cyclic lipopeptide consisting of 11 amino acids, including five D-form amino acid residues, which was discovered by the authors in 1993 from a soil bacterium in Shizuoka Prefecture [59]. Arthrofactin is one of the most effective BS with CMC (critical micelle concentration) value ~ 0.01 mM and minimum surface tension reduced to 24 mN/m.

These lipopeptides are synthesized without ribosomes by a huge non-ribosomal peptide synthetase (NRPS), in which substrate amino acids are activated and linked one by one. NRPS has a modular structure with an activation domain and a condensation domain before and after the domain that binds the substrate amino acid, thiolation domain. Interestingly, the gene structure of NRPS has a co-linearity rule with that of the product peptide. Moreover, a novel cyclic lipopeptide can be synthesized by replacing the gene module.

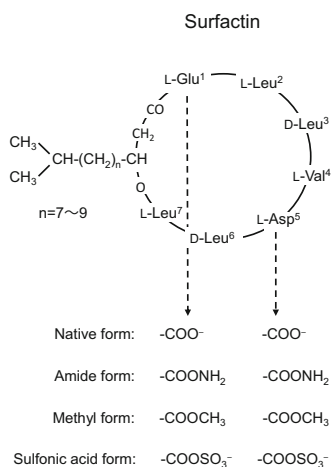
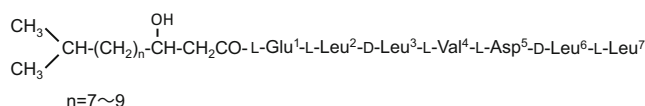


Fig. 12 Chemical modification of surfactin. Methyl form was obtained by keeping surfactin overnight in anhydrous methanol with conc. HCl. Amide form was obtained from surfactin by keeping two hours at 22° C in methanol containing 5.5 M NH_4Cl (pH 5.0) with 0.1 M 1-ethyl-3-(3-dimethylaminopropyl)-carbodiimide (EDC). Sulfonic acid form was obtained by keeping in aminomethane sulfonic acid (pH 8.0) and solubilized by the addition of appropriate amount of acetonitrile and EDC up to 0.1 M

Linear form Surfactin



Linear form Arthrofactin

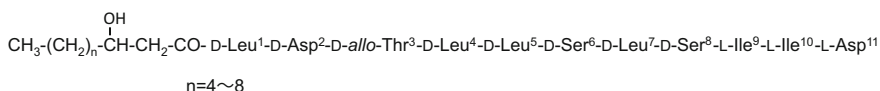


Fig. 13 Linearization of surfactin and arthrofactin. Linear forms were obtained by dissolving each BS in NaOH/40% methanol and incubated at 37° C for 18 h

3.4 Structure-Activity Relationships of BS

BS, especially lipopeptide-type, have very diverse and complex structures. There is yet a limited knowledge available to understand rationality of its structure. In order to investigate the structural inevitability of arthrofactin and surfactin, we have attempted several structural modifications [67]. The first question was both have two acidic amino acids in common. The experimental results showed that either amidation or methylation of the Asp and Glu residues which eliminates negative charge of the molecule resulted in an increase in surfactant activity but also lost water solubility (Fig. 12). On the other hand, sulfonation to make the molecule more strongly acidic maintained the water solubility but drastically reduced the surface activity. Furthermore, when the lactone was saponified and cleaved lactone ring to form a linear structure, the activity was reduced to one-third in both cases (Fig. 13). These results allow us to conclude that lactone formation can increase the biosurfactant activity by three folds. When the activity was carefully measured by HPLC fractionating the arthrofactin according to their fatty acid chain length, relative biosurfactant activity ($/A_{210}$) of the most major product was found to be the highest (Fig. 14). Furthermore, the three-dimensional structure of arthrofactin in DMSO solution was investigated using high-performance NMR. It was found that arthrofactin formed a unique helmet-like structure, with hydrophobic amino acids, Ile and Leu, oriented on the upper outer side and hydrophilic amino acids, Asp, Ser, *allo*-Thr, on the lower inner side (Fig. 15). Higher surface activity of BS than chemical surfactants can be probably attributed to this steric distribution of hydrophilic and hydrophobic part in a biosurfactant molecule which enables to occupy larger interfacial area. Our experimental results demonstrated that the complex BS structure successfully harmonized high surfactant activity and water solubility in a perfect manner. Here, we could see a wonderful aspect of rational natural selection over million years.

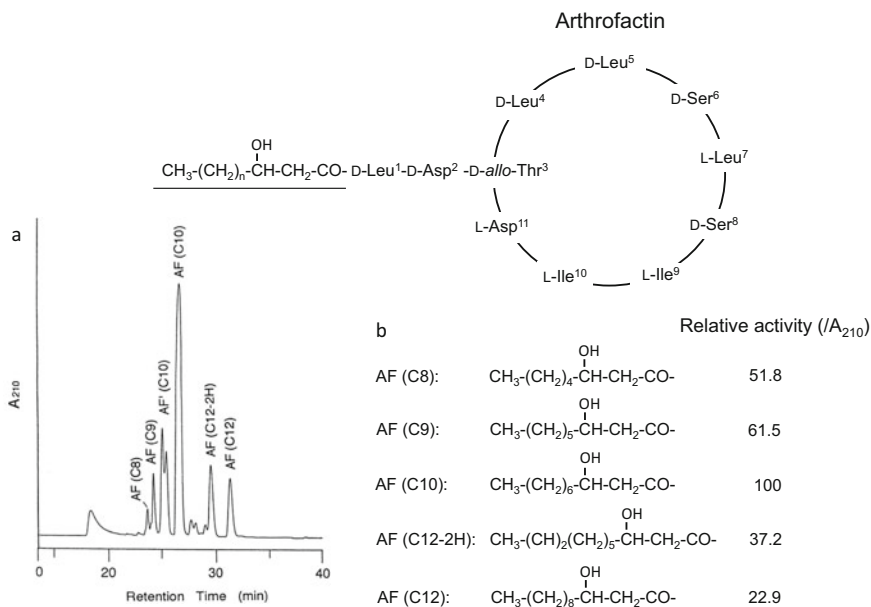


Fig. 14 Separation and relative activity of arthrofactin (AF) structural family. **(a)** Elution pattern of AF family on reverse-phase HPLC with MS detector. **(b)** Chemical structure and relative oil displacement activity of AF family. Relative activity was determined as follows: the oil displacement circle area was divided by A210 units and each value was compared with the major AF (C10)

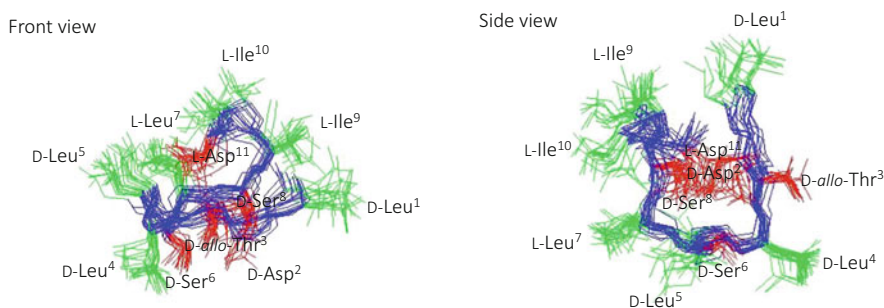


Fig. 15 3D structure of arthrofactin in DMSO

3.5 Synthetic Mechanisms of Arthrofactin and Encoding Gene Cluster

Gram-positive *Bacillus* and Gram-negative *Pseudomonas* strains produce a variety of lipopeptides with remarkable surface and biological activities. In contrast to the structural diversity of these lipopeptides, their biosynthetic mechanism is basically conserved. They are synthesized nonribosomally by a mega-peptide synthetase unit,

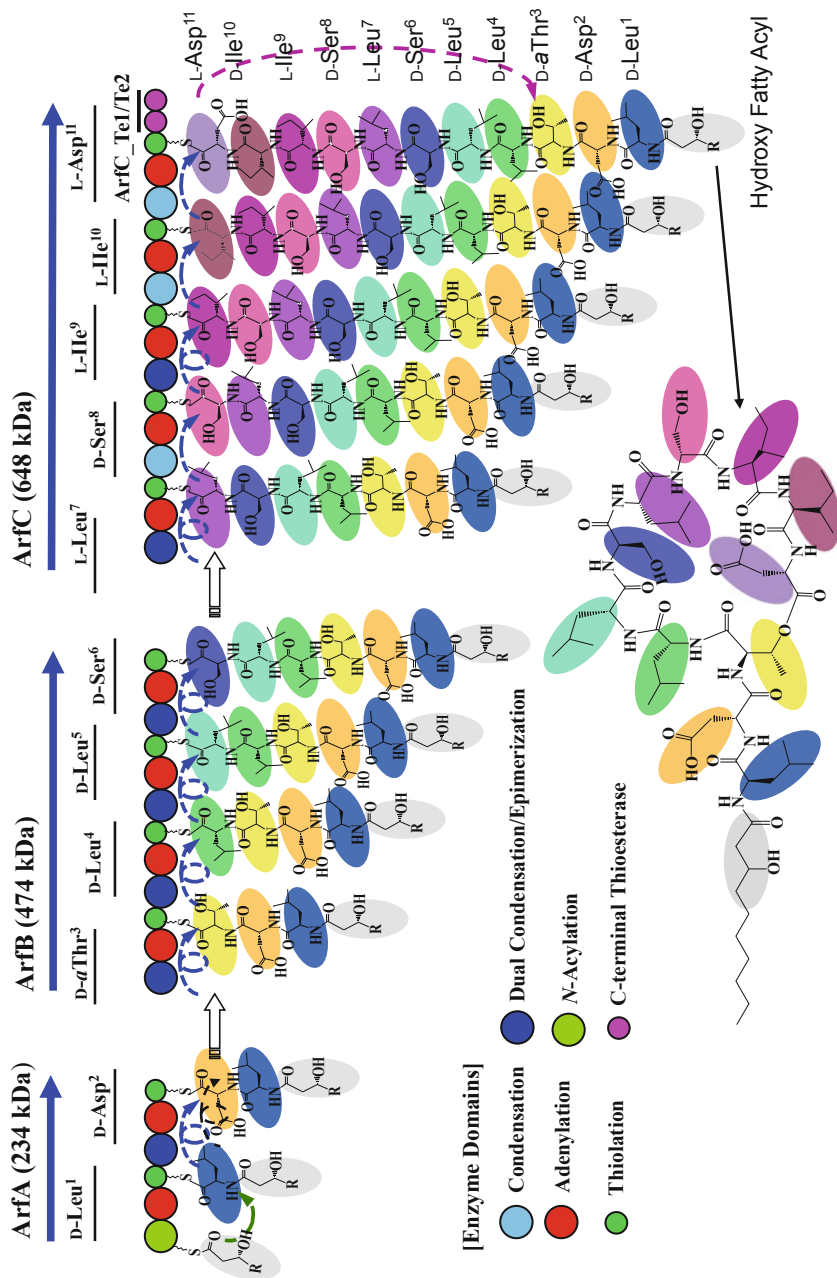


Fig. 16 The arthrofactin biosynthesis assembly line. Arthrofactin synthetase is composed of ArfA, ArfB, and ArfC enzyme complex. Each enzyme contains several sets of domains responsible for adding aminoacylated substrate amino acid residues. The last dual thioesterase Te1/Te2 releases and cyclizes arthrofactin

non-ribosomal peptide synthetase, NRPS which is composed of several cooperating multifunctional modules, each capable of performing one cycle of peptide elongation. To become an active form, they are post-translationally modified by a phosphopantetheinyl transferase. However, recent analysis of the lipopeptide synthetases suggests that there are several variants of NRPS architecture.

Biosynthesis of arthrofactin is catalyzed by the arthrofactin synthetase (Arf), which consists of three non-ribosomal peptide synthetase, NRPS protein subunits, ArfA (234 kDa), ArfB (474 kDa), and ArfC (648 kDa), which contain two, four, and five functional modules, respectively (Fig. 16, [57]). An additional C-domain was identified in the first module of ArfA, suggesting that the first amino acid could be initially acylated with a fatty acid. Site-directed mutagenesis changing the histidine residue of conserved core motif (HHXXXDG) to alanine impairs arthrofactin production (N. Roongsawang and M. Morikawa, unpublished data). This result suggested that the first C-domain is essential for biosynthesis of lipopeptide. Indeed, the β -hydroxydecanoyl thioester may be coupled to the activated leucine by the action of this C-domain to yield β -hydroxydecanoyl-L-Leu as the initial intermediate. A phylogenetic tree showed that the first C-domain of Arf belongs to *N*-acyl groups that use fatty acyl-CoA as their starter unit [68]. Although seven out of the 11 amino acid residues in arthrofactin are in the D-form, Arf contains no E-domains, as found in syringomycin and syringopeptin. The A-domain of D-Leu¹ specifically recognizes only L-Leu in vitro. Based on these observations, we initially hypothesized that an external racemase may be responsible for incorporation of the D-amino acids in arthrofactin. Different amino acid sequences downstream of a conserved core motif [FFELGGHSLLA(V/M)] in the T-domains were expected to reflect the recognition by external racemase. However, Balibar and coworkers demonstrated in 2005 that Arf contains unique dual C/E domains, which contribute to the conversion of L-amino acids to the D-form [69]. This novel C/E domain is cryptically embedded with the C-domain located downstream of the D-amino acid-incorporating modules. Dual C/E domains can be recognized by an elongated His motif (HHI/LXXXXGD). This feature was also identified in the Syr and Syp synthetases. Another unique characteristic of Arf is the presence of C-terminal tandem Te-domains like syringopeptin. By site-directed mutagenesis, the first Te-domain (ArfC-Te1) was shown to be essential for the completion of macrocyclization and the release of the final product. The second Te-domain (ArfC-Te2) was suggested to be involved in the evolution of Arf to improve the macrocyclization efficiency. Moreover, we found that the gene encoding putative ArfA/B/C exists in the genome sequence of *Pseudomonas fluorescens* Pf0-1 (YP_347943/YP_347944/YP_347945). Arf represents a novel NRPS architecture that features tandem Te-domains and dual C/E domains. Interestingly, another type of NRPS involved in biosynthesis of a siderophore, pyoverdine, was also identified in arthrofactin-producing *Pseudomonas* sp. MIS38. A gene encoding NRPS for the chromophore part of pyoverdine contains a conventional E-domain [70]. This observation shows that different NRPS systems with dual C/E domains and a conventional E-domain are both functional in *Pseudomonas* spp.

Our current knowledge is still not enough to understand the evolutionary history of biosurfactants. On the other hand, modification of NRPS by genetic engineering

of the encoding genes is a potential method to produce useful variants. Accumulation of genetic information for lipopeptide synthetases should contribute to design biosurfactants with higher surface activity and/or novel features [71]. Moreover, understanding their biosynthetic pathways and genetic regulation mechanisms will facilitate not only uncovering the evolution of NRPS mechanisms, but also the development of cost-effective methods for large-scale production of useful lipopeptides.

4 Conclusion

Bioremediation is one of the excellent functions that have been naturally acquired in the evolution of microorganisms, whose history is more than one billion years. Therefore, there is no doubt that it is an environmentally friendly technology. However, it has a disadvantage of requiring time much longer than physicochemical methods. When considering the return on investment on the scale of human time, it has been not yet practically used in many occasions. In the future, in order to realize a sustainable biosphere without being bound by human self-convenience in a short span of view, research and development to further improve bioremediation while understanding its characteristics is desired.

References

1. Kato T, Haruki M, Imanaka T, Morikawa M, Kanaya S (2001a) Isolation and characterization of psychrotrophic bacteria from oil reservoir water and oil sands. *Appl Microbiol Biotechnol* 55: 794–800
2. Kato T, Haruki M, Imanaka T, Morikawa M, Kanaya S (2001b) Isolation and characterization of long-chain-alkane degrading *Bacillus thermoleovorans* from deep subterranean petroleum reservoirs. *J Biosci Bioeng* 91(1):64–70
3. Kunihiro N, Haruki M, Takano K, Morikawa M, Kanaya S (2005) Isolation and characterization of *Rhodococcus* sp. strains TMP2 and T12 that degrade 2,6,10,14-tetramethylpentadecane (pristane) at moderately low temperatures. *J Biotechnol* 115:129–136
4. Morikawa M (2010) Dioxygen activation responsible for oxidation of aliphatic and aromatic hydrocarbon compounds: current state and variants. *Appl Microbiol Biotechnol* 87:1596–1603
5. Ahlborg UG, Becking GC, Birnbaum LS, Brouwer A, Derks HJGM, Feeley M, Color G, Hanberg A, Larsen JC, Liem AKD, Safe SH, Schlatter C, Wvorn F, Younes M, Yrjainheikki E (1994) Toxic equivalency factors for dioxin-like PCBs. *Chemosphere* 28(6):1049–1067
6. Leigh MB, Prouzová P, Macková M, Macek T, Nagle DP, Fletcher JS (2006) Polychlorinated biphenyl (PCB)-degrading bacteria associated with trees in a PCB-contaminated site. *Appl Environ Microbiol* 72(4):2331–2342
7. Payne KAP, Quezada CP, Fisher K, Dunstan MS, Collins FA, Sjuts H, Levy C, Hay S, Rigby SEJ, Leys D (2015) Reductive dehalogenase structure suggests a mechanism for B12-dependent dehalogenation. *Nature* 517:513–516
8. van Beilen JB, Funhoff EG (2007) Alkane hydroxylases involved in microbial alkane degradation. *Appl Microbiol Biotechnol* 74:13–21

9. Rieske JS, MacLennan DH, Coleman R (1964) Isolation and properties of an iron-protein from the (reduced coenzyme Q)-cytochrome C reductase complex of the respiratory chain. *Biochem Biophys Res Commun* 15(4):338–344
10. Parales RE (2003) The role of active-site residues in naphthalene dioxygenase. *J Ind Microbiol Biotechnol* 30(5):271–278
11. Karlsson A, Parales JV, Parales RE, Gibson DT, Eklund H, Ramaswamy S (2003) Crystal Structure of naphthalene dioxygenase: side-on binding of dioxygen to iron. *Science* 299(5609): 1039–1042
12. Bugg TDH, Ramaswamy S (2008) Non-heme iron-dependent dioxygenases: unravelling catalytic mechanisms for complex enzymatic oxidations. *Curr Opin Chem Biol* 12(2):134–140
13. Alexander M (1999) *Biodegradation and bioremediation*. 2nd edn. Academic Press
14. Bouchez T, Patureau D, Dabert P, Juretschko S, Doré J, Delgenès P, Moletta R, Wagner M (2000) Ecological study of a bioaugmentation failure. *Environ Microbiol* 2:179–190
15. El-Fantroussi S, Agathos SN (2005) Is bioaugmentation a feasible strategy for pollutant removal and site remediation? *Curr Opin Microbiol* 8:268–275
16. van Veen JA, van Overbeek LS, van Elsas JD (1997) Fate and activity of microorganisms introduced into soil. *Microbiol Mol Biol Rev* 61:121–135
17. Thompson IP, van-der-Gast CJ, Ciric L, Singer AC (2005) Bioaugmentation for bioremediation: the challenge of strain selection. *Environ Microbiol* 7:909–915
18. Dejonghe W, Boon N, Seghers D, Top EM, Verstraete W (2001) Bioaugmentation of soils by increasing microbial richness: missing links. *Environ Microbiol* 3:649–657
19. Silva E, Fialho AM, Sá-Correia I, Burns RG, Shaw LJ (2004) Combined bioaugmentation and biostimulation to cleanup soil contaminated with high concentrations of atrazine. *Environ Sci Technol* 38:632–637
20. Moslemy P, Neufeld RJ, Giot SR (2002) Biodegradation of gasoline by gellan gum-encapsulated bacterial cells. *Biosci Bioeng* 80:175–184
21. Mrozik A, Piotrowska-Seget Z (2010) Bioaugmentation as a strategy for cleaning up soils contaminated with aromatic compounds. *Microbiol Res* 182:2675–2679
22. Watnick P, Kolter R (2000) Biofilms, city of microbes. *J Bacteriol* 13:20–26
23. Shemesh M, Kolter R, Losick R (2010) The biocide chlorine dioxide stimulates biofilm formation in *Bacillus subtilis* by activation of the histidine kinase KinC. *J Bacteriol* 192: 6352–6356
24. Morikawa M (2006) Beneficial biofilm formation by industrial bacteria *Bacillus subtilis* and related species. *J Biosci Bioeng* 101:1–8
25. Iijima S, Washio K, Okahara R, Morikawa M (2009) Biofilm formation and proteolytic activities of *Pseudoalteromonas* bacteria that were isolated from fish farm sediments. *J Microbiol Biotechnol* 2:361–369
26. Qureshi N, Annous BA, Ezeji TC, Karcher P, Maddox IS (2005) Biofilm reactors for industrial bioconversion processes: employing potential of enhanced reaction rates. *Microb Cell Fact* 4:24
27. Singh R, Paul D, Jain RK (2006) Biofilms: implications in bioremediation. *Trends Microbiol* 14:389–397
28. Yamaga F, Washio K, Morikawa M (2010) Sustainable biodegradation of phenol by *Acinetobacter calcoaceticus* P23 isolated from the rhizosphere of duckweed *Lemna aoukikusa*. *Environ Sci Technol* 44:6470–6474
29. Shimada K, Itoh Y, Washio K, Morikawa M (2012) Efficacy of forming biofilms by naphthalene degrading *Pseudomonas stutzeri* T102 toward bioremediation technology and its molecular mechanisms. *Chemosphere* 87(3):226–233
30. Lalucat J, Bennisar A, Bosch R, García-Valdés E, Palleroni NJ (2006) Biology of *Pseudomonas stutzeri*. *Microbiol Mol Biol Rev* 70:510–547
31. Hirano S, Kitauchi F, Haruki M, Imanaka T, Morikawa M, Kanaya S (2004) Isolation and characterization of *Xanthobacter polyaromaticivorans* sp. nov. 127W that degrades polycyclic and heterocyclic aromatic compounds under extremely low oxygen conditions. *Biosci Biotechnol Biochem* 68:557–564

32. Gross R, Hauer B, Otto K, Schmid A (2007) Microbial biofilms: new catalysts for maximizing productivity of long-term biotransformations. *Biotechnol Bioeng* 98:1123–1134
33. Ma Q, Wood TK (2009) OmpA influences *Escherichia coli* biofilm formation by repressing cellulose production through the CpxRA two-component system. *Environ Microbiol* 11:2735–2746
34. Werner E, Roe F, Bugnicourt A, Franklin MJ, Heydom A, Molin S, Pitts B, Stewart PS (2004) Stratified growth in *Pseudomonas aeruginosa* biofilms. *Appl Environ Microbiol* 70:6188–6196
35. Lewis K (2007) Persister cells, dormancy and infectious disease. *Nat Rev Microbiol* 5:48–56
36. Rani SA, Pitts B, Beyenal H, Veluchamy RA, Lewandowski Z, Davison WM, Buckingham-Meyer K, Stewart PS (2007) Spatial patterns of DNA replication, protein synthesis, and oxygen concentration within bacterial biofilms reveal diverse physiological states. *J Bacteriol* 189:4223–4233
37. Gilbert P, Collier PJ, Brown MR (1990) Influence of growth rate on susceptibility to antimicrobial agents: biofilms, cell cycle, dormancy, and stringent response. *Antimicrob Agents Chemother* 34:1865–1868
38. Ensley BD, Gibson DT, Laborde AL (1982) Oxidation of naphthalene by a multicomponent enzyme system from *Pseudomonas* sp. strain NCIB 9816. *J Bacteriol* 149:948–954
39. Takei D, Washio K, Morikawa M (2008) Identification of alkane hydroxylase genes in *Rhodococcus* sp. strain TMP2 that degrades a branched alkane. *Biotechnol Lett* 30:1447–1452
40. Park W, Jeon CO, Madsen EL (2002) Interaction of NahR, a LysR-type transcriptional regulator, with the alpha subunit of RNA polymerase in the naphthalene degrading bacterium, *Pseudomonas putida* NCIB 9816-4. *FEMS Microbiol Lett* 213:159–165
41. Park JW, Crowley DE (2006) Dynamic changes in nahAc gene copy numbers during degradation of naphthalene in PAH-contaminated soils. *Appl Microbiol Biotechnol* 72:1322–1329
42. Chang WS, van-de-Mortel M, Nielsen L, Nino-de-Guzman G, Li X, Halverson LJ (2007) Alginate production by *Pseudomonas putida* creates a hydrated microenvironment and contributes to biofilm architecture and stress tolerance under water-limiting conditions. *J Bacteriol* 189:8290–8299
43. Bossé JT, Sinha S, Li MS, O'Dwyer CA, Nash JH, Rycroft AN, Kroll JS, Langford PR (2010) Regulation of pga operon expression and biofilm formation in *Actinobacillus pleuropneumoniae* by sigma E and H-NS. *J Bacteriol* 192:2414–2423
44. Halan B, Schmid A, Buehler K (2011) Real-time solvent tolerance analysis of *Pseudomonas* sp. strain VLB1206C catalytic biofilms. *Appl Environ Microbiol* 77:1563–1571
45. Lang S (2002) Biological amphiphiles (microbial biosurfactants). *Curr Opin Colloid Interface Sci* 7(1–2):12–20
46. Ron EZ, Rosenberg E (2001) Natural roles of biosurfactants. *Environ Microbiol* 3(4):229–236
47. Jahan R, Bodratti AM, Tsiannou M, Alexandridis P (2020) Biosurfactants, natural alternatives to synthetic surfactants: physicochemical properties and applications. *Adv Colloid Interface Sci* 275:102061
48. Zhang Y, Maier WJ, Miller RM (1997) Effect of rhamnolipids on the dissolution, bioavailability, and biodegradation of phenanthrene. *Environ Sci Technol* 31:2211–2217
49. Calvo C, Manzanera M, Silva-Castro GA, Uad I, González-López J (2009) Application of bioemulsifiers in soil oil bioremediation processes. Future prospects. *Sci Total Environ* 407(12):3634–3640
50. Sriram MI, Gayathiri S, Gnanaselvi U, Jenifer PS, Raj SM, Gurunathan S (2011) Novel lipopeptide biosurfactant produced by hydrocarbon degrading and heavy metal tolerant bacterium *Escherichia fergusonii* KLU01 as a potential tool for bioremediation. *Bioresour Technol* 102(19):9291–9295
51. Cameotra SS, Bollag J-M (2003) Biosurfactant-enhanced bioremediation of polycyclic aromatic hydrocarbons. *Crit Rev Environ Sci Technol* 33(2):111–126
52. Bezza FA, Chirwa EMN (2017) The role of lipopeptide biosurfactant on microbial remediation of aged polycyclic aromatic hydrocarbons (PAHs)-contaminated soil. *Chem Eng J* 309:563–576

53. Lamichhane S, Krishna KCB, Sarukkalige R (2017) Surfactant-enhanced remediation of polycyclic aromatic hydrocarbons. *J Environ Manage* 199:46–61
54. Matsuyama T, Kaneda K, Nakagawa Y, Isa K, Hara-Hotta H, Yano I (1992) A novel extracellular cyclic lipopeptide which promotes flagellum-dependent and -independent spreading growth of *Serratia marcescens*. *J Bacteriol* 174(6):1769–1776
55. Nielsen TH, Sørensen D, Tobiasen C, Andersen JB, Christophersen C, Givskov M, Sørensen J (2002) Antibiotic and biosurfactant properties of cyclic lipopeptides produced by fluorescent *Pseudomonas* spp. from the sugar beet rhizosphere. *Appl Environ Microbiol* 68(7):3416–3423
56. Pamp SJ, Tolker-Nielsen T (2007) Multiple roles of biosurfactants in structural biofilm development by *Pseudomonas aeruginosa*. *J Bacteriol* 189(6):2531–2539
57. Roongsawang N, Hase K, Haruki M, Imanaka T, Morikawa M, Kanaya S (2003) Cloning and characterization of the gene cluster encoding arthrofactin synthetase from *Pseudomonas* sp. MIS38. *Chem Biol* 10(9):869–880
58. Marchant R, Banat IM (2012) Biosurfactants: a sustainable replacement for chemical surfactants? *Biotechnol Lett* 34(9):1597–1605
59. Morikawa M, Daido H, Takao T, Murata S, Shimonishi Y, Imanaka T (1993) A new lipopeptide biosurfactant produced by *Arthrobacter* sp. strain MIS38. *J Bacteriol* 175(20):6459–6466
60. Youssef NH, Duncan KE, Nagle DP, Savage KN, Knapp RM, McInerney MJ (2004) Comparison of methods to detect biosurfactant production by diverse microorganisms. *J Microbiol Methods* 56(3):339–347
61. Ohno A, Ano T, Shoda M (1995) Production of a lipopeptide antibiotic, surfactin, by recombinant *Bacillus subtilis* in solid state fermentation. *Biotechnol Bioeng* 47(2):209–214
62. Jarvis FG, Johnson MJ (1949) A glyco-lipid produced by *Pseudomonas aeruginosa*. *J Am Chem Soc* 71(12):4124–4126
63. Hisatsuka K, Nakahara T, Sano N, Yamada K (1971) Formation of rhamnolipid by *Pseudomonas aeruginosa* and its function in hydrocarbon fermentation. *Agric Biol Chem* 35(5):686–692
64. Gorin PAJ, Spencer JFT, Tullock AP (1961) Hydroxy fatty acid glycosides of sophorose from *Torulopsis magnoliae*. *Can J Chem* 39:846–895
65. Arima K, Kakinuma A, Tamura G (1968) Surfactin, a crystalline peptidelipid surfactant produced by *Bacillus subtilis*: Isolation, characterization and its inhibition of fibrin clot formation. *Biochem Biophys Res Commun* 31(3):488–494
66. Raaijmakers JM, Bruijn ID, Nybroe O, Ongena M (2010) Natural functions of lipopeptides from *Bacillus* and *Pseudomonas*: more than surfactants and antibiotics. *FEMS Microbiol Rev* 34(6):1037–1062
67. Morikawa M, Hirata Y, Imanaka T (2000) A study on the structure–function relationship of lipopeptide biosurfactants. *Biochim Biophys Acta* 1488(3):211–218
68. Roongsawang N, Lim SP, Washio K, Takano K, Kanaya S, Morikawa M (2005) Phylogenetic analysis of condensation domains in the nonribosomal peptide synthetases. *FEMS Microbiol Lett* 252(1):143–151
69. Balibar CJ, Vaillancourt FH, Walsh CT (2005) Generation of D amino acid residues in assembly of arthrofactin by dual condensation/epimerization domains. *Chem Biol* 12(11):1189–1200
70. Lim SP, Roongsawang N, Washio K, Morikawa M (2007) Functional analysis of a pyoverdine synthetase from *Pseudomonas* sp. MIS38. *Biosci Biotechnol Biochem* 71(8):2002–2009
71. Roongsawang N, Washio K, Morikawa M (2011) Diversity of nonribosomal peptide synthetases involved in the biosynthesis of lipopeptide biosurfactants. *Int J Mol Sci* 12(1):141–172

Part IV
Design of Environmental Materials

Environmentally Friendly Adsorbents



Eko Siswoyo, Yingjie Dai, Masanobu Mori, Nobuhiko Wada,
and Hideyuki Itabashi

Contents

1	Introduction	294
2	Adsorbent Based on Solid Waste Materials	296
2.1	Paper Sludge for Removal of Cadmium Ion in Water	296
2.2	Adsorbent Based on Drinking Water Treatment Plant Sludge	298
2.3	Adsorbent Based on Platanus Leaf	302
2.4	Conclusion	306
3	Agricultural Products and Waste-Based Absorbents	306
3.1	Konjac Glucomannan Gel Embedded with Activated Carbon	306
3.2	Spent Coffee Ground	308
3.3	Auricularia Auricularia	309
3.4	Biochar from AA Dregs	312
3.5	Carbon Material	313
3.6	Conclusion	315
4	Utilization of a Fermented Bark Amendment That Can Be Assimilated into Soil	315
4.1	Suppression of Cadmium Uptake in Rice Using Fermented Bark	316
4.2	Application of FBA to Large-Scale Crop Cultivation	320
4.3	Simultaneous Suppression of Magnetic Nanoscale Powder and Fermented Bark Amendment for As and Cd Uptake by Radish Sprouts Grown in Agar Medium ...	324
4.4	Conclusion	328
5	Conclusion	328
	References	329

E. Siswoyo (✉)

Department of Environmental Engineering, Universitas Islam Indonesia, Yogyakarta, Indonesia
e-mail: eko_siswoyo@uui.ac.id

Y. Dai

College of Resources and Environment, Northeast Agricultural University, Harbin, China
e-mail: yingjiedai@neau.edu.cn

M. Mori

Faculty of Science and Technology, Kochi University, Kochi, Japan
e-mail: mori@kochi-u.ac.jp

N. Wada and H. Itabashi

Graduate School of Science and Technology, Gunma University, Kiryu, Gunma, Japan
e-mail: t15807009@gunma-u.ac.jp; itabashi@gunma-u.ac.jp

Shunitz Tanaka, Masaaki Kurasaki, Masaaki Morikawa, and Yuichi Kamiya (eds.), 293
Design of Materials and Technologies for Environmental Remediation,
Hdb Env Chem (2023) 115: 293–334, DOI 10.1007/698_2021_827,
© The Author(s), under exclusive license to Springer Nature Singapore Pte Ltd 2022,
Published online: 24 August 2022

Abstract Contamination of organic and inorganic substances in water, such as heavy metal ions and dyes, is found in almost every country, including developed and developing countries. The presence of these pollutants in the environment frequently resulted in negative effects on the human body and also ecosystem. So far, many technologies to remove pollutants, filtration, precipitation, ion exchange, phytoremediation, adsorption, and so on have been developed. Among these, adsorption is regarded as one of the most promising methods due to its high adsorption capacity and easiness of operation, and then many kinds of adsorbent materials have been researched. The most common adsorbent material used in many places is activated carbon; however, this adsorbent is quite expensive. This chapter introduces some environmentally friendly adsorbents, which are low-cost, safe, and non-harmful adsorbents based on natural products and solid waste materials. Especially, natural materials like plants, solid waste, and agricultural waste investigated in our laboratories are described here. Most of them have the large surface area and some useful functional groups for adsorbing, and then they originally have the high adsorption capacity for pollutants. The treatment of the adsorbents with chemicals like citric acid and phosphoric acid improved their adsorption capacities for metal ions. Some agricultural waste, such as konjac glucomannan, spent coffee grounds, and biochar, have the ability to remove organic compounds and dyes from water. Furthermore, it is introduced that the fermented bark amendment from the thinning of cedar can suppress the uptake of cadmium ion in rice.

Keywords Biochar, Drinking water treatment sludge, Environmentally friendly adsorbent, Fermented bark, Konjac glucomannan, Platanus leaf, Spent coffee ground

1 Introduction

Many water and wastewater treatment technologies have been developed in order to solve the contamination of heavy metal, including membrane filter [1], bio-sorption [2], neutralization [3], phytoremediation [4], ion exchange [5], precipitation [6], and adsorption [7]. Adsorption is known as one of the most effective for water and wastewater treatment, especially activated carbon is frequently employed. It is considered as the most common long-term adsorbent and has been used for the removal of many organic pollutants and also metal ions in water. Due to its large surface area and the presence of certain functional groups that are significant for metal binding, it has the high adsorption ability even for metal ions. However, its comparatively high cost puts it at a disadvantage for other sorts of adsorbents, such as biosorbents [8, 9]. Therefore, the development of low-cost and environmentally friendly adsorbent has been required. The term “environmentally friendly” literally means friendly for the earth and not harmful to the environment. Then environmentally friendly adsorbent is the safe and not-harmful adsorbent, in a narrow sense which is prepared from natural or waste materials and useful for removing pollutants

Table 1 Classification of the environmentally friendly adsorbents

Category	Adsorbent materials	Target	Characteristic	References
Natural material	Scallop shell	Metal ions	The large surface area	[10]
	Freshwater snail shell	Metal ions	The main functional groups responsible for chelation are OH, C=O, C=C, and C-C	[11]
Plant	Platanus leaf	Cadmium	Main element is cellulose with carboxylate group	[12]
	<i>Eucalyptus camaldulensis</i>	Metal ions	The thick wall structure along with a well-developed wider porosity	[9]
	<i>Jujube</i>	Metal ions	The irregular and inflexed surface morphology	[13]
	<i>Auricularia auricularia</i>	Neutral red (NR)	Has -OH/NH, -COH, C=C, -CO, and benzene ring skeletons	[14]
	Mango peel waste	Metal ions	The carboxyl and hydroxyl functional groups	[15]
Solid waste	Paper sludge	Cadmium	The phosphate functional group	[16]
	DWTP sludge	Cadmium	Main elements are Al and Si	[17]
	Coal fly ash	Metal ions	The large surface area	[8]
Agricultural waste	Konjac glucomannan	Organic compounds	Contains activate carbon	[18]
	Spent coffee ground	Metal ions and dye	The large surface area	[19, 20]
	Biochar	Tetracycline	The porous surface	[21]
	Carbon material from the combustion of forest branches	Methyl orange (MO) and methylene blue (MB)	Has a partial tubular or rope-like structure	[22]
	Bark	Cadmium uptake in rice	Consists of natural polymers, such as lignin and cellulose	[23]

from the environment. The environmentally friendly adsorbents are classified into several kinds as shown in Table 1.

The environmentally friendly adsorbents classified in Table 1 have a high ability in removing contaminants including heavy metal ions and organic substances from water and soil. The presence of some functional groups, porous structure, and large surface area of these adsorbents plays important role in removing the target contaminants. Considering the availability and cost performance of the environmentally friendly adsorbent, the development of these adsorbent materials is very promising for environmental remediation in the near future.

2 Adsorbent Based on Solid Waste Materials

Recently, the development of adsorbent for the removal of metal ions based on solid waste materials has been studied by many researchers because of its high ability in removing some metal ions, low cost in preparation, and easiness in getting these materials. Sludge from drinking water treatment plant and from paper industry and some kinds of biomass such as leaves and seeds have their potency to be utilized as environmentally friendly and low-cost adsorbent. The characteristic of each adsorbent material is so interesting to be examined to understand the adsorption mechanism and its adsorption capacity for the removal of metal ions in water. In this section, some adsorbents based on solid waste materials that we have developed are introduced.

2.1 Paper Sludge for Removal of Cadmium Ion in Water

The amount of pulp and paper production is rising every year in many countries around the world and the production process has still problems with the appearance of solid waste. The top ten pulp producers are the USA, China, Canada, Brazil, Sweden, Finland, Japan, Russia, Indonesia, and Chile. Approximately 40–50 kg of sludge (dry) is generated by the processing of 1 ton of paper at a paper mill, of which approximately 70% is primary sludge and 30% secondary sludge [24]. Japan's paper industry remains to produce a large paper sludge as solid waste material that is disposed of in landfills. The amount of paper sludge disposed of by the Japanese paper industry in landfills is about five million tons per year [25]. The treatment of paper sludge in landfill or incineration is expensive and may create newly environmental problems such as the elution of heavy metals and pollution with dioxins. The use of paper sludge as a raw adsorbent material has many benefits, decreasing the amount of solid waste and treatment costs and providing a low-cost adsorbent for the removal of heavy metals. Paper sludge as an adsorbent medium has a high capacity to remove metal ions from water [16].

The characteristics of the paper sludge are defined on the basis of SEM, surface analyzer (BET), and FTIR data. The surface structure of the paper sludge before and after treatment with phosphoric acid as a modifier for the surface is shown in Fig. 1. It is quite difficult to find out the effect of activation with some chemicals on adsorbent materials only by using SEM image because the images of these adsorbents are almost similar. However, from the image of both adsorbents we can state that the adsorbent becomes more porous after the treatment using phosphoric acid. The result of surface analyzer test based on BET strengthened the data of SEM. The surface area of raw paper sludge was $50 \text{ m}^2/\text{g}$ and then increased into $83.5 \text{ m}^2/\text{g}$ after treatment with phosphoric acid maybe because of the ability of this acid in releasing dirty particles from the paper sludge.

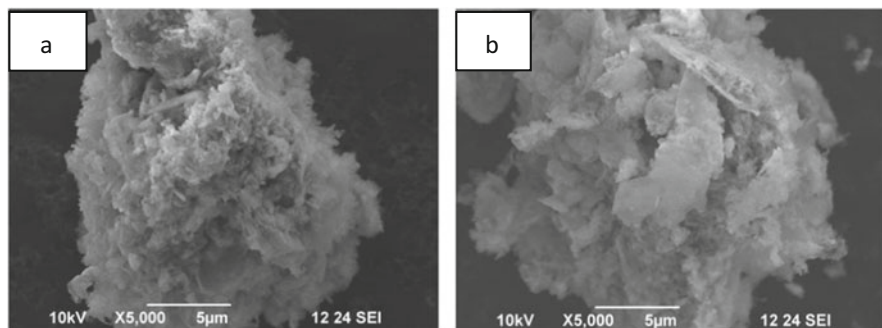


Fig. 1 SEM images of paper sludge before (a) and after treatment with H_3PO_4 (b)

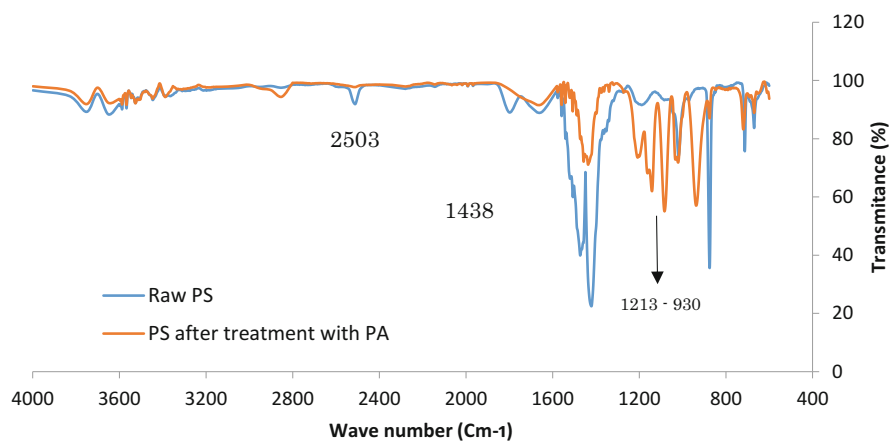


Fig. 2 FTIR spectra of paper sludge (PS) before and after treatment with H_3PO_4

Paper sludge has some functional groups which are important to bind metal ions. Based on the data of FTIR spectra as shown in Fig. 2, we can see that the activated paper sludge has some new peaks between 930 and $1,213\text{ cm}^{-1}$ and they indicate the presence of the functional groups generated by the activation process with phosphoric acid. These functional groups have an important role in binding some metal ion such as cadmium in water. Therefore, the adsorption capacity increased significantly after the modification with phosphoric acid.

Figure 3 clearly shows that the impregnation ratio during the activation process influences the performance of the adsorbent for removing metal ion in water. The impregnation ratio is the ratio between adsorbent material and the chemicals used for the activation (weight/weight). The best impregnation ratio for the removal of cadmium by using phosphoric acid is 0.5 (paper sludge: phosphoric acid = 50%: 50% of weight). The highest adsorption removal for 10 mg/L of cadmium ion by using 200 mg of the activated adsorbent at pH 6.0 was 97.74%.

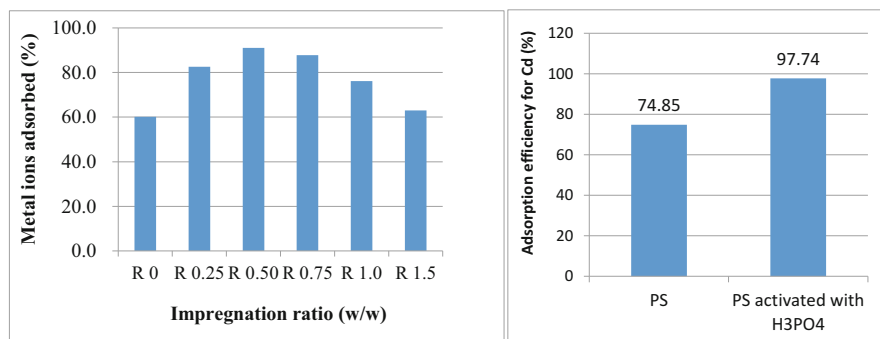


Fig. 3 The effect of the treatment with H_3PO_4 on Cd removal by the paper sludge

2.2 Adsorbent Based on Drinking Water Treatment Plant Sludge

Drinking water treatment plant sludge (DWTPS) is a by-product of the precipitation process that uses coagulant, and it is produced in large quantities in most municipalities around the world on a daily basis. In the developed countries, this sludge is mostly disposed as solid waste to the landfill, however, in some developing countries, it is discharged into the river because of the high processing cost at landfill. The quality of the drinking water source, the type of coagulant, and the treatment plant system all have an impact on the property of the DWTP sludge. If water sources for drinking water would be contaminated, DWTPS could contain some contaminants in it. However, ordinary clean water sources are preferred for drinking water production, and then the levels of contaminants or hazardous substances in DWTP sludge are low enough to use it as an adsorbent. As a result, using DWTP sludge as an adsorbent material may be feasible.

Adsorption of metal ion on the adsorbent is influenced by some factors, and among them pH of the solution is one of the most important factors [17, 26]. The surface charge of the adsorbent is strongly influenced by the pH of the solution. There are several ways how the initial pH of the solution can influence the adsorption capacity: (1) the electrostatic repulsion and affinity between adsorbent and adsorbate [8, 27, 28]; (2) the process of ion exchange between adsorbent and adsorbate [15, 29]; and (3) the distribution of metal species, such as soluble or insoluble and cationic or anionic [26, 30]. In extreme acidic conditions the surface of the adsorbent has dominantly positive charges, and therefore the adsorbent has the low adsorption capacity for metal ion with positive charge such as cadmium (Cd^{2+}), lead (Pb^{2+}), and copper (Cu^{2+}) because of the electrostatic repulsion between the adsorbent and adsorbate.

The results of the adsorption study using the DWTPS for removal of Cd^{2+} at different pH are shown in Fig. 4. For all types of the adsorbents (powdery raw sludge, powdery treated sludge, treated sludge encapsulated in alginate gel and

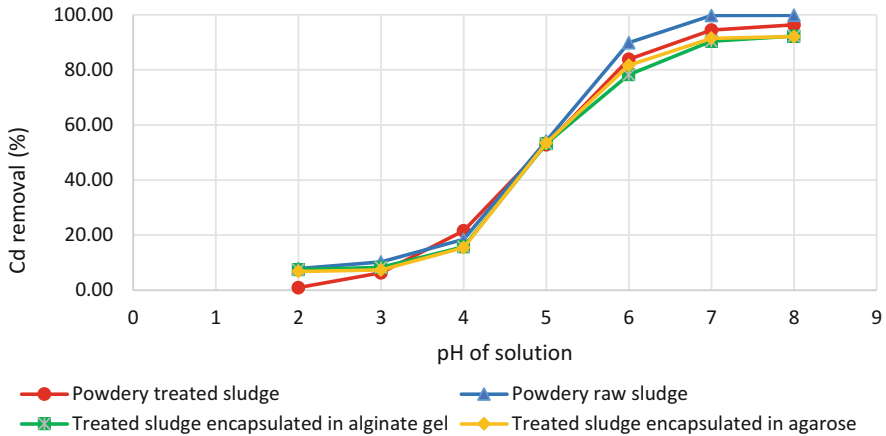


Fig. 4 The influence of pH solution on the adsorption of Cd ion in water

treated sludge encapsulated in agarose adsorbents), the removal efficiency increased as pH of the solution increased. Under pH 5, the adsorbent has positive charges, therefore it has a low cadmium adsorption removal due to the electrostatic repulsion between the adsorbent and cadmium ion. The favorable pH for cadmium removal was 6–7. The adsorption removal of cadmium becomes constant around pH 8 and cadmium ion in water will be precipitated at higher pH than pH 8.2 [17].

The adsorption potential of the adsorbent for metal ions can be evaluated using the Langmuir isotherm model. The Langmuir isotherm model was used to achieve the constant balance of the adsorption equilibrium by the following equation:

$$\frac{C_e}{q_e} = \frac{1}{q_m} C_e + \frac{1}{K_L q_m} \tag{1}$$

where C_e is the equilibrium concentration (mg/L), q_e is the amount of metal ion adsorbed at the equilibrium (mg/g), q_m and K_L are the Langmuir isotherm constants related to the adsorption capability and adsorption energy, respectively. From the above equation, a plot of C_e/q_e versus C_e will be employed to calculate the values of q_m and K_L as the tangent of the estimated straight line and its vertical axis intercept.

Beside Langmuir isotherm model, the Freundlich isotherm model can also be used to evaluate the isotherm process of adsorption. The equation of this model is:

$$q_e = K_f C_e^{1/n} \tag{2}$$

$$\text{Log} (q_e) = \text{log} (K_f) + 1/n \text{log} (C_e) \tag{3}$$

where q_e is the amount of metal ion adsorbed at the equilibrium (mg/g), C_e is the equilibrium concentration (mg/L), and K_f and n are the constants. We can determine the amount of K_f and n by plotting between $\text{log} C_e$ and $\text{log} q_e$.

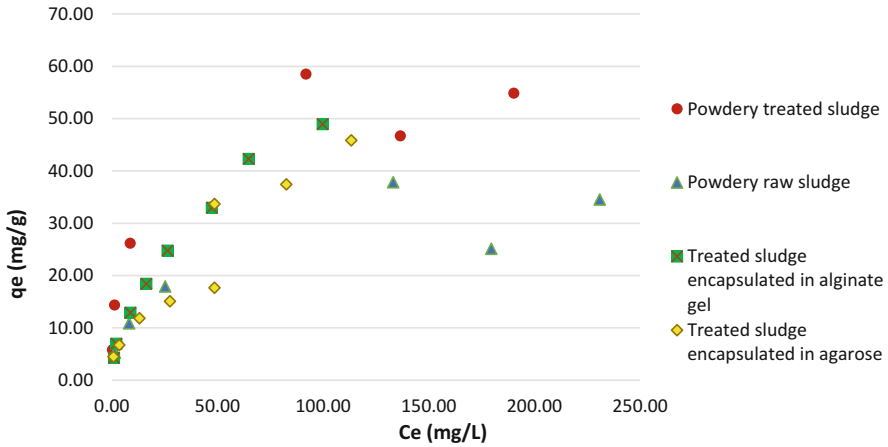


Fig. 5 Langmuir adsorption isotherm for Cd removal

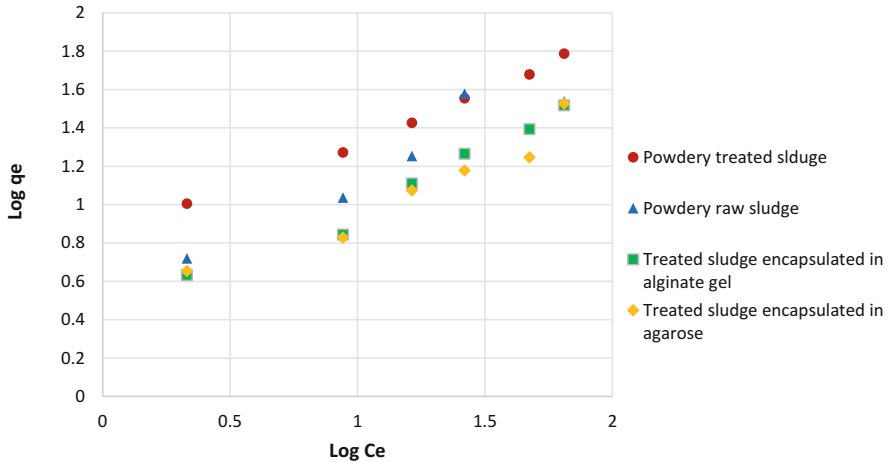


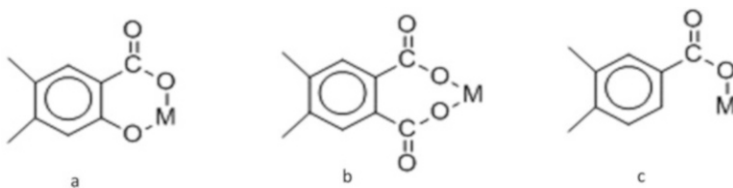
Fig. 6 Freundlich adsorption isotherm for Cd removal

Figures 5 and 6 show the Langmuir and Freundlich isotherms of those adsorbents based on sludge of drinking water treatment plant for the removal of cadmium ion in water.

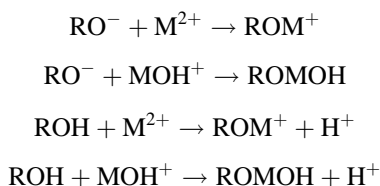
Most drinking water treatment plants in many countries use river water as their raw water because of its high quality, the stable supply in quantity and continuity. Compared to other water sources, river water is better in terms of the above criteria. In order to use the river water as the raw water for the drinking water treatment plant (by public water company) sustainably, the government needs to protect the river from contamination. The turbidity of raw water is one of the key parameters to be treated in the sedimentation tank. Most public water providers use some coagulants

to minimize the turbidity to meet drinking water requirements. The condition of the raw water and the type of coagulant affected the quality of the sludge from the sedimentation tank. Humic substances (natural organic matters) and iron hydroxide (from iron including in the coagulant) are commonly present in the DWTPS. Both components play an important role in the adsorption of metal ions by using an adsorbent obtained from a drinking water treatment facility.

The possible binding mechanism of cadmium ion with the DWTPS is suggested by considering the functional groups in the structure of humic substances: (a) by chelation between carboxyl and phenolic hydroxyl, (b) by chelation between two carboxyl groups, and (c) by complexation with a carboxyl group.



The presence of iron hydroxide as explained in the above paragraph also is suggested to have an important role in adsorption of metal ions. The possible mechanisms of adsorption by iron hydroxide are shown as follows.



where RO^- denotes a negatively charged surface of iron hydroxide, ROH denotes a neutral surface, and M denotes metal such as Cd . The mechanism of cadmium adsorption by using DWTP sludge is investigated by preparing the sludge similar to the DWTPS artificially. The artificial sludge were constructed by using the following process, in which kaolin, a white clay mineral, was used as the sludge's basic material and then combined with other elements such as Fe(III) , Mn(II) , and humic acid. In order to make a flock from these components, aluminium sulfate ($\text{Al}_2(\text{SO}_4)_3$) was used instead of coagulant (PAC) in the real drinking water treatment plant. Several types of artificial sludge were generated using various types and amounts of chemicals in order to search for the key constituents of the adsorbent for cadmium ion adsorption in solution. The amounts of each substance were determined by referring to the actual DWTPS as follows. In 1,000 mL of distilled water, 10 g of kaolin, 10 g of $\text{Al}_2(\text{SO}_4)_3$, 0.2 mg of Fe(III) , 0.05 mg of Mn(II) , and 1.2–2.4 mg of humic acid were added. A jar test using the mixed solution containing those components was carried out at 150 rpm for 5 min, and followed by a 10-min jar test at 40 rpm. The mixed solution was then rested for around 30 min until

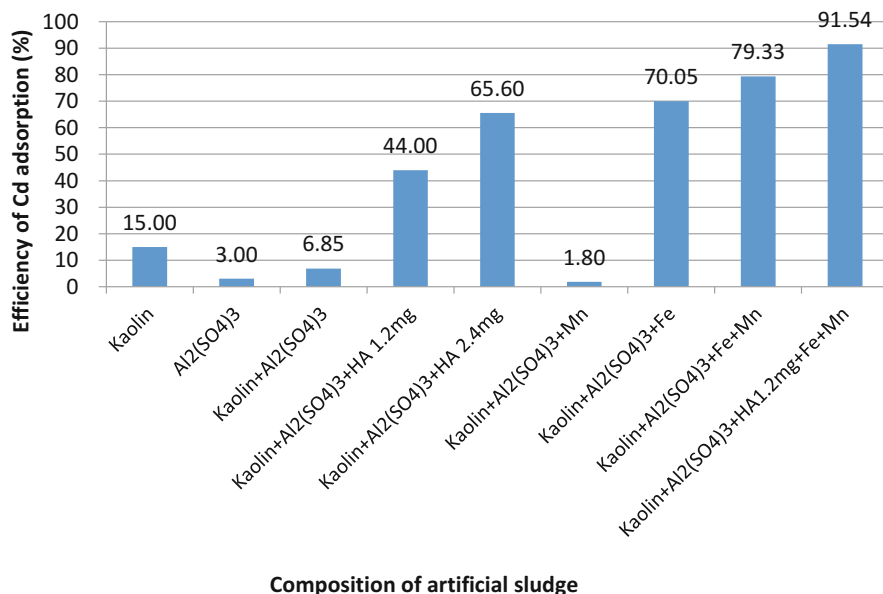


Fig. 7 Cd removal of some artificial sludge

precipitation occurred entirely to form sediment. According to the original sludge treatment, the sediment was removed from the solution by decantation, dried at 100°C for 24 h, and then crushed into powder. The amounts of humic substances and iron hydroxide are adjusted and then some kinds of the prepared artificial sludge were applied to the removal of cadmium ion in water. The results of the cadmium removal are shown in Fig. 7. The artificial sludge with the higher amount of humic substances and iron hydroxide showed the higher adsorption capacity, and therefore two components of the artificial sludge are suggested to play the most important role in the adsorption process [17].

2.3 Adsorbent Based on *Platanus Leaf*

The *Platanus* tree is common in Japan and many other Northern Hemisphere countries, where it is used as an ornamental and roadside tree. In Japan, the fall leaves of this tree are typically collected and discarded as garbage. The leaf of this tree has the potential to be a low-cost and environmentally friendly adsorbent material. However, the research on the use of the leaf of the *Platanus* tree as an adsorbent material is still limited. It is known that the modification of plant based adsorbents with citric acid is effective to improve the adsorbing ability for metal ions [31]. Therefore, in this section, the adsorbing ability of *Platanus* leaf modified with citric acid is introduced.

Table 2 The main elements of Platanus leaf before and after citric acid modification

Element (%w/w)	Type of adsorbent	
	Raw adsorbent	Citric acid modified adsorbent
Carbon (C)	49.98	49.90
Hydrogen (H)	5.78	6.14
Oxygen (O)	23.03	40.22
Nitrogen (N)	1.10	1.95
Ash	20.11	1.79

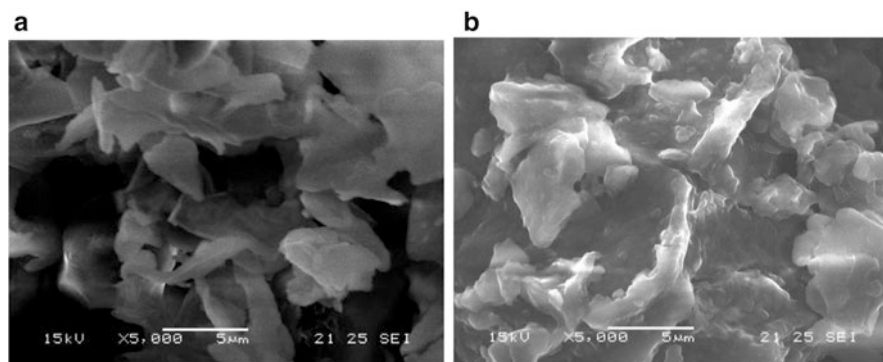
**Fig. 8** SEM images of Platanus leaf before (a) and after treatment (b) with citric acid

Table 2 shows the contents of principal elements of Platanus leaf before and after the treatment with citric acid. The content of oxygen (O) increased significantly after the treatment with citric acid because carboxyl groups (COOH) of citric acid are probably bound to the leaf by the reaction shown later. The presence of the carboxyl group in the adsorbent material is important for the adsorption of metal ions due to the complex formation.

The micromorphology of Platanus leaf before and after the treatment with citric acid can be seen in Fig. 8. The surface of Platanus leaf after treatment with citric acid seems to be brighter and more porous compared to that of the raw Platanus leaf. The increase in the porosity is also proved by the data obtained from the BET analysis. The surface area and pore volume of the raw leaf and treated leaf are $19 \text{ m}^2 \text{ g}^{-1}$ and $4 \text{ cm}^3 \text{ g}^{-1}$, and $32 \text{ m}^2 \text{ g}^{-1}$ and $7 \text{ cm}^3 \text{ g}^{-1}$, respectively. The surface area and pore volume are important to improve the adsorption capacity of the adsorbent, and therefore the larger surface area and pore volume of the adsorbent are, the higher adsorption capacity the adsorbent has usually.

The concentration of carboxylic acid of adsorbent materials was determined by titration method using NaOH as a titrant. The concentration of carboxylic acid of Platanus leaf before and after treatment with citric acid were 0.26 and 1.4 mmol/g,

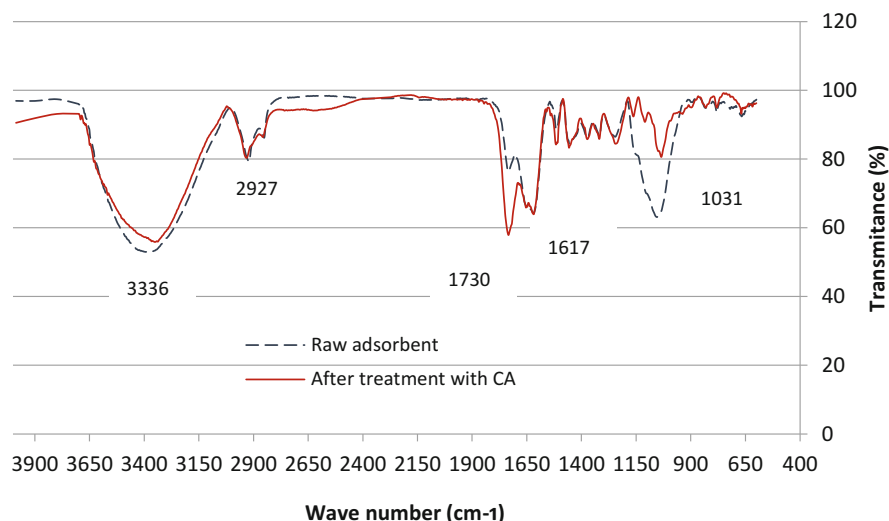


Fig. 9 FTIR spectra of *Platanus* leaf before (a) and after treatment (b) with citric acid

respectively. It was clear that the amount of carboxylic acid increased almost five times as the effect of treatment with citric acid.

The concentration of carboxylic acid in citric acid used for activation was 15.6 mmol/g and few parts of them (about 1.14 mmol/g) were bonded with *Platanus* leaf. Figure 10 presented the possible mechanism of the modification for *Platanus* leaf treated with citric acid. Cellulose, a main component of *Platanus* leaf, was bonded with carboxylic acid of citric acid to form the citric acid modified cellulose that has some carboxyl groups, which is important for metals binding. As shown in Fig. 9, the strong absorption band at $1,730\text{ cm}^{-1}$ of the modified adsorbent indicates the presence of carboxyl groups in *Platanus* leaf as the result of citric acid modification.

Powdery adsorbent has a larger surface area than granular adsorbent. However, the separation of the powdery adsorbent after adsorption process is difficult in comparison with granular adsorbent. Therefore, granular adsorbent is suitable for the application to real samples. The encapsulation of powdery adsorbent into alginate or agarose gel sometimes gives a solution for the separation of the adsorbent after adsorption. In this study, the adsorbent treated with citric acid was encapsulated in agarose gel. The adsorption capacities of the adsorbent before and after encapsulation are shown in Table 3. The adsorption capacity decreased largely after the encapsulation because of covering of the adsorbing sites with the gel. However, the encapsulated adsorbent still has enough adsorption capacity in comparison with that of the untreated adsorbent.

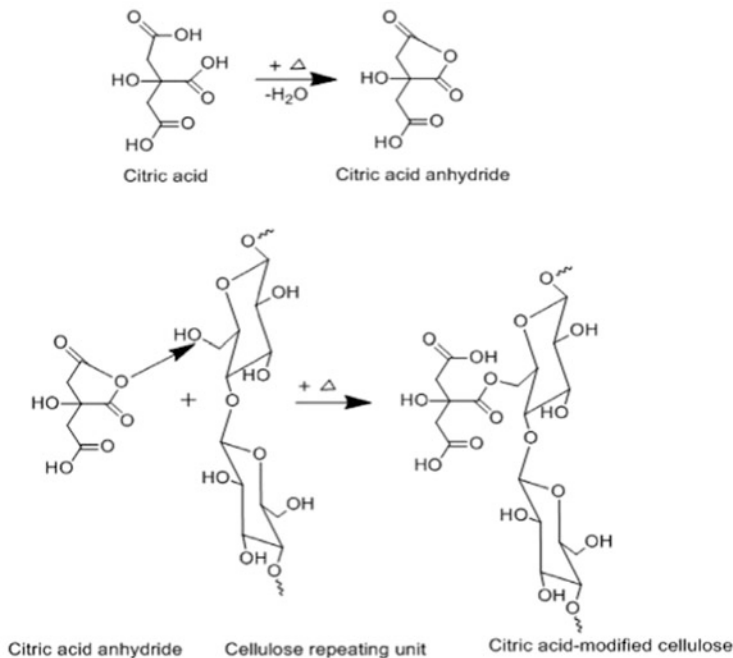


Fig. 10 Possible mechanism of modification for Platanus leaf with citric acid

Table 3 The adsorption capacities of Platanus leaf before and after encapsulation

Adsorbent	Langmuir model			Freundlich model		
	q_m (mg/g)	K_L (l/mg)	R^2	K_f	n	R^2
Raw Platanus	3.69	6.29	0.978	4.403	2.61	0.972
Platanus treated with CA	15.31	1.36	0.939	6.725	3.27	0.993
Platanus treated and encapsulated in agarose	6.89	2.48	0.948	4.709	2.64	0.991

The basic features of the Langmuir isotherm can be described by the dimensionless separation factor constant or by the equilibrium parameter R_L defined as: $R_L = 1 / (1 + K_L C_0)$, where K_L is the Langmuir constant and C_0 is the initial concentration of the adsorbate in the solution. The R_L value shows the shape of the isotherm:

$R_L > 1$	Unfavorable
$R_L = 1$	Linear
$0 < R_L < 1$	Favorable
$R_L = 0$	Irreversible

The R_L value between 0 and 1 is favorable for adsorption [32]. The R_L values of raw, treated (powdery), and encapsulated adsorbents for 10 mg/L of cadmium ion

are 0.016, 0.069, and 0.039, respectively. It was proved that *Platanus* leaf-based adsorbents are favorable for the removal of cadmium ion in water.

2.4 Conclusion

The adsorbents based on paper sludge, drinking water treatment plant sludge, and leaf of *Platanus* have good performance in reducing cadmium ion in water. The presence of some functional groups, humic acid, and iron (for DWTPS) are considered as the major elements for metal adsorption. These developed adsorbents are suggested to be the low-cost and environmentally friendly adsorbents for the removal of heavy metal ions in water.

3 Agricultural Products and Waste-Based Adsorbents

There have been many kinds of the adsorbent that can effectively adsorb harmful and toxic substances in the environments. Moreover, with the vigorous development of environmental protection technologies, many new adsorbents have emerged in an endless stream. For the application of these adsorbents to the actual polluted sites, adsorbents should be low cost, easy to obtain, and environment-friendly in addition of the conventional functions like the high capacity and selectivity. Especially, among agricultural products and wastes, there are many candidates for the adsorbents having these properties, which illustrate significant benefits in the environmental field, and some of them surpass the traditional adsorbents. In this section, the author's recent researches on the development of the adsorbents based on agricultural products and waste are introduced. Five kinds of the adsorbents developed by authors, konjac glucomannan gel embedded with activated carbon, spent coffee ground, *Auricularia auricularia*, biochar and carbon material, are described.

3.1 Konjac Glucomannan Gel Embedded with Activated Carbon

Konjac plant is grown in some Asian countries for its edible use. Konjac glucomannan (KGM) is a high-molecular weight water-soluble nonionic natural polysaccharide isolated from the konjac plants, which is nontoxic and low cost, and the chemical structure is shown in Fig. 11 [33]. KGM gel (KGMG) is formed by heating a KGM solution in the presence of alkali compound or higher amount of neutral salt [34]. In the food industry of China and Japan [35–37], KGMG has been used widely as a non-caloric health-care food. The KGM itself has a low adsorption

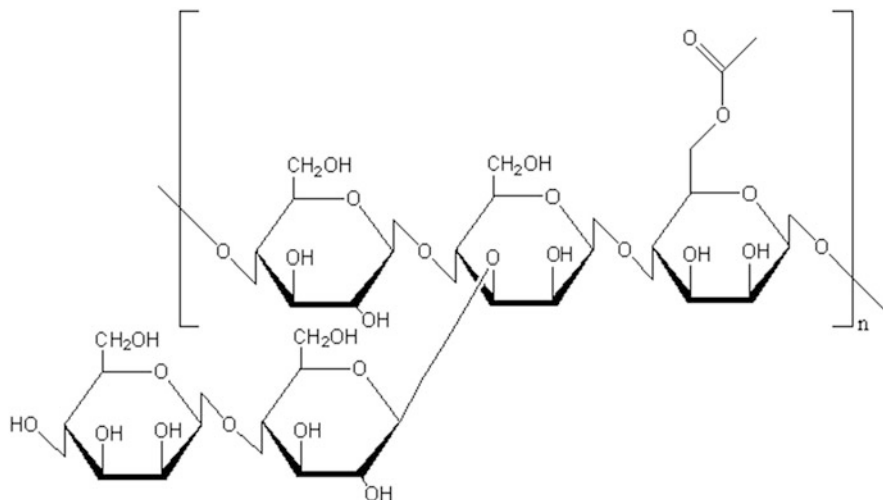


Fig. 11 Chemical structure of konjac glucomannan (KGM) [32]

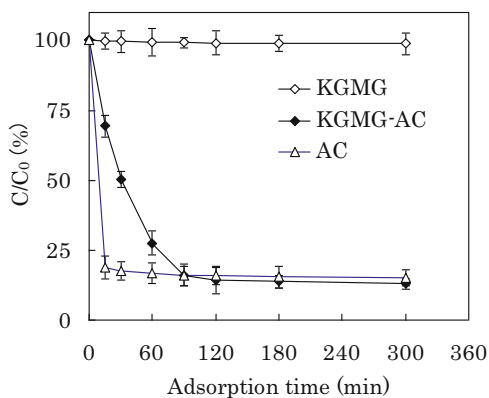


Fig. 12 The removal ratio of nitrobenzene (NB) as a function of time using AC(10 mg), KGMG (1 g) and KGMG-AC(1 g containing 10 mg AC)

ability, but can act as a carrier for the adsorbent by the encapsulation of the adsorbent like activated carbon with the KGM's gel network structure (KGMG-AC). The encapsulation of adsorbent with the gel network can make only small molecules participate in the adsorption process but block macromolecules like humic substances as pointed out in the study using alginate gel beads by Fugetsu et al. [38]. Therefore, it can improve the selectivity of adsorption and consequently extend the lifetime of the adsorbent.

The experimental results using the KGMG-AC showed that the KGMG-AC adsorbed NB well, slightly better than AC itself as shown in Fig. 12. Some organic dyes such as Methylene Blue (MB) and Rose Bengal (RB) in solution could be

removed by KGMG-AC. Humic substances play an important role in supplying nutrients to plants and microbial organisms and also in maintaining the crumb structure of soil. The use of AC to remove pollutants in agriculture water sometimes leads to the removal of precious humic substances. Therefore, we attempted to avoid the adsorption of humic acid by the encapsulation of AC with KGMG.

100 mg/L humic acid solution was shaken with 10 mg of AC or 1 g KGMG containing 10 mg AC for 5 h at 25°C. As a result, 47% of humic acid in the solution adsorbed on AC, however, it is noteworthy that humic acid did not adsorb at all KGMG-AC. The gel structure of KGM around the AC might suppress the transport of humic acid to the AC entrapped within the KGMG. It shows that KGMG-AC has the potential for the selective removal of agricultural chemicals from the wastewater [18].

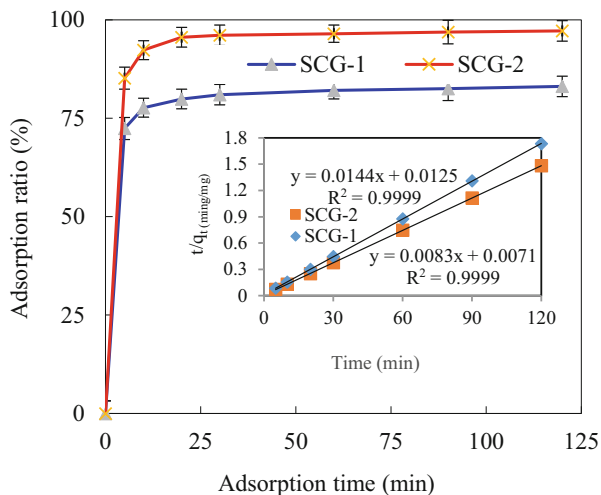
In conclusion, KGMG-AC prepared from a safe food processing material showed the high efficiency in the adsorption of some organic contaminants, slightly higher than that of AC itself. More importantly, it provided the possibility of selective adsorption for small molecules avoiding the adsorption of large molecules such as humic substances. Consequently, KGMG-AC will be a complete safe, low-cost, and environment-friendly adsorbent.

3.2 Spent Coffee Ground

Coffee is one of the most consumed beverages in the world. According to the latest International Coffee Organization (ICO) statistics, global coffee consumption for the year 2019–2020 has reached 10 billion kg [39], which cause a release of a notable amount of solid and liquid residues. About 90% in weight of coffee berries is discarded during manufacturing as agricultural waste and by-products. Spent coffee ground (SCG) is a waste residue from the ground coffee beans after extracting them with hot water and the porous structure of the SCG can act as the adsorbing sites. The dry SCG has been used for the removal of the moisture and smell in a refrigerator and room. In this study, the ability of the SCG to absorb tetracycline (TC) in water was investigated. TC is widely used in aquaculture as the antibiotics. Since not degradable easily in environment, it stays for a long time in environment and has a possibility to affect the ecosystem. In this section, we introduce the removal of TC with the SCG as an adsorbent. In this study, two kinds of the SCG were used; SCG-1 produced from coffee Arabica beans of Hainan Province of China and SCG-2 produced from coffee Arabica beans of Yunnan Province of China.

It can be retrieved from Fig. 13 that the adsorption reaction reached equilibrium quickly within about 20 min. At the initial stage of adsorption, the removal ratio of TC was high, and the adsorption ratio slowed down over time until the adsorption equilibrium reached. The pseudo-first-order model and the pseudo-second-order model were used to analyze the kinetic experiment data, the R^2 of pseudo-second-order had a higher degree of fitting compared the correlation coefficients of pseudo-first-order with that of pseudo-second-order kinetic. Therefore, it was concluded that

Fig. 13 Effect of adsorption time and Pseudo-second-order kinetic plots of TC by SCG-1 and SCG-2



the adsorption of TC by the SCGs progresses according to the pseudo-second-order model.

Although the BET surface area of SCG-1 ($451 \text{ m}^2/\text{g}$) was slightly larger than that of SCG-2 ($419 \text{ m}^2/\text{g}$), the adsorption equilibrium constant of TC by SCG-2 was almost twice as high as that of SCG-1. This indicated that the adsorption capacity of SCG-2 to TC depended mainly on the chemical properties of the surface, rather than the BET surface area [19, 20, 40]. The SCG-2 surface has a large amount of oxygen-containing functional groups in which the carboxyl group, the lactone group, and the phenol group can form a hydrogen bond on the TC molecules with the hydroxyl groups of C10 and C12 (see Fig. 14) [41]. The adsorption mechanism is through the hydrogen bond, and also the π - π interaction occurs at the interface between the TC molecule and the SCG. The results showed that second-hand coffee grounds had a great potential to be an inexpensive alternative adsorbent for tetracycline removal in wastewater treatment.

3.3 *Auricularia Auricularia*

In China's textile mills, as the working environment is full of cotton wadding, the factory often distributes fungus (such as *Auricularia auricularia*) free of charge. Because the colloid of *Auricularia auricular*(AA) has strong adsorption capacity, it can adsorb and gather the dust and dregs remaining in the human digestive system and discharge them out of the body. It has the function of cleaning the stomach. Based on this fact, we came up with the idea of using AA in dye removal. AA, one of the four most important cultivated edible fungi in the world, is nutrient-rich and has pharmacological functions. AA grows on the rot and is like a gelatinous sheet. The

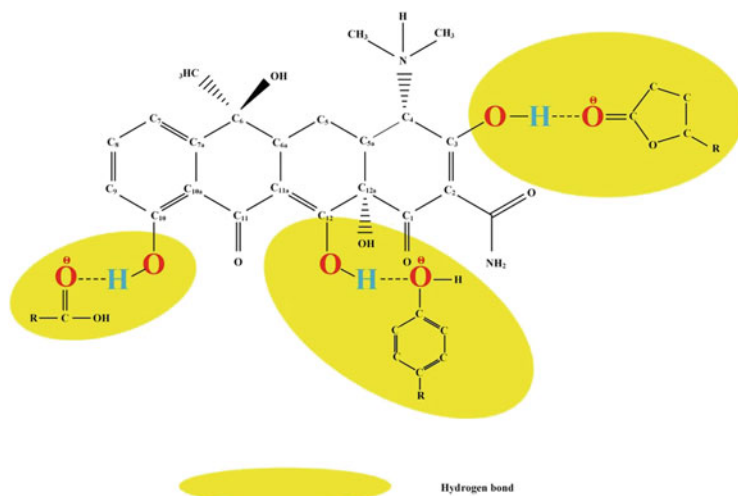


Fig. 14 The mechanism of hydrogen bonds for TC adsorption on SCGs

origin of AA is mainly in China, Thailand, Japan, and other countries in Asia. AA not only plays an important role in the field of food, but also can be used in the field of environment.

Two kinds of AA, AA-*Se*, and AA-*I* were selected in our studies. The content of Se in AA-*Se* was significantly higher than that of AA-*I*. As one of the essential micronutrients for humans and animals, Se is involved in the synthesis of more than 30 proteins and enzymes in mammals. Selenium deficiency can cause a variety of diseases in human body. By eating selenium enriched AA, we can supplement the selenium needed by human body. The results of the adsorption experiments showed that the AA-*Se* adsorbed Neutral Red (NR) better than AA-*I*. After AA-*I* adsorbed NR, there was no change in the type of functional group, and only the position of the absorption peak of some functional groups changed. Figure 15 shows that the functional groups of AA-*Se* mainly include $3,418.81\text{ cm}^{-1}$ ($-\text{OH}$ functional group), $2,926.18\text{ cm}^{-1}$ (lipid CH functional group), $1,735.78\text{ cm}^{-1}$ ($-\text{COH}$), and $1,655.06\text{ cm}^{-1}$ ($\text{C}=\text{O}$ stretching or aromatic $\text{C}=\text{C}$ and $\text{C}=\text{O}/\text{C}=\text{C}$ stretching), $1,560.44\text{ cm}^{-1}$ (secondary amine group), $1,377.69\text{ cm}^{-1}$ (CH bending, symmetric bending of $-\text{CH}$), $1,254.48\text{ cm}^{-1}$ (CN. stretching), $1,064.40\text{ cm}^{-1}$ (COH stretching), 605.45 cm^{-1} ($\text{Fe}-\text{O}$) [42, 43]. After adsorption of NR, some functional groups of AA-*Se* shifted or decreased. These results suggest that the $-\text{OH}/\text{NH}$, $-\text{COH}$, $\text{C}=\text{C}$, $-\text{CO}$, and benzene ring skeletons in AA-*Se* participate in the reaction with NR.

The adsorption mechanism diagram is shown in Fig. 16 [14]. The adsorption isotherm results showed that the adsorption of NR on AA-*I* and AA-*Se* was based on electrostatic adsorption. FTIR analysis showed that the functional groups in AA-*I* and AA-*Se* played a key role in NR adsorption, including aromatic skeleton vibration, C-H, C-O and Si-O-Si groups through π - π stacking and hydrogen bonding,

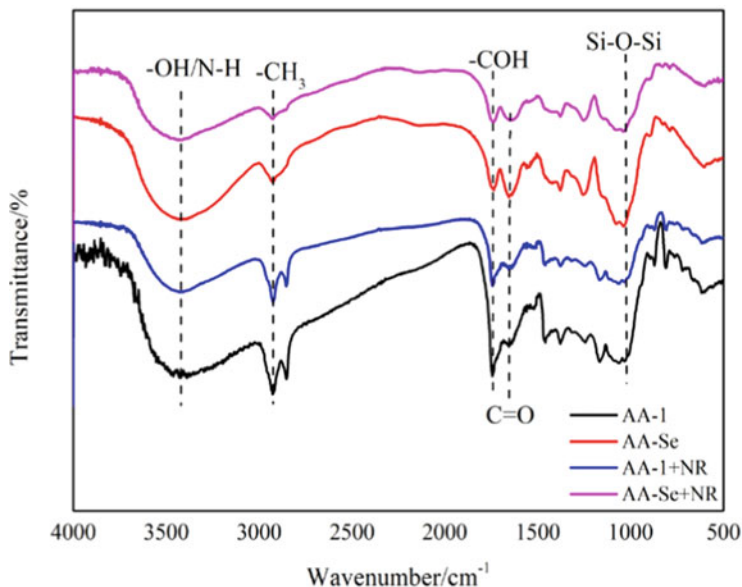


Fig. 15 FTIR spectra of AA-1 and AA-Se

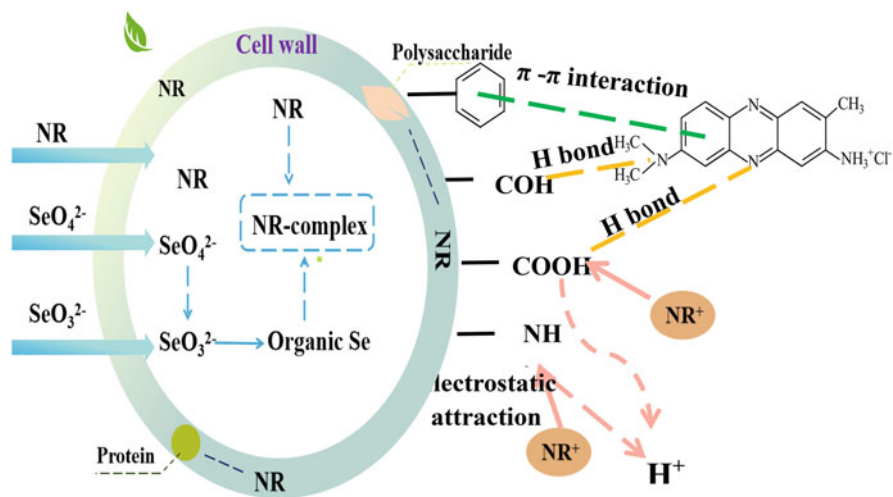


Fig. 16 Possible adsorption mechanism of NR on AA-1 and AA-Se

etc. The aromatic benzene rings of AA-1 and AA-Se easily form π - π stacking with the benzene ring of NR. In addition, the chemisorption mechanism plays an important role in the adsorption of NR by AA-1 and AA-Se. The mechanism involved in chemisorption is the formation of covalent bonds and ion exchange, and it is speculated that NR may cooperate with proteins and polysaccharides on the cell

wall of the adsorbent to immobilize NR on the cell wall. The experimental data also speculate that NR can be removed by the above oxidation-reduction reaction.

AA is a nontoxic and harmless food material, which can effectively adsorb some chemical dyes. The AAs are an environmentally friendly adsorbent with low cost and easy to obtain.

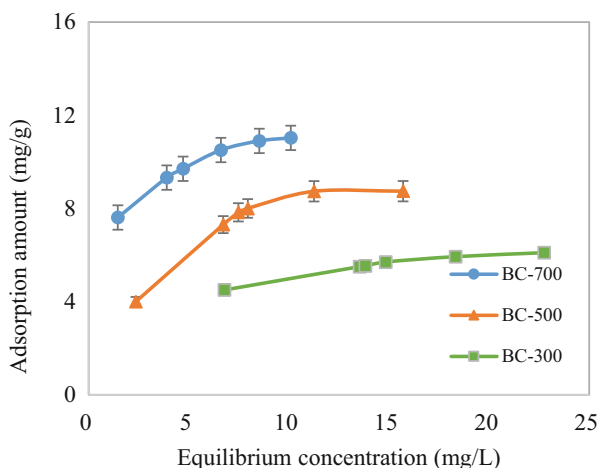
3.4 Biochar from AA Dregs

Biochar (BC) is a widely used adsorbent, because of its cost efficiency and adsorption properties [44]. The methods used for preparing raw materials to obtain BC are important, where the raw materials should not pollute the environment as well as being ready and available [45]. BC has a wide range of sources, such as *Pinus taeda*, rice husk, sawdust, tires, *Fargesia* leaves, and waste *Auricularia auricula* (AA) dregs.

AA dregs are a by-product of the edible AA industry, comprising a mixture of wood chips, wheat bran, corncob granules, lime and gypsum, which are used to cultivate AA. After bagging the mixture, it is sterilized at 100°C for 12 h, before inoculating the raw AA. The AA dregs are usually disposed of after harvesting the AA. China is the largest producer of edible AA with an annual output 22.6 million tons, which accounts for more than 75% of the total production [46]. Previous studies have showed that the production of 1 kg of edible AA generates 5 kg of waste AA dregs [47].

Waste AA dregs can be utilized as raw materials to produce BC for removing tetracycline (TC) from aqueous solutions in order to develop a cheap and readily available adsorbent. During the preparation process of BC from waste AA dregs, three different pyrolysis temperatures comprising 300, 500, and 700°C were tested. The results of adsorption isotherms obtained for the BCs are shown in Fig. 17 [21].

Fig. 17 Adsorption isotherm curves obtained for TC on BC-300, BC-500, and BC-700



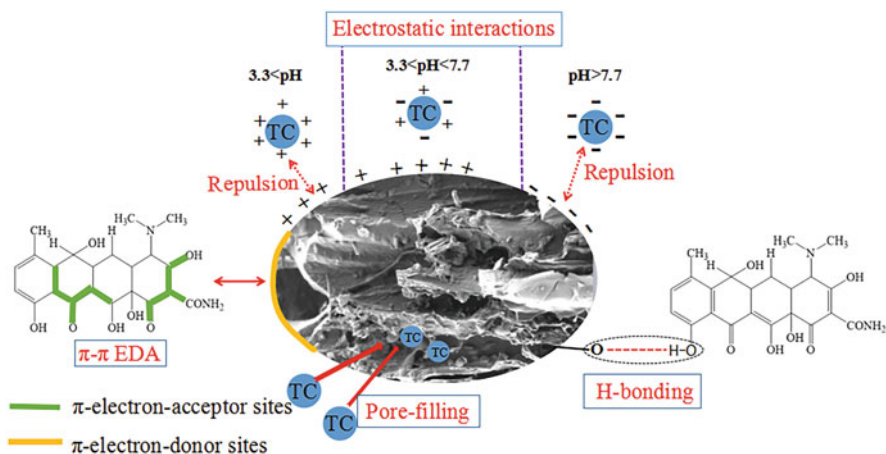


Fig. 18 Possible mechanisms responsible for adsorption of TC on BCs

Langmuir, Freundlich, Temkin, and D-R isotherm models were utilized to fit the isotherm data in order to explore the adsorption mechanisms [48]. The Langmuir model represents a process with monolayered adsorbents on a homogeneous surface [49], and obtained the best fit in previous studies of the adsorption of TC [50]. The results showed that the saturated adsorption capacities of BC-300, BC-500, and BC-700 were 7.22 mg/g, 9.90 mg/g, and 11.90 mg/g, respectively. After three cycles of ultrasonic vibration, the TC removal rates decreased for the three BCs. But given the low cost and ready availability of the waste AA dregs used as the raw material to produce the BCs, the dosages of the BCs could be increased during the reusability process to achieve the higher removal efficiencies.

The TC adsorption mechanisms for the BCs are shown in Fig. 18. The adsorption isotherm data fitted well with the D-R model and the Temkin isotherm model. H-bonds form readily when TC is adsorbed on BC. It is indicated that the pore filling effect, the formation of hydrogen bonds, and electrical recycling are all the principles of adsorption of TC. Finally, π - π electron-donor acceptor (EDA) interactions may have played a major role in the adsorption of TC onto the BCs according to the FTIR results. BC from AA dregs is a possible economical and environment-friendly adsorbent for the removal of TC from wastewater. Through the experiment, we knew that the BC prepared at the higher temperature had the greater capacity for removing TC.

3.5 Carbon Material

Carbon material (CM) derived from the combustion of forest branches has been widely used for the adsorption of nitrobenzene [51]. In this section, we are going to

introduce the removal of Methyl Orange (MO) and Methylene Blue (MB) from an aqueous solution using a CM derived from the combustion of forest branches. The CM used in this study was produced during combustion of wood chips in a gasification power plant (Thomas Koch Corporation, Denmark) in Oshu City in Japan. The wood chips were obtained from logging or thinning of trees (Japanese cedar and red pine after approximately 25 years of growth) during the summer of 2006. After dried and pyrolyzed, the part of the wood chips is inverted into CM. In order to observe the adsorption characteristics of the CM and the effect of the functional groups on the surface of the CM on the removal of dyes more clearly, we oxidized the CM for 4 h to obtain the oxidized version (Ox-CM), whose adsorption properties were compared with those of the CM.

The SEM pictures of the CM and the Ox-CM are shown in Fig. 19. These pictures show the surface texture and porosity of the adsorbents. A high porosity and large surface area are essential for highly efficient adsorbents. The SEM picture of the CM displays a partial tubular or rope-like structure, but the surface of the Ox-CM shows no such structure probably due to the oxidization with nitric acid. We have studied some factors affecting the adsorption, such as pH, ion concentration, and contact time. The removal ratio of MO decreased as the pH was increasing while the removal ratio of MB increased with the pH increased. The higher cationic strength and valence of salts showed the stronger adsorption of dye. An increase in temperature had a slight influence on the adsorption isotherms of this CM. The adsorption ratios of MO and MB on the CM after 3 h were 96.3% and 90.2%, respectively. The removal rates of the MO and the MB were quite fast during the initial 5 min, and then the removal ratio slowly increased and reached equilibrium after 3 h. This result is important because the equilibrium time is one of the considerations for application to the removal of dyes in a wastewater treatment plant [52]. The effect of the adsorption time on the MO and MB adsorption by the CM (initial concentration of MO (50 mg/L) and MB (50 mg/L), adsorbent dose = 0.40 g/L, pH = 7.0, at 25°C) was also investigated. The adsorbed dyes were almost completely released by the regeneration process, while the capacity for dye adsorption of the reused CMs remained unchanged. The adsorptive capacity was regained even after three cycles of

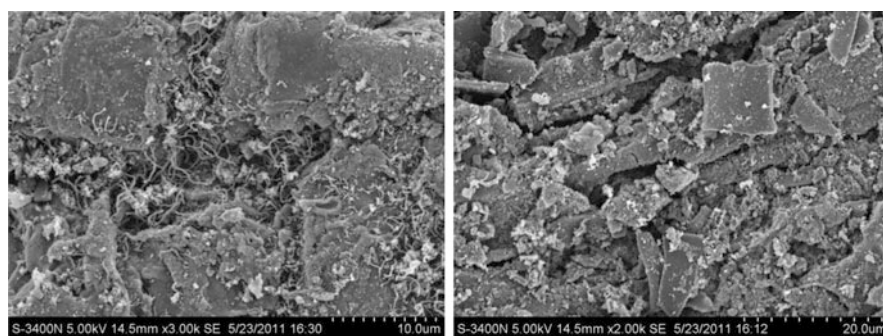


Fig. 19 SEM and FTIR images of the CM (left) and the Ox-CM (right)

adsorption and elution. So, the CM can be regenerated and reused many times [22]. The CM derived from the combustion of forest branches can be an inexpensive and environment-friendly adsorbent for the removal of organic dyes such as MO and MB from aqueous solutions.

3.6 Conclusion

It is very pleased to see that the discovery and application of environmental adsorbents are growing vigorously. But so far, there are still many pollution problems in the environments around us in spite of many efforts by various people. Therefore, more practical application, exploration and development of adsorbents still need to remediate our environments. Although the discovery of new adsorbents plays an important role in the field of environmental protection, it causes a new challenge to gradually improve the defects of adsorption process and give full play to the benefits of adsorbents to achieve maximum adsorption benefits. It is hoped that readers can understand the characteristics of these five types of adsorbents through this paper and promote the optimization and application of these five types of adsorbents, as looking forward to a greater breakthrough in the field of environmental adsorbents in the future.

4 Utilization of a Fermented Bark Amendment That Can Be Assimilated into Soil

We have investigated the properties of lignin in woody bark, which can adsorb heavy metals, and applied the fermented bark to fixing the heavy metals in soil and accelerating plant growth, considering as a mild recycle that woody biomass can be assimilated into soil.

Here, we introduce the suppression of cadmium uptake from soil to rice by the amendment produced from fermented bark (fermented bark amendment:FBA), and its application of FBA to large-scale rice farmland in China. In addition, we also describe simultaneous uptake suppression of arsenic and cadmium from a cultivation agar to radish by mixing a mixture of magnetic nanoscale powder (MNP) and FBA.

4.1 *Suppression of Cadmium Uptake in Rice Using Fermented Bark*

4.1.1 Introduction

We considered the potential of bark, an environmentally friendly material produced in abundance from the thinning of cedar in Gunma Prefecture, Japan, for soil restoration. Bark consists of natural polymers, such as lignin and cellulose, and has been primarily used for fuel production or as a soil substitute [53] in horticulture. Lignin, which represents about 20–35% of the cell wall of conifer wood, is particularly known for absorbing heavy metals [54, 55], since it is not easily decomposed by bacteria or hydrolyzed as happens with cellulose. However, white-rot fungus found in humic soil is known to decompose bark [56, 57]. The assimilation of bark in the soil can be accelerated by applying it in a decomposed state, instead of using it directly. Bark composts consist of decomposing bark that is rapidly assimilated into the soil to improve plant growth and soil quality [58]. However, the preparation of bark compost is time consuming and requires approximately 6–12 months for the decomposition to small organic compounds such as aliphatic carboxylic acids, aromatic carboxylic acids, or carbon dioxide (CO₂).

Our group has developed a soil amendment that could be used to reduce Cd uptake in brown rice. The fermented bark amendment (FBA) was produced by mixing recycled bark, rice bran, and white-rot fungus to accelerate the fermentation process and was obtained in 2–10 days using a rapid fermentation procedure (Fig. 20).

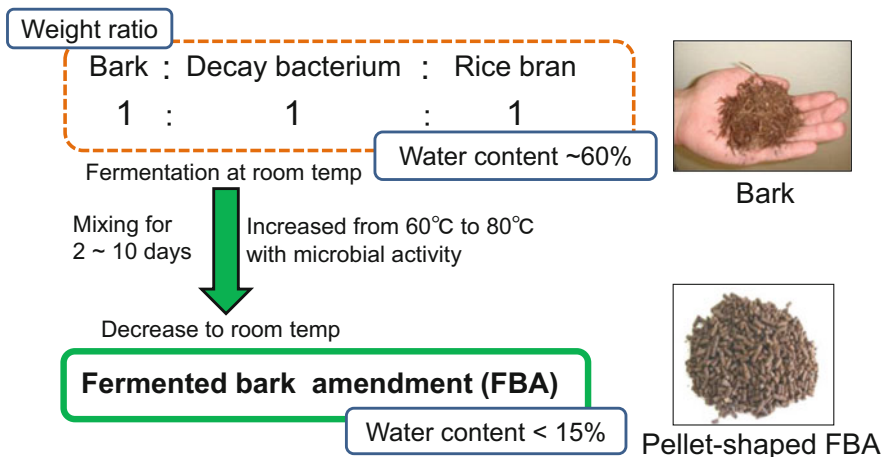


Fig. 20 Preparation process of FBA. Reproduced from Elsevier Copyright with permission

4.1.2 N, P, and K Contents in FBA

The N, P, and K contents in FBA were 3.2%, 0.6%, and 1.2%, respectively, giving a total content of less than 5.0%. Considering that the recommended total content of N, P, and K in commercial chemical fertilizers is 30%, the FBA has significantly lower N, P, and K levels and thus an inferior quality.

4.1.3 Rice Cultivation in Pot

Rice was cultivated for approximately 120 days between July and November in 2009–2014 on a rooftop at Gunma University, Gunma, Japan. The soil was collected from a site close to a Cu-Cd mine, with a Cd content of $2.2 \pm 0.7 \text{ mg kg}^{-1}$, which was lower than the reference value of 150 mg kg^{-1} for contaminated soil.

The FBA was mixed with 5 kg of soil at weight ratios ranging from 0.1 to 2.0%. At the same time, a high-grade compound fertilizer (N:P:K, 1:1:1) was added to all test soil samples at a rate of 0.5 g per pot (530 cm^2). The water regime was applied under “water-filling with midterm drying” (approximately 5 cm water depth), which is a common method for rice cultivation in Japan, which strengthens the roots of plants by temporarily allowing the soil to dry-out during paddy cultivation.

4.1.4 Effects of FBA Application and Water Regimes

We studied the effects of different FBA application amounts (0.1–2%, w/w) under water-filling on soil pH and ORP and the uptake of Cu, Zn, Cd and Pb in brown rice. The pH of soil supplemented with chemical fertilizers and FBA increased from 4 to 7, however, no significant differences were identified between the treatments. On the other hand, the ORP in soil supplemented with chemical fertilizers and FBA rapidly declined, probably due to the activities of methanogens or sulfate-reducing bacteria in the soil and water, which promote oxidative decomposition and generate CO_2 [59]. In fact, the amount of CO_2 and CH_4 increased with the amount of FBA due to the rapid reduction of soil.

The suppression of Cd uptake was clearly dependent on the amount of FBA applied to the soil. Cd concentration in rice cultivated in FBA-supplemented (0.1–2%, w/w) soil was significantly lower ($P < 0.05$) than that of rice cultivated in soil without FBA supplementation (i.e., chemical fertilizer only). When FBA (2%, w/w) was applied, the level of Cd absorption was reduced to about one-tenth of that obtained when only chemical fertilizers were used (Fig. 21). However, rice growth was poor in soils supplemented with more than 1% FBA (Fig. 22).

We also investigated the application effect of 1% (w/w) fertilizer that ferments rice bran (RB) and 1% (w/w) compost that ferments bark by water (BC) on the uptake of heavy metals in brown rice. The results indicated that the content of heavy metals in rice cultivated with RB and BC was lower than that cultivated with

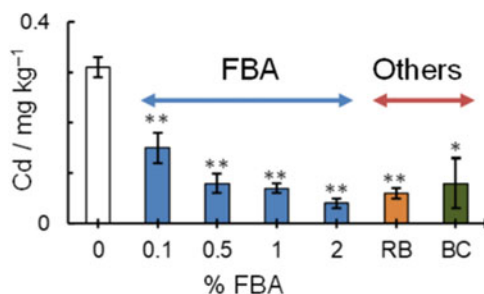


Fig. 21 Cd concentrations in brown rice after the application of FBA and other organic fertilizers to the soil under water-filling with midterm drying. RB, rice bran; BC, bark compost. RB and BC were applied to the soil at a rate of 1.0% (w/w). Asterisks indicate significant differences between bars at $P < 0.05$ (*), and $P < 0.01$ (**). Reproduced from Elsevier Copyright with permission

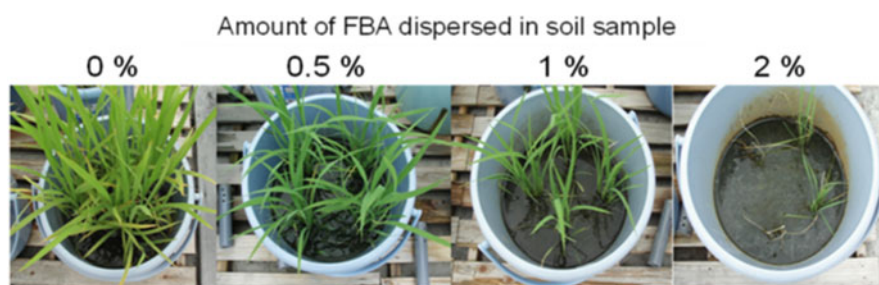


Fig. 22 Photos of paddies cultivated in FBA-supplemented soil for 30 days under medium drying conditions. Reproduced from Elsevier Copyright with permission

chemical fertilizers alone. However, the supplementation of RB provided strong odor during water-filling. The supplementation of BC did not obtain strong odor; however, the production of BC requires about 6–12 months.

4.1.5 Effect of a Timing for FBA Application

The application of FBA effectively suppressed the uptake of Cd in brown rice; when the roots of the paddy were still immature under water-filling conditions, it led to the failure of rice growth with a rapid decline in the ORP of the soil. Therefore, we applied 1% (w/w) FBA at 2, 4, 6, 8, and 9 weeks after rice planting and did not change the other conditions before. As the results, the crop failure could be minimized, because the roots are sufficiently grown to survive the reduction of ORP in the soil after 2 weeks after planting the seedlings.

Chino reports that the heavy metal uptakes into rice plants are maximal between 3 weeks before heading and 1 week after heading [60]. Based on the amount of Cd uptake in brown rice, the changes in soil ORP, and the growth of rice plants, we

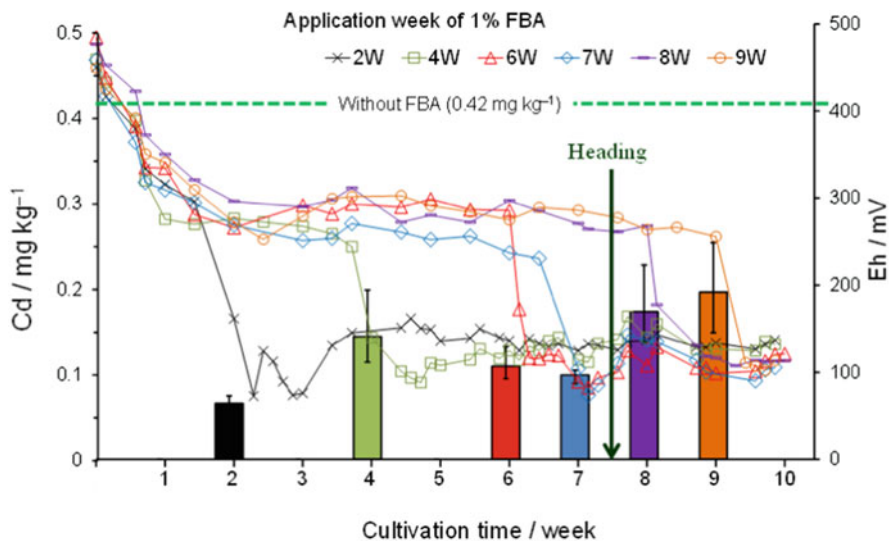


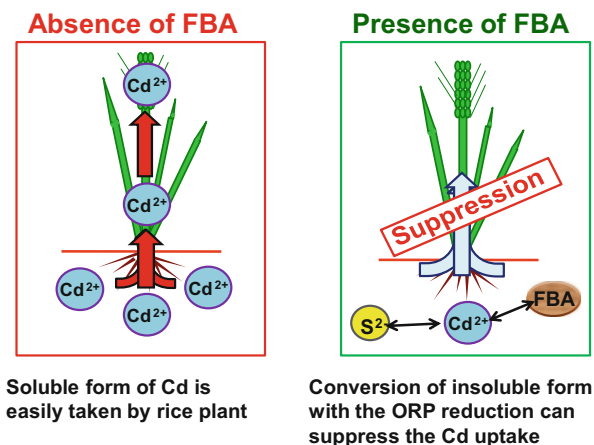
Fig. 23 Effect of FBA (1%) application timing (2, 4, 6, 7, 8, and 9 weeks after rice planting) on Cd concentrations and oxidation-reduction potential (OPR) in rice under water-filling with midterm drying conditions. Reproduced from Elsevier Copyright with permission

found that the optimum period for the application of FBA was 2 weeks after planting. The suppressions of Cd uptake in brown rice and the variation of ORP are shown in Fig. 23.

4.1.6 Suppression Mechanism of Cd Uptake with FBA

Cd uptake in brown rice was suppressed when rice plants were grown in FBA-supplemented soil under ordinary water-filling conditions, mainly because: (1) the complexation of Cd with the decomposed materials of bark and (2) the generation of sulfide form, e.g., CdS, with generation of sulfide ion in the soil (Fig. 24). Under no water-filling conditions, FBA did not reduce the mobility and uptake of specific heavy metals as occurred under water-filling conditions. In FBA-supplemented soil under water-filling conditions, the microbial decomposition of bark on the soil surface consumes O₂ and generates CO₂ and CH₄. At that time, SO₄²⁻ content in the soil is reduced with activation on sulfate-reducing bacteria in soil, causing the generation of S²⁻, which combines with heavy metals and forms insoluble sulfide precipitates.

Fig. 24 Suppression mechanism of Cd expected by this study. Reproduced from Elsevier Copyright with permission



4.2 Application of FBA to Large-Scale Crop Cultivation

4.2.1 Introduction

Next, we investigated whether the variations of the Cd concentration in harvested brown rice and rice yields were affected by adding the FBA derivative onto a large-scale farmland soil contaminated by Cd continuously for 3 years.

A schematic representation of the farmland used in the study is shown in Fig. 25. A field trial was conducted in the western part of Jiangsu Province, China at ~5 m altitude. Both rice and wheat were cultivated there annually. The area of the experimental farmland was 9,635.4 m² (90.9 m E–W and 106.0 m N–S). The farmland was situated both east and west of a 20-m-wide canal. Several pottery and chemical factories are located to the south of the farmland.

The experimental farmland consisted of six plots (A–F) and an embankment passage 30–40 cm wide. For each plot, the rice plant samples were collected within the 1 m × 1 m of area of three equal parts (1–3) per each plot (Fig. 26). The rice plants were pulled out from the center and for corners in each plot.

The fermented bark was produced from woody and food wastes locally obtained in China, so-called fermented botanical waste-based amendment (FBWA), which is a kind of FBA. Before evaluating the effect of FBWA spraying on the Cd uptake in rice, the heavy metal concentration was measured in irrigation water pumped from canals adjacent to the farmland. The average Cd concentration was <0.20 μg L⁻¹, which was well below the environmental quality threshold for farmland used for edible agricultural product cultivation in China (5.0 μg L⁻¹). However, the Cd concentrations in the farmland soil were 7–10 times higher than the environmental quality standard (0.30 mg kg⁻¹) and also exceeded the averages for farmlands in Hunan Province (0.73 mg kg⁻¹), Guangxi Province (0.70 mg kg⁻¹), and Sichuan Province (0.46 mg kg⁻¹).

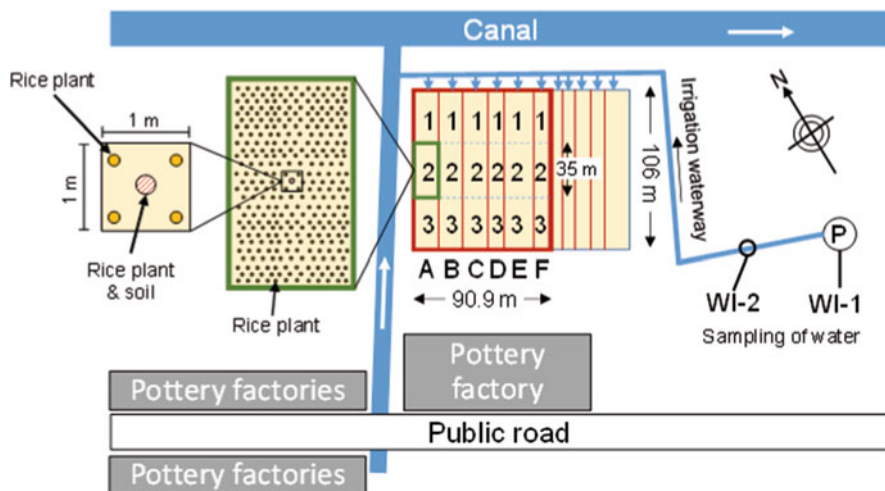


Fig. 25 Location of the farmland in Jiangsu Province, China. P: Pumping facilities. WI-1 and WI-2: water intake positions. The numbers in the experimental farmland represent the sampling points divided in three equal parts per plot. Reproduced from the Japan Society for Analytical Chemistry Copyright with permission

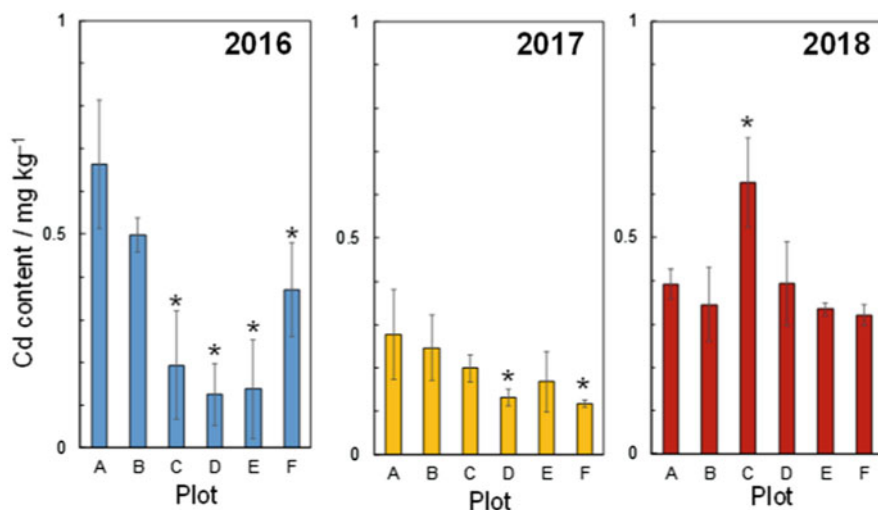


Fig. 26 Cd content in rice harvested from the farmland. Farmland was divided into blocks according to the irrigation water inflow. FBWA was sprayed onto the paddy soil at the following rates: A, 0%; B and F, 0.1%; C and E, 0.5%; and D, 1.0%. The variety of rice seed sprayed on the experimental farmland in 2017 was different to those in 2016 and 2018. Asterisks indicate significant differences between the Cd levels in the rice harvested from amended soil and those in the rice harvested from unamended soil at $P < 0.05$ (*). Triplicate samples were taken for each plot. Reproduced from the Japan Society for Analytical Chemistry Copyright with permission

4.2.2 Variations of Cd Content in Rice after Spraying FBWA onto Contaminated Soil

The effects of the FBWA application rate on soil were assessed in terms of the Cd uptake in rice and yield. On August 11, 2016, FBWA was sprayed about 2 weeks before the rice was headed. The quantities of FBWA sprayed were determined from the soil weight calculated using the depth of a rice root (15 cm) and the area in each plot, based on the soil specific gravity (1.2 g cm^{-3}). 0.1% FBWA was applied in plots B and F, 0.5% FBWA was applied in plots C and E, and 1.0% FBWA was applied in plot D. FBWA was not sprayed onto plot A (control plot). The variations in the Cd contents in brown rice were compared between plots amended with FBA and the control plot over a period of 3 years.

In 2016, the Cd concentration of the rice harvested from control plot A was 0.66 mg kg^{-1} , and those from plots B and F (where 0.1% FBWA was sprayed) were 0.50 mg kg^{-1} and 0.37 mg kg^{-1} , respectively (Fig. 29). Those in rice harvested from plots C and E (where 0.5% FBWA was sprayed) were 0.19 mg kg^{-1} and 0.14 mg kg^{-1} , respectively, lower than that of the rice harvested from plot A. Furthermore, the Cd concentration in rice harvested from plot D (0.13 mg kg^{-1}), where 1% FBA was sprayed, was reduced by 80% compared with that in plot A. Accordingly, rice harvested from plots amended with 0.5–1% FBWA had 66–80% less Cd than that derived from control plots, while rice harvested from plots B and F amended with 0.1% FBWA had 24% and 44% less Cd, respectively, than that derived from control plots.

In 2017, the rice crop was sown after the wheat harvest and soil conditioning. FBWA was not added to the cultivation soil to determine the longevity of its initial application. Because the rice variety seeded in that year was different to that in 2016, the Cd contents taken up by brown rice were lower than those in 2016 but the trends in the Cd contents among plots were similar. Because the Cd concentration in rice also decreased in plot A, the differences between the FBWA-amended plots and the control plot in 2017 were smaller than those in 2016.

In 2018, the suppressive effect of FBWA on the Cd uptake by rice was almost eliminated, that is, there were no significant differences between the amended plots and the control plot A. In addition, the Cd concentration in rice harvested from plot C amended with 0.5% FBWA was higher than that in plot A.

As mentioned above, we concluded that the longevity of the suppression of Cd uptake by rice was 2 years from the initial application of FBWA.

4.2.3 Rice Yield

Applying the technique evaluated in the present study to real farmland restoration requires not only decreases of the Cd content in rice, but also validation of the rice yield. The variation in the theoretical rice yield (Y_t) estimated from Eq. (4) for each year is plotted in Fig. 27.

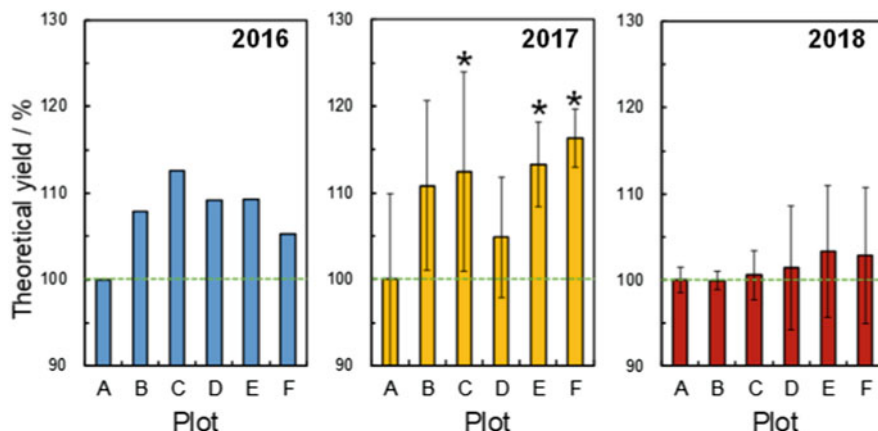


Fig. 27 Rice yield in each FBWA-sprayed farmland plot relative to that for the unamended control (plot A) in 2016–2018. FBWA was sprayed onto the paddy soil at the following rates: A, 0%; B and F, 0.1%; C and E, 0.5%; and D, 1.0%. Asterisks indicate significant differences between rice yields in soils amended with FBWA (B–F) and the unamended (A) at $P < 0.05$ (*). Statistical analyses were conducted using three replicates per plot. In 2016, the rice yield was calculated by collecting all the rice harvested in each plot. Reproduced from the Japan Society for Analytical Chemistry Copyright with permission

$$Y_t(\text{kg}) = N_p (\text{m}^{-2}) \times N_r \times G_{1000} (\text{g}) / 10^6 \times 0.85 \quad (4)$$

where N_p is the number of panicles to unit of surface area, N_r is the number of rice grains, G_{1000} is the 1,000-grain weight of ripe rice, and 0.85 is the weight loss ratio of the samples after drying.

When the yield in control plot A, which was a normal chemical fertilizer only, was compared with those for plots B–F after the FBWA treatment in 2016, plots C and E (0.5% FBWA) in 2016 had the maximum yields of 13% higher rice yields than all other plots ($P < 0.05$). Therefore, FBWA-amended soils promoted higher yields than unamended soil.

The rice yield trend obtained in 2016 did not change in 2017, though the species of rice seed in 2017 was different to that in 2016 and 2018. Because the cultivation situation, such as crop rotation, soil type, and water flow, except for rice species, remained, the soil remediation with spraying FBWA would lead to the acceleration of plant growth. In 2017, the rice yields in the amended plots were increased by 5–16% over that of the control plot A. The rice harvested from plots C–F had lower Cd concentration than the standard level ($<0.2 \text{ mg kg}^{-1}$) in China. However, in the third year, no significant differences in yields were observed.

4.3 Simultaneous Suppression of Magnetic Nanoscale Powder and Fermented Bark Amendment for As and Cd Uptake by Radish Sprouts Grown in Agar Medium

4.3.1 Introduction

We here attempted to hybridize multiple compounds to simultaneously reduce the uptake of As and Cd, considering the influence of plant growth.

Honma et al. describes that it is difficult to simultaneously reduce As and Cd uptakes using a single countermeasure, such as water management practice or soil amendment application [61]. For example, filling water to paddy fields reduces the Cd concentrations in the rice under the anaerobic conditions in paddy soil. However, because it consequently accelerates the As uptake by rice due to the increases of solubilities of arsenite or arsenate in the water [62]. Thus, it has become widely recognized that there is a trade-off between the uptake of arsenic and cadmium by rice [63].

We attempted the suppression of the inorganic species uptake by plant in the agar medium including magnetic nanoparticle powder (MNP, α -Fe₃O₄) and FBA [64].

4.3.2 Preparation of MNP

MNP was prepared in Kanto Denka Kogyo Co., Ltd. (Shibukawa, Japan). Briefly, 0.6 mol FeCl₂ and 4.8 mol FeCl₃ were added to 1.0 L of pure water. Next, 500 mL of an aqueous solution containing 0.1 M NaOH was added, after which a colloid suspension was obtained. During this procedure, nitrogen gas was flowed over the mixture at a rate of 10 L min⁻¹ at 60°C, and air was then bubbled into the sample at 20 L min⁻¹ to oxidize the iron species for 6 h. The suspension was separated into particles and aqueous solution by centrifuging at 3,000 rpm for 3 h. The nanoparticles were washed with 200 L of deionized water at 60°C. The MNP obtained was dried at 120°C under a nitrogen stream.

4.3.3 Adsorption Capabilities for Arsenate, Arsenic, and Cadmium

The adsorption-saturation capacities of As(III), As(V), and Cd(II) to MNP and FBA at pH 6 were estimated from the adsorption amounts (q_e) reached during the saturated state after mixing for 30 min into the residual concentration (C_e).

As the adsorption-saturation capacities (Q) of MNP and FBA were estimated from the intercept of the calibration curve in Eq. (1), the Q values of arsenic species to MNP were 10-fold higher than that of Cd(II), and the opposite tendency was observed for FBA, as summarized in Table 4. In addition, the Q value of As(III) to MNP was higher than those to the adsorbents cited in this paper [65, 66], though that of As(V) was lower than several materials complexing multiple adsorbents

Table 4 Adsorption-saturation capacity (Q) of arsenic and cadmium to MNP and FBA and the comparative data by adsorbents obtained from industrial wastes and iron oxide in previous researches [64]

Adsorbents	Analyte	Q ($\mu\text{mol/g}$)	References
MNP	As(III)	303 ± 12	
FBA		76.9 ± 5.3	
Pine cone-magnetite		227	[65]
Hematite-coated Fe_3O_4		13.3	[66]
MNP	As(V)	303 ± 10	
FBA		38.5 ± 7.2	
Hematite-coated Fe_3O_4		28.0	[66]
Granular ferric hydroxide		30.9	[72]
Synthesized magnetite		887	[67]
Chitosan-coated $\text{Cu}(\text{OH})_2$		520	[68]
MNP	Cd(II)	27.4 ± 1.1	
FBA		558 ± 36	
<i>Pinus halepensis</i> sawdust		65.6	[70]
Magnetic biochar derived from kelp		207	[71]
Pyrolyzed coffee residues and clay		527	[69]

Average and standard deviations in MNP and FBA were estimated from three different samples

[67, 68]. The Q value of Cd(II) to FBA indicated much higher than biomass materials presented in reports by several researchers [69–71].

4.3.4 Determination of the As and Cd Concentrations in Radish Sprouts

Radish sprouts were cultivated in agar medium, according to the cultivation method described by [73]. Three different radish cultivations were performed for each condition. First, the FBA and/or MNP, 0.2 g agar powder, and 25 mL Tris (hydroxymethyl) aminomethane buffer containing both As(III) and Cd(II) (100 $\mu\text{g/L}$) were cooled to 25°C and then solidified by heating to 90°C. MNP and FBA were added in range of 0.025–2.5 g per 25 mL agar: the solid-to-liquid ratio (g/mL) was 0.001–0.1. The radish seeds were cultivated in agar medium for 18 days and then harvested. The radishes produced were dried in an oven at 80°C for 3 h, following the measurement of the length of the roots and edible portions. The dried radish samples were mashed using an agate mortar and completely dissolved in nitric acid. As and Cd concentrations in the solution were quantified by ICP-MS.

4.3.5 Suppression of As and Cd Uptakes into Radish Sprouts

When the radish sprouts were grown in the agar media with As and Cd (each initial concentration: 100 $\mu\text{g/L}$ for As(III) (arsenite) and Cd(II)), the effects of MNP and FBA added to the medium were compared by determining the amounts of As and Cd

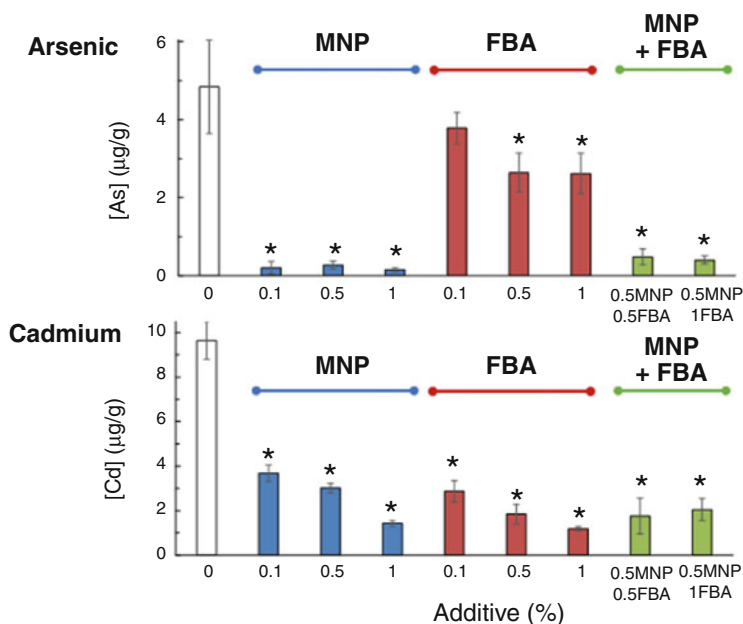


Fig. 28 Contents of arsenic (upper trace) and cadmium (lower trace) absorbed into radishes planted in agar medium supplemented with MNP, FBA, and a mixture thereof (0.5% MNP/0.5% FBA or 0.5% MNP/1% FBA). The initial concentrations of arsenic(III) and cadmium(II) in the agar were 100 µg/L. The error bars in bar graphs were estimated from the standard deviations of analytes in radishes, obtained in triplicate experiments. Significant differences ($p < 0.05$, $n = 3$) between the results of the blank and those of the treatments with MNP and/or FBA are indicated by asterisk above bar. Reproduced from Springer Copyright with permission

absorbed in the sprouts. In this experiment, they were co-mixed in the agar media. The amount of FBA and MNP added to the agar media ranged from 0.1 to 1.0%.

As shown in Fig. 28, the absorption of As into the sprouts was almost quantitatively suppressed by adding MNP in the medium at concentrations higher than 0.1% MNP. In addition, the As content decreased by approximately 50% in the blank condition by the addition of 1% FBA. The amount of Cd absorbed by the sprouts in the agar medium with FBA was reduced by approximately fivefold versus the blank. Interestingly, Cd uptake by the sprouts was also reduced by 60–85% by adding MNP, although Cd adsorption to MNP in aqueous solution was much lower than its As adsorption. The cation-exchanger or chelating complex site such as the carboxyl and hydroxyl groups in FBA promoted by decomposing bark by activation of white-rot fungus would relate to binding to metals. According to a report by [74], the carboxyl and phenolic hydroxyl groups in the humus bind to metal cations by forming complexes with the adsorption site. The suppression of As uptake by the radish sprouts in the agar media with FBA was lower than that of Cd. This would be because of the low binding capability for As (anionic species) to materials with carboxyl groups and phenolic hydroxyl groups in the FBA [75].

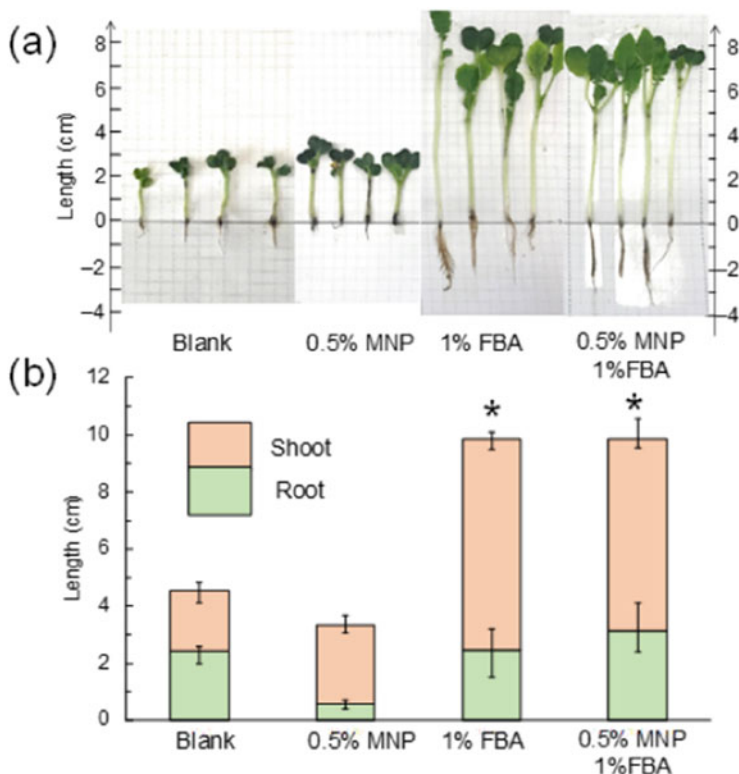


Fig. 29 Growths of radishes harvested after growth in blank medium, or medium containing 0.5% MNP, 1% FBA and 0.5% MNP, and 1% FBA. Trace: (a) photographs and (b) bar graphs. Significant differences ($p < 0.05$, $n = 4$) between the results of the blank and those of the treatments with MNP and/or FBA are indicated by asterisk above bar. Addition of As and Cd in the agar mediums used in the tests was not carried out. Reproduced from Springer Copyright with permission

Many researchers provided that iron hydroxides and oxides could efficiently bind and remove arsenic from aqueous solution [76–79]. In this study, MNP composed of iron oxide could bind negatively charged arsenic ions; thus, the binding mechanism of MNP to arsenic species is comparable to that for iron oxide.

Japanese radish was cultivated in the agar medium containing a mixture of 0.5% MNP/0.5% FBA or 0.5% MNP/1% FBA, of which concentrations were obtained after reasonable suppression of As and Cd. As shown in Fig. 29 their uptakes were suppressed by the presence of the mixed additive. However, the capability of the mixture for suppressing each analyte uptake was slightly lower than found for As with 1% MNP alone and cadmium with 1% FBA alone. This would be because the adsorption capabilities of MNP and FBA for analytes were offset. Indeed, the suppression of analyte uptake did not change even when the amount of FBA was increased to 1% and mixed with 0.5% MNP to further reduce the Cd contents in

radishes. Inversely, when the MNP amount was increased to 1% and mixed with 0.5% FBA, As content was not different to that with 0.5% MNP and 0.5% FBA but the radish growth was largely suppressed (data not shown).

According to a report by [80] when both iron oxide and dissolved organic matter (DOM) co-exist in medium, the cadmium preferentially binds to functional carboxyl groups on aromatic rings in humic acid than to iron oxide. DOM contained in FBA may adsorb to both heavy metal cations and arsenite on mineral surfaces [81–83] demonstrated to reduce the arsenic content when iron and DOM coexisted in aqueous medium. Arsenic adsorption might be due to the formation of Fe-bridged As–Fe–DOM complexes and surface complexation of arsenic on DOM-stabilized Fe colloids [84, 85]. In this case, the FBA–MNP complex in agar might be formed dominantly over the complex with As or Cd in the agar medium.

Interestingly, the combination of MNP and FBA was found to be effective for the plant growth. In fact, the elongations of root and stem in radish cultivated in agar with FBA were larger than those in agars without FBA or with MNP only (Fig. 29a). As shown in Fig. 29b, in addition to the 0.5% MNP only, the growth of radish was obviously defected compared to other conditions, that is, the MNP might suppress the absorption of arsenic but cannot supply the nutrients such as potassium and phosphorus concerning the growth of plant. Also, the average length of stem and root cultivated in the agar with 0.5% MNP and 1% FBA were 2.7-fold and 3.4-fold longer, respectively, than those without additive, indicating almost comparative to those in the agar medium with 1% FBA.

4.4 Conclusion

The supplementation of FBA in the heavy metal-contaminated soil provides sustainable suppression of Cd uptake by rice plant, because the Cd is converted into insoluble form with the reduction of ORP on the soil surface. Also, since FBA is made from waste materials and food waste, it has a high affinity for soil and is considered to be an environmentally friendly amendment. Mixing different adsorbents such as a combination of FBA and MNP provides a synergy effect that can simultaneously suppress the uptake of different metal species by plant. As the further investigation, the FBA will be applied to soils contaminated by other toxic elements such as mercury or radioisotope cesium.

5 Conclusion

The environmentally friendly adsorbents proposed in the study, which is based on natural products, plants, solid waste material, and agricultural waste, have a high potential for removing organic and inorganic materials, including heavy metal ions and dyes, from water or soil. All of the adsorbent materials proposed in this chapter

are widely available and easily developed by using low-cost and waste materials. Furthermore, they have a high capacity for metal ions and also some organic materials in water. The use of these adsorbents has many advantages, including low cost and easiness of production, safety for the environment, and the conversion of waste materials into valuable materials for the environmental remediation.

References

1. Khulbe KC, Matsuura T (2018) Removal of heavy metals and pollutants by membrane adsorption techniques. *Appl Water Sci* 8(19):1–30
2. Baysal A, Ozbek N, Akman S (2013) Determination of trace metals in wastewater and their removal processes wastewater – treatment technologies and recent analytical developments. Chapter 7. <https://doi.org/10.5772/52025>, ISBN: 978-953-51-0882-5
3. Markovic R, Bessho M, Masuda N, Stevanovic Z, Bozic D, Trujic TA, Gardic V (2020) New approach of metals removal from acid mine drainage. *Appl Sci* 10:1–16
4. Emiliani J, Oyarce W, Bergara CD, Salvatierra LM, Novo LAB, Perez LM (2020) Variations in the phytoremediation efficiency of metal-polluted water with *Salvinia biloba*: prospects and toxicological impacts. *Water* 12:1–15
5. Edeballi S, Pehlivan E (2016) Evaluation of chelate and cation exchange resins to remove copper ions. *Powder Technol* 301:520–525
6. Pohl A (2020) Removal of heavy metal ions from water and wastewaters by sulfur-containing precipitation agents. *Water Air Soil Pollut* 231. 503:1–17
7. Namasivayam C, Ranganathan K (1995) Removal of Cd (II) from wastewater by adsorption on waste Fe (III)/Cr (III) hydroxide. *Water Res* 29:1737–1744
8. Papandreou AD, Stourmaras CJ, Panias D, Paspaliaris I (2011) Adsorption of Pb (II), Zn (II) and Cr (III) on coal fly ash porous pellets. *Miner Eng* 24:1495–1501
9. Gebretsadik H, Gebrekidan A, Demlie L (2020) Removal of heavy metals from aqueous solutions using *Eucalyptus Camaldulensis*: an alternate low-cost adsorbent. *Cogent Chem* 6(1):1–16
10. Hasan AF, Hrdina R (2018) Chitosan/nanohydroxyapatite composite based scallop shells as an efficient adsorbent for mercuric ions: static and dynamic adsorption studies. *Int J Biol Macromol* 109:507–516
11. Hossain A, Bhattacharyya SR, Aditya G (2015) Biosorption of cadmium from aqueous solution by shell dust of the freshwater snail *Lymnaea luteola*. *Environ Technol Innov* 4:82–91
12. Siswoyo E, Nozomi E, Yoshihiro M, Shunitz T (2014) Agar-encapsulated adsorbent based on leaf of *Platanus* sp. to adsorb cadmium ion in water. *Water Sci Technol* 70(1):89–94
13. Jae WC, Seung GC, Seok WH, Dong JK, Sang HL (2011) Development of an environmentally friendly adsorbent for the removal of toxic heavy metals from aqueous solution. *Water Air Soil Pollut* 2012(223):1837–1846
14. Dai Y, Li J, Sun Q, Liu Z (2020) Adsorption isotherm, kinetic modeling and mechanism of neutral red on *Auricularia auricularia*. *Desalin Water Treat* 198:335–344
15. Iqbal M, Saeed A, Zafar SI (2009) FTIR spectrophotometry, kinetics and adsorption isotherms modeling, ion exchange, and EDX analysis for understanding the mechanism of Cd²⁺ and Pb²⁺ removal by mango peel waste. *J Hazard Mater* 164:161–171
16. Siswoyo E, Tanaka S (2013) Development of eco-adsorbent based on solid waste of paper industry to adsorb cadmium ion in water. *J Clean Energy Technol* 1(3):198–201
17. Siswoyo E, Mihara Y, Tanaka S (2014) Determination of key components and adsorption capacity of a low-cost adsorbent based on sludge of drinking water treatment plant to adsorb cadmium ion in water. *Appl Clay Sci* 97–98:146–152

18. Dai Y, Yan H, Zhang B, Wu W, Yang L, Li S, Li W, Li H, Yan L, Shan D, Feng Y, Terui N, Tanaka S (2014) A novel adsorbent obtained by caging activated carbon by konjac glucomannan gel for elimination of organic compounds. *J Appl Polym Sci* 131:40542
19. Dai Y, Du C, Yu H, Zhang D, Zhang K (2016) Influence of spent coffee ground treated by nitric acid on Pb (II)-biosorption from aqueous solution. *Int Agric Eng J* 25:20–28
20. Dai Y, Zhang D, Yan H, Ji Y, Wu W, Tanaka S (2016) Study on the mechanism of methylene blue adsorption on spent coffee grounds. *Fresenius Environ Bull* 25:3423–3429
21. Dai Y, Li J, Shan D (2020) Adsorption of tetracycline in aqueous solution by biochar derived from waste *Auricularia auricula* dregs. *Chemosphere* 238:124432
22. Dai Y, Li J (2020) Adsorption behavior of methyl orange and methylene blue onto carbon material in an aqueous solution. *Desalin Water Treat* 180:387–397
23. Mori M, Kotaki K, Gunji F, Kubo N, Kobayashi S, Ito T, Itabashi H (2016) *Chemosphere* 148: 487–494
24. Bajpai P (2015) Generation of waste in pulp and paper mills. In: *Management of pulp and paper mill waste*. Springer, Cham. https://doi.org/10.1007/978-3-319-11788-1_2
25. Prasetyo J, Naruse K, Kato T, Boonchird C, Harashima S, Park EY (2011) Bioconversion of paper sludge to biofuel by simultaneous saccharification and fermentation using a cellulose of paper sludge origin and thermotolerant *saccharomyces cerevisiae* TJ14. *Biotechnol Biofuels* 4: 35
26. Qin Q, Wang Q, Fu D, Ma J (2011) An efficient approach for Pb(II) and Cd(II) removal using manganese dioxide formed in situ. *Chem Eng J* 172:68–74
27. Rao M, Parwate AV, Bhole AG (2002) Removal of Cr^{6+} and Ni^{2+} from aqueous solution using bagasse and fly ash. *Waste Manag* 22:821–830
28. Vitela-Rodríguez AV, Rangel-Mendez JR (2013) Arsenic removal by modified activated carbons with iron hydro(oxide) nanoparticles. *J Environ Manage* 114:225–231
29. Su Q, Pan B, Wan S, Zhang W, Lv L (2010) Use of hydrous manganese dioxide as a potential sorbent for selective removal of lead, cadmium, and zinc ions from water. *J Colloid Interface Sci* 349:607–612
30. Zhang Y, Jiang J, Chen M (2008) MINTEQ modeling for evaluating the leaching behavior of heavy metals in MSWI fly ash. *J Environ Sci (China)* 20:1398–1402
31. Zhou Y, Zhang R, Gu X, Lu J (2014) Adsorption of divalent heavy metal ions from aqueous solution by citric acid modified pine sawdust. *Sci Technol* 50(2):245–252
32. Mckay G, Blair HS, Gardener JR (1982) Adsorption of dyes on chitin I. Equilibrium studies. *J Appl Polym Sci* 27:3043–3057
33. Alonso-Sande M, Teijeiro-Osorio D, Remuñán-López C, Alonso MJ (2009) Glucomannan, a promising polysaccharide for biopharmaceutical purposes. *Eur J Pharm Biopharm* 72:453–462
34. Case SE, Knopp JA, Hamann DD, Schwartz SJ (1992) Characterisation of gelation of konjac mannan using lyotropic salts and rheological measurements. In: Phillips GO, Williams PA, Wedlock DJ (eds) *Gums and stabilisers for the food industry* 6. IRL Press, Oxford, pp 489–500
35. Gao S, Nishinari K (2004) Effect of degree of acetylation on gelation of konjac glucomannan. *Biomacromolecules* 5:175–185
36. Huang L, Takahashi R, Kobayashi S, Kawase T, Nishinari K (2002) Gelation behaviour of native and acetylated konjac glucomannan. *Biomacromolecules* 3:1296–1303
37. Nishinari K (2000) Konjac glucomannan. *Dev Food Sci* 41:309–330
38. Fugetsu B, Satoh S, Shiba T, Mizutani T, Lin Y, Terui N, Nodasaka Y, Sasa K, Shimizu K, Akasaka T, Shindo M, Shibata K, Yokoyama A, Mori M, Tanaka K, Sato Y, Tohji K, Tanaka S, Nishi N, Watari F (2004) Caged multiwalled carbon nanotubes as the adsorbents for affinity-based elimination of ionic dyes. *Environ Sci Technol* 38:6890–6895
39. Gokhan Z, Sinan K, Fawzi M, Mahomoodally, Simone, A., Ahmed, M., Mustafa., Sauro, V., Filippo, M., Giovanni, C. (2020) Chemical composition, antioxidant and enzyme inhibitory properties of different extracts obtained from spent coffee ground and coffee silverskin. *Foods* 9(6):713

40. Dai Y, Zhang D, Zhang K (2016) Nitrobenzene adsorption capacity of NaOH modified spent coffee ground from aqueous solution. *J Taiwan Inst Chem Eng* 68:232–238
41. Kulshrestha P, Giese FR, Aga DS (2004) Investigating the molecular interactions of oxytetracycline in clay and organic matter: insights on factors affecting its mobility in soil. *Environ Sci Technol* 38:4097–4105
42. Liao YK, Li LX, Fan SS (2019) Removal behavior and mechanism of methylene blue in aqueous solution by rice straw and rice straw-Fe₃O₄ composite. *Acta Sci Circumcision* 39:359–370
43. Yao S, Zhang MS, Li LX, Liao YK, Zhou N, Fan SS, Tang J (2018) Preparation of tea waste-nano Fe₃O₄ composite and its removal mechanism of methylene blue from aqueous solution. *Environ Chem* 37:96–107
44. Ahmed M, Rajapaksha A, Lim JE, Zhang M, Bolan N, Mohan D, Vithanage M, Lee SS, Ok YS (2014) Biochar as a sorbent for contaminant management in soil and water: a review. *Chemosphere* 99:19–33
45. Li YL, Ruan GD, Jalilov AS, Tarkunde YR, Fei HL, Tour JM (2016) Biochar as a renewable source for high-performance CO₂ sorbent. *Carbon* 107:344–351
46. Lou ZM (2016) Research on physio-chemical characteristics of spent mushroom substrate and its environmental impact during recycling process, Master thesis. Zhejiang University
47. Zhang L, Sun X (2014) Changes in physical, chemical, and microbiological properties during the two-stage co-composting of green waste with spent mushroom compost and biochar. *Bioresour Technol* 172:274–284
48. Ahmed M, Zhou JL, Ngo HH, Guo W (2015) Adsorptive removal of antibiotics from water and wastewater: progress and challenges. *Sci Total Environ* 532:112–126
49. Li Y, Wang Z, Xie X, Zhu J, Li R, Qin T (2017) Removal of norfloxacin from aqueous solution by clay-biochar composite prepared from potato stem and natural attapulgite. *Colloids Surf, A* 514:126–136
50. Fu B, Ge C, Yue L, Luo J, Feng D, Deng H, Yu H (2016) Characterization of biochar derived from pineapple peel waste and its application for sorption of oxytetracyclines from aqueous solution. *Bio Resources* 11(4):9017–9035
51. Dai Y, Mihara Y, Tanaka S, Watanabe K, Terui N (2010) Nitrobenzene-adsorption capacity of carbon materials released during the combustion of woody biomass. *J Hazard Mater* 174:776–781
52. Rocher V, Siaugue JM, Cabui V, Bee A (2008) Removal of organic dyes by magnetic alginate beads. *Water Res* 42:1290–1298
53. Yoshioka T, Hirata S, Matsumura Y, Sakanishi K (2005) Woody biomass resources and conversion in Japan: the current situation and projections to 2010 and 2050. *Biomass Bioenergy* 29:336–346
54. Guo X, Zhang S, Shan X (2008) Adsorption of metal ions on lignin. *J Hazard Mater* 151:134–142
55. Sciban MB, Klasnja MT, Antov MG (2011) Study of the biosorption of different heavy metal ions onto Kraft lignin. *Ecol Eng* 37:2092–2095
56. Tuomela T, Oivanen P, Hatakka A (2002) Degradation of synthetic ¹⁴C-lignin by various white-rot fungi in soil. *Soil Biol Biochem* 34:1613–1620
57. Vane CH, Drage TC, Snape CE (2006) Bark decay by the white-rot fungus *Lentinula edodes*: polysaccharide loss, lignin resistance and the unmasking of suberin. *Int Biodeter Biodegr* 57:14–23
58. Fukushima M, Yamamoto K, Ootsuka K, Komai T, Aramaki T, Ueda S, Horiya S (2009) Effects of the maturity of wood waste compost on the structural features of humic acids. *Bioresour Technol* 100:791–797
59. Asakawa S, Asagawa M, Koga Y, Hayano K (1998) Communities of methanogenic bacteria in paddy field soils with long-term application of organic matter. *Soil Biol Biochem* 30:299–303
60. Chino M (2006) The distribution of heavy metals in rice plants as influenced by the time and the path of supply. *Jpn Soc Soil Sci Plant Nutr* 77:119–124. In Japanese with English title

61. Honma T, Ohba H, Kaneko A, Nakamura K, Makino T, Katou H (2016) Effects of soil amendments on arsenic and cadmium uptake by rice plants (*Oryza sativa* L. cv. Koshihikari) under different water management practices. *Soil Sci Plant Nutr* 62:349–356
62. Koyama T (1975) Behavior of arsenic in soil and crops. *Jpn J Soil Sci Plant Nutr* 46:491–502. in Japanese
63. Arai T, Kawasaki A, Baba K, Mori S, Matsumoto S (2009) Effects of water management on cadmium and arsenic accumulation and dimethylarsinic acid concentrations in Japanese rice. *Environ Sci Technol* 43:9361–9367
64. Sun X, Mo H, Hatano K, Itabashi H, Mori M (2019) Simultaneous suppression of magnetic nanoscale powder and fermented bark amendment for arsenic and cadmium uptake by radish sprouts grown in agar medium. *Environ Sci Pollut Res* 26: 14483–14493
65. Ouma ILA, Naidoo EB, Ofomaja AE (2018) Thermodynamic, kinetic and spectroscopic investigation of arsenite adsorption mechanism on pine cone-magnetite composite. *J Environ Chem Eng* 6:5409–5419
66. Simeonidis K, Gkinis T, Tresintsi S, Martinez-Boubeta C, Vourlias G, Tsiaoussis I, Stavropoulo G, Mitrakas M, Angelakeris M (2011) Magnetic separation of hematite-coated Fe₃O₄ particles used as arsenic adsorbents. *Chem Eng J* 168:1008–1015
67. Iconaru SL, Guégan R, Popa CL, Motelica-Heino M, Ciobanu CS, Predoi D (2016) Magnetite (Fe₃O₄) nanoparticles as adsorbents for As and Cu removal. *Appl Clay Sci* 134:128–135
68. Elwakeel KZ, Guibal E (2015) Arsenic(V) sorption using chitosan/Cu(OH)₂ and chitosan/CuO composite sorbents. *Carbohydr Polym* 134:190–204
69. Boonamnuayvitaya V, Chaiya CY, Tanthapanichakoon W, Jarudilokkul S (2004) Removal of heavy metals by adsorbent prepared from pyrolyzed coffee residues and clay. *Sep Purif Technol* 35:11–22
70. Semerjian L (2010) Equilibrium and kinetics of cadmium adsorption from aqueous solutions using untreated *Pinus halepensis* sawdust. *J Hazard Mater* 173:236–242
71. Son E-B, Poo K-M, Chang J-S, Chae K-J (2018) Heavy metal removal from aqueous solutions using engineered magnetic biochars derived from waste marine macro-algal biomass. *Sci Total Environ* 615:161–168
72. Saldaña-Robles A, Saldaña-Robles N, Saldaña-Robles AL, Damian-Ascencio C, Rangel-Hernandez VH, Guerra-Sanchez R (2017) Arsenic removal from aqueous solutions and the impact of humic and fulvic acids. *J Clean Prod* 159:425–431
73. Hatano K, Kanazawa K, Tomura H, Yamatsu T, Tsunoda K, Kubota K (2016) Molasses melanoidin promotes copper uptake for radish sprouts: the potential for an accelerator of phytoextraction. *Environ Sci Pollut Res* 23:17656–17663
74. Baker H, Khalili F (2005) A study of complexation thermodynamic of humic acid with cadmium (II) and zinc (II) by Schubert's ion-exchange method. *Anal Chim Acta* 542:240–248
75. Fakour H, Lin T (2014) Experimental determination and modeling of arsenic complexation with humic and fulvic acids. *J Hazard Mater* 279:569–578
76. Rahman IMM, Begum ZA, Sawai H, Maki T, Hasegawa H (2013) Decontamination of spent iron-oxide coated sand from filters used in arsenic removal. *Chemosphere* 92:196–200
77. Xu X, Chen C, Wang P, Kretzschmar R, Zhao FJ (2017) Control of arsenic mobilization in paddy soils by manganese and iron oxides. *Environ Pollut* 231:37–47
78. Mishra T, Mahato DK (2016) A comparative study on enhanced arsenic(V) and arsenic(III) removal by iron oxide and manganese oxide pillared clays from ground water. *J Environ Chem Eng* 4:1224–1230
79. Siddiqui SI, Chaudhry SA (2017) Iron oxide and its modified forms as an adsorbent for arsenic removal: a comprehensive recent advancement. *Process Saf Environ Prot* 111:592–626
80. Du H, Peacock CL, Chen W, Huang Q (2018) Binding of Cd by ferrihydrite organo-mineral composites: implications for Cd mobility and fate in natural and contaminated environments. *Chemosphere* 207:404–412
81. Wang S, Mulligan CN (2006) Effect of natural organic matter on arsenic release from soils and sediments into groundwater. *Environ Geochem Health* 28:197–214

82. Sharma P, Ofner J, Kappler A (2010) Formation of binary and ternary colloids and dissolved complexes of organic matter, Fe and As. *Environ Sci Technol* 44:4479–4485
83. Bauer M, Blodau C (2009) Arsenic distribution in the dissolved, colloidal and particulate size fraction of experimental solutions rich in dissolved organic matter and ferric iron. *Geochim Cosmochim Acta* 73:529–542
84. Liu G, Fernandez A, Cai Y (2011) Complexation of arsenite with humic acid in the presence of ferric iron. *Environ Sci Technol* 45:3210–3216
85. Lin HT, Wang MC, Li GC (2004) Complexation of arsenate with humic substance in water extract of compost. *Chemosphere* 56:1105–1112

Preparation and Modification of Activated Carbon Surface and Functions for Environments



Motoi Machida and Yoshimasa Amano

Contents

1	Pollution of Aquatic Environment	336
2	Adsorbents for Organic Pollutants	336
3	Adsorbents for Ionic Pollutants	340
3.1	Cationic Contaminants	341
3.2	Anionic Contaminants	347
4	Conclusion	362
	References	363

Abstract Preparation and modification of activated carbon (AC) and activated carbon fiber (ACF) were described for the adsorptive removal of contaminants from aqueous phase. For hydrophobic and nonpolar organic pollutants, specific surface area and pore distribution of hydrophobic carbon surface play an important role. On the contrary, hydrophilic carbon surface containing heterolytic oxygen-, nitrogen-, and sulfur-containing functional groups is required for capturing ionic pollutants rather than specific surface area. Carboxy groups was successfully introduced onto carbon surface to remove cationic contaminants as heavy metal cations of Pb^{2+} , Ni^{2+} , Cd^{2+} , Cu^{2+} , etc., while quaternary nitrogen could be formed to some extent on carbon surface for uptaking anionic pollutants of nitrate, phosphate, $\text{Cr}_2\text{O}_4^{2-}$, AsO_4^{3-} , etc. However, introduction of sulfonic functional groups onto carbon surface for cationic pollutants and alkylamine groups for anionic pollutants has still been challenging subjects.

M. Machida (✉) and Y. Amano
Safety and Health Organization, Chiba University, Chiba, Japan
Graduate School of Engineering, Chiba University, Chiba, Japan
e-mail: machida@faculty.chiba-u.jp; amanoy@faculty.chiba-u.jp

Shunitz Tanaka, Masaaki Kurasaki, Masaaki Morikawa, and Yuichi Kamiya (eds.), 335
Design of Materials and Technologies for Environmental Remediation,
Hdb Env Chem (2023) 115: 335–366, DOI 10.1007/698_2020_673,
© The Author(s), under exclusive license to Springer Nature Singapore Pte Ltd 2020,
Published online: 26 October 2020

Keywords Activated carbon fiber, Adsorption of ionic pollutants, Oxygen- and nitrogen-containing functional groups, Positively charged quaternary nitrogen, Surface chemistry, Textural properties

1 Pollution of Aquatic Environment

In this chapter, porous carbonaceous materials and their surface modification for adsorptive removal of contaminants in aquatic environments were described based on our previous study and some literature survey. Before detail description regarding carbon, char, and fiber, we would like to mention the background of the study to show significance of the developments of new type of porous carbonaceous materials with hetero-atom (N, O, S) functionalized surface.

Pollution of aquatic environment can be defined as contaminations of undesired materials of organic and inorganic compounds found in sea, river, lake, and groundwater. In the pollution of organic materials, not only conventional polycyclic and mono-aromatic organic compounds mainly originated from crude oil but also pesticides and insecticides [1], and nowadays pharmaceuticals and antibiotics [2, 3] are involved for the study field. In regard to inorganic pollutants in aquatic system, heavy metals such as lead (Pb), cadmium (Cd), nickel (Ni), chromium (Cr), arsenic (As), and mercury (Hg) are frequently found worldwide, especially in China, due to rapid urbanization and industrialization [4, 5], and heavy metals penetrated in soil are greatly connected with aquatic environment as well [6–8]. Nitrogen, phosphorous, and potassium are widely known as three main macronutrients, and they are not harmful themselves. But, once excess amounts of nitrogen (ammonia N) and phosphorous (P) are discharged into environment, N and P induce eutrophication of lake (particularly in shallow lake) [9], shallow estuary at coastal area [10], and pollution by nitrate in river [11] and groundwater [12–14]. In this section, relationship between properties of carbonaceous adsorbents and the above various pollutants in water will be described in terms of reduction of the pollution level by adsorptive removal of contaminants.

2 Adsorbents for Organic Pollutants

Carbonaceous adsorbents such as activated carbons/chars and activated carbon fibers have been frequently utilized for the removal of organic compounds from aqueous phase for a long time. Activated carbons consist of a numerous number of curved graphene sheets intertangled each other. Principally, adsorption kinetics is dependent on pore distribution and particle size of adsorbents, and adsorption capacity of organic pollutants is governed by specific surface area and surface nature. For

granular activated chars and carbons, adsorption speed of organic pollutants into pore structure is controlled by diffusion in most of the cases. When we attempt to apply pseudo-first-order and pseudo-second-order kinetics to the experimental data, pseudo-second-order kinetics will be more suitable than pseudo-first-order analysis because pseudo-second-order kinetics is said to be appropriately represented for diffusion controlled mechanism [15–18]. On the contrary, in case of using fine particles of carbonaceous adsorbents including dried leaves, rapid adsorption was observed, and the kinetics obeyed pseudo-first-order kinetics [19] indicating that the rate-limiting step should be collision of the solute onto adsorption sites of the adsorbent surface. The pseudo-first-order kinetics could be also more suitably applied to mesoporous activated carbon than pseudo-second-order for heavy metal adsorption as described latter section [20].

Adsorption capacities of organic compounds on carbon surface are usually proportional to specific surface area of activated char if no or a little oxygen-containing strong acidic surface functional groups are present on the surface. Goto et al. examined the influence of the oxygen species on activated carbon (AC) and found that any sort of oxygen functional group more or less inhibited the adsorption of benzene and nitrobenzene in aqueous solution [21]. Figure 1 shows adsorption isotherms of benzene and nitrobenzene (NBz) on bead-shaped AC (BAC, Kureha Corporation, Japan), AC oxidized with concentrated nitric acid (AC-Ox), and AC-Ox outgassed at 900°C in helium flow (AC-OxOG) together with Langmuir fitting of the isotherms [21]. In case of benzene adsorption, adsorption amount was drastically altered by the oxidation of AC (AC-Ox) from 10 mmol/g to close to zero, while consecutive outgassing treatment led to regaining some amount of capacity. The Langmuir maximum adsorption amounts of 11.4 mmol/g of benzene and 5.5 mmol/g of nitrobenzene on AC are corresponding to the amounts of monolayer coverage of specific surface area of 1,360 m²/g. Significant amount of carboxy groups (3.75 mmol/g by Boehm titration) was introduced to carbon surface by the oxidation, whereas no carboxy groups were detected before the oxidation. The result

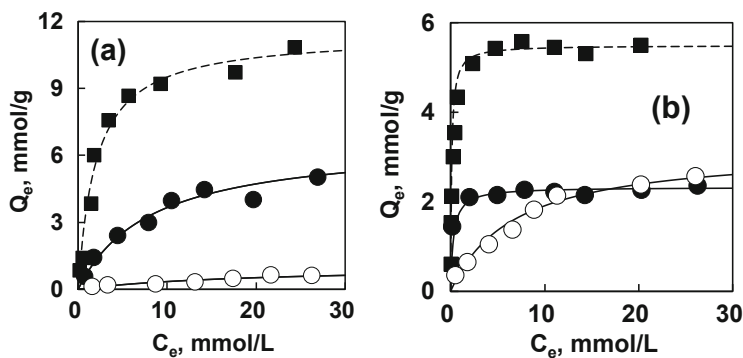


Fig. 1 Langmuir isotherms of benzene (a) and nitrobenzene (NBz) adsorption (b) in aqueous solution onto activated carbon (AC, filled square), AC oxidized with conc. HNO₃ (AC-Ox, open circle) and AC oxidized and outgassed at 900°C (AC-OxOG, filled circle) [21]

implied that the presence of carboxy groups could inhibit the benzene adsorption by the withdrawal of $C\pi$ -electrons on the graphene layer of AC. The decrease in $C\pi$ -electron density could significantly bring the weakness of π - π interaction between AC graphene and benzene by the fact that the amount of basic site was decreased from 0.60 meq/g to 0.00 meq/g (Boehm titration) by the oxidation. Specific surface area was also decreased from 1,360 m^2/g to 140 m^2/g by the oxidation. This is partly caused by physical inhibition by oxygen functional groups such as carboxy, lactone, and phenol groups. But the outgassing treatment at 900°C regained basic site from 0.00 meq/g to 0.48 meq/g, and some amount of benzene could adsorb again on AC-OxOG in Fig. 1. Specific surface area also increased again from 140 m^2/g to 650 m^2/g corresponding to adsorption amount of benzene [21].

As for nitrobenzene (NBz), the adsorption performance was a little different from benzene. Adsorption amount of NBz was not close to zero, but moderate adsorption of NBz could be observed on AC-Ox. The different performance may be caused by difference in dipole moments (D) between benzene and NBz; dipole moment of NBz is 4.22, whereas that of benzene is 0.00. When ACs are oxidized, carbon surface will be altered from hydrophobic to hydrophilic, and then π - π interaction between benzene ring and graphene will be weakened. In case of NBz, adsorption configuration can be estimated to switch from flat-on adsorption via π - π interaction to end-on adsorption via weak electrostatic interaction between NBz and acidic oxygen functional groups. We have not direct evidence for the end-on adsorption of NBz on oxidized BAC(BAC-Ox), but as displayed in Fig. 1b, the adsorption amount of NBz on AC-Ox exceeded that on AC-OxOG at equilibrium solution concentration (C_e) beyond 20 mmol/L in spite of a small specific surface area of only 140 m^2/g of AC-Ox. Ramis et al. examined adsorption of benzene and NBz on TiO_2 , ZrO_2 , and Fe_2O_3 (hydrophilic surface) and observed flat-on orientation for benzene adsorption but side-on (perpendicular) orientation for NBz [22]. This is caused by strong π -electron withdrawal effect by nitro group in NBz. Chen et al. also observed the alternation of adsorption orientation of phenyl hydroquinone (PHQ) on graphene nanoplatelets from Langmuirian flat-on at low concentration and then to endwise orientation at higher PHQ concentration in aqueous phase [23].

As long as strong oxygen functional groups like carboxy groups are not present in graphene structure of ACs, the adsorption amount of mono-aromatics will be approximately proportional to specific surface area due to the mechanism of mono-layer Langmuir-type adsorption with π - π interaction between benzene ring and graphene. When we use granular activated carbon (GAC) and remove large organic molecules such as dyes dissolved in aqueous phase, larger pore diameter is needed to accommodate the pollutants. Figure 2 represents adsorption performance of small (NBz, mono-aromatics) and large (tannic acid) molecules to ACs as a function of mesopore volume [24]. Normally ACs are rich in micropore and have hydrophobic graphene surface; therefore, they are suitable for small organic molecules as mono-aromatics. The adsorption amounts of mono-aromatics are usually proportional to specific surface area and/or micropore volume. However, large bulky molecules as tannic acid can adsorb only larger pore surface as mesopore and macropore. As clearly shown in Fig. 2, although the amounts of nitrobenzene

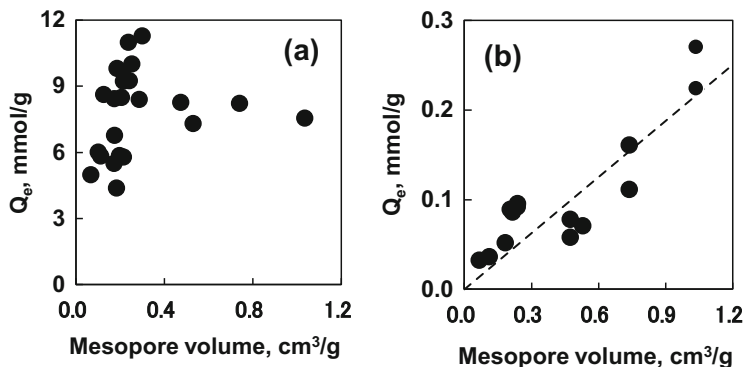


Fig. 2 Adsorption amount of nitrobenzene (NBz) (a) and tannic acid (b) as a function of mesopore volume of various modified activated carbons (ACs) [24]

adsorption exhibit poor relationship with mesopore volume, those of tannic acid uptake have a good relationship with mesopore volume [24]. Large bulky molecules as dyes and tannic acid dissolved in water have ionic parts in their molecules; therefore, large pore size is more important to capture them for AC structure than small molecules. Mono-aromatics rather adsorb via π - π interaction (HOMO-LUMO system) between aromatics adsorbates (MOMO) and carbon adsorbents (LUMO) [25]. In adsorptive removal of organic contaminants in water, the following conditions may be essential for activated chars and their surface:

- Some amount of specific surface area will be needed, probably at least 500 m²/g.
- Oxygen content should be minimized in the carbonaceous adsorbents at any stage of production, storage, practical usage, and regeneration because oxygen functional groups, particularly carboxy groups, always cause poor adsorption behavior for the organic pollutants. Carbon materials can accumulate oxygen in air even at the ambient conditions, and then the surface will be gradually degraded with time.
- Adsorption speed is controlled by diffusion of organic contaminants in the pore structure, and then fine powder and/or mesoporous structure will be required for increasing the adsorption speed especially in aqueous phase. For example, fine activated carbon powder was sprayed at the outlet of exhaust gas to even capture gas phase dioxins in the waste incineration plant in Japan.

Since removal of organic pollutants has been a major role of activated carbons (ACs) for a long time, above conditions for organic pollutants were fully satisfied in the commercial production base of activated carbons (commercially available ACs), thanks for the efforts in industries. Ideally when activated carbon (AC) and activated carbon fiber (ACF) are composed of carbon and hydrogen and condensed poly aromatic ring is formed, the size of graphene structure can be estimated as shown in Fig. 3 [26]. Using the simple model, chemical formula and the number of benzene ring can be easily estimated as an ideal case; e.g., if only 99.8 wt% carbon and 0.2 wt

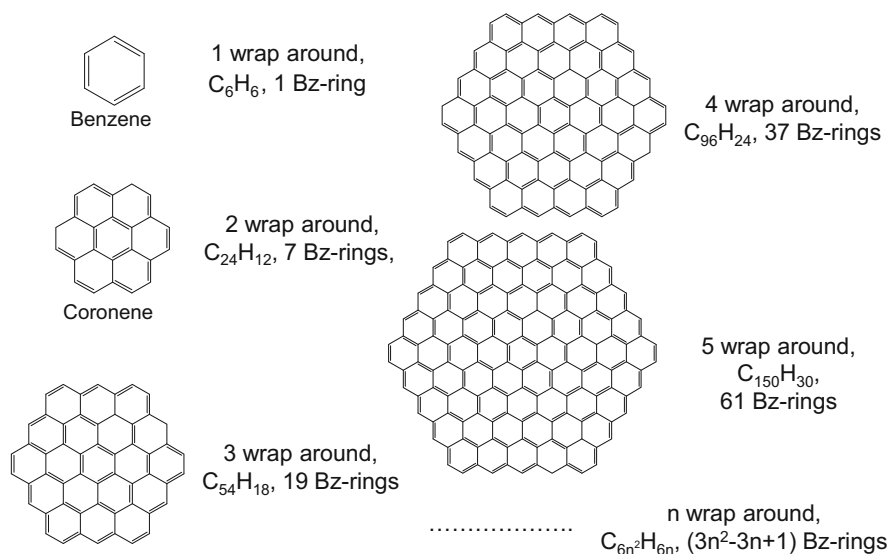


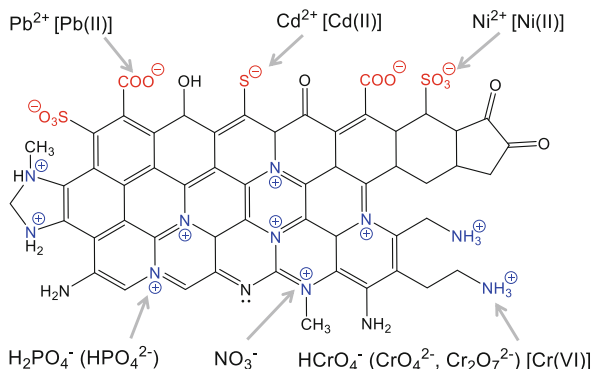
Fig. 3 Model of unit crystal graphene size of activated carbon (AC) [26]

% hydrogen are contained in AC or ACF, we can obtain chemical formula of C₁₀₀₀₀₀₀H₂₅₀₀ and the number of benzene ring per one graphene sheet of 5.2×10^5 . In practice, graphene sheet is not flat because curved three-dimensional graphene unit structure containing 5 and 7 membered rings and heterolytic atoms as oxygen, nitrogen, and sulfur must be formed [27]. The porous structure is constructed by the curved structure of graphene units; otherwise, all graphene sheets become two dimensional with only sp² hybrid bonds (no sp³ hybridization), and then graphene sheets are binding each other resulting in little porous structure (small specific surface area).

3 Adsorbents for Ionic Pollutants

There are various ionic pollutants in water environment such as heavy metals, halogens, oxoacids, and some kinds of dyes. For adsorptive removal of the ionic pollutants, ion-exchange resins [28] and metal oxides [29] have been utilized, but carbonaceous materials can be used as well if suitable carbon surface modifications can be made [26]. In this chapter, applicability of carbonaceous adsorbents of ACs and ACFs for the removal of ionic contaminants in aqueous phase together with current developments of new carbon/char adsorbents with heteroatom functions. Some of them are successfully developed superior to ion-exchange resins, and the others are under the development in the laboratory scale. Figure 4 displays the

Fig. 4 Some surface functions on graphene layer required to effectively capture cationic and anionic contaminants from aqueous phase [30]



concept of the modification on the heteroatom functionalized carbonaceous adsorbent [30].

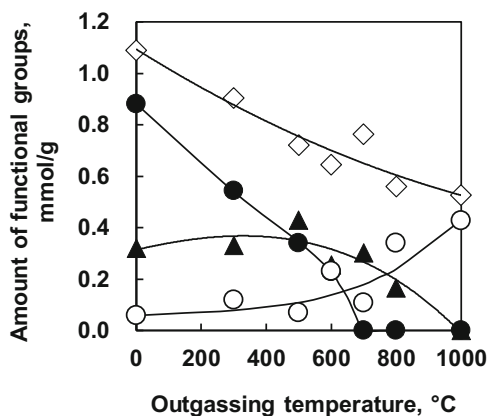
3.1 Cationic Contaminants

3.1.1 Surface Functional Groups for Cations

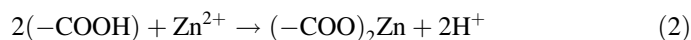
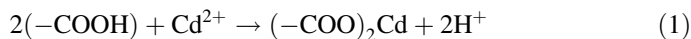
As represented in Fig. 4, carboxy ($-\text{COO}^- \text{H}^+$, $-\text{COO}^- \text{Na}^+$), sulfonic ($-\text{SO}_3^- \text{H}^+$, $-\text{SO}_3^- \text{Na}^+$), and thiol ($-\text{S}^- \text{H}^+$, $-\text{S}^- \text{Na}^+$) groups on carbon are widely proven to be effective for the adsorption of cationic pollutants, such as lead(II) (Pb^{2+}), cadmium (II) (Cd^{2+}), nickel(II) (Ni^{2+}), and Cs(I) (Cs^+) dissolved in water. Weakly negatively charged $\text{C}\pi$ site is working as well for the adsorption sites of heavy metal ions. Carboxy groups can be introduced to the carbon surface with oxidation by H_2O_2 , HNO_3 , and $(\text{NH}_4)_2\text{S}_2\text{O}_8$ [31], whereas it is hardly achieved that sulfonic acid can be individually introduced on graphene layer of ACs although several attempts have been done [32, 33]. Thiol functional groups ($-\text{SH}$) on carbon surface are also applicable especially for the capture of cadmium(II) [34]. Thiol groups may be more suitable for cadmium(II) uptake than for lead(II) on mesoporous silica materials, while carboxy groups on carbon are better for lead(II) than for cadmium (II) [35]. Assuming that thiol groups ($\text{Ar}-\text{S}^- \text{H}^+$) could work as soft base and carboxy groups ($\text{Ar}-\text{COO}^- \text{H}^+$) as hard base according to HSAB theory for Lewis acids and bases, the pair of soft acid of cadmium ion (Cd^{2+}) and soft base of thiol groups ($\text{Ar}-\text{S}^-$) and that of medium acid of lead ion (Pb^{2+}) and hard base of carboxy groups ($\text{Ar}-\text{COO}^-$) should be better combination than the opposite pairs of the heavy metals and the surface functional groups.

In practice, the introduction of carboxy groups is probably the most feasible for the modification of carbon surface to remove heavy metal cations. The amounts of carboxy groups can be ultimately introduced with the order of $(\text{NH}_4)_2\text{S}_2\text{O}_8 > \text{HNO}_3 > \text{H}_2\text{O}_2$. In case of using HNO_3 as an oxidant, mixture of activated carbon (AC) and concentrated HNO_3 is boiled generating blown colored NO_2 gas as the oxidation progressed, and

Fig. 5 Surface oxygen-containing acidic functional groups and basic sites ($C\pi$ sites) of HNO_3 oxidized AC as a function of outgassing temperature from 300°C to 1,000°C. The functional groups were determined with Boehm titration; carboxy groups (filled circle), lactone groups (filled triangle), hydroxy groups (open diamond), basic sites (open circle) [36]



acidic oxygen function as carboxy and lactone groups can be introduced on AC surface. Figure 5 shows the changes in oxygen functional groups and basic sites on activated carbon (AC) oxidized with 6 M HNO_3 and their outgassed materials [36]. And Fig. 6 represents corresponding adsorption amounts of cadmium(II) and zinc(II) cations and the ratio of discharged proton (H^+) over adsorbed cadmium(II) and zinc(II), respectively [36]. By the oxidation of AC, significant amounts of carboxy ($-COOH$), lactone ($-OCO-$), and hydroxy ($-OH$) groups were introduced and gradually decreased in carboxy and hydroxy groups by increasing outgassing temperature, and the carboxy groups were disappeared until 700°C (Fig. 5). In contrast, basic sites ($C\pi$ sites) were increased as electron withdrawal carboxy functions were decreased. On the other hand, the lactone groups exhibit relatively constant values until 700°C indicating that lactone groups can be converted to CO/CO_2 by decomposition, while a part of lactone can be newly generated by dehydration of carboxy and hydroxyl groups. As clearly seen in Fig. 6, the adsorption of cadmium(II) and zinc(II) was taken place with ion-exchange mechanism because two protons were discharged, while one divalent metal(II) cation was adsorbed when more than the stoichiometric amount of carboxy groups was available on carbon surface as shown in Fig. 5.



Contrarily when most of carboxy groups were removed from graphene layers as CO/CO_2 and H_2O , and/or converted to lactone on the graphene, adsorption mechanism was switched from ion-exchange mechanism (Eqs. (1) and (2)) to electrostatic interactions between heavy metal cations and $C\pi$ -electrons on the graphene that could have slightly negative charged properties. Similar electrostatic interactions could be observed for lead(II) adsorption [37]. Electron density of $C\pi$ sites could be corresponding to basic sites of Boehm titration as also displayed in Fig. 5. The electron density might be able to be easily reduced by electron withdrawing groups

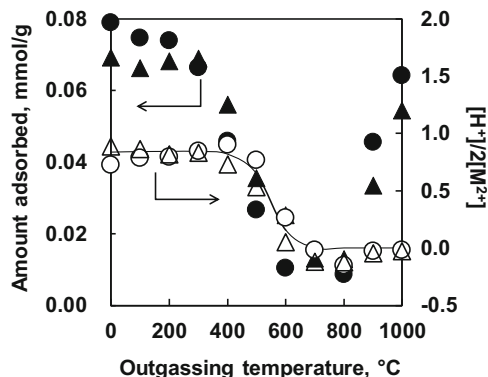


Fig. 6 Adsorption amounts of cadmium(II) (filled circle) and zinc(II) (filled triangle) as a function of outgassing temperature from 100°C to 1,000°C, corresponding molar ratios of discharged proton (H^+)/adsorbed cadmium(II) (open circle) and zinc(II) (open triangle) ($[H^+]/2[M^{2+}]$) in which $[H^+]/2[M^{2+}]$ is 1.0 and 0.0 which represent ion-exchange mechanism and $C\pi$ sites adsorption, respectively [36]

of carboxy and lactone at the edge of graphene layer, but the $C\pi$ electron density might be increased by the reduction of them leading to the rise in the adsorption amounts of metal cations as could be seen in Fig. 6.

When greater amounts of heavy metal cations should be accommodated in ACs and ACFs, oxidation with ammonium peroxodisulfate (APS, $(NH_4)_2S_2O_8$) solution is one of the most effective options to introduce abundant amounts of oxygen functional groups [38, 39]. The APS oxidation can be conducted using ambient temperature, although a few days or longer will be required to generate enough carboxy groups on AC and ACF surface. Effective carboxy groups can be formed on carbon surface by destructing the graphene edges and whole graphene basal plane. Figure 7 shows changes in adsorption amounts of lead(II) cation (Pb^{2+}) as a function of APS oxidation time [38]. The adsorption amount of lead(II) is greatly improved from only 0.1 mmol/g (non-oxidized BAC) to as much as 2.3 mmol/g (ca. 0.5 g-lead (II)/g-AC oxidized). On the other hand, specific surface area (S_{BET}) was unilaterally declined during the oxidation as represented in Fig. 8 in which maximum adsorption amounts of day 4 (30°C oxidation) and day 8 (20°C oxidation) were consistent with the days losing their specific surface area (close to zero) [38]. The results indicated that carboxy groups available for lead(II) adsorption could reach the maximum after measurable porous structures were completely destroyed (Fig. 8). As shown in Fig. 9 [38], carbon content was decreased from 94% down to 65% within first 2 days, whereas oxygen was increased from 5% up to 35%, but after that the adsorption amounts of lead(II) went up until day 4 (30°C oxidation) and day 8 (20°C oxidation) revealing that oxygen functional groups would be introduced by forming precursors of carboxy groups (hydroxyl and/or carbonyl, etc.) until day 2 and then they might be further converted to carboxy groups that were only effective function for the adsorptive removal of heavy metal cations. Adsorption amount of lead(II) can be

Fig. 7 Increase in the adsorption amounts of lead (II) (Pb^{2+}) as a function of oxidation time. Starting materials; beaded-shaped activated carbon (BAC, Kureha Corporation). Oxidation with ammonium peroxodisulfate ($(\text{NH}_4)_2\text{S}_2\text{O}_8$) solution at 20°C (filled circle) and 30°C (filled triangle). Solution equilibrium pH (pH_e) > 4.0 . Initial lead (II) concentration; 4.8 mmol/L [38]

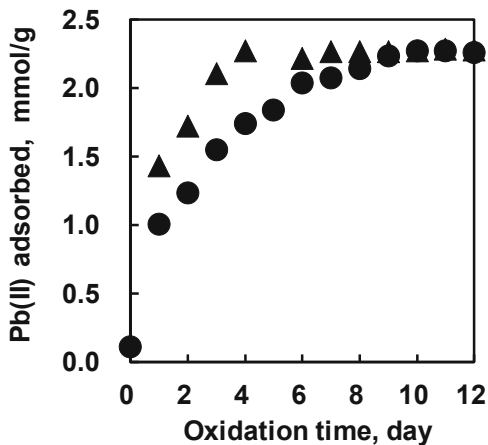


Fig. 8 Decrease in B.E.T. specific surface area of BAC from $1,380 \text{ m}^2/\text{g}$ to less than $25 \text{ m}^2/\text{g}$ during oxidation in peroxodisulfate ($(\text{NH}_4)_2\text{S}_2\text{O}_8$) solution at 20°C (filled circle) and 30°C (filled triangle) [38]

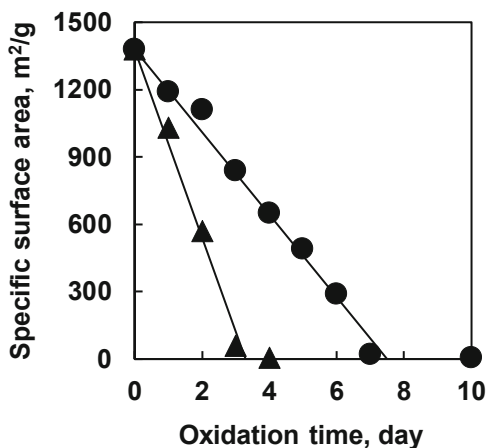


Fig. 9 Changes in carbon (filled circle and triangle) and oxygen (open circle and triangle) content during oxidation in peroxodisulfate ($(\text{NH}_4)_2\text{S}_2\text{O}_8$) solution at 20°C (open circle) and 30°C (open triangle) [38]

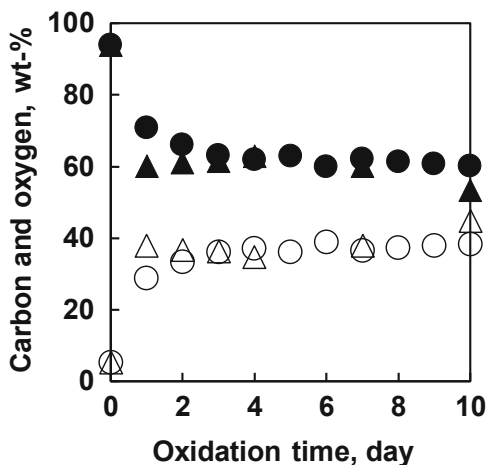
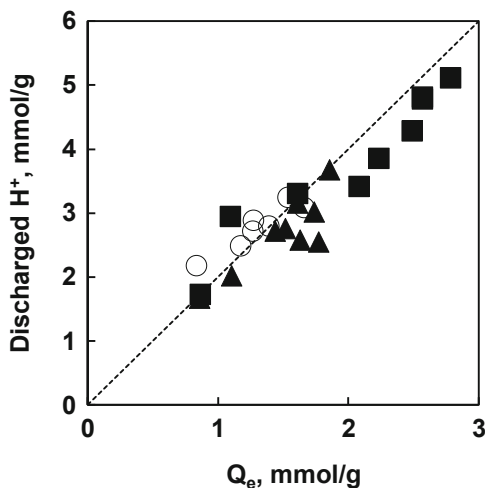


Fig. 10 Relationship of the proton discharged into water (H^+ [mmol/g]) and the amount of lead(II) (Pb^{2+}) adsorbed onto oxidized activated carbon fiber (Q_e [mmol/g]) by ion-exchange process. Oxidized ACF (KF1500) by $(NH_4)_2S_2O_8$ (filled triangle and square), carboxy functionalized ion-exchange resin (open circle) [39]



significantly improved for activated carbon fiber (ACF) by the oxidation with ammonium peroxodisulfate (APS, $(NH_4)_2S_2O_8$) as well. Figure 10 shows an evidence of ion-exchange mechanism for the adsorption of lead(II) onto oxidized ACF (Toyobo Co., Ltd., Japan) and carboxy functionalized ion-exchange resin (AMBERLITE™ IRC86) [39]. When one lead(II) cation is uptaken on the adsorbents, two protons (H^+) are instead released from carboxy groups ($-COO^-H^+$) into water, supporting ion-exchange mechanism. However, only 4.01 mmol/g of carboxy groups was measured by Boehm titration despite as much as 2.79 mmol/g of lead (II) (Pb^{2+}) adsorbed. The results reveal that an excess amount ($2.79 \times 2 - 4.01 = 1.57$ mmol/g) of lead(II) could adsorb on the oxidized ACF. We are not sure, but some unknown sites may participate in the adsorption via ion-exchange. In both AC and ACF, APS oxidation leads to the destruction of carbon structure introducing nearly a half portion of oxygen in the total elemental composition. Oxidized AC and ACF with the abundant oxygen are easily dissolved in the basic solution (e.g., NaOH solution), thereby the extent of oxidation should be controlled not to be dissolved in a practical use [38, 39], although much amount of carboxy groups can be easily introduced onto graphene layers for AC and ACF. In our oxidation procedure, 2 M (mol/L) APS ($(NH_4)_2S_2O_8$) in 1 M H_2SO_4 solution was mixed with AC (or ACF) at APS solution/AC ratio of 50 mL/g or more at 20–30°C [38]. The 2 M APS solution and the mixing ratio of 50 mL/g-AC were most important points to introduce sufficient amounts of carboxy groups ($-COOH$) introduced onto graphene layer of ACs and ACFs. Since higher oxidation temperature and longer oxidation period also cause the destruction of graphite structure of AC and ACF, the temperature and period of APS oxidation should be suitably adjusted depending on the properties of each AC and ACF [40].

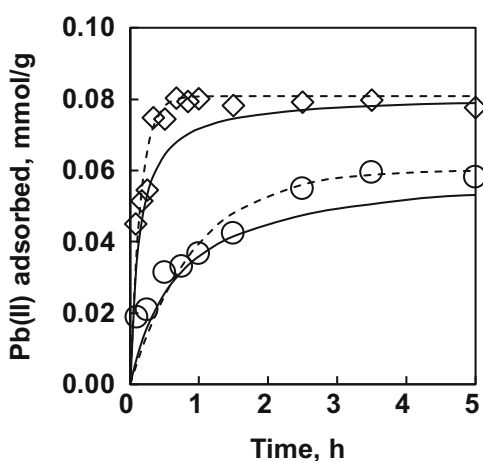
In addition, even if AC surface can be successfully filled with carboxy groups by the oxidation, as increase in the adsorption amount of heavy metal cations, pH of aqueous solution will be decreased less than 4 by discharging corresponding

amounts of protons (Fig. 10) resulting in stopping further adsorption caused by competitive adsorption of abundant amounts of protons. Thereby, protons of carboxy groups ($-\text{COO}^{-}\text{H}^{+}$) should be replaced by sodium ions in NaCl/NaOH solution forming $-\text{COO}^{-}\text{Na}^{+}$ as well as ion-exchange resin from the practical points of view.

3.1.2 Adsorption Kinetics

Not only adsorption capacity but adsorption kinetics is an important aspect from the practical point of view. In general, fine powder AC exhibits much faster adsorption speed than granular AC. However, fine powder has disadvantage because it is hard to be recovered after use for regeneration. On the other hand, pseudo-second-order kinetics can be observed for granular AC in which diffusion control kinetics is progressed [16]. To increase kinetic efficiency of granular AC, mesoporous and/or macroporous AC should be prepared. As mentioned in the previous section, mesoporous granular ACs were prepared from bamboo chips and measured adsorption kinetics of lead(II) as displayed in Fig. 11 [20] in which pseudo-first-order kinetics rather than pseudo-second-order was fitted to the experimental results, indicating that adsorption process was controlled by not diffusion in the porous structure but collision to the adsorption sites in which no sterically restriction in approaching the adsorption sites occurred. In this case, since non-oxidized AC was examined ($\text{C}\pi$ sites), oxidized mesoporous AC (carboxy groups) has not been clarified for kinetics yet. But, as long as we have examined, pseudo-second-order kinetics is more applicable for oxidized ACF which is microporous one before oxidation [39] and for most of other oxidized ACs and ACFs.

Fig. 11 Adsorption kinetics of lead(II) on mesoporous activated carbons (ACs) derived from bamboo chips (BC). ZnCl_2/BC ratio of 1.0 (open circle) and 6.0 (open diamond) in activation at 500°C . Dashed and solid lines represent the approximation curves by pseudo-first-order and pseudo-second-order kinetic models, respectively. Initial lead(II) concentration; 0.48 mmol/L [20]

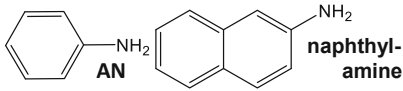
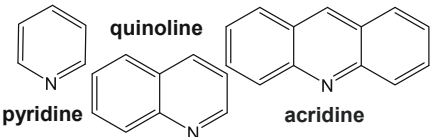
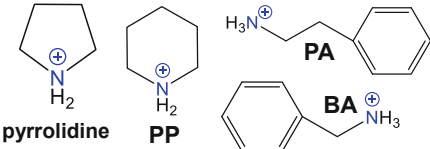
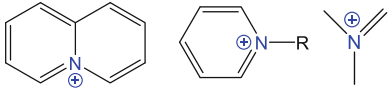


3.2 Anionic Contaminants

3.2.1 Surface Functional Groups/Sites (Nitrogen and C π Sites) for Anions

Sodium, chloride, and hydroxy ions are not regarded as pollutants, but not only fluoride, bromide, arsenic, and chromate but also nitrate and phosphate are also regarded as contaminants in aqueous phase to be removed as mentioned in the previous section. For the adsorption of cationic pollutants, oxygen-containing (carboxy) and sulfur-containing (sulfonic and thiol) groups are effective to capture Cs^+ , Pb^{2+} , Cd^{2+} , Ni^{2+} , Cu^{2+} , etc., while for adsorptive removal of anionic pollutants, nitrogen-containing functions on the adsorbents are said to be desirable to attract anionic impurities as F^- , Br^- , H_2AsO_4^- , HCrO_4^- , $\text{Cr}_2\text{O}_7^{2-}$, NO_2^- , NO_3^- , H_2PO_4^- , etc. Table 1 displays some typical nitrogen-containing compounds and their nitrogen hybridization (sp^2 , sp^3 orbital) and pK_a range that represents the degree of affinity to protons (H^+) in aqueous phase. Aromatic amine (aniline, pK_a 3–5)- and pyridine (pK_a 5–7)-type nitrogen species (N-6) cannot accept protons at pH above 7, and they are negatively charged around neutral to basic region implying that repulsive force is working between anionic pollutants and carbon surface. Alternatively, aliphatic amine ($\text{pK}_a > 9$) and quaternary nitrogen species (N-Q) are positively charged in a wide range of solution pH. The aliphatic amine types can easily attract protons (H^+)

Table 1 Nitrogen hybridization and pK_a ranges of nitrogen-containing compounds assuming solution pH 7–8

Nitrogen-containing compound	Nitrogen hybridization	pK_a range
 AN naphthyl-amine	sp^3	3–5
 pyridine acridine	sp^2	5–7
 pyrrolidinium piperidinium PA BA	sp^3 (Aliphatic amines)	9<
 quaternary nitrogen (N-Q) family	sp^2 (N-Q)	Positively charged

Prepared using the data in refs. [41, 42]

from weak acidic to weak basic region [41, 42]. They are sometimes detected on carbon surface. Dioum and Hamoudi examined nitrate adsorption onto mesoporous silica materials functionalized with propyl-ammonium (alkyl amine) and propyl-*N,N,N*-trimethylammonium (N-Q) and observed effective progress in adsorption on the surface nitrogen species in which nitrate (NO_3^-) adsorption capacities of 0.9–1.0 mmol/g-adsorbent were achieved [43]. On the carbonaceous materials, such sufficient amount of effective nitrogen has not been introduced yet. Other than effective nitrogen species of alkyl amine and quaternary nitrogen (N-Q), $\text{C}\pi$ electrons on graphene layers play a role of nitrate adsorption as well as heavy metal cations because $\text{C}\pi$ electrons can accommodate protons at acidic region (pH 3–5) and the positively charged surface attracts nitrate anion. In the same way of the adsorption of heavy metal cations, $\text{C}\pi$ electrons can show their ability only in the absence of electron-withdrawing oxygen functional groups. Figure 12 shows adsorption isotherms of nitrate on de-ashed activated carbon (AC, Calgon F400) and ACs oxidized and outgassed at 600°C and 900°C, respectively [44]. The properties of adsorbents including oxidized AC are tabulated as well in Table 2 [44]. The de-ashed AC adsorbed nitrate by 0.1 mmol/g. The de-ashed AC was oxidized with 8 M HNO_3 solution at 95°C to introduce acidic oxygen functional groups, washed with pure water using Soxhlet extractor, and calcined in air for 6 h to completely decompose the nitrate ions remained in the carbon. The oxidized AC was referred to as Ox in Table 2. Ox was outgassed by heat treatment in inert gas at 600°C (Ox-6OG) and 900°C (Ox-9OG) to remove oxygen as CO/CO_2 and H_2O [45]. There are some amounts of carboxy and lactone groups in de-ashed AC (F400). The acidic oxygen functional groups increased by oxidation (Ox). We could not observe any nitrate adsorption on Ox revealing that acidic oxygen functional groups of carboxy and lactone might withdraw $\text{C}\pi$ electrons on graphene layers leading to inhibiting nitrate adsorption. Some adsorption occurred on Ox-6OG, but the adsorption amounts were less than those of F400 because carboxy and lactone groups on Ox-6OG were considerably reduced from those on Ox, but they are greater than F400. No detection

Fig. 12 Adsorption isotherms of nitrate on activated carbons (AC, F400) at 25°C. Original de-ashed F400 AC (open square, Ox), oxidized F400 and outgassed at 600°C (filled triangle, Ox-6OG), and oxidized F400 and outgassed at 900°C (filled circle, Ox-9OG) [44]

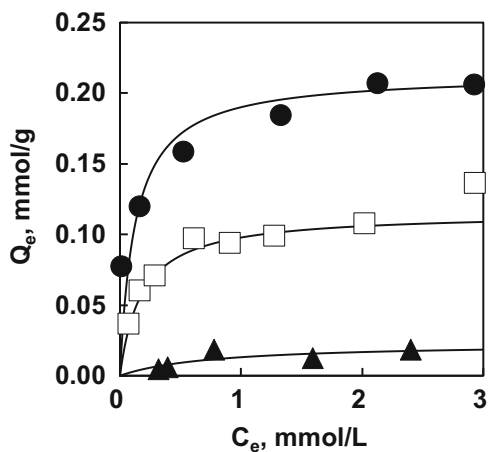


Table 2 Textural, bulk, and surface properties for F400-activated carbon (AC) and modified ACs [44]

AC	Surface area and pore volumes			Elemental composition			Surface functional groups/sites ^a					
	S _{ges} m ² /g	V _{total} cm ³ /g	V _{micro} cm ³ /g	V _{meso} cm ³ /g	Carbon, wt%	Hydrogen, wt%	Nitrogen, wt%	Oxygen ^b , wt%	Carboxy, mmol/g	Lactone, mmol/g	Phenol, mmol/g	Basic sites, mmol/g
F400 ^c	1,290	0.612	0.421	0.191	90.8	0.1	0.6	8.5	0.15	0.13	0.32	0.29
Ox	820	0.406	0.223	0.183	80.2	0.2	0.9	18.8	0.90	0.52	1.19	0.06
Ox-6OG	1,110	0.665	0.446	0.219	90.0	0.3	0.9	8.9	0.27	0.29	0.67	0.21
Ox-9OG	1,120	0.666	0.467	0.199	95.2	0.2	1.2	3.5	0.00	0.00	1.04	0.27

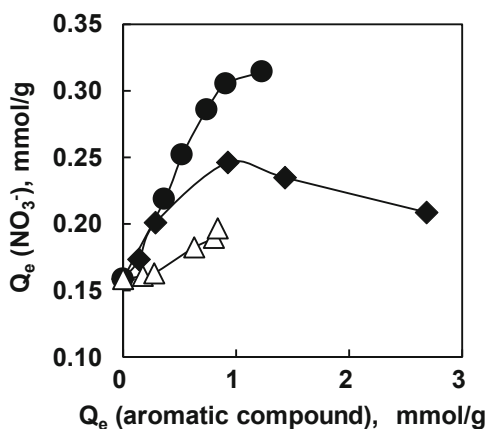
^aMeasured by Boehm titration^bCalculated by difference^cF400: de-ashed Filtrasorb 400

of carboxy and lactone groups and the largest adsorption amount of nitrate could be observed for Ox-9OG. Thereby, the amounts of carboxy and lactone groups might be adversely proportional to the adsorption amounts of nitrate.

3.2.2 Surface Nitrogen (Alkyl Amine Type)

As shown in Table 1, alkyl amine type of nitrogen such as benzylamine (BA), phenethylamine (PA), and piperidine (PP) can accommodate protons (H^+) in a wide range from acidic to weak basic region (solution $pH < 9$) [41, 42]. Although adsorption capacity of $C\pi$ electrons sites is greatly influenced by solution pH , principally alkyl amines are always positively charged as long as pH is less than 9. For the present, alkyl amines have never been detected on carbon surfaces. Alternatively, mono-aromatic amine compounds were mixed with solution to inspect the effect of the amines on the adsorption of nitrate onto AC surface. Figure 13 represented the possibility of the effectiveness of alkyl amine on the carbon for nitrate adsorption [46]. The adsorption of nitrate was conducted in the presence of aniline (AN), benzylamine (BA), and phenethylamine (PP). Comparing to absence of the amines, co-existence of the molecular amines in aqueous phase could improve the adsorption amount of nitrate. The enhancement of nitrate adsorption was most pronounced for phenethylamine and then benzylamine and slightly effective of aniline. The order of the effectiveness is consistent with pK_a values (acidity) of phenethylamine (pK_a 9.83) > benzylamine (9.33–9.34) > aniline (4.87) [41, 42]. The results were supported by the fact that the propyl-ammonium (alkyl amine, $R-NH_2$) on mesoporous silica materials became suitable adsorption sites as well [43], whereas aromatic amine like aniline in which amine groups were directly bound to aromatic ring (aromatic amine, $Ar-NH_2$) cannot be effective function to capture nitrate anion. Consequently, improvement of nitrate adsorption might be promising for ACs if amine groups possessing pK_a values greater than 9, e.g., benzylamine, phenethylamine, and piperidine, can be successfully introduced on the carbon surface.

Fig. 13 Adsorption of nitrate on activated carbon (AC, de-ashed F400) at 25°C in the presence of aniline (AN, open triangle), benzylamine (BA, filled diamond), and phenethylamine (PA, filled circle). Equilibrium solution pH (pH_e) 2.0, initial concentration of chloride $[Cl]_0$: 30 mM [46]



In addition to anionic pollutants, alkyl amine function, in the case of mesoporous silica materials, is useful for cationic pollutants such heavy metal ions as cadmium(II) and lead(II) in neutral and basic region (solution pH > 7–8) in which lone pair of nitrogen atom in amine groups can preferably accommodate cationic ions as well as protons (H^+) by forming covalent bond with the lone pair of nitrogen [47, 48]. Therefore, alkyl amine functionalized carbon can be utilized for adsorptive removal of both anions (acidic and neutral region) and cations (neutral and basic region) when it will be successfully prepared in the future as well as mesoporous silica materials.

3.2.3 Surface Nitrogen (Quaternary Nitrogen, N-Q)

In our previous study, the introduction of alkyl amine, piperidine, and quaternary nitrogen (N-Q) was attempted. In the several trials, only quaternary nitrogen (N-Q) has been able to be doped on the carbonaceous adsorbents to some extent. According to the procedure of the research group in Pennsylvania State University in which AC was oxidized first and then ammonia gas treated at 700°C [49], bead-shaped activated carbon (BAC, Kureha Corporation) was oxidized with APS ($(NH_4)_2S_2O_8$) solution followed by ammonia gas treatment at 950°C and then supplied for adsorption experiment of nitrate [50]. In our study, ammonia treatment temperature was altered from 700°C (Penn State temperature) to 950°C due to thermodynamically favorable temperature to form quaternary nitrogen (N-Q) at 950°C referring to the study by Pel et al. [51]. In principle, carbonization is the endothermic reaction of dehydrogenation releasing hydrogen and oxygen as CO/CO₂ and H₂O and also nitrogen and sulfur as ammonia and hydrogen sulfide. Rising treatment temperature, transformation of pyrrolic nitrogen (N-5) to pyridinic nitrogen (N-6) is firstly taken place, and then condensation of carbon matrix will be progressed to spread graphene unit together with incorporation of nitrogen as N-Q ($=N^+<$) in the graphene layers as a result [51]. Figure 14 represents adsorption isotherms of nitrate on as-received AC (BAC) and AC oxidized followed by

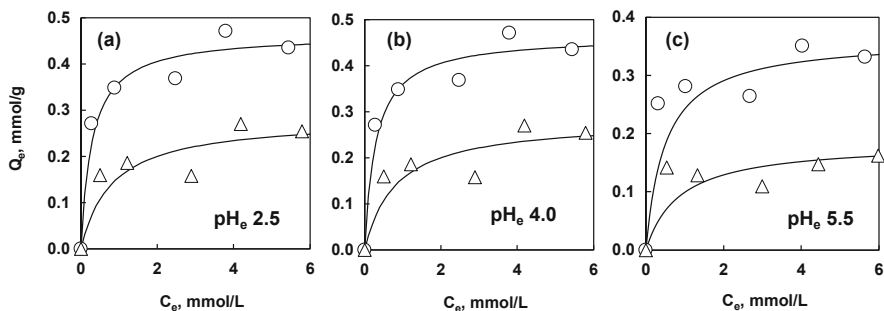


Fig. 14 Langmuir isotherms of nitrate adsorption on as-received AC (open triangle) and oxidized and ammonia gas-treated (950°C) AC (open circle) in ambient temperature at equilibrium solution pH (pH_e) 2.5 (a), 4.0 (b), 5.5 (c) [50]

ammonia treated AC (Ox-9.5AG) as a function of equilibrium solution pH (pH_e) 2.5–5.5 [50]. The as-received AC has neither acidic oxygen groups nor nitrogen species, and then all adsorption sites are estimated to be $C\pi$ sites, thereby adsorption amounts of nitrate increase with lowering pH_e due to larger proton concentration at low pH_e indicating that more positively charged surface can attract nitrate anion. The difference between as-received AC and Ox-9.5AG could be attributed to the difference in N-Q content introduced to Ox-9.5AG. The specific surface area of AC ($1,380 \text{ m}^2/\text{g}$) is much larger than Ox-9.5AG ($770 \text{ m}^2/\text{g}$) also supporting that N-Q sites on Ox-9.5OG can play a specific role for the greater nitrate adsorption [50].

A high nitrogen content material of melamine form was also supplied for the preparation of nitrogen-containing carbonaceous adsorbent. Melamine sponge (ML, Fuji Gomu Co., Ltd.) was impregnated with ZnCl_2 solution (ML to ZnCl_2 ratio of 3 and 6), dried at 110°C , and activated at 500°C [52]. The carbonized materials were named as Z3 and Z6. Specific surface area of the melamine sponge (ML) was only $1 \text{ m}^2/\text{g}$, but it improved by the ZnCl_2 activation to 58 and $99 \text{ m}^2/\text{g}$ for Z3 and Z6, respectively. The Z3 and Z6 were further treated with methyl iodide (CH_3I) to principally convert N-6 remaining on Z3 and Z6 to N-Q (Z3-Q and Z6-Q) via nucleophilic substitution reaction ($\text{S}_{\text{N}}2$) as displayed in Eq. (3).

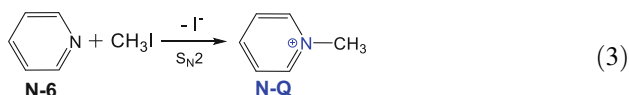


Figure 15 shows the results of screening test of nitrate adsorption on the melamine form-derived carbonaceous materials [52]. Surprisingly starting material of melamine form itself adsorbed nitrate ion to some extent even though specific surface area was only $1 \text{ m}^2/\text{g}$ (0.1% of usual values of ACs). We are not sure but nitrogen species and/or some sponge structure may contribute to the adsorption. The

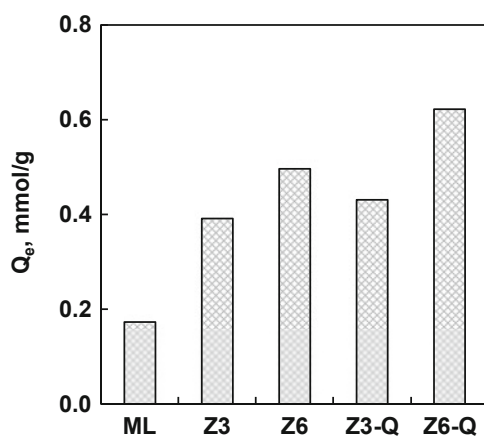


Fig. 15 Adsorption of nitrate on melamine sponge (ML), ML activated with ZnCl_2 at 500°C by ML/ ZnCl_2 ratio of 3 and 6 (Z3, Z6) and their CH_3I treated (N-6 to N-Q converted) materials (Z3-Q, Z6-Q). Initial nitrate concentration: 200 mg/L , equilibrium solution pH (pH_e) 3–4 [52]

Fig. 16 Adsorption isotherms of nitrate on ZnCl_2 activated melamine sponge (Z6, open circle) and post- CH_3I -treated Z6 to convert N-6 to N-Q (Z6-Q, filled circle). Equilibrium solution pH (pH_e) 3–4 [52]

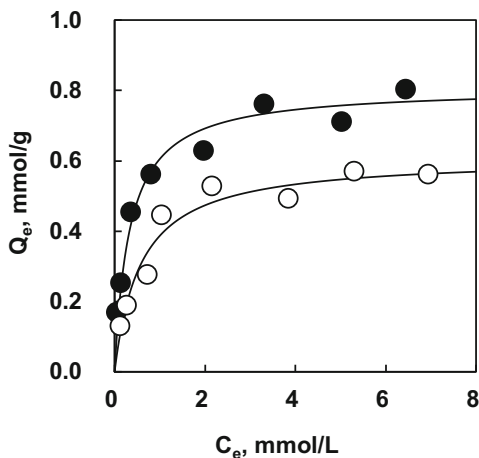
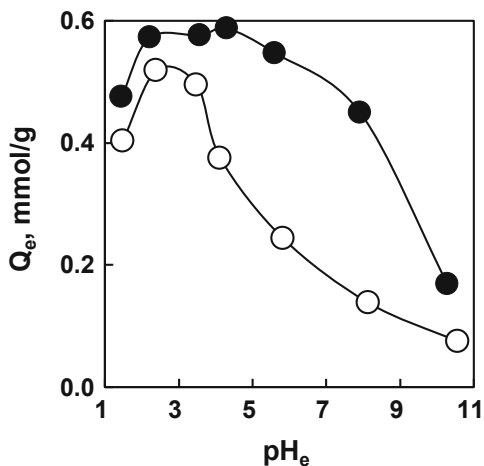


Fig. 17 Influence of equilibrium solution pH (pH_e) on the adsorption of nitrate onto ZnCl_2 -activated melamine sponge (Z6, open circle) and post- CH_3I -treated Z6 to convert N-6 to N-Q (Z6-Q, filled circle) [52]

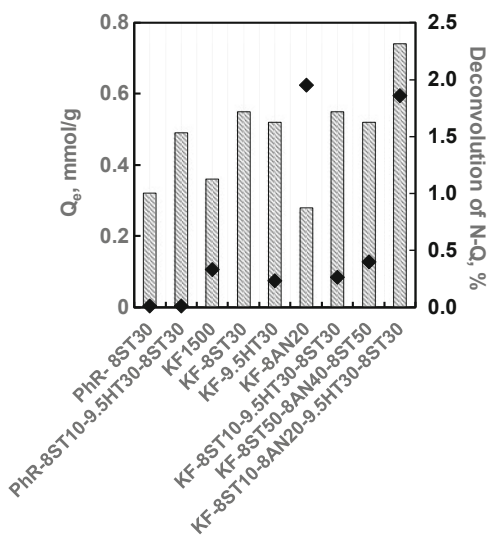


ZnCl_2 activation improved nitrate adsorption from 0.2 mmol/g to 0.4–0.5 mmol/g for Z3 and Z6. Post methyl iodide (CH_3I) reaction could slightly increase the nitrate adsorption amount for Z6. As representing adsorption isotherms of nitrate on Z6 and Z6-Q in Fig. 16 [52], Z6-Q is superior to Z6 at equilibrium solution pH (pH_e) 3–4 probably due to greater amount of quaternary nitrogen (N-Q) on Z6-Q. The above estimation was supported by Fig. 17 [52] because Z6-Q maintained the adsorption amounts of nitrate ranging pH_e 2–8, but steep decline of nitrate adsorption was observed from pH_e 4 to 8 for Z6 sample. The results implied that constant positively charged N-Q could be dominant on Z6-Q. In this case, N-Q sites were only influenced by chloride ions (Cl^-) in acidic region and hydroxy ions (OH^-) in basic region. On the other hand, the surface of Z6 might be occupied with other nitrogen species (N-5, N-6) and/or $\text{C}\pi$ sites which is always influenced by solution

pH leading to the wide range of surface proton (H^+) concentrations from acidic (higher proton concentration) to basic region (lower proton concentration).

Activated carbon fiber (ACF) is a useful carbon material from the point of handling. Nitrogen doping into ACF was conducted by thermal chemical vapor deposition (CVD) by charging acetonitrile (CH_3CN) into ACF [53]. Rayon-based ACF (Toyobo Co., Ltd.), namely, KF1500, was employed as a starting material. KF1500 is microporous ACF produced as a commercial product from cellulose (rayon polymer), and it has average pore diameter (D_{avg}) of 1.8 nm and specific surface area (S_{BET}) of 1,540 m^2/g . In our study at first KF1500 was further activated with super heat steam at 800°C to expand pore volume by sending pure water to quartz tube readily heated in a tube furnace at the desired temperature in which KF1500 sample (2–3 g) was placed on a boat. In the next step, the flow of steam was switched to the acetonitrile liquid under inert gas flow, and nitrogen deposition with thermal CVD started, and nitrogen was continuously doped inside KF1500 accompanied by plugging the pore structure with carbonization of acetonitrile. Since the resultant KF1500 must have contained more than 4% nitrogen but very small specific surface area around 10 m^2/g , post-heat treatment at 950°C and steam activation at 800°C were carried out to raise the N-Q content by converting N-6 in doped nitrogen to N-Q [51] and increase specific surface area [54], respectively. Figure 18 shows nitrate adsorption onto modified KF1500 ACFs compared with those derived from phenol resin referred to as PhR (Kynol, Gun Ei Chemical Industry Co., Ltd.) [53]. The pristine material of KF1500 adsorbs nitrate by 0.36 mmol/g, and it contains 0.33% of quaternary nitrogen (N-Q) because some nitrogen compounds were mixed with rayon resin in the process of manufacturing KF1500. The further steam activation of KF1500 at 800°C (KF-8ST30) in our laboratory resulted in the increase in adsorption amount of nitrate from 0.36 to 0.55 mmol/g by expanding specific surface area from 1,560 to 1960 m^2/g , but no

Fig. 18 Adsorption amount of nitrate on ACFs derived from phenol resin (PhR) and ACFs modified of KF1500 (KF) and corresponding quaternary nitrogen content (N-Q, filled diamond) in ACFs. 8ST10; steam activation at 800°C by charging 10 mL water, 9.5HT30; heat treated at 950°C for 30 min, 8AN20; thermal CVD at 800°C by charging 20 mL of acetonitrile. Initial nitrate concentration of 200 $mg-NO_3^-/L$, equilibrium solution pH (pH_e) 3.0 [53]



N-Q was detected. Thereby the increase in nitrate adsorption is attributed to not N-Q content but $C\pi$ sites increased by enlarging graphene sheets exposed. While just heat treatment of KF1500 (KF-9.5HT30) makes the adsorption amount increase up to 0.52 mmol/g, only nitrogen doping with acetonitrile into KF1500 (KF-8AN20) could not improve nitrate adsorption even though N-Q content is increased as great as 1.95%. This is caused by plugging of pore during nitrogen doping with acetonitrile at 800°C supported by the fact that only 10 m²/g of specific surface area could be measured for KF-8AN20. Then several combinations of steam activation at 800°C (8ST), nitrogen doping with acetonitrile at 800°C (8AN), and heat treatment to form N-Q at 950°C (9.5HT) were attempted, and the order of steam activation, nitrogen doping, heat treatment, and steam activation again (KF-8ST10-8AN20-9.5HT30-8ST30) was found to be the optimum for nitrate adsorption of 0.74 mmol/g among all combinations examined in the study. At the same time N-Q content is 1.86% next to 1.95% of KF-8AN20, although specific surface area is a little declined from 1,540 m²/g (KF1500) to 1,360 m²/g (KF-8ST10-8AN20-9.5HT30-8ST30). On the other hand, for phenol resins (PhRs) similar treatments without nitrogen doping (PhR-8ST10-9.5HT30-8ST30) were conducted, and no N-Q was detected and adsorption amount of nitrate attained 0.49 mmol/g. Similar treatments also applied to KF1500 (KF-8ST10-9.5HT30-8ST30) and similar results with PhR were obtained for nitrate uptake. The above results imply that nitrogen doping at 800°C followed by heat treatment at 950°C and finally steam activation may be one of the best procedures to maximize both specific surface area and N-Q contents exposed on ACF surface. Figure 19 represents XPS N1s signals of pristine KF1500 and nitrogen-doped KF1500 (KF-8ST10-8AN20-95HT30-8ST30) [53]. When trimethylammonium (quaternary amino groups, a kind of N-Q)-functionalized ion-exchange resin was used for nitrate adsorption, adsorption amount of nitrate was constant for a wide range of equilibrium solution pH as shown in Fig. 20 [55]

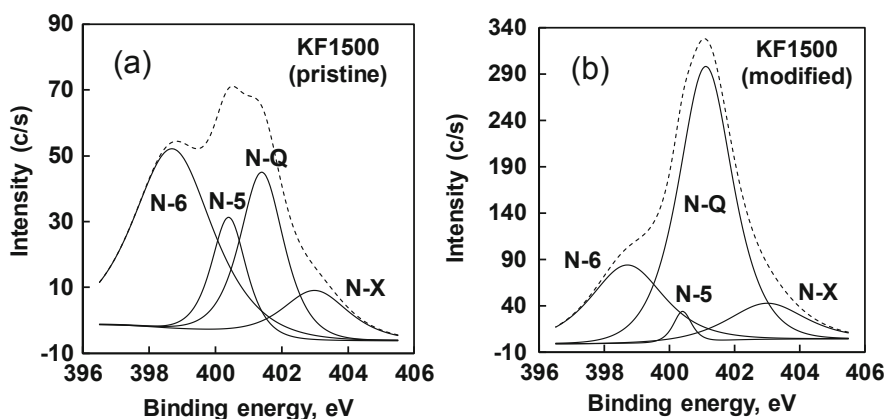


Fig. 19 XPS N1s spectra and deconvolution results of KF1500 (pristine (a) and modified (b)). Modified conditions; steam activation at 800°C by 10 mL water, nitrogen thermal CVD doping at 800°C with 20 mL acetonitrile solvent, heat treatment at 950°C in inert gas for 30 min, and steam activation at 800°C by 30 mL water again (KF-8ST10-8AN20-95HT30-8ST30) [53]

Fig. 20 Influence of equilibrium solution pH (pH_e) on nitrate adsorption onto trimethylammonium (quaternary amino groups)-functionalized ion exchange resin (HP555). Initial nitrate concentration of 200 mg- NO_3^-/L [55]

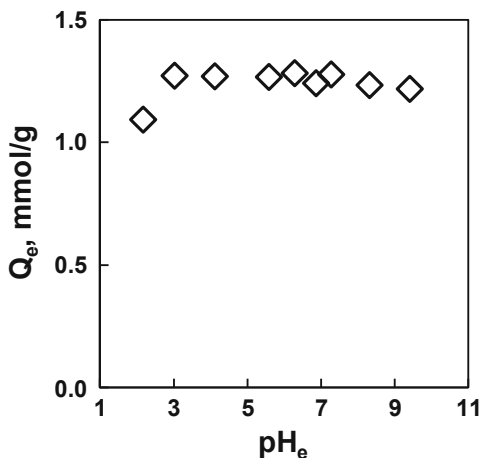
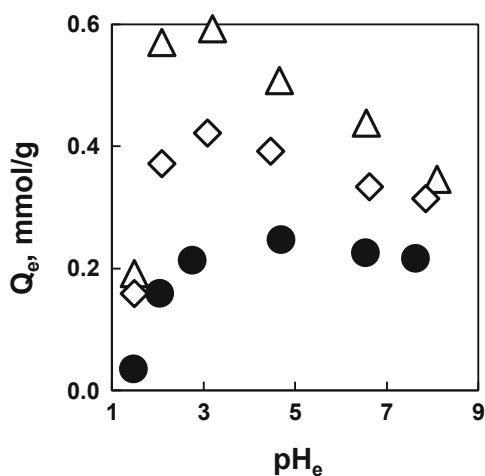


Fig. 21 Influence of equilibrium solution pH (pH_e) on nitrate adsorption onto modified KF1500 (KF-8ST10-8AN20-9.5HT30-8ST10). Initial nitrate concentration of 200 mg- NO_3^-/L (open triangle), 100 mg/L (open diamond), and 40 mg/L (filled circle) at ambient temperature [56]



indicating that N-Q could adsorb nitrate independent on solution pH due to positively charged nitrogen of N-Q ($\text{R-N}^+(\text{CH}_3)_3\text{Cl}^-$) which strongly attracted nitrate anion. N-Q composition and content of the nitrogen-doped KF1500 compared with N-6 are much greater than the pristine KF1500. Based on the results, specific surface area and N-Q content are estimated to play an important role for the nitrate adsorption. To inspect the hypothesis, influence of solution pH on the adsorption of nitrate onto the nitrogen-doped KF1500 was inspected using various initial concentrations of nitrate as displayed in Fig. 21 [56]. In the figure, the number of variations of initial concentrations of nitrate was limited to 3, but we can explain the adsorption sites of the nitrogen-doped KF1500. As long as we understand considering our previous study, $\text{C}\pi$ sites are strongly influenced by solution pH; when solution pH is adjusted with HCl and NaOH, in acidic region protons (H^+) are concentrated on $\text{C}\pi$ sites, and the positively charged graphene attracts nitrate anion, but much amount of Cl^- anion

(strong HCl acid) hinders the approach of nitrate (NO_3^-) onto the positive surface charge with competitive adsorption between Cl^- and NO_3^- . In NaOH basic region, OH^- is competitive with NO_3^- , and graphene layer itself becomes negative charge causing the decline of nitrate adsorption. As can be seen in Fig. 21, equilibrium adsorption amount of nitrate (Q_e) exhibits the maximum value (0.59 mmol/g) at pH 3 and gradually decreased toward 0.3 mmol/g at pH 5 to 8 in case of the initial nitrate concentration of 200 mg/L. Similar tendency was observed for the initial nitrate concentration of 100 mg/L, but nearly constant amounts could be seen for 40 mg/L. The results reveal that there are strong adsorption sites that can be always positively charged in changing solution pH and weak adsorption sites that are easily influenced by solution pH; the former should be N-Q sites, and the latter can be $\text{C}\pi$ sites. When the total adsorption amount is about 0.6 mmol/g, a part of it can be attributed to $\text{C}\pi$ sites (0.3 mmol/g); the other part will be come from N-Q sites (0.3 mmol/g).

Polyacrylonitrile (PAN) fiber is one of the promising materials to prepare nitrogen-containing adsorbents because it contains 20% nitrogen in the PAN structure at the flame-resistant forms [57]. White colored polymer of polyacrylonitrile (PAN) resin is at first carefully treated in air to stabilize the PAN resin [58–60]; otherwise, PAN fiber will be easily turned to carbon cake without remaining fiber morphology in the post-activation process at 500°C or more. In the first stage, we prepared the flame-resistant PAN fiber to optimize air treatment conditions [60], but commercially available black colored insolubilized PAN fiber, namely, PYROMEX was purchased from Teijin Co., Ltd. (former Toho Tenax Co., Ltd.), to accelerate the examination of post-activation treatments. Since PYROMEX fiber is supplied as a felt shaped material, we can easily handle PYROMEX for the various treatments. At first, PYROMEX (hereafter designated as PYR) was activated with steam at 800°C to improve the porous structure. Three grams of PYR were placed in a quartz tube and heated up to 800°C, and then 20 mL pure water was charged into quartz tube to develop porous structure in PYR with super-heated steam (PYR-8ST20). PYR-8ST20 was further treated at 950°C in inert gas to convert N-6 to N-Q species [51]. For the comparison, cellulose-based KF1500 was heat-treated at 950°C as well. Figure 22 displays the SEM images of the materials revealing that original morphology can be maintained after the steam and heat treatments. In Table 3 were shown properties of the prepared samples [57]. Specific surface area of PYR went up from 9 m²/g to 790 m²/g (PYR-8ST20) by the steam activation, whereas nitrogen content significantly declined from 20.9% to 5.6%. Post-treatment of PYR-8ST20 at 950°C for 30 min (PYR-8ST20-9.5HT30) resulted in the decline of specific surface area and nitrogen and oxygen content. N-Q content was also decreased from 0.56% to 0.51%, but adsorption amount of nitrate went up from 0.47 mmol/g (PYR-8ST20) to 0.64 mmol/g (PYR-8ST20-9.5HT30) [57]. The increase in adsorption amount of nitrate can be attributed to not only N-Q content but also lower oxygen content, because oxygen including acidic functional groups on carbon surface can inhibit nitrate adsorption [57]. KF1500-9.5HT30 was used as a reference material because heat treatment at 950°C could reduce acidic oxygen functional groups. Resultant oxygen content was 10.6% close to the value of PYR-8ST20-9.5HT30 (9.3%), and it has twice larger specific surface area but less N-Q content than PYR-8ST20-

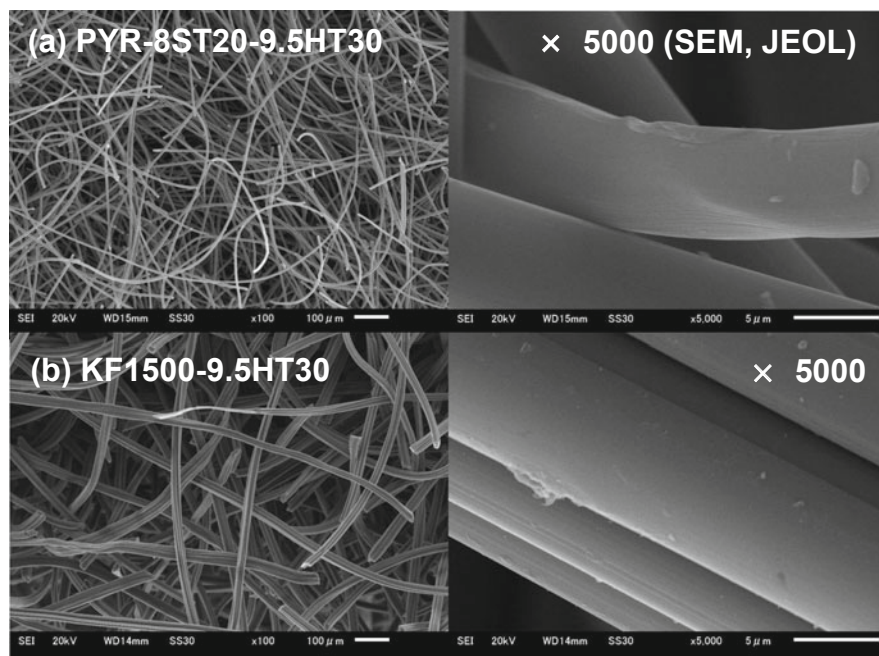


Fig. 22 SEM image of PAN-based ACF (a) (upper pictures, PYR-8ST20-9.5HT30) and cellulose-based ACF (b) (lower pictures, KF1500-9.5HT30) as a reference material using scanning electron microscope (JEOL JSM-6510) [57]

9.5HT30. Figure 23 shows the adsorption of nitrate as a function of equilibrium solution pH (pH_e) at the initial nitrate concentration of 50 mg/L (a) and 200 mg/L (b) [57]. PYR-8ST20-9.5HT30 is always better than KF1500-9.5HT30 at any condition; however, maximum points can be observed at the initial nitrate concentration of 50 mg/L for the both adsorbents, but not at 200 mg/L. In the lower nitrate concentration, adsorption amount is easily influenced by co-existing anions as chloride (Cl^-) and hydroxide (OH^-) in acidic and basic regions, respectively. Furthermore, decreasing slopes toward neutral region are more pronounced for PYR-8ST20-9.5HT30 than KF1500-9.5HT30 indicating that pH-insensitive N-Q sites are dominant for PYR-8ST20-9.5HT30, whereas pH-sensitive $\text{C}\pi$ sites are predominant for KF1500-9.5HT30 as well.

Other than nitrate, anionic contaminant of phosphate can be removed with the PYR adsorbents. In our experiences, adsorbents suitable to nitrate cannot be directly applied to the capture of phosphate, although phosphate is also present in aqueous phase as negatively charged anions in a wide range of solution pH above 2 (non-ionic H_3PO_4 species at solution pH less than 2). In case of PAN ACF (PYROMEX), activation with K_2CO_3 may be the best procedure for the preparation of adsorbent to remove phosphate. The original fiber morphology is not changed even though the chemical activation with K_2CO_3 is employed. When other chemicals such as ZnCl_2 , H_3PO_4 , and KOH were used for activation, fiber morphology was broken from the pristine PYROMEX status. The K_2CO_3 activation was conducted at 800°C in the

Table 3 Properties of PAN-based and cellulose-based activated carbon fibers (ACFs) activated by steam and annealed [57]

Sample name	Textural and surface properties				Elemental composition				Nitrogen configuration				
	S_{BET} , m^2/g	Pore volume (V_{total}), cm^3/g	Micropore volume (V_{micro}), cm^3/g	Mesopore volume (V_{meso}), cm^3/g	pH_{pzc}	Carbon, %	Hydrogen, %	Nitrogen, %	Oxygen, %	Pyridine (N-6), %	Pyrrole (N-5), %	Quaternary (N-Q), %	Pyridine- N-oxide, etc. (N-X), %
PYROMEX	9	0.004	0.003	0.001	-	59.6	3.6	20.9	15.9	-	-	-	-
PYR-8ST20	790	0.34	0.33	0.01	-	73.0	0.8	5.6	20.6	2.60	0.86	0.56	1.58
PYR-8ST20- 9.5HT30	710	0.32	0.32	0.005	5.3	86.7	0.5	3.6	9.3	0.92	0.36	0.51	1.78
KFI500- 9.5HT30	1,530	0.68	0.66	0.03	5.4	87.4	0.3	1.7	10.6	0.65	0.25	0.28	0.51

^aCalculated by difference

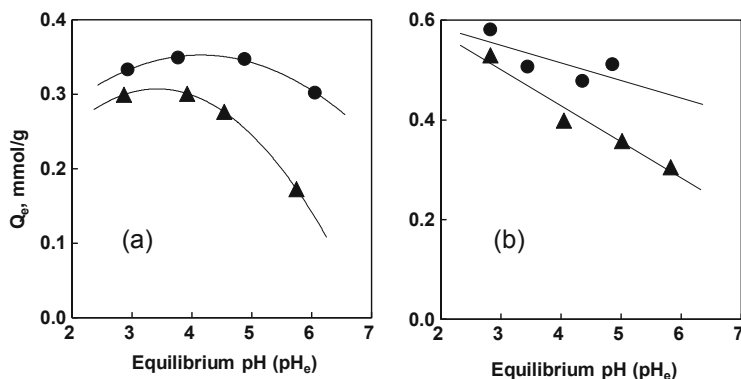


Fig. 23 Influence of equilibrium solution pH (pH_e) on the amount of nitrate adsorption onto PYR-8ST20-9.5HT30 (filled circle) and KF1500-9.5HT30 (filled triangle) at the initial nitrate concentrations of 50 mg- NO_3^- /L (a) and 200 mg- NO_3^- /L (b). Adsorption conditions; 30 mg adsorbent dosage into 15 mL nitrate solution [57]

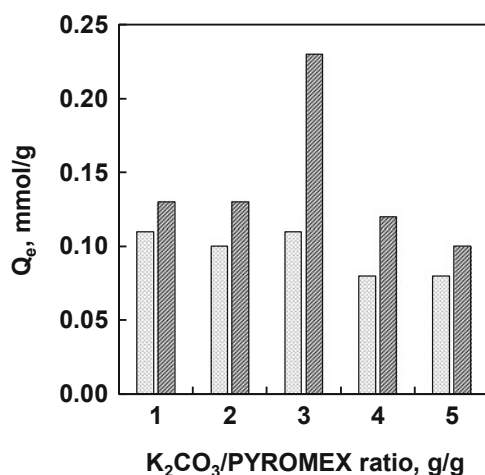


Fig. 24 Equilibrium adsorption amount of phosphate (Q_e) on PYR-KC1 (or 2, 3, 4, 5) (light bar) and PYR-KC1 (or 2, 3, 4, 5)-9.5HT30 (dark bar). Initial KH_2PO_4 concentration; 3 mmol/L, adsorbent dosage; 2 g/L [61]

impregnation ratio of K_2CO_3 /PYROMEX ranging 1–5 by step 1, referred to as PYR-KC3 in case of the impregnation ratio of 3. Post-heat treatment at 950°C for 30 min was carried out for PYR-KC1 (and 2, 3, 4, 5) to obtain PYR-KC1 (and 2, 3, 4, 5)-9.5HT30 as well. Figure 24 displays the adsorption of phosphate on the ten prepared samples from PYROMEX [61]. All heat treatment samples captured greater amount of phosphate than all corresponding samples before the heat treatment. In the PYR-KC-9.5HT30 series, PYR-KC3-9.5HT30 exhibited exceptionally better adsorption performance than the other PYR-KC-9.5HT30 series. Table 4

Table 4 Textural, bulk and surface properties of ACFs derived from PYROMEX using K_2CO_3 activation and annealing [61]

Sample from PYROMEX	Textural analysis		Elemental analysis, wt%				XPS analysis, wt%			
	S_{BET} , m^2/g	V_{total} , cm^3/g	Carbon	Hydrogen	Nitrogen	Oxygen ^a	N-6	N-5	N-Q	N-X
PYR-KC1	2,040	0.998	74.8	0.5	6.7	18.0	-	-	-	-
PYR-KC3	1,720	0.807	89.4	<0.1	0.9	9.6	0.14	0.49	0.33	0.11
PYR-KC5	1,800	0.675	89.1	<0.1	0.6	10.2	-	-	-	-
PYR-KC1-9.5HT30	870	0.411	87.9	<0.1	1.3	10.7	0.19	0.19	0.50	0.30
PYR-KC3-9.5HT30	1,280	0.559	90.0	<0.1	1.2	8.7	0.30	0.40	0.46	0.19
PYR-KC5-9.5HT30	1,940	0.911	85.6	<0.1	0.5	13.8	0.05	0.24	0.25	0.20

^aCalculated by difference

shows textural and surface properties of the ten samples prepared from PYROMEX using K_2CO_3 activation [61]. For PYR-KC series, lower N-Q and higher oxygen content (oxygen functional groups) might reduce the adsorption amounts of phosphate compared to PYR-KC-9.5HT30 series. After the heat treatment, oxygen-containing functional groups must have been removed, and N-Q content was increased. PYR-KC3-9.5HT30 is better than PYR-KC1-9.5HT30 because pore structure has not been sufficiently developed although N-Q in PYR-KC1-9.5HT30 (0.50 wt%) is slightly larger than PYR-KC3-9.5HT30 (0.46 wt%); effective adsorption sites of N-Q might not be exposed to phosphate anion due to lower specific surface area. On the other hand, even though PYR-KC5-9.5HT30 has larger specific surface area than PYR-KC3-9.5HT30, adsorption amount of phosphate of the latter is greater than the former. This is caused by significant decrease in N-Q content of PYR-KC5-9.5HT30 (0.25 wt%) compared with PYR-KC3-9.5HT30 (N-Q, 0.46 wt%). Consequently PYR-KC3-9.5HT30 is the optimum adsorbent for phosphate removal under the balance of N-Q and oxygen content and specific surface area including the extent of exposure of N-Q on the carbon surface.

Nitrogen-doped ACs and ACFs can be derived from numerous materials and procedures; thereby, we believe that there are still much room to develop more excellent materials to capture anionic contaminants such as bean dregs (by-product in the production of bean cake that is “TOFU” in Japanese) that contains nitrogen by 4.6 wt% in dry base [62] and bamboo activated with $ZnCl_2$ followed by ammonia (NH_3) gas treatment at $950^\circ C$ [63]. Nitrogen doping with thermal CVD treatment of ACF by aniline in place of acetonitrile was effective for arsenic ($As(V)$; $HAsO_4^{2-}$, AsO_4^{3-}) adsorption as well [64, 65]. Hexavalent chromium ($Cr(VI)$) is dissolved in aqueous phase as anions such as $Cr_2O_7^{2-}$, CrO_4^{2-} , and $HCrO_4^-$ [66]. These $Cr(VI)$ species can be captured with above N-doped materials [62, 63].

4 Conclusion

Modification of activated carbon is effective for improving adsorption affinity and capacity of organic and inorganic pollutants in water. Small and large molecules, e.g., mono-aromatics and tannic acids, respectively, are included as organic molecules. Heavy metals of cations (Cd^{2+} , Pb^{2+} , Ni^{2+} , etc.) and anions (NO_3^- , $H_2PO_4^-$, $HAsO_4^{2-}$, $Cr_2O_7^{2-}$, etc.) are involved in inorganic pollutants. For adsorptive removal of organic contaminants, high specific surface area sometimes with meso- and macropore and less oxygen content are preferable for ACs and ACFs. To capture cationic heavy metals, carboxy, sulfonic, and thiol groups ACs and ACFs are effective on, although only sulfonic function has not been sufficiently formed yet on carbon surface. For the adsorptive removal of anionic contaminants, nitrogen functional groups such as quaternary nitrogen (N-Q) and alkyl amine and less oxygen groups may be essential to effective uptake of anions. N-Q functional ACs and ACFs are now under development, but binding alkyl amine onto carbon surface has still been challenging subject.

Acknowledgments This review study was supported in part Grants-in-Aid for Scientific Research (C) from the Japan Society for the Promotion of Science (KAKENHI Grant No. JP20K05187). Prof. Dr. Fumio Imazeki, the head of Safety and Health Organization, Chiba University, is sincerely acknowledged for his encouragement and the financial support of our study. Gratitude is greatly extended to Ms. Shizuka Ishibashi, Safety and Health Organization, Chiba University, for her dedicated support in preparing the review manuscripts.

References

1. Konstantinou IK, Hela DG, Albanis TA (2006) The status of pesticide pollution in surface waters (rivers and lakes) of Greece. Part I. review on occurrence and levels. *Environ Pollut* 141 (3):555–570. <https://doi.org/10.1016/j.envpol.2005.07.024>
2. Jones OAH, Voulvoulis N, Lester JN (2004) Potential ecological and human health risks associated with the presence of pharmaceutically active compounds in the aquatic environment. *Crit Rev Toxicol* 34(4):335–350. <https://doi.org/10.1080/10408440490464697>
3. Kleywegt S, Pileggi V, Yang P, Hao C, Zhao X, Rocks C, Thach S, Cheung P, Whitehead B (2011) Pharmaceuticals, hormones and bisphenol A in untreated source and finished drinking water in Ontario, Canada — occurrence and treatment efficiency. *Sci Total Environ* 409 (8):1481–1488. <https://doi.org/10.1016/j.scitotenv.2011.01.010>
4. Pan K, Wang W-X (2012) Trace metal contamination in estuarine and coastal environments in China. *Sci Total Environ* 421-422:3–16. <https://doi.org/10.1016/j.scitotenv.2011.03.013>
5. Wang S-L, Xu X-R, Sun Y-X, Liu J-L, Li H-B (2013) Heavy metal pollution in coastal areas of South China: a review. *Mar Pollut Bull* 76(1–2):7–15. <https://doi.org/10.1016/j.marpolbul.2013.08.025>
6. Li Z, Ma Z, van der Kuijp TJ, Yuan Z, Huang L (2014) A review of soil heavy metal pollution from mines in China: pollution and health risk assessment. *Sci Total Environ* 468-469:843–853. <https://doi.org/10.1016/j.scitotenv.2013.08.090>
7. Yang Q, Li Z, Lu X, Duan Q, Huang L, Bi J (2018) A review of soil heavy metal pollution from industrial and agricultural regions in China: pollution and risk assessment. *Sci Total Environ* 642:690–700. <https://doi.org/10.1016/j.scitotenv.2018.06.068>
8. Wei B, Yang L (2010) A review of heavy metal contaminations in urban soils, urban road dusts and agricultural soils from China. *Microchem J* 94(2):99–107. <https://doi.org/10.1016/j.microc.2009.09.014>
9. Qin B, Zhou J, Elser JJ, Gardner WS, Deng J, Brookes JD (2020) Water depth underpins the relative roles and fates of nitrogen and phosphorus in lakes. *Environ Sci Technol* 54:3191–3198. <https://doi.org/10.1021/acs.est.9b05858>
10. Kraal P, Burton ED, Rose AL, Cheetham MD, Bush RT, Sullivan LA (2013) Decoupling between water column oxygenation and benthic phosphate dynamics in a shallow eutrophic estuary. *Environ Sci Technol* 47(7):3114–3121. <https://doi.org/10.1021/es304868t>
11. Sprague LA, Hirsch RM, Aulenbach BT (2011) Nitrate in the Mississippi river and its tributaries, 1980 to 2008: are we making progress? *Environ Sci Technol* 45(17):7209–7216. <https://doi.org/10.1021/es201221s>
12. Burow KR, Nolan BT, Rupert MG, Dubrovsky NM (2010) Nitrate in groundwater of the United States, 1991-2003. *Environ Sci Technol* 44(13):4988–4997. <https://doi.org/10.1021/es100546y>
13. Leone A, Ripa MN, Uricchio V, Deák J, Vargay Z (2009) Vulnerability and risk evaluation of agricultural nitrogen pollution for Hungary's main aquifer using DRASTIC and GLEAMS models. *J Environ Manag* 90(10):2969–2978. <https://doi.org/10.1016/j.jenvman.2007.08.009>
14. Liu GD, Wu WL, Zhang J (2005) Regional differentiation of non-point source pollution of agriculture-derived nitrate nitrogen in groundwater in northern China. *Agric Ecosyst Environ* 107(2–3):211–220. <https://doi.org/10.1016/j.agee.2004.11.010>

15. Wang J, Guo X (2020) Adsorption kinetic models: Physical meanings, applications, and solving methods. *J Hazard Mater* 390:122156. <https://doi.org/10.1016/j.jhazmat.2020.122156>
16. Hubbe MA, Azizian S, Douven S (2019) Implications of apparent pseudo-second-order adsorption kinetics onto cellulosic materials: a review. *Bio Res* 14(3):7582–7626
17. Fan S, Wang Y, Wang Z, Ji T, Tang J, Li X (2017) Removal of methylene blue from aqueous solution by sewage sludge-derived biochar: adsorption kinetics, equilibrium, thermodynamics and mechanism. *J Environ Chem Eng* 5:601–611. <https://doi.org/10.1016/j.jece.2016.12.019>
18. Wu F-C, Tseng R-L, Juang R-S (2001) Kinetic modeling of liquid-phase adsorption of reactive dyes and metal ions on chitosan. *Water Res* 35(3):613–618. [https://doi.org/10.1016/S0043-1354\(00\)00307-9](https://doi.org/10.1016/S0043-1354(00)00307-9)
19. Bhattacharyya KG, Sharma A (2005) Kinetics and thermodynamics of Methylene Blue adsorption on Neem (*Azadirachta indica*) leaf powder. *Dyes Pigments* 65:51–59. <https://doi.org/10.1016/j.dyepig.2004.06.016>
20. Oishi S, Amano Y, Aikawa M, Machida M (2011) Adsorption of Pb(II) ion on mesoporous activated carbon prepared by ZnCl₂ activation. *TANSO* 2011(250):231–237. <https://doi.org/10.7209/tanso.2011.231>
21. Goto T, Amano Y, Machida M, Imazeki F (2015) Effect of polarity of activated carbon surface, solvent and Adsorbate on adsorption of aromatic compounds from liquid phase. *Chem Pharm Bull* 63(9):726–730. <https://doi.org/10.1248/cpb.c15-00039>
22. Ramis G, Busca G, Lorenzelli V (1993) Determination of the geometry of adsorbed unsaturated molecules through the analysis of the CH out-of-plane deformation modes. *J Electron Spectrosc Relat Phenom* 64–65:297–305. [https://doi.org/10.1016/0368-2048\(93\)80091-Y](https://doi.org/10.1016/0368-2048(93)80091-Y)
23. Chen L, Tanner EEL, Richard G, Compton RG (2017) Adsorption on graphene: flat to edge to end transitions of phenyl hydroquinone. Adsorption on graphene: flat to edge to end transitions of phenyl hydroquinone. *Phys Chem Chem Phys* 19:17521–17525. <https://doi.org/10.1039/c7cp03261g>
24. Sakazaki T, Oishi S, Amano Y, Machida M (2011) Adsorption properties of large molecule on activated carbons prepared from Urame oak and coconut shell char. *Kagaku Kogaku Ronbunshu* 37(5):381–387. <https://doi.org/10.1252/kakoronbunshu.37.381>
25. Tamon H, Okazaki M (1996) Desorption characteristics of aromatic compounds in aqueous solution on solid adsorbents. *J Colloid Interface Sci* 179(1):181–187. <https://doi.org/10.1006/jcis.1996.0200>
26. Machida M, Amano Y, Imazeki F (2015) Water purification with activated carbons (ACs): a short review - influence of the textural and surface properties of ACs on the adsorptive removal of pollutants. *Carbon* 2015(270):241–249. <https://doi.org/10.7209/tanso.2015.241>
27. Harris PJF, Tsang SC (1997) High-resolution electron microscopy studies of non-graphitizing carbons. *Philos Mag A* 76(3):667–677. <https://doi.org/10.1080/01418619708214028>
28. Huang J-JS, Lin S-C, Lowemark L, Liou SYH, Chang Q, Chang T-K, Wei K-Y, Croudace IW (2019) Rapid assessment of heavy metal pollution using ion-exchange resin sachets and micro-XRF core-scanning. *Sci Rep* 9(1):1–6. <https://doi.org/10.1038/s41598-019-43015-x>
29. Ming Hua M, Shujuan Zhang S, Bingcai Pan B, Weiming Zhang W, Lu Lv L, Quanxing Zhang Q (2012) Heavy metal removal from water/wastewater by nanosized metal oxides: a review. *J Hazard Mater* 211–212:317–331. <https://doi.org/10.1016/j.jhazmat.2011.10.016>
30. Machida M, Amano Y (2020) Development of carbonaceous porous adsorbents to remove ionic pollutants from aqueous solution. *Shokubai* 62(3):190–196. <https://cats.jp/jnl/pageview?articlecd=62030010000>
31. Moreno-Castilla C, Ferro-Garcia MA, Joly JP, Bautista-Toledo I, Carrasco-Marin F, Rivera-Utrilla J (1995) Activated carbon surface modifications by nitric acid, hydrogen peroxide, and ammonium peroxydisulfate treatments. *Langmuir* 11:4386–4392. <https://doi.org/10.1021/la00011a035>
32. Nemoto Y, Iitsuka Y, Watanabe K, Amano Y, Machida M (2016) Adsorptive removal of Ni (II) from water using oxidized activated carbon derived from sulfur containing petroleum coke. *Kagaku Kogaku Ronbunshu* 42(4):142–147. <https://doi.org/10.1252/kakoronbunshu.42.142>

33. Sato K, Izza A, Watanabe K, Hagiwara K, Kato M, Amano Y, Machida M (2019) Preparation of sulfur-contained activated carbon from petroleum coke. *J Jpn Pet Inst* 62(5):205–210. <https://doi.org/10.1627/jpi.62.205>
34. Kim D, Jung YW, Kwon S, Park J-W (2011) Adsorption of cadmium(II) from aqueous solutions by thiol-functionalized activated carbon. *Water Sci Technol Water Supply* 11(1):61–66. <https://doi.org/10.2166/ws.2011.009>
35. Machida M, Fotoohi B, Amano Y, Mercier L (2012) Cadmium(II) and lead(II) adsorption onto hetero-atom functional mesoporous silica and activated carbon. *Appl Surf Sci* 258:7389–7394. <https://doi.org/10.1016/j.apsusc.2012.04.042>
36. Sato S, Yoshihara K, Moriyama K, Machida M, Tatsumoto H (2007) Influence of activated carbon surface acidity on adsorption of heavy metal ions and aromatics from aqueous solution. *Appl Surf Sci* 253:8554–8559. <https://doi.org/10.1016/j.apsusc.2007.04.025>
37. Machida M, Mochimaru T, Tatsumoto H (2006) Lead(II) adsorption onto the graphene layer of carbonaceous materials in aqueous solution. *Carbon* 44(13):2681–2688. <https://doi.org/10.1016/j.carbon.2006.04.003>
38. Machida M, Chensun S, Amano Y, Imazeki F (2015) Adsorptive removal of Pb(II) ions from aqueous solution by $(\text{NH}_4)_2\text{S}_2\text{O}_8$ oxidized activated carbon. *Bull Chem Soc Jpn* 88:127–132. <https://doi.org/10.1246/bcsj.20140124>
39. Mena Aguilar KM, Amano Y, Machida M (2016) Ammonium persulfate oxidized activated carbon fiber as a high capacity adsorbent for aqueous Pb(II). *J Environ Chem Eng* 4:4644–4652. <https://doi.org/10.1016/j.jece.2016.10.028>
40. Li N, Ma X, Zha Q, Kim K, Chen Y, Song C (2011) Maximizing the number of oxygen-containing functional groups on activated carbon by using ammonium persulfate and improving the temperature-programmed desorption characterization of carbon surface chemistry. *Carbon* 49:5002–5013. <https://doi.org/10.1016/j.carbon.2011.07.015>
41. Weast RC (1994) *Handbook of chemistry and physics*. 75th edn. CRC Press, Boca Raton, pp D159–D161
42. Bitter JH, van Dommele S, de Jong KP (2010) On the virtue of acid-base titrations for the determination of basic sites in nitrogen doped carbon nanotubes. *Catal Today* 150:61–66. <https://doi.org/10.1016/j.cattod.2009.09.008>
43. Dioum A, Hamoudi S (2014) Mono- and quaternary-ammonium functionalized mesoporous silica materials for nitrate adsorptive removal from water and wastewaters. *J Porous Mater* 21:685–690. <https://doi.org/10.1007/s10934-014-9815-6>
44. Ota K, Amano Y, Aikawa M, Machida M (2012) Removal of nitrate ions from water by activated carbons (ACs) - influence of surface chemistry of ACs and coexisting chloride and sulfate ions. *Appl Surf Sci* 276:838–842. <https://doi.org/10.1016/j.apsusc.2013.03.053>
45. Figueiredo JL, Pereira MFR, Freitas MMA, Órfão JJM (1999) Modification of the surface chemistry of activated carbons. *Carbon* 37(9):1379–1389. [https://doi.org/10.1016/S0008-6223\(98\)00333-9](https://doi.org/10.1016/S0008-6223(98)00333-9)
46. Iida T, Amano Y, Aikawa M, Machida M (2013) The effect of the surface property of activated carbon on nitrate adsorption. *Kankyo Kagaku* 23(2):91–94. <https://doi.org/10.5985/jec.23.91>
47. Machida M, Fotoohi B, Amano Y, Mercier L (2012) Cadmium(II) and lead(II) adsorption onto hetero-atom functional mesoporous silica and activated carbon. *Appl Surf Sci* 258:7389–7394. <https://doi.org/10.1016/j.apsusc.2012.04.042>
48. Machida M, Fotoohi B, Amano Y, Ohba T, Kanoh H, Mercier L (2012) Cadmium (II) adsorption using functional mesoporous silica and activated carbon. *J Hazard Mater* 221-222:220–227. <https://doi.org/10.1016/j.jhazmat.2012.04.039>
49. Byrne TM, Gu X, Hou P, Cannon FS, Brown NR, Nieto-Delgado C (2014) Quaternary nitrogen activated carbons for removal of perchlorate with electrochemical regeneration. *Carbon* 73:1–12. <https://doi.org/10.1016/j.carbon.2014.02.020>
50. Machida M, Goto T, Amano Y, Iida T (2016) Adsorptive removal of nitrate from aqueous solution using nitrogen doped activated carbon. *Chem Pharm Bull* 64:1555–1559. <https://doi.org/10.1248/cpb.c16-00368>

51. Pels JR, Kapteijn F, Moulijn JA, Zhu Q, Thomas KM (1995) Evolution of nitrogen functionalities in carbonaceous materials during pyrolysis. *Carbon* 33(11):1641–1653. [https://doi.org/10.1016/0008-6223\(95\)00154-6](https://doi.org/10.1016/0008-6223(95)00154-6)
52. Goto T, Amano Y, Machida M (2017) Surface modification of carbonized melamine sponge by methyl iodide for the efficient removal of nitrate ions. *Tanso* 2017(276):2–7. <https://doi.org/10.7209/tanso.2017.2>
53. Yuan J, Amano Y, Machida M (2019) Surface modified mechanism of activated carbon fibers by thermal chemical vapor deposition and nitrate adsorption characteristics in aqueous solution. *Colloids Surf A Physicochem Eng Asp* 580:123710. <https://doi.org/10.1016/j.colsurfa.2019.123710>
54. Machida M, Yoo P, Amano Y (2019) Adsorption of nitrate from aqueous phase onto nitrogen-doped activated carbon fibers (ACFs). *SN Appl Sci* 1(4):1–7. <https://doi.org/10.1007/s42452-019-0333-7>
55. Kino K, Sakamoto T, Yuan J, Amano Y (2020) Quaternary nitrogen functionalized carbonaceous adsorbents to remove nitrate from aqueous phase. *Catal Today*. <https://doi.org/10.1016/j.cattod.2020.06.036>
56. Yuan J, Amano Y, Machida M (2019) Study on the characteristics of nitrogen-doped activated carbon fibers to remove nitrate ions by multi-factor analysis. *Int J Environ Sci Technol* 17(5):2563–2570. <https://doi.org/10.1007/s13762-020-02663-7>
57. Machida M, Sakamoto T, Sato K, Goto T, Amano Y (2018) Adsorptive removal of nitrate from aqueous phase using steam activated and thermal treated polyacrylonitrile (PAN) fiber. *J Fiber Sci Technol* 74(7):158–164. <https://doi.org/10.2115/fiberst.2018-0023>
58. Surianarayanan M, Vijayaraghavan R, Raghavan KV (1998) Spectroscopic investigations of polyacrylonitrile thermal degradation. *J Polym Sci Part A Polym Chem* 36(14):2503–2512. [https://doi.org/10.1002/\(SICI\)1099518\(199810\)36:14<2503::AID-POLA9>3.0.CO;2-T](https://doi.org/10.1002/(SICI)1099518(199810)36:14<2503::AID-POLA9>3.0.CO;2-T)
59. Dalton S, Heatley F, Budd PM (1999) Thermal stabilization of polyacrylonitrile fibers. *Polymer* 40(20):5531–5543. [https://doi.org/10.1016/S0032-3861\(98\)00778-2](https://doi.org/10.1016/S0032-3861(98)00778-2)
60. Zaini MAA, Amano Y, Machida M (2010) Adsorption of heavy metals onto activated carbons derived from polyacrylonitrile fiber. *J Hazard Mater* 180(1–3):552–560. <https://doi.org/10.1016/j.jhazmat.2010.04.069>
61. Sakamoto T, Amano Y, Machida M (2020) Phosphate ion adsorption properties of PAN-based activated carbon fibers prepared with K_2CO_3 activation. *SN Appl Sci* 2(4):702–709. <https://doi.org/10.1007/s42452-020-2465-1>
62. Chu B, Amano Y, Machida M (2020) Preparation of bean dreg derived N-doped activated carbon with high adsorption for Cr(VI). *Colloids Surf A Physicochem Eng Asp* 586:124262. <https://doi.org/10.1016/j.colsurfa.2019.124262>
63. Chu B, Terao K, Amano Y, Machida M (2020) Adsorption behavior of Cr(VI) by N-doped biochar derived from bamboo. *Water Pract Technol* 15(1):170–181. <https://doi.org/10.2166/wpt.2020.008>
64. Yoo P, Amano Y, Machida M (2020) Investigating the effective carbon material for thermal chemical vapor deposition using aniline to enhance as(V) adsorption capacity of activated carbon. *SN Appl Sci* 2:1179. <https://doi.org/10.1007/s42452-020-2974-y>
65. Yoo P, Amano Y, Machida M (2020) Effective preparation of nitrogen-doped activated carbon by aniline thermal chemical vapor deposition for arsenate adsorption. *Environ Eng Res* 25(5):707–713. <https://doi.org/10.4491/eer.2019.217>
66. Peng Z, Xiong C, Wang W, Tan F, Xu Y, Wang X, Qiao X (2017) Facile modification of nanoscale zero-valent iron with high stability for Cr (VI) remediation. *Sci Total Environ* 596:266–273. <https://doi.org/10.1016/j.scitotenv.2017.04.121>

Pyrolysis to Produce Hydrochar and Biochar Carbon Material for Carbon Removal and Sustainable Environmental Technology



Kim Yrjälä, Muthusamy Ramakrishnan, Huabao Zheng,
and Eglantina Lopez-Echartea

Contents

1	Introduction	368
2	Biowaste Streams for Thermal Treatment	370
2.1	Composition of Agroforestry Waste (AFWs)	370
2.2	Municipal Solid Waste	371
3	Hydrothermal Carbonization (HGT)	371
3.1	Feedstock Nature	372
4	Pyrolysis for Biochar Production	373
4.1	Slow Pyrolysis, Temperature Regulation	374
4.2	Pyrolysis Atmosphere	375

K. Yrjälä (✉)

State Key Laboratory of Subtropical Silviculture, Zhejiang A&F University, Hangzhou, Zhejiang, China

Department of Forest Sciences, University of Helsinki, Helsinki, Finland

e-mail: kim.yrjala@helsinki.fi

M. Ramakrishnan

Co-Innovation Center for Sustainable Forestry in Southern China, Nanjing Forestry University, Nanjing, Jiangsu, China

Bamboo Research Institute, Nanjing Forestry University, Nanjing, Jiangsu, China

e-mail: ramky@njfu.edu.cn

H. Zheng

Zhejiang Province Key Laboratory of Soil Contamination Bioremediation, Zhejiang A&F University, Hangzhou, Zhejiang, China

e-mail: zhenghuabao@zafu.edu.cn

E. Lopez-Echartea

Department of Biochemistry and Microbiology, University of Chemistry and Technology, Prague, Czech Republic

Shunitz Tanaka, Masaaki Kurasaki, Masaaki Morikawa, and Yuichi Kamiya (eds.),

Design of Materials and Technologies for Environmental Remediation,

Hdb Env Chem (2023) 115: 367–392, DOI 10.1007/698_2022_845,

© The Author(s), under exclusive license to Springer Nature Singapore Pte Ltd 2022,

Published online: 26 February 2022

4.3	Co-Pyrolysis of Biomass with Activator/Dopant	375
4.4	Activation by Chemical Agents	377
4.5	The Quality and Safety of the Produced Biochars	378
5	Biochar for the Remediation of Contaminated Soil and Water	379
5.1	Heavy Metals	379
5.2	Phytoremediation and Related Microbes	380
5.3	Organic Pollutants	381
6	Toward Circular Economy: Recycled Waste for Biochar Production	383
6.1	Novel Applications of Biochar	383
7	Conclusion	385
	References	385

Abstract Natural resources are continuously depleted globally, and accelerated climate change is a consequence of irresponsible human action. Planetary resources have to be better utilized not to threaten living ecosystems, the biodiversity and cause further land degradation. New nature-based and cost-effective materials are appearing for remediation purposes but need continued development since they require extra knowledge about structure-function relations. Within emerging circular economy new waste streams are detected which can serve as substrate for new valuable and smart materials and at the same time provide energy and even carbon removal. Biomass has been generated from both agriculture and forestry but lately also municipal solid waste has been recognized as resource in waste valorization. Waste can be converted to new products by hydrothermal processes that yield hydrochar and thermal pyrolysis processes to produce biochar; a multiuse carbon material. Ideal waste utilization processes have good energy yield at the same time as new materials are formed. Carbon removal can become a part of environmental societal solutions dealing with sustainable waste processing and application of new value-added products coming from development of new smart materials. Carbon removal efforts are currently supported through the voluntary market and the total value of global carbon markets grew by over 20% in 2020 – the fourth consecutive year of record growth. This chapter displays different waste streams and their suitability for thermal treatments to produce hydrochar or biochar for understanding of how the choice of feedstock together with optimization of thermal process parameters will give best smart products.

Keywords Carbon removal, Chemical and physical activation, Municipal solid waste (MSW), Remediation, Waste streams

1 Introduction

The rise of standard of living globally is virtuous but it's always connected to increased consumption and demand for consumer goods followed by increased generation of municipal solid waste (MSW) [1]. Several competing technologies

are available for treating this waste and their sustainability is becoming a prominent factor. In addition to ecological and societal sustainability technologies need to be economically feasible to be applied on larger scale. One important quality criterion for waste treatment is suitability for energy and fuel production. In Europe the main renewable energy source is wood, which represents over 60% of all non-conventional energy used in the EU-27 [2]. Lignocellulosic woody biomass constitutes arborous forestry residues and residues from the wood processing industry. The activated sludge process produces solids that have mostly been considered as a waste without any good reuse and sewage sludge from biogas reactors has created challenges for reuse [3]. Sludge is, however, a suitable biomass for fuel production. The advantage with the hydrothermal process (HGT) is that the biomass does not need drying pretreatment and requires less energy. The yield of solid product, hydrochar, is greater in lower temperature pyrolysis (200–300°C) [4].

From the prospect of climate change, there is a great demand for swift and efficient methods to capture and sequester carbon away from the atmosphere. It was very recently reported that production, use and storage of biochar are carbon negative, and if applied into practice an estimated sequestration of 0.3–2 Gt CO₂ year⁻¹ by 2050 could be achieved [5]. The most relevant technologies offering carbon removal from atmosphere are forestation, direct air carbon capture with utilization and storage, carbon sequestration into soil, and wooden building elements for biochar production. The carbon fees on the voluntary carbon markets range from 12 to 1,045 European euro per ton CO₂ [5]. These carbon removal services by means of biochar are currently offered through full-bodied marketplaces that require wide-ranging certification, verification, and monitoring to add credibility and authenticity. Simultaneously biochar production is hopefully improving with increasing knowledge on feedstock usability, pyrolysis and in future more tailored applications to show that the biochar system is realistic to be applied at large scale [6].

Just as there are new usable waste streams, so are their potential uses that require more studies to become effective in environmental remediation, which is an actual field application of biochars [7]. Biochar production from lightly contaminated waste timber (WT) has been coined as a promising waste handling option for valorization of such residues into biochar sorbents that can be used for contaminant stabilization [8]. A challenge with wood waste is the presence of trace environmental pollutants that threaten the sustainable recycling of this waste. Impurities comprise adhesives, paints, trace metals fire retardants, waxes and plastics. Very recent studies have proposed thermochemical treatment of wood waste like gasification and pyrolysis that can give different new products, but also energy. Polycyclic aromatic hydrocarbons (PAHs), volatile organic compounds (VOCs), and trace metals are formed and/or emitted during thermochemical conversion. Their formation depends on both the operating conditions and the type of feedstock used. These pollutants may also appear in the resulting biochar [9, 10].

2 Biowaste Streams for Thermal Treatment

2.1 *Composition of Agroforestry Waste (AFWs)*

Timber logging generates large amounts of forestry waste residue. The global forests cover 4 billion ha, which is almost 30% of total land area, and on average 0.62 ha/capita [11]. Around 50% of this forest area is in developing countries [12]. The forest residue is typically stumps, branches, and leaves, and wood processing waste in form of logs and sawdust. The recovery of different residues depends on geography and related conditions, like type of tree species. For every cubic meter of logged material removed from the forest it has been estimated that a cubic meter of waste remains in the forest. The types of processing waste are bark removal and branch trimming (about 12% of this material arrives at mill facilities, slabs/blocks/further trimmings (about 34%) and sawdust constitutes about 12%. Waste comes also from kiln drying, shavings (about 6%), and sawdust/trimming (about 2%). On the scale woody biomass contributes around 4.6 Gt annually, from which 60% is used for energy, 20% is used as industrial “round wood,” and the remaining 20% is in the primary production pool remaining in the forest where it decays. A surprisingly large part, ~80% of forest tree mass is then lost as waste, and from that wood about 20% ends up in kiln-dried sawn product [13].

Agricultural biomass wastes and residues are mainly crop stalks, leaves, roots, fruit peels, and seed/nut shells. These residues are mainly discarded or burned although they are valuable supplies of feedstock material [13]. It imposes challenges to estimate the degree of produced crop biomass in relation to what is the “loss” in production, including harvesting and processing, and also in relation to what is considered as “waste” that again entails retail or consumer loss. The production of “food” seems to be measured as the edible parts of a crop (harvest index), which again is not taking into account non-edible biomass parts, that are crops or not. One example to stress this point is sugarcane that requires processing generating waste streams in addition to the primary biomass waste in harvesting.

Based on Food and Agricultural Organization [14] estimations, Russia, Indonesia, USA, Brazil, and China produce most AFWs and industrial wood wastes. The potential production of residues could be more than 700 Mt./p.a. This large loss is a resource that could be used as fuel source. Typically, in the developing countries they are main household fuel and major energy source as part of industrial energy consumption [15]. The composition of AFW greatly influences the performance of AFW conversion system. In developing countries, most of the biomass residues are left in the field to decompose or alternatively burned on the spot, resulting in major environmental impacts. In the urbanization process the demand for products increase and alternative sustainable energy sources and raw material supplies are in need. So far, the biomass wastes are not efficiently taken into reuse as material and source of energy. Even less activity has been devoted to develop “low-carbon” solutions for valorization.

Forest residue amounts are defined as 46% of total forest stock [16]. Globally Russian Federation, Indonesia, USA, and Brazil produce most the forest residue, 5,718, 2,221, 2078 and 1,613 million tons (Mt), respectively. China, Sweden, France, and Finland are the next largest producers of forest residues of which Sweden and Finland represent Nordic countries with large proportion of forests land cover.

2.2 *Municipal Solid Waste*

Municipal solid wood waste (MSWW) constitutes a quite low share of total MSW, but the relatively high volume and inadequate prospects for reuse are causing cities difficulties in treatment, selection, and transport of the waste with the goal to mitigate MSWW environmental impacts [17, 18]. The common solution has often been the incineration of MSWW to produce energy [18]. In the time of circular economy worldwide [19], alternative policies have become the norm to reduce the environmental impact of incineration and instead promote the reuse of this waste category and prolong its life cycle [17]. In the present situation incineration should only be used as last of options since wood waste entails great reuse potential, and by recycling MSWW many opportunities arise still including efficient energy recovery.

3 Hydrothermal Carbonization (HGT)

Biochar has long been a known way of carbonization of different types of biomasses and in recent years hydrothermal carbonization (HTC) has in parallel been developed as an alternative method of processing biomass for value-added products [20, 21]. The solid char product formed during HTC is called hydrochar to be distinguished from biochar which is formed in pyrolysis process in temperatures from 300–650°C [22]. During the HTC process, biomass is heated in an oxygen free environment in presence of subcritical water under autogenous 2–10 MPa pressure [23]. The HTC process has several benefits compared to pyrolysis, including a lower energy consumption and the generation of less emissions. It is especially suited for high moisture feedstocks with a high moisture content that produces lower amounts of solid material after drying, and that makes them inadequate sources for pyrolysis [23]. This gives possibilities for a variety of feedstocks to be used for the production of hydrochar when drying the feedstock is not necessary [24]. Another gain compared to biochar is that by HTC the char yield is larger and produced with lower amounts of energy. Since the feedstock does not need to be dried, and operating temperatures for HTC (200–300°C) are lower, the yield is greater with less energy compared to biochar pyrolysis [25]. The char biomass is activated in the presence of liquid heating up the process, which enables lower process temperature compared to biochar production. The heating of the biomass initiates hydrolysis, dehydration,

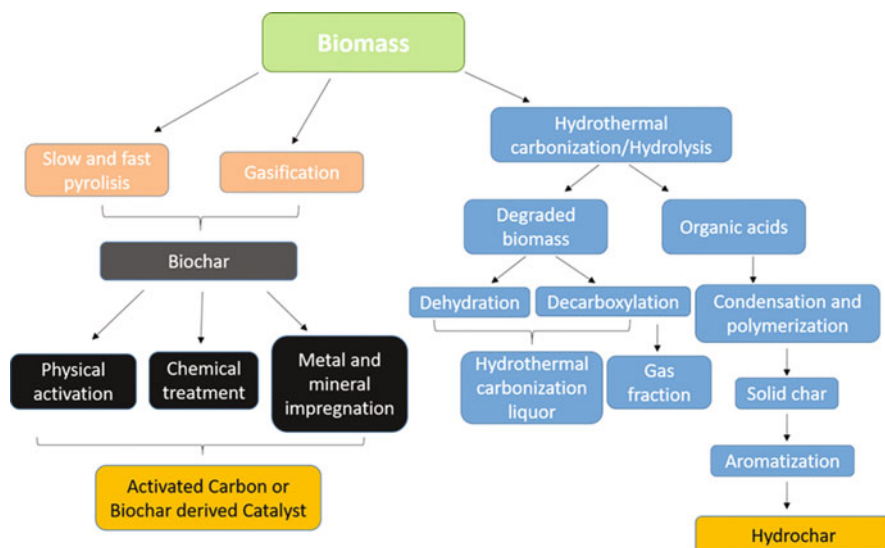


Fig. 1 Processes involved in the production biochar and hydrochar from biomass

decarboxylation, and aromatization that changes the physical structure of the biomass (Fig. 1) [26]. The hydrolysis is the primary reaction in HTC, and it has lower activation energy than the other reactions.

3.1 Feedstock Nature

The classification of feedstocks into wet and dry biomass can be done based on initial moisture content. Newly harvested biomass like sewage sludge, vegetable residues, algae, animal wastes, etc. often has high moisture content (>400%) and is then called “wet biomass.” Agricultural residues and some wood species have low moisture content (<30%) when they are harvested and are thus called “dry biomass” [24]. The wet biomass can be dried to become low moisture content feedstock with complementing drying techniques, but their downside is the high-energy requirement that will be economically costly.

Biomass is an excellent source for bioenergy [27], that basically is clean energy and HTC can be applied to large varieties of feedstock like lignocellulosic residues [28], animal wastes [29], agricultural residues, food wastes [30], municipal wastes [31], and wastewater treatment plants’ (WWTPs) activated sludge [32] that have detrimental effects on the quality of hydrochar. Overall, both hydrochar and biochar have their advantages and disadvantages. In future research biomass treatment can be combined with the hydrothermal carbonization process and pyrolysis process. The catalytic performance of the product materials needs to be further investigated [33].

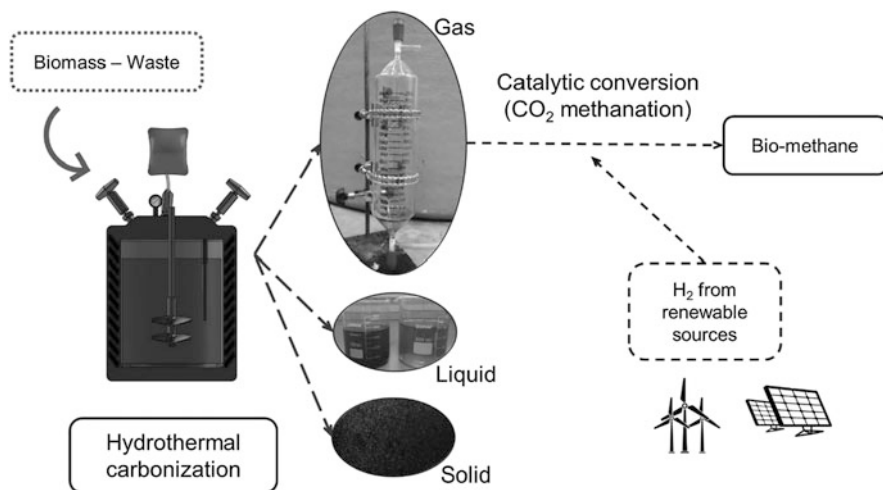


Fig. 2 Integration of HTC with methanation of gas phase [34]

Alternative fuels are sought to achieve required process temperatures in industrial processes as electricity becomes more expensive [34]. The gas phase obtained in hydrothermal carbonization can be subjected to a methanation stage, when the resulting methane could be used to fuel the process. Such process idea is depicted in Fig. 2. Such solution could be a step forward for integrated process according to circular economy principles. Moreover, the needed hydrogen for methanation should come from renewable sources.

Biomass has so far been utilized in many ways, but pyrolysis is a new way of dealing with biomass sustainably. The biological conversion has been applied with biogas reactors in fermentation and anaerobic digestion where the crucial step is what to do with the sludge to avoid it becoming a waste. Densified biomass like pelletization of forest residue has the challenge that it has mainly been used for heat production instead of channeling it into the biochar system (FAO) according to the principles of circular economy. The forms of biomass utilization are compared with pyrolysis and hydrothermal processes in Table 1.

4 Pyrolysis for Biochar Production

Biochar is a solid, carbon-rich product acquired from the pyrolysis process under an oxygen-limited atmosphere and high temperature [22]. The handling of all kinds of agriculture and forestry has become a priority. In the EU, about 23 Mt/p.a. of biomass (dry) is available as residual straw from cereals [16] whereas from example emerging economies like India, ca. 368 Mt/p.a. straw residue is available [35].

Table 1 Evaluations of waste biomass use

Biomass processing	Advantages	Disadvantages	Technology and objective
Pyrolysis	High efficiency and flexibility with sustainability prospects	Requires pretreatment of especially wet biomass waste	Slow or fast pyrolysis to receive biochar, bio-oil, and gases
Hydrothermal process	Direct application for wet biomass	The products not easily separated and demanding equipment	Carbonization, liquefaction, and gasification to receive hydrochar, bio-oil and gas
Anaerobic digestion	Low energy needs and large capacity	Requires large investments and is time consuming	Anaerobic digestion in biogas plant (bioreactor)
Solid fuel	Densified fuel into smaller space	High hydrophilicity catching moisture	Pelletization and briquette production

Biochar can be produced in different types of units and reactors to achieve the desired yield and quality. Reactors are similar, but the oxygen use, heating rate, and final temperature affect the quality and distribution of final products [36]. The thermal process for optimizing biochar yield is slow pyrolysis, which is conducted in 300–700°C in the absence of air producing bio-oil and biogas as by-products. Torrefaction is another process optimizing biochar yield, carried out at 200–300°C in the absence of air and it does not produce by-products. By prolonging the biochar residence time at ~400°C for more hours a higher yield and quality could be obtained [36].

4.1 *Slow Pyrolysis, Temperature Regulation*

In slow pyrolysis the temperature range is 300–600°C, with a long residence time (several hours to several days) and requires only low heating rate. It is generally believed that slow pyrolysis is the best pyrolysis method optimizing the biochar yield and structure [36, 37]. Zhang et al. [38] prepared three types of cow dung biochar under slow pyrolysis which revealed differences in morphology, surface area, pore structure, surface charge, and oxygen-containing functional groups where the biochar yield was 30–60% and the specific surface area <400 m²/g.

The temperature is an important parameter in the design of biochar that governs physicochemical properties of the pyrolyzed product. It affects the aromatic condensation and aromaticity of biochar. With increased pyrolysis temperature the liquefied aromatic ring structure in biochar increases, at the same time as the unstable nonaromatic ring structure decreases [39]. Along with aromaticity hemicellulose, cellulose, lignin, protein, polysaccharide, and other macromolecules decrease in the resulting biochar. This leads to lower polarity of the solid product, but also lower hydrophilicity of the surface, forming separated aromatic rings. Zhang et al. [39] found that the pyrolysis temperature played a significant role in the properties of

biochar. The temperature correlated positively with the carbon content, ash content, pH, surface roughness, and conductivity. The (O + N)/C, O/C, and H/C ratios, however, correlated negatively with temperature [39]. The higher temperatures favor formation of crystal structures. Biochar produced in lower temperatures becomes acidic, polar with low aromaticity and hydrophobicity. With the increasing temperature functional acidic groups like –OH and –COOH decrease along with biochar yield. This leads to appearance of more alkaline functional groups, higher pH and ash when the biochar surface area increases as volatiles evaporate from the biomass.

4.2 *Pyrolysis Atmosphere*

In recent years the biochar synthesis has been refined and a number of different functional structures of biochar are better controlled through adjustment of synthesis parameters, not only pyrolysis time and pyrolysis temperature, but also by choice of biomass, and different pretreatment process. It is the gap between functional structures and mechanisms that needs to be bridged for achieving better results with biochar applications [40].

It is possible to optimize the pyrolysis process by changing the atmosphere in-situ activation for production of more potent biochars. This has been reported in several studies where the conventional N₂ atmosphere has been changed, for instance, to CO₂ as carrier gas [41, 42]. The activation with CO₂ improved the aromatic surface properties of biochar in temperatures of 500, 600, and 700°C [43].

Using spent coffee ground (SCG) the authors Cho, Chang [44] found two key roles of CO₂: the thermal cracking of VOCs appearing from the thermal degradation and the reaction of CO₂ with VOCs. They concluded that the morphological modification was initiated after depleting VOCs by the thermal degradation of the SCG sample in CO₂ atmosphere.

4.3 *Co-Pyrolysis of Biomass with Activator/Dopant*

When biochar is going to be used as a catalyst or adsorbent sufficient surface functionality is wanted providing more active sites for catalysis and adsorption of pollutants. High porosity and large surface areas are also advantageous for biochar utilized for storage of energy since they enable higher fluxes of mass transfer and active loading [45]. For biochar use, porosity and surface area of biochar and surface are critical and need to be properly assessed, or else desirable biochar features must be stimulated through suitable activation strategies (Table 2). Directly after the production process the biochar has low tendency to absorb or adsorb compounds. The surface area, pore size, pore volume, and the amount of pores present contribute to the reaction characteristics [56]. The produced biochars without proper activation

Table 2 The surface area, pore volume, and pore size of different biochars [46]

Surface area, pore size, and pore volume of various biochar-derived catalysts					
Catalyst support	Catalyst support	Surface area (m ² /g)	Pore size (nm)	Pore volume (cm ³ /g)	References
Glucose solid acid catalyst	Un sulfonated glucose solid acid catalyst	3.65 ± 0.26	–	–	[47]
	Sulfonated glucose solid acid catalyst	10.67 ± 0.90	–	–	
Douglas fir wood chip biochar	Biochar catalyst	3.51	–	–	[48]
Polyethylene terephthalate waste	Activated carbon	1,105	–	–	[49]
	Carbon acid catalyst	624.20	–	–	
Palm kernel shell biochar	Biochar	0.02	–	–	[50]
	Biochar-based catalyst	290.44	–	–	
Peat biochar	Peat biochar	83.78	89.26	106.90	[51]
	30 K/PB-600	20.04	42.02	31.55	
	30 K/PB-600 (fresh)	20.04	–	31.55	
	30 K/PB-600 (recovered)	17.81	–	26.62	
Chicken manure biochar	Silica (commercial)	451.1	5.98	0.88	[52]
	Biochar (350°C)	0.043	31.47	0.043	
	Biochar (450°C)	0.072	19.595	0.072	
	Biochar (550°C)	0.067	22.198	0.067	
Oat hull-derived biochar	B600	49.32	1.04	0.008	[53]
	BS100	30.59	2.30	0.055	
	BS140	5.43	1.03	0.008	
Waste pig meat and bone meal biochar	Meat and bone meal biochar	142.6	45.3	190.6	[54]
	AMB	430.5	128.6	586.5	
	30 K/AMB-550, fresh	80.0	59.4	61.4	
	30 K/AMB-550, recovered	91.6	66.4	74.5	
Wood char	Wood char	354	3.8	0.34	[55]
	Wood char-derived acid catalyst	337	2.7	0.24	

contain (1) abundant intermolecular spaces as a result of bond breakage between the organic components (2) clogged pores that cause generation of tar (3) inadequate pore size reducing the distribution of surface area (4) condensate contaminants like, ashes, etc. that decrease the pore size and volume.

4.4 Activation by Chemical Agents

Chemical activation methods are generally one-step processes where the agents are added to biochar and subjected to further pyrolysis. An activated biochar is usually washed for removing excess chemical, and after that the surface is ready for adsorptive reactions depending on target use. Typical chemical activation is oxidation, sulfonation, and amination and agents used are H_2O_2 , SO_3H , $ZnCl_2$, acids like HNO_3 , bases like KOH , $NaOH$. The activation agent is selected on the bases of the target use of biochar. Adsorbing negatively charged elements requires activation with bases imposing positive surface giving affinity to adsorbate. For adsorbing positively charged element, biochar is in turn activated with acid for improving adsorption of positively charged elements [57].

4.4.1 Activation by H_2O_2

H_2O_2 is a low-cost activation agent used at ambient temperature that splits into H_2O and O_2 and it is used as oxidizing agent because of the following reasons (1) low cost, (2) works at low temperature, (3) end products are H_2O and O_2 . Biochar made from grape wood activated by H_2O_2 at $350^\circ C$ has been shown to effectively adsorb the cyhalofop herbicide (35.4%) due to strong affinity of herbicide to biochar [58].

4.4.2 Activation by Metals

Metal ions are often applied as agents for catalysis [59]. Iron, cobalt, and other metallic biomass elements have been used in advanced oxidation systems [60]. Loading metal is thought as one of the operational ways for expanding the catalytic ability of biochar. When metal particles are dispersed in biochar, they can lower metal leaching. Biochar can prevent the aggregation of metal nanoparticles and thus offers many more accessible active sites. Compared to other catalysis supports, biochar has economical and efficiency advantages.

Zn-Co-layered double hydroxide (Zn-Co- LDH) nanostructures were incorporated with biochar through hydrothermal process [61]. After loading on biochar, the specific surface declined from 112.9 to 95.7 m^2/g . At the same time gemifloxacin degradation efficiency was raised from 60.4% to 92.7%.

There are several techniques to analyze biochar properties. The surface chemistry can best be studied by Fourier transformation infrared spectroscopy, X-ray diffraction analysis, and X-ray photoelectron spectroscopy. Structural analysis is done by scanning electron microscopy and Brunauer-Emmett-Teller analysis. The elements in biochar can be revealed by energy-dispersive-X-ray spectroscopy. The acidity and basicity can be determined by temperature-programmed desorption using ammonia [46].

Usually before co-pyrolysis biomass is premixed by impregnation or mechanical mixing with an activator/dopant, and then pyrolyzed. Co-pyrolysis of biomass with activators/dopants such as KOH, Ca(OH)₂, ZnCl₂, MgCl₂, FeCl₃, chlorapatite, Fe(NO₃)₃, KMnO₄, melamine, and urea has been explored. By using hazelnut shells as a raw material, Zhao et al. [62] undertook the chemical activation of ZnCl₂ for co-pyrolysis and found that hazelnut shells were an effective material for producing a microporous structure. Liu et al. [63] pretreated straw with a Ca(OH)₂ water solution, and then synthesized the calcium-rich biochar in-situ with black liquor as a precursor, whereby Ca(OH)₂ was found to be a mesoporous forming agent in the synthesis process. With corn stalk as raw material and urea as nitrogen source, Li et al. [64] prepared a nitrogen-doped fractional porous biochar by in-situ co-pyrolysis. The addition of urea promoted the formation of biochar pores, and nitrogen atoms successfully became a part of the biochar skeleton. Biochar attained through the co-pyrolysis of biomass with activators/dopants has a larger surface area and more surface oxygen-containing functional groups in comparison with original biochar.

4.5 The Quality and Safety of the Produced Biochars

Waste material is an important resource in Circular economy [65]. The recycling and upgrading of waste require detailed evaluation of possible waste contaminants. In pyrolysis there is the need to assess them in the biochar product. In the pyrolysis process enrichment of metals takes place since most of them are not released by emissions [66]. Pyrolysis can release metals as a volatile metal mixture together with aerosols from the gases. Organic compounds like polyaromatic hydrocarbons (PAHs) can leak during pyrolysis as aromatic rings condensation, fused into PAH-like sheet assemblies [67]. The quantity of toxic elements in biochars has been examined [68]. PAHs are especially produced during incomplete combustion of biomass, and thus are integrally generated during biochar production. Due to their well-known toxicity and carcinogenic traits, they constitute an environmental risk.

The quality of biochars is an important issue especially in the commercial market where the biochar is intended for a spectrum of different uses. The European Biochar Certificate highlights the specific contaminant threshold levels in biochar for agricultural soil improvement [69]. The threshold levels are given as total content in the solid phase. Concerning contaminants, the bioavailable concentrations are crucial in accurate risk assessment and need some attention [70]. The heavy metal contents are dependent on both feedstock and process parameters of the performed pyrolysis [71]. The rise in pH supports lower heavy metal solubility [72]. The pH increase in biochar may not last due to leaching where soil pH might in the long term be reduced. Biochar application in agriculture requires thorough assessment of biochar quality since toxic organic contaminants of biochar may end up in the environment. European Biochar Certificate (EBC) values of the molar ratio of H/Corg <0.7 and O/Corg <0.4 does not ensure that biochar will not cause phytotoxicity [10].

5 Biochar for the Remediation of Contaminated Soil and Water

Soil amendment is the most common application of biochar and several studies have demonstrated the benefits of such practice [73, 74]. Biochar as an amendment in soil has been shown to improve soil properties such as soil C content, increase water holding capacity, and increase aggregate formation, stability [75] and plant growth [76]. It could also improve soil quality and fertility [77, 78]. The high porosity of biochar has taken advantage to immobilize heavy metals in soils [79], and in consequence reduce their uptake by plants [80], and remediate organic pollutant-contaminated soils [81].

5.1 Heavy Metals

Soil pollution poses a threat to human and environmental health as contamination can migrate into groundwater, or drain into other water bodies. But it may also get into the food chain and eventually reach humans [79]. Just in the USA more than 100,000 contaminated sites have been identified [82] and in Europe the estimate for the total number of potentially contaminated sites is 2.5 million [83]. Due to their high toxicity and health risks the remediation of heavy metal (HM)-contaminated soil has become a priority in the environmental agenda [84]. The use of biochar for the remediation of HM-contaminated soil has become a sustainable solution (Fig. 3). Biochar as a porous material has the capacity to bind HMs from soil and that way reduce the uptake of HMs by plants [80, 85, 86]. The raw materials and feedstock for biochar production together with the pyrolysis temperatures are the most important

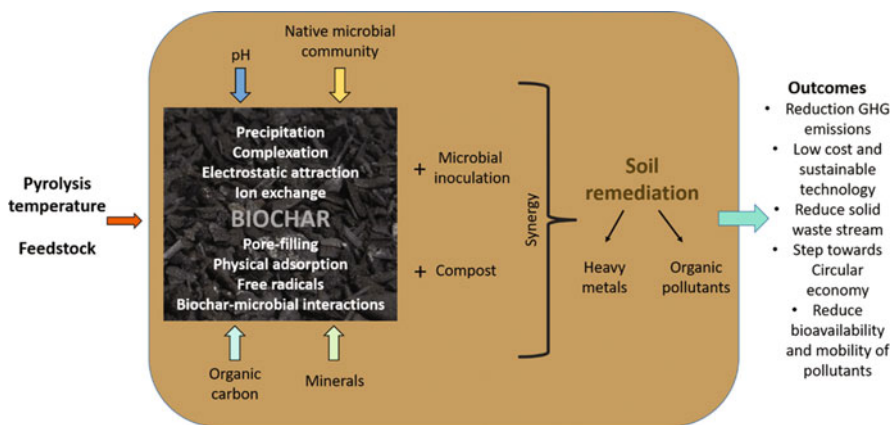


Fig. 3 Factors influencing the remediation of contaminated soil with biochar as an amendment and its advantages

criteria affecting the binding capacity of biochar. The interactions between biochar and HMs in soil can be direct in precipitation, complexation, or electrostatic attraction. The interactions can also be relatively indirect depending on soil pH, minerals, or organic carbon [87]. Biochar adsorbs the metal ions from contaminated soils due to its stronger sorption sites and high affinity to metal ions [88].

Choudhary et al. [89] used biochar from pine needle litter to serve for Pb adsorption from contaminated water. The study showed that Pb adsorption increased significantly as pH and temperatures increased and desorption results were promising with a lead recovery of 90–93%. They concluded that biochars possess the potential for aqueous removal of other metal cations [89].

5.2 Phytoremediation and Related Microbes

The most recent studies have been testing biochar as a carrier of HM-reducing strains or HM-tolerant bacteria and its effects upon its addition into contaminated soil [90]. Cr contaminated soil is of great concern due to the high toxicity of Cr(IV). A recent study successfully immobilized a Cr(IV)-reducing strain into biochar to treat Cr-polluted soil. Soil properties improved with aggregate formation, organic carbon content, and cation exchange increased. The Cr(IV) was transformed into less toxic Cr(III) and that Cr-residue fraction increased by 63.38% compared with control. The aggregates also reduced the Cr absorption of *Ryegrass* from the root and enhanced its growth [91]. Biochar inoculation with a HM-tolerant strain was reported to significantly increase residual fraction of Cd and Cu leading to the decreased bioavailability of the metals in soil. The inoculated biochar enhanced soil enzyme activity and the soil microbial community recovered at the end of the incubation, showing improved soil function after metal stabilization [92].

It has been demonstrated that solubility of Pb and Cd decreased significantly with biochar produced from agriculture residues providing evidence that biochar decreased HM toxicity [93]. Soil properties improved; pH increased together with organic matter and nutrient content. Maize planted on the treated soil with biochar performed better compared to the control demonstrated as an increase in biomass [93].

The interaction among biochar, plants, and microbes might alter the HMs behavior in the soil [94]. The beneficial roles of biochar on plant growth and on the enhancement of microbial activity were likely to improve the phytoremediation efficiency of the hyperaccumulators [95]. Biochar incorporation does not decrease the total heavy metal content of the soil but it reduces the bioavailability and phytotoxicity of heavy metals. Therefore, phytostabilization of metal-contaminated soils can be enhanced by combining metal immobilizing plants with biochar [96]. Biochar was used in Cd soil contamination for cell immobilization of two cadmium resistant bacteria (CRB), *Arthrobacter* sp. and *Micrococcus* sp. [97]. Biochar-immobilized (BC) CRB were able to survive in cadmium-contaminated soil (Fig. 4). The inoculation of BC-*Micrococcus* sp. increased the

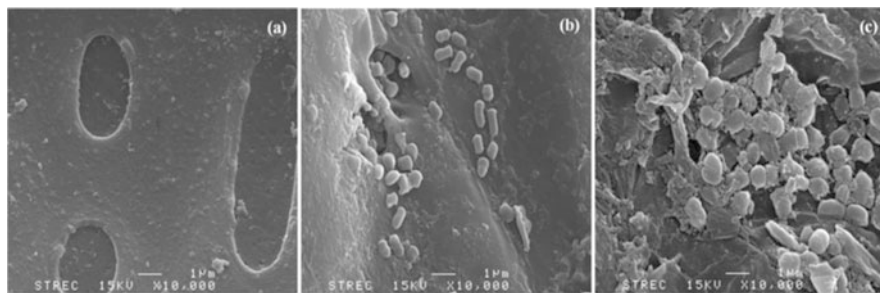


Fig. 4 Biochar of cassava stem (*Manihot esculenta L. Crantz*). HM Phytoremed with bacterial immobilization. Characteristics of (a) biochar, (b) BC-*Arthrobacter* sp., and (c) BC-*Micrococcus* sp. observed under SEM at $\times 10,000$ magnification remove 5 [97]

root dry weight of *C. laxum* planted in cadmium-contaminated soil. Plants inoculated with either BC-*Arthrobacter* sp. or BC-*Micrococcus* sp. had the highest cadmium contents in the shoots and the roots. They concluded that *C. laxum* combined with BC-*Arthrobacter* sp. or BC-*Micrococcus* sp. inoculation achieved a high efficiency of cadmium phytoextraction in metal-contaminated soil.

5.3 Organic Pollutants

Biochar from biomass waste has successfully been used for remediation of organic pollutants [98]. Interactions of free radical-based chemical reactions and biochar-microbial communities are the most important mechanisms involved in the degradation of soil organic pollutants using biochar. Pollutants are preferentially adsorbed onto the surface and pores of the biochar in free radical-based chemical reactions. The radicals formed in advance oxidation process degrade the pollutants [73].

Colored contaminated water has been treated with different types of biochar with good results. An example is the recent study where engineered biochar was produced from food waste digestate to remove azo dye pollutant from water. Results were promising with a removal of $>99\%$ of the dye upon the addition of biochar (0.5 g/L) and peroxymonosulfate (1 mM) to wastewater. The removal efficiency was attributed to the catalytic sites in the biochar which could activate peroxymonosulfate to produce reactive oxygen species [99]. Biochar from wood apple fruit shell waste was used in the removal phenol and chlorophenols (4-CPh and 2,4-DCPh) from contaminated aqueous media [100]. The study revealed that this biochar was an effective adsorbent of these organic pollutants with pH and temperature being vital parameters to take into account for a rapid uptake and high sorption capacity: it could be used for the treatment of contaminant wastewater [100]. Efficient removal of Rhodamine B dye was achieved by a magnetic biochar produced from waste wood [101]. The adsorption process was governed by a chemical reaction and the adsorption process was a single-layer and heterogeneous surface adsorption. The equilibrium was

established within 1 min, indicating an excellent adsorption efficiency making this magnetic biochar a prospect in wastewater treatment [101].

Modified biochars with active oxidation agents, e.g. persulfate, peroxymonosulfate, chlorine, iodine, etc., have been utilized to generate free radicals and improve the degradation of organic pollutants [73]. Biochar from waste lychee branches was together with persulfate used for the removal of bisphenol A (BPA) in soils [102]. This type of biochar activates persulfate to generate sulfate and hydroxyl radicals for BPA degradation. Liu et al. 2020 [102] concluded that the combination of biochar and persulfate could be used for in-situ remediation of organic contaminated sites.

Herbicides are organic chemicals that may undesirably impact human, wildlife, beneficial plants and soil organisms. In a multifaceted experiment by Wu, Liu [103] different types of biochar (peanuts (BCP), chestnuts (BCC), bamboo (BCB), maize straw (BCM), and rice hull (BCR) were applied to soil to study their sorption capacity, degradation, and effect on the bioavailability of the herbicide oxyfluorfen. The most important results showed that the biochars exhibited different sorption capacities for oxyfluorfen in the following order: BCR > BCB > BCM > BCC > BCP and that the addition of biochar to soil reduced the bioavailability of oxyfluorfen. Oxyfluorfen degraded faster in BCR-amended soil compared to unamended soil, i.e., degradation increased by ~1.2-fold with addition of just 2% BCR. Interestingly, the adsorption capacity of amended soil for oxyfluorfen decreased with increased aging time, however, it was still higher on the amended soil compared to the unamended soil after 6 months. In conclusion, the study indicates that the introduction of biochar is an effective method to modify soil contaminated with oxyfluorfen and to decrease the risk of contamination [103]. Sugarcane top-derived biochar was added to different types of soils to evaluate the sorption capacity toward atrazine herbicide [104]. The sorption coefficients had a positive correlation with the amount of biochar added into soil. The study indicated, however, that as a result of adsorption the degradation of atrazine decreased and that it could be a method to prevent atrazine leaching into groundwater [104].

The combination of biochar and compost has proven to be effective in the remediation of organic pollutants, when both amendments improve soil quality and fertility. The application of compost and biochar amendment decreased the concentration and bioavailability of PHCs [105]. The addition of compost enhanced biodegradation, while biochar contributed to lock the hydrocarbons in contaminated soils [105]. Hussain, Khan [106] observed that the combination of biochar, compost, and immobilized microorganisms resulted in the highest PHCs removal from soil compared to the control or the treatments alone.

6 Toward Circular Economy: Recycled Waste for Biochar Production

Pyrolysis and hydrothermal carbonization of biomass have attracted attention as expedient waste management methods [107]. Biochar has been produced from several organic waste material such as guayule bagasse, cotton gin waste [108], coconut shell [109], empty fruit bunches [110], and rice husk [111]. Biochar pyrolysis has been reported for food waste digestate and food waste [99], straw from crops (corn, wheat and bulrush) [112, 113], pig manure [107], and wood waste materials.

When waste wood is used as heating energy it will release CO₂ to the atmosphere, which is against current policies in Europe for reaching carbon neutrality. Furthermore, waste wood in landfills will create methane emission as product of the decomposition of lignocellulose compounds [114]. The construction and demolition industry produces waste wood that has become a viable source of biomass for the production of biochar. Countries including Taiwan have already implemented the reuse of waste wood as material and energy resource in carbon-negative policies, to reduce greenhouse gases (GHG) emissions [114]. Waste wood like wood shavings, waste timber, bark and pine needles litter has already successfully been produced [89, 109, 115]. The increase of the production of biochar from waste wood could become a global solution to reduce the landfills. It has been estimated that just in Finland wood waste accounts for 3,268,000 t from which 401,000 t comes from construction industry [116, 117].

Differently produced biochars have increasingly been used for soil amendment but also contributing to carbon sequestration. An interesting application is the introduction of biochar into building material like cement and concrete.

6.1 Novel Applications of Biochar

The use of biochar as soil amendment is the most common application of this material [78], however in recent years there has been several other useful and sustainable applications. Some of these examples are briefly mentioned in this chapter as in Fig. 5.

6.1.1 Carbon Sequestration for Carbon Neutrality

For achieving the goals of carbon (C) neutrality, municipalities need worldwide to apply negative emission technologies. The application of biochar as soil amendment represents a sustainable long-term carbon storage [118, 119] that has a mitigating influence on climate change and global warming. The conversion of waste wood into biochar has a positive effect on carbon sequestration. Around 50% of the carbon in waste wood is retained in biochar instead of being released into the atmosphere. In

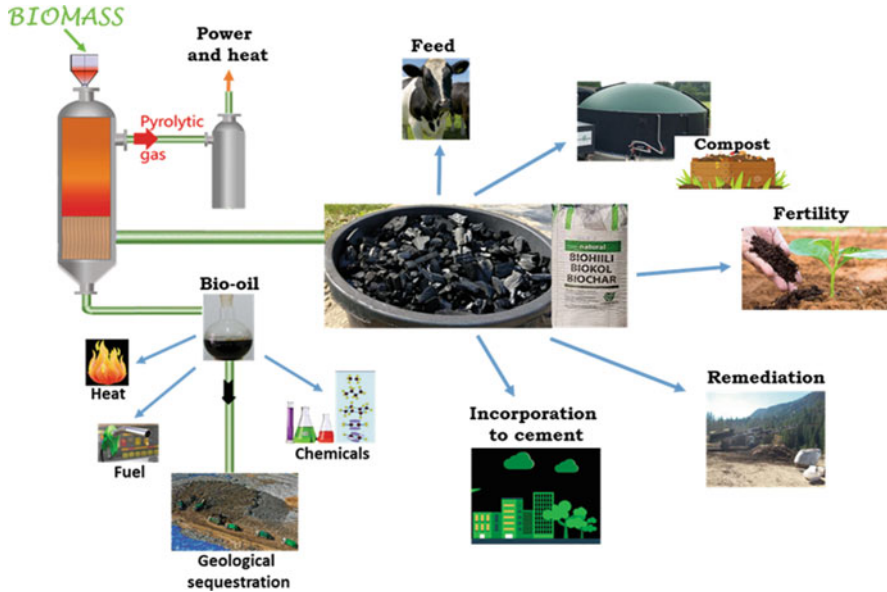


Fig. 5 Pyrolysis presenting the three main products, biochar, gas, and bio-oil. Potential applications for the carbon sequestered in biochar including soil fertility, feed in livestock farming, incorporation to building material, organic fertilizer, and environmental remediation. Bio-oil can be used for heating, but especially for upgrading to fuel, chemicals and even deposited as geological sequestration

this procedure the organic carbon is moved to a slower carbon cycle reservoir (biochar) that can remain in soil even for centuries [120]. Urban demonstration areas using trees and biochars for C sequestration have been implemented in Helsinki, Finland to show that urban C sinks in public parks need to be visible and scientifically sound for reliable cost-effective verification of carbon sequestration. Valuable synergies emerged from co-creation of urban C sink parks between stakeholders (scientists, city officials, companies, and citizens) for increasing impact of biochar application [121].

6.1.2 Composting

The addition of biochar into compost (Fig. 5) could increase the aeration process as biochar is a porous material with low density [122]. Moreover, due to its high sorption capacity it could reduce the loss of nitrogen and immobilize HMs and organic pollutants present in the compost materials [123]. It has also been demonstrated that it could reduce the emission of GHGs [124]. Moreover, research has demonstrated that the combined application of biochar and compost to soils could increase both; their agronomic value and reduce nutrients losses [125].

6.1.3 Livestock

Significant benefits of biochar in feed (Fig. 5) to improve animal health have been reported [126]. In an extensive survey (>100 scientific publications) on biochar in animal feeding, positive effects on digestion, feed efficiency, toxin adsorption, blood values, and meat quality were widely observed. GHG emissions were also reduced when biochar was added to feed [126]. In Europe it has recently been approved to add biochar to livestock feed at 1–2% for reducing vet and medical costs [127]. Biochar has further been effective in animal bedding for odor control [128].

6.1.4 Concrete

Other biochar applications include the incorporation of biochar into the concrete mixture for building (Fig. 5), with positive results and as carbon sequestration opportunity. Akhtar and Sarmah [129] tested three different waste sources of biochar to replace cement content up to 1%. The study concluded that biochar has the potential to improve the concrete properties, e.g. flexural strength while replacing minor fractions of cement [129]. Biochar from residual biomass of a bio-ethanol industry in mixture with concrete improved the sound absorption coefficient [130]. Biochar-concrete mixtures have also shown an improved water tightness, mechanical strength and minimal internal damage to concrete micro-structure [131].

7 Conclusion

The utilization of waste biomass for pyrolysis opens up great avenues for valorization of it to hydrochar and biochar. These higher value products may find a wide environmental range of applications ranging from fertilizers to remediation tools and use in building material to support the transition toward carbon neutral societies. The future success of these materials requires good separation of waste and channeling of waste streams into economic valorization. This will further depend on the ability to tailor various biomasses for specific purposes in an economically feasible way. The removal of carbon from atmosphere through biochar systems and the growth of the voluntary carbon market will speed up new applications for these very stable carbon products helping to reach carbon neutrality.

References

1. Drews S, Antal M, van den Bergh JC (2018) Challenges in assessing public opinion on economic growth versus environment: considering European and US data. *Ecol Econ* 146: 265–272

2. EUROSTAT (2019) Share of energy from renewable sources 2019 data. European Commission
3. Lu X et al (2021) Co-hydrothermal carbonization of sewage sludge with wood chip: fuel properties and heavy metal transformation behavior of hydrochars. *Energy Fuel* 35(19): 15790–15801
4. Fang J et al (2018) Minireview of potential applications of hydrochar derived from hydrothermal carbonization of biomass. *J Ind Eng Chem* 57:15–21
5. Fawzy S et al (2021) Industrial biochar systems for atmospheric carbon removal: a review. *Environ Chem Lett.* <https://doi.org/10.1007/s10311-021-01210-1>
6. Kim Y et al (2022) Agricultural waste streams as resource in circular economy for biochar production towards carbon neutrality. *Curr Opin Environ Sci Health*. Accepted
7. Oleszczuk P et al (2014) Effect of pesticides on microorganisms, enzymatic activity and plant in biochar-amended soil. *Geoderma* 214:10–18
8. Sørmo E et al (2020) Waste timber pyrolysis in a medium-scale unit: emission budgets and biochar quality. *Sci Total Environ* 718:137335
9. Freddo A, Cai C, Reid BJ (2012) Environmental contextualisation of potential toxic elements and polycyclic aromatic hydrocarbons in biochar. *Environ Pollut* 171:18–24
10. Ruzickova J et al (2021) A comprehensive assessment of potential hazard caused by organic compounds in biochar for agricultural use. *J Hazard Mater* 403:123644
11. d'Annunzio R et al (2015) Projecting global forest area towards 2030. *For Ecol Manag* 352: 124–133
12. van den Born GJ, van Minnen JG, Olivier JGJ, Ros JPM (2014) Integrated analysis of global biomass flows in search of the sustainable potential for bioenergy production. P.N.E.A. Agency, The Hague
13. Tripathi N et al (2019) Biomass waste utilisation in low-carbon products: harnessing a major potential resource. *NPJ Clim Atmos Sci* 2(1):1–10
14. Forestry Department FAO (2018) Global forest products facts and figures. Food and Agriculture Organization of the United Nations, p 20
15. Rafael S et al (2015) Impact of forest biomass residues to the energy supply chain on regional air quality. *Sci Total Environ* 505:640–648
16. Baruya P (2015) World forest and agricultural crop residue resources for cofiring. International Centre for Sustainable Carbon, London, p 66
17. Faraca G et al (2017) Environmental assessment of presence of impurity materials and chemical pollutants in wood waste meant for recycling. In: Abstract from SETAC Europe 27th Annual Meeting. Brussels, Belgium
18. Zhou H et al (2014) An overview of characteristics of municipal solid waste fuel in China: physical, chemical composition and heating value. *Renew Sust Energy Rev* 36:107–122
19. Winans K, Kendall A, Deng H (2017) The history and current applications of the circular economy concept. *Renew Sust Energy Rev* 68:825–833
20. Stemann J, Putschew A, Ziegler F (2013) Hydrothermal carbonization: process water characterization and effects of water recirculation. *Bioresour Technol* 143:139–146
21. Oliveira I, Blöhse D, Ramke H-G (2013) Hydrothermal carbonization of agricultural residues. *Bioresour Technol* 142:138–146
22. Lehmann J, Joseph S (2015) *Biochar for environmental management: science, technology and implementation*. Routledge
23. He C, Giannis A, Wang J-Y (2013) Conversion of sewage sludge to clean solid fuel using hydrothermal carbonization: Hydrochar fuel characteristics and combustion behavior. *Appl Energy* 111:257–266
24. Kambo HS, Dutta A (2015) A comparative review of biochar and hydrochar in terms of production, physico-chemical properties and applications. *Renew Sust Energy Rev* 45:359–378
25. Takaya CA et al (2016) Phosphate and ammonium sorption capacity of biochar and hydrochar from different wastes. *Chemosphere* 145:518–527

26. Funke A, Ziegler F (2010) Hydrothermal carbonization of biomass: a summary and discussion of chemical mechanisms for process engineering. *Biofuels Bioprod Biorefin* 4(2):160–177
27. Azzaz AA et al (2020) Hydrochars production, characterization and application for wastewater treatment: a review. *Renew Sust Energy Rev* 127:109882
28. Li D-C, Jiang H (2017) The thermochemical conversion of non-lignocellulosic biomass to form biochar: a review on characterizations and mechanism elucidation. *Bioresour Technol* 246:57–68
29. Heilmann SM et al (2014) Phosphorus reclamation through hydrothermal carbonization of animal manures. *Environ Sci Technol* 48(17):10323–10329
30. Cantero-Tubilla B et al (2018) Characterization of the solid products from hydrothermal liquefaction of waste feedstocks from food and agricultural industries. *J Supercrit Fluids* 133:665–673
31. Bevan E, Fu J, Zheng Y (2020) Challenges and opportunities of hydrothermal carbonisation in the UK; case study in Chirside. *RSC Adv* 10(52):31586–31610
32. Danso-Boateng E et al (2015) Hydrothermal carbonization of primary sewage sludge and synthetic faeces: effect of reaction temperature and time on filterability. *Environ Prog Sustain Energy* 34(5):1279–1290
33. He X et al (2021) Hydrothermal and pyrolytic conversion of biomasses into catalysts for advanced oxidation treatments. *Adv Funct Mater* 31(7):2006505
34. González-Arias J et al (2021) Hydrothermal carbonization of biomass and waste: a review. *Environ Chem Lett*. <https://doi.org/10.1007/s10311-021-01311-x>
35. Hiloidhari M, Das D, Baruah D (2014) Bioenergy potential from crop residue biomass in India. *Renew Sust Energy Rev* 32:504–512
36. Wang D et al (2020) Biochar production and applications in agro and forestry systems: a review. *Sci Total Environ* 723:137775
37. Wang L et al (2020) New trends in biochar pyrolysis and modification strategies: feedstock, pyrolysis conditions, sustainability concerns and implications for soil amendment. *Soil Use Manag* 36(3):358–386
38. Zhang P et al (2019) Characteristics of tetracycline adsorption by cow manure biochar prepared at different pyrolysis temperatures. *Bioresour Technol* 285:121348
39. Zhang X et al (2020) Effect of pyrolysis temperature and correlation analysis on the yield and physicochemical properties of crop residue biochar. *Bioresour Technol* 296:122318
40. Zhou X et al (2021) New notion of biochar: a review on the mechanism of biochar applications in advanced oxidation processes. *Chem Eng J* 416:129027
41. Sørmo E et al (2021) Stabilization of PFAS-contaminated soil with activated biochar. *Sci Total Environ* 763:144034
42. Kończak M et al (2020) Carbon dioxide as a carrier gas and mixed feedstock pyrolysis decreased toxicity of sewage sludge biochar. *Sci Total Environ* 723:137796
43. Godlewska P et al (2019) Adsorption capacity of phenanthrene and pyrene to engineered carbon-based adsorbents produced from sewage sludge or sewage sludge-biomass mixture in various gaseous conditions. *Bioresour Technol* 280:421–429
44. Cho S-T et al (2015) Genome analysis of *Pseudomonas fluorescens* PCL1751: a rhizobacterium that controls root diseases and alleviates salt stress for its plant host. *PLoS One* 10(10):e0140231
45. Liu W-J, Jiang H, Yu H-Q (2015) Development of biochar-based functional materials: toward a sustainable platform carbon material. *Chem Rev* 115(22):12251–12285
46. Balajii M, Niju S (2019) Biochar-derived heterogeneous catalysts for biodiesel production. *Environ Chem Lett* 17(4):1447–1469
47. Lokman IM, Rashid U, Taufiq-Yap YH (2015) Production of biodiesel from palm fatty acid distillate using sulfonated-glucose solid acid catalyst: characterization and optimization. *Chin J Chem Eng* 23(11):1857–1864
48. Dong T et al (2015) Two-step microalgal biodiesel production using acidic catalyst generated from pyrolysis-derived bio-char. *Energy Convers Manag* 105:1389–1396

49. Fadhil AB, Aziz AM, Al-Tamer MH (2016) Biodiesel production from *Silybum marianum* L. seed oil with high FFA content using sulfonated carbon catalyst for esterification and base catalyst for transesterification. *Energy Convers Manag* 108:255–265
50. Nuradila D, Ghani W, Alias AB (2017) Palm kernel shell-derived biochar and catalyst for biodiesel production. *Malays J Anal Sci* 21(1):197–203
51. Wang S et al (2017) A novel peat biochar supported catalyst for the transesterification reaction. *Energy Convers Manag* 139:89–96
52. Jung J-M et al (2017) Biodiesel synthesis using chicken manure biochar and waste cooking oil. *Bioresour Technol* 244:810–815
53. González ME et al (2017) Functionalization of biochar derived from lignocellulosic biomass using microwave technology for catalytic application in biodiesel production. *Energy Convers Manag* 137:165–173
54. Wang S et al (2017) Transesterification of vegetable oil on low cost and efficient meat and bone meal biochar catalysts. *Energy Convers Manag* 150:214–221
55. Ahmad J et al (2018) Synthesis of char-based acidic catalyst for methanolysis of waste cooking oil: an insight into a possible valorization pathway for the solid by-product of gasification. *Energy Convers Manag* 158:186–192
56. Anto S et al (2021) Activation strategies for biochar to use as an efficient catalyst in various applications. *Fuel* 285:119205
57. Tan X-F et al (2017) Biochar as potential sustainable precursors for activated carbon production: multiple applications in environmental protection and energy storage. *Bioresour Technol* 227:359–372
58. Gámiz B et al (2019) Understanding activation effects on low-temperature biochar for optimization of herbicide sorption. *Agronomy* 9(10):588
59. Luo H et al (2020) Recent progress on metal-organic frameworks based-and derived-photocatalysts for water splitting. *Chem Eng J* 383:123196
60. Cao X et al (2020) Preliminary study on the electrocatalytic performance of an iron biochar catalyst prepared from iron-enriched plants. *J Environ Sci* 88:81–89
61. Gholami P et al (2020) Photocatalytic degradation of gemifloxacin antibiotic using Zn-Co-LDH@ biochar nanocomposite. *J Hazard Mater* 382:121070
62. Zhao B et al (2017) Surface characteristics and potential ecological risk evaluation of heavy metals in the bio-char produced by co-pyrolysis from municipal sewage sludge and hazelnut shell with zinc chloride. *Bioresour Technol* 243:375–383
63. Liu X et al (2019) Black liquor-derived calcium-activated biochar for recovery of phosphate from aqueous solutions. *Bioresour Technol* 294:122198
64. Li Y et al (2019) Nitrogen-doped hierarchical porous biochar derived from corn stalks for phenol-enhanced adsorption. *Energy Fuel* 33(12):12459–12468
65. European Commission (2019) Report from the Commission to the European Parliament, the Council, the European Economic and Social Committee, and the Committee of the Regions, on the implementation of the Circular Economy Action Plan. European Commission, Brussels
66. Dong J et al (2015) Partitioning of heavy metals in municipal solid waste pyrolysis, gasification, and incineration. *Energy Fuel* 29(11):7516–7525
67. Kołowski M, Oleszczuk P (2015) Toxicity of biochars after polycyclic aromatic hydrocarbons removal by thermal treatment. *Ecol Eng* 75:79–85
68. Hale SE et al (2012) Quantifying the total and bioavailable polycyclic aromatic hydrocarbons and dioxins in biochars. *Environ Sci Technol* 46(5):2830–2838
69. European Biochar Certificat (EBC) (2012) Summary of the EBC certification. <https://www.european-biochar.org/en/ct/29-Summary-of-the-EBC-certification>. Accessed 30 Oct 2021
70. Reichenberg F, Mayer P (2006) Two complementary sides of bioavailability: accessibility and chemical activity of organic contaminants in sediments and soils. *Environ Toxicol Chem* 25(5):1239–1245
71. Beesley L et al (2015) Biochar and heavy metals. In: Lehmann J, Joseph S (eds) *Biochar for environmental management* 2nd edn. Taylor & Francis, pp 563–594

72. Devi P, Saroha AK (2014) Risk analysis of pyrolyzed biochar made from paper mill effluent treatment plant sludge for bioavailability and eco-toxicity of heavy metals. *Bioresour Technol* 162:308–315
73. Kamali M et al (2022) Biochar for soil applications-sustainability aspects, challenges and future prospects. *Chem Eng J* 428:131189
74. Zhu X et al (2017) Effects and mechanisms of biochar-microbe interactions in soil improvement and pollution remediation: a review. *Environ Pollut* 227:98–115
75. Diatta AA et al (2020) Effects of biochar on soil fertility and crop productivity in arid regions: a review. *Arab J Geosci* 13(14):1–17
76. Rafique M et al (2020) Residual effects of biochar and phosphorus on growth and nutrient accumulation by maize (*Zea mays* L.) amended with microbes in texturally different soils. *Chemosphere* 238:124710
77. Alkharabsheh HM et al (2021) Biochar and its broad impacts in soil quality and fertility, nutrient leaching and crop productivity: a review. *Agronomy* 11(5):993
78. Zhanhua Z et al (2022) Organic amendments combined with biochar for improving soil and plant quality in a *Torreyia grandis* plantation. *J Soils Sediments*. <https://doi.org/10.1007/s11368-021-03127-2>
79. Shakya A, Agarwal T (2020) Potential of biochar for the remediation of heavy metal contaminated soil. In: *Biochar applications in agriculture and environment management*. Springer, Berlin, pp 77–98
80. Seleiman MF et al (2020) Effects of ZnO nanoparticles and biochar of rice straw and cow manure on characteristics of contaminated soil and sunflower productivity, oil quality, and heavy metals uptake. *Agronomy* 10(6):790
81. Rao MA et al (2017) Biochar based remediation of water and soil contaminated by phenanthrene and pentachlorophenol. *Chemosphere* 186:193–201
82. Connell DW et al (2005) *Basic concepts of environmental chemistry*. CRC/Taylor & Francis
83. Van Liedekerke M et al (2014) *Progress in the management of contaminated sites in Europe*. EUR 26376. Publications Office of the European Union, Luxembourg, p 68
84. Selvi A et al (2019) Integrated remediation processes toward heavy metal removal/recovery from various environments-a review. *Front Environ Sci* 7:66
85. Bashir S et al (2018) Cadmium immobilization potential of rice straw-derived biochar, zeolite and rock phosphate: extraction techniques and adsorption mechanism. *Bull Environ Contam Toxicol* 100(5):727–732
86. Lahori AH et al (2017) Use of biochar as an amendment for remediation of heavy metal-contaminated soils: prospects and challenges. *Pedosphere* 27(6):991–1014
87. He L et al (2019) Remediation of heavy metal contaminated soils by biochar: mechanisms, potential risks and applications in China. *Environ Pollut* 252:846–855
88. Adnan M et al (2020) Coupling phosphate-solubilizing bacteria with phosphorus supplements improve maize phosphorus acquisition and growth under lime induced salinity stress. *Plan Theory* 9(7):900
89. Choudhary V et al (2020) Batch and continuous fixed-bed Lead removal using Himalayan pine needle biochar: isotherm and kinetic studies. *ACS Omega* 5(27):16366–16378
90. Yrjälä K, Lopez-Echartea E (2021) Structure and function of biochar in remediation and as carrier of microbes. In: Sarmah AK (ed) *Biochar: fundamentals and applications in environmental science and remediation technologies*. Elsevier
91. Chen Y et al (2021) Remediation of chromium-contaminated soil based on bacillus cereus WHX-1 immobilized on biochar: Cr(VI) transformation and functional microbial enrichment. *Front Microbiol* 12(408):641913
92. Tu C et al (2020) Biochar and bacteria inoculated biochar enhanced Cd and Cu immobilization and enzymatic activity in a polluted soil. *Environ Int* 137:105576
93. Alaboudi KA, Ahmed B, Brodie G (2019) Effect of biochar on Pb, Cd and Cr availability and maize growth in artificial contaminated soil. *Ann Agric Sci* 64(1):95–102

94. Kiran BR, Prasad MNV (2019) Biochar and rice husk ash assisted phytoremediation potentials of *Ricinus communis* L. for lead-spiked soils. *Ecotoxicol Environ Saf* 183:109574
95. Gong X et al (2019) Biochar facilitated the phytoremediation of cadmium contaminated sediments: metal behavior, plant toxicity, and microbial activity. *Sci Total Environ* 666: 1126–1133
96. Edenborn S et al (2015) Influence of biochar application methods on the phytostabilization of a hydrophobic soil contaminated with lead and acid tar. *J Environ Manag* 150:226–234
97. Chuaphasuk C, Prapagdee B (2019) Effects of biochar-immobilized bacteria on phytoremediation of cadmium-polluted soil. *Environ Sci Pollut Res* 26(23):23679–23688
98. Abbas S et al (2021) Chapter 30 - alteration of plant physiology by the application of biochar for remediation of organic pollutants. In: Hasanuzzaman M, Prasad MNV (eds) *Handbook of bioremediation*. Academic Press, pp 475–492
99. Huang S et al (2020) Engineered biochar derived from food waste digestate for activation of peroxymonosulfate to remove organic pollutants. *Waste Manag* 107:211–218
100. Kumar NS et al (2021) Engineered biochar from wood apple shell waste for high-efficient removal of toxic phenolic compounds in wastewater. *Sci Rep* 11(1):2586
101. Zhang Y et al (2019) Synthesis of porous Fe/C bio-char adsorbent for rhodamine B from waste wood: characterization, kinetics and thermodynamics. *PRO* 7(3):150
102. Liu J et al (2020) Activation of persulfate with biochar for degradation of bisphenol A in soil. *Chem Eng J* 381:122637
103. Wu C et al (2019) Sorption, degradation and bioavailability of oxyfluorfen in biochar-amended soils. *Sci Total Environ* 658:87–94
104. Huang H et al (2018) Effects of biochar amendment on the sorption and degradation of atrazine in different soils. *Soil Sediment Contam Int J* 27(8):643–657
105. Cipullo S et al (2019) Linking bioavailability and toxicity changes of complex chemicals mixture to support decision making for remediation endpoint of contaminated soils. *Sci Total Environ* 650(Pt 2):2150–2163
106. Hussain F et al (2021) Soil conditioners improve rhizodegradation of aged petroleum hydrocarbons and enhance the growth of *Lolium multiflorum*. *Environ Sci Pollut Res*. <https://doi.org/10.1007/s11356-021-16149-7>
107. Gascó G et al (2018) Biochars and hydrochars prepared by pyrolysis and hydrothermal carbonisation of pig manure. *Waste Manag* 79:395–403
108. Ndoun MC et al (2021) Adsorption of pharmaceuticals from aqueous solutions using biochar derived from cotton gin waste and guayule bagasse. *Biochar* 3(1):89–104
109. Silvani L et al (2019) Can biochar and designer biochar be used to remediate per- and polyfluorinated alkyl substances (PFAS) and lead and antimony contaminated soils? *Sci Total Environ* 694:133693
110. Yavari S et al (2017) Synthesis optimization of oil palm empty fruit bunch and rice husk biochars for removal of imazapic and imazapyr herbicides. *J Environ Manag* 193:201–210
111. Bielská L et al (2018) Sorption, bioavailability and ecotoxic effects of hydrophobic organic compounds in biochar amended soils. *Sci Total Environ* 624:78–86
112. Wang Y et al (2017) Remediation of petroleum-contaminated soil using bulrush straw powder, biochar and nutrients. *Bull Environ Contam Toxicol* 98(5):690–697
113. Cao Y et al (2016) Wheat straw biochar amendments on the removal of polycyclic aromatic hydrocarbons (PAHs) in contaminated soil. *Ecotoxicol Environ Saf* 130:248–255
114. Tsai W-T (2021) Carbon-negative policies by reusing waste wood as material and energy resources for mitigating greenhouse gas emissions in Taiwan. *Atmos* 12(9):1220
115. Hagemann N et al (2020) Wood-based activated biochar to eliminate organic micropollutants from biologically treated wastewater. *Sci Total Environ* 730:138417
116. Official Statistics of Finland (OSF) (2018) Waste statistics [e-publication]. Appendix table 1. Waste generation by industry, 2018, 1,000 tonnes
117. Official Statistics of Finland (OSF) (2018) Waste statistics [e-publication]. Appendix table 2. Waste treatment in 2018, 1,000 tonnes

118. Ma Y et al (2019) The global warming potential of straw-return can be reduced by application of straw-decomposing microbial inoculants and biochar in rice-wheat production systems. *Environ Pollut* 252(Pt A):835–845
119. Shen H et al (2020) Intense warming will significantly increase cropland ammonia volatilization threatening food security and ecosystem health. *One Earth* 3:126–134
120. Yargicoglu EN et al (2015) Physical and chemical characterization of waste wood derived biochars. *Waste Manag* 36:256–268
121. Tammeorg P et al (2021) Co-designing urban carbon sink parks: case carbon lane in Helsinki. *Front Environ Sci* 9:672468
122. Antonangelo JA, Sun X, Zhang H (2021) The roles of co-composted biochar (COMBI) in improving soil quality, crop productivity, and toxic metal amelioration. *J Environ Manag* 277: 111443
123. Sanchez-Monedero MA et al (2018) Role of biochar as an additive in organic waste composting. *Bioresour Technol* 247:1155–1164
124. Guo X-X, Liu H-T, Zhang J (2020) The role of biochar in organic waste composting and soil improvement: a review. *Waste Manag* 102:884–899
125. Bong CPC et al (2021) Integrating compost and biochar towards sustainable soil management. *Chem Eng Trans* 86:1345–1350
126. Schmidt H-P et al (2019) The use of biochar in animal feeding. *PeerJ* 7:e7373
127. Redling A (2019) Why producing biochar from wood is more viable than ever for C&D recyclers. In: *Construction & Demolition Recycling*
128. O'Toole A et al (2016) Current and future applications for biochar. In: *Biochar in European soils and agriculture*. Routledge, pp 275–302
129. Akhtar A, Sarmah AK (2018) Novel biochar-concrete composites: manufacturing, characterization and evaluation of the mechanical properties. *Sci Total Environ* 616–617:408–416
130. Cuthbertson D et al (2019) Biochar from residual biomass as a concrete filler for improved thermal and acoustic properties. *Biomass Bioenergy* 120:77–83
131. Gupta S, Kua HW, Pang SD (2020) Effect of biochar on mechanical and permeability properties of concrete exposed to elevated temperature. *Constr Build Mater* 234:117338

Graphene Oxide for Elimination of Dyes



Ling Sun and Bunshi Fugetsu

Contents

1	Introduction	394
1.1	Water Pollution	394
1.2	Adsorbent from Macro Through Micro to Nano	396
1.3	Nano Planar Carbon Adsorbent	398
2	Synthesis of Graphene Oxide	399
2.1	From Pristine Graphite	399
2.2	From Graphite with Expanded Structure	401
3	Frequently-Used Process Theories for Adsorption on Graphene Oxide	402
3.1	Isotherms	402
3.2	Kinetics	404
3.3	Route Models of Adsorption	405
4	Dye Removal by Pristine GO	406
4.1	SER Adsorption	406
4.2	MER Adsorption	410
5	Dye Adsorption by Modified GO	411
5.1	Via Surface Functionalization	412
5.2	Via Immobilization	414
6	Conclusion and Outlook	416
	References	418

Abstract Organic pollution such as dyes is unignorable to hazard the livings. To decontamination, high-performance adsorption is the priority due to the cost-effectiveness and widely-available adsorbents. Instead of commonly-seen activated carbon (AC), novel carbon nanomaterials are these years under the spotlight and still being abundantly researched. This chapter put the eyes on graphene oxide (GO), a

L. Sun (✉)
Beijing University of Technology, Beijing, China

Beijing Guyue New Materials Research Institute, Beijing, China
e-mail: sunling@bjut.edu.cn

B. Fugetsu
Policy Alternative Research Institute, The University of Tokyo, Tokyo, Japan

derivative of the Wonder-material graphene, as the emerging nanoscopic two-dimension carbon adsorbent for the application to eliminating cationic or anodic dyes from the aqueous phase. In the introduction, two key factors influencing an adsorbent's performance are briefly profiled as the spatial dimension of adsorbent varies less from AC to GO. The comparative advantages of such a two-dimension GO adsorbent are then pointed out, for which to mass prepare GO turns out to be much desirable. In the second part, typical ways are summarized, and significant attention is drawn to identify the differences if GOs are made from two different graphites as the starting materials. In the third, typically-used theories are collected to study the isotherms and kinetic specifically in GO cases. Besides, route-dependent adsorption models of GO are proposed, which necessarily help understand the following consecutive parts. The fourth part focuses on dye eliminations from water using pristine GO as an adsorbent, while the fifth part leaves on the modified GO. The conclusion and outlook are also integrated in terms of GO as the high-performance dye pollutant carrier in water remediation in the last part.

Keywords Dye removal, Enhanced adsorption, Graphene oxide, In situ reduction, Multiple-equilibrium route (MER), Nanocarbon adsorbent

1 Introduction

1.1 Water Pollution

Forty percent of freshwater resources shortage by 2030 amid a rising world population has the world trapped in a global water crisis, unveiled by the Water Action Decade 2018–2028. Over 80% of wastewater generated by human activities remains discharged untreated into water bodies (www.un.org/sustainabledevelopment/zh/water-and-sanitation/). Unprecedented urbanization, product innovation, increasing industrialization, and exponential growth of the online fashion sector are in trend accompanying extensive use of dyestuffs comprising several types, like Vat dye, Reactive dye, Basic dye, Acid dye, and Disperse dye [1]. Production of dyes goes up to ~2 million tons per year worldwide, and approximately 15% of dye wastes after dyeing are being released into the environment [2].

Besides, wastewater containing the dyes is mostly refractory, featuring a high organic matter concentration, high chroma, serious demulsification, and small quantity, but high pollution intensity. A substandard discharge has a severe impact on the environment and poses a significant threat to human health. Typically, as a nucleic acid selective fluorescent weakly basic dye, acridine orange (AO, 3,6-Bis(dimethylamino) acridine) is often used to probe DNA structure in drug–DNA and protein–DNA interactions, together with another cell-stain basic dye methylene blue [3–5]. On the one hand, it can provide specific fluorescent tumor labeling for photo diagnostics and viable cell count as a vital strain of bacteria [5, 6]. On the other, as mentioned above, AO intercalates the DNA base pairs and can cause gene coding

mutation, which was regarded as a potential carcinogen for human beings. Once it leaks out into the environment and gets live-beings being touched, such dye has already historically evidenced its potentially detrimental health effects dating back to the late 1960s [5, 7]. From an environmental perspective, developing an effective method for the complete removal of dyes of such kind from wastewater is urgently demanded.

Given the simplicity of design, availability, and ease of operation, adsorption has been preferred over other techniques, such as coagulation, flocculation, and biological [2, 8, 9]. Adsorption defines the process that some of the components separate from the fluid/liquid phase onto the surface of the adsorbent, consisting of both the external and internal. This process typically comprises two steps. Initially, molecules/ions approach the external surface of the adsorbent. After a while, an internally diffusive transfer occurs so that substances could penetrate the depth of the adsorbent, that is, to the interior surfaces. The process ends up with the formation of an equilibrium adsorptive layer on the surface of active pores. Adsorption is then a fast and relatively cost-effective technology for water treatment [9, 10].

The occurrence of adsorption often refers to physical and/or chemical mechanisms (Fig. 1) [2]. In the physical adsorption, target molecules/ions bind to the walls of adsorbents by the Van der Waals force, consuming a low adsorption heat. Adsorbent traits, including the surface area, and pore size, would play critical roles. In the chemical, the target pollutant attaches to specific sites of the adsorbent via a chemical covalent reaction. Much more heat is consumed than that of physical adsorption and is nearly equivalent to the reaction heat. Furthermore, such a process is hardly reversible, and the materials thereof unlikely recyclable.

In the past few decades, carbon materials have been widely used, beneficial from their flexible porous structures as physically functioning sites and surface functionalities as chemically functioning sites. Research in this field is still stepping forwards [2, 9, 11]. And the dimension of materials has evolved from macroscopic such as activated carbon (AC) to nano-size such as graphene oxide (GO). With the surface characters altering much, this evolvement has significantly advanced high-performance adsorption.

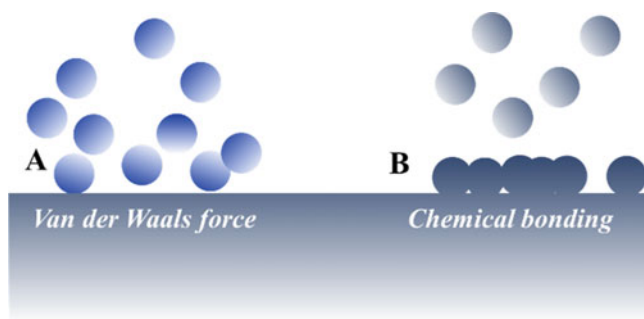


Fig. 1 Types of adsorption. (a) Van der Waals force-guided physical adsorption. (b) Chemical mechanism

1.2 *Adsorbent from Macro Through Micro to Nano*

Nowadays, AC is the typically commonly-used adsorbent. Many materials are used as the starting materials for industrially scalable AC production, including coal, oil pitch, and coconut shell. They are transformed to AC to form the desired porosity after sequentially going through physiochemical processing, mainly including carbonization and activation. More recently, much research is still ongoing with the utilization of the agricultural waste biomass as the starting, such as sunflower piths [12], rice husk [13], and crop straws [14, 15]. Therefore, AC turns out to be relatively cost-effective.

Since the physical dimension of commercial AC, namely the particle size, is of the magnitude of up to tens of millimeters or higher, AC is conventionally regarded as typically macro-sized. Notably, inside the particles, tens of thousands of macro/micro-sized channels or pores contribute to the considerable functioning area and large oxygen-containing functional groups attached to internal surfaces during the processing, as mentioned above. It is these traits that help build the interactions between the adsorbate molecules or ions. With the merits of extensive surface area nature and relative cost-effectiveness, such a macro-sized carbon adsorbent has succeeded in playing an essential role for centuries for water purification or decontamination [14–17].

1.2.1 **Surface Area**

The influence of surface area as one key factor matters much to the decontaminative performances of AC. Take the removal of methylene blue dye from water as examples. André L. Cazetta et al. [18] synthesized three ACs (250–450 μm) from coconut husk through a 200°C hydrothermal carbonization and NaOH chemical activation process (respective mass ratio of NaOH/waste-derived Char = 1/1, 2/1, 3/1, activation at 700°C for 1.5 h). The corresponding surface area had the order from 783, 1,842 to 2,825 $\text{m}^2 \text{g}^{-1}$, and the maximum adsorption capacity at 30°C was up to 916 mg/g . Contrastly, Md. Azharul Islam et al. [19] modified the above strategy (NaOH/waste-derived Char = 3/1) with a lower activation temperature at 600°C and a shorter time of 1 h. As-formed AC (1,000–2,000 μm) produced a surface area of up to 876.14 $\text{m}^2 \text{g}^{-1}$, and correspondingly the capacity fell to 200.01 mg g^{-1} , much lower than that of the group above.

With further modifications, I.A.W. Tan et al. [20] used KOH as the activated agent together with a higher temperature of 850°C but setting the mass ratio of KOH to char 1/1. The surface area of AC (1,000–2,000 μm) reached 1,940 $\text{m}^2 \text{g}^{-1}$ higher than that of Islam. As a consequence, the capacity was improved to 434.78 mg g^{-1} . With the comparison, the larger the surface area it is for the AC, the higher value for the adsorptive capacity. From this perspective, adsorbents titled with higher surface area values become in general much more desirable. In practice, such adsorbent production cost is often of several magnitudes higher than that regular carbon

product with the specific area only tens of to hundreds of square meters per gram. This point, to some extent, has limited AC in high-performance water-related applications.

1.2.2 Interfacial Functionalities

Another critical factor comes to the functionalities that are randomly located at the surface of an adsorbent. For macro-sized AC, on the surfaces of its carbon backbone usually hold only a few numbers of oxygenated or hydrogenated carbon groups [21] such as C–H, C–OH, C=O, and C–O–C, O=C–OH, all of which possibly function as chemically reactive sites to target dye pollutants, in any case. Therefore, most AC intrinsically behaves in somewhat hydrophobicity and especially poor adsorptive selectivity, which adversely affects the adsorption [22]. From this point of view, it is desirable to modify carbon surface to enhance its affinity with target pollutants using some physical (e.g., entrapment), chemical (e.g., surfactant grafting, acid soak), or biological (e.g., bacteria immobilization) methods.

Lin et al. [23] prepared calcium-crosslinked alginate-entrapped AC gel beads specifically targeting the positively-charged and neutral compounds, while the ferric beads for the negatively charged, thus highlighting highly selective adsorption. Both can be attributed to the bead surfaces electrocharged during the activation carbon entrapment, which resulted in the foreign ions/molecules partly entering insides onto carbon surfaces. Kuang et al. [22] investigated the adsorption by anionic or cationic surfactant-modified AC to remove methylene blue. The significantly improved adsorption performance by anionic surfactant-modified AC, whereas the cationic surfactant-modified AC suffered a reduction. For biological, Sun et al. [24] immobilized a strain of bacteria onto the surface of commercially available activated carbon to form nitrobenzene-targeted biocarbon. It demonstrated that compared to the bare carbon with no recyclability, the biocarbon became capable of recyclable use and, most importantly, decomposing nitrobenzene with a concentration of up to 600 ppm, practically available in river water remediation. However, it is also true that chemical modification could produce an adverse effect on adsorption. Wang et al. [16] treated coal-derived carbons by covering them in the HCl or HNO₃ solution. As-modified carbons failed to enhance the adsorption of methylene blue due to the surface loss of hydroxyl groups and the formation of acidic functional groups, although both of them were increased in surface area.

Both surface area and functionality have played essential roles in a satisfactory performance for the macroscopic AC, whereas its production and regeneration remain rather expensive. AC is not primarily used to remove pollutants in water because of its widely-known low adsorption capacity [22, 25]. As such, adsorbents in micro or nano sizes featuring the structure (Fig. 2) of high surface area and a wide variety of functionalities have been gradually recognized as emergent high-performance decontaminants.

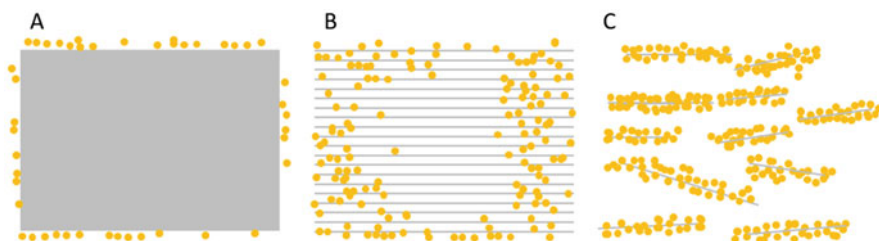


Fig. 2 Influence of structure over adsorption (Yellow: Adsorbate ions/molecules; Gray: Adsorbent). Adsorbents vary with structures in the forms of (a) solid bulk, (b) macro-sized porous bulk containing inner pores or channels or spaced layers (e.g., ac), and (c) micro/nanosized 2D sheets (e.g., graphene or GO) or 1D tubes (e.g., carbon nanotube)

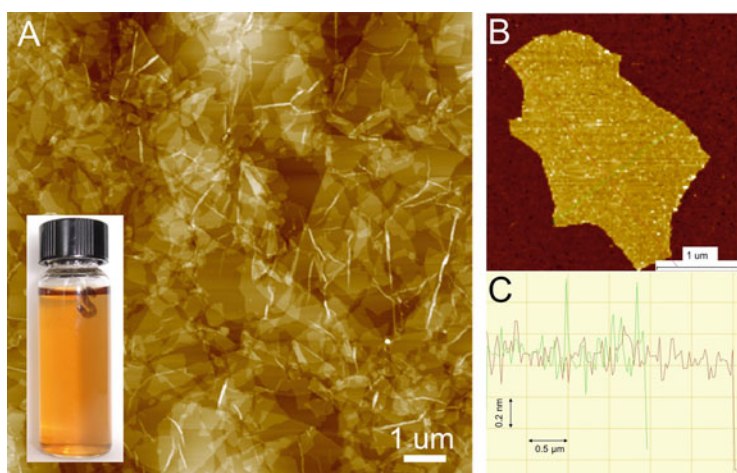


Fig. 3 Characterization of GO. (a) Atomic Force Microscopic (AFM) image of graphene air-dried film made from the solution (inset); (b) AFM image of GO sheet with lateral dimensions of about several micrometers and a thickness of one nanometer; (c) a cross-sectional profile, respectively, corresponding to the lines drawn in the image (b), showing the sheet lateral and vertical sizes calculated from either trace or retrace modes

1.3 Nano Planar Carbon Adsorbent

It is ubiquitous that with sizes changing from macroscopic to microscopic, the surface area of a particle is exponentially increased, consequently accompanying the structure-dependent variation of adsorbing amount as illustrated in Fig. 2. This law also suits the selection of high-performance carbon-sourced adsorbent.

GO (Fig. 3) is regarded as a chemical compound with a non-stoichiometric ratio of carbon, oxygen, and hydrogen, which correlates to production techniques. Resembling graphene, it also features a carbon skeleton network yet combining extra lots of oxygen functional groups such as epoxide groups (bridging oxygen

atoms), carbonyl (C=O), phenol, hydroxyl (-OH), and even organosulfate groups (impurity of sulfur) during the exfoliation of graphite [26].

Contrary to AC, GO is one to several atoms nano thick, firstly showing more surface area. Secondly, both sides of GO exposed outside stand many oxygen-containing functionalities, much more than activated carbon, rendering itself with high hydrophilicity and molecule-like dispersibility in water. Most importantly, GO is scalably made from cheap graphites such as flake graphite, microcrystalline graphite, and expandable graphite [26]. Therefore, research around such an emerging nano adsorbent has undergone an explosion, especially after 2010 its reductive analog graphene being awarded [27–29].

2 Synthesis of Graphene Oxide

Graphite-originated GO has become the most prevalent across the scientific community. Graphite treated with intercalation and oxidation and exfoliation in the sequence (Fig. 4) has been the central methodology for decades [30]. Two typical graphites are commercially available, flake graphite (Fig. 4a) and expanded graphite (Fig. 4b). The former highlights the structure consisting of Van der Waals forces-driven stacked graphene sheets, while for the latter, its internal graphene sheets have already been processed to become somewhat chemically space-loosened and even size-reduced.

2.1 From Pristine Graphite

Pristine graphite has been widely used as the starting material for converting to GO (the vast majority in Table 1) [28]. The most prevalent method refers to the “water-free” synthesis ever proposed by Hummers and Offeman in 1958, who at the earliest introduced concentrated sulfuric acid, potassium nitrate, and potassium

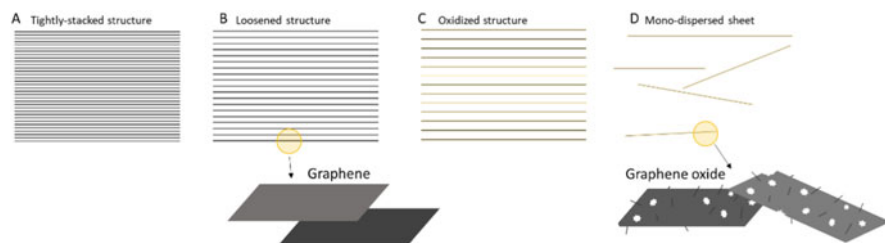


Fig. 4 The top-down method from graphite to GO: (a) Pristine graphite with a tightly stacked structure; (b) Intercalated graphite having loosened structure by alien molecule or ions; (c) Intermediate graphite being further expanded and oxidized; (d) Water-dispersed exfoliated GO sheets

Table 1 Methods to the preparation of GO

Year	First Author	Materials	Reagents	Reaction	Temperature
1859	Brodie [30]	Graphite	KClO ₃ , HNO ₃	3–4 days	60°C
1898	Staudenmaier [31]	Graphite	KClO ₃ , HNO ₃ , H ₂ SO ₄	4 days	RT
1958	Hummers [32]	Graphite ~44 μm	KMnO ₄ , NaNO ₃ , H ₂ SO ₄	2 h	20–35–98°C
2005	Fu [33]	Graphite	KMnO ₄ , H ₂ SO ₄	2 h	35°C
2009	Su [34]	Graphite <3,000 μm	KMnO ₄ , H ₂ SO ₄	4 h	RT
2010	Marcano [35]	Graphite ~150 μm	H ₂ SO ₄ , H ₃ PO ₄ , KMnO ₄	12 h	50°C
2011	Huang [36]	Graphite	H ₂ SO ₄ , H ₃ PO ₄ , KMnO ₄	3 days	RT
2013	Eigler [37]	Graphite ~300 μm	KMnO ₄ , NaNO ₃ , H ₂ SO ₄	16 h	10°C
2015	Chen [38]	Graphite 3-20 μm	KMnO ₄ , H ₂ SO ₄	1 h	20–40–95°C
2015	Panwar [39]	Graphite	H ₂ SO ₄ , H ₃ PO ₄ , KMnO ₄ , HNO ₃	3 h	50 °C
2015	Peng [40]	Graphite >10 μm	K ₂ FeO ₄ , H ₂ SO ₄	1 h	RT
2016	Yu [41]	Graphite ~44 μm	K ₂ FeO ₄ , KMnO ₄ , H ₂ SO ₄ , H ₃ BO ₃	5 h	5–35–95°C
2016	Dimiev [42]	Graphite	(NH ₄) ₂ S ₂ O ₈ , 98% H ₂ SO ₄ , fuming H ₂ SO ₄	3–4 h	RT
2018	Ranjan [43]	Graphite	H ₂ SO ₄ , H ₃ PO ₄ , KMnO ₄	>24 h	RT-35–95°C
2013	Sun [44]	Expanded graphite	KMnO ₄ , H ₂ SO ₄	1.5 h	RT-90°C

permanganate to treat graphite of 325 mesh [32]. It remarkably improved the synthesis efficiency and safety compared to the earlier methods [30, 31]. More measures were also studied and adopted, such as eliminating NaNO₃ [33] and alternating the oxidants [40, 41]. However, they still have to face such a procedure simultaneously that may have something to do with a long reaction even up to days, and large consumption of strong acid [32, 33, 35, 37, 42, 43] or mysterious instability of acids [40], implying high tediousness and risk, though readiness. As such, the cons also include costly post purification and disposal of used acids [28]. Therefore, it necessitates turning back to alter the starting material better on large-scale GO production for environmental use.

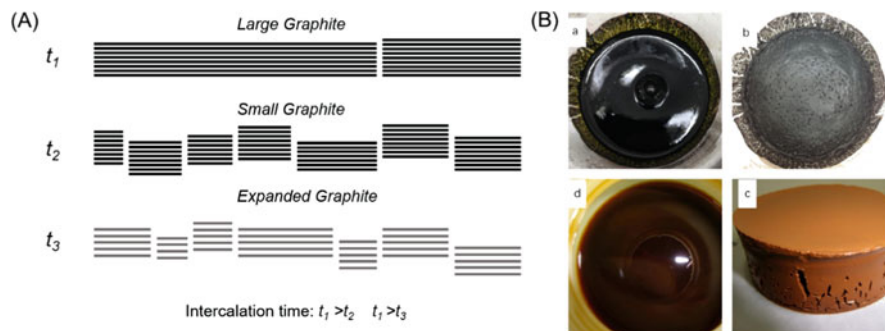


Fig. 5 Influence of expanded graphite on the preparation of GO. (A) conceptualization of intercalation of graphite varying at size and structure: graphite of varying sizes and textures undergoing oxidation will result in different lengths of time: large graphite particles have longer intercalation than the smaller ones in the same context, and also the tight structure also takes longer time over the loosened structure; (B) brief imagination of the procedure with expanded graphite as the starting material: (a) an ice-bath mixing of the raw expanded graphite with chemicals, (b) room temperature expansion of graphite resulted from the intercalation and simultaneous oxidation, (c) high-temperature hydrolysis and exfoliation, resulting in a homogeneous “GO cake,” (d) a purified concentrated GO solution in dark brown. Reproduced from Ref. [28, 44] with permission from Elsevier

2.2 From Graphite with Expanded Structure

In addition to tightly stacked graphite, there comes the expanded graphite (EG) as the alternative. EG features its pre-expanded structure and relatively confined sizes. EG has also been comparatively cheap for the development of GO-based adsorbent. As shown in Figs. 5A and 6, EG at a suitable size range favors a fast and distinctly volumetric expansion as the reaction goes, and the water addition without fearing the dangerous explosion, and the less use of acids (10 mL vs. 13 mL of sulfuric acid per gram of graphite before) [28]. Simultaneously, during the process, a fast macroscopic change would occur with the formation of a “form-like intermediate.” With this transformation as an indicator, the preparation from EG turned out to be with a high conversion efficiency of nearly 100% (Fig. 5B) and procedural safety [44]. This method demonstrated suitable suitability for scaleup due to the entire-process simplicity as compared to those previously published. Holding these findings, Sun and Fugetsu [44] investigated the EG-based massive GO production with methodological modifications (Fig. 6).

It is of note that a complete exfoliation of EG into single dispersed oxidized sheets was easily accomplished without alien mechanical forces of extremes, such as hours of sonication or milling, which may affect the size. As-obtained GO sheets could furthest maintain the sizes as the initial graphite crystals have [45]. The merit is unique and meaningful to obtain subsequent EG-derived size-specific GO. Hu et al. found that with EG as starting material, the GO could be exfoliated out quickly, even having higher-degree oxidation and better hydrophilicity [26]. On the contrary, for

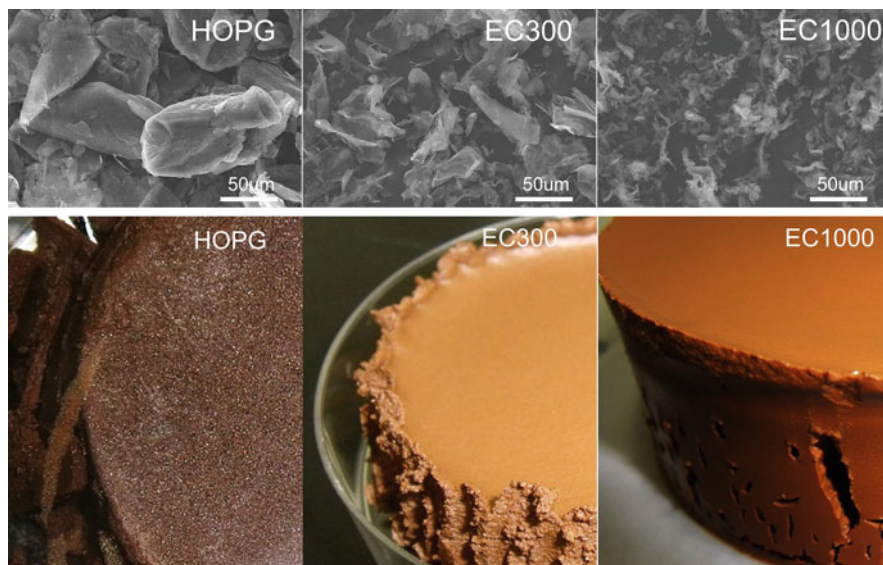


Fig. 6 Various graphite resources and corresponding GO cakes. (HOPG) graphite flake. Its GO cake was the smallest among all, and the color is the darkest, indicative of a low oxidation degree, (EC300) expanded graphite with a median diameter $\sim 50 \mu\text{m}$. Coarse particles were included homogeneously in the cake with a light-yellow color, indicative of suffering heavy oxidation but insufficient intercalation; (EC1000) expanded graphite with a median diameter $\sim 15 \mu\text{m}$. The cake with the most enormous volume and the lightest color was observed, demonstrating the occurrence of full interaction and oxidation. Reproduced from Ref. [44] with permission from Elsevier

the conventional graphite, this result takes place to some extent if the oxidation procedure is extended long enough [35, 36] or with an amplified oxidants dosages [35].

Furthermore, it is worth pointing out that a small number of defects [44] (functionalities, vacancies) are unavoidable for the EG due to the industrial chemical procedure. However, they could play a positive role in promoting GO formation, e.g., by attracting many more charged radicals outside-in. With these merits, 2D nanocarbon adsorbents from EG render GO with great water remediation promise.

3 Frequently-Used Process Theories for Adsorption on Graphene Oxide

3.1 Isotherms

Isotherm studies are common applied to describe the extent of interaction between adsorbent and adsorbate in adsorption because they bring meaningful insights into

Table 2 Typical isotherms and kinetics for adsorptions

	Type	Equation	Linearized form
Isotherm	Langmuir	$q_e = \frac{q_m K_L C_e}{1 + K_L C_e}$	$\frac{1}{q_e} = \frac{1}{q_m} + \frac{1}{q_m K_L C_e}$
	Freundlich	$q_e = K_F (C_e)^{1/n}$	$\ln q_e = \ln K_F + \frac{1}{n} \ln C_e$
	Temkin	$q_e = \frac{RT}{b_T} \ln A_T + \frac{RT}{b_T} \ln C_e$	–
	Redlich–Peterson (R-P)	$q_e = \frac{a_R C_e}{1 + b_R C_e}$	$\ln \left(\frac{a_R C_e}{q_e} - 1 \right) = \ln b_R + g \ln C_e$
	Brunauer–Emmett–Teller (BET)	$q_e = \frac{q_m K_b C_e}{(C_s - C_e) [1 + (K_b - 1) \frac{C_e}{C_s}]}$	$\frac{C_e}{(C_s - C_e) q_e} = \frac{1}{K_b q_m} + \frac{(K_b - 1) C_e}{q_m K_b C_s}$
Kinetics	Pseudo-first-order	$q_t = q_e (1 - e^{-K_1 t})$	$\ln(q_e - q_t) = \ln q_e - K_1 t$
	Pseudo-second-order	$q_t = \frac{k_2 q_e^2 t}{1 + K_2 q_e t}$	$\frac{t}{q_t} = \frac{1}{K_2 q_e} + \frac{1}{q_e} t$
	Weber–Morris	$q_t = K_{int} t^{0.5} + C$	–
	Elovich	$q_t = K'' \ln(K' K'') + K'' \ln t$	–

Note

R is the gas constant, $\sim 8.314 \text{ J mol}^{-1} \text{ K}^{-1}$

T is the working temperature, unit by Kelvin

q_m is the maximum amount per gram adsorbent of adsorption, (mg g^{-1})

q_e is the adsorptive capacity per gram adsorbent at equilibrium time, (mg g^{-1})

q_t is the adsorptive capacity at the time t , (mg g^{-1})

C_e is the equilibrium concentration at the time t , (mg L^{-1})

K_L is the Langmuir equilibrium constant, (L mg^{-1})

$K_F (\text{mg}^{1-1/n} \text{ L}^{1/n} \text{ g}^{-1})$ is the Freundlich distribution coefficient, equivalent to $q_m' A$, where A is preexponential coverage coefficient, q_m' is the characteristic adsorption capacity [63]

n , is a dimensionless correction factor, if $0.1 < 1/n \leq 0.5$, easy to adsorb; $0.5 < 1/n \leq 1$, some difficult going on with the absorption; $1/n > 1$, quite difficult to adsorb

A_T is the Temkin isotherm equilibrium binding constant (mL g^{-1})

b_T is the Temkin isotherm constant

$a_R (\text{L mg}^{-1}), b_R$ and g are the Redlich–Peterson equation empirical coefficients [55]

K_b is a constant expressive of the energy of interaction with the surface

C_s is the saturation concentration of adsorbate or solute, (mg L^{-1}) [53]

K_1 is the first-order rate constant (h^{-1})

K_2 is the rate constant of pseudo-second-order, ($\text{g mg}^{-1} \text{ h}^{-1}$)

K_{int} is the pore diffusion rate constant, ($\text{mg g}^{-1} \text{ h}^{-0.5}$)

C relates to the thickness of the boundary [62]

K' is the initial adsorption rate ($\text{mg g}^{-1} \text{ h}^{-1}$)

K'' is the desorption constant (mg g^{-1})

the adsorption mechanism, surface properties, and the affinity of an adsorbent. To this end, it is essential to establish a reasonable correlation reflecting the interaction. Form the equilibrium profiling, isotherms can be built up and further modeled by the Langmuir model, Freundlich model, Brunauer–Emmett–Teller model, and Temkin model. All equations in the integrated and linearized forms are listed in Table 2.

The Langmuir model has been the most utilized isothermal equation in practical applications since introduced about 90 years ago [46]. This model relies on several hypothesized bases: monolayer adsorption, dynamic balance, no interaction between

sorbate entities, and every adsorption site with the same adsorptive power [47, 48] in other words, it can be valid only for monolayer adsorption onto a surface with a finite number of identical sites. To date, the Langmuir isotherm has been successfully applied to a large number of pollutant adsorptions.

The Freundlich model is one other widely used equation originating from the description of gas-phase adsorption and solute adsorption [49]. It is an empirical expression encompassing the surface heterogeneity and the exponential distribution of active sites and their energies. This model predicts infinite surface coverage without any saturation of the adsorbent surface, and therefore, it depicts physisorption on the surface [48].

The Temkin model introduces a factor by explicitly taking into account indirect adsorbent–adsorbate interactions. Its derivation assumes the decrease of adsorption heat of molecules or micro-entities in the layer is linearized with coverage, other than logarithmic as implied from the Freundlich equation [50, 51].

The Brunauer–Emmett–Teller (BET) model is based on the assumption of multilayer adsorption, of which each layer follows the Langmuir model [52, 53]. This model allows exterior layers can be initiated even before an interior layer is completely formed [53].

The Redlich–Peterson (R-P) model characters three parameters and combines the Langmuir and Freundlich isotherms features, implying a hybrid mechanism. The equation has a linear dependence on concentration in the numerator and an exponential function in the denominator [50, 54, 55].

3.2 Kinetics

It is crucial to predict kinetical behavior necessary for consequent column design of batch adsorption. However, due to the inseparable effects of transport phenomena and chemical reactions, it often produces incredible bias to describe adsorption kinetics with simple first- or second-order rate equations, especially involving rarely homogeneous solid surfaces [56].

So mechanisms are more frequently used, including typical pseudo-first-order equation (PFO), pseudo-second-order equation (PSO), Weber–Morris equation, and Elovich equation (Table 2).

The PFO model [57] describes the adsorption between the liquid and solid phases based on the assumption that the rate is proportional to the number of unoccupied adsorptive sites of the solid. In contrast, the PSO model assumes that the rate is proportional to the square of the available number of adsorptive sites [48, 58–60].

Adsorption by using a porous adsorbent usually comprises three sequential steps: (1) film diffusion, where adsorbate molecules migrate from the boundary film to the external surface of the adsorbent; (2) intraparticle diffusion, where these molecules travel within the pores; (3) site adsorption on the surface. Among all, the slowest step holds back the overall rate of adsorption. The Weber–Morris model, also known as

the intraparticle diffusion equation, describes mass transport of adsorbate from a liquid phase to a solid phase [59].

The Elovich model assumes that the adsorption rate decreases with time due to decreasing of unoccupied sites. It is usually used to describe the adsorption process at a fast rate, especially in chemisorption [61, 62].

3.3 Route Models of Adsorption

Adsorption could be conducted through two routes, as illustrated in Fig. 7. Always, the single-equilibrium route (SER, Fig. 7A) is adopted using only an adsorbent. The multiple-equilibrium route (MER, Fig. 7B) is worthy of notice, which intrinsically performed with high removal efficiency ascribed to more equilibriums occurring along with additional characteristic variations of the adsorbent such as alteration of surface groups and vacancies.

Specific to GO, it has a large number of different functionalities (Fig. 8a) except for the large surface area, especially for the EG-derived GO as discussed above. Nevertheless, all these functionalities hardly function as enabling sites at one time toward a specific contaminant dye. Some of the functionalities would devote primarily to the first equilibrium with higher reactivity, while some remain unused as “inert sites” (Fig. 8b). If some measures such as chemical redox are adopted to activate these functionalities in the course of adsorption, additional active sites will be formed and become instantly available to use without severe structural deformation (Fig. 8c). Then, the adsorption will advance to the second equilibrium (Fig. 8c) and end up with better decontamination than that with one equilibrium.

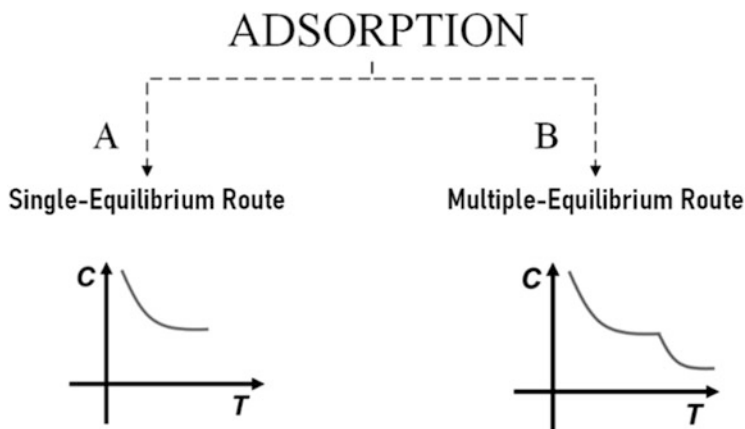


Fig. 7 Route models of adsorption. (A) Single-equilibrium route (SER): adsorbent functions directly with the adsorbate, reflected by the concentration falling to reach an equilibrium as depicted from the time (T)-residual concentration (C) curve; (B) Multiple-equilibrium route (MER): adsorbent functions via multiple equilibriums to best approach its removal efficiency

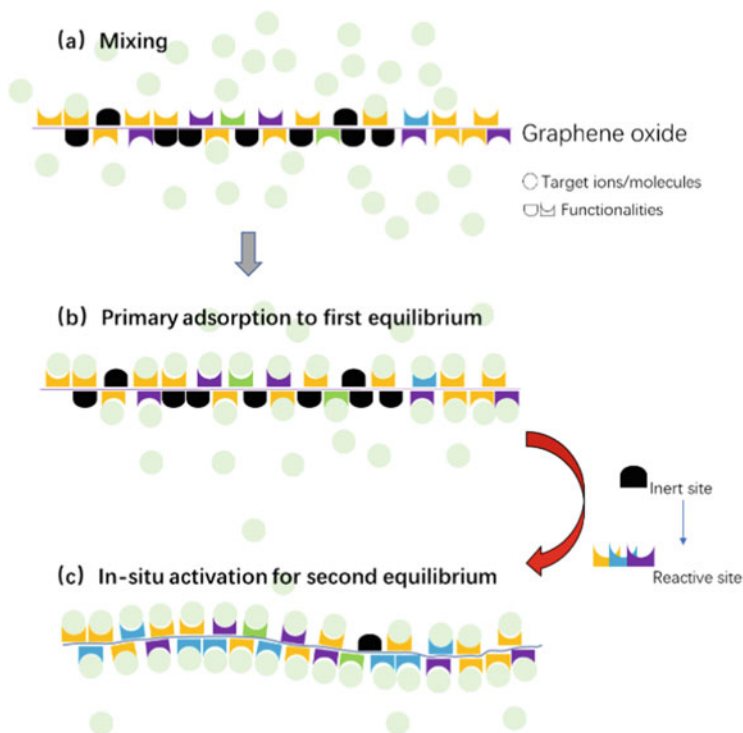


Fig. 8 Schematic of MER adsorption by GO. (a) Mixing, (b) a first equilibrium due to the adsorptive saturation of GO, (c) a second equilibrium follows an in situ conversion of inert functionality of GO to reactive sites

4 Dye Removal by Pristine GO

4.1 SER Adsorption

As mentioned, the SER adsorption has been widely adopted. Therefore, it is familiar for applying pristine GO as a nano adsorbent to the application in dye removal. Herein the term “pristine GO” is intended to indicate those used as prepared via the methods listed in Table 1. It covers both unexfoliated or partly exfoliated graphite oxide (loosely stacked GO) and thoroughly exfoliated graphite oxide, namely GO [64]. As early as in the 1970s, Lopez Gonzalez et al. used the Staudenmaier method-derived graphite oxide toward adsorbing various polar alcohols, showing an impressive capability because of the interlamellar effect and polar attribute of the internal region they explained [65]. Research themed on dye adsorption by graphene-based adsorbents stepped onto the fast track from that time on.

As listed in Table 3, pristine GO was prepared from various graphites and was artificially termed as GO, sGO, 3D GO, GO_p, and more, respectively, in different adsorptions. Almost all SER adsorptions had better fit by the Langmuir isotherm and

Table 3 Summary of SER adsorption for dye removal

Adsorbent	Targets	Isotherm	Exp. q_e (Calc. q_m) mg g ⁻¹ at RT	Kinetics	Resource
GO	MB MG	Langmuir	220 (351) 180 (248)	–	Bradder et al. [25]
GO	MB RhB CV1	–	199.2 ^a 154.8 ^a 195.4 ^a	PSO	Jin et al. [66]
GO	AO	Langmuir	1,382 (1,428)	–	Sun et al. [11]
GO	MB	Langmuir	240.65 (243.9)	PSO	Li et al. [68]
GO	MB BG	Langmuir	927 (476.19) 724 (416.67)	PSO	Ghaedi et al. [67]
GO	AO	–	229.8	–	Fiallos et al. [9]
GO	BR12 MO	Langmuir	(63.69) (16.83)	– –	Robati et al. [51]
GO	AO8 DR23	Langmuir	25.6 (29) 14.0 (15.3)	PSO PSO	Konicki et al. [72]
GO-VG GO-LG GO-FG GO-AG	CB	Langmuir	3,071.47 (3,206.66) 3,261.25 (3,414.92) 3,404.80 (3,587.92) 3,953.92 (4,248.79)	PSO	Jiao et al. [71]
sGO	AO MB CV	–	94.6 123.3 125.0	PSO	Coello-Fiallos et al. [61]
GO	MB	Langmuir	(286.9)	PSO	Sabzevari et al. [69]
GO _p NGO _p -1 wt % NGO _p -2 wt % NGO _p -3 wt % GO _f NGO _f -1 wt % NGO _f -2 wt % NGO _f -3 wt %	CR	Langmuir	(12.56) (11.06) (16.84) (19.49) (12.42) (9.59) (11.64) (14.17)	PSO	Yokwana et al. [73]

Note: *MB* methylene blue, *MG* malachite green, *RhB* rhodamine B, *CV1* crystal violet, *AO* Acridine orange, *CV* Cresyl violet, *AO8* acid Orange 8, *DR23* direct red 23, *BR12* basic red 12, *MO* methyl orange, *CB* cationic blue X-GRRL, *CR* Congo red, *BG* brilliant green, *PSO* the pseudo-second-order kinetic equation; –, no mention in the publication

^aThe value estimated by the kinetical fitting; RT, room temperature

the PSO kinetics. Specific to the methylene blue as the example, Bradder et al. [25] investigated the SER adsorption of incompletely exfoliated graphite oxide as one earliest case. The surface area was found no larger than that of graphite. The surface

chemistry, such as acidity and several oxygen functional groups, played a significant role in cationic dye adsorption through intrinsic electrostatic attraction. A large capacity $\sim 220 \text{ mg g}^{-1}$ was found for the GO through a Langmuir monolayer adsorptive manner. Apart from that, Jin et al. [66], Ghaedi et al. [67], Coello-Fiallos et al. [61], Li et al. [68], and Sabzevari et al. [69] had also experimentally prepared GO for the same purpose. Also, Ma et al. [70] theoretically studied such adsorption by molecular dynamics simulation. The capabilities of the adsorbents were found to vary much from each other. GO reported by Jin et al. [66] was made from a modified Hummers method that was partly replaced by a 12-h 70°C sealed autoclave reaction, which demonstrated a high capacity of 199.2 mg g^{-1} due to surface oxygen functional groups and the existence of the multilayers of dye molecules between the layers. Li et al. [68] unveiled that the maximal capacity reached 243.9 mg g^{-1} for the nitric acid-treated expanded graphite-derived GO. With the superiority in surface area accessibility, its normalized adsorption capacity was beyond that of the AC and CNT. Ghaedi et al. [67] prepared the GO from a pre-oxidation-involved modified Hummers method. It demonstrated a capacity of 476.2 mg g^{-1} contributed by the large surface area via π - π -electron donor-acceptor interactions and electrostatic attraction between oppositely charged dye ions and adsorbents. Coello-Fiallos et al. [61] synthesized graphite oxide by oxidizing the graphite and giving a further sonication, comprising conglomerates of nanoparticles with a radius of the order of tens of nanometers, and the capacity was about 123.3 mg g^{-1} . Sabzevari et al. [69] prepared the incompletely exfoliated GO with a maximal capacity of 286.9 mg g^{-1} through a monolayer uptake and a PSO kinetics mechanism.

Ma et al. [70] concluded, by simulations, that arising from the electrostatic attraction of oxygen-containing functionalities, the molecule of methylene blue could move to the GO, vertically approached its surface, and parallelly concentrated on it to form a stable monolayer. This interaction could be further intensified by extra hydrogen bonds, which are introduced by uplifting the oxidation degree of carbon adsorbent. These inspirations explained the dramatic capacitive differences and were also applicable to more cationic dyes such as Malachite green [25], Rhodamine B [66], Basic red 12 [51], Cationic blue X-GRRL [71], and Acridine orange [9, 11, 61] and even the oppositely charged dyes such as Cresyl Violet [61], Direct Red 23 [72], Methyl orange [51], Crystal violet [66], Acid Orange 8 [72], Congo red [73] though electrostatically repelling the negatively charged GO.

Noteworthy, the specific surface area of graphene was reported $\sim 2,630 \text{ m}^2 \text{ g}^{-1}$, while for chemically derived graphene powder, this value could fall to $705 \text{ m}^2 \text{ g}^{-1}$ as measured by the N_2 adsorption BET method since the sheets locating within the agglomerated particles were incompletely accessible [74, 75]. Besides, GO sheets being naturally of labile structure, readily agglomerate or re-stack likewise in the absence of hydrogen bonding-providing polar solvents [76], like water. Moreover, GO powder often somewhat deteriorates when re-dissolving in water as an example, negatively influencing the consequent performances compared to that freshly-prepared solution-in GO [77]. For such GO, little has been known concerning the surface area for a long time. To this end, Zhang et al. [75] determined the specific

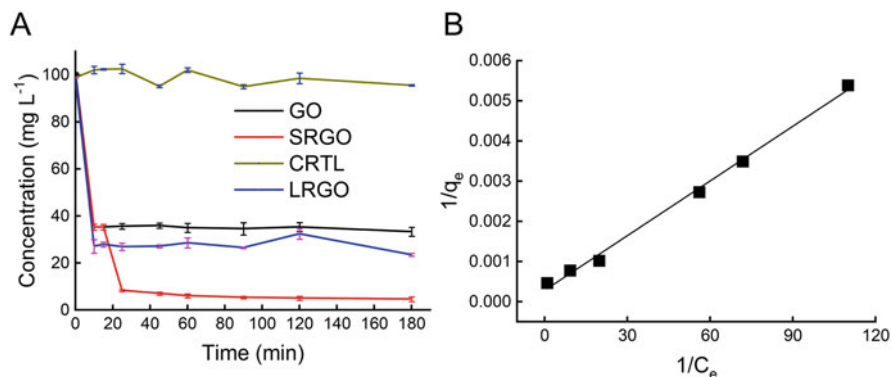


Fig. 9 Adsorption of AO by the graphene oxide. (a) the Time-Concentration curves of SER adsorptions by the pristine GO assigned as the “GO” and the three-hour-long reduced GO as the “LRGO” and a MER adsorption by GO termed as “SRGO” which undertook two-equilibrium adsorption, and a reference group with only the AO ~ 100 mg/L as “CTRL,” all being conducted in the 50-mL tubes; (b) Fitting of the linearized Langmuir model. Reproduced from Ref. [11] with permission from Elsevier

surface area of monolayer water-in GO to be $2,391(\pm 1,292)$ m² g⁻¹ using a rheology-based method, close to the theoretically calculated of about 2,418 m² g⁻¹. The fact that aqueous-in GO outperformed most of the previously reported solid adsorbents confirmed single dispersed GO turned out to be of great potential as a liquid adsorbent.

Nearly a decade ago, Sun et al. [11] used freshly-prepared aqueous GO to study the SER adsorption with AO as the target. The GO sheet was chosen to have the sizes by centrifugation from 2,000 to 5,000 rounds per minute. As shown in Table 3 and Fig. 9A, at first, an instant color change was observed within less than 10 min, and an equilibrium fast approached, demonstrative of high-efficiency elimination of AO (molecular weight ~ 265.4 g mol⁻¹). The GO reached a record capacity of 1,382 mg g⁻¹, highly coincident to its maximal Langmuir capacity of 1,428 mg g⁻¹ (~ 5.5 mmol g⁻¹). On the contrary, Coello-Fiallos et al. [9, 61] investigated two powdered GO as solid sorbents. Neither succeeded in surpassing the aqueous GO mentioned above in terms of the adsorption capacity, fully confirming the latter’s superiority [11]. Recently, Jiao et al. [71] applied a given amount of GO suspension to removing cationic dye CB with a higher molecular weight ~ 484.6 g mol⁻¹. The GO capacity experimentally reached up to 3,953.92 mg g⁻¹ (~ 8.16 mmol g⁻¹) and was much close to the Langmuir isotherm-derived capacity (4,248.79 mg g⁻¹, ~ 8.76 mmol g⁻¹).

Also mentioned above, GO is of multiple functionalities that will not entirely function in a SER adsorption. For example, most cationic dyes are electrostatically attracted onto GO due to its negatively charged surface that results from the deionization of surface carboxyl groups and π - π interactions [78]. Part functionalities take on reactivity while the other part appears to be inert. Imagine that in situ

transformations of the latter part would bring additional functioning sites. It will thereby definitely enhance the final performances.

4.2 MER Adsorption

In contrast to the SER adsorption featuring one equilibrium, low utilization of functioning sites is often unavoidable, as has been exemplified and discussed in the above section. The MER model turned out into consideration being an option. GO contains at least four types of oxygen-containing functional groups. Carbonyl group was ever more than 30%, but it just played a minor role in the AO adsorption [11]. Using aqueous GO as the sorbent together, Sun et al. [11], for the first time, applied the MER model in adsorption and dye removal as the target. Two equilibriums were in all achieved through a room temperature viable chemical transformation. As shown in Fig. 9, a typical two-equilibrium adsorption profile appeared, simultaneously with a far lower AO concentration than the SER adsorption marked as GO and LRGO. The process consisted of two steps. At first, a small volume of freshly-prepared GO (1 mL, ~0.48% w/v) was added into the 50-mL AO solution (0.1 g L^{-1}), and the liquid was kept stirring. Minutes later, the first equilibrium reached as the color got no further change. After that, a several-microliter solution was added containing a highly-reducing reagent known as sodium hydrosulfite ($10 \text{ }\mu\text{L}$, 0.2 g mL^{-1}). An additional change was observed in depigmented color, which indicated another equilibrium had taken place. Characterizations confirmed the surface carbonyl groups were converted to the hydroxyl groups that interacted with AO. With such, the adsorption capacity of GO was further elevated up to $2,158 \text{ mg g}^{-1}$, and theoretically to be a maximal capacity of $3,300 \text{ mg g}^{-1}$ following Langmuir uptake mechanism, two-fold high over the SER [11].

Notice that this MER operation involved an in situ configuration amid adsorption. It is necessary to point out that Sun et al. [11] had even compared it to that with the GO being treated before adsorption. As a result, it outperformed the latter, and the inaccessible sufficient surfaces of GO could be found to interpret their gap. It realized highly efficient adsorption and facilitated the spontaneous separation of GO in composite from the aqueous. Thus, it significantly reduced the cost and simplified operations for water treatment [79]. Most importantly, the MER model's effectiveness was well verified by, e.g., consistently activating inert groups for higher performance adsorbent.

In terms of economy and efficiency, Hao et al. modified the MER adsorption by introducing a Zinc- NH_4Cl system (Fig. 10A) to tune the surface functionality of GO instead of sodium hydrosulfite [79]. It separated five example pollutants from water, i.e., MB (Fig. 10B), CR, lemon yellow, cadmium ions (Cd^{2+}), and lead ions (Pb^{2+}), within 10 min and had removal efficiency up to 98.46%. A series of record monolayer capacities were up to 2,630.85, 7,630.15, 3,166.13, 8,435.26, and 17,904.75 mg g^{-1} , respectively, far beyond those reported. This modified method was also applied to real water, including a heavy metal-ion containing turbid soil

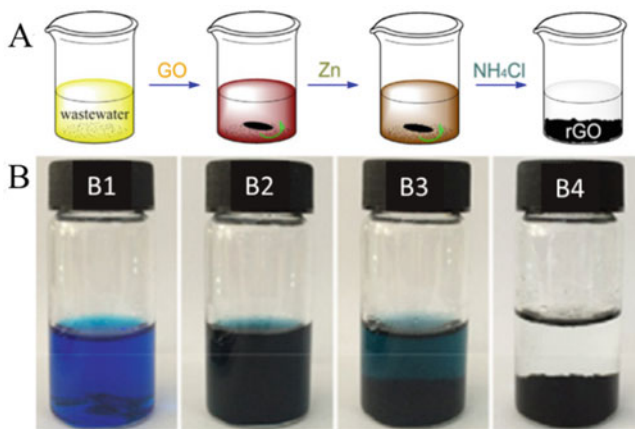


Fig. 10 (a) Schematic of MER adsorption using Zn-NH₄Cl converting GO for removal of methylene blue. (b) Photographic images for the MB (B1) at 217 mg L⁻¹ by the in situ conversion/reduction of 4.34 mg GO (B2) with 17.36 mg Zn powder (B3) and 86.80 mg NH₄Cl (B4). Reproduced from Ref. [79] with permission from Elsevier

water, milk, yogurt, protein, and fats containing water, indicating broad applicability. However, even though such MER adsorption byproducts demonstrated utilization in energy or agricultural fields, the treatment is hard to work at a low cost. Notably, the environmental risk is not so slight to ignore due to extensive chemical use ($\text{GO}/\text{Zn}/\text{NH}_4\text{Cl} = 1/4/20$ [79] vs. $\text{GO}/\text{Na}_2\text{S}_2\text{O}_4 = 1/40$ [11]). Under such circumstances, it necessitates further effort to investigate green chemical reduction or alternative ways to sustainable adsorption.

5 Dye Adsorption by Modified GO

First, many SER adsorptions have displayed the GO capable of adsorbing dyes in the magnitude of grams of dye per gram due to intrinsically multiple functionalities existing on both sheet sides. Second, with adopting the MER adsorption, an enhancement of adsorptive capability occurred to GO itself via the in situ modification. However, it still suffers some hard-to-overcome difficulties in conducting the MER adsorption currently, such as the selection of regulating agents or other reducing ways alike. Therefore, in addition to the sole GO, much research mainly focuses on developing the high-performance additively-modified GO as an advance or prerequisite measure. Typically, foreign moieties or matrixes are intentionally brought in to modify GO via surface functional grafting or immobilization, respectively, to enhance the targeting adsorption.

5.1 Via Surface Functionalization

Wu et al. [52] modified the GO surface with the rhamnolipid through a three-hour-long ultrasonication-assisted reaction (Fig. 11) conceived as RL-GO and then used for artificial and real MB-containing wastewater treatment. The RL-GO was characterized to have abundant functional groups and a mesopore structure and insensitive to ionic strength variation during adsorption. Due to the electrostatic attraction, π - π interaction, and hydrogen bonding interactions, its adsorption of MB was spontaneous, endothermic, and multilayered with the PSO kinetics. The Brunauer–Emmett–Teller model best fitted the adsorption isotherm from which a capacity at room temperature was concluded only 309 mg g^{-1} , but this value deviated much from the experimental ($\sim 494.9 \text{ mg g}^{-1}$) as shown in Table 4. The Freundlich and Langmuir isotherms turned out to be more convincing than the BET. A maximal capacity predicted by the Langmuir description was about 529.1 mg g^{-1} that agreed well with the fact.

Wang et al. [80] functionalized the surface of magnetic GO (MGO) by 1-amine-3-methyl imidazole chloride ion liquid to form LI-MGO. Its surface was then less negatively charged, leading to higher adsorptive capacity for the anionic dyes such as OIV and GR, yet fewer capacities for the cationic dyes such as AO and CV. All adsorptions of the LI-MGO were rate-limiting implied by the PSO modeling and monolayer manner in coverage. Sabzevari et al. [69] reported a chitosan-crosslinked composite (GO-LCTS) by bonding chitosan chains to GO via the reactions between the amine and carboxyl groups. The surface area of composited GO increased and the microscopic morphology also varied. Similarly, monolayer uptake occurred with the maximal capacity of 286.9 mg g^{-1} , and the adsorptions were all rate-limiting. Wang et al. [81] deposit the CS phase ($\text{Ca}_5\text{Si}_6\text{O}_{16}(\text{OH})_2 \cdot 8\text{H}_2\text{O}$) and oleic acid-coated Fe_3O_4 nanoparticles onto the surface of GO to obtain an easily-separable magnetic calcium silicate GO adsorbent (MGSi). Due to more substantial electropositivity than MB and less steric hindrance than CV, a higher adsorption selectivity occurred

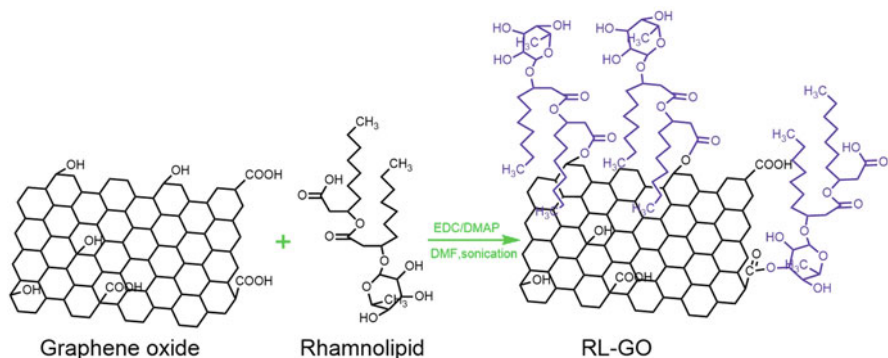


Fig. 11 Schematic of the formation of RL-GO. Reproduced from Ref. [52] with permission from Elsevier

Table 4 Dye adsorption with modified GO

Types	Adsorbent	Targets	Isotherm	Exp. q_e (Calc. q_m) mg g^{-1} at RT	Kinetics	Reference
Surface functional grafting	RL-GO	MB	BET, Langmuir	~494.9 (309, 529.1)	PSO	Wu et al. [52]
	MGSi	AO	Freundlich	193.05	PSO	Wang et al. [81]
	LI-MGO	AO CV OIV GR	Langmuir	62.08 (132.80) 37.88 (69.44) 39.46 (57.37) 147.8 (588.24)	PSO	Wang and Wei [80]
	GO-LCTS	MB	Langmuir	(402.6)	PSO	Sabzevari et al. [69]
	GO/I-OA	MG ER	Freundlich	2,687.56 1,189.1	PSO	Lv et al. [82]
	p(AA)-g- GO	MB	Langmuir	634.3 (1,448.2)	PSO	Wang et al. [96]
	DES/GO- Fe ₃ O ₄	MB	Langmuir	116.28	–	Mehrabi et al. [83]
	GO immobilization	SA-GO-N SA-GO-M	AO	Langmuir	797 (836) 1,351 (1,420)	PFS PFS
5wt% GOCB		MG	Langmuir	(17.862)	PSO	Zhang et al. [88]
KGM		MO MB	Freundlich	51.6 92.3	PSO	Gan et al. [93]
polyHIPEs/ GO		MB RhB	–	1.2503 ^a 1.0541 ^a	PSO	Huang et al. [95]
GO/A		MB	Freundlich	221.7155	PSO	Liu et al. [92]
CTS/PAA/ GO		MB FY3	–	296.5±31.7 280.3±23.9	PFO PSO	Chang et al. [94]

Note: *MB* methylene blue, *MG*, malachite green, *RhB* rhodamine B, *AO* Acridine orange, *CV* Cresyl violet, *OIV* Orange IV, *MO* methyl orange, *ER* Eriochrome blue black R, *CB* cationic blue X-GRRL, *CR* Congo red, *FY3* food yellow 3, *GR* Glenn black R, *BET*, the Brunauer–Emmett–Teller method used for surface area measurement, *PFS* the first-order kinetics, *PSO* the pseudo second-order kinetics; –, the publication does not note; *RT* room temperature

^a The data predicted by the kinetics model

to AO than the CV and MB. By the electrostatic, hydrophobic, and π – π interactions, the removal of AO much agreed with the behavior depicted by the PSO model and the Freundlich isotherm. Interestingly, since the Langmuir isotherm fitting has a coefficient over 99% that rivaled the Freundlich, the maximal capacity for MGSi was

estimated $\sim 193.05 \text{ mg g}^{-1}$ accordingly. Lv et al. [82] developed two-component non-covalently surface-functionalized GO with 1, 3-di(1H-tetrazol-5-yl) benzene and octadecylamine. The resultant GO/1-OA could structurally provide multiple synergistic non-covalent interactions at a time to decontamination, such as π - π stacking from tetrazolyl moiety and GO backbone, electrostatic interactions from charged NH^{3+} and tetrazolyl/oxygen-containing functional groups of GO, H_2O -assisted hydrogen bonding supported by tetrazolyl and amine groups, the chelating effect from tetrazolyl groups, and hydrophobicity from alkyl chains. Not only it adsorbed nine dyes experimentally out of the water with high performance, but it also eliminated the multiple contaminants simultaneously, i.e., pharmaceutical Ciprofloxacin, endocrine-disruptor bisphenol A, and metal ion Cu^{2+} . Furthermore, targeting at selected cationic malachite green (MG) and anionic eriochrome blue black R (ER), their isotherm fitted well with the Freundlich model, while the kinetics much resembled those sorbents mentioned above, being the PSO model.

Deep eutectic solvents (DESs) promise to substitute ionic liquids as coupling agents due to their low cost and enhanced biodegradability. They can be used for surface modification of GO with different functional groups. Mehrabi et al. [83] used a mixture of choline chloride and urea as a typical DES to functionalize GO sheets and conjugated metallic nanoparticles of Fe_3O_4 homogeneously onto the modified GO sheets to form nanohybrid adsorbent DES/GO- Fe_3O_4 with three hybrid ratios of GO to Fe_3O_4 . As a result, the nanohybrid at the dosage of 0.3 mg mL^{-1} had an optimized removing efficiency at $\sim 100\%$ of 25 mg L^{-1} MB within 5 min when the ratio was 1/2, faster than the bare GO. The adsorption behavior depended closely on the variation of ratio. However, the Langmuir model was found to better describe the adsorption than the Freundlich, even when GO was half of the total weight. Then, the maximal capacity of the DES/GO- Fe_3O_4 could be speculated about 116 mg g^{-1} . Although the capacity was lower than the GO, the modified adsorbent was quickly separated. Overall, it had demonstrated a high potential for environmental use in this way.

5.2 Via Immobilization

Exposure to GO has demonstrated a potential risk to the environment in pristine form or with superficial modifications [84, 85]. In fact, practical application of GO has been to some extent restricted in the water treatment due to the high water dispersibility for which ultrahigh centrifugation was necessary after the adsorption [47, 86]. Immobilization of GO as an alternative measure can effectively address the above issue via the confinement of nanoscopic GO in host matrixes. The procedure is simple and controllable with respect to the composition and dimension of the consequent structure. The structure can be long-term stable and endowed with good performance. Unlike GO, these adsorbents can be collected with many conveniences and recovered by state-of-art methods such as filtration and centrifugation [29, 87, 88].

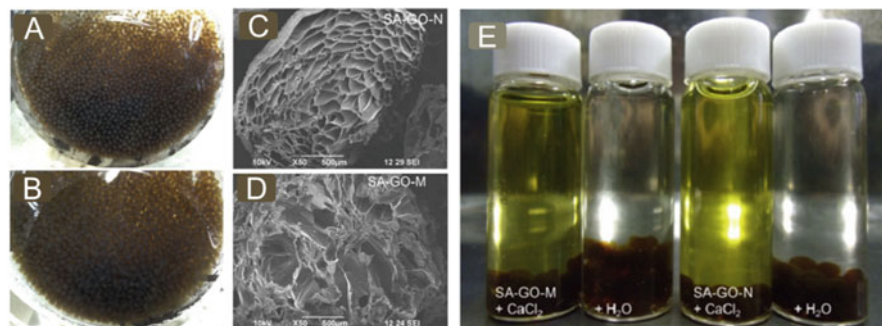


Fig. 12 Adsorption of alginate modified GO. (a) Ca^{2+} cross-linked GO-alginate composite beads as the SA-GO-N; (b) H^+ -gelled beads as the SA-GO-M; (c) the electronic scanning image of a freezing-dry bead SA-GO-N; (d) the electronic scanning image of the bead SA-GO-M; (e) Comparison of changes upon the dye-adsorbing beads (SA-GO-M and SA-GO-N) being immersed in either the Ca^{2+} $\sim 0.5 \text{ mol L}^{-1}$ solution or the deionized water. Reproduced from Ref. [87] with permission from Elsevier

Bio-extract polysaccharides such as alginate, cellulose, and Konjac glucomannan are typical host matrixes [69, 89–91]. Amid a sol–gel process, chelation could transform highly dissolved polysaccharides colloid to a water-rich gel framework. For dye removal, Sun et al. [87] immobilized GO as the minor constituent (GO/alginate = 1/100) into the Ca^{2+} or H^+ gelled alginate beads, of which the dimensions were millimeter-sized (Fig. 12a, b), by the interaction of carboxyl and hydroxyl groups between alginate and GO. The addition of GO visibly thinned the alginate walls and uplifted the porosity concluded from the observatory structure variation via electronic scanning microscopy (Fig. 12c, d), and specific surface area changes via N_2 adsorption–desorption isotherms. The calcium alginate with GO was $\sim 22.9 \text{ m}^2 \text{ g}^{-1}$, two magnitudes high over the pure one $\sim 0.4 \text{ m}^2 \text{ g}^{-1}$, and so was the alginic acid from 11.4 to $31.3 \text{ m}^2 \text{ g}^{-1}$. In other words, GO immobilized alginates were to expose additional functional sites outside for dye-targeting ion exchanging (Fig. 12e). Besides, they also showed wide-pH adaptability (Table 4) as compared. And all the adsorptions followed Langmuir-type adsorptions and PFO kinetics, resulting from the chemical adsorptive mechanism.

Liu et al. [92] raised the proportion of GO in alginate to 1/10 and prepared lyophilized GO-immobilizing alginate for the removal of MB. The maximal capacity of alginate was 357.14 mg g^{-1} predicted using Langmuir modeling, which was yet quite distant from the experimental. As a contrast, the Freundlich model fitted the isotherm better, implying a multilayered adsorptive manner. Even though the GO increased much in content, the capacity ($\sim 221.7155 \text{ mg g}^{-1}$) was significantly lower than that with wet beads by Sun et al. [87].

Similarly, Zhang et al. [88] incorporated GO into cellulose beads (GOCB) with a mass ratio estimated at 1/1–1/10 by a modified sol–gel method. After GO and cellulose were mixed with a strong alkali, the suspension was ultrasonically transformed into a mixture colloid. The size of GO sheets was gradually reduced,

and the intermolecular interactions were intensified. In the acid treatment, the coalescence of GO and cellulose was further gelled into a solid one. GO was thereby firmly entrapped inside. Again, the internal structure was changed with much porosity. The removal of MG was over 96%, and the reusability reached five times by simple filtration. Gan et al. [93] suggested that the presence of GO could intensify the cross-linking interactions between GO and konjac glucomannan (KGM), and therefore stabilize the network structures via the interactions such as hydrogen bonding. To this end, dried hydrogel beads were made from GO and KGM at a mass ratio $\sim 1/32$ and used for aqueous removal of cationic MB and anionic MO (Table 4). Since the adsorptions followed the PSO kinetics and the Freundlich isotherm, it is reasonable to understand dye molecules formed multilayers on bead walls. However, the capacities for two dyes were found less than those by wet hydrogel beads. Chang et al. [94] integrated GO homogeneously in polyacrylate (PAA)-chitosan matrix to conceive tri-component freeze-dried hydrogel to remove cationic MB and anionic FY3, for there naturally existed electrostatic interactions between carboxyl groups of GO and PAA and amino groups of chitosan. Triggered by gaseous acetic acid fumigation, the sol-gel transition was easily accomplished in a componential homogeneity. During the process, the chitosan dissolved and expanded. GO-chitosan cross-linking network was densified. The tensile strength enhanced, and the swelling was also inhibited, beneficial to the dual adsorption targeting oppositely charged dyes. The MB was found chemisorbed out ($296.5 \pm 31.7 \text{ mg g}^{-1}$), while the FY3 was separated via simultaneously-occurring chemisorption and physisorption ($280.3 \pm 23.9 \text{ mg g}^{-1}$). However, the capacity remained low, even when employing dried hydrogels with an optimized mass ratio of GO, PAA, and chitosan at 1/200/200. GO played a role of great importance, as the authors expected.

Besides, polymerization also acts as an immobilization. Huang et al. [95] introduced high-internal-phase-emulsions to polymerize polyvinylpyrrolidone-modified GO to form a macroporous polymer monolith (polyHIPEs/GO). It was found that such GO improved the structural stability of macropores and imparted more organic groups [95]. Increasing the GO would strengthen the electrostatic interaction and π - π interaction, resulting in a higher uptake of cationic and anionic dyes. Thus, either polyHIPEs/GO or its aminated form (polyHIPEs_(NH₂)/GO) demonstrated enhanced adsorption to the MB, RB, and anionic Eosin Y compared to the GO-free polymer. Unlike those GO-rich adsorbents above, due to higher bulk density, such polymer adsorbents did not show great superiority in the capacity per gram. The capacities of polyHIPEs/GO for MB and RB were 1.2503 and 1.0541 mg g^{-1} , respectively, and the aminated polyHIPEs_(NH₂)/GO showed only 1.9673 mg g^{-1} on eosin Y.

6 Conclusion and Outlook

Carbon adsorbents have long been used in water decontamination, given considerable capacity, relative durability, and cost-efficiency. However, adsorption technologies are still progressing due to the need for high-performance environmental

remediation in rapid human civilization. On the one hand, as the material dimension degrades, the micro/nano effect accounts for the prominence in adsorption, partly owing to high surface energy that intensifies the interactions with alien ions/molecules. On the other hand, traditional ways to adsorption have possibly developed to an edge of transformation since that MER model featuring high capability becomes available, especially when the 2D materials with structures bearing multiple intertransformable functionalities emerge, resembling the GO.

It appears that the scalable synthesis of GO has been well solved. For now, there has been no advance across the scientific community. In other words, whatever for lab or industry, the present syntheses are mostly using harsh acids and/or corrosive salts as summarized (Table 4). Then, post purification and recyclability are unavoidable and have-to-overcome issues. This reality explains the dilemma that the price per kilogram remains so high that it has contained wide-spectrum environmental applications, including the nano adsorbent. To this end, substantial breakthroughs become urgent and desire more contributions by scientists from multi-disciplinary fields.

Further, GO has proven itself high capability for cationic dye removal. With additional surface treatments, it has been able to isolate anodic dyes or else. We noticed that nearly all the studies were run in the SER model. This model features insufficient functionalities as enabling sites for the targeted contaminant, especially for the GO with additive modification. Although the MER model was schematically proposed in 2012 as early and GO, an emerging high-performance adsorbent, had proven its theoretical feasibility, no example of modified GO has ever worked with the MER adsorption. Such a model is still thousands of miles away from prevalence. As speculated, three primary reasons are in possible consideration.

First, the fact that GO-basis adsorbents and adsorptions are hard to replicate precisely and to produce massively, besides being costly, is quite self-evident. As to adsorbents such as AC and zeolite, constituting the second reason, they intrinsically lack a variety of functionalities. This way, it is unrealistic or no driving force to conduct MER adsorption for these adsorbents only through functionalities variation. Therefore, different ways are needed, accompanying with researches. Third, the MER, as mentioned in earlier reports, has exhibited critical dependence of the in situ reductive mechanisms of GO for enhanced adsorption. They also deliver that an appropriate reducing agent matters much. However, only a few cases have been reported over this issue. Except for the reductive mechanism, there are other analogous mechanisms concerning in situ oxidation or non-electron transfer mechanism, although relevant progress has not been at the stage. Nonetheless, at least for GO, the in situ mechanism-based MER way is continuing to fascinate us as the complexity of its structure–performance correlations reveals.

Acknowledgement The contribution was partly supported by Beijing Municipal Education Commission (No. KM201910005007) and NSFC (No. 51902007). Great thanks are dedicated to Prof. Shunitz Tanaka for his kind and meticulous supervision in Hokkaido University and the faculty members of Beijing University of Technology. Besides, special thanks are given to those who helped much while shaping this manuscript, such as Mrs. Fei, Xian-Di, Mr. Sun, Yi-Bing, Dr. Chen, Wen-Ya, Mrs. Sun Ya-Lan, and Ms. Sun, Tang-Yue.

References

1. Allied Analytics LLP (2020) Textile dyes market by dye type, and fiber type: global opportunity analysis and industry. Forecast:2019–2026
2. Moosavi S, Lai CW, Gan S, Zamiri G, Akbarzadeh Pivezhzani O, Johan MR (2020) Application of efficient magnetic particles and activated carbon for dye removal from wastewater. *ACS Omega* 5(33):20684–20697
3. Lv G, Li Z, Jiang W-T, Chang P-H, Jean J-S, Lin K-H (2011) Mechanism of acridine orange removal from water by low-charge swelling clays. *Chem Eng J* 174(2–3):603–611
4. Miao Y, Li Y, Zhang Z, Yan G, Bi Y (2015) “Turn off–on” phosphorescent biosensors for detection of DNA based on quantum dots/acridine orange. *Anal Biochem* 475:32–39
5. Byvaltsev VA, Bardanova LA, Polkin RA, Ochkal SV, Shepelev VV, Aliyev MA et al (2019) Acridine orange: a review of novel applications for surgical cancer imaging and therapy. *Front Oncol* 9:925
6. Francisco DE, Mah RA, Rabin AC (1973) Acridine orange-epifluorescence technique for counting bacteria in natural waters. *Trans Am Microsc Soc* 92(3):416
7. Fucic A, Maric T, Vivic Bockor V, Jezek D (2020) In vivo acridine orange human spermatozoa staining – a new perspective for RNA detection and spermatozoa morphology evaluation. *Anat Histol Embryol* 50(1):102–107
8. Nayeri D, Mousavi SA (2020) Dye removal from water and wastewater by nanosized metal oxides-modified activated carbon: a review on recent researches. *J Environ Health Sci Eng* 18:1671–1689
9. Fiallos DC, Gómez CV, Usca GT, Pérez DC, Tavolaro P, Martino G et al (2015) Removal of acridine orange from water by graphene oxide. *AIP Conf Proc* 1646(1):38–45
10. Ali I, Gupta VK (2006) Advances in water treatment by adsorption technology. *Nat Protoc* 1(6):2661–2667
11. Sun L, Yu H, Fugetsu B (2012) Graphene oxide adsorption enhanced by in situ reduction with sodium hydrosulfite to remove acridine orange from aqueous solution. *J Hazard Mater* 203–204:101–110
12. Baysal M, Bilge K, Yilmaz B, Papila M, Yurum Y (2018) Preparation of high surface area activated carbon from waste-biomass of sunflower piths: kinetics and equilibrium studies on the dye removal. *J Environ Chem Eng* 6(2):1702–1713
13. Chen Y, Zhu Y, Wang Z, Li Y, Wang L, Ding L et al (2011) Application studies of activated carbon derived from rice husks produced by chemical-thermal process – a review. *Adv Colloid Interface Sci* 163(1):39–52
14. Hu S, Hsieh Y-L (2014) Preparation of activated carbon and silica particles from rice straw. *ACS Sustain Chem Eng* 2(4):726–734
15. Ren X, Wang S, Jin Y, Xu D, Yin H (2020) Adsorption properties of reactive dyes on the activated carbon from corn straw prepared by microwave pyrolysis. *Desalin Water Treat* 200:296–303
16. Wang S, Zhu ZH, Coomes A, Haghseresht F, Lu GQ (2005) The physical and surface chemical characteristics of activated carbons and the adsorption of methylene blue from wastewater. *J Colloid Interface Sci* 284(2):440–446
17. Chen X, Chen G, Chen L, Chen Y, Lehmann J, McBride MB et al (2011) Adsorption of copper and zinc by biochars produced from pyrolysis of hardwood and corn straw in aqueous solution. *Bioresour Technol* 102(19):8877–8884
18. Cazetta AL, Vargas AMM, Nogami EM, Kunita MH, Guilherme MR, Martins AC et al (2011) NaOH-activated carbon of high surface area produced from coconut shell: kinetics and equilibrium studies from the methylene blue adsorption. *Chem Eng J* 174(1):117–125
19. Islam MA, Ahmed MJ, Khanday WA, Asif M, Hameed BH (2017) Mesoporous activated coconut shell-derived hydrochar prepared via hydrothermal carbonization-NaOH activation for methylene blue adsorption. *J Environ Manage* 203(1):237–244

20. Tan IAW, Ahmad AL, Hameed BH (2008) Adsorption of basic dye on high-surface-area activated carbon prepared from coconut husk: equilibrium, kinetic and thermodynamic studies. *J Hazard Mater* 154(1–3):337–346
21. Youssef AM, Ahmed AI, El-Bana UA (2012) Adsorption of cationic dye (MB) and anionic dye (AG 25) by physically and chemically activated carbons developed from rice husk. *Carbon Lett* 13(2):61–72
22. Kuang Y, Zhang X, Zhou S (2020) Adsorption of methylene blue in water onto activated carbon by surfactant modification. *Water* 12(2):587
23. Lin YB, Fugetsu B, Terui N, Tanaka S (2005) Removal of organic compounds by alginate gel beads with entrapped activated carbon. *J Hazard Mater* 120(1–3):237–241
24. Sun L, Li Y, Hu H (2009) Biodegradation of nitrobenzene by a strain biodegradation of nitrobenzene by a strain immobilized on granular activated carbon. *China Environ Sci* 29(9): 941–945
25. Bradder P, Ling SK, Wang SB, Liu SM (2011) Dye adsorption on layered graphite oxide. *J Chem Eng Data* 56(1):138–141
26. Hu X, Yu Y, Zhou J, Song L (2014) Effect of graphite precursor on oxidation degree, hydrophilicity and microstructure of graphene oxide. *Nano* 9(3)
27. Stankovich S, Dikin DA, Dommett GHB, Kohlhaas KM, Zimney EJ, Stach EA et al (2006) Graphene-based composite materials. *Nature* 442(7100):282–286
28. Sun L (2019) Structure and synthesis of graphene oxide. *Chin J Chem Eng*
29. Wang Y, Panl C, Chu W, Vipin AK, Sun L (2019) Environmental remediation applications of carbon nanotube and graphene oxide: adsorption and catalysis. *Nanomaterials (Basel)* 9(3):439
30. Brodie BC (1859) On the atomic weight of graphite. *Philos Trans R Soc Lond* 149:249–259
31. Staudenmaier L (1898) Verfahren zur Darstellung der Graphitsäure. *Ber Dtsch Chem Ges* 31(2):1481–1487
32. Hummers WS, Offeman RE (1958) Preparation of graphitic oxide. *J Am Chem Soc* 80(6):1339
33. Fu L, Hongbo L, Yanhong Z, Bo L (2005) Technology research on oxidative degree of graphite oxide prepared by Hummers method (in Chinese). *Carbon* 124(4):10–14
34. Su C-Y, Xu Y, Zhang W, Zhao J, Tang X, Tsai C-H et al (2009) Electrical and spectroscopic characterizations of ultra-large reduced graphene oxide monolayers. *Chem Mater* 21(23): 5674–5680
35. Marcano DC, Kosynkin DV, Berlin JM, Sinitskii A, Sun Z, Slesarev A et al (2010) Improved synthesis of graphene oxide. *ACS Nano* 4(8):4806–4814
36. Huang NM, Lim HN, Chia CH, Yarmo MA, Muhamad. (2011) Simple room-temperature preparation of high-yield large-area graphene oxide. *Int J Nanomedicine* 6(1):3443–3448
37. Eigler S, Enzelberger-Heim M, Grimm S, Hofmann P, Kroener W, Geworski A et al (2013) Wet chemical synthesis of graphene. *Adv Mater* 25(26):3583–3587
38. Chen J, Li Y, Huang L, Li C, Shi G (2015) High-yield preparation of graphene oxide from small graphite flakes via an improved Hummers method with a simple purification process. *Carbon* 81:826–834
39. Panwar V, Chattree A, Pal K (2015) A new facile route for synthesizing of graphene oxide using mixture of sulfuric–nitric–phosphoric acids as intercalating agent. *Physica E* 73:235–241
40. Peng L, Xu Z, Liu Z, Wei Y, Sun H, Li Z et al (2015) An iron-based green approach to 1-h production of single-layer graphene oxide. *Nat Commun* 6:5716
41. Yu H, Zhang B, Bulin C, Li R, Xing R (2016) High-efficient synthesis of graphene oxide based on improved hummers method. *Sci Rep* 6:36143
42. Dimiev AM, Ceriotti G, Metzger A, Kim ND, Tour JM (2016) Chemical mass production of graphene Nanoplatelets in ~100% yield. *ACS Nano* 10(1):274–279
43. Ranjan P, Agrawal S, Sinha A, Rao TR, Balakrishnan J, Thakur AD (2018) A low-cost non-explosive synthesis of graphene oxide for scalable applications. *Sci Rep* 8(1):12007
44. Sun L, Fugetsu B (2013) Mass production of graphene oxide from expanded graphite. *Mater Lett* 109:207–210

45. Chhowalla M, Eda G (2010) Chemically derived graphene oxide: towards large-area thin-film electronics and optoelectronics. *Adv Mater* 22(22):2392–2415
46. Langmuir I (1916) The constitution and fundamental properties of solids and liquids. Part I. solids the constitution and fundamental properties of solids and liquids. *J Am Chem Soc* 38(11):2221–2295
47. Cheng C, Deng J, Lei B, He A, Zhang X, Ma L et al (2013) Toward 3D graphene oxide gels based adsorbents for high-efficient water treatment via the promotion of biopolymers. *J Hazard Mater* 263:467–478
48. Faghihi A, Vakili MH, Hosseinzadeh G, Farhadian M, Jafari Z (2016) Synthesis and application of recyclable magnetic freeze-dried graphene oxide nanocomposite as a high capacity adsorbent for cationic dye adsorption. *Desalin Water Treat* 57(47):22655–22670
49. Freundlich H (1907) Über die adsorption in Lösungen. *Z Phys Chem* 57U(1):385–470
50. Arami M, Yousefi Limae N, Mahmoodi NM (2006) Investigation on the adsorption capability of egg shell membrane towards model textile dyes. *Chemosphere* 65(11):1999–2008
51. Robati D, Mirza B, Rajabi B, Moradi O, Tyagi I, Agarwal S et al (2016) Removal of hazardous dyes-BR 12 and methyl orange using graphene oxide as an adsorbent from aqueous phase. *Chem Eng J* 284:687–697
52. Wu Z, Zhong H, Yuan X, Wang H, Wang L, Chen X et al (2014) Adsorptive removal of methylene blue by rhamnolipid-functionalized graphene oxide from wastewater. *Water Res* 67: 330–344
53. Ramakrishna KR, Viraraghavan T (1997) Dye removal using low cost adsorbents. *Water Sci Technol* 36(2–3):189–196
54. Ho YS, Huang CT, Huang HW (2002) Equilibrium sorption isotherm for metal ions on tree fern. *Process Biochem* 37(12):1421–1430
55. Redlich O, Peterson DL (1959) A useful adsorption isotherm. *J Phys Chem* 63(6):1024
56. Ho YS, McKay G (1998) The kinetics of sorption of basic dyes from aqueous solution by sphagnum moss peat. *Can J Chem Eng* 76(4):822–827
57. Sten Yngve Lagergren (1899) Zur Theorie der sogenannten Adsorption gelöster Stoffe. *Bihang till Kongl Svenska vetenskaps-akademiens handlingar* 24(2):1–39
58. Wu X-L, Xiao P, Zhong S, Fang K, Lin H, Chen J (2017) Magnetic ZnFe₂O₄@chitosan encapsulated in graphene oxide for adsorptive removal of organic dye. *RSC Adv* 7(45): 28145–28151
59. Sahraei R, Hemmati K, Ghaemy M (2016) Adsorptive removal of toxic metals and cationic dyes by magnetic adsorbent based on functionalized graphene oxide from water. *RSC Adv* 6(76): 72487–72499
60. Ho YS, McKay G (2002) Application of kinetic models to the sorption of copper(II) on to peat. *Adsorption Sci Technol* 20(8):797–815
61. Coello-Fiallos D, Cazzanelli E, Tavolaro A, Tavolaro P, Arias M, Caputi LS (2018) Cresyl violet adsorption on sonicated graphite oxide. *J Nanosci Nanotechnol* 18(4):3006–3011
62. Du Q, Sun J, Li Y, Yang X, Wang X, Wang Z et al (2014) Highly enhanced adsorption of Congo red onto graphene oxide/chitosan fibers by wet-chemical etching off silica nanoparticles. *Chem Eng J* 245:99–106
63. Sheindorf C, Rebhun M, Sheintuch M (1981) A Freundlich-type multicomponent isotherm. *J Colloid Interface Sci* 79(1):136–142
64. Nebol'sin VA, Galstyan V, Silina YE (2020) Graphene oxide and its chemical nature: multi-stage interactions between the oxygen and graphene. *Surf Interfac* 21:100763
65. Lopezgonzalez JD, Martinrodriguez A, Martinpozuolo A, Rodriguezreinoso F (1977) Adsorption of alcohols on several graphite oxides. *Carbon* 15(6):416–417
66. Jin Q-Q, Zhu X-H, Xing X-Y, Ren T-Z (2012) Adsorptive removal of cationic dyes from aqueous solutions using graphite oxide. *Adsorpt Sci Technol* 30(5):437–447
67. Ghaedi M, Zeinali N, Ghaedi AM, Teimuori M, Tashkhourian J (2014) Artificial neural network-genetic algorithm based optimization for the adsorption of methylene blue and brilliant green from aqueous solution by graphite oxide nanoparticle. *Spectrochim Acta A Mol Biomol Spectros* 125:264–277

68. Li Y, Du Q, Liu T, Peng X, Wang J, Sun J et al (2013) Comparative study of methylene blue dye adsorption onto activated carbon, graphene oxide, and carbon nanotubes. *Chem Eng Res Des* 91(2):361–368
69. Sabzevari M, Cree DE, Wilson LD (2018) Graphene oxide–chitosan composite material for treatment of a model dye effluent. *ACS Omega* 3(10):13045–13054
70. Ying M, Tian W, Heng Z (2019) Molecular dynamics simulation of adsorption of methylene blue by graphene oxide. *Chem J Chinese Universities* 40(12):2534–2541
71. Jiao X, Zhang L, Qiu Y, Guan J (2017) Comparison of the adsorption of cationic blue onto graphene oxides prepared from natural graphites with different graphitization degrees. *Colloids Surf A Physicochem Eng Aspects* 529:292–301
72. Konicki W, Aleksandrak M, Moszynski D, Mijowska E (2017) Adsorption of anionic azo-dyes from aqueous solutions onto graphene oxide: equilibrium, kinetic and thermodynamic studies. *J Colloid Interface Sci* 496:188–200
73. Yokwana K, Kuvarega AT, Mhlanga SD, Nxumalo EN (2018) Mechanistic aspects for the removal of Congo red dye from aqueous media through adsorption over N-doped graphene oxide nanoadsorbents prepared from graphite flakes and powders. *Phys Chem Earth* 107:58–70
74. Stoller MD, Park SJ, Zhu YW, An JH, Ruoff RS (2008) Graphene-based ultracapacitors. *Nano Lett* 8(10):3498–3502
75. Zhang S, Wang H, Liu J, Bao C (2019) Measuring the specific surface area of monolayer graphene oxide in water. *Mater Lett*:127098
76. Dubin S, Gilje S, Wang K, Tung VC, Cha K, Hall AS et al (2010) A one-step, solvothermal reduction method for producing reduced graphene oxide dispersions in organic solvents. *ACS Nano* 4(7):3845–3852
77. Shen L, Wang D, Jin Z, Che L, Cai N, Wang Y et al (2019) The effect of drying modes on aqueous dispersion of graphene oxide solids. *Funct Mater Lett* 12(04):1950043
78. Gao J, Liu F, Liu YL, Ma N, Wang ZQ, Zhang X (2010) Environment-friendly method to produce graphene that employs vitamin C and amino acid. *Chem Mater* 22(7):2213–2218
79. Hao J, Ji L, Li C, Hu C, Wu K (2018) Rapid, efficient and economic removal of organic dyes and heavy metals from wastewater by zinc-induced in-situ reduction and precipitation of graphene oxide. *J Taiwan Inst Chem Eng* 88:137–145
80. Wang H, Wei Y (2017) Magnetic graphene oxide modified by chloride imidazole ionic liquid for the high-efficiency adsorption of anionic dyes. *RSC Adv* 7(15):9079–9089
81. Wang H, Chen Y, Wei Y (2016) A novel magnetic calcium silicate/graphene oxide composite material for selective adsorption of acridine orange from aqueous solutions. *RSC Adv* 6(41):34770–34781
82. Lv M, Yan L, Liu C, Su C, Zhou Q, Zhang X et al (2018) Non-covalent functionalized graphene oxide (GO) adsorbent with an organic gelator for co-adsorption of dye, endocrine-disruptor, pharmaceutical and metal ion. *Chem Eng J* 349:791–799
83. Mehrabi N, Haq UFA, Toufiq Reza M, Aich N (2020) Application of deep eutectic solvent for conjugation of magnetic nanoparticles onto graphene oxide for lead(II) and methylene blue removal. *J Environ Chem Eng* 8(5):104222
84. Fadeel B, Bussy C, Merino S, Vázquez E, Flahaut E, Mouchet F et al (2018) Safety assessment of graphene-based materials: focus on human health and the environment. *ACS Nano* 12(11):10582–10620
85. Zhao Y, Liu Y, Zhang X, Liao W (2021) Environmental transformation of graphene oxide in the aquatic environment. *Chemosphere* 262:127885
86. Zhang X, Cheng C, Zhao J, Ma L, Sun S, Zhao C (2013) Polyethersulfone unwrapped graphene oxide porous particles for water treatment. *Chem Eng J* 215:72–81
87. Sun L, Fugetsu B (2014) Graphene oxide captured for green use: influence on the structures of calcium alginate and macroporous alginate beads and their application to aqueous removal of acridine orange. *Chem Eng J* 240:565–573
88. Zhang X, Yu H, Yang H, Wan Y, Hu H, Zhai Z et al (2015) Graphene oxide caged in cellulose microbeads for removal of malachite green dye from aqueous solution. *J Colloid Interface Sci* 437:277–282

89. Li LB, Fang YP, Vreeker R, Appelqvist I (2007) Reexamining the egg-box model in calcium-alginate gels with X-ray diffraction. *Biomacromolecules* 8(2):464–468
90. Bai H, Chen J, Wang Z, Wang L, Lamy E (2020) Simultaneous removal of organic dyes from aqueous solutions by renewable alginate hybridized with graphene oxide. *J Chem Eng Data* 65(9):4443–4451
91. Vipin AK, Ling S, Fugetsu B (2014) Sodium cobalt hexacyanoferrate encapsulated in alginate vesicle with CNT for both cesium and strontium removal. *Carbohydr Polym* 111:477–484
92. Liu X, Cui B, Liu S, Ma Q (2019) Methylene blue removal by graphene oxide/alginate gel beads. *Fibers Polym* 20(8):1666–1672
93. Gan L, Shang S, Hu E, Wah C, Yuen M, Jiang S (2015) Konjac glucomannan/graphene oxide hydrogel with enhanced dyes adsorption capability for methyl blue and methyl orange. *Appl Surf Sci* 357:866–872
94. Chang Z, Chen Y, Tang S, Yang J, Chen Y, Chen S et al (2020) Construction of chitosan/polyacrylate/graphene oxide composite physical hydrogel by semi-dissolution/acidification/sol-gel transition method and its simultaneous cationic and anionic dye adsorption properties. *Carbohydr Polym* 229:115431
95. Huang Y, Ruan G, Ruan Y, Zhang W, Li X, Du F et al (2018) Hypercrosslinked porous polymers hybridized with graphene oxide for water treatment: dye adsorption and degradation. *RSC Adv* 8(24):13417–13422
96. Wang G, Li G, Huan Y, Hao C, Chen W (2020) Acrylic acid functionalized graphene oxide: high-efficient removal of cationic dyes from wastewater and exploration on adsorption mechanism. *Chemosphere* 261

Heterogeneous Catalysts for Environmental Purification



Yuichi Kamiya

Contents

1	Catalysts as Indispensable Materials in Today's Lives	424
2	How Does a Catalysts Work?	429
3	Purification of Water with Catalytic Reactions	431
3.1	Groundwater Pollution with Nitrate	432
3.2	Purification Methods for the Polluted Groundwater	434
3.3	Catalytic Reduction of NO_3^- for Purification of the Polluted Groundwater	435
3.4	Purification of Real Groundwater by the Catalytic Method with the CuPd Catalyst ..	441
3.5	A Supported SnPd Catalyst for Purification of Real Polluted Groundwater	446
3.6	Alternative Methods Without Gaseous Hydrogen On-Site	450
4	Prospect	455
	References	458

Abstract In this chapter, the basics and applications of heterogeneous catalysts for environmental purification, especially for groundwater purification is described. First, it is introduced that catalysts are deeply involved in our lives and as key materials in supporting modern society by taking some practical applications. Then, basic knowledge of the reaction mechanism over a solid catalyst is outlined to facilitate understanding of the catalytic reaction for groundwater purification. Finally, the catalytic reaction for the purification of groundwater polluted with nitrate is described in detail as an example of how solid catalysts are developed. Later, remaining issues and prospect for practical applications of the catalytic purification of groundwater are given.

Keywords Heterogeneous catalyst, Hydrogenation, Nitrate, Photocatalysis, Water purification

Y. Kamiya (✉)

Faculty of Environmental Earth Science, Hokkaido University, Sapporo, Hokkaido, Japan
e-mail: kamiya@ees.hokudai.ac.jp

This chapter introduces the basics and applications of heterogeneous catalysts for environmental purification, especially for groundwater purification. Heterogeneous catalysts are often called solid catalysts, and this term is used throughout this chapter. First, it is introduced that catalysts are deeply involved in our lives and as key materials in supporting modern society (Sect. 1). In Sect. 2, basic knowledge of the reaction mechanism over a solid catalyst is outlined to facilitate understanding of the catalytic reaction for groundwater purification. Finally, the catalytic reaction for the purification of groundwater polluted with nitrate (NO_3^-) is described in detail as an example of how solid catalysts are developed. Later, it is discussed that the background of the research, what kind of viewpoint was taken to proceed with the catalyst development, and elaborate on remaining issues for practical applications (Sect. 3), which are centered on the research of this author.

1 Catalysts as Indispensable Materials in Today's Lives

In our daily lives, we rarely see a catalyst in its form and are rarely aware of how it works. Nevertheless, catalysts are important functional materials, indispensable for the construction of the current society, because catalysts play an important role in the production of materials and in keeping our living environment clean (Fig. 1).

Iron oxide (Fe_3O_4), to which Al_2O_3 and K_2O are added as promoters, is used as a catalyst in the production of NH_3 from N_2 in air and H_2 , while Fe_3O_4 is reduced to Fe when it acts as a catalyst under reaction conditions [1]. The development of NH_3 production on an industrial scale by Haber and Bosch has been saving humankind

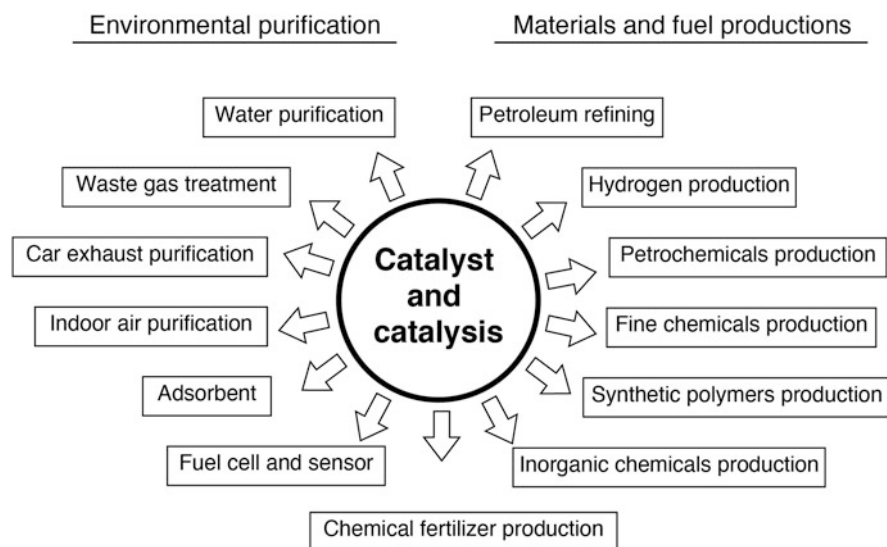
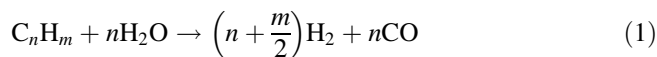


Fig. 1 Active roles played by catalysts in modern society

from food shortages, because NH_3 is predominantly used to produce nitrogen fertilizer. Catalysts are indispensable for the production of petroleum products such as gasoline, light oil, jet fuel, and heavy oil from crude oil [2]. The catalytic reactions convert fractions distilled from crude oil into hydrocarbons with an appropriate number of carbon atoms, carbon skeleton, and hydrogen to carbon ratio (H/C) for each petroleum product (Fig. 2). In addition, hydrogenation reactions, including hydrodesulfurization and hydrodenitrogenation over solid catalysts, are used to remove sulfur and nitrogen compounds, which produce air pollutants, including SO_x and NO_x , through combustion of gasoline and light oil. Hydrogen (H_2), which is an expected next-generation clean fuel, is mainly produced by the reaction of carbon resources such as petroleum and natural gas with steam at high temperature in the presence of a supported NiO catalyst (Eq. 1).



To mitigate global warming, replacement of fossil fuels such as coal, oil, and natural gas with renewable carbon resources, typically biomass, is essential. Currently, catalysts for the hydrolysis of cellulose, a non-edible biomass, into monosaccharides and oligosaccharides, and further conversion of the obtained saccharides into more useful chemicals (Scheme 1), are being actively developed [3]; however, such catalysts have not yet been put into practical use.

Catalysts are also indispensable for making daily commodities, such as plastic and synthetic fibers. Polymers are the raw materials for plastic and synthetic fibers and are synthesized mainly through the polymerization of monomers using high-performance catalysts [4]. In addition to polymers, various monomers are produced via catalytic reactions. Catalysts are also used in the production of high value-added chemical products, called fine chemicals, and in the organic synthesis of functional organic compounds such as pesticides and pharmaceuticals [5]. Without catalysts, these products could not be obtained. In other words, catalysts are important functional materials for efficiently advancing chemical reactions to produce fuels and chemicals. In fact, catalysts are used in approximately 70% of industrial chemical processes worldwide [1]. Catalysts are also active in the generation of energy used in our daily lives. For example, a high-performance electrode catalyst is required in fuel cells [6], which are expected to be next-generation power generation devices (Fig. 3).

Catalysts are also widely used to keep our environment clean by the decomposition of harmful chemicals into harmless chemicals before they are released into the environment [7]. For example, catalysts are installed in a gas purification system for nitrogen oxides (NO_x) generated in thermal power plants, boilers, and waste incinerators; such NO_x is known as thermal NO_x because it is generated by the thermal reaction of N_2 with O_2 at high temperatures. In this purification system, NO_x is decomposed by reaction with NH_3 into harmless N_2 through a honeycomb-structured reactor, on which the $\text{V}_2\text{O}_5/\text{TiO}_2$ catalyst is fixed (Fig. 4) [8]. Automobile exhaust gases contain NO_x , CO, and unburned fuel. These air pollutants are

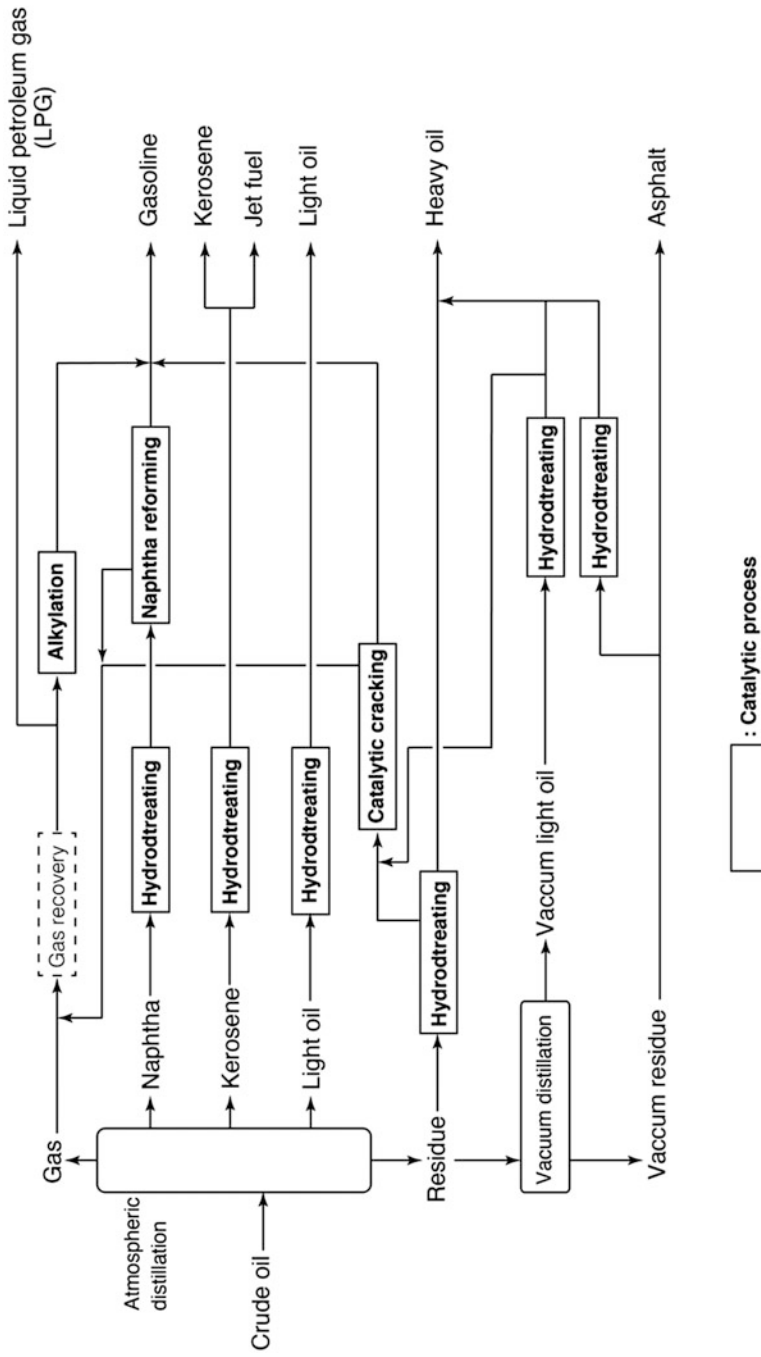
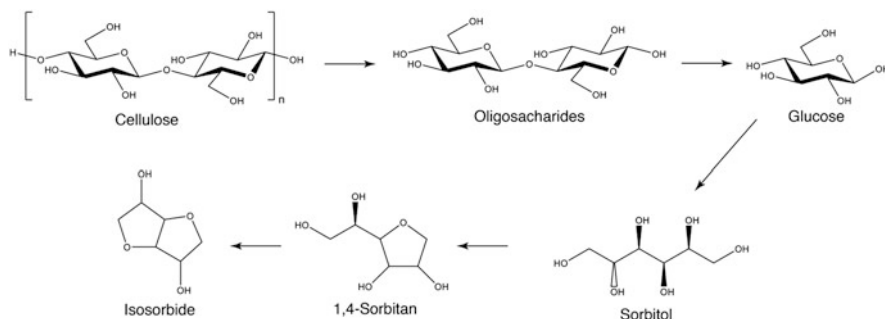


Fig. 2 Catalytic processes in a refinery



Scheme 1 Production of useful chemicals from non-edible biomass via catalytic reactions

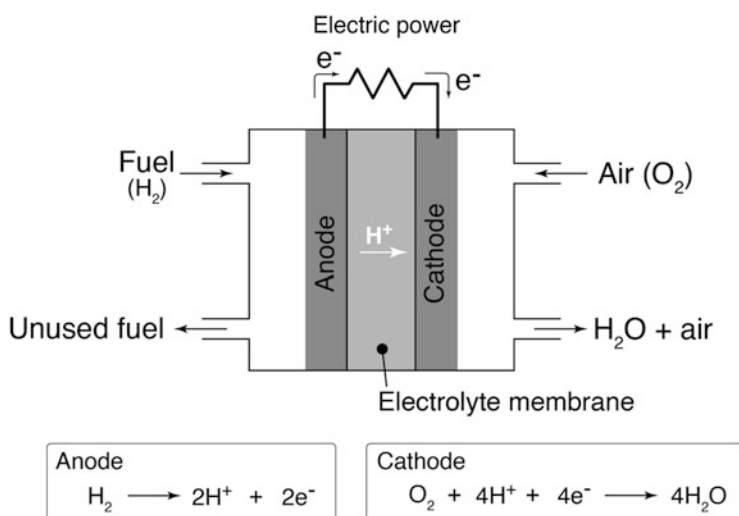


Fig. 3 Schematic illustration of a fuel cell

concurrently decomposed in a catalytic converter installed in an automobile, and the cleaned exhaust gas is released into the environment [9]. Particulate matter (PM) contained in the exhaust gas of buses and trucks with diesel engines is captured on a porous ceramic filter coated with a catalytically active component to burn them out.

The catalyst not only contributes to the purification of exhaust gas, but also to the purification of wastewater containing harmful chemical substances. For example, organic compounds contained in wastewater discharged from factories are decomposed by wet air oxidation using a supported precious metal catalyst such as Pt/Al_2O_3 (Fig. 5) [10]. Through this treatment, the biodegradability of the organic compounds in the wastewater is enhanced. Consequently, these compounds can be treated through an activated sludge process in the subsequent stage, whereby organic

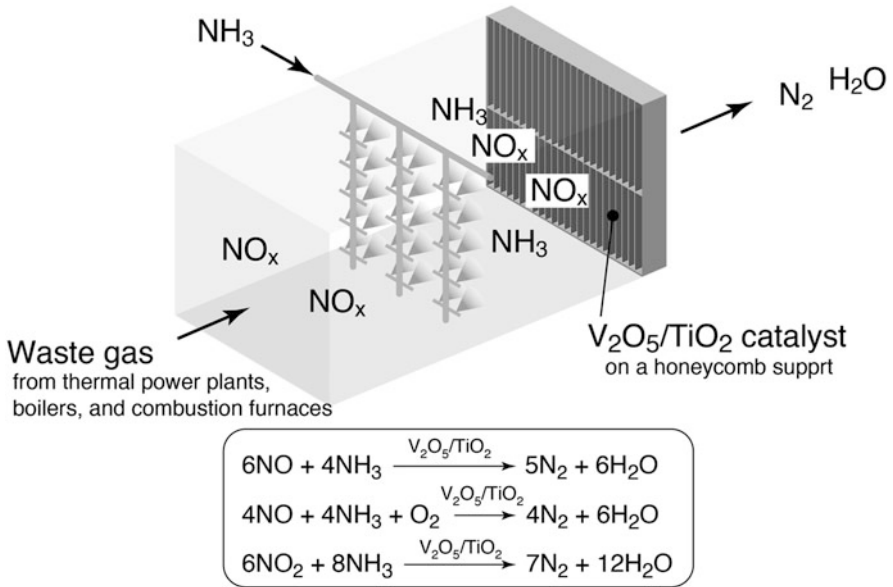


Fig. 4 Waste gas treatment system for NO_x using $\text{V}_2\text{O}_5/\text{TiO}_2$ catalyst

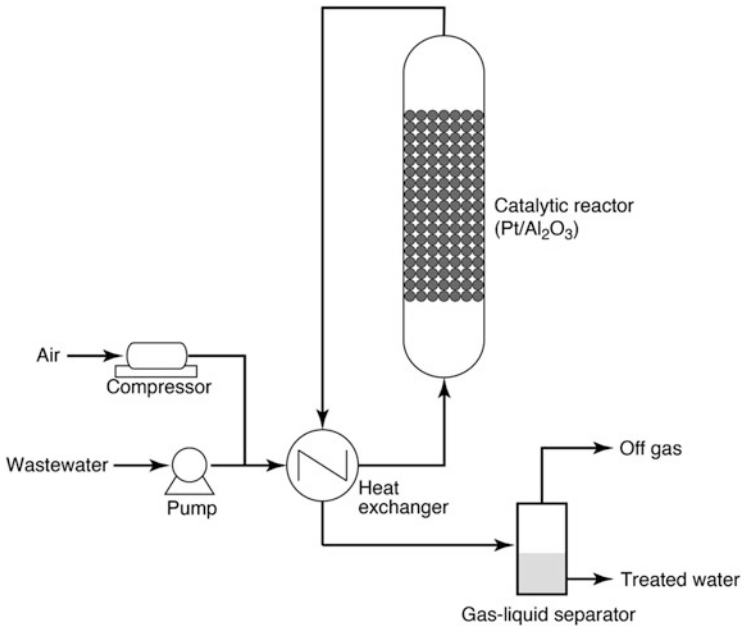


Fig. 5 Process flow of catalytic wet air oxidation for wastewater treatment

compounds in wastewater are completely decomposed into CO_2 and H_2O and released into the environment.

In summary, fuels can be stably supplied by catalytic reactions, and chemical products can be obtained by using catalysis in large quantities at low cost, which is the basis for today's rich material society. Furthermore, an increase in food production that supports the world's population growth is supported by the production of NH_3 and pesticides through catalytic reactions. In addition, catalysts play an important role in environmental protection, such as the purification of exhaust gas and wastewater. In this way, modern society cannot exist without catalysts, and it is obvious that catalysts are key materials, and catalytic technologies are indispensable for our lives.

2 How Does a Catalysts Work?

A catalyst is defined as a substance that significantly increases reaction rate by adding only a small amount to the reaction system without itself changing after the reaction. Thus, a catalyst is not consumed by the reaction and does not appear in a stoichiometric equation for the overall reaction. However, a catalyst is involved in the reaction, and it causes a significant increase in the reaction rate. Such action of a catalyst is called "catalysis."

Taking the combustion reaction of hydrogen ($2\text{H}_2 + \text{O}_2 \rightarrow 2\text{H}_2\text{O}$) as an example, the mechanism by which a catalyst exhibits catalysis is explained. For instance, even if a mixed gas of H_2 and O_2 is heated to approximately 200°C , the reaction hardly occurs (Note: it is very dangerous, so never actually do it!). However, if a small amount of copper powder is added to the mixed gas and the reaction system is heated, the reaction proceeds explosively. At this time, no change occurs in the copper powder at first glance. In other words, the copper powder acts as a catalyst.

The catalysis of copper powder in this reaction is shown in Fig. 6. Here, the surface of the copper powder before the reaction was in a reduced state (Cu^0). The Cu^0 on the surface was oxidized to CuO by O_2 . Subsequently, CuO was reduced back to Cu^0 by H_2 , and H_2O was produced. In these series of reactions, the Cu atoms on the surface change in the order $\text{Cu}^0 \rightarrow \text{CuO} \rightarrow \text{Cu}^0$. One molecule of H_2O is formed in one cycle of the reaction. If the surface of the copper powder is oxidized, the reaction starts with CuO and changes in the order $\text{CuO} \rightarrow \text{Cu}^0 \rightarrow \text{CuO}$. After one cycle of the reaction, the copper atom on the surface returned to its original state. As in this example, the important thing to understand regarding catalysis is that (1) a

Fig. 6 Catalysis of copper powder for hydrogen combustion

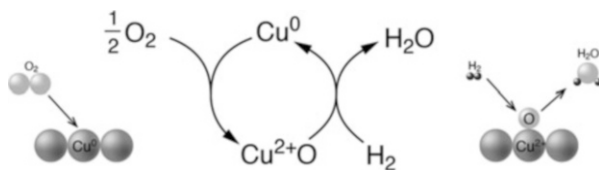
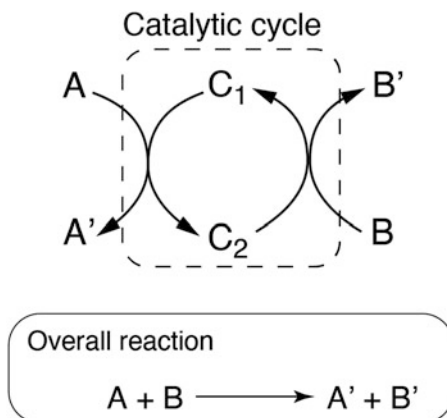


Fig. 7 A generalized catalytic cycle



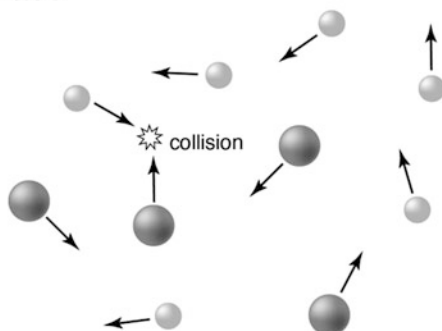
series of reactions involving a catalyst forms a cycle, (2) a reaction proceeds once for each cycle, and (3) an active site on the catalyst returns to its original state after one cycle of the reaction.

Next, the catalysis of a more general reaction ($A + B \rightarrow A' + B'$) shown in Fig. 7 is addressed. In this reaction, C_1 or C_2 is the catalyst. If C_2 is stable, the reaction forming C_2 proceeds smoothly, but the reaction returning to C_1 is difficult because of the high stability of C_2 . On the contrary, if C_1 is stable, the reaction giving C_1 proceeds quickly, but the reaction going to C_2 is slow. According to the theory of a rate-determining step in a sequential reaction, the overall reaction rate is governed by the rate of the slowest step, which is called the rate-determining step; if either C_1 or C_2 is too stable, the overall reaction rate is slow. In other words, it is important for a catalyst to exhibit high catalytic performance in that both C_1 and C_2 are not too stable or too unstable.

Now, let us consider why the reaction is accelerated by a catalyst, taking a simple gas phase reaction $A + B \rightarrow C$ as an example. For this reaction to occur without any catalyst, namely the non-catalytic reaction, reactants A and B must collide at one point in three-dimensional space (Fig. 8). Such collisions are unlikely to occur. Moreover, if the translational velocities of the reactant molecules are slow, the kinetic energy of the molecules is too small to exceed the activation energy of the reaction, and thus no reaction occurs if they collide. In general, because the activation energy of such a non-catalytic reaction is customarily large, a high reaction temperature is necessary to cause a reaction.

On the other hand, if a solid catalyst is present in the reaction system, reactants A and B are easily adsorbed onto the surface of the catalyst to form chemical bonds with atoms on the surface, which is called chemisorption. Because the surface of the catalyst has a coordination number smaller than that in the bulk, the surface of the catalyst is unstable. Therefore, the surface of the catalyst is stabilized by adsorbing molecules. Because the entropy change associated with adsorption is negative, the adsorption of molecules is exothermic in all cases. As a result, the densities of A and B on the catalyst surface are significantly higher than those of A and B in the gas

In gas phase



On catalyst surface

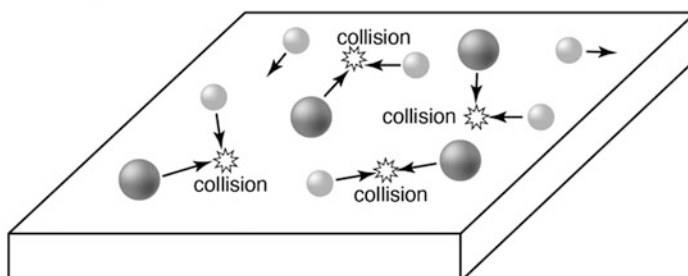


Fig. 8 Non-catalytic reaction in gas phase and catalytic reaction occurring on a solid catalyst

phase, namely, concentrations of A and B. The adsorbed A and B move around the surface and collide. The collision probability between A and B was significantly greater than that in the gas phase (Fig. 8). This effect caused by a solid catalyst is called the concentration effect, which is one of the reasons for the acceleration of the reaction by a catalyst. In addition to the concentration effect, the formation of a reaction route with a low activation energy on the catalyst surface is another reason for the catalytic reaction being fast (Fig. 9).

3 Purification of Water with Catalytic Reactions

The earth is said to be a water planet, but the freshwater that can be used by humans, excluding permanently frozen ground and glaciers, constitutes only 0.7% of the water that exists on the earth. Demand for water continues to rise significantly as the population is increasing, and as living standards are improving. However, water supply is not secured to meet the increase in demand. Thus, serious water shortages,

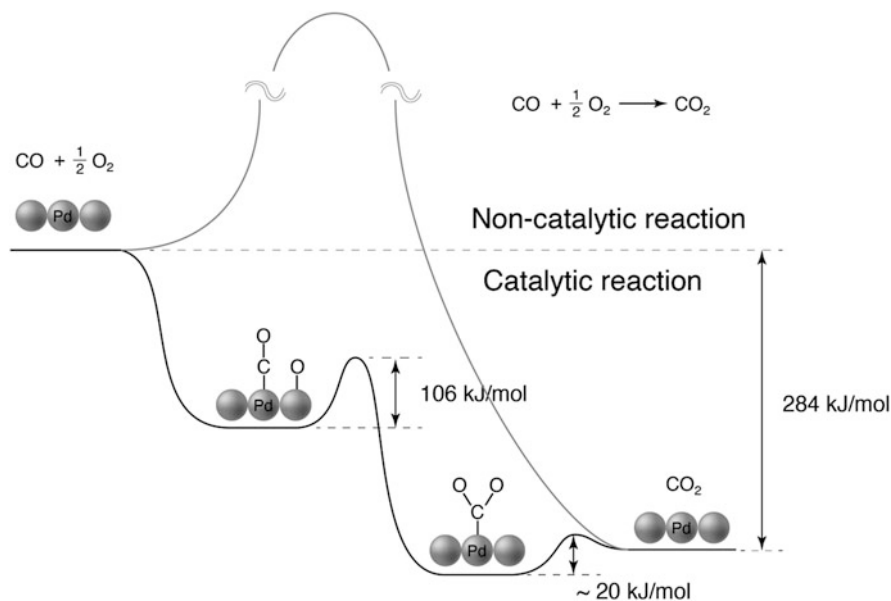


Fig. 9 Energy diagram for non-catalytic and catalytic reactions for CO oxidation

which are called water crises, have begun to occur in various parts of the world. In the future, water shortages will become even more serious, and it is predicted that by 2050, as many as 40% of the population will not be able to obtain enough clean fresh water (Fig. 10) [11]. In the twentieth century, there have been conflicts around the world over oil. Similarly, it is said that the battle for water will occur in the twenty-first century. As such, we must immediately, and actively develop technologies to ensure sufficient amounts of clean fresh water, and it is a mission that researchers and engineers like readers of this chapter should address.

3.1 Groundwater Pollution with Nitrate

Of the fresh water that humans can use, 98% is groundwater. Groundwater has been used as a daily water source for a long time because its quality is generally good owing to the soil purification effect. In addition, the annual fluctuation in water volume is small for groundwater. In Japan, which has abundant rainfall and steep terrain, the quality of river water is good, so the utilization rate of river water as a water source for tap water is high. Consequently, the dependence on groundwater is not very strong. However, in Europe, where there are many long rivers that straddle the countries, the quality of river water in the downstream area deteriorates significantly; thus, groundwater is a major source of daily-use water. In developing countries, where the development of water supply systems is delayed, groundwater

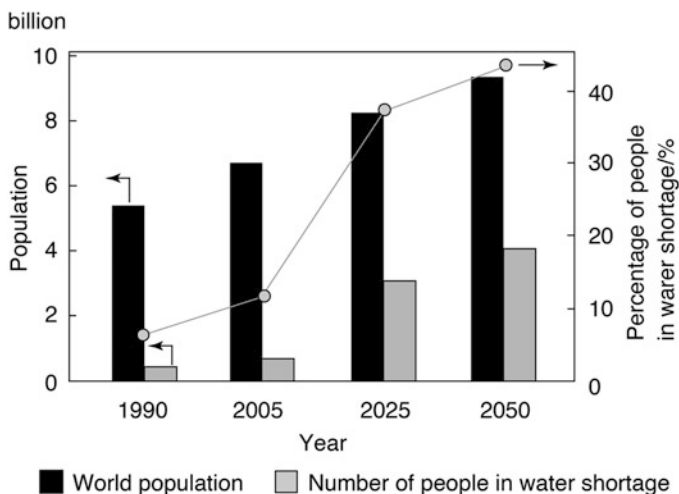


Fig. 10 World population, number of people suffering from water shortage, and percentage of people suffering from water shortage in the past, present, and future. Availability of less than 1,000 m³/year of clean fresh water is defined as water shortage

is an important water source for daily usage. However, in the latter half of the 1970s, groundwater pollution with nitrate nitrogen (NO₃⁻) became apparent in various parts of the world, and it continues to be a problem worldwide [12].

According to a report by the European Environment Agency [13], more than 20% of wells in the European Union have found NO₃⁻ at concentrations exceeding the allowable concentration for drinking water (50 mg/L) recommended by the World Health Organization (WHO). In addition, 25 mg/L or more of NO₃⁻, considered desirable by the WHO, is detected in approximately 40% of the survey wells. A few studies have extensively investigated the pollution situation of developing countries, but wells polluted with extremely high concentrations of NO₃⁻, especially shallow wells, have been found, and urgent comprehensive investigation is needed. In Japan, the combined nitrogen concentration of NO₃⁻ and nitrite nitrogen (NO₂⁻) must be below 10 mg/L (as N), as per the water quality standard for groundwater. In considering only NO₃⁻, the concentration is below 44 mg/L for NO₃⁻. As such, the water quality standard for tap water in Japan was determined according to this regulation, with a guideline of 44 mg/L for NO₃⁻. The Ministry of the Environment of Japan conducts a water quality survey of about 5,000 wells every year, and NO₃⁻ concentrations exceeding the water quality standard are detected in 3–5% of the wells. Unfortunately, the situation has not improved.

The main causes of groundwater pollution with NO₃⁻ are excessive fertilizer application on farmland and improper treatment of livestock manure (Fig. 11) [14, 15]. A large amount of fertilizer is spread on farmland to increase crop yield. Excess nitrogen fertilizer that is not absorbed by crops is oxidized to NO₃⁻ via NO₂⁻ by the action of microorganisms, which is called nitrification. Because soil has a weak retention capacity for NO₃⁻, it gradually moves deep into the ground along

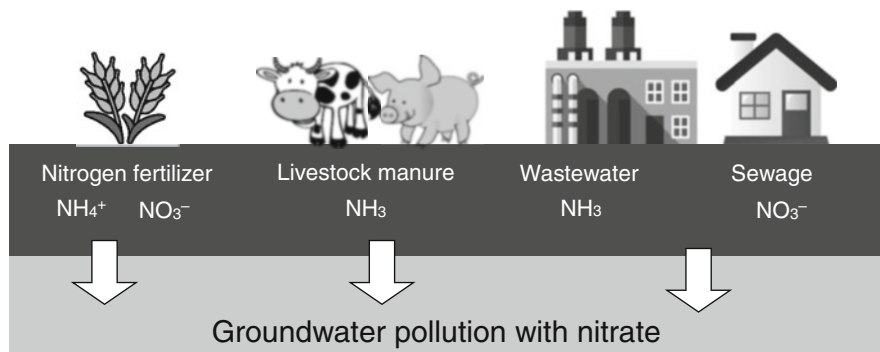


Fig. 11 Causes of groundwater pollution with nitrate

with the underground penetration of rainwater, and finally reaches groundwater causing pollution. Improper treatment of livestock manure, such as field piles and digging, causes groundwater pollution through the same process as that from overfertilization of farmland. In urban areas, leakage of sewage from damaged sewer pipes to the soil is another cause of groundwater pollution by NO₃⁻.

Nitrate ions taken orally through drinking water are reduced to NO₂⁻ in the stomach. If NO₂⁻ is absorbed into the blood, it combines with hemoglobin to form methemoglobin. Since methemoglobin is incapable of carrying oxygen, high levels of blood methemoglobin cause cyanosis; this is called methemoglobinemia, and in severe cases, it results in death. Infants are particularly vulnerable to serious health hazards owing to their low tolerance for NO₃⁻.

3.2 Purification Methods for the Polluted Groundwater

In general, the removal of a pollution source from a polluted environment is a permanent and effective way to solve the environmental pollution problem. However, because groundwater pollution with NO₃⁻ is mainly caused by overfertilization of nitrogen fertilizer on farmland, it is practically challenging to take such measures against the problem. In addition, because it takes decades for NO₃⁻ to reach groundwater from the farmland, although it depends on the depth of aquifer and farmland conditions, it will take a long time for the effect to appear such that the polluted groundwater can be restored. Thus, even if the pollution source is removed, the quality of the groundwater is not recovered immediately. Therefore, the purification of polluted groundwater is a realistic initiative for solving the problem of groundwater pollution with NO₃⁻.

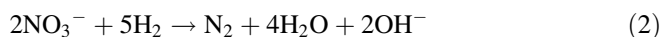
Techniques used for desalination of seawater to provide fresh water, such as ion exchange [16], reverse osmosis [17], and electrodialysis [18, 19] have been widely studied as a method for the purification of groundwater polluted with NO₃⁻. However, all of these are separation techniques, and wastewater with concentrated

NO_3^- is inevitably generated; as such, secondary treatment is needed. Therefore, a method for decomposing NO_3^- into harmless compounds, ideally N_2 and H_2O , is desirable.

An activated sludge method (biological treatment) commonly used for sewage treatment is available as a purification technology for this purpose. The application of this method to the purification of groundwater polluted with NO_3^- has been studied [20]. The activated sludge method utilizes the action of denitrifying bacteria in activated sludge that can use NO_3^- as an oxygen source under anaerobic conditions. Through this action, NO_3^- is decomposed into N_2 . The activated sludge method is an excellent method for the decomposition of NO_3^- , but because it is a biological treatment, the reaction is slow, and large purification equipment is necessary. In addition, strict operation control is required to maintain the activated sludge in an active state. The biggest and most serious problem with the activated sludge method to produce drinking water is the potential contamination of treated water with pathogenic microorganisms. Even if the treated water is completely sterilized, people have a high resistance to drinking water, and it takes a lot of work and time to attain social tolerance for practical use of the active sludge method in producing drinking water.

3.3 Catalytic Reduction of NO_3^- for Purification of the Polluted Groundwater

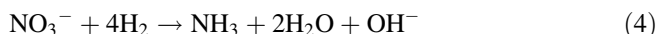
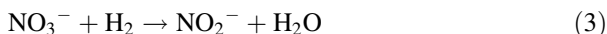
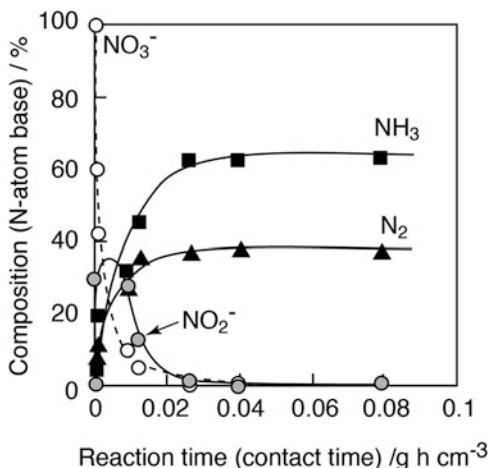
Chemical reduction of NO_3^- with H_2 in the presence of a solid catalyst has been proposed (Eq. 2) as a promising method to decompose NO_3^- into harmless products. This method is called the catalytic method.



The decomposition of NO_3^- in the catalytic method is several orders of magnitude faster than that in the activated sludge method. Unlike in the activated sludge method, which utilizes the action of microorganisms, the reaction in the catalytic method can be accelerated by increasing the reaction temperature or the catalyst amount because this method is based on only a chemical reaction. Therefore, a large amount of polluted groundwater can be purified using a small amount of chemical reactor. In contrast to the activated sludge method, the catalytic process is easy for daily start-up and shut-down, which is a major advantage for obtaining the required amount of purified water whenever needed.

In the catalytic method, NH_3 and NO_2^- , which are products of hydrogenation and partial reduction, respectively, can be by-products (Eqs. 3 and 4).

Fig. 12 Contact time dependence of reduction of NO_3^- over CuPd/active carbon taken in a fixed-bed flow reactor [27]



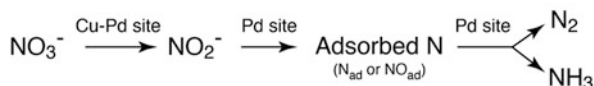
NO_2^- is more harmful to the human body than NO_3^- , whereas NH_3 gives off an unpleasant odor, their presence is not suitable for drinking, thus, the formation of by-products should be avoided in the catalytic method. Therefore, the catalyst must have high activity as well as high selectivity to N_2 .

The catalytic method was first reported by Vorlop et al. in 1989 [21]. They investigated catalysts with single and binary metals for the reduction of NO_3^- with H_2 in water. They found that CuPd bimetal supported on Al_2O_3 shows catalytic activity and forms a relatively small amount of undesirable NH_3 [22]. With this paper as a trigger, the catalyst search was advanced to find more active and selective catalysts, and InPd, SnPd, and CuPt were found to act as catalysts for the reaction [23, 24].

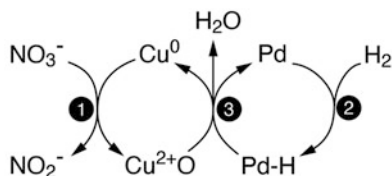
The reaction mechanism of the reduction of NO_3^- was investigated in detail using supported CuPd catalysts [25, 26]. As shown in Fig. 12, the reaction result of the NO_3^- reduction in water clearly indicates that the reaction proceeds sequentially through NO_2^- as an intermediate, when performed by changing the reaction time; this is the contact time in the case of the reaction with a fixed-bed flow reactor [27]. Moreover, since the formation of NO_2^- is observed only in the very early stage of the reaction, namely in the short contact time region, the reaction from NO_3^- to NO_2^- is the rate-determining step. Furthermore, (1) a single metal catalyst consisting of only one of Cu and Pd does not show any catalytic activity for NO_3^- reduction, but (2) the single metal Pd catalyst shows extremely high catalytic activity for the reduction of NO_2^- , and (3) metallic copper powder (Cu^0) can reduce NO_3^- stoichiometrically, but non-catalytically. Based on these findings, the reaction mechanism shown in Fig. 13 is proposed [25]. Accordingly, the catalytic reduction of NO_3^- to NO_2^- proceeds on the Cu-Pd pair site, on which Cu^0 stoichiometrically

Fig. 13 Proposed reaction mechanism for reduction of NO_3^- over a supported CuPd catalyst

Reaction rate for reduction of NO_3^-



Reaction from NO_3^- to NO_2^- on a Cu-Pd site

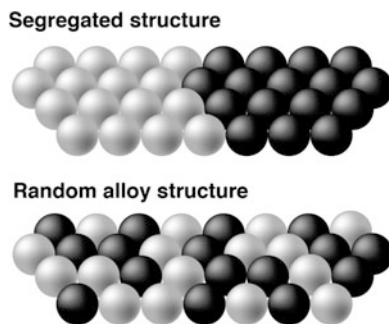


reduces NO_3^- to NO_2^- ; then, the Cu^{2+}O generated by this reaction is reduced by the atomic H activated on Pd, returning Cu^{2+}O to the original state (Cu^0). On the other hand, the subsequent reactions after NO_2^- , which is the reaction to form the final product N_2 or NH_3 via the adsorbed N species as an intermediate, proceed on the Pd site. The activation of H_2 , which generates atomic H, occurs only on the Pd site, and the Cu sites do not activate H_2 under the reaction conditions.

Details of the reaction mechanism, for example, whether the adsorbed N species is an atomic N or an adsorbed NO, etc., are still under discussion, but there is no doubt that the reaction of the adsorbed N species that occurs on the Pd site is an important reaction step that determines selectivity. When the adsorbed N species reacts with another adsorbed N species, N_2 is generated, while the reaction with adsorbed H atoms results in the formation of NH_3 . According to this, the surface densities of adsorbed N species and adsorbed H atoms on the Pd site are important parameters for determining the selectivity. If the surface density of the adsorbed N species is high or if the surface density of adsorbed H atoms is low, it is considered that the formation of N_2 occurs preferentially over that of NH_3 . Thus, it is considered that high N_2 selectivity could be achieved if the catalyst is designed to achieve such a situation (high density of the adsorbed N species and low density of the adsorbed H atoms) on the surface.

There are two typical alloy structures of the CuPd alloy nanoparticles (Fig. 14): (1) segregated structures in which Cu and Pd domains are separately present, and (2) a random alloy structure in which Cu and Pd atoms are randomly mixed. On the surface of the CuPd alloy nanoparticles with a segregated structure, Cu-Pd pair sites are formed only at the interface between the two domains. On the other hand, it is apparent that the CuPd alloy nanoparticles with random alloy structures have many Cu-Pd pair sites on their surfaces. Based on this discussion, the catalytic properties of the two CuPd alloy particles were predicted as follows: For the segregated structured CuPd alloy particles, because there are few Cu-Pd pair sites where the reaction from NO_3^- to NO_2^- progresses, it is expected that the supply rate of NO_2^- to the Pd site is slow. Consequently, the surface density of the adsorbed N species

Fig. 14 Typical two structures on the surface of CuPd alloy particles



remained low. This state also leads to a decrease in the consumption of H atoms adsorbed on the Pd site, because less Cu^{2+}O is generated on the Cu-Pd site. As a result, it is considered that the surface density of the adsorbed H atoms on the Pd site remains high.

In contrast, because the CuPd alloy particle with the random alloy structure has many Cu-Pd pair sites on the surface, the formation rate of NO_2^- is high, leading to a high surface density of adsorbed N species on the Pd sites. This state results in the consumption of large amounts of adsorbed H atoms for the reduction of both NO_2^- and Cu^{2+}O , so that the surface density of adsorbed H atoms is kept low. Based on these expectations, it was thought that the CuPd alloy particles with a random alloy structure would be an excellent catalyst with high activity and high N_2 selectivity for the reduction of NO_3^- with H_2 in water, which is promising for the purification of polluted groundwater.

To demonstrate this, we applied a CuPd alloy cluster protected by polyvinyl pyrrolidone (PVP) to the catalyst [28], because extended X-ray absorption fine structure analysis (EXAFS) revealed that the alloy cluster had a random alloy structure [29]. The catalytic activity for the reduction of NO_3^- changed significantly depending on the Cu/Pd ratio, when using the CuPd alloy cluster supported on activated carbon (CuPd_{-PVP}/AC) (Fig. 15). In this case, CuPd_{-PVP}/AC with Cu/Pd = 1 showed the highest activity. This result is reasonable because the CuPd alloy cluster with Cu/Pd = 1 has the largest number of Pd pair sites on the surface. However, the CuPd alloy cluster protected by PVP is problematic, as it entails complicated preparation procedures and large amounts of waste generation to obtain the cluster. In addition, only a small amount of CuPd cluster (less than 1 wt.% for total weight of the catalyst) can be fixed on AC due to electrostatic repulsion between the protecting agent (PVP) and the surface of AC.

To solve these problems, the CuPd cluster protected by sodium citrate was applied instead of that protected by PVP [30], because the preparation procedure was much simpler and easier, and less waste was generated during the preparation of the cluster. Furthermore, more than 2 wt.% of the cluster was able to be fixed on AC, which was advantageous to obtain more active catalysts. Here, the CuPd cluster protected by sodium citrate supported on AC was named CuPd/AC_{-random}. For comparison, the CuPd/AC catalyst – named CuPd/AC_{-segre}, in which Pd and Cu

Fig. 15 Influence of Cu/Pd ratio in CuPd clusters protected by PVP on activity for reduction of NO_3^- [28]. The total amount of metals (Cu + Pd) was fixed to be $0.0234 \text{ mmol g}_{\text{cat}}^{-1}$

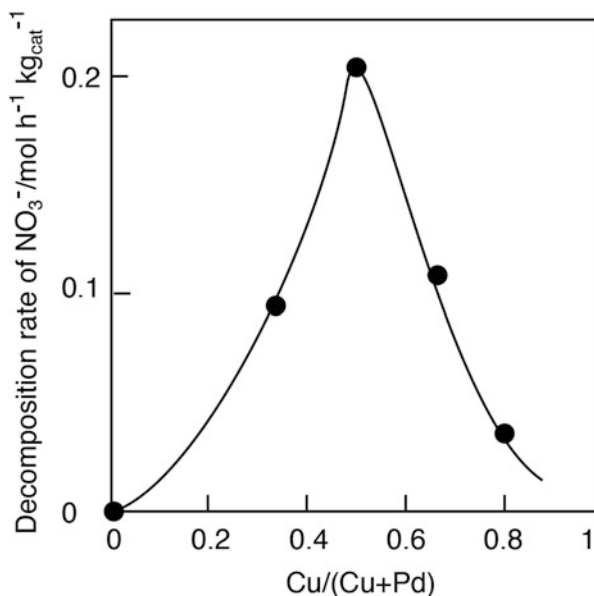


Table 1 Catalytic performance of the CuPd catalysts with random alloy and segregated structures for reduction of NO_3^- in water

Catalyst	P_{H_2} ^a (atm)	Selectivity (%)		Decomposition rate of nitrate ($\text{mol h}^{-1} \text{ kg}_{\text{cat}}^{-1}$)
		$\text{N}_2 + \text{N}_2\text{O}$	NH_3	
CuPd/AC_random	0.5	89	9	21
	0.05	>99	<1	8
CuPd/AC_segre	0.5	70	26	5
	0.05	96	4	<1

Reaction conditions: temperature, 298 K; reactant, NO_3^- , 100 mg/L from NaNO_3 ; H_2 (0.5 atm) or H_2 (0.05 atm), CO_2 (0.5 atm)

^aPartial pressure of H_2

were sequentially supported on AC to form a segregated structure of CuPd particles – was prepared.

The random alloy and segregated structures of the CuPd particles on AC were confirmed by powder X-ray diffraction and EXAFS analyses. As shown in Table 1, the NH_3 selectivity of CuPd/AC_random was 9% for the reaction, with a hydrogen partial pressure of 0.5 atm ($=P_{\text{H}_2}$); in contrast, a larger amount of NH_3 was formed over CuPd/AC_segre, with the NH_3 selectivity being 26%. Moreover, the reduction rate (catalytic activity) of NO_3^- was approximately four times higher than that of CuPd/AC_segre because CuPd/AC_random had many Cu-Pd pair sites. In the reaction experiments mentioned above, an aqueous solution of NaNO_3 with 100 mg/L NO_3^- ($=1.6 \text{ mmol/L}$), approximately twice the concentration of the water quality standard, was used. Thus, if the groundwater polluted with the same

concentration of NO_3^- is purified by the catalytic method, the selectivity to NH_3 must be 2% or less. In other words, the selectivity to N_2 must be 98% or more to meet the permissible concentration of NH_3 in drinking water (0.5 mg/L as NH_3). Thus, hoping for further decrease in the surface density of the adsorbed H on the catalyst, the partial pressure of H_2 was lowered from 0.5 to 0.05 atm, and the reaction was carried out at $P_{\text{H}_2} = 0.05$ atm. The results showed that even at a NO_3^- removal rate near 100%, the formation of NH_3 was completely suppressed (Table 1). Under these reaction conditions, N_2 was produced as a gaseous product with a selectivity of approximately 30%, and the remaining gaseous product was N_2O . Since N_2O is a gas with a large warming coefficient, 298 times larger than that of CO_2 , its release into the atmosphere must be avoided. The problem of N_2O formation was solved by post-treatment of exhaust gas with a supported Pd catalyst. Supported Pd catalysts are known to effectively promote the reduction of N_2O to N_2 with H_2 . In the gas phase at the outlet of the reactor for NO_3^- reduction, excess H_2 which was not used for the NO_3^- reduction was present. Thus, the formed N_2O was rapidly reduced with excess H_2 over Pd/ Al_2O_3 placed at the outlet of the reactor, even at room temperature (Fig. 16).

As described hitherto, it has been demonstrated that the CuPd alloy cluster with a random alloy structure can reduce NO_3^- with H_2 selectively to N_2 and N_2O with a high reaction rate. However, the synthesis of the CuPd alloy cluster protected with sodium citrate is cumbersome in practice; this is because both Pd^{2+} and Cu^{2+} in the aqueous solution must be reduced slowly in the presence of sodium citrate under an inert atmosphere such as N_2 , using a large amount of a diluted FeSO_4 solution, which is a mild reducing agent. This catalyst preparation caused problems such as a large

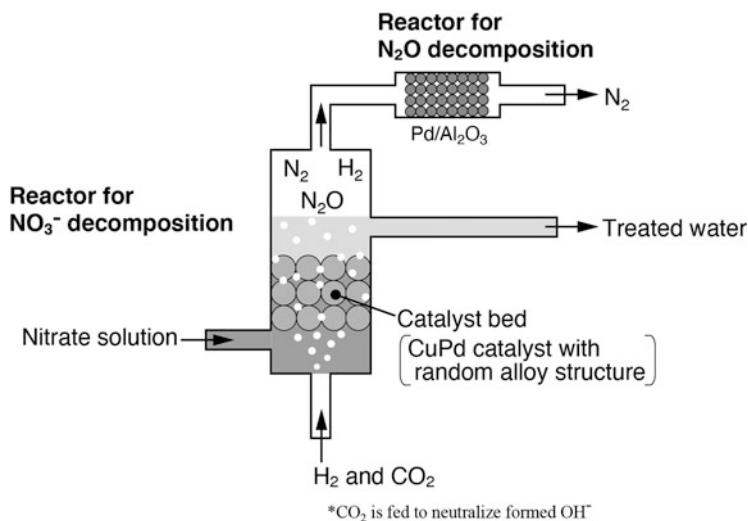
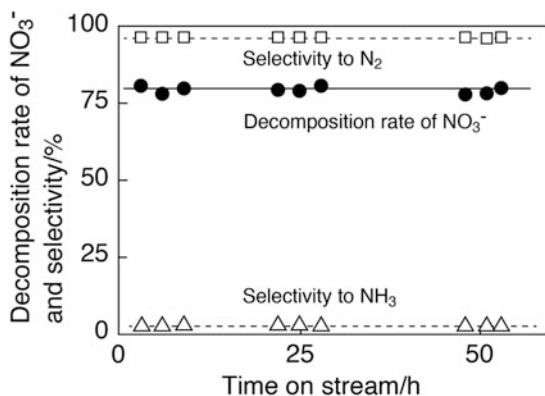


Fig. 16 Schematic of a combined purification system comprising a NO_3^- reduction reactor and a N_2O decomposition reactor

Fig. 17 Time course for reduction of NO_3^- over the CuPd/AC_impreg coupled with Pd/Al₂O₃ placed at the gas exit of a NO_3^- reduction reactor for NO_3^- decomposition



amount of liquid waste generation, and difficulty in scaling up the catalyst preparation. Thus, it was necessary to develop a simpler preparation method with less waste generation and ease of scale-up.

It is known that the alloys of Cu and Pd form a solid solution in the entire composition region in a thermodynamically stable form. As such, if the preparation conditions and procedures are precisely controlled, it is expected that CuPd nanoparticles with a random alloy structure on a support can be obtained, in spite of using common impregnation method, whereby a carrier is added to a solution containing a catalytically active component and the solvent is evaporated to immobilize the active component on the carrier. Thus, this author systematically investigated the Cu/Pd ratio, preparation procedure, addition order, reductants used for the reduction of Cu^{2+} and Pd^{2+} , reduction conditions, type of carrier, etc., and found that the Cu/Pd ratio and reductant were the key parameters for obtaining CuPd alloy nanoparticles with a random alloy structure [31, 32]. In this preparation, excess Cu was added ($\text{Cu/Pd} > 1$), and NaBH_4 was used as a reducing agent for Cu^{2+} and Pd^{2+} fixed on AC in the liquid phase. By such a preparation, a high-performance catalyst showing the same performance as CuPd/AC_random was successfully obtained using a simple and conventional impregnation method. This catalyst, referred to as CuPd/AC_impreg, showed excellent stability, activity, and selectivity for the reduction of NO_3^- in water and maintained high catalytic performance for at least 50 h (Fig. 17).

3.4 Purification of Real Groundwater by the Catalytic Method with the CuPd Catalyst

In the development of the catalyst described in Sect. 3.3, a pure aqueous solution of NO_3^- prepared by dissolving NaNO_3 or KNO_3 in distilled water was used as a reaction solution instead of real groundwater. Groundwater contains various inorganic cations and anions, as well as water-soluble organic matter such as humic acid,

Table 2 Components of the groundwater taken from a well beside a farmland in Kitami, Hokkaido prefecture, Japan

Component		Concentration (mg L ⁻¹)
Anion ^a	NO ₃ ⁻	66.1
	Cl ⁻	37.3
	SO ₄ ²⁻	114.5
	Silicate (Si _x O _y ⁿ⁻) ^b	34.0
Cation ^a	Na ⁺	2.8
	K ⁺	25.1
	Mg ²⁺	18.7
	Ca ²⁺	59.7
Water-soluble organic matter ^c		5.2

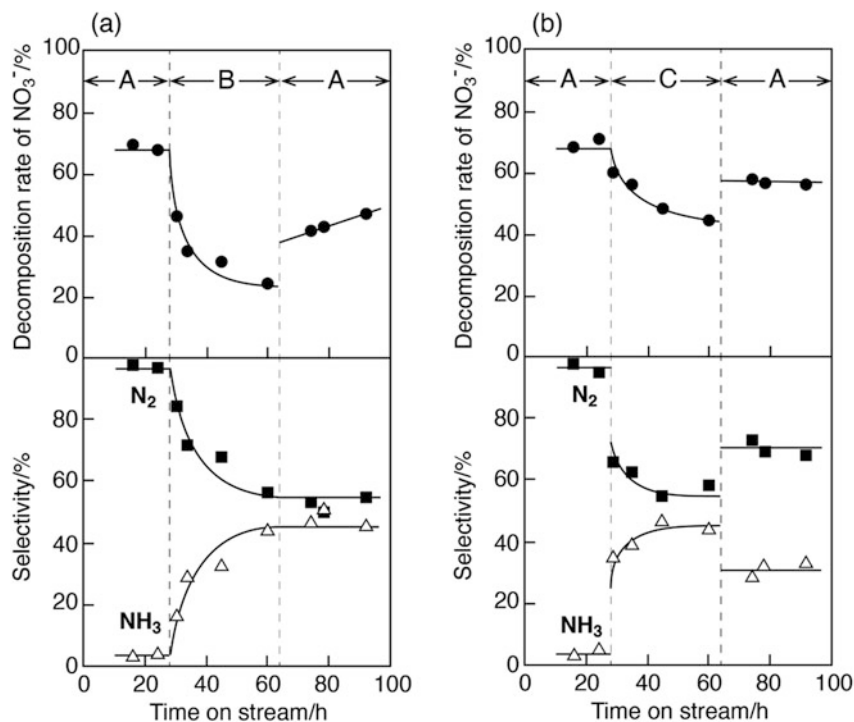
^aDetermined using ion chromatography

^bDetermined using inductively coupled plasma-atomic emission spectrometry (ICP-AES)

^cTotal organic carbon (TOC) determined using a TOC analyzer

in addition to pollutant NO₃⁻. Because the catalytic reaction occurs on the catalyst surface and such compounds in groundwater adsorb on the catalyst surface as NO₃⁻ does, these adsorptions are expected to affect the catalytic performance of the CuPd catalyst. To investigate the effect of co-existing compounds in real groundwater on the catalytic performance, purification of real groundwater collected from a well beside a farmland on Hokkaido Island using CuPd/AC_impreg was performed [32]. Table 2 summarizes the cations, anions, and soluble organic matter contained in the groundwater. Figure 18a shows the catalytic reaction date for CuPd/AC_impreg obtained using a fixed-bed flow reactor. A pure aqueous solution of NO₃⁻ was fed to the reactor filled with the catalyst for approximately 30 h. During this time, the catalyst showed high activity and high selectivity toward N₂. However, after the reaction solution was changed to real polluted groundwater, both the decomposition rate of NO₃⁻ and selectivity to N₂ decreased significantly. Even though the reaction solution was returned to the pure aqueous solution of NO₃⁻ at 65 h, the catalytic performance was not recovered, indicating that CuPd/AC_impreg was irreversibly deteriorated in the groundwater.

The groundwater contained 5.2 mg/L of water-soluble organic matter as total organic carbon (TOC). It was determined that such organic matter caused the irreversible deterioration of CuPd/AC_impreg. Because water-soluble organic matter has hydrophilic functional groups such as hydroxyl and carboxylic groups, these functional groups strongly interact with the catalyst surface, leading to irreversible adsorption to cover the active sites on the catalyst. Ozone, a well-known strong oxidant, was blown into the groundwater at room temperature for 8 h to decompose the water-soluble organic matter in groundwater. This pretreatment of the groundwater reduced the concentration of the water-soluble organic matter from 5.2 to 1.6 mg/L as TOC and considerably inhibited the irreversible deterioration of CuPd/AC_impreg. In fact, the catalytic performance was restored to some extent when the reaction solution was changed from the pretreated groundwater to the pure aqueous NO₃⁻ solution (Fig. 18b). However, the catalytic performance in terms of both activity and selectivity was still lower, even in O₃-pretreated groundwater. A further



A: aqueous NO_3^- solution, B: groundwater, C: O_3 -treated groundwater

Fig. 18 Time courses for reduction of NO_3^- over the CuPd/AC_impreg. In the first 30 h, pure aqueous solution of NO_3^- was fed to the reactor; then, the reaction solution was changed to (a) groundwater and (b) groundwater pretreated with O_3 for 8 h to decompose water-soluble organic matter. At 65 h, the reaction solution was changed back to the pure aqueous solution of NO_3^- .

study revealed that the water-soluble organic matter contained in the groundwater was almost completely decomposed by photocatalytic oxidation, which was performed in the presence of photocatalyst Pt/TiO₂ under UV irradiation. However, despite such pretreatment for groundwater, the catalytic performance of CuPd/AC_impreg was still degraded in the pretreated groundwater. Thus, it was supposed that the inorganic cations or anions contained in the groundwater deteriorated the catalytic performance of CuPd/AC_impreg.

To investigate the influence of the cations or anions contained in groundwater, an aqueous solution of NO_3^- with a cation or anion contained in the groundwater was prepared, and the catalytic performance of CuPd/AC_impreg was evaluated using aqueous solutions as a reaction solution [32]. The obtained results clearly indicate that Cl^- was responsible for the deterioration of the catalytic performance of CuPd/AC_impreg (Table 3). As shown in Fig. 19, the removal rate of NO_3^- gradually decreased, and the selectivity to NH_3 increased as the concentration of Cl^- in the

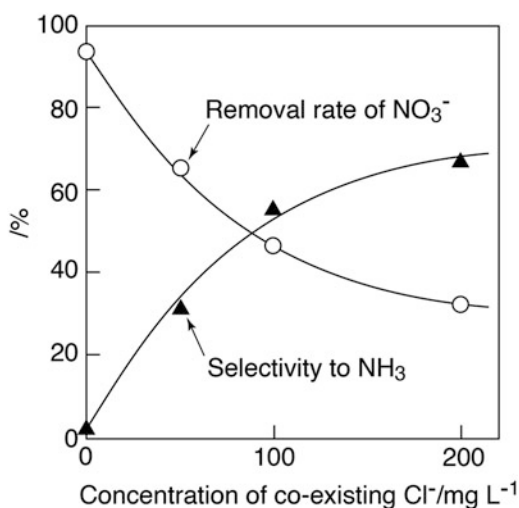
Table 3 Influence of co-existing ions in the reaction solution on the catalytic performance of CuPd/AC_impreg for the reduction of NO_3^-

Co-existing ion ^a	Removal rate of NO_3^- (%)	Selectivity (%)		
		N_2	N_2O	NH_3
None	83	61	37	2
Cl^-	55	48	18	34
SO_4^{2-}	79	40	53	7
K^+	79	64	29	7
Mg^{2+}	82	63	29	7
Ca^{2+}	81	61	35	4

Reaction conditions: catalyst weight, 0.5 g; temperature, 298 K; reactant NO_3^- , 1.6 mmol L^{-1} (100 ppm), 81.6 mmol h^{-1} ; gas composition, $\text{H}_2/\text{He}/\text{CO}_2 = 5/45/50$; total pressure, 1.0 atm; total flow rate of gas, 3 $\text{cm}^3 \text{min}^{-1}$

^aConcentration of co-existing ion was 50 mg L^{-1}

Fig. 19 Influence of concentration of co-existing Cl^- on the catalytic performance of CuPd/AC_impreg. Reaction conditions: catalyst weight, 0.3 g; temperature, 298 K; reactant NO_3^- , 1.6 mmol L^{-1} (100 ppm), 40.3 $\mu\text{mol h}^{-1}$; gas composition, $\text{H}_2/\text{He}/\text{CO}_2 = 5/45/50$; total pressure, 1.0 atm; total flow rate of gas, 3 $\text{cm}^3 \text{min}^{-1}$



solution increased. Furthermore, when the reaction solution was switched from an aqueous solution of NO_3^- with Cl^- to a pure aqueous solution without Cl^- , the catalyst performance was almost completely restored to the original state; thus, the reduction in the catalyst performance caused by Cl^- was reversible. It is noted that Cl^- had no impact on the reduction of NO_2^- over CuPd/AC_impreg, indicating that Cl^- affected only the Cu site and not the Pd site. Because the effect of Cl^- was reversible, it was presumed that Cl^- competed with NO_3^- for adsorption on the Cu sites, causing a tentative reduction in catalytic performance. As mentioned earlier, the reaction of NO_3^- to NO_2^- , which is the rate-determining step, proceeds on the Cu-Pd pair site, and it is considered that the number of effective Cu sites was reduced by the adsorption of Cl^- on the Cu sites, thereby reducing the removal rate of NO_3^- (Fig. 20). In addition, because the reaction rate for the formation of NO_2^- decreased in the presence of Cl^- , the amount of Cu^{2+}O produced by the reduction of NO_3^-

Fig. 20 Schematic showing tentative deactivation of the CuPd catalyst caused by adsorption of Cl^- on the Cu site

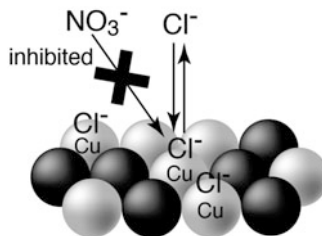
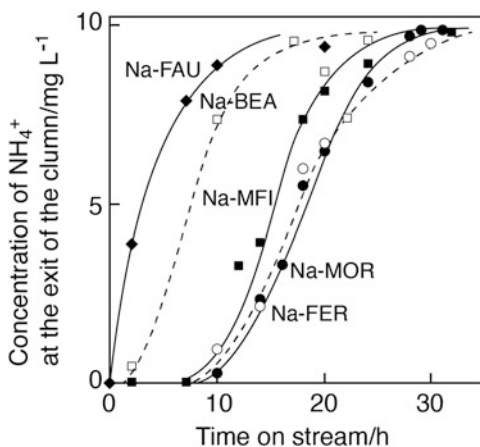


Fig. 21 Time courses of NH_3 concentration at the outlet of columns filled with various Na-type zeolites including Na-faujasite (Na-FAU), Na-mordenite (Na-MOR), Na-beta (Na-BEA), Na-ZSM-5 (Na-MFI), and Na-ferrierite (Na-FER). Conditions: Na-type zeolite, 0.2 g; inlet concentration of NH_3 , 10 mg L^{-1} ; flow rate of aqueous ammonia, $24 \text{ cm}^3 \text{ h}^{-1}$; column temperature, 333 K; and flow rate of CO_2 , $96 \text{ cm}^3 \text{ h}^{-1}$



with Cu^0 decreased as well. As a result, the adsorbed H atoms on the Pd sites was surplus, leading to an increase in the selectivity to NH_3 .

It is assumed that the formation of NH_3 is suppressed by the reaction at P_{H_2} of less than 0.05 atm. However, this is undesirable and unfeasible because the decrease in P_{H_2} also brings about a further decrease in the decomposition rate of NO_3^- , which makes the catalytic reactor larger. The addition of post-treatment equipment to remove or decompose the formed NH_3 is additive to the problem of NH_3 formation in the catalytic reduction of NO_3^- in real groundwater. Among the methods for NH_3 removal and decomposition, ion-exchange adsorption using zeolites is one of the most promising because of its ease of operation and relatively low cost. The authors investigated the removal of low concentrations of NH_3 (10 ppm) using various synthetic zeolites [33]. As shown in Fig. 21, Na-mordenite (Na-MOR) and Na-ferrierite (Na-FER) had the largest NH_3 uptake, as evaluated from breakthrough curves with a column. By using a column filled with Na-MOR as a post-treatment equipment, which was connected at the exit of the catalytic reactor for the reduction of NO_3^- , and the pretreatment of groundwater with O_3 , the real groundwater polluted with NO_3^- was successfully purified without any leaching of NH_3 in the treated water for 40 h (Fig. 22) [32].

Through a combination of the catalytic reduction of NO_3^- over the CuPd catalyst with ion-exchange removal of formed NH_3 over Na-MOR, real polluted

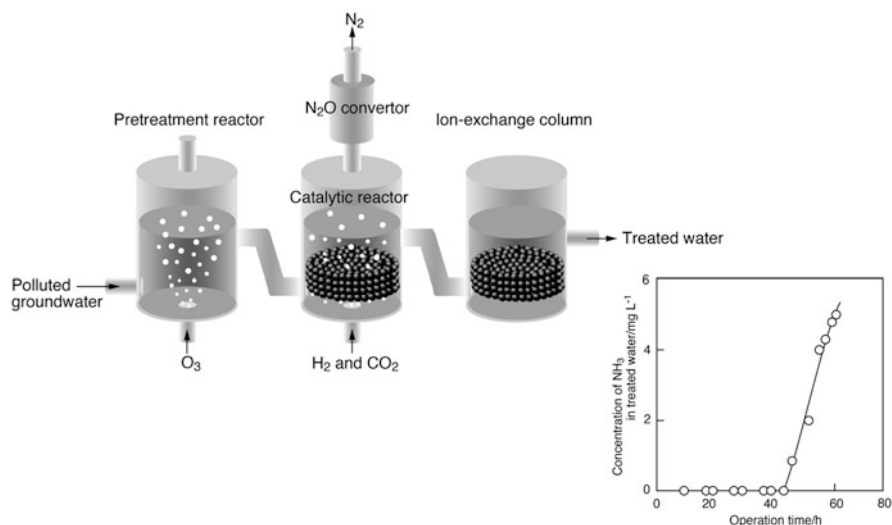


Fig. 22 Schematic of a combined purification system composed of a O_3 -pretreatment reactor, a NO_3^- reduction reactor coupled with a N_2O decomposition reactor, and an ion-exchange column filled with Na-mordenite

groundwater can be purified to a drinkable level. However, post-treatment of the treated water is not very elegant, and the entire treatment process is complicated and large. Because the adsorption of Cl^- on the Cu sites over the CuPd catalyst is an unavoidable phenomenon, it was necessary to develop a catalyst whose performance is unaffected by ionic species in groundwater; and ensure a treatment process that does not require any post-treatment equipment. To do so, a combination of Pd with base metals active for NO_3^- but not Cu was necessary for such a catalyst. This is the next target for catalyst development.

3.5 A Supported SnPd Catalyst for Purification of Real Polluted Groundwater

As mentioned before, there are not many alloy catalysts that are active in the reduction of NO_3^- with H_2 in water. The catalysts showing activity for the reaction should be a combination of precious metals, such as Pd, that activate H_2 at ambient temperature with base metals, and should stoichiometrically reduce NO_3^- and the oxidized form, regenerated with H_2 . In addition to Cu, In and Sn are known as base metals. Therefore, the author investigated the influence of co-existing ions in water on the catalytic properties of the InPd and SnPd catalysts and found that the supported SnPd catalyst ($SnPd/Al_2O_3$) was not significantly affected by the presence of Cl^- in water (Fig. 23) [34, 35]. To clarify why $SnPd/Al_2O_3$ was not affected by Cl^- in water, the adsorption isotherm of Sn/Al_2O_3 for Cl^- in water was measured

Fig. 23 Influence of co-existing ions in the reaction solution on the catalytic performance of the SnPd/Al₂O₃ for the reduction of NO₃⁻. The reactions were performed in a batch-type reactor. Reaction conditions: catalyst, SnPd/Al₂O₃, 10 mg; concentration of NO₃⁻, 1.0 mmol dm⁻³; volume of reaction solution, 250 cm³; gas composition, H₂/CO₂ = 1/1; gas flow rate, 30 cm³ min⁻¹

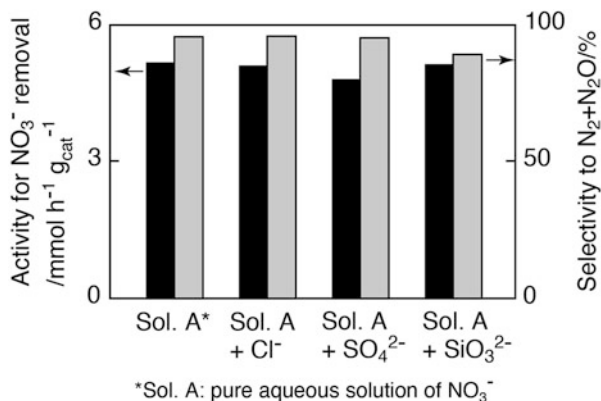
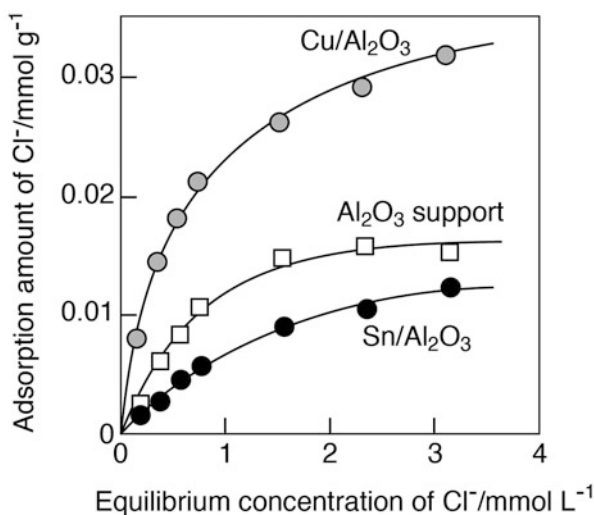


Fig. 24 Adsorption isotherms of Cl⁻ for Sn/Al₂O₃, Cu/Al₂O₃, and Al₂O₃ support. Conditions: adsorbent, 30 mg; temperature, 303 K; volume of solution, 10 cm³; and adsorption time, 24 h



and was compared with that of Cu/Al₂O₃ (Fig. 24). It was found that the equilibrium constant for the adsorption of Cl⁻ on Sn/Al₂O₃ assuming the Langmuir model was approximately one-third of that on Cu/Al₂O₃, indicating weak interaction of Cl⁻ with the Sn site. A kinetic analysis of the reduction of NO₃⁻ over SnPd/Al₂O₃ and CuPd/Al₂O₃ revealed that the reaction order of CuPd/Al₂O₃ for NO₃⁻ was 0.4, whereas that of SnPd/Al₂O₃ was only 0.1 (Fig. 25). The small reaction order of SnPd/Al₂O₃ for NO₃⁻ indicated that Sn had a high affinity for NO₃⁻. These two factors, i.e., weak and strong affinities for Cl⁻ and NO₃⁻, respectively, are the reasons for the high catalytic performance of SnPd/Al₂O₃ in the presence of Cl⁻ in water. In addition, SnPd/Al₂O₃ was more resistant than CuPd/Al₂O₃ to anions other than Cl⁻, like SO₄²⁻ and SiO₃²⁻, which are found in abundance in groundwater (Fig. 23). From these results, it is expected that SnPd/Al₂O₃ can be used for the purification of real groundwater polluted with NO₃⁻.

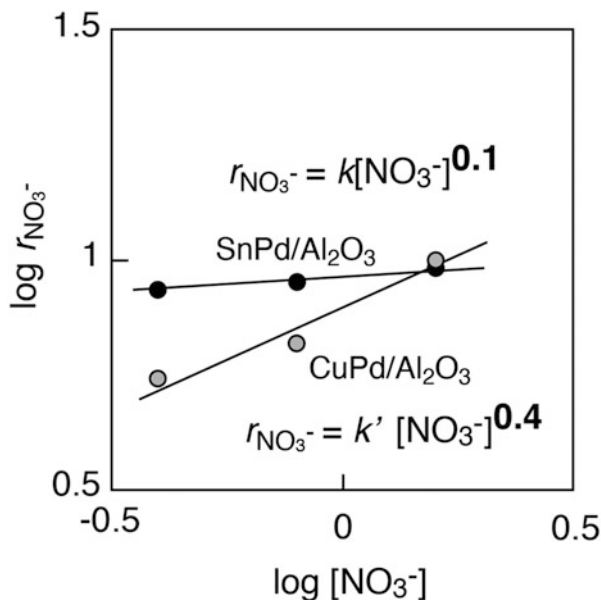


Fig. 25 Dependence of decomposition rate of NO_3^- ($r_{\text{NO}_3^-}$) on concentration of NO_3^- ($[\text{NO}_3^-]$) for the reduction of NO_3^- over SnPd/ Al_2O_3 and CuPd/ Al_2O_3 . Reaction conditions: catalyst weight, 10 mg; reactant NO_3^- , 0.4–1.6 mmol dm^{-3} ; reaction volume, 250 cm^3 ; gas composition, $\text{H}_2/\text{CO}_2 = 1/1$, and gas flow rate, 30 $\text{cm}^3 \text{min}^{-1}$

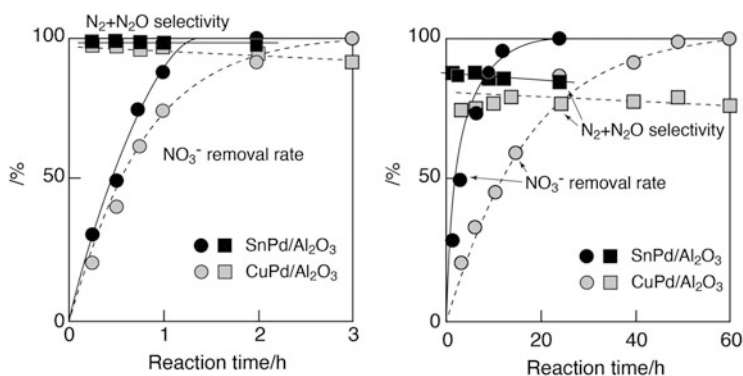


Fig. 26 Time courses for removal rate of NO_3^- and selectivity to $\text{N}_2 + \text{N}_2\text{O}$ for the reduction of NO_3^- over SnPd/ Al_2O_3 and CuPd/ Al_2O_3 . Left: pure aqueous solution of NO_3^- , right: groundwater pretreated through photo-oxidation with Pt/ TiO_2 and UV irradiation. Reaction conditions: catalyst weight, 10 mg; reactant NO_3^- , 0.4–1.6 mmol dm^{-3} ; reaction volume, 250 cm^3 ; gas composition, $\text{H}_2/\text{CO}_2 = 1/1$, and gas flow rate, 30 $\text{cm}^3 \text{min}^{-1}$

Thus, the next stage involved an attempt to purify real polluted groundwater using SnPd/ Al_2O_3 [35]. The reaction results for SnPd/ Al_2O_3 are shown in Fig. 26.

For comparison, the data for CuPd/Al₂O₃ are also shown in the figure, which presents the reaction results obtained in a pure aqueous solution of NO₃⁻. The water-soluble organic matter contained in the groundwater was almost completely removed upon photo-oxidation treatment with Pt/TiO₂ and UV irradiation. In these reactions, a batch reactor was used to evaluate catalytic performance. In the pure aqueous solution of NO₃⁻, the catalytic performance of SnPd/Al₂O₃ was comparable to that of CuPd/Al₂O₃, with both showing high catalytic activity and minimal NH₃ formation. However, SnPd/Al₂O₃ exhibited a much higher catalytic performance than CuPd/Al₂O₃ in groundwater, as expected. In the case of SnPd/Al₂O₃, all NO₃⁻ in the groundwater was decomposed after 24 h in the groundwater, whereas the same process required 60 h for CuPd/Al₂O₃. In particular, the decrease in the reaction rate for the reduction of NO₃⁻ in the region of high decomposition rate of NO₃⁻ was remarkable for CuPd/Al₂O₃; thus, the difference in the catalytic performance between SnPd/Al₂O₃ and CuPd/Al₂O₃ is significant in this region. This is because the concentration of Cl⁻ relative to that of NO₃⁻ became high, and its influence on the reaction was more evident. In addition to the decomposition rate of NO₃⁻, SnPd/Al₂O₃ was superior to CuPd/Al₂O₃ for NH₃ formation. SnPd/Al₂O₃ suppressed NH₃ formation to a low level of about 10% selectivity, even for the groundwater treatment, whereas the selectivity to NH₃ for CuPd/Al₂O₃ increased to about 25% in the groundwater. These results clearly demonstrate that SnPd/Al₂O₃ is a suitable catalyst for the purification of polluted groundwater.

However, even with SnPd/Al₂O₃, a decrease in catalytic performance, especially activity, was observed in the groundwater (Fig. 27). To clarify the cause of this deterioration observed in the groundwater, all cationic or anionic species were removed from the groundwater by ion-exchange removal of all cations or anions using cation or anion-exchange resin, and the pretreated groundwater samples were allowed to react with SnPd/Al₂O₃. It was found that SnPd/Al₂O₃ exhibited almost the same performance in the pure aqueous solution of NO₃⁻ as that in the groundwater from which all the anions were removed, while no change in the catalytic performance was observed for the reaction in the groundwater from which all the cations were removed (Fig. 27). In other words, the anionic species in the groundwater deteriorated the catalytic performance of SnPd/Al₂O₃ in groundwater.

The real polluted groundwater used for this experiment contained 1.0 and 0.5 mmol/L of Cl⁻ and SO₄²⁻, respectively. However, these concentrations of Cl⁻ or SO₄²⁻ did not decrease the catalytic performance of SnPd/Al₂O₃ if they were present in water. Groundwater contains soil-derived silicate ions. The groundwater used in the study also contained 0.3 mmol/L of Si, as determined through inductively coupled plasma-atomic emission spectrometry (ICP-AES) analysis. Silicate ions in groundwater exist in various condensed states as SiO₃²⁻, Si₂O₅²⁻, Si₄O₉²⁻, and so on. The catalytic performance of SnPd/Al₂O₃ was examined using an aqueous solution of NO₃⁻ supplemented with metasilicate ion (SiO₃²⁻) and it was found that 0.3 mmol/L or less of SiO₃²⁻ did not decrease the catalytic performance. Unfortunately, it is not known how silicate ions are present in groundwater because of the complexity of silicate ion chemistry in water. Consequently, we speculate that silicate ions with a high degree of condensation and a large formula mass strongly

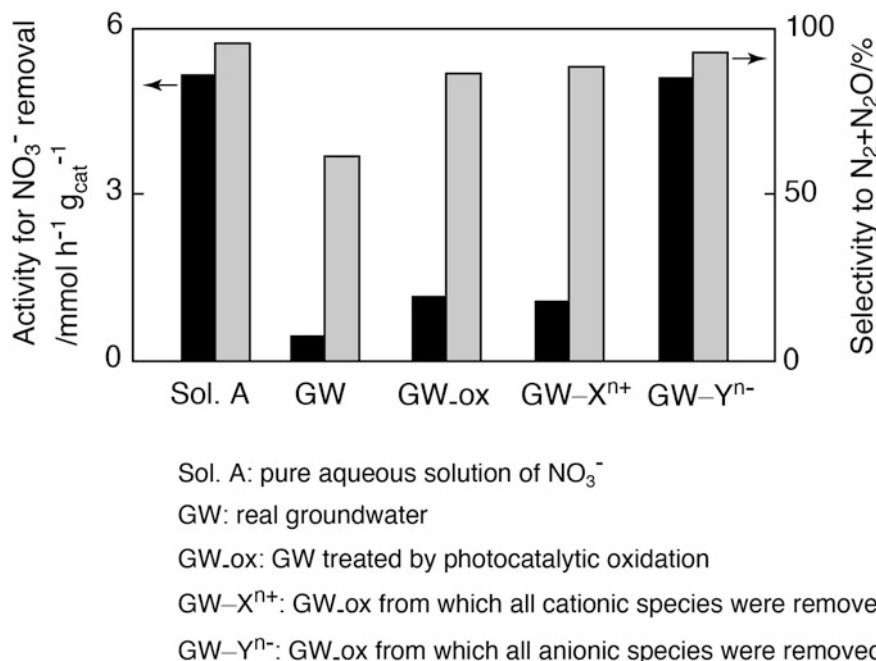


Fig. 27 Catalytic performance of SnPd/ Al_2O_3 for the reduction of NO_3^- in pure aqueous solution of NO_3^- and groundwater treated using various methods

adsorbed on the active sites of SnPd/ Al_2O_3 , thus reducing the catalytic performance in the real polluted groundwater. To put the purification of groundwater by the catalytic method into practical use, the problem of silicate ions must be solved.

3.6 Alternative Methods Without Gaseous Hydrogen On-Site

In the case where purification of polluted groundwater by the catalytic method can be applied, a relatively small number of water purification facilities and well water treatment in ordinary households can be considered with regard to hydrogen. Unlike large-scale water purification plants with well-equipped facilities and excellent personnel, gaseous H_2 cannot be used as a reducing agent in small-scale facilities and well water treatment from the viewpoint of safety. The catalytic reduction of NO_3^- in water using reducing reagents commonly used in organic synthesis, such as formic acid and NaBH_4 , was investigated. Indeed, in some cases, the reaction proceeded rapidly with high selectivity, but also reduced the reagent itself, whereby harmful substance to the human body may have been generated. Thus, these

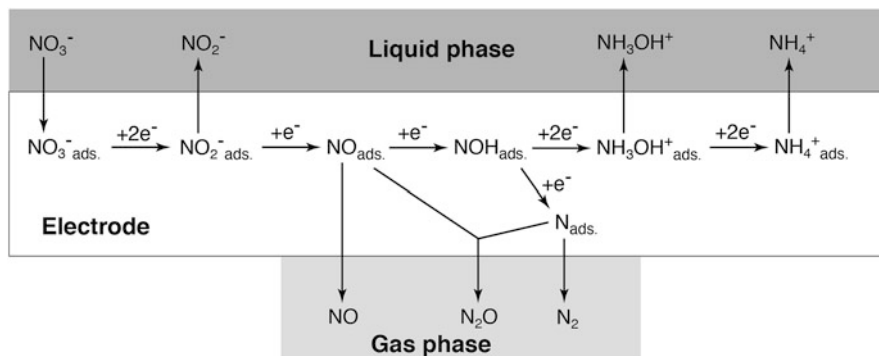
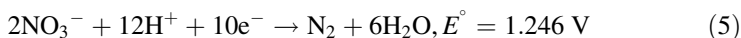


Fig. 28 Proposed reaction scheme for electrocatalytic reduction of NO_3^-

reducing agents cannot be used for the treatment of groundwater to ensure the safety of drinking water.

There are three major ways to avoid the use of gaseous H_2 on-site: (1) electrocatalytic reduction, (2) photocatalytic reduction, and (3) separation of NO_3^- on-site and decomposition of NO_3^- off-site. In the case of electrocatalytic reduction, electrons can be regarded as a reducing reagent, and ideally NO_3^- is reduced to N_2 and H_2O according to Eq. 5 [36].



As a catalytic reduction, the electrocatalytic reduction of NO_3^- proceeds sequentially via NO_2^- as an intermediate (Fig. 28). The order of electrocatalytic activity of a single metal electrode is as follows: $\text{Rh} > \text{Ru} > \text{Ir} > \text{Pt}$, Pd (or $\text{Ru} > \text{Rh} > \text{Ir} > \text{Pt}$, Pd) [37]. Rh and Ru electrodes exhibit activity, but the maximum activity is not very high (0.3 mA cm^{-2} at 0.1 V (RHE)). Large amounts of NO_2^- , NH_3 (or NH_4^+), and NH_2OH (or NH_3OH^+) are produced as by-products; which make the water unsuitable for drinking. The rate-determining step is the electrochemical reduction of NO_3^- to NO_2^- as that for the catalytic reduction. To improve the reaction rate in this rate-determining step, the addition of a second metal (base metal) to the noble metal electrode was investigated, and it was found that modification of the Pd electrode with Cu and Sn enhanced the electrocatalytic activity, being 10 mA cm^{-2} or more [38]. However, even with these binary metal electrodes, the selectivity to N_2 was only about 50% at the maximum, and a significant improvement was still required.

In electrocatalytic reduction using a common three-pole electrochemical cell, an electrolyte such as perchlorate or sulfuric acid is added to the reaction solution for the reaction to proceed smoothly. However, it is not desirable to add an electrolyte to polluted groundwater to obtain drinking water. To avoid this problem, the application of an electrolytic cell in which electrodes are attached to both sides of a proton-conducting polymer electrolyte membrane has been proposed [39]. In this

Fig. 29 Schematic of an electrolytic cell for electrocatalytic reduction of NO_3^- in water. A Pt electrode is used as an anode

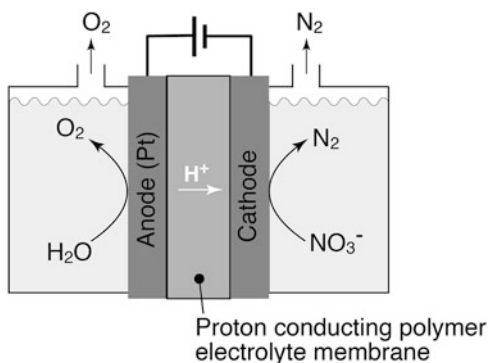


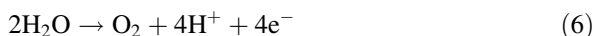
Table 4 Performance of the electrolytic cell for electrocatalytic reduction of NO_3^- in pure aqueous solution of NO_3^- and real groundwater

Solution	Removal rate of NO_3^- (%)	Selectivity (%)	
		NO_2^-	NH_4^+
Pure aqueous NO_3^- solution ^a	88	2	1
Real groundwater ^b	74	11	36

^aPrepared from KNO_3 , $[\text{NO}_3^-] = 10.1 \text{ mg L}^{-1}$

^b $[\text{NO}_3^-] = 12.2 \text{ mg L}^{-1}$, $[\text{F}^-] = 3.6 \text{ mg L}^{-1}$, $[\text{Cl}^-] = 9.2 \text{ mg L}^{-1}$, $[\text{SO}_4^{2-}] = 25.4 \text{ mg L}^{-1}$, $[\text{Na}^+] = 13.1 \text{ mg L}^{-1}$, $[\text{K}^+] = 4.1 \text{ mg L}^{-1}$, $[\text{Mg}^{2+}] = 8.2 \text{ mg L}^{-1}$, and $[\text{Ca}^{2+}] = 17.5 \text{ mg L}^{-1}$

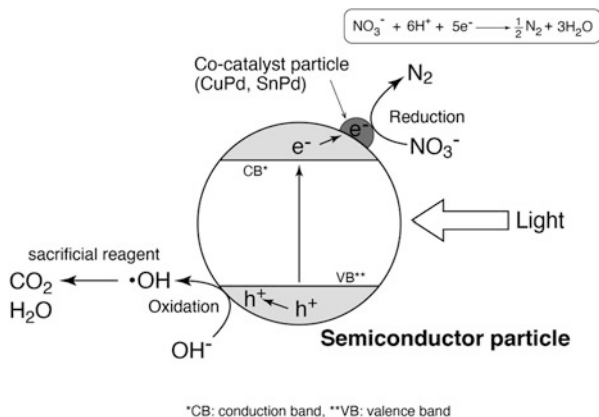
electrolytic cell, an electrode catalyst for reducing NO_3^- in water was used as the cathode, and a Pt electrode was used as the anode (Fig. 29). When voltage is applied between the electrodes, H_2O is oxidized at the anode, and O_2 is generated (Eq. 6).



The protons generated on the anode move to the cathode through the proton-conducting polymer electrolyte membrane and react with NO_3^- together with electrons supplied from a DC power supply on the cathode (Eq. 5). In this system, it is not necessary to add an electrolyte to the reaction solution, as such, only electrons and water are used to reduce NO_3^- .

Nafion[®]-117 has been used as a proton-conducting polymer electrolyte membrane, and a binary metal electrode consisting of CuPd or CuPt has been used as a cathode [39]. When CO_2 was bubbled into the solution to neutralize the OH^- generated at the cathode during the reaction, NO_3^- was rapidly decomposed on the cathode. The amount of formed NH_3 was approximately 1% of that of the decomposed NO_3^- , indicating that NO_3^- was selectively reduced to N_2 . This electrocatalytic system efficiently reduced NO_3^- even when other anions coexisted in the reaction solution. However, in real groundwater, the amounts of formed NO_2^- and NH_3 were larger than those for the reaction in a pure aqueous solution of NO_3^- ; this indicates that the performance deteriorated because of co-existing ions and/or water-soluble organic matter, as in the catalytic method (Table 4).

Fig. 30 Schematic showing photocatalytic reduction of NO_3^- over a semiconductor photocatalyst



The photocatalytic reduction of NO_3^- in the presence of a sacrificial reagent has been studied as a method for decomposing NO_3^- in water without using gaseous H_2 [40, 41]. Semiconductor photocatalysts in which a semiconductor particle is modified with co-catalysts, such as Cu and Sn active for NO_3^- , in addition to precious metals such as Pt and Pd, have been widely studied. In the photocatalytic reduction of NO_3^- in water using semiconductor photocatalysts, the semiconductor particles absorb light with energy equal to or higher than the band gap energy of the semiconductor, and excited electrons generated in the conduction band of the semiconductor move to the co-catalyst particle to reduce NO_3^- (Fig. 30). On the other hand, electron holes generated in the valence band of the semiconductor particles show a strong oxidizing action, which are consumed for the oxidation of sacrificial reagents such as ethanol added to the solution. In the photocatalytic reduction of NO_3^- , H_2 is generated if the photoexcited electrons react with H_2O instead of NO_3^- . The reduction in H_2O (Eq. 7) reduces the efficiency of light utilization, that is, quantum yield, which is a problem in the photocatalytic reduction of NO_3^- .



In fact, in the photoreduction reaction of NO_3^- in water by a semiconductor photocatalyst modified with co-catalysts (SnPd/TiO_2), the utilization efficiency of the photoexcited electrons (UE) defined by Eq. 8 was only approximately 50% [42].

$$UE = \frac{\text{The number of photoexcited electrons for nitrate reduction}}{\text{Total number of photoexcited electrons}} \times 100 \quad (8)$$

To improve UE , the author proposed a tandem photocatalytic system in which both a photocatalyst that produces H_2 via a photocatalytic reaction (Pt/TiO_2), and a supported SnPd catalyst ($\text{SnPd}/\text{Al}_2\text{O}_3$) that promotes NO_3^- reduction with H_2 is suspended in a reaction solution (Fig. 31) [34, 43]. The great merit of the tandem

Fig. 31 Schematic of a tandem-type photocatalytic reaction system for photocatalytic reduction of NO_3^- . Pt/TiO₂ and SnPd/Al₂O₃ have roles in photocatalytic H₂ generation and selective reduction of NO_3^- with H₂ to N₂, respectively

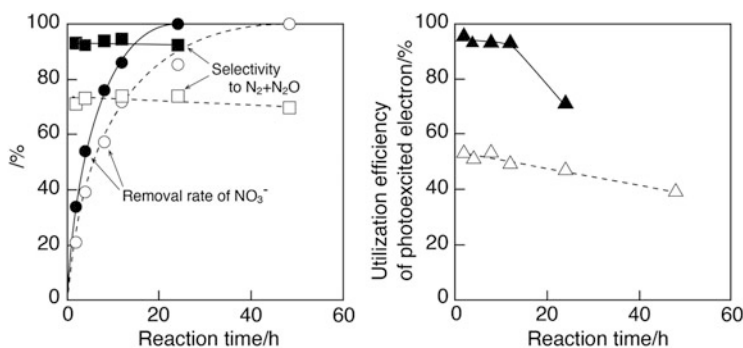
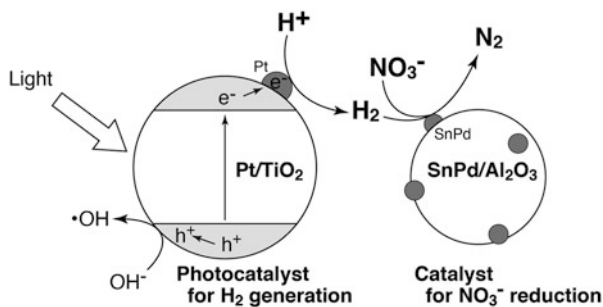


Fig. 32 Comparison of photocatalytic performance of the tandem-type reaction system composed of Pt/TiO₂ and SnPd/Al₂O₃ (filled circles/squares/triangles) with SnPd/TiO₂ (hollow circles/squares/triangles)

photocatalytic system is that the production rate of H₂ by the photocatalytic reaction and the consumption rate of H₂ by the catalytic reduction of NO_3^- can be well matched by adjusting the amount of photocatalyst and catalyst added to the reaction solution. As a result, the generated H₂ can be fully used for the reduction of NO_3^- , leading to almost 100% UE. In addition to this merit, in this reaction system, the photocatalytic and catalytic functions of the photocatalyst for H₂ generation and of the catalyst for the reduction of NO_3^- are assigned to different particles, that is, Pt/TiO₂ and SnPd/Al₂O₃, respectively. Thus, each of the two can be designed and developed independently, such that efficient and highly selective photocatalytic reduction of NO_3^- can be realized. In fact, the tandem photocatalytic system composed of optimum amounts of Pt/TiO₂ and SnPd/Al₂O₃ was added to a pure aqueous solution of NO_3^- , which decomposed NO_3^- rapidly under ultraviolet irradiation without the formation of gaseous H₂. The photocatalytic performance of the tandem photocatalytic system was superior in activity, selectivity to N₂, and UE to the optimized photocatalyst TiO₂ modified with Sn and Pd (Fig. 32). This photocatalytic system was also effective in purifying groundwater polluted with NO_3^- [34].

As a method that does not use gaseous H_2 on-site, the author proposed a combination of ion-exchange removal of NO_3^- using an ion-exchange resin on-site and catalytic reduction of NO_3^- off-site. Ion-exchange removal of anions from water using an anion-exchange resin (AER) has already been widely put into practical use as a technique for the desalination of seawater to produce fresh water, as well as for the removal of NO_3^- from polluted groundwater. However, wastewater containing a high concentration of NO_3^- is generated when the anion-exchange resin is regenerated using brine.

To avoid the generation of wastewater, the author devised a method in which NO_3^- was reduced in the anion-exchange resin without removing it from the resin. For this purpose, an anion-exchange resin containing fine metal particles active for the reduction of NO_3^- with H_2 was developed. In the metal-incorporated resin (Metal-AER), NO_3^- was reduced to N_2 , H_2O , and OH^- (Eq. 8) by contacting Metal-AER with H_2 . Since the reaction proceeds in the resin, no wastewater containing NO_3^- is generated for the regeneration of Metal-AER. For on-site operation, NO_3^- in polluted groundwater was removed with Metal-AER by an anion-exchange reaction. When the ion-exchange capacity of Metal-AER reaches saturation, it is regenerated off-site. Using this method, polluted groundwater can be treated quickly on-site without gaseous H_2 , and no waste other than H_2O is generated in the off-site regeneration treatment.

Based on this idea, the author employed an anion-exchange resin (Amberlite[®] IRA410 OH AG) as an anion exchanger. After the introduction of the Au complex ($AuCl_4^-$) to the resin through an anion-exchange reaction, Au complex was reduced by $NaBH_4$ to form Au nanoparticles in the resin (Fig. 33). The incorporation of Au nanoparticles in the resin did not affect the anion-exchange properties of the resin. The anion-exchange resin containing Au nanoparticles (Au-IRA410) rapidly removed NO_3^- from water. By contacting Au-IRA410 that incorporated NO_3^- with H_2 at $80^\circ C$, NO_3^- was reduced and Au-IRA410 was completely regenerated. Au-IRA410 was reusable for the removal of NO_3^- at least three times without performance deterioration. Using this metal-incorporated anion-exchange resin, it is possible to make a cartridge-type water purifier for rapid purification of polluted groundwater applicable in small water purification facilities and well water treatment systems. The cartridge was collected and reprocessed in a cartridge-regeneration factory (Fig. 34).

4 Prospect

Regarding the use of solid catalysts for water treatment, commercial treatment plants have already been utilizing oxidative decomposition of organic matter in wastewater. In contrast, treatment of water with reduction reaction, which includes purification of NO_3^- -polluted groundwater introduced in this chapter, is still at the research stage and requires a lot of time to be put into practical use. In particular, as explained in detail in this chapter, real groundwater contains various ionic compounds and

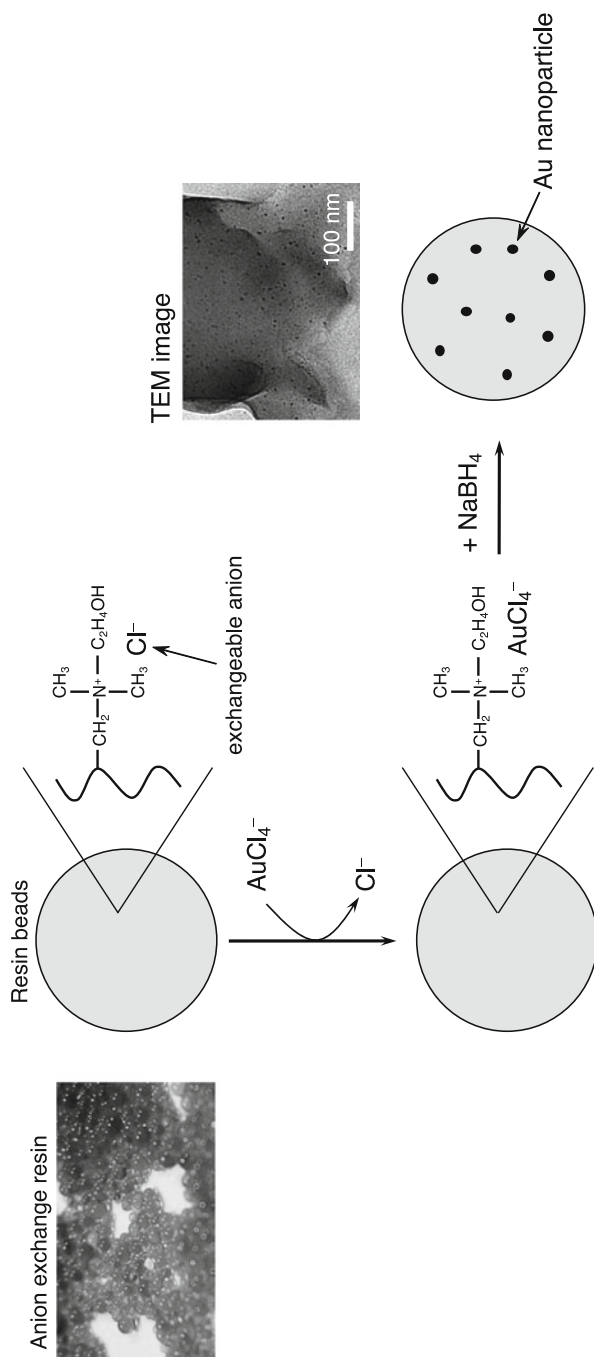


Fig. 33 Preparation scheme for anion-exchange resin containing gold nanoparticles

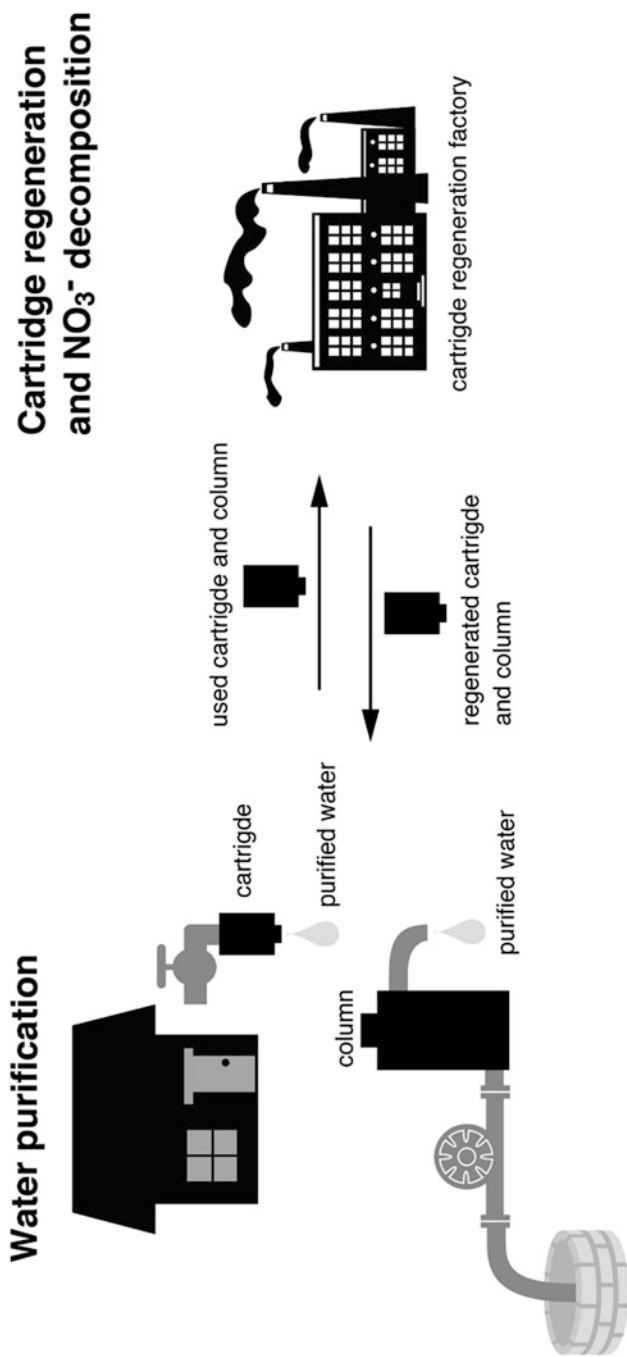


Fig. 34 Proposed system for rapid on-site treatment of polluted groundwater with a cartridge and column filled with gold nanoparticle-incorporated anion-exchange resin, which is applicable for small water purification facilities and well-water treatment. The used cartridge and column are reprocessed at a cartridge-regeneration factory

water-soluble organic matter in addition to pollutants, which cause a decrease in the performance of catalysts. The types and concentrations of such compounds vary from water sources to water sources, which complicate this problem. In any case, to expand the use of solid catalysts for water treatment with reduction reactions and to lead to practical use, it is necessary to proceed with research and development considering these influences from the initial stage of catalyst and process development. However, it cannot be said that its basic knowledge has been sufficiently accumulated. The author hopes that this chapter gives an opportunity to especially young researchers to enter this field, and anticipates future developments on this topic.

References

1. Bartholomew CH, Farrauto RJ (2006) Fundamentals of industrial catalytic processes. 2nd edn. Wiley, Hoboken, pp 371–382. <https://doi.org/10.1002/9780471730071>
2. Topsøe H, Clausen BS, Massoth FE (1996) Hydrotreating catalysis. Springer. https://doi.org/10.1007/978-3-642-61040-0_1
3. Dhepe PL, Fukuoka A (2008) Cellulose conversion under heterogeneous catalysis. *ChemSusChem* 1:969–975. <https://doi.org/10.1002/cssc.200800129>
4. Matthias Beller, Albert Renken, Rutger van Santen (Eds.), “Catalysis: from principle to applications”, Wiley-VCH, 2012, pp. 261–285. ISBN: 978-3-527-32349-4
5. Roberts SM, Poignant G (eds) (2002) Catalysts for fine chemical synthesis. Wiley. <https://doi.org/10.1002/0470855800>
6. O’Hayre R, Cha S-W, Colella W, Prinz FB (2016) Fuel cell fundamentals. 3rd edn. Wiley. ISBN-10 1119113806
7. Ertl G, Knözinger H, Weitkamp J (eds) (1999) Environmental catalysis. Wiley-VCH. ISBN-10 3527298274
8. Bartholomew CH, Farrauto RJ (2006) Fundamentals of industrial catalytic processes. 2nd edn. Wiley, Hoboken, pp 754–776. <https://doi.org/10.1002/9780471730071>
9. Bartholomew CH, Farrauto RJ (2006) Fundamentals of industrial catalytic processes. 2nd edn. Wiley, Hoboken, pp 705–743. <https://doi.org/10.1002/9780471730071>
10. Kim K-H, Ihm S-K (2011) Heterogeneous catalytic wet air oxidation of refractory organic pollutants in industrial wastewaters: a review. *J Hazard Mater* 186:16–34. <https://doi.org/10.1016/j.jhazmat.2010.11.011>
11. United Nations Development Program (UNDP) (2006) Human development report 2006. Palgrave Macmillan. ISBN 0-230-50058-7
12. Razowska-Jaworek L, Sadurski A (2005) Nitrate in groundwater. Taylor and Francis, London. ISBN: 9789058096647
13. European Environment Agency (EEA) (2007) Present concentration of nitrate in groundwater bodies in European countries, 2003. <http://dataservice.eea.europa.eu/atlas/viewdata/viewpub.asp?id=2027>
14. Bijay Singh GSS (1978/1979) Nitrate pollution of groundwater from farm use of nitrogen fertilizers – a review. *Agric Environ* 4:207–225. [https://doi.org/10.1016/0304-1131\(79\)90022-5](https://doi.org/10.1016/0304-1131(79)90022-5)
15. Wakida FT, Lerner DN (2005) Non-agricultural sources of groundwater nitrate: a review and case study. *Water Res* 39:3–16. <https://doi.org/10.1016/j.watres.2004.07.026>
16. Samatya S, Kabay N, Yüksel Ü, Arda M, Yüksel M (2006) Removal of nitrate from aqueous solution by nitrate selective ion exchange resins. *React Funct Polym* 66:1206–1214. <https://doi.org/10.1016/j.reactfunctpolym.2006.03.009>

17. Bohdziewicz J, Bodzek M, Wasik E (1999) The application of reverse osmosis and nanofiltration to the removal of nitrates from groundwater. *Desalination* 121:1390147. [https://doi.org/10.1016/S0011-9164\(99\)00015-6](https://doi.org/10.1016/S0011-9164(99)00015-6)
18. Sata T, Yamaguchi T, Matsusaki K (1995) Anion exchange membranes for nitrate ion removal from groundwater by electrodialysis. *J Chem Soc Chem Commun*:1153–1154. <https://doi.org/10.1039/C39950001153>
19. Menkouchi Sahli MA, Tahaikt M, Achary I, Taky M, Elhanouni F, Hafsi M, Elmghari M, Elmidaoui A (2006) Technical optimization of nitrate removal for groundwater by ED using a pilot plant. *Desalination* 189:200–208. <https://doi.org/10.1016/j.desal.2005.06.025>
20. Mohseni-Bandpi A, Elliott DJ, Zazouli MA (2013) Biological nitrate removal processes from drinking water supply – a review. *J Environ Health Sci Eng* 11:35. <https://doi.org/10.1186/2052-336X-11-35>
21. Vorlop K-D, Tacke T (1989) First step towards noble metal catalyzed removal of nitrate and nitrite from drinking water. *Chem Ing Tech* 61:836–837. <https://doi.org/10.1002/cite.330611023>
22. Hörold S, Vorlop K-D, Tacke T, Sell M (1993) Development of catalysts for a selective nitrate and nitrite removal from drinking water. *Catal Today* 17:21–30. [https://doi.org/10.1016/0920-5861\(93\)80004-K](https://doi.org/10.1016/0920-5861(93)80004-K)
23. Barrabés N, Sá J (2011) Catalytic nitrate removal from water, past, present and future perspectives. *Appl Catal Environ* 104:1–5. <https://doi.org/10.1016/j.apcatb.2011.03.011>
24. Tokazhanov G, Ramazanova E, Hamid S, Bae S, Lee W (2020) Advances in the catalytic reduction of nitrate by metallic catalysts for high efficiency and N₂ selectivity: a review. *Chem Eng J* 384:123252. <https://doi.org/10.1016/j.cej.2019.123252>
25. Prüsse U, Vorlop K-D (2001) Supported bimetallic palladium catalysts for water-phase nitrate reduction. *J Mol Catal A Chem* 173:313–328. [https://doi.org/10.1016/S1381-1169\(01\)00156-X](https://doi.org/10.1016/S1381-1169(01)00156-X)
26. Prüsse U, Hähnlein M, Daum J, Vorlop K-D (2000) Improving the catalytic nitrate reduction. *Catal Today* 55:79–90. [https://doi.org/10.1016/S0920-5861\(99\)00228-X](https://doi.org/10.1016/S0920-5861(99)00228-X)
27. Yoshinaga Y, Akita T, Mikami I, Okuhara T (2002) Hydrogenation of nitrate in water to nitrogen over Pd-Cu supported on active carbon. *J Catal* 207:37–45. <https://doi.org/10.1006/jcat.2002.3529>
28. Sakamoto Y, Kamiya Y, Okuhara T (2006) Selective hydrogenation of nitrate to nitrite in water over Cu-Pd bimetallic clusters supported on active carbon. *J Mol Catal* 250:80–86. <https://doi.org/10.1016/j.molcata.2006.01.041>
29. Bian C-R, Suzuki S, Kiyotaka Asakura L, Ping NT (2002) Extended X-ray absorption fine structure studies on the structure of the poly(vinylpyrrolidone)-stabilized Cu/Pd nanoclusters colloiddally dispersed in solution. *J Phys Chem B* 106:8587–8598. <https://doi.org/10.1021/jp0204861>
30. Sakamoto Y, Kanno M, Okuhara T, Kamiya Y (2008) Highly selective hydrogenation of nitrate to harmless compounds in water over copper-palladium bimetallic clusters supported on active carbon. *Catal Lett* 125:392–395. <https://doi.org/10.1007/s10562-008-9574-6>
31. Wang Y, Kasuga T, Mikami I, Kamiya Y, Okuhara T (2007) Palladium-copper/hydrophobic active carbon as a highly active and selective catalyst for hydrogenation of nitrate in water. *Chem Lett* 36:994–995. <https://doi.org/10.1246/cl.2007.994>
32. Wang Y, Sakamoto Y, Kamiya Y (2009) Remediation of actual groundwater polluted with nitrate by the catalytic reduction over a copper-palladium supported on active carbon. *Appl Catal A* 361:123–129. <https://doi.org/10.1016/j.apcata.2009.04.006>
33. Wang Y, Kamiya Y, Okuhara T (2006) Removal of low-concentration ammonia in water by ion-exchange of Na-mordenite. *Water Res* 41:269–276. <https://doi.org/10.1016/j.watres.2006.10.035>
34. Hirayama J, Kamiya Y (2014) Combining the photocatalyst Pt/TiO₂ and the non-photocatalyst SnPd/Al₂O₃ for effective photocatalytic purification of groundwater polluted with nitrate. *ACS Catal* 4:2207–2215. <https://doi.org/10.1021/cs5003564>

35. Hirayama J, Kamiya Y (2018) Tin-palladium supported on alumina as a highly active and selective catalyst for hydrogenation of nitrate in actual groundwater polluted with nitrate. *Cat Sci Technol* 8:4985–4993. <https://doi.org/10.1039/C8CY00730F>
36. Garcia-Segura S, Lanzarini-Lopes M, Hristovski K, Westerhoff P (2018) Electrocatalytic reduction of nitrate: fundamentals to full-scale water treatment applications. *Appl Catal Environ* 236:546–568. <https://doi.org/10.1016/j.apcatb.2018.05.041>
37. Dima GE, de Vooy's ACA, Koper MTM (2003) Electrocatalytic reduction of nitrate at low concentration on coinage and transition-metal electrodes in acid solutions. *J Electroanal Chem* 554-555:15–23. [https://doi.org/10.1016/S0022-0728\(02\)01443-2](https://doi.org/10.1016/S0022-0728(02)01443-2)
38. Motahar Hossain M, Nakata K, Kawaguchi T, Shimazu K (2013) Reduction of nitrate on electrochemically pre-reduced tin-modified palladium electrodes. *J Electroanal Chem* 707:59–65. <https://doi.org/10.1016/j.jelechem.2013.08.015>
39. Abul HM, Isao I, Kiwako S, Ryoko A, Tsuyoshi Y, Keita I, Masato M (2008) Electrocatalytic reduction of nitrate using Cu-Pd and Cu-Pt cathodes/H⁺-conducting solid polymer electrolyte membrane assemblies. *Bull Chem Soc Jpn* 81:1675–1680. <https://doi.org/10.1246/bcsj.81.1675>
40. Zhang F, Jin R, Chen J, Shao C, Gao W, Li L, Guan N (2005) High photocatalytic activity and selectivity for nitrogen in nitrate reduction on Ag/TiO₂ catalyst with fine silver clusters. *J Catal* 232:424–431. <https://doi.org/10.1016/j.jcat.2005.04.014>
41. Kominami H, Nakaseko T, Shimada Y, Furusho A, Inoue H, Murakami S-y, Kera Y, Ohtani B (2005) Selective photocatalytic reduction of nitrate to nitrogen molecules in an aqueous suspension of metal-loaded titanium(IV) oxide particles. *Chem Commun*:2933–2935. <https://doi.org/10.1039/B502909K>
42. Hirayama J, Kamiya Y (2017) Highly selective and efficient photocatalytic reduction of nitrate in water by a tandem reaction system consisting of Pt/TiO₂ and SnPd/Al₂O₃: a comparative study of the tandem reaction system with a typical semiconductor photocatalyst, SnPd/TiO₂. *J Catal* 348:306–313. <https://doi.org/10.1016/j.jcat.2016.12.019>
43. Hirayama J, Kondo H, Miura Y-k, Abe R, Kamiya Y (2012) Highly effective photocatalytic system comprising semiconductor photocatalyst and supported bimetallic non-photocatalyst for selective reduction of nitrate to nitrogen in water. *Catal Commun* 20:99–102. <https://doi.org/10.1016/j.catcom.2012.01.011>

Coal Fly/Bottom Ash, Hydroxylapatite, and Hydrotalcite



Mudasir Mudasir, Roto Roto, Yoshinori Kuboki, and Parvin Begum

Contents

1	Coal Ash for the Adsorption of Dyes and Heavy Metal Ions in the Environments	462
1.1	Introduction to Coal Ash	462
1.2	Coal Bottom Ash (CBA)	463
1.3	Coal Fly Ash (CFA)	464
1.4	Acid Activation of Coal Ash	466
1.5	Modification of Coal Ash with Organic Ligand	467
1.6	Examples of Applications	470
1.7	Conclusion	473
2	New Functions of Hydroxyapatite in the Environmental and Medical Applications	474
2.1	Introduction	474
2.2	The Importance of Geometrical in the Scaffolds for Bone Reconstruction	476
2.3	Removal of Arsenate from Environmental Water by Hydroxyapatite Chromatographic System	483
2.4	Conclusion	489
3	Layered Double Hydroxides (LDHs) for Removal of Drug Trace in the Environment ...	489
3.1	Introduction to Layered Double Hydroxide (LDHs)	489
3.2	Syntheses of LDHs	491
3.3	Anion Exchange Properties of LDHs	493
3.4	Common Applications	494
4	Conclusion	498
	References	498

Abstract In this chapter, some inorganic materials such as coal ash, hydroxyapatite, and hydrotalcite are taken up as the adsorbents to remove pollutants in contaminated water and soil. Coal ash is a residual material that exists after all combustible

M. Mudasir (✉) and R. Roto
Faculty of Science, University of Gadjah Mada, Yogyakarta, Indonesia
e-mail: mudasir@ugm.ac.id; roto05@ugm.ac.id

Y. Kuboki and P. Begum
Faculty of Environmental Earth Science, Hokkaido University, Sapporo, Japan
e-mail: parvinchy@ees.hokudai.ac.jp

Shunitz Tanaka, Masaaki Kurasaki, Masaaki Morikawa, and Yuichi Kamiya (eds.), 461
Design of Materials and Technologies for Environmental Remediation,
Hdb Env Chem (2023) 115: 461–506, DOI 10.1007/698_2022_844,
© The Author(s), under exclusive license to Springer Nature Singapore Pte Ltd 2022,
Published online: 24 August 2022

material in coal has been burned. The main components of coal ash are silica (SiO_2) and alumina (Al_2O_3) and other metal oxides also exist. Although coal ash has some ability to adsorb pollutants, the ability increases by activation with acids and modification with an organic ligand like dithizone. The activated and modified coal ash were applied to the adsorption of cationic, anionic dyes and also Hg(II) . Hydroxyapatite (HAP), one form of Ca-phosphate compound, is a main component in bone as well as collagen. HAP is an important material biologically and it becomes an excellent adsorbent for arsenate. Firstly, our studies of HAP as the geometrical scaffolds for bone reconstruction are introduced and then the removal of arsenate from environmental water by HAP is discussed using a chromatographic system. Lastly, the adsorbing property of layered double hydroxides (LDHs), which are called hydrotalcite minerals, with the unique structure, is discussed as well as the synthesis methods.

Keywords Coal ash, Environmental applications, Hydrotalcite, Hydroxyapatite, Multifunctional materials

1 Coal Ash for the Adsorption of Dyes and Heavy Metal Ions in the Environments

1.1 Introduction to Coal Ash

Coal, as an energy source, in its combustion process produces several by-products. If the by-products are not used properly, it can cause environmental pollution. Based on the particle size, coal combustion ash is divided into two types, namely fly ash and bottom ash. The amount and characteristics of ash produced from coal combustion are determined by the type of coal and the combustion system used [1]. Coal ash is a residual material that exists after all combustible material in coal has been burned [2].

Based on energy use data, Indonesia uses a lot of energy sourced from coal. According to Oplas [3], the use of coal energy in Indonesia ranks first in ASEAN and tenth in the world. The rate of waste recycling of coal ash is not proportional to its production, hence it has the opportunity to cause pollution for the environment. Coal ash is a hazardous waste whose accumulation can trigger an explosion due to the formation of methane gas (CH_4). The accumulation of coal ash waste can also produce acid seepage which can damage soil fertility. To balance the rate of coal ash waste production, efforts are needed to utilize coal ash waste other than as a mixture of cement and construction materials [4].

The presence of silica (SiO_2) and alumina (Al_2O_3) content in ash allows coal ash to be used as an adsorbent. In its use as an adsorbent, fly ash is more common than bottom ash. This is because fly ash contains more silica and alumina, namely 56.13%

and 18.49%, while bottom ash is 50.98% and 14.99%, respectively. Production of fly ash waste is also higher, namely 80–90%, while bottom ash is 10–20% [5].

1.2 Coal Bottom Ash (CBA)

Coal ash is an amorphous adsorbent and comes from coal combustion. Coal burning produces coal bottom ash and fly ash by-products. Coal bottom ash is the ash left in the furnace. In Indonesia, the volume of this waste reaches 500–1,000 tons/day and is classified as hazardous waste. Coal bottom ash has a gray-black physical property and has a rougher surface than fly ash. The particle size of coal bottom ash is 10–100 μm .

The composition of coal ash depends on the type, source, application, and not the conditions of the kiln [6, 7]. Comparison of the compositions of coal bottom ash obtained from the coal burning at some Indonesian electricity power plants and sugar factory is presented in Table 1 [8–10]. Based on the table, bottom ash has the main components of silica and alumina. The presence of silica and alumina is the main reason why coal ash is used as an adsorbent. Silica present on the surface of the oxide particles is a weakly acidic silica monomer [11]. SiO_2 , CaO , Fe_2O_3 compounds can raise the pH, because metal oxides such as CaO can interact with water to form $\text{Ca}(\text{OH})_2$.

Some works have [12–14] reported that coal bottom ash has the main content of quartz and mullite. According to Murniati [15], characterization using XRD showed that the bottom ash was dominated by minerals quartz (SiO_2), mullite ($2\text{SiO}_2\cdot\text{Al}_2\text{O}_3$), and amorphous solids of silica and alumina. Other researchers [16, 17] have observed that coal ash before activation was amorphous, whereas

Table 1 Comparison of the composition of some coal bottom ash in Indonesia

Minerals	Percentage (% w/w)		
	PLTU paiton ^a [8]	PLTU IPMOMI ^a [9]	PG madukismo ^b [10]
Silica (SiO_2)	49.73	24.10	41.50
Alumina (Al_2O_3)	19.51	6.80	28.12
Iron oxide (Fe_2O_3)	16.18	33.59	15.37
Titania (TiO_2)	0.99	–	–
Magnesium oxide (MgO)	2.96	–	1.37
Calcium oxide (CaO)	5.40	26.30	1.25
Na_2O	1.23	–	4.25
K_2O	0.84	–	1.25
Mn_2O	0.17	0.32	–
Carbon (C)	–	11.50	–

Note: (–) not determined

^a Electricity power plant company

^b Sugar factory

after activation it was in the form of coarser (crystalline) deposits. Londar et al. [9] added that carbon inhibits crystal formation. Crystal formation is triggered by high temperatures, therefore carbon removal can be carried out through combustion (calcination). Ash with amorphous structure is more advantageous when used as a silica gel preparation material. The amorphous structure is easy to melt so as to produce optimal silica [18]. According to Padi [19], amorphous adsorbents have small pores so that their adsorption capacity is low.

An adsorbent with a high silica content is stable to high temperatures. Silica is resistant to temperatures up to 2,200°C. Coal fly ash and bottom ash have different levels of silica. Kula and Olgun [5] stated that coal fly ash contains more Si and Al than coal bottom ash. As a result, fly ash is more likely to be used as a geopolymer, cement additive, zeolite, and others. In the case of zeolites, Padi [19] found that the surface of the zeolite has oxide impurities that cover the pores and reduce absorption, so it must be activated first. NaOH and HCl can activate the adsorbent. According to Padi [19] and Mufrodi et al. [20], reflux using HCl solvent aims to enlarge pores, reduce impurities, partially dissolve alumina, and deionize Na metal. Other researchers [8, 17, 21] have used NaOH in the manufacture of zeolites. Smelting with NaOH aims to activate silica and alumina into soluble minerals. Sodium silica is soluble in water, while sodium alumina is soluble in alkali. NaOH can also expel silica and alumina from inside of the framework to the surface silica and alumina. Based on this result, coal bottom ash also has been treated and activated in the same manner as zeolite to remove oxide impurities.

The preparation of adsorbent from coal bottom ash has been studied by several researchers. Sunarti [8] has synthesized zeolite from coal bottom ash by smelting with NaOH and hydrothermal reaction. XRD data showed that smelting with NaOH produced amorphous silica and alumina and the adsorption study showed that the synthetic zeolite from bottom ash adsorbed more Pb(II) than the original bottom ash. The synthetic zeolite prepared from coal bottom ash is able to adsorb 99.74% Zn (II) [21]. The same adsorbent, e.g. synthetic zeolite prepared from coal bottom ash, is also able to adsorb Cu(II) with an adsorption capacity of 25 mg/g and the adsorption takes place chemically by involving the active site of the synthetic zeolite [15].

1.3 Coal Fly Ash (CFA)

Fly ash is a by-product of coal combustion which accounts for about 60–88% of the total coal combustion residue. Globally, its annual production is estimated at 0.75–1 billion tons. So far, fly ash is generally used as a mixture of concrete and road or dam construction [22]. The release of fly ash into the atmosphere is very dangerous for health if it is inhaled directly because fly ash is a particulate material that can affect DNA repair mechanisms through the formation of reactive organic species [23]. Currently, many studies use fly ash as a coagulant, catalyst, membrane filtration, photocatalysis, and the Fenton process [24].

Coal fly ash consists of a complex mixture of organic (1–9%) and inorganic (90–99%) constituents of which it is about 30–84% amorphous and 17–63% crystalline which is between 1 and 500 μm in size and has a particle size distribution of tri-modal which is mostly located below 75 μm . The color of coal fly ash depends on the unburnt carbon and iron content, it can be reddish brown due to iron or gray to black due to carbon content. The different components of coal fly ash induce the different structures or shapes, which are different from the aluminosilicate glass phase which is spherical, while in the crystalline phase quartz and unburned carbon are irregularly shaped particles [25]. The density of coal fly ash ranges from 0.54 to 0.86 g/cm^3 [22] and the surface area usually lies between 0.2 and 10 m^2/g , coal fly ash with unburned carbon content has a surface area of approx. 200 m^2/g [26].

Coal fly ash has properties such as particle size distribution, surface area, hydrophilicity, and porosity that are complex according to their origin and composition [27]. The main constituents of coal fly ash are silica, alumina, iron oxide, calcium oxide, and varying amounts of carbon [28]. Coal fly ash has an irregular structure (amorphous) above 90%. More than 80% of the inorganic composition consists of Al_2O_3 , SiO_2 , and Fe_2O_3 . Coal fly ash also contains small amounts of transition metal oxides which are active components of many catalytic systems such as Mn, Cr, Co, Ni, Zn, Cu [29, 30] (Table 2).

The classification of coal fly ash is based on the CaO content. If chemical elements such as silica, iron oxide, and alumina make up more than 70% of all raw ash, then it is categorized as F-type ash according to American Society for Testing and Materials (ASTM) C 618. If the content of silica, iron oxide, and alumina is <70% of the total raw ash, fly ash is categorized as C-type ash [31]. Another criterion according to the ASTM standard is that fly ash obtained from burning bituminous or anthracite coal is classified as Class-F and that obtained from burning subbituminous coal or lignite is classified as Class-C fly ash [32]. Most of the F-type coal fly ash have been used by researchers for water treatment applications and very few studies have used C-type fly ash [33].

Coal fly ash can be used as a gas adsorbent such as CO_2 [25], SO_2 , NO_x [34], and H_2S , because it has a high alkali content, namely calcium which is usually used as an adsorbent for acid gas in the process of controlling air pollution [35]. Coal fly ash can also be used for adsorption of dyes such as reactive black-5 (RB5) azo dye [36], methyl orange [37], acid blue-113 and tartrazine [38], indigo carmine and acid orange-52 [39], active red X-3B [40]. The adsorption of anthraquinone-dye (acid blue-127) and acid yellow-17 must be carried out at a pH lower than the pK_a of the dye, in order to form a stable cationic site so that adsorption can take place optimally [41].

Single or simultaneous adsorption of heavy metals with coal fly ash has been widely carried out. Metal adsorption is generally carried out with a batch system so that the adsorption runs optimally [42]. Before being used, the adsorbent is usually activated first to make it more effective. Activation can be done physically by heating or chemically by extracting coal fly ash with acids such as HCl [43] and base NaOH [44]. The purpose of activation is to enlarge the pores and remove

Table 2 Metal oxide compositions of Coal fly ash from PT Petrokimia Gresik, Indonesia [30]

No.	Metal oxides	Chemical composition (% w/w)
1.	SiO ₂	36.10
2.	Al ₂ O ₃	19.80
3.	Fe ₂ O ₃	24.1
4.	CaO	9.18
5.	MgO	–
6.	P ₂ O ₅	1.10
7.	SO ₃	0.40
8.	K ₂ O	1.27
9.	TiO ₂	1.88
10.	V ₂ O ₅	0.07
11.	Cr ₂ O ₃	0.03
12.	MnO	0.20
13.	ZnO	0.07
14.	MoO ₃	5.10
15.	BaO	0.30

impurity of metal oxides in coal fly ash so that the adsorption ability becomes better [27].

1.4 Acid Activation of Coal Ash

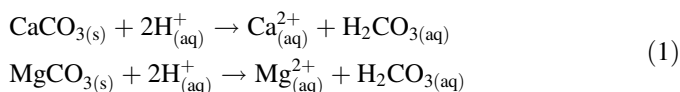
The existence of impurities in coal bottom ash including metal salts such as CaCO₃, MgCO₃, Fe₂S, and FeS and free heavy metals causes the ability of coal bottom ash for pollutants such as heavy metals and dyes to become less optimal, and therefore its adsorption capacity toward a certain pollutants is low [45]. In addition, if the impurities are not removed from the adsorbent, the presence of heavy metals in coal bottom ash can pollute the environment when coal ash is used as an adsorbent on a large scale. Therefore, it is necessary to do a treatment to remove impurities in the coal bottom ash. Various methods have been used to remove metal oxides from aluminasilica materials. One of them is activation with strong acids such as HCl, HNO₃, and H₂SO₄ [46].

Activation with strong acids usually has a strong influence on the structure and properties of the material because of the chemical interactions that occur between the strong acid and the surface of the material or adsorbent [47]. This method increases the adsorptive properties or adsorption capacity of coal ash by producing a more specific surface [45]. Inorganic acids or mineral acids such as HCl, H₂SO₄, HNO₃ are more commonly used in the activation process because they have a more significant effect than organic acids such as acetic, formic, oxalic acids [48]. Wang et al. [49] have reported that most of the metal oxides contained in coal ash dissolve in low pH. The dissolution intensity of metal oxides increases as the pH of the solution decreases. When coal ash is activated by strong inorganic acids like HCl,

Table 3 Analytical results of major components of coal fly ash from PT. Petrokimia Gresik before and after activation using AAS

Components	Coal fly ash before acid activation	Coal fly ash after acid activation
	Content (% w/w)	Content (% w/w)
SiO ₂	33.3	41.7
Al ₂ O ₃	16.0	17.0
CaO	0.57	0.38
Fe ₂ O ₃	12.7	4.87

the content of other minerals (metal oxides) except silica minerals will interact with the acid, then dissolve and cause the active site in the coal ash to be more open. This causes the active site of the adsorbent to become more accessible so that the adsorption capacity of coal ash increases [45]. An example of the dissolution reaction of metal oxides with strong acids is shown as Eq. (1) (Table 3).



1.5 Modification of Coal Ash with Organic Ligand

Dithizone is an organic ligand which is commonly used in spectrometric analysis and metal extraction. The chemical properties of dithizone are having the molecular formula C₁₃H₁₂N₄S, molecular weight 256.32 g/mol, boiling point 168°C, unstable to heat, non-polar at pH < 7, and when dissolved it produces a green solution. Dithizone is soluble in non-polar solvents such as ethanol, tetrachloride, chloroform, and benzene. Figure 1 shows the structure of dithizone in the keto and enol forms. According to Suseno [50], in the keto form, metal ions interact with -NH and in the enol form interact with -SH.

Dithizone is a ligand that can form coordinate covalent bonds with metal ions, through one or more of its donor atoms. Based on the number of donor atoms owned, ligands are grouped into monodentate, bidentate, and so on. Some complexes form weak ligand-metal bonds, so they decompose when dissolved in water. Metal ions that can form metal complexes with dithizone include Ag, Au, Bi, Cd, Co, Cu, Fe, Hg, Ni, Pb, Pd, Te, and Zn. The complex formed is generally neutral so that it can be extracted into the organic phase. According to Kunarti [51], ligands experience deprotonation at alkaline pH, so that their surface is negatively charged. The large number of OH⁻ ions causes competition between the OH⁻ ions in the solvent and the ligands. Under increasingly acidic conditions, the metal-dithizone complex becomes less stable. Meanwhile, under more alkaline conditions, the dithizonate complex was more stable. The gradual addition of ligands causes complex formation

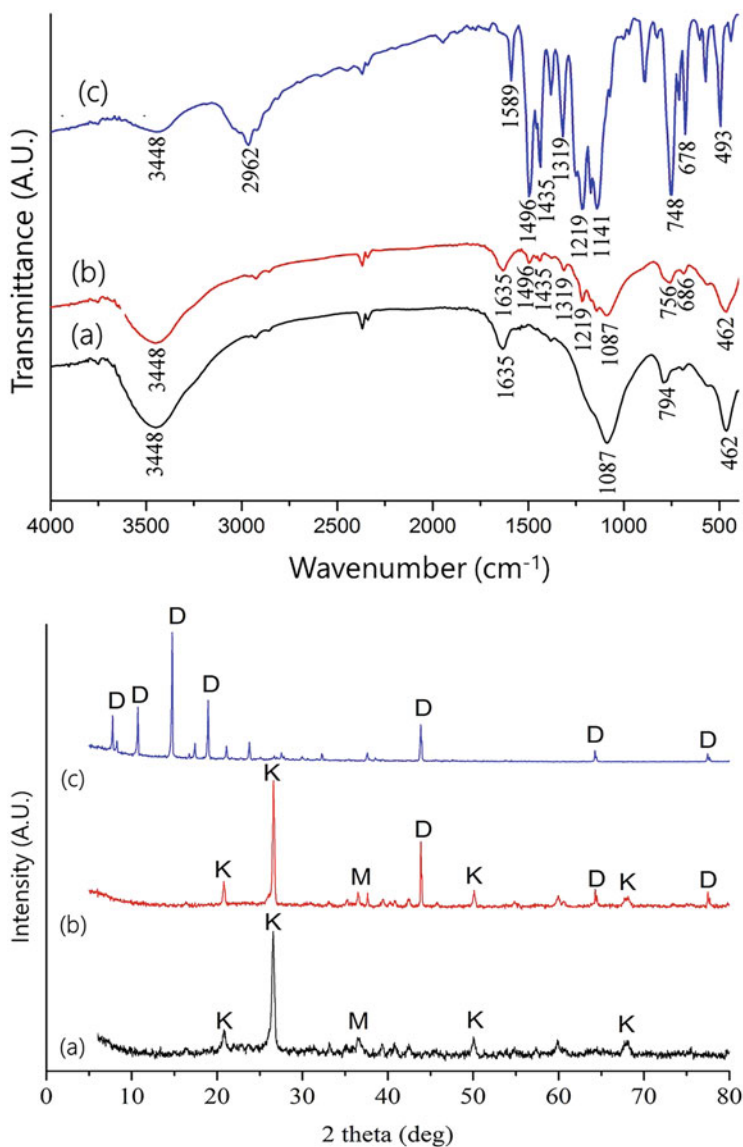


Fig. 1 Chemical structure of dithizone, showing keto and enol forms

to occur gradually. If there is excess ligand, the equilibrium reaction for complex formation shifts toward the product.

Because it has many donor atoms, dithizone can bind to both metal ions and solid supports. The most effective technique for binding dithizone to a solid support is through immobilization. Another technique that is often used is impregnation [18],

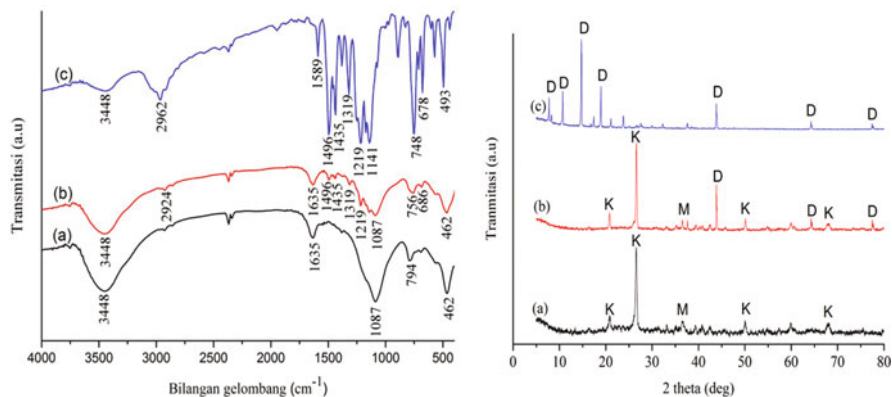


Fig. 2 Typical FTIR Spectra (left) and XRD pattern of Act-CBA (a), Dtz-CBA (b) and free dithizone (c)

but it is less effective because the interaction between the adsorbent and dithizone is less strong. Wogo et al. [52] stated that the modification of dithizone did not change the silica crystallization, but the surface area was reduced. Dithizone-immobilized silica gel shows a color change from gray to brick red, the more dithizone, the darker the color [53]. Several other researchers reported that dithizone can bind to poly EGDMA-co-HEMA (ethylene glycol dimethacrylate and 2-hydroxyethyl methacrylate), silica gel, chitin, natural zeolites, and others. Salih, et al. [54] reported that the order of single metal adsorption on dithizone-poly EGDMA-co-HEMA beads was Pb(II) > Cr(II) > Hg(II) > Cd(II).

Several dithizone immobilization methods have been used by previous researchers. Salih et al. [54] carried out the immobilization of dithizone on poly EGDMA-co-HEMA by refluxing 0.5 g of dithizone, 3 g of polymer, and 4 g of NaOH. Reflux was carried out for 24 h, at a speed of 400 rpm and a temperature of 80°C. Another procedure was carried out by Absalan and Goudi [55], namely mixing 10 mL of dithizone with 40 mL of a suspension containing 1.5 g of alumina. The adsorbent is then used to adsorb Ag(I). Dithizone immobilized triacetylcellulosic membranes were prepared by Savafi and Bagheri [56] and used to adsorb Hg(II). The researchers also designed the same adsorbent to adsorb Cu (II) [57]. Immobilization of dithizone on chitin from shrimp shells has also been carried out by refluxing 4 g of biopolymer with 1 g of dithizone at 70°C. Reflux was carried out for 6 h and the adsorbent was used to adsorb Cd(II) [58]. The optimum adsorption of Cd(II) occurred at pH 6 with an adsorption capacity of 5.67 mol/g.

Silica-dithizone adsorbent was also prepared by refluxing 20 mL of silica suspension with 5 g of dithizone. Reflux was carried out for 24 h, then the adsorbent was used to study the kinetics and equilibrium of Hg(II) [53]. Yu et al. [59] have used dithizone immobilized silica gel to adsorb Cu(II). Silica gel activation was carried out by refluxing 20 g of silica gel with 10 mL of 6 M HCl for 5 h. The solids were washed to neutral and dried. The mixture was stirred for 48 h in 30 mL of dithizone

solution. The solid was washed with toluene, ethanol, water, then dried. Dithizone immobilized chitin for Cu(II) adsorption has also been reported [60].

Based on these various methods, in our study on the modification of coal ash, we have modified the previously reported method [19, 20, 59], which first used HCl to activate coal ash and then the activated adsorbent was modified with dithizone by immobilization. As reported by Jundu [18], immobilization with organic ligands is an effective way to get a higher adsorption capacity. The adsorbent modified with dithizone showed higher selectivity and capacity for heavy metals [58, 61–63]. Figure 2 gives the examples of typical FTIR spectra and XRD pattern of (a) activated coal bottom ash (Act-CBA), (b) dithizone-immobilized CBA (Dtz-CBA), and (c) free dithizone.

1.6 Examples of Applications

1.6.1 Adsorption of Cationic and Anionic Dyes

We have studied the adsorption of anionic dyes of coomassie brilliant blue (CBB) and cationic malachite green (MG) dyes using activated coal bottom ash (Act-CBA) as well as non-activated coal bottom ash (CBA). Coal bottom ash was activated by acid method by refluxing it in hydrochlorid acid (HCl) for 4 h. Adsorption processes was conducted in batch method and some parameters influencing the adsorption performance were examined, including the effects of pH, adsorbent mass, contact time, and initial concentration of adsorbate. From this data then the kinetic models and isotherm adsorption were evaluated, and the example of dyes removal from synthetic samples containing both CBB or MG using Act-CBA was also carried out.

As expected the optimum removal of anionic CBB from solution of 50 mL, 20 ppm CBB using both CBA and Act-CBA is obtained at acidic solution of pH 3–4 because at this condition the surface of the adsorbent is positively charged (PZC of CBA = 5–6) [63], the optimum adsorbent mass is 0.3 g with the contact time of 90 min and initial dye concentration of 125 ppm. In contrast, the optimum adsorption of cationic MG from 50 mL, 40 ppm solution using either CBA or Act-CBA is obtained at alkaline pH of 8 with 0.2 g of adsorbent mass, 90 min of contact time; and 125 ppm of initial MG dye concentration. This is also easily understood as the surface of CBA will have negative net-charge at pH > 6. Effect of pH on the adsorption of dyes is given in Fig. 3. From the figure, it is obviously observed that Act-CBA adsorbs dyes more efficiently than the non-activated CBA. This is probably due to the dissolution of some metal oxide impurities that cover the active sites of the adsorbents.

The adsorption kinetics and isotherms were also studied in this research. The adsorption of the dyes by Act-CBA and CBA is best described by pseudo-second order kinetic models with the rate constants (k_2) for anionic CBB are 9.91×10^{-2} and 2.16×10^{-2} g/mg.min, respectively, and those for cationic MG are 2.16×10^{-2} and 1.52×10^{-2} g/mg.min, respectively. Isotherm adsorption studies indicate that

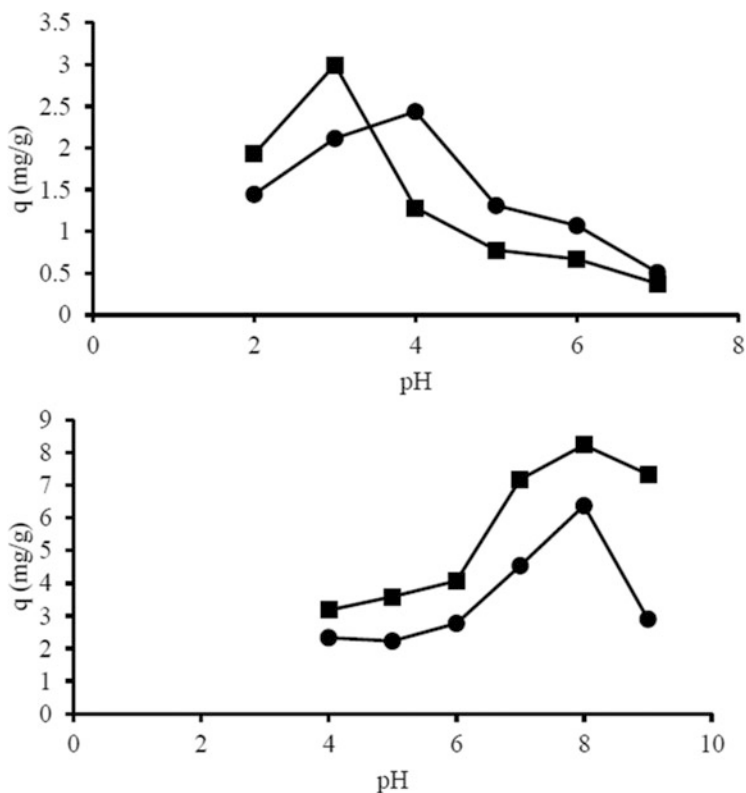


Fig. 3 Effect of pH on the adsorption capacity of CBB (upper) and MG (lower) dyes on CBA (circle) and Act-CBA (square)

Freundlich isotherm model best fits the adsorption of CBB with the Freundlich constants (K_F) for Act-CBA and CBA are respectively 5.54×10^{-4} and 2.73×10^{-4} mol/g. Meanwhile, the adsorption of cationic MG fits Langmuir isotherm model with the adsorption capacity (q_m) for Act-CBA and CBA are 1.98×10^{-5} and 6.63×10^{-5} mol/g, indicating the significant effect of acid activation on adsorption capacity of the adsorbent.

The adsorbent application for the adsorption of CBB and MG dyes in synthetic samples is shown in Fig. 4. From this figure, it can be seen that the concentration of coomassie brilliant blue dye decreased from 198.5 to 7.8 mg/L after five adsorption processes using HCl-activated coal bottom ash. The concentration of coomassie brilliant blue dye continuously decreased after the repetition of the adsorption process, which was 143.4; 97.2; 51.2; 20.9; and 7.8 mg/L, respectively. The adsorption percentage of the 1-fifth consecutive adsorption process also increased, namely 27.7; 51.0; 74.2; 89.4; and 96.1%, respectively. Figure 4 shows that the concentration of malachite green dye also decreased from 199.1 to 6.1 mg/L after three consecutive adsorption processes using HCl-activated coal bottom ash. The

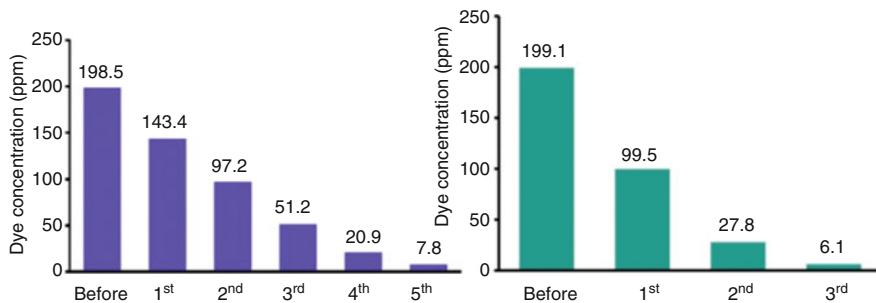


Fig. 4 Consecutive adsorption of MBB (left) and MG (right) from synthetic samples using Act-CBA at their optimum condition

decrease in the concentration of malachite green dye after the first to third adsorption process was 99.5; 27.8; and 6.1 mg/L, respectively, while the adsorption percent increased by 50.0; 86.0; and 96.9%. From these results, it is evident that coal bottom ash after activation can be used for the adsorption of cationic and anionic dyes by adjusting the pH of the solution.

1.6.2 Adsorption of Metal Ions

Many applications of coal ash for the adsorption of metal ions have been reported [58, 61–64]. Here we give one example of the application of coal bottom ash after being immobilized with dithizone (Dtz-CBA) for the adsorption of Hg(II) ions. The immobilization of dithizone was conducted in toluene medium, and the products were confirmed by some analytical methods [58, 61, 62]. The aims of dithizone immobilization is to increase adsorption selectivity and capacity of CBA toward Hg(II) ion. The parameters influencing the adsorption performance of Dtz-CBA and CBA toward Hg(II) ion such as pH solution, adsorbent mass, interaction time, and initial concentration (Fig. 5) were systematically optimized.

Results of our study have shown that the morphology of coal bottom ash characterized by SEM-EDS shows spherical and irregular shapes. The CBA contains mainly SiO₂ and Al₂O₃. FTIR spectra of Dtz-CBA show new peaks at 1,319 and 1,489 cm⁻¹ which are characteristics for –NH stretching and –CN bending of dithizone. XRD data shows basal spacing (d) at 4.28, 3.36, 3.72 Å for Dtz-CBA, while CBA shows basal spacing at 4.25, 3.69, 3.34 Å, indicating that both adsorbents are dominated by quartz and mullite minerals. GSA analysis shows the CBA surface area, pore volume, and pore radius were, respectively, 126.66 m²/g, 15.22 Å, and 0.10 mL/g and Dtz-CBA gives 13.48 m²/g, 17.02 Å, and 0.05 mL/g, respectively.

Adsorption study shows that Hg(II) is adsorbed chemically, and fitted well pseudo-second order kinetic models, and Freundlich isotherm models. At optimum condition the adsorption of Hg(II) on CBA is 68.958% using the initial concentration

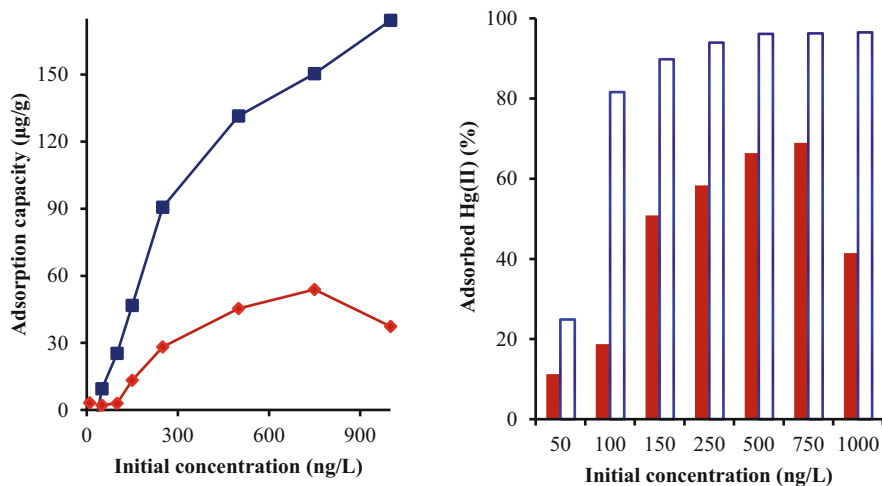


Fig. 5 Effect of initial concentration of Hg(II) on the adsorption performance of CBA (red) and Dtz-CBA

Table 4 Equilibrium constants (K), adsorption capacity (Q), and adsorption energy (E) for the adsorption of Hg(II) ion on coal bottom ash (CBA) and Dithizone-CBA (Dtz-CBA)

Adsorbents	R^2	K (L/mol)	Q (mol/g)	E (kJ/mol)
CBA	0.930	22,872.27	2.685×10^{-7}	24.869
Dtz-CBA	0.999	212×10^5	8.685×10^{-7}	41.795

of Hg(II) 750 ppb, and that of Dtz-CBA reaches 96.531% using the initial concentration of Hg(II) 1,000 ng/L. The adsorption capacity (Q), equilibrium constant (K), adsorption energy (E) (Table 4), and adsorption rate (k) for Hg(II) on Dtz-CBA are much higher than those on CBA, suggesting the effectiveness of dithizone immobilization in enhancing the adsorption ability of CBA. This is most probably due to the fact that Dtz-CBA has larger pore radius, and much more donating atom originating from dithizone so that the complexation between metal ion and active site of adsorbent is readily facilitated. These results have clearly proved that immobilization of specific organic ligand on the surface of certain adsorbents is able to increase the adsorption capacity of the adsorbents toward certain metal ions.

1.7 Conclusion

It has been shown that coal fly/bottom ash contains mainly silica and mullite minerals which are potential to be used as adsorbent for pollutants. Coal fly/bottom ash also contains impurities of metal oxides such as calcium and iron oxides. Acid activation of the coal fly/bottom ash before it is being used as adsorbent has proved

to be very effective and efficient methods to remove impurities of metal oxides that cover the surface of the adsorbents, so that their adsorption capacity toward either cationic or anionic dyes is significantly improved. Moreover, modification of the surface of coal fly/bottom ash with organic ligands such as dithizone has also increased the adsorption selectivity and capacity of the adsorbents to the heavy metal ions. In case of Hg(II) ion, it has been demonstrated that the adsorption capacity of dithizone-immobilized coal bottom ash is more three times higher than that of unmodified coal bottom ash. These results clearly demonstrated that coal fly/bottom ash can potentially be used for the adsorption of cationic and anionic dyes by adjusting the pH of the solution and that the modification of coal fly/bottom ash with specific organic ligand can be used as suitable strategy in enhancing the selectivity and capacity of coal fly/bottom ash toward heavy metal ions.

Acknowledgements The first author (M.M.) would like to acknowledge the partial financial support from Directorate General of Higher Education (DGHE), The Republic of Indonesia through research grants of Penelitian Dasar (PD), and Penelitian Dasar Unggulan Perguruan Tinggi (PDUPT) for fiscal year of 2021.

2 New Functions of Hydroxyapatite in the Environmental and Medical Applications

2.1 Introduction

Hydroxyapatite and collagen, as we see in this section, are the two main components of bone that exist as an exquisite molecular hybrid structure. Let us look at hydroxyapatite from the viewpoint of animal evolution. Mother Nature selected this mineral as the main component of bone about 0.4 billion years ago, in the Ordovician period. Surprisingly, there is one exception. In the Cambrian period, about 0.2 billion years before the appearance of HAP as a bone component, a brachiopod named *Lingulidae* equipped hydroxyapatite as a component of their exoskeleton, and they are still living only in Ariake Bay, Japan [65, 66]. From the above historical facts, we conceive that hydroxyapatite should be discussed with collagen as the extracellular matrices to understand the actual function. Therefore, this article will first discuss the latest medical application of hydroxyapatite to reconstruct bone tissue. Then, we will describe our new findings that hydroxyapatite: a component of bone, can remove the toxin (As) from environmental water.

What is hydroxyapatite?

To answer this question, we attempted a kind of decalogue for hydroxyapatite, by which we hope to give a glance at this exciting mineral.

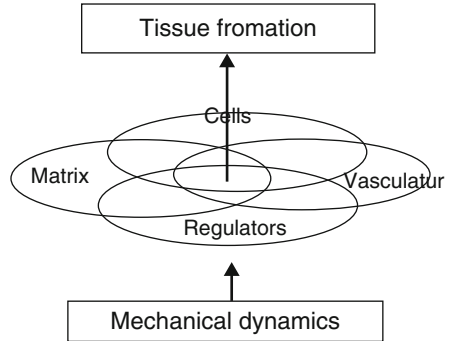
1. Hydroxyapatite (HAP) is one form of Ca-phosphate compound made of the 18 atomic groups, named by Werner, after the Greek word $\alpha\pi\alpha\tau\alpha\omega$ meaning “to deceive,” because of difficulty to distinguish from other minerals [67].

2. HAP is chemically and thermodynamically the most stable form among the many Ca-phosphate compounds, being highly insoluble in water but readily soluble in aqueous solvents at pH below 5.5 and can be used as a Ca-nutrient.
3. The unit cell of HAP crystal is composed of 18 atomic groups: $\text{Ca}_{10}(\text{PO}_4)_6(\text{OH})_2$, with the lattice: $a = 9.43 \text{ \AA}$, $c = 6.888 \text{ \AA}$, rhombic shape in ab-plane, rectangle in ac-plane.
4. HAP and collagen constitute the two main components of bone invertebrates, and both substances exist in bone tissue as the systematic hybrid at the nano-meter level [68].
5. HAP possesses strong adsorbing abilities for many minerals and organic compounds. The primary application of this property is for chromatography. Biochemically, HAP possesses a higher affinity for double chain DNA than the single one. This critical fact may suggest the involvement of HAP in animal evolution. (A hypothesis in this article.)
6. Adsorbing ability of HAP helps us to remove various harmful substances from the environment. One of the valuable medical applications is the preventive methods for athlete's foot [69].
7. HAP can be sintered to fine solid-state ceramics, which is highly valuable for orthopedic and dental fields. Aoki et al. developed this method (1972) [70]. Also, a traditional beautiful ceramics called "bone china" has probably contained HAP.
8. HAP is highly useful for bone reconstruction and cell substrates for cell culture: the powerful tool regenerative medicine.
9. The powders of pure HAP were shown to invest the micro defects on the surface of tooth enamel, thus believed to prevent the early development of tooth decay (micro-investing theory by Kuboki et al. 1972) [71, 72].
10. From the calcium resource of scallop shell composed of CaCO_3 , Kuboki et al. synthesized HAP in a recycled manner, performed HAP chromatography, and produced a HAP toothpaste [73].

For the past 60 years, our research group has engaged in the biochemistry of the hard tissues: bone and teeth. We had tried to clarify the mechanism of hard tissues (bone and teeth) formation and developed new technologies to reconstruct these tissues when they were disturbed. We concluded that the five factors must be considered: they are (1) cells, (2) extracellular matrices (ECM), (3) activating factors, (4) nutrition by vascularization, and (5) mechano-dynamic factors as illustrated in Fig. 6. For successful results in regenerative medicine, in our proposal, we must combine these five factors properly to lead the growth and differentiation of cells into specific active tissues and organs.

We have proposed that we consider five factors for the successful reconstruction of local tissues. These are (1) cells directly involved in tissue formation, (2) natural extracellular matrices (ECM) produced by the cells, or artificial ECM, (3) nutrition, provided by vascularization, (4) regulators for cellular activities, and (5) mechano-dynamic factors.

Fig. 6 Five factors that influence tissue formation and reconstruction



Among five factors, the cell is the primary importance, and the stem is the almighty cell that can create all kinds of tissues and organs. However, stem cell alone creates any tissue or organ. The stem cells first need their matrices. The matrices include natural and artificial HAP; the latter is often called a scaffold. Also, the cells need regulators, such as cytokines and vasculature, to supply nutrients, and people have often forgotten the mechano-dynamic factors. Still, we quickly understand if we imagine in utero situations [74].

This article concentrates on the matrix since HAP is one of the most valuable materials in constructing artificial ECM for bone reconstruction.




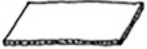







We have already pointed out that there are four fundamental requisites for the artificial ECM (scaffold), (1) physical, (2) chemical, (3) biochemical, and (4) geometrical properties [74, 75]. Because of the former three properties we see in all references in regenerative medicine, we will pay attention to the geometrical property hereafter.

2.2 *The Importance of Geometrical in the Scaffolds for Bone Reconstruction*

We can mold HAP into various geometrical shapes in the milli- and micro-meter scales during ceramic production. The desirable geometries of ceramics are crucial for inducing the cells to migrate, adhere, and grow into the normal tissues to reconstruct bone. Furthermore, we gradually understood that these 3D geometrical fabrications of HAP and related ceramic (scaffolds) were vital tools for the regeneration therapy of bone. Thus, we have developed more than twelve scaffolds of different geometry for bone formation [74–84] and classified them into eleven categories, as shown in Table 5. And we showed which geometry was practical and which was not.

This section focuses on the various geometrical scaffolds made of HAP and related ceramics and their efficacies in producing bone tissues.

Table 5 Eleven categories of geometries found in artificial ECM at micrometer level (0.1–1,000 nm). Modified from reference [74]

Categories of Geometry	Fundamental Shape		Example
Convex type	Fibers		Titanium web, Fibrous collagen membrane
	Particles		Insoluble bone Matrix, Particles with pores
Plane type	Planes		Conventional dishes
	Sheets (Membrane)		Porous sheets
	Blocks		Porous blocks of hydroxyapatite
Concave	Connected Pores		Bone is easily induced
	Straight tunnel (Honeycomb)		Rapid vasculature and bone formation
	Concavities		Bone formation on the inner surface
	Micro-pits		Cell growth at the corners
	Grooves		Directional growth of nerve cell & fibroblast
Room type	Chamber		Equipped with windows, floor & ceiling lead rapid bone formation

2.2.1 Preparation of HAP-Derived Geometrical Scaffolds

There are many fascinating methods of preparation of micro-geometrical HAP scaffolds. We classified them into two categories: molding and spacing methods. In the molding method, the paste made of HAP powders was pressed out with high pressure through the various nozzles: noodle-, macaroni-, and reverse multi-noodle-types, each of which produces rods or fibers, pipes, and honeycomb structure, respectively. We compressed the paste and let it go out from the nozzles to obtain

smaller diameters to even micron order, dried, and finally sintered to prepare geometric HAP ceramics. The spacing method, on the other hand, the HAP paste is mixed with combustible materials, such as plastic beads, fibers, or the piece of the plates with the convex dotted surface and sintered to prepare porous HAP ceramics. The temperature of sintering is usually 900–1,000°C. To our previous studies [74–83], these scaffolds induce bone effectively if they have porous structures, the pore size of which ranged 300–500 μm , which facilitate the penetration of cells.

2.2.2 Application of a Vital Growth Factor: Bone Morphogenetic Proteins (BMP)

To test the efficacy of geometric HAP scaffolds, we combined them with a bone-inducing growth factor named BMP, which Urist discovered in 1965 [84]. A remarkable characteristic of BMP was that it needed a particular scaffold to induce bone when implanted into soft tissues. Thus, to test the bone-inducing efficacy of the given scaffold, we combined it with BMP and implanted it into animal skin or muscle to see how much bone formed after 2–3 weeks.

2.2.3 Early Findings in the Geometry that Induce Bone Effectively

Historically, Reddi et al. [85] were the first to show the importance in the geometry of bone-inducing scaffold. They showed that the optimal size of granular ECM (decalcified bone powder) in BMP-induced bone formation to be around 420–850 μm in particle size. Cartilage and bone scarcely formed with the smaller particles (<74 μm). Inspired by their pioneering work, we prepared the HAP granules within which we gave the continuous and interconnected pores, and called them “porous particles of HAP,” abbreviated as PPHAP. The PPHAP induced a much higher bone induction than the granules without porosity (the smooth particles of HAP) [80].

Size and Shape of Pores

Thus, we found that the porosity of ECM is an essential determinant for tissue formation [64–66, 80], but previously there were no systematic studies.

Therefore, we systematically compared the bone-inducing efficacies by using the HAP block of the same size but five different porous pore sizes. We concluded that the optimal pore size for bone formation is 300–400 μm [81].

Concept of Optimal Spaces for Tissue Formation

We also noted generally that most of the initial bone formation started at the concave area of ECM. Furthermore, several authors have reported that bone tissue formed without the addition of BMP in the concavities and pores of ceramics *in vivo* [86].

These observations led us to the concept of “optimal spaces for tissue formation in artificial ECM.” We proposed that scaffolds had an optimal geometrical shape and size for each kind of tissue, which facilitates its cells to differentiate, proliferate, and develop tissue in a particular direction. These optimal spaces are not limited to tube- or sphere-types but include specific “spaces” between the solid ECM structures, such as fibers, particles, and flat planes. The size of the optimal spaces is assumed to be approximately 300–400 nm, which is dependent upon tissues.

The above results urged us to classify all the scaffold geometry into eleven categories, as shown in Table 5. First, the table categorized the geometries into four groups: convex-, flat-, concave-, and chamber-type. Then the convex group is divided into the fibers and particles, the flat group into the plane, sheets and blocks, and the concave group into the irregular connected pores, straight tunnel (honeycomb), concavity, micro-pits, groove, finally, the chamber type. This classification table is valuable when we design a new scaffold to regenerate certain tissues or organs because stem cells need specific geometrical circumstances to grow into the target tissue of an organ.

2.2.4 Side by Side Induction of Blood Vessel and Bone in the Tunnel Structure

In Fig. 7, we introduce an example of three-dimensional (3D) geometric artificial ECM of honeycomb-shaped ceramics with 37 tunnels made of β -TCP (Pilot Corporation, Japan). This honeycomb structure was made essentially through the unique nozzle of reverse noodle type, and extension into the micro-scale. In this bio-resorbable artificial ECM, the numbers and size of the tunnels are strictly controllable in the production process. The length of the ECM can be varied from 1 to 10 cm. Many kinds of cells and tissues can migrate into the tunnels, and develop in specific ways, dependent upon their characteristics.

There are intermediate cells between the osteoblasts and endothelial cells, which we hypothesized to be the common precursor cells for osteoblasts and endothelial cells.

We implanted the honeycomb β -TCP (3 mm in outer diameter, 4 mm in length, and 0.3 mm in tunnel size) combined with 1 mg of rhBMP-2 (a kind gift from Yamanouchi) into the subcutaneous tissue of the Wistar rat. Active vascular formation occurred along with bone formation, side by side through inside the tunnel, as shown in Fig. 8. When we looked at the enlarged view of the same sample in Fig. 9, we could see the closer relationship between erythrocytes and osteoblasts. We hypothesized the presence of common precursor cells between both cells, which we observed, but needs further verification.

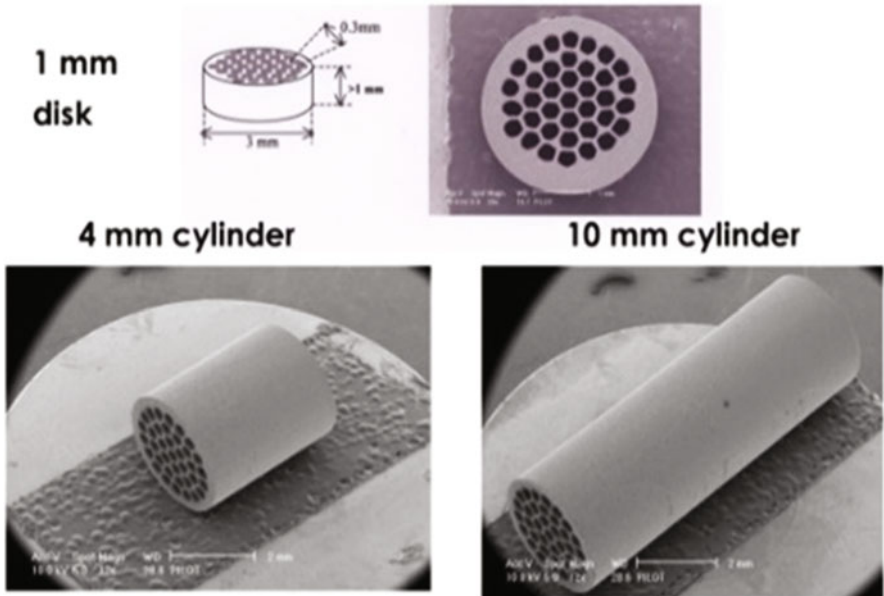


Fig. 7 An example of the geometric artificial ECM of honeycomb-shaped ceramics with 37 tunnels made of β -tricalcium phosphate (Pilot Corporation, Japan). In this bio-resorbable artificial ECM, the numbers and size of the tunnels are strictly controllable in the production process. The length of the ECM can be varied from 1 to 10 cm. Various cells and tissues can enter into the tunnels, and develop in specific ways

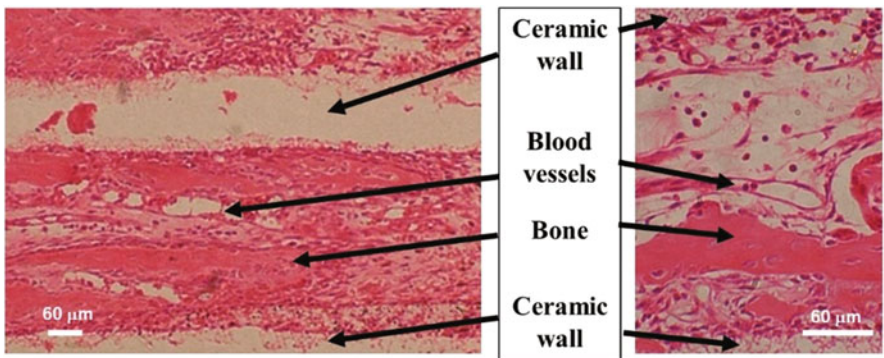


Fig. 8 Side by side induction of bone and blood vessel by the scaffold of the honeycomb structure

Furthermore, when we implanted the same honeycomb scaffolds without BMP-2, we could not observe bone formation, but only the active vascular formation, as illustrated in Fig. 10. These results indicated that the honeycomb scaffold is feasible for vascular formation, which led to bone formation when BMP supplied. This

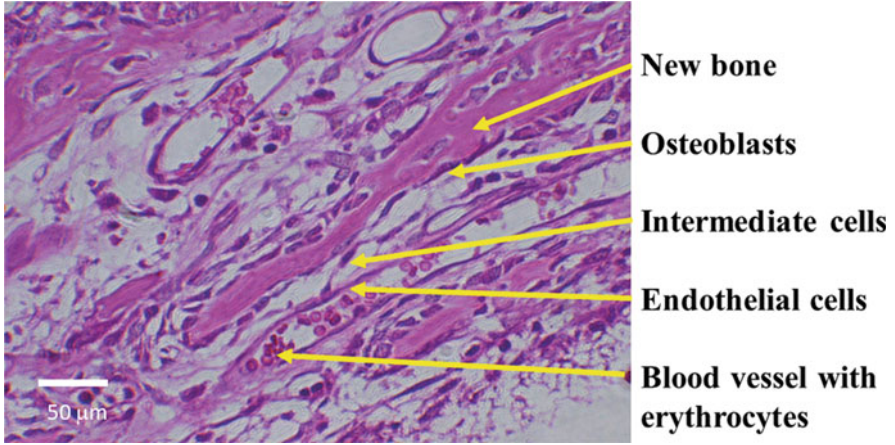


Fig. 9 Enlarged view of the relationship between the new bone and capillary

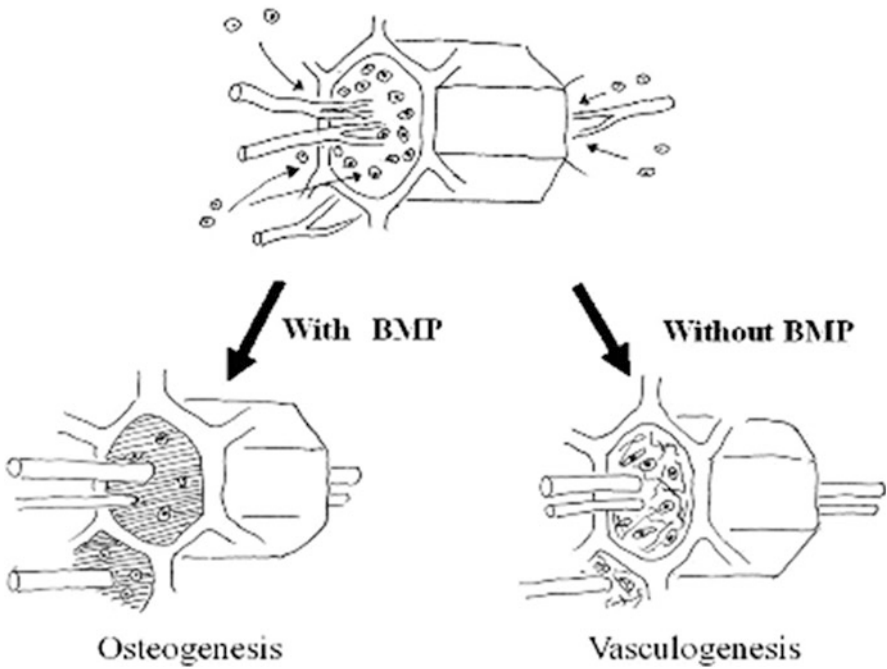
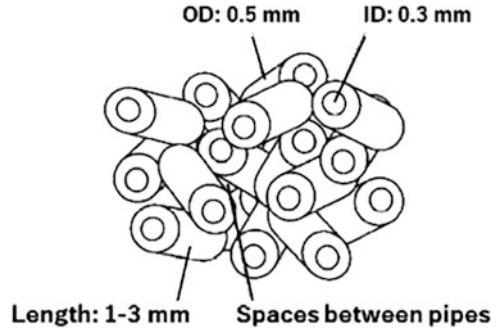


Fig. 10 Schematic explanation for the induction of osteogenesis and vasculogenesis by honeycomb scaffold

Fig. 11 Random tunnel β -TCP in that the short pipes were sintered into blocks



system of bone formation proved to be an excellent tool to clarify the relationship between blood vessels and bone formation.

Next, we extended the idea of a tunnel to the “random tunnel” β -TCP, in that the short pipes were sintered together to form the structure of random-directed tunnels. The merit of this scaffold was the increase in the 3-dimensional volume of bone formation as shown in Fig. 11.

Mechanism of Tunnel Effects

Among the 3D geometrical functions of HAP-related scaffold, tunnel-type scaffold and tunnel effect are the most eminent phenomenon. We attribute the tunnel effect to the flow of tissue fluid that facilitates cell immigration and directional growth into tissue.

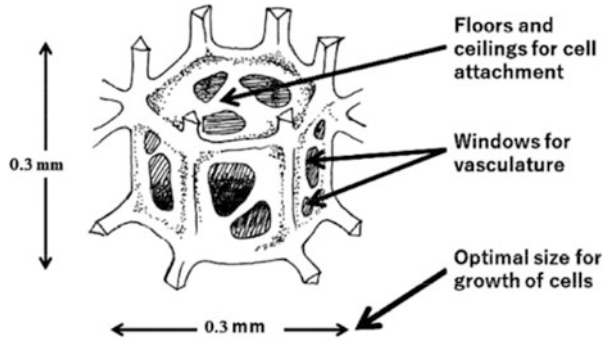
An Example of a Chamber-Type Scaffold

Figure 12 shows an example of the chamber-type scaffold that was fabricated by replicating a certain polyurethane foam, which was first calcified and sintered to a ceramic. Their geometry is proved to be ideal for bone tissue formation [74].

The above results of the geometry of scaffold indicate the common principles and recipes applicable both for the medical and environmental application of HAP-related ceramics, which we summarize as follows.

1. We studied systematically the effective geometry of scaffold for bone formation. We have divided all the geometries of ECM into three large groups: the convex-, plane- and concave-geometries, and also into the eleven practical groups. The concave geometry is generally advantageous over convex or flat, as far as the bone formation is concerned.
2. The possible mechanisms involved are as follows: (1) concave geometry permits a higher concentration of cells, (2) it leads to effective accumulation of cytokine

Fig. 12 Chamber-type scaffold that provides the osteoblasts their houses where they can grow into bone tissue



and other active bio-molecules, (3) there is a closer chance of the cell–cell communication, and (4) faster creation of three-dimensional (3D) environments, rather than two-dimensional (2D).

3. Among the concave geometries, the tunnel structures are shown to be particularly effective for bone formation. The optimal diameter of the tunnel structures was concluded to be 300–400 μm , and the effective radius of curvature is up to about 250 μm , as shown in the previous experiment.
4. These conclusions concerning the size of concave geometry are not only applicable to the tunnel structures but also may be partially eligible to open pore structures (concavities), rectangular concavities, and grooves as shown in Table 5. Furthermore, the concept of the geometry of HAP will be also applicable for use of these ceramics for water purification, which we will discuss in the next section.

2.3 Removal of Arsenate from Environmental Water by Hydroxyapatite Chromatographic System

2.3.1 Needs for Water Purification in Asian Countries

Hydroxyapatite and active carbon (charcoal) are the two effective adsorbent materials of the natural origin for environmental purification. On the other hand, it was only recently that arsenate was confirmed to exist in the raw water in Bangladesh and her vicinity. In 1998, a British scientist team reported 4,600,000–5,700,000 people (out of 122,500,000 the population of related areas) were drinking the natural well water containing more than ten ppm of arsenate, which is the maximum expected value by the WHO. The source of the arsenate is the underground water from the Himalayas [87–90]. Since the sufficient city water system is still under construction in this country, developing a low-cost and effective water purification method is very important for the local people.

Several authors have already applied HAP for the arsenate-removal method from drinking water [91–94]. But in most of their works, HAP was combined with other factors to increase the efficiency of arsenate removal, and we could not find the report in that the pure HAP was tested on the column chromatography. We developed a method of HAP chromatography for testing the arsenate removal. We synthesized hydroxyapatite (HAP) using a scallop shell as a calcium source. And we found that the shell-derived HAP could remove the arsenate effectively from water. Also, we found that the commercial bone-derived charcoal has the arsenate binding ability.

Therefore, we compared the arsenate removing abilities between the other HAP and the active carbon preparations. We have used a chromatographic system equipped with a refractive index detector. Surprisingly, we found the highest arsenate removing abilities in the hybrid of apatite and active carbon. This product was produced by carbonizing the bovine bone under the usual thermal process. This bone-derived hybrid of apatite and active carbon (abbreviated “Bone AC”) is valuable for its high arsenate-adsorbing ability. Also, we especially noticed that from the biological viewpoint of bone structure, the origin of the carbon part of this hybrid is collagen in bone. As we already described, HAP and collagen construct bone highly geometrically. This fact may cause the geometric effect of adsorption of both substances.

In this chapter, two types of HAP of biological origin: shell-derived HAP and bone apatite carbon (Bone AC) are discussed, describing their preparation methods, adsorbing function, merits for environmental water purification, and further application prospects.

2.3.2 Preparation of Hydroxyapatite from a Scallop Shell and Bovine Bone

We obtained shells of Japanese scallop (*Mizuhopecten yessoensis*) from a local fishery company in Hokkaido, Japan, cleaned of all adhering soft tissues, crushed into small pieces (<1 cm size), heated 900°C for 2 h. After cooled down to room temperature, the white product (CaO MW = 56) was transferred into distilled water at a slow step while stirring to obtain a final concentration of 9.33% (1.66 M). The homogenous suspension of Ca(OH)₂, thus prepared, is technically called lime water (pH 11).

To the 9.33% (1.66 M) lime water suspension, an equal volume of 1 M H₃PO₄ solution was slowly added stepwise with vigorous stirring. We adjusted and maintained the pH around 7.4, and we left the mixture for maturation overnight with stirring, and again adjusting pH was 7.4.

The next step is to filtrate the suspension, which was done effectively by the chromatographic system. The suspension is poured into the chromatographic column of a large scale with a 20 cm diameter, equipped with a polyester filter at the bottom, and drained the extra water. Then a sufficient volume of distilled water was added to the top of the column and drained again. We washed out all the non-reacted

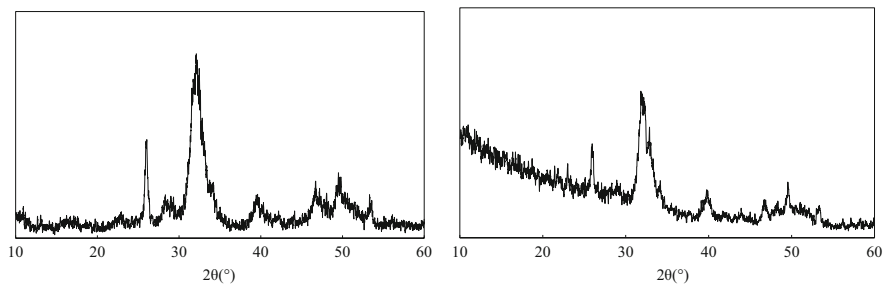


Fig. 13 X-ray diffraction patterns of the shell-derived (a) and bone-derived (b) hydroxyapatite. Both samples were analyzed by the X-ray diffraction analyzer Ultima-IV (Rigaku Corp., Japan) with a $\text{CuK}\alpha$ radiation source operating at 40 kV and a 30 mA excitation current. They showed peaks at $2\theta = 25.8^\circ$, 31.8° , and 39.8° corresponding to HAP. Analyses were done by Associate Professor Kazuhide Ozeki, Ibaraki University

soluble chemicals from the solid product, hydroxyapatite, by repeating this process. We dried the wet hydroxyapatite first in the air, then in the oven at $80\text{--}120^\circ\text{C}$. We crushed the solid mass of the dried HAP, and filtered to obtain the powder with a diameter of 1–2 mm.

Naruto Chemical Co., Tokushima, Japan, provided Bone-AC. (Commercial name: Fish-Cal). Briefly, adult bovine femora were cleaned off bone marrow and soft tissues and removed the metatarsus portions of the femora. They cleaned the hard part of bone tissue and is composed of two main components: collagen and HAP of about 25 and 65 wt.%, respectively. This raw material was processed under the usual anaerobic thermal condition and converted into Bone-AC. As mentioned in the introduction part of this article, bone collagen and HAP in the animal tissues are constructed by a unique hybrid structure with a highly ordered three-dimensional arrangement at the nanometer level [68, 95]. Since the carbon component of the Bone AC is entirely derived from the highly cross-linked type I collagen, the 3D-geometry may reflect the previous one in bone tissue, which is under investigation by SEM in this laboratory.

The products were fabricated as either fine powders of 0.05 mm or granules about 1 mm.

Figure 13a, b are the results of the X-ray diffraction analysis of Shell HAP (a) and Bone AC (b). They show the characteristic peaks at $2\theta = 25.8^\circ$, 31.8° , and 39.8° corresponding to HAP, and indicate that both samples are composed of typical hydroxyapatite of mediate crystallinity for biological origins such as bone

2.3.3 The Chromatographic Estimation of Adsorbing Ability for Arsenate

We need the rapid and straightforward method to test the various samples for adsorbing ability for arsenate and concluded that chromatography is the best one,

considering Bangladesh's present urgent environmental situation. We used a commercial glass chromatography column (Bio-Rad, Japan). We packed the various test materials into the column to obtain a $\varnothing 10 \times 50$ mm bed volume. Before packing, we removed finer particles from the test materials by repeated decantation from a suspension in distilled water. We washed the column with a large amount of distilled water and ran it at a flow rate of 80 mL/h at 15°C, using a ceramic pump (VSP-3200 W, Eyela, Tokyo, Japan). We monitored the arsenate concentration in the elution by their refraction index using a differential refraction meter (YRD-880 Shimamura Technology, Tokyo). We checked that concentrations of arsenate follow Lambert-Beer's law by the optical density and diffractive index. In addition to their refraction index, we also monitored the elution by absorbance at 254 nm with an ATTO Bio-Mini-UV monitor (Atto Co., Tokyo, Japan). We chose several HAP and active carbon preparations from different sources as the samples for testing were:

1. Shell-derived hydroxyapatite (Shell HAP),
2. Bone-derived active carbon (Bone AC),
3. Pollack bone apatite: hydroxyapatite prepared from pollack bone [Naruto Chemical (N-C) Co., Tokushima, Japan), which was designed into the particles by the method described above for scallop shell apatite.
4. Jatropha charcoal was prepared from the seeds of *Jatropha curcas* and kindly given by Jissen Kankyo Kenkyusho Co., Nagoya, Japan.

We applied a fixed amount of arsenate (As_2O_3 , 5 mg in 1 mL on the columns 10×50 mm in the bed volume), packed with different adsorbents, and ran with distilled water at a flow rate of 80 mL/h. Eluted solutions were monitored by a differential refraction meter (YRD-880 Shimamura Technology, Tokyo). Peak areas in the chromatogram were measured using Image-J software.

2.3.4 Results of as-Removal by HAPs from Shell and Bone

Figure 14 shows the chromatogram of 5 mg arsenate applied on the column 10×50 mm, which was packed with the glass beads (0.1 mm in diameters) as control of non-adsorbent material. The same arsenate amount (5 mg) was applied and ran three times successively with distilled water at the flow rate of 80 mL/h. The black arrows indicated injection points. The refractive index monitored the formers of double-peak each, and the latter was at an optical density at 254 nm. The areas of peaks were calculated using Image-J and turned out to be highly reproducible. Figure 14b shows the same chromatographic peaks of arsenate solution, except that the column was packed with the apatite beads (0.2 mm in diameters) made from scallop shells. The average peak areas of Shell HAP column (B) were 46% of glass beads column (A), which meant the remaining 54% of the charged arsenate was adsorbed in this column.

This study aimed to devise a new method to estimate the adsorption ability for arsenate of a particular material. The assay principle compares the peak areas of chromatograms produced by columns packed with glass beads (non-adsorbing

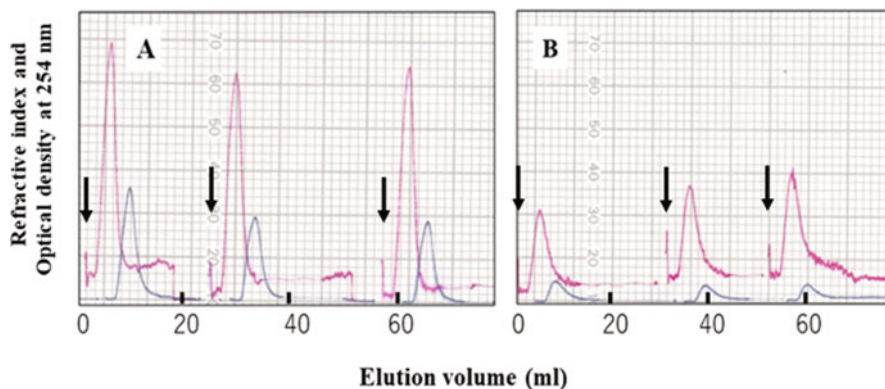


Fig. 14 Chromatographic profiles when we applied 5 mg arsenate on the column. We packed the column with the glass beads (0.1 mm in diameters) as control of non-adsorbent material (a). The same chromatographic peaks except that the column was packed with Shell-HAP (b)

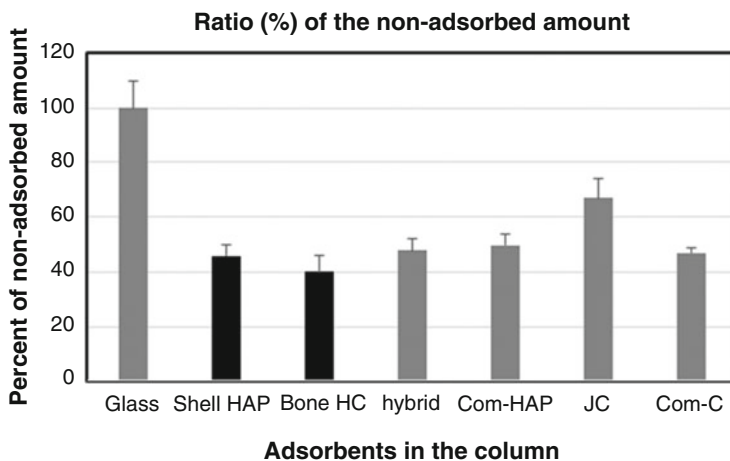


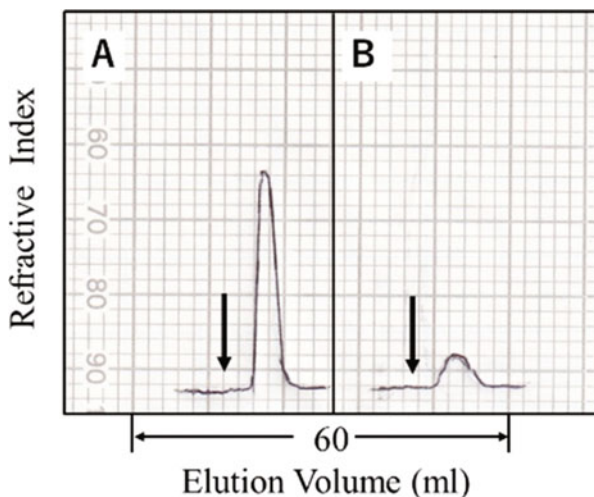
Fig. 15 Comparisons of the ratios (%) of the non-adsorbed per total applied amount of arsenate on the column packed with the different adsorbents

ability) and the testing materials. Figure 15 shows the ratios (%) of the non-adsorbed amounts per the total quantity of arsenate applied. We can estimate by comparing the peak areas of chromatograms of each sample with that of the column packed with the glass beads, which was a non-adsorbent control.

We applied the same amount of arsenate (5 mg taken as 100%), compared to the ratio of the peaks areas by Image-J, and expressed it as a percent.

Glass indicates the glass beads as a non-adsorbent control, Shell-HAP: scallop shell-derived HAP, Bone AC: Bone-derived complex of HAP and active carbon, hybrid: hybrid column packed with the commercial charcoal and commercial HAP

Fig. 16 Chromatograms of the arsenate (0.2 mg) applied on the columns packed with glass beads (a) and the bone-derived complex of HAP and active carbon (b). The peak area of B was 25% of that of a



in the upper and lower half, Com-HAP: a commercial HAP, JC: Jatropha-seed charcoal, and Com-C: commercial charcoal.

The lowest peak area (40%) indicated the highest adsorption was the bone-derived active carbon (Bone AC), which meant the highest adsorbent ability among the tested adsorbents. Other adsorbents remained within 45–50%, except for Jatropha charcoal 67%.

Figure 16 shows the chromatographic peak of 0.2 mg arsenate (2 mL of 100 ppm solution) applied on the column (10 × 50 mm), which was packed with the glass beads (0.1 mm in diameters) as control and ran at the flow rate of 120 mL/h. Figure 14b results from the same chromatography as Fig. 14a, except that the column's content was the bone-derived active carbon (Bone AC) instead of glass beads. Figure 4 showed the chromatogram with glass beads and the Bone AC on that we applied a smaller amount of arsenate (5 mg taken as 100%). Comparing the two chromatograms, we will find the peak area by the Bone AC column was 25% of glass beads. The reduction of 75% when we applied 0.2 mg was much eminent 40% when using 5 mg arsenate.

Namely, the applied amount reduced, the absorbed amount increased. We explained the reason for this situation as follows. According to the isotherm theory by Freundlich and Langmuir [96–98], the adsorbed amount of the soluble materials (adsorbate) on the solid substance (adsorbent) is dependent on the concentration of the soluble materials. The higher the concentration of the soluble materials (adsorbate), the lower the ratio of adsorbed amount/the concentration of the soluble material. The above situation occurs at least within a specific range of concentrations. Therefore, we can estimate the maximum amount of adsorbed material on a certain amount of solid materials by repeating the experiments changing the concentration of soluble materials.

We showed by chromatography that we can estimate the maximum amount of arsenate adsorbed on a certain amount of materials with adsorbing ability. The

chromatographic method we developed would be helpful for arsenate removal from water by apatite.

The mechanism of the adsorption of arsenate by HAP is an exciting issue. It is still not clear whether it is a pure adsorption phenomenon or accompanying the exchange with the atomic components of HAP. Recycling adsorbed arsenate in HAP is another promising subject.

2.4 Conclusion

1. Simple and economic adsorbing materials for arsenate (As compounds) are ardently needed in Bangladesh, where the natural well water contains arsenate originating from the Himalayas Mountains.
2. Natural sources of calcium for HAP production are available quickly, from seashell (scallop), bovine bone, pollack bone, eggshell (a hen). We propose simple methods of HAP production from these calcium resources.
3. We developed a new chromatographic method to measure the efficacy of arsenate removal from water by HAP and other materials.
4. The hybrid product of HAP and active carbon from bovine bone (bone AC) seemed to be relatively higher efficient among the HAP samples tested this time. Previously, we have no study on the bone AC for arsenate removal, and only the positive affinities of bone AC for metals: Mn, Fe, Ni, and Cu were so far reported [99]. Therefore, our first trial study of arsenate removal by bone AC is highly expected for further studies, considering the urgent water purification needs in Bangladesh.

Acknowledgements Collaborations did with Associate Professor Kazuhide Ozeki (Ibaraki University, Japan) and Dr. Iku Shouhei (Jiangsu Alphas Biological Technology Co., Ltd., Nantong, China). Their efforts are equivalent to those by Yoshinori Kuboki and Purvin Bergun, and we regarded them to possess the same authorships as us.

3 Layered Double Hydroxides (LDHs) for Removal of Drug Trace in the Environment

3.1 Introduction to Layered Double Hydroxide (LDHs)

Layered double hydroxides (LDHs) are the only known group of layered inorganic materials that have net positively charged sheets [100, 101]. Figure 17 shows a representation of the LDH layers. The layers are formed by edge sharing metal

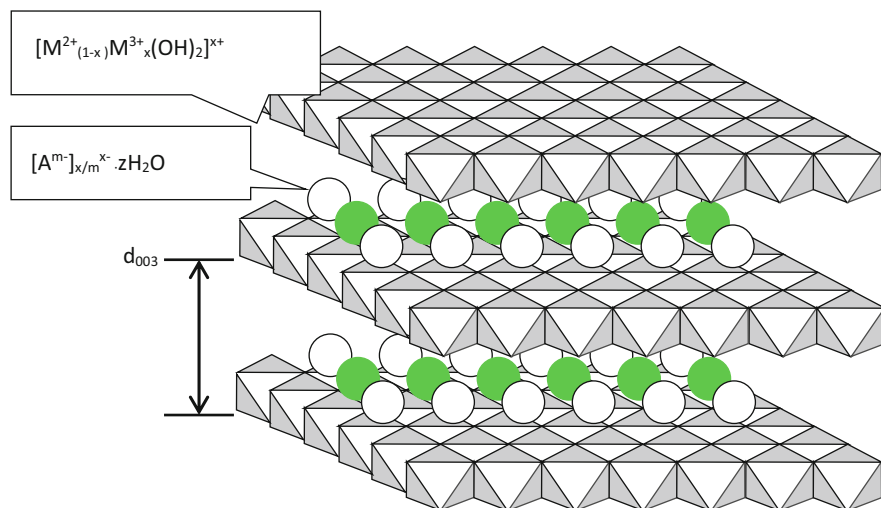


Fig. 17 Schematic structure of a layered double hydroxide. White ball: anion, green ball: water molecule

hydroxide octahedra similar to those of brucite, $Mg(OH)_2$ [102]. Substitution of some of the divalent metals by trivalent metals results in net positive charges on the layers that are neutralized by counterbalancing anions intercalated between the layers. The chemical formula of the layers can be expressed as $[M^{2+}_{(1-x)}M^{3+}_x(OH)_2][A^{m-}]_{x/m} \cdot zH_2O$ where M^{2+} and M^{3+} are di- and trivalent metals, A^{m-} is an exchangeable anion, and x normally ranges from 0.17 to 0.33 [103–105]. LDHs are also called hydrotalcite minerals, mixed metal hydroxides, or anionic clays.

A wide range of metals can form LDH layers provided certain conditions are met. First, the ionic radii of the M^{2+} and M^{3+} ions must be within 30% of each other. Second, the solubility products of the divalent metal hydroxide (S_1) and trivalent metal hydroxide (S_2) must be within 10 orders of magnitude of each other. LDHs containing divalent metals such as iron(II), magnesium, manganese(II), nickel, zinc and trivalent metals such as iron(III), aluminum, cobalt(III), and chromium(III) can be synthesized. LDHs containing monovalent and tetravalent cations such as lithium and tin(IV) have also been reported [106, 107].

Any anions or anionic complexes can function as counterbalancing species provided that they do not form complexes with the metals of the octahedral sheets during the formation of the LDH [102]. They range from inorganic anions such as CO_3^{2-} , Cl^- , SO_4^{2-} , PO_4^{3-} , polyoxometalates, etc. to organic anions such as acetate, acrylate, oxalate, benzoate, benzene sulfonate, etc. However, CO_3^{2-} is preferred and is found in almost all-natural minerals of the LDH family. Water molecules are also always found in the interlayer space. The unit cell of LDHs can contain from 1 to 6 H_2O , but usually has 4 H_2O . The prototype of the naturally occurring minerals is hydrotalcite, an Mg-Al LDH with carbonate as the charge balancing anion,

Table 6 Naturally occurring minerals with the layered double hydroxide structure

Mineral name	Empirical formula
Hydrotalcite	$Mg_6Al_2(OH)_{16}CO_3 \cdot 4H_2O$
Stichtite	$Mg_6Cr_2(OH)_{16}CO_3 \cdot 4H_2O$
Desautelsite	$Mg_6Mn_2(OH)_{16}CO_3 \cdot 4H_2O$
Pyroaurite	$Mg_6Fe_2(OH)_{16}CO_3 \cdot 4H_2O$
Reevesite	$Ni_6Fe_2(OH)_{16}CO_3 \cdot 4H_2O$
Comblainite	$Ni_6Co_2(OH)_{16}CO_3 \cdot 4H_2O$
Caresite	$(Fe^{2+}, Mg)_4Al_2(OH)_{12}CO_3 \cdot 3H_2O$
Sergeevite	$Ca_2Mg_{11}(OH)_4(CO_3)_9(HCO_3)_4 \cdot 6H_2O$
Takovite	$Ni_6Al_2(OH)_{16}(CO_3)_{0.75}(OH)_{0.25} \cdot 4H_2O$

$Mg_6Al_2(OH)_{16}CO_3 \cdot 4H_2O$. Other examples of naturally available minerals in the LDH family are listed in Table 6.

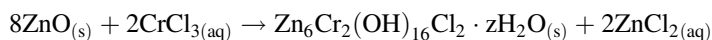
Hydrotalcite has cell parameters $a = b = 3.07 \text{ \AA}$, $\alpha = \beta = 90^\circ$, $\gamma = 120^\circ$, and $c = 23.23 \text{ \AA}$ for those with the CO_3^{2-} counter anion. Stacking of the layers can be accomplished in two ways, leading to two polytypes with a rhombohedral (3R symmetry) or a hexagonal cell (2H symmetry); hydrotalcite has 3R symmetry, while the 2H analogue is known as manasseite [102]. The density of the LDH depends on the metal cations in the layers, the interlayer anions, and the interlayer water content. For example, hydrotalcite has a density of 2.06 g/mL. The density increases to 3.05 g/mL for comblainite [102].

3.2 Syntheses of LDHs

Naturally available minerals of the LDH family are rare. Fortunately, hydrotalcite-like minerals can be synthesized very easily in the laboratory. There are numerous routes to synthetic LDHs. Some of the most significant methods will be briefly described here.

3.2.1 Salt-Oxide Method

In this method, a trivalent metal salt is added to the aqueous suspension of a divalent metal oxide. For example, Boehm and co-workers used this method in 1977 to prepare Zn-Cr-Cl LDH by adding chromium(III) chloride to the aqueous suspension of zinc oxide [103].



Zn-Al-Cl and Cu-Cr-Cl LDHs can also be synthesized using this route. Not all oxides, however, can be dispersed in the aqueous medium, limiting the range of LDHs that can be made by this method.

3.2.2 Salt-Base Method

This method, first introduced by Feicknecht in 1942, is probably the simplest [105]. It consists of the titration of the aqueous solution of a mixture of the di- and trivalent salts with a base. For example, reaction (2) shows the preparation of hydrotalcite with chloride in the interlayer space by this method.



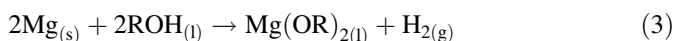
The titration itself can be performed by increasing the pH (addition of the base to the salt mixture) or decreasing the pH (addition of the salt mixture to the base). The final pH of the titration mixture must be adjusted in order to obtain well-crystallized products. Ni-Cr-Cl LDH, for example, forms well in a pH range of 3.5 to 6.8, Zn-Al-Cl LDH in a pH range of 4 to 10, Zn-Cr-Cl LDH in a pH range of 4.5 to 5, and Cu-Cr-Cl LDH at pH 5.5 [103]. In 1975, Miyata modified this method by simply adjusting the pH of the solution mixture to 10 with the base rather than by titration [105]. There was a work on LDH containing multiple metals [106].

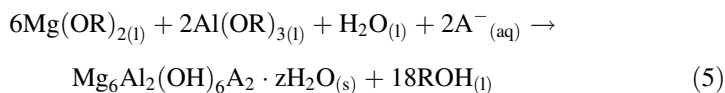
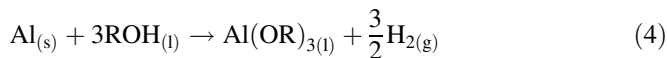
3.2.3 Stoichiometric Method

This is very similar to the salt-base method except that instead of maintaining the pH at a predetermined value, only the stoichiometric amount of the base required to form the LDH is added. For example, to produce the $\text{Mg}_6\text{Al}_2(\text{OH})_{16}\text{Cl}_2$ LDH 8 mol of NaOH is added to an aqueous solution mixture containing 3 mol of MgCl_2 and 1 mol of AlCl_3 . This is simple since no pH adjustment is required [107].

3.2.4 Metal Alcoholate Method

This method yields the very pure LDHs that are needed for some applications, such as for drug use. Heating a primary alcohol (preferably C_2 to C_{10}) and the pure metal at about 160 °C produces metal alcoholate. Hydrolysis of the metal alcoholate mixture in water containing the desired interlayer anions produces the LDHs.





This process has been patented recently [108]. However, hydrogen gas produced in these reactions needs to be handled carefully. And, some transition metals react slowly with alcohol limiting the range of LDHs that can be prepared. There are methods generally employed for the synthesis of transition metal alkoxides [109] that could probably be used to prepare LDHs.

3.2.5 Heat Treatment of Metal Oxides Suspensions

Heating a mixture of metal oxides with a small amount of water at elevated temperatures, about 450–500 °C, in an oxygen free environment will produce a slurry of LDH precursors. Hydrolysis of the slurry at room temperature in an aqueous medium containing the desired anion gives LDHs with good crystallinity. MgO and Al₂O₃ have been successfully converted into LDH using this method [110]. The hydrolysis can be done at room temperature. As of the salt-oxide method, the difficulty is to develop a good aqueous suspension of the precursors. This limits this method to the synthesis of LDHs containing main group metals.

3.3 Anion Exchange Properties of LDHs

The counterbalancing anions in the LDH interlayer are exchangeable. LDHs are one of the main classes of inorganic anion exchangers. Thermodynamically, ion exchange in the LDH depends mainly on the electrostatic interactions between positively charged hydroxylated sheets and the exchanging anions, and on the free energy involved in the changes of the hydration state of these ions. The equilibrium is constant for adsorption increases with the decrease of the ionic radius of the unhydrated (bare) anion. Ion exchange is therefore favored for incoming anions with a high charge density. In 1983, Miyata suggested a comparative list of ion selectivity for monovalent anions as $\text{OH}^- > \text{F}^- > \text{Cl}^- > \text{Br}^- > \text{NO}_3^- > \text{I}^-$, and for divalent anions $\text{CO}_3^{2-} > \text{C}_{10}\text{H}_4\text{N}_2\text{O}_8\text{S}^{2-} > \text{SO}_4^{2-}$. For oxoanions the order is HPO_4^{2-} ; $\text{HAsO}_4^{2-} > \text{CrO}_4^{2-} > \text{SO}_4^{2-} > \text{MoO}_4^{2-}$ [111]. According to these guidelines, nitrate-LDHs and iodide-LDHs are the best anion exchangers. Also, the selectivity for divalent anions is higher than for monovalent anions.

Although LDHs have complementary structures to the smectite clays, they are not easily pillared [3]. They have relatively high layer charge density ($\sim 0.04 \text{ e}^+/\text{X}^2$ for LDHs versus $0.01 \text{ e}^-/\text{X}^2$ for smectites) [3]. Thus, the galleries of the LDHs tend to

become crowded with the pillaring anions themselves. Nonetheless, polyoxometalate anions that have high charge density have been found effective in pillaring LDHs. The pillaring ions, however, must have a high negative charge density to balance the high positive charge density of the octahedral sheets, and be stable to hydrolysis reactions at above neutral pH. The first polyoxometalate ion that was successfully intercalated into the LDH gallery was $V_{10}O_{28}^{6-}$ by using Zn_2Al , Zn_2Cr , and Ni_3Al LDHs [111]. Keggin ions, $[X^{n+}M_{12}O_{40}]^{(8-n)-}$, have also shown a possibility to occupy the interstitial space. Anions formed at a lower pH require LDHs that are stable at a lower pH. Recently, Mg-Al LDH pillared with the decamolybdodicobaltate(III)anion, $[H_4Co_2Mo_{10}O_{38}]^{6-}$, has been found to remain intact at a pH as low as 4.7 [112].

3.4 Common Applications

LDHs have been used in various fields. Very pure synthetic Mg-Al- CO_3 layered double hydroxides have found applications as a pharmaceutical antacid (Talcid® by Bayer, Germany, and Altacite® by Peckforton Pharmaceuticals Ltd., England). These LDH-based antacids are especially good for patients that also suffer from hypertension and diabetes because of their low sodium and calcium contents. Another potential use of LDHs in the pharmaceutical industry is in drug delivery systems, especially for anionic drugs such as Ibuprofen. Mg-Al-Ibuprofen can be prepared by the ion exchange of Mg-Al-Cl LDH. The drug can then be slowly released into the digestive tract as the LDH framework dissolves in the gastric fluid to prolong the pharmacologic effect of the drug [113].

Another promising application of the LDHs is as gene reservoirs. Phosphate groups in DNA double helices that have negative charges can form weak ionic bonds with the positively charged sheets of LDHs [114]. The DNA stored in the LDH interlayer space can be released back into the aqueous solution simply by lowering the pH of the system.

There are numerous reports on the use of LDHs in organic syntheses as catalysts and catalyst supports. The recent work by Choudory et al. showed that the tetrachloropaladate anion could be intercalated into the LDH interlayer to produce catalysts for Heck-, Suzuki-, and Stille-coupling reactions with excellent yields [115]. Mg-Al hydrotalcite itself has been found to catalyze the reaction between aldehydes and nitroalkanes to afford nitroalkanols. Mg-Al-O-t-Bu LDH is an efficient catalyst for the 1,4-Michael addition [116]. Ruthenium-grafted LDHs are good catalysts for direct alpha-alkylation of nitriles with primary alcohols [117]. LDHs with OsO_4^{2-} counterbalancing anion have been prepared as catalysts for asymmetric dihydroxylation of olefins to vicinal diols [118] and LDHs with MnO_4^- for alcohol oxidation. In environmental remediation, Cu-Mg-Al LDH has proven to be a new catalyst for the simultaneous removal of SO_x and NO_x , gases that cause acid rain [119].

One large-scale application of LDHs is as polymer additives. They are used in polyolefin syntheses to neutralize residual acidic substances from Ziegler-Natta or other polymerization catalysts. The addition of the LDHs to the polymers prevents degradation and improves their heat and weathering resistance. They have been used in the stabilization of halogen containing polymers, particularly polyvinylchloride (PVC) [120], where they function as scavengers for the HCl released from the PVC. This is an excellent development since most acid scavengers are generally made of compounds containing lead, tin, or barium. LDHs that have carbonate and acrylate in the interlayer space are particularly good fire retardants. Some new materials based on polymer-LDH nanocomposites have begun to be studied. Polyacrylate-LDH nanocomposite might be useful in the design of fireproof material. Conducting polymers such as doped polyaniline, polythiophene, and polyacetylene are prospective candidates for electronic applications and can be inserted into the LDH interlayer to obtain a desirable range of electrical conductivity [121].

3.4.1 LDH for Removal of Drug Traces in the Environment

Research on the application of layered double hydroxide (LDH) as an anion exchanger in the pharmaceutical field is still being developed. The pharmaceutical drugs and their metabolites are a subclass of detectable organic contaminants in wastewater, and aquatic environments, the concentration of which keeps increasing. A diverse group of pharmaceuticals, potential endocrine disrupting compounds (EDCs), and other unregulated organic contaminants were screened. The 11 most frequently detected compounds in the US drinking water were atenolol, atrazine, carbamazepine, estrone, gemfibrozil, meprobamate, naproxen, phenytoin, sulfamethoxazole, TCEP, and trimethoprim [122]. Antibiotics are the focus of many studies because of the high frequency of detection in the environment and the increased incidence of bacterial resistance. Nowadays, there is increasing use of antibiotics as means of treating infectious diseases, especially those caused by microorganisms. Surveys conducted within the country and abroad found that β -lactam antibiotics are the most widely prescribed antibiotics. Amoxicillin is semisynthetic penicillin that has antibiotic properties of the β -lactam ring. The increased presence of β -lactam antibiotics such as amoxicillin in aquatic environments will lead to reduced water quality, be a threat to ecosystems, and affect the quality of drinking water source [123].

Several studies on the application of LDH as anion exchanger in the pharmaceutical field have been widely reported, e.g., the application of Ni-Al-NO₃ LDH in the determination of salicylic acid in blood serum, willow leaves, and aspirin tablets [124]. The extracts of salicylic acid were measured using spectrofluorometry with obtained percent recovery of 96–101%. Other works have been carried out in the determination of mesalamine content in human serum through the process of preconcentration by SPE with Ni-Al LDH as an anion exchanger and obtained percent recovery of up to 99% [125]. Ni-Al-NO₃ LDH as an anion exchanger was reported to have successfully analyzed the level of mefenamic acid in human serum

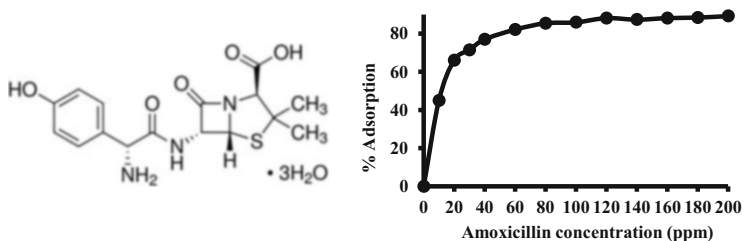


Fig. 18 Chemical structure of amoxicillin and adsorption profile of amoxicillin by Mg-Al LDH

and pharmaceutical wastewater samples and gave results between 94.7 and 104%. Mg-Al-diclofenac LDH has been successfully prepared by the ion-exchange method with initial CO_3^- anion present in the LDH [126]. The adsorption capacity of the calcined hydrotalcite was about 1.9 mmol g^{-1} .

One good example of LDH application is in the removal of antibiotic drug in the environment. Amoxicillin (Am) drug has been successfully intercalated into the interlayer of Mg-Al hydrotalcite through anion exchange [127]. Amoxicillin in slight alkaline media has a negative charge. Mg-Al- NO_3 LDH was synthesized, exchanged with oxalate ion, and applied as an adsorbent for amoxicillin. Figure 18 shows the structure of the compound and the adsorption reaction, whereas Fig. 19 displays the XRD and FTIR data. The process of amoxicillin adsorption is carried out through an ion-exchange method. The XRD of the Mg-Al- NO_3 , Mg-Al-Ox, and Mg-Al-Am is displayed. The Mg-Al- NO_3 LDH gives 2 θ peaks at 11.34° , 23.07° , and 34.55° . They correspond to the $d_{(003)}$, $d_{(006)}$, and $d_{(009)}$ spacings, respectively. It confirms the data reported in the previous works. The XRD pattern could be fitted to the hexagonal phase of a typical Mg-Al LDH (JCPDS file 22-0700). After ion exchange with oxalate, the diffraction peak at 2θ 5.33° is detected. It is also consistent with the data in the literature for LDH with oxalate ion. The Mg-Al-Am LDH gives diffraction peaks at 2θ 8.9° and 18.1° , corresponding to the $d_{(006)}$ and $d_{(009)}$ spacing and gives large basal spacing to indicate the insertion of the drug.

The FTIR spectra of Mg-Al- NO_3 , Mg-Al-Ox before and after the exchange are shown in Fig. 19. The band at $3,400\text{--}3,500 \text{ cm}^{-1}$ could be assigned as an O-H stretching vibration of the LDH octahedral layer and water molecules in the interlayer. For Mg-Al- NO_3 LDH, there is a weak band at $1,620 \text{ cm}^{-1}$, which could be associated with O-H bending vibrations. A sharp peak that appears at $1,381 \text{ cm}^{-1}$ may be attributed to NO_3^- asymmetric stretching vibration. According to the previous study, the LDH-FTIR spectra give a band at $3,463 \text{ cm}^{-1}$, which could be ascribed as an O-H vibration mode of free water molecules, M-OH lattices, and interlayer water molecules. The peak at $1,635 \text{ cm}^{-1}$ is the corresponding bending vibration of O-H. The band at $1,381 \text{ cm}^{-1}$ could be attributed to the asymmetric stretching vibration of nitrate ions. The peaks detected at 617 , 447 , and 409 cm^{-1} could be due to the stretching vibration of M-O. After ion exchange, the NO_3^- asymmetric vibration is no longer seen. In the Mg-Al-Ox LDH spectrum, the peaks that appear at $1,635 \text{ cm}^{-1}$ could be attributed to the C=O vibration mode. The appearance at $1,389 \text{ cm}^{-1}$ is due to the C-O asymmetric stretching of carboxylate

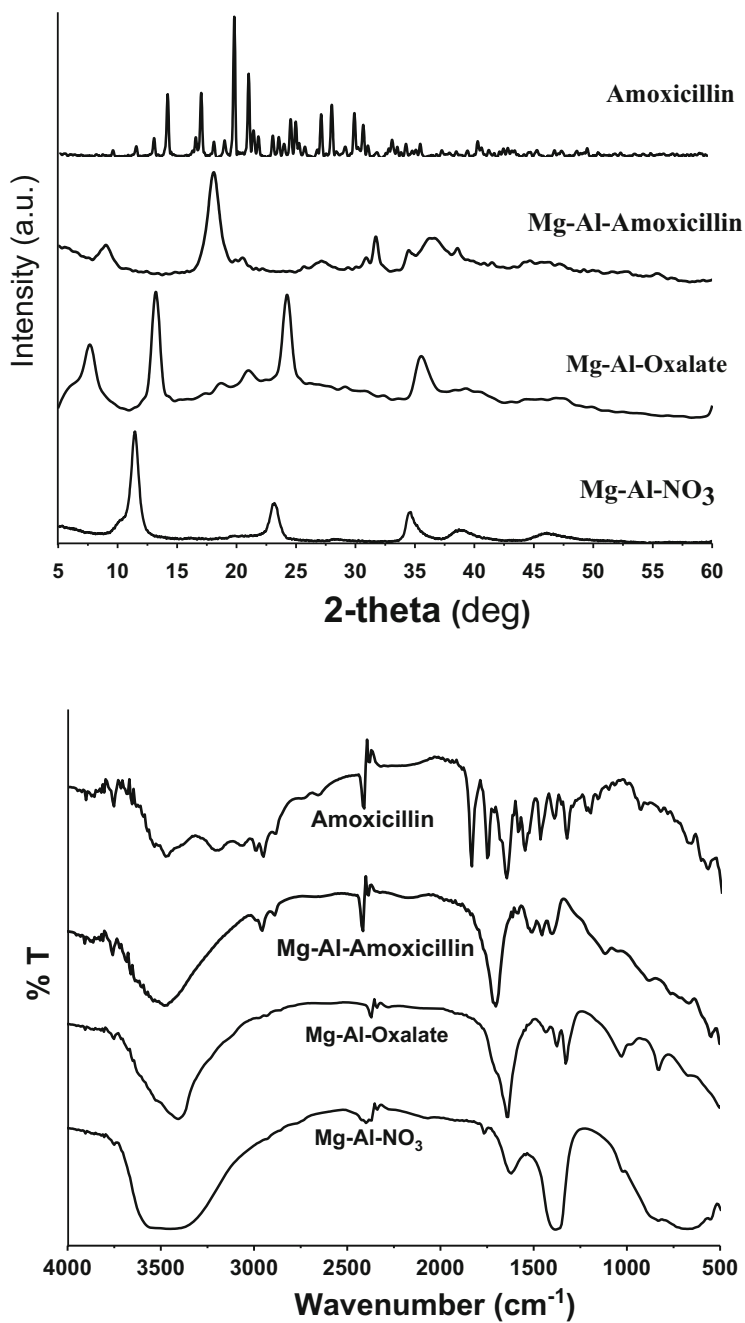


Fig. 19 XRD pattern and FTIR of Mg-Al LDH before and after adsorption of amoxicillin

ions. Multiple peaks in the fingerprint region of 400–800 cm^{-1} are believed to be due to the bending vibrations of the metal oxide of Mg-O, Al-O, Mg-O-Al, and O-Mg-O or O-Al-O.

After ion exchange, the peaks at 2,924, 1,774, 1,690 cm^{-1} might be assigned as the stretching vibration modes of the C_{sp^3} -H, C=O, and C=C bonds of the drug, respectively. The peaks observed at 1,582, 1,481, and 1,090–1,020 cm^{-1} could be assigned as bending vibration modes of the N-H, C-H, and C-N bonds. The bending vibration modes of the C-H and C-S are viewed at 1,000–675 and 563 cm^{-1} , respectively. The peak at 3,071 cm^{-1} is believed to be the stretching vibration mode of the benzene C_{sp^2} -H bond. Also, the peaks at 1,597 and 1,543 cm^{-1} could be attributed to the vibration mode of the benzene ring. It means that the amoxicillin has replaced the oxalate ion. All these prove that trace amoxicillin in the environment could be immobilized by the use of layered double hydroxides. Other negatively charged drug molecules may have similar interactions.

4 Conclusion

It has been demonstrated in this chapter that coal bottom/fly ash, hydroxyapatite, and hydrotalcite are potential inorganic materials that can be modified and applied in many applications such as environmental remediation and health areas. Coal ash can be found naturally and is normally classified as hazardous waste of coal burn, because of its high content of silica and alumina, it can be activated and modified to become selective adsorbents of heavy metals and dyes, so it can support zero-waste policy as well as innovation motto “form pollution to solution.” Hydroxyapatite and hydrotalcite are all environmentally benign materials. Both of them are also easy to prepare. Further modification and activation may be required to solve the target environmental and health issues. These can be basically achieved by considering the phenomena underlying the process such as the interaction between adsorbent and the target molecules and the properties of both the active site of the adsorbents and adsorbates as described in some examples of applications given in this chapter. In the future, these three types of materials may be modified further to address the developed environmental issues as well as to explore their possible applications in supporting many areas such as health, medicinal, and agricultural issues as multifunctional materials.

References

1. Jumaeri J (2015) Synthesis of zeolite A from coal fly ash and its modification using HDTMAB as a multifunctional adsorbent. PhD Disertasi, Chemistry Department Gadjah Mada University, Yogyakarta, Indonesia
2. Hessley RK, Reasoner JW, Riley JT (1986) Coal Science. Wiley, New York, pp 81–87

3. Oplas N (2014) Coal use and growth development potential of the economy. <http://Funwithgovernment.blogspot.com>
4. Kikuchi R (1999) Application of coal ash to environmental improvement transformation into zeolite, potassium fertilizer and FGD absorbent. *J Res Conserv Recycl* 27:333–346. <http://hdl.handle.net/1975/211>
5. Kula I, Olgun A, Erdogan Y, Sevinc V (2000) Effect of colemanite waste, coal bottom ash and fly ash on the properties of cement. *Cem Concr Res* 32:491–494. [https://doi.org/10.1016/s0008-8846\(00\)00486-5](https://doi.org/10.1016/s0008-8846(00)00486-5)
6. Mukhtar S, Kenimel AL, Sadaka SS, Mathis JG (2002) Evaluation of bottom ash and composite manur blends as a soil amandement material. *J Bioresour Technol* 89:217–228. [https://doi.org/10.1016/s0960-8524\(03\)00085-3](https://doi.org/10.1016/s0960-8524(03)00085-3)
7. Kuncoro MP, Fahmi MZ (2013) Removal of Hg and Pb in aqueous solution using coal fly ash adsorbent. *J Procedia Earth Planet Sci* 6:377–382. <https://doi.org/10.1016/j.proeps.2013.01.049>
8. Sunarti (2008) Preparation of modified adsorbent from coal bottom ash and its application for adsorption of heavy metal lead (Pb). M.Sc. thesis, Chemistry Department, Gadjah Mada University, Yogyakarta, Indonesia
9. Londar E, Fansuri H, Widiastuti N (2010) Effect of carbon on the formation of zeolite from bottom ash by direct hydrothermal method. Master thesis, Surabaya Institute of Technology, Surabaya, Indonesia
10. Wicaksono D (2014) Competitive adsorption of methylene blue and methyl orange using coal base ash. B.Sc. final project, Chemistry Department, Gadjah Mada University, Yogyakarta, Indonesia
11. Anderson AM, Rubin JA (1981) Adsorption of inorganics at solid-liquid interfaces. An Arbor Science Publishers
12. Tanjungsari R (2008) Pb(II) metal ion adsorption study by coal bottom ash. B.Sc. final project, Chemistry Department, Gadjah Mada University, Yogyakarta, Indonesia
13. Jati RA (2012) Methylene blue and methyl orange adsorption using coal bottomash in a binary system. B.Sc. final project, Chemistry Department, Gadjah Mada University, Yogyakarta, Indonesia
14. Septiana A (2013) Adsorption study of Pb(II), Cu(II) and Cr(II) metal ions using coal bottom ash. B.Sc. final project, Chemistry Department, Gadjah Mada University, Yogyakarta, Indonesia
15. Murniati M (2009) Preparation of zeolite from coal bottom ash and its application as Cu (II) adsorbent. M.Sc. thesis, Chemistry Department, Gadjah Mada University, Yogyakarta, Indonesia
16. Sutarno S, Arryanto Y, Yulianto I (2000) Utilization of fly ash waste as a basic material for faujisite synthesis with hydrothermal interaction smelting method. In: Proceedings of the 8th national chemistry seminar, Gadjah Mada University, Yogyakarta, Indonesia. pp. 265–270
17. Ratnasari M, Widiastuti N (2011) Adsorption of Cu(II) metal ions on zeolite synthesized from coal base ash of PT IPMOMI paiton by column method. In: Proceedings of the Unesa chemistry national seminar
18. Jundu R (2012) Thermodynamics of simultaneous adsorption of Mg(II) and Ca(II) influenced by heavy metals on dithizone modified silica gel. www.wordpress.com. Accessed 10 Feb 2014
19. Padi P (2009) The effect of HCl treatment on the character of klaten natural zeolite. M.Sc. thesis, Chemistry Department, Gadjah Mada University, Yogyakarta, Indonesia
20. Mufrodi Z, Sutrisno B, Hidayat A (2011) Modification of fly ash waste as a new adsorbent material. In: Proceedings of the chemical engineering national seminar
21. Wahyuni S, Widiastuti N (2009) Zn(II) metal ion adsorption on zeolite A synthesized from coal base ash of PT IPMOMI paiton with batch method. In: Proceeding of 2008 final project, Surabaya Institute of Technology, Surabaya, Indonesia

22. Yao ZT, Ji XS, Sarker PK, Tang JH, Ge LG, Xia MS, Xi YQ (2015) A comprehensive review on the applications of coal fly ash. *Earth-Sci Rev* 141:105–121. <https://doi.org/10.1016/j.earscirev.2014.11.016>
23. Matzenbacher CA, Garcia ALH, Dos Santos MS, Nicolau CC, Premoli S, Correa DS, De Souza CT, Niekraszewicz L, Dias JF, Delgado TV (2017) DNA damage induced by coal dust, fly and bottom ash from coal combustion evaluated using the micronucleus test and comet assay in vitro. *J Hazard Mater* 324:781–788. <https://doi.org/10.1016/j.jhazmat.2016.11.062>
24. Mushtaq F, Zahid M, Bhatti IA, Nasir S, Hussain T (2019) Possible applications of coal fly ash in wastewater treatment. *J Environ Manag* 204:27–46. <https://doi.org/10.1016/j.jenvman.2019.03.054>
25. Dindi A, Quang DV, Vega LF, Nashef E, Abu-Zahra MRM (2019) Applications of fly ash for CO₂ capture, utilization, and storage. *J CO₂ Util*:82–102. <https://doi.org/10.1016/j.jcou.2018.11.011>
26. Valer MMM, Lu Z, Zhang Y, Tang Z (2008) Sorbents for CO₂ capture from high carbon fly ashes. *Waste Manag* 28:2320–2328. <https://doi.org/10.1016/j.wasman.2007.10.012>
27. Kanarac M, Dolic M, Veljonic D, Ognjanovic VR, Velickovic Z, Pavicevic V, Marinkovic A (2018) The removal of Zn²⁺, Pb²⁺, and As(V) ions by lime activated fly ash and valorization of the exhausted adsorbent. *J Waste Manag* 78:366–378. <https://doi.org/10.1016/j.wasman.2018.05.052>
28. Xiyili H, Cetintas S, Bingol D (2017) Removal of some heavy metals onto mechanically activated fly ash: modeling approach for optimization, isotherms, kinetics and thermodynamics. *Process Saf Environ PRO* 109:288–300. <https://doi.org/10.1016/j.psep.2017.04.012>
29. Serrano D, Kwapinska M, Sánchez-Delgado S, Leahy JJ (2018) Fly ash characterization from *Cynara Cardunculus* L. Gasification. *Energy Fuels* 32(5):5901–5909. <https://doi.org/10.1021/acs.energyfuels.7b04050>
30. Sari DK, Setyaningsih EP, Fansuri H, Susanto TE (2018) Study of the chemical and physical characteristics of fly ash which determines the mechanical strength of fly ash based geopolymer adhesives. *Akta Kimindo* 3(2):222–235
31. Wang N, Zhao Q, Zhang A (2017) Catalytic oxidation of organic pollutants in wastewater via a fenton-like process under the catalysis of HNO₃-modified coal fly ash. *RSC Adv* 7:27619–27628. <https://doi.org/10.1039/C7RA09925H>
32. Blissett R, Rowson N (2012) A review of the multi-component utilisation of coal fly ash. *Fuel* 97:1–23. <https://doi.org/10.1016/j.fuel.2012.03.024>
33. Giribabu P, Swaminathan G (2016) Synergetic degradation of reactive dye acid red-1 by cobalt-doped lignite fly ash. *Desalin Water Treat* 57:16955–16962. <https://doi.org/10.1080/19443994.2015.1082509>
34. Ji L, Yu H, Wang X, Grigore M, French D, Gözükarar YM, Yu J, Zeng M (2017) CO₂ sequestration by direct mineralisation using fly ash from Chinese Shenfu coal. *Fuel Process Technol* 156:429–437. <https://doi.org/10.3390/cryst11111314>
35. Wu H, Zhu Y, Bian S, Ko JH, Li SM, Xu Q (2018) H₂S adsorption by municipal solid waste incineration (MSWI) fly ash with heavy metals immobilization. *Chemosphere* 195:40–47. <https://doi.org/10.1016/j.chemosphere.2017.12.068>
36. Kumar THV, Sivasankar V, Fayoud N, Oualid HA, Sundramoorthy AK (2018) Synthesis and characterization of coral-like hierarchical Mgo incorporated fly ash composite for the effective adsorption of azo dye from aqueous solution. *Appl Surf Sci* 449:719–728. <https://doi.org/10.1016/j.apsusc.2018.01.060>
37. Patra G, Barnwal R, Bahera SK, Meikap BC (2018) Removal of dyes from aqueous solution by sorption with fly ash using a hydrocyclone. *J Environ Chem Eng* 6:5204–5211. <https://doi.org/10.1016/j.jece.2018.08.011>
38. Pura S, Atun G (2009) Adsorptive removal of acid blue 113 and tartrazine by fly ash from single and binary dye solutions. *Sep Sci Technol* 44:75–101. <https://doi.org/10.1080/01496390802437057>

39. Alouani ME, Achhouri ME, Taibi M (2017) Potential use of moroccan fly ash as low cost adsorbent for the removal of two anionic dyes (indigo carmine and acid orange). *J Mar Sci Eng* 8(9):3397–3409. <https://www.jmaterenvironsci.com>
40. Jimping LI, Jinhua G, Liang W, Juan Y (2016) Preparation of fly ash based adsorbents for removal active red X-3B from dyeing wastewater. *MATEC Web Conf* 67:07004. <https://doi.org/10.1051/mateconf/20166707004>
41. Atun G, Ayar N, Kurtoglu AE, Ortoboy S (2019) A comparison of sorptive removal of anthraquinone and azo dyes using fly ash from single and binary solutions. *J Hazard Mater* 371:94–107. <https://doi.org/10.1016/j.jhazmat.2019.03.006>
42. Liu J, Mwamulima T, Wang Y, Fang Y, Song S, Peng C (2017) Removal of Pb(II) and Cr (VI) from aqueous solutions using the fly ash-based adsorbent material-supported zero-valent iron. *J Mol Liq* 243:205–211. <https://doi.org/10.1016/j.molliq.2017.08.004>
43. Soni R, Shukla DP (2019) Synthesis of fly ash based zeolite-reduced graphene oxide composite and its evaluation as an adsorbent for arsenic removal. *Chemosphere* 219:504–509. <https://doi.org/10.1016/j.chemosphere.2018.11.203>
44. Feng W, Wan Z, Daniels J, Li Z, Xiao G, Yu J, Xu D, Guo H, Zhang D, May EF, Li G (2018) Synthesis of high quality zeolites from coal fly ash: mobility of hazardous elements and environmental applications. *J Clean Prod* 202:390–400. <https://doi.org/10.1016/j.jclepro.2018.08.140>
45. Zhuannian L, Anning Z, Guirong W, Xiaoguang Z (2009) Adsorption behavior of methyl orange onto ultrafine coal powder. *Chin J Chem Eng* 17(6):942–948. <http://cjche.cip.com.cn>
46. Jarusiripot C (2014) Removal of reactive dye by adsorption over chemical pretreatment coal based bottom ash. *Procedia Chem* 9:121–130. <https://doi.org/10.1016/j.proche.2014.05.015>
47. Valaskova M, Martynkova GS, Matejka V, Kratosova G (2007) Chemically activated kaolin-ites after deintercalation of formamide. *Ceramics-Silikaty* 51(1):24–29
48. Terrazas CGD, Ibarra RJ, Ortiz-Méndez U, Torres-Martínez LM (2005) Iron leaching of a Mexican clay of industrial interest by oxalic acid. *Adv Technol Mat Mat Process* 7(2): 161–166. <https://doi.org/10.2240/azojomo0168>
49. Wang Y, Ren D, Zhao F (1999) Comparative leaching experiments for trace elements in raw coal, laboratory ash, fly ash and bottom ash. *Int J Coal Geol* 40:103–108. <http://www.paper.edu.cn>
50. Suseno S (2006) Physical immobilization of dithizone in natural zeolite and study of its adsorption ability towards Pb(II) and Cd(II) metals. M.Sc. thesis, Chemistry Department, Gadjah Mada University, Yogyakarta, Indonesia
51. Kunarti ES (1994) Formation and chromatographic separation characteristics of diethylthiocarbamate and dithizonate complex compounds. M.Sc. thesis, Chemistry Department, Gadjah Mada University, Yogyakarta, Indonesia
52. Wogo HE, Segu JO, Ola P (2011) Synthesis of dithizone immobilized silica gel through sol gel process. *J Sci Appl Chem* 5:84–95. <https://ppjp.ulm.ac.id/journal/index.php/jstk>
53. Cestari AR, Vieira EF, Lopes EC, Silva RA (2004) Kinetics and equilibrium parameters of Hg (II) adsorption on silica-dithizone. *J Colloid Interf Sci* 272:271–276. <https://doi.org/10.1016/j.jcis.2003.09.019>
54. Salih B, Denizli B, Kavakli C, Say R, Piskin E (1998) Adsorption of heavy metal ions onto dithizone-anchored poli(EGDMA-HEMA) microbeads. *Talanta* 46:1205–1213. [https://doi.org/10.1016/S0039-9140\(97\)00362-7](https://doi.org/10.1016/S0039-9140(97)00362-7)
55. Absalan G, Goudi AA (2004) Optimizing the immobilized dithizone on surfactant-coated alumina as a new sorbent for determination of silver. *Sep Purific Technol* 38:209–214. <https://doi.org/10.1016/j.seppur.2003.11.008>
56. Savafi A, Bagheri M (2004) Design and characteristics of a mercury(II) optode based on immobilization of dithizone on a triacetylcellulose membrane. *Sensor Actuat B* 99:608–612. <https://doi.org/10.1016/j.snb.2004.01.022>

57. Savafi A, Bagheri M (2005) Design of a copper(II) optode based on immobilization of dithizone on a triacetylcellulose membrane. *Sensor Actuat B* 107:53–58. <https://doi.org/10.1016/j.snb.2004.10.062>
58. Mudasir M, Raharjo G, Tahir I, Wahyuni ET (2008) Imobilization of dithizone onto chitin isolated from prawn seawater shells (*P.marguensis*) and preliminary study for the adsorption of Cd(II) ion. *J Phys Sci* 19:63–78. <https://jps.usm.my/wp-content/uploads/2014/11/Article-19-1-6.pdf>
59. Yu HM, Song H, Chen ML (2011) Dithizone immobilized silica gel on-line preconcentration of trace copper with detection by flame atomic absorption spectrometry. *Talanta* 85:625–630. <https://doi.org/10.1016/j.talanta.2011.04.039>
60. Rohyami Y (2011) Study of Cu(II) preconcentration with solid phase extraction method using dithizone immobilized chitin as adsorbent. M.Sc. thesis, Chemistry Department, Gadjah Mada University, Yogyakarta, Indonesia
61. Mudasir M, Karelius K, Aprilita NH, Wahyuni ET (2016) Adsorption of mercury(II) on dithizon-immobilized natural zeolite. *J Environ Chem Eng* 4:1839–1849. <https://doi.org/10.1016/j.jece.2016.03.016>
62. Mudasir M, Baskara RA, Suratman A, Yunita KS, Perdana R, Puspitasari W (2020) Simultaneous adsorption of Zn(II) and Hg(II) ions on selective adsorbent of dithizone-immobilized bentonite in the presence of Mg(II) ion. *J Environ Chem Eng* 8:104002. <https://doi.org/10.1016/j.jece.2020.104002>
63. Huda BN, Wahyuni ET, Mudasir M (2021) Eco-friendly immobilization of dithizone on coal bottom ash for the adsorption of lead(II) ion from water. *Results Eng* 10:100221. <https://doi.org/10.1016/j.rineng.2021.100221>
64. Aminy DE, Rusdiarso B, Mudasir M (2021) Adsorption of Cd(II) ion from the solution using selective adsorbent of dithizone-modified commercial bentonite. *Int J Environ Sci Technol*. <https://doi.org/10.1007/s13762-021-03570-1>
65. Kato Y et al (2003) Biomineralization (BIOM2001): formation, diversity, evolution and application. In: Kobayashi, Ozawa (eds) *Proceedings of the 8th int sympo biomineral*. Tokai Univ Press, Kanagawa, pp 194–201
66. Iijima M, Takita H, Moriwaki Y, Kuobki Y (1991) Difference on the organic components between the mineralized and the non-mineralized layers of lingula shell. *Comp Biochem Phys* 98A:379–382
67. Paselo M et al (2010) Nomenclature of the apatite supergroup minerals. *Eur J Mineral* 22:163–179
68. Landis WL (1999) An overview of vertebrate mineralization with emphasis on collagen-mineral interaction. *Gravit Space Bull* 12(2):15–26
69. Aoki H, Kato K, Tabata T (1977) Osteo-compatibility of apatite ceramics in mandibles, official report of the Institute for Medical Instruments. *Tokyo Med Den Univ* 11:33
70. Kuboki Y et al (1988) Remedy for a skin disease, Japanese Patent Showa 63-107938
71. Kuboki Y, Tazaki M, Mizuno M, Fujita K (1987) Mechanical filling of the micro-defects of enamel surface with HAP: the interaction between the solid surface and fine powders of the same material. *Dent J* 26(2):215–223
72. Kuboki Y et al (1989) Dental micro-investment method and its material, Japanese Patent Heisei 01-11608
73. Kuboki Y et al (2007) Development of a new purification method of active organic factors from sea shell. *Annu Sci Rep North Adv Center Sci Tech* 2007:77
74. Kuboki Y, Yagami G, Furusawa T (2017) New principles of regenerative medicine: with special reference to mechano-dynamic factors. *J Oral Tissue Eng* 14(3):128–152
75. Kuboki Y, Jin Q, Takita H (2001) Geometry of carriers controlling phenotypic expression in BMP-induced osteogenesis and chondrogenesis. *J Bone Joint Surg* 83-A:A:S1–S105
76. Kuboki Y, Jin Q, Kikuchi M, Mamood J, Takita H (2002) Geometry of artificial ECM: sizes of pores controlling phenotype expression in BMP-induced osteogenesis and chondrogenesis. *Connect Tissue Res* 43:529–534

77. Kuboki Y, Sasaki M, Saito A, Takita H, Kato H (1998) Regeneration of periodontal ligament and cementum by BMP-applied tissue engineering. *Eur J Oral Sci* 106(Suppl 1):197–203
78. Kuboki Y, Saito T, Murata M, Takita H, Mizuno M, Inoue M, Nagai N, Poole AR (1995) Two distinctive BMP-carriers induce zonal chondrogenesis and membranous ossification, respectively; geometrical factors of matrices for cell-differentiation. *Connect Tissue Res* 32:219–226
79. Kuboki Y, Takita H, Kobayashi D, Tsuruga E, Inoue M, Murata M, Nagai N, Dohi Y, Ohgushi H (1998) BMP-induced osteogenesis on the surface of hydroxyapatite with geometrically feasible and nonfeasible structures: topology of osteogenesis. *J Biomed Mater Res* 39:190–199
80. Itoh H, Wakisaka Y, Ohnuma Y, Kuboki Y (1994) A new porous hydroxyapatite ceramic prepared by cold isostatic pressing and sintering synthesized flaky powder. *Dent Mater J* 13: 25–35
81. Tsuruga E, Takita H, Itoh H, Wakisaka Y, Kuboki Y (1997) Pore size of porous hydroxyapatite as the cell-substratum controls BMP-induced osteogenesis. *J Biochem* 121:317–324
82. Kuboki Y, Iku S, Yoshimoto R, Kaku T, Takita H (2008) Modification of titanium surfaces based on the principles of the geometry of the artificial extracellular matrix (ECM). In: Tanaka J, Itoh S, Chen G (eds) *Surface design and modification of the biomaterials for clinical application*. Transworld Research Network, Kerala, pp 1–27
83. Kuboki Y et al (2009) Calcified honeycomb-shaped collagen maintains its geometry *in vivo* and effectively induces vasculature and osteogenesis. *Nano Biomed* 1:85–94
84. Urist MR (1965) Bone: formation by autoinduction. *Science* 150(3698):893–899
85. Reddi AH, Huggins CB (1973) Influence of geometry of transplanted tooth and bone on transformation of fibroblasts. *Proc Soc Exp Biol Med* 143:634–637
86. Ripamonti U, Crooks J, Kirkbride AN (1999) Sintered porous hydroxyapatite with intrinsic osteoinductive activity: geometric induction of bone formation. *S Afr J Sci* 95:335–343
87. Smith AH, Lingas EO, Rahman M (2000) Contamination of drinking-water by arsenic in Bangladesh: a public health emergency. *Bull World Health Organ* 78(9):1093–1103
88. Smith AH (1997) Report and action plan for arsenic in drinking water focusing on health, Bangladesh. Assignment report, WHO project BAN CWS 001, March 1997. <http://socrates.berkeley.edu/~asrg/>
89. Smith AH (1998) Technical report and review of action plan for arsenic in drinking water in Bangladesh focusing on health. Assignment Report, WHO project BAN CWS 001/D, February 1998. <http://socrates.berkeley.edu/~asrg/>
90. Smith AH (1998) Technical report. Assignment report, WHO project BAN CWS 001, June 1998. <http://socrates.berkeley.edu/~asrg/>
91. Sasaki K, Hayashi Y, Toshiyuki K, Guo (2018) Simultaneous immobilization of borate, arsenate, and silicate from geothermal water derived from mining activity by co-precipitation with hydroxyapatite. *Chemosphere* 207(9):139–146
92. Islam M, Mishra PC, Patel R (2011) Arsenate removal from aqueous solution by cellulose-carbonated hydroxyapatite nanocomposites. *J Hazard Mater* 189(3):755–763. <https://doi.org/10.1016/j.jhazmat.2011.03.051>
93. Liu G, Talley JW, Na C, Larson SL, Wolfe LG (2010) Copper doping improves hydroxyapatite sorption for arsenate in simulated groundwaters. *Environ Sci Technol* 44(4):1366–1372
94. Rouff AA, Ma N, Kustka AB (2016) Adsorption of arsenic with struvite and hydroxylapatite in phosphate-bearing solutions. *Chemosphere* 146(3):574–581
95. Katz EP, Li S-T (1973) Structure and function of bone collagen fibrils. *J Mol Biol* 80(1):1–15
96. Freundlich HMF (1906) Over the adsorption in solution. *J Phys Chem B* 57:385–470
97. Langmuir I (1918) The adsorption of gases on plane surfaces of glass, mica, and platinum. *J Am Chem Soc* 40:1361–1403
98. Langmuir I (1916) The constitution and fundamental properties of solids and liquids. Part I. Solids *J Am Chem Soc* 38:2221–2295
99. Moreno JC, Rigoberto G, Liliana G (2010) Removal of Mn, Fe, Ni and Cu ions from wastewater using cow bone charcoal. *Materials* 3:452–466

100. Meyn M, Beneke K, Lagaly G (1990) Anion-exchange reactions of layered double hydroxides. *Inorg Chem* 29:5201–5207
101. Dimotakis ED, Pinnavaia TJ (1990) New route to layered double hydroxides intercalated by organic anions: precursors to polyoxometalate-pillared derivatives. *Inorg Chem* 29:2393–2394
102. De Roy A, Forano C, El Malki K, Besse J-P (1992) Anionic clays: trends in pillaring chemistry. In: Ocelli ML, Ronson H (eds) *Expanded clays and other microporous solids. Synthesis of microporous materials*. Springer, p 108
103. Ocelli ML, Robson HE (1992) *Expanded clays and other microporous solids*. In: *Synthesis of microporous materials, vol vol II*. Van Nostrand Reinhold
104. Taylor RM (1984) The rapid formation of crystalline double hydroxy salts and other compounds by controlled hydrolysis. *Clay Miner* 19:591–603
105. Miyata S (1975) The syntheses of hydrotalcite-like compounds and their structures and physico-chemical properties-i: the systems Mg^{2+} - Al^{3+} - No^{3-} , Mg^{2+} - Al^{3+} - Cl^{-} , Mg^{2+} - Al^{3+} - ClO^{4-} , Ni^{2+} - Al^{3+} - Cl^{-} and Zn^{2+} - Al^{3+} - Cl^{-} . *Clay Clay Miner* 23:369–375
106. Velu S, Suzuki K, Osaki T (1999) Selective production of hydrogen by partial oxidation of methanol over catalysts derived from CuZnAl-layered double hydroxides. *Catal Lett* 62:159–167
107. Bocclair JW, Baterman PS (1999) Synthesis and characterisation of layered double hydroxide dispersions in organic solvents. *Chem Mater* 11:298–302
108. Klaus Noweck B, Klaus Dibilitz S, Jan Sohiefler H, Andrea Brasch M (2003) United States patent
109. Mehrotra RC (1988) Synthesis and reactions of metal alkoxides. *J Non-Cryst Solids* 100:1–15
110. Vierheilig AA (1999) US patent
111. Miyata S (1983) Anion-exchange properties of hydrotalcite-like compounds. *Clay Clay Miner* 31:305–311
112. Barriga C, Jones W, Malet P, Rives V, Ulibarri MA (1998) Synthesis and characterization of polyoxovanadate-pillared Zn-Al layered double hydroxides: an x-ray absorption and diffraction study. *Inorg Chem* 37:1812–1820
113. Ambroggi V, Fardella G, Grandolini G, Perioli L (2001) Intercalation compounds of hydrotalcite-like anionic clays with antiinflammatory agents - I. intercalation and in vitro release of ibuprofen. *Int J Pharm* 220:23–32
114. Choy JH, Park JS, Kwak SY, Jeong YJ, Han YS (2000) Layered double hydroxide as gene reservoir. *Mol Cryst Liq Cryst Sci Technol Sect A Mol Cryst Liq Cryst* 341:425–429
115. Choudary BM, Madhi S, Chowdari NS, Kantam ML, Sreedhar B (2002) Layered double hydroxide supported nanopalladium catalyst for Heck-, Suzuki-, Sonogashira-, and Stille-type coupling reactions of chloroarenes. *J Am Chem Soc* 124:14127–14136
116. Choudary BM, Kantam ML, Neeraja V, Koteswara Rao K, Figueras F, Delmote L (2001) Layered double hydroxide fluoride: a novel solid base catalyst for C-C bond formation. *Green Chem* 3:257–260
117. Motokura K, Mizugaki T, Ebitani K, Kaneda K (2004) Multifunctional catalysis of a ruthenium-grafted hydrotalcite: one-pot synthesis of quinolines from 2-aminobenzyl alcohol and various carbonyl compounds via aerobic oxidation and aldol reaction. *Tetrahedron Lett* 45:6029–6032
118. Friedrich HB, Govender M, Makhoba X, Ngcobo TD, Onani MO (2003) The Os/Cu-Al-hydrotalcite catalysed hydroxylation of alkenes. *Chem Commun* 3:2922–2923
119. Corma A, Palomares AE, Rey F, Márquez F (1997) Simultaneous catalytic removal of SOx and NOx with hydrotalcite-derived mixed oxides containing copper, and their possibilities to be used in FCC units. *J Catal* 170:140–149
120. Fearon PK, Marshall N, Billingham NC, Bigger SW (2001) Evaluation of the oxidative stability of multiextruded polypropylene as assessed by physicochemical testing and simultaneous differential scanning calorimetry-chemiluminescence. *J Appl Polym Sci* 79:733–741
121. Leroux F, Besse J (2001) Polymer interleaved layered double hydroxide: a new emerging class of nanocomposites. *Chem Mater* 13:3507–3515

122. Benotti MJ, Trenholm RA, Vanderford BJ, Holady JC, Stanford BD, Snyder SA (2009) Pharmaceuticals and endocrine disrupting compounds in U.S. drinking water. *Environ Sci Technol* 43:597–603
123. Maichin F, Freitas LC, Ortiz N (2013) The use of converter slag (magnetite) and bentonite clay for amoxicillin adsorption from polluted water, orbital electron. *J Chem* 5:1–5
124. Abdolmohammad-Zadeh H, Kohansal S, Sadeghi GH (2011) Nickel-aluminum layered double hydroxide as a nanosorbent for selective solid-phase extraction and spectrofluorometric determination of salicylic acid in pharmaceutical and biological samples. *Talanta* 84:368–373
125. Abdolmohammad-Zadeh H, Kohansal S (2012) Determination of mesalamine by spectrofluorometry in human serum after solid-phase extraction with Ni-Al layered double hydroxide as a nanosorbent. *J Braz Chem Soc* 23:473–481
126. Khatem R, Miguel RO, Bakhti A (2015) Use of synthetic clay for removal of diclofenac anti-inflammatory. *Eurasian J Soil Sci* 4:126
127. Dwiasi DW, Mudasir M, Roto R (2020) Solid-phase extraction of amoxicillin in aqueous system by using Mg-Al-oxalate ldh as a stationary phase. *Rasayan J Chem* 13:2523–2529

Bio-Inspired Materials for Environmental Remediation



Sayaka Fujita and Nobuo Sakairi

Contents

1	Background	508
1.1	Micropollutants	508
1.2	Adsorbents for Removing Contaminants	509
1.3	Designing Biomimetic Adsorbents	510
2	Cyclodextrin Linked Chitosan	511
2.1	Cyclodextrin	511
2.2	Characteristics of Chitosan	513
2.3	Pioneering Researches on CD Linked Chitosan	514
2.4	CD-Linked Chitosan Gel Beads	517
2.5	Adsorbents for MPs Removal	518
2.6	Recent Progress in CD-Based Adsorbents for MPs Removal	519
3	Encapsulated Biomass for MPs Removal	521
3.1	Immobilized Biomass	521
3.2	Nonyl Phenol Removal by Immobilized Biomass	522
3.3	Recent Applications to Removal of MPs	523
4	DNA Based Adsorbent	525
4.1	DNA Intercalation	525
4.2	DNA Based Adsorbents	526
4.3	Application to MPs Uptake	527
5	EDTA-Chitosan	528
5.1	Chelation	528
5.2	Preparation of Water-Soluble EDTA-Linked Chitosan	528
5.3	Metal Ion Removal by ED-ch Flocculation	530
5.4	Some Applications of EDTA-Linked Chitosan	532
6	Conclusion	533
	References	534

S. Fujita

National Institute of Technology, Tomakomai College, Tomakomai, Hokkaido, Japan
e-mail: fujita@tomakomai-ct.ac.jp

N. Sakairi (✉)

Hokkaido University, Sapporo, Hokkaido, Japan
e-mail: nsaka@ees.hokudai.ac.jp

Shunitz Tanaka, Masaaki Kurasaki, Masaaki Morikawa, and Yuichi Kamiya (eds.), 507
Design of Materials and Technologies for Environmental Remediation,
Hdb Env Chem (2023) 115: 507–538, DOI 10.1007/698_2021_820,
© The Author(s), under exclusive license to Springer Nature Singapore Pte Ltd 2022,
Published online: 1 January 2022

Abstract Highly organized structures and functions in living organisms have been a source of inspiration of new materials, of which properties are beyond the artificially synthesized materials. This chapter describes the development of design and synthesis of new adsorbents mimicking remarkable biological system of molecular recognition. These adsorbents are expected to apply to selective and efficient removal of organic micropollutants.

Cyclodextrin (CD), a cyclic oligosaccharide, with unique property to form inclusion complex, was utilized as recognition site in the new adsorbent. Coupling with CD derivatives and polysaccharide, chitosan, provided CD-based adsorbents, which had a high affinity toward various organic and hydrophobic pollutants with appropriate molecular sizes. Furthermore, importance of soft, flexible, and swelling polymer support of CD such as polysaccharides was revealed to demonstrate their high selectivity and high adsorption capacity. The importance of the soft scaffold was also shown in the preparation of biomass-immobilized adsorbents. Their bio-compatible nature of polysaccharide hydrogel beads was useful for the growth of various bacteria and fungi with pollutant degradation ability, and their multifunctionality was useful for structural modification such as introducing molecular recognition sites and cross-linking.

Furthermore, adsorbents having intercalation and chelation ability are also received much attention. DNA-immobilized materials inspired by interaction between DNA and genotoxins are shown to be useful for the removal and the detoxification of water containing various polycyclic aromatic pollutants. Chitosan derivative with pendant EDTA showed potential chelation ability toward various metal ions, and its zwitterionic property resulted in pH dependent dynamic morphology change, which could apply to the removal of heavy metals by flocculation.

Furthermore, this chapter also highlights recent advances in these biomimetic adsorbents for the selective and efficient removal of target pollutants.

Keywords Biomass-immobilized adsorbents, Biomimetic adsorbents, Chelation, Genotoxins, Inclusion, Intercalation, Micropollutants

1 Background

1.1 Micropollutants

Contamination of water has been one of the major concerns of global environment. The problems of water contamination of toxic heavy metals and harmful organic chemicals from a point source such as a factory or a mine have been existed since before. Nowadays, non-point source pollution is the leading course of water pollution. Development of microanalytical technology reveals that water resources contain a variety of organic substances at extreme low concentration ranging from ppb (parts per billion, $\mu\text{g}/\text{kg}$) level to ppt (parts per trillion, ng/kg) level, and that the

Table 1 Examples of micropollutants (MPs)

Source	Chemicals
Industrial products	Chlorinated alkane, polycyclic aromatics, bisphenol A (BPA), phthalates, PCB
Pesticides	Atrazine, DDT
Pharmaceuticals	Acetaminophen, codeine, antibiotics, ibuprofen
Steroid hormones	Estradiol (E2), ethynilestradiol (EE2)

pollution spreads through the world. These pollutants are called micropollutants (MPs) or emerging pollutants. Although there is a little toxicological data of MPs, they are becoming serious threat of ecosystem and human health due to their undesirable developmental, reproductive, and endocrine disrupting effects [1, 2] (Table 1).

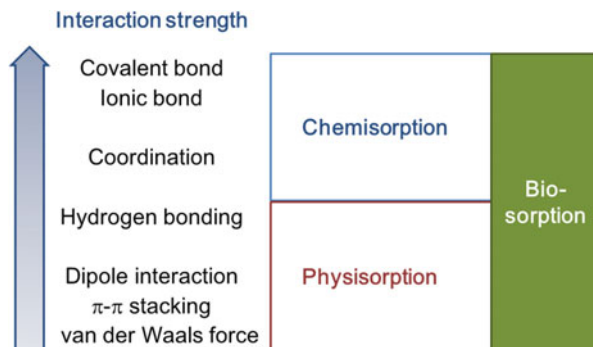
A most intractable problem concerning MPs is their bio-accumulation and bio-magnification. MPs are hydrophobic organic compounds. Because MPs have a nature of persistent and biological inefficiency, MPs captured by an organism tend not to be eliminated by catabolism or excretion. Therefore, MPs are accumulated in tissue of the organism. Moreover, in the ecosystem, the system of food web transfers the MPs accumulated in an organism to that of higher level with increasing MPs concentration. It means that higher level animals on the food chain build up greater and more dangerous amounts of toxic materials than animals in lower level.

1.2 Adsorbents for Removing Contaminants

In order to remove harmful contaminants from water, various technologies, e.g., adsorption, chemical precipitation, flocculation, membrane filtration, biological treatment, and photocatalytic degradation, have been extensively investigated. Some of them are contributing in the actual process of water purification. Among these removal technologies, an adsorption process has been the most widely employed due to its low cost and easy operation, as well as a little production of undesired secondary pollutants.

Adsorption is generally classified into three categories, chemisorption, physisorption, and biosorption. Chemisorption process occurs by a specific reaction between an adsorbent surface and adsorbate, and creates such a strong electronic linkage as covalent bond and ionic bond. Although its selectivity is extremely high, the adsorption process is irreversible. On the other hand, physisorption is caused by weaker interactions such as van der Waals interactions and dipole–dipole interaction between the adsorbate and the surface. Activated carbon (AC) is a typical example of physisorption, and is regarded as the most widely used adsorbent to remove organic pollutants. AC has high surface areas and nanostructured pores, and attracts the adsorbate through van der Waals force in the surrounding medium [3]. Since AC has various advantages such as low cost and decent absorption capacity, AC has been the

Fig. 1 Three categories of adsorbents used for environmental remediation



most widely used adsorbents for water treatment. However, AC based approaches are subject to limitations including slow uptake kinetics, low affinities for many relatively hydrophilic pollutants and low selectivity (Fig. 1).

Living organisms synthesize a large number of polymer materials such as proteins, polysaccharides, lignin, and humic acid. *Biosorption* is a property of certain bio-material to bind and concentrate organic and inorganic chemical substances from aqueous solution through physico-chemical process. For example, bacteria produce extracellular polymeric substances, a complex mixture of bio-materials, which aid in resistance to harmful exogenous materials [4]. Bio-materials have extremely complicated structures and many functional groups, which bind the adsorbates through non-covalent multivalent interactions.

Biosorption, especially using biomass waste, is currently considered to be one of the most promising environmentally benign techniques for removing various pollutants from aqueous solutions [5]. Biosorption-based processes are expected to have a number of advantages including low production cost of adsorbents, simple operation, high efficiency, as well as improved selectivity for specific pollutants of interest.

1.3 Designing Biomimetic Adsorbents

In living organisms, biomaterials play essential biological roles including structural support, signal transduction, sensing, catalysis, light-harvesting, molecular recognition, and self-organization. These highly sophisticated and well-organized biological functions basically rely on non-covalent and multivalent interactions. This is important for not only understanding many biological processes but also designing novel artificial materials and systems. The remarkable phenomena such as self-assembly, molecular recognition, and molecular complexation frequently seen in biological processes have stimulated chemists to mimic in artificial systems. Extensive studies are performed to create new bio-inspired materials, and some examples are seen in

construction of artificial self-assembly system [6], synthesis and application of hybrid materials [7], and inorganic materials [8].

Molecular recognition plays an important role in biological systems, such as highly specific binding between enzyme–substrate, receptor–ligand, lectin–sugar, and antibody–antigen. Two or more molecules specifically interact with each other by non-covalent bonding, such as van der Waals force, π – π stacking, hydrogen bonding, and metal coordination to form a complex. In a typical enzymatic reaction, an enzyme recognizes its substrate, specifically forms an enzyme–substrate complex, and subsequently displays an excellent catalytic efficiency. This process has been encouraged us to develop. Since the 1990s, key applications of mimicking biological molecular recognition and complex formation have been the construction of artificial molecular sensors and artificial enzymes [9, 10]. Macrocyclic compounds are very useful for synthesis of artificial enzyme, because they provide appropriate cavities that can surround the substrate molecules to form host–guest complex. Cyclodextrins, calixarenes, and crown ethers have been used for constructing the artificial systems [11]. In order to solve the problem of organic MPs, the development of novel adsorbents having molecular recognition ability has been expected. An adsorbent having highly selective molecular recognition site would be useful for environmental remediation.

Another approach to efficient adsorbents is thought to be biomimetic design of the structure surrounding the adsorption site. Cell membranes are complex and highly dynamic systems, which consist of amphipathic lipids and polymeric substances such as protein and polysaccharides. Their major function is to protect the cell, to transport various materials in and out through a passive or an active way, and to communicate with its surroundings. These biopolymers have soft, flexible, and highly swelling properties. The investigations of cell surface mimics are performed with biomedical interest. Since the biosorption is involved in these biological function [12], novel adsorbents with soft and flexible constituents mimicking cell surface would be expected to improve their adsorption ability.

This chapter describes important consideration in designing and synthesizing new adsorbents mimicking remarkable biological system such as molecular recognition and cell surface structure, and also highlights recent advances in biomimetic adsorbents for the selective and efficient removal of target pollutants.

2 Cyclodextrin Linked Chitosan

2.1 Cyclodextrin

Cyclodextrins (CDs), cyclic oligosaccharides, are produced by enzymatic degradation (cyclodextrin glucanotransferase) of starch in an industrial scale. CDs mainly consist of six, seven, and eight α -linked D-glucopyranose units, which are called α -, β -, and γ -CD, respectively. The most remarkable feature of CDs is to form inclusion complex with various hydrophobic compounds [13]. As shown in Fig. 2, CDs have

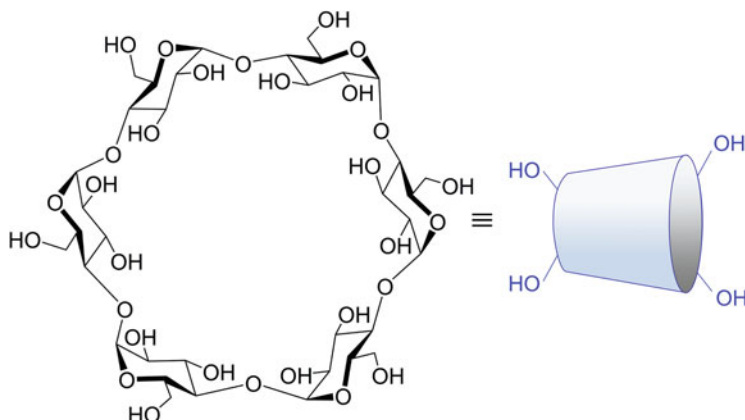


Fig. 2 Chemical structure and schematic representation of α -CD

Table 2 Physical property of CDs

CDs	α	β	γ
Number of Glc units	6	7	8
Molecular weight	972	1,135	1,297
Outer diameter (nm)	1.37	1.53	1.69
Inner diameter (nm)	0.53	0.65	0.83
Height (nm)	0.79	0.79	0.79
Cavity volume (nm ³)	0.174	0.267	0.427

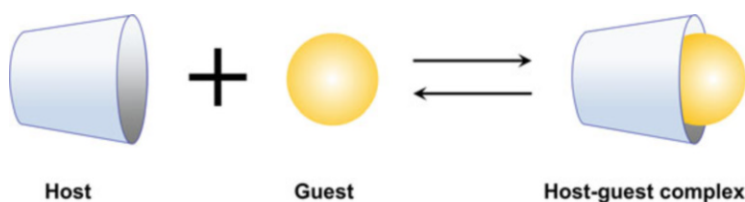


Fig. 3 Schematic drawing of the host-guest inclusion complexation on the more favorable wider rim of CD molecule

cone-shape structures, where the secondary hydroxyl groups and the primary hydroxyl groups are located on wider rim and narrow rim, respectively. Physical properties of three kinds of CDs are summarized in Table 2. The interior of CD cavity is less hydrophilic than the exterior because of the absence of hydrophilic functional groups. Consequently, in aqueous media, CDs can interact with appropriately sized hydrophobic guest molecules to result in the formation of inclusion complexes (Fig. 3). Removal of water molecules from the cavity of the CDs to make room for the guest molecule for accommodation while formation of inclusion complex, increases entropy of the process. Estimating from the diameters of inner cavities of α -, β -, and γ -CD (0.53, 0.65, and 0.83 nm, respectively), appropriate sizes

of the guests are similar to benzene, naphthalene, and anthracene, respectively. Due to this unique property, CDs have been singled out for studies on host–guest chemistry. Numerous investigations have been carried out to construct artificial enzymes and receptors and to apply in pharmaceutical, cosmetic, and food industries [14]. Moreover, CDs have also been investigated for the removal of toxic substances from industrial effluent. For example, toxicity of an insecticide, tetramethrin, was reduced by formation of inclusion complex with β -CD [15], and CD oligomers and polymers prepared by cross-linking with epichlorohydrin have been investigated as encapsulation materials [16]. The unique inclusion ability of CDs attracted us to create new CD-based adsorbents for the pollutant removal.

2.2 Characteristics of Chitosan

In order to synthesize biomimetic adsorbents bearing CDs, chitosan was first chosen as a polymer scaffold. Cellulose and chitin are the most abundant extracellular polysaccharides found in cell wall or extracellular matrix of various organisms. Chitin is isolated from several sources including cuticles of arthropods such as crab, shrimps, and insects, and fungal biomass. Chitin of β -*N*-acetylglucosamine residues and its basic hydrolysis affords chitosan, a linear polymer of β (1 \rightarrow 4) linked 2-amino-2-deoxyglucopyranose (Fig. 4). Since the amino groups of chitosan are protonated in numerous dilute mineral and organic acids, it shows polycationic character and high solubility. Chitosan has been extensively studied as an adsorbent of heavy metals, as an ion exchanger, as an antifungal agent, and so on. Furthermore, these properties of chitosan make it possible to introduce various functional groups by chemical modifications [17]. Chitosan-based hydrogel beads can be easily

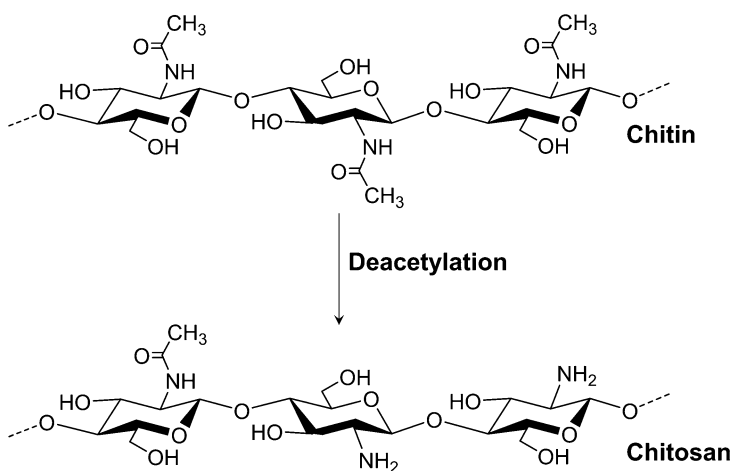


Fig. 4 Chemical structure and transformation of chitin to chitosan

prepared by dropping chitosan solution in aqueous acetic acid into an alkaline solution. They have been extensively studied as micro- or nano-particulate carriers in the pharmaceutical and medical fields such as drug delivery and as adsorbent for pollutants such as heavy metal ions and dyes [18, 19]. Considering the versatility of chitosan, it seemed to be a promising candidate of the supporting material of CD-based adsorbent.

2.3 Pioneering Researches on CD Linked Chitosan

Among three kinds of functional group in chitosan, the amino group at 2-position is the most reactive, and a large number of chitosan derivatives have been synthesized mainly by chemical modifications of this group [17]. Furusaki et al. synthesized for the first time β -CD-linked chitosan (β -CD-ch-A) through formation of amido bond (Fig. 5) [20]. Water-soluble low molecular weight chitosan ($M_w = 7,300$) was coupled with carboxymethylated β -CD in the presence of water-soluble carbodiimide (WSC) as a condensation reagent in water. The degree of substitution

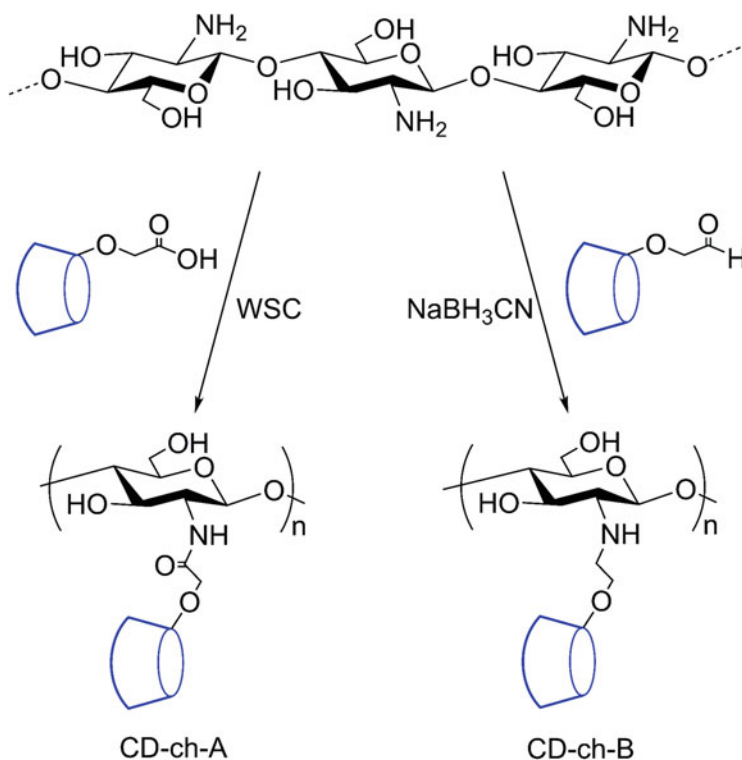


Fig. 5 Two possible routes for the synthesis of CD pendant chitosan derivatives

(DS) of the product (β -CD-ch-A) estimated by ^1H NMR spectrum was 20%. Inclusion ability of β -CD-chitosan-A with 1:1 stoichiometry was determined by spectroscopic titration using a fluorescent dye, 6-(*p*-toluidino)-2-naphthalene-6-sulfonate (TNS). Association constants (K_a) of β -CD-ch-A and TNS complex was $1.13 \times 10^3 \text{ mol}^{-1} \text{ L}$ at pH 7.0 and that of β -CD was $2.54 \times 10^3 \text{ mol}^{-1} \text{ L}$, showing that the inclusion ability of β -CD is maintained after coupling with chitosan.

Another major route of chitosan modification is to use reductive amination, which involves Schiff's base formation between the amino group of chitosan and carbonyl reagents and subsequent reduction of the C=N double bond [21]. An advantage of this route is that the reaction proceeds in aqueous acidic solution, which is suitable to perform the reaction under homogeneous conditions and without isolation of any intermediates. Tojima et al. described synthesis of α -CD-linked chitosan (α -CD-ch-B) by this route [22]. Thus, mono-*O*-allyl- α -CD was oxidized with ozone to generate 2-*O*-(formylmethyl)- α -CD having an aldehyde function, which was subjected to Schiff's base formation with medium molecular weight chitosan (Mw = 40,000) in acetate buffer at pH 4.4 and subsequent to reduction with NaBH_3CN . Purification by dialysis afforded α -CD-ch-B with D.S. from 15 to 60%. The product was soluble in water even under neutral and alkaline conditions. Inclusion property of α -CD-ch-B determined by UV-visible and circular dichroism spectroscopic titration using *p*-nitrophenolate confirmed that it had the almost similar ability of original α -CD [22].

The reductive amination route can be applicable to various CD derivatives having an aldehyde function to convert into the corresponding CD-chitosan-B derivatives. In a similar way as above, β -CD-ch-B having different length of cross-linker moieties, β -CD-ch-B C0, C2, and C4 (Fig. 6) were synthesized [23, 24]. Their inclusion properties of β -CD-ch-B C4 (D.S. 18%), β -CD-ch-B C2, and β -CD-ch-B C0 (D.S. 17%) with TNS were investigated in acetate buffer (pH 4.3) at 25°C. Job's continuous variation plot showed the stoichiometry of inclusion complex of C2 and C4 cross-linker derivatives and TNS was 1:1, whereas that of C0 derivatives was not

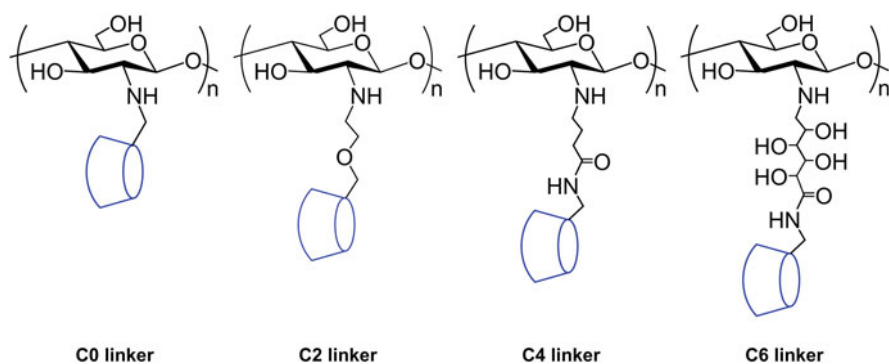


Fig. 6 Partial structures of β -CD-ch-B with various cross-linkers synthesized via reductive amination route

fit 1:1 stoichiometry. Furthermore, a viscose solution was formed when β -CD-ch-B C0 and TNS were mixed. The association constants of β -CD-ch-B C2 and C4 determined by Benesi–Hildebrand plot were almost same as that of native β -CD, suggesting the inclusion ability of CD is maintained after immobilized on polysaccharide backbone [24]. The distance between CD moiety and polymer main chain is influenced on their inclusion property. The unusual inclusion property of directly linked C0 derivative is probably due to lack of flexibility of the β -CD residue. The constrained conformation around the CD residue may interfere the guest molecule approaching from the wider rim of the CD cavity as shown in Fig. 3.

Since hemiacetal group of a reducing sugar is a potential aldehyde function, reducing sugars are used as starting materials for the reductive amination reaction. Therefore, chitosan and CD residue can be linked with hydrophilic group. Thus, 6-amino- β -CD was coupled with a galacturonic acid derivative, and then underwent similar reductive amination with chitosan. The product (α -CD-ch-B C6) had a polyol-type cross-linker, and showed inclusion ability toward 4-tert-butylbenzoic acid and (+)-catechin (Fig. 7) as model guests [25]. In case of such a large guest as catechin, CD grafting on chitosan left its inclusion ability unaffected relative to the original CD.

Using reductive amination, various CD derivatives found to be efficiently grafted on chitosan, yielding highly water-soluble CD-polymers, which exhibit the same inclusion properties toward hydrophobic guests as the native CD (Fig. 7).

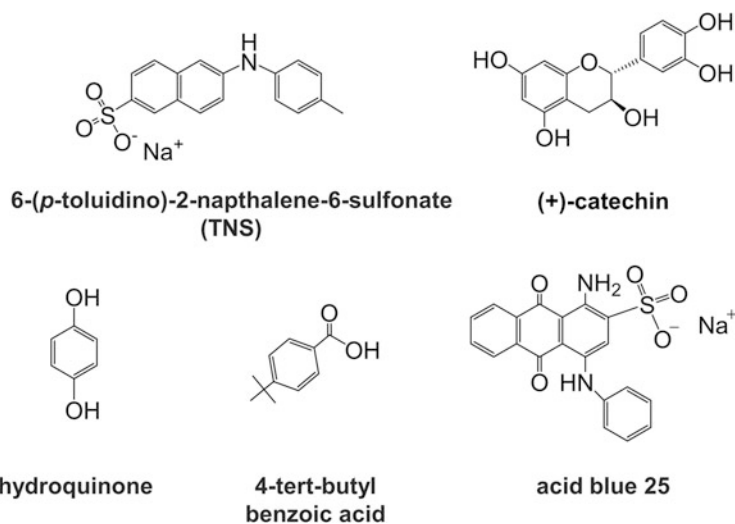
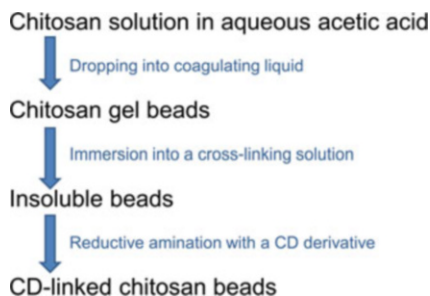


Fig. 7 Chemical structures of guest molecules for CD-based adsorbents

Fig. 8 Flowchart for the preparation of CD-linked chitosan beads



2.4 CD-Linked Chitosan Gel Beads

In order to apply CD-chitosan to adsorbent for pollutant removal, similar reductive amination of water-insoluble chitosan beads was examined. Chitosan gel beads were prepared according to the flowchart shown in Fig. 8. An aqueous acetic acid solution of chitosan was dropped into a coagulating liquid such as ethanolic aqueous sodium hydroxide. The spherical chitosan gel was subsequently undergone cross-linking with hexamethylene diisocyanate. Glutaraldehyde, epichlorohydrin, ethylene glycol diglycidyl ether, and molybdate salt are also reported as the useful cross-linking reagents. Formation of chitosan beads provides solid material with high porosity and large surface area [26]. The beads were converted into α -CD chitosan beads (α -CD@ch) by reductive amination with 2-*O*-formylmethyl- α -CD in the presence of NaBH₃CN in acetate buffer at pH 4.4 [27].

As a preliminary experiment for the utilization of α -CD@ch as adsorbent, column chromatographic adsorption–desorption was examined by use of a mixed aqueous solution of 4-nitrophenol and 3-methyl-4-nitrophenol. The former is a preferable guest for α -CD, while the latter has a bulky methyl group that inhibits formation of the inclusion complex with α -CD. The chromatogram (Fig. 9) showed 3-methyl-4-nitrophenol was quickly eluted with water, while 4-nitrophenol was adsorbed by α -CD@ch during elution with water. 4-Nitrophenol was readily recovered by eluting the α -CD@ch column with methanol, less hydrophobic solvent [27]. This experiment shows that CD@ch has an ability of size selective adsorption of guests and desorption.

Furthermore, other type of insoluble CD@ch was synthesized and its adsorption behavior was examined by several groups. Martel et al. prepared different types of insoluble β -CD-chitosan with triazinyl cross-linker (β -CD-TZ@ch), which exhibited adsorption ability toward such textile azo dyes as acid blue 15 and acid blue 25 (Fig. 7). The adsorption capacity was superior to a conventional CD-polymer prepared from chitosan and CD-epichlorohydrin [28]. Zha et al. introduced β -CD into chitosan beads by subsequent treatment with hexamethylene isocyanate and β -CD, giving insoluble β -CD linked chitosan beads (β -CD-HMC@ch), and its adsorption behavior was examined with hydroquinone. This adsorption process was found to be a spontaneous, endothermic, and a random process [29].

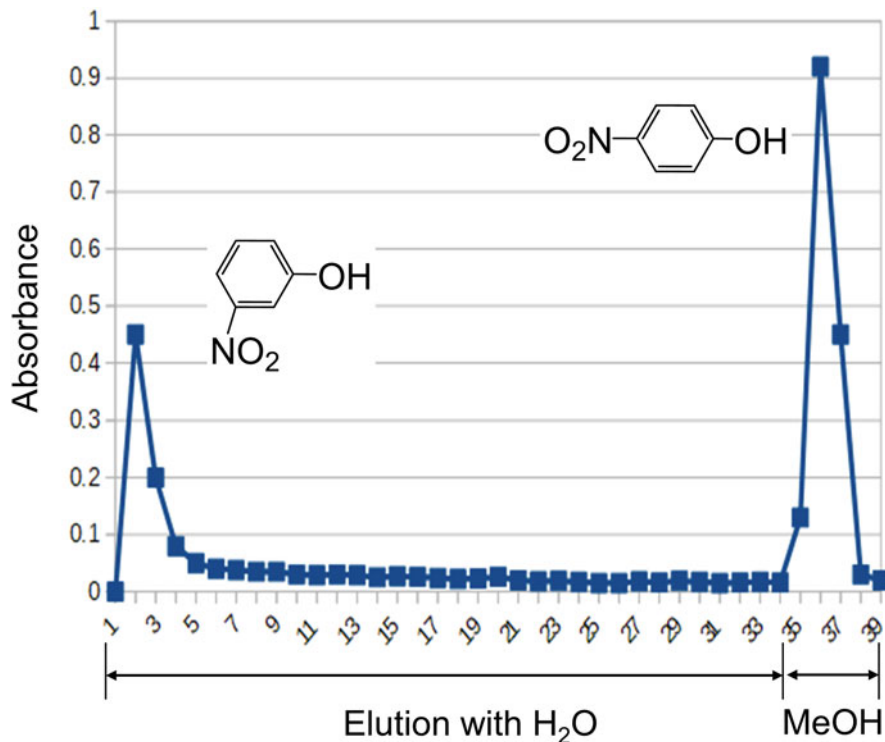


Fig. 9 Chromatogram of nitrophenols separation with β -CD-chitosan beads (β -CD@ch) observed at 400 nm

2.5 Adsorbents for MPs Removal

Adsorption behavior of these CD-based adsorbents was also examined for the purpose of MPs removal. Nishiki et al. prepared water-insoluble and highly porous β -CD linked chitosan beads (β -CD@ch) in a similar way as above, and preliminary experiments for its application to removal of bisphenol A (BPA), an endocrine disrupting chemical (Fig. 10), was carried out using β -CD@ch gel beads. More than 90% removal of BPA from aqueous solution was successful by the use of β -CD@ch column, and washing the column with methanol recovered BPA. Furthermore, this procedure was applicable to the removal of BPA at concentrations <1 ppm [30]. Aoki et al. reported coupling 6-amino- β -CD with succinylated chitosan gave insoluble β -CD linked SU-chitosan (β -CD-SU@ch). Adsorption experiments with β -CD-SU@ch showed excellent adsorption ability toward BPA and NP and initial adsorption rates with BPA and NP were 40 and 1.3 times larger than those of AC, respectively [31]. Removal of non-ionic surfactants, 4-nonylphenol ethoxylates (NPEs), was compared with three kinds of adsorbents (α -, β -, and γ -CD@ch), and found that β -CD@ch was the most suitable for the

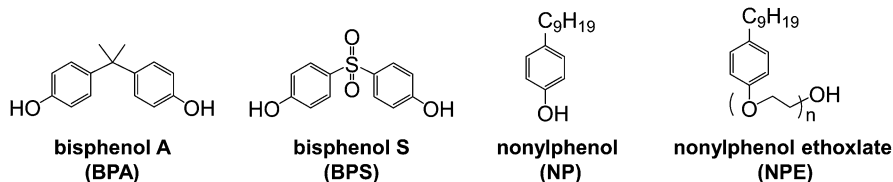


Fig. 10 Structures of MPs captured by CD-based adsorbents

adsorption of the phenol derivatives (Fig. 10). Most of the NPE adsorbed on β -CD@ch was successfully released by the treatment of β -CD@ch with aqueous alcohol solutions and its adsorption ability was maintained after 20 cycles of the adsorption–desorption [32]. Other examples of CD-chitosan based adsorbents and CD-polymer are mentioned in several reviews [33, 34].

2.6 Recent Progress in CD-Based Adsorbents for MPs Removal

Based on the fundamental investigations mentioned above, various CD-based adsorbents were synthesized and applied to MPs removal. Orelma et al. reported that surface modification of cellulose fiber yarns with CD-chitosan gave a new adsorbent for removal of 17 α -ethinyl estradiol (EE2) [35]. A deep eutectic solution of cellulose was subjected to dry jet spinning in choline chloride-urea to give cellulose fiber yarns. The yarns were immersed in a chitosan solution in acetate buffer, and then treated with a TEMPO-oxidized β -CD derivative in the presence of WSC as a condensation agent. Surface plasmon resonance (SPR) experiments showed the EE2 adsorption capacity of the β -CD modified fiber yarn was 2.5 mg g⁻¹.

Very recently, porous β -CD polymer (β -CD@P) with rigid aromatic cross-linker was synthesized by aromatic nucleophilic substitution, and it rapidly adsorbed various MPs. The co-polymerization was performed by β -CD, tetrafluoroterephthalonitrile (TFN), and K₂CO₃ in aprotic solvents (Fig. 11). β -CD@P showed an excellent property to adsorb various MPs, e.g., BPA, bisphenol S (BPA-S), EE2, propranolol with adsorption rate constants 15 to 200 times greater than those of AC [36].

Furthermore, the property of β -CD@P was found to be remarkably changed by the property of cross-linker group. When the polymerization was carried out using two cross-linking reagents, TFN and flexible cross-linker (epichlorohydrin), the product β -CD@P showed highly swellable property [37]. Owing to the porous structure and easy access of adsorption sites, these β -CD@P exhibited ultra-rapid adsorption of organic micropollutants, such as bisphenol A (BPA), 3-phenylphenol (3-PH), and ethinyl estradiol (EE2). The polymer adsorbent could be easily regenerated by methanol at room temperature and reused many times without a

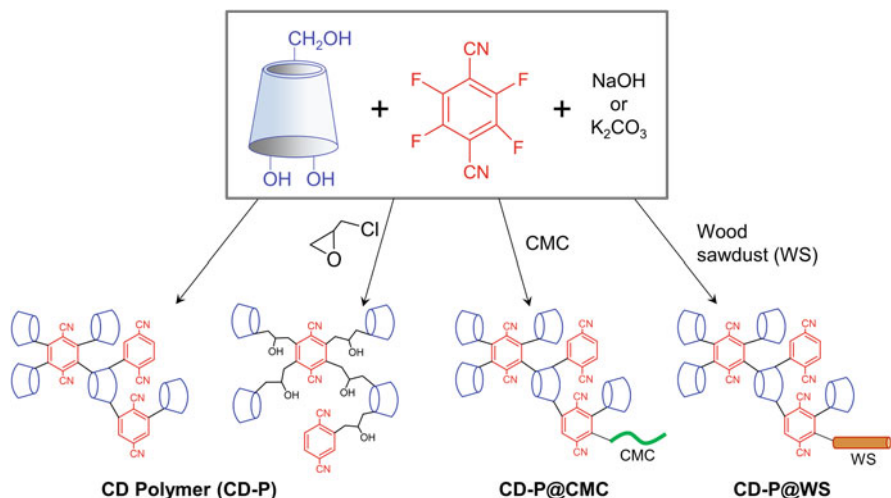


Fig. 11 Schematic representations for the synthesis of cross-linked CD polymers for MPs removal

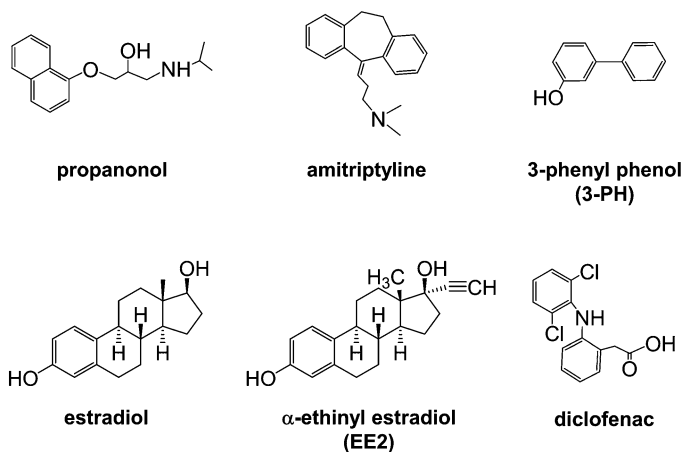


Fig. 12 Chemical structures of pharmaceuticals captured by CD-polymer adsorbents

significant decrease in the adsorption performance. Thus, β -CD-P could effectively remove many organic pollutants (Fig. 12) from water at environmentally relevant concentrations and without being affected by the pH level, ionic strength, and humic acid concentration, indicating that it is very suitable for application in practical water treatment [37].

Versatility of this polymerization procedure of β -CD-P was applicable to surface modification of various materials. Alzate-Sánchez et al. synthesized an adsorbent with a core/shell structure by incorporation of β -CD-P onto cellulose microcrystals

(CMC) [38]. Batch adsorption experiments using β -CD-P@CMC demonstrated rapid pollutant uptake and high accessibility of the CD on the adsorbent. Similarly, column experiments demonstrate rapid uptake of a model pollutant with minimal back-pressure, demonstrating potential for use in packed-bed adsorption processes. Furthermore, the pollutant-saturated columns were regenerated using methanol and reused three times with almost no change in performance [38]. Similarly, Guo et al. incorporated β -CD@P onto wood sawdust (WS), a byproduct of the wood-processing industry, and applied β -CD-P@WS to cross-flow filtration to remove some pharmaceutical pollutants. Consequently, the β -CD-P@WS filter device shows a high removal efficiency of over 97.5% within 90 s for various pharmaceutical contaminants including propranolol, amitriptyline, chlortetracycline, diclofenac, and levofloxacin, and a high saturation uptake capacity of 170, 156, 257, 159, and 185 mg/g, respectively [39].

Utilizing the unique inclusion property of cyclodextrins, new type of adsorbents have been synthesized and shown to have a high affinity toward various organic and hydrophobic pollutants with appropriate molecular sizes. In addition to CD residue, consideration of structure and property of the polymer support and/or the cross-linker is also important for designing. Selection of soft, flexible, and swelling polymer such as polysaccharide scaffolds of CD is found to demonstrate their high selectivity and high adsorption capacity of CD-based adsorbents.

3 Encapsulated Biomass for MPs Removal

3.1 *Immobilized Biomass*

Various living and dead biomass obtained from bacteria, algae, fungi, and yeast have been used for remediation of polluted water through adsorption, biosorption, biodegradation, and bioprecipitation [40]. However, there are some drawbacks to use biomass, such as low stability (storage, pH, and temperature), high price of production, poor reusability, and difficult separation from reaction media.

Immobilized biomass on various supporting materials has been extensively investigated to overcome these problems [41]. Swelling and porous polysaccharide gel beads are a candidate of supporting materials for environmental remediation [42]. Enzyme immobilization can improve these problems. Fixing the enzymes in solid supports makes it easier to separate them from solutions, and improves the reusability. However, in some of the cases, activity of the immobilized enzyme decreases probably due to undesired interactions between the support and the enzyme, lower movement of the enzymes, or inhibited interaction between the enzyme and substrate.

3.2 Nonyl Phenol Removal by Immobilized Biomass

Lang et al. reported introduction of a fungal biomass into chitosan beads and utilization for biosorption of NP [43]. The beads were prepared by a modified procedure shown in Fig. 8. Spore of *Rhizopus arrhizus* TISTR 3606, a fungal strain, was mixed with an autoclaved acetic acid solution of chitosan. It was dropped into a sterilized coagulating liquid containing sodium tri-polyphosphate, which forms polyion complex with chitosan to yield stable beads without any affection of the living spores. The resulting beads were incubated in TGY medium for 5 days, inactivated by autoclaving at 121°C, filtered, washed with water, and vacuum dried to give the beads encapsulating dead fungal biomass inside (fungus@ch). During the 5-days incubation, the diameter of dried *R. arrhizus*@ch was increased from 1 to 1.5 mm (original beads) to 4 mm, and the whole bead surface was homogeneously covered with outward growing mycelia. The dry weight of immobilized fungus was 0.97 mg/bead.

Adsorption and desorption experiments of NP using *R. arrhizus*@ch were performed by batch method. It was found that Fritz–Schluender model was the best fit with the experimental data and the adsorption capacity was 30.25 mg/g. The entrapped NP on the beads could be released by washing with methanol, and the regenerated dead beads were reusable for NP uptake. Table 3 shows the usefulness repeated adsorption–desorption of NP. However, by the end of the fifth batch use, the recovery of NP was decreased to 38% of the first batch and the weight loss of dead beads was 43% probably due to physical decomposition of fine mycelia immobilized on the beads.

Sphingomonas cloacae, which has a degradation ability of NP, was immobilized in calcium alginate beads covalently linked with α -cyclodextrin (*S. cloacae*@CD-alg). Column chromatographic experiment using *S. cloacae*@CD-alg beads showed a strong affinity for NP adsorption. Incubation of *S. cloacae*@CD-alg in NP containing medium at 25°C in a shallow incubation tube for 10 days showed 83% NP removal. Furthermore, cell numbers of the bacteria in the beads were increased from 400 to 1,200 during the incubation (Fig. 13). Scanning electron microscopic photographs revealed that multiplied bacteria were present both on the surface and inside the beads [44].

Table 3 Sorption–desorption of nonyl phenol by repeated use of *R. arrhizus*@ch

Cycle	Recovery of NP (%)	Beads weight (%)
1	100	100
2	78	63
3	77	61
4	76	60
5	38	43

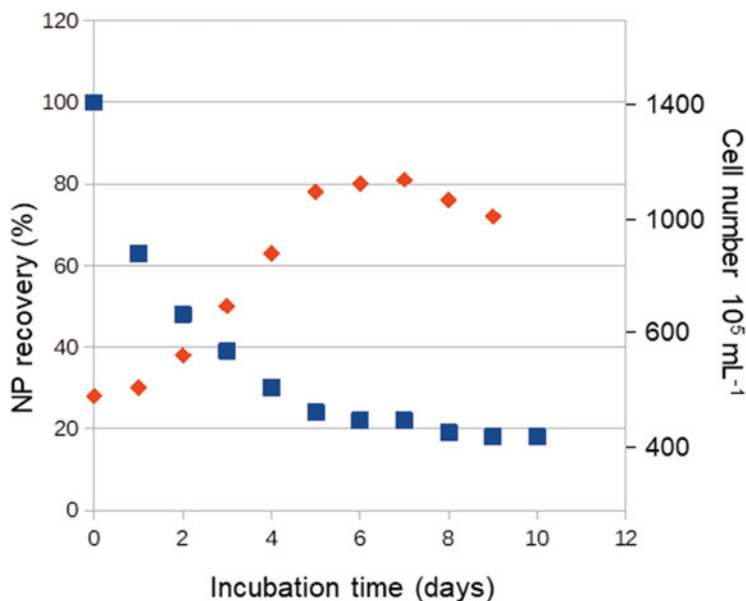


Fig. 13 Time-course of NP degradation and bacterial growth with *S. cloacae*@CD-alg. Percentage of NP remaining unchanged (blue square) and cell number (orange diamond)

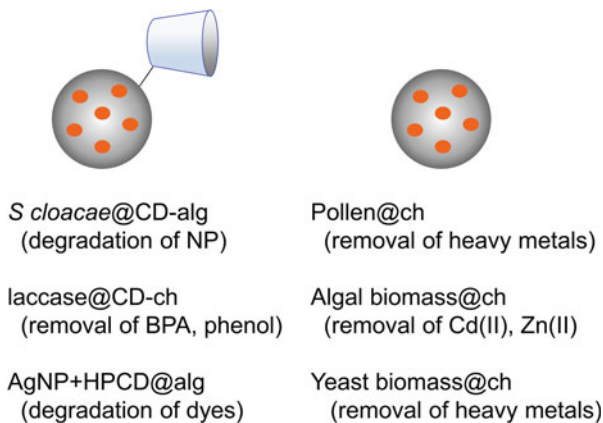
3.3 Recent Applications to Removal of MPs

A large number of biomass encapsulated polysaccharide beads have been prepared and evaluated mainly their ability of heavy metal removal (Fig. 14), e.g., pollens containing chitosan micro capsule (pollen@ch) [45], chitosan–algal biomass composite (algal@ch) [46], and yeast immobilized in chitosan/lignosulphonate matrix (yeast@ch) [47]. Application to the removal of micropollutants has also been extensively investigated.

Tarasi et al. reported synthesis of CD-chitosan conjugated with Fe_3O_4 magnetic nanoparticle (laccase@CD-ch) is useful for laccase immobilization and degradation of some phenolic compounds [48]. Laccase is known to catalyze one-electron oxidation of phenolic compounds. The immobilized enzyme maintained 70% of its initial activity up to 12 days, and showed maximal removal with 96.4 and 85.5% for phenol and BPA, respectively. One of the advantages of the magnetic beads is that they could be collected or transported by an external magnetic field at specific positions. Furthermore, laccase immobilization on chitosan beads using WSC resulted in significant improvement of the enzyme activity [49]. Removal experiment of indigo carmine as a model micropollutant showed the activity remained almost constant of up to 80% during 10-cycle of reuse and that the residual activities were 85% after 32 days of storage.

Similarly horseradish peroxidase catalyzed oxidation of various organic compounds by hydrogen peroxide. Bilal et al. immobilized this enzyme onto the self-

Fig. 14 Some examples of living or dead biomass encapsulated polysaccharide gel beads for the removal of MPs and metal ions



fabricated polyvinyl alcohol-alginate (peroxidase@alg-PVA) beads using sodium nitrate as a cross-linker. They reported simple and shorter time for preparation method, high reusability, and minimum enzyme leakage. They applied it to the degradation of an azo dye, ethyl orange [50].

Reduction of 2-hydroxypropyl- β -CD (HPCD) and Ag(I) encapsulated calcium alginate gel using aqueous extract of *Jasminum subtriplinerve* leaves as a reducing agent gave Ag nanoparticles and HPCD containing nanocomposites (AgNP + HPCD@alg). The AgNP + HPCD@alg showed excellent catalytic performance for degradation of pollutants within industrial effluents including 4-nitrophenol, methyl orange, and rhodamine B [51] (Fig. 14).

Furthermore, Zhang et al. synthesized magnetic chitosan beads immobilized *Aspergillus sydowii* (*A. sydowii*@ch), and examined simultaneous removal of Cd (II) and trichlorfon, an insecticide [52]. The beads were prepared from a chitosan solution of aqueous citric acid containing Fe_2O_3 and the fungal spore and incubated at 28°C for 24 h. During the incubation, the surface area of the beads was significantly increased to 55.38 m² g⁻¹. Using *A. sydowii*@ch, simultaneously removal of both organic pollutant and heavy metal ion was examined. The equilibrium removal capacities of TCF and Cd(II) were 135.43 and 56.40 mg g⁻¹, respectively. *A. sydowii*@ch exhibited excellent recyclability up to four cycles.

Chitosan and calcium alginate hydrogel beads are flexible and highly swelling scaffold of a large number of living or dead biomass, which have an ability of pollutant accumulation and degradation. Their biocompatible nature helps the growth of various bacteria and fungi with pollutant degradation ability, and their multi-functionality is useful for structural modification such as introducing molecular recognition sites and cross-linking.

4 DNA Based Adsorbent

4.1 DNA Intercalation

Deoxyribonucleic acid (DNA) carrying genetic instructions is a biopolymer, which has a unique three-dimensional structure. A combination of hydrogen bonding and π - π stacking between the nucleobases constituting DNA makes a double-helical ladder structure. Double-helical DNA most commonly has B-form, in which distance between nucleobase pairs is 0.34 nm and 10 base pairs makes one turn in 3.4 nm. Large amounts of DNA-enriched materials can be available from the waste of food industry such as salmon milts and shellfish gonads. DNA is highly water-soluble and biochemically unstable, which have been making it difficult to utilize as a functional material. Immobilization of DNA on solid supports such as cellulose powder or gold nanoparticle, or by making a stable complex with other polymers, such as cationic amphiphilic lipids or acrylamide has been reported [53]. Conjugation of DNA with alginic acid [54], chitosan, or collagen was also attempted [55] to expand the scope of DNA material for medical use.

Intercalation is a phenomenon that a guest molecule or ion is inserted into a material with layered structure. In biochemistry, intercalation mainly means the insertion of guest molecules between the ladder structure of double-helical DNA (Fig. 15). The DNA intercalator has an appropriate size and chemical nature to fit between the base pairs of DNA through sharing of the π -electrons. The suitable structures of intercalators are mostly polycyclic, aromatic, and planar compounds (Fig. 16). DNA intercalators are often carcinogenic, which leads structural change of DNA and often to inhibition of transcription and replication. Inspiring this biological process, harmful DNA intercalating pollutants uptake of immobilization of double-stranded DNA was investigated as follows.

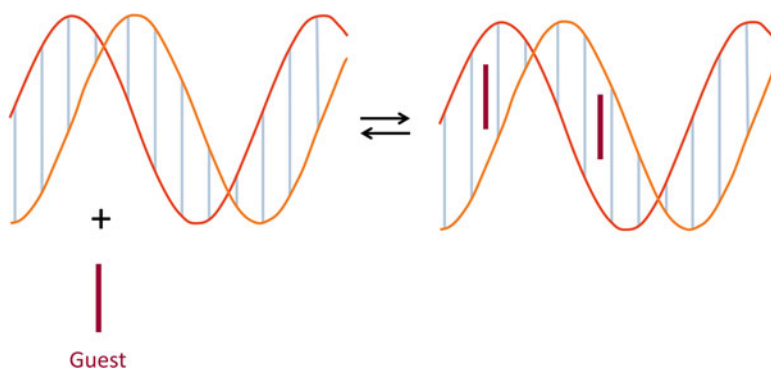


Fig. 15 Schematic representation of double-stranded DNA and its intercalation complex

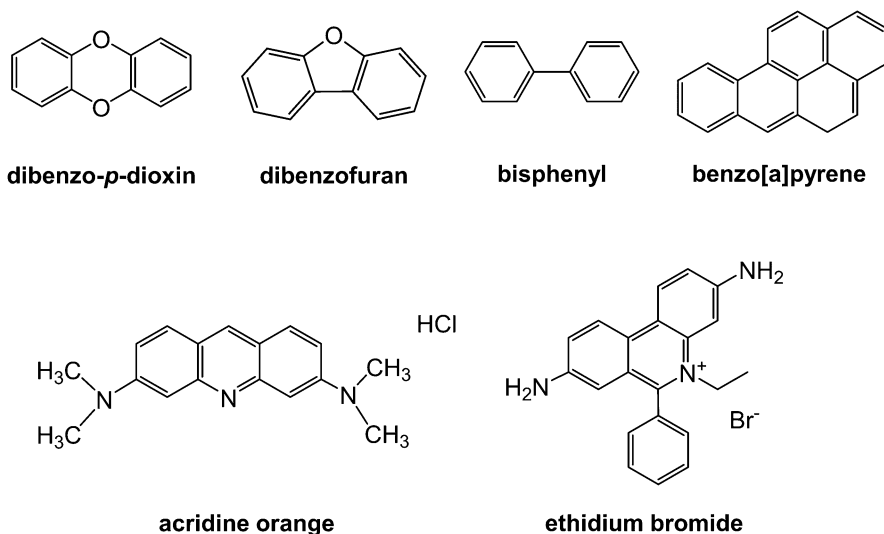


Fig. 16 Chemical structures of DNA intercalators

4.2 DNA Based Adsorbents

Immobilized DNA film was first investigated as an accumulator of intercalating substances [56]. Although native DNA is a high water-soluble biopolymer, exposure of DNA to UV light makes irreversible change to give insoluble material. The mechanism is explained by [2 + 2] cycloaddition reaction between two adjacent pyrimidine bases to form cyclobutane pyrimidine dimer, which crosslinks between two DNA chains [57]. The starting DNA film was prepared by casting an aqueous double-stranded DNA ($M_w = 5 \times 10^3$ kDa) solution onto glass plates, and dried at room temperature. The film was irradiated with UV light at 254 nm for several times, giving a water-insoluble film. Since addition of a radical scavenger, galvinoxyl, inhibited this change, the reaction is revealed to proceed through a radical reaction mechanism. Agarose gel electrophoresis of the short UV-irradiated product showed significant increase of the molecular weight of DNA. The longer irradiated DNA film showed both physical and biological stability because it did not dissolve in water even after incubation for a long time and the UV-irradiated DNA films showed resistance to hydrolysis by nuclease. Circular dichroism spectra of the DNA film, which have a maximum peak at 280 nm and a minimum peak at 240 nm, revealed it has the B-form structure, which suggested native double-stranded DNA structure in water was maintained.

Intercalation property of the UV-irradiated DNA film was examined by UV-vis spectroscopy using ethidium bromide and acridine orange. When the UV-irradiated DNA film was incubated with a dilute aqueous ethidium bromide solution for 24 h, the color of DNA film changed from clear to red, and the absorption peak of the solution at 480 nm disappeared completely. The binding constant for ethidium

bromide was calculated to be $6.8 \times 10^4 \text{ mol}^{-1} \text{ L}$, which was consistent with the data of native double-stranded DNA [56]. The UV-irradiated DNA films have potential uses as a bio-material filter for the removal of harmful DNA intercalating compounds.

4.3 Application to MPs Uptake

Immobilization of double-stranded DNA onto nonwoven cellulose fabric by UV irradiation and utilization of DNA-immobilized cloth were examined. The immobilized DNA was found to be stable in water, with the maximum amount of fabric-immobilized DNA being approximately $20 \text{ mg}\cdot\text{g}^{-1}$ of nonwoven fabric. The DNA-immobilized cloth could effectively accumulate endocrine disruptors and harmful DNA intercalating pollutants, such as dibenzo-p-dioxin, dibenzofuran, biphenyl, benzo[a]pyrene, and ethidium bromide [58]. Additionally, DNA-immobilized cloth was found to bind metal ions such as Ag(I), Cu(II), and Zn(II) due to the polyanionic property of DNA.

Furthermore, DNA was immobilized on a glassy carbon electrode by UV irradiation, and the electrochemical oxidation of tetracycline (TC) was detected by cyclic voltammetry. The applicability of the DNA modified electrode was demonstrated by detection of TC in such complicated samples as pharmaceutical formulations and milk [59].

Polycyclic aromatic hydrocarbons (PAHs) are combustion related pollutants and are also members of micropollutant. Some carcinogenic PAHs are genotoxic and induce mutations. Since PAHs are planar molecule, intercalation of PAHs with DNA occurs through physical interaction with the hydrophobic spaces between adjacent base pairs of DNA strands. Upon contact with DNA, stable PAH–DNA adducts form rapidly as the first step toward their toxic effects. Topuz et al. prepared by cross-linking of inverse miniemulsion of double-stranded DNA molecules using poly(ethylene oxide) diglycidyl ether [60]. Their biomimetic approach relies on interaction between PAHs and the complete network that constitutes the water swelling DNA nanogels. PAH adsorption capacity of the DNA nano gel $720 \text{ }\mu\text{g}\cdot\text{g}^{-1}$, which means that 1 mg of DNA nanogel is sufficient to purify a liter of water containing the critical PAH concentration for cancer risk ($600 \text{ ng}\cdot\text{L}^{-1}$). Double-stranded DNA nanogels showed larger phenanthrene uptake than that of single-stranded ones. As a result of short diffusion pathways, PAH uptake is rapid, reaching 50% loading after 15 min.

DNA-immobilized materials have been developed on the basis of mechanistic study of interaction between DNA and genotoxins. They are expected to be useful for the removal and the detoxification of water containing various polycyclic aromatic pollutants.

5 EDTA-Chitosan

5.1 Chelation

Metal ions play important roles of many natural proteins, providing structural, catalytic, and electron transfer functions. Some metalloproteins act as such important biological roles as oxygen transfer, metabolism, and signal transduction, and have transition metal ions through a coordination bonds with nitrogen, oxygen, or sulfur atoms of side-chains of constituted amino acid residues or their cofactors. Although some bio-materials have an ability to bind various metal ions, introduction of a chelation site is expected to enhance the ability. Chelation involves the formation or presence of two or more separate coordinate bonds between a polydentate (multiple bonded) ligand and a single central metal atom. Focusing on the coordination ability of amino group with transition metals, chitosan-based materials have been extensively investigated to remove heavy metal ions [61].

5.2 Preparation of Water-Soluble EDTA-Linked Chitosan

Ethylenediaminetetraacetic acid (EDTA) is the most useful hexadentate ligand and chelating agent, which is used for sequestering metal ions, reducing water hardness, removing metal ions, and so on. In order to enhance the metal binding ability of chitosan, introduction of EDTA residue was investigated. In the previous work, solid EDTA-linked chitosan (ED-ch) was synthesized and evaluated its heavy metal ions uptake [62]. Fujita et al. reported the synthesis and property of the corresponding water-soluble derivative [63]. Behavior of metal ion chelation and property of polyelectrolyte in water have received much attention. Since chitosan skeleton has positive charge and EDTA residue has negative charge, the water-soluble ED-ch was expected to have a zwitterionic property. The charge density is changeable by pH of the solution and amount of chelated metal ions (Fig. 17), which is useful to apply to metal ion removal by flocculation.

In the previous study, introduction of EDTA residue was simply performed by a reaction between chitosan amino group and EDTA dianhydride underwent cross-linking reaction to give insoluble ED-ch. In order to avoid the cross-linking, an acetic acid solution of high molecular weight chitosan ($M_w = 50\text{--}100$ kDa) was treated with EDTA monoanhydride. This reaction proceeded smoothly and homogeneously by addition of aqueous NaHCO_3 to control the pH of the reaction mixture to slightly basic. The degree of substitution (DS) of EDTA residues in the product was changeable from 20 to 80% by the amount of the acylation reagent used. ED-ch thus obtained was highly soluble in water and it was purified by dialysis or ultrafiltration.

ED-ch is a polyelectride having amino groups and carboxylic acid, and positive charge and negative charge should present predominantly under acidic and basic

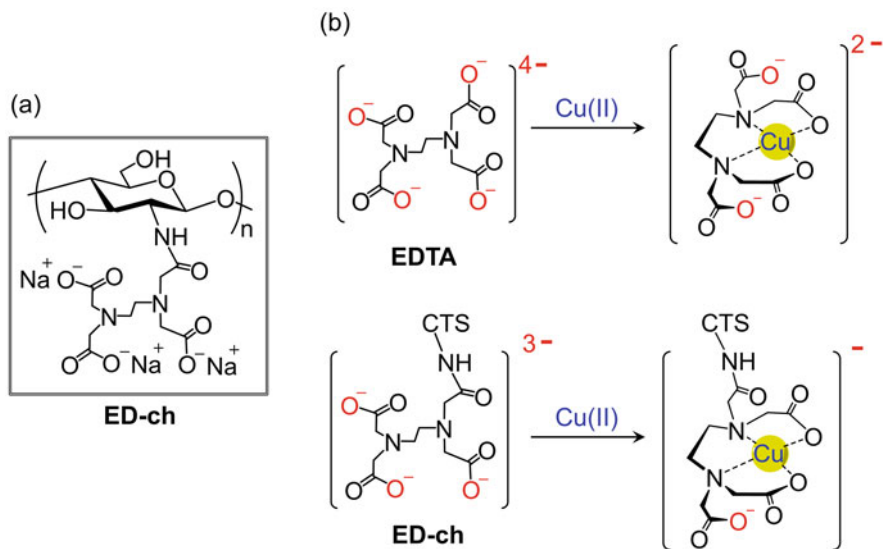


Fig. 17 Structures of EDTA-linked chitosan (ED-ch) (a) and its chelation complex with Cu(II) (b)

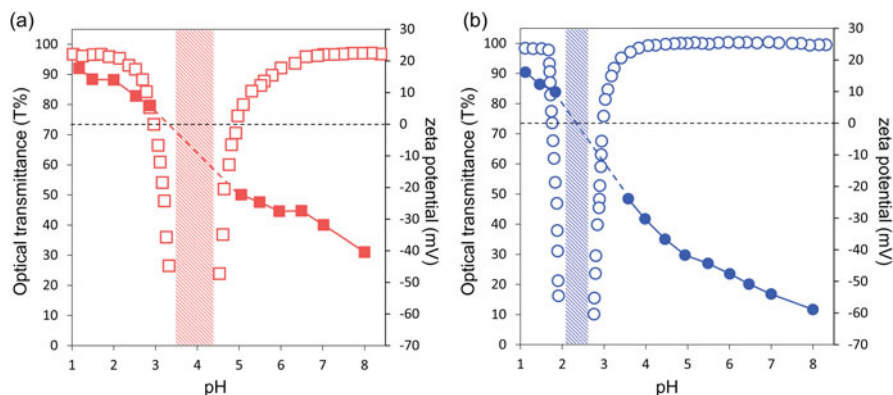


Fig. 18 pH dependent solubility of ED-cd observed by transmittance at 600 nm (a) and its zeta potential (b)

conditions, respectively. The amphoteric property of ED-ch with D.S. 39 and 70% was confirmed by relation between pH and zeta potential (Fig. 18b). Furthermore, the potential curve suggested that charge neutralization of ED-ch with D.S. 39 and 70% occurred at around pH 3.5 and pH 2.5, respectively. Turbidity experiment shown in Fig. 18a revealed that ED-ch had good water solubility in both acidic and basic regions, whereas turbidity was increased at around the isoelectric pH and almost complete precipitation was observed at the narrow pH region. These pH

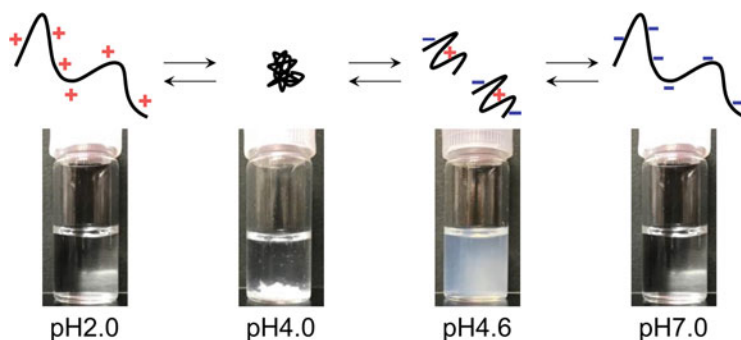


Fig. 19 Schematic drawing of pH controlled flocculation of ED-ch 39 and photos of ED-ch samples

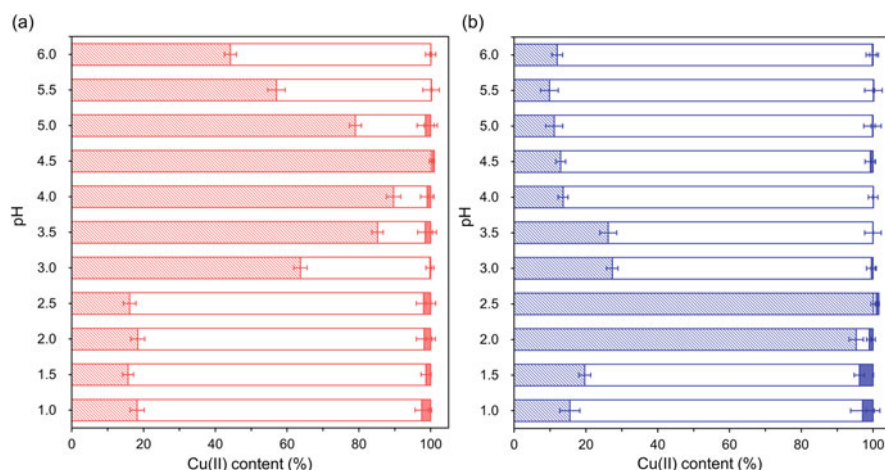


Fig. 20 pH dependent Cu(II) distribution in the presence of ED-ch 39 (a) and ED-ch 73 (b) (closed bar: free Cu(II), open bar: chelated Cu(II) in solution, dotted bar: precipitated Cu(II))

dependence properties of ED-ch suggested that the flocculation occurs by charge neutralization of the polymers (Fig. 19).

5.3 Metal Ion Removal by ED-ch Flocculation

Using ED-ch that has pH dependent flocculation property, removal of Cu(II) was performed under various pH conditions. After mixing with ED-ch with D.S. 39% or 73%, each sample was separated by centrifuge to obtain precipitate, and then the resulting supernatant was fractionated into polymer gel and filtrate by ultrafiltration. Content of Cu(II) was estimated by atomic absorption and summarized in Fig. 20.

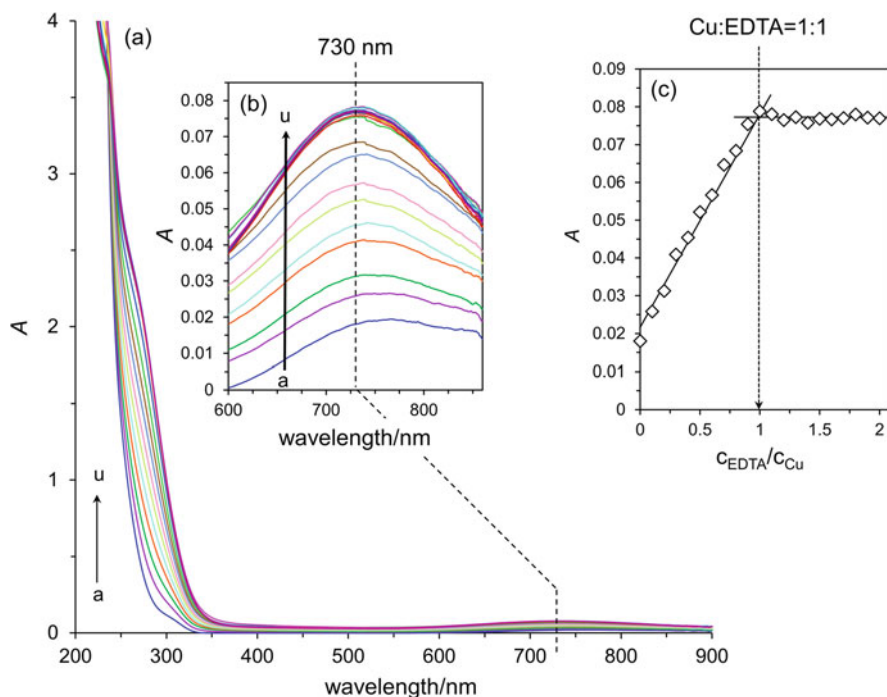


Fig. 21 Spectroscopic titration of ED-ch with Cu(II). UV-vis spectrum with different amounts of Cu(II) (a), (b), and the titration curve (c)

Table 4 Removal of various metal ions by ED-ch determined by atomic absorption spectrometry

	Cu (II)	Cd (II)	Pb (II)	Zn (II)	Ag (I)	Fe (III)	Hg (II)	Mn (II)	Cr (VI)	Ca (II)	Mg (II)
ED-ch 39	89%	84	94	82	94	90	95	85	35	20	3
ED-ch 73	96%	96	92	96	95	99	98	95	34	70	5

All filtrate fractions found to contain <5% of Cu(II) suggesting that almost all Cu (II) is captured by ED-ch. The ratio of Cu(II) containing the precipitate and the polymer gel was dependent on pH of the samples and the best removal by ED-ch 39 and ED-ch 73 was achieved at pH 4.5 and 2.5, respectively. Furthermore, spectroscopic titration of ED-ch with Cu(II) (Fig. 21) showed formation of EDTA-Cu(II) chelation complex in the ratio of 1:1.

The ability of metal chelation and flocculation abilities of ED-ch could be useful for the removal of various metal ions. ED-ch was added to a metal ion containing solution, and then pH was adjusted to form precipitate, which was separated by centrifuge. As shown in Table 4, Cu(II), Cd(II), Pb(II), Zn(II), Ag(I), Fe(III), Hg(II), and Mn(II) were successfully removed more than 90%. However, removal of Cr

(VI) was unsuccessful because of low chelation ability of its oxyanion. Since flocculation is one of the most efficient methods for the waste water treatment, the unique property of water-soluble ED-ch extends this procedure to metal ion removal.

5.4 Some Applications of EDTA-Linked Chitosan

In order to extend applicability of the pollutant removal, further chemical modification of ED-ch was performed by several groups as shown in Fig. 22. Moreira et al. described introduction of two functional groups, EDTA and pyridyl amino, into chitosan skeleton increased its affinity toward Cr(VI) [64]. Reductive amination of chitosan was conducted with 2-pyridinecarboxaldehyde and NaBH_4 . Subsequently, the product was acylated with EDTA dianhydride (EDTAD) to give a cross-linked insoluble material (ED-py-ch). ED-py-ch has both cationic functional group of ammonium group and chelation site of EDTA group. The removal of Cu(II) and oxyanion of Cr(VI) from a single aqueous solution using the novel bifunctionalized adsorbent material revealed that the maximum adsorption capacities for Cu(II) 2.60 mmol g^{-1} at pH 5.5, whereas that of Cr(VI) was 3.50 mmol g^{-1} at pH 2.0. These results were explainable by consideration of the zwitterionic structure of the adsorbent. Presence of rich ammonium cations at low pH conditions enhances Q_{max} for oxyanion of Cr(VI), while deprotonation of carboxyl group occurred at higher pH region stabilizes chelation complex of Cu(II) and EDTA.

Furthermore, biodegradable adsorbent for the heavy metal ion removal was synthesized by thermal condensation of three components, namely EDTA tosylate, chitosan, and carboxymethyl cellulose (CMC) [65]. This composite material (ED-ch@CMC) was insoluble in water, and efficiently removed Cu(II) from an aqueous medium. Washing ED-ch@CMC with an EDTA solution resulted in desorption of Cu(II), which means possibility of the repeated use of this adsorbent. As an excellent advantage, this material was shown to be decomposed when it was buried under the soil for 50 days.

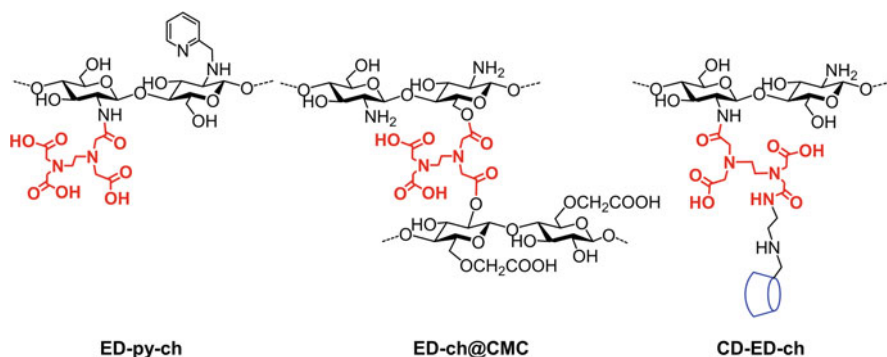


Fig. 22 Partial structures of multi-functional ED-ch adsorbents

The global contamination of water resources with inorganic and organic micropollutants, such as metals and pharmaceuticals, poses a critical threat to the environment and human health. Zhao et al. reported on a bio-derived trifunctional adsorbent (CD-ED@ch), which consisted of chitosan, EDTA, and β -CD [66]. They fabricated via a simple one-pot synthesis method, which involves cross-linking chitosan and 6-amino- β -CD derivative using EDTAD as a cross-linker. In this 3-component-system, chitosan chain is considered as the backbone, the immobilized β -CD cavities capture the organic compounds via host-guest inclusion complexation, and EDTA-groups form chelation complexes with metal ions. CD-ED@ch displayed a monolayer adsorption capacity of 0.803 and 1.258 mmol g⁻¹ for Pb(II) and Cd(II), respectively. While a heterogeneous adsorption capacity of 0.177, 0.142, 0.203, 0.149 mmol g⁻¹ for BPS, ciprofloxacin, procaine, and imipramine, respectively. Importantly, the adsorbent performed an effective role in the simultaneous removal of metals and organic pollutants at environmentally relevant concentrations.

Chitosan derivative with pendant EDTA showed potential chelation ability toward various metal ions, and its zwitterionic property resulted in pH dependent dynamic morphology change, which could apply to the removal of heavy metals by flocculation. Further chemical modification of ED-ch provides multi-functional adsorbents for simultaneous removal of different types of pollutants.

6 Conclusion

Over the past few decades, the biological systems represent a successful strategy for the design of materials. Highly organized structures and functions in living organisms have been a source of inspiration of new materials, of which properties are beyond the artificially synthesized materials. This chapter describes important consideration in designing and synthesizing new adsorbents mimicking remarkable biological system of molecular recognition, and also highlights recent advances in biomimetic adsorbents for the selective and efficient removal of target pollutants.

Utilizing the inclusion ability of CDs, new type of adsorbents have been synthesized by CD derivatives and polysaccharide, chitosan, and shown to have a high affinity toward various organic and hydrophobic pollutants with appropriate molecular sizes. In these studies, employing soft, flexible, and swelling polymer such as polysaccharide scaffolds of CD demonstrated their high selectivity and high adsorption capacity of CD-based adsorbents. The importance of the soft scaffold is also shown in the preparation of biomass-immobilized adsorbents. Chitosan and calcium alginate hydrogel beads have flexible and highly swelling property and they act as a scaffold of a large number of living or dead biomass, which have an ability of pollutant accumulation and degradation. Their biocompatible nature helps the growth of various bacteria and fungi with pollutant degradation ability, and their multi-functionality is useful for structural modification such as introducing molecular recognition sites and cross-linking.

Furthermore, adsorbents having intercalation and chelation ability are designed. DNA-immobilized materials inspired by interaction between DNA and genotoxins are shown to be useful for the removal and the detoxification of water containing various polycyclic aromatic pollutants. Chitosan derivative with pendant EDTA showed potential chelation ability toward various metal ions, and its zwitterionic property resulted in pH dependent dynamic morphology change, which could apply to the removal of heavy metals by flocculation. Further chemical modification of ED-ch provides multi-functional adsorbents for simultaneous removal of different types of pollutants.

Although the efficiency of novel synthetic adsorbents designed based on biomimetic approaches is still far away from that of our request, further improvement of adsorbent structures will possibly surpass conventional adsorbents. Further investigations on fundamental comprehension of supramolecular chemistry and study on mechanism of action of pollutants would be necessary.

References

1. Lapworth DJ, Baran N, Stuart ME et al (2012) Emerging organic contaminants in groundwater: a review of source, fate and occurrence. *Environ Pollut* 163:287–303
2. Kim MK, Zoh KD (2016) Occurrence and removals of micropollutants in water environment. *Environ Eng Res* 21:319–332
3. Dias JM, Alvim-Ferraz MCM, Almeida MF et al (2007) Waste materials for activated carbon preparation and its use in aqueous-phase treatment: a review. *Aust J Environ Manag* 85:833–846
4. Pal A, Paul AK (2008) Microbial extracellular polymeric substances: central elements in heavy metal bioremediation. *Indian J Microbiol* 48:49–64
5. Akuz Z (2005) Application of biosorption for the removal of organic pollutants: a review. *Process Biochem* 40:997–1026
6. Fiammengo R, Crego-Calama M, Reinhoudt DN (2002) Synthetic self-assembled models with biomimetic functions. *Curr Opin Chem Biol* 5:660–673
7. Zhang C, Mcadams II DA, Grunlan JC (2016) Nano/micro-manufacturing of bioinspired materials: a review of methods to mimic natural structures. *Adv Mater* 28:6292–6321
8. Böhm CF, Harris J, Schodder PI et al (2019) Bioinspired materials: from living systems to new concepts in materials chemistry. *Materials* 12:2117–2136
9. Breslow R, Dong SD (1998) Biomimetic reactions catalyzed by cyclodextrins and their derivatives. *Chem Rev* 98:1997–2012
10. Dong Z, Luo Q, Liu J (2012) Artificial enzymes based on supramolecular scaffolds. *Chem Soc Rev* 41:7890–7908
11. Hu Q-D, Tang G-P, Chu PK (2014) Cyclodextrin-based host-guest supramolecular nanoparticles for delivery: from design to applications. *Acc Chem Res* 47:2017–2025
12. Vijayaraghavan K, Balasubramanian R (2015) Is biosorption suitable for decontamination of metal-bearing wastewaters? A critical review on the state-of-the-art of biosorption processes and future directions. *J Environ Manag* 160:283–296
13. Szejtli J (1998) Introduction and general overview of cyclodextrin chemistry. *Chem Rev* 98:1743–1754
14. Hedges AR (1998) Industrial applications of cyclodextrins. *Chem Rev* 98:2035–2044
15. Alonso ML, Laza JM, Alonso RM et al (2014) Pesticides microencapsulation. A safe and sustainable industrial process. *J Chem Technol Biotechnol* 89:1077–1085

16. Gidwani B, Vyas A (2014) Synthesis, characterization and application of epichlorohydrin- β -cyclodextrin polymer. *Colloid Surf B* 114:130–137
17. Mourya VK, Inamdar NN (2008) Chitosan-modifications and applications: opportunities galore. *React Funct Polym* 68:1013–1051
18. Rani M, Agarwal A, Negi YS (2010) Chitosan-modifications and applications: opportunities galore. *Bioresources* 5:2765–2807
19. Crini G (2006) Non-conventional low-cost adsorbents for dye removal: a review. *Bioresour Technol* 97:1061–1085
20. Furusaki E, Ueno Y, Sakairi N et al (1996) Facile preparation and inclusion ability of a chitosan derivative bearing carboxymethyl- β -cyclodextrin. *Carbohydr Polym* 29:29–34
21. Bentley MD, Roberts MJ, Harris JM (1998) Reductive amination using poly(ethylene glycol) acetaldehyde hydrate generated in situ: applications to chitosan and lysozyme. *J Pharm Sci* 87: 1446–1449
22. Tojima T, Katsura H, Han SM et al (1998) Preparation of an α -cyclodextrin-linked chitosan derivative via reductive amination strategy. *J Polym Sci Polym Chem* 38:1965–1968
23. Tanida F, Tojima T, Han SM et al (1998) Novel synthesis of a water-soluble cyclodextrin-polymer having a chitosan skeleton. *Polymer* 39:5261–5263
24. Buranaboripan W, Lang W, Motomura E et al (2014) Preparation and characterization of polymeric host molecules, β -cyclodextrin linked chitosan derivatives having different linkers. *Int J Biol Macromol* 69:27–34
25. Auzély-Velty R, Rinaudo M (2001) Chitosan derivatives bearing pendant cyclodextrin cavities: synthesis and inclusion performance. *Macromolecules* 34:3574–3580
26. Dambies L, Vincent T, Domard A et al (2001) Preparation of chitosan gel beads by ionotropic molybdate gelation. *Biomacromolecules* 2:1198–1205
27. Tojima T, Katsura H, Han SM et al (1999) Chitosan beads with pendant α -cyclodextrin: preparation and inclusion property to nitrophenolates. *Carbohydr Polym* 40:17–22
28. Martel B, Devassine M, Crini G et al (2001) Preparation and sorption properties of a β -cyclodextrin-linked chitosan derivative. *J Polym Sci Part A Polym Chem* 39:169–176
29. Zha F, Li S, Chang Y (2008) Preparation and adsorption property of chitosan beads bearing β -cyclodextrin cross-linked by 1,6-hexamethylene diisocyanate. *Carbohydr Polym* 72:456–461
30. Nishiki M, Tojima T, Nishi N et al (2000) β -Cyclodextrin-linked chitosan beads: preparation and application to removal of bisphenol A from water. *Carbohydr Lett* 4:61–67
31. Aoki N, Nishikawa M, Hattori K (2003) Synthesis of chitosan derivatives bearing cyclodextrin and adsorption of *p*-nonylphenol and bisphenol A. *Carbohydr Polym* 52:219–223
32. Aoki N, Kinoshita K, Mikuni K et al (2007) Adsorption of 4-nonylphenol ethoxylates onto insoluble chitosan beads bearing cyclodextrin moieties. *J Incl Phenom Macrocycl Chem* 57: 237–241
33. Prabaharan M, Mano JF (2006) Chitosan derivatives bearing cyclodextrin cavities as novel adsorbent matrices. *Carbohydr Polym* 63:153–166
34. Manakker F, Vermonden T, Nostrum CF et al (2009) Cyclodextrin-based polymeric materials: synthesis, properties, and pharmaceutical/biomedical applications. *Biomacromolecules* 10: 3157–3175
35. Orelma H, Virtanen T, Spoljaric S et al (2018) Cyclodextrin-functionalized fiber yarns spun from deep eutectic cellulose solutions for nonspecific hormone capture in aqueous matrices. *Biomacromolecules* 19:652–661
36. Alsbaiee A, Smith BJ, Xiao L et al (2016) Rapid removal of organic micropollutants from water by a porous β -cyclodextrin polymer. *Nature* 529:190–194
37. Xu G, Xie X, Qin L et al (2019) Simple synthesis of a swellable porous β -cyclodextrin-based polymer in the aqueous phase for the rapid removal of organic micro-pollutants from water. *Green Chem* 21:6062–6072
38. Alzate-Sánchez DM, Ling Y, Li C et al (2019) β -Cyclodextrin polymers on microcrystalline cellulose as a granular media for organic micropollutant removal from water. *ACS Appl Mater Interfaces* 11:8089–8096

39. Guo R, Liu H, Yang K et al (2020) β -Cyclodextrin polymerized in cross-flowing channels of biomass sawdust for rapid and highly efficient pharmaceutical pollutants removal from water. *ACS Appl Mater Interfaces* 12:32817–32826
40. Kapoor A, Viraraghavan T (1995) Fungal biosorption – an alternative treatment option for heavy metal bearing wastewaters: a review. *Bioresour Technol* 53:195–206
41. Mallick N (2001) Biotechnological potential of immobilized algae for wastewater N, P and metal removal: a review. *Biomaterials* 15:377–390
42. He JS, Chen JP (2014) A comprehensive review on biosorption of heavy metals by algal biomass: materials, performances, chemistry, and modeling simulation tools. *Bioresour Technol* 160:67–78
43. Lang W, Dejma C, Sirisansaneeyakul S et al (2009) Biosorption of nonylphenol on dead biomass of *Rhizopus arrhizus* encapsulated in chitosan beads. *Bioresour Technol* 100:5616–5623
44. Pluemsab W, Fukazawa Y, Furuike T et al (2007) Cyclodextrin-linked alginate beads as supporting materials for *Sphingomonas cloacae*, a nonylphenol degrading bacteria. *Bioresour Technol* 98:2076–2081
45. Sargin I, Kaya M, Arslan G et al (2015) Preparation and characterisation of biodegradable pollen–chitosan microcapsules and its application in heavy metal removal. *Bioresour Technol* 177:1–7
46. Sargin I, Arslan G, Kaya M (2015) Efficiency of chitosan–algal biomass composite microbeads at heavy metal removal. *React Funct Polym* 98:38–47
47. Saifuddin N, Raziha AZ (2007) Removal of heavy metals from industrial effluent using *Saccharomyces cerevisiae* (Baker’s yeast) immobilised in chitosan/lignosulphonate matrix. *J Appl Sci Res* 3:2091–2099
48. Tarasi R, Alipour M, Gorgannezhad L et al (2018) Laccase immobilization onto magnetic β -cyclodextrin-modified chitosan: improved enzyme stability and efficient performance for phenolic compounds elimination. *Macromol Res* 26:755–762
49. Aricov L, Leonties AR, Gifu IC et al (2020) Enhancement of laccase immobilization onto wet chitosan microspheres using an iterative protocol and its potential to remove micropollutants. *J Environ Manag* 276:111326
50. Bilal M, Iqbal HMN, Hu H et al (2017) Development of horseradish peroxidase-based cross-linked enzyme aggregates and their environmental exploitation for bioremediation purposes. *J Environ Manag* 188:137–142
51. Nguyen TD, Dang CH, Mai DT (2018) Biosynthesized AgNP capped on novel nanocomposite 2-hydroxypropyl- β -cyclodextrin/alginate as a catalyst for degradation of pollutants. *Carbohydr Polym* 197:29–37
52. Zhang C, Chen Z, Tao Y et al (2020) Enhanced removal of trichlorfon and Cd(II) from aqueous solution by magnetically separable chitosan beads immobilized *Aspergillus sydowii*. *Int J Biol Macromol* 148:457–465
53. Mucic RC, Storhoff JJ, Mirkin CA et al (1998) DNA-directed synthesis of binary nanoparticle network materials. *J Am Chem Soc* 120:12674–12675
54. Kitamura H, Matsuura E, Nagata A et al (1997) DNA-alginate complex recognized by autoantibodies against DNA. *Int J Biol Macromol* 20:75–77
55. Kitamura H, Iwamoto C, Sakairi N et al (1997) Marked effect of DNA on collagen fibrillogenesis in vitro. *Int J Biol Macromol* 20:241–244
56. Yamada M, Kato K, Nomizu M et al (2002) Preparation and characterization of DNA-films induced by UV irradiation. *Chem Euro J* 8:1407–1412
57. Yamamoto Y, Nishiguchi K, Manabe K et al (2011) Photosensitized [2 + 2] cycloaddition of *N*-acetylated cytosine affords stereoselective formation of cyclobutane pyrimidine dimer. *Nucleic Acid Res* 39:1165–1175
58. Yamada M, Kato K, Nomizu M et al (2002) UV-irradiated DNA matrixes selectively accumulates endocrine disruptors. *Environ Sci Technol* 36:949–954

59. Yamada M, Kato K, Shindo K et al (2001) UV-irradiation-induced DNA immobilization and functional utilization of DNA on nonwoven cellulose fabric. *Biomaterials* 22:3121–3126
60. Topuz F, Singh S, Albrecht K et al (2016) DNA nanogels to snare carcinogens: a bioinspired generic approach with high efficiency. *Angew Chem Int Ed* 55:12210–12213
61. Kawamura Y, Mitsuhashi M, Tanibe H et al (1993) Adsorption of metal ions on polyaminated highly porous chitosan chelating resin. *Ind Eng Chem Res* 32:386–391
62. Inoue K, Ohto K, Yoshizuka K et al (1997) Adsorption of lead(II) ion on complexation types of chemically modified chitosan. *Bull Chem Soc Jpn* 70:2443–2447
63. Fujita S, Sakairi N (2016) Water soluble EDTA-linked chitosan as a zwitterionic flocculant for pH sensitive removal of Cu(II) ion. *RSC Adv* 6:10385–10392
64. Moreira ALSL, Pereira AS, Speziali MG et al (2018) Bifunctionalized chitosan: a versatile adsorbent for removal of Cu(II) and Cr(VI) from aqueous solution. *Carbohydr Polym* 201:218–227
65. Manzoor K, Ahmad M, Ahmad S et al (2019) Synthesis, characterization, kinetics, and thermodynamics of EDTA-modified chitosan-carboxymethyl cellulose as Cu (II) ion adsorbent. *ACS Omega* 4:17425–17437
66. Zhao F, Repo E, Yin D (2017) One-pot synthesis of trifunctional chitosan-EDTA- β -cyclodextrin polymer for simultaneous removal of metals and organic micropollutants. *Sci Rep* 7:15811

Zero-Valent Iron and Some Other Nanometal Particles for Environmental Remediation



Mahmuda Akter, Md. Tajuddin Sikder, and A. K. M. Atique Ullah

Contents

1	General Introduction	540
2	Zero-Valent Iron in Environmental Remediation	540
2.1	Synthesis	542
2.2	Composites of nZVI/Modification	544
2.3	Environmental Application	549
2.4	Toxicity of nZVI and Future Prospects	553
3	Nanomaterials in Environmental Remediation	553
3.1	Synthesis of Nanomaterials	553
3.2	Nanoparticles with Potential Remediation Applications	556
4	Conclusion	560
	References	561

Abstract The global environment has been continuously dealing with numerous natural and anthropogenic sources of pollutants leading threatening to the ecosystem and human health. In accordance with the removal of environmental pollutants, environmental chemical science and engineering science are facing challenges to upgrade the remediation technologies. This chapter is aimed to deal with nano zero-valent iron (nZVI) and other functional nanomaterials (TiO₂, Ag, Mn, Au, etc.) having the properties of environmental pollutant remediation. Recently, nano zero-

M. Akter

Group of Environmental Adaptation Science, Faculty of Environmental Earth Sciences,
Hokkaido University, Sapporo, Japan

M. Tajuddin Sikder (✉)

Department of Public Health and Informatics, Jahangirnagar University, Dhaka, Bangladesh
e-mail: sikder@juniv.edu

A. K. M. Atique Ullah

Nanoscience and Technology Research Laboratory, Chemistry Division, Atomic Energy
Centre, Bangladesh Atomic Energy Commission, Dhaka, Bangladesh

Shunitz Tanaka, Masaaki Kurasaki, Masaaki Morikawa, and Yuichi Kamiya (eds.), 539

Design of Materials and Technologies for Environmental Remediation,

Hdb Env Chem (2023) 115: 539–568, DOI 10.1007/698_2021_821,

© The Author(s), under exclusive license to Springer Nature Singapore Pte Ltd 2022,

Published online: 1 January 2022

valent iron (nZVI) and some functional nanomaterials have become an integral part of remediation technologies for both of the inorganic and organic pollutants. These functional materials have the potentiality to convert the toxic pollutants into more environmentally friendly chemical or to reduce into a concentration acceptable for environmental discharge. The synthesis procedure of these functional materials is facile, and a tremendous effort has been given for the enhancement of their functionality, reactivity, and efficiency throughout the remediation researches. The authors have given emphasis to draw a clear outline of the function, application, and overall significant contribution of nZVI and other nanomaterials in the sector of environmental pollutant remediation.

Keywords Green synthesis, Heavy metal removal, Nanoscale zero-valent iron, Nanotoxicity, Organic pollutant removal, Soil remediation, Wastewater remediation, Wastewater treatment

1 General Introduction

The applications of reactive materials to the remediation of environmental pollutants and their promising results demonstrated the great potential of them in the field of materials science. Among the reactive materials, functional metals, e.g. iron, silver, gold, titanium, manganese, etc. are of great interest for their distinct characteristics of reactivity, binding capacity, electronegativity, reducing capability, surface morphology, etc. [1]. The technologies related to the synthesis and design of these reactive materials/metals thereafter acquired intensive scientific attention for the removal of environmental contaminants from agricultural and industrial wastewaters. Introduction of nanotechnological attribution into these metals makes them not only more functional but also efficient to separate pollutants from contaminated environment. Nanotechnology deals with manipulation of matter at the atomic and molecular scale with the particles having at least one dimension 1–100 nm. In this chapter, we will give a brief discussion with zero-valent iron and other functional nanomaterials in respect of their function, synthesis, and overall contribution in the sector of environmental remediation.

2 Zero-Valent Iron in Environmental Remediation

One of the most engineered metals in this emerging field of nanotechnology is iron which has markedly different properties from one form to another [2]. Nanosized zero-valent iron (nZVI) is such a form of metallic iron which is relatively inexpensive; and highly reactive towards a large number of organic and inorganic compounds, including halogenated hydrocarbons, organic dyes, antibiotics, heavy metal

ions, etc. [3]. In addition, nZVI has large specific surface area, better mobility, strong adsorption capacity, and reducing power that made it superior over a variety of conventional and modern methods including chemical precipitation, electrochemical treatment, electrodialysis, evaporative recovery, ultra-filtration, solvent extraction, reverse osmosis, filtration, and membrane technologies [4]. nZVI, the most prevalent environmentally benign nanomaterials, has strong bactericidal effect and toxicity towards microorganisms, which in turn confirms its wide adaptability to remove pollutants from aquatic environment [5]. The unique excellent reactive longevity of nZVI along with its controllable particle size (1–100 nm) has made it compatible to treat successfully a wide variety of toxic chemicals, e.g. biosolids, tetracycline, chlorinated ethylene, trichloroethylene, organo-chlorine pesticides, herbicides, atrazine, antibiotic metronidazole, organic dyes, nitrate and nitrite, phosphorous and various metal ions, e.g., Pb(II), Ba(II), Zn(II), As(III), Cr(VI), As(V), Cu(II), Cd(II), Ni(II) and Co(II), from the environment [5–15].

nZVI reacts rapidly with oxygen and water, and has a high tendency to agglomerate; therefore, these nanoparticles, NPs, are usually capped with various inorganic and organic materials or supported on various supports (Fig. 1) [16]. Capping and support agents consequently reduce the reactivity to some extent, what is gained by the small size of NPs, but increase stability and transport properties, what is essential for environmental, e.g., soil and groundwater, remediation [17]. The potential of nZVI for environmental remediation has initiated numerous laboratory works for investigating the reactivity and toxicity of these NPs with distinct inorganic and organic contaminants and microorganisms and plants, respectively [18]. Zero-valent iron takes part in corrosion in solution through an electrochemical process which involves both its dissolution and association with redox species. Its dissolution forms soluble ionic products or insoluble oxide/hydroxide and is called anodic reactions,

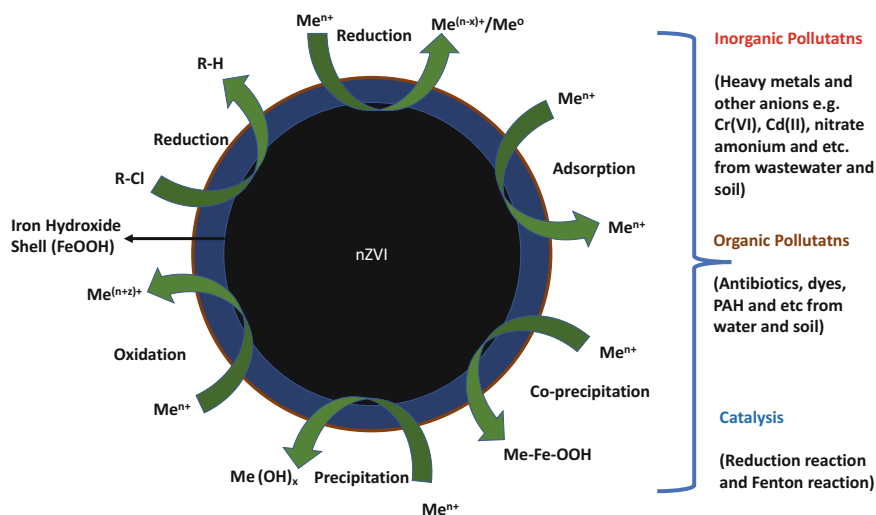


Fig. 1 Various mechanisms for the removal of inorganic and organic pollutants from water and soil

whereas the reduction at the cathode is termed as cathodic reactions. In aqueous solution, the corrosion is triggered by dissolved oxygen and water [19, 20]. In the first phase of this chapter, the facile synthesis of both bare nZVI and its different composites along with its environmental applicability is discussed. In the later part, nanomaterials for environmental remediation other than nZVI are presented.

2.1 Synthesis

2.1.1 Synthesis of Pristine nZVI

Pristine nZVI for the environmental application usually is produced by the reduction of dissolved iron using sodium borohydride solutions or by milling or grinding processes of metal iron [21]. In general, nZVI used in water treatment has been developed using two basic categories: physical methods and chemical methods. These two methods are further divided into top-down approach and bottom-up approach. In top-down approach, bulk iron reduces its size into nanoscale whereas nZVI generated from ions or molecules in bottom-up approach [22, 23].

Physical Methods

The main advantages of physical methods, e.g. gas condensation processing and ball milling, are its easy operation and naive separation of products over chemical methods. Nano iron particles are obtained by condensing the vapor of iron atoms under an inert gas atmosphere via cooling with liquid nitrogen in gas condensation processing (GPC). In this process, the yield of nanoparticles is low and the preparing conditions are exclusive, e.g. high temperature, high pressure, and substantial coolant, whereas this process has well control over the particle size and its distribution [24]. Metallic balls or beads are used as media in ball milling method to decrease the size of materials, where micro iron particles as raw materials could effectively produce nZVI of uniform size and high surface area [25–27]. This process is environmentally friendly and has suitability on commercial scale but requires high energy and specialized equipment to form nano particles.

Chemical Methods

Chemical routes for nZVI preparation have potential advantages in respect of suitability, applicability, cost-effectiveness, and easiness for synthesis over physical methods. The borohydride reduction for nZVI preparation is the most acceptable one which involves the reduction of Fe^{3+} or Fe^{2+} by NaBH_4 under ambient temperature and pressure. This method can result in secondary pollution of toxic reagents and chemicals [28]. Few supplementary means, e.g. ionic liquids (ILs) are also used to

obtain smaller, more uniform, and stable nZVI. Besides reduction methods and ultrasound method have been used to change the morphology of nZVI from spherical to plate-like and then to needlelike. Thus, the typical attributes of nZVI, e.g. smaller particle size, a larger specific surface area and higher crystallinity can be achieved under high ultrasonic power.

Carbothermal synthesis and thermal decomposition method are now-a-days considering significant ones to generate nZVI where the former one requires the use of C or CO to reduce iron oxide, ferrous or ferric ions, and the latter one involves organometallic molecules for thermal decomposition to yield nZVI. Carbothermal synthesis received wider attention due to the availability of inexpensive raw materials whereas a good quality of small size nZVI up to 2 nm with perfect homogeneity can yield from thermal decomposition method. Thermal decomposition of $\text{Fe}(\text{CO})_5$ combined with both ionic liquids and microwave irradiation can control formation, stabilization, size distribution of nZVI precisely. Chemical vapor condensation, on the other hand, combines chemical thermal decomposition and physical condensation at high temperature (400–1,100°C) followed by cooling down at liquid nitrogen to yield nZVI of good physical and chemical homogeneity. These methods require elevated temperatures and thus energy-intensive. In addition, toxic carbon monoxide and other unstable by-product are usually produced from these methods.

The hydrothermal method uses glucose and ferric nitrate as precursors to obtain encapsulated nano-size iron particles of high stability and reusability via a one-pot hydrothermal method followed by self-reduction under a N_2 atmosphere [29]. The synthesis of size and shape controlled iron NPs ranging between 10 and 90 nm in liquid polyols such as tri-methylene glycol, propylene glycol, and ethylene glycol through heterogeneous nucleation is called polyol process [30]. This method uses different degree of H_2PtCl_6 as a nucleation agent to control the size and shape of nZVI and the polyol medium prevents possible oxidation of particles by atmospheric oxygen. In the reverse micelle method (microemulsion synthetic method), Fe^{2+} is reduced to Fe^0 by hydrazine injected into a system of cetyl trimethyl ammonium bromide (CTAB) as the surfactant, butanol as the co-surfactant, and octane as the oil phase, to control the size and shape of iron NPs [31].

In ultrasound assisted electrochemical method, Fe^{3+} or Fe^{2+} is reduced to Fe^0 on the cathode to obtain very small size particles (1–20 nm) with the large surface area ($25.4 \text{ m}^2 \text{ g}^{-1}$) [32]. Green synthesis, on the other hand, is the recent addition into the methods of preparation of iron nano particles where environmental safety and sustainable approaches are the key focuses. Natural reducing agents, e.g. polyphenol and caffeine from green tea, oolong tea, black tea, oak, pomegranate and other plant extracts [33, 34] can produce small size (10–20 nm) nZVI. These agents are safe, secured, available, eco-friendly, low-cost, and energy-saving. These qualities are the top priority in every physical and chemical method.

2.2 Composites of nZVI/Modification

nZVI possesses many disadvantages despite having many desirable traits in environmental remediation, e.g. aggregation into the system leading to a decrease of mobility and reactivity [35]. In addition, post treatment of nZVI in respect of separation from the media makes difficult its functionality and applicability and thus demands further modification. Notable approaches have been proposed so far in the literature to remove the above-mentioned disparities of nZVI, including surface modification, bimetallic nanoparticles, conjugation with supports, magnetization modification, and integrated methods.

2.2.1 Surface Modification

Surface modification is the first effort in this dealing which can be achieved by coating materials to confirm stability, surface adherence, low diffusion, and cost-effective. The modifiers induce electrostatic repulsion to prevent possible aggregation of nZVI. Surfactants in this list of modifiers are the ideal ones that impede aggregations by their hydrophilic heads whereas the hydrophobic tails confirm the adsorption on their surface. These amphiphilic organic compounds, e.g. nonionic, anionic, and cationic surfactants, contribute improved functionality and transportation capability of nZVI in environmental remediation sector. Polymers with negative surface charges can serve as a good choice for making effective nZVI to work in against aquifer materials [36], for example, polyacrylic acid, polyacrylamide [37], and polyethylene glycol [38]. Polymers containing multi-functional groups in conjunction with nZVI exhibit desirable properties for water treatment. For example, carboxyl groups anchored to the surface of iron NPs impart good affinity to water and colloidal stability with strong electrostatic interparticle repulsions [39–42]. Likewise, biopolymers, another kind of surface modifiers, e.g. alginate [43], agar [44], chitosan [5], natural polysaccharides, cellulose and its derivatives are widely used in the modification of nZVI. The polysaccharide derivatives named carboxymethyl cellulose (CMC) are used widely in this regard to modify nZVI for water treatment applications which exhibit better dispersity, stability, antioxidizability, discoloration efficiency, high reaction rate, and less toxicity. Surface modified nZVI was reported in many studies of having low toxicity but high reactivity due to the cover of bare surface with the coating [45].

One of the significant processes to increase the reactivity and decrease the aggregation and oxidation of nZVI is to form bimetallic NPs (B-NPs). In this process, the incorporation of less active metals, e.g. Pd, Pt, Ni, Ag, Cu with nZVI makes a cell where the iron acts as anode and the other metal acts as cathode. This cell along with the electrochemical effects, catalytic hydrogenation, accelerates the overall reactivity and thus increases the degradation of contaminants [46, 47]. B-NPs are formed usually by chemical solution deposition (CSD) which has drawbacks of secondary pollution and instability [48]. In addition, less active metals conjugated

with nZVI in this method have distinct reactivity performance and ranked as $\text{Cu} > \text{Pd} > \text{Pt} > \text{Ag} > \text{Ni}$ [49–51].

2.2.2 Conjugation with Supports

To reduce aggregation and to facilitate easy separation of nZVI, composites of nZVI by the conjugation with supportive materials work better than bare nZVI. The composites are formed with a number of materials: clays (bentonite and kaolinite), carbon carriers (graphene nanosheet, activated carbon, biochar, carbon black, mesoporous carbon), membranes, resins, silica, boron nitride nanosheets, chitosan, and $\text{Mg}(\text{OH})_2$ that have enhanced adsorption capability of contaminants before degradation [52]. These supportive materials are convenient in terms of high porosity, easy availability, mechanical strength, low cost, ion exchange capacity, adsorption, low aggregation, high dispersion, accelerated mobility [53–59]. Immobilization of nZVI by conjugation with large pore size of membranes (polyacrylic acid, polyvinyl alcohol) is another sophisticated composite formation way to increase specific surface area, porosity, and the effectiveness of contaminant degradation with excellent reusability. Resins, on the other hand, e.g. polymeric exchange resins, polystyrene cation-exchange resin, anion-exchange resin, nonionic resins, give to the nZVI good chemical stability, robust mechanical strength, and low environmental leaking risks [60–62]. Supported nZVI in different conjugated adsorbents or composites along with the morphology and surface characteristics are shown in Fig. 2.

Conjugation of nZVI with silica fume or coating with SiO_2 is also frequently used to increase the stability, mobility, and reactivity of nZVI in soil. Boron nitride nanosheets give nZVI magnetic properties with high specific surface area and density so that the efficiency of this composite becomes twice when compared with the bare nZVI. These magnetic properties help the composite in easy separation from solution and thus ensure its reusability [63]. Clays, carbon carriers, membranes, resins silica, and boron nitride nanosheets are well capable to remove toxic heavy metals, e.g. $\text{Pb}(\text{II})$, $\text{Cr}(\text{VI})$, $\text{As}(\text{III})$, $\text{As}(\text{V})$ and other inorganic ions, e.g. phosphorus, chlorine, bromine, nitrate, trichloroethylene, etc. But, these all supporting materials are suffering from few limitations, e.g. complexity of preparation, high cost, and uneven loading of nZVI [64].

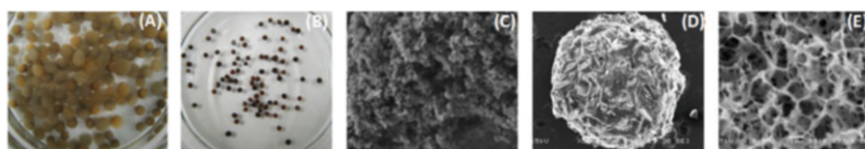


Fig. 2 Images of (a) chitosan supported nZVI beads; (b) nZVI impregnated in polymer; (c) SEM images of bare nZVI; (d) surface morphology of supported nZVI; and (e) distribution of pore spaces and nZVI in a supported adsorbent

Chitosan is the most available, easily synthesized, and commercially abundant polysaccharide in which nZVI can be entrapped and eventually chitosan gives nZVI increased dispersity, stability, reactivity and impedes aggregation [7, 65]. On the other hand, $\text{Mg}(\text{OH})_2$ can also be used as an effective carrier and on its surface nZVI can be uniformly immobilized on the surface to minimize aggregation and to acquire excellent synergistic adsorption capacity [64].

2.2.3 Magnetism and Emulsification

One of the major shortcomings of nZVI for its application in the aqueous media is the post treatment or separation easiness which eventually confirms its reusability. Different methods are used now-a-days to provide magnetism to the nZVI using boron nitride nanosheets, magnetic carbon, graphene, Fe_3O_4 , etc. [66]. These materials induced superparamagnetism, also prevented agglomeration of nZVI, and gave enough mechanical strength to the composites to prevent possible breakdown into the solution [67]. Emulsifying agents or surfactants containing nZVI in water are surrounded by an oil-liquid membrane that generates a hydrophobic aqueous environment. This comes into contact with dense non-aqueous phase contaminants and degrades them rapidly [68, 69]. Hybrid composites also receive wide attention in recent times. The attributes of every materials used in the hybrid composites give added advantages of high activity, stability, efficiency, synergistic effects, and reusability of the obtained product [5]. The chitosan, magnetic agents, emulsifying agents, and hybrid composites are well studied for the removal of heavy metals, e.g. lead, chromium, and trichlorophenol. To ensure improved applicability and effectiveness, it is important to synthesize selective adsorbents of targeted contaminants to ensure sustainable performance of nZVI. In order to arrive at an optimal nZVI modification method, the choice of a modified nZVI variant for the elimination of a contaminant should depend on the removal mechanism, modification effect, removal efficiency, the cost, and so on. From the above discussion it is evident that the desirable attributes of nZVI for environmental application are their small size, high surface area, high reactivity and mobility, and easy separation from solution. It is also palpable that the shortcomings of the nZVI are their high particle aggregation and subsequent gelation, high oxidation and corrosion rate and inadequate separation capacity from solution make them difficult for environmental application. Various alternatives discussed above are now widely used to improve the remediation quality of nZVI. The use of surfactants, supports and coating and composite formation or integrated/hybrid composites enable this excellent material to give a nano boom in environmental remediation sector. Particularly, the surface modified nZVI, porous material supported nZVI, and the inorganic clay mineral supported nZVI are the most promising ones that have lower aggregation property, higher efficiency, higher sorption capacity, and more stability in the removal of heavy metal ions from aqueous solutions. The synthesis process of nZVI and its different derivatives along with other characteristics are given in Table 1.

Table 1 Synthesis of bare nZVI and modified nZVI

Methods	Raw materials	Synthesis parameters	Characteristics	Advantages	Disadvantages	Reference
<i>Physical methods</i>						
Gas condensation processing	Vapor of iron atoms; inert gas and liquid nitrogen	Condensation of iron atoms	Nano iron particles are obtained	Good particle size and size distribution	Energy-intensive; low yield	[24]
Ball mining	Micro iron particles; metallic balls and beads	Heavy milling media	Highly effective	Nontoxic and no secondary pollution	Energy-intensive; poor homogeneity	[25, 26]
<i>Chemical methods</i>						
Borohydride reduction method	Fe^{3+} or Fe^{2+} and NaBH_4	Reduction of Fe^{3+} or Fe^{2+} by NaBH_4	Mild operating conditions	Good homogeneity; large scale applications	Expensive; toxic and secondary pollution	[28]
Ultrasound assisted method	Ultrasound machine	Increased ultrasonic power	Impact the growth and coalescence of iron NPs	Small particle size; large specific surface area	Poor crystallinity; agglomeration	[32]
Carbothermal synthesis	C or CO, goethite	Elevated temperature	Iron or iron oxide reduced by C or CO	Available and inexpensive raw materials	Energy-intensive; flammable and toxic gas (CO)	[110]
Thermal decomposition method	$\text{Fe}(\text{CO})_5$; trioctylphosphine oxide	320°C; argon atmosphere	Highly effective method	Small size; good homogeneity	Toxic; unstable and energy-intensive	[109]
Chemical vapor condensation	$\text{Fe}(\text{CO})_5$	400–1,100°C; liquid nitrogen media	Combination of chemical thermal decomposition and physical condensation	Good physical and chemical homogeneity	Toxic; unstable and energy-intensive	[108]
Hydrothermal method	Glucose and ferric nitrate	Encapsulation process	Self-reduction under a N_2 atmosphere	An enhancement of transportation, suspension, and stability; relatively good reusability	Complex preparation and separation processes	[29]

(continued)

Table 1 (continued)

Methods	Raw materials	Synthesis parameters	Characteristics	Advantages	Disadvantages	Reference
Polyol process	H_2PtCl_6 , NaOH; Trimethylene glycol, propylene glycol, and ethylene glycol.	The reaction takes place in liquid medium	Common route for the synthesis of metallic and alloy NPs	Controllable size; high stability in air	Agglomeration	[30]
Reverse micelle method (microemulsion synthetic method)	Fe^{2+} ; Cetyltrimethylammonium bromide; butanol and octane	The reaction takes place in liquid medium	Fe^{2+} is reduced to Fe^0 by hydrazine injected into the system	Good homogeneity	Agglomeration; unstable	[31]
Electrochemical method	Fe^{3+} or Fe^{2+}	Fe^{3+} or Fe^{2+} reduced to Fe^0 to the cathode	Physical energy provided by ultrasound	Simplicity; low cost	Agglomeration	[32]
Green synthesis	Different polymers, plant extracts, polyphenols, ferric nitrate	Ferric nitrate	Reduction is the key reaction of green synthesis	High reactivity; eco-friendly; energy-saving; low cost	Incomplete reduction of iron ions; agglomeration	[33, 34]
<i>Supports and modification</i>						
Surfactants	Non-ionic surfactants, such as polysorbate; polyethylene glycol; anionic surfactants, such as sodium dodecyl sulfate; and sodium dodecyl benzene sulfonate, etc.	The reaction takes place in liquid medium	Hydrophilic heads and hydrophobic tails impede aggregation; good surface modifier	Minimizing aggregation and improving the transportation of nZVI	Toxic by-products can be generated	[36–45]
Polymers, bio-polymers and resins	Polyacrylic acid; polyvinyl pyrrolidone, etc.	Facile synthesis process	Amphiphilicity induces into the nZVI	Stable and low aggregation	Secondary pollution	[43, 44, 52]

2.3 Environmental Application

2.3.1 Removal of Heavy Metals

Considering the current pace of the development and application of nZVI, it appears to be an extremely promising technology for water treatment. Heavy metals and metalloids are the most serious concerns now-a-days and therefore effective cleaning technologies are extensively searched. nZVI is found as an electron source (core) and a site for surface complexation (shell) which make it enable for possible sequestration mechanism of metal ion removal. The redox potential of the system and capping layer of the nZVI adsorb most of the metal ions. The interaction between nZVI and metal and metalloid ions can be categorized [21, 70] as follows:

Reduction (examples: Cr, As, Cu, U, Pb, Ni, Se, Co, Pd, Pt, Hg, and Ag ions),
Adsorption (examples: Cr, As, U, Pb, Ni, Se, Co, Cd, Zn, and Ba ions),
Oxidation/reoxidation (examples: As, U, Se, and Pb ions),
Cocprecipitation (examples: Cr, As, Ni, and Se ions),
Precipitation (examples: Cu, Pb, Cd, Co, and Zn ions).

In situ remediation of heavy metal ions by adsorption mechanism of nZVI is found beneficial in water remediation sector. Heavy metal ions express adsorption, redox, aggregation, ion exchange, hydroxylation as well as subsequent precipitation reaction with nZVI. Among them, adsorption, reduction, and oxidation processes are the predominant processes in this regard. The most typical one is adsorption where oxygen-containing functional groups on the surface of various adsorbents including nZVI-based materials have been confirmed with large number of active sites or functional groups [71–72]. The main mechanism in nZVI/H₂O system occurs in the presence of an oxygen environment and Cr(VI), Cu(II), Cd(II), Ni(II), and Zn (II) ions can be effectively adsorbed on its surface [71, 73–75]. For heavy metals, especially the divalent metals, the possible mechanism of the interaction with nZVI supported/impregnated composites is shown in Fig. 3.

Multivalent heavy metal ions undertake the multistep process where Fe⁰ acts as an electron donor to many heavy metal ions [76–77]. Reduction reaction includes two distinct mechanisms: (1) the reduction of heavy metals by Fe⁰ directly [78]; (2) the primarily adsorption of heavy metals on the core–shell structure of nZVI and then gradually reduction of adsorbed heavy metals by Fe²⁺ derived from nZVI [79]. In the reduction process, the initial valence of heavy metal ions reduced and formed more stable valence and sometimes it gives synergistic effect [78]. nZVI showed possible reduction process of Pb(II) to Pb(0); Sb(III) to Sb(0), and Cr(VI) to Cr(III) [5]. Reduction process could be useful and beneficial to the in situ remediation of some unstable heavy metal ions from the natural environment. The oxidation process could be rare in the removal of heavy metal ions on nZVI-based materials but with the aid of Fenton reaction in the presence of oxygen, the oxidization of heavy metal ions in aqueous solutions is possible [80]. As(III) could be oxidized partially to As(V) by nZVI using H₂O₂ as oxidizing agent where Fe⁰

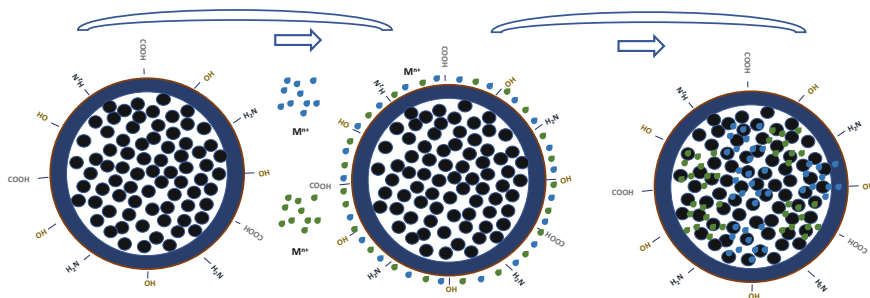


Fig. 3 Schematic representation of polymer coated (chitosan) zero-valent iron beads for the removal of heavy metals. The polymer coated nZVI at the left hand figure representing the functional groups on the surface. In the middle figure, the synthesized beads are exposed in aquatic heavy metals where the surface functional groups are occupied by metal ions. Subsequently at the right hand figure, the metal ions further penetrates into the core of the beads

accelerates the oxidizing capacity and forms various derivatives of iron, and it was beneficial for the separation of heavy metal ions. Other than the above-mentioned removal processes, magnetic interaction forces, van der Waals forces, electrostatic interactions and specific surface bonding are also effective for nZVI to acquire synergistic effect. As(III), Cr(III), and Pb(II) from the mixture solutions can be effectively removed by nZVI where the interaction mechanisms between adsorbents and target metals were attributed to adsorption, reduction, ion exchange reaction, hydroxylation, and even subsequent precipitation, which is beneficial for the aggregation of pollutants. Thus, the true interaction mechanism between heavy metal ions and nZVI-based materials could be understood via to real reaction conditions. nZVI is found effective to remedy heavy metals in batch experiments from aqueous solution where some experimental parameters, e.g. pH, contact time, dosage of adsorbent, temperature, coexisting oxy-anions, and cations are very important to consider. Various kinds of nZVI-based materials have shown great adsorption capacity for heavy metal ions from environment, and the main adsorption parameters were summarized in Table 2.

2.3.2 Removal of Organic Compounds

nZVI is found effective for the removal of persistent, toxic, and non-biodegradable pollutants from environment. Toxic and persistent organic compounds are now-a-days being used and emitted into the environment from various industries, such as stabilizers, preservatives, insecticides, pharmaceuticals industries, etc. These compounds also originated from our household operation and, pharmaceuticals and personal care products, e.g. antibiotics, and posing threat to the ecosystem and human health. The adsorption and reducing capacity of nZVI is capable to reduce and modify many organic functional groups, thereby to transform toxic compounds to less harmful derivatives. Polycyclic aromatic hydrocarbons (PAHs), anthracene

Table 2 Application of nZVI and its derivatives for the removal of both heavy metals and organic compounds from water

nZVI derivatives	Target pollutants	Interaction mechanism	Surface area ($\text{m}^2 \text{g}^{-1}$)	Effective pH	Removal capacity (mg g^{-1})	References
Bare nZVI $\text{FeCl}_3 \cdot 6\text{H}_2\text{O} + \text{NaBH}_4$	As(III), As(V), Ba(II), Cd(II), Co(II), Cu(II), Cr (VI)	Adsorption, reduction, ion exchange, hydroxylation, precipitation.	14.2–33.5	6.5–8	~769.2	[9–14]
Amino-functionalized nZVI (APS-nZVI) nZVI- Fe_3O_4 ; siniguelas waste-modified (S-NaOH- nZVI); coated nZVI; G-nZVI; $\text{Mg}(\text{OH})_2$ -supported nZVI	Pb(II)	Adsorption and reduction	5–40.2	5–7	100–1,986	[19]
MWCNT-nZVI- $\text{FeSO}_4 \cdot 7\text{H}_2\text{O} + \text{NaBH}$	Cr(VI)	Adsorption, reduction	–	7	200	[17]
Magnetic Fe_3O_4 /graphene-supported nZVI	Cr(VI)	Van der Waals force, magnetic interaction	–	8	66.2	[20]
Activated carbon supported-nZVI (nZVI/AC)	As(III)	Adsorption	69.4	6.5	18.2	[16]
Bentonite supported nZVI	Cr(VI)	Reduction, electron transport	39.94	6	73	[18]
Zeolite supported nZVI	Pb(II)	Adsorption	29.1	5.5	105.5	[8]
$\text{Al}(\text{OH})_3$ supported nZVI	4-Nitrophenol	Adsorption	–	7.3	4- Aminophenol	[103]
Diatomite supported nZVI	Bisphenol A	Adsorption	–	5.75	CO_2 , H_2O	[104]
Polyphenols supported nZVI	Amoxicillin	Adsorption	–	3	CO_2 , H_2O	[105]
PVP supported nZVI	Tetracycline	Adsorption	–	6.5	$\text{C}_{19}\text{H}_{26}\text{O}$	[106]
Cellulose supported nZVI	Methylene blue, methylene blue, methyl orange	Decomposition	–	5.96	–	[87]
Graphene supported nZVI	Trichloronitromethane	Adsorption	–	6.5	Methylamine	[107]

and phenanthrene from aqueous systems [81] can be removed by nZVI/SiO₂ adsorbent which exhibited good reusability over 10 cycles. Coated or supported nZVI has suspension stability, longevity, and low corrosion and is also active in the reductive 4-nitrophenol removal from water.

The coated nZVI, e.g. carbon coat mediated by Pd, accelerated the Fenton reaction and thus effectively removed phenol [82]. The bentonite-supported nZVI/persulfate system attained synergistic effect for the dual removal of Cr(VI) and phenol. Bisphenol A (BPA) can be interacted on an nZVI/diatomite/organosilane composite that is prepared by grafting an acid precursor, 3-mercaptopropyl trimethoxysilane, onto diatomite [83]. The steroidal estrogen 17 α -ethinylestradiol (EE2) is a model endocrine disrupting chemical which can be degraded by using commercial nZVI at pH 3, 5, and 7 under different oxygen conditions [84]. The degradation of amoxicillin (AMX), a common antibiotic, in water can be performed using green nZVI made by oak leaves extract [85]. nZVI triggers Fenton reaction and was applied as a reductant to remove antibiotic metronidazole (MNZ) from deoxygenated water [86]. The removal of amoxicillin (AMX) and ampicillin (AMP) from water are found effective on the supported nZVI than bare one. The ultrasound bound nZVI effectively reduced both norfloxacin and nitrate through and de-passivating nZVI. Polyvinylpyrrolidone (PVP) modified nZVI can be effectively used for tetracycline removal from water [87]. Several degradation products were identified on both the composite surface and treated solution originating from tetracycline degradation via loss of N-methyl, amino, hydroxyl, carbonyl, and formyl groups, indicating that nZVI/PVP adsorbed both tetracycline and its degradation products.

Organic dyes are not-biodegradable and toxic, therefore they seek special attention for their possible removal from industrial wastewater in the form of discoloration, degradation, and physical adsorption processes. Organic dyes such as methylene blue (MB) in water utilize adsorption, reduction, degradation, and/or precipitation processes, all four reaction paths, depending on the pH of the solution and oxygen content [88]. Other than methylene blue, malachite green (MG), methyl violet 2B (MV), Rhodamine B (RhB) [89], Orange II dye [90], azo dye [91], acid red organic dye [92], methyl orange dye can also be removed from solution using both bare nZVI and modified nZVI. Removal of halogenated compounds, perfluorinated compounds, perfluorooctanoic acid, perfluorooctane sulfonate, and halonitromethanes trichloronitromethane from water and wastewater is technically challenging. nZVI flakes are highly effective to degrade them under certain experimental conditions (Table 2). In addition, chlorinated aliphatic compounds, namely 1,1-dichloroethane, 1,1,1-trichloroethane, tetrachloromethane, 1,2-dichloroethane, trichloroethene, tetrachloroethene, 1,1,2,2-tetrachloroethane [93], trichloroethylene, tetrachloroethylene [94] along with chloramphenicol, florfenicol [95], diazepam (DZP), organophosphorus insecticides [96], polybrominated diphenyl ethers, decabromodiphenyl ether [97], decabromodiphenyl ether [98] are all successfully eradicated by nZVI and its composites where capping layer on nZVI strongly influences the reactivity of NPs. Other than surface water, nZVI flakes are similarly applicable and effective to eliminate the halogenated compounds from groundwater

and soil [99]. Other than heavy metals, metalloids and organic compounds, nZVI acts as an effective reducing material for the removal of bromate [100], nitrate [101], ammonium, and perchlorate ions [102] from water.

2.4 Toxicity of nZVI and Future Prospects

Heavy metals and its composites along with the other organic pollutants into the environment are inevitable and poisonous, therefore, their remediation in the environment is particularly important and urgent. Iron is regarded as a green material but sometimes it raises concerns as it generates reactive radical species and reduces many vital components and eventually forms a more toxic material. nZVI may impact on some essential microorganisms and alter the overall sensitivity of bacterial communities. Bare nZVI has strong bactericidal effect and able to generate reactive oxygen species at the presence of oxygen, which can cause oxidative stress for microorganisms [145]. nZVI was found to cause oxidative damage to both proteins and lipids [146] and the toxicity depends on its particle size and dose. Apart from few limitations of bare nZVI, e.g. high reactivity with oxygen and water, and tendency to aggregate, it possesses several advantages due to its small size, higher surface area, reactivity, higher adsorption capacity, and higher mobility which enable nZVI reactive to many organic and inorganic toxic pollutants in the environment. The in-situ application capability of nZVI makes it a good alternative to the contaminated groundwater, soil, industrial, and municipal wastewaters treatment. In addition, modified composites of nZVI display synergistic effect with increased stability, mobility, and adsorption properties. The recent addition in the synthesis sector of nZVI is the green methods which trigger the volume production and economic benefit. The future researches focus on to reduce the toxicity and other disadvantages of the application of nZVI in water purification and environmental remediation. Most importantly, the sustainable application for environmental remediation along with its long-term impact on environment should be accomplished in reference to future endeavor. Alongside, the effort should be continued to improve properties and to understand reaction mechanisms and long-term biological effects.

3 Nanomaterials in Environmental Remediation

3.1 Synthesis of Nanomaterials

Recently, nanomaterials have been raised immense attention in the sector of environmental remediation due to their unique chemical, physical, thermal, and mechanical properties [111]. The size and shape of the nanomaterials keeps pivotal role in controlling their properties and subsequently applications. Therefore, to obtain efficient size, shape, and stable nanomaterials researchers are searching various

synthesis methods [112]. Up to date two major methods have been found for the synthesis of nanoparticles. First one is the top-down (breakdown) method where external force is applied to a solid leading to its breakup into the smaller particles. And, second one is the bottom-up (build up) method where particles are produced from the atom of gas or liquid based on atomic transformation or molecular condensation [113].

Top-Down Method In top-down method solid substances are broken down following several techniques such as photolithography, scanning lithography, laser machining, soft lithography, nanocontact printing, nanosphere lithography, colloidal lithography, scanning probe lithography, ion implantation, diffusion, and deposition [114]. Though top-down method has been playing significant role in the process of nanomaterial synthesis, several limitations have also arisen in this process such as imperfections of the developed materials, high expense, requisite of finished materials with high surface area and longer etching times [115].

Bottom-Up Method In the bottom-up approach, nanomaterials are synthesized by building upon single atoms or molecules, where controlled segregation of atoms or molecules is assembled to get the desired nanoparticles (2–10 nm size range) [114]. Bottom-up approach is roughly divided into solid phase method and liquid phase method where solid phase method is of mainly two types: chemical method and physical method. In chemical method, a chemical reaction involves in chemical vapor deposition method (CVD), whereas evaporated material is cooled down in physical vapor deposition method (PVD). In CVD method, less than 1 μm sized nanoparticles can be produced. Therefore, CVD method is more suitable for the production of ultrafine structured nanoparticles due to the chemical reaction in gaseous phase. In CVD method to perform the high temperature chemical reaction, heat source is required such as chemical flame, plasma process, laser, or electric furnace. On the other hand, in PVD method evaporation of the solid or liquid material resulting vapor is cooled down rapidly in order to yield the desired nanoparticles [116]. However, among all of the methodologies liquid phase synthesis methods are preferred for the preparation of inorganic nanoparticles due to the several advantages, such as security, comparatively low energy consumption, possibility of reactant recovery, and homogeneity of the precursors and control of particle sizes and morphologies [117]. Liquid phase methods are roughly divided into chemical reduction method and sedimentation methods. Generally, sedimentation method is a sol gel process and this method is extensively used in the fabrication of metal oxide nanoparticles. In this technique a solution of metal alkaloid is transformed into a sol by hydrolysis. Other methods included in sedimentation method are co-precipitation, hydrolysis, alkaline precipitation, and colloidal chemistry [116]. Various methods of nanoparticles synthesis have been summarized in Fig. 4. In chemical reduction method chemical reduction is carried out in the metal ion to their oxidation states; the process is cost-effective, requires easily handled equipment or instruments and able to yield large quantities of nanoparticles in a short time; thus, this method is widely used in the environmental remediation. Chemical reduction method includes ozone/UV radiation/ H_2O_2 oxidation, photocatalytic

degradation, supercritical water oxidation, the Fenton method, sonochemical degradation, electrochemical method, electron beam process, solvated electron reduction, permeable reactive barriers of iron, and other valent metals and enzymatic treatment methods and green synthesis [118].

Green Synthesis Method Recently, green synthesis method for the synthesis of nanoparticles has created immense attention to the researchers. In this synthesis process no other toxicant is needed to achieve the nanoparticles. Moreover, this process is cost-effective and environmentally friendly, thus this process is named as green synthesis. For instance, researchers place a great deal of effort for the biosynthesis of inorganic nanoparticles especially metal nanoparticles, using microorganisms and plants [112]. Both live and dead microorganisms are used for the fabrication of nanoparticles. A bunch of studies reported about the biosynthesis of nanoparticles using prokaryotic bacteria such as *Pseudomonas stutzeri*, *Lactobacillus*, and *Desulfovibrio desulfuricans* for silver, gold, and palladium nanoparticles, respectively [119]. However, synthesis of metal nanoparticles by eukaryotic organisms later accomplished with some excellent works based on fungi. This shifting from bacteria to fungi is a milestone of developing nano factories that added advantages in the processing of nanomaterials. Due to the simplicity of processing biosynthetic method using plant extracts it raises the attention as an alternative to chemical and physical methods of synthesis [119]. In this process usually plant or any part of the plant is used as extraction which acts as reducing and capping agent. Water is the most available and well-accepted solvent for the preparation of aqueous extraction of plant; though ethanolic or methanolic extraction has been also used by several researchers in nanoparticle synthesis. Plant extraction is then mixed with the metal ion solution in a controlled environment, subsequently after certain period nanometal precipitation settled down (Fig. 4). After washing and centrifugation, the

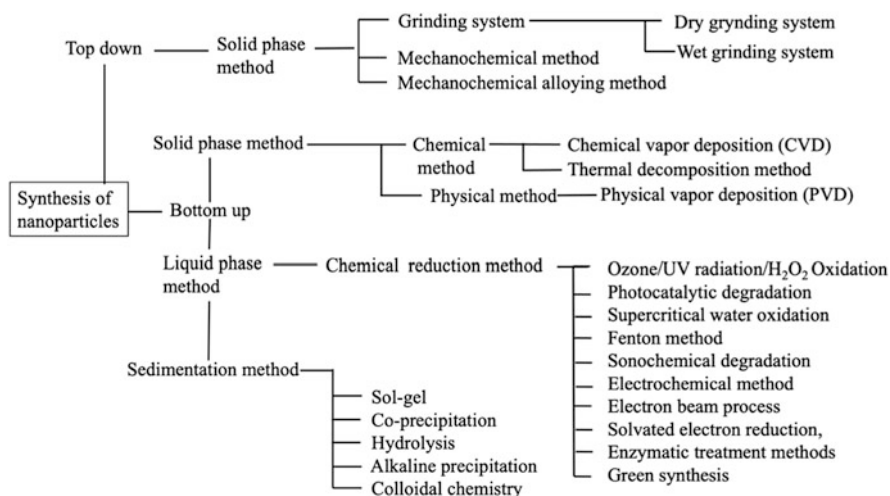


Fig. 4 Overview of synthetic and green methods for nanoparticle synthesis



Fig. 5 Green synthesis of nanoparticles using plant extract

precipitate was dried and the desired nanoparticles were collected in a desiccator. However, still clear information about reducing agent, stabilizing or capping agent responsible in green synthesis of nanoparticles is not found yet. A lot of studies reported about the reducing agent in green synthesis process. From our study we claimed that amino acid ($R-CH(NH_2)-COOH$) containing lone pairs of electrons facilitates the reduction of metallic ion for the formation of Ag-NPs in the ambient condition [120]. Flavonoids and alkaloids present in the leaf extracts also can act as a reducing and capping agent in the synthesis of Ag, TiO_2 , and MnO nanoparticle synthesis [121, 122, 123]. According to Jiale et al., polyols are responsible for the reduction of silver and chloraurate ions in silver and gold nanoparticles synthesis, whereas alkaloids, flavones, and anthracenes are acted as the capping ligands of the nanoparticles [119] (Fig. 5).

3.2 Nanoparticles with Potential Remediation Applications

Nanoscale materials are developing for the potential use in the environmental remediation either in situ or ex situ processes. Titanium dioxide (TiO_2), silver (Ag), manganese oxide (MnO), gold (Au), nanotubes, ferritin, dendrimers, metalloporphyrinogens, and swellable organically modified silica (SOMS) are some nanoscale materials used in environmental remediation [118]. Table 3 summarizes some of the nanoscale materials that have already been used for various environmental remediation applications. Here we will briefly discuss some of the advanced nanomaterials that are recently used in environmental remediation of a variety of pollutants.

Titanium Dioxide Nanoparticles (TiO_2 -NPs) TiO_2 -NPs acquire unique physiochemical properties such as high specific surface area, proper electronic

Table 3 Nanoscale materials in environmental remediation

Nanomaterials	Application in remediation	Reference
TiO ₂	Purification and treatment of contaminant air, water, and bacteria	[124, 125]
Titanate nanotubes	Nitric oxide	[126]
Ag	Disinfection of water	[118]
MnO	Methylene blue	[127]
Au	Inorganic mercury from drinking water	[128]
Ag-doped TiO ₂	2,4,6-Trichlorophenol	[129]
Ag-doped TiO ₂ nanofibers	Methylene blue	[130]
Cu/Fe/Ag-doped TiO ₂	Nitrate (NO ₃ ⁻)	[131]
Silica nanoparticles	Polycyclic aromatic hydrocarbons from aqueous solutions	[132]
PAMAM dendrimer composite membrane	CO ₂ separation from a feed gas mixture of CO ₂ and N ₂ on porous substrates	[133]
Gold NPs with chitosan polymer coating	Zn ²⁺ , Cu ²⁺ in aqueous solution	[134]
Poly(methacrylic acid)-grafted chitosan/bentonite	Th ⁴⁺	[135]
Carbon nanotubes	Fluoride	[136]
Multiwall carbon nanotube	Zn ²⁺	[137]
Bimetallic NPs	Water, soil from chlorinated and brominated contaminants	[138]
Amine-modified xerogels	Gaseous CO ₂ , H ₂ S	[139]
Amine-modified aluminosilicates and porous silica	Gaseous – CO ₂ , aldehydes, ketones	[140]
Carboxylic acid-functionalized mesoporous silica	Wastewater-cationic dyes, heavy metals	[141]
Amino-functionalized mesoporous silica	Heavy metals from wastewater	[142]
Thiol-functionalized mesoporous silica	Heavy metals from water	[143]

band structure, high quantum efficiency and stability, and thus, TiO₂-NPs perform numerous applications in cosmeceutical, pharmaceutical, optical, and in commercial sectors [144]. However, nanoscale TiO₂ has potentiality to mineralize a variety of herbicides, insecticides, and pesticides via photocatalysis. These particles have unique ability to convert highly toxic contaminants into lower toxic compounds; for example, TiO₂ nanotubes are effective at high temperatures and capable to reduce concentrations of the chemical contaminants by more than 50% [145]. Another important application of TiO₂ NPs is the removal of cyanide from the wastewater. Annual world production of cyanide is 1.4 million tons that is mainly used in the gold mining, but a part of the cyanide used in the industry directly comes into the environment as it is highly toxic. Though many removal techniques of cyanide remediation are offered, most of them are costly and time consuming. Thus, photocatalytic techniques of TiO₂ NPs can remediate cyanide from the wastewater

through the hydrolysis and this process is much convenient than others [145]. Similarly, TiO₂ activated carbon composite shows photocatalytic degradation application of β -naphthol from the wastewater [145]. During photocatalysis when TiO₂ suspension is irradiated with more than 3.2 eV of light energy, then TiO₂ being activated combines with water or dissolved oxygen or both and forms highly reactive species. Thus, these reactive species including hydroxyl radical and the superoxide radical anion can oxidize and degrade a wide range of contaminants [146].

Silver Nanoparticles (Ag-NPs) Ag-NPs have been received a great interest due to their cost-effectivity, synthetic versatility, and chemical-physical properties. Therefore, Ag-NPs are widely used in versatile sectors such as medicine, medicinal device, cosmetics, industry, electronics, environmental studies, etc. [112]. However, another recent application of Ag-NPs is found as monitoring and remediation of water pollution. Ag-NPs are widely used in plasmonic sensors for monitoring and oxidative degradation for remediation of pollutant such as heavy metals and organic compounds. In this aspect, surface functionalization could be changed with a specific ligand and thus selective particles are created for a particular analyte. Also, the sensitivity of the NPs can be improved through the optimization of the degree of surface functionalization [146]. For the detection and monitoring of the Hg in water environment, the authors [147] developed Ag-NPs with amine functionalized silicate sol-gel matrix using different combination of silicate, surfactant, and cyclodextrin. Here, the authors found the formation of anisotropic Ag amalgam crystals which influenced the blue shift up or quenching of surface plasma resonance (SPR) band [147]. Based on this phenomena Sharma et al. developed a colorimetric sensor based on thiol-modified chitosan Ag-NPs which is simple, label-free, cost-effective, portable, selective, and sensitive; moreover, usable for the real-time detection of toxic Hg (II) ions in water. In the UV-vis spectra, blue shift of LSPR was observed in the solution of Md-Ch-Ag-NPs after addition of Hg²⁺. However, the change in SPR occurred due to the redox interaction between the Hg (II) ions and Ag-NPs. [148]. Another important potentiality of Ag-NPs is their photocatalytic activity which can be classified into two categories: plasmonic photocatalysts and semiconductor photocatalysts based on the LSPR effect of Ag-NPs and band gap excitation of Ag-containing compounds. In plasmonic excitation upon light irradiation, hot electron is released from Ag-NPs while in bandgap excitation a semiconductor containing Ag generates electron hole pair undergoing charge separation and transfer, and thus finally catalytic reaction happened. Recent studies showed that Ag-based visible light responsive photocatalysts is highly potential for the decomposition of organic pollutant, selective organic transformation, bacteria destruction, water oxidation, and purification [146]. Antibacterial activity of Ag-NPs is an imperative property which lifts them lucrative to the remediation sector. In searching of the mechanism by which Ag-NPs work as antibacterial agent, various activities have been proposed which can be summarized in three actions: (1) alteration of bacterial membrane (2) ionization of Ag-NPs (3) generation of ROS and subsequently damage of DNA/RNA, protein and finally cell death [120].

Manganese Oxide Nanoparticles (MnO_x-NPs) Manganese oxides (MnO_x) have chemical stability in both the acidic and basic conditions with excellent potentiality to form complex with heavy metal ions (e.g., Cd, Cu, Zn, Pb), and thus MnO_x is considered as the potential adsorbent for the pollutant remediation. Manganese exists in nature with different single valence states such as MnO, Mn₂O₃, and MnO₂ as well as mixed valence states such as Mn₃O₄ and Mn₅O₈ [149]. Manganese dioxide (MnO₂) nanoparticles exhibit potential adsorption of Pb (II), Cd (II), and Cu (II) ions in aqueous solution without being affected by coexisting ions (Na⁺ and Mg²⁺) [150]. According to Wang et al., heavy metal adsorption mechanism by layered MnO₂ nanoparticle depends on the complexation of the Mn-OH groups on its surface [151]. However, it is to be noted that only nanosized MnO₂ contains an active surface area but due to its high surface energy it is likely to form aggregation which greatly reduces specific surface area and subsequently decreases the capacity of adsorbing heavy metal ions. Due to the large surface area MnO-NPs can be supported on a carrier to enhance its dispersibility and adsorption capacity [152]. For instance, MnO₂ NPs loaded on the graphene oxide (Wang 2005) ordered mesoporous silica, [153] and ordered mesoporous carbon materials [152] and exhibited higher energy storage, catalysis, and adsorption capacity than that of the aggregated MnO₂-NPs. Manufacturing of materials with large specific surface area is costly and difficult, thus loading of MnO₂ NPs on the low-cost materials having large specific surface area is a promising approach [152]. Mn oxides are considered as the powerful oxidants having high-reducing potentiality for remediation purpose including degradation of organic pollutants [127]. Oxides and hydroxides of Mn³⁺ and Mn⁴⁺ are reported as potential for the oxidation of a variety of natural and xenobiotic organic compounds such as catechol, quinines, substituted phenols, aromatic amines, pesticides, and trimanganese tetraoxide [152]. However, Mn₃O₄ contains both di- and tri-valents of Mn and has strong reducing potential than that of other Mn oxides and thus in our previous study we have reported the efficiency of Mn₃O₄ in oxidative degradation and mineralization of methylene blue [127]. The synthesis of different oxides of manganese can be performed with various methods. However, in our previous study we have synthesized three different oxides of Mn such as Mn₃O₄, Mn₅O₈, and Mn₂O₃ via a single gel formation route with different surface morphology as shown in Fig. 6 [149]. Briefly, aqueous solution of KMnO₄ was reduced with the aqueous solution of glycerol at 80°C and a gel network was

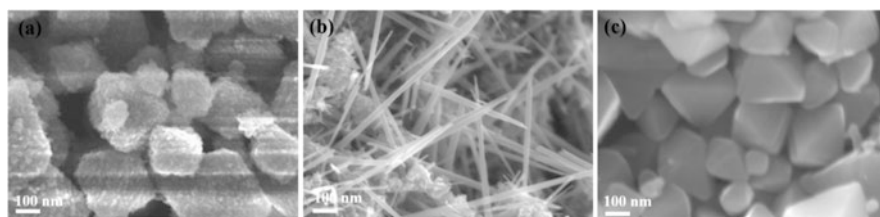


Fig. 6 Synthesis of three different oxides of Mn, (a) Mn₃O₄, (b) Mn₅O₈, and (c) Mn₂O₃ via a single route at 80, 350 and 700°C, respectively

formed. The solid portion was separated through centrifugation which was identified as Mn_3O_4 . Then the Mn_3O_4 was heated at different temperatures and two other oxides of Mn, Mn_5O_8 , and Mn_2O_3 were formed at 350 and 700°C, respectively. The three different oxides of Mn, i.e., Mn_3O_4 , Mn_5O_8 , and Mn_2O_3 were found to show distinct magnetic property [154]. Thus, it can be assumed that the three oxides can be used in different types of remediation purposes.

Gold Nanoparticles (Au-NPs) Au-NPs have also been used in both the detection and remediation of contaminants from the water. Large surface area per volume creates large adsorption capacity in comparison with the conventional adsorbents. In addition, strong and high SPR in the visible region allows them to be utilized as colorimetric agents for the water pollutant detection. Colorimetric agent prepared by Au-NPs is highly sensitive and selective to detect water pollutant in comparison with the conventional colorimetric agents. Therefore, Au-NPs are used in the detection of toxic heavy metals such as Pb, Hg, and also pesticides [155]. Analyte induced color shift is the main property of detection of the pollutant in the water. Heavy metal ion and pesticides can be remediated from the water by Au-NPs but in that case after adsorption the separation of the Au-NPs from the pollutant is difficult. To solve this problem Lisha et al. prepared very stable Au-NPs where the authors enable to recover and reuse Au-NPs after adsorption, though still more intensive research is needed to finalize their approach [156].

4 Conclusion

Though various nanomaterials deal with various aspects of environmental remediation, there is a fact of its own toxicity. Various studies talk with the intensity of nanomaterials induced toxicity in their research. Nanoparticles having the size of 5–20 nm can penetrate into the skin and thus interact with the biological systems. These nanoparticles are also very effective for the healing of acne, eczema, or wounds and thus subsequently reduce complications [120]. Several studies reported that NPs induced toxicity in different organisms. However, researchers are concerned about the issue of toxicity reduction of nanoparticles. In our previous study, we also tried to synthesize Ag-NPs having antibacterial activity with reduced toxicity [120]. For the better implementation of the NPs in remediation it is important to understand the mechanism of reactivity of NPs. Therefore, more intensive research is still needed in this sector. With unveiling the mechanism of reactivity of NPs, engineered NPs can be used in various sectors of environmental remediation.

References

1. Lu HJ, Wang JK, Ferguson S et al (2016) Mechanism, synthesis and modification of nano zerovalent iron in water treatment. *Nanoscale* 8:9962
2. Zou Y, Wang X, Khan A et al (2016) Environmental remediation and application of nanoscale zero-valent iron and its composites for the removal of heavy metal ions: a review. *Environ Sci Technol* 50:7290–7304
3. Chen X, Ji D, Wang X et al (2017) Review on nano zerovalent iron (nZVI): from modification to environmental applications. *Earth Environ Sci* 51:012004
4. Pasinszki T, Krebsz M (2020) Synthesis and application of zero-valent iron nanoparticles in water treatment, environmental remediation, catalysis, and their biological effects. *Nano* 10: 917
5. Sikder MT, Mihara Y, Islam MS et al (2014) Preparation and characterization of chitosan-cboxymethyl- β -cyclodextrin entrapped nano zerovalent iron composite for Cu (II) and Cr (IV) removal from waste water. *Chem Eng J* 236:378–387
6. Sikder MT, Kubota R, Akter M et al (2019) Adsorption mechanism of Cu(II) in water environment using chitosan- nano zero valent iron-activated carbon composite beads. *Desalin Water Treat* 145:202–210
7. Sikder MT, Tanaka S, Saito T et al (2014) Synthesis and application of a arsenic sorbent using zerovalent iron impregnated chitosan-cboxymethyl- β -cyclodextrin composite beads. *J Environ Chem Eng* 2:370–376
8. Miranda NA, Baltazar SE, Garcia A et al (2016) Nanoscale zero valent supported by zeolite and montmorillonite: template effect of the removal of lead ion from an aqueous solution. *J Hazard Mater* 301:371–380
9. Yuan C, Lien HL (2006) Removal of arsenate from aqueous solution using nanoscale iron particles. *Water Qual Res J Can* 41:210–215
10. Kanel SR, Manning B, Charlet L et al (2005) Removal of arsenic (III) from groundwater by nanoscale zero-valent iron. *Environ Sci Technol* 39:1291–1298
11. Kanel SR, Greneche JM, Choi H et al (2006) Arsenic(V) removal from groundwater using nano scale zero-valent iron as a colloidal reactive barrier material. *Environ Sci Technol* 40: 2045–2050
12. Celebi O, Uzum C, Shahwan T et al (2007) A radiotracer study of the adsorption behavior of aqueous Ba²⁺ ions on nanoparticles of zero-valent iron. *J Hazard Mater* 148:761–767
13. Uzum C, Shahwan T, Eroglu AE et al (2008) Application of zero-valent iron nanoparticles for the removal of aqueous Co²⁺ ions under various experimental conditions. *Chem Eng J* 144: 213–220
14. Boparai HK, Joseph MO, Carroll DM (2011) Kinetics and thermodynamics of cadmium ion removal by adsorption onto nano zerovalent iron particles. *J Hazard Mater* 186:458–465
15. Karabelli D, Uzum C, Shahwan T et al (2008) Batch removal of aqueous Cu²⁺ ions using nanoparticles of zero-valent iron: a study of the capacity and mechanism of uptake. *Ind Eng Chem Res* 47:4758–4764
16. Zhu HJ, Jia YF, Wu X et al (2009) Removal of arsenic from water by supported nano zero-valent iron on activated carbon. *J Hazard Mater* 172:1591–1596
17. Lv XS, Xu J, Jiang GM et al (2011) Removal of chromium (VI) from wastewater by nanoscale zero-valent iron particles supported on multiwalled carbon nanotubes. *Chemosphere* 85:1204–1209
18. Shi LN, Zhang X, Chen ZL (2011) Removal of chromium (VI) from wastewater using bentonite-supported nanoscale zero-valent iron. *Water Res* 45:886–892
19. Jabeen H, Kemp KC, Chandra V et al (2013) Synthesis of nano zerovalent iron nanoparticles-graphene composite for the treatment of lead contaminated water. *J Environ Manage* 130:429–435

20. Lv XS, Xue XQ, Jiang GM et al (2014) Nanoscale zero-valent iron (nZVI) assembled on magnetic Fe₃O₄/graphene for chromium (VI) removal from aqueous solution. *J Colloid Interface Sci* 417:51–59
21. Crane RA, Scott TB (2012) Nanoscale zero-valent iron: future prospects for an emerging water treatment technology. *J Hazard Mater*:112–125. <https://doi.org/10.1016/j.jhazmat.2011.11.073>
22. Adusei-Gyamfi J, Acha V (2016) Carriers for nano zerovalent iron (nZVI): synthesis, application and efficiency. *RSC Adv* 6:91025–91044
23. Mackenzie K, Georgi A (2019) nZVI synthesis and characterization. In: Phenrat T, Lowry GV (eds) *Nanoscale zerovalent iron particles for environmental restoration, fundamental science to field scale engineering applications*. Springer, Cham, pp 45–95
24. Hahn H (1997) Gas phase synthesis of nanocrystalline materials. *Nanostruct Mater* 9:3–12
25. Suryanarayana C (2001) Mechanical alloying and milling. *Prog Mater Sci* 46:1–184
26. Li S, Yan W, Zhang WX (2009) Solvent-free production of nanoscale zero-valent iron (nZVI) with precision milling. *Green Chem* 11:1618–1626
27. Wang CB, Zhang WX (1997) Synthesizing nanoscale iron particles for rapid and complete dechlorination of TCE and PCBs. *Environ Sci Technol* 31:2154–2156
28. Kończak M, Oleszczuk P, Ok YS (2015) Review on nano zerovalent iron (nZVI): from synthesis to environmental applications. *Environ Sci Technol*. <https://doi.org/10.1016/j.cj.2015.11.046>
29. Sun H, Zhou G, Liu S et al (2012) Nano-Fe₀ encapsulated in microcarbon spheres: synthesis, characterization, and environmental applications. *ACS Appl Mater Interfaces* 4:6235–6241
30. Joseyphus RJ, Kodama D, Matsumoto T et al (2007) Role of polyol in the synthesis of Fe particles. *J Magn Magn Mater* 310:2393–2395
31. Seip CT, Connor CJO (1999) The fabrication and organization of self-assembled metallic nanoparticles formed in reverse micelles. *Nanostruct Mater* 12:183–186
32. Chen SS, Hsu HD, Li CW (2004) A new method to produce nanoscale iron for nitrate removal. *J Nanopart Res* 6:639–647
33. Huang L, Weng X, Chen Z et al (2014) Green synthesis of iron nanoparticles by various tea extracts: comparative study of the reactivity. *Spectrochim Acta A* 130:295–301
34. Machado S, Pinto SL, Grosso JP et al (2013) Green production of zero-valent iron nanoparticles using tree leaf extracts. *Sci Total Environ* 445:1–8
35. Phenrat T, Navid S, Kevin S et al (2007) Aggregation and sedimentation of aqueous nanoscale zerovalent iron dispersions. *Environ Sci Technol* 41:284–290
36. Phenrat T, Lowry GV (2014) Nanotechnology applications for clean water. *Ch* 30, pp 473–490
37. Kanel SR, Goswami RR, Clement TP et al (2008) Two dimensional transport characteristics of surface stabilized zero-valent iron nanoparticles in porous media. *Environ Sci Technol* 42: 896–900
38. Bonder MJ, Kiick KL, Papaefthymiou V et al (2007) Controlling synthesis of Fe nanoparticles with polyethylene glycol. *J Magn Magn Mater* 311:658–664
39. Phenrat T, Fritjof F, Tissa I et al (2011) Polymer-modified Fe₀ nanoparticles target entrapped NAPL in two dimensional porous media: effect of particle concentration, NAPL saturation, and injection strategy. *Environ Sci Technol* 45:6102–6109
40. Jiemvarangkul P, Zhang WX, Lien HL (2011) Enhanced transport of polyelectrolyte stabilized nanoscale zero-valent iron (nZVI) in porous media. *Chem Eng J* 170:482–491
41. Sita K, Harjyoti K, Chisholm BJ et al (2012) Simulating adsorption of organic pollutants on finite (8,0) single-walled carbon nanotubes in water. *Environ Sci Technol* 46:8887–8894
42. Saleh N, Sirk K, Liu Y et al (2007) Inorganic nanoparticles synthesis, applications and perspectives. *Environ Eng Sci* 24:45–57
43. Bezbaruah AN, Krajangpan S, Chisholm BJ et al (2009) Entrapment of iron nanoparticles in calcium alginate beads for groundwater remediation applications. *J Hazard Mater* 166:1339–1343

44. Velimirovic M, Schmid D, Wagner S et al (2015) Agar agar-stabilized milled zerovalent iron particles for in situ groundwater remediation. *Sci Total Environ.* <https://doi.org/10.1016/j.scitotenv.2015.11.007>
45. Dror I, Jacov OM, Cortis A et al (2012) Catalytic transformation of persistent contaminants using a new composite material based on nanosized zero-valent iron. *ACS Appl Mater Interfaces* 4:3416–3423
46. Cwiertny DM, Bransfield SJ, Livi KJT et al (2006) Exploring the influence of granular iron additives on 1,1,1-trichloroethane reduction. *Environ Sci Technol* 40:6837–6843
47. Zhang WX, Wang CB, Lien HL (1998) Treatment of chlorinated organic contaminants with nanoscale bimetallic particles. *Catal Today* 40:387–395
48. Xu FY, Deng SB, Xu J et al (2012) Mechanically synthesized SiO₂-Fe metal matrix composite for effective dechlorination of aqueous 2-chlorophenol: the optimum of the preparation conditions. *Environ Sci Technol* 46:4576–4582
49. Hosseini SM, Ataie-Ashtiani B, Kholghi M (2011) Nitrate reduction by nano-Fe/Cu particles in packed column. *Desalination* 276:214–221
50. Pasinszki T, Krebsz M (2020) Synthesis and application of zero-valent iron nanoparticles in water treatment, environmental remediation, catalysis, and their biological effects. *Nano* 10: 917
51. Kalhapure RS, Sonawane SJ, Sikwal DR et al (2015) Solid lipid nanoparticles of clotrimazole silver complex: an efficient nano antibacterial against *Staphylococcus aureus* and MRSA. *Colloids Surf B* 136:651–658
52. Singh R, Misra V (2015) *Handbook of nanoparticles*. Springer, pp 985–1007
53. Hoch LB, Mack EJ, Hydutsky BW et al (2008) Carbothermal synthesis of carbon-supported nanoscale zero-valent iron particles for the remediation of hexavalent chromium. *Environ Sci Technol* 42:2600–2605
54. Sun Z, Zheng S, Ayoko GA et al (2013) Degradation of simazine from aqueous solutions by diatomite-supported nanosized zero-valent iron composite materials. *J Hazard Mater* 263:768–777
55. Liu ZT, Gu CG, Mao Y et al (2015) Debromination of polybrominated diphenyl ethers by attapulgite-supported Fe/Ni bimetallic nanoparticles: Influencing factors, kinetics and mechanism. *J Hazard Mater* 298:328–337
56. Li XY, Ai LH, Jiang J (2016) Nanoscale zerovalent iron decorated on graphene nanosheets for Cr(VI) removal from aqueous solution: Surface corrosion retard induced the enhanced performance. *Chem Eng J* 288:789–797
57. Wang CB, Luo HJ, Zhang ZL et al (2014) Environmental nanotechnology for water purification. *J Hazard Mater* 268:124–131
58. Liu FL, Yang JH, Zuo J et al (2014) Graphene-supported nanoscale zero-valent iron: removal of phosphorus from aqueous solution and mechanistic study. *J Environ Sci* 26:1751–1762
59. Dai Y, Hu YC, Jiang BJJ et al (2016) Enhancing cleanup of environmental pollutants. *J Hazard Mater* 309:249–258
60. Tesh SJ, Scott TB (2014) Nano-composites for water remediation: a review. *Adv Mater* 26: 6056–6068
61. Ghaffar A, Zhang L, Zhu X et al (2018) Porous PVdF/GO nanofibrous membranes for selective separation and recycling of charged organic dyes from water. *Environ Sci Tech* 52. <https://doi.org/10.1021/acs.est.7b06081>
62. Li A, Tai C, Zhao ZS et al (2007) Debromination of decabrominated diphenyl ether by resin-bound iron nanoparticles. *Environ Sci Technol* 41:6841–6846
63. Li YC, Xiu ZM, Li TL et al (2013) Stabilization of Fe₀ nanoparticles with silica for enhanced transport and remediation of hexavalent chromium in groundwater. *ACS Symp Ser* 1124:307–326
64. Ling X, Li J, Zhu W et al (2012) Synthesis of nanoscale zero-valent iron/ordered mesoporous carbon for adsorption and synergistic reduction of nitrobenzene. *Chemosphere* 87:655–660

65. Liu TY, Zhao L, Sun DS et al (2010) Entrapment of nanoscale zero-valent iron in chitosan beads for hexavalent chromium removal from wastewater. *J Hazard Mater* 184:724–730
66. Lv XS, Xu J, Jiang GM et al (2011) Highly active nanoscale zero-valent iron (nZVI)-Fe₃O₄ nanocomposites for the removal of chromium(VI) from aqueous solutions. *J Colloid Interface Sci* 369:460–469
67. Lv XS, Xue XQ, Jiang GM et al (2014) Nanoscale zero-valent iron (nZVI) assembled on magnetic Fe₃O₄/graphene for chromium (VI) removal from aqueous solution. *J. Colloid Interface Sci* 417:51–59
68. Berge ND, Andrew RC (2009) Oil-in-water emulsions for encapsulated delivery of reactive iron particles. *Environ Sci Technol* 43:5060–5066
69. Shu HY, Chang MC, Chen CC et al (2010) Using resin supported nano zero-valent iron particles for decoloration of acid blue 113 azo dye solution. *J Hazard Mater* 184:499–505
70. Jiang ZM, Lv L, Zhang WM et al (2011) Nitrate reduction using nanosized zero-valent iron supported by polystyrene resins: role of surface functional groups. *Water Res* 45:2191–2198
71. Li J, Chen CL, Zhu K (2016) Nanoscale zero-valent iron particles modified on reduced graphene oxides using a plasma technique for Cd(II) removal. *J Taiwan Inst Chem Eng* 59: 389–394
72. Wang C, Luo HJ, Zhang ZL et al (2014) Removal of As(III) and As(V) from aqueous solutions using nanoscale zero valent iron-reduced graphite oxide modified composites. *J Hazard Mater* 268:124–131
73. Lv XS, Xue XQ, Jiang GM et al (2014) Nanoscale zero-valent iron (nZVI) assembled on magnetic Fe₃O₄/graphene for chromium (VI) removal from aqueous solution. *J Colloid Interface Sci* 417:51–59
74. Lazar P, Otyepka M (2012) Dissociation of water at iron surfaces: generalized gradient functional and range-separated hybrid functional study. *J Phys Chem C* 116:25470–25477
75. Wang CM, Baer DR, Amonette JE (2009) Morphology and electronic structure of the oxide shell on the surface of iron nanoparticles. *J Am Chem Soc* 131:8824–8832
76. Shu HY, Chang MC, Yu HH et al (2007) Reduction of an azo dye acid black 24 solution using synthesized nanoscale zerovalent iron particles. *J Colloid Interface Sci* 314:89–97
77. Zhang Y, Li YM, Zheng XM (2011) Removal of atrazine by nanoscale zero valent iron supported on organobentonite. *Sci Total Environ* 409:625–630
78. Liu MH, Wang YH, Chen LT et al (2015) Mg (OH)₂ supported nanoscale zero valent iron enhancing the removal of Pb(II) from aqueous solution. *ACS Appl Mater Interfaces* 7:7961–7969
79. Li YM, Cheng W, Sheng GD et al (2015) Synergetic effect of a pillared bentonite support on SE(VI) removal by nanoscale zero valent iron. *Appl Catal B* 174:329–335
80. Elsner M, Chartrand M, Vanstone N et al (2008) Identifying abiotic chlorinated ethene degradation: characteristic isotope patterns in reaction products with nanoscale zero-valent iron. *Environ Sci Technol* 42:5963–5970
81. Li J, Zhou Q, Liu Y et al (2017) Recyclable nanoscale zero-valent iron-based magnetic polydopamine coated nanomaterials for the adsorption and removal of phenanthrene and anthracene. *Sci Technol Adv Mater* 18:3–17
82. He D, Niu H, He S et al (2019) Strengthened Fenton degradation of phenol catalyzed by core/shell Fe-Pd@C nanocomposites derived from mechanochemically synthesized Fe-Metal organic frameworks. *Water Res* 62:151–160
83. Ma L, He H, Zhu R et al (2016) Bisphenol A degradation by a new acidic nano zero-valent iron diatomite composite. *Cat Sci Technol* 6:6066–6075
84. Karim S, Bae S, Greenwood D et al (2017) Degradation of 17 α -ethinylestradiol by nano zero valent iron under different pH and dissolved oxygen levels. *Water Res* 125:32–41
85. Machado S, Pacheco JG, Nouws HPA et al (2017) Green zero-valent iron nanoparticles for the degradation of amoxicillin. *Int J Environ Sci Technol* 14:1109–1118
86. Chen J, Qiu X, Fang Z et al (2012) Removal mechanism of antibiotic metronidazole from aquatic solutions by using nanoscale zero-valent iron particles. *Chem Eng J* 181:113–119

87. Chen H, Luo H, Lan Y et al (2011) Removal of tetracycline from aqueous solutions using polyvinylpyrrolidone (PVP-K30) modified nanoscale zero valent iron. *J Hazard Mater* 192: 44–53
88. Sun X, Kurokawa T, Suzuki M et al (2015) Removal of cationic dye methylene blue by zero-valent iron: Effects of pH and dissolved oxygen on removal mechanisms. *J Environ Sci Health A* 50:1057–1071
89. Son YH, Lee JK, Soong Y et al (2012) Heterostructured zero valent iron-montmorillonite nanohybrid and their catalytic efficacy. *Appl Clay Sci* 62:21–26
90. Yang Y, Sun M, Zhou J et al (2020) Degradation of orange II by Fe@Fe₂O₃ core shell nanomaterials assisted by NaHSO₃. *Chemosphere* 244:125588
91. Barreto-Rodrigues M, Silveira J, Zazo JA et al (2017) Synthesis, characterization and application of nanoscale zero-valent iron in the degradation of the azo dye Disperse Red 1. *J Environ Chem Eng* 5:628–634
92. Xu H, Tian W, Zhang Y et al (2018) Reduced graphene oxide/attapulgite-supported nanoscale zero-valent iron removal of acid red 18 from aqueous solution. *Water Air Soil Pollut* 229:388
93. Li S, Yan W, Zhang WX (2009) Solvent-free production of nanoscale zero-valent iron (nZVI) with precision milling. *Green Chem* 11:1618–1626
94. Ribas D, Peskova K, Jubany I et al (2019) High reactive nano zero-valent iron produced via wet milling through abrasion by alumina. *Chem Eng J* 366:235–245
95. Cao Z, Liu X, Xu J et al (2017) Removal of antibiotic florfenicol by sulfide-modified nanoscale zero-valent iron. *Environ Sci Technol* 51:11269–11277
96. Mehrotra N, Tripathi RM, Zafar F et al (2017) Catalytic degradation of dichlorvos using biosynthesized zero valent iron nanoparticles. *IEEE Trans Nanobioscience* 16:280–286
97. Tan L, Lu S, Fang Z et al (2017) Enhanced reductive debromination and subsequent oxidative ring-opening of decabromodiphenyl ether by integrated catalyst of nZVI supported on magnetic Fe₃O₄ nanoparticles. *Appl Catal B Environ* 200:200–210
98. Tan L, Liang B, Cheng W et al (2016) Effect of solvent on debromination of decabromodiphenyl ether by Ni/Fe nanoparticles and nano zero-valent iron particles. *Environ Sci Pollut Res* 23:22172–22182
99. Chen SS, Hsu HD, Li CW (2004) A new method to produce nanoscale iron for nitrate removal. *J Nanopart Res* 6:639–647
100. Wang Q, Snyder S, Kim J et al (2009) Aqueous ethanol modified nanoscale zero valent iron in bromate reduction: synthesis, characterization, and reactivity. *Environ Sci Technol* 43:3292–3299
101. Ryu A, Jeong SW, Jang A et al (2011) Reduction of highly concentrated nitrate using nano scale zero-valent iron: effects of aggregation and catalyst on reactivity. *Appl. Cat. B: Environ.* 105:128–135
102. Cao J, Elliott D, Zhang (2005) Perchlorate reduction by nanoscale iron particles. *J Nanopart Res* 7:499–506
103. Hu YB, Li XY (2018) Influence of a thin aluminum hydroxide coating layer on the suspension stability and reductive reactivity of nanoscale zero-valent iron. *Appl Catal B Environ* 226:554–564
104. Ma L, He H, Zhu R et al (2016) Bisphenol A degradation by a new acidic nano zero-valent iron diatomite composite. *Cat Sci Technol* 6:6066–6075
105. Machado S, Pacheco JG, Nouws HPA et al (2017) Green zero-valent iron nanoparticles for the degradation of amoxicillin. *Int J Environ Sci Technol* 14:1109–1118
106. Wang X, Wang P, Ma J et al (2015) Synthesis, characterization, and reactivity of cellulose modified nano zero-valent iron for dye discoloration. *Appl Surf Sci* 345:57–66
107. Chen HF, Cao Y, Wei E et al (2016) Facile synthesis of graphene nano zero-valent iron composites and their efficient removal of trichloronitromethane from drinking water. *Chemosphere* 146:32–39
108. Choi CJ, Tolochko O, Kim BK (2002) Nanoparticles in the fight against parasites. *Mater Lett* 56:289–294

109. Park SJ, Kim S, Lee S et al (2000) ChemInform abstract: synthesis and magnetic studies of uniform iron nanorods and nanospheres. *ChemInform* 31:8581–8582
110. Hoch LB, Mack EJ, Hydutsky BW et al (2008) Carbothermal synthesis of carbon-supported nanoscale zero-valent iron particles for the remediation of hexavalent chromium. *Environ Sci Technol* 42:2600–2605
111. Guerra FD, Attia MF, Whitehead DC, Frank A (2018) Nanotechnology for environmental remediation: materials and applications. *Molecules* 23:1760. <https://doi.org/10.3390/molecules23071760>
112. Akter M, Sikder MT, Rahman MM et al (2018) A systematic review on silver nanoparticles-induced cytotoxicity: physicochemical properties and perspectives. *J Adv Res* 9:1–16. <https://doi.org/10.1016/j.jare.2017.10.008>
113. Stewart ME, Anderton CR, Thompson LB, Maria J, Gray SK, Rogers JA, Nuzzo RG (2008) Nanostructured plasmonic sensors. *Chem Rev* 108:494–521
114. Kumar S, Bhushan P, Bhattacharya S (2018) Fabrication of nanostructures with bottom-up approach and their utility in diagnostics, therapeutics, and others. In: Bhattacharya S, Agarwal A, Chanda N, Pandey A, Sen A (eds) *Environmental, chemical and medical sensors. Energy, environment, and sustainability*. Springer, Singapore. https://doi.org/10.1007/978-981-10-7751-7_8
115. Biswas A, Bayer IS, Biris AS, Wang T, Dervishi E, Faupel F (2012) Advances in top–down and bottom–up surface nanofabrication: techniques, applications & future prospects. *Adv Colloid Interface Sci* 170:2–27
116. Horikoshi S, Serpone N (2013) *Microwaves in nanoparticle synthesis: fundamentals and applications, introduction to nanoparticles*. Wiley, pp 1–24. <https://doi.org/10.1002/9783527648122.ch1>
117. Filho S, Paulo CD, Osvaldo SA (2015) Liquid phase synthesis methodologies for the obtainment of rare earth-based inorganic nanomaterials. *Quím Nova* 38:679–696
118. Khin MM, Nair AS, Jagadeesh VB et al (2012) A review on nanomaterials for environmental remediation. *Energ Environ Sci* 5:8075. <https://doi.org/10.1039/c2ee21818f>
119. Huang J, Li Q, Sun D et al (2007) Biosynthesis of silver and gold nanoparticles by novel sundried *Cinnamomum camphora* leaf. *Nanotechnology* 18:105104. 11 pp
120. Akter M, Rahman MM, Ullah AKMA et al (2018) Brassica rapa var. japonica leaf extract mediated green synthesis of crystalline silver nanoparticles and evaluation of their stability, cytotoxicity and antibacterial activity. *J Inorg Organomet Polymer Mater* 28:1483–1493
121. Ullah AKMA, Kabir MF, Akter M (2018) Green synthesis of bio-molecule encapsulated magnetic silver nanoparticles and their antibacterial activity. *RSC Adv* 8:37176–37183
122. Ullah AKMA, Tamanna AN, Hossain A et al (2019) In vitro cytotoxicity and antibiotic application of green route surface modified ferromagnetic TiO₂ nanoparticles. *RSC Adv* 9. <https://doi.org/10.1039/c9ra01395d>
123. Ullah AKMA, Haque MM, Akter M et al (2020) Green synthesis of Bryophyllum pinnatum aqueous leaf extract mediated bio-molecule capped dilute ferromagnetic α -MnO₂ nanoparticles. *Mater Res Express*. <https://doi.org/10.1088/2053-1591/ab6c20>
124. Chen Y, Crittenden JC, Hackney S et al (2005) Preparation of a novel TiO₂-Based p–n junction nanotube photocatalyst. *Environ Sci Technol* 39:1201–1208. <https://doi.org/10.1021/es049252g>
125. Park JY, Lee IH (2014) Photocatalytic degradation of 2-chlorophenol using Ag-doped TiO₂ nanofibers and a near-UV light-emitting diode system. *J Nanomater* 2014:250803. <https://doi.org/10.1155/2014/250803>
126. Chen X, Cen C, Tang Z (2013) The key role of pH value in the synthesis of titanate nanotubes-loaded manganese oxides as a superior catalyst for the selective catalytic reduction of NO with NH₃. *J Nanomater* 2013:871528. <https://doi.org/10.1155/2013/871528>
127. Ullah AKMA, Kibria AKMF, Akter M (2017) Oxidative degradation of methylene blue using Mn₃O₄ nanoparticles. *Water Conserv Sci Eng* 1:249–256

128. Pradeep T, Anshup (2009) Noble metal nanoparticles for water purification: a critical review. *Thin Solid Films* 517:6441–6478
129. Rengaraj S, Li XZ (2006) Enhanced photocatalytic activity of TiO₂ by doping with Ag for degradation of 2,4,6-trichlorophenol in aqueous suspension. *J Mol Catal A Chem* 243:60–67
130. Srisithirathkul C, Pongsorarith V, Intasanta N (2011) The potential use of nanosilver-decorated titanium dioxide nanofibers for toxin decomposition with antimicrobial and self-cleaning properties. *Appl Surf Sci* 257:8850–8856
131. Sa J, Agüera CA, Gross S, Anderson JA (2009) Photocatalytic nitrate reduction over metal modified TiO₂. *Appl Catal Environ* 85:192–200
132. Diallo MS, Falconer K, Johnson JH et al (2007) Dendritic anion hosts: perchlorate uptake by G5-NH₂ poly (propyleneimine) dendrimer in water and model electrolyte solutions. *Environ Sci Technol* 41:6521–6527
133. Kouketsu T, Duan S, Kai T et al (2007) PAMAM dendrimer composite membrane for CO₂ separation: formation of a chitosan gutter layer. *J Membr Sci* 287:51–59
134. Sugunan A, Thanachayanont C, Dutta J, Hilborn JG (2005) Heavy-metal ion sensors using chitosan-capped gold nanoparticles. *Sci Technol Adv Mater* 6:335–340
135. Baybas D, Ulusoy U (2019) The use of polyacrylamide-aluminosilicate composites for thorium adsorption. *Appl Clay Sci* 51:138–146
136. Li YH, Wang S, Cao A et al (2001) Adsorption of fluoride from water by amorphous alumina supported on carbon nanotubes. *Chem Phys Lett* 350:412–416
137. Lu C, Chiu H (2006) Adsorption of zinc (II) from water with purified carbon nanotubes. *Chem Eng Sci* 61:1138–1145
138. Lien HL, Zhang W (2005) Hydrodechlorination of chlorinated ethanes by nanoscale Pd/Fe bimetallic particles. *J Environ Eng* 131:4–10
139. Huang HY, Yang RT, Chinn D et al (2003) Amine-grafted MCM-48 and silica xerogel as superior sorbents for acidic gas removal from natural gas. *Ind Eng Chem Res* 42:2427–2433
140. Nomura A, Jones CW (2013) Amine-functionalized porous silicas as adsorbents for aldehyde abatement. *ACS Appl Mater Interfaces* 5:5569–5577
141. Tsai CH, Chang WC, Saikia D et al (2016) Functionalization of cubic mesoporous silica SBA-16 with carboxylic acid via one-pot synthesis route for effective removal of cationic dyes. *J Hazard Mater* 309:236–248
142. Wang S, Wang K, Dai C (2015) Adsorption of Pb²⁺ on amino-functionalized core-shell magnetic mesoporous SBA-15 silica composite. *Chem Eng J* 262:897–903
143. Arencibia A, Aguado J, Arsuaga JM (2010) Regeneration of thiol-functionalized mesostructured silica adsorbents of mercury. *Appl Surf Sci* 256:5453–5457
144. Lai Y, Wang L, Liu D et al (2015) TiO₂-based nanomaterials: design, synthesis and applications. *J Nanomater* 2015:1–3
145. Waghmode MS, Gunjal AB, Mulla JA et al (2019) Studies on the titanium dioxide nanoparticles: biosynthesis, applications and remediation. *SN Appl Sci*. <https://doi.org/10.1007/s42452-019-0337-3>
146. U.S. EPA 2008 Nanotechnology for site remediation fact sheet. Solid waste and emergency response. EPA 542-F-08-009. <http://www.clu-in.org/download/remed/542-f-08-009.pdf>
147. Manivannan S, Ramaraj R (2013) Silver nanoparticles embedded in cyclodextrin-silicate composite and their applications in Hg(II) ion and nitrobenzene sensing. *Analyst* 138:1733–1739
148. Sharma P, Mourya M, Choudhary D et al (2018) Thiol terminated chitosan capped silver nanoparticles for sensitive and selective detection of mercury (II) ions in water. *Sens Actuators B Chem* 268:310–318
149. Ullah AKMA, Kibria AKMF, Akter M et al (2017) Synthesis of Mn₃O₄ nanoparticles via a facile gel formation route and study of their phase and structural transformation with distinct surface morphology upon heat treatment. *J Saudi Chem Soc* 21:830–836
150. Zhang HP, Gu L, Zhang L et al (2017) Removal of aqueous Pb(II) by adsorption on Al₂O₃-pillared layered MnO₂. *Appl Surf Sci* 406:330–338

151. Wang Z, Qin Y, Pan F et al (2018) Mesoporous silica-supported manganese oxides for complete oxidation of volatile organic compounds: Influence of mesostructure, redox properties, and hydrocarbon dimension. *Ind Eng Chem Res* 57:7374–7382
152. Zhang H, Xu F, Xue J et al (2020) Enhanced removal of heavy metal ions from aqueous solution using manganese dioxide-loaded biochar: behavior and mechanism. *Sci Rep.* <https://doi.org/10.1038/s41598-020-63000-z>
153. Wang LZ, Sakai N, Ebina Y (2005) Inorganic multilayer films of manganese oxide nanosheets and aluminum polyoxocations: fabrication, structure, and electrochemical behavior. *Chem Mater* 17:1352–1357
154. Ullah AKMA, Hossain A, Akter M et al (2019) Room temperature ferromagnetic behavior of Mn/Manganese oxides nanocomposites. *Mater Lett* 238:51–54
155. Nitti F (2014) Synthesis of gold nanoparticles and their application for detection and removal of water contaminants. *Rev Media Sains* 13:221–232
156. Lisha KP, Pradeep T (2009) Towards a practical solution for removing inorganic mercury from drinking water using gold nanoparticles. *Gold Bull* 42:144–152

Part V
Easily Collectable Adsorbents

Magnetic Separation of Pollutants for Environmental Remediation



Takahiro Sasaki, Satya Candra Wibawa Sakti, Nuryono Nuryono,
and Philip Anggo Krisbiantoro

Contents

1	Materials for Magnetic Separation	572
1.1	Features of Magnetic Separation	572
1.2	Magnetic Materials for Magnetic Separation	573
1.3	Preparation of Magnetic Adsorbent	573
1.4	Application of Magnetic Adsorbents in Environmental Science	574
2	Surface-Modified Magnetic Adsorbents	575
2.1	Surface Modification for Magnetic Materials	575
2.2	Hydrophobic Group Modified Magnetic Adsorbents	575
2.3	Cyclodextrin Modified Magnetic Adsorbent	579
2.4	Prussian-Blue Modified Magnetic Adsorbents	582

T. Sasaki (✉)

School of Pharmaceutical Sciences, Health Sciences University of Hokkaido, Ishikari-gun,
Japan

e-mail: tsasaki@hoku-iryo-u.ac.jp

S. C. W. Sakti

Department of Chemistry, Faculty of Science and Technology, Universitas Airlangga,
Surabaya, Indonesia

Supramodification Nano-Micro Engineering Research Group, Universitas Airlangga, Surabaya,
Indonesia

e-mail: satya.sakti@fst.unair.ac.id

N. Nuryono

Department of Chemistry, Faculty of Mathematics and Natural Sciences, Universitas Gadjah
Mada, Yogyakarta, Indonesia

e-mail: nuryono_mipa@ugm.ac.id

P. A. Krisbiantoro

International Graduate Program of Molecular Science and Technology (NTU-MST), National
Taiwan University, Taipei, Taiwan

Molecular Science and Technology, Taiwan International Graduate Program, Academia Sinica,
Taipei, Taiwan

e-mail: d09551004@ntu.edu.tw

Shunitz Tanaka, Masaaki Kurasaki, Masaaki Morikawa, and Yuichi Kamiya (eds.),

571

Design of Materials and Technologies for Environmental Remediation,

Hdb Env Chem (2023) 115: 571–616, DOI 10.1007/698_2021_822,

© The Author(s), under exclusive license to Springer Nature Singapore Pte Ltd 2022,

Published online: 1 January 2022

3	Magnetic Polysaccharide Composites	585
3.1	Remediation of Dyes and Heavy Metal Ion Contaminated Water by Magnetic Adsorbent	585
3.2	Chitosan Based Magnetic Adsorbent	587
3.3	Alginate Based Magnetic Adsorbent	589
3.4	Cellulose Based Magnetic Adsorbent	591
3.5	Pectin Based Magnetic Adsorbent	594
3.6	Future Perspectives	596
4	Functionalized Natural Magnetic Materials	596
4.1	Natural Magnetic Materials from Iron Sand	596
4.2	Functionalization of Natural Magnetic Materials with Functional Groups and the Application as Adsorbents	599
5	Conclusion	604
	References	605

Abstract Magnetic adsorbents are composed of magnetic materials for magnetic separation and functional molecules for adsorption of substances. Depending on the properties of the functional molecules used, it is possible to adsorb various pollutants such as harmful organic compounds, heavy metals, and radioactive substances. The selectivity, rate, conditions, and maximum amount of adsorption depend on the material used and its design of adsorbents. This chapter summarizes the adsorption characteristics of pollutants in environmental samples for three types of adsorbents: surface-modified magnetic adsorbents, magnetic polysaccharide composites, and functionalized natural magnetic materials.

Keywords Functionalized natural magnetic materials, Heavy metals, Magnetic adsorbent, Magnetic polysaccharide composites, Organic compounds, Radioactive substances, Surface modification

1 Materials for Magnetic Separation

1.1 Features of Magnetic Separation

Magnetic separation is a method of separating a target substance from other substances by the differences in magnetic response. If a target substance is magnetic, it can be easily separated from non-magnetic substances by the application of a magnetic field. Even though a target substance is non-magnetic, which is a common case, the target substance can be moved together if the substance is attached to a magnetic material by some means. The magnetic material that can attach the target substance is a magnetic adsorbent.

The separation method using a magnetic adsorbent has been used in various fields due to its simplicity and high selectivity. Some examples are solid-phase extraction in analytical chemistry [1], purification of biological macromolecules (proteins, antibodies, nucleic acids) [2–4], microorganisms [5], and cells [6] in biochemistry,

recovery of catalysis for reuse in catalytic chemistry [7], and removal of toxic contaminants in environmental remediation [8]. Their common technical advantages of magnetic separation are rapid separation and good cost-performance. Furthermore, magnetic separation can be applied to large-scale and flow processing.

1.2 Magnetic Materials for Magnetic Separation

The magnetic materials used for magnetic adsorbent are mainly iron oxides. There are various magnetic materials such as iron, nickel, cobalt, their oxides, and so on, but iron is mainly used for magnetic separation materials due to its cost [9]. In addition, iron oxides are more often used than metallic iron because of the advantages of easy synthesis, size control, and morphology control [10].

Typical ferrimagnetic materials used as magnetic separation materials are magnetite (Fe_3O_4) and maghemite ($\gamma\text{-Fe}_2\text{O}_3$) [11]. Cobalt ferrite (CoFe_2O_4), in which the iron element in magnetite is partially replaced by cobalt to improve the magnetic properties, is also generally used as a magnetic material for magnetic separation [12]. These magnetic materials are relatively inexpensive to synthesize and are also found in nature, and magnetic separation materials using natural iron sand have also been studied as described later.

1.3 Preparation of Magnetic Adsorbent

Magnetic adsorbents can be obtained by two methods. One is to provide the magnetism to functional materials, and the other is to functionalize magnetic materials. One of the studies on the imparting of the magnetism to functional materials is to impregnate magnetic particles into porous carbon materials, such as activated carbon, one of excellent [13]. Concretely, it is obtained by the depositing generated iron oxide nanoparticles on the surface or inside of the porous adsorbent by mixing iron salt aqueous solution and the porous carbon materials. The method is especially prevalent in the studies of the magnetic adsorbents using natural porous materials [14].

Functionalization of magnetic materials includes the methods for modifying their surfaces with functional molecules or combining magnetic materials with functional materials. Magnetic adsorbents require a site to interact with the target substance. The interactions used for this purpose are mainly hydrophobic interactions [15], electrostatic interactions [16], van der Waals forces [17], coordination bonds [18], and covalent bonds [19]. Modifiers for functionalizing magnetic materials include small molecules [20], synthetic polymers [21], and biopolymers [22]. Composites of functional molecules and magnetic materials can be created by combining various polymers with magnetic particles [23], or by combining small molecules with magnetic particles via polymerization [24].

1.4 Application of Magnetic Adsorbents in Environmental Science

Magnetic adsorbents are used for both of the removal of hazardous substances from the environment [25] and the solid-phase extraction in environmental analysis [26]. Since the scale of the experiments in environmental science research is relatively large, conventional separation processes such as filtration and centrifugation to recover the adsorbent are lower efficient and higher cost in the operation [27]. On the other hand, the magnetic adsorbents can be recovered in a large-scale experiment and have the potential for in situ environmental remediation [28, 29].

Some applications of magnetic adsorbents in environmental sciences are shown in Table 1 [30–38]. Magnetic adsorbents are often used for decontamination and analysis of samples from aqueous targets, lakes, river water, and seawater. In the following sections, our researches on three categories of magnetic adsorbents, i.e. surface-modified magnetic adsorbents, magnetic polysaccharide composites, and adsorbents using functionalized natural magnetic materials, in environmental sciences will be mainly introduced, and the types and characteristics of magnetic adsorbents prepared in our laboratories and their applications to aqueous system and soil will be described in detail.

Table 1 Applications of magnetic adsorbents for environmental water samples

Adsorbents	Adsorbates	Applications	Water samples	Reference
Ionic liquid-based magnetic carbon nanotube	Triazole fungicides	SPE	River	[30]
Magnetic graphene oxide adsorbent	As	Removal	Spring water, river, lake, tap water	[31]
Magnetic and hydrophilic molecularly imprinted polymer	Dyes	Removal	River	[32]
Fe ₃ O ₄ @alkali-treated calcium-silicate composite	Phosphate	Removal	Lake	[33]
Hydrous lanthanum oxide loaded silica-coated magnetite	Phosphate	Removal	Lake	[34]
γ-Mercaptopropyl trimethoxysilane modified silica-coated magnetic nanoparticle	Te	SPE	Sea	[35]
Graphene-based magnetic nanocomposite	Triazole fungicides	SPE	Sea, river, reservoir water	[36]
Magnetic hydrogel	Heavy metals	Removal	Tap water, sea	[37]
Sodium-copper hexacyanoferrate-functionalized magnetic nanoadsorbent	Cs	Removal	Sea	[38]

2 Surface-Modified Magnetic Adsorbents

2.1 *Surface Modification for Magnetic Materials*

Surface-modified magnetic adsorbent has a feature of being simple in design. This design for modification is based on only two points: what to use as a magnetic material and what to use as a modifier. Iron oxide is often used as a reasonable magnetic material [9]. Modifiers can be selected from a variety of materials such as organic, organometallic, and inorganic compounds [13].

The surface modifier must satisfy two requirements. One is to interact with the surface of the magnetic particles for modification. The interaction with the surface of magnetic particle is caused by some means of coordination bonds with Fe or hydrogen bonds with O and OH groups on its particle surface [39, 40]. The other is to interact with the target compounds you want to remove. The affinity with the target compounds plays an essential function as the adsorbent.

The adsorption principles are classified into chemical adsorption and physical adsorption. Chemical adsorption is due to the strong bonds (covalent, ionic, metallic, and coordination bonds) through the transfer of electrons. In this adsorption, monolayer adsorption mainly occurs [41]. Physical adsorption is due to the weak interactions between substances (van der Waals forces, hydrophobic interactions, π - π interactions, CH- π interactions, hydrogen bonds, etc.) and is fast and reversible [42]. The reversibility of adsorption facilitates the reuse of the adsorbent. In this adsorption, not only monolayer adsorption but also multilayer adsorption may occur [43].

Upon determining the modifier for the adsorbent, you can then modify the surface of the magnetic particles using the selected modifier. Many methods for the surface modification methods are relatively simple, and the simplest method to prepare a surface-modified magnetic adsorbent is only to mix the modifier with magnetic particles [44]. Some studies of the surface-modified magnetic adsorbent are shown in the below sections.

2.2 *Hydrophobic Group Modified Magnetic Adsorbents*

In this study, the adsorption behavior of monocyclic aromatic compounds due to hydrophobic interactions was investigated using hydrophobized magnetite (Fe_3O_4), one of iron oxides [44].

This study was prompted by heavy oil spills into the ocean that were triggered by tanker and oil rig accidents, and pollution with organic compounds spilled into rivers from chemical plant accident [45–47]. Sudden pollution of oceans and rivers, for which no countermeasures have been made in advance, and the rapid spread of contaminants require rapid countermeasures. For the rapid treatment of the contaminations, hydrophobic magnetic adsorbents, which is a type of physical adsorption, is

suitable because the adsorption reaction is rapid and less sensitive to the environmental matrix.

Aromatic hydrocarbons, one of the hydrophobic compounds, include monocyclic aromatic compounds with a single aromatic ring, and polycyclic aromatic hydrocarbons (PAHs), dioxins, and PCBs composed of multiple aromatic rings. In general, PAHs, dioxins, and PCBs are highly hydrophobic and can be easily adsorbed and removed from water by hydrophobic interactions [48–50]. In contrast, the adsorption behavior of less hydrophobic aromatic hydrocarbons due to hydrophobic interactions has rarely been investigated. Some low hydrophobic aromatic compounds are used as raw materials for chemical products and have a high risk of spilling into the environment. In fact, large amounts of low hydrophobic compounds such as benzene, nitrobenzene, and aniline flowed into rivers from chemical plants in China [47].

Therefore, in this study, the adsorption behavior of relatively low hydrophobic monocyclic aromatic compounds was systematically investigated based on the following two factors. Their factors were the hydrophobicity of the monocyclic aromatic compound and the type of hydrophobic functional groups modified onto the adsorbent. The hydrophobicity of the compounds was indicated by the water/octanol partition coefficient ($\log P_{ow}$). The monocyclic aromatic compounds in this study are benzene and its mono-substitutes, which can be divided into three groups based on the values of $\log P_{ow}$: $1 < \log P_{ow} < 2$, $2 < \log P_{ow} < 3$ and $3 < \log P_{ow}$ (Fig. 1). The use of such different types of hydrophobic modifiers may provide useful information in investigating the adsorption mechanism to the adsorbent.

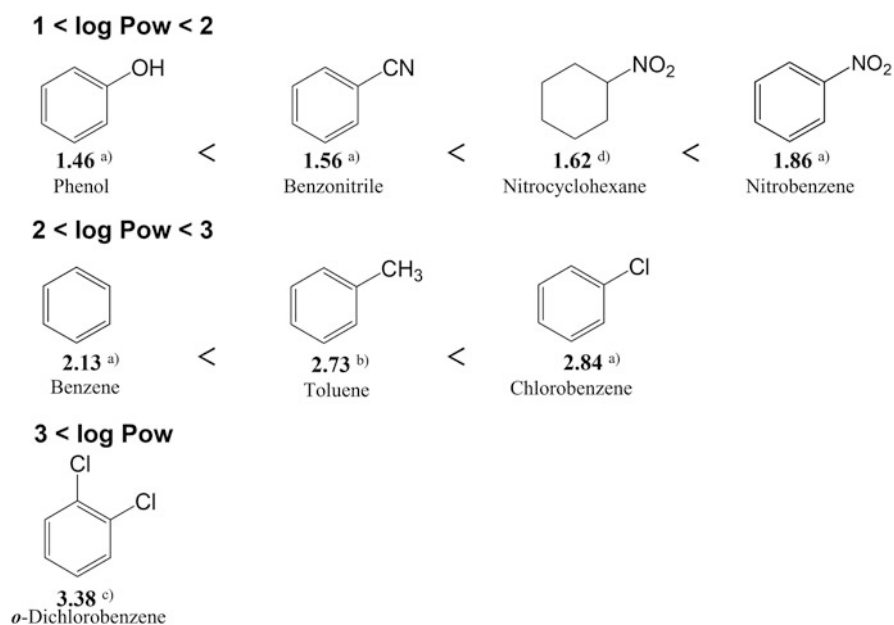


Fig. 1 Structures and $\log P_{ow}$ s of aromatic compounds and nitrocyclohexane [44]

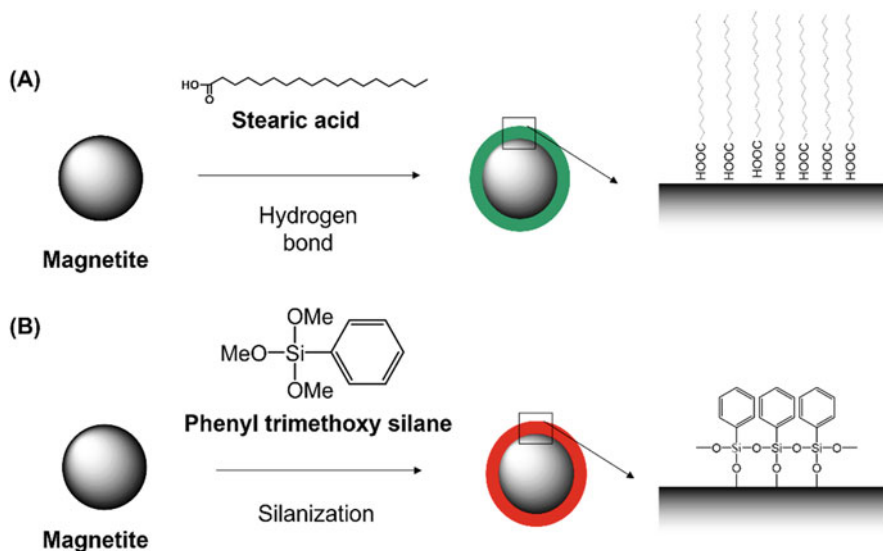


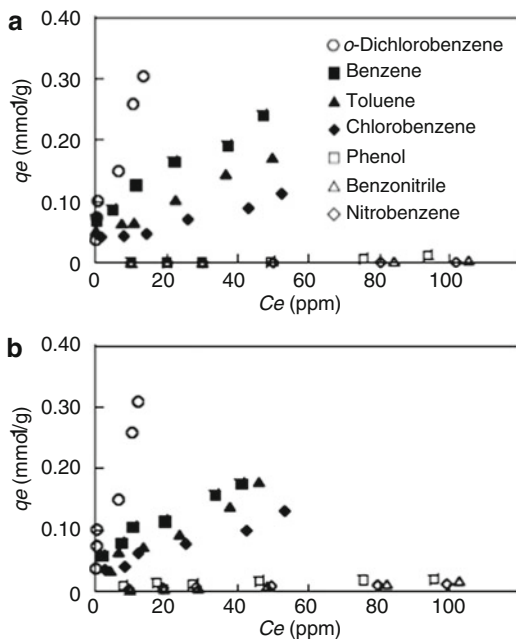
Fig. 2 Hydrophobization of magnetite surface (a) is modification with stearic acid and (b) is with phenyl group on magnetite surface [44]

The hydrophobic functional groups used as the modifier for the adsorbent in this study were stearyl from stearic acid and phenyl groups from phenyltrimethoxysilane (Fig. 2). Stearic acid was immobilized to magnetic particle by coordinate and/or hydrogen bonding between the carboxy groups of the modifier and the particle surface. Furthermore, the modification layer was stable in water due to hydrophobic interactions between its alkyl chains. The phenyltrimethoxysilane was immobilized to magnetic particle by hydrogen bonding between silanol groups formed by the hydrolysis of their methoxy groups and hydroxyl groups on the particle surface. In addition, the silanol groups are self-condensed intermolecularly to form a stable silica layer with phenyl groups on the particle surface. Both hydrophobic layers of the obtained magnetic adsorbent were confirmed to be thin and have no pores by the modification amount analysis and N_2 BET analysis, respectively. Therefore, the contribution of hydrophobic and π -electron interactions in adsorption can be evaluated.

The adsorption behaviors of monocyclic aromatic hydrocarbons to hydrophobic adsorbents were investigated by the adsorption isotherm. Adsorption isotherms are obtained from the relationship between the equilibrium concentration of a compound and its adsorbed amount at a constant temperature and the shapes of the isotherm give the information of some interaction between the adsorbent and the adsorbed compound.

The results of the adsorption experiments are shown in Fig. 3. The magnitude of the slope of each adsorption isotherm correlates with the strength of the adsorption. Comparing the slopes across the groups, the order of hydrophobic strength and the

Fig. 3 The adsorption amounts of aromatic compounds onto (a) Stearyl-mag and (b) Phenyl-mag in various initial concentrations (10–100 ppm) [44]



magnitude of slope were in agreement. In the groups of $3 < \log P_{ow}$ and $2 < \log P_{ow} < 3$, the adsorption behavior on the adsorbent modified with stearyl and phenyl groups was almost the same. This indicates that the main interaction in the adsorption is due to hydrophobic interaction.

In contrast, the compounds with $1 < \log P_{ow} < 2$ had the different adsorption behavior on the adsorbents modified with stearyl and phenyl groups, and adsorbed only on the surface of phenyl group. Furthermore, nitrocyclohexane, which has a $\log P_{ow}$ similar to nitrobenzene but no aromatic ring, was not adsorbed on the phenyl group-modified magnetic adsorbent, indicating that the effective interaction for adsorption of compounds with low hydrophobicity is not hydrophobic interaction but π -electron interaction.

In addition, we also have confirmed that it is possible to magnetically separate oil droplets by introducing a hydrophobic magnetic adsorbent into the oil droplets (Fig. 4), and the magnetic separation method with this magnetic adsorbent has the potential to be used for large-scale contamination with the lower hydrophobic aromatic compounds.

Grbic et al. reported a study of the removal of microplastics (MPs) from environmental water by magnetic adsorbents modified hexadecylsilyl group on its surface [51]. MPs, which are low-degradable and hydrophobic, have attracted much attention in recent years due to their widespread distribution in the environment and ecosystems [52, 53].

The magnetic separation system in this study is unique. The MPs to be removed are considerably larger than the magnetic adsorbent, and it is contrary to the general

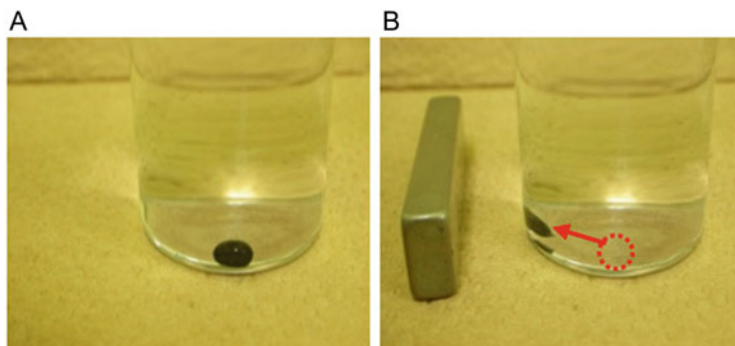


Fig. 4 Photographs of an oil droplet containing the hydrophobic magnetites in water (a) and the oil droplet containing the hydrophobic magnetites moved by magnet (b)

relationship between the size of the adsorbent and the target material. The MPs surrounded by the fine hydrophobic magnetic adsorbent behave like a magnetic material and can be separated by a magnet (Fig. 5b).

The spike and recovery tests were performed by using different size and types of plastics. The sizes on MPs were in the range of 1–8 mm (large), 200 μm to 1 mm (medium), and $<20 \mu\text{m}$ (small). The types of MPs were polypropylene (PP), polyvinyl chloride (PVC), polyurethane (PU), polystyrene (PS), high-density polyethylene (HDPE), and polyethylene terephthalate (PET). In addition, the matrix effects on the removal of MPs were investigated by using freshwater, seawater, and sediments.

The results of the spike and recovery tests are shown in Fig. 5. For large size fraction, the recovery rate in seawater was ranged from 74 to 105%, which was generally good. For middle size fraction, the recovery rates in freshwater or sediments were ranged from 59 to 100% and from 49 to 90%, respectively. The recovery rate of PVC was lowest in sediments and that of PP was lowest in freshwater. At present, no clear relationship has been found between the different matrices or plastic types and the lower recovery rates. For small size fraction, the recovery rates in seawater were 96% for PE and 88% for PS, respectively. The smaller MPs are, the harder the recovery and analysis are, while the larger MPs are, the easier the recover and analysis are by conventional methods. This study is important for future research on small MPs in environment.

2.3 Cyclodextrin Modified Magnetic Adsorbent

Ji et al. reported the study for removal of harmful organic compounds from environmental water using β -cyclodextrin (β -CD) modified magnetic particles [54]. Although the purpose of this study is to develop a solid-phase extraction (SPE) technology for environmental analysis, this study can also be considered as

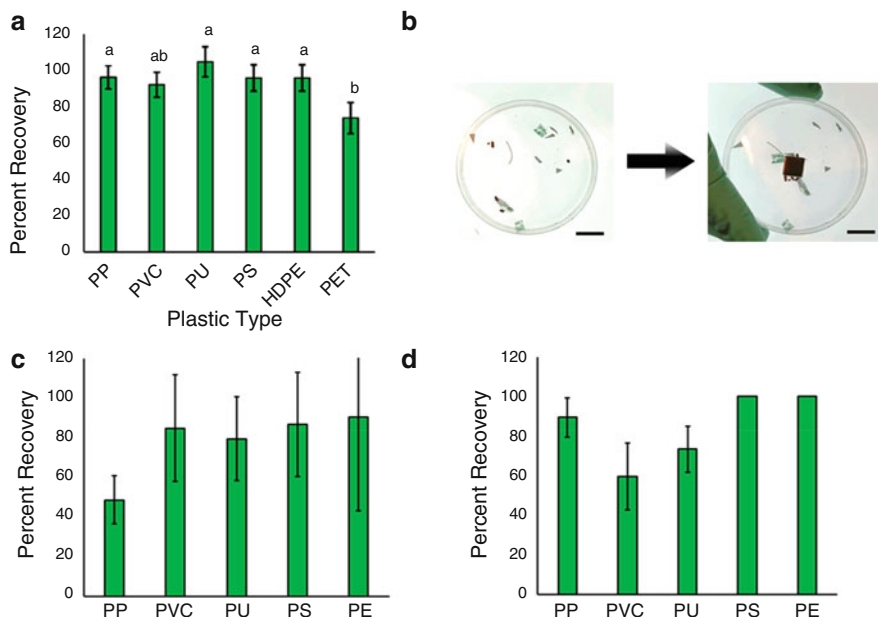


Fig. 5 Results from the spike and recovery experiments with large MPs. **(a)** Percent recoveries of large MPs spiked into seawater with 5–10 pieces of each type spiked into 200 mL of seawater ($n = 3$ trials). Error bars show standard deviations. Letters denote statistical significance between groups. **(b)** Photograph of large MPs exposed to modified Fe nanoparticles being attracted to a magnet at the center of the dish. The scale bar is 20 mm. Spike and recovery of medium MPs (from 200 μm to 1 mm) in **(c)** sediment and **(d)** RO water ($n = 3$ trials for all cases). Error bars show standard deviations. Note that for PS and PE error bars are not visible because all trials resulted in 100% recovery [51]

an environmental remediation technology, since SPE and adsorption technologies for environmental remediation require almost the same functions as the materials used there [55].

CD is a cyclic oligosaccharide composed of glucose and has a truncated cone-like structure [56]. The rim of CD is hydrophilic, and the inside of its cavity is hydrophobic. CDs consisting of 6, 7, or 8 glucoses, called α -, β -, or γ -, respectively, have different sized cavities. CDs can selectively collect hydrophobic compounds having an appropriate size for their cavity size and are known to be representative materials in host-guest chemistry [57]. The chemical industry additives bisphenol A (BPA) and diethylstilbestrol (DES) were selected as the model compounds to compare the performance of hydrophobic CTAB-coated MNPs and β -CD MNPs.

In this study, the characterization of the synthesized materials and the functional evaluation of the adsorbent have been carried out, and the functional evaluation includes the effect of pH, ionic strength, and contact time on adsorption. Briefly, the material was synthesized by constructing a silica layer on the surface of magnetic

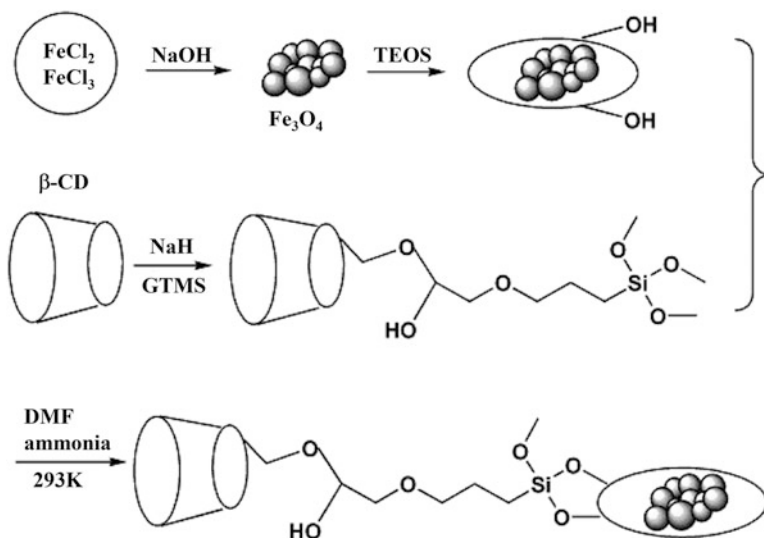


Fig. 6 Scheme for the preparation of Fe₃O₄@SiO₂/β-CD [54]

particles using tetraethoxysilane (TEOS) and then modifying it with a silane coupling agent coupled with β-CD (Fig. 6).

The adsorption behavior was investigated in the pH 2–10 range, and both BPA and DES adsorbed well in the range of pH 4.3–8.5. The decrease in the amount adsorbed under more acidic and basic conditions was due to a change in the electrostatic state of the target compounds. At the same time, the adsorbent surface was also covered with hydrated ions and the adsorption amount was reduced. The effect of ionic strength on adsorption was studied in the range 0–30% salt concentration. The increased ionic strength enhanced the adsorption efficiency of BPA. On the contrary, the adsorption amount of DES decreased. This is due to a decrease in the amount of dissolution in water by the salt effect, which is inherently favorable to extraction. The hydrophobicity and water solubility of BPA ($\log P = 3.32$, water solubility 120 mg/L) and DES ($\log P = 5.07$, water solubility 12 mg/L) support the result of decreasing the adsorbed amount of DES only when the ion strength was increased. Adsorption of both BPA and DES was completed in 8 min. The adsorption kinetics is sufficiently fast compared to conventional solid-phase microextraction or stir bar sorptive extraction, which takes 30 or 60 min to reach the adsorption equilibrium [58, 59]. These adsorbed compounds could be eluted by sonication in methanol (1% acetic acid) for 30 s. The efficient elution of adsorbed compounds under mild conditions is great advantageous for adsorbent reuse.

Aggregation sometimes occurs in the case of the adsorbent utilizing hydrophobic interactions with target compounds, because of the hydrophobicity of the adsorbent itself. However, the hydrophobic site of CD is only inside the CD cavity. This feature can avoid the problem of poor dispersibility in water due to its hydrophobic

nature, which is often seen in hydrophobic adsorbents. For this reason, magnetic adsorbents based on materials from host-guest chemistry including CD are very attractive as environmental remediation materials.

2.4 Prussian-Blue Modified Magnetic Adsorbents

The research on Prussian blue modified magnetic adsorbent was accelerated after the Fukushima Daiichi Nuclear Power Plant accident caused by the Great East Japan Earthquake in 2011. This incident resulted in the release of various radioactive species, which contaminated a wide area of the water and soil environments [60–62]. In this subsection, cesium-contaminated water is discussed first and then the treatment of contaminated soil.

Contaminated water of radioactive substances has been treated by adsorption, and a variety of adsorbents have been developed for this purpose. Many studies on the adsorbents for Cs removal have been conducted by using Prussian blue (PB) as the adsorbent [63]. PB is a organometallic coordination polymer composed of ferric ions (Fe^{3+}) and ferrocyanide ions ($[\text{Fe}(\text{CN})_6]^{4-}$), and is known to be an excellent adsorbent for cesium ion [64]. PB has a cubic lattice structure whose cavity size in the lattice is similar to the hydrated ionic diameter of cesium. The structural features of PB allow it to selectively adsorb cesium among alkali metals with property similar to that of cesium. Zeolite is also used as materials with the similar adsorption mechanism [65].

PB has small particle size, ca. 100 nm, which makes it difficult to recover after the adsorption process. Therefore, PB is usually used as an adsorbent supported on some material for easy recovery. Adsorbents modified with PB have been developed in various forms such as particles, sponges, filters, fibers, gel beads, and fabrics [66–71].

PB-modified magnetic adsorbent, which can be collected by magnetic field, is currently one of the most studied adsorbents for the removal of Cs. This adsorbent can overcome the disadvantage of PB, which is difficult to recover due to its small crystal size, i.e. it is one of the solutions of the trade-off between the adsorption ability and the recovery easiness in adsorbent size. Here, one of the studies on magnetic adsorbents with PB modified on the surface is presented.

In this study, the characterization, adsorption performance, and magnetic separation efficiency of PB-modified magnetic adsorbents were investigated (Fig. 7) [66]. PB-modified magnetic adsorbent (PB-mag) was prepared by a unique build-up method. In addition, some other methods for the immobilization of PB onto various materials also have been reported, such as modification of electrode surfaces by electrochemical reactions, formation of crystals in gel beads, and so on.

The size of PB grains immobilized on magnetite was about 100 nm and the thickness of layer composed of PB was 200–400 nm. The amount of modified PB was about 25% of PB-mag weight. The maximum adsorption capacity, adsorption kinetics, and selectivity of PB-mag for Cs ion were investigated by adsorption

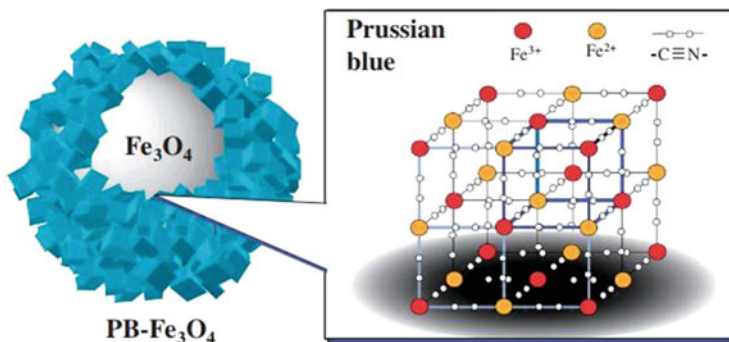


Fig. 7 Schematic representation of PB-Fe₃O₄ (PB-mag) and lattice structure of PB [66]

experiments using non-radioactive ¹³³Cs in water. To evaluate the amount of Cs adsorbed, Cs ions were eluted from PB-mag recovered after the adsorption experiment and measured by inductively coupled plasma mass spectrometry (ICP-MS). The results of adsorption experiments showed that the maximum adsorption capacity was 16.2 mmol g⁻¹, and 0.1 mM of Cs was completely adsorbed on 10 mg of PB-mag in 24 h. The adsorption rate did not decrease in the presence of 3 wt% NaCl, the same concentration as in the seawater. The recovery of PB-mag from 1 L of water was achieved within about 6 min by magnetic separation.

For the contaminated water with radioactive Cs, many treatment methods have been developed and the applicable treatment technology has been almost established on the basis of ion-exchange mechanism [72]. While any efficient treatment methods for contaminated soil have not yet been established and the development is required as soon as possible.

Generally, adsorbents cannot be used to treat contaminated soil. There are three reasons for this. First, the target substance for adsorption is attached to the soil particles strongly and is difficult to remove it directly by an adsorbent. Therefore, it is necessary to elute the target substance with an appropriate eluting agent in advance. Second, the soil eluate contains high concentrations of multicomponent coexisting substances, i.e., matrix, which may inhibit the adsorption of the target substance. Third, it is difficult to recover the adsorbent from the eluate containing soil particles. Thus, few removal studies using adsorbents for soil have been reported.

PB-mag has a high Cs selectivity in adsorption and can be efficiently separated from other components by magnetic separation. Therefore, we attempted to treat contaminated soil by a combination of Cs eluting and magnetic adsorbent [73]. The eluting process is important in this treatment method, and the eluting behavior of Cs from the contaminated soil was evaluated in detail using a speciation analysis.

The speciation analysis was performed by the sequential extraction method, which is a method for sequentially eluting Cs in contaminated soil with multiple conditions and analyzing the eluted Cs quantitatively in each condition [74]. In this study, Cs in the soil was classified into five chemical species, Fraction 1–5. Fraction

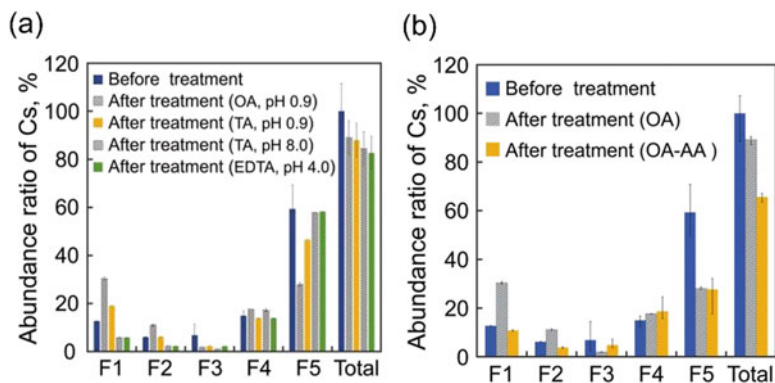


Fig. 8 Fraction analysis of Cs in the simulated contaminated soil before and after the elution process using organic acids. (a) Fraction analysis of Cs in clay by a treatment with oxalic acid (OA) and oxalic acid-ammonium acetate (OA-AA) (b) [73]

1 (F1) is ion-exchangeable, Fraction 2 (F2), 3 (F3), 4 (F4), and 5 (F5) are bound with a carbonate, iron, and manganese oxides, and an organic substance, and a clay, respectively. The order of difficulty in elution is $F5 > F4 > F3 > F2 > F1$ [75].

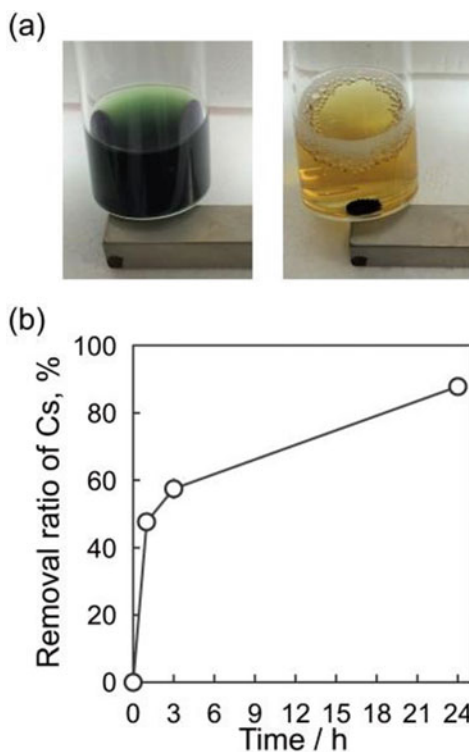
Firstly, the effective eluting agents for Cs were searched for among various organic acids, and it was found that the oxalic acid effectively eluted Cs of F5, which is difficult to elute in most cases (Fig. 8a). However, there were still two problems in the use of oxalic acid: one was the re-absorption of the eluted Cs onto F1 and F2, and the other was the dissolution of magnetite by the oxalic acid.

Fortunately, however, these two problems were solved by a simple method of adding ammonium acetate (AcNH_4). This is because AcNH_4 was an eluent of F1 and F2 in the sequential extraction method, which can inhibit the re-adsorption of Cs to F1 and F2 (Fig. 8b), and also deactivated the excess oxalic acid.

The stability and the adsorption ability of PB-mag in the eluate were confirmed by adding with and without AcONH_4 , respectively. As shown in Fig. 9a (right), the PB-mag was attracted to the magnet in the eluate with AcONH_4 . On the other hand, the magnetite of PB-mag was dissolved and PB crystalline dispersed in the eluent without AcONH_4 (Fig. 9a (left)). The results showed that the addition of AcONH_4 was essential for the stability of PB-mag in the eluate. Then, the adsorption capacity of Cs in the eluate was examined, and most of Cs was adsorbed by PB-mag in the eluate, although the adsorption rate was slightly decreased (Fig. 9b).

This method was applied to the treatment of actual contaminated soil in a scale-up. In this treatment experiment, two factors were assumed to influence the treatment effectiveness: the differences in soil type and scale of treatment. In particular, the results are often very different before and after scale-up. However, not only the total removal rate but also the Cs removal rate in each fraction was the same as in the laboratory experiments, indicating the robustness and usefulness of this treatment method.

Fig. 9 (a) Photographs of PB-mag after shaking in the eluate with oxalic acid (left) and the OA-AA elution system (right) for 5 h and (b) the removal ratio of Cs by PB-mag in the OA-AA system [73]



In this study, the detailed investigation by speciation analysis had been able to overcome the disadvantages of the adsorbent and expand the range of the applications of the adsorbent. For environmental remediation research, which often needs the approaches in the hard conditions that are far from the ideal experimental systems, it is important to understand the properties of the target substance, its behavior in the environment, and the characteristics of the adsorbent and the eluting agent to overcome the technical difficulties.

3 Magnetic Polysaccharide Composites

3.1 Remediation of Dyes and Heavy Metal Ion Contaminated Water by Magnetic Adsorbent

Water contamination is one of environmental challenging issues that mainly caused by releasing untreated pollutant to the water body. Dyes and heavy metal ions are two common types of toxic and hazardous substances that are present in wastewater or industrial effluents. The presence of dyes can hinder penetration of sunlight, interfere photosynthesis, reduce dissolved oxygen value, and increase both of

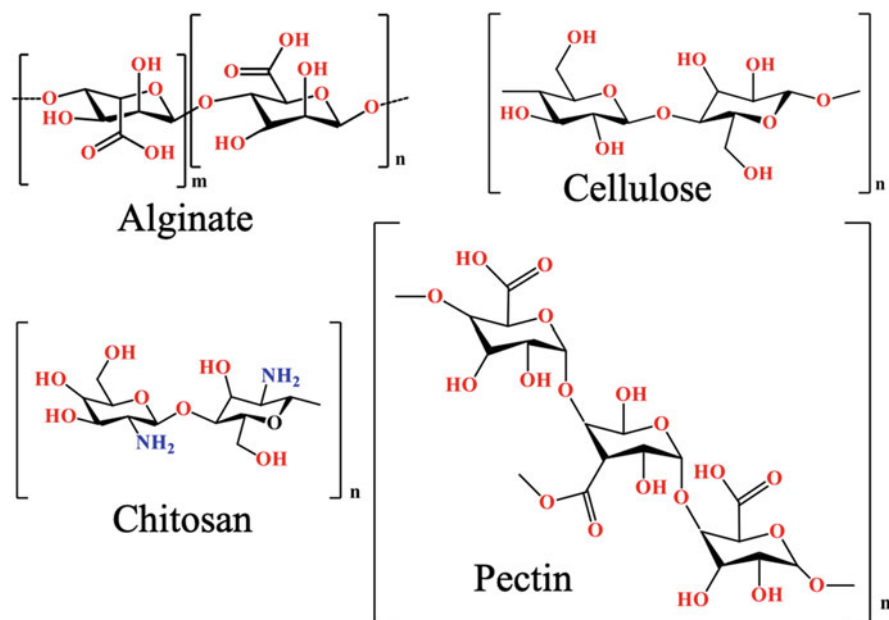


Fig. 10 Chemical structure of alginic acid, cellulose, chitosan, and pectin

chemical and biological oxygen demand [76]. Even in low concentration, presence of dyes in water leads to unpleasant water color and odor. Annually, around 7×10^5 tons of dyes is synthesized and more than 100,000 types of dyes are available in the market [77]. Reactive, acid, basic, direct and dispersed type are the most common dyes used by industries. Unfortunately, more than 15% of manufactured dyes are untreated properly and ended as contaminant in water body [78]. The As (III), Cd (II), Co(II), Cr(III), Cr(VI), Cs(I), Cu(II), Pb(II), and Se(IV) are the common detected heavy metal ions in electroplating, metal and steel, electronic, and metal finishing industries. There are various methods which have been developed to remediate heavy metal ions and dyes polluted water. However, adsorption by using magnetic adsorbent is probably one of the best methods to be applied due to its simplicity, cost-effective, easy recollection, and possible regeneration. Polysaccharides-based magnetic adsorbents such as magnetic chitosan, magnetic alginic acid, magnetic cellulose, and magnetic pectin are the main polysaccharides-based adsorbents which have been applied extensively. Chemical structure of alginic acid, cellulose, chitosan, and pectin are presented in Fig. 10.

Chitosan, structurally known as poly (1-4)-2-amino-2-deoxy-D-Glucan, is one of the polysaccharides which is widely applied for magnetite coating to obtain magnetic chitosan. Chitosan can be extracted from crustacean shells by series of deproteinization, demineralization, and deacetylation step to partially convert amide groups of chitin into free amine groups. Presence of hydroxyl groups and amine groups play important roles in hydrogen bond formation and electrostatic interaction between chitosan and various types of adsorbate [79].

Alginate is polymer of (1-4) linked β -D-mannuronate (M unit) and α -L-guluronate (G unit), where M and G unit are linked in various sequences [80]. It can be extracted from brown algae by basic solution followed by precipitation with calcium chloride and calcium carbonate, respectively [81]. In the presence of divalent ion such as Ba^{2+} and Ca^{2+} , L-guluronate fragments are crosslinked to each other, which leads to alginate phase transition from liquid to gel [82]. Induced gelation by the presence of divalent ion is called ionic gelation. Due to the extensive amount of carboxylate group, biocompatibility, biodegradability, and non-toxic property, alginate has been used for water treatment especially for oil, dyes, heavy metal ion removal [83–85]. Powder and beads are the most common form of synthesized magnetic alginate as adsorbent.

Cellulose is polysaccharide consisted of β -linked D-glucose in linear structure [86]. Together with lignin and hemicellulose, cellulose constructs plant cell wall. Cellulose is also the main component of cell wall of some type of bacteria. Based on its shape, cellulose can be divided into two main groups, namely cellulose crystal and cellulose fibril [87]. The presence of abundant amount of hydroxyl groups have made cellulose versatile to be functionalized with other active compounds or materials [88].

Pectin can be extracted from plant cell wall. Orange peel [89] and apple peel [90] are the most well-known source of pectin. Chemically, pectin is constructed by both linear and branched fragments that consist of homogalacturonan (HG), rhamnogalacturonan I (RGI), rhamnogalacturonan II (RGII), apiogalacturonan (APG), and xylogalacturonan (KG). Linear fragment of homogalacturonan (HG) consists of (1 \rightarrow 4) glycosidic bond linked α -D galacturonate while branched fragment of rhamnogalacturonan is constructed by simple sugar such as D-galactose, D-glucose, D-xylose, L-arabinose, and L-rhamnose [91]. Similar to alginate, pectin forms “egg-box” structure with divalent ions depend on degree of methylation (DM). Pectin can be classified into low methylated pectin with $\text{DM} < 50\%$ and high methylated pectin with $\text{DM} > 50\%$ [92]. There are some published reports that focus on adsorption performance of magnetic pectin on removal of heavy metal ion and dyes.

3.2 Chitosan Based Magnetic Adsorbent

Magnetic chitosan probably is the most studied polysaccharide based magnetic adsorbent. Applications of magnetic chitosan on removal of heavy metal ion and dyes are presented in Table 2. Adsorption ability of chitosan mainly caused by the presence of $-\text{NH}_2$ group which can be protonated to form $-\text{NH}_3^+$ group in acidic solution. Anionic species such as H_2AsO_4^- and HAsO_4^{2-} were reported forming electrostatic bond with $-\text{NH}_3^+$ group of magnetic chitosan [93]. Number of $-\text{NH}_3^+$ determined the number of adsorbed anionic species. Therefore, Q_{max} value of glutaraldehyde crosslinked chitosan was lower than that of non-crosslinked one since glutaraldehyde consumes $-\text{NH}_2$ for crosslinking [94]. Adsorption at higher pH was possible to be conducted via complexation mechanism instead of

Table 2 Removal of various heavy metal ions and dyes by magnetic chitosan

No.	Adsorbent	Synthesis of magnetic chitosan	Modification	Ms (emu/g)	Adsorption					Recycle	Reference	
					pH	Equilibrium time (min)	Kinetics model	Qmax (mg/g)	Isotherm model			Description
1	Fe ₃ O ₄ -chitosan nanoparticle	Blending	Crosslinking with glutaraldehyde	–	3–4	120	PSO	10.81	Langmuir	0.1 M HCl	4	[94]
2	Pyridinium functionalized magnetic chitosan	In situ coprecipitation	Grafting with Pyridinium group	13.6	3.6 and 9	5	PSO	176 (pH 3), 124 (pH 6) and 86 (pH 9)	Langmuir	0.001 M NaOH-0.1 M NaCl mixture solution	5	[97]
3	Hexacyanoferrate modified magnetic Fe ₃ O ₄ -chitosan nanoparticles	Blending	In situ modification of Cu-hexacyanoferrate	53.54	5–6	200	PSO	161.3	Langmuir	0.05 M EDTA	5	[99]
4	Chitosan/clinoptilolite/magnetic nanocomposite	Blending	Clinoptilolite	9.5	6	30	PSO	137	Langmuir	NaCl, CaCl ₂ , HNO ₃	4	[125]
5	Multi-cyanoguanidine modified magnetic chitosan	Blending	Cyanoguanidine crosslinking and grafting	21.6	44,017	60	PSO	285.7	Langmuir	Saturated EDTA	6	[126]
6	Glutamine modified chitosan magnetic composite microspheres	w/o emulsion	Blending with glutamine	3.48	7	20	PSO	699	Langmuir	0.1 M EDTA	5	[127]
7	Double-stranded DNA immobilized on quaternary ammonium magnetic chitosan	Blending	Quaternized with glycidyltrimethylammonium chloride followed by DNA immobilization	17.6	7.5	5	PSO	48.02 (AO), 31.54 (EiBr) and 30.01 (MB)	Freundlich	–	–	[103]
8	Ethylendiamine-modified-TEOS-coated magnetized chitosan beads	Blending	Coating with TEOS, grafting with ethylenediamine	4.53	2	30–45	PSO	179.45 (CBY) and 377.60 (CBR)	Langmuir	–	–	[128]
9	Chitosan grafted poly (quaternary ammonium)/Fe ₃ O ₄ nanoparticle	w/o emulsion	Grafting with trimethylallyl ammonium chloride	21.57	4	80	PSO	1.13 mmol/g	Langmuir	0.5 M NaOH	5	[101]
10	Magnetic Fe ₃ O ₄ / chitosan nanoparticles	In situ reduction and coprecipitation	–	17.1	2	5 h	PSO	476.8	Langmuir	1 M NaOH	5	[129]

electrostatic mechanism. Complex formation between -NH_2 with adsorbate in solution was reported less affected by the presence of Cl^- , NO_3^- , or SO_4^{2-} [95]. XPS study confirmed that N atom donated electron during complex formation between Cu^{2+} with poly aniline functionalized magnetic chitosan [96]. Electrostatic interaction between -NH_3^+ with anionic species was also reported strongly which depends on the pH of solution. In neutral and basic condition mechanism is less effective. Converting -NH_2 group into -pyridinium group depressed pH influence on adsorption. Pyridinium functionalized magnetic chitosan shows pH-independent nature during removal of Cr(VI) in acidic, neutral, and basic solution [97]. Incorporation of selective material or grafting with specific organic groups is reported enhancing selectivity of magnetic chitosan. Ferrofluid modified chitosan-mesoporous carbon nanohybrid adsorbs Cd^{2+} selectively in the presence of Cu^{2+} , Pb^{2+} , Co^{2+} , NO_3^- , PO_4^{2-} , K^+ , Mg^{2+} , Fe^{3+} , Zn^{2+} , CO_3^{2-} , and Cl^- [98]. In situ formation of Cu-hexacyanoferrate in magnetic chitosan increased its selectivity towards Cs^+ without being interfered by the presence of Mg^{2+} , K^+ , or Ca^{2+} [99]. Imprinting techniques are widely used to synthesize magnetic adsorbent which has selective cavity. Imprinting of alizarin red on magnetic chitosan structure showed high capacity and selectivity toward alizarin red and not being interfered by the presence of other organic dyes such as acid orange 7, acid orange 10, methylene blue, or remazol black 5 [100]. Similar to heavy ion adsorption, adsorption of dyes is dominated by electrostatic interaction. Positively charged ammonium groups on the surface of chitosan grafted poly (quaternary ammonium)/ Fe_3O_4 nanoparticles form electrostatic interaction with food yellow 3 with being less affected by solution pH [101]. Other mechanisms such as hydrogen bonding, π - π interaction, and affinity interaction were also reported to play important role in removal of dye [102]. Double-stranded DNA immobilized on quaternary ammonium magnetic chitosan adsorbs cationic dyes not only by electrostatic mechanism but also by intercalation between two-helix of DNA [103].

3.3 Alginate Based Magnetic Adsorbent

Utilization of magnetic alginate for removal of pollutant in water or wastewater has been studied extensively. Application of magnetic alginate on removal of heavy metal ion and dyes is presented in Table 3. Magnetic alginate was reported to adsorb As(V) effectively at pH 3 within 48 h. The study indicated that adsorption was followed by reduction of As(V). The XPS study showed that oxygen atom of hydroxyl group of alginate and oxygen of magnetite lattice contributed to reduction by donating electrons to As(VI) [104]. ^{88}Sr and ^{90}Sr could be removed by magnetic alginate from seawater within 6 h with Q_{max} value of 400 mg/g without being affected by the presence of cations such as Na^+ , K^+ , Mg^{2+} , and Ca^{2+} [105]. Electrostatic interaction between cerium-magnetic alginate bead with Cr(VI) was strongly interfered by the presence of HCO_3^- in the solution and less affected by Cl^- , SO_4^{2-} , or NO_3^- [106]. Selective adsorption by magnetic alginate can be achieved by

Table 3 Removal of various heavy metal ions and dyes by magnetic alginate

No.	Adsorbent	Synthesis of magnetic alginate	Modification	Ms (emu/g)	Adsorption				Desorption	Recycle	Reference	
					Adsorbate	pH	Equilibrium time (min)	Kinetics				Qmax (mg/L)
1	Alginate-encapsulated Fe ₃ O ₄	Blending	–	–	As(V)	3	48 h	–	–	–	[104]	
2	Magnetite graphene oxide encapsulated in alginate beads	Blending	Fe ₃ O ₄ coated with graphene oxide	25	Cr (VI) and As(V)	5 (Cr (VI) and 7 (As (V))	24 h	PSO	14,903 (Cr (VI) and 6,859 (As(V))	Freundlich (Cr(VI) and Langmuir (As (V))	5	[130]
3	Magnetic carboxymethyl chitosan/graphene oxide @ Fe ₃ O ₄ gel beads	Blending	Fe ₃ O ₄ was composited with GO	14.1	Cd(II), Cu and Pb(II)	5–6	400	PSO	86.28 (Cd (II)), 35.96 (Cu(II)) and 189.04 (Pb (II))	Langmuir	5	[131]
4	DNA aptamer magnetic alginate	In situ coprecipitation	Immobilization of DNA aptamer	51	Hg(II)	7	20	–	–	–	–	[107]
5	Bio-magnetic alginate membrane capsule	Blending	Blending with PVA and crosslinked with Ca(II), glutaraldehyde or boric acid	11.02	Pb(II) and Cd(II)	6–8	25	PSO	548 (Pb (II) and 610.67 (Cd (II))	Langmuir	7	[132]
6	Magnetic/activated charcoal/Cyclodextrin/alginate polymer nanocomposite	In situ coprecipitation	Blending with activated carbon and grafting of beta cyclodextrin	0.12849	MB	6	90	PSO	2,079	Langmuir	5	[133]
7	Magnetic zeolite-alginate-polyanetholesulfonic acid gel beads	Blending	Fe ₃ O ₄ was composited with zeolite and blended with alginate and polyanetholesulfonic acid	31.5	MB, MG	6	240	PSO	400 (MB) and 164 (MG)	Langmuir	10	[109]
8	Magnetic alginate/rice husk bio-composite	In situ coprecipitation	Blending with rice husk	9.97	MB	6–10	90	PSO	274.9	Freundlich	–	[110]
9	Sodium alginate-coated Fe ₃ O ₄ nanoparticles	In situ coprecipitation	–	43	MG	9	20	PSO	47.84	Langmuir	–	[134]
10	Magnetic alginate beads crosslinked with epichlorohydrin	In situ coprecipitation	Crosslinking with epichlorohydrin	–	MO, MB	7.5	30–60	PSO	0.02 mmol/g MO and 0.7 mmol/g MB	Langmuir	–	[135]

introducing active organic group which can recognize specific heavy metal ion as a target. Immobilization of DNA aptamer in magnetic alginate enhanced its selectivity toward Hg^{2+} ion. DNA aptamer specifically recognizes and binds Hg^{2+} in the aqueous solution without being interfered by the presence of Fe^{2+} , Zn^{2+} , Cr^{3+} , Cu^{2+} , Pb^{2+} , Ca^{2+} and Cl^- [107]. Other study reported that magnetic alginate functionalized with L-cysteine showed high selectivity toward Pb^{2+} . The XPS survey results indicated the chelation and ion exchange between $-\text{COO}-$ and $-\text{NH}_2$ groups with Pb^{2+} with high selectivity in the presence of Cu^{2+} , As^{3+} , Cd^{2+} , Ni^{2+} , and Zn^{2+} [108]. Electrostatic interaction was also reported to be the main mechanism on removal of dyes. Cationic dyes such as methylene blue and malachite green were adsorbed by magnetic zeolite-alginate-polyanetholesulfonic acid gel beads effectively due to the presence of new additional sulfonic group. The formed electrostatic interaction can be interrupted by ionic solution. Therefore NaCl solution is desorption solution for regeneration of the used adsorbent [109]. In order to achieve high performance adsorption, parameters such as pH, contact time, and initial concentration have to be optimized. pH of solution showed less effect on the adsorption of methylene blue by magnetic alginate/rice husk bio-composite [110]. Adsorption optimization by using Taguchi method showed that removal of methylene blue by magnetic alginate is highly influenced by adsorbent dose, contact time, initial methylene blue concentration, and intensity of external magnetic field [111].

3.4 Cellulose Based Magnetic Adsorbent

Application of magnetic cellulose on removal of heavy metal ion and dyes is presented in Table 4. Particle size is an important parameter which determines the adsorptive performance of synthesized adsorbent. Magnetic cellulose nanofluid with size ranged from 21 to 41 nm showed adsorption ability towards methylene blue. Due to higher specific area, smaller nanofluid has higher Q_{max} value compared to bigger nanofluid. The adsorption experiment showed that adsorption of methylene blue by magnetic cellulose follows physisorption mechanism [112]. The carboxylate ($-\text{COOH}$) and hydroxyl ($-\text{OH}$) groups interact with dyes via electrostatic interaction. Several efforts have been conducted to increase the number of such groups of magnetic cellulose including grafting and co-polymerization. Grafting of polyacrylic acid on magnetic cellulose increased its ability to adsorb methylene blue in aqueous medium up to 332 mg/g due to high content of $-\text{COOH}$ and $-\text{OH}$ [113]. Glutaric acid functionalized magnetic cellulose beads showed higher ability on removal of methylene blue and rhodamine B [114]. Not only methylene blue, but other cationic dyes such as crystal violet were also adsorbed by functionalized magnetic cellulose via electrostatic interaction [115]. Co-grafting of 3-chloro-2-hydroxypropyl trimethyl ammonium chloride and 2-acrylamide-2-methylpropane sulfonic acid provided magnetic cellulose with new organic groups, ammonium (cationic group) and sulfonic (anionic group) which actively contributed to adsorption. The obtained amphiprotic adsorbent can be used to remove both anionic (Congo Red) and cationic

Table 4 Removal of various heavy metal ions and dyes by magnetic cellulose

No.	Adsorbent	Synthesis of magnetic cellulose	Modification	Ms (emu/g)	Adsorption				Reference				
					Adsorbate	pH	Equilibrium time (min)	Kinetics		Qmax (mg/L)	Isotherm	Description	Recycle
1	2-mercaptobenzamide modified itaconic acid-grafted-magnetic nanocellulose composite carboxyl functionalized magnetic nanocellulose composite	In situ coprecipitation	Itaconic acid and 2 mercaptobenzamide grafting	0.18	Co(II)	6.5	60	PSO	349.62	Sips	0.1 M HCl	6	[118]
2	PEI-grafted magnetic cellulose	Blending	Blending with polyethyleneimine	–	Cr(VI)	3	10	Avrami	421.8	Langmuir	0.1 M NaOH	6	[136]
3	Nano-magnetic cellulose	In situ coprecipitation	Grafting with tetraethylenepentamine by using glycidyl methacrylate as bridging agent	–	Hg(II), Cu (II) and Ag(I)	2 (Hg(II)), 5.4 (Cu(II)) and 6.3 (Ag(I))	3–5 min	PSO	2 mmol/g (Hg(II)), 1.5 mmol/g (Cu(II)), and 1.2 mmol/g (Ag(II))	Langmuir	0.5 M thiourea-0.2 M H ₂ SO ₄ mixture solution	8	[137]
4	Amphiprotic cellulose mediated graphene oxide magnetic aerogels	Blending	Fe3O4 dispersed in premodified microcrystalline cellulose with 3-chloro-2-hydroxypropyl trimethyl ammonium chloride and 2-acrylamide-2-methylpropane sulfonic acid	8.61	Dyes (CR and MB) and heavy metal ions (Cu(II), Pb(II), Cd (II), and Cr(III))	3 (CR), 6 (MB) and 4–6 (heavy metal ions)	200	PSO	222.22 (Cu (II)), 568.2 (Pb(II)), 185.5 (Cd (II)), 122.2 (Cr(III)), 1015.1 (CR) and 781.3 (MB)	Langmuir	Weak acidic solution (pH 5)	5	[116]

5	Starch grafted copolymers of 2-acrylamido-2-methyl propane sulfonate and acrylic acid (starch-g-(AMPS-co-AA)) hydrogel with magnetite-functionalized cellulose nanocrystals (MCNCs)	In situ coprecipitation	Copolymerization with starch, 2-Acrylamido-2-methylpropanesulfonic acid and acrylic acid	0.46	CV and MB	9	71 (CV) and 16 (MB)	PSO	2500 (CV) and 1.428 (MB)	Langmuir	Diluted HCl solution (pH 4)	6	[115]
6	Functionalized porous magnetic cellulose/Fe ₃ O ₄ beads	Blending	Glutaric anhydride grafting	9.34	MB and RhB	9 (MB) and 7 (RhB)	120	PSO	1186.8 (MB) and 151.8 (RhB)	Langmuir	0.1 M HCl	5	[114]

dyes (methylene blue). It also showed high affinity toward heavy metal ions such as Cu(II), Pb(II), Cd(II), and Cr(III) [116]. Adsorption mechanism of magnetic carboxymethyl cellulose with heavy metal ion can be studied by XPS. Oxygen peak of mono- and bi-dentate carboxylate of magnetic carboxymethyl cellulose shifted from 529.9 to 531.1 eV and 533.1 to 531.9 eV, respectively, after adsorption of Pb(II), which indicated Pb(II)-O bond formation via electrostatic interaction [117]. Since electrostatic interaction seems to be the main mechanism on removal of magnetic cellulose, the presence of other anion and cation could interfere the adsorption of heavy metal ion. Adsorption of Co(II) by 2-mercaptobenzamide modified itaconic acid-grafted-magnetite nanocellulose composite was interfered by the presence of other cation in the following order: $\text{Ca}^{2+} > \text{Mg}^{2+} > \text{K}^+ > \text{Na}^+$ due to competition of such cation with Co(II) to bind with the active surface of adsorbent [118]. On the other hand, adsorption of As(V) was not interfered by the presence of cation such as Ca^{2+} , Fe^{2+} , and Mg^{2+} . However, anions such as PO_4^{3-} , NO_3^- , SO_4^{2-} and Cl^- competed with Co(II) during the adsorption process. Beside the nature of adsorbent, adsorption of heavy metal ion by magnetic cellulose was strongly influenced by pH, contact time, adsorbent dose, and initial concentration of adsorbate.

3.5 Pectin Based Magnetic Adsorbent

Adsorption removal performance of magnetic pectin based adsorbent mainly depends on the number of active adsorption sites on its structure. Application of magnetic pectin on removal of heavy metal ion and dyes is presented in Table 5. Grafting of poly(N-hydroxyethyl acrylamide) on magnetic pectin was reported to enhance its performance on removal of Cu(II), Hg(II), and Rhodamine 6G from aqueous solution [119]. Blending other active materials often conducted to increase the removal adsorption performance of magnetic pectin. Co-blending of graphene oxide (GO) and Prussian blue with magnetic pectin show higher adsorption capacity toward Cs(I) ion in comparison with magnetic graphene oxide-Prussian blue, magnetic pectin Prussian blue, and magnetic Prussian blue nanocomposites. The number of adsorbed Cs(I) mainly depended on the amount of Prussian blue of adsorbent. Surface composition survey by XPS showed that the presence of -OH and -COOH groups of pectin and graphene oxide increased the number of attached Prussian blue on the magnetic adsorbent [120], therefore to increase its adsorption performance. Magnetic pectin blended with polymers such as gluten increased its capability on adsorption of As, Ba, Cd, Pb, and Hg from the surface water of Lake Urmia (Iran) sediment. Presence of gluten on the structure of composite depressed its solubility while highly swelling pectin played the main role in removal of heavy metal ions [121]. Blending of starch with magnetic pectin showed ability on removal of methylene blue from aqueous solution at pH 8 [122]. Similar result was obtained by magnetic silica-pectin nanocomposite. Cationic dyes such as crystal violet and methylene blue were removed effectively in basic media. On the other hand, anionic

Table 5 Removal of various heavy metal ions and dyes by magnetic pectin

No.	Adsorbent	Synthesis of magnetic pectin	Modification	Ms (emu/gr)	Adsorption				Kinetics model	Qmax (mg/g)	Isotherm model	Desorption	Recycle	Reference
					Adsorbate	pH	Equilibrium time (min)							
1	Pectin/Prussian blue/Fe ₃ O ₄ /graphene oxide	In situ reduction	Blending with GO	8	Cs(I)	7	24 h	PSO	1–90 mmol	Langmuir (1.6 mmol/g)	–	–	[120]	
2	Gluten/pectin/Fe ₃ O ₄ /Nano-hydrogel	Blending	Blending with gluten		As, Ba, Cd, Pb, Hg	–	–						[121]	
3	Fe ₃ O ₄ embedded pectin-graft-poly (N-hydroxyethyl acrylamide) hydrogel	In situ coprecipitation	Pre-grafting with poly (N-hydroxyethyl acrylamide)	0.7367	Rh6G, Cu (II), Hg (II)	–	–	PFO	10–500 mg/L (dye), 20–1,000 mg/L (metal ion)	Langmuir, 169.49 mg/g (R6G), 5,000 mg/g (Cu(II)) and 770 mg/g (Hg(II))	–	–	[119]	
4	Fe ₃ O ₄ -silica/pectin double shell	Blending	–	24.4	CV	8 (CV, MB) and 2 (EBT, MO)	120	PSO	197.18 (CV), 180.29 (MB), 65.35 (EBT) and 26.75 (MO)	Sips	Acetic acid/methanol or NaOH/methanol	3	[123]	
5	Starch/pectin/Fe ₃ O ₄ nanoparticles	In situ coprecipitation	–	–	MB	8	–	–	–	–	–	–	[122]	
6	Fe ₃ O ₄ /pectin-Chlorella vulgaris biomass	In situ coprecipitation	Pre-blending with Chlorella vulgaris	–	MB, MR, MO, TB, CV, SO, BB, BP, MG and its mixture	–	30	–	–	109.11–287.05 mg/g	Microwave assisted	10	[124]	

dyes such as eriochrome black T and methyl orange were adsorbed at acidic condition. Electrostatic interaction was the main adsorption mechanism for such dyes [123]. Blending of magnetic pectin with *Chlorella vulgaris* biomass showed outstanding performance on removal of single and multi-dyes in aqueous media with maximum capacity range from 109.11 to 287.05 mg/g within 30 min of contact time. Applied adsorbent can be regenerated easily by microwave reactor and can be re-used up to 10 cycles of adsorption-desorption [124].

3.6 Future Perspectives

Polysaccharides-based magnetic adsorbents have attracted greatly researchers and environmentalist's attention due to its superiority over numerous conventional adsorbents especially its simple recollection under magnetic field and regeneration. Published reports showed that electrostatic attraction, hydrogen bonding, π - π stacking as well as chemical bonding are the main adsorption mechanisms between polysaccharides-based magnetic adsorbent with dyes or heavy metal ions. Its cost-effective, simple recollection, and regeneration have made polysaccharides-based magnetic adsorbent prospective to be applied in larger scale. However, there are some issues that need to consider as future perspectives: (1) Preparation and modification of polysaccharides-based magnetic adsorbent are complex and troublesome. Therefore, a simple preparation method is encouraged to be developed so then energy and production costs can be minimized, (2) Stability and mechanical strength of polysaccharides-based magnetic adsorbents are considerably low in comparison with conventional adsorbents which leads to a low regeneration performance, (3) Adsorptive performance should be optimized by established method such as response surface method (RSM) prior to its larger scale application especially for continuous adsorption system, (4) Most of the reported adsorption studies were performed at lab scale with single pollutant as adsorbate. On the other hand, dyes and heavy metal ion in real contaminated water or wastewater are present in complex structures of multi-pollutant, and (5) Fate and toxicity of prepared adsorbent should be evaluated as well in order to ensure its environmental friendliness (Fig. 11).

4 Functionalized Natural Magnetic Materials

4.1 Natural Magnetic Materials from Iron Sand

4.1.1 Resources and Composition of Iron Sand

Iron sand is one type of sand with high concentration of natural magnetic material (NMM) [138]. In nature, iron sand is formed by the weathering process of iron-rich volcanic rocks and thus, it appears blackish in color and can be found worldwide but

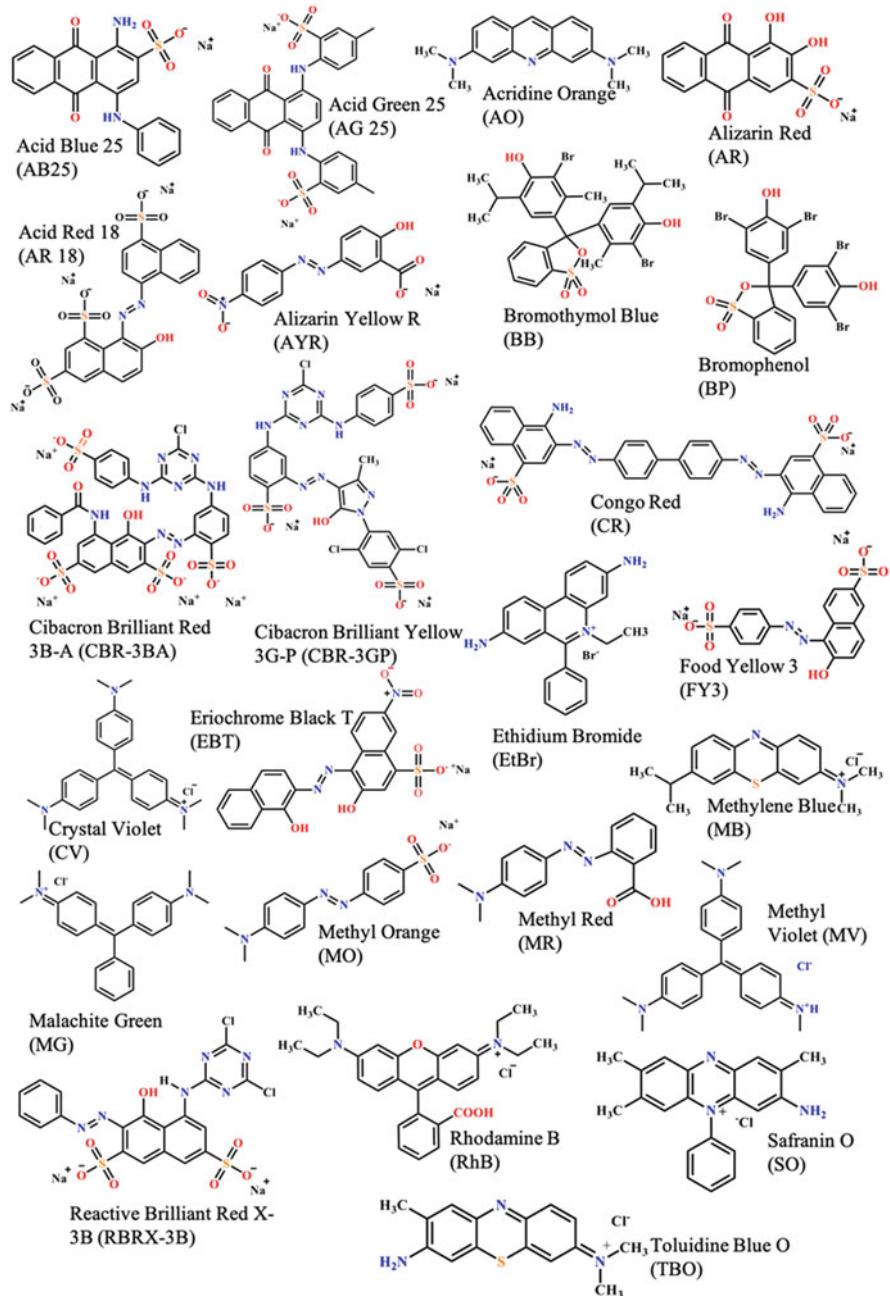


Fig. 11 Various types of dyes used as pollutant target on water remediation by magnetic polysaccharides

Table 6 The composition of iron sand from different areas

Country	Area	Fe ₂ O ₃ (%)	Fe ₃ O ₄ (%)	TiO ₂ (%)	SiO ₂ (%)	Al ₂ O ₃ (%)	Reference
Black Sea	Black Sea	15.4	–	1.0	45.6	5.1	[150]
Costa Rica	Atlantic coast, Cahuita	13.97	86.03% as titanomagnetite		–	–	[146]
Indonesia	Bugel Beach, Yogyakarta	70.18	–	6.61	11.0	5.0	[151]
	Bonto Kanang, South Sulawesi	–	59	–	–	11	[152]
	Glagah Beach, Yogyakarta	37.5	–	4.18	40.0	8.07	[142]
	North coast of Java (disclosed area)	35	55	–	–	–	[143]
	Syiah Kuala beach, Aceh	–	85.80	5.65	2.92	1.51	[144]
	Tor River Estuary, Papua	54.4	–	4.27	21.6	6.34	[149]
Italia	Mediterranean Sea	<12.6	87.4	<12.6			[153]
Japan	Sanin-Shirakawa belt	1.47	–	0.47	66.96	17.06	[154]
	Shimane prefecture	73.72	–	1.95	3.84	0.72	[154]
New Zealand	New Zealand	43.36	–	7.95	2.34	3.78	[155]
	Waikato north head	57.2	–	7.43	2.17	3.59	[156]
	Waitakere coast, Auckland	0–6	0–40% as titanomagnetite		–	–	[145]

prevalent in volcano-rich countries like New Zealand, Japan, and Indonesia. In New Zealand, the extensive volcanic areas of North Island produce heavy coastal and offshore concentrations of iron sand [139, 140], while in Japan, iron sand can be found in coastal areas of Kuji in Iwate, Tanegashima island in Kagoshima, Hiroshima in Chugoku, Funkawan in Hokkaido, and Naarai in Chiba [141]. Meanwhile, in Indonesia, the southern coast of Java island is the main source of iron sand. Table 6 shows the reported composition of iron sand from different areas. It is obvious that the composition of iron sand depends on the area where the iron sand is taken. While the south and north coasts of Java island, Indonesia, are dominated by maghemite [142, 143], in Syiah Kuala beach, which is one of the westernmost coasts of the country, is dominated by magnetite [144]. In New Zealand, on the other hand, most resources are predominated by titanomagnetite [139, 145].

4.1.2 Separation of Magnetic Materials from Iron Sand

The preparation of NMM from iron sand is typically initiated by air-drying the iron sand followed by separation of NMM from other non-magnetic compounds with an external magnet. The physical appearance change of iron sand after and before being magnetically separated is presented in Fig. 12. Separated iron sand NMM is then

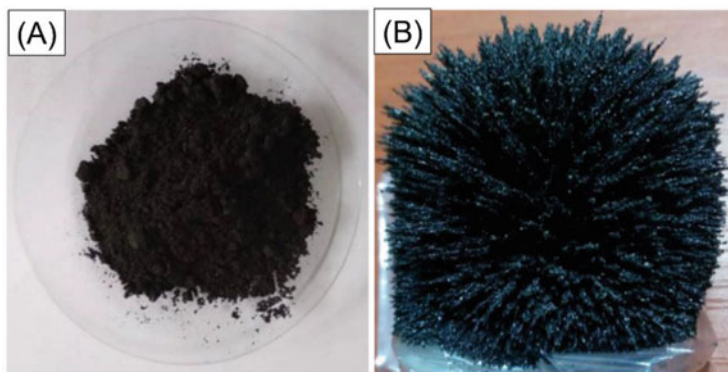


Fig. 12 Iron sand obtained from Bugel beach, Kulon Progo, Indonesia (a) before and (b) after physically separation process (obtained with permission from [151])

crushed to an intended size using sieve apparatus and subsequently washed with pure water in a batch with the help of ultrasound radiation to further separate the remaining non-magnetic compounds. After drying at moderate temperature (60–80°C), iron sand NMM is obtained [148, 151, 157]. The content of NMM depends on the sampling location even though from the same district of Yogyakarta. In the western part of Yogyakarta southern coast (Bugel), the content of NMM reaches 89.5% and it is higher than that in iron sand sampled from the eastern part (Bantul) (66.32% (w/w)) [151]. The content of metal oxides in iron sand affects the magnetic properties of the iron sand as well as NMM obtained. For instance, iron sand NMM from Atlantic coast of Costa Rica which predominated by titanomagnetite is a semi-hard magnet with H_c value of 39.6 Oe ($3.151 \times 10^3 \text{ A m}^{-1}$) [146], while the iron sand NMM from coastal areas in Yogyakarta, Indonesia, where maghemite and hematite are predominant, are soft magnet ($H_c < 10^3 \text{ A m}^{-1}$) [147, 148]. On the other hand, Togibasa et al. [149] reported that iron sand NMM from Top River, Estuary Papua, which has high content of magnetite (54.4%), is a semi-hard magnet ($H_c = 1.591 \times 10^3 \text{ A m}^{-1}$).

4.2 Functionalization of Natural Magnetic Materials with Functional Groups and the Application as Adsorbents

Table 7 shows the functional groups that have been used for the modification of NMM as well as their application as adsorbents for the removal of pollutants in water. Unfortunately, only few numbers of studies on the functionalization of NMM with functional groups and their application for wastewater treatment are reported

Table 7 Compounds used for the modification of iron sand NMM and the application for the adsorption of pollutants in water

Organic compound	Pollutant	pH	$q_{\max}/\text{mg g}^{-1}$	Reference
Chitosan	Au^{3+}	5	149.20	[147]
	Au^{3+} from PCBs waste solution	3	94.34	[158]
	Hg^{2+}	4	9.53	[159]
	Methylene blue	4–12	20.408	[160]
Diethylenetriamine	Au^{3+}	2	285.71	[157]
1-(o-tolyl)biguanide	Au^{3+}	1	9.44	[148]
2-aminobenzimidazole	Au^{3+}	1	17.15	[148]

despite the fact that magnetic particle prepared from iron sand is far cheaper than the synthetic ones (Fig. 13).

4.2.1 Functionalization with Amine Groups

So far, only four papers have reported the modification of iron sand NMM with amine groups [148, 157, 161, 162]. One of them is our recent work on the functionalization of silica-coated iron sand NMM with 3-chloropropyltrimetoxisilane (CPTS)-coupled 1-(o-tolyl)biguanide (NMM@[OB-CPTS-SiO₂]) and 2-aminobenzimidazole (NMM@[AB-CPTS-SiO₂]) used for the adsorption of Au^{3+} [148]. The composites were prepared by using conventional sol-gel method. CPTS in this case acts as a linker between silica-coated NMM and OB or AB. The results showed that the coating of iron sand NMM with OB and AB indeed reduced the crystallinity of magnetite, while it was also significantly decreased the saturation field (M_s) of iron sand NMM from 44.90 to 10.60 and 23.30 emu g⁻¹ for OB and AB, respectively (Fig. 14). Nevertheless, both adsorbents were still strongly affected by an external magnet. Further, the adsorption test showed that the adsorption capacity of NMM@[OB-CPTS-SiO₂] (9.44 mg g⁻¹) was lower than that of NMM@[AB-CPTS-SiO₂] (17.5 mg g⁻¹) regardless of the fact that OB has more amine (-NH₂) functional group than AB. The steric hindrance of adsorbed Au^{3+} on OB is likely the factor causing such phenomena [148]. This is supported by the fact that diethylenetriamine, which possessed a simpler geometry than OB and AB, showed adsorption capacity to Au^{3+} more than 15 times higher than that of OB and AB (Table 7).

4.2.2 Functionalization with Chitosan

Functionalization of magnetic materials, especially magnetite, with chitosan has been widely reported, mainly because of its low cost and abundant availability in nature. Moreover, amine group of chitosan is very reactive compared to other functional groups in binding metal ions [97]. The high reactivity is owing to the

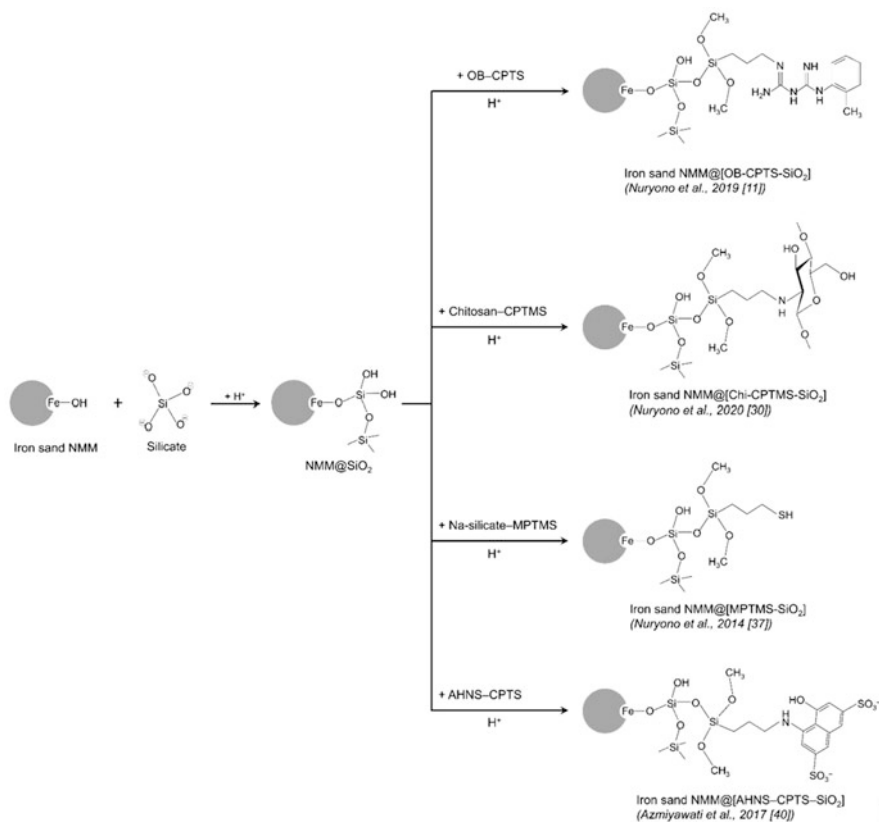


Fig. 13 Schematic illustration of the functionalization of iron sand NMM with 1-(o-tolyl)biguanide (OB), chitosan, (3-mercaptopropyl)trimethoxysilane (MPTMS), and 4-amino-5-hydroxy-naphtalene-2,7-disulfonic acid (AHNS)

ability of amine in adsorbing metal ions through different mechanisms, depending on the metal, reaction pH, and matrix of the solution [163]. While two free electrons of nitrogen atom of amine give the ability to adsorb metal ions at neutral pH, the protonation under acidic condition makes amine behave as a cation which thus has the potential for binding metal anions [163–165].

Functionalization of iron sand NMM with chitosan is generally performed in the presence of crosslinkers, such as glutaraldehyde [159], sulfuric acid (H₂SO₄) [160], sodium silicate [147, 158], 3-glycidyloxypropyltrimethoxysilane (GPTMS) [158], and 3-chloropropyltrimethoxysilane (CPTMS) [166], in order to increase the mechanical performance of the composite. Among them, sodium silicate is the most used crosslinker. Typically, the functionalization process is initiated by the surface activation of iron sand NMM with an acidic solution, such as acetic acid [159, 160] and HCl [147, 158]. The as-activated iron sand NMM is then introduced into a mixture of chitosan and a fixed concentration of crosslinker solution which

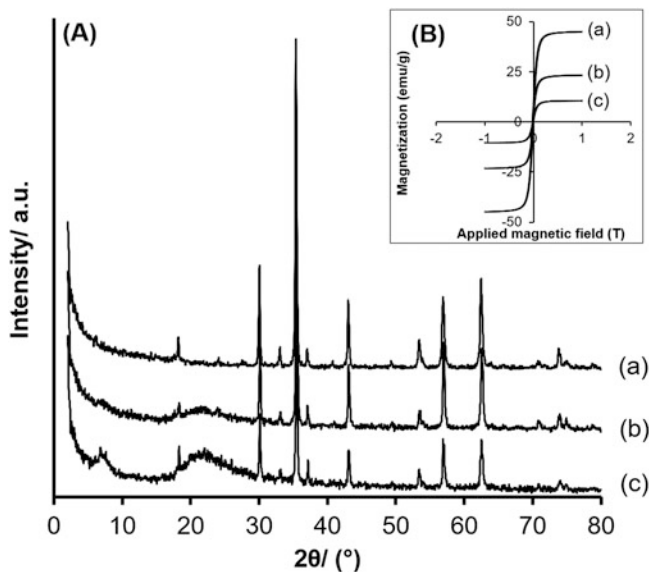


Fig. 14 (A) XRD spectra and (B) magnetic moments for (a) iron sand NMM, (b) NMM@[AB-CPTS-SiO₂] and (c) NMM@[OB-CPTS-SiO₂] (obtained with permission from [148])

subsequently followed with the addition of acidic solution to produce chitosan silica-coated iron sand NMM.

As shown in Table 7, in the last 5 years, chitosan-coated iron sand NMM has been used for the removal of Au³⁺ (including from PCBs solution), Hg²⁺, and methylene blue. Muflikhah et al. [147] reported that the coating of iron sand NMM with natural chitosan significantly decreased the saturation field M_s value from 43.40 to 20.15 emu g⁻¹. Nevertheless, the material was still able to be physically separated from aqueous medium by an external magnet and showed relatively high adsorption capacity toward Au³⁺, being 149.2 mg g⁻¹. In addition, Harumi et al. [158] also reported that chitosan-coated NMM was stable with repeated use and showed high selectivity toward Au³⁺ over Cu²⁺ and Ni²⁺ in PCBs solution. Recently, our research group also reported that the use of CPTMS as crosslinker between iron sand NMM with chitosan significantly improved the stability of adsorbent under acidic condition [166]. Although the adsorption capacity of CPTMS-crosslinked iron sand NMM/chitosan (112 mg g⁻¹) is slightly lower than that of siloxane-crosslinked NMM/chitosan (149.2 mg g⁻¹), it was reusable at least two times without significant decrease of Au³⁺ recovery while keeping high selectivity to Au³⁺ over Cu²⁺ and Zn²⁺ (Fig. 15).

Interestingly, we found that Au³⁺ was not only adsorbed onto MP@[Chi-CPTMS-SiO₂] but also reduced into Au⁰ on the surface of adsorbent. This was confirmed through the appearance of diffraction lines due to cubic plane of Au in the X-ray diffractogram of adsorbent after adsorption [166]. According to Adlim and Bakar, primary hydroxyl functional group of chitosan is the one responsible for

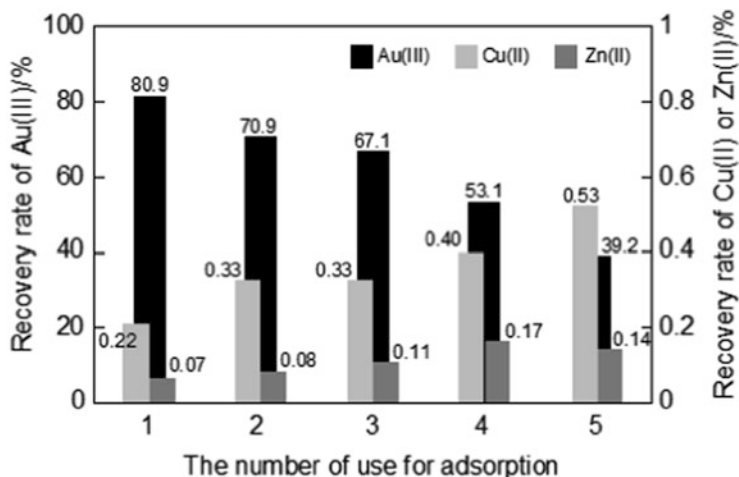


Fig. 15 Recovery rates of Au(III), Cu(II), and Zn(II) and repeated use of MP@[Chi-CPTMS(1/4)-SiO₂] for the adsorption experiments (obtained with permission from [166])

the reduction of Au³⁺ to Au⁰ [167]. Moreover, Rahmi et al. [159] reported that chitosan-coated iron sand NMM can be used repeatedly for the removal of Hg²⁺ without significant loss in adsorption capacity.

4.2.3 Functionalization with Mercaptans

Mercapto group or mercaptan is a group of any compounds that contain –SH (thiol) functional group in the structure. Since thiol is a superior ligand that has strong affinity to various heavy metal ions, it has been especially used for the modification of adsorbent materials [168, 169]. This is because, in aqueous solution, thiol is readily interacting with metal ions, notably Hg²⁺, Ag⁺, Cu²⁺, Ni²⁺, and Zn²⁺, through a Lewis acid–base interaction [170]. Although the use of mercaptan for the functionalization of synthetic magnetic materials has been vastly reported, for iron sand NMM, the number of papers reported is low. To the best of the authors' knowledge, our research group was the first to report the modification of iron sand NMM with mercaptan [171, 172].

Modification of iron NMM with mercaptan could be performed through a sol-gel method under acidic condition with the help of sodium silicate as described in [171, 173]. Being similar to that modification with amino groups and chitosan, a crosslinker is indispensable to connect mercaptan with NMM. Generally, the reaction mechanism for the process is as follows. Under acidic condition, silicate anion is protonated to form negatively charged siloxane species which readily interacts with iron sand NMM to produce silica-coated iron sand NMM. Further, the addition of mercaptan would then lead to an interaction between negatively charged siloxane and mercaptan to produce mercapto silica-coated iron sand NMM [171, 173].

We demonstrated that the functionalization of mercaptobenzimidazole ($C_7H_6N_2S$) into silica-coated iron sand NMM significantly increased the adsorption capacity toward Au(III) from 45.83 to 156.11 mg g^{-1} [172]. Further, we also confirmed that mercapto silica-coated iron sand NMM was able to withstand strong acid condition [171] and thus it is highly potential for the adsorption of heavy metal ions which require strong acidic condition to proceed the process.

4.2.4 Functionalization with Sulfonate

Sulfonate groups have been reported to have strong affinity to chemically bind with metal ions. We previously reported that the hybrid of sulfonate and silica showed high adsorption performance toward Mg^{2+} , Ca^{2+} , Pb^+ , and Ag^+ [174, 175], and thus modification of iron sand NMM with sulfonate group is an interesting topic since a paper by Azmiyawati et al. [176] is the only published report on the matter so far. Being similar to those previously discussed functional groups, sulfonate-modified iron sand NMM can be prepared through conventional sol-gel method in the presence of siliceous crosslinkers. In the case of Azmiyawati [176], 4-amino-5-hydroxy-naphthalene-2,7-disulfonic acid (AHNS) is the source of sulfonate functional group, while sodium silicate and CPTS are the crosslinkers (Fig. 13). Unfortunately, the application of iron sand NMM@[AHNS-CPTS-SiO₂] has not yet been reported. Therefore, the window for the development as well as the application of sulfonate-modified NMM for the removal of pollutants, especially heavy metal ions, is widely open.

5 Conclusion

As we have seen here, the magnetic adsorbents can adsorb a large variety of targets (polyaromatic hydrocarbons, pesticides, dyes, heavy metal ions, radioactive ions, and so on) by changing their designs.

The elements of their designs are magnetic materials, functional materials, and the structure of the magnetic adsorbent. The magnetic materials can be either synthetic or natural, and the functional materials for adsorption are available in a wide range of materials, from various small molecules to polymers, depending on the targets. The structure of the magnetic adsorbent consisting of magnetic materials and functional materials can be selected from the types of surface modification or composite.

A great number of magnetic adsorbents of various designs have been developed, but their adsorption properties and recoverability need to be further improved. The adsorption properties such as molecular recognition and adsorption selectivity are particularly important in the environment. For this purpose, the knowledge in the field of materials chemistry, including metal-organic frameworks (MOFs) such as Prussian blue and host-guest chemistry such as cyclodextrin may be a key to the

development of adsorbents with highly functional adsorption properties [177, 178]. The well-defined structural control of magnetic adsorbents has the potential to provide multiple adsorption properties, which will be important in the development of a magnetic adsorbent for removal of multiple targets [179]. In addition, there is still room for improvement in the efficiency of magnetic separation in the processing of a large and open system such as ocean and river, although it has been better than the efficiency of other conventional separation methods. More efficient magnetic separation could be achieved if the functional materials could provide the advanced functions like a controlled self-assembly to the adsorbents.

References

1. Zhang W, Zhang Y, Jiang Q, Zhao W, Yu A, Chang H, Lu X, Xie F, Ye B, Zhang S (2016) Tetraazacalix[2]arene[2]triazine coated Fe₃O₄/SiO₂ magnetic nanoparticles for simultaneous dispersive solid phase extraction and determination of trace multitarget analytes. *Anal Chem* 88:10523–10532. <https://doi.org/10.1021/acs.analchem.6b02583>
2. Kim J, Piao Y, Lee N, Park YI, Lee I-H, Lee J-H, Paik SR, Hyeon T (2010) Magnetic nanocomposite spheres decorated with NiO nanoparticles for a magnetically recyclable protein separation system. *Adv Mater* 22:57–60. <https://doi.org/10.1002/adma.200901858>
3. Ta DT, Vanella R, Nash MA (2017) Magnetic separation of elastin-like polypeptide receptors for enrichment of cellular and molecular targets. *Nano Lett* 17(12):7932–7939. <https://doi.org/10.1021/acs.nanolett.7b04318>
4. Kang K, Choi J, Nam JH, Lee SC, Kim KJ, Lee S-W, Chang JH (2009) Preparation and characterization of chemically functionalized silica-coated magnetic nanoparticles as a DNA separator. *J Phys Chem B* 113(2):536–543. <https://doi.org/10.1021/jp807081b>
5. Sutarlie L, Ow SY, Su X (2017) Nanomaterials-based biosensors for detection of microorganisms and microbial toxins. *Biotechnol J* 12:1500459. <https://doi.org/10.1002/biot.201500459>
6. Bohmer N, Demarmels N, Tsolaki E, Gerken L, Keevend K, Bertazzo S, Lattuada M, Herrmann IK (2017) Removal of cells from body fluids by magnetic separation in batch and continuous mode: influence of bead size, concentration, and contact time. *ACS Appl Mater Interfaces* 9(35):29571–29579. <https://doi.org/10.1021/acsami.7b10140>
7. Tukhani M, Panahi F, Khalafi-Nezhad A (2018) Supported palladium on magnetic nanoparticles–starch substrate (Pd-MNPSS): highly efficient magnetic reusable catalyst for C–C coupling reactions in water. *ACS Sustain Chem Eng* 6(1):1456–1467. <https://doi.org/10.1021/acssuschemeng.7b03923>
8. Tang W, Su Y, Li Q, Gao S, Shang JK (2013) Superparamagnetic magnesium ferrite nanoadsorbent for effective arsenic (III, V) removal and easy magnetic separation. *Water Res* 47(11):3624–3634. <https://doi.org/10.1016/j.watres.2013.04.023>
9. Hao L, Liu M, Wang N, Li G (2018) A critical review on arsenic removal from water using iron-based adsorbents. *RSC Adv* 8:39545–39560. <https://doi.org/10.1039/C8RA08512A>
10. Lu H, Salabas EL, Schüth F (2007) Magnetic nanoparticles: synthesis, protection, functionalization, and application. *Angew Chem Int Ed* 46:1222–1244. <https://doi.org/10.1002/anie.200602866>
11. Kharisov BI, Dias HVR, Kharissova OV, Vázquez A, Peña Y, Gómez I (2014) Solubilization, dispersion and stabilization of magnetic nanoparticles in water and non-aqueous solvents: recent trends. *RSC Adv* 4:45354–45381. <https://doi.org/10.1039/C4RA06902A>

12. Song Q, Zhang ZJ (2006) Correlation between spin–orbital coupling and the superparamagnetic properties in magnetite and cobalt ferrite spinel nanocrystals. *J Phys Chem B* 110(23):11205–11209. <https://doi.org/10.1021/jp060577o>
13. Shokry H, Elkady M, Salama E (2020) Eco-friendly magnetic activated carbon nano-hybrid for facile oil spills separation. *Sci Rep* 10:10265. <https://doi.org/10.1038/s41598-020-67231-y>
14. Yi Y, Huang Z, Lu B, Xian J, Tsang EP, Cheng W, Fang J, Fang Z (2020) Magnetic biochar for environmental remediation: a review. *Bioresour Technol* 298:122468. <https://doi.org/10.1016/j.biortech.2019.122468>
15. Wang P, Shi Q, Shi Y, Clark KK, Stucky GD, Keller AA (2009) Magnetic permanently confined micelle arrays for treating hydrophobic organic compound contamination. *J Am Chem Soc* 131(1):182–188. <https://doi.org/10.1021/ja806556a>
16. Honda H, Kawabe A, Shinkai M, Kobayashi T (1999) Recovery of recombinant *Escherichia coli* by chitosan-conjugated magnetite. *Biochem Eng J* 3(2):157–160. [https://doi.org/10.1016/S1369-703X\(99\)00009-1](https://doi.org/10.1016/S1369-703X(99)00009-1)
17. Yang L, Zhang Y, Liu X, Jiang X, Zhang Z, Zhang T, Zhang L (2014) The investigation of synergistic and competitive interaction between dye Congo red and methyl blue on magnetic $MnFe_2O_4$. *Chem Eng J* 246(15):88–96. [https://doi.org/10.1016/S1369-703X\(99\)00009-1](https://doi.org/10.1016/S1369-703X(99)00009-1)
18. Warner CL, Addleman RS, Cinson AD, Droubay TC, Engelhard MH, Nash MA, Yantasee W, Warner MG (2010) High-performance, superparamagnetic, nanoparticle based heavy metal sorbents for removal of contaminants from natural waters. *Chem Sus Chem* 3:749–757. <https://doi.org/10.1002/cssc.201000027>
19. Zhang H, Deng J, Wu Y (2017) Biobased magnetic microspheres containing aldehyde groups: constructed by vanillin-derived polymethacrylate/ Fe_3O_4 and recycled in adsorbing amine. *ACS Sustain Chem Eng* 5:658–666. <https://doi.org/10.1021/acssuschemeng.6b02018>
20. Parham H, Zargar B, Shiralipour R (2012) Fast and efficient removal of mercury from water samples using magnetic iron oxide nanoparticles modified with 2-mercaptobenzothiazole. *J Hazard Mater* 205–206:94–100. <https://doi.org/10.1016/j.jhazmat.2011.12.026>
21. Bayramoğlu G, Arica MY (2008) Adsorption of Cr(VI) onto PEI immobilized acrylate-based magnetic beads: isotherms, kinetics and thermodynamics study. *Chem Eng J* 139:20–28. <https://doi.org/10.1016/j.cej.2007.07.068>
22. Xiong B, Wang N, Chen Y, Peng H (2018) Self-assembly of alginate/polyethyleneimine multilayer onto magnetic microspheres as an effective adsorbent for removal of anionic dyes. *J Appl Polym Sci* 45876. <https://doi.org/10.1002/app.45876>
23. Luo J, Gao Y, Tan K, Wei W, Liu X (2016) Preparation of a magnetic molecularly imprinted graphene composite highly adsorbent for 4-Nitrophenol in aqueous medium. *ACS Sustain Chem Eng* 4:3316–3326. <https://doi.org/10.1021/acssuschemeng.6b00367>
24. Zhou L, Hu Y, Li G (2016) Conjugated microporous polymers with built-in magnetic nanoparticles for excellent enrichment of trace hydroxylated polycyclic aromatic hydrocarbons in human urine. *Anal Chem* 88:6930–6938. <https://doi.org/10.1021/acs.analchem.6b01708>
25. Zhu J, Wei S, Chen M, Gu H, Rapole SB, Pallavkar S, Ho TC, Hopper J, Guo Z (2013) Magnetic nanocomposites for environmental remediation. *Adv Powder Technol* 24(2):459–467. <https://doi.org/10.1016/j.apt.2012.10.012>
26. Huang D, Deng C, Zhang X (2014) Functionalized magnetic nanomaterials as solid phase extraction adsorbents for organic pollutants in environmental analysis. *Anal Methods* 6:7130–7141. <https://doi.org/10.1039/c4ay01100g>
27. Elkady M, Shokry H, Hamad H (2018) Microwave-assisted synthesis of magnetic hydroxyapatite for removal of heavy metals from groundwater. *Chem Eng Technol* 41(3):553–562. <https://doi.org/10.1002/ceat.201600631>
28. Matlochová A, Plachá D, Rapantová N (2013) The application of nanoscale materials in groundwater remediation. *Pol J Environ Stud* 22(5):1401–1410

29. Nuñez L, Buchholz BA, Vandegrift GF (1995) Waste remediation using in situ magnetically assisted chemical separation. *Sep Sci Technol* 30(7–9):1455–1471. <https://doi.org/10.1080/01496399508010357>
30. Chen F, Song Z, Nie J, Yu G, Li Z, Lee M (2016) Ionic liquid-based carbon nanotube coated magnetic nanoparticles as adsorbent for the magnetic solid phase extraction of triazole fungicides from environmental water. *RSC Adv* 6:81877. <https://doi.org/10.1039/c6ra16682b>
31. Nodeh HR, Ibrahim WAW, Ali I, Sanagi MM (2016) Development of magnetic graphene oxide adsorbent for the removal and preconcentration of As(III) and As(V) species from environmental water samples. *Environ Sci Pollut Res* 23:9759–9773. <https://doi.org/10.1007/s11356-016-6137-z>
32. Luo X, Zhana Y, Huang Y, Yanga L, Tua X, Luo S (2011) Removal of water-soluble acid dyes from water environment using a novel magnetic molecularly imprinted polymer. *J Hazard Mater* 187:274–282. <https://doi.org/10.1016/j.jhazmat.2011.01.009>
33. Jiang D, Amano Y, Machida M (2017) Removal and recovery of phosphate from water by a magnetic Fe₃O₄@ASC adsorbent. *J Environ Chem Eng* 5(5):4229–4238. <https://doi.org/10.1016/j.jece.2017.08.007>
34. Funes A, Martínez FJ, Alvarez-Manzaneda I, Conde-Porcuna JM, de Vicente J, Guerrero F, de Vicente I (2018) Determining major factors controlling phosphorus removal by promising adsorbents used for lake restoration: a linear mixed model approach. *Water Res* 141:377–386. <https://doi.org/10.1016/j.watres.2018.05.029>
35. Huang C, Hu B (2008) Speciation of inorganic tellurium from seawater by ICP-MS following magnetic SPE separation and preconcentration. *J Sep Sci* 31:760–767. <https://doi.org/10.1002/jssc.200700405>
36. Wang W, Ma X, Wu Q, Wang C, Zang X, Wang Z (2012) The use of graphene-based magnetic nanoparticles as adsorbent for the extraction of triazole fungicides from environmental water. *J Sep Sci* 35:2266–2272. <https://doi.org/10.1002/jssc.201200285>
37. Ozay O, Ekici S, Baran Y, Aktas N, Sahiner N (2009) Removal of toxic metal ions with magnetic hydrogels. *Water Res* 43(17):4403–4411. <https://doi.org/10.1016/j.watres.2009.06.058>
38. Yang HM, Hwang KS, Park CW, Lee KW (2017) Sodium-copper hexacyanoferrate-functionalized magnetic nanoclusters for the highly efficient magnetic removal of radioactive caesium from seawater. *Water Res* 125(15):81–90. <https://doi.org/10.1016/j.watres.2017.08.037>
39. Sahoo Y, Goodarz A, Swihart MT, Ohulchanskyy TY, Kaur N, Furlani EP, Prasad P (2005) Aqueous ferrofluid of magnetite nanoparticles: fluorescence labeling and magnetophoretic control. *J Phys Chem B* 109:3879–3885. <https://doi.org/10.1021/jp045402y>
40. Liu B, Zhang W, Yang F, Feng H, Yang X (2011) Facile method for synthesis of Fe₃O₄@polymer microspheres and their application as magnetic support for loading metal nanoparticles. *J Phys Chem C* 115:15875–15884. <https://doi.org/10.1021/jp204976y>
41. Stanciu MC, Nichifor M (2019) Adsorption of anionic dyes on a cationic amphiphilic dextran hydrogel: equilibrium, kinetic, and thermodynamic studies. *Colloid Polym Sci* 297:45–57. <https://doi.org/10.1007/s00396-018-4439-z>
42. Zhu Z, Zhang M, Wang W, Zhou Q, Liu F (2018) Efficient and synergistic removal of tetracycline and Cu(II) using novel magnetic multi-amine resins. *Sci Rep* 8:4762. <https://doi.org/10.1038/s41598-018-23205-9>
43. Khalfaoui M, Knani S, Hachicha MA, Lamine AB (2003) New theoretical expressions for the five adsorption type isotherms classified by BET based on statistical physics treatment. *J Colloid Interface Sci* 263:350–356. [https://doi.org/10.1016/S0021-9797\(03\)00139-5](https://doi.org/10.1016/S0021-9797(03)00139-5)
44. Sasaki T, Tanaka S (2011) Adsorption behavior of some aromatic compounds on hydrophobic magnetite for magnetic separation. *J Hazard Mater* 196:327–334. <https://doi.org/10.1016/j.jhazmat.2011.09.033>

45. Kasai Y, Kishira H, Syutsubo K, Harayama S (2001) Molecular detection of marine bacterial populations on beaches contaminated by the Nakhodka tanker oil-spill accident. *Environ Microbiol* 3(4):246–255. <https://doi.org/10.1046/j.1462-2920.2001.00185.x>
46. Boehm PD, Murray KJ, Cook LL (2016) Distribution and attenuation of polycyclic aromatic hydrocarbons in Gulf of Mexico seawater from the deepwater horizon oil accident. *Environ Sci Technol* 50:584–592. <https://doi.org/10.1021/acs.est.5b03616>
47. Yan Z, Zhang Z, Wang H, Liang F, Li J, Liu H, Sun C, Liang L, Liu Z (2012) Development of aquatic life criteria for nitrobenzene in China. *Environ Pollut* 162:86–90. <https://doi.org/10.1016/j.envpol.2011.11.007>
48. Gong Z, Alef K, Wilke BM, Li P (2007) Activated carbon adsorption of PAHs from vegetable oil used in soil remediation. *J Hazard Mater* 143(1–2):372–378. <https://doi.org/10.1016/j.jhazmat.2006.09.037>
49. Long RQ, Yang RT (2001) Carbon nanotubes as superior sorbent for dioxin removal. *J Am Chem Soc* 123(9):2058–2059. <https://doi.org/10.1021/ja003830l>
50. Vasilyeva GK, Strijakova ER, Nikolaeva SN, Lebedev AT, Shea PJ (2010) Dynamics of PCB removal and detoxification in historically contaminated soils amended with activated carbon. *Environ Pollut* 158(3):770–777. <https://doi.org/10.1016/j.envpol.2009.10.010>
51. Grbic J, Nguyen B, Guo E, You JB, Sinton D, Rochman CM (2019) Magnetic extraction of microplastics from environmental samples. *Environ Sci Technol Lett* 6:68–72. <https://doi.org/10.1021/acs.estlett.8b00671>
52. van Sebille E, Wilcox C, Lebreton L, Maximenko N, Hardesty BD (2015) A global inventory of small floating plastic debris. *Environ Res Lett* 10:124006. <https://doi.org/10.1088/1748-9326/10/12/124006>
53. de Souza Machado AA, Kloas W, Zarfl C, Hempel S, Rillig MC (2017) Microplastics as an emerging threat to terrestrial ecosystems. *Glob Chang Biol* 24:1405–1416. <https://doi.org/10.1111/gcb.14020>
54. Ji Y, Liu X, Guan M, Zhao C, Huang H, Zhang H, Wang C (2009) Preparation of functionalized magnetic nanoparticulate sorbents for rapid extraction of biphenolic pollutants from environmental samples. *J Sep Sci* 32:2139–2145. <https://doi.org/10.1002/jssc.200900018>
55. Kaur R, Hasan A, Iqbal N, Alam S, Saini MK, Raza SK (2014) Synthesis and surface engineering of magnetic nanoparticles for environmental cleanup and pesticide residue analysis: a review. *J Sep Sci* 37:1805–1825. <https://doi.org/10.1002/jssc.201400256>
56. Ozmen EY, Sezgin M, Yilmaz A, Yilmaz M (2008) Synthesis of β -cyclodextrin and starch based polymers for sorption of azo dyes from aqueous solutions. *Bioresour Technol* 99(3):526–531. <https://doi.org/10.1016/j.biortech.2007.01.023>
57. Szejtli J (1998) Introduction and general overview of cyclodextrin chemistry. *Chem Rev* 98:1743–1753. <https://doi.org/10.1021/cr970022c>
58. Ouyang G, Pawliszyn J (2006) Recent developments in SPME for on-site analysis and monitoring. *Trends Anal Chem* 25(7):692–703. <https://doi.org/10.1016/j.trac.2006.05.005>
59. David F, Sandra P (2007) Stir bar sorptive extraction for trace analysis. *J Chromatogr A* 1152(1–2):54–69. <https://doi.org/10.1016/j.chroma.2007.01.032>
60. Koarashi J, Nishimura S, Atarashi-Andoh M, Matsunaga T, Sato T, Nagao S (2018) Radiocesium distribution in aggregate-size fractions of cropland and forest soils affected by the Fukushima nuclear accident. *Chemosphere* 205:147–155. <https://doi.org/10.1016/j.chemosphere.2018.04.092>
61. Ochiai A, Imoto J, Suetake M, Komiya T, Furuki G, Ikehara R, Yamasaki S, Law GTW, Ohnuki T, Grambow B, Ewing RC, Satoshi U (2018) Uranium dioxides and debris fragments released to the environment with Cesium-rich microparticles from the Fukushima Daiichi nuclear power plant. *Environ Sci Technol* 52:2586–2594. <https://doi.org/10.1021/acs.est.7b06309>

62. Grambow B, Mostafavi M (2014) State of Fukushima nuclear fuel debris tracked by Cs137 in cooling water. *Environ Sci: Processes Impacts* 16:2472–2476. <https://doi.org/10.1039/C4EM00103F>
63. Wang J, Zhuang S (2019) Removal of cesium ions from aqueous solutions using various separation technologies. *Rev Environ Sci Biotechnol* 18:231–269. <https://doi.org/10.1007/s11157-019-09499-9>
64. Beneš J, Kyrš M (1963) The isolation of caesium-137 from liquid radioactive fall-out. *Anal Chim Acta* 29:564–568. [https://doi.org/10.1016/S0003-2670\(00\)88665-1](https://doi.org/10.1016/S0003-2670(00)88665-1)
65. Nakamura H, Okumura M, Machida M (2013) First-principles calculation study of mechanism of cation adsorption selectivity of zeolites: a guideline for effective removal of radioactive Cesium. *J Physical Soc Japan* 82:023801. <https://doi.org/10.7566/JPSJ.82.023801>
66. Sasaki T, Tanaka S (2012) Magnetic separation of Cesium ion using Prussian blue modified magnetite. *Chem Lett* 41:32–34. <https://doi.org/10.1246/cl.2012.32>
67. Chang S, Fu H, Wu X, Liu C, Li Z, Dai Y, Zhang H (2018) Batch and fixed-bed column studies for selective removal of cesium ions by compressible Prussian blue/polyurethane sponge. *RSC Adv* 8:36459. <https://doi.org/10.1039/c8ra07665k>
68. Kim H, Wi H, Kang S, Yoon S, Bae S, Hwang Y (2019) Prussian blue immobilized cellulosic filter for the removal of aqueous cesium. *Sci Total Environ* 670(20):779–788. <https://doi.org/10.1016/j.scitotenv.2019.03.234>
69. Yamashita Y, Sasaki T, Tanaka S (2017) Electrochemical synthesis and immobilization of a beadwork-like Prussian blue on carbon fiber and the removal of cesium. *J Environ Chem Eng* 5(3):2912–2920. <https://doi.org/10.1016/j.jece.2017.05.043>
70. Mihara Y, Sikder MT, Yamagishi H, Sasaki T, Kurasaki M, Itoh S, Tanaka S (2016) Adsorption kinetic model of alginate gel beads synthesized micro particle-prussian blue to remove cesium ions from water. *J Water Process Eng* 10:9–19. <https://doi.org/10.1016/j.jpwe.2016.01.001>
71. Yasutaka T, Kawamoto T, Kawabe Y, Sato T, Sato M, Suzuki Y, Nakamura K, Komai T (2013) Rapid measurement of radiocesium in water using a Prussian blue impregnated nonwoven fabric. *J Nucl Sci Technol* 50(7):674–681. <https://doi.org/10.1080/00223131.2013.797936>
72. Olatunji MA, Khandaker MU, Mahmud HNME, Amin YM (2015) Influence of adsorption parameters on cesium uptake from aqueous solutions- a brief Kenji review. *RSC Adv* 5: 71658–71683. <https://doi.org/10.1039/c5ra10598f>
73. Sasaki T, Yamashita A, Terui N, Hattori T, Tanaka S (2020) Evaluation of removal behavior of Cesium in contaminated soil based on speciation analysis. *Anal Sci* 36:589–594. <https://doi.org/10.2116/analsci.19SBP12>
74. Tessier A, Campbell PGC, Bisson M (1979) Sequential extraction procedure for the speciation of particulate trace metals. *Anal Chem* 51(7):844–851. <https://doi.org/10.1021/ac50043a017>
75. Bunzl K, Seblmmaek W, BeHi M, Riccardi M (1997) Sequential extraction of fallout radiocesium from the soil: small scale and large scale spatial variability. *J Radioanal Nucl Chem* 226:47–53. <https://doi.org/10.1007/BF02063623>
76. Vikrant K, Giri BS, Raza N, Roy K, Kim KH, Rai BN, Singh RS (2018) Recent advancements in bioremediation of dye: current status and challenges. *Bioresour Technol* 253:355–367. <https://doi.org/10.1016/j.biortech.2018.01.029>
77. Sen TK, Afroze S, Ang HM (2011) Equilibrium, kinetics and mechanism of removal of methylene blue from aqueous solution by adsorption onto pine cone biomass of *Pinus radiata*. *Water Air Soil Pollut* 218:499–515. <https://doi.org/10.1007/s11270-010-0663-y>
78. Ajmal A, Majeed I, Malik RN, Idriss H, Nadeem MA (2014) Principles and mechanisms of photocatalytic dye degradation on TiO₂ based photocatalysts: a comparative overview. *RSC Adv* 4:37003–37026. <https://doi.org/10.1039/c4ra06658h>
79. Reddy DHK, Lee SM (2013) Application of magnetic chitosan composites for the removal of toxic metal and dyes from aqueous solutions. *Adv Colloid Interface Sci* 201–202:68–93. <https://doi.org/10.1016/j.cis.2013.10.002>

80. Yang JS, Xie YJ, He W (2011) Research progress on chemical modification of alginate: a review. *Carbohydr Polym* 84:33–39. <https://doi.org/10.1016/j.carbpol.2010.11.048>
81. Hambali E, Sakti SCW, Fahmi MZ, Wahyudianto FE, Nuryono, Yessi P, Yani M, Sinurat E, Pratama BS (2018) Effect of extraction time and Na₂CO₃ concentration on the characteristics of alginate extracted from sargassum sp. *IOP Conf Ser Earth Environ Sci* 209. <https://doi.org/10.1088/1755-1315/209/1/012033>
82. Fernando IPS, Lee WW, Han EJ, Ahn G (2020) Alginate-based nanomaterials: fabrication techniques, properties, and applications. *Chem Eng J* 391:123823. <https://doi.org/10.1016/j.cej.2019.123823>
83. Quesada HB, de Araújo TP, Vareschini DT, de Barros MASD, Gomes RG, Bergamasco R (2020) Chitosan, alginate and other macromolecules as activated carbon immobilizing agents: a review on composite adsorbents for the removal of water contaminants. *Int J Biol Macromol* 164:2535–2549. <https://doi.org/10.1016/j.ijbiomac.2020.08.118>
84. Sakti SCW, Wijaya RA, Indrasari N, Fahmi MZ, Widati AA, Abdulloh N, Chen CH (2021) Magnetic hollow buoyant alginate beads achieving rapid remediation of oil contamination on water. *J Environ Chem Eng* 9:104935. <https://doi.org/10.1016/j.jece.2020.104935>
85. Gao X, Guo C, Hao J, Zhao Z, Long H, Li M (2020) Adsorption of heavy metal ions by sodium alginate based adsorbent—a review and new perspectives. *Int J Biol Macromol* 164:4423–4434. <https://doi.org/10.1016/j.ijbiomac.2020.09.046>
86. Oyewo EE, Elemike DC, Onwudiwe MS (2020) Onyango, metal oxide-cellulose nanocomposites for the removal of toxic metals and dyes from wastewater. *Int J Biol Macromol* 164:2477–2496. <https://doi.org/10.1016/j.ijbiomac.2020.08.074>
87. Peter Z (2020) Order in cellulose: historical review of crystal structure research on cellulose. *Carbohydr Polym*:117417. <https://doi.org/10.1016/j.carbpol.2020.117417>
88. Dong YD, Zhang H, Zhong GJ, Yao G, Lai B (2021) Cellulose/carbon composites and their applications in water treatment – a review. *Chem Eng J* 405:126980. <https://doi.org/10.1016/j.cej.2020.126980>
89. Tovar AK, Godínez LA, Espejel F, Ramírez-Zamora RM, Robles I (2019) Optimization of the integral valorization process for orange peel waste using a design of experiments approach: production of high-quality pectin and activated carbon. *Waste Manag* 85:202–213. <https://doi.org/10.1016/j.wasman.2018.12.029>
90. Shivamathi CS, Moorthy IG, Kumar RV, Soosai MR, Maran JP, Kumar RS, Varalakshmi P (2019) Optimization of ultrasound assisted extraction of pectin from custard apple peel: potential and new source. *Carbohydr Polym* 225:115240. <https://doi.org/10.1016/j.carbpol.2019.115240>
91. Zaitseva O, Khudyakov A, Sergushkina M, Solomina O, Polezhaeva T (2020) Pectins as a universal medicine. *Fitoterapia* 146:104676. <https://doi.org/10.1016/j.fitote.2020.104676>
92. Cao L, Lu W, Mata A, Nishinari K, Fang Y (2020) Egg-box model-based gelation of alginate and pectin: a review. *Carbohydr Polym* 242:116389. <https://doi.org/10.1016/j.carbpol.2020.116389>
93. Kloster GA, Valiente M, Marcovich NE, Mosiewicki MA (2020) Adsorption of arsenic onto films based on chitosan and chitosan/nano-iron oxide. *Int J Biol Macromol* 165:1286–1295. <https://doi.org/10.1016/j.ijbiomac.2020.09.244>
94. Gogoi P, Thakur AJ, Devi RR, Das B, Maji TK (2017) Adsorption of As(V) from contaminated water over chitosan coated magnetite nanoparticle: equilibrium and kinetics study. *Environ Nanotechnol Monit Manag* 8:297–305. <https://doi.org/10.1016/j.enmm.2017.09.002>
95. Sherlala AIA, Raman AAA, Bello MM, Buthiyappan A (2019) Adsorption of arsenic using chitosan magnetic graphene oxide nanocomposite. *J Environ Manage* 246:547–556. <https://doi.org/10.1016/j.jenvman.2019.05.117>
96. Kavosi Rakati K, Mirzaei M, Maghssoodi S, Shahbazi A (2019) Preparation and characterization of poly aniline modified chitosan embedded with ZnO-Fe₃O₄ for Cu(II) removal from aqueous solution. *Int J Biol Macromol* 130:1025–1045. <https://doi.org/10.1016/j.ijbiomac.2019.02.033>

97. Sakti SCW, Narita Y, Sasaki T, Nuryono ST (2015) A novel pyridinium functionalized magnetic chitosan with pH-independent and rapid adsorption kinetics for magnetic separation of Cr(VI). *J Environ Chem Eng*. <https://doi.org/10.1016/j.jece.2015.05.004>
98. Yadaei H, Beyki MH, Shemirani F, Nouroozi S (2018) Ferrofluid mediated chitosan@mesoporous carbon nanohybrid for green adsorption/preconcentration of toxic Cd (II): Modeling, kinetic and isotherm study. *React Funct Polym* 122:85–97. <https://doi.org/10.1016/j.reactfunctpolym.2017.10.011>
99. Xia T, Yin L, Xie Y, Ji Y (2020) Efficiently remove of Cs(I) by metals hexacyanoferrate modified magnetic Fe₃O₄-chitosan nanoparticles. *Chem Phys Lett* 746. <https://doi.org/10.1016/j.cplett.2020.137293>
100. Fan L, Zhang Y, Li X, Luo C, Lu F, Qiu H (2012) Removal of alizarin red from water environment using magnetic chitosan with alizarin red as imprinted molecules. *Colloids Surf B Biointerfaces* 91:250–257. <https://doi.org/10.1016/j.colsurfb.2011.11.014>
101. Yu C, Geng J, Zhuang Y, Zhao J, Chu L, Luo X, Zhao Y, Guo Y (2016) Preparation of the chitosan grafted poly (quaternary ammonium)/Fe₃O₄ nanoparticles and its adsorption performance for food yellow 3. *Carbohydr Polym* 152:327–336. <https://doi.org/10.1016/j.carbpol.2016.06.114>
102. Lu F, Dong A, Ding G, Xu K, Li J, You L (2019) Magnetic porous polymer composite for high performance adsorption of acid red 18 based on melamine resin and chitosan. *J Mol Liq* 294. <https://doi.org/10.1016/j.molliq.2019.111515>
103. Narita Y, Sakti SCW, Akemoto Y, Tanaka S (2019) Ultra-rapid removal of cationic organic dyes by novel single- and double-stranded DNA immobilized on quaternary ammonium magnetic chitosan. *J Environ Chem Eng* 7:103308. <https://doi.org/10.1016/j.jece.2019.103308>
104. Lim SF, Zheng YM, Zou SW, Chen JP (2009) Uptake of arsenate by an alginate-encapsulated magnetic sorbent: process performance and characterization of adsorption chemistry. *J Colloid Interface Sci* 333:33–39. <https://doi.org/10.1016/j.jcis.2009.01.009>
105. Hong HJ, Jeong HS, Kim BG, Hong J, Park IS, Ryu T, Chung KS, Kim H, Ryu J (2016) Highly stable and magnetically separable alginate/Fe₃O₄ composite for the removal of strontium (Sr) from seawater. *Chemosphere* 165:231–238. <https://doi.org/10.1016/j.chemosphere.2016.09.034>
106. Gopalakannan V, Viswanathan N (2015) Synthesis of magnetic alginate hybrid beads for efficient chromium (VI) removal. *Int J Biol Macromol* 72:862–867. <https://doi.org/10.1016/j.ijbiomac.2014.09.024>
107. Deepuppha N, Thongsaw A, Rutnakornpituk B, Chaiyaisith WC, Rutnakornpituk M (2020) Alginate-based magnetic nanosorbent immobilized with aptamer for selective and high adsorption of Hg²⁺ in water samples. *Environ Sci Pollut Res* 27:12030–12038. <https://doi.org/10.1007/s11356-020-07809-1>
108. Feng J, Zhang J, Song W, Liu J, Hu Z, Bao B (2020) An environmental-friendly magnetic bio-adsorbent for high-efficiency Pb(II) removal: preparation, characterization and its adsorption performance. *Ecotoxicol Environ Saf* 203:111002. <https://doi.org/10.1016/j.ecoenv.2020.111002>
109. Metin Ü, Doğan D, Can M (2020) Novel magnetic gel beads based on ionically crosslinked sodium alginate and polyanetholesulfonic acid: synthesis and application for adsorption of cationic dyes. *Mater Chem Phys* 256. <https://doi.org/10.1016/j.matchemphys.2020.123659>
110. Alver E, Metin AÜ, Brouers F (2020) Methylene blue adsorption on magnetic alginate/rice husk bio-composite. *Int J Biol Macromol* 154:104–113. <https://doi.org/10.1016/j.ijbiomac.2020.02.330>
111. Rezaei H, Haghshenasfard M, Moheb A (2017) Optimization of dye adsorption using Fe₃O₄ nanoparticles encapsulated with alginate beads by Taguchi method. *Adsorpt Sci Technol* 35: 55–71. <https://doi.org/10.1177/0263617416667508>

112. Anushree C, Philip J (2019) Efficient removal of methylene blue dye using cellulose capped Fe₃O₄ nanofluids prepared using oxidation-precipitation method. *Colloids Surf A Physicochem Eng Asp* 567:193–204. <https://doi.org/10.1016/j.colsurfa.2019.01.057>
113. Samadder R, Akter N, Roy AC, Uddin MM, Hossen MJ, Azam MS (2020) Magnetic nanocomposite based on polyacrylic acid and carboxylated cellulose nanocrystal for the removal of cationic dye. *RSC Adv* 10:11945–11956. <https://doi.org/10.1039/d0ra00604a>
114. Li B, Zhang Q, Pan Y, Li Y, Huang Z, Li M, Xiao H (2020) Functionalized porous magnetic cellulose/Fe₃O₄ beads prepared from ionic liquid for removal of dyes from aqueous solution. *Int J Biol Macromol* 163:309–316. <https://doi.org/10.1016/j.ijbiomac.2020.06.280>
115. Moharrami P, Motamedi E (2020) Application of cellulose nanocrystals prepared from agricultural wastes for synthesis of starch-based hydrogel nanocomposites: efficient and selective nanoadsorbent for removal of cationic dyes from water. *Bioresour Technol* 313:123661. <https://doi.org/10.1016/j.biortech.2020.123661>
116. Xiong J, Zhang D, Lin H, Chen Y (2020) Amphiprotic cellulose mediated graphene oxide magnetic aerogels for water remediation. *Chem Eng J* 400:125890. <https://doi.org/10.1016/j.cej.2020.125890>
117. Fan H, Ma X, Zhou S, Huang J, Liu Y, Liu Y (2019) Highly efficient removal of heavy metal ions by carboxymethyl cellulose-immobilized Fe₃O₄ nanoparticles prepared via high-gravity technology. *Carbohydr Polym* 213:39–49. <https://doi.org/10.1016/j.carbpol.2019.02.067>
118. Anirudhan TS, Shainy F, Deepa JR (2019) Effective removal of cobalt(II) ions from aqueous solutions and nuclear industry wastewater using sulfhydryl and carboxyl functionalised magnetite nanocellulose composite: batch adsorption studies. *Chem Ecol* 35:235–255. <https://doi.org/10.1080/02757540.2018.1532999>
119. Kulal P, Badalamoole V (2020) Magnetite nanoparticle embedded pectin-graft-poly (N-hydroxyethylacrylamide) hydrogel: evaluation as adsorbent for dyes and heavy metal ions from waste water. *Int J Biol Macromol* 156:1408–1417. <https://doi.org/10.1016/j.ijbiomac.2019.11.181>
120. Kadam AA, Jang J, Lee DS (2016) Facile synthesis of pectin-stabilized magnetic graphene oxide Prussian blue nanocomposites for selective cesium removal from aqueous solution. *Bioresour Technol* 216:391–398. <https://doi.org/10.1016/j.biortech.2016.05.103>
121. Pirsra S, Asadzadeh F, Karimi Sani I (2020) Synthesis of magnetic gluten/pectin/Fe₃O₄ nano-hydrogel and its use to reduce environmental pollutants from Lake Urmia sediments. *J Inorg Organomet Polym Mater* 30:3188–3198. <https://doi.org/10.1007/s10904-020-01484-y>
122. Nsom MV, Etape EP, Tendo JF, Namond BV, Chongwain PT, Yufanyi MD, William N (2019) A green and facile approach for synthesis of starch-pectin magnetite nanoparticles and application by removal of methylene blue from textile effluent. *J Nanomater* 2019. <https://doi.org/10.1155/2019/4576135>
123. Attallah OA, Al-Ghobashy MA, Nebsen M, Salem MY (2016) Removal of cationic and anionic dyes from aqueous solution with magnetite/pectin and magnetite/silica/pectin hybrid nanocomposites: kinetic, isotherm and mechanism analysis. *RSC Adv* 6:11461–11480. <https://doi.org/10.1039/c5ra23452b>
124. Khorasani AC, Shojaosadati SA (2019) Magnetic pectin-*Chlorella vulgaris* biosorbent for the adsorption of dyes. *J Environ Chem Eng* 7:103062. <https://doi.org/10.1016/j.jece.2019.103062>
125. Javanbakht V, Ghoreishi SM, Habibi N, Javanbakht M (2016) A novel magnetic chitosan/clinoptilolite/magnetite nanocomposite for highly efficient removal of Pb(II) ions from aqueous solution. *Powder Technol* 302:372–383. <https://doi.org/10.1016/j.powtec.2016.08.069>
126. Wang Y, Qi Y, Li Y, Wu J, Ma X, Yu C, Ji L (2013) Preparation and characterization of a novel nano-adsorbent based on multi-cyanoguanidine modified magnetic chitosan and its highly effective recovery for Hg(II) in aqueous phase. *J Hazard Mater* 260:9–15. <https://doi.org/10.1016/j.jhazmat.2013.05.001>
127. Tao X, Li K, Yan H, Yang H, Li A (2016) Simultaneous removal of acid green 25 and mercury ions from aqueous solutions using glutamine modified chitosan magnetic composite microspheres. *Environ Pollut* 209:21–29. <https://doi.org/10.1016/j.envpol.2015.11.020>

128. Zheng X, Zheng H, Xiong Z, Zhao R, Liu Y, Zhao C, Zheng C (2020) Novel anionic polyacrylamide-modify-chitosan magnetic composite nanoparticles with excellent adsorption capacity for cationic dyes and pH-independent adsorption capability for metal ions. *Chem Eng J* 392:123706. <https://doi.org/10.1016/j.cej.2019.123706>
129. Cao C, Xiao L, Chen C, Shi X, Cao Q, Gao L (2014) In situ preparation of magnetic Fe₃O₄/chitosan nanoparticles via a novel reduction-precipitation method and their application in adsorption of reactive azo dye. *Powder Technol* 260:90–97. <https://doi.org/10.1016/j.powtec.2014.03.025>
130. Vu HC, Dwivedi AD, Le TT, Seo SH, Kim EJ, Chang YS (2017) Magnetite graphene oxide encapsulated in alginate beads for enhanced adsorption of Cr(VI) and As(V) from aqueous solutions: role of crosslinking metal cations in pH control. *Chem Eng J* 307:220–229. <https://doi.org/10.1016/j.cej.2016.08.058>
131. Wu Z, Deng W, Zhou W, Luo J (2019) Novel magnetic polysaccharide/graphene oxide @Fe₃O₄ gel beads for adsorbing heavy metal ions. *Carbohydr Polym* 216:119–128. <https://doi.org/10.1016/j.carbpol.2019.04.020>
132. Ali I, Peng C, Lin D, Saroj DP, Naz I, Khan ZM, Sultan M, Ali M (2019) Encapsulated green magnetic nanoparticles for the removal of toxic Pb²⁺ and Cd²⁺ from water: development, characterization and application. *J Environ Manage* 234:273–289. <https://doi.org/10.1016/j.jenvman.2018.12.112>
133. Yadav S, Asthana A, Chakraborty R, Jain B, Singh AK, Carabineiro SAC, Susan MABH (2020) Cationic dye removal using novel magnetic/activated charcoal/β-cyclodextrin/alginate polymer nanocomposite. *Nanomaterials (Basel)* 10:170. <https://doi.org/10.3390/nano10010170>
134. Mohammadi A, Daemi H, Barikani M (2014) Fast removal of malachite green dye using novel superparamagnetic sodium alginate-coated Fe₃O₄ nanoparticles. *Int J Biol Macromol* 69:447–455. <https://doi.org/10.1016/j.ijbiomac.2014.05.042>
135. Rocher V, Bee A, Siaugue JM, Cabuil V (2010) Dye removal from aqueous solution by magnetic alginate beads crosslinked with epichlorohydrin. *J Hazard Mater* 178:434–439. <https://doi.org/10.1016/j.jhazmat.2010.01.100>
136. Li Y, Zhu H, Zhang C, Cheng M, He H (2018) PEI-grafted magnetic cellulose for Cr(VI) removal from aqueous solution. *Cellul* 25:4757–4769. <https://doi.org/10.1007/s10570-018-1868-2>
137. Donia AM, Atia AA, Abouzayed FI (2012) Preparation and characterization of nano-magnetic cellulose with fast kinetic properties towards the adsorption of some metal ions. *Chem Eng J* 191:22–30. <https://doi.org/10.1016/j.cej.2011.08.034>
138. Cornell RM, Schwertmann U (2003) *The iron oxides: structure, properties, reactions, occurrences and uses*. 2nd edn. Wiley. <https://doi.org/10.1002/3527602097>
139. Wright JB (1964) Iron-titanium oxides in some New Zealand ironsands. *New Zealand J Geol Geop* 7:424–444. <https://doi.org/10.1080/00288306.1964.10422094>
140. McDougall JC (1961) Ironsand deposits offshore from the west coast, North Island, New Zealand. *New Zealand J Geol Geop* 4:283–300. <https://doi.org/10.1080/00288306.1961.10423129>
141. Erselcuk M (1947) Iron and Steel Industry in Japan. *Econ Geogr* 23(2):105–129. <https://doi.org/10.2307/141318>
142. Mar KK, Karnawati D, Sarto, Putra DPE, Igarashi T, Tabelin CB (2013) Comparison of arsenic adsorption on lignite, bentonite, shale, and iron sand from Indonesia. *Proc Earth Planet Sci* 6:242–250. <https://doi.org/10.1016/j.proeps.2013.01.033>
143. Yulianto A, Sulhadi S, Isnaeni Azis AL, Dayati E (2014) Synthesis of iron sand into nano Mn-ferrite. *Mal J Fund Appl Sci* 9. <https://doi.org/10.11113/mjfas.v9n4.112>
144. Jalil Z, Rahwanto A, Mustanir A, Handoko E (2017) Magnetic behavior of natural magnetite (Fe₃O₄) extracted from beach sand obtained by mechanical alloying method. *AIP Conf Proc* 1862:030023. <https://doi.org/10.1063/1.4991127>

145. Hamill PF, Ballance PF (1985) Heavy mineral rich beach sands of the Waitakere coast, Auckland, New Zealand. *New Zealand J Geol Geop* 28:503–511. <https://doi.org/10.1080/00288306.1985.10421203>
146. Cruz-Sánchez E, Álvarez-Castro JF, Ramírez-Picado JA, Matutes-Aquino JA (2004) Study of titanomagnetite sands from Costa Rica. *J Alloys Compd* 369:265–268. <https://doi.org/10.1016/j.jallcom.2003.09.064>
147. Muflikhah M, Rusdiarso B, Putra EGR, Nuryono N (2017) Modification of silica coated on iron sand magnetic material with chitosan for adsorption of Au(III). *Indones J Chem* 17:264. <https://doi.org/10.22146/ijc.22549>
148. Nuryono N, Rosiati NM, Rettob AL, Suyanta S, Arryanto Y (2019) Coating of 2-aminobenzimidazole and 1-(o-toly)lbiguanide functionalized silicas on iron sand magnetic material for sorption of $[\text{AuCl}_4]^-$. *Indones J Chem* 19:395. <https://doi.org/10.22146/ijc.34653>
149. Togibasa O, Bijaksana S, Novala G (2018) Magnetic properties of iron sand from the Tor River estuary, Sarmi, Papua. *Geosciences* 8:113. <https://doi.org/10.3390/geosciences8040113>
150. Tylecote RF (1981) Iron Sands from the Black Sea. *Anatol Stud* 31:137–139. <https://doi.org/10.2307/3642764>
151. Fahmiati N (2017) Suyanta, characteristics of iron sand magnetic material from Bugel Beach, Kulon Progo, Yogyakarta. *IOP Conf Ser Mater Sci Eng* 172:012020. <https://doi.org/10.1088/1757-899X/172/1/012020>
152. Tiwow VA, Arsyad M, Palloan P, Rampe MJ (2018) Analysis of mineral content of iron sand deposit in Bontokanang Village and Tanjung Bayang Beach, South Sulawesi, Indonesia. *J Phys Conf Ser* 997:012010. <https://doi.org/10.1088/1742-6596/997/1/012010>
153. Braccini S, Pellegrinelli O, Krämer K (2013) Mössbauer, X-ray and magnetic studies of black sand from the Italian Mediterranean Sea, world. *J Nucl Sci Technol* 03:91–95. <https://doi.org/10.4236/wjnst.2013.33016>
154. Tsusue A, Ishihara S (1975) “Residual” iron-sand deposits of Southwest Japan. *Econ Geol* 70:706–716. <https://doi.org/10.2113/gsecongeo.70.4.706>
155. Wang Z, Pinson D, Chew S, Rogers H, Monaghan BJ, Pownceby MI, Webster NAS, Zhang G (2016) Behavior of New Zealand ironsand during iron ore sintering. *Metall Mater Trans B Process Metall Mater Process Sci* 47:330–343. <https://doi.org/10.1007/s11663-015-0519-3>
156. Park E, Lee S-B, Ostrovski O, Min D-J, Rhee C-H (2004) Reduction of the mixture of titanomagnetite ironsand and hematite iron ore fines by carbon monoxide. *ISIJ Int* 44:214–216. <https://doi.org/10.2355/isijinternational.44.214>
157. Fahmiati A (2020) Armid, Suyanta, Nuryono, adsorption of Au(III) on diethylenetriamine-functionalized silica coated on iron sand magnetic material. *AIP Conf Proc* 2237:020051. <https://doi.org/10.1063/5.0005579>
158. Harumi M, Santosa SJ (2019) Nuryono, recovery of Au(III) from printed circuit board waste by chitosan/SiO₂ coated on iron sand magnetic material. *Mater Today Proc* 19:1101–1110. <https://doi.org/10.1016/j.matpr.2019.11.002>
159. Rahmi, Fathurrahmi, Lelifajri, PurnamaWati F (2019) Preparation of magnetic chitosan using local iron sand for mercury removal. *Heliyon* 5:e01731. <https://doi.org/10.1016/j.heliyon.2019.e01731>
160. Rahmi I, Mustafa I (2019) Methylene blue removal from water using H₂SO₄ crosslinked magnetic chitosan nanocomposite beads. *Microchem J* 144:397–402. <https://doi.org/10.1016/j.microc.2018.09.032>
161. Rettob AL (2019) Coating of iron sand magnetic material with aminobenzimidazole modified silica via green process. *IOP Conf Ser Earth Environ Sci* 235:012075. <https://doi.org/10.1088/1755-1315/235/1/012075>
162. Rettob AL (2019) Characterization of iron sand magnetic materials coated with 2-aminobenzimidazole modified silica. *Int J Mech Eng Technol* 10:620–627
163. Guibal E (2004) Interactions of metal ions with chitosan-based sorbents: a review. *Sep Purif Technol* 38:43–74. <https://doi.org/10.1016/j.seppur.2003.10.004>

164. Qian S, Huang G, Jiang J, He F, Wang Y (2000) Studies of adsorption behavior of crosslinked chitosan for Cr(VI), Se(VI). *J Appl Polym Sci* 77:3216–3219. [https://doi.org/10.1002/1097-4628\(20000929\)77:14<3216::AID-APP240>3.0.CO;2-P](https://doi.org/10.1002/1097-4628(20000929)77:14<3216::AID-APP240>3.0.CO;2-P)
165. Guibal E, Ruiz M, Vincent T, Sastre A, Navarro-Mendoza R (2001) Platinum and palladium sorption on chitosan derivatives. *Sep Sci Technol* 36:1017–1040. <https://doi.org/10.1081/SS-100103634>
166. Nuryono N, Miswanda D, Sakti SCW, Rusdiarso B, Krisbiantoro PA, Utami N, Otomo R, Kamiya Y (2020) Chitosan-functionalized natural magnetic particle@silica modified with (3-chloropropyl) trimethoxysilane as a highly stable magnetic adsorbent for gold(III) ion. *Mater Chem Phys* 255:123507. <https://doi.org/10.1016/j.matchemphys.2020.123507>
167. Adlim A, Bakar MA (2010) Preparation of chitosan-gold nanoparticles: part 2. The role of chitosan. *Indones J Chem* 8:320–326. <https://doi.org/10.22146/ijc.21585>
168. Li G, Zhao Z, Liu J, Jiang G (2011) Effective heavy metal removal from aqueous systems by thiol functionalized magnetic mesoporous silica. *J Hazard Mater*. <https://doi.org/10.1016/j.jhazmat.2011.05.015>
169. Kang T, Park Y, Yi J (2004) Highly selective adsorption of Pt²⁺ and Pd²⁺ using thiol-functionalized mesoporous silica. *Ind Eng Chem Res* 43:1478–1484. <https://doi.org/10.1021/ie030590k>
170. Vieira EFS, Simoni J d A, Airoidi C (1997) Interaction of cations with SH-modified silica gel: thermochemical study through calorimetric titration and direct extent of reaction determination. *J Mater Chem* 7:2249–2252. <https://doi.org/10.1039/a704286h>
171. Karbeka M (2020) Nuryono, Suyanta, synthesis of silica coated on iron sand magnetic materials modified with 2- mercaptobenzimidazole through sol-gel. *Mor J Chem* 8:44–52
172. Karbeka M (2020) Nuryono, Suyanta, coating of mercapto modified silica on iron sand magnetic material for Au(III) adsorption in aqueous solution. *IOP Conf Ser Mater Sci Eng* 823:012031. <https://doi.org/10.1088/1757-899X/823/1/012031>
173. Nuryono N, Rosiati NM, Rusdiarso B, Sakti SCW, Tanaka S (2014) Coating of magnetite with mercapto modified rice hull ash silica in a one-pot process. *SpringerPlus* 3:515. <https://doi.org/10.1186/2193-1801-3-515>
174. Sulastri S, Nuryono N, Kartini I, Kunarti ES (2011) Adsorption of Ca(II), Pb(II) and Ag(I) on sulfonato-silica hybrid prepared from rice hull ash. *Indones J Chem* 11:273–278. <https://doi.org/10.22146/ijc.21392>
175. Azmiyawati C, Nuryono N, Narsito N (2012) Adsorption of Mg(II) and Ca(II) on disulfonato-silica hybrid. *Indones J Chem* 12:223–228. <https://doi.org/10.22146/ijc.21334>
176. Azmiyawati C, Suyati L, Taslimah RDA (2017) Coating of sulfonic silica onto magnetite from Marina Beach iron sand, Semarang, Indonesia. *IOP Conf Ser Mater Sci Eng* 172:012009. <https://doi.org/10.1088/1757-899X/172/1/012009>
177. Khan NA, Hasan Z, Jung SH (2013) Adsorptive removal of hazardous materials using metal-organic frameworks (MOFs): a review. *J Hazard Mater* 244–245(15):444–456. <https://doi.org/10.1016/j.jhazmat.2012.11.011>
178. Wang Q, Astruc D (2020) State of the art and prospects in metal – organic framework (MOF)-based and MOF-derived nanocatalysis. *Chem Rev* 120:1438–1511. <https://doi.org/10.1021/acs.chemrev.9b00223>
179. Misra A, Zambrzycki C, Kloker G, Kotyrba A, Anjass MH, Castillo IF, Mitchell SG, Ggittel R, Streb C (2020) Water purification and microplastics removal using magnetic polyoxometalate-supported ionic liquid phases (magPOM-SILPs). *Angew Chem Int Ed* 59:1601–1605. <https://doi.org/10.1002/anie.201912111>

Easily Collectable Floating-Up Adsorbents to Remove Pollutants



Yoshihiro Mihara and Shunitz Tanaka

Contents

1	Background of Floating Adsorbents (Collection of Adsorbents)	618
2	Design of Floating-Up Adsorbent by Controlling the Specific Gravity of Adsorbent	621
2.1	Introduction	621
2.2	Preparation of Alginate Gel Beads with a Weight and a Float	622
2.3	The Effect of NaHCO_3 and CaCO_3 on the Specific Gravity of Alginate Gel Beads ..	623
2.4	Floating Time of Alginate Gel Beads	623
2.5	Removal of Lead Ion Existing at the Bottom of Water Using $\text{CaCO}_3\text{-CO}_2$ Bubble-AG	625
2.6	Conclusion	627
3	Use of Shirasu Balloon as a Floating Adsorbent	628
3.1	Introduction	628
3.2	Preparation of SB Adsorbents	628
3.3	Removal of Cadmium Ion	629
3.4	Collection of SB from Soil	630
3.5	Conclusions	632
4	Adsorbent Which Can Repeat Floating and Sinking	632
4.1	Introduction	632
4.2	Fermentation Model and Kinetics	633
4.3	Floating Profile of the Beads	635
4.4	Vertical Migration Behavior of the Beads	637
4.5	Conclusion	638

Y. Mihara (✉)

Department of Medicinal Chemistry, Faculty of Pharmaceutical Sciences, Hokkaido University of Science, Sapporo, Hokkaido, Japan

e-mail: mihara-y@hus.ac.jp

S. Tanaka

Hokkaido Environmental Science and Technology Center, Hokkaido University, Sapporo, Hokkaido, Japan

ES General Laboratory Co., Sapporo, Hokkaido, Japan

e-mail: shunitz@ees.hokudai.ac.jp

Shunitz Tanaka, Masaaki Kurasaki, Masaaki Morikawa, and Yuichi Kamiya (eds.),

Design of Materials and Technologies for Environmental Remediation,

Hdb Env Chem (2023) 115: 617–650, DOI 10.1007/698_2021_826,

© The Author(s), under exclusive license to Springer Nature Singapore Pte Ltd 2022,

Published online: 8 January 2022

617

5	Adsorption Kinetic Model of Alginate Gel Beads Synthesized Micro Particle-Prussian Blue to Remove Cesium Ions from Water	639
5.1	Introduction	639
5.2	Preparation of PB-AG Beads	640
5.3	Characterization of PB-AG Beads	641
5.4	Removal of Cs Ions by PB-AG Beads	643
5.5	Removal of Cesium Ion in Water Column Using a Vertical Migration System of Alginate Gel Beads	645
5.6	Conclusion	645
6	Conclusion	647
	References	648

Abstract The novel adsorbents with controlled specific gravity were developed, which can firstly sink in the bottom of water and then float up on the surface of water after the process of adsorption. In order to introduce the unique property into the adsorbent, the specific gravity of alginate gel composite was controlled by adding a float and a weight. In this study, three different adsorbents with various floating mechanisms were developed and the floating behaviors were investigated.

The first one is to control the specific gravity of the beads by adding CO₂ gas bubbles as a float and CaCO₃ as a weight dissolving into water. In this case, by changing the amount of a weight, the floating time of the gel beads after the completion of adsorption of metal cation could be controlled. The second is to use the surface functionalized Shirasu balloons of as a float. Octadecylsilyl (ODS) modified Shirasu balloons were prepared and the strong floatability had been demonstrated. SH modified Shirasu balloons were also prepared and by using them the removal of heavy metal ions in water and soil was attempted. The third is to develop an adsorbent having a repeated vertical migration system by introducing a fermentation process using yeast and glucose into the alginate gel bead. This adsorbent can move in water from the bottom to the surface many times repeatedly.

By introducing a simple concept like the control of the specific gravity of adsorbent, the easy collection of adsorbent could be achieved.

Keywords Adsorption kinetics, Buoyancy-control, Easily collectable adsorbent, Vertical migration, Water purification

1 Background of Floating Adsorbents (Collection of Adsorbents)

Many kinds of pollutants have being discharged in aquatic environments from daily human and industry activities, and sometimes by accidents. For example, about 100 tons of nitrobenzene were spilled into the Son-hua River by the explosion of a petrochemical factory at Jilin in China (2005). A great deal of crude oil was emitted

into the Gulf of Mexico by the accident at the deep-water horizon drilling rig (2010). Pollution of water and soil with radioactive species such as ^{134}Cs and ^{137}Cs ions released from Fukushima Daiichi nuclear power plants after the mega earthquakes and tsunami is still now one of the most severe environmental pollution problems in Japan (2011).

The pollutants described above have the different specific gravity. The specific gravity of crude oil is lighter than that of water, and that of nitrobenzene is heavier than that of water. Therefore, crude oil floats on the surface of water, while nitrobenzene sinks to the bottom of water [1]. Most of water-soluble pollutants like heavy metal ions must exist homogeneously in the body of water after a sufficient period since the inflow. Although the use of adsorbents is one of the most promising methods to remove pollutants, the adsorbents should be selected as taking account on the specific gravity of pollutants in order to guarantee the sufficient contact with these pollutants [2]. For pollutants that are floating on the surface of water, an adsorbent that is lighter than water is favorable. An adsorbent heavier than water is suitable for the pollutants that sink to the bottom of water.

Many kinds of adsorbents have been used to remove hazardous substances in water and soil, that is, activated carbon [3, 4], ion-exchange resin [5, 6], zeolite [7], bio-surfactants [8], clay-soils [9], etc. Moreover, many researches have made much effort to improve the adsorbing ability and selectivity. When these adsorbents are injected directly into the environment to remove pollutants, those adsorbents should be collected from the environment after adsorption of pollutants. Even if the adsorbent has a superior adsorption ability for a pollutant, if the adsorbents cannot be collected after adsorption, the pollutants would diffuse into the environment again. Therefore, it is very important to develop adsorbents that can be easily collected. The easy collection is an essential feature as an adsorbent for the application of the adsorbents to actual contaminated sites.

In this viewpoint, the collection of adsorbents can be a new concept in the development of adsorbents as well as the environmentally-friendly and low cost. Many studies have been performed to develop the environmentally-friendly and low-cost adsorbents [10–12], however, few studies focused on the collection of adsorbents, especially on the collection by controlling the specific gravity of adsorbent. In the case that a pollutant exists in the bottom of water, if we can prepare an adsorbent that at first sinks to the bottom of water to adsorb pollutants there and then float up on the surface of water, the adsorption of pollutant will be achieved effectively and the adsorbent will be collected easily. If we can develop an adsorbent which can repeat sinking and floating between the surface and bottom of water, the adsorbent may adsorb pollutants in the bulk of water without stirring. Moreover, if the floating adsorbent has the magnetism, we can collect the floating adsorbent by a magnet easily, as shown schematically in Fig. 1 [13].

Here we describe some types of the easily collectable adsorbent to remove pollutants in water and soil, which we have developed for a long time, especially on the basis of the control of the specific gravity of the adsorbent. All of the developed adsorbents can be collected on the surface of water because the adsorbents can float up on the surface of water after adsorption. At first, in order to realize

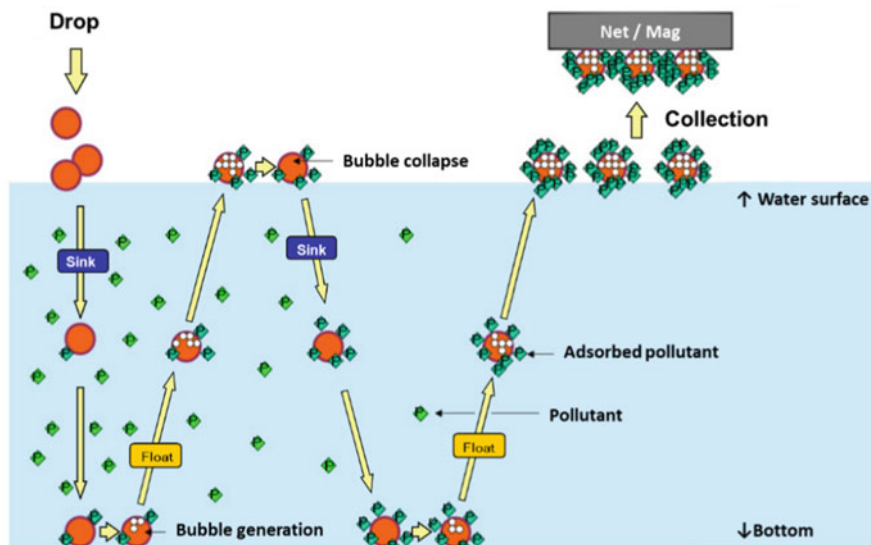


Fig. 1 Conceptual image of the removal of a pollutant from aquatic environments using gravity-controlled adsorbents. “S.G.” refers to the specific gravity of materials [13]

such adsorbent, a prototype of the easily collectable adsorbent was developed by using alginate gel beads whose specific gravity was controlled by introducing both a weight and a float. By attaching a weight exceeding the buoyancy due to the float, the prepared adsorbent sinks and stays at the bottom of water. However, if the weight in the gel beads can be dissolved, the specific gravity of the adsorbent gradually becomes lighter and at last begins to float upward. The floating adsorbents on the surface of water can be collected easily (Sect. 2) [14]. The usefulness of the floating adsorbent was demonstrated by using the adsorbent to remove lead salts set at the bottom of water. Sodium alginate contains anionic groups, i.e. carboxyl and hydroxyl groups in its structure, which exhibit the properties of electrostatic and complexing interaction with metal cations. The adsorbent which sank at the bottom of water adsorbed lead ions there and then floated up the surface of water. The floating gel beads could be collected on the water surface. It was confirmed that the adsorbent could transfer the pollutant from the bottom of water to the surface.

Next, we developed another type of the floating adsorbent by using Shirasu balloon, whose specific gravity is lighter than that of water. The surface of Shirasu balloons was modified with the functional groups or materials to introduce the adsorbing ability and improve the stability of the balloon in water. The modified Shirasu balloons could be collected easily by the buoyancy of the balloons themselves after the adsorption of pollutants. The usefulness of this type of the adsorbent was demonstrated by applying to the removal of Cd^{2+} in soil (Sect. 3) [15].

During these developments of the floating adsorbents, fortunately we found out an interesting adsorbent, which repeated floating and sinking between the bottom

and surface of water. The repeated movement of the alginate gel bead could be achieved through the introduction of a fermentation system with glucose and yeast (Sect. 4) [13]. In addition, the alginate gel bead encapsulating Prussian blue (PB-AG) was developed to remove cesium ion in water [16]. The combination of PB-AG and the fermentation system was attempted and the usefulness of the adsorbent was demonstrated by removing cesium ions in the water column (Sect. 5) [17].

2 Design of Floating-Up Adsorbent by Controlling the Specific Gravity of Adsorbent

2.1 Introduction

When a pollutant exists at the bottom of water, how can we remove the pollutant by an adsorbent? If we have an adsorbent which adsorbs well the pollutant at the bottom, we can collect the pollutant on the adsorbent, but how to collect the adsorbent used at the bottom of water? If we can prepare an adsorbent that at first sinks at the bottom of water to adsorb pollutants there and then floats up on the surface of water, both of the adsorption of pollutant and the collection of adsorbents could be achieved effectively as shown schematically in Fig. 2. In order to realize such an adsorbent, we attempted to develop a new type of adsorbent on the basis of

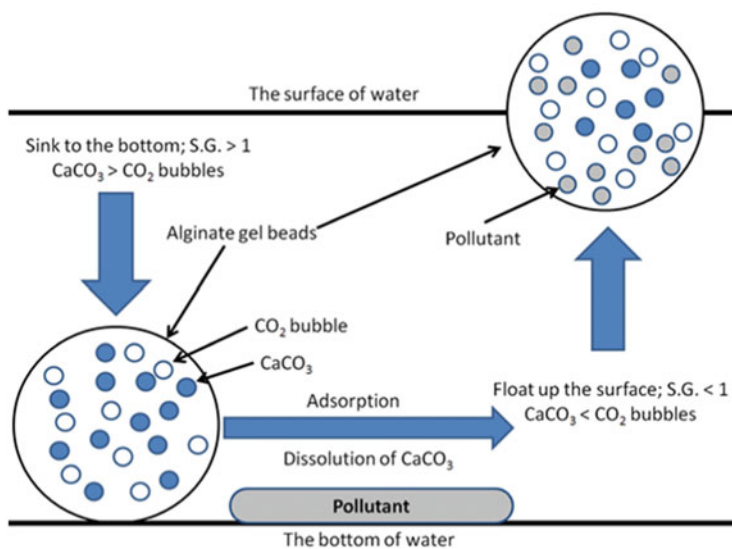


Fig. 2 Conceptual image of the removal of a pollutant from aquatic environments using the gravity-controlled alginate gel beads. "S.G." refers to the specific gravity of alginate gel beads [14]

the control of the specific gravity of the adsorbent. The specific gravity of the adsorbent was controlled by introducing both a weight and a float into the adsorbent. When the weight of the adsorbent exceeds the buoyancy of a float, the adsorbent sinks at the bottom of water. However, if the weight is dissolved gradually to water, the buoyancy of the float exceeds the weight to float up to the surface of water. To build up a prototype of such adsorbent, we chose alginate gel bead as an adsorbing material, and CaCO_3 and bubbles of CO_2 as a weight and a float, respectively [18, 19]. At first the adsorbent would sink and stay at the bottom of water because the weight of CaCO_3 exceeds the buoyancy of CO_2 bubbles. However, when the weight of CaCO_3 in the gel beads begins to dissolve under the weak acidic condition, the specific gravity of the adsorbent would gradually become lighter and at last the adsorbent begins to float upward [20]. The floating-up adsorbents on the surface of water can be collected easily.

We show here how to prepare such adsorbent using alginate gel bead and introducing the weight and float into the gel bead. The usefulness of this adsorbent was demonstrated by removing lead ion set at the bottom of the water column as PbSO_4 powder.

2.2 Preparation of Alginate Gel Beads with a Weight and a Float

By adding drop-wisely the mixed solution of 1–3 wt% sodium alginate solution, 3 wt% sodium hydroxyl carbonate solution and fine powder of calcium carbonate (0–10 wt%) into 100 mL of 0.1 M calcium nitrate solution at 5°C , we could get calcium alginate gel beads entrapping CO_2 gas bubbles as a float and CaCO_3 as a weight. The prepared gel beads were washed in a 20 wt% solution of $\text{Ca}(\text{NO}_3)_2$ at 5°C for 3 h and then they were stored in distilled water at room temperature. The diameter of the alginate gel beads was 5.0 ± 0.2 mm. The specific gravity (S.G.) of the alginate gel beads was measured using a 25 mL of classical pycnometer. The S.G. of a liquid can be expressed as follows (Eq. 1).

$$\text{S.G.} = \frac{W_1}{(W_1 + (W_2 - W_0))} \times \rho_{\text{H}_2\text{O}} \quad (1)$$

where ρ = the density of fluid or substance (g/cm^3), $\rho_{\text{H}_2\text{O}}$ = the density of water (g/cm^3), W_0 = Weight of the pycnometer containing 10 number of alginate gel beads and water (g), W_1 = Weight of 10 numbers of alginate gel beads (g), W_2 = Weight of the pycnometer containing water (g).

It is common to use the density of water at 25°C as a reference – the density of water at 25°C is $0.9971 \text{ g}/\text{cm}^3$.

Table 1 Specific gravity of alginate gel bead prepared under different conditions [14]

Alginate gel (wt%)	NaHCO ₃ (wt%)	CaCO ₃ (wt%)	Specific gravity
1	0	0	1.0083 ± 0.0005
1	0	3	1.0658 ± 0.0007
1	0	5	1.0941 ± 0.0010
1	0	10	1.1652 ± 0.0008
1	0.5	0	1.0077 ± 0.0015
1	1	0	0.9880 ± 0.0021
1	3	0	0.9524 ± 0.0025
1	3	3	1.0239 ± 0.0016
1	3	5	1.0489 ± 0.0015
1	3	10	1.1081 ± 0.0022

2.3 *The Effect of NaHCO₃ and CaCO₃ on the Specific Gravity of Alginate Gel Beads*

The specific gravities of an alginate gel bead prepared under different conditions are shown in Table 1. The plain alginate gel bead has the slight heavier S.G. than that of water. However, the addition of the weight of CaCO₃ in the bead made it heavier almost linearly depending on the added amount of CaCO₃. On the other hand, the addition of NaHCO₃ in the alginate solution resulted in the formation of many small bubbles in the bead and consequently made it lighter than that of water. The addition of both NaHCO₃ and CaCO₃ into the alginate solution enabled to control the specific gravity of the prepared gel bead from lighter to heavier than that of water by changing the ratio of CaCO₃ to NaHCO₃. The results of Table 1 suggested us that the specific gravity of the alginate gel bead could be controlled by balancing the amount of a float and a weight. Even though at first the gel bead sank to the bottom of water by the weight of CaCO₃, the bead could float up to the surface of water when the CaCO₃ in the gel beads was dissolved in the acidic solution. The size and numbers of the bubbles formed in the bead depended on the reaction condition of NaHCO₃, especially the solution pH. Figure 2 shows the optical microscope images of cross-sectional alginate gel beads prepared at pH 6.0, 5.0, 4.0, and 3.0. The closer the pH to neutral like 6.0, the more numbers and smaller bubbles were formed in the gel bead. In order to evaluate the stability of CO₂ bubbles in alginate gel beads, the prepared alginate gel beads were introduced in the solutions adjusted to pH = 3.0, 6.0, and 10.0 with nitric acid or NaOH. Consequently, the bubbles in the gel beads were stably maintained for 3 days.

2.4 *Floating Time of Alginate Gel Beads*

The migration behavior of the prepared adsorbent with the weight and float was investigated using one hundred alginate gel beads. These gel beads were put into 5 L

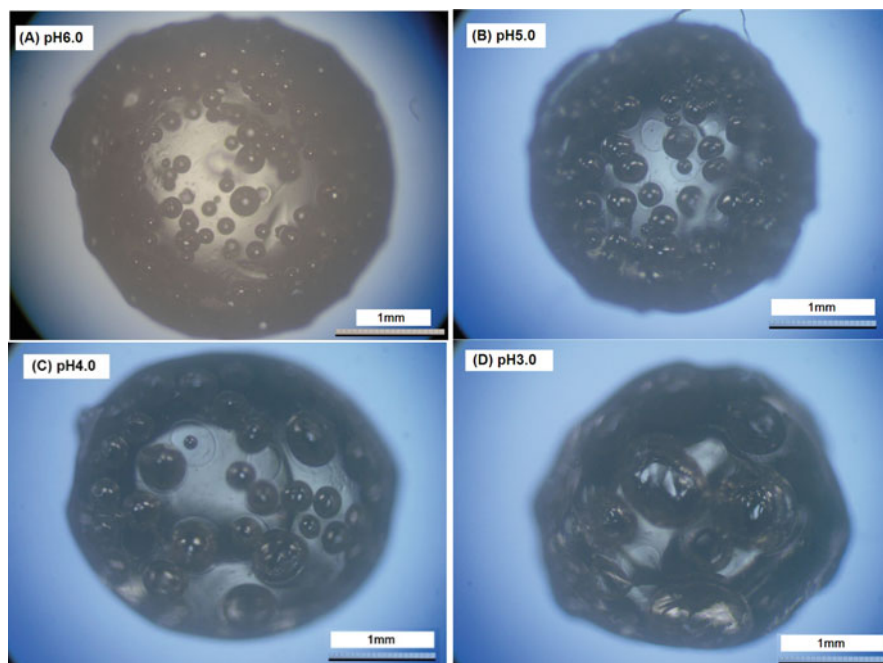


Fig. 3 Optical microscope images of cross-sectional alginate gel beads prepared at pH (a) 6.0, (b) 5.0, (c) 4.0, and (d) 3.0 [14]

of the acidic solution and the movement of the beads was observed. The alginate gel beads prepared from a 1% alginate solution containing 10 wt% of CaCO_3 and 3 wt% of NaHCO_3 firstly sank at the bottom of the solution and then the beads began to float up on the surface of the water after staying at the bottom in some delay period. The floating profile of 100 beads of CaCO_3 - CO_2 bubbles-AG in the solution with pH 3.0 is shown in Fig. 3. The numbers of the floating beads at the pH 3 showed an almost normal distribution with the maximum at 260 min and the range of 200 to 300 min. Within the first 200 min (the delay period), all of the alginate gel beads stayed at the bottom of the water and after 300 min all beads floated up on the surface of the water. The floating time was defined as the time when 50% of the added beads floated up on the surface of water. The delay period means a time necessary for the dissolution of the CaCO_3 in the gel beads in an acidic solution. When the specific gravity of the beads became lighter than that of water by the dissolution of the CaCO_3 during the delay period, the gel beads began to float up on the surface. The delay period can be varied by changing the amount of CaCO_3 in the bead and the pH of the solution. Actually, the delay period extended as the amount of CaCO_3 increased and shortened as the pH decreased. In the solution of pH 2.0, every types of alginate gel bead floated up after a short delay period, 4 min for 3 wt% of CaCO_3 , 12 min for 5 wt% of CaCO_3 , and 24 min for 10 wt% of CaCO_3 . In the case

of pH 3.0, a delay period for each alginate gel beads was 48 min for 3 wt% of CaCO_3 , 120 min for 5 wt% of CaCO_3 , and 210 min for 10 wt% of CaCO_3 . The floating time of the alginate gel beads increased as increasing the amount of CaCO_3 in the alginate solution. The dissolution speed of CaCO_3 became almost 10-fold faster when the pH of the solution was changed from 3.0 to 2.0.

The wide range of the distribution in the delay period of each bead may be due to the variation of a float and a weight in an alginate gel bead. That is, the number of CO_2 bubble and the amount of CaCO_3 in each bead are somewhat different in the current production process. Another reason might be a change in the pH of the solution during the experiment where the dissolved components from CaCO_3 neutralized the unbuffered acidic solution. In order to confirm that the floating of an alginate gel bead was attributed to the dissolution of CaCO_3 as the weight in the gel bead, the concentration of Ca^{2+} in the solution used for the floating experiment was measured as a function of time. Simultaneously, the specific gravity of the gel beads was measured every 30 min during the floating experiment. The concentration of calcium ion eluted from the Ca-AG without a weight of CaCO_3 was very low. The concentration of calcium ion in the solution was linearly increased until all alginate gel beads floated up. The increase in the calcium concentration in the solution was due to the dissolution of CaCO_3 as a weight in the gel beads. The specific gravity of alginate gel beads was initially 1.0489 ± 0.0015 , when the weight of the gel beads gradually decreased in the acidic solution (pH 3.0), the specific gravity of the alginate gel beads was 1.0157 ± 0.0018 after 150 min, at that time all of the alginate gel beads still remained at the bottom of water. After about 210 min, however, the specific gravity of the gel bead had decreased to 0.9996 ± 0.0032 and the beads began to float up. Therefore, it was confirmed that the floating mechanism of the alginate gel beads was due to the decrease in the specific gravity by the dissolution of CaCO_3 in the acidic solution. The gel bead having CaCO_3 but not CO_2 gas bubbles could not float up. Therefore, CO_2 gas generated from the dissolution of CaCO_3 as a weight did not contribute to the increase in the floatability of alginate gel beads.

2.5 Removal of Lead Ion Existing at the Bottom of Water Using $\text{CaCO}_3\text{-CO}_2$ Bubble-AG

It is known that Ca-alginate gel has the binding sites for metal ions because of the presence of the functional groups like carboxyl and hydroxyl groups [21]. Then the $\text{CaCO}_3\text{-CO}_2$ bubble-AG has the binding ability for heavy metal ions. In order to confirm the usefulness of the floating-up adsorbent, we demonstrated the removal of lead ions, 80 mg powder of PbSO_4 set at the bottom of water column (the length of 80 cm), by using 5 wt% of $\text{CaCO}_3\text{-CO}_2$ bubble-AG. This experimental condition was prepared as a model where the source of pollutant exists at the bottom of water.

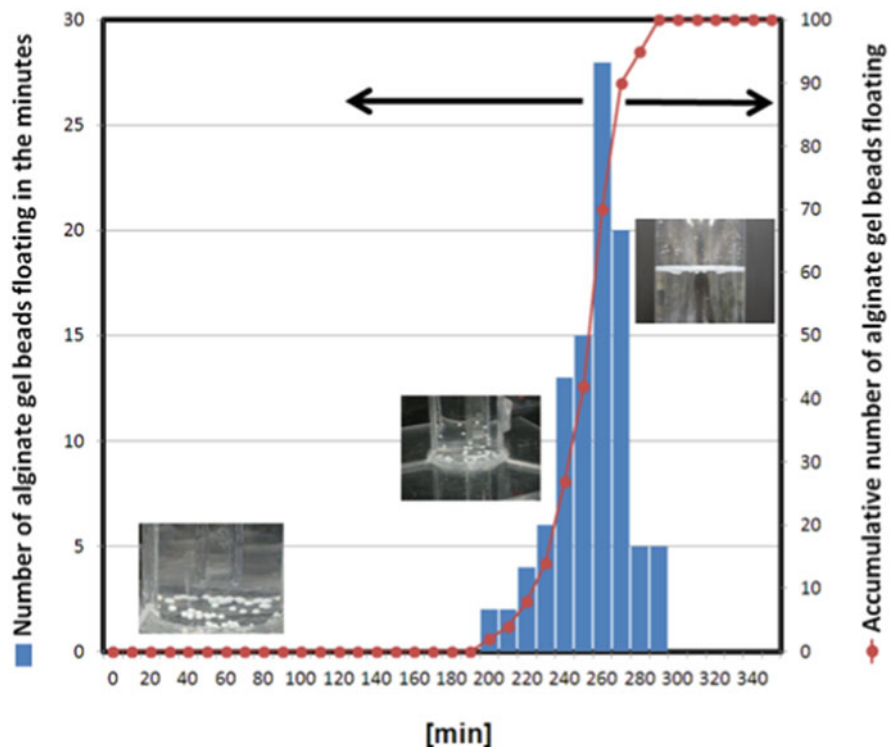


Fig. 4 The number of alginate gel beads floating up in every 10 min (left) and accumulative number of alginate gel beads floating (right) in the floating experiment at pH 3.0 [14]

All of the added 300 of CaCO_3 -alginate gel beads sank at the bottom, stayed there, and then floated up. All of the beads could be collected on the surface of water within 3 h. This process was repeated eight times, after 24 h 98.4 wt% of total lead ions at the bottom of water could be removed. During this process, the concentrations of lead ion at the bottom and the middle of water column were monitored. As shown in Fig. 4, the concentration of lead ion was suppressed to a low level at the bottom and also the middle. On the other hand, in the case without the treatment by the CaCO_3 - CO_2 bubble-AG, the concentration of lead ion at the bottom and the middle increased with increasing time.

Consequently, the use of CaCO_3 - CO_2 bubble-AG shifted the equilibrium in the solubility of PbSO_4 to bind lead ions on the binding sites of alginate, prevented lead ion from spreading to the whole water, and facilitated to collect lead ions on the surface of water (Fig. 5).

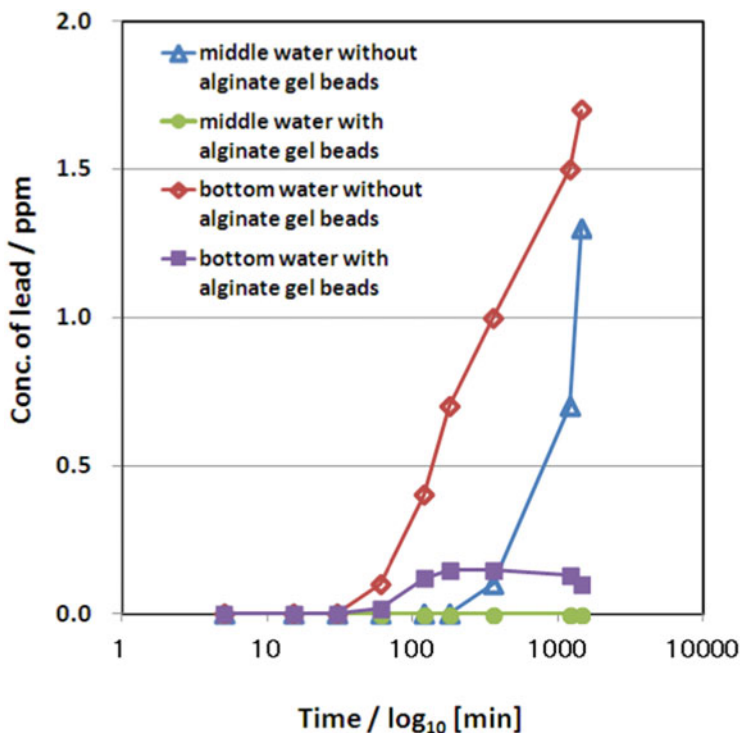


Fig. 5 Concentration of lead ion in the bottom and the middle of water column [14]

2.6 Conclusion

A new type of adsorbent, which can float up to the surface of water after sinking at the bottom of water to adsorb pollutants, was developed by controlling the specific gravity of alginate gel beads through introducing CaCO_3 as a weight and CO_2 gas bubbles as a float. The specific gravity of the prepared beads was larger than that of water due to the enough amount of the weight and therefore the beads sank to the bottom of water. However, by the dissolution of the weight in acidic water, the alginate gel beads could float up to the surface of water by the buoyancy of the CO_2 gas bubbles. The floating time of the alginate gel beads could be controlled by the amount of the weight if the amount of bubbles in the gel beads was constant. The concentration of NaHCO_3 as a CO_2 forming agent and the pH were also the important factors to achieve the uniformity in the size and the number of the CO_2 gas bubbles. CaCO_3 in the alginate gel bead also acted as a reagent to keep the pH of the inside of the bead basic. Therefore, even in the acidic solution, the gel beads have the adsorbing ability for lead ions. Consequently, CaCO_3 - CO_2 bubble-AG could remove lead ions at the bottom of water and be collected on the surface of water.

3 Use of Shirasu Balloon as a Floating Adsorbent

3.1 Introduction

In the previous section, we described the floating-up adsorbent based on the introduction of CaCO_3 and CO_2 bubbles into the alginate gel beads. Next, we describe the use of “Shirasu balloon” as the floating adsorbent in this section. “Shirasu” is fine-grained pumice and volcanic ash and distributes in a thick stratum throughout the southern Kyushu, Japan [22]. “Shirasu balloon (SB)” is a hollow glassy microsphere, which is produced by heating vitric volcanoclastic materials, named as Shirasu or Hakudo (a kind of the “perlite”) [23]. The mean particle size of plain SB is several micrometers when they are prepared in a fluidized sand bed furnace by the rapid heating of pulverized Shirasu. SB has a high potential as an eco-material in industry and also civilian use. Actually, SB is used in a house wall as the thermal insulating material because of including air in the hollow structure [24]. Moreover, it is used for the treatment of waste water and soil [25]. Since the specific gravity of SB is lighter than that of water (the specific gravity was about 0.5 at 25°C), SB floats on the surface of water so that can be collected easily on the surface of water. However, the SB particles are not so mechanically stable in water because water sometimes invades into the cavities of balloons through the cracks and holes to lose the buoyancy. SB has not the strong binding sites for the specific pollutant. In order to solve these problems, the modification of the surface of the SB by introducing chelating and hydrophobic groups seems to be effective.

The purpose of this study is to enhance the stability of the balloons in water and soil and to develop a novel floating adsorbent by modifying the surface of SB, which has a well adsorbing ability for heavy metal ions, and can be collected from contaminated water or soil easily (Fig. 6).

3.2 Preparation of SB Adsorbents

Shirasu balloons (SB-201 type) obtained from Silax Co., Ltd. (Kagoshima prefecture, Japan) are foamed hollow glass microspheres, which are produced by heating Shirasu (perlite), one of the volcanic materials, at about 1,000°C [22]. In this study, two kinds of modified SB were prepared. One is hydrophobized SB modified with *n*-octadecyldimethylchlorosilane (ODS-SB). The hydrophobization of the surface of the SB is expected to prevent water from invading into the inside of the balloon through the holes and cracks. Another is modified SB with 3-mercaptopropyltrimethoxysilane [26] to introduce thiol groups on the SB. The introduction of thiol groups on the SB (SH-SB) is expected to increase in the cadmium adsorption capacity. In addition, the modification with both of hydrophobic and thiol groups were conducted by using a mixture of *n*-octadecyltrichlorosilane and (3-mercaptopropyl)-trimethoxysilane (SH-ODS-SB). According to a report by

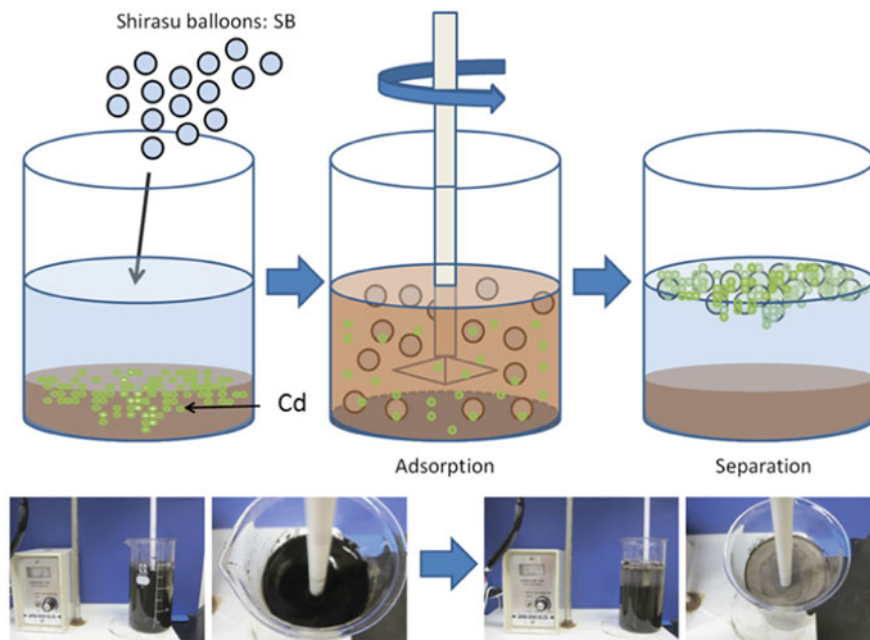


Fig. 6 Conceptual image of the removal of cadmium ion from soil and water using the modified SB [15]

Sodeyama et al., the main components of the SB are SiO_2 , Al_2O_3 , K_2O , Na_2O , CaO , Fe_2O_3 , and their percentages are 69.7, 12.6, 3.36, 2.89, 1.59, and 1.56, respectively [23]. It was confirmed by optical microscopy observation that the SB particles have an average particle size of 15–25 μm . The density of SB was determined to be 0.5 g/cm^3 by pycnometry. The amounts of C, H, and S of the plain and modified SB were determined by the elemental analysis. Carbon and sulfur were not found in the plain SB. The sulfur content was 11.36 wt% for SH-SB and 5.12 wt% for SH-ODS-SB. The presence of sulfur on the modified SB suggested the successful implementation of the modification of SB with thiol groups. FTIR spectra of the SB before and after modifications were measured in the range of 600–4,000 cm^{-1} . The broad peak at around 3,000–4,000 cm^{-1} might be due to OH stretching vibrations of silanol groups on the modified SB. A new peak that appeared at 2,900–3,000 cm^{-1} was assigned to CH stretching vibrations of alkyl groups introduced by the modification, and a small peak at 2,540–2,560 cm^{-1} was assigned to SH stretching vibrations of the thiol groups.

3.3 Removal of Cadmium Ion

Cadmium ions in solution hardly adsorb on the plain SB (Fig. 7a) because the plain SB just has silanol groups, and but neither thiol groups nor other binding sites.

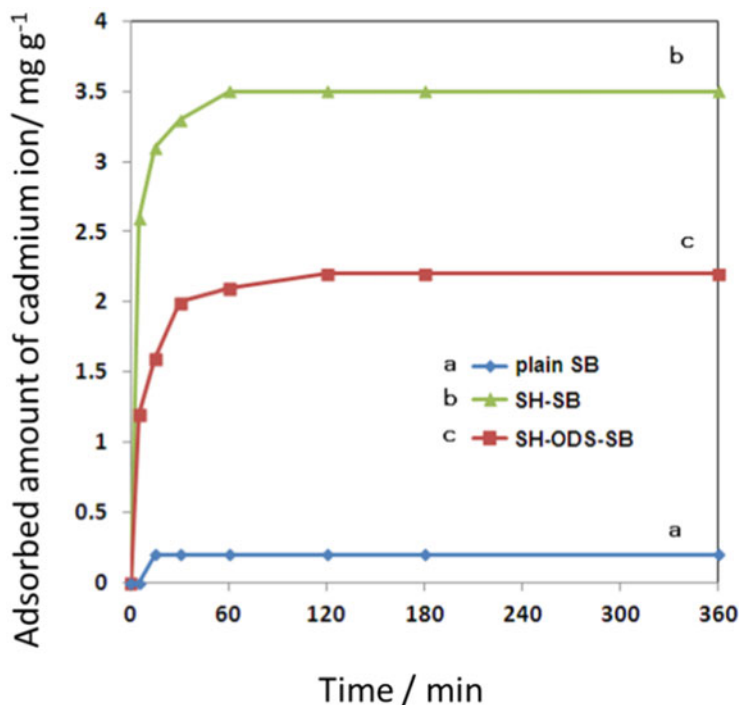


Fig. 7 Adsorption of cadmium ion on SB. pH; 3.0, temperature, 25°C; concentration of the Cadmium ion, 10 mg/L; (a) plain SB; (b) SH-SB; (c) SH-ODS-SB [15]

ODS-SB also did not show the ability to adsorb cadmium ions. However, SH-SB and SH-ODS-SB showed the strong adsorbing ability for cadmium ions and reached to the equilibrium within 2 h (Fig. 7b, c). The interaction depended on the pH of the soil and water strongly. The removal ratio of cadmium ion increased with increasing pH of the solution. The adequate pH for the adsorption with SH-ODS-SB was in the range of 3–7. The adsorption capacity of the modified SB seemed to depend on the amounts of the thiol group modified on the SB. SH-SB and SH-ODS-SB have the potential for removing a variety of metal ions from contaminated soils under the condition of weakly acidic solution.

3.4 Collection of SB from Soil

The collection of the SBs in water is relatively easy because the SB, whose specific gravity is lighter than that of water, floats up on the surface of water after the use. How to collect the SBs when they are used for the treatment of contaminated soil? Therefore, the separation of SB used for the treatment of soil contaminated with cadmium ions for 1 week was demonstrated by putting the soil containing the SB

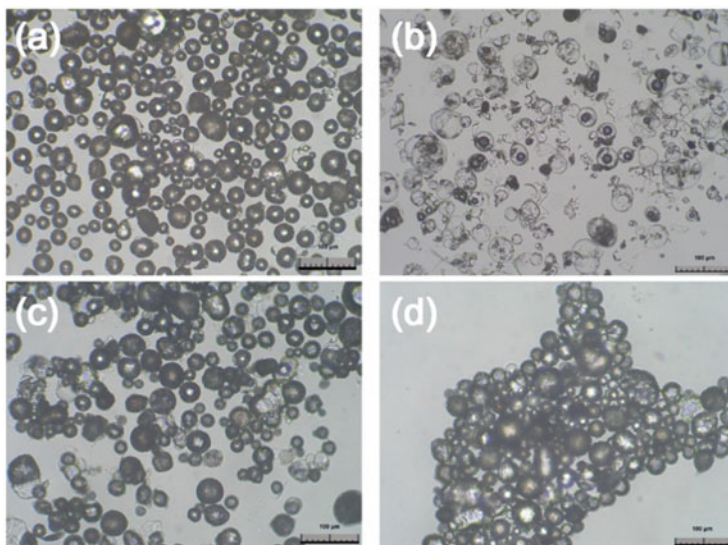


Fig. 8 Photograph of the adsorbent in solution by an optical microscope.; (a) plain SB; (b) plain SB after 1 week; (c) SH-SB after 1 week; (d) SH-ODS-SB after 1 week [15]

into water and shaking it for 24 h. The separation efficiency of the plain SB and the SH-SB from soil was 11 wt% and 73 wt%, respectively. On the other hand, the separation efficiency of ODS-SB and SH-ODS-SB was 103 wt% and 98 wt%, respectively. Figure 8a shows the surface morphology of the SBs before the use for the treatment of soil. On the other hand, the surface morphologies shown in Fig. 8b–e were of the SBs collected from the surface water after contact with the soil sample for 1 week. Most of the plain SBs after 1 week seems to have been damaged by the penetration of water into the cavity of the SB as shown in Fig. 8b. On the other hand, the SH-SBs after 1 week have maintained the initial state without any holes and cracks on the surface of the SH-SB (Fig. 8c). The modification with alkyl chains on the surface of the SB played an important role to prevent the balloons from the physical deterioration and damage as well as the penetration of water into the cavity of the SB. In the case of SH-ODS-SB, the high assembling property was observed on the basis of hydrophobic interaction as shown in Fig. 8d. This property is favorable to improve the collection efficiency and shorten the separation time. The removal of cadmium ions deliberately added in paddy soil was investigated by using SH-ODS-SB at various pH values. The efficiency of cadmium ion desorbed from soil and the adsorption of cadmium ion on the SH-ODS-SB are summarized in Table 2.

84.5% of cadmium ions in soil could be removed from soil at pH 3 and most of the cadmium ion was collected on the SH-ODS-SB within 6 h. However, the desorbing efficiency of cadmium ion decreased remarkably in the higher pH range of 4–6. The desorbing of cadmium ions from soil is due to the ion-exchanging mechanism between Cd^{2+} and proton. The decrease in the proton concentration leads to the decrease in the desorbing efficiency due to a reduction of the ion-exchange

Table 2 The rates of cadmium ion desorption from soil and adsorption on SH-ODS-SB [15]

Eluants (100 mL)	Soil pH	Desorbed, %	Adsorbed, %		
	Final	Cadmium ion/soil (0.01 mg/10 g)	SH-ODS-SB (0.25 g)	SH-ODS-SB (0.5 g)	SH-ODS-SB (1.0 g)
Nitric acid	1.13	99.8	0.0	1.2	1.2
Citric acid/NaOH	2.23	93.0	35.0	45.1	60.1
Citric acid/NaOH	3.28	84.5	70.4	84.2	84.2
Citric acid/NaOH	4.49	48.0	40.0	48.0	48.0
Citric acid/NaOH	5.39	15.0	15.0	15.0	15.0
Citric acid/NaOH	6.09	6.0	6.0	6.0	6.0
Pure water	6.59	2.2	2.2	2.1	2.1

ability. Therefore, the lower pH is suitable to elute cadmium ions from soil. On the other hand, for the binding of cadmium ion with the SH group, the acid dissociation of SH group is necessary, and the relatively higher pH is suitable for this condition. The pH that can satisfy these two conditions was at around pH 3, and under this condition the maximum values were obtained in the elution of cadmium ion from soil and the collection of cadmium ion with the SH-ODS-SB.

3.5 Conclusions

The use of SBs, whose specific gravity is lighter than water, and the modification of the surface made it easy to remove Cd^{2+} in water and soil and to collect the adsorbents after adsorption. The introduction of an alkyl group on the surface of SB increased the mechanical strength of SB by suppressing the inflowing of water into the cavity of SB. In addition, the higher assembling property based on the hydrophobic surface on the SB has a large advantage in the collection of SB. Consequently, the high collection of SB led to the improvement of the removal efficiency of Cd^{2+} from soil. We successfully developed the easily collectable adsorbent by using the modified Shirasu balloon. The easily collectable adsorbent will probably enable the direct injection of adsorbent to the contaminated site without using a column system. After adsorption of pollutant, the adsorbent can be collected on the surface of water easily. It will be a low-cost remediation technology to remove pollutants from water and soil.

4 Adsorbent Which Can Repeat Floating and Sinking

4.1 Introduction

In the previous two sections, we described the floating adsorbents using the modified Shirasu balloons or alginate gel beads with a weight and a float. The later adsorbent

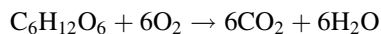
firstly sinks at the bottom of water but thereafter floats up on the surface of water. These adsorbents can be applied to the removal of pollutants in water and soil and can be collected easily after adsorption because these adsorbents float up on the surface of water. When we were trying to develop another type of the floating adsorbent by introducing a fermentation system into the bead, we found that the adsorbent repeated the movement of sinking and floating and finally floated up the surface of water. The repeat of sinking and floating of the adsorbent probably enables the significant contact with pollutants distributing in the whole bulk of water. Generally, for the treatment of a huge amount of polluted water, a column filled with adsorbent is used and the polluted solution is passed through the column. However, the column method needs a piping and pumping system. If we could develop the adsorbent which has the vertical migration system, that is, the adsorbent repeats floating and sinking between the bottom and surface of the bulk water many times, it could exhibit the advantage that the removal of pollutants from plenty amount of water could be achieved without the pumping or stirring system. The objective of the present study was to develop such an adsorbent having a vertical migration system. In order to build up this system into an adsorbent, the introduction of a fermentation process using glucose and yeast into alginate gel beads was attempted [27, 28].

The alginate hydrogel composite was prepared in the alginate solution containing both glucose and yeast to introduce the fermentation system in the bead.

In this study, at first the kinetics of glucose in the fermentation process was investigated and then the adsorbent having the fermentation system was prepared. The repeated vertical migration of the adsorbent was observed and finally the mechanism of the repeated migration was discussed.

4.2 Fermentation Model and Kinetics

The fermentation system introduced in the alginate gel bead in this study is based on the decomposition of glucose by yeast. In the aerobic condition, the fermentation process by yeast decomposed glucose easily to produce CO₂ gas. This process can be represented by the following equation:



It is nothing but the fermentation process by yeast is the conversion of glucose to CO₂ gas. The kinetic model of the fermentation process depends on the amount of glucose and temperature. Therefore, the alginate gel beads having the fermentation process can produce CO₂ gas bubbles in the bead and can float up on the surface of water because of the buoyancy of the generated CO₂ gas bubbles. During the generation of CO₂ gas bubbles in alginate gel beads, the concentration of glucose in alginate gel beads, [C]_{gel}, is decreased. The concentration of glucose in alginate gel beads is also decreased by the elution of glucose from alginate gel beads because

the size of glucose is too small to retain it in the gel network structure. The kinetics of the decrease of glucose by the fermentation process is described by a first-order kinetics, as shown by Eq. (2),

$$\frac{-d[C]_{\text{gel}}}{dt} = -k_1[C]_{\text{gel}} \quad (2)$$

$$\text{Ln} \left(\frac{[C]_{\text{gel}}}{[C_0]_{\text{gel}}} \right) = -k_1 t \quad (3)$$

where $[C_0]_{\text{gel}}$ (mg/L) is the initial concentration of glucose in the bead, $[C]_{\text{gel}}$ (mg/L) is the concentration of glucose at the time t , and k_1 is the first-order constant as the decreasing rate of glucose in alginate gel beads. The value of k_1 was obtained from the slope of the plot $\text{Ln} ([C]_{\text{gel}}/[C_0]_{\text{gel}})$ against t as Eq. (3). The amount of glucose in alginate gel beads without yeast was also decreased by the elution process.

The kinetic model of glucose fermentation process using yeast could be evaluated by adopting the pseudo first-order kinetic equation [29]. It is important to clarify the factors and conditions which determines the fermentation kinetics, in order to apply this process to the development of the adsorbent having a vertical migration system. A kinetic modeling of floatation using fermentation process has been reported by some researchers [30]. However, there are few studies on developing the adsorbent on the basis of the fermentation process involving yeast and glucose.

The fermentation kinetics of glucose by yeast was investigated at different temperatures of 5, 15, and 25°C using the initial concentration of 5, 10, and 30 wt % glucose in the alginate solution (Fig. 9). The consumption of glucose in the alginate solution after 48 h was 40% at 5°C, 80% at 15°C, and 95% at 25°C. As shown in Fig. 9, the first-order kinetics constant could be obtained from the kinetics data. The first-rate constant of the fermentation activity (k_1) by yeast at 25°C was 0.0697, which was higher than those at 5°C (0.0181) and 15°C (0.0456). Therefore, the fermentation rate constant for glucose depended on the temperature of the

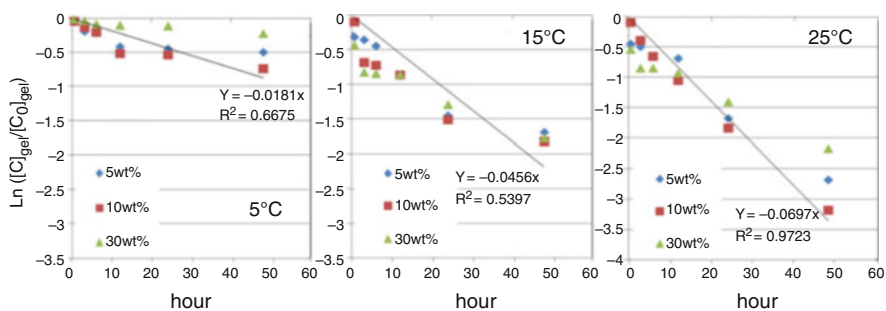


Fig. 9 Typical kinetics results for 5, 10, and 30% glucose fermentation using yeast in alginate solution at 5°C, 15°C, and 25°C

Fig. 10 Floating alginate gel beads by fermentation



solution. The production of CO_2 gas by fermentation of glucose using yeast is expected to act as a temporary buoyancy of alginate gel beads.

4.3 Floating Profile of the Beads

The vertical migration behavior of the alginate gel beads having the fermentation system in a water column was observed for a long time by a video camera. The gel beads repeated the vertical migration in the water column (the depth of the column was 80 cm), that is, the gel beads at first sank to the bottom of water and then floated up on the surface of water after some delay time at the bottom. Moreover, the floating gel bead sank to the bottom of water and then floated up to the water surface again. Surprisingly this process of sinking and floating was repeated in water many times (Fig. 10). The track of the repeated migration of a gel bead is shown in Fig. 11.

The solid line in the figure shows the track of a gel bead in water as a function of time. At the zero time, the bead exists at the bottom of water, that is, the bead sinks to the bottom when the bead is added to water. After staying there some time, the bead floats up on the surface of water. After staying there, the bead sinks to the bottom and this migration is repeated several times. The migration behavior of sinking and

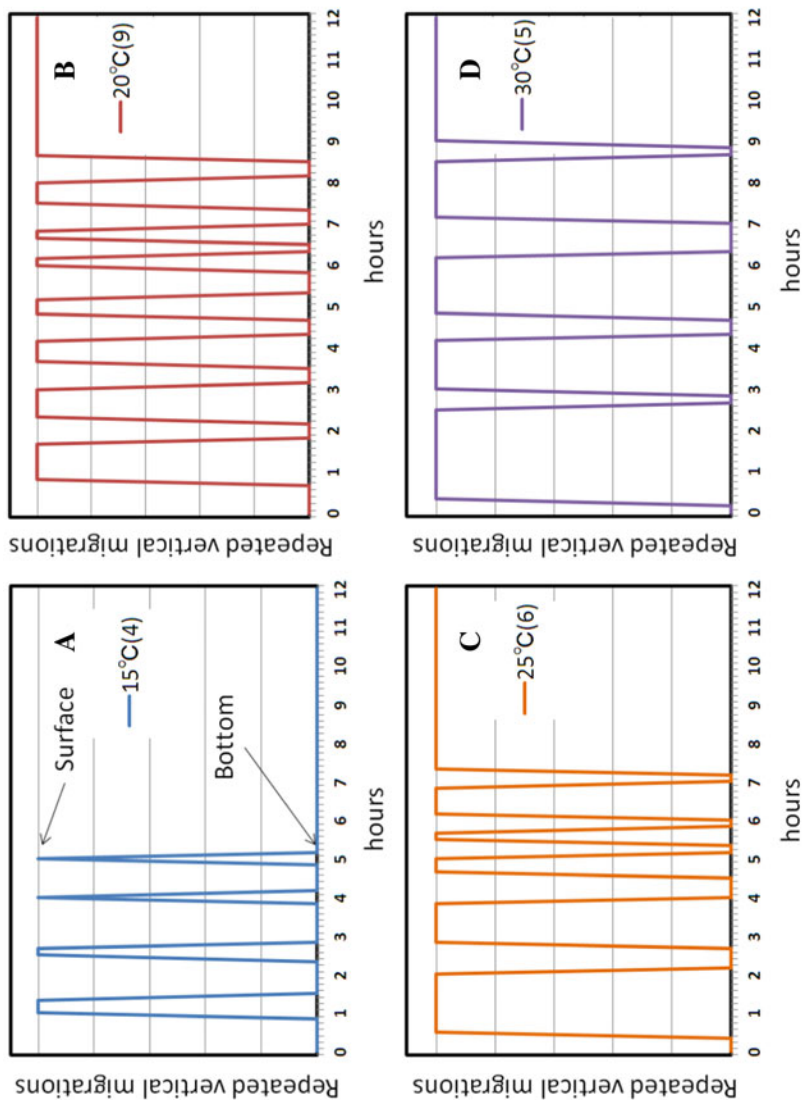


Fig. 11 Repeated behavior of the alginate gel beads having vertical migration system. The repeated vertical migration times was four at 15°C (a), and the repeated vertical migration times was nine at 20°C (b), and the repeated vertical migration times was six at 25°C (c), and the repeated vertical migration times was five at 30°C, (d) [13]

floating of alginate gel bead depended on the temperature, because the suitable temperature for the glucose fermentation is around 10–30°C. Glucose in the alginate gel bead was converted to CO₂ gas by fermentation process at 25°C. CO₂ gas, which was produced and accumulated in the alginate gel beads, acted as a buoyancy for the alginate gel beads. At the lower temperature, the rate of generation of CO₂ gas is slow, the bead stays longer at the bottom of water but shorter on the surface of water. The specific gravity of the alginate gel beads was decreased by the consumption of glucose during the fermentation process and also the elution. From the consumption amount of glucose could be evaluated from the amount of CO₂ gas formed by the fermentation process. The beads containing 10 wt% of glucose stayed in the bottom of water for 30 min and began to float up after 40 min and repeated this behavior.

The repeated behavior of the beads having the frequency rate of the vertical migration system at 15–30°C. The alginate gel beads kept for a longer time at the bottom of water at 15°C. On the other hand, in the case of at 30°C, the alginate gel beads kept for a longer time on the surface of the water although the repeated vertical migration was just five times. It can be explained by the temperature dependency of the activity of yeast to produce the CO₂ gas during the glucose fermentation process.

4.4 Vertical Migration Behavior of the Beads

The vertical migration behavior of the bead in water also depended on the concentration of glucose in the bead. The repeated vertical migration of a bead containing 5, 10, and 30 wt% glucose is shown in Fig. 12. The bead containing 5 wt% of glucose showed a sharp floatability, that is, after the first 30 min the bead started to float up to the surface of water, and stayed the surface of water for 30 min and sank to the bottom of water. Then, the bead repeated just four times the vertical migration between the bottom and the surface of the water column for 12 h. The higher concentration of glucose was in the bead, the more frequent vertical migration of the bead was observed for 12 h. On the other hand, the interval of the repeated action of the bead containing 30 wt% glucose shifted to the longer. It became clear that the interval can be varied by changing the amount of glucose in the beads. As shown in Fig. 12, the repeated interval of the alginate gel beads was 30–40 min for 5 wt% of glucose, 60 min for 10 wt% of glucose, and 120–380 min for 30 wt% of glucose. In the case of 10 wt% of glucose, the fermentation rate was stable for 12 h and in the case of 30 wt% of glucose, it was stable for 48 h. This fact suggests that the concentration of glucose in the alginate gel beads was decreased by two different processes. One is the elution process; the amount of glucose was eluted directly from alginate gel beads to water. Another is due to the consumption by the fermentation process. The decrease in the amount of glucose affected more largely the specific gravity of alginate gel beads by eluting rather than the increase in the buoyancy of CO₂ bubbles produced by the fermentation process.

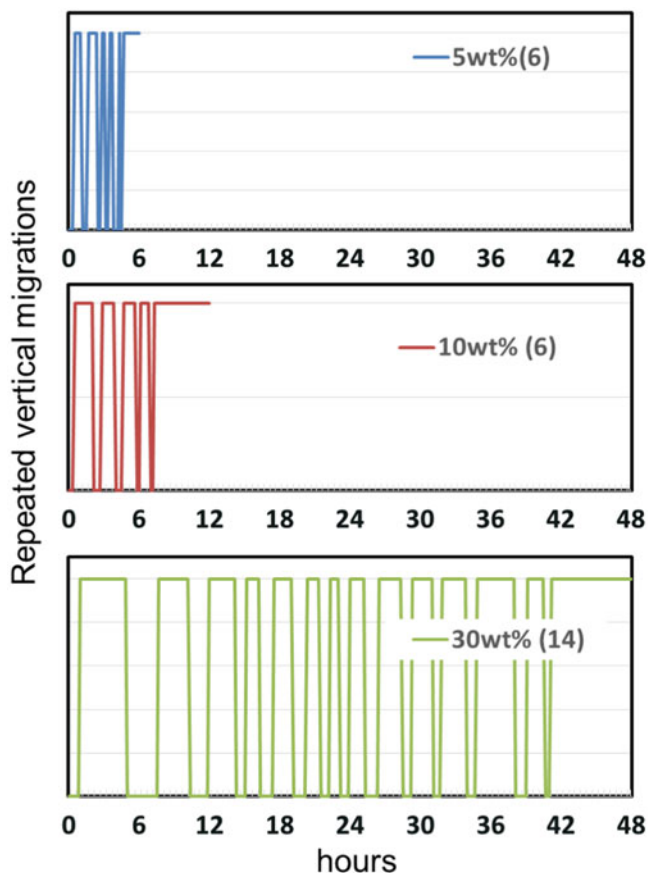


Fig. 12 The floating profile of the gel beads containing 5, 10, and 30 wt% glucose [13]

4.5 Conclusion

In order to build up another type of the floating-up adsorbent, the alginate gel beads into which the fermentation process was introduced were prepared. The obtained beads firstly sank to the bottom of water, however, 30 min later, most of the beads floated up to the surface of water by the generation of carbon dioxide bubbles by the fermentation. During the flotation of the alginate beads, glucose reacted with yeast to produce CO_2 gas bubbles as a buoyancy for the gel beads. When the alginate gel beads floated on the surface of the water, the accumulated CO_2 gas bubbles in alginate gel beads might come off from the gel due to the decrease of the water pressure or the evaporation of a water film covering around the bead and then the bead sank to the bottom. This behavior was repeated many times during the continuation of the fermentation process. The expected mechanism of the repetition

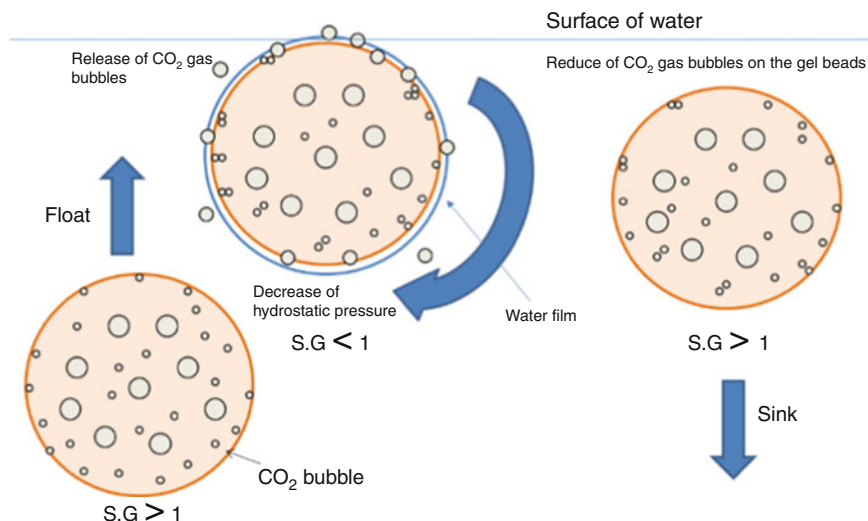


Fig. 13 The expected mechanism of repetition of vertical migration by the release of CO₂ gas bubbles from the alginate gel beads

of vertical migration of the alginate gel beads is shown in Fig. 13. It was confirmed that the repeated motion was based on the repetition of accumulation and the release of CO₂ gas bubbles on the gel beads. The repeated vertical migration of the gel beads has a great potential to remove pollutants distributed in the bulk water without column and stirring system.

5 Adsorption Kinetic Model of Alginate Gel Beads Synthesized Micro Particle-Prussian Blue to Remove Cesium Ions from Water

5.1 Introduction

Prussian blue (PB) is well known to be as an effective adsorbent for removing radioactive Cs ions from wastewater [31, 32]. PB has the three-dimensional network structure with a face-centered cubic structure consisting Fe (III) (coordinated to nitrogen) and Fe (II) (coordinated to carbon atom) ions linked via the bridging of cyanide ligands [33, 34]. Cs ion penetrates into the lattice of PB and is trapped there. Generally, the fine crystals of PB are more favorable to gain the high capacity and fast adsorption of cesium ions. However, for the collection and reuse of the fine form of the adsorbent, the process such as filtration or centrifugation, which is time and energy-consuming, is necessary after adsorption [35]. A possible solution is entrapping the fine crystals of PB in supporting materials for preparation of new

class conjugate adsorbent [36]. Vipin et al. developed Ca-alginate gel beads encapsulating PB powder and investigated their use in the removal of cesium ions from water [37]. However, the high dispersion of the PB powder in the alginate gel beads and the production of huge sludge after the use of the adsorbent have been made it as major hurdle in the large-scale use for the removal of Cs. The key adsorbing materials such as Prussian blue (PB) particulates in alginate gel beads should be synthesized and purified systematically and the characterization should be scientifically completed using various techniques such as Scanning Electron Microscope (SEM), X-ray Diffraction (XRD) measurement [38]. Then the micro-particles of PB were encapsulated in hydrogels using sodium alginate as the immobilizer and ferric ions (Fe^{3+}) as the cross-linker. Two types of beads, PB-AG(syn) and PB-AG(mix) were prepared. The developed beads were examined by means of SEM and Brunauer–Emmett–Teller (BET) analysis to understand the morphological and porous peculiarities [39]. A series of experiments were performed to aim at applying the adsorbents practically to the removal of cesium from aqueous solutions under batch conditions. Various issues such as the characteristics, effects of pH, foreign ions, organic acids, and so on were discussed systematically. The PB-AG(syn) beads were successfully synthesized and their effectiveness were compared with other PB derivatives. As a result, the adsorption of Cs ions onto PB-AG(syn) could attain a more stable and much faster adsorption equilibrium than that of PB-AG(mix) and other PB derivatives.

5.2 Preparation of PB-AG Beads

The impregnation of Prussian blue into alginate gel beads was carried out by two different methods (PB-AG(syn.) and PB-AG(mix.)). One is a PB-AG(syn) method, where PB was synthesized in the gel beads. First, Ca^{2+} -AG beads containing $\text{K}_4\text{Fe}(\text{CN})_6$ were prepared by adding alginate solution containing $\text{K}_4\text{Fe}(\text{CN})_6$ drop-wisely from a burette into a calcium chloride solution. And then, the Ca^{2+} -AG beads containing $\text{K}_4\text{Fe}(\text{CN})_6$ were immersed in a Fe (III) chloride solution. After that, the PB particulate was synthesized by the reaction of $\text{Fe}(\text{CN})_6^{4-}$ in the gel with Fe (III) when ferric ions in the solution diffused into the Ca^{2+} -AG beads. Calcium ions in Ca^{2+} -AG beads was exchanged with ferric ions to form Fe(III)-AG beads. After that, these gel beads were filtered and washed with distilled water and designated as PB-AG(syn) beads.

Another one is a PB-AG(mix) method, where the powder of PB was entrapped in the Ca-alginate gel. A sodium alginate solution was added to 50.5 mg powder of Prussian blue under the constant stirring. The solution was kept for 20 min under stirring. The aqueous PB particle-alginate colloidal solution was added drop-wisely into a beaker containing calcium chloride solution under magnetic stirring to produce the PB-encapsulated beads (PB-AG(mix)). After maturation for 3 h, the PB-AG (mix) beads were exchanged with ferric ions to form Fe(III)-AG beads for 3 h.

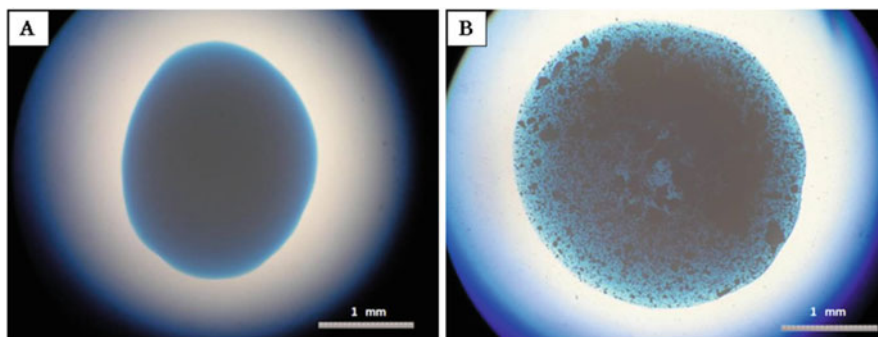


Fig. 14 Optical microscope image of a PB particle synthesized in an alginate gel bead (a) and PB powder mixed with an alginate gel bead (b) [16]

Finally, they were collected by filtration, washed three times with deionized water, and stored in calcium chloride solution.

5.3 Characterization of PB-AG Beads

The powder X-ray diffraction patterns of the PB particulate in PB-AG(syn) revealed the totally same as the diffraction peaks of the PB crystals at 17.5° , 24.8° , and 30.66° , 35.7° , 39.14° , 43.32° , 50.32° , 53.26° , and 56.42° . This pattern is completely consistent with that of Prussian blue having a face-centered cubic structure with space group, Fm3m [40, 41]. The difference in dispersion of PB particles between PB-AG(syn) and (mix) could be observed in an optical microscope, SEM, and particle size distribution measurement. Figure 14 shows the optical microscope images of the cross section of the PB-AG(syn) and PB-AG(mix) beads. The PB particles in the PB-AG(syn) beads is more uniformly dispersed (Fig. 14a). On the other hand, the dispersion of the PB particles in PB-AG(mix) beads seems to be heterogeneous (Fig. 14b). The SEM images of PB particle in PB-AG(syn) and PB-AG(mix) are shown in Fig. 15a, b. We can find the cubic structures of the uniformly dispersed PB in PB-AG(syn), whose average particle diameter of these particles is almost $0.1 \mu\text{m}$. On the other hand, the particles in PB-AG(mix) are comparatively bigger than that of PB-AG(syn) because of the agglomeration of the PB particles. The particle size distributions of PB-AG(syn) and (mix) measured by a dynamic light scattering method are shown in Fig. 16. The particle size was almost 107 nm (Fig. 3a), consisted with the observation by SEM. On the other hand, the particle size distribution of PB-AG(mix) was a wide range of distribution 275–5,390 nm and the particle average size was 2,035 nm (Fig. 16b). Particularly, for achieving better dispersion of PB particles in alginate gel beads, PB-AG(syn) which was stable in colloidal PB particle to enhance the uniformity of PB particle density was preferable.

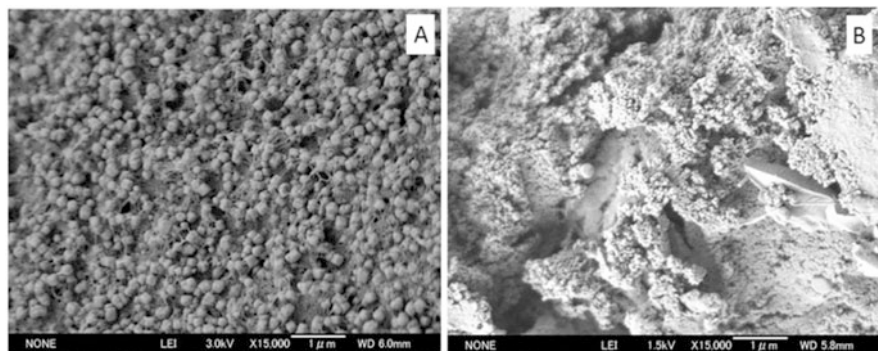


Fig. 15 SEM images of Prussian blue impregnated alginate gel bead with cross section: (a) PB-AG (syn.) and (b) PB-AG(mix.) [16]

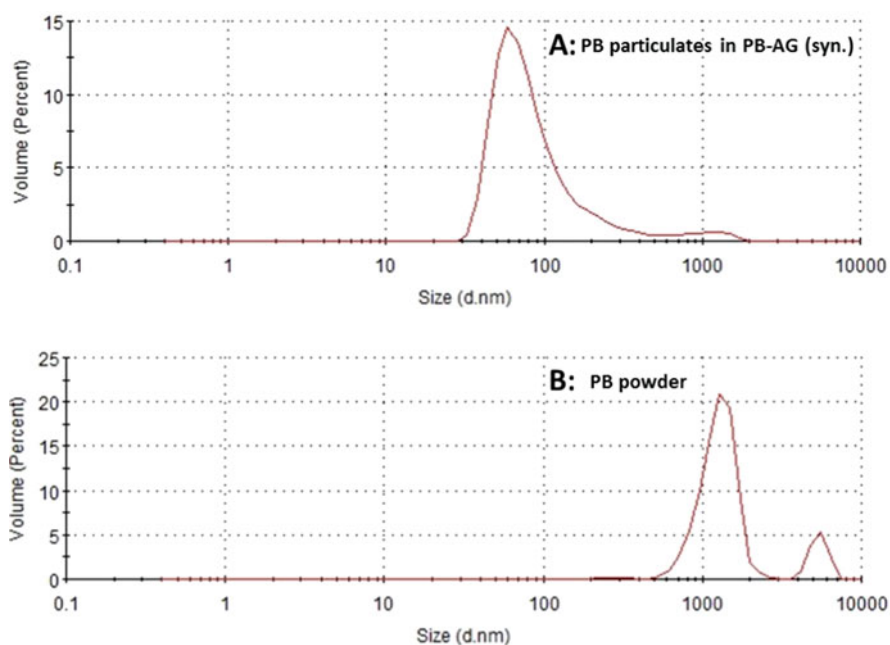


Fig. 16 Particle size distribution of PB particles: (a) PB particulate in PB-AG(syn) and (b) PB powder [16]

Surface area and porosity are important factors, which affect the quality and utility of materials in adsorption. In addition, they are helpful in understanding the structure, formation, and applications of materials. Therefore, these factors were measured by BET method. The results for the PB powder and PB particulate in

Table 3 The BET specific surface areas of the samples [16]

Samples	Conc. of alginate gel (wt %)	Surface area (m ² /g)
Alginate gel bead	1.0	16.2
PB powder	–	52.3
PB-AG (mix.)	1.0	155
PB-AG (syn.)	1.0	309

alginate gel beads, PB-AG(syn), are given in Table 3. The surface area of the plane alginate gel beads was 16.2 m²/g and that of PB powder was 52.3 m²/g. In addition, the pore size distribution of PB powder for micro-pores was 0.18 mg/g and that of meso-pores was 0.36 mg/g. On the other hand, the surface area of PB particulate in PB-AG(syn) was 309 m²/g, because of the relatively small particle size. The surface area of beads depended on the encapsulated adsorptive particle. The PB particulates impregnated in the alginate gel with the high hydrophilic property can give more chance to contact with cesium. From the SEM and BET studies, we could confirm the importance of PB particulate in PB-AG(syn.).

5.4 Removal of Cs Ions by PB-AG Beads

The adsorption isotherm and kinetics of Cs ion on PB-AG(mix) and PB-AG(syn) were investigated. Both of PB-AG(mix) and (syn) beads could adsorb Cs ions within 24 h, where PB played main binding sites for Cs ions. The adsorption equilibrium constant (K) and the saturated amount of adsorption at the equilibrium (Q_{\max}) were estimated by fitting to the Langmuir adsorption isotherm equation. The parameters of this isotherm are summarized in Tables 4. The Q_{\max} of PB powder and PB-AG (syn.) increased slightly with increasing in pH (1.0–6.0). The Q_{\max} of PB-AG(syn.) was slightly larger than that of PB powder. On the other hand, the K value of PB-AG (syn.) was about twice that of the PB powder and it indicated that PB-AG(syn.) has higher effectiveness to remove Cs ions. These results confirmed that the adsorption capacity of PB in AG mainly depended on the amount of PB in the bead if sufficient time is taken to achieve the equilibrium. The amount of cesium adsorption for PB-AG(syn.) was calculated 55.6 mg per 1 g of the PB powder as estimated by the Langmuir model.

The adsorption of Cs ions onto PB-AG(syn) reached to the equilibrium within 12 h, while in a case of PB-AG(mix), it took 24 h to reach the equilibrium. To clarify the kinetic characteristics, the adsorption processes were described by both pseudo-first-order and pseudo-second-order kinetics. The maximum adsorption capacities of the PB-AG(syn) beads were 0.557 mg. bead⁻¹ and the kinetic rate was found to be $1.72 \times 10^{-1} \text{ min}^{-1}$ at pH 6.0 for the pseudo first order, and $4.65 \times 10^{-1} \text{ bead}^{-1} \text{ mg}^{-1} \text{ min}^{-1}$ at pH 6.0 for the pseudo second order. In the

Table 4 Effect of pH on the pseudo-first-order and pseudo-second-order model constants for the adsorption of Cs⁺ ions [16]

PB-AG	pH	Pseudo-first-order		Pseudo-second-order				R^2
		k_1 (min ⁻¹)	Q_e (mg bead ⁻¹)	k_2 (bead mg ⁻¹ min ⁻¹)	$t_{1/2}$ (min)	h (mg bead ⁻¹ min)	Q_e (mg bead ⁻¹)	
PB(mix.)								
1.0		7.96×10^{-2}	0.348	9.63×10^{-2}	28	0.01292	0.366	0.9994
2.0		8.30×10^{-2}	0.439	1.32×10^{-1}	17	0.02730	0.454	0.9999
3.0		8.69×10^{-2}	0.476	1.25×10^{-1}	17	0.02920	0.483	0.9995
4.0		8.80×10^{-2}	0.497	1.12×10^{-1}	18	0.02835	0.502	0.9993
5.0		9.19×10^{-2}	0.503	1.32×10^{-1}	15	0.03528	0.517	0.9981
6.0		9.63×10^{-2}	0.536	1.21×10^{-1}	15	0.03803	0.561	0.9998
PB(syn.)								
1.0		1.16×10^{-1}	0.398	2.54×10^{-1}	10	0.04264	0.409	0.9999
2.0		1.23×10^{-1}	0.489	2.01×10^{-1}	10	0.05246	0.510	0.9998
3.0		1.42×10^{-1}	0.500	1.92×10^{-1}	10	0.05384	0.530	0.9995
4.0		1.47×10^{-1}	0.523	2.06×10^{-1}	9	0.05955	0.537	0.9999
5.0		1.49×10^{-1}	0.540	3.13×10^{-1}	6	0.09315	0.546	0.9999
6.0		1.72×10^{-1}	0.557	4.65×10^{-1}	4	0.14498	0.558	0.9999

case of PB-AG(mix), most of the binding sites of the PB are present in relatively large PB crystals and therefore it has taken a longer time for the Cs^+ to arrive at the binding sites in the bulk of the PB crystals. The concentration of AG also affected the adsorption kinetics for Cs ions onto the PB-AG gel beads due to the change in the permeability of the Cs ions in the AG gel. The diffusion velocity of the Cs ions in the gel was decreased with an increase in the concentration of the alginate solution. These results confirmed that the AG gel and ferric ions surrounding PB particles played important roles in controlling the adsorption of Cs ions onto PB particles.

5.5 Removal of Cesium Ion in Water Column Using a Vertical Migration System of Alginate Gel Beads

The combination of two functions of adsorption and floating leads to the development of a novel adsorbent. In order to confirm the usefulness of the novel adsorbent, the PB-AG gel beads with a vertical migration system were prepared by introducing 30 wt% of glucose, 1 wt% of yeast, and 25 mg of PB into an alginate gel bead and the removal of cesium ions was demonstrated using a water column (1.5 m height) of 1 ppm Cs^+ solution. One hundred alginate gel beads were added to the water column and the concentrations of cesium ion at the bottom and the middle of water were measured as a function of time. All of the added beads repeated sinking and floating between the bottom and the surface of water column for 48 h. During this vertical migration process, the concentration of cesium ion in the water column was monitored. As shown in Fig. 17, the concentration of cesium ion was decreased with increase of the time due to the adsorption during the vertical migration. After 48 h, 99.2 wt% of total cesium ions in the water column could be removed when the PB alginate gel beads having repeated vertical migration system were used. On the other hand, when the same numbers of the PB gel beads which have no vertical migration property were used, that is, the beads were set only at the surface or the bottom of the water column, the removal of cesium ions was 65.9% by the floating beads and 50.6% by the sinking beads. Figure 18 shows the relationships between the repeated numbers of the vertical migration of PB alginate gel beads and the removal ratio of cesium ion from water column. In this case, all of the alginate gel beads containing 5 wt% of glucose repeated the vertical migration four times and could be collected on the surface of water within 6 h. During this process, the concentration of cesium ion in the water column was monitored.

5.6 Conclusion

Prussian blue (PB) impregnated in Alginate gel (AG) beads was synthesized in order to test their viability for removing cesium (Cs) ions from wastewater. Two types of

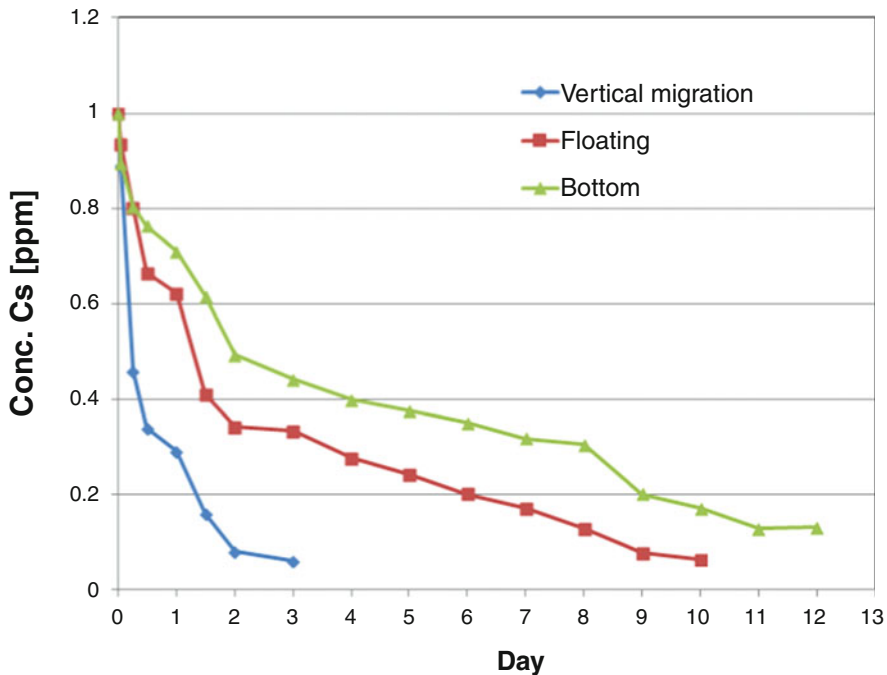


Fig. 17 The concentration of cesium ion using the PB alginate gel beads having a vertical migration system [17]

AG beads that contained Prussian blue (PB-AG(syn) and PB-AG(mix)) were successfully prepared and their ability to adsorb Cs ions was investigated. Both types of PB-AG beads showed an efficient adsorption of Cs ions. In particular, PB-AG(syn), where PB was synthesized in the gel, had very fine particulates and demonstrated a high dispersion of PB in the gel beads. The interaction between PB-AG(syn) beads and Cs ions was investigated by adsorption experiments and analyzed using Langmuir and adsorption kinetic models. Consequently, the PB-AG(syn) beads showed a high capacity for the removal of Cs ions from water.

In order to introduce the unique property into the adsorbent, the removal of cesium ions in a water column was demonstrated by using Prussian blue modified alginate gel beads, which have a repeated vertical migration system. As the result, this adsorbent showed the faster removal of cesium than that by the adsorbent without the system. The system can be applied to the treatment of plenty amount of wastewater which cannot be stirred and pumping. Therefore, the novel adsorbent developed in this study is expected to contribute to the environmental remediation in future.

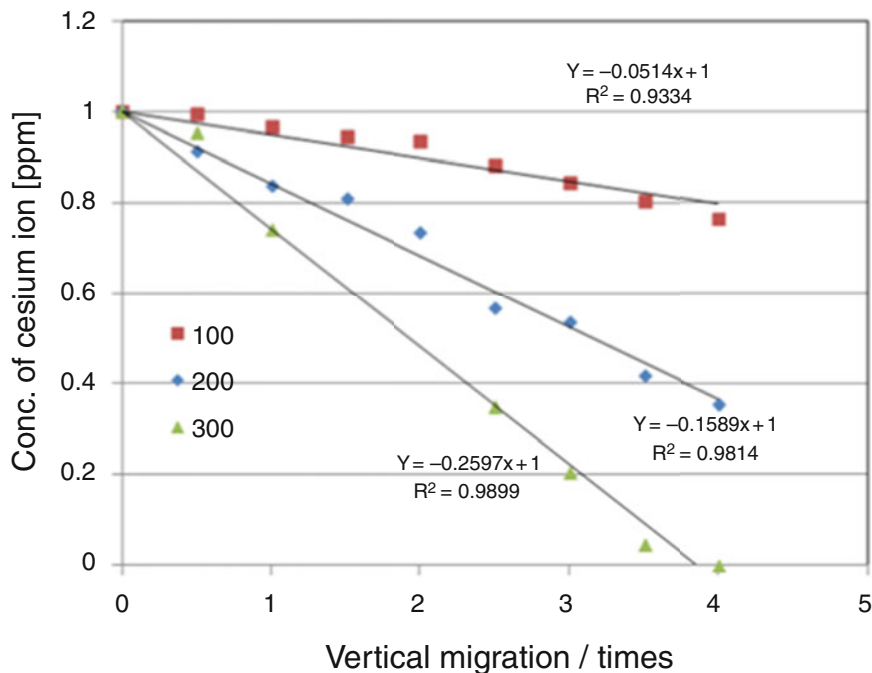


Fig. 18 The relationships between the concentration of cesium ion and the repeated times of the vertical migration of the PB alginate gel beads

6 Conclusion

In the present study, to realize an easy collection of adsorbents from water environment, our attempt is to develop a new type of adsorbent based on alginate gel beads whose specific gravity could be controlled by introducing both a weight and a float. At first a prototype adsorbent was built up by using Shirasu balloon or CO_2 gas bubbles as a float and CaCO_3 as a weight in alginate gel beads. This adsorbent sank and stayed at the bottom of water because the weight of salts exceeds the buoyancy at first. In order to build up another type of the floating-up adsorbent, the alginate gel beads into which the fermentation process was introduced were prepared. In this case, CO_2 bubbles generated by the fermentation process of glucose with yeast were expected to act as a float. The gel bead with the fermentation system could float up on the surface of water. Moreover, the gel bead not only floated up but also repeated floating and sinking many times. After the repeated vertical migration, the gel beads floated up on the surface of water, therefore, these gel beads could be collected easily on the surface of water. This unique motion in water, that is, the repeated vertical migration of the gel beads in water, provides us the useful advantage in the removal of pollutant in water where stirring and pumping system cannot be used.

Since there are many other methods to control the specific gravity of adsorbent, the more sophisticated adsorbents will be developed according to the situation of the contaminated sites. These new type adsorbents are expected to contribute to the remediation of environments in future.

References

1. Dai Y et al (2010) Nitrobenzene-adsorption capacity of carbon materials released during the combustion of woody biomass. *J Hazard Mater* 174(1–3):776–781. <https://doi.org/10.1016/j.jhazmat.2009.09.119>
2. Wu G et al (2010) A critical review on the bio-removal of hazardous heavy metals from contaminated soils: issues, progress, eco-environmental concerns and opportunities. *J Hazard Mater* 174(1–3):1–8. <https://doi.org/10.1016/j.jhazmat.2009.09.113>
3. Madhava Rao M et al (2006) Removal of copper and cadmium from the aqueous solutions by activated carbon derived from Ceiba pentandra hulls. *J Hazard Mater* 129(1–3):123–129. <https://doi.org/10.1016/j.jhazmat.2005.08.018>
4. Lin YB et al (2005) Removal of organic compounds by alginate gel beads with entrapped activated carbon. *J Hazard Mater* 120(1–3):237–241. <https://doi.org/10.1016/j.jhazmat.2005.01.010>
5. Avramenko V et al (2011) Colloid stable sorbents for cesium removal: preparation and application of latex particles functionalized with transition metals ferrocyanides. *J Hazard Mater* 186(2–3):1343–1350. <https://doi.org/10.1016/j.jhazmat.2010.12.009>
6. Chen R et al (2013) Selective removal of cesium ions from wastewater using copper hexacyanoferrate nanofilms in an electrochemical system. *Electrochim Acta* 87:119–125. <https://doi.org/10.1016/j.electacta.2012.08.124>
7. Liu H et al (2013) Magnetic zeolite NaA: synthesis, characterization based on metakaolin and its application for the removal of Cu^{2+} , Pb^{2+} . *Chemosphere* 91(11):1539–1546. <https://doi.org/10.1016/j.chemosphere.2012.12.038>
8. Scaglia B et al (2016) Chlorpyrifos-methyl solubilisation by humic acids used as bio-surfactants extracted from lignocelluloses and kitchen wastes. *Chemosphere* 159:208–213. <https://doi.org/10.1016/j.chemosphere.2016.06.008>
9. Siswoyo E, Tanaka S (2013) Development of eco-adsorbent based on solid waste of paper industry to adsorb cadmium ion in water. *J Clean Energy Technol* 1(3):198–201. <https://doi.org/10.7763/jocet.2013.v1.45>
10. Ye X et al (2008) Comparison of strontium and calcium adsorption onto composite magnetic particles derived from Fe_3O_4 and bis(trimethoxysilyl)propylamine. *Colloids Surf A Physicochem Eng Asp* 330(1):21–27. <https://doi.org/10.1016/j.colsurfa.2008.07.019>
11. Walsh PK et al (2010) Remediation of soil contaminated with the heavy metal (Cd^{2+}). *J Hazard Mater* 358(1–2):81–91. <https://doi.org/10.1016/j.ijpharm.2008.02.024>
12. Ramdas S (2012) Cruel disease, cruel medicine: self-treatment of cutaneous leishmaniasis with harmful chemical substances in Suriname. *Soc Sci Med* 75(6):1097–1105. <https://doi.org/10.1016/j.socscimed.2012.04.038>
13. Mihara Y, Tanaka S. Patent JP6468639B2
14. Mihara Y, Tanaka S (2013) Development of a new type of adsorbent that can be collected easily on the surface of water after adsorption at the bottom of water. *J Environ Chem* 23(4):187–194. <https://doi.org/10.5985/jec.23.187>
15. Mihara Y et al (2020) Functionalization of shirasu-balloons surface for removal of cadmium ions from contaminated soil. *Anal Sci* 36(5):553–560. <https://doi.org/10.2116/ANALSCI.19SBP06>

16. Mihara Y et al (2016) Adsorption kinetic model of alginate gel beads synthesized micro particle-Prussian blue to remove cesium ions from water. *J Water Process Eng* 10:9–19. <https://doi.org/10.1016/j.jwpe.2016.01.001>
17. Mihara Y, Sano K, Minai H, Haneda N. Patent, JP2019-195792
18. Choi BY et al (2002) Preparation of alginate beads for floating drug delivery system: effects of CO₂ gas-forming agents. *Int J Pharm* 239(1–2):81–91. [https://doi.org/10.1016/S0378-5173\(02\)00054-6](https://doi.org/10.1016/S0378-5173(02)00054-6)
19. Tønnesen HH, Karlsen J (2002) Alginate in drug delivery systems. *Drug Dev Ind Pharm* 28(6): 621–630. <https://doi.org/10.1081/DDC-120003853>
20. Minor AM et al (2008) Development and evaluation of new sustained-release floating microspheres. *Int J Pharm* 358(1–2):82–90. <https://doi.org/10.1016/j.ijpharm.2008.02.024>
21. Jang LK et al (1995) Effect of pH on the absorption of Cu(II) by alginate gel. *Water Res* 29(1): 315–321. [https://doi.org/10.1016/0043-1354\(94\)E0091-J](https://doi.org/10.1016/0043-1354(94)E0091-J)
22. Sodeyama K et al (1999) Preparation of fine expanded perlite. *J Mater Sci* 34(10):2461–2468. <https://doi.org/10.1023/A:1004579120164>
23. Sodeyama K et al (2000) The manufacturing process of fine Shirasu balloons using a fluidized sand-bed furnace. *Adv Powder Technol* 11(4):503–516. <https://doi.org/10.1163/156855200750172097>
24. Kimura K et al (1972) On the hollow glass micro-sphere made from the “Shirasu” (Silas Balloons). *J Ceram Assoc* 80(918):84–91. https://doi.org/10.2109/jcersj1950.80.918_84
25. Lin CC, Lin HL (2005) Remediation of soil contaminated with the heavy metal (Cd²⁺). *J Hazard Mater* 122(1–2):7–15. <https://doi.org/10.1016/j.jhazmat.2005.02.017>
26. Angela de MFG et al (2009) Smectite organo functionalized with thiol groups for adsorption of heavy metal ions. *Appl Clay Sci* 42(3–4):410–414. <https://doi.org/10.1016/j.clay.2008.04.006>
27. Huberts DHEW et al (2013) Construction and use of a microfluidic dissection platform for long-term imaging of cellular processes in budding yeast. *Nat Protoc* 8(6):1019–1027. <https://doi.org/10.1038/nprot.2013.060>
28. Grillitsch K et al (2011) Lipid particles/droplets of the yeast *Saccharomyces cerevisiae* revisited: lipidome meets proteome. *Biochim Biophys Acta* 1811(12):1165–1176. <https://doi.org/10.1016/j.bbalip.2011.07.015>
29. Hansen RJ et al (1977) Effects of glucose and nitrogen source on the levels of proteinases, peptidases, and proteinase inhibitors in yeast. *Biochim Biophys Acta* 496(1):103–114. [https://doi.org/10.1016/0304-4165\(77\)90119-2](https://doi.org/10.1016/0304-4165(77)90119-2)
30. Fujita J et al (2001) Critical importance of phytase for yeast growth and alcohol fermentation in Japanese sake brewing. *Biotechnol Lett* 23(11):867–871. <https://doi.org/10.1023/A:1010599307395>
31. Hu B et al (2012) Prussian blue caged in spongiform adsorbents using diatomite and carbon nanotubes for elimination of cesium. *J Hazard Mater* 217–218:85–91. <https://doi.org/10.1016/j.jhazmat.2012.02.071>
32. Pearce J (1994) Studies of any toxicological effects of Prussian blue compounds in mammals – a review. *Food Chem Toxicol* 32(6):577–582. [https://doi.org/10.1016/0278-6915\(94\)90116-3](https://doi.org/10.1016/0278-6915(94)90116-3)
33. Sasaki T, Tanaka S (2012) Magnetic separation of cesium ion using Prussian blue modified magnetite. *Chem Lett* 41(1):32–34. <https://doi.org/10.1246/cl.2012.32>
34. Itaya K et al (1982) Spectroelectrochemistry and electrochemical preparation method of Prussian blue modified electrodes. *J Am Chem Soc* 104:4767–4772. <https://doi.org/10.1021/ja00382a006>
35. Ding Y et al (2009) Controllable synthesis and formation mechanism investigation of prussian blue nanocrystals by using the polysaccharide hydrolysis method. *J Phys Chem C* 113(33): 14838–14843. <https://doi.org/10.1021/jp905704c>
36. Le Gall B et al (2006) Comparison of Prussian blue and apple-pectin efficacy on ¹³⁷Cs decorporation in rats. *Biochimie* 88(11):1837–1841. <https://doi.org/10.1016/j.biochi.2006.09.010>

37. Vipin AK et al (2013) Prussian blue caged in alginate/calcium beads as adsorbents for removal of cesium ions from contaminated water. *J Hazard Mater* 258–259:93–101. <https://doi.org/10.1016/j.jhazmat.2013.04.024>
38. Wu X et al (2006) Sonochemical synthesis of Prussian blue nanocubes from a single-source precursor. *Cryst Growth Des* 6(1):26–28. <https://doi.org/10.1021/cg050371x>
39. Ladavos AK et al (2012) The BET equation, the inflection points of N₂ adsorption isotherms and the estimation of specific surface area of porous solids. *Micropor Mesopor Mater* 151:126–133. <https://doi.org/10.1016/j.micromeso.2011.11.005>
40. Yang HM et al (2016) Prussian blue-functionalized magnetic nanoclusters for the removal of radioactive cesium from water. *J Alloy Compd* 657:387–393. <https://doi.org/10.1016/j.jallcom.2015.10.068>
41. Farah AM et al (2012) Fabrication of prussian blue/multi-walled carbon nanotubes modified glassy carbon electrode for electrochemical detection of hydrogen peroxide. *Int J Electrochem Sci* 7(5):4302–4313

Remediation by Floating Plants



Masaaki Morikawa

Contents

1	What Is Phytodegradation Mechanism?	652
2	Phytodegradation of Phenolic EDCs by Enhanced Common Reed <i>Phragmites</i>	654
2.1	Rhizobacterial Strains TIK1 and IT4 That Are Capable of Degrading Phenolic EDCs	654
2.2	Demonstration of TIK1 and IT4 to Degrade Phenolic EDCs with Organic Compounds Exuded by <i>Phragmites</i> Roots	655
2.3	Construction of <i>Phragmites</i> /TIK1 or <i>Phragmites</i> /IT4 Association Systems and Degradation of Phenolic EDCs	656
2.4	Continuous Removal of Phenolic EDCs from Polluted Effluent by Use of a Sequencing Batch Reactor (SBR) System Containing <i>Phragmites</i> /TIK1 or <i>Phragmites</i> /IT4	657
3	Tiny Floating Plant, Duckweeds, a Multi-Talented Phytoremediation Device	659
3.1	Isolation of Phenol-Degrading Bacteria from the Surface of the Duckweed, <i>Lemna aoukikusa</i>	660
3.2	Preparation of Enhanced Duckweed on Which Surface Is Dominated by <i>Acinetobacter</i> P23, the <i>L. aoukikusa</i> /P23 System	662
3.3	Stability of Phenol Degradation by <i>L. aoukikusa</i> /P23 Association System	663
3.4	Growth Promotion of Duckweed by P23 Colonization	666
4	Water Purification and Biomass Production Using Two Ponds System Toward Practical Use for Enhanced Duckweeds	667
4.1	Nutrients Removal, Phytoextraction, and Biomass Production Capacity of Enhanced Duckweeds in Two-Step Cultivation	668
4.2	Duration of Plant Growth-Promoting Effects After Pre-inoculation of P23	671
4.3	Persistence of P23 on Duckweed Surface	672
4.4	Shifts in Duckweed-Associated Microbial Community	673
4.5	Outlook for Future	674
5	Environmental Technologies “to the Duckweed and from the Duckweed” That Have Potentials to Contribute to Establishing Sustainable Society	675
5.1	Duckweed as a Protein Resource	675
5.2	Duckweed as a Starch Resource	676

M. Morikawa (✉)

Faculty of Environmental Earth Science, Hokkaido University, Sapporo, Japan

e-mail: morikawa@ees.hokudai.ac.jp

5.3 Utilization of PGPB for Accelerating Duckweed Industries	678
References	679

Abstract One of the environmental remediation technologies for next-generation could be not just to remove pollutants, but conversely to consider this process as an inexpensive biomass resource production. In particular, plant biomass that grows on light energy and CO₂ is a key material that supports sustainable society. The use of the produced biomass maybe changed depending on the type of pollutants treated. The plants used to adsorb heavy metals are clearly unsuitable for food and livestock feed, and will be limited to, for example, produce biofuels. On the other hand, as to the water pollutants contained in sewage and food factory wastewater, they are on the contrary at the same time essential elements for plants to grow such as nitrogen and phosphorous. In this case, the product biomass can be regarded even similar to ordinary crops. This chapter reviews phytoremediation technology using aquatic plants that can be applied from purification of toxic phenol related compounds to removal of nutrient minerals.

Keywords Endocrine disrupting compounds, Nutrient removal, Biomass production, Plant growth-promoting bacteria, Symbiosis

1 What Is Phytodegradation Mechanism?

Phytoremediation, which is a type of bioremediation, is defined as the use of plants to remove pollutants from the environment or to render them harmless [1]. Phytoremediation can be categorized by “phytoextraction,” “phytodegradation,” “rhizofiltration,” “phytostabilization,” and “phytovolatilization” depending on the mechanism of pollutant removal or transformation (Fig. 1). Root exudates acidify the rhizosphere by lowering soil pH, which promotes solubilization of heavy metals from insoluble complexes to free ion form, thus increasing the ability of phytoremediation, especially phytoextraction, rhizofiltration, phytostabilization, and phytovolatilization. On the other hand, phytodegradation is mostly caused by the activity of microorganisms in the rhizosphere, an area of enriched microbial activity close to the surface of plant roots. The rhizosphere was first defined by Lorenz Hiltner as the zone influenced by the root system [2]. Plant roots support the growth and metabolic activities of a wide variety of microbes that in return have profound effects on the growth and/or health of plants. The advantage of phytodegradation is that microorganisms in the rhizosphere benefit from the nutrients provided by plant root exudates and oxygen exchange in the root system, enhancing the rate and extent of pollutant degradation [3, 4]. The rhizosphere is therefore a “hotspot” for bacterial growth and aerobic biodegradation that transforms organic pollutants into CO₂ and H₂O.

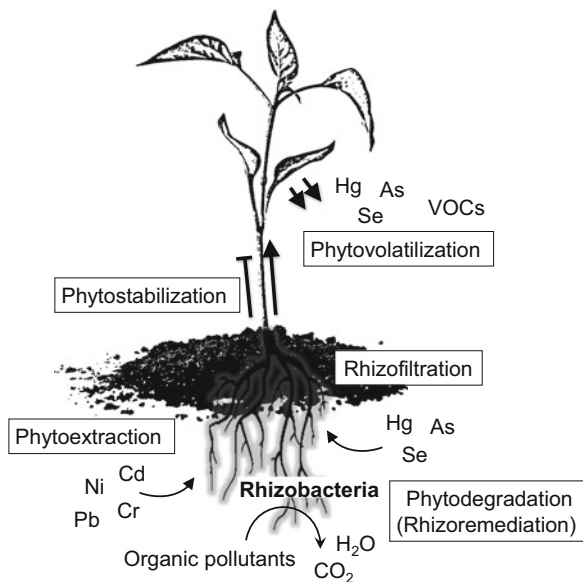
Phytodegradation, in another word rhizoremediation, in soil has been reported for a wide range of organic pollutants, such as chlorinated ethenes, polycyclic aromatic hydrocarbons, and polychlorinated biphenyls [3]. In the last decade, accelerated

Fig. 1 Mechanisms of phytoremediation.

Rhizosphere (gray color) is the area around the roots, where direct symbiosis with rhizobacteria is formed.

Rhizosphere accumulates high concentration of root exudates, changes soil conditions, and provides nutrition to the rhizobacteria.

Phytodegradation is mostly due to the activity of rhizobacteria. Heavy metals extracted by plants will be either fixed in the plant body (phytostabilization) or further transpired from the leaves (phytovolatilization). VOCs means volatile organic compounds



biodegradation of recalcitrant organic pollutants such as petroleum hydrocarbons [5], pesticides [6], chlorinated solvents [7], and polycyclic aromatic hydrocarbons [8] in the rhizosphere of terrestrial plant–soil systems have been shown. The introduction of specific pollutant-degrading bacteria to the rhizosphere has great potential to enhance the efficacy of rhizoremediation [4, 9–11], and bacteria that efficiently colonize roots and degrade pollutants markedly enhance the process. Introduction of such bacteria into the rhizosphere can make possible the design of an ideal plant–bacteria association depending on the target pollutants.

However, potentials of rhizoremediation in hydrosphere environments are yet intensively examined as compared to soil environments. Comparing the rhizodegradation technologies in the soils and hydrosphere environments from the viewpoint of sustainability and effectiveness, the number of microorganisms is estimated approximately 100 million to 1 billion per gram of soil, while the number of microorganisms in the hydrosphere is two to four orders of magnitude lower. In other words, the number of microorganisms that compete for survival with rhizosphere microorganisms is overwhelmingly low in the latter. This is a major advantage of the latter technology. Furthermore, as will be discussed in more detail later, many rhizosphere microorganisms in aquatic plants have acquired the ability to adhere more strongly to the host plant to prevent them from being swept away by water flows. This feature may also be advantageous when pollutant-degrading microorganisms are removed along with the plants from the environment after remediation is completed.

Contamination of environmental water is a serious issue for conservation of the biosphere. Pollutants in water are more diffusive and at lower concentrations than those in soils. Thus, the immobilization for stabilization and stimulation of contaminant-degrading bacteria remains critical for the complete restoration of

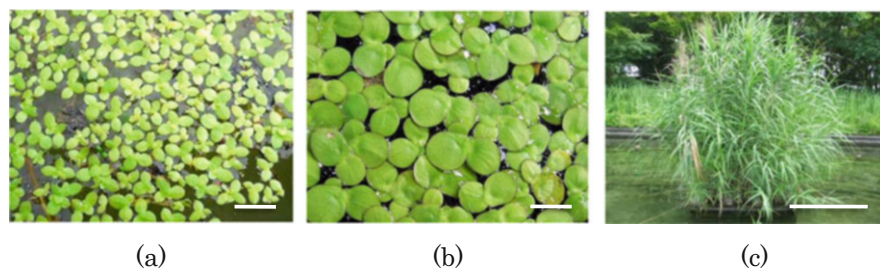


Fig. 2 Popular aquatic plants. *Lemna minor* (a), *Spirodela polyrhiza* (b), *Phragmites australis*. Bars indicate 1 cm (a, b) and 100 cm (c)

contaminated aquatic environments [11]. The microbial rhizosphere is ubiquitous in natural aquatic environments, as it is in the soil [12, 13]. There are examples that clearly demonstrates the importance of mutualisms, a type of symbiosis both species benefit each other, between a host plant and its associated microorganisms that are capable of degrading organic pollutants. The rhizospheres of aquatic plants, *Phragmites australis* (common reed), and the floating aquatic plants *Spirodela polyrhiza* (giant duckweed) and *Lemna aquinoctialis* or *Lemna minor* (lesser duckweed) have also been shown to be efficient in acceleration of biodegradation in both water and sediment of single aromatic compounds (Fig. 2.) [10, 14, 15]. First example is phenolic EDCs by use of specially designed plant–bacteria associations.

2 Phytodegradation of Phenolic EDCs by Enhanced Common Reed *Phragmites*

A series of 4-alkylphenols, including 4-nonylphenol (4-NP), 4-tert-octylphenol (4-tert-OP), and 4-tert-butylphenol (4-tert-BP), have been used in the production of nonylphenol polyethoxylate surfactants, phenolic resins, and polycarbonate resins. 4-alkylphenols are persistent, toxic compounds classified as endocrine-disrupting chemicals (EDCs); they are capable of interfering with the hormonal systems of numerous organisms [16, 17].

2.1 *Rhizobacterial Strains TIK1 and IT4 That Are Capable of Degrading Phenolic EDCs*

It was previously observed accelerated removal of 4-tert-BP [18] and branched 4-NP [19] in a *Phragmites* rhizosphere sediment system collected from a natural pond, whereas both 4-tert-BP and 4-NP persisted in non-rhizosphere sediment. In the rhizosphere sediment associated with a *Phragmites* plant, 91% of 4-tert-BP initially

added to the sediment (initial concentration, 25 mg 4-tert-BP/kg dry sediment) was removed after 42 days, and 53% of 4-NP added to the sediment (initial concentration, 25 mg 4-NP/kg dry sediment) was removed in the same period. Toyama et al. successfully isolated a 4-tert-BP-degrading bacterium strain *Sphingobium fuliginis* TIK1 and a 4-NP-degrading *Sphingobium* sp. IT4 from the *Phragmites* rhizosphere, respectively. In contrast, there were no substantial degradation of 4-tert-BP and 4-NP in the non-rhizosphere sediment of the same pond, and the efforts to enrich and isolate 4-tert-BP-degrading bacteria and 4-NP-degrading bacteria from the non-rhizosphere sediment were unsuccessful. Therefore, it was indicated that 4-tert-BP-degrading bacteria and 4-NP-degrading bacteria were present only in the rhizosphere sediment. The successful enrichment and obtaining 4-tert-BP-degrading bacterium and 4-NP-degrading bacterium from the rhizosphere must also be attributable to “the rhizosphere effects” of *Phragmites*.

2.2 Demonstration of TIK1 and IT4 to Degrade Phenolic EDCs with Organic Compounds Exuded by Phragmites Roots

TIK1 can utilize 4-tert-BP as a sole carbon source via phenolic ring hydroxylation and a meta-cleavage pathway. On the other hand, IT4 can utilize branched 4-NP or 4-tert-OP as a sole carbon source via an ipso-substitution mechanism. The abilities of TIK1 and IT4 to degrade 4-alkylphenols and bisphenols are summarized in Table 1. TIK1 was capable of degrading various 4-alkylphenols and bisphenols via phenolic ring hydroxylation followed by a meta-cleavage pathway. IT4 was also capable of degrading 4-alkylphenols and bisphenols by an ipso-substitution mechanism. These two bacterial strains have wide scope for degradation of phenolic EDCs and are potentially useful for the treatment of waters polluted with multiple species of phenolic EDCs. The effects were examined of organic compounds released from *Phragmites* roots on cell growth and the degradation activity of TIK1 and IT4. *Phragmites* root extracts were prepared from crushed roots of 2-month-old, sterile *Phragmites* plants [20]. Cells of each bacterium TIK1 or IT4 were incubated in 100 mL of basal salt medium containing the sterilized root extract (140 mg/L of dissolved organic carbon) at 28°C and 120 rpm. They were able to grow with *Phragmites* root extracts as source of carbons. The yield coefficients of cell mass were 0.74 mg dry-weight/mg carbon of root extract for TIK1 and 0.61 mg dry-weight/mg carbon of root extract for IT4. For comparison, when TIK1 used 4-tert-BP or glucose as a sole carbon source, the yield coefficients of cell growth for 4-tert-BP and glucose were 0.91 mg dry-weight/mg carbon of 4-tert-BP and 1.05 mg dry-weight/mg carbon of glucose, respectively. When IT4 used 4-tert-OP or glucose as a sole carbon source, the yield coefficients of cell growth for 4-tert-OP and glucose were 0.18 mg dry-weight/mg carbon of 4-tert-OP and 0.87 mg dry-weight/mg carbon of glucose, respectively. In addition, TIK1 and IT4 grown

Table 1 *Sphingobium fuliginis* strain TIK1 and *Sphingobium* sp. strain IT4 display exceptionally high abilities to degrade phenolic EDCs [18–20]

Phenolic EDC	Strain TIK1	Strain IT4
	Transformation ratio (%) ^a	Transformation ratio (%) ^a
4- <i>n</i> -Butylphenol	100.0	70.2
4- <i>sec</i> -Butylphenol	100.0	95.5
4- <i>tert</i> -Butylphenol	100.0	100.0
4- <i>n</i> -Pentylphenol	100.0	68.0
4- <i>tert</i> -Pentylphenol	100.0	98.9
4- <i>n</i> -Hexylphenol	100.0	82.2
4- <i>n</i> -Heptylphenol	100.0	96.1
4- <i>n</i> -Octylphenol	100.0	91.6
4- <i>tert</i> -Octylphenol	98.0	100.0
4- <i>n</i> -Nonylphenol	100.0	91.9
Branched 4-nonylphenol	64.0	92.6
Bisphenol A	100.0	100.0
Bisphenol B	99.0	100.0
Bisphenol E	100.0	100.0
Bisphenol F	100.0	100.0
Bisphenol P	78.2	91.1
Bisphenol S	100.0	100.0

^aTransformation ratio (%) refers to the percent reduction in the concentration of the phenolic EDC in cultures after a 24-h incubation relative to the concentration in a sterile control. Concentrations were obtained from HPLC chromatograms

with root organic compounds were highly capable of degrading various phenolic EDCs. Therefore, organic compounds from *Phragmites* roots function as carbon and energy sources for cell growth and enhance the degradation activity, the result being elevated cell numbers and activities of the bacteria.

2.3 Construction of *Phragmites*/TIK1 or *Phragmites*/IT4 Association Systems and Degradation of Phenolic EDCs

Enhanced *Phragmites* systems associating with TIK1 or IT4 (*Phragmites*/TIK1 and *Phragmites*/IT4) were prepared using the following simple method. Bacterial cells of each were suspended at $OD_{600} = 0.3$ (about 0.15 mg/dry-weight mL) in 200 mL of sterilized Hoagland solution in a 500-mL flask containing a 2-month-old plant (about 0.05 g dry root biomass and 0.14 g dry above-ground biomass). The flask containing the plant and cells of each strain was incubated statically for 1 h. The cell suspension was then removed from the flask, and the roots were gently washed three times with sterilized Hoagland solution to remove suspended cells. The *Phragmites* plant was then presumptively termed either *Phragmites*/TIK1 or *Phragmites*/IT4 dependent on the strain it was inoculated with. To determine whether the bacteria

had successfully colonized the roots and were able to express degradation activity on the root surfaces of the previously sterile *Phragmites*, we conducted a phenolic EDC degradation assay (five cycles, each with a 24-h reaction time) with the *Phragmites*/TIK1 or *Phragmites*/IT4. One *Phragmites*/TIK1 or *Phragmites*/IT4 was placed in a 500-mL flask with 200 mL of Hoagland solution containing phenolic EDCs (5 mg/L BPA, 5 mg/L BPS, 5 mg/L 4-tert-BP, 2.5 mg/L 4-tert-OP, and 2.5 mg/L branched 4-NP). The flask was then statically incubated in a chamber ($28 \pm 1^\circ\text{C}$, 8,000 lx, 16-h light and 8-h dark cycle). After 24 h, the EDCs–Hoagland solution was removed completely from the flask and replaced with 200 mL of fresh EDCs–Hoagland solution. This 24-h cycle was repeated a total of five times in triplicate.

After preparation of a *Phragmites*/TIK1 or *Phragmites*/IT4 association system, each bacterium easily colonized the roots, TIK1 at a density of $9.08 \pm 2.32 \times 10^{10}$ CFU (colony-forming units)/g dry root and IT4 at a density of $3.13 \pm 0.83 \times 10^{10}$ CFU/g dry root. At the end of five cycles, the populations on the roots remained at $5.37 \pm 0.83 \times 10^{11}$ CFU/g dry root for TIK1 and $3.24 \pm 0.24 \times 10^{11}$ CFU/g dry root for IT4. The changes in EDC concentrations during the degradation experiments are shown in Fig. 3. The *Phragmites*/TIK1 and *Phragmites*/IT4 associations both consistently removed all EDCs from the EDC-dosed Hoagland solutions within the 24-h reaction time throughout all five cycles. In the control experiments with sterile *Phragmites*, the concentrations of BPA, BPS, and 4-tert-BP did not decline at all; 4-tert-OP declined by about 20%, and 4-NP declined by about 30% within the 24-h reaction time throughout all five cycles. Strains TIK1 and IT4 therefore appear capable of sustainably colonizing sterilized *Phragmites* roots and degrading phenolic EDCs for at least 120 h, presumably with support from organic compounds exuded from the *Phragmites* roots.

2.4 Continuous Removal of Phenolic EDCs from Polluted Effluent by Use of a Sequencing Batch Reactor (SBR) System Containing *Phragmites*/TIK1 or *Phragmites*/IT4

A laboratory-scale sequencing batch reactor (SBR) experiment using the *Phragmites* associations was conducted to treat 500-mL samples of effluent polluted with EDCs (10 cycles, each with a 12-h reaction time) to evaluate the potential for using *Phragmites*/TIK1 and *Phragmites*/IT4 associations to treat waters polluted with phenolic EDCs. Synthetic effluent containing EDCs was prepared by dissolving 5 mg/L BPA, 5 mg/L BPS, 5 mg/L 4-tert-BP, 2.5 mg/L 4-tert-OP, and 2.5 mg/L branched 4-NP into a secondary-treated effluent sample of sewage treatment plant. The *Phragmites*/TIK1 and *Phragmites*/IT4 systems were prepared by inoculating roots of 3-month-old, non-sterile *Phragmites* (about 2.5 g dry root biomass and 10 g dry above-ground biomass) with cells of either TIK1 or IT4 at $\text{OD}_{600} = 0.3$. EDC-polluted effluent (500 mL) was placed in the bottle with one *Phragmites*/TIK1 or one *Phragmites*/IT4 system. The bottle was statically incubated in a

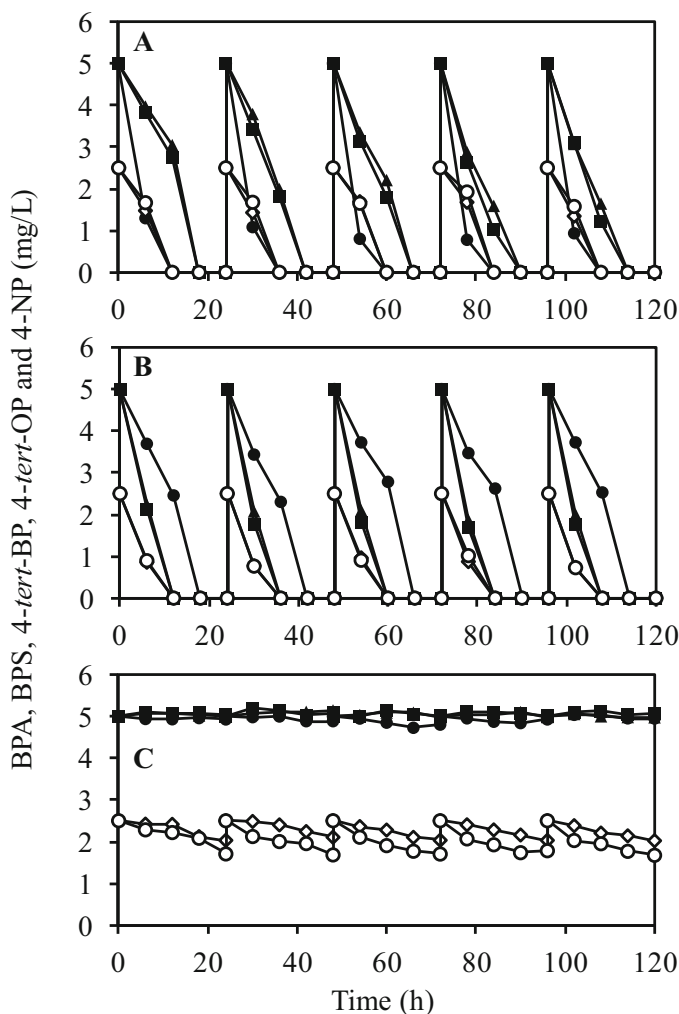


Fig. 3 Changes in concentrations of the phenolic EDCs BPA (■), BPS (▲), 4-tert-BP (●), 4-tert-OP (◇), and branched 4-NP (○) in Hoagland solution. The changes reflect degradation in the presence of (a) *Phragmites*–TIK1 association, (b) *Phragmites*–IT4 association, and (c) sterile and uninoculated *Phragmites*. Values are means from triplicate experiments. The Hoagland solution containing the EDCs was replaced with fresh solution every 24 h [20]

chamber ($28 \pm 1^\circ\text{C}$, 8,000 lx, 16-h light and 8-h dark cycle). After 12 h, the EDC-polluted effluent was completely removed from the flask and replaced with 500 mL of fresh, EDC-polluted effluent. This 12-h cycle was repeated 10 times in triplicate.

Uninoculated *Phragmites* removed small amounts of BPA (1.9–10.3%), BPS (0.5–3.8%), 4-tert-BP (1.7–4.1%), 4-tert-OP (22.0–26.8%), and 4-NP (31.2–33.6%)

Table 2 Removal of phenolic EDCs by *Phragmites*/TIK1, *Phragmites*/IT4, and uninoculated *Phragmites* in sequencing batch reactors. Values shown are the reduction in contaminant concentrations at the end of a reaction cycle as a percentage of the concentration at the beginning of the cycle. The initial concentration was 5.0 mg/L for BPA, BPS, and 4-*tert*-BP and 2.5 mg/L for 4-*tert*-OP and branched 4-NP [20]

Contaminant	<i>Phragmites</i> /TIK1			<i>Phragmites</i> /IT4			Uninoculated <i>Phragmites</i>		
	Cycle number			Cycle number			Cycle number		
	1	5	10	1	5	10	1	5	10
BPA	100	100	100	100	100	100	1.9	2.6	9.0
BPS	100	100	100	100	100	100	1.7	3.5	1.4
4- <i>tert</i> -BP	100	100	100	100	100	100	2.1	2.5	4.1
4- <i>tert</i> -OP	100	100	100	100	100	100	23.4	26.8	25.2
Branched 4-NP	100	100	100	100	100	100	31.8	33.6	33.2

from the effluent (Table 2). Partial removal of these EDCs from polluted effluent in the presence of uninoculated *Phragmites* might have resulted from adsorption onto the roots and biodegradation by indigenous bacteria in the secondary effluent. In contrast, both the *Phragmites*/TIK1 and *Phragmites*/IT4 repeatedly achieved complete removal of all phenolic EDCs from the dosed water throughout all 10 cycles (Table 2). TIK1 and IT4 were able to thoroughly colonize the surface of non-sterile *Phragmites* roots. Both *Phragmites*/TIK1 and *Phragmites*/IT4 systems could therefore be used for long-term, simultaneous removal of phenolic EDCs from polluted effluent. It was concluded that the use of hydroponic systems using *Phragmites*/TIK1 and *Phragmites*/IT4 systems would be a successful strategy for the sustainable treatment of polluted water containing various phenolic EDCs.

3 Tiny Floating Plant, Duckweeds, a Multi-Talented Phytoremediation Device

Duckweeds, typified by the family *Lemnaceae*, are small free-floating aquatic angiosperm plants without distinct stems and leaves. The whole plant body is reduced to form a flat small leaf-like structure called a frond. This unique morphological feature of the duckweeds provides them with substantial rhizosphere and phyllosphere communities that may interact directly the plant and surrounding aquatic environment [13]. It is noteworthy that chlorophylls are contained not only in frond but also in the root of duckweed. It is then possible that oxygen produced by photosynthetic activity is directly supplied from the roots to rhizobacteria, thereby elevating the activities of rate-limiting mono- and dioxygenase enzymes for hydroxylation reaction that is essential for the breakdown of most organic pollutants (Chapter “Bioremediation – from key enzymes to practical technologies”) [21].

Phenol is a toxic compound for particular aquatic species [22] and is also harmful to human health when ingested or inhaled even at very low concentrations

[23]. Therefore, it is also meaningful to develop strategies for the efficient and continuous biodegradation of phenols with minimum impact to the environment. Here, we present an example of developing mutualisms between duckweed and its surface associated bacteria, which is useful for the continuous and ecologically safe degradation of phenol [10].

3.1 Isolation of Phenol-Degrading Bacteria from the Surface of the Duckweed, *Lemna aoukikusa*

Mature duckweed plants (*Lemna aoukikusa*/*Lemna minor*) were collected from a small pond in the botanical garden of Hokkaido University (Sapporo, Japan). The duckweed plants were gently washed with sterile water and cultivated in a flask containing Hoagland medium [24] supplemented with 200 mg L⁻¹ phenol at 25°C with a day/night photoperiod of 16 h/8 h at 8,500 lx. After 3 weeks of incubation, ten fronds of the duckweed were washed with sterilized water and then sonicated to disperse the surface-attached bacteria. The bacterial suspension was serially diluted with sterilized water and spread onto basal salt medium (BM) [25] agar plates supplemented with phenol as the sole carbon source. Colonies that appeared on the plates were picked and subcultured several times to obtain pure isolates of phenol-degrading bacteria. Finally, five strains exhibited marked abilities to degrade phenol (Fig. 4a). Partial 16S rRNA gene fragments were sequenced for the five strains which revealed that these strains belong to *Pseudomonas* (P02), *Rhodococcus* (P11c), and *Acinetobacter* (P22, P23, and P24a). Further analysis revealed that P22, P23, and P24a tightly clustered with *A. rhizosphaerae*, *A. calcoaceticus*, and *A. tandoii*, respectively.

The property of adherence is a critical trait of surface associated bacteria, including in the rhizosphere especially for aquatic environments [26, 27]. Biofilm formation, which is an indicator of adherence to solid surfaces, was first examined each strain using a crystal violet assay (Fig. 4b) [28]. Each bacterial strain was grown in a 1.5 mL polypropylene tube without shaking for 24 h in Hoagland medium, basal medium, or Luria-Bertani (LB) medium. The three *Acinetobacter* strains formed robust biofilms when grown in the LB medium, whereas *Pseudomonas* sp. P02 and *Rhodococcus* sp. P11c formed marginal biofilms under all of the tested conditions. These results are in accordance with the classification of the genus *Acinetobacter*, species of which are non-motile and grow attached to a variety of solid surfaces in nature [29]. It has been reported that a toluene-degrading *Acinetobacter* sp. Tol5 has a highly hydrophobic cell surface and preferably adheres to a solid phase [30]. Because P23 exhibited the best phenol degradation and substantial biofilm formation abilities among the tested strains, we hypothesized that P23 could be a potential candidate for effective degradation of phenol in association with *L. aoukikusa*. Thus, we used P23 for further experiments. When we examined the ability of this strain to degrade a range of carbon sources, almost all of the tested

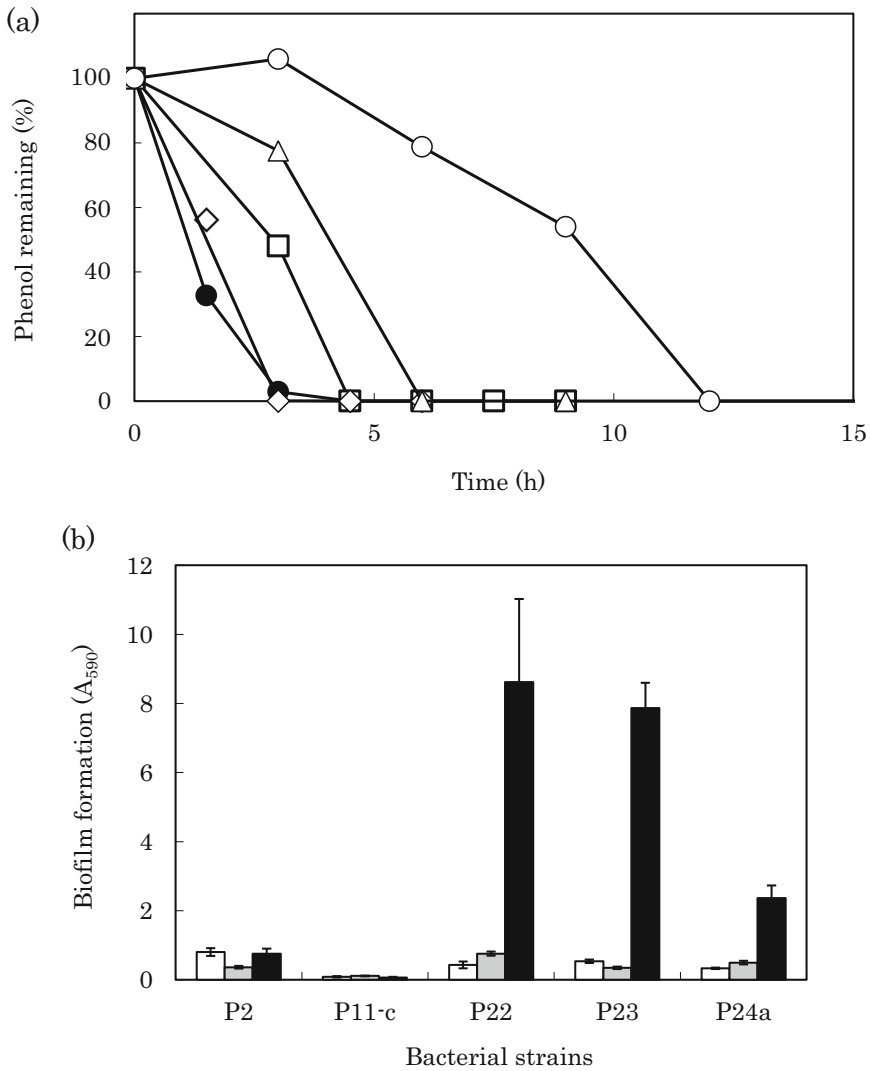


Fig. 4 (a) Phenol degrading activity of bacteria isolated from the surface of *L. aoukikusa*. Degradation test of 20 mg L⁻¹ phenol was performed at 25 °C with shaking at 150 rpm. Each data point is the average of triplicate experiments. Closed circle (●), P23; open diamond (◇), P11c; open square (□), P02; open triangle (△), P22; open circle (○), P24a. P23 and P11c similarly showed the highest activity of phenol among the bacterial strains [10]. (b) Biofilm formation by phenol degrading bacteria isolated from the surface of *L. aoukikusa*. Bacterial strains were cultured in Hoagland medium (white bar), basal medium (gray bar) each contained 10 mg mL⁻¹ phenol or LB medium (black bar)

compounds, including glucose, maltose, cellobiose, sucrose, trehalose, inositol, 5-ketogluconic acid, pyruvate, arabinose, mannitol, arabitol, sorbitol, galacturonic acid, benzene, toluene, failed to support the growth of P23, except for phenol and ethanol. Because phenolic compounds are major exudates of plant roots [4], we hypothesized that the surface of duckweed should provide favorable growth conditions for P23.

3.2 Preparation of Enhanced Duckweed on Which Surface Is Dominated by Acinetobacter P23, the *L. aoukikusa*/P23 System

To eliminate or reduce the abundance of indigenous microorganisms that coexist with duckweeds, *L. aoukikusa* fronds were either (1) submerged in 0.5% (v/v) NaClO/0.05% (v/v) Triton X-100 and gently stirred for 30 min or (2) treated with a sonicator for 5 s 6 times. These plants were then washed twice for 10 min with sterilized water and transferred into Hoagland medium. P23 cells from the late exponential growth phase, cultured in LB media supplemented with 2 mg L⁻¹ phenol, were recovered by centrifugation at 10,000 × g for 10 min and suspended in Hoagland medium. This cell suspension (1 mL) and 30 surface-cleansed fronds were transferred into a 100-mL flask with 50 mL of Hoagland medium supplemented with 20 mg L⁻¹ phenol (final OD₆₀₀ = 0.3) and incubated under the day/night photoperiod for 72 h at 25°C. During incubation of duckweed plants with P23 in Hoagland medium, most of the P23 cells adhered to the duckweed, and culture turbidities (OD₆₀₀) significantly declined from 0.3 at 0 h to 0.02 at 72 h (Fig. 5a).

When the *L. aoukikusa*/P23 cultures were stained with the LIVE/DEAD BacLight kit and observed by fluorescence microscopy, many green fluorescent spots, indicating living bacteria, were observed on the surface of the roots at 72 h, whereas there was less green fluorescence on the *L. aoukikusa* plants without P23 (Fig. 5b). The bacterial cells were dispersed from the *L. aoukikusa*/P23 plants by sonication and spread on LB agar plates so that we could confirm that P23 was the dominant strain of adhered bacteria (>99% 16S rRNA gene fragment sequence similarity; data not shown). Thus, the small colonies and biofilms formed on the root of duckweeds should be that of P23. We further measured the number of attached bacterial cells separately for the leaf-like part of fronds and the roots. It was revealed that most P23 (about 90%) are colonized on the leaf-like frond, 3.0 × 10⁶ CFUs/frond rather than the roots, 3.2 × 10⁵ CFUs/root. This probably reflects that the surface area of the frond is much larger than that of roots.

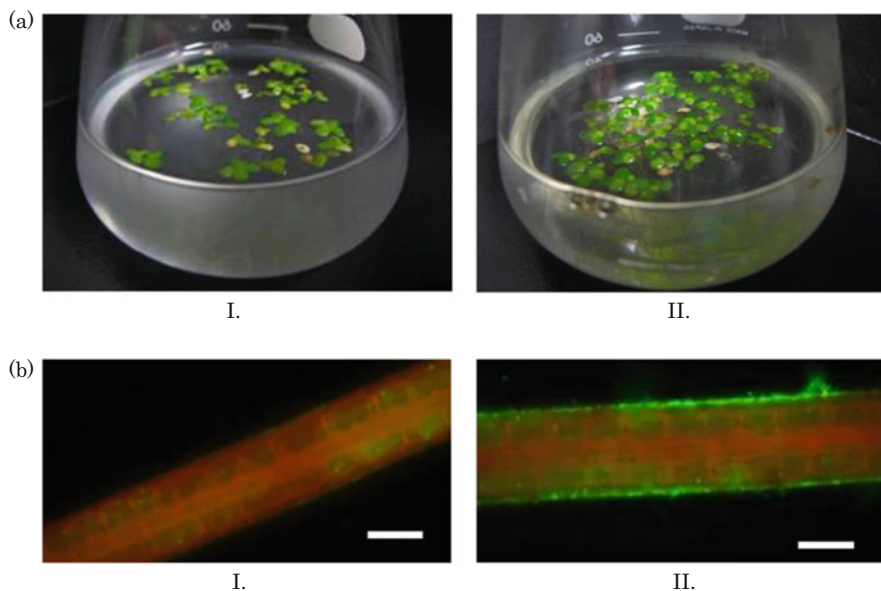


Fig. 5 (a) Flask culture of *L. aoukikusa*/P23 system, Turbidities of the culture (OD_{600}) significantly declined from 0.3 at 0 h (I) to 0.02 at 72 h (II). (b) Fluorescent microscopy of a root of sterile *L. aoukikusa* (I) *L. aoukikusa*/P23 system (II)

3.3 Stability of Phenol Degradation by *L. aoukikusa*/P23 Association System

To determine whether the reinforcement of the specific single species P23 on the surface-cleansed *L. aoukikusa* plants, namely *L. aoukikusa*/P23 system, could be useful for effective biodegradation, several treatment systems of *L. aoukikusa* with P23 were tested for long-term phenol degradation ability (Fig. 6). These were natural *L. aoukikusa* (intact as they are), surface-cleansed *L. aoukikusa*, P23, and *L. aoukikusa* inoculated with P23. Ten fronds of the *L. aoukikusa*/P23 prepared as described above were transferred into a 100-mL flask containing 50 mL of Hoagland medium supplemented with 40 mg mL⁻¹ phenol and further cultivated under the photoperiod at 25°C. For the degradation test by P23 alone, 0.5 × 10¹⁰ cells (ten times of the number of P23 cells adhered to ten fronds as counted by an assay of colony-forming units at 72 h) were applied. Culture medium (0.25 mL) was collected at different times and subjected to HPLC analysis to determine phenol concentrations. After 40 h and 88 h, the culture volume and the concentration of phenol were re-adjusted to 50 mL and 40 mg L⁻¹, respectively.

In the first period of 40 h, the intact *L. aoukikusa* (triangle) and the *L. aoukikusa*/P23 system (closed circle) completely eliminated 40 mg L⁻¹ phenol in the culture, whereas neither the surface-sterilized duckweed nor P23 alone effectively eliminated phenol. These observations are consistent with a previous report for giant duckweed

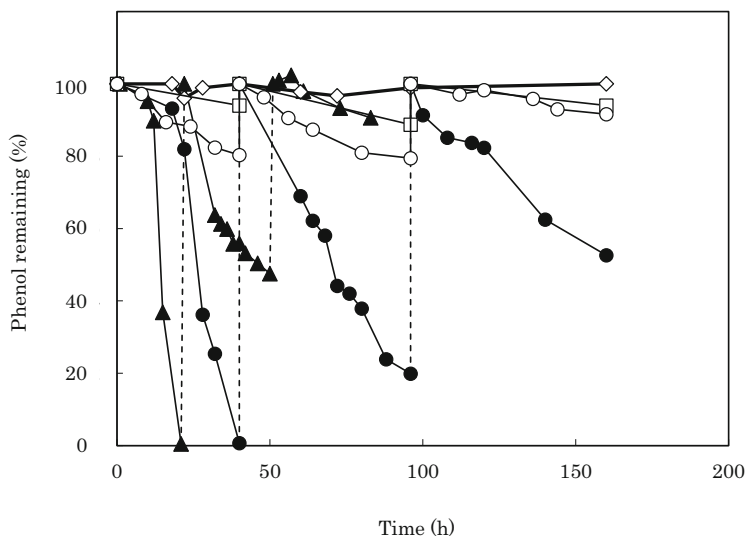


Fig. 6 Long-term performance test of phenol degradation. The elimination of phenol was examined for the different combination systems of *L. aoukikusa* and P23. Wild duckweeds (closed triangle, ▲), P23 only (open circle, ○) was tested using ten times more cells than that of attached to *L. aoukikusa* (closed circle, ●). Controls were set for the experiment without *L. aoukikusa* (open square, □) and P23 (open diamond). Each data point is the average of triplicate experiments

Spirodela polyrhiza that phenol degradation activity of sterilized duckweed plant is negligible and that indigenous rhizobacteria of natural duckweed are responsible for degrading phenol [14]. In the second period (40–88 h), there was roughly 80% and 50% elimination of phenol by *L. aoukikusa*/P23 and the natural duckweed, respectively. P23 alone showed less degradation ability, accounting for the elimination of ca. 20% of the phenol. At the end of the third period (160 h), *L. aoukikusa*/P23 maintained a 50% phenol elimination level, whereas the other systems eliminated <10% of the phenol. The long-term performance test (88–160 h) under nutrient-starvation conditions resulted in a severe reduction of phenol degradation activity for all combinations except for the *L. aoukikusa*/P23 system. These results also suggest that indigenous plant surface bacteria capable of degrading phenol were rapidly attenuated, probably because of competition in the complex microbial community. The exact mechanisms are unclear; however, these experimental results indicate that the durable and continuous removal of phenol by the *L. aoukikusa*/P23 system may be attributed to the beneficial interaction between P23 and the duckweed. Decrease in the phenol degradation activity of the *L. aoukikusa*/P23 system during the periods was due to decreased numbers of P23 cells, from 5.1×10^5 CFUs (day 0) to 1.6×10^4 CFUs (day 7). This happened probably because metabolic wastes were accumulated and/or minerals for plant growth were depleted in the flasks.

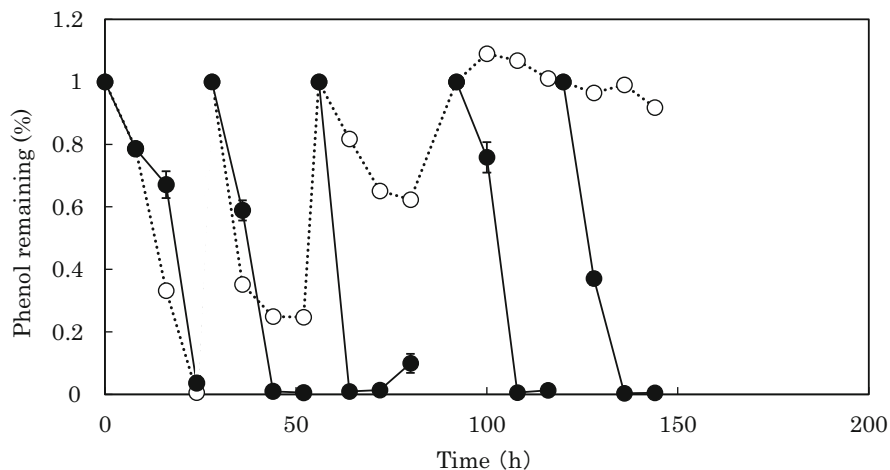


Fig. 7 Stability of phenol degradation by *L. aoukikusa*/P23 during five cultivation cycles. *L. aoukikusa*/P23 were transferred after every 24 h cultivation to a new 50 mL Hoagland medium containing 40 mg ml⁻¹ phenol in 100 mL flask, closed circle (●). A flask containing *L. aoukikusa*/P23 was added with 40 mg ml⁻¹ phenol at 0, 28, 56, 92, and 120 h for every 24 h cultivation, open circle (○)

In order to address this point, *L. aoukikusa*/P23 was transferred after every 24 h to a new Hoagland medium containing 40 mg mL⁻¹ phenol. It was clearly shown that the *L. aoukikusa*/P23 system maintained high phenol degradation activity for 1 week, over five transfer cycles (Fig. 7). In contrast, degradation activity of *L. aoukikusa*/P23 system in a flask without transfer was decreased after three cycles as similar to Fig. 6 (closed circle).

One of the major advantages of biodegradation among phytodegradation that utilizes mutualism of host plants and pollutant degrading bacteria is its energy saving low-carbon technology with less impact to the environment. Another advantage of using bacteria that colonize floating plants, including duckweeds, is the ease with which these bacteria and plants may be recovered after site remediation. In fact, the turbidity of *L. aoukikusa*/P23 culture remained at an OD₆₀₀ < 0.01 during the long-term performance test over 160 h. This feature should be useful for reducing risks of microbial community disruption caused by the introduction of foreign bacteria. When we used completely surface-sterilized *L. aoukikusa*, the number of P23 cells attached to the plant was significantly decreased. This observation suggests that there were unknown microorganisms remained on the surface-washed plants that helped attachment of P23 to the plants. The next challenge maybe to design beneficial multi-species microbial community biofilms on plant surfaces, further advancing opportunities for sustainable water purification technologies [27].

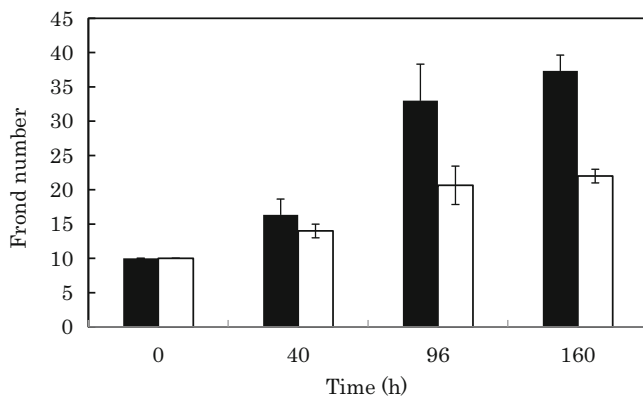


Fig. 8 The effects of *A. calcoaceticus* P23 on the growth of *L. aoukikusa*. Frond number was compared between surface-cleansed *L. aoukikusa* carrying P23 (*L. aoukikusa*/P23), black bar, ■, and surface-cleansed *L. aoukikusa* only, white bar, □, during growth. Significant growth-promotion was observed for *L. aoukikusa*/P23. Error bars are standard deviation ($n = 3$)

3.4 Growth Promotion of Duckweed by P23 Colonization

During the long-term performance test of the *L. aoukikusa*/P23 system in a flask (Figs. 6 and 7), we noticed that the number of fronds, leaf like structure, markedly increased as compared with the system containing surface-cleansed *L. aoukikusa* plants without P23. The number of *L. aoukikusa*/P23 fronds increased by 3.7-fold at 160 h, whereas the surface-cleansed *L. aoukikusa* plants increased by only ca. 2.2-fold (Fig. 8). This result indicates that P23 promoted the growth of *L. aoukikusa*, especially multiplication rate. It should be notable that the growth-promoting activity of P23 for duckweeds was also observed in the phenol free Hoagland medium. This result eliminates a possibility that the growth promotion is caused by the removal of toxic phenol by P23. It has been reported that *A. calcoaceticus* SE370 isolated from soil produces plant growth-promoting hormones (gibberellins) and also carries phosphate-solubilizing activity [31]. However, our preliminary result indicates that the plant growth-promoting factor of P23 is not gibberellins [32]. Moreover, phosphate-solubilizing activity of the associated bacteria may be not the case in the liquid culture systems that we adopted. Further studies are needed to clarify the environmental factors and cellular responses of P23 that involve the beneficial function to duckweed. To our best knowledge, P23 is the first growth-promoting bacterium, PGPB, identified from the duckweed plants in the genus *Lemna*.

4 Water Purification and Biomass Production Using Two Ponds System Toward Practical Use for Enhanced Duckweeds

We have previously demonstrated that growth promotion by *A. calcoaceticus* P23 is useful for a wide range of duckweed species and environmental conditions, even in non-sterile environmental waters [33]. The studies suggest the prospects of enhanced water purification coupled with high yield duckweed biomass production by inoculating them with PGPB. However, it is also suggested that inoculating PGPB at a high cell density is required to effectively induce growth-promoting effects in the presence of indigenous environmental microbes. This may not be feasible for full-scale duckweed cultivation because the large water volume and flow lead to the massive consumption of PGPB cells, resulting in environmental risks posed by PGPB discharge. Therefore, a reasonable methodology is desired to utilize PGPB for large hydroponic systems.

Here, we propose a two-step cultivation process as a novel strategy, which comprises colonization and mass cultivation steps utilizing PGPB, to achieve a higher yield of duckweed biomass production associated with water purification (Fig. 9) [34]. In the colonization step, duckweeds are co-cultured with PGPB in a small and closed tank for a short period of time to enable PGPB colonization on duckweeds. The duckweeds colonized by PGPB are then used as the inoculum for a mass and open-pond cultivation step, in which they produce biomass and remove nutrients from wastewater. Since in this two-step method, PGPB are inoculated only

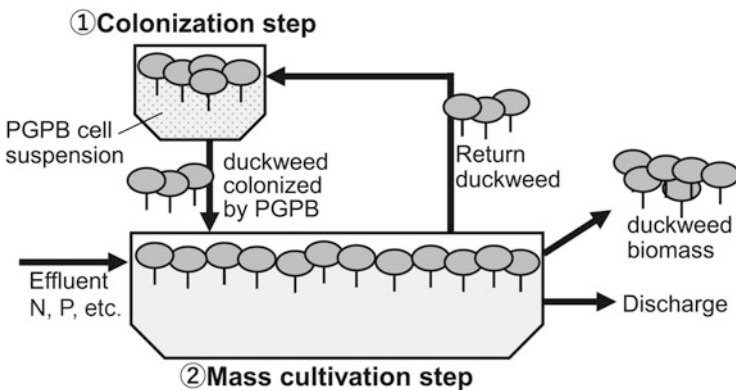


Fig. 9 Outline of the two-step cultivation process proposed in this study. The colonization of plant with PGPB, including P23, was initiated by culturing duckweeds in a cell suspension containing a higher density of PGPB. In the next mass cultivation step, duckweeds colonized by PGPB are cultured in wastewater effluent for enhanced biomass production and nutrient removal. After a certain cultivation period, a part of duckweeds was returned to colonization step to again prepare PGPB-colonized duckweeds

in the small and closed tank at the colonization step, we can expect a reduction of the cost for PGPB cultivation and the ecological risk of PGPB outflow.

Thus, a series of cultivation experiments were conducted to test the ability of the proposed method for improving duckweed production. We first determined the effects of the pre-inoculation of the PGPB strain, *A. calcoaceticus* P23, on the growth and nutrient removal of duckweed (*Lemna minor*) in three non-sterile environmental waters. Because a sufficient growth-promotion effect was observed, we evaluated the duration of such growth-promoting effects through flask-scale experiments. Molecular analyses were also performed for a deeper understanding of the survival of the colonized strain P23 on the duckweed surface and the relationships between duckweed growth and its surface microbial community.

4.1 Nutrients Removal, Phytoextraction, and Biomass Production Capacity of Enhanced Duckweeds in Two-Step Cultivation

The two-step cultivation of *L. minor* was conducted in bucket-scale experiments. Wild *L. minor* plants were cultured for 3 days with or without inoculating the PGPB strain P23 in the first step. The cultured plants in the first step were transplanted into the second mass cultivation step, in which plant growth and nutrient removal were monitored. Our results indicate that *L. minor* plants co-cultured with P23 apparently showed a rapid growth in the following 7 days cultivation (Fig. 10). The biomass yields of pre-inoculated plants in 7 days increased by 2.3, 1.9, and 2.3 times more in

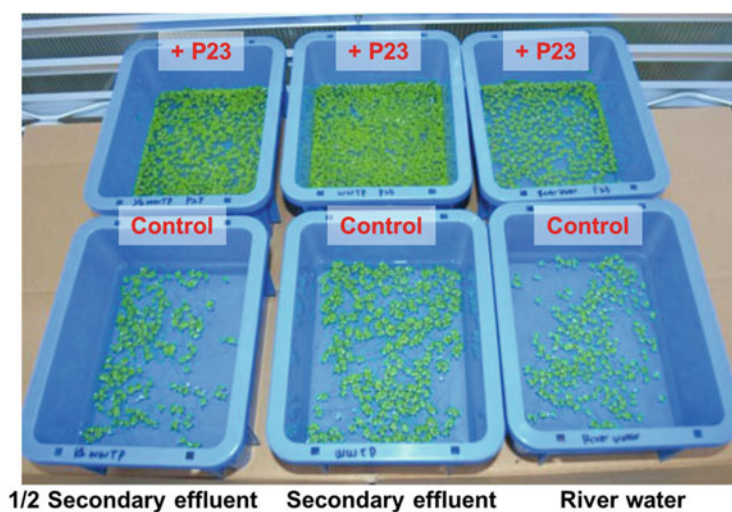
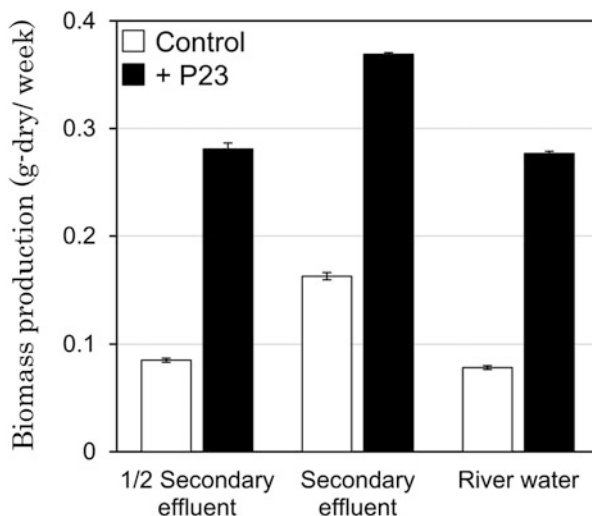


Fig. 10 The photograph of duckweed cultivation in three environmental waters with and without inoculation of strain P23. The image was taken on day 6 of mass cultivation step

Fig. 11 The weekly yield of *L. minor* by the inoculation of P23. Error bars show the standard deviations ($n = 2$). The plants had 0.07 g dry biomass at the start of cultivation



1/2 secondary effluent, secondary effluent, and river water, respectively, when compared with control plants (Fig. 11). Our previous study reported 1.7–2.4 times increase of *L. minor* growth by direct co-cultivations with 0.15 mg dry-weight/mL (equivalent to $OD_{600} = 0.3$) of P23 in pond water and secondary effluent [33]. Consistently, the present results indicate that similar extents of growth promotion can be achieved by the two-step cultivation process using the same PGPB strain.

Table 3 shows the nutrient removal capacity of the P23-inoculated and control plants in the bucket-scale cultivation. These environmental waters contained ammonium, nitrate, and negligible amounts of nitrite as the inorganic nitrogen. We observed that ammonium was completely removed in all cultures whereas not all nitrate was removed from the culture media, which is consistent with an earlier report that duckweed preferentially consumes ammonium to nitrate [35]. Additionally, P23-inoculated plants almost completely removed nitrate and phosphate, while significant amounts of these nutrients remained in the culture media of control plants. These results indicate, for the first time, that PGPB can also enhance nutrient removal from environmental waters. On the other hand, the increment of nitrogen and phosphorus removal was not as high as the extent of growth promotion by P23, probably due to the depletion of inorganic nitrogen and phosphorus in P23-inoculated cultures.

The two-step cultivation process proposed in this study (Fig. 9) was designed to improve duckweed production with minimal or reduced use of PGPB cells. To attain this, the scale, cultivation term, and PGPB cell density in the colonization step should be minimized as far as the PGPB can sufficiently colonize the plant and exert its growth-promoting effect. Although we co-cultured duckweed with P23 ($OD_{600} = 0.3$) for 3 days for the colonization step in the present study, the parameters of the colonization step need to be optimized toward minimizing the

Table 3 Removal of nutrient salts by *Lemma minor* with and without inoculation of P23. Concentrations in the unit of mg/L and percent removal are shown

	1/2 Secondary effluent			Secondary effluent			River water		
	Initial	7 days	% Removal	Initial	7 days	% Removal	Initial	7 days	% Removal
NH ₄ -N + P23	3.04 ± 0.07	n.d.	100%	6.01 ± 0.13	n.d.	100%	1.77 ± 0.12	n.d.	100%
Control	3.04 ± 0.07	n.d.	100%	6.01 ± 0.13	n.d.	100%	1.77 ± 0.12	n.d.	100%
NO ₂ -N + P23	n.d.	n.d.	–	0.07 ± 0.00	n.d.	100%	n.d.	n.d.	–
Control	n.d.	n.d.	–	0.07 ± 0.00	n.d.	100%	n.d.	n.d.	–
NO ₃ -N + P23	4.82 ± 0.06	0.09 ± 0.02	98.2%	8.63 ± 0.10	0.10 ± 0.03	98.9%	4.47 ± 0.20	0.09 ± 0.03	98.1%
Control	4.82 ± 0.06	2.78 ± 0.08	83.9%	8.63 ± 0.10	5.06 ± 0.12	41.3%	4.47 ± 0.20	2.33 ± 0.17	48.0%
PO ₄ -P + P23	1.01 ± 0.09	n.d.	100%	1.84 ± 0.09	n.d.	100%	0.52 ± 0.03	n.d.	100%
Control	1.01 ± 0.09	0.17 ± 0.01	97%	1.84 ± 0.09	0.15 ± 0.05	92.0%	0.52 ± 0.03	0.15 ± 0.05	72.5%

n.d. not detected

cost. In this regard, it was recently found that the kinetics of bacterial duckweed colonization differs depending on bacterial strains and inoculation densities, and some bacterial strains can fully colonize on duckweed within 3 to 24 h even with smaller cell densities ($OD_{600} < 0.02$) [36]. The detailed conditions of colonization step should be determined based on the colonization behavior of each PGPB strain used for the two-step cultivation process.

4.2 Duration of Plant Growth-Promoting Effects After Pre-inoculation of P23

Although the bucket-scale experiments successfully demonstrated the efficiency of the proposed two-step cultivation strategy, the duration of such growth-promoting effect is quite important for the application in full-scale duckweed cultures. We examined this by a repeated batch cultivation experiment using non-sterile pond water according to the procedure depicted in Fig. 12. Although the extent of plant growth promotion was restricted unlike in the bucket-scale experiments as shown in Fig. 10, in the first and second batches after the colonization step, P23-colonized plants showed significantly faster growth, and average frond numbers after 5-day cultivations were 27.7% and 16.9% higher than those of control plants, respectively (Fig. 13). In contrast, such differences were not observed in the third batch, indicating the growth-promoting effect disappeared before the third batch. We, therefore, set up the re-colonization step between the third and fourth batches, which successfully restored growth-promoting effects in the fourth batch. However, the effect was again lost in the next fifth batch. Overall, these results indicate that the growth-promoting effect of P23 can last for up to one to two batches (5 to 10 days) and, therefore, the re-colonization step is requisite for the restoration of an accelerated duckweed growth.

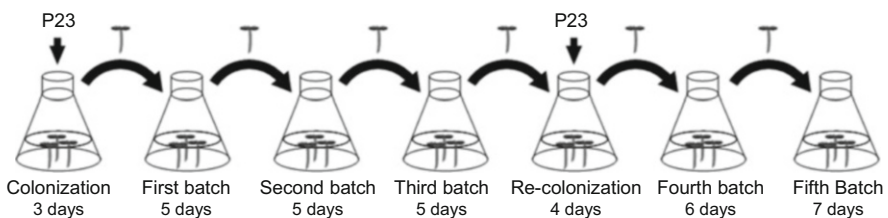


Fig. 12 The procedure of repeated batch cultivation experiments. Control experiments were performed without inoculation of P23 in “Colonization” and “Re-colonization” steps. The number of plant fronds was counted during each batch. DNA quantification and microbial community analysis were conducted after each cultivation step

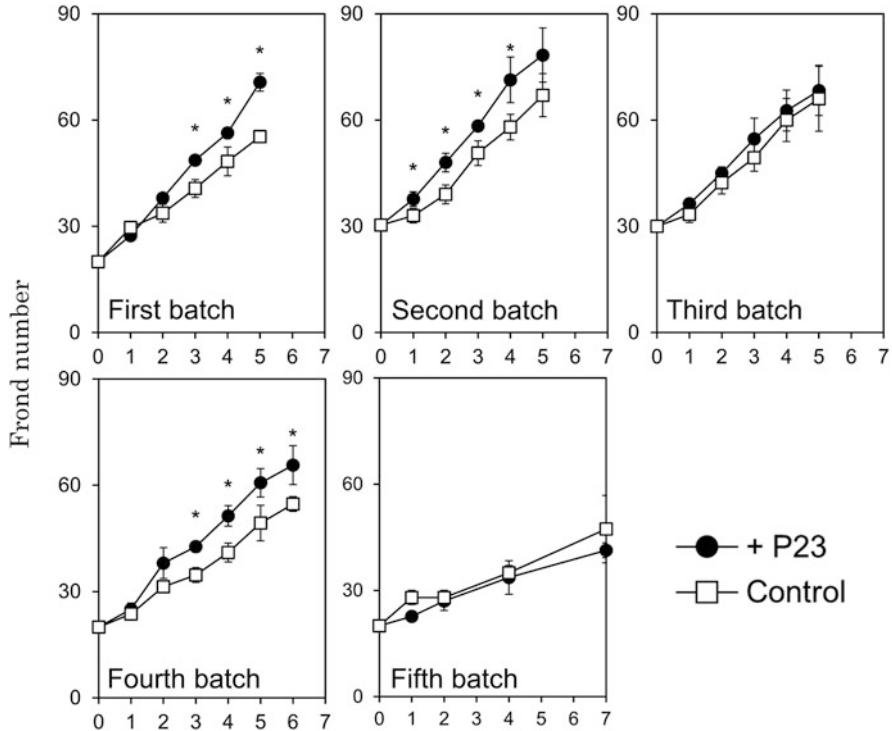
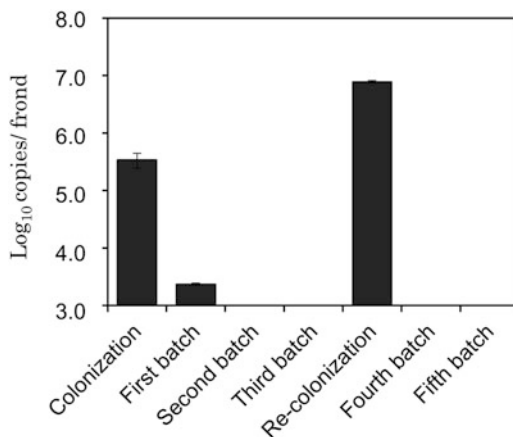


Fig. 13 Increase of frond number of *L. minor* in the repeated batch cultivation experiments. Error bars show the standard deviations ($n = 3$). Asterisks indicate a significant difference ($p < 0.05$) among P23-treated and control plants

4.3 Persistence of P23 on Duckweed Surface

The survival of inoculated bacteria in plant rhizosphere is one of the most significant concerns of PGPB application. We performed the real-time PCR to monitor the persistence of P23 on duckweed surface during the repeated batch cultivation experiments. Our results showed that each plant contained approximately 10^5 to 10^7 copies of P23 after the colonization and re-colonization steps (Fig. 14). These data are similar to that of P23 inoculated with *L. minor* in sterilized pond water (10^5 to 10^6 copies per frond; data not shown) and to those reported for three other duckweed-associated bacteria in axenic culture media (10^5 to 10^7 cells per frond). Therefore, our data confirmed that maximum colonization of P23 could be possible by each colonization and re-colonization steps. However, no colonization was detected at the subsequent cultivation steps, except for the end of the first batch. These data strongly suggest that P23 was excluded from the plant surface through the competition with indigenous microbes, as reported in the previous studies [37, 38]. Since a significant rapid plant growth was observed in the first, second,

Fig. 14 The abundance of strain P23 on the plant surface by estimating the copy numbers of P23-specific gene after each cultivation step. Error bars show the standard deviations ($n = 3$)



and fourth batches (Fig. 13), it is likely that a better plant growth promotion is possible only when more than 10^3 copies/frond of P23 bacteria remain on the plant surface at the start of each batch. Therefore, maintaining a certain density of P23 on the plant surface would be essential to extend the duration of growth-promoting effects, and rotating duckweeds between colonization step and mass cultivation step, as shown in Fig. 9, is useful for maintaining high growth of duckweeds.

4.4 Shifts in Duckweed-Associated Microbial Community

In order to understand the dynamics of the whole microbial community formed on *L. minor*, culture-independent microbial community profiling was performed by T-RFLP during the repeated batch cultivation experiments. Similar to the results of real-time PCR, the T-RF representing P23 (205-bp) was detected after the colonization and re-colonization steps, but not in the subsequent cultivation steps (Fig. 15). Among the T-RFs detected, many were commonly observed in duckweed-associated microbial communities, irrespective of P23 inoculation, suggesting the strong selectivity of the host plant. These data indicate that inoculation of P23 strongly impacted the duckweed-associated microbial community, and the effect persisted even after the disappearance of P23 from the plant surface. Additionally, we found that the relative abundances of the most dominant T-RFs (563–566 bp, 918–925 bp, and 967–975 bp) were extremely different among different batch plants (Fig. 15). Similarly, a previous study that conducted high-throughput sequencing analyses of duckweed-associated bacterial communities reported the shifts of dominant bacterial taxa depending on the environmental context [39]. These observations suggest the possible multistability of duckweed microbiome, whose mechanisms and implications on culturing systems are yet to be proved. Since the

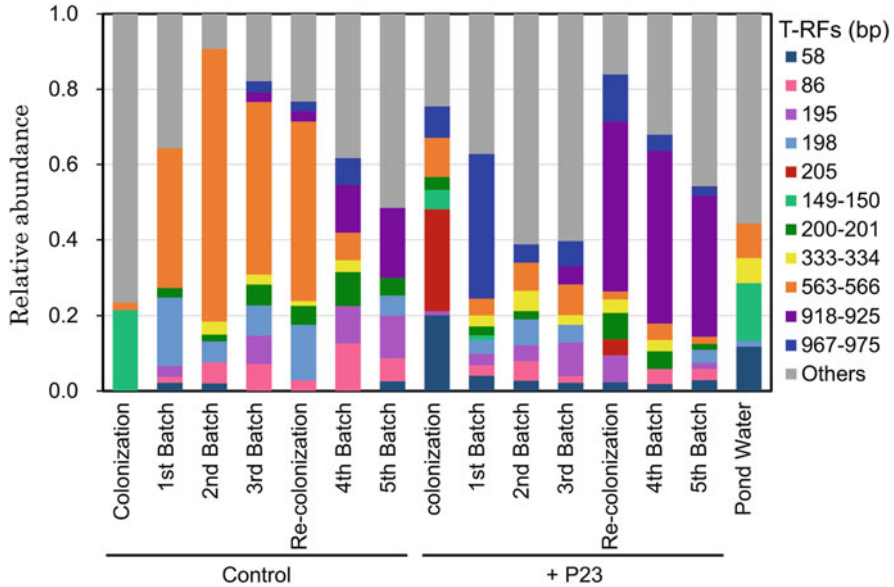


Fig. 15 Microbial communities on the plant surface of *L. minor* after each cultivation step, evaluated by terminal restriction fragment length polymorphism (T-RFLP). The red bar, 205 bp T-RFs, indicates abundance of P23 in the microbial community. Population of P23 decreases to undetectable level even after 5 day, one batch

different microbial communities can affect the plant growth [40, 41] such dynamics of duckweed-associated bacterial communities should be further analyzed in detail.

4.5 Outlook for Future

In this section, we demonstrated that significant increase in duckweed production could be achieved by two-step cultivation with a PGPB strain, *Acinetobacter calcoaceticus* P23. The remarkable improvements in biomass yield and nutrient removal in bucket-scale cultivations indicate the prospect of the two-step cultivation process as an effective strategy for maximizing duckweed yield without extensive use of PGPB and ecological risks associated with PGPB discharge into the environment. Repeated batch cultivation experiments revealed that P23 influenced overall microbial community structures of the plant surface, and exerted growth-promoting effects until no colonization of P23 was detected. These results indicate that the effect of the two-step cultivation process is quite dependent on the persistence of PGPB in the duckweed-associated microbial community. The rotation of duckweed between the colonization step and mass cultivation step, as proposed, would facilitate the maintenance of a high growth rate of duckweed. Understanding multiple

symbiotic mechanisms among different microorganisms and host plants is one of the subjects in biology of next generation. It is also an interesting question if further continuous inoculation of P23 in this rotation system will have chance to recruit specific microbial community benefits to stabilize P23 colonization.

5 Environmental Technologies “to the Duckweed and from the Duckweed” That Have Potentials to Contribute to Establishing Sustainable Society

Duckweeds, family *Lemnaceae* plants, is a vascular plant with the fastest growth rate, which usually has a life cycle of the so-called clonal propagation (asexual reproduction) in which the fronds increase by vegetative reproduction and then each plant body separates naturally. The longer the day time, the better the vegetative growth of duckweeds, and their optimum temperature is from 20 to 30°C (growth temperature range is from 6 to 33°C) at water temperature. Aquatic plants such as duckweeds and microalgae can absorb nutrient minerals necessary for growth such as nitrogen, phosphorus, and potash from dirty water such as drainage and sewage. This means that the fertilizer cost required for biomass production can be significantly reduced than that of soil plants. They are also capable of degrading organic pollutant compounds in association with potential bacteria as above described (Sects. 1 and 2). From the viewpoint of water treatment technology, it is possible to purify water as the plants grow while using light energy, so there is almost no need for a large amount of power consumption associated with aeration, which is essential for conventional activated sludge treatment in the wastewater treatment processes. The first advantage of the duckweed production in wastewater is its potential contribution to SDGs 13 – Climate Action, through energy saving water purification process. Recently, the value of the product duckweed biomass is very much spotlighted, which may accelerate introduction of the duckweed to the process.

5.1 Duckweed as a Protein Resource

Duckweed is named after “*the weed which ducks eat,*” and is known to have high nutritional value. In particular, the protein content reaches 20–45% per dry-weight of the whole plant, which score is more than 10% of corn (seed only) and comparable to 36% of soybean (seed only). It has also been confirmed that, similar to soybeans, duckweeds almost meets the recommended feed composition values for chickens [42]. On the other hand, regarding the nutritional value of chicken eggs fed with duckweeds, cholesterol, vitamin A, vitamin E, and beta-carotene remained unchanged, and omega-3 fatty acids increased 1.6 times. More interestingly, the score of yolk color was improved from 7 for the soybean-blended feed to 11 for the

duckweed-blended feed on a 14-full score scale. In Japan, duckweed (especially *Wolffia globosa*) has long been used as raw feed for the coloring of Nishikigoi and Goldfish (e.g., Ranchu). There is also an anecdote that when the duckweed was removed from the pond where the carp was kept, the orange body color became lighter. This is expected to relate to the fact that duckweed contains a large amount of carotenoid compounds such as lutein and zeaxanthin in addition to chlorophyll. In addition, it has been reported that the lipid and fatty acid contents of wild duckweed (*L. minor*) are 3.1% and 0.8%, respectively, which are not so high. However, 72% of the fatty acids are unsaturated fatty acids in which α -linolenic acid (omega-3 series) and linoleic acid (omega-6 series) account for 58%. It is nutritionally interesting that the former ratio is higher than latter [43, 44]. It is also known to contain 0.015% coumaric acid, which is reported to reduce the risk of stomach cancer by suppressing the production of nitrosamines. In addition, vitamin B12, which is mainly contained in animal foods, is also attracting attention from vegans (strict vegetarians) as plants contain almost no vitamin B12. Duckweed is also considered a candidate for space food in the United States with its excellent capacity for elemental circulation. In this way, duckweed is not only a tool for purifying water but can be a resource for livestock feed and even highly nutritious functional crops, which is the second advantage of the duckweed in relation to SDGs 15 – Life on Land.

5.2 Duckweed as a Starch Resource

Duckweed is also capable of accumulating large amount of carbohydrates such as starch, as it can be inferred from the fact that it is taxonomically classified into the family Araceae. Although it depends on the environmental conditions, wild duckweed has a carbohydrate content up to 50%, of which starch accounts for 20% under some stress condition [43]. On the other hand, the content of phenolic compounds such as persistent lignin is only 2.4% compared to 12 to 20% of energy biomass such as rice straw and wheat, which makes the duckweed as a soft biomass with high utilization efficiency. Furthermore, the content of glucose, including as starch or cellulose is 33% per biomass, which is a high quality substrate material for bioethanol fermentation or a raw material for petroleum alternative products. In other words, duckweed glucose can supply non-petroleum chemical intermediates such as 1,3-propanediol, hydroxymethylfurfural, and succinic acid, which are important in the field of green chemistry, at a low production cost to replace corn and potatoes that compete with food. Duckweeds are the plants that change protein and carbohydrate contents freely according to the environmental conditions. For example, in a well-nourished environment, the growth rate of duckweed is high and a large amount of protein is accumulated up to about 45%. On the contrary, in a stress environment such as nutrient depletion and high salt environment, the growth rate decreases and the starch content increases. When duckweed is transferred to tap water containing no nutrient minerals and left for a week, the protein content decreases from 30% to 11% and the amount of starch accumulation increases to

about 45%. Interestingly, despite the absence of nutrient minerals, the amount of biomass increases about 1.5 times in wet weight or 3 times in dry-weight in tap water condition. Similar tendency has been confirmed even in a salty water environment in which seawater is diluted about 3 times. In addition, the starch content is also increased by applying low temperature stress of about 5°C. In particular, the starch content of winter buds reaches higher than 50%. One of the multi-benefits of duckweed is that it can increase the protein content or starch content according to the needs. Xu et al. [45] reported that duckweed in anaerobic digested pig effluent produced 9.4-tons of starch per hectare per year. It has been also reported that 6.4-kL of ethanol can be produced per hectare per year by saccharification treatment with an enzyme cocktail (conversion yield of 94.7%) and subsequent yeast fermentation. This ethanol production yield by duckweed was about 50% higher than that of ethanol production using corn. It has been also verified by other groups that the yields of ethanol and methane gas produced by duckweeds are sufficiently high [46–48]. It is also noteworthy that the content of recalcitrant lignins is significantly low (3–5% of dry mass) compared with other land plants (12–14% in *Arabidopsis thaliana*) and trees (20–40%). This can be probably explained by the fact that the duckweeds live floating on the water and do not need to have a tough cell wall to resist gravity for stand straight. The ability to accumulate a large amount of starch, which is easily saccharified, is the third advantage of the duckweed contributing to SDGs 12 – Responsible Production and Consumption.

Various platform chemicals have been produced in biorefinery and it has been shown that renewable biomass can be used as a resource, the so-called green chemistry. These include ethanol, lactic acid, succinic acid, levulinic acid, sorbitol, 1,3-propanediol, hydroxymethylfurfural, and 2,5-furandicarboxylic acid. In addition, several value-added chemicals and biobased and biodegradable polymers produced in biorefinery have been commercialized including polylactic acid and polyhydroxybutyrate. However, solving the energy problems required by biorefinery is essential for building a truly sustainable society. Therefore, in order to develop a sustainable biorefinery, it is important to produce high value-added bioproducts along with bioenergy in an integrated biorefinery system [49]. Additional advantage of duckweed in biomass production is the ease of recovery. In other words, you just scoop the water surface with a net or a belt conveyor. There is no need for driving large tractors for harvesting crops such as corn and soybeans. Microalgae are also attracting attention as inexpensive and useful biomass resource with the ability of water purification, however, there is a fact that they need for a harvesting filter that boosts production costs. Although duckweeds have a number of advantageous features, the bottleneck of its industrial production is the technology for further accelerating the growth rate.

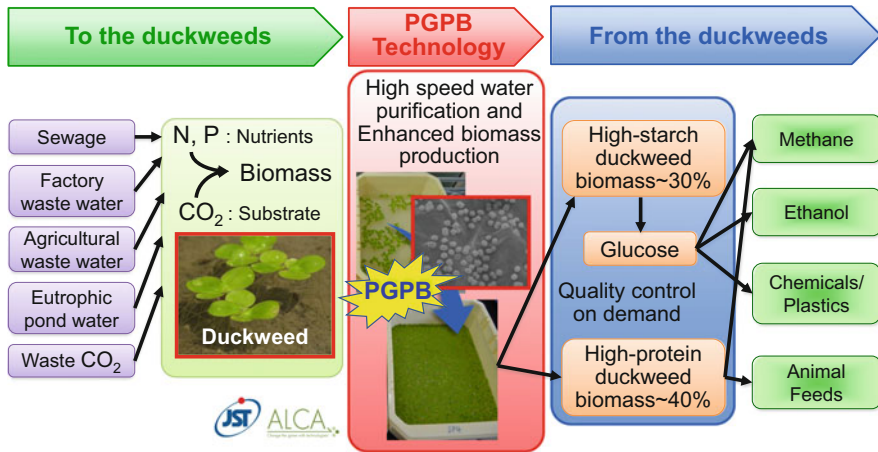


Fig. 16 Conceptual illustration of the duckweed industry. Waste water or eutrophic water can be cost-free N and P nutrients for the duckweed growth. Waste CO₂ from the factory can be fixed into the duckweed biomass. Introduction and enrichment of plant growth-promoting bacteria, PGPB, accelerates the growth of duckweeds leading to high speed water purification and enhanced biomass production. The duckweeds accumulate proteins up to 40% of the dry mass under favorable conditions. On the other hand, the duckweeds start to reduce proteins and accumulate starch up to 30% under stressful conditions including nutrient poor or high salt. High-protein duckweeds are useful feedstock for animal feeds and methane fermentation. High-starch duckweeds are useful feedstock for methane and ethanol fermentation and chemicals/plastics

5.3 Utilization of PGPB for Accelerating Duckweed Industries

The total number of bacteria living on the earth is estimated about 10^{30} . It weighs as much as 5×10^{17} g. On the other hand, 7.4 billion people live on the earth today and their total weight is only 4×10^{14} g. To our great surprise, total bacteria are 1,000 times heavier than total humans, and it is no exaggeration to say that the earth is a bacterial planet. Looking at the human body, indigenous bacteria live at various places from the epidermis to the oral cavity and intestines, their number is estimated to be about 100 trillion to 1,000 trillion. The number of human cells is only about 37 trillion. The power of bacteria, truly indigenous living organisms on the earth, with such a huge number and a long history of more than 3 billion years, is still far from our understanding. In the field of biology, the importance of treating animals and plants as holobionts, totality of hosts and coexisting microorganisms, or hologenomes has been pointed out in recent years. Regarding research on holobiont in the aquatic plant duckweeds, our Japanese research teams are recognized as global pioneers leading this field. JST-ALCA, Advanced Low Carbon Technology Research and Development Program, 2011–2015 Biotechnology Subcommittee “Development of Higher-order Vegetation Bioprocess Utilizing Rhizosphere Microbial Symbiotic System” and subsequent 2016–2019 Practical Enabling Technology

Project “Effective Aquatic Biomass Production Utilizing Mutualistic Microorganisms”, we have developed basic technologies for duckweed holobiont control and low-carbon type water purification system (Fig. 16) [13, 20, 27, 32–34, 39, 41, 48, 50]. This is based on an innovative game changing technology concept of deep knowing their interacting mechanisms and making the best use of the natural symbiotic systems, which is not based on genetic recombination or excessive fertilization that causes ecological or environmental issues. We should remind that “nature is the best teacher.”

References

1. Salt DE, Smith RD, Raskin I (1998) Phytoremediation. *Annu Rev Plant Physiol Plant Mol Biol* 49:643–668
2. Hiltner L (1904) Über neue erfahrungen und problem auf dem gebiet der bodenbakteriologie und unter besonderes berücksichtigung der grundungen und brauche. *Arb Dtsch Landwirt Ges Berl* 98:59–78
3. Kuiper I, Lagendijk EL, Bloemberg GV, Lugtenberg BJ (2004) Rhizoremediation: a beneficial plant-microbe interaction. *Mol Plant-Microbe Interact* 17:6–15
4. Chaudhry Q, Blom-Zandstra M, Gupta S, Joner EJ (2005) Utilizing the synergy between plants and rhizosphere microorganisms to enhance breakdown of organic pollutants in the environment. *Environ Sci Pollut Res* 12:34–48
5. Radwan S, Sorkhoh N, el-Nemr, I. (1995) Oil biodegradation around roots. *Nature* 376:302
6. Hsu TS, Bartha R (1979) Accelerated mineralization of two organophosphate insecticides in the rhizosphere. *Appl Environ Microbiol* 37:36–41
7. Walton BT, Anderson TA (1990) Microbial degradation of trichloroethylene in the rhizosphere: potential application to biological remediation of waste sites. *Appl Environ Microbiol* 56:1012–1016
8. Binet P, Portal JM, Leyval C (2000) Dissipation of 3–6-ring polycyclic aromatic hydrocarbons in the rhizosphere of ryegrass. *Soil Biol Biochem* 32:2011–2017
9. Shaw LJ, Burns RC (2001) Biodegradation of organic pollutants in the rhizosphere. *Adv Appl Microbiol* 53:1–60
10. Yamaga F, Washio K, Morikawa M (2010) Sustainable biodegradation of phenol by *Acinetobacter calcoaceticus* P23 isolated from the rhizosphere of duckweed *Lemma aoukikusa*. *Environ Sci Technol* 44:6470–6474
11. Lear G (ed) (2016) *Biofilms in bioremediation: current research and emerging technologies*. Caister Academic Press
12. Acosta K, Xu J, Gilbert S, Denison E, Brinkman T, Lebeis S, Lam E (2020) Duckweed hosts a taxonomically similar bacterial assemblage as the terrestrial leaf microbiome. *PLoS One* 15(2): e0228560
13. Iwashita T, Tanaka Y, Tamaki H, Yoneda T, Makino A, Tateno Y, Li Y, Toyama T, Kamagata Y, Mori K (2020) Comparative analysis of microbial communities in the fronds and roots of three duckweed species: *Spirodela polyrrhiza*, *Lemma minor*, and *Lemma aequinoctialis*. *Microb Environ* 35:ME20081
14. Toyama T, Yu N, Kumada H, Sei K, Ike M, Fujita M (2006) Accelerated aromatic compounds degradation in aquatic environment by use of interaction between *Spirodela polyrrhiza* and bacteria in its rhizosphere. *J Biosci Bioeng* 101:346–353
15. Toyama T, Sato Y, Inoue D, Sei K, Chang Y-C, Kikuchi S, Ike M (2009) Biodegradation of bisphenol A and bisphenol F in the rhizosphere sediment of *Phragmites australis*. *J Biosci Bioeng* 108:147–150

16. Ying G-G, Williams B, Kookana R (2002) Environmental fate of alkylphenols and alkylphenol ethoxylates—a review. *Environ Int* 28:215–226
17. Soares A, Guieysse B, Jefferson B, Cartmell E, Lester JN (2008) Nonylphenol in the environment: a critical review on occurrence, fate, toxicity and treatment in wastewaters. *Environ Int* 34:1033–1049
18. Toyama T, Momotani N, Ogata Y, Miyamori Y, Inoue D, Sei K, Mori K, Kikuchi S, Ike M (2010) Isolation and characterization of 4-tert-butylphenol-utilizing *Sphingobium fuliginis* strains from *Phragmites australis* rhizosphere sediment. *Appl Environ Microbiol* 76:6733–6740
19. Toyama T, Murashita M, Kobayashi K, Kikuchi S, Kanunari S, Tanaka Y, Ike M, Mori K (2011) Acceleration of nonylphenol and 4-tert-octylphenol degradation in sediment by *Phragmites australis* and associated rhizosphere bacteria. *Environ Sci Technol* 45:6524–6530
20. Toyama T, Ojima T, Tanaka Y, Mori K, Morikawa M (2013) Sustainable biodegradation of phenolic endocrine-disrupting chemicals by *Phragmites australis*-rhizosphere bacteria association. *Water Sci Technol* 68:522–529
21. Morikawa M (2010) Dioxygen activation responsible for oxidation of aliphatic and aromatic hydrocarbon compounds: current state and variants. *Appl Microbiol Biotechnol* 87:1596–1603
22. Brown VM, Jordan DHM, Tiller BA (1967) The effect of temperature on the acute toxicity of phenol to rainbow trout in hard water. *Water Res* 1(8–9):587–594
23. Pedersen G, Brynskov J, Saermark T (2002) Phenol toxicity and conjugation in human colonic epithelial cells. *Scand J Gastroenterol* 37(1):74–79
24. Arnon DI, Hoagland DR (1939) A comparison of water culture and soil as media for crop production. *Science* 89(2318):512–514
25. Kunihiro N, Haruki M, Takano K, Morikawa M, Kanaya S (2005) Isolation and characterization of *Rhodococcus* sp. strains TMP2 and T12 that degrade 2,6,10,14-tetramethylpentadecane (pristane) at moderately low temperatures. *J Biotechnol* 115(2):129–136
26. Ramey BE, Koutsoudis M, von Bodman SB, Fuqua C (2004) Biofilm formation in plant-microbe associations. *Curr Opin Microbiol* 7(6):602–609
27. Yamakawa Y, Jog R, Morikawa M (2018) Effects of co-inoculation of two different plant growth-promoting bacteria on duckweed. *Plant Growth Regul* 86(2):287–296
28. Iijima S, Washio K, Okahara R, Morikawa M (2009) Biofilm formation and proteolytic activities of *Pseudoalteromonas* bacteria that were isolated from fish farm sediments. *Microbial Biotechnol* 2:361–369
29. Juni E (1978) Genetics and physiology of *Acinetobacter*. *Annu Rev Microbiol* 32:349–371
30. Ishii S, Koki J, Unno H, Hori K (2004) Two morphological types of cell appendages on a strongly adhesive bacterium *Acinetobacter* sp. strain Tol 5. *Appl Environ Microbiol* 70(8):5026–5029
31. Kang SM, Joo GJ, Hamayun M, Na CI, Shin DH, Kim HY, Hong JK, Lee IJ (2009) Gibberellin production and phosphate solubilization by newly isolated strain of *Acinetobacter calcoaceticus* and its effect on plant growth. *Biotechnol Lett* 31(2):277–281
32. Utami D, Kawahata A, Sugawara M, Jog R, Miwa K, Morikawa M (2018) Effect of exogenous general plant growth regulators on the growth of the duckweed *Lemna minor*. *Front Chem* 6: 251
33. Toyama T, Kuroda M, Ogata Y, Hachiya Y, Quach A, Tokura K, Tanaka Y, Mori K, Morikawa M, Ike M (2017) Enhanced biomass production of duckweeds by inoculating a plant growth-promoting bacterium, *Acinetobacter calcoaceticus* P23, in sterile medium and non-sterile environmental waters. *Water Sci Technol* 76(6):1418–1428
34. Ishizawa H, Ogata Y, Hachiya Y, Tokura K, Kuroda M, Inoue D, Toyama T, Tanaka Y, Mori K, Morikawa M, Ike M (2020) Enhanced biomass production and nutrient removal capacity of duckweed via two-step cultivation process with a plant growth-promoting bacterium, *Acinetobacter calcoaceticus* P23. *Chemosphere* 238:124682
35. Cedergreen N, Madsen TV (2002) Nitrogen uptake by the floating macrophyte *Lemna minor*. *New Phytol* 155(2):285–292

36. Ishizawa H, Kuroda M, Inoue K, Inoue D, Morikawa M, Ike M (2019) Colonization and competition dynamics of plant growth-promoting/inhibiting bacteria in the phytosphere of the duckweed *Lemna minor*. *Microbial Ecol* 77(2):440–450
37. Liu W, Yang C, Shi S, Shu W (2014) Effects of plant growth-promoting bacteria isolated from copper tailings on plants in sterilized and non-sterilized tailings. *Chemosphere* 97:47–53
38. Qiao J, Yu X, Liang X, Liu Y, Borriss R, Liu Y (2017) Addition of plant-growth-promoting *Bacillus subtilis* PTS-394 on tomato rhizosphere has no durable impact on composition of root microbiome. *BMC Microbiol* 17(1):1–12
39. Xie W, Su J, Zhu Y (2015) Phyllosphere bacterial community of floating macrophytes in paddy soil environments as revealed by Illumina high-throughput sequencing. *Appl Environ Microbiol* 81(2):522–532
40. Anderson M, Habiger J (2012) Characterization and identification of productivity-associated rhizobacteria in wheat. *Appl Environ Microbiol* 78(12):4434–4446
41. Ishizawa H, Kuroda M, Morikawa M, Ike M (2017) Evaluation of environmental bacterial communities as a factor affecting the growth of duckweed *Lemna minor*. *Biotechnol Biofuels* 10(1):62
42. Anderson KE, Lowman Z, Stomp A-M, Cheng J (2011) Duckweed as a feed ingredient in laying hen diets and its effect on egg production and composition. *Int J Poultry Sci* 10(1):4–7
43. Zhao X, Moates GK, Wellner N, Collins SRA, Coleman MJ, Waldron KW (2014) Chemical characterisation and analysis of the cell wall polysaccharides of duckweed (*Lemna minor*). *Carbohydr Polym* 111:410–418
44. Appenroth K-J, Sree S, Bohm V, Hammann S, Vetter W, Leiterer M, Jahreis G (2017) Nutritional value of duckweeds (Lemnaceae) as human food. *Food Chem* 217:266–273
45. Xu J, Cui W, Cheng J, Stomp A (2011) Production of high-starch duckweed and its conversion to bioethanol. *Biosyst Eng* 110(2):67–72
46. Ge X, Zhang N, Phillips GC, Xu J (2012) Growing *Lemna minor* in agricultural wastewater and converting the duckweed biomass to ethanol. *Bioresour Technol* 124:485–488
47. Verma R, Suthar S (2015) Utility of duckweeds as source of biomass energy: a review. *Bioenergy Res* 8(4):1589–1597
48. Toyama T, Hanaoka T, Tanaka Y, Morikawa M, Mori K (2018) Comprehensive evaluation of nitrogen removal rate and biomass, ethanol, and methane production yields by combination of four major duckweeds and three types of wastewater effluent. *Bioresour Technol* 250:464–473
49. Takkellapati S, Li T, Gonzalez MA (2018) An overview of biorefinery derived platform chemicals from a cellulose and hemicellulose biorefinery. *Clean Techn Environ Policy* 20(7):1615–1630
50. Khailina Y, Jog R, Boonmak C, Oyama T, Toyama T, Morikawa M (2021) Indigenous bacteria, an excellent reservoir of functional plant growth promoters for enhancing duckweed biomass yield on site. *Chemosphere* 268:129247